Transactions of the ASME®

Technical Editor, LEWIS T. WHEELER (1997)

Department of Mechanical Engineering,
University of Houston,
Houston, TX 77204-4792

APPLIED MECHANICS DIVISION

Chairman, J. W. HUTCHINSON
Secretary, L. ANAND
Associate Technical Editors,
R. ABEYARATNE (1994)
T. R. AKYLAS (1994)
D. M. BARNETT (1996)
S. A. BERGER (1994)
I. M. DANIEL (1996)
W. DRUGAN (1997)
G. J. DVORAK (1995)
E. J. HAUG, JR. (1996)
J. T. JENKINS (1996)
S. KYRIAKIDES (1997)
S. LICHTER (1995)
W. K. LIU (1996)
X. MARKENSCOFF (1994)
D. M. PARKS (1995)
J. N. REDDY (1995)
W. N. SHARPE, JR. (1996)
S. W. SHAW (1997)
C. F. SHIH (1995)
M. SHINOZUKA (1997)
M. TAYA (1996)

BOARD ON COMMUNICATIONS

Chairman and Vice-President
R. D. ROCKE

Members-at-Large
T. BARLOW, N. H. CHAO, A. ERDMAN,
G. JOHNSON, L. KEER, W. MORGAN,
E. M. PATTON, S. PATULSKI, R. E. REDER,
S. ROHDE, R. SHAH, F. WHITE,
J. WHITEHEAD

OFFICERS OF THE ASME
President, P. J. TORPEY
Exec. Director
D. L. BELDEN
Treasurer
R. A. BENNETT

PUBLISHING STAFF
Mng. Dir., Publ.,
CHARLES W. BEARDSLEY
Managing Editor,
CORNELIA MONAHAN
Production Editor,
JUDITH SIERANT
Production Assistant,
MARISOL ANDINO

Transactions of the ASME, Journal of Applied Mechanics (ISSN 0021-8936) is published quarterly (Mar., June, Sept., Dec.) for $185.00 per year by The American Society of Mechanical Engineers, 345 East 47th Street, New York, NY 10017. Second class postage paid at New York, NY and additional mailing office. POSTMASTER: Send address changes to Transactions of the ASME, Journal of Applied Mechanics, c/o THE AMERICAN SOCIETY OF MECHANICAL ENGINEERS, 22 Law Drive, Box 2300, Fairfield, NJ 07007-2300.

CHANGES OF ADDRESS must be received at Society headquarters seven weeks before they are to be effective. Please send old label and new address.

PRICES: To members, $40.00, annually: to nonmembers, $185.00.
Add $30.00 for postage to countries outside the United States and Canada.

STATEMENT from By-Laws. The Society shall not be responsible for statements or opinions advanced in papers or ... printed in its publications (B7.1, Par. 3).

COPYRIGHT © 1994 by The American Society of Mechanical Engineers. Authorization to photocopy material for internal or personal use under circumstances not falling within the fair use provisions of the Copyright Act is granted by ASME to libraries and other users registered with the Copyright Clearance Center (CCC) Transactional Reporting Service provided that the base fee of $3.00 per article is paid directly to CCC, 27 Congress St., Salem, MA 01970. Request for special permission or bulk copying should be addressed to Reprints/Permission Department.

INDEXED by Applied Mechanics Reviews and Engineering Information, Inc. Canadian Goods & Services Tax Registration #126148048

Journal of Applied Mechanics

Published Quarterly by The American Society of Mechanical Engineers

VOLUME 61 • NUMBER 3 • SEPTEMBER 1994

509 In Memoriam

TECHNICAL PAPERS

511 Constrained Elastic-Plastic Materials
H. C. Lin and P. M. Naghdi

519 Some Remarks on the Wedge Paradox and Saint-Venant's Principle
X. Markenscoff

524 Plastic Spin and Related Issues in Phenomenological Plasticity
V. A. Lubarda and C. F. Shih

530 An Energy Criterion for the Onset of Shear Localization in Thermal Viscoplastic Materials, Part I: Necessary and Sufficient Initiation Conditions
T. G. Shawki

538 An Energy Criterion for the Onset of Shear Localization in Thermal Viscoplastic Materials, Part II: Applications and Implications
T. G. Shawki

548 Interactions Between Dislocations and Anisotropic Elastic Elliptical Inclusions
Wen J. Yen and Chyanbin Hwu

555 Analysis of the Second Mixed Boundary Value Problem for a Thin Plate
Norio Hasebe, Takuji Nakamura, and Yoshihiro Ito

560 Crack Propagation at and Near Bimaterial Interfaces: Linear Analysis
P. H. Geubelle and W. G. Knauss

567 Load Diffusion and Absorption Problems From a Finite Fiber to Elastic Infinite Matrix
Ven-Gen Lee and Toshio Mura

575 Hilbert Transform Generalization of a Classical Random Vibration Integral
P. D. Spanos and S. M. Miller

582 A Circular Crack System in an Infinite Elastic Medium Under Arbitrary Normal Loads
Zhou Yong and M. T. Hanson

589 Simulation of Cone Bore Growth in Bearings With a Three-Ring Model
R. W. Neu and Huseyin Sehitoglu

596 Propagation of Surface Waves Across an Anisotropic Layer
E. N. Its and J. S. Lee

605 Swerve During Three-Dimensional Impact of Rough Rigid Bodies
W. J. Stronge

612 Bending of a Layered Isotropic Plate With Periodic Debondings
E. Danicki

618 Equivalent Nonlinear System Method for Stochastically Excited Hamiltonian System
W. Q. Zhu, T. T. Soong, and Y. Lei

624 An Inverse Mode Problem for the Continuous Model of an Axially Vibrating Rod
Y. M. Ram

629 An Exact Solution of the Unsteady Navier-Stokes Equations Resulting From a Stretching Surface
S. H. Smith

634 A Theory of Hydrodynamic Lubrication Involving the Mixture of Two Fluids
F. Dai and M. M. Khonsari

642 Finite Element Analysis of Quasi-static Contact Problems Using Minimum Dissipation of the Energy Principle
N. N. Kishore, A. Ghosh, S. K. Rathore, and P. V. Kishore

649 Exact Transient Full-Field Analysis of an Antiplane Subsurface Crack Subjected to Dynamic Impact Loading
Chien-Ching Ma and Szu-Kuzi Chen

656 Transient Response of Multiple Rigid Foundations on an Elastic, Homogeneous Half-Space
F. Guan and M. Novak

664 Nondimensional Parameters and Equations for Buckling of Anisotropic Shallow Shells
M. P. Nemeth

670 Thermodynamics of Duffing's Oscillator
V. Berdichevsky, O. Özbek, and W. W. Kim

676 Reconsideration of the Stress-Focusing Effect in a Uniformly Heated Solid Cylinder
T. Hata

681 Marangoni Convection With a Deformable Surface
F. McCaughan

689 On the Geometry of Nonholonomic Dynamics
H. Essén

695 Plausibility of Structural Constitutive Equations for Isotropic Soft Tissues in Finite Static Deformations
Y. Lanir

703 Three-Dimensional Frictional Contact Analysis Using the Homotopy Method
J. K. Park and B. M. Kwak

(Contents continued on Outside Back Cover)

Downloaded 04 May 2010 to 171.66.16.52. Redistribution subject to ASME license or copyright; see http://www.asme.org/terms/Terms_Use.cfm

CONTENTS (CONTINUED)

BRIEF NOTES

On the Modeling of Fracture of Brittle Solids — 710
Y. V. Petrov and N. F. Morozov

A Note on Peel Stresses in Single-Lap Adhesive Joints — 712
Ming-Yi Tsai and J. Morton

A Sufficient Stability Condition for Linear Conservative Gyroscopic Systems — 715
Jinn-Wen Wu and Tsu-Chin Tsao

Buckling Load of Composite Conical Shells Under Axial Compression — 718
Liyong Tong

Stress Intensity Factors for Plate Bending and Shearing Problems — 719
A. T. Zehnder and Chung-Yuen Hui

Response of a Disk Mass on a Half-Space to Dilatational Waves — 722
Tierang Liu and Xiangzhou Zhang

Rayleigh Waves on a Rotating Surface — 724
N. S. Clarke and J. S. Burdess

Linear Flow and Deformation in a Poroelastic Disk With a Free Surface — 726
J. R. Sachs, M. R. Glucksberg, O. E. Jensen, and J. B. Grotberg

729 Weakly Nonlinear Deformation of a Thin Poroelastic Layer With a Free Surface
O. E. Jensen, M. R. Glucksberg, J. R. Sachs, and J. B. Grotberg

731 Stress Intensity Factors of Two-Dimensional and Three-Dimensional Cracks Next to a Thermally Mismatched Inclusion
W. H. Müller, D. O. Harris, and D. D. Dedhia

736 Coupled Transient Thermoelastic Contact Problem in an Edge-Cracked Plate
Cha'o-Kuang Chen and Bor-Lih Kuo

738 Crack-Tip Singular Fields in Nonhomogeneous Materials
Zhi-He Jin and Naotake Noda

740 An Analytical Solution for Adsorption and Desorption Problems in Porous Media
K. Muralidhar and J. Swarup

742 Half-Space Instabilities and Short Wavelength Bifurcations in Cylinders and Rectangular Blocks
K. T. Chau

744 To the Construction of Uniformly Valid Forward-Area Asymptotics in Terms of the Ray Method in Dynamic Problems in Linear Viscoelasticity
Y. A. Rossikhin and M. V. Shitikova

DISCUSSION

747 **Characteristics of Modal Coupling in Nonclassically Damped Systems Under Harmonic Excitation, by I. W. Park, J. S. Kim, and F. Ma—Discussion by S. M. Shahruz with Authors' Closure**

BOOK REVIEWS

749 ***Elasticity*, by J. R. Barber . . .** Reviewed by **C. O. Horgan**

749 ***Plasticity and Creep*, by J. J. Skrzypek . . .** Reviewed by **Z. Mróz**

ANNOUNCEMENTS AND SPECIAL NOTES

529 9th International Conference on Numerical Methods for Thermal Problems—Call for Papers

604 Symposium on Recent Developments in Theories of Viscoplasticity—Call for Papers

641 Change of Address Form

648 19th International Congress of Theoretical and Applied Mechanics—Announcement

663 9th International Conference on Numerical Methods in Laminar and Turbulent Flow—Call for Papers

688 Books Received by the Office of the Technical Editor

748 Thermal Stress '95—Announcement

751 Worldwide Mechanics Meetings List

753 Reviewers List for 1993-1994

Downloaded 04 May 2010 to 171.66.16.52. Redistribution subject to ASME license or copyright; see http://www.asme.org/terms/Terms_Use.cfm

Paul M. Naghdi
1924–1994

Mechanics lost one of its most ardent proponents with the recent death of Paul Naghdi. Having been diagnosed as suffering from lung cancer at the beginning of the year, Naghdi faced the disease with fortitude, and continued to devote himself to his field. However, his condition worsened rapidly in June and he finally succumbed on July 9, 1994 at his home in Berkeley. He is dearly missed by his children and grandchildren, and by his friends and colleagues from around the world.

Paul Naghdi was born in Tehran on March 29, 1924. In 1943, he undertook a perilous voyage to the U.S. to pursue his education. He studied mechanical engineering at Cornell University and was graduated in 1946. After a short period in the U.S. Army, he enrolled in the graduate program in the Engineering Mechanics Department of The University of Michigan. He was granted U.S. citizenship in 1948. He received his M.S. degree in 1948, and his doctorate in 1951. During the period 1949–1951, he held the position of Instructor in Engineering Mechanics, and upon receipt of his Ph.D., he was appointed Assistant Professor at Ann Arbor. He was promoted rapidly, to Associate Professor in 1953 and to full Professor the following year. He moved to the University of California at Berkeley in 1958 as Professor of Engineering Science, and spearheaded the establishment of a Division of Applied Mechanics in the Department of Mechanical Engineering there. From 1964 to 1969, he served as Chairman of the Division. From 1991 onwards, he held the Roscoe and Elizabeth Hughes Chair in Mechanical Engineering, and in 1994 he was advanced to the newly instituted position of Professor in the Graduate School.

Throughout his long career, Professor Naghdi participated vigorously in academic life. For him, both the discovery and the transmission of knowledge were deeply satisfying activities which continually enhanced each other. He valued the strongly democratic ideals and processes that exist on the Berkeley campus, and did not shirk the onerous committee work which such institutions entail. He enjoyed the company and conversation of friends and colleagues, especially over dinner with a good bottle of wine.

Naghdi's work on continuum mechanics extended over a period of more than 40 years and encompassed almost all aspects of the mechanical behavior of solids and fluids. A consummate theoretician, he was most strongly attracted by fundamental questions in mechanics and always sought to treat these at the highest level of generality. He is best known for his work in the areas of shell theory and plasticity, but is also recognized for his contributions to linear and nonlinear elasticity, viscoelasticity, the theories of fluid sheets and jets, continuum thermodynamics, mixture theory, etc.

Naghdi's interest in elastic shells and plates dated back to his graduate student days at The University of Michigan, where he attended summer lectures in 1949 on elastic plates by Stephen Timoshenko (who had immigrated to the U.S. in 1922). Working along classical lines, Naghdi subsequently developed a systematic treatment of elastic shells and plates undergoing small deformations.[1]

During the 1950s, the modern renaissance in continuum mechanics was gathering momentum. It had started out in the 1940s as an interest in nonlinear elastic materials and non-Newtonian fluids, but quickly spread to envelop a much broader range of material behavior. Naghdi embraced the emerging theoretical developments and began to consider in a new light

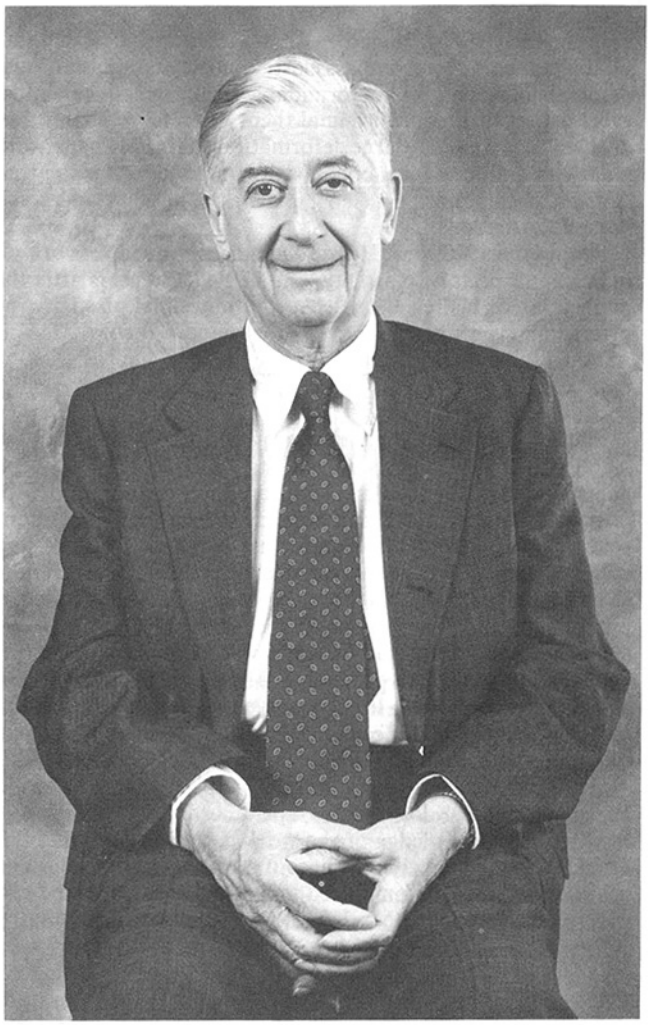


Photo credit: Geoffry Johnson, Berkeley (1994)

the mechanics which he had learned from the classical authors, such as Love, Lamb, and Whittaker. As regards shell theory, he soon realized that a completely new viewpoint could be taken which would lead to an essential clarification of the subject. This is the theory of the *Cosserat surface* (named after the early 20th-century French elasticians Eugène and Francois Cosserat). The Cosserat surface is a mathematical model which idealizes a shell-like structure as a curved surface upon which additional independent vector fields are defined. Naghdi was able to show that inertia, momentum, and angular momentum could be ascribed to the additional fields in such a way that a set of general dynamical equations for the deformations of shells could be obtained. He was invited to write the Handbuch der Physik article on shells and plates.[2] This appeared in 1972 and is universally recognized as the definitive treatment of the subject.

The second major focal area that attracted Naghdi from the beginning of his career until the very end is the behavior of elastic-plastic materials. By the mid 1950s, a reasonably satisfactory theory of plasticity had been developed for materials

[1] Naghdi, P. M., 1963, "Foundations of Elastic Shell Theory," *Progress in Solid Mechanics*, Vol. 4, pp. 1–90.

[2] Naghdi, P. M., 1972, "The Theory of Shells and Plates," *Handbuch der Physik*, S. Flügge, ed., Vol. VIa/2, Springer-Verlag, New York, pp. 425–640.

Copyright © 1994 by ASME
Downloaded 03 May 2010 to 171.66.16.20. Redistribution subject to ASME license or copyright; see http://www.asme.org/terms/Terms_Use.cfm

undergoing small deformations. Naghdi and his co-workers performed a number of experimental studies and also contributed several analytical papers on infinitesimal plasticity. Naghdi's review paper of 1960 set forth a comprehensive treatment of the theory of infinitesimal plasticity and is still widely cited.[3]

In the early 1960s, Naghdi set himself the task of extending plasticity theory to encompass elastic-plastic materials at finite deformations. This was a formidable challenge, since almost every aspect of the infinitesimal theory had to be changed in order to accommodate large deformations. His 1965 paper with his friend and long-term collaborator A. E. Green is the first systematic treatment of elastic-plastic materials undergoing large deformations.[4]

During the 1970s and 1980s, Naghdi continued to work on important aspects of plasticity, and in 1990, 30 years after the publication of his review article on infinitesimal plasticity, he offered an even finer account of the modern theory.[5] This is a thought-provoking analysis of the subject, and as was the case with the 1960 review, it unveils many unexplored avenues for future research.

Paul Naghdi had a long and enjoyable association with the Applied Mechanics Division and its Journal. His very first paper (on elastoplastic plates) appeared in the *Journal of Applied Mechanics* in 1952, and a steady stream of contributions followed throughout his career. Just before his death—and with a considerable degree of physical discomfort—he carefully checked the page proofs of a paper on plasticity which is published in the present issue of the Journal.

Naghdi's service to the Division was exemplary. Over the years, he was an active member of numerous committees. During the period 1967–1972, he served on the Executive Committee of the Applied Mechanics Division, and was Chairman of the Committee in 1972. For its 50th Anniversary in 1977, Naghdi undertook the preparation of a history of the Division.[6] Based on archival documents, tape-recorded interviews, and his first-hand knowledge of the workings of The ASME, this article provides a valuable account of the aspirations and achievements of the committed individuals who founded and promoted the Applied Mechanics Division.[7]

Naghdi's professional role extended beyond the AMD, to The ASME at large, and to national and international organizations. He rarely (if ever) missed a Winter Annual Meeting of The ASME. From 1972 to 1984, he served on the U.S. National Committee on Theoretical and Applied Mechanics, and was Chairman of the Committee in 1979–1980. During the period 1978–1984, he was a member of the General Assembly of the International Union of Theoretical and Applied Mechanics. His last appointment was to the ASME Committee on Honors (1986–1994); of which he was Chairman during 1991–1994. At great personal hardship, he flew to Denver in April of 1994 to chair the Committee's final meeting under his stewardship.

Naghdi's talents as a teacher are legendary. At Berkeley, he introduced and continually refined a magnificent series of courses on theoretical mechanics. These incorporate modern ideas on finite deformations, shell theory, plasticity, fluid sheets and jets, and many other topics of research interest. Naghdi's lectures were well-prepared, clearly delivered, highly original, and intellectually provocative. They also reflected his deep understanding of the history of mechanics and his encyclopedic knowledge of the modern literature.

In recognition of his achievements, Naghdi received many prestigious awards. For his fundamental contributions to plasticity and to shell theory, he was awarded the Timoshenko medal in 1980, which justly placed his name on the list of the top engineering scientists of this century (i.e., Timoshenko himself, G. I. Taylor, T. von Kármán, W. Prager, J. P. Den Hartog, and others). He was made an Honorary Member of The ASME in 1983, and a Member of the National Academy of Engineering in 1984. In 1986, he was awarded the Eringen medal of the Society of Engineering Science. He held Honorary Doctor's Degrees from the National University of Ireland (1987) and Université Catholique de Louvain (1992). In 1994, he was honored with the Berkeley Citation (which is Berkeley's equivalent to an honorary doctoral degree). In celebration of his 70th birthday, a collection of research papers by his former students and colleagues is being published.[8]

Through his scientific papers (which number over 200), inspired teaching, and dedicated professional efforts, Paul Naghdi contributed immeasurably to the revitalization of continuum mechanics in the 20th century. His influence on our field will be distinctly felt for a long time to come.

James Casey
University of California at Berkeley

[3] Naghdi, P. M., 1960, "Stress-Strain Relations in Plasticity and Thermoplasticity," *Proceedings of the Second Symposium on Naval Structural Mechanics*, Pergamon Press, New York, pp. 121–167.

[4] Green, A. E., and Naghdi, P. M., 1965, "A General Theory of an Elastic-Plastic Continuum," *Archive for Rational Mechanics and Analysis*, Vol. 18, pp. 251–281.

[5] Naghdi, P. M., 1990, "A Critical Review of the State of Finite Plasticity," *Journal of Applied Mathematics and Physics (ZAMP)*, Vol. 41, pp. 315–394.

[6] Naghdi, P. M., 1979, "A Brief History of the Applied Mechanics Division of ASME," ASME JOURNAL OF APPLIED MECHANICS, Vol. 46, pp. 721–749.

[7] Because of its immense historical value to the AMD, the source material for Naghdi's article was placed by him in December 1980 with the Smithsonian Institution in Washington, D.C. It is archived in the Division of Engineering and Industry, Department of the History of Science and Technology, at the National Museum of American History, under the title: *A.S.M.E. Applied Mechanics Division Archives*.

[8] Casey, J., and Crochet, M. J., eds., 1994, *Theoretical, Experimental, and Numerical Contributions to the Mechanics of Fluids and Solids* (Special issue of *Journal of Applied Mechanics and Physics (ZAMP)*. Here, an essay on Naghdi's work, as well as a list of his papers, can be found.

Downloaded 03 May 2010 to 171.66.16.20. Redistribution subject to ASME license or copyright; see http://www.asme.org/terms/Terms_Use.cfm

H. C. Lin

P. M. Naghdi
Hon. Mem. ASME.

Department of Mechanical Engineering,
University of California,
Berkeley, CA 94720

Constrained Elastic-Plastic Materials

The main purpose of this paper is to present a general (purely mechanical) constrained theory of finitely deforming elastic-plastic materials. Our development is based on a strain-space formulation of plasticity and requires a detailed examination of the effect of constraint on various constitutive ingredients in the unconstrained theory, including the yield functions (in both the stress and strain spaces), the loading criteria, and various response functions. Also examined is the effect of constraint on the restrictions arising from the work inequality of Naghdi and Trapp (1975b).

1 Introduction

The general theory of constrained materials in classical mechanics of deformable media is characterized by a restriction on the class of possible motions. Interest in the general problem of the effect of such constraints on material response is longstanding and hardly needs emphasis here. Background information on the modern treatment of internal constraints is given by Truesdell and Noll (1965, pp. 69–73) who have also supplied a systematic procedure for dealing with purely mechanical constraints. For a related exposition of mechanical constraints see also Sections 2-3 of a paper by Green et al. (1970) which deals with thermomechanical constraints and constrained directed media.

One of the simplest mechanical constraints, namely the condition of incompressibility, has played a central role in the formulation and utilization of constitutive equations for elastic solids (both linear and nonlinear) and Newtonian viscous fluids, as well as the development of constitutive theories of other media including plasticity. Indeed, one version of the oldest constitutive equations for elastic-perfectly plastic materials undergoing small deformations, i.e., the Prandtl-Reuss constitutive relations, employs a constraint of incompressibility. Moreover, interest in the utilization of constraints in the context of plasticity has not diminished, as is evident from the papers of Spencer (1972, 1984) whose work is motivated by certain applications to a fiber-reinforced composite material with metal matrix. The developments just referred to are all carried out for small deformation plasticity. Also, mention should be made here of a paper by Casey (1986) which includes an illuminating derivation of the theory of finitely deforming rigid-plastic materials as a limiting case of a general theory of elastic-plastic materials formulated in a strain-space setting.

The main purpose of the present paper is to present a general constrained theory for finitely deforming elastic-plastic materials with a fairly wide range of applicability, including application to fiber-reinforced composites. The constraint is not necessarily integrable (except during unloading or neutral loading) and the theory is constructed in the context of the strain-space formulation of plasticity; a concise summary of the strain-space formulation can be found in a recent review article by Naghdi (1990, Section 5). After summarizing the basic constitutive ingredients of a strain-space formulation of a purely mechanical nonlinear theory of (rate-dependent) plasticity in Section 2, some motivation and preliminary development for our main objective is provided in Section 3, where the implication of a simple constraint imposed on a tranversely isotropic elastic-plastic material is discussed. The discussion in Section 3 is also of interest for application to a class of composite materials in which the metal matrix may be elastic-plastic (or even rigid plastic) while the deformation in a certain direction is constrained. General developments for constrained elastic-plastic materials, including the consequences of the work inequality of Naghdi and Trapp (1975b) in the presence of constraints, are carried out in Section 4. This is followed by a brief development of constrained rigid-plastic materials in Section 5 as a limiting case of the results in Section 4. Some of the details of the intermediate steps, which require a careful analysis of limiting cases or proofs of a number of results recorded in Sections 3 and 4 are placed in Appendices A to C.

2 General Background

We summarize in this section the basic constitutive ingredients of a strain-space formulation of (rate-independent) plasticity that was initiated in a paper of Naghdi and Trapp (1975a). In this fairly general nonlinear theory of inelastic behavior—which has been developed during the past 15 years—the strain space and its loading criteria are regarded as primary, but many of its features draw from the original thermodynamical theory of Green and Naghdi (1965, 1966) formulated relative to stress space. Additional relevant references on the subject can be found in a recent review article by Naghdi (1990). In particular

Contributed by the Applied Mechanics Division of THE AMERICAN SOCIETY OF MECHANICAL ENGINEERS for publication in the ASME JOURNAL OF APPLIED MECHANICS.

Discussion on this paper should be addressed to the Technical Editor, Professor Lewis T. Wheeler, Department of Mechanical Engineering, University of Houston, Houston, TX 77204-4792, and will be accepted until four months after final publication of the paper itself in the ASME JOURNAL OF APPLIED MECHANICS.

Manuscript received by the ASME Applied Mechanics Division, Dec. 17, 1992; final revision, July 27, 1993. Associate Technical Editor: R. M. Bowen.

Copyright © 1994 by ASME
Downloaded 03 May 2010 to 171.66.16.20. Redistribution subject to ASME license or copyright; see http://www.asme.org/terms/Terms_Use.cfm

we discuss here a system of Lagrangian constitutive equations which incorporates strain-hardening characterization that includes loading surfaces in both strain and stress spaces (Naghdi, 1990, Section 5).

Let the set of variables consisting of the total strain $\mathbf{E}$, the plastic strain $\mathbf{E}_p$, the work-hardening parameter κ, and the shift tensor (or the "back stress") α be designated as

$$U=(\mathbf{E},\ W),\ W=(\mathbf{E}_p,\ \kappa,\ \alpha) \tag{1}$$

and introduce a constitutive assumption for the stress response and its inverse in the form

$$\mathbf{S}=\hat{\mathbf{S}}(U),\ \mathbf{E}=\hat{\mathbf{E}}(W), \tag{2}$$

where $\mathbf{S}$ denotes the symmetric Piola-Kirchhoff stress tensor and we have assumed that for fixed values of the variables W, the expression $(2)_1$ is invertible in the form $(2)_2$ with

$$V=(\mathbf{S},\ W). \tag{3}$$

Further, we admit a loading function f in stress space as a function of the variables (3) and note that for fixed values of W the equation

$$f(V)=0 \tag{4}$$

represents the loading surface in stress space, i.e., a hypersurface in the six-dimensional space of the symmetric stress $\mathbf{S}$. In view of $(2)_1$, the left-hand side of (4) can be rewritten as a different function g of the variables $(1)_1$, i.e.,

$$\begin{aligned} f(V)&=f(\mathbf{S},\ W)\\ &=f[\hat{\mathbf{S}}(U),\ W]=g(U). \end{aligned} \tag{5}$$

It follows that for fixed values of $(\mathbf{E}_p,\ \kappa,\ \alpha)$ the equation

$$g(U)=0 \tag{6}$$

is the loading surface in strain space, i.e., a hypersurface in the six-dimensional space of the symmetric strain $\mathbf{E}$. Moreover, as noted in (5) the relation $g(U)\leftrightarrow f(V)$ always holds, but the set of *loading criteria* for the strain-space formulation and the (derived) loading conditions of the stress space are not *equivalent* (see Table 1 on p. 339 of Naghdi, 1990) throughout elastic-plastic deformation. We recall that the loading criteria of the strain-space formulation are defined by

(a) $g<0$ (elastic state),

(b) $g=0$ and $\hat{g}<0$ (unloading from an elastic-plastic state),

(c) $g=0$ and $\hat{g}=0$ (neutral loading),

(d) $g=0$ and $\hat{g}>0$ (loading), (7)

$$\hat{g}=\frac{\partial g}{\partial \mathbf{E}}\bullet\dot{\mathbf{E}}. \tag{8}$$

The constitutive assumptions for the rate of plastic strain $\dot{\mathbf{E}}_p$, the rate of work-hardening $\dot{\kappa}$ and the rate of shift tensor (or "back stress") $\dot{\alpha}$ that are linear in the rate of strain $\dot{\mathbf{E}}$ during loading, i.e., when $g=0$, $\hat{g}>0$, as well as the so-called "consistency" condition that during loading the strain trajectory remains on the yield surface ($\dot{g}=0$, $\hat{g}>0$), can be shown to yield the reduced expressions (Naghdi and Trapp, 1975; Casey and Naghdi, 1984b)

$$\dot{\mathbf{E}}_p=\rho\hat{g},\quad \dot{\kappa}=\lambda\hat{g},\quad \dot{\alpha}=\beta\hat{g}\ \ (g=0,\ \hat{g}\geq 0) \tag{9}$$

and the consistency condition

$$1+\lambda\frac{\partial g}{\partial\kappa}+\frac{\partial g}{\partial\alpha}\bullet\beta+\frac{\partial g}{\partial\mathbf{E}_p}\bullet\rho=0. \tag{10}$$

In (9)–(10), a superposed dot denotes the material time derivative, ρ and β are symmetric second-order tensor-valued functions of U and λ is a scalar-valued function of U. The above equations and the loading criteria constitute the *flow rules* of the strain-space formulation of finite plasticity. Then, in addition to the response function for the stress, an elastic-plastic material is completely specified by four functions g, λ, ρ, and β subject to the restriction demanded by the consistency condition. In fact, if $\partial g/\partial\kappa\neq 0$, the consistency condition may be used to solve for λ.

The constitutive results outlined above must be augmented with appropriate criteria for strain-hardening behavior of the material pertaining to hardening, softening and perfectly plastic behavior as discussed by Casey and Naghdi (1981, 1984a) and summarized in Naghdi (1990, Eqs. (4.19)–(4.20)). It should be clear that the basic loading criteria of the theory are those of the strain-space formulation in terms of $\hat{g}$, but $\hat{f}$ plays an important role in the strain-hardening characterization; in this connection, see Table 1 in Naghdi (1990).

As noted above (following (10)), the constitutive equations of the (rate-independent) theory of finitely deforming elastic-plastic materials during loading, i.e., when $\dot{\mathbf{E}}_p$, $\dot{\kappa}$, and $\dot{\alpha}$ are not zero, require the knowledge of

$$\left\{\begin{matrix}\text{the stress response } \hat{\mathbf{S}},\ \text{the loading function } g\\ \text{the tensor functions } \rho \text{ and } \beta \text{ and the scalar function } \lambda\end{matrix}\right\}. \tag{11}$$

Moreover, once g and $\mathbf{S}$ (as listed in (11)) are specified, then f is determined also and no additional constitutive specification is needed for the determination of $\hat{f}$, $\hat{g}$.

For later reference, we also recall the expressions for the stress rate and the strain rate (Casey and Naghdi, 1984b,c) in the forms

$$\dot{\mathbf{S}}=\boldsymbol{L}[\dot{\mathbf{E}}]+\frac{\partial\hat{\mathbf{S}}}{\partial W}[\dot{W}],\quad \dot{\mathbf{E}}=\boldsymbol{M}[\dot{\mathbf{S}}]+\frac{\partial\hat{\mathbf{E}}}{\partial W}[\dot{W}]. \tag{12}$$

In $(12)_{1,2}$, the operators $\boldsymbol{L}$ and $\boldsymbol{M}$ defined by

$$\boldsymbol{L}=\frac{\partial\hat{\mathbf{S}}}{\partial\mathbf{E}},\quad \boldsymbol{M}=\frac{\partial\hat{\mathbf{E}}}{\partial\mathbf{S}} \tag{13}$$

are assumed to be symmetric positive definite and satisfy the identity

$$\boldsymbol{L}\boldsymbol{M}=\boldsymbol{M}\boldsymbol{L}=\boldsymbol{I},\ \ \boldsymbol{I}=\frac{1}{2}(\delta_{KP}\delta_{LQ}+\delta_{KQ}\delta_{LP})\mathbf{e}_K\otimes\mathbf{e}_L\otimes\mathbf{e}_P\otimes\mathbf{e}_Q, \tag{14}$$

where $\boldsymbol{I}$ is the fourth-order unit tensor, the symbol $\otimes$ denotes tensor product and δ_{KL} is the Kronecker delta representing the components of the second-order unit tensor referred to the basis $\mathbf{e}_K\otimes\mathbf{e}_L$. Also, we need to recall the symmetric second-order tensor $\hat{\sigma}$ and $\hat{\epsilon}$ given by

$$\begin{aligned} \hat{\sigma}&=\frac{\partial\hat{\mathbf{S}}}{\partial\mathbf{E}_p}[\rho]+\frac{\partial\hat{\mathbf{S}}}{\partial\kappa}\lambda+\frac{\partial\hat{\mathbf{S}}}{\partial\alpha}[\beta],\\ \hat{\epsilon}&=\frac{\partial\hat{\mathbf{E}}}{\partial\mathbf{E}_p}[\rho]+\frac{\partial\hat{\mathbf{E}}}{\partial\kappa}\lambda+\frac{\partial\hat{\mathbf{E}}}{\partial\alpha}[\beta], \end{aligned} \tag{15}$$

which can be related to $(12)_1$, as shown in Casey and Naghdi (1984b).

Substituting $(12)_1$ into $(12)_2$ and using the identity $\boldsymbol{M}\boldsymbol{L}=\boldsymbol{I}$ in (14) results in an expression which is linear in the rate quantities $\dot{W}=(\dot{\mathbf{E}},\ \dot{\kappa},\ \dot{\alpha})$ with an operator independent of $\dot{W}$. Since this expression must remain valid for every choice of the rate quantities $(\dot{\mathbf{E}}_p,\ \dot{\kappa},\ \dot{\alpha})$, it readily follows that

$$\begin{aligned} &\frac{\partial\hat{\mathbf{E}}}{\partial\mathbf{E}_p}+\boldsymbol{M}\frac{\partial\hat{\mathbf{S}}}{\partial\mathbf{E}_p}=0,\quad \frac{\partial\hat{\mathbf{E}}}{\partial\kappa}+\boldsymbol{M}\left[\frac{\partial\hat{\mathbf{S}}}{\partial\kappa}\right]=0,\\ &\frac{\partial\hat{\mathbf{E}}}{\partial\alpha}+\boldsymbol{M}\frac{\partial\hat{\mathbf{S}}}{\partial\alpha}=0. \end{aligned} \tag{16}$$

In addition, we recall the related relationships given previously by Casey and Naghdi (1984c, Eqs. (26)) between $\hat{\sigma}$ and $\hat{\epsilon}$, namely

$$\hat{\epsilon}=-\boldsymbol{M}[\hat{\sigma}],\quad \hat{\sigma}=-\boldsymbol{L}[\hat{\epsilon}]. \tag{17}$$

Although the structure of the basic theory is quite elegant, the solution of the general problem in terms of the constitutive ingredients (11) represents a formidable task. Because of this

Downloaded 03 May 2010 to 171.66.16.20. Redistribution subject to ASME license or copyright; see http://www.asme.org/terms/Terms_Use.cfm

complexity, it is desirable to simplify the theory by placing physically plausible restrictions on the form of the constitutive response functions. With this background and a desire for obtaining some systematic constitutive restrictions in the purely mechanical theory, the following work assumption was proposed by Naghdi and Trapp (1975b): *The external work done on the body by surface tractions and by body forces in any sufficiently smooth spatially homogeneous cycle $C(t_o, t_f)$ during the time interval (t_o, t_f) is non-negative.* This work assumption was shown by Naghdi and Trapp (1975b) to imply the inequality

$$\int_{t_o}^{t_f} \mathbf{S}\cdot\dot{\mathbf{E}}\, dt \geq 0, \tag{18}$$

where the times t_o and t_f designate, respectively, the time of the beginning and end of the cycle.

Background information concerning the derivation of (18) and an account of the restrictions that can be derived from the work inequality (18) is given in Naghdi (1990, Subsection 5C), where references to the original sources of contributions can also be found. These restrictions are

$$\mathbf{S} = \frac{\partial \hat{\psi}}{\partial \mathbf{E}}, \quad \psi = \hat{\psi}(U), \tag{19}$$

$$H(t)/\hat{g} \geq 0 \quad (g(U) = 0,\ g(\tilde{U}) \leq 0), \tag{20}$$

$$\hat{\sigma}\cdot\dot{\mathbf{E}} \leq 0 \quad (g(U) = 0,\ \hat{g} > 0) \tag{21}$$

where the second-order tensor $\hat{\sigma}$ is given by $(15)_1$ and the scalar function H is defined by

$$H(t)\left[\left(\frac{\partial \hat{\psi}}{\partial \mathbf{E}_p}(\tilde{U}(t)) - \frac{\partial \hat{\psi}}{\partial \mathbf{E}_p}(U(t))\right)\rho(U) + \left(\frac{\partial \hat{\psi}}{\partial \alpha}(U(t)) - \frac{\partial \hat{\psi}}{\partial \alpha}(U(t))\right)\beta(U) + \left(\frac{\partial \hat{\psi}}{\partial \kappa}(\tilde{U}(t)) - \frac{\partial \hat{\psi}}{\partial \kappa}(U(t))\right)\lambda(U)\right]\hat{g}(t), \tag{22}$$

and

$$\tilde{U} = U|_{\mathbf{E}=\mathbf{E}_0} = (\mathbf{E}_o,\ W), \quad g(\tilde{U}) \leq 0. \tag{23}$$

From (21) follows the restriction

$$\hat{\sigma} = -\gamma \frac{\partial g}{\partial \mathbf{E}}, \quad \gamma = \gamma(U) \geq 0 \quad (g(U) = 0). \tag{24}$$

The two restrictions (19)–(20) are both necessary and sufficient for the validity of (18) but (21) is only necessary.

The results (19), (20), and (21) or (24) were derived (during the period 1975–1987) by considering a smooth homogeneous cycle of motion $C(t_o, t_f)$ which begins at an interior point $e_{MN}(t_o) = e^o_{MN}$ of the yield (or loading) surface ∂E and returns to the same value of strain $e^o_{MN} = e_{MN}(t_f)$ at the completion of the cycle. In the derivation of (19) a special cycle is used in which loading does not occur, but in the derivation of (20) and (21) a part of the cycle of motion involves loading ($g = 0$, $\hat{g} > 0$). The condition (19) establishes the existence of a stress potential ψ for the elastic-plastic materials under consideration. The condition (20) represents an additional constitutive restriction on the first partial derivatives of ψ which is also related to convexity of yield surfaces. Finally, according to (21), the symmetric second-order tensor $\hat{\sigma}$ is directed along the normal to the yield surface in *strain space*.

The result (19) was first given in Casey and Naghdi (1984b) although it was implied in the final results discussed in Section 5 of Naghdi and Trapp (1975b). The normality condition (24) was first derived by Naghdi and Trapp (1975b) from (18), although a much simpler proof was supplied later by Casey (1984). The restriction (20) was derived by Casey and Tseng as a necessary condition from (18). More recently, it has been shown by Lin and Naghdi (1989) that the two conditions (19)–(20) are also sufficient for the validity of inequality (18).

3 Some Preliminary Development for Constrained Elastic-Plastic Materials

In order to motivate the nature of constraints and their effects on the full constitutive response of the variables (11) for elastic-plastic materials, we consider in this section a simple constraint such that the component of the strain rate is zero in one direction, say in the x_3-direction of the rectangular Cartesian coordinates x_i $(i = 1, 2, 3)$. To this end, suppose the stress response of an elastic-plastic material and its inverse are of the form (2), and confine attention to tranversely isotropic material (for example, a finite cylindrical body with the x_3-axis coincident with the axis of cylinder). Consider now a sequence of such elastic-plastic cylinders, each of which has a higher value of the stiffness coefficient $\mathfrak{L}_{3333}$ while the remaining constitutive coefficients $\mathfrak{L}_{KLMN}$ have constant values. It is clear that for an arbitrary fixed value of the stress rate $\dot{s}_{33}$, the sample with a higher value of $\mathfrak{L}_{3333}$ can only sustain a lower value of the strain rate $\dot{e}_{33}$. In fact, in the limit

$$\mathfrak{L}_{3333} \to \infty, \quad \dot{e}_{33} \to 0, \quad \text{with } \dot{s}_{33} = \text{arbitrary finite.} \tag{25}$$

We recall from Section 2 the expressions for the rate of stress and rate of strain, which for our immediate purpose can be conveniently recorded as

$$\dot{s}_{KL} = \mathfrak{L}_{KLMN}\dot{e}_{MN} + \frac{\partial \hat{s}_{KL}}{\partial W}\dot{W},$$

$$\dot{e}_{KL} = \mathfrak{M}_{KLMN}\dot{s}_{MN} + \frac{\partial \hat{e}_{KL}}{\partial W}\dot{W}, \tag{26}$$

where the coefficients $\mathfrak{L}_{KLMN}$ and $\mathfrak{M}_{KLMN}$ are defined by

$$\mathfrak{L}_{KLMN} = \frac{\partial \hat{s}_{KL}}{\partial e_{MN}}, \quad \mathfrak{M}_{KLMN} = \frac{\partial \hat{e}_{KL}}{\partial s_{MN}} \tag{27}$$

and satisfy the identity

$$\mathfrak{M}_{KLMN}\mathfrak{L}_{MNRS} = \frac{1}{2}(\sigma_{KR}\delta_{LS} + \delta_{KS}\delta_{LR}). \tag{28}$$

Similarly, the component forms of the identities (16) may conveniently be recorded as

$$\frac{\partial \hat{e}_{KL}}{\partial e^p_{MN}} + \mathfrak{M}_{KLPQ}\frac{\partial \hat{s}_{PQ}}{\partial e^p_{MN}} = 0, \quad \frac{\partial \hat{e}_{KL}}{\partial \kappa} + \mathfrak{M}_{KLPQ}\frac{\partial \hat{s}_{PQ}}{\partial \kappa} = 0,$$

$$\frac{\partial \hat{e}_{KL}}{\partial \alpha_{MN}} + \mathfrak{M}_{KLPQ}\frac{\partial \hat{s}_{PQ}}{\partial \alpha_{MN}} = 0. \tag{29}$$

We continue our discussion on a sequence of elastic-plastic cylinders and examine the identity (28) for the limiting case in which (25) holds. Then, since all the stiffness coefficients $\mathfrak{L}_{KLMN}$ except $\mathfrak{L}_{3333}$ remain constant, in the limiting case of the sequence (for details see Appendix A)

$$\mathfrak{M}_{33RS} \to 0 \quad \text{as} \quad \mathfrak{L}_{3333} \to \infty. \tag{30}$$

Moreover, since we have assumed that the quantities

$$\left\{\frac{\partial \hat{s}_{PQ}}{\partial e^p_{MN}}, \quad \frac{\partial \hat{s}_{PQ}}{\partial \kappa}, \quad \frac{\partial \hat{s}_{PQ}}{\partial \alpha_{MN}}\right\}$$

remain finite for the sequence under consideration, we may conclude from the identities (29) that the first term in each of $(29)_{1,2,3}$ for $K = L = 3$ will tend to zero in view of (30) so that

$$\left\{\frac{\partial \hat{e}_{33}}{\partial e^p_{MN}}, \quad \frac{\partial \hat{e}_{33}}{\partial \kappa}, \quad \frac{\partial \hat{e}_{33}}{\partial \alpha_{MN}}\right\} \to 0 \quad \text{when (30) holds.} \tag{31}$$

Next, we note the following relationship between the component forms of $(17)_2$, namely

$$\hat{\sigma}_{KL} = -\mathfrak{L}_{KLMN}\hat{\epsilon}_{MN}. \tag{32}$$

Downloaded 03 May 2010 to 171.66.16.20. Redistribution subject to ASME license or copyright; see http://www.asme.org/terms/Terms_Use.cfm

Since the quantities $\{\rho_{MN}, \lambda, \alpha_{MN}\}$ which occur in $(15)_2$ are assumed to have finite values in the limiting case (25), it follows from the component form of $(15)_2$, (31), and (32) that in the limiting case of the sequence for which (25) holds

$$\hat{\epsilon}_{33} \to 0, \quad \hat{\sigma}_{33} = \text{indeterminate, when (30) holds.} \tag{33}$$

The result $(25)_2$, namely $\dot{e}_{33} \to 0$, suggests that an elastic-plastic material which is constrained such that

$$\dot{e}_{33} = 0 \tag{34}$$

can be regarded as a limiting case of the sequence of elastic-plastic materials introduced in the first paragraph of this section. An example of such a constrained material is a finite cylindrical body—regarded as a fiber-reinforced composite—consisting of a set of unidirectional inextensible, densely populated fibers embedded in an elastic-plastic matrix. It is important to note that the components $\hat{\sigma}_{KL}$ of the second-order tensor $\hat{\boldsymbol{\sigma}}$ in the presence of the constraint (34) can only be determined to within an arbitrary component $\hat{\sigma}_{33}$, in view of $(33)_2$. Moreover, in the limiting case of the sequence $\dot{e}_{33} = 0$, $e_{33} = \text{constant}$ (determined by its initial value) and the yield function g in (6) now becomes

$$g(U) \to g(U)\,|_{e_{33}=\text{const.}} \to \bar{g}(e_{\alpha\beta}, e_{\alpha 3}, W), \quad (\alpha, \beta = 1, 2). \tag{35}$$

Further, remembering

$$\frac{\partial f}{\partial s_{33}} = \mathfrak{M}_{33MN} \frac{\partial g}{\partial e_{MN}},$$

which readily follows from (5) to $(13)_2$, in the limiting case of the sequence discussed above we also have

$$\frac{\partial f(V)}{\partial s_{33}} \to 0. \tag{36}$$

The results (35)–(36) represent additional effects of a constraint on e_{33}. According to (35), in the presence of (34) the yield function g is necessarily a hypersurface in five-dimensional space of the strain $(e_{\alpha\beta}, e_{\alpha 3})$, while by (36) the yield function f must be independent of s_{33}, i.e., the particular component of the stress $\mathbf{S}$ which is indeterminate by virtue of (34). These, in turn, have additional effects on the loading criteria but we postpone a further discussion of these until the next section.

4 Mechanical Constraints in Elastic-Plastic Materials

In the previous section motivation was provided for a relatively simple mechanical constraint of the form (34) and its effect was partially examined on various constitutive response functions which occur in a general theory of elastic-plastic materials summarized in Section 2. Here we consider a more general constraint and expect that the form of the constitutive assumptions (9) for the rates of the variables W remain valid during loading. Thus, we proceed to consider a general mechanical constraint in the form

$$\phi(\mathbf{E}, W; \mathbf{X}) = 0, \tag{37}$$

where ϕ is a scalar-valued function and any dependence on inhomogeneity is indicated through the argument $\mathbf{X}$. Differentiating (37) with respect to t leads to an equation of the form

$$\mathbf{A} \cdot \dot{\mathbf{E}} = 0, \quad \mathbf{A} = \mathbf{A}(\mathbf{E}, W; \mathbf{X}), \tag{38}$$

where the second-order tensor coefficient function $\mathbf{A}$ is to be specified by a constitutive equation. For example, corresponding to the sequence of elastic-plastic material in Section 3, the coefficient function $\mathbf{A}$ in $(38)_2$ may be specified as $\mathbf{A} = \delta_{K3}\delta_{L3}\mathbf{e}_K \otimes \mathbf{e}_L$. Then, with this specification of $\mathbf{A}$, (38) reduces to (34) and we have $\mathbf{A} \cdot \boldsymbol{L}[\mathbf{A}] = \mathfrak{L}_{3333}$ along with other results given in Section 3.

A general consideration of constraints in the theory of elastic-plastic materials necessarily requires separate discussions during *loading* and *unloading* as defined by the conditions (7). During loading ($g = 0$, $\hat{g} > 0$), the constraint Eq. $(38)_1$ is not necessarily integrable and cannot in general be expressed in terms of a potential. However, during unloading and neutral loading ($g = 0$, $\hat{g} \le 0$) in which $W = \text{constant}$, we assume that $(38)_1$ is integrable and admit a constraint in the form (37). Then, during unloading and neutral loading, we may differentiate (37) with respect to t and obtain an equation of the form $(38)_1$ with $\mathbf{A}$ given by

$$\mathbf{A} = \frac{\partial \phi}{\partial \mathbf{E}} \text{ during unloading and neutral loading } (g = 0, \hat{g} \le 0). \tag{39}$$

In the remainder of this section, we concentrate on the analysis pertaining to the implication of the constraint (38) during loading of elastic-plastic materials. During unloading and neutral loading, the effect of constraint with $\mathbf{A}$ given by (39) would be similar to that of an elastic material and will not be discussed here. Thus, in Subsection 4.1, we consider a sequence of elastic-plastic materials and carefully examine the limiting behavior of this sequence in order to exploit the effect of the constraint (38) during loading as can be seen from (44)–(47) below. Next, the main features of constrained elastic-plastic materials are presented in Subsection 4.2 and this is followed by a detailed development of the consequences of the work inequality (18) for constrained elastic-plastic materials in Subsection 4.3.

4.1 Implication of the Limiting Case of a Sequence of Elastic-Plastic Materials. In the previous section, a sequence of material behavior was considered which motivated the simple constraint (34) on the basis of the limiting results (25), (30), (32), and (36). A generalization of such limiting results for a constraint of the form (38) is far from obvious and requires further elaboration and this is the main purpose of this subsection. Thus, we again consider a sequence of elastic-plastic materials and suppose that each member of the sequence has a higher value (than the previous one) of the quantity

$$\mathbf{A} \cdot \boldsymbol{L}[\mathbf{A}] \tag{40}$$

and recall that the fourth order tensor $\boldsymbol{L}$ and its inverse $\boldsymbol{M}$ [see (13) and (14)] are both symmetric and positive definite. Also for this sequence of elastic-plastic materials we assume that $\partial \hat{\mathbf{S}}/\partial W$ and $\boldsymbol{L}[\mathbf{N}]$ remain finite and that the scalar $\mathbf{N} \cdot \boldsymbol{L}[\mathbf{N}]$ remains finite and positive for every symmetric second-order tensor $\mathbf{N}$ which is orthogonal to $\mathbf{A}$ in a six-dimensional strain space, i.e., $\mathbf{N} \cdot \mathbf{N} = 0$.

Now recall the identity $\boldsymbol{L}\boldsymbol{M} = \boldsymbol{I}$ in (14) and write $\mathbf{A} \cdot (\boldsymbol{L}\boldsymbol{M})\mathbf{A} = \mathbf{A} \cdot \boldsymbol{I}\mathbf{A}$, the right-hand side of which is the square of the norm $\|\mathbf{A}\|^2 = |\mathbf{A} \cdot \mathbf{A}|$. Hence, we conclude that

$$\boldsymbol{L}[\mathbf{A}] \cdot \boldsymbol{M}[\mathbf{A}] = \|\mathbf{A}\|^2 > 0. \tag{41}$$

Next, we observe that the operation of $\boldsymbol{L}\boldsymbol{M}$ on $\mathbf{A}$, after also using (14), yields $\boldsymbol{L}\boldsymbol{M}[\mathbf{A}] = \boldsymbol{I}[\mathbf{A}] = \mathbf{A}$. Taking the inner product of both sides of the last result with $\mathbf{N}$, we have

$$\boldsymbol{L}[\mathbf{N}] \cdot \boldsymbol{M}[\mathbf{A}] = \mathbf{N} \cdot \mathbf{A} = 0. \tag{42}$$

The scalar $\mathbf{A}/\|\mathbf{A}\| \cdot \boldsymbol{L}[\mathbf{A}]$ represents the components of $\boldsymbol{L}[\mathbf{A}]$ in the direction of the unit tensor $\mathbf{A}/\|\mathbf{A}\|$ in a six-dimensional strain space. Keeping this in mind, the components $\mathbf{A} \cdot \boldsymbol{L}[\mathbf{A}]$, and similarly $\mathbf{A} \cdot \boldsymbol{M}[\mathbf{A}]$ and $\mathbf{A} \cdot \dot{\mathbf{E}}$ may be interpreted as representing the components of the second-order tensors $\boldsymbol{L}[\mathbf{A}]$, $\boldsymbol{M}[\mathbf{A}]$ and $\dot{\mathbf{E}}$ along directions parallel to the direction of $\mathbf{A}/\|\mathbf{A}\|$ in a six-dimensional vector space. Since the right-hand side of (41) is positive and finite, it follows from (41) that for the sequence of elastic-plastic materials under consideration, the sample with a higher value of $\mathbf{A} \cdot \boldsymbol{L}[\mathbf{A}]$ corresponds to a lower value of $\mathbf{A} \cdot \boldsymbol{M}[\mathbf{A}]$. Moreover, it follows from $(12)_1$ that for arbitrary fixed values of $\dot{\mathbf{S}}$ the sample with a higher value of $\mathbf{A} \cdot \boldsymbol{L}[\mathbf{A}]$ can only sustain a lower value of $\mathbf{A} \cdot \dot{\mathbf{E}}$. We therefore conclude that when the components of $\boldsymbol{L}[\mathbf{A}]$ in the direction of $\mathbf{A}/\|\mathbf{A}\|$ increase *indefinitely*, then the components of $\boldsymbol{M}[\mathbf{A}]$

Downloaded 03 May 2010 to 171.66.16.20. Redistribution subject to ASME license or copyright; see http://www.asme.org/terms/Terms_Use.cfm

and $\dot{\mathbf{E}}$ in the direction of $\mathbf{A}/\|\mathbf{A}\|$ diminishes *indefinitely* so that in the limit

$$\mathbf{A}\cdot\boldsymbol{L}[\mathbf{A}]\to\infty,\quad \mathbf{A}\cdot\boldsymbol{M}[\mathbf{A}]\to 0,$$
$$\mathbf{A}\cdot\dot{\mathbf{E}}\to 0 \text{ with } \dot{\mathbf{S}} = \text{arbitrary finite.} \quad (43)$$

In view of the fact that scalar $\mathbf{N}\cdot\boldsymbol{N}[\mathbf{N}]$ remains finite and positive in the limit of the sequence for which (43) holds, it can be shown that in this limit the tensor $\mathbf{A}$ is linearly independent of all tensors of the type $\boldsymbol{L}[\mathbf{N}]$ with $\mathbf{N}$ satisfying the condition $(42)_2$ (for details, see (1) of Appendix B). It then follows from (42) and $(43)_2$ that in the limit of the sequence

$$\boldsymbol{M}[\mathbf{A}]\to 0. \quad (44)$$

Moreover, with the help of $(15)_2$–(17) and the result (44) in the limit of the sequence we also have (for details, see (2) of Appendix B):

$$\mathbf{A}\cdot\hat{\boldsymbol{\varepsilon}}\to 0,\quad \mathbf{A}\cdot\hat{\boldsymbol{\sigma}}\to\text{indeterminate form.} \quad (45)$$

Further, assuming that the yield function $g(U)$ remains unchanged in the limit of the sequence under discussion, from (5), $(13)_2$ and the result (44) we obtain

$$\mathbf{A}\cdot\frac{\partial f}{\partial\mathbf{S}}=\frac{\partial g}{\partial\mathbf{E}}\cdot\boldsymbol{M}[\mathbf{A}]\to 0. \quad (46)$$

In summary, we note that the conclusion $(43)_3$ suggests that a constrained elastic-plastic material characterized by (38) may be regarded as a limiting case of the sequence of elastic-plastic materials discussed in this subsection. Indeed, the results[1] (43)–(46) suggest that in this limit the functional form (but not the arguments) of tensors $\boldsymbol{L}$, $\boldsymbol{M}$ and the yield function f remain the same as those in Section 2, but as will become evident later (see Theorem 4.1) the same is not necessarily true for $\hat{\boldsymbol{\sigma}}$ defined by $(15)_1$.

4.2 Development of the Constrained Theory. Returning to our main objective in this section, we assume that the coefficient function $\mathbf{A}$ does not depend explicitly on $\dot{\mathbf{E}}$, at least one component of the coefficient is nonzero, and each term of the inner product (on the left-hand side of (38)) is unaltered under superposed rigid-body motions. Moreover, we assume that the stress tensor $\mathbf{S}$ defined by $(2)_1$ is determined to within an additive constraint response $\bar{\mathbf{S}}$ so that

$$\mathbf{S}=\bar{\mathbf{S}}+{}_d\mathbf{S},\quad {}_d\mathbf{S}={}_d\hat{\mathbf{S}}(U). \quad (47)$$

In (47), the determinant part ${}_d\mathbf{S}$ of $\mathbf{S}$ is to be specified by a constitutive equation while the constraint response $\bar{\mathbf{S}}$ has the following properties: It is (i) an arbitrary function of $\mathbf{X}$ and t, (ii) may depend on some kinematical variables but is independent of the rate of strain $\dot{\mathbf{E}}$, and (iii) is *workless*, i.e.,

$$\bar{\mathbf{S}}\cdot\dot{\mathbf{E}}=0. \quad (48)$$

It follows from the constraint Eq. (38) and the condition (48) that $\bar{\mathbf{S}}$ is parallel to $\mathbf{A}$ and is given by (for details, see Appendix C):

$$\bar{\mathbf{S}}=C\mathbf{A}, \quad (49)$$

where $C=C(\mathbf{X}, t)$ is an arbitrary scalar function. For fixed value of $(1)_2$, the constitutive Eq. $(47)_2$ can be inverted in the form

$${}_d\mathbf{E}={}_d\hat{\mathbf{E}}({}_dV),\quad {}_dV=({}_d\mathbf{S}, W) \quad (50)$$

where W is still defined by $(1)_2$. With the use of the response functions in $(47)_2$ and $(50)_1$, much of the basic structure of the constrained theory will have the same forms as those summarized in Section 2 with $\mathbf{S}$ replaced by ${}_d\mathbf{S}$, $\hat{\mathbf{S}}$ replaced by ${}_d\hat{\mathbf{S}}$ in $(47)_2$ and $\hat{\mathbf{E}}$ now replaced by the response function on the right-hand side of $(50)_1$. For example, the expressions $(13)_{1,2}$ and the identities $(14)_{1,2}$ remain valid but now $\hat{\mathbf{S}}$ and $\hat{\mathbf{E}}$ are replaced by those in $(47)_2$ and $(50)_1$ and the response coefficients $\boldsymbol{L}$ and $\boldsymbol{M}$ in the constrained theory will not necessarily have the same values as those in the absence of constraints. Also, now instead of (5), we have (compare (5) and (51))

$$g(U)=g({}_d\hat{\mathbf{E}}({}_dV), W)=f({}_dV), \quad (51)$$

where the variables ${}_dV$ are defined by $(50)_2$. The loading criteria (7) involves $\dot{\mathbf{E}}$ through $\hat{g}$ defined by (8), but now $\dot{\mathbf{E}}$ must be compatible with that in (38) or, said differently, now $\hat{g}$ must satisfy the constraint condition (38). Also, the strain-hardening criteria given by Eqs. (55)–(56) of Naghdi (1990, p. 339) remain valid but with $\hat{f}$ now replaced by $f({}_dV)$ on the right-hand side of (51). We omit details of the modifications of the various results in Section 2 in the presence of constraint condition (38) but elaborate on the nature of the modification of the consequences of the work inequality (18) in the next subsection.

4.3 The Consequence of the Work Inequality in the Constrained Theory. The inequality (18) which is derived from the work assumption of Naghdi and Trapp (1975b) still holds. But now, in view of worklessness of $\bar{\mathbf{S}}$ [see $(47)_1$ and (48)], the integrand of (18) must be replaced by the determinate part ${}_d\mathbf{S}$ of the stress. It is then evident that the restrictions in the constrained theory will differ from (19)–(21) as follows:

(i) the result $(19)_1$ remains valid with $\mathbf{S}$ replaced by ${}_d\mathbf{S}$, which is determined from the function $\hat{\psi}(U)$; (ii) the inequality (20) remains valid but with $\hat{\psi}$ being that specified in (i) for the constrained theory; and (iii) the inequality (21), which restricts the second-order tensor $\hat{\boldsymbol{\sigma}}$, also remains valid but now $\hat{\mathbf{S}}$ in $(15)_1$ is replaced with ${}_d\hat{\mathbf{S}}$ in $(47)_2$. (52)

Despite the relatively simple modification for $\hat{\mathbf{S}}$ in the expression $(15)_1$ indicated under (iii) of (52) the implication of (21) in the constrained theory requires further analysis which depends on the nature of the direction of $\mathbf{A}$ in (38) relative to the normal to the yield surface. To elaborate, consider an arbitrary regular point P on the yield surface (6) in the six-dimensional space of the strain $\mathbf{E}$ and let the second-order tensor $\mathbf{A}$ in (38) be resolved into two components: one component along the normal $\partial g/\partial\mathbf{E}$ to the yield surface and another $\mathbf{A}_T$ in the tangent plane to the yield surface at P. Thus, we write

$$\mathbf{A}=c_1\frac{\partial g}{\partial\mathbf{E}}+\mathbf{A}_T,\quad \mathbf{A}_T\cdot\frac{\partial g}{\partial\mathbf{E}}=0,\quad (g(U)=0), \quad (53)$$

where $\mathbf{A}_T$ in $(53)_2$ is not necessarily zero. Similarly, it is convenient to decompose the second-order tensor $\hat{\boldsymbol{\sigma}}$ (at the regular point P on the yield surface $g=0$) into a component along the normal and a component $\hat{\boldsymbol{\sigma}}_T$ in the tangent plane at P, i.e.,

$$\hat{\boldsymbol{\sigma}}=-\tilde{\gamma}\frac{\partial g}{\partial\mathbf{E}}+\hat{\boldsymbol{\sigma}}_T,\quad \hat{\boldsymbol{\sigma}}_T\cdot\frac{\partial g}{\partial\mathbf{E}}=0\quad (g(U)=0). \quad (54)$$

The coefficient $c_1=c_1(U)$ in $(53)_1$ is a known function determined from the inner product of both sides of $(53)_1$ with $\partial g/\partial\mathbf{E}$ resulting in

$$c_1=\mathbf{A}\cdot\frac{\partial g/\partial\mathbf{E}}{\|\partial g/\partial\mathbf{E}\|^2}, \quad (55)$$

and in (54) the scalar $\tilde{\gamma}$ depends only on U and the minus sign on the right-hand side of $(54)_1$ is introduced for later convenience.

We now state and prove the following:

Theorem 4.1 Under the constraint condition (38), the implication of the inequality $(21)_1$ depends on the direction of the second order tensor $\mathbf{A}$ according to whether (a) $\mathbf{A}_T\neq 0$ or (b) $\mathbf{A}_T=0$. In case (a), $(21)_1$ implies

$$\hat{\boldsymbol{\sigma}}=-\bar{\gamma}\frac{\partial g}{\partial\mathbf{E}}+c_2\mathbf{A},\quad \bar{\gamma}=\bar{\gamma}(U)\geq 0\quad (g(U)=0), \quad (56)$$

where the scalar coefficient

[1] These are the generalizations of the special results (30), (33), and (36).

Downloaded 03 May 2010 to 171.66.16.20. Redistribution subject to ASME license or copyright; see http://www.asme.org/terms/Terms_Use.cfm

$$c_2 = c_2(U) = \frac{\|\hat{\sigma}_T\|^2}{\mathbf{A}\cdot\hat{\sigma}_T}, \quad \hat{\sigma}_T \neq \mathbf{0}. \tag{57}$$

In case (b), $\hat{\sigma} \| \partial g/\partial \mathbf{E}$ and is given by an expression of the form $(24)_1$.

Proof. We first consider the proof of case (a). In view of the decomposition $(53)_1$, it can easily be verified that during neutral loading ($g=0$, $\hat{g}=0$) the scalar quantity $\mathbf{A}\cdot\dot{\mathbf{E}}$ in $(38)_1$ reduces to $\mathbf{A}_T\cdot\dot{\mathbf{E}}$; and, hence, it may be concluded that the constraint condition (38) is equivalent to

$$\mathbf{A}_T\cdot\dot{\mathbf{E}} = 0 \quad \text{during neutral loading } (g=0,\ \hat{g}=0). \tag{58}$$

Substituting of (54) into $(21)_1$ results in the inequality

$$\left(-\tilde{\gamma}\frac{\partial g}{\partial \mathbf{E}} + \hat{\sigma}_T\right)\cdot\dot{\mathbf{E}} \leq 0 \quad (g=0,\ \hat{g}\geq 0), \tag{59}$$

which must hold for all values of $\dot{\mathbf{E}}$ subject to the constraint condition $(38)_1$. Since continuity of various results from *neutral loading* to *loading* demands that (59) remain valid during neutral loading for which $\hat{g}=0$, $(59)_1$ reduces to $\hat{\sigma}_T\cdot\dot{\mathbf{E}}\leq 0$. But from the fact that this latter inequality must hold for all $\dot{\mathbf{E}}$ in the tangent plane, including $-\dot{\mathbf{E}}$, we obtain

$$\hat{\sigma}_T\cdot\dot{\mathbf{E}} = 0 \quad (g=0,\ \hat{g}=0) \tag{60}$$

for all $\dot{\mathbf{E}}$ satisfying the constraint condition (58) during neutral loading. Since both $\hat{\sigma}_T$ and $\mathbf{A}_T$ can be regarded as vector-like quantities in the five-dimensional hyperplane tangent to the yield surface at the point P, by an argument similar to that presented for a different situation[2] in Appendix C, we conclude that $\hat{\sigma}_T$ is parallel to $\mathbf{A}_T$ and hence write

$$\hat{\sigma}_T = c_2\mathbf{A}_T = c_2\left(\mathbf{A} - c_1\frac{\partial g}{\partial \mathbf{E}}\right), \tag{61}$$

where the values of the coefficients c_2 and c_1 are given by (57) and (55), respectively.

Substitution of $(61)_2$ and $(59)_1$ after invoking $(38)_1$, yields an inequality which can be displayed as

$$-\bar{\gamma}\,\hat{g} \leq 0 \quad (g=0,\ \hat{g}\geq 0) \tag{62}$$

where we have set

$$\bar{\gamma} + c_2 c_1 = \bar{\gamma}. \tag{63}$$

Since (63) must hold during loading for which $\hat{g}>0$, it follows from (62) that $\bar{\gamma}\geq 0$. Substitution of $(63)_2$ for $\hat{\sigma}$ into $(56)_1$, together with the restriction for $\bar{\gamma}$ leads to (56) and this completes the proof of case (a).

We now turn to the proof of case (b). With $\mathbf{A}_T=\mathbf{0}$, $\mathbf{A}$ can be displayed as

$$\mathbf{A} = c_1\frac{\partial g}{\partial \mathbf{E}}, \quad (g(U)=0), \tag{64}$$

where c_1 is still given by (55) as can be easily verified by taking the inner product of both sides of (64) with $\partial g/\partial \mathbf{E}$. Using (64) and recalling (8), the left-hand side of $(38)_1$ takes the form

$$\mathbf{A}\cdot\dot{\mathbf{E}} = c_1\,\hat{g}, \quad (g(U)=0). \tag{65}$$

Next, recall the decomposition of $\hat{\sigma}$ in the form $(54)_1$ and note that the steps between (54)–(55) and (59)–(60) still hold but thereafter the argument in the proof is different. In the proof of case (a), Eq. (60) holds for *all* $\dot{\mathbf{E}}$ satisfying the constraint condition (58). But in case (b), the constraint $(38)_1$ is automatically satisfied during neutral loading by virtue of (65) and hence Eq. (60) holds for all $\dot{\mathbf{E}}$ in the five-dimensional hyperplane tangent to the yield surface at P. Furthermore, since $\hat{\sigma}_T$ (which also lies in the five-dimensional tangent hyperplane at P) is independent of $\dot{\mathbf{E}}$, from $(60)_1$ we conclude that $\hat{\sigma}_T = \mathbf{0}$. Then, remembering $(54)_1$, it follows that $\hat{\sigma} \| \partial g/\partial \mathbf{E}$ and this completes the proof of case (b).

[2] Recall that Appendix C provides a proof of parallelism of $\bar{\mathbf{S}}$ and $\mathbf{A}$ from (48) subject to the constraint condition (38). The corresponding parallelism of $\hat{\sigma}_T$ and $\mathbf{A}_T$ here derives from (60) subject to the condition (58).

5 Constrained Rigid-Plastic Materials

We briefly present here the analysis leading to constrained rigid-plastic materials as a limiting case of the theory of Section 4. Our development parallels that of Casey (1986) who obtained results appropriate for the unconstrained rigid-plastic materials as a limiting case of the strain-space formulation of elastic-plastic materials. We begin by introducing the set of variables $\bar{U}$, namely

$$\bar{U} = (\mathbf{E}-\mathbf{E}_p,\ W), \tag{66}$$

the use of which is equivalent to the set U defined by (1). In terms of the variables (66) the stress response $(47)_2$ and similarly $(50)_1$ can be rewritten as

$$\begin{aligned} {}_d\mathbf{S} = {}_d\hat{\mathbf{S}}(U) = {}_d\bar{\mathbf{S}}(\bar{U}), \quad \mathbf{E}-\mathbf{E}_p \\ = {}_d\hat{\mathbf{E}}({}_dV) - \mathbf{E}_p = {}_d\bar{\mathbf{E}}({}_dV), \end{aligned} \tag{67}$$

where the variables ${}_dV$ are defined by $(50)_2$. Keeping in mind the forms (67) and remembering the definition $(13)_{1,2}$, with the use of chain rule we have

$$\boldsymbol{L} = \frac{\partial \hat{\mathbf{S}}}{\partial \mathbf{E}} = \frac{\partial_d \bar{\mathbf{S}}}{\partial(\mathbf{E}-\mathbf{E}_p)}, \quad \boldsymbol{M} = \frac{\partial_d \hat{\mathbf{E}}}{\partial_d \mathbf{S}} = \frac{\partial_d \bar{\mathbf{E}}}{\partial_d \mathbf{S}}. \tag{68}$$

Then, analogously to $(12)_{1,2}$ and in terms of the variables (66) we may write

$$\begin{aligned} {}_d\dot{\mathbf{S}} &= \boldsymbol{L}[\dot{\mathbf{E}} - \dot{\mathbf{E}}_p] + \frac{\partial_d \bar{\mathbf{S}}}{\partial W}[\dot{W}], \\ \dot{\mathbf{E}} - \dot{\mathbf{E}}_p &= \boldsymbol{M}[{}_d\dot{\mathbf{S}}] + \frac{\partial_d \bar{\mathbf{E}}}{\partial W}[\dot{W}], \end{aligned} \tag{69}$$

and by a procedure similar to that which led to (17), we obtain

$$\begin{aligned} \boldsymbol{L}\frac{\partial_d \bar{\mathbf{E}}}{\partial \mathbf{E}_p} + \frac{\partial_d \bar{\mathbf{S}}}{\partial \mathbf{E}_p} = 0, \quad \boldsymbol{L}\left[\frac{\partial_d \bar{\mathbf{E}}}{\partial \kappa}\right] + \frac{\partial_d \bar{\mathbf{S}}}{\partial \kappa} = 0, \\ \boldsymbol{L}\frac{\partial_d \bar{\mathbf{E}}}{\partial \boldsymbol{\alpha}} + \frac{\partial_d \bar{\mathbf{S}}}{\partial \boldsymbol{\alpha}} = 0. \end{aligned} \tag{70}$$

Consider now a sequence of the constrained elastic-plastic materials of the type discussed in Section 4 and suppose that the tensor-valued coefficient $\mathbf{A}$ in (38) is the same for every member of the sequence. Moreover, assume that for arbitrary values of the variables ${}_dV$ each member of the sequence has a lower value of the Euclidean norm $\|{}_d\bar{\mathbf{E}}({}_dV)\|$ than the previous ones so that in the limit of the sequence

$${}_d\bar{\mathbf{E}}({}_dV) \to 0 \quad \text{as} \quad \mathbf{E}-\mathbf{E}_p \to 0, \tag{71}$$

which is the rigid-plastic limit of the sequence of constrained elastic-plastic materials. Assuming sufficient smoothness (i.e., differentiability, continuity, and boundedness) of ${}_d\bar{\mathbf{E}}({}_dV)$, we may deduce from $(71)_1$ and $(68)_2$ that

$$\mathfrak{M} \to 0, \quad \frac{\partial_d \bar{\mathbf{E}}}{\partial \mathbf{E}_p} \to 0, \quad \frac{\partial_d \bar{\mathbf{E}}}{\partial \kappa} \to 0, \quad \frac{\partial_d \bar{\mathbf{E}}}{\partial \boldsymbol{\alpha}} \to 0. \tag{72}$$

Since the tensors $\boldsymbol{L}$ and $\boldsymbol{M}$ satisfy (14), it follows from (72) that

$$\boldsymbol{L} \to \infty \tag{73}$$

in the limit (71) of the sequence. It should be noted that (71)–(73) are analogous to corresponding results derived previously by Casey (1986, Eqs. (48)–(50)).

Next, we assume that the stress response functions in (67), namely ${}_d\bar{\mathbf{S}}$, become indeterminate as $\mathbf{E}-\mathbf{E}_p \to 0$ while the current value of the stress ${}_d\mathbf{S}$ at each material point remains finite, i.e.,

$${}_d\bar{\mathbf{S}} \to \text{indeterminate form and bounded.} \tag{74}$$

Also, it is clear from (70) and the results (72)–(73) that

$$\frac{\partial_d \bar{\mathbf{S}}}{\partial \mathbf{E}_p}, \quad \frac{\partial_d \bar{\mathbf{S}}}{\partial \kappa}, \quad \frac{\partial_d \bar{\mathbf{S}}}{\partial \boldsymbol{\alpha}} \to \text{indeterminate forms,} \tag{75}$$

in the limit $(71)_2$ of the sequence.

Downloaded 03 May 2010 to 171.66.16.20. Redistribution subject to ASME license or copyright; see http://www.asme.org/terms/Terms_Use.cfm

In the remainder of this section, we summarize the main limiting forms of other constitutive aspects of the constrained theory, but omit details since they are similar to those in Subsection III.1 of Casey (1986). Thus, we assume that the yield function $f({}_dV)$ in (51) has a definite limiting form denoted by "$\lim f$" but because of the stress response ${}_d\bar{\mathbf{S}}$ becomes indeterminate in the rigid-plastic limit, while the strain space becomes a point, so that

$$f \to \lim f \quad \text{as} \quad \mathbf{E} - \mathbf{E}_p \to 0. \tag{76}$$

We also assume that during loading (with finite values of $\dot{\mathbf{E}}$), the values of $(\dot{\mathbf{E}}_p, \dot{\kappa}, \dot{\boldsymbol{\alpha}})$ remain finite in the limit $(71)_2$ of the sequence. It then follows that in the rigid-plastic case, the loading criteria (see Eqs. (55)–(64) of Casey (1986)) reduce to:

$$\text{(a) } \dot{\mathbf{E}} = \mathbf{0} \quad \text{(for unloading)},$$
$$\text{(b) } \dot{\mathbf{E}} \neq 0 \quad \text{(for loading)}. \tag{77}$$

Moreover, during loading, the constitutive Eqs. (9) reduce to the same forms as those in Eqs. (122) of Casey (1986), i.e.,

$$\dot{\mathbf{E}} = \gamma\boldsymbol{\rho}, \quad \dot{\kappa} = \gamma\lambda, \quad \dot{\boldsymbol{\alpha}} = \gamma\boldsymbol{\beta}, \quad (\gamma > 0,\ \dot{\mathbf{E}} \neq 0,\ \lim f = 0), \tag{78}$$

in the limit $(71)_2$ of the sequence, but the response functions $(\boldsymbol{\rho}, \lambda, \boldsymbol{\beta})$ in (78) now depend on ${}_d\mathbf{S}$ (rather than $\mathbf{S}$) in addition to their dependence on the variables W. Moreover, no modifications are needed in Eqs. (68)–(75) of Casey (1986).

Acknowledgment

The results reported here were obtained in the course of research supported by the Solid Mechanics Program of the U.S. Office of Naval Research under contract N00014-90-J-1959, R&T 4324-436 with the University of California at Berkeley. The work of H.-C. Lin was supported by a grant from Lawrence Livermore National Laboratory.

References

Casey, J., 1984, "A Simple Proof of a Result in Finite Plasticity," *Quarterly of Applied Mathematics*, Vol. 42, pp. 61–71.

Casey, J., 1986, "On Finitely Deforming Rigid-Plastic Materials," *International Journal of Plasticity*, Vol. 2, pp. 247–277.

Casey, J., and Naghdi, P. M., 1981, "On the Characterization of Strain-Hardening in Plasticity," ASME JOURNAL OF APPLIED MECHANICS, Vol. 48, pp. 285–296.

Casey, J., and Naghdi, P. M., 1984a, "Strain-Hardening Response of Elastic-Plastic Materials." *Mechanics of Engineering Materials*, C. S. Desai and R. H. Gallagher, eds., John Wiley and Sons Ltd., U.K., pp. 61–89.

Casey, J., and Naghdi, P. M., 1984b, "Further Constitutive Results in Finite Plasticity," *Quarterly Journal of Mechanics and Applied Mathematics*, Vol. 37, pp. 231–249.

Casey, J., and Naghdi, P. M., 1984c, "Constitutive Results for Finitely Deforming Elastic-Plastic Materials," *Constitutive Equations: Macro and Computational Aspects*, K. J. Willam, ed., ASME, New York, pp. 53–71.

Casey, J., and Tseng, M., 1984, "A Constitutive Restriction Related to Convexity of Yield Surfaces in Plasticity," *Journal of Applied Mathematics and Physics (ZAMP)*, Vol. 35, pp. 478–496.

Green, A. E., and Naghdi, P. M., 1965, "A General Theory of an Elastic-Plastic Continuum," *Archive for Rational Mechanics and Analysis*, Vol. 18, pp. 251–281.

Green, A. E., and Naghdi, P. M., 1966, "A Thermodynamic Development of Elastic-Plastic Continua," *Proceedings of the IUTAM Symposium on Irreversible Aspects of Continuum Mechanics and Transfer of Physical Characteristics in Moving Fluids*, H. Parkus and L. I. Sedov, eds., Springer-Verlag, New York, pp. 117–131.

Green, A. E., Naghdi, P. M., and Trapp, J. A., 1970, "Thermodynamics of a Continuum with Internal Constraints," *International Journal of Engineering Science*, Vol. 8, pp. 891–908.

Lin, H.-C., and Naghdi, P. M., 1989, "Necessary and Sufficient Conditions for the Validity of a Work Inequality in Finite Plasticity," *Quarterly Journal of Mechanics and Applied Mathematics*, Vol. 42, pp. 13–21.

Naghdi, P. M., 1990, "A Critical Review of the State of Finite Plasticity," *Journal of Applied Mathematics and Physics (ZAMP)*, Vol. 41, pp. 315–394.

Naghdi, P. M., and Trapp, J. A., 1975a, "The Significance of Formulating Plasticity Theory with Reference to Loading Surfaces in Strain Space," *International Journal of Engineering Science*, Vol. 13, pp. 785–797.

Naghdi, P. M., and Trapp, J. A., 1975b, "Restrictions on Constitutive Equations of Finitely Deformed Elastic-Plastic Materials," *Quarterly Journal of Mechanics and Applied Mathematics*, Vol. 28, pp. 25–46.

Noble, B., and Daniel, J. W., 1977, *Applied Linear Algebra*, 2nd ed., Prentice-Hall, Englewood Cliffs, NJ.

Spencer, A. J. M., 1972, *Deformations of Fibre-Reinforced Materials*, Oxford University Press, Oxford, U.K.

Spencer, A. J. M., 1984, "Constitutive Theory for Strongly Anisotropic Solids," *Continuum Theory of the Mechanics of Fibre-Reinforced Composites*, A. J. M. Spencer, ed., Springer-Verlag, New York, pp. 1–32.

Truesdell, C., and Noll, W., 1965, "The Non-linear Field Theories of Mechanics," *S. Flügge's Handbuch der Physik*, Vol. III/3, Springer-Verlag, New York, pp. 1–602.

APPENDIX A

The purpose of this Appendix is to verify the truth of the limiting result $(30)_1$ for the sequence of elastic-plastic cylinders considered in Section 3.

In view of the assumed symmetry properties of the fourth-order tensors $\boldsymbol{L}$ and $\boldsymbol{M}$, their components $\mathfrak{L}_{KLMN}$ and $\mathfrak{M}_{KLMN}$ for the purpose of this Appendix may be regarded as symmetric 6×6 matrices $\overline{\mathfrak{L}}_{IJ}$ and $\overline{\mathfrak{M}}_{IJ}$ $(I, J = 1, \ldots, 6)$ in the six-dimensional strain space, respectively; and, similarly, the right-hand side of (28) may be viewed as a 6×6 identity matrix. The indices I, J in this Appendix take the values $1, 2, \ldots, 6$. Thus, with this notational agreement, $\overline{\mathfrak{L}}_{66}$ stands for the stiffness coefficient $\mathfrak{L}_{3333}$ and so on, and the reciprocal relation (28) assumes the form

$$\overline{\mathfrak{M}}_{IJ}\overline{\mathfrak{L}}_{JK} = \delta_{IK}. \tag{A1}$$

We also indicate here the relationships between some of the components of $\overline{\mathfrak{M}}_{IJ}$ and the corresponding components of $\mathfrak{M}_{KLMN}$ as follows:

$$\begin{aligned} &\overline{\mathfrak{M}}_{16} = \mathfrak{M}_{1133}, && \overline{\mathfrak{M}}_{26} = \mathfrak{M}_{2233}, \\ &\overline{\mathfrak{M}}_{36} = \sqrt{2}\,\mathfrak{M}_{1233}, && \overline{\mathfrak{M}}_{46} = \sqrt{2}\,\mathfrak{M}_{2333}, \\ &\overline{\mathfrak{M}}_{56} = \sqrt{2}\,\mathfrak{M}_{1333}, && \overline{\mathfrak{M}}_{66} = \mathfrak{M}_{3333}. \end{aligned} \tag{A2}$$

Let L and $\mathfrak{L}^*_{IJ}$ denote, respectively, the determinant of $\overline{\mathfrak{L}}_{IJ}$ and its cofactor, and recall standard results from linear alegebra (see, for example, Noble and Daniel, 1977, pp. 198 and 205–208), namely

$$\begin{aligned} &\mathfrak{L}^*_{IJ} = L\delta_{IK}, \\ &\overline{\mathfrak{M}}_{IJ} = \frac{1}{L}\mathfrak{L}^*_{JI}. \end{aligned} \tag{A3}$$

From consideration of $(A3)_1$ with $I = K = 6$ and after observing that the left-hand side of $(A3)_1$ represents a sum of six terms, we readily obtain

$$L = \mathfrak{L}^*_{66}\overline{\mathfrak{L}}_{66} + \sum_{J=1}^{5} \mathfrak{L}^*_{6J}\overline{\mathfrak{L}}_{6J}. \tag{A4}$$

Since all stiffness coefficients $\overline{\mathfrak{L}}_{IJ}$ remain constant, except $\overline{\mathfrak{L}}_{66}$ $(= \mathfrak{L}_{3333})$, for the sequence of cylinders, by the definition of cofactors the cofactor components $\mathfrak{L}^*_{6J}$, $(J = 1, 2, \ldots, 6)$, also remain constant. Hence, by (A4), we have

$$L \to \infty \quad \text{as} \quad \overline{\mathfrak{L}}_{66}\ (= \mathfrak{L}_{3333}) \to \infty. \tag{A5}$$

Next, considering the relation $(A3)_2$ with $J = 6$ and remembering that the coefficients $\mathfrak{L}^*_{6I}$ remain constant, with the use of (A5) we obtain

$$\overline{\mathfrak{M}}_{I6} \to 0 \quad \text{as} \quad \overline{\mathfrak{L}}_{66} \to \infty. \tag{A6}$$

The result (30) now follows at once from (A6) after remembering the notations in (A2).

APPENDIX B

The purpose of this Appendix is to provide detailed proofs of a number of intermediate results which are used in the derivation of (44) and $(45)_{1,2}$ of the main text.

(1) Linear Independence Property of Tensor A. We show here that, in the limiting case of the sequence for which (43)

Downloaded 03 May 2010 to 171.66.16.20. Redistribution subject to ASME license or copyright; see http://www.asme.org/terms/Terms_Use.cfm

holds, the second-order tensor $\mathbf{A}$ in (38) is linearly independent of all second-order tensors $\boldsymbol{L}[\mathbf{N}]$ satisfying the orthogonality condition $(42)_2$. The proof (by contradiction) is as follows. Let $\mathbf{N}^i$, $(i=1, 2, \ldots, 5)$, be a set of five nonzero tensors satisfying $\mathbf{N}^i\mathbf{A}=0$ and designate $\overline{\mathbf{N}}^i$ the limiting values of $\boldsymbol{L}(\mathbf{N}^i)$, i.e.,

$$\boldsymbol{L}[\mathbf{N}^i]\rightarrow\overline{\mathbf{N}}^i \quad \text{when (43) holds.} \tag{B1}$$

Now suppose that the tensor $\mathbf{A}$ admits a linearly dependent representation of the form

$$\mathbf{A}=\sum_{i=1}^{5} a_i\overline{\mathbf{N}}^i, \tag{B2}$$

where at least one of the coefficients a_i is nonzero.

Defining

$$\mathbf{N}^*=\sum_{i=1}^{5} a_i\mathbf{N}^i, \tag{B3}$$

it is clear that this quantity is orthogonal to $\mathbf{A}$, i.e.,

$$\mathbf{N}^*\cdot\mathbf{A}=0. \tag{B4}$$

Next, by considering the operation of $\boldsymbol{L}$ on $\mathbf{N}^*$ we deduce that

$$\boldsymbol{L}[\mathbf{N}^*]=\boldsymbol{L}\left[\sum_{i=1}^{5} a_i\mathbf{N}^i\right]=\sum_{i=1}^{5} a_i\boldsymbol{L}[\mathbf{N}^i] \tag{B5}$$

where in the last step of (B5) the order of summation and linear operation has been interchanged. Then, in the limit of the sequence under consideration, it follows from (B5), (B1), and (B2) that

$$\boldsymbol{L}[\mathbf{N}^*]\rightarrow\mathbf{A} \quad \text{when (43) holds.} \tag{B6}$$

Next, recalling (from Subsection 4.1) that the scalar $\mathbf{N}\cdot\boldsymbol{L}[\mathbf{N}]$ must remain finite and positive for every $\mathbf{N}$ satisfying $(42)_2$, and examination of the inner product of $\mathbf{N}^*$ and $\boldsymbol{L}[\mathbf{N}^*]$ in the limit of the sequence leads to

$$\mathbf{N}^*\cdot\boldsymbol{L}[\mathbf{N}^*]\rightarrow 0 \quad \text{when (43) holds,} \tag{B7}$$

where in obtaining (B7) we have made use of (B6) and (B4). The result (B7) contradicts the positiveness of $\mathbf{N}\cdot\boldsymbol{L}[\mathbf{N}]$ in the limit of the sequence for which (43) holds and the proof is complete.

(2) Proofs of $(45)_{1,2}$. From the inner product of $(16)_2$ with the tensor $\mathbf{A}$ we have

$$\frac{\partial\hat{\mathbf{E}}}{\partial\kappa}\cdot\mathbf{A}+\frac{\partial\hat{\mathbf{S}}}{\partial\kappa}\cdot\mathfrak{M}[\mathbf{A}]=0. \tag{B8}$$

Similarly, from the operation of the transposes of the left-hand sides of $(16)_{1,3}$ with $\mathbf{A}$ we may obtain

$$\left(\frac{\partial\hat{\mathbf{E}}}{\partial\mathbf{E}_p}\right)^T[\mathbf{A}]+\left(\frac{\partial\hat{\mathbf{S}}}{\partial\mathbf{E}_p}\right)^T\mathfrak{M}[\mathbf{A}]=\mathbf{0}, \tag{B9}$$

$$\left(\frac{\partial\hat{\mathbf{E}}}{\partial\alpha}\right)^T[\mathbf{A}]+\left(\frac{\partial\hat{\mathbf{S}}}{\partial\alpha}\right)^T\mathfrak{M}[\mathbf{A}]=\mathbf{0}. \tag{B10}$$

Given the fact that $\partial\hat{\mathbf{S}}/\partial W$ remains finite in the limit of the sequence, it readily follows from (B8)–(B10) that in the limit of the sequence for which (43)and (44) holds, we also have

$$\frac{\partial\hat{\mathbf{E}}}{\partial\kappa}\cdot\mathbf{A}\rightarrow 0, \quad \left(\frac{\partial\hat{\mathbf{E}}}{\partial\mathbf{E}_p}\right)^T[A]\rightarrow\mathbf{0}, \quad \left(\frac{\partial\hat{\mathbf{E}}}{\partial\alpha}\right)^T[\mathbf{A}]\rightarrow\mathbf{0}. \tag{B11}$$

Now, the inner product of $\mathbf{A}$ with $(15)_2$ is

$$\mathbf{A}\cdot\hat{\boldsymbol{\epsilon}}=\boldsymbol{\rho}\cdot\left(\frac{\partial\hat{\mathbf{E}}}{\partial\mathbf{E}_p}\right)^T[\mathbf{A}]+\lambda\frac{\partial\mathbf{E}}{\partial\kappa}\cdot\mathbf{A}+\boldsymbol{\beta}\cdot\left(\frac{\partial\hat{\mathbf{E}}}{\partial\alpha}\right)^T[\mathbf{A}], \tag{B12}$$

the right-hand side of which after an appeal to (B11) yields $(45)_1$.

Next, we consider the inner product of $\mathbf{A}$ with $(17)_2$, namely

$$\mathbf{A}\cdot\hat{\boldsymbol{\sigma}}=-\hat{\boldsymbol{\epsilon}}\cdot\boldsymbol{L}[\mathbf{A}], \tag{B13}$$

and proceed to examine the quantity on the right-hand side of (B13) in the limit of the sequence. As is evident from $(43)_1$ and $(45)_1$, in the limit of the sequence for which (43) holds, the components of the tensor $\boldsymbol{L}[\mathbf{A}]$ in the direction of the unit tensor $\mathbf{A}/\|\mathbf{A}\|$ increases indefinitely and the components of $\hat{\boldsymbol{\epsilon}}$ in the same direction diminishes indefinitely, while the right-hand side of (B13) remains arbitrary finite and $(45)_2$ follows.

APPENDIX C

Given the condition (48) for all $\dot{\mathbf{E}}$ satisfying (38), the purpose of this Appendix is to show that the tensor $\overline{\mathbf{S}}$ in (48) is parallel to $\mathbf{A}$. The proof (by contradiction) is as follows: suppose that $\overline{\mathbf{S}}$ is not parallel to $\mathbf{A}$. Then, we may choose a particular value of $\dot{\mathbf{E}}$ in the form

$$\dot{\mathbf{E}}=\overline{\mathbf{S}}-(\overline{\mathbf{S}}\cdot\mathbf{A})\frac{\mathbf{A}}{\|\mathbf{A}\|^2}. \tag{C1}$$

It can be easily verified that the choice (C1) satisfies the constraint condition (38) as follows:

$$\begin{aligned}\mathbf{A}\cdot\dot{\mathbf{E}}&=\mathbf{A}\cdot(\text{right-hand side of (C1)})\\&=\mathbf{A}\cdot\overline{\mathbf{S}}-(\overline{\mathbf{S}}\cdot\mathbf{A})\frac{\mathbf{A}\cdot\mathbf{A}}{\|\mathbf{A}\|^2}=0.\end{aligned} \tag{C2}$$

Next, taking the inner product of both sides of (C1) with $\overline{\mathbf{S}}$ and invoking the condition (48), we obtain

$$(\overline{\mathbf{S}}\cdot\mathbf{A})^2=\|\overline{\mathbf{S}}\|^2\|\mathbf{A}\|^2. \tag{C3}$$

Using the result (C3), it follows from the value of $\dot{\mathbf{E}}$ in (C1) that

$$\begin{aligned}\|\dot{\mathbf{E}}\|^2&=\left\{\overline{\mathbf{S}}-(\overline{\mathbf{S}}\cdot\mathbf{A})\frac{\mathbf{A}}{\|\mathbf{A}\|^2}\right\}\cdot\left\{\overline{\mathbf{S}}-(\overline{\mathbf{S}}\cdot\mathbf{A})\frac{\mathbf{A}}{\|\mathbf{A}\|^2}\right\}\\&=\|\overline{\mathbf{S}}\|^2-\frac{2}{\|\mathbf{A}\|^2}(\overline{\mathbf{S}}\cdot\mathbf{A})^2+\frac{1}{\|\mathbf{A}\|^2}(\overline{\mathbf{S}}\cdot\mathbf{A})^2\\&=0.\end{aligned} \tag{C4}$$

Therefore, $\dot{\mathbf{E}}=0$ or equivalently

$$\overline{\mathbf{S}}=(\overline{\mathbf{S}}\cdot\mathbf{A})\frac{\mathbf{A}}{\|\mathbf{A}\|^2}, \tag{C5}$$

and hence $\overline{\mathbf{S}}$ is parallel to $\mathbf{A}$ and can be expressed in the form (49).

Downloaded 03 May 2010 to 171.66.16.20. Redistribution subject to ASME license or copyright; see http://www.asme.org/terms/Terms_Use.cfm

Some Remarks on the Wedge Paradox and Saint-Venant's Principle

X. Markenscoff
Professor of Applied Mechanics,
Department of Applied Mechanics
and Engineering Sciences,
University of California, San Diego,
La Jolla, CA 92093
Fellow ASME

The solutions for the wedge loaded by a concentrated couple at its vertex, known as the Carothers-Sternberg-Koiter problem, are examined critically. The cause of the divergence are terms which are fundamental self-equilibrated solutions with unbounded energy arising from the eigenvalues of the wedge and with exponent depending on the angle. The "paradox" occurs at the angle at which the term of the (angle-independent exponent) r^{-2} stress singularity is superseded by the next eigenvalue. These terms are conjectured to be the weight functions of the wedge. The breaking down of St. Venant's principle for the wedge in connection with these terms is also demonstrated. As for the definition of a concentrated couple, it can only exist if the limiting solutions are independent of the path of loading (stable node); for wedge angles bigger than a half-space, they depend on the path of loading, and the loadings that give path independence are characterized.

1 Introduction

A problem that has bewildered elasticians over the last 40 years is the wedge loaded by a concentrated couple at its vertex. For a complete survey of the literature we refer the reader to Dundurs and Markenscoff (1989); here only the more fundamentally different references will be reviewed.

While the phenomenon examined here will be the concentrated couple, there is a larger class of phenomena that manifest the same behavior: a center of dilation or a dipole of dislocations approaching the tip of a crack or an anticrack (Markenscoff, 1991) also exhibit divergent solutions. Also, an embedded wedge with a concentrated couple (Dundurs and Markenscoff, 1989) or with a disclination exhibits analogous behavior (Belov, 1991). In fluid mechanics a similar paradox occurs in the Jeffrey-Hamel viscous flow problem.

This paper is a critical review of the existing solutions in the process of which a new understanding has been achieved. By a "wedge loaded by a concentrated couple" drawn schematically in Fig. 1, we may mean any of the following limiting loading configurations depicted in Fig. 2:

(a) a truncated wedge loaded by distributed tractions on an arc of radius r_i having resultant force zero and resultant moment M, and taking the limit as $r_i \to 0$ (Fig. 2(*a*)). This is the Carothers problem.
(b) a wedge loaded by distributed tractions $p(r)$ on its flanks as in Fig. 2(*b*) having zero resultant force and resultant moment M and taking the limit as the length a of the distribution of the applied tractions vanishes. This is the Sternberg-Koiter problem.
(c) a wedge with a concentrated couple—considered to be the limit of a twisting plug of vanishing radius—applied at an interior point and taking a limit as the concentrated couple approaches the vertex from the inside (Fig. 2(*c*)). This is the approach of Dundurs-Markenscoff (1989).

For angles of the wedge smaller or equal to a half-space, all three problems have the same solution, and then we can talk about a wedge loaded by a concentrated couple represented schematically as in Fig. 1. However, for angles of the wedge bigger than a half-space, the solution of each of the three problems may exist depending on the path of loading, and then the problems are not equivalent. In that case we cannot talk about a concentrated couple at the tip of a wedge. We will examine now each of the three problems separately, and we shall see the connection of this behavior to Saint-Venant's principle.

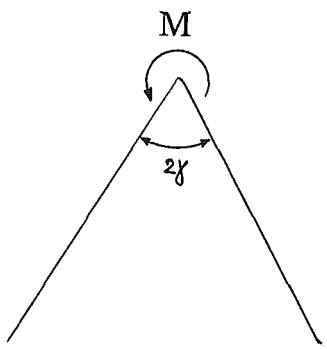


Fig. 1 A wedge "loaded by a concentrated couple"

Contributed by the Applied Mechanics Division of THE AMERICAN SOCIETY OF MECHANICAL ENGINEERS for publication in the ASME JOURNAL OF APPLIED MECHANICS.

Discussion on this paper should be addressed to the Technical Editor, Professor Lewis T. Wheeler, Department of Mechanical Engineering, University of Houston, Houston, TX 77204-4792, and will be accepted until four months after final publication of the paper itself in the ASME JOURNAL OF APPLIED MECHANICS.

Manuscript received by the ASME Applied Mechanics Division, Dec. 21, 1992; final revision, Mar. 23, 1993. Associate Technical Editor: L. T. Wheeler.

Copyright © 1994 by ASME
Downloaded 03 May 2010 to 171.66.16.20. Redistribution subject to ASME license or copyright; see http://www.asme.org/terms/Terms_Use.cfm

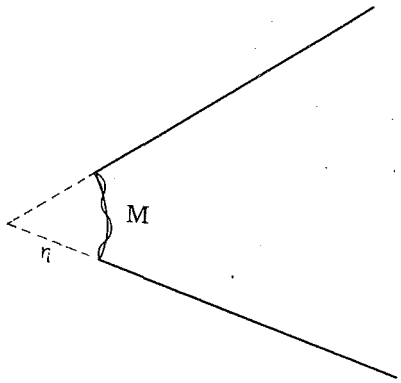


Fig. 2(*a*) The Carothers problem

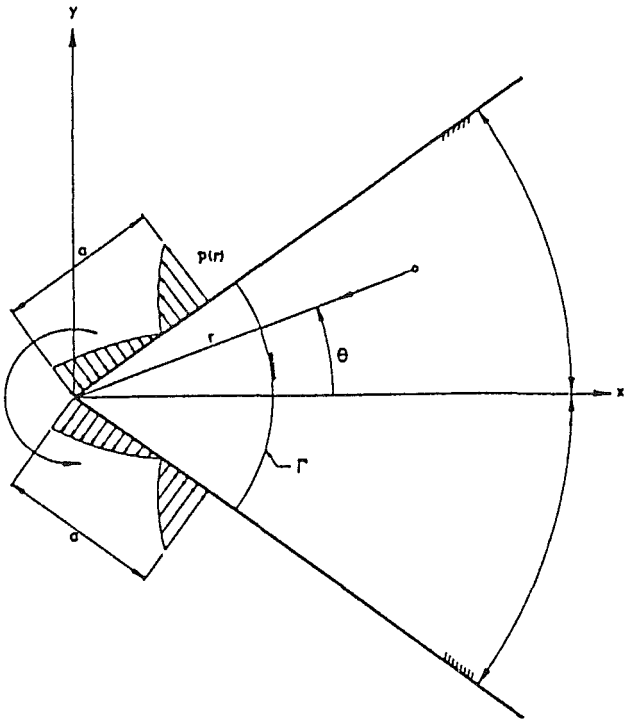


Fig. 2(*b*) The Steinberg-Koiter problem

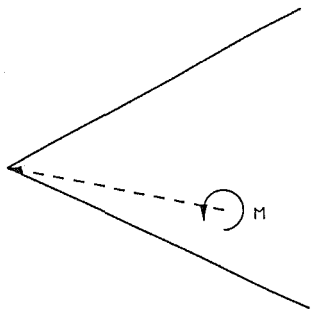


Fig. 2(*c*) The wedge with a concentrated couple approaching from the interior (Dundurs and Markenscoff)

2 The Carothers—Leguillon Solution

Carothers (1912) considered the Airy stress function

$$\phi = \frac{M}{D}\left(\theta \cos 2\gamma - \frac{1}{2}\sin 2\theta\right) \qquad D = \sin 2\gamma - 2\gamma \cos 2\gamma \tag{1}$$

and observed that it has the property to clear the flanks of the wedge of tractions (Fig. 1) and to produce stresses which are as $\sim 1/r^2$ so that they produce a constant resultant moment M on arcs of constant r. These stresses are

$$\sigma_{\theta\theta} = 0 \qquad \sigma_{rr} = \frac{M}{Dr^2} 2 \sin 2\theta \qquad \sigma_{r\theta} = \frac{M}{Dr^2}(\cos 2\gamma - \cos 2\theta). \tag{2}$$

At the critical angle γ^* which satisfies $D = 0$, the stresses are self-equilibrated not only for the force but also for the resultant couple on r = constant surfaces, which means that they cannot be scaled so as to provide a finite resultant M. Thus for $\gamma = \gamma^*$, the stresses in (2) diverge for all r.

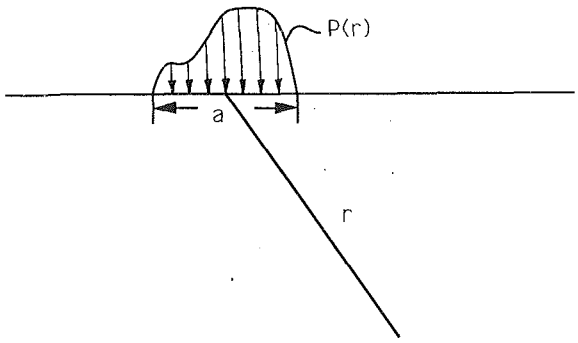
However, Carothers' stress function was only an intelligent guess and the solution for the critical angle has been obtained by Ting (1985) and Leguillon (1988). Leguillon considered the eigenfunctions of the wedge for displacement fields of the form $r^\alpha u(\theta)$ where α is determined by the satisfaction of the homogeneous boundary conditions on the flanks, and he examined the properties of the ensuing eigenvalue problem. While the eigenvalues are in general functions of the wedge angle, the eigenvalue -1 is independent of the angle and corresponds to the Carothers stress field. The eigenvalue 1 corresponds to rigid-body motion, and the other eigenvalues are excluded either for giving $M \to 0$ or $M \to \infty$, as $r \to 0$. Actually these other eigenvalues play a prominant role in this phenomenon as is discussed in the next section. At the critical angle γ^*, the Carothers eigenvalue -1 coincides with one of the others producing a double eigenvalue with geometric multiplicity 1. The corresponding eigenvector (Leguillon, 1988) is

$$v_{-1}(r, \theta) = \frac{\log r}{r} u_{-1}(\theta) + \frac{1}{r} v_{-1}(\theta) \tag{3}$$

where u_{-1} is the Carothers eigenvector and v_{-1} is an associated eigenvector. The contributions to the stress field come from both terms in (3). The first term corresponds to the Carothers distribution $u_{-1}(\theta)$ multiplied by $\log r$, but, since the resultant moment of it is zero, it does not contribute to the total moment. However, it gives stresses, which are $\log r/r^2$ singular at the vertex. The second term contributes stresses which are $\sim 1/r^2$ singular and give a constant moment (calculated numerically to be nonzero) at r = constant surfaces. Thus, the total stress gives a resultant moment independent of r and (3) is a solution to the wedge problem at γ^*. The Leguillon solution is, however, deficient in the sense that it gives infinite moment resultant on arcs of arbitrary length at infinity. Only on the total wedge angle the resultant moment is M (being the finite difference of two infinities).

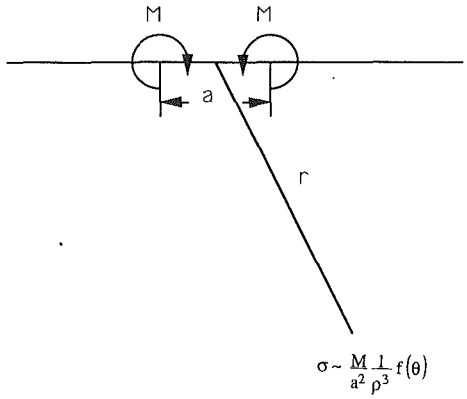
Although the above solution solves the Carothers paradox in the sense that it finds one elasticity field of stresses distributed on r = constant surfaces having zero force resultant and resultant moment M, the meaning of the above solution is limited, since it corresponds only to a specific loading given by the Leguillon distribution. It is obvious that the Saint-Venant's principle does not hold for the critical angle, since it requires that when a distributed loading has zero resultant force and zero resultant moment the stress decays at infinity *faster* than r^{-2} (in two dimensions). However, at the critical angle, the *Carothers stress field is just the solution for such a loading* (*with zero resultant force and zero resultant moment*) and it decays only as r^{-2}. So the principle does not hold. Apparently between the half-space, where the stresses (of a zero resultant force and zero resultant moment distribution of tractions) decay as r^{-3} (Fig. 4), and the critical Carothers angle where they decay as r^{-2}, there is a transition. It would be of interest to know what is happening at intermediate angles, in the sense how the exponent of r varies as a function of the angle. This question is answered in the discussion of the Stern-

Downloaded 03 May 2010 to 171.66.16.20. Redistribution subject to ASME license or copyright; see http://www.asme.org/terms/Terms_Use.cfm



$$\sigma \sim \frac{P}{a}\frac{1}{\rho} f_1(\theta) + \frac{M}{a^2}\frac{1}{\rho^2} f_2(\theta) + \frac{M^{(2)}}{a^2}\frac{1}{\rho^3} f_3(\theta)$$

Fig. 3 The far-field due to a distributed loading (two-dimensional) on a half-space



$$\sigma \sim \frac{M}{a^2}\frac{1}{\rho^3} f(\theta)$$

Fig. 4 The far-field due to a couple of a couple ($M^{(2)}$) on a half-space

berg-Koiter problem in the next section. There may also exist other loading stress distributions which give solutions that go to zero faster than r^{-2}, but these would form a much smaller space than the space of all loadings.

3 The Sternberg-Koiter (S-K) Problem

Sternberg and Koiter (1958) considered the wedge loaded by distributed normal loading on its flanks (Fig. 2(*b*)). It should be noted here that the S-K loadings on the flanks are a subset of the loadings on r = constant surfaces, since to each S-K loading corresponds a stress distribution (loading) on r = constant surfaces. However, the converse is not necessarily true, and no completeness of the eigenfunctions of the wedge has been proven except for fields with finite strain energy or bounded displacements (Gregory, 1979), which is not the case when the loading is a concentrated couple. Sternberg and Koiter solved the boundary value problem by the Mellin transform and concluded that

for $0 \le \gamma < \pi/2$, (i.e., a wedge smaller than a half-space), the solution exists,
for $\pi/2 \le \gamma < \gamma^*$ the solution exists for antisymmetric loadings only,
for $\gamma^* \le \gamma \le \pi$ the solution does not exist.

Actually in the paper the proof only appears for the antisymmetric loading, which is well behaved until the angle γ^*. The symmetric case (which diverges for wedges bigger than a half-space) has not been treated in the main paper, but there is a note added in proof to this effect. Sternberg and Koiter found (in the antisymmetric loading case) that for angles $\gamma^* < \gamma < \pi$, the asymptotic expansion for the stress as $\rho = r/a \to \infty$ is

$$\tau_{r\theta} = \frac{M\hat{\varphi}(\lambda)\,(\lambda+2)[\cos(\lambda+2)\gamma\,\cos\lambda\theta - \cos\lambda\gamma\,\cos\,(\lambda+2)\theta]}{2a^2[\sin\,2\gamma - 2\gamma\,\cos\,2(\lambda+1)\gamma]\rho^{\lambda+2}} \tag{4}$$

with

$$\hat{\varphi}(\lambda) = \int_0^1 \rho^{\lambda+1}\varphi(\rho)d\rho, \quad \varphi(\rho) = \frac{2a^2}{M}\,p(r) \tag{5}$$

in the notation of S-K. The first term in this expansion diverges as $a \to 0$ but if $M\hat{\phi}(\lambda)/a^2$ is a constant, then the leading order term is $1/\rho^{\lambda+2}$, with λ taking negative values $-1 < \lambda < 0$, while the $1/\rho^2$ term, which corresponds to the Carothers solution, is of smaller order. Thus in this range of angles, the third term is *taking the lead* over the $1/\rho^2$ term, and this is happening because this problem has an eigenvalue independent of the angle.

4 Saint-Venant's Principle for the Wedge

For the half-space we may (intuitively, but we conjecture that it can be formally proved) formulate Saint-Venant's principle as follows: When a normal load is distributed over a finite region a of a half-plane (Fig. 3), the stresses at infinity have terms that decay as $1/\rho$ (where $\rho = r/a$), the coefficients of which depend on the resultant force P/a; terms that decay as $1/\rho^2$, the coefficients of which depend on the resultant moment M/a^2; terms decaying as $1/\rho^3$ the coefficients of which depend on the moment of the moment $M^{(2)}/a^3$ (Timoshenko and Goodier, p. 101 for a couple of moments), and so on. The question is whether the above is also true when the load is distributed on the flanks of a wedge. The S-K solution shows the following: for angles smaller than a half-space this is true for the $1/\rho$ and $1/\rho^2$ terms. (The $1/\rho$ term can be also extracted from the S-K solution when the resultant of the distributed load is $\neq 0$, in which case $s = -1$ is a pole yielding the $1/\rho$ additional term.) The third term, however, for angles between a half-space and the critical is $\sim(1/\rho)^{\lambda+2}$ where λ is a function of the angle and the coefficient of which depends on $(M/a^2)\hat{\varphi}(\lambda)$ and where

$$\hat{\varphi}(\lambda) = \int_0^1 \rho^{\lambda+1}\varphi(\rho)d\rho$$

is a dimensionless "moment" of exponent $(\lambda + 1)$ of the distributed loading $\varphi(\rho)$. Actually, beyond the critical angle (for antisymmetric loadings), λ takes negative values so that this term becomes more dominant than the $1/\rho^2$ singularity. If the region of distribution of the loading vanishes, then the coefficient of it diverges $\sim a^{-\lambda}$ as $a \to 0$ (hence the nonexistence of the limit). Thus the quantity $\hat{\varphi}(\lambda)$, which is "between a force and a moment" for negative values of λ, is constant on r = constant surfaces and controls the phenomenon, because the $(1/\rho)^{\lambda+2}$ solution is then energetically more favorable than the $1/\rho^2$ solution with the moment constant (on r = constant surfaces). In the case of a half-space, $\lambda = 1$ satisfies

$$(\lambda+1)\,\sin\,2\gamma - \sin\,2(\lambda+2)\gamma = 0, \tag{6}$$

and gives

$$\hat{\varphi}(\lambda) = \int_0^1 \rho^2\varphi(\rho)d\rho,$$

i.e., reduces to the second moment, and the corresponding term $(1/\rho)^{\lambda+2}$ yields the $1/\rho^3$ term of the second moment (couple of moments) solution (Fig. 4) (Timoshenko and Goodier, p. 101). It is thus confirmed that for a half-space the next term in the far-field expansion comes from that zero force and zero moment distribution which has the second moment $\int \rho^2\varphi(\rho)d\rho$ constant. However, for other wedge angles, the exponent of

Downloaded 03 May 2010 to 171.66.16.20. Redistribution subject to ASME license or copyright; see http://www.asme.org/terms/Terms_Use.cfm

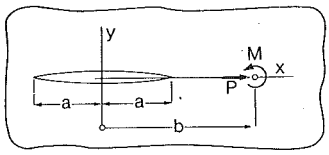


Fig. 5 A concentrated couple approaching the tip of a crack

ρ is a function of the angle and the intuitive order of affairs for the half-space is no longer valid.

For cracks, the solutions that satisfy the homogeneous equations of elasticity with homogeneous (traction) boundary conditions and have the right order of singularity are the weight functions (Bückner, 1970; Rice, 1972). The Bückner-Rice functions are solutions of the elasticity equations (with unbounded energy) that satisfy zero boundary conditions on the whole boundary. The first term in the solution (4) is exactly that. It is a stress field that possesses a self-equilibrated singularity of order $\rho^{\lambda+2}$ at the vertex and satisfies zero boundary conditions over the whole boundary including the one at infinity. When the wedge angle becomes two-dimensional and the wedge becomes a semi-infinite crack they yield the weight function of a crack (Dundurs and Markenscoff, 1989). We conjecture that these terms are the weight functions of the wedge and research is under way to formulate a weight function for the wedge theory (Markenscoff, 1994).

5 The Wedge With a Concentrated Couple Approaching From the Interior

Dundurs and Markenscoff (1989) proposed the problem of a concentrated couple, (i.e., a twisting moment, op. cit., Timoshenko and Goodier, p. 126) approaching the vertex of the wedge from the interior (Fig. 3). For this problem it is conjectured here that

for $0 \le \gamma \le \pi/2$ the solution exists for any direction of approach to the vertex,
for $\pi/2 \le \gamma < \gamma^*$ the solution exists only if the couple approaches the vertex along the bisector,
for $\gamma^* \le \gamma \le \pi$ the solution does not exist in the limit.

For $\gamma = \pi$ the wedge becomes a semi-infinite crack. Instead of solving the problem of a twisting couple approaching the tip of a semi-infinite crack, Dundurs and Markenscoff (1989) solved in closed form the finite crack of length $2a$ with a moment in front of it. While this problem has a characteristic length $2a$—in contrast to the semi-infinite crack—still the solution does not exist in the limit. The loss of characteristic length of the area of distribution of the load was attributed as the reason for the nonexistence of the solution in the S-K problem by Barenblatt (1979). Apparently the characteristic length of the crack is not important.

Dundurs and Markenscoff (1989) obtained the closed-form solution at the front of a crack-tip due to a moment M at position b (Dundurs and Markenscoff) (Fig. 5) which as the moment approaches the crack tip, i.e., as $b - a \to 0$ gives

$$\sigma_{xy} \sim \frac{Ma \operatorname{sng} xH(|x|-a)}{2\pi(b^2-a^2)^{1/2}(x+a)^{1/2}(x-a)^{3/2}}. \tag{10}$$

As they observed, this stress corresponds to a Bückner fundamental field if $M/(b^2 - a^2)^{1/2}$ is set to a constant. Again it is apparent from this closed-form solution that the moment does not appear in the leading term and the solution picks up the fractional moment $M/(b^2 - a^2)^{1/2}$ corresponding exactly to $\hat{\varphi}(\lambda)$ with $\lambda = -1/2$ at $\gamma = \pi$. If the load was distributed (instead of a point moment), then the terms associated with the fractional moment $\int \rho^{1/2}\varphi(\rho)d\rho$ = constant, would be the leading ones (as discussed in the previous section) being energetically more favorable than those corresponding to $\int \rho\varphi(\rho)d\rho$ = constant. Both terms satisfy the equations of equilibrium and stress-free boundary conditions on the wedge, but the first ones have a singularity of a lower order. This whole paradox is happening because when the energy is unbounded there is no uniqueness of solution in elasticity theory.

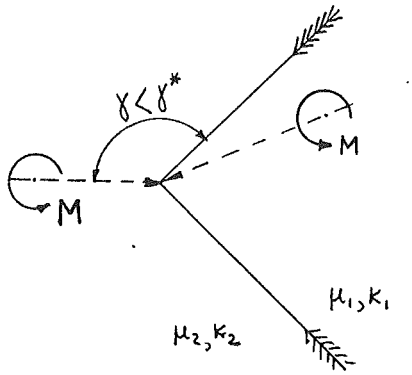


Fig. 6 A concentrated couple approaching the vertex of a bimaterial wedge

It should be pointed out that this anomaly of the nonexistence of the solution of the finite crack and moment problem is not due to the infinity of the domain of the problem. The solution for a finite domain containing a crack and a couple (Fig. 5) can be obtained from the infinite problem by superposing on the tractions at the boundary of the finite body—due to the infinite domain problem—(which have a resultant moment M), self-equilibrated tractions, so that the sum of the total tractions yields the boundary conditions pertaining to the finite domain, which will be stress-free in the case of Fig. 5. Obviously the solution of the second problem (self-equibrated tractions on the finite boundary) has a square-root singularity at the crack tip but no divergence.

6 The Bimaterial Wedge

A bimaterial wedge loaded at its vertex by a concentrated couple exhibits the Carothers anomaly (Dundurs and Markenscoff, 1989) and a similar anomaly when loaded by a disclination (Belov, 1991). There is no anomaly when loaded by a concentrated force or dislocation. The Dundurs and Markenscoff (1989) analysis shows that there are two wedge angles, γ^*, depending on the Dundurs' constant α, for which the solution diverges everywhere. However, this suffers from the same path dependence of the solution and the nonapplicability of the Saint-Venant's principle as the single wedge, and thus the solution of the bimaterial wedge depends on the direction of approach of the concentrated couple (Fig. 6). If the concentrated couple approaches the tip of the wedge along the bisector, then the solution should exist for wedge angles $2\gamma < 2\gamma^*$. If the concentrated couple approaches the vertex along any arbitrary direction then the solution exists only if it approaches the vertex from the side of the embedded wedge smaller than a half-space. If the concentrated couple approaches the vertex from an inside angle $2\gamma > 2\gamma^*$, then the solution does not exist for any direction of approach. Also, the two limits of the solution when a concentrated couple reaches the interface of two half-spaces depend on the side from which the interface has been approached, which means that there is again path dependence. An analogous phenomenon of dependence on the direction of approach should be expected to occur in the embedded wedge problems treated by Belov for disclinations.

7 The Definition of a Concentrated Couple and a Definition of Saint-Venant's Principle

For a moment approaching the vertex of a wedge, and for a wedge smaller or equal to a half-space, all paths of loading (giving resultant concentrated moment M at the vertex) con-

Downloaded 03 May 2010 to 171.66.16.20. Redistribution subject to ASME license or copyright; see http://www.asme.org/terms/Terms_Use.cfm

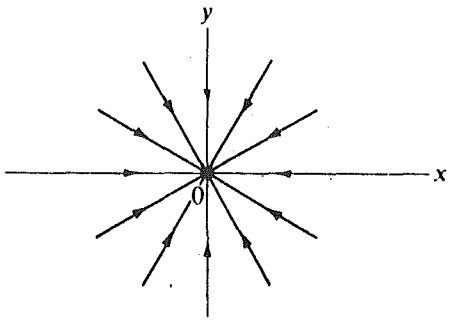


Fig. 7 A stable node for different paths of loading

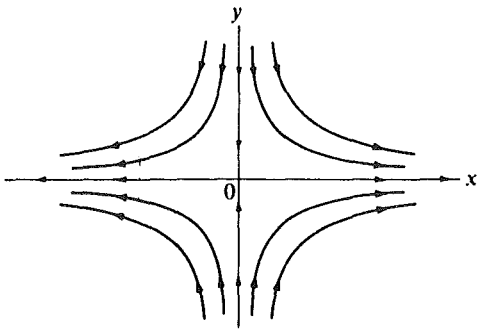


Fig. 8 A saddle point for different paths of loading

verge to the same limiting solution. We may depict then the behavior of the solution as one of a stable node in analogy to dynamical systems with a length variable instead of the time variable (Fig. 7). However, the space of loadings for which there is convergence of the solution reduces to the antisymmetric ones when the wedge angle is between the half-space and a critical, and only to the Carothers-Leguillon loading for wedge angles bigger or equal to the critical. In this case we may draw the solution schematically in two dimensions as a saddle point (Fig. 7). Obviously we can only meaningfully talk about a concentrated couple in the case of a stable node. *If all paths of loading form a stable node, we can view that as one definition of Saint-Venant's principle.* The paths of loading that give convergent solutions for angles bigger than the critical are characterized as those with constant a "fractional" moment $\hat{\varphi}(\lambda)$, of power depending on the angle, and it is of this problem that the solutions would form a stable node, i.e., independent of the path of loading. This phenomenon of path dependence of the solution manifests itself in other physical phenomena as well as mentioned in the Introduction, and only then can we talk about steady-state entities if they are limits of physically meaningful limiting processes.

Acknowledgment

This research was supported by NSF grant #INT-9115553, and the University of California, San Diego.

References

Barenblatt, G. I., 1979, *Similarity, Self-similarity, and Intermediate Asymptotics*, translated from Russian by Norman Stein, Consultant Bureau, New York.

Belov, A. Yu., 1991, "The Analogue of the Carothers' Effect and Stress Anomalies in the Theory of Disclinations," *Philosophical Magazine Letters*, Vol. 64, pp. 207–211.

Bückner, H. F., 1970, "A Novel Principle for the Computation of Stress Intensity Factors," *Zeitschrift für angewandte Mathematik und Mechanik*, Vol. 50, pp. 529–565.

Carothers, S. D., 1912, "Plane Strain in a Wedge," *Proceedings of the Royal Society of Edinburgh*, Vol. 23, p. 292.

Dundurs, J., and Markenscoff, X., 1989, "The Sternberg-Koiter Conclusion and Other Anomalies of the Concentrated Couple," ASME JOURNAL OF APPLIED MECHANICS, Vol. 56, pp. 240–245.

Gregory, R. D., 1979, "Green's Functions, Bi-linear Forms, and Completeness of the Eigenfunctions for the Elastostatic Strip and Wedge," *Journal of Elasticity*, Vol. 9, pp. 283–309.

Leguillon, D., 1988, "Sur le Moment Ponctuel Appliqué à un Secteur: le Paradoxe de Sternberg-Koiter," *C. R. Acad. Sci. Paris*, Vol. 307, Série II, pp. 1741–1746.

Markenscoff, X., 1993, "Interaction of Dislocations and Dislocation Dipoles with Cracks and Anticracks," *Materials Science Forum*, Vol. 123–125, pp. 525–530.

Markenscoff, X., 1994, "On the Weight Function and the Stress Intensity Factor for the Wedge (or Notch)," *Philosophical Magazine Letters* (in press).

Rice, J. R., 1972, "Some Remarks on Elastic Crack-tip Stress Fields," *Int. J. Solids Structures*, Vol. 8, pp. 751–758.

Timoshenko, S. P., and Goodier, J. N., 1970, *Theory of Elasticity*, 3rd ed., McGraw-Hill, New York.

Ting, T. C. T., 1985, "A Paradox of the Elastic Wedge Subjected to a Concentrated Couple and the Jeffrey-Hamel Viscous Flow Problem," *Zeitschrift für Angewandte Mathematik und Mechanik*, Vol. 65, pp. 188–190.

Downloaded 03 May 2010 to 171.66.16.20. Redistribution subject to ASME license or copyright; see http://www.asme.org/terms/Terms_Use.cfm

V. A. Lubarda
Department of Mechanical and Aerospace Engineering, Arizona State University, Tempe, AZ 85287-6106

C. F. Shih
Division of Engineering, Brown University, Providence, RI 02912
Mem. ASME

Plastic Spin and Related Issues in Phenomenological Plasticity

The role of plastic spin within the framework of a phenomenological polycrystalline plasticity is examined. We show that if elastic and plastic strain rates are properly identified, partitioning of total spin and identification of its "plastic" part is not required in the elastoplastic constitutive analysis of elastically isotropic materials.

1 Introduction

In recent years the subject of the partitioning of the total spin into its elastic and plastic parts has received a considerable attention within the framework of polycrystalline phenomenological plasticity theory. We will show that such partitioning is arbitrary in the absence of a physical structure that describes the process of the plastic flow as in single crystal plasticity. In fact, within a phenomenological plasticity theory, there is no need to partition the total spin into its constituents nor make any reference to them.

To introduce the so-called plastic spin within a polycrystalline, phenomenological plasticity theory is a consequence of the improper identification of elastic and plastic parts of the total strain rate. This led to the statement in the literature that a tacit assumption of the Prandtl-Reuss equations is that the plastic spin is zero. Furthermore, it has been interpreted by some that a more complete plasticity theory can be obtained by including a constitutive law for plastic spin. Advocates of such an approach have made a superficial parallel between polycrystalline plasticity and single crystal plasticity, in which an additional physical structure is introduced to describe material flowing through the crystal lattice.

Within a phenomenological plasticity of polycrystalline materials, plastic spin has been introduced to describe certain features of anisotropic hardening (Dafalias, 1983; Loret, 1983). These attempts were motivated by the observation that spurious oscillations of shear stress occurred in the analysis of monotonically increasing simple shear (Nagtegaal and de Jong, 1982). Various plastic spin measures were subsequently introduced and discussed by many authors; i.e., Dafalias (1985, 1987), Dashner (1986), Zbib and Aifantis (1988), Aravas and Aifantis (1991), and others. Earlier work on the subject of plastic spin and its significance also includes Mandel (1973) and Kratochvil (1973). Since most of the work on plastic spin utilizes the multiplicative decomposition of deformation gradient into its elastic and plastic parts, introduced by Lee (1969), the same is done here. Elastoplastic constitutive analysis based on this decomposition has been a topic of active research in the last several decades (Willis, 1969; Freund, 1970; Mandel, 1973; Sidoroff, 1975; Kleiber 1975; Lubliner 1978; Lubarda and Lee 1981; Needleman 1985; Agah-Tehrani et al. 1987; Moran et al., 1990; Lubarda, 1991a, 1991b, etc.). Various issues related to applicability of the decomposition in elastoplasticity were discussed by Green and Naghdi (1971), Nemat-Nasser (1979, 1982), Casey and Naghdi (1980), and Naghdi (1990). In the context of single crystal plasticity, the multiplicative decomposition was used by Asaro and Rice (1977), Hill and Havner (1982), Asaro (1983a, 1983b), Mohan et al. (1992), and others.

2 Partition of Elastoplastic Strain Rate and Spin into Their Constituents

To elucidate our ideas we restrict attention to elastically isotropic polycrystalline materials that can harden in an arbitrary manner during the course of elastoplastic deformation. Let $\mathbf{F}$ be the deformation gradient that deforms the body to its current configuration. Following Lee (1969), we introduce an intermediate configuration which is obtained from the current configuration by (possibly virtual) elastic distressing to zero stress. The multiplicative decomposition then holds

$$\mathbf{F} = \mathbf{F}_e \mathbf{F}_p, \tag{1}$$

where $\mathbf{F}_e$ is the elastic and $\mathbf{F}_p$ the plastic part of deformation gradient $\mathbf{F}$. The intermediate configuration is not uniquely defined since it remains unstressed after any superposed rigid-body rotation. Alternatively, the intermediate configuration can be obtained by the mapping $\mathbf{F}_p$ applied to the initial configuration. To the extent that $\mathbf{F}_p$ contains an unspecified rotation the intermediate configuration is also nonunique.

We adopt the assumption that plastic deformation does not affect the elastic characteristics of the material. In this case, the response of elastically isotropic material does not depend on any rotation superposed to the intermediate configuration.

Contributed by the Applied Mechanics Division of THE AMERICAN SOCIETY OF MECHANICAL ENGINEERS for publication in the ASME JOURNAL OF APPLIED MECHANICS.

Discussion on this paper should be addressed to the Technical Editor, Professor Lewis T. Wheeler, Department of Mechanical Engineering, University of Houston, Houston, TX 77204-4792, and will be accepted until four months after final publication of the paper itself in the ASME JOURNAL OF APPLIED MECHANICS.

Manuscript received by the ASME Applied Mechanics Division, Jan., 1992; final revision, June 28, 1992. Associate Technical Editor: L. M. Keer.

Copyright © 1994 by ASME
Downloaded 03 May 2010 to 171.66.16.20. Redistribution subject to ASME license or copyright; see http://www.asme.org/terms/Terms_Use.cfm

The hyperelasticity law defined with respect to any intermediate configuration is (Truesdell and Noll, 1965)

$$\tau = 2\mathbf{F}_e \frac{\partial \psi_e(\mathbf{C}_e)}{\partial \mathbf{C}_e} \mathbf{F}_e^T. \tag{2}$$

Here ψ_e, the strain energy per unit unstressed volume, is an isotropic function of the right Cauchy-Green deformation tensor $\mathbf{C}_e = \mathbf{F}_e^T\mathbf{F}_e$ and $\tau = (\det\mathbf{F}_e)\boldsymbol{\sigma}$ is the Cauchy stress $\boldsymbol{\sigma}$ weighted by $\det\mathbf{F}_e$. If plastic deformation is taken to be incompressible, $\det\mathbf{F}_e = \det\mathbf{F}$ and τ is then the Kirchhoff stress.

Using (1) in the velocity gradient expression $\mathbf{L} = \dot{\mathbf{F}}\mathbf{F}^{-1}$, we obtain

$$\mathbf{L} = \dot{\mathbf{F}}_e\mathbf{F}_e^{-1} + \mathbf{F}_e(\dot{\mathbf{F}}_p\mathbf{F}_p^{-1})\mathbf{F}_e^{-1}, \tag{3}$$

where superimposed dot denotes the material time derivative. The strain rate $\mathbf{D}$ and spin $\mathbf{W}$ are given by the symmetric and antisymmetric parts of $\mathbf{L}$:

$$\mathbf{D} = (\dot{\mathbf{F}}_e\mathbf{F}_e^{-1})_s + [\mathbf{F}_e(\dot{\mathbf{F}}_p\mathbf{F}_p^{-1})\mathbf{F}_e^{-1}]_s \tag{4}$$

$$\mathbf{W} = (\dot{\mathbf{F}}_e\mathbf{F}_e^{-1})_a + [\mathbf{F}_e(\dot{\mathbf{F}}_p\mathbf{F}_p^{-1})\mathbf{F}_e^{-1}]_a. \tag{5}$$

The first term on the right-hand side of (4) has often been identified as the elastic strain rates and the second term as the plastic strain rate. Other definitions of elastic and plastic strain rates have also been proposed. These identifications are made without taking full use of the kinetics of elastoplastic deformation. Similarly, the first term on the right-hand side of (5) has often been identified as the elastic spin and the second term as the plastic spin. However, the later partitioning is arbitrary in the absence of a relevant physical structure upon which spin can be defined. We shall show that the need for the partitioning $\mathbf{W}$ arises from an improper identification of the elastic and plastic strain rates in (4). When the elastic and plastic strain rates are properly identified, only the total spin enters the elastoplastic constitutive formulation. Thus the partitioning of $\mathbf{W}$ is unnecessary.

We begin with partitioning $\mathbf{D}$ into $\mathbf{D}_e$ and $\mathbf{D}_p$. We note that the elastic and plastic strain rate cannot be identified from (4) and the corresponding kinematics, since $\mathbf{F}_e$ or $\mathbf{F}_p$ are not uniquely defined. Furthermore, any proposed partitioning of $\mathbf{D}$ which does not take into considerations the kinetics of elastoplastic deformation is insufficiently specified and arbitrary.

To develop this line of reasoning, we begin by differentiating the hyperelasticity relation (2) to obtain

$$\dot{\tau} - (\dot{\mathbf{F}}_e\mathbf{F}_e^{-1})\tau - \tau(\dot{\mathbf{F}}_e\mathbf{F}_e^{-1})^T = \hat{\mathbf{\Lambda}}_e : (\dot{\mathbf{F}}_e\mathbf{F}_e^{-1})_s. \tag{6}$$

Here : denotes the trace product and $\hat{\mathbf{\Lambda}}_e$ is the corresponding tensor of elastic moduli, with the components

$$\hat{\Lambda}^e_{ijkl} = 4F^e_{im}F^e_{jn}\frac{\partial^2\psi_e(\mathbf{C}_e)}{\partial C^e_{mn}\partial C^e_{pq}}F^e_{kp}F^e_{lq}. \tag{7}$$

The left-hand side of (6) is the Lie (or convected) derivative of stress τ, with respect to $\mathbf{F}_e$ (e.g., Simo and Ortiz, 1985). Equation (6) can be equivalently rewritten in terms of the Jaumann derivative with respect to the spin $(\dot{\mathbf{F}}_e\mathbf{F}_e^{-1})_a$, as

$$\dot{\tau} - (\dot{\mathbf{F}}_e\mathbf{F}_e^{-1})_a\tau + \tau(\dot{\mathbf{F}}_e\mathbf{F}_e^{-1})_a = \mathbf{\Lambda}_e : (\dot{\mathbf{F}}_e\mathbf{F}_e^{-1})_s. \tag{8}$$

The elastic moduli tensor $\mathbf{\Lambda}_e$ has the components

$$\Lambda^e_{ijkl} = \frac{1}{2}(\delta_{ik}\tau_{jl} + \delta_{il}\tau_{jk} + \tau_{ik}\delta_{jl} + \tau_{il}\delta_{jk}) + \hat{\Lambda}^e_{ijkl}, \tag{9}$$

where δ_{ij} is the Kronecker delta.

If deformation is purely elastic, i.e., $\mathbf{F} = \mathbf{F}_e$, then clearly $(\dot{\mathbf{F}}_e\mathbf{F}_e^{-1})_s$ in (8) is the elastic strain rate. In that case, $\mathbf{F}_e$ is defined relative to a nonchanging (initial) configuration. However, if deformation is elastoplastic, $\mathbf{F}_e$ is defined relative to an intermediate configuration, which is changing during elastoplastic deformation. Consequently, two difficulties can arise in the identification of the elastic strain rate. First, since $\mathbf{F}_e$ and $\mathbf{F}_p$ are specified only to within an arbitrary rotation, $\dot{\mathbf{F}}_e\mathbf{F}_e^{-1}$ and its symmetric and antisymmetric parts are nonunique. Therefore, a precise physical interpretation of strain rate measure $(\dot{\mathbf{F}}_e\mathbf{F}_e^{-1})_s$ and the assertion that it represents the elastic part of the total strain rate cannot be made. Secondly, the deforming intermediate configuration also contributes to the elastic strain rate so that it is not in general given by $(\dot{\mathbf{F}}_e\mathbf{F}_e^{-1})_s$. These difficulties are resolved in the treatment presented below.

The elastic strain rate is defined by the kinetic relation $\mathbf{D}_e = \mathbf{\Lambda}_e^{-1} : \overset{\circ}{\tau}$, where $\mathbf{D}_e$ represents the reversible part of $\mathbf{D}$ in the sense that the strain increment $\mathbf{D}_e dt$ is recovered upon loading-unloading cycle of the stress increment $\overset{\circ}{\tau}dt$. Here, $\overset{\circ}{\tau} = \dot{\tau} - \mathbf{W}\tau + \tau\mathbf{W}$ is the Jaumann derivative relative to the material spin $\mathbf{W}$ of the Kirchhoff stress $\tau = (\det\mathbf{F})\boldsymbol{\sigma}$. With $\mathbf{D}_e$ defined in this way, the remaining part of the total strain rate, $\mathbf{D}_p = \mathbf{D} - \mathbf{D}_e$, is plastic (residual) contribution. This $\mathbf{D}_p$ can be shown to be governed by plastic potential and codirectional with the outward normal to current yield surface in the Cauchy stress space (Hill and Rice, 1973). When the reference state is taken to momentarily coincide with the current state, these strain rates correspond to the choice of the logarithmic strain and its conjugate stress, as discussed in Hill (1978).

To obtain the desired form, $\mathbf{D}_e = \mathbf{\Lambda}_e^{-1} : \overset{\circ}{\tau}$, plastic incompressibility is assumed so that τ appearing in (8) and (9) is the Kirchhoff stress. We then use (5) to eliminate $(\dot{\mathbf{F}}_e\mathbf{F}_e^{-1})_a$ from (8) to get

$$\overset{\circ}{\tau} = \mathbf{\Lambda}_e : \{(\dot{\mathbf{F}}_e\mathbf{F}_e^{-1})_s - \mathbf{\Lambda}_e^{-1} : \{[\mathbf{F}_e(\dot{\mathbf{F}}_p\mathbf{F}_p^{-1})\mathbf{F}_e^{-1}]_a\tau - \tau[\mathbf{F}_e(\dot{\mathbf{F}}_p\mathbf{F}_p^{-1})\mathbf{F}_e^{-1}]_a\}\}. \tag{10}$$

Therefore, with the elastic strain rate given by

$$\mathbf{D}_e = (\dot{\mathbf{F}}_e\mathbf{F}_e^{-1})_s - \mathbf{\Lambda}_e^{-1} : \{[\mathbf{F}_e(\dot{\mathbf{F}}_p\mathbf{F}_p^{-1})\mathbf{F}_e^{-1}]_a\tau - \tau[\mathbf{F}_e(\dot{\mathbf{F}}_p\mathbf{F}_p^{-1})\mathbf{F}_e^{-1}]_a\}, \tag{11}$$

the inversion of (10) provides the desired relation

$$\mathbf{D}_e = \mathbf{\Lambda}_e^{-1} : \overset{\circ}{\tau}. \tag{12}$$

Note from (7) and (9) that the elastic compliance tensor $\mathbf{\Lambda}_e^{-1}$ possesses the following symmetry and reciprocity properties:

$$(\Lambda_e^{-1})_{ijkl} = (\Lambda_e^{-1})_{ijlk} = (\Lambda_e^{-1})_{jikl} = (\Lambda_e^{-1})_{klij}. \tag{13}$$

As a consequence $\mathbf{\Lambda}_e^{-1} : \overset{\circ}{\tau}$ is derivable from elastic rate potential $\phi_e = 1/2\,\mathbf{\Lambda}_e^{-1} : (\overset{\circ}{\tau} \otimes \overset{\circ}{\tau})$ as its gradient $\partial\phi_e/\partial\overset{\circ}{\tau}$ ($\otimes$ denotes the tensor product) and, therefore, $\mathbf{D}_e$, defined by (12), gives the reversible strain increment that is recovered upon unloading of the Jaumann stress increment associated with $\overset{\circ}{\tau}$.

We note that the second part of the strain rate $\mathbf{D}_e$ in its representation (11) makes no contribution to elastic work, which follows by observing that, in view of elastic isotropy, the strain rate $\mathbf{\Lambda}_e^{-1} : \{[\mathbf{F}_e(\dot{\mathbf{F}}_p\mathbf{F}_p^{-1})\mathbf{F}_e^{-1}]_a\tau - \tau[\mathbf{F}_e(\dot{\mathbf{F}}_p\mathbf{F}_p^{-1})\mathbf{F}_e^{-1}]_a\}$ has parallel principal directions to those of the associated stress rate $[\mathbf{F}_e(\dot{\mathbf{F}}_p\mathbf{F}_p^{-1})\mathbf{F}_e^{-1}]_a\tau - \tau[\mathbf{F}_e(\dot{\mathbf{F}}_p\mathbf{F}_p^{-1})\mathbf{F}_e^{-1}]_a$. Since the direction of the above stress rate is normal to τ, their trace is zero. Hence, $\psi_e = \tau : \mathbf{D}_e \equiv \tau : (\dot{\mathbf{F}}_e\mathbf{F}_e^{-1})_s$.

After identifying elastic strain rate, as given by (11) and (12), the remaining part of the total strain rate is the plastic (residual) part, which is governed by plastic potential and normal to the corresponding yield surface. From (4) and (11), therefore,

$$\mathbf{D}_p = [\mathbf{F}_e(\dot{\mathbf{F}}_p\mathbf{F}_p^{-1})\mathbf{F}_e^{-1}]_s + \mathbf{\Lambda}_e^{-1} : \{[\mathbf{F}_e(\dot{\mathbf{F}}_p\mathbf{F}_p^{-1})\mathbf{F}_e^{-1}]_a\tau - \tau[\mathbf{F}_e(\dot{\mathbf{F}}_p\mathbf{F}_p^{-1})\mathbf{F}_e^{-1}]_a\}. \tag{14}$$

Observe that $\mathbf{\Lambda}_e^{-1}$ and $\overset{\circ}{\tau}$, appearing in (12), are independent of any superposed rotation on the intermediate configuration. *Therefore* (12) *specifies* $\mathbf{D}_e$ *uniquely*. In contrast, the constituents of $\mathbf{D}_e$, namely $(\dot{\mathbf{F}}_e\mathbf{F}_e^{-1})_s$ and $[\mathbf{F}_e(\dot{\mathbf{F}}_p\mathbf{F}_p^{-1})\mathbf{F}_e^{-1}]_a$, do depend on the choice of an intermediate configuration. Similar remarks apply to $\mathbf{D}_p$ and its representation (14).

We have shown that the right-hand side of (11) is the correct relation for the elastic strain rate, and not $(\dot{\mathbf{F}}_e\mathbf{F}_e^{-1})_s$ alone. Nevertheless, the latter has been taken to be the elastic strain

Downloaded 03 May 2010 to 171.66.16.20. Redistribution subject to ASME license or copyright; see http://www.asme.org/terms/Terms_Use.cfm

rate in many studies. The following question arises naturally. Is there a choice of intermediate configuration for which $(\dot{\mathbf{F}}_e\mathbf{F}_e^{-1})_s$ is exactly $\mathbf{D}_e$? From (12) it can be seen that this is the case when the intermediate configuration is chosen such that the so-called "plastic spin," $[\mathbf{F}_e(\dot{\mathbf{F}}_p\mathbf{F}_p^{-1})\mathbf{F}_e^{-1}]_a$, vanishes identically.

Within the framework under discussion, the above choice of spin represents a geometric (kinematic) specification of the intermediate configuration. It is not a constitutive assumption and has no consequences on (12). For any other choice of intermediate configuration, $(\dot{\mathbf{F}}_e\mathbf{F}_e^{-1})_s$ is not the elastic strain rate $\mathbf{D}_e$ $(= \mathbf{\Lambda}_e^{-1} : \mathring{\tau})$, as can be seen from (11).

We could just as well define an intermediate configuration by requiring that the "elastic spin," $(\dot{\mathbf{F}}_e\mathbf{F}_e^{-1})_a$ vanish identically. In this case the plastic spin is exactly equal to total spin, $[\mathbf{F}_e(\dot{\mathbf{F}}_p\mathbf{F}_p^{-1})\mathbf{F}_e^{-1}]_a = \mathbf{W}$. The end result is still Eq. (12), as can be checked by inspection. Therefore, the partitioning of the total spin into elastic and plastic parts by direct identification of the terms in (5), or more elaborate kinematical considerations, is superficial and unnecessary. These aspects appear to be overlooked in much of the related work on this subject.

3 An Alternative Derivation

We now present an alternative derivation of the expression for $\mathbf{D}_e$, which gives additional insight in the kinematics of elastoplastic deformation and partitioning of the strain rate. To that end and in light of the assumed isotropy of the strain energy function ψ_e, we rewrite the hyperelasticity law (2) in the form

$$\tau = 2\mathbf{V}_e \frac{\partial \psi_e(\mathbf{B}_e)}{\partial \mathbf{B}_e}\mathbf{V}_e, \tag{15}$$

where $\tau = (\det \mathbf{V}_e)\sigma$ is the Kirchhoff stress since plastic incompressibility is assumed. Note that only the elastic stretch tensor $\mathbf{V}_e$ and the deformation tensor $\mathbf{B}_e = \mathbf{V}_e^2$ appear in this representation, since the stress response does not depend on rotation $\mathbf{R}_e$ associated with $\mathbf{F}_e$ in its stretch-rotation decomposition $\mathbf{F}_e = \mathbf{V}_e\mathbf{R}_e$.

Introduce the spin $\mathbf{\Omega}$, which is defined as the solution of the following equation (Lubarda, 1991a):

$$\mathbf{W} = (\dot{\mathbf{V}}_e\mathbf{V}_e^{-1})_a + (\mathbf{V}_e\mathbf{\Omega}\mathbf{V}_e^{-1})_a. \tag{16}$$

$\mathbf{\Omega}$ is an invariant quantity, independent of the choice of intermediate configuration, as neither $\mathbf{W}$ nor $\mathbf{V}_e$ and its material derivative depend on the chosen intermediate configuration. It then follows by applying to (15) the Jaumann derivative with respect to $\mathbf{\Omega}$

$$\overset{*}{\tau} = (\overset{*}{\dot{\mathbf{V}}}_e\mathbf{V}_e^{-1})\tau + \tau(\mathbf{V}_e^{-1}\overset{*}{\dot{\mathbf{V}}}_e) + 2\mathbf{V}_e\left[\frac{\partial^2\psi_e(\mathbf{B}_e)}{\partial\mathbf{B}_e\otimes\partial\mathbf{B}_e} : \overset{*}{\mathbf{B}}_e\right]\mathbf{V}_e, \tag{17}$$

where the superposed $*$ is the Jaumann derivative with respect to the spin $\mathbf{\Omega}$; i.e., $(^*) = (\dot{}) - \mathbf{\Omega}(\,) + (\,)\mathbf{\Omega}$. To obtain the desired form in terms of $\mathring{\tau}$, we rearrange (16) to get

$$(\overset{*}{\dot{\mathbf{V}}}_e\mathbf{V}_e^{-1})_a = \mathbf{W} - \mathbf{\Omega}, \tag{18}$$

and substitute (18) in (17) to reach the form

$$\mathring{\tau} = (\overset{*}{\dot{\mathbf{V}}}_e\mathbf{V}_e^{-1})_s\tau + \tau(\overset{*}{\dot{\mathbf{V}}}_e\mathbf{V}_e^{-1})_s + 4\mathbf{V}_e\left\{\frac{\partial^2\psi_e(\mathbf{B}_e)}{\partial\mathbf{B}_e\otimes\partial\mathbf{B}_e} : [\mathbf{V}_e(\overset{*}{\dot{\mathbf{V}}}_e\mathbf{V}_e^{-1})_s\mathbf{V}_e]\right\}\mathbf{V}_e. \tag{19}$$

Therefore, Eq. (19) can be written in the form

$$\mathring{\tau} = \mathbf{\Lambda}_e : \mathbf{D}_e, \tag{20}$$

where $\mathbf{\Lambda}_e$ is the well-known elastic moduli tensor with components

$$\Lambda^e_{ijkl} = \frac{1}{2}(\delta_{ik}\tau_{jl} + \delta_{il}\tau_{jk} + \tau_{ik}\delta_{jl} + \tau_{il}\delta_{jk}) + 4V^e_{im}V^e_{jn}\frac{\partial^2\psi_e(\mathbf{B}_e)}{\partial B^e_{mn}\partial B^e_{pq}}V^e_{pk}V^e_{ql}, \tag{21}$$

provided that the elastic strain rate is defined by

$$\mathbf{D}_e = (\overset{*}{\dot{\mathbf{V}}}_e\mathbf{V}_e^{-1})_s. \tag{22}$$

This alternative representation of the elastic strain rate involves only kinematic quantities ($\mathbf{V}_e$ and $\mathbf{\Omega}$), while the previous representation (11) involves both, kinematic and kinetic quantities. Of course, the two representations are equivalent, as has been established by the preceding derivation. Note also that elastic moduli tensor (21) exactly coincides with that in (9), due to isotropy of the strain energy function ψ_e. Inversion of (20) therefore again gives the elastic strain rate expression (12).

Kinematic interpretation of (22) is more clear when (22) is written in the form

$$\mathbf{D}_e = (\dot{\mathbf{V}}_e\mathbf{V}_e^{-1})_s + (\mathbf{V}_e\mathbf{\Omega}\mathbf{V}_e^{-1})_s. \tag{23}$$

The above shows that $\mathbf{D}_e$ has two contributions. One contribution is from the elastic stretching rate $(\dot{\mathbf{V}}_e\mathbf{V}_e^{-1})_s$ and the other from the spin $\mathbf{\Omega}$. This contribution is in general related to both, $\dot{\mathbf{R}}_e\mathbf{R}_e^{-1}$ and $\dot{\mathbf{F}}_p\mathbf{F}_p^{-1}$, and represents the effect of deforming and rotating intermediate configuration, as well as of the rotation due to $\mathbf{R}_e$. Note that this term has no contribution to the work, i.e., the rate of work (per unit initial volume) expended in elastic deformation is $\dot{\psi}_e = \tau : \mathbf{D}_e \equiv \tau : (\dot{\mathbf{V}}_e\mathbf{V}_e^{-1})_s$, since in view of elastic isotropy, $\mathbf{V}_e^{-1}\tau\mathbf{V}_e \equiv \tau$, and $\tau : \mathbf{V}_e\mathbf{\Omega}\mathbf{V}_e^{-1} \equiv \tau : \mathbf{\Omega} \equiv 0$.

The derivation presented here, (15)–(23), is analogous to a rate-type finite elasticity formulation. The spin $\mathbf{\Omega}$ is then simply $\mathbf{\Omega} = \dot{\mathbf{R}}\mathbf{R}^{-1}$, where $\mathbf{R}$ is the rotation from the polar decomposition of deformation gradient $\mathbf{F} = \mathbf{V}\mathbf{R}$. In elastoplasticity the spin $\mathbf{\Omega}$ is uniquely defined by (16), with the total spin on the left-hand side and elastic stretch on the right-hand side.

As we have shown, elastic strain rate $\mathbf{D}_e$ in both representations (11) or (22), does not depend on a superposed rotation on the intermediate configuration. For example, one can choose $\mathbf{R}_e = \mathbf{I}$; i.e., define intermediate configuration to be obtained by distressing without rotation (Lee, 1969), or one can choose distressing program which makes the spin of intermediate configuration to vanish, $(\dot{\mathbf{F}}_p\mathbf{F}_p^{-1})_a = \mathbf{0}$, etc. In each case the final constitutive equation is given by (12) and the numerical values of $\mathbf{D}_e$ and $\mathbf{\Omega}$ are not affected by the choice of an intermediate configuration. However, their form in terms of kinematic quantities $\mathbf{F}_e$, $\mathbf{F}_p$ and their rates do depend on the intermediate configuration. For example, in the case of intermediate configuration defined by $\mathbf{R}_e = \mathbf{I}$, the spin $\mathbf{\Omega}$ has (for isotropic hardening) a simple, explicit representation $\mathbf{\Omega} = (\dot{\mathbf{F}}_p\mathbf{F}_p^{-1})_a$, while the plastic strain rate becomes $\mathbf{D}_p = (\dot{\mathbf{F}}_p\mathbf{F}_p^{-1})_s$. If the intermediate configuration is defined by distressing such that $[\mathbf{F}_e(\dot{\mathbf{F}}_p\mathbf{F}_p^{-1})\mathbf{F}_e^{-1}]_a = \mathbf{0}$, from (5) and polar decomposition of $\mathbf{F}_e$ it follows that $\mathbf{\Omega} = \dot{\mathbf{R}}_e\mathbf{R}_e^{-1}$, while $\mathbf{D}_p = \mathbf{F}_e(\dot{\mathbf{F}}_p\mathbf{F}_p^{-1})\mathbf{F}_e^{-1}$. Additional kinematic analysis of the elastic strain rate expression and spin $\mathbf{\Omega}$ is given in Section 6.

A comment should also be made regarding the definition of elastic strain rate used in some related work. In those studies, elastic strain rate is defined by an equation of the type (22), but with the Jaumann rate of $\mathbf{V}_e$ taken relatively to the spin of the director vectors triad, which is introduced to cope with the anisotropic hardening features (referred to as substructural spin). However, for elastically isotropic material the elastic strain rate should not depend on such a spin, nor on any other variable that is introduced to handle the anisotropic hardening. These variables directly effect only the constitutive expression for the plastic strain rate, but should not be present in the definition of the elastic part of the total strain rate. Indeed, in our definition of the elastic strain rate (22), the Jaumann

Downloaded 03 May 2010 to 171.66.16.20. Redistribution subject to ASME license or copyright; see http://www.asme.org/terms/Terms_Use.cfm

rate of $\mathbf{V}_e$ is taken relatively to spin Ω which depends only on $\mathbf{V}_e$, $\dot{\mathbf{V}}_e$ and the total material spin $\mathbf{W}$ as shown in (16), regardless of the type of (isotropic or anisotropic) plastic hardening, or any variable that is introduced to describe it.

4 Elastoplastic Constitutive Structure

With the elastic (reversible) part of the strain rate identified by (12), the remaining part, $\mathbf{D}_p = \mathbf{D} - \mathbf{D}_e$, is plastic (residual) contribution. This is governed by the plastic potential and codirectional with the outward normal to current yield surface in the Cauchy stress space (Hill, 1967; Hill and Rice, 1973). It is $\mathbf{D}_p$ (in its entirety) that has to be constructed at the phenomenological level. In the case of isotropic hardening, with the yield function g as an isotropic scalar function of σ, one has the well-known representation

$$\mathbf{D}_p = \frac{1}{h}\left(\frac{\partial g}{\partial \sigma} : \overset{\circ}{\tau}\right)\frac{\partial g}{\partial \sigma}. \tag{24}$$

Here h is a scalar function of plastic deformation history and $\overset{\circ}{\tau}$ is defined for a reference configuration chosen to coincide, instantaneously, with the current configuration. This definition differs from the one used in Sections 2 and 3 by a scalar multiplier $\det\mathbf{F}_e$ which can be absorbed into h. Equations (12) and (24) complete the constitutive description of the considered model of material behavior, giving

$$\mathbf{D} = \boldsymbol{\Lambda}^{-1} : \overset{\circ}{\tau}, \quad \boldsymbol{\Lambda}^{-1} = \boldsymbol{\Lambda}_e^{-1} + \frac{1}{h}\frac{\partial g}{\partial \sigma} \otimes \frac{\partial g}{\partial \sigma}, \tag{25}$$

where $\boldsymbol{\Lambda}^{-1}$ is the instantaneous elastoplastic compliance tensor. The inverted form of (25) is

$$\overset{\circ}{\tau} = \boldsymbol{\Lambda} : \mathbf{D}, \quad \boldsymbol{\Lambda} = \boldsymbol{\Lambda}_e - \frac{1}{H}\boldsymbol{\Lambda}_e : \left(\frac{\partial g}{\partial \sigma} \otimes \frac{\partial g}{\partial \sigma}\right) : \boldsymbol{\Lambda}_e, \tag{26}$$

where $H = h + (\partial g/\partial\sigma) : \boldsymbol{\Lambda}_e : (\partial g/\partial\sigma)$. Transition from this elastoplastic constitutive structure, with the Jaumann derivative of stress $\overset{\circ}{\tau} = \dot{\tau} - \mathbf{W}\sigma + \sigma\mathbf{W}$, to one with the convected derivative $\overset{\circ}{\tau} = \dot{\tau} - \mathbf{L}\sigma - \sigma\mathbf{L}^T$, is direct via $\overset{\circ}{\tau} = \overset{\circ}{\tau} + \mathbf{D}\sigma + \sigma\mathbf{D}$. The corresponding elastoplastic moduli tensors differ by terms of the order of stress.

It is seen that the so-called plastic spin does not appear in the constitutive equations at all. Therefore, the statement recently often made in the literature that isotropic hardening Prandtl-Reuss equations are obtained when the so-called plastic spin is assumed to vanish is incorrect.

If hardening is anisotropic, the constitutive structure of $\mathbf{D}_p$ has to be accordingly constructed. In doing this, one introduces in the analysis some additional ingredients. For example, the back stress and its evolution law have been introduced in the case of the kinematic hardening model. However, the back stress model does not include any statement regarding plastic spin. It can be useful to introduce in the analysis a new spin measure, say the spin of the material line that instantaneously coincides with an eigendirection of the back stress (Lee et al., 1983), but this spin can be directly calculated in terms of the total spin and strain rate. Therefore, an additional constitutive equation for such a back stress (plastic) spin is not required.

As discussed previously, the identification of the constituents of the total spin must be carried out within the framework of a physical structure. This is outlined in the next section.

5 Crystal Plasticity

In single crystal plasticity, a definite additional structure is attached to intermediate configuration: material flows through the crystal lattice via dislocation motion, while the lattice preserves its orientation (Asaro 1983a, 1983b). In that way the intermediate configuration differs from the initial, undeformed configuration by deformation solely due to crystallographic slip, i.e.,

$$\dot{\mathbf{F}}_p\mathbf{F}_p^{-1} = \sum_i \dot{\gamma}^{(i)}\mathbf{s}^{(i)} \otimes \mathbf{m}^{(i)}. \tag{27}$$

Here $\dot{\gamma}^{(i)}$ is the shearing (slipping) rate of the ith active slip system, with the slip direction $\mathbf{s}^{(i)}$ in the slip plane with the normal $\mathbf{m}^{(i)}$. Hence, both symmetric and antisymmetric parts of $\dot{\mathbf{F}}_p\mathbf{F}_p^{-1}$, i.e., the strain rate and spin of the intermediate configuration are prescribed by (27). Integration of (27) leads to a unique $\mathbf{F}_p$. The elastic part of $\mathbf{F}$, $\mathbf{F}_e$, can be obtained from the solution of (1) and is also unique. In the context of crystal plasticity, $\mathbf{F}_e$ represents the stretching and rotation of the lattice with the material embedded on it. The intermediate configuration is therefore uniquely specified and it can be called isoclinic, in the sense of Mandel (1973).

Elastic strain rate can again be expressed by (11), i.e.,

$$\mathbf{D}_e = (\dot{\mathbf{F}}_e\mathbf{F}_e^{-1})_s - \boldsymbol{\Lambda}_e^{-1} : (\mathbf{W}_p\tau - \tau\mathbf{W}_p), \tag{28}$$

with

$$\mathbf{W}_p = [\mathbf{F}_e(\dot{\mathbf{F}}_p\mathbf{F}_p^{-1})\mathbf{F}_e^{-1}]_a. \tag{29}$$

The first term in the right-hand side of (28) is the lattice strain rate while the remaining term is the contribution from the deforming intermediate configuration induced by crystallographic slip.

Since $(\dot{\mathbf{F}}_e\mathbf{F}_e^{-1})_a$ represents the lattice spin, from (5) we see that $\mathbf{W}_p = \mathbf{W} - (\dot{\mathbf{F}}_e\mathbf{F}_e^{-1})_a$ is the spin of the material relative to the lattice. In single crystal plasticity, $\mathbf{W}_p$ is customarily called plastic spin, but essential additional structure of the crystal plasticity is all contained in the kinematics of crystallographic slip, attached to intermediate configuration and described by (27), and associated kinetics which specifies the shearing rates $\dot{\gamma}^{(i)}$ in terms of stress and stress rate. From (4) and $\mathbf{D} = \mathbf{D}_e + \mathbf{D}_p$, the plastic strain rate is

$$\mathbf{D}_p = [\mathbf{F}_e(\dot{\mathbf{F}}_p\mathbf{F}_p^{-1})\mathbf{F}_e^{-1}]_s + \boldsymbol{\Lambda}_e^{-1} : (\mathbf{W}_p\tau - \tau\mathbf{W}_p). \tag{30}$$

It is $\mathbf{D}_p$ that is normal to the yield surface, and not $[\mathbf{F}_e(\dot{\mathbf{F}}_p\mathbf{F}_p^{-1})\mathbf{F}_e^{-1}]_s$. In other words, in transforming the slip deformation $\dot{\mathbf{F}}_p\mathbf{F}_p^{-1}$ from intermediate to current configuration by elastic deformation $\mathbf{F}_e$, the corresponding strain rate $[\mathbf{F}_e(\dot{\mathbf{F}}_p\mathbf{F}_p^{-1})\mathbf{F}_e^{-1}]_s$ is equal to plastic strain rate $\mathbf{D}_p$ with an elastic contribution, due to stress rate $(\mathbf{W}_p\tau - \tau\mathbf{W}_p)$, subtracted off (see also Hill and Havner, 1982). Note that in the foregoing derivation, the lattice elasticity does not have to be isotropic (Lubarda, 1991b).

6 General Expression for Elastic Strain Rate

We show here that the elastic strain rate can also be represented in terms of an arbitrary $\mathbf{F}_e$, in the form

$$\mathbf{D}_e = (\overset{*}{\dot{\mathbf{F}}}_e\mathbf{F}_e^{-1})_s, \tag{31}$$

where $\overset{*}{\dot{\mathbf{F}}}_e = \dot{\mathbf{F}}_e - \Omega\mathbf{F}_e + \mathbf{F}_e\Omega_p$ is the Jaumann derivative of $\mathbf{F}_e$, taken relatively to spins Ω and Ω_p, which are associated with the current and intermediate states, respectively. Physically, so defined $\overset{*}{\dot{\mathbf{F}}}_e$ gives the change of elastic deformation gradient $\mathbf{F}_e$ observed in the coordinate systems that rotate with spin Ω in the current, and spin Ω_p in the intermediate configuration. Spin Ω is independent of the choice of intermediate configuration, whereas spin Ω_p does depend on that choice, as will be seen as follows. By equating (31) and (22),

$$(\overset{*}{\dot{\mathbf{F}}}_e\mathbf{F}_e^{-1})_s = (\overset{*}{\dot{\mathbf{V}}}_e\mathbf{V}_e^{-1})_s, \tag{32}$$

we therefore have

$$[\mathbf{V}_e(\dot{\mathbf{R}}_e\mathbf{R}_e^{-1} + \mathbf{R}_e\Omega_p\mathbf{R}_e^T)\mathbf{V}_e^{-1}]_s = (\mathbf{V}_e\Omega\mathbf{V}_e^{-1})_s, \tag{33}$$

from which, by a simple matrix argument, it follows that

$$\Omega_p = \mathbf{R}_e^T(\Omega - \dot{\mathbf{R}}_e\mathbf{R}_e^{-1})\mathbf{R}_e. \tag{34}$$

This expresses the spin Ω_p in terms of the spin Ω, rotation $\mathbf{R}_e$, and its rate $\dot{\mathbf{R}}_e$. Recall that the spin Ω is uniquely determined

Downloaded 03 May 2010 to 171.66.16.20. Redistribution subject to ASME license or copyright; see http://www.asme.org/terms/Terms_Use.cfm

by (16). Clearly from (34), Ω_p depends on a particular choice of intermediate configuration. For example, if the intermediate configuration is defined by distressing without rotation ($\mathbf{R}_e = \mathbf{I}$), $\Omega_p \equiv \Omega$. If the intermediate configuration is defined by $[\mathbf{F}_e(\mathbf{F}_p\mathbf{F}_p^{-1})\mathbf{F}_e^{-1}]_a = \mathbf{0}$, we have shown in Section 3 that $\Omega = \dot{\mathbf{R}}_e\mathbf{R}_e^{-1}$, and therefore $\Omega_p \equiv \mathbf{0}$. Of course, in each case the elastic strain rate is the same.

We can also write (31) in the expanded form

$$\mathbf{D}_e = (\dot{\mathbf{F}}_e\mathbf{F}_e^{-1})_s + (\mathbf{F}_e\Omega_p\mathbf{F}_e^{-1})_s, \tag{35}$$

which shows that besides the usual contribution given by the first term on the right-hand side, the elastic strain rate $\mathbf{D}_e$, has an additional contribution, given by the second term, which is caused by the spin Ω_p due to deforming and rotating intermediate configuration. If intermediate configuration is defined by distressing without rotation ($\mathbf{F}_e = \mathbf{V}_e$), above coincides with (23). Comparing (35) with (11), we in addition have

$$(\mathbf{F}_e\Omega_p\mathbf{F}_e^{-1})_s = -\mathbf{\Lambda}_e^{-1} : \{[\mathbf{F}_e(\dot{\mathbf{F}}_p\mathbf{F}_p^{-1})\mathbf{F}_e^{-1}]_a\tau - \tau[\mathbf{F}_e(\dot{\mathbf{F}}_p\mathbf{F}_p^{-1})\mathbf{F}_e^{-1}]_a\}. \tag{36}$$

We note that the representation (31) can be established directly, by applying the Jaumann derivative $*$ to both sides of the hyperelasticity law (2). By demanding $\Omega + (\overset{*}{\mathbf{F}}_e\mathbf{F}_e^{-1})_a = \mathbf{W}$ in an analogous procedure to that described in Section 3, we again arrive at (31) and (34).

Finally, if we rewrite (34) in the form

$$\Omega = \dot{\mathbf{R}}_e\mathbf{R}_e^{-1} + \mathbf{R}_e\Omega_p\mathbf{R}_e^T, \tag{37}$$

we see that the invariant spin Ω has two contributions: one from spin $\dot{\mathbf{R}}_e\mathbf{R}_e^{-1}$, and another which is induced from spin Ω_p and which represents the effect of deforming and rotating intermediate configuration. Both of these contributions depend on the choice of an intermediate configuration, but their combination giving Ω does not.

Results presented in this and previous sections should remove disagreements that appeared in the literature over a long period of time regarding the invariance requirements and independence of the final constitutive equations of the selected intermediate configuration used in developing the theory.

7 Concluding Remarks

We have shown in this paper that, within the framework of a phenomenological plasticity theory, there is no basis and no necessity for partitioning the total spin into its elastic and plastic constituents. Statements to the contrary in literature are the result of improper partitioning of total strain rate and subsequent misinterpretations. The introduction of various ingredients to treat anisotropic hardening, such as back stress or similar internal variables, only affects the structure of the constitutive equation for the plastic strain rate, but does not provide a basis for the identification of the plastic spin. Indeed, we have shown that such identification in the context of a phenomenological theory is unnecessary.

The situation is quite different in single crystal plasticity, where a specific additional structure is introduced in the model (that of material flowing through the crystal lattice) while the lattice preserves its orientation. Material and lattice then have different spins, and it is this difference that is identified as the plastic spin.

A remark should be also made regarding the elastically anisotropic, say persistently orthotropic materials. In this case the rotation of the principal axes of orthotropy is not given by the overall deformation gradient but must be independently determined. This can be accomplished by introducing a constitutive equation for an associated spin, but a reliable procedure for doing this is yet to be proposed. In analogy with single crystal plasticity, one could define the intermediate configuration to be isoclinic, i.e., material "flows" through the structure with fixed oriented axes of orthotropy (director vectors). However, the kinematic and kinetic description of such a process for the polycrystalline material is currently not available. In single crystal plasticity this process is crystallographic slip, i.e., the kinematics of simple shearing and kinetic relationships specifying the shearing rates in terms of stress and stress rate.

Acknowledgment

The authors would like to thank Professor Li Cheng for helpful discussions.

References

Agah-Tehrani, A., Lee, E. H., Mallett, R. L., and Onat, E. T., 1987, "The Theory of Elastic-Plastic Deformation at Finite Strain with Induced Anisotropy Modeled as Combined Isotropic-Kinematic Hardening," *J. Mech. Phys. Solids*, Vol. 35, pp. 519–539.

Aravas, N., and Aifantis, E. C., 1991, "On the Geometry of Slip and Spin in Finite Plasticity Deformation," *Int. J. of Plasticity*, Vol. 7, pp. 141–160.

Asaro, R. J., 1983a, "Crystal Plasticity," ASME JOURNAL OF APPLIED MECHANICS, Vol. 50, pp. 921–934.

Asaro, R. J., 1983b, "Micromechanics of Crystals and Polycrystals," *Advances in Applied Mechanics*, Vol. 23, J. W. Hutchinson and T. Y Wu, eds., Academic Press, New York, pp. 1–115.

Asaro, R. J., and Rice, J. R., 1977, "Strain Localization in Ductile Single Crystals," *J. Mech. Phys. Solids*, Vol. 25, pp. 309–338.

Casey, J., and Naghdi, P. M., 1980, "Remarks on the Use of the Decomposition $F = F_eF_p$ in Plasticity," ASME JOURNAL OF APPLIED MECHANICS, Vol. 47, pp. 672–675.

Dafalias, Y. F., 1983, "Corotational Rates for Kinematic Hardening at Large Plastic Deformations," ASME JOURNAL OF APPLIED MECHANICS, Vol. 50, pp. 561–565.

Dafalias, Y. F., 1985, "The Plastic Spin," ASME JOURNAL OF APPLIED MECHANICS, Vol. 52, pp. 865–871.

Dafalias, Y. F., 1987, "Issues in Constitutive Formulation at Large Elastoplastic Deformation, Part 1: Kinematics," *Acta Mech.*, Vol. 69, pp. 119–138.

Dashner, P. A., 1986, "Invariance Considerations in Large Strain Elasto-Plasticity," ASME JOURNAL OF APPLIED MECHANICS, Vol. 53, pp. 55–60.

Freund, L. B., 1970, "Constitutive Equations for Elastic-Plastic Materials at Finite Strain," *Int. J. Solids Struct.*, Vol. 6, pp. 1193–1209.

Green, A. E., and Naghdi, P. M., 1971, "Some Remarks on Elastic-Plastic Deformation at Finite Strain," *Int. J. Engg. Sci.*, Vol. 9, pp. 1219–1229.

Hill, R., 1967, "On Constitutive Inequalities for Simple Materials—II," *J. Mech. Phys. Solids*, Vol. 16, pp. 315–322.

Hill, R., 1978, "Aspects of Invariance in Solid Mechanics," *Advances in Applied Mechanics*, Vol. 18, C.-S. Yih, ed., Academic Press, New York, pp. 1–75.

Hill, R., and Havner, K. S., 1982, "Perspectives in the Mechanics of Elastoplastic Crystals," *J. Mech. Phys. Solids*, Vol. 30, pp. 5–22.

Hill, R., and Rice, J. R., 1973, "Elastic Potentials and the Structure of Inelastic Constitutive Laws," *SIAM J. Appl. Math.*, Vol. 25, pp. 448–461.

Kleiber, M., 1975, "Kinematics of Deformation Processes in Materials Subjected to Finite Elastic-Plastic Strains," *Int. J. Eng. Sci.*, Vol. 13, pp. 513–525.

Kratochvil, H., 1973, "On a Finite Strain Theory of Elastic-Inelastic Materials," *Acta Mech.*, Vol. 16, pp. 127–142.

Lee, E. H., 1969, "Elastic-Plastic Deformation at Finite Strains," ASME JOURNAL OF APPLIED MECHANICS, Vol. 36, pp. 1–6.

Lee, E. H., Mallett, R. L., and Wertheimer, T. B., 1983, "Stress Analysis for Anisotropic Hardening in Finite-Deformation Plasticity," ASME JOURNAL OF APPLIED MECHANICS, Vol. 50, pp. 554–560.

Loret, B., 1983, "On the Effects of Plastic Rotation in the Finite Deformation of Anisotropic Elastoplastic Materials," *Mech. Matls.*, Vol. 2, pp. 287–304.

Lubarda, V. A., 1991a, "Constitutive Analysis of Large Elasto-Plastic Deformation Based on the Multiplicative Decomposition of Deformation Gradient," *Int. J. Solids Struct.*, Vol. 27, pp. 885–895.

Lubarda, V. A., 1991b, "Some Aspects of Elasto-Plastic Constitutive Analysis of Elastically Anisotropic Materials," *Int. J. Plasticity*, Vol. 7, pp. 625–636.

Lubarda, V. A., and Lee, E. H., 1981, "A Correct Definition of Elastic and Plastic Deformation and its Computational Significance," ASME JOURNAL OF APPLIED MECHANICS, Vol. 48, pp. 35–40.

Lubliner, J., 1978, "A Thermodynamic Yield Criterion in Viscoplasticity," *Acta Mech.*, Vol. 30, pp. 165–174.

Mandel, J., 1973, "Equations Constitutives et Directeurs dans les Milieux Plastiques et Viscoplastiques," *Int. J. Solids Struct.*, Vol. 9, pp. 725–740.

Mohan, R., Ortiz, M., and Shih, C. F., 1992, "An Analysis of Cracks in Ductile Single Crystals: Part I—Anti-plane Shear," *J. Mech. Phys. Solids*, Vol. 40, pp. 291–314.

Moran, B., Ortiz, M., and Shih, C. F., 1990, "Formulation of Implicit Finite Element Methods for Multiplicative Finite Deformation Plasticity," *Int. J. Numer. Methods Eng.*, Vol. 29, pp. 483–514.

Naghdi, P. M., 1990, "A Critical Review of the State of Finite Plasticity," *Z. angew. Math. Phys.*, Vol. 41, pp. 315–394.

Nagtegaal, J. C., and de Jong, J. E., 1982, "Some Aspects of Nonisotropic Work Hardening in Finite Strain Plasticity," *Plasticity of Metals at Finite Strain:*

Downloaded 03 May 2010 to 171.66.16.20. Redistribution subject to ASME license or copyright; see http://www.asme.org/terms/Terms_Use.cfm

Theory, Experiment and Computation, E. H. Lee and R. L. Mallett, eds., pp. 65–102.

Needleman, A., 1985, "On Finite Element Formulations for Large Elastic-Plastic Deformations," *Comp. Struct.*, Vol. 20, pp. 247–257.

Nemat-Nasser, S., 1979, "Decomposition of Strain Measures and their Rates in Finite Deformation Elastoplasticity," *Int. J. Solids Struct.*, Vol. 15, pp. 155–166.

Nemat-Nasser, S., 1982, "On Finite Deformation Elasto-Plasticity," *Int. J. Solids Struct.*, Vol. 18, pp. 857–872.

Sidoroff, F., 1975, "On the Formulation of Plasticity and Viscoplasticity with Internal Variables," *Arch. Mech.*, Vol. 27, pp. 807–819.

Simo, J. C., and Ortiz, M., 1985, "A Unified Approach to Finite Deformation Elastoplastic Analysis based on the Use of Hyperelastic Constitutive Equations," *Comput. Methods Appl. Mech. Engng.*, Vol. 49, pp. 221–245.

Truesdell, C., and Noll, W., 1965, "The Nonlinear Field Theories of Mechanics," *Handbuck der Physik*, Band III/3, Springer-Verlag, Berlin.

Willis, J. R., 1969, "Some Constitutive Equations Applicable to Problems of Large Dynamic Plastic Deformation," *J. Mech. Phys. Solids*, Vol. 17, pp. 359–369.

Zbib, H. M., and Aifantis, E. C., 1988, "On the Concept of Relative and Plastic Spins and its Implications to Large Deformation Theories. Part II: Anisotropic Hardening," *Acta Mechanica*, Vol. 75, pp. 35–56.

Downloaded 03 May 2010 to 171.66.16.20. Redistribution subject to ASME license or copyright; see http://www.asme.org/terms/Terms_Use.cfm

An Energy Criterion for the Onset of Shear Localization in Thermal Viscoplastic Materials, Part I: Necessary and Sufficient Initiation Conditions

T. G. Shawki
Department of Theoretical and Applied Mechanics,
University of Illinois at Urbana—Champaign,
Urbana, IL 61801

Necessary and/or sufficient conditions for the onset of shear flow localization in thermal viscoplastic materials are derived. Initiation of shear band formation is examined through the analysis of a one-dimensional model of dynamic simple shear with velocity-controlled boundaries. An exact energy estimate is derived for the fully nonlinear initial boundary value problem which illustrates the weak effect of elasticity as regards the onset of localization. The existence, uniqueness and well-posedness properties of a spatially homogeneous solution are also examined. A unique homogeneous solution is shown to exist for the dynamic simple shear problem with velocity controlled and thermally insulated boundaries. The former solution is also shown to be the unique static *solution of the simple shear problem, with no elastic or heat conduction effects, consistent with the foregoing boundary conditions. A linear system of equations is derived for the perturbations superposed on the reference,* time-dependent *homogeneous (static) solution. A discussion regarding the notions of instability and localization motivates the introduction of a novel localization criterion, based on an appropriately selected energy norm, that takes full account of the time variation of the homogeneous solution. Taking advantage of the admissible spatial form of the perturbations together with the foregoing criterion allows for the association of the positive rate of change of the total kinetic energy of the absolute perturbations with the onset of shear strain localization.*

1 Introduction

The term *shear strain localization* is frequently used to describe the concentration of plastic deformation within local regions (known as *shear bands*) in an otherwise homogeneous deformation field. Shear strain localization, in the dynamical sense, denotes the continual evolution of an inhomogeneous deformation field from an initially homogeneous (near-homogeneous) reference field. The appearance of narrow bands of intense shearing deformation has been observed during the low and high rate deformations of many materials (e.g., ferrous metals, nonferrous metals, polymeric glasses). Extensive reviews of experimental observations of shear bands in various applications are given by Rogers (1974, 1979, 1983). Shawki and Clifton (1989) recently presented a review of the different mechanisms proposed for the analysis of shear strain localization as it is observed in different materials, geometries, scales of observation, and loading conditions.

The term *adiabatic* shear bands is commonly used in connection with shear band formation at high strain rates where the time scale of the deformation is much shorter than that required for local heat conduction, between sufficiently distant material points, and global heat diffusion, from the body to its surroundings, to be considered significant. Early observations of adiabatic shear bands can be traced back to Henri Tresca (1878) who described them as *heat lines* (see Johnson, 1987). Clear identification of the relation between the initiation of adiabatic shear bands and the negative slope of the adiabatic stress-strain curve is attributed to Zener and Hollomon (1944). The primary mechanism for shear band formation at high rates of loading is believed to be a thermo-mechanical mechanism, through which the localization of plastic flow is the outcome of a *net* material softening. Furthermore, the primary softening mechanism, in this framework, is that related to *thermal softening* which is manifested by the decrease in the flow stress associated with temperature increase in a constant strain and

Contributed by the Applied Mechanics Division of JOURNAL OF APPLIED MECHANICS for publication in the ASME THE AMERICAN SOCIETY OF MECHANICAL ENGINEERS.

Discussion on this paper should be addressed to the Technical Editor, Professor Lewis T. Wheeler, Department of Mechanical Engineering, University of Houston, Houston, TX 77204-4792, and will be accepted until four months after final publication of the paper itself in the ASME THE AMERICAN SOCIETY OF MECHANICAL ENGINEERS.

Manuscript received by the ASME Applied Mechanics Division, Apr. 5, 1991; final revision, July 29, 1993. Associate Technical Editor: C. F. Shih.

Copyright © 1994 by ASME
Downloaded 03 May 2010 to 171.66.16.20. Redistribution subject to ASME license or copyright; see http://www.asme.org/terms/Terms_Use.cfm

strain-rate test. At high strain rates, the lack of time for local and global heat diffusion allows nonuniform straining to cause nonuniform heating. The rate of heat generation is highest at the sites of the highest strain rates. As the temperature is increased (nonuniformly), the material local resistance to further plastic flow decreases and the cycle continues with the deformation being eventually localized in the form of shear bands. The foregoing mechanism applies formally to the *pre-initiation regime*. Subsequent propagation and intensification of a shear band are topics related to the *post-initiation regime*. Shawki and Clifton (1989) have presented late-time numerical solutions that illustrate the band narrowing mechanism and the associated elastic unloading away from the band. Shawki and Sherif (1988) have constructed a steady-state solution, valid at late times, to determine the characteristic band *thickness* (if any) at which all the locally generated heat is diffused to the colder outside material. This model provides closed-form expressions for the shear band thickness.

Most of the analytic literature on shear localization focuses on the analysis of the pre-initiation regime where necessary and sufficient conditions for the *onset* of localization are sought. A linear stability approach has been adopted by many authors in an attempt to examine the stability of a spatially homogeneous reference solution (if any) to small initial spatial perturbations. We present a brief review of these efforts since they represent the background to our paper. Clifton (1979) examined the stability of quasi-static, simple shear including the effects of heat conduction, strain hardening, strain rate sensitivity, and thermal softening. Bai (1981, 1982) presented a similar perturbation analysis where he considered the dynamic simple shear problem. The foregoing works do not account for the time variation of the homogeneous solution since they take the homogeneous solution to be constant in both time and space. Burns and Trucano (1982) examined the stability of the time-dependent, homogeneous, simple shear solution for the special case of a Newtonian fluid with temperature-dependent viscosity. Shawki, Clifton, and Majda (1983) considered the rate of growth of an energy norm while retaining the time dependence of the homogeneous solution. The former effort established necessary conditions for the *well-posedness* of solutions to the linear system of absolute perturbations. Clifton et al. (1984) presented a general linear stability analysis for the dynamic, simple shear of a thermal elastic-viscoplastic solid while assuming that the homogeneous solution is "frozen" at a reference initial time. Burns (1985) presented a two-timing asymptotic expansion, for a particular constitutive model, to include the time dependence of the homogeneous solution. Fressengeas and Molinari (1985) examined the effects of inertia and heat conduction on flow localization in dynamic, uniaxial tension of a thermal viscoplastic material. Anand, Kim, and Shawki (1987) presented a three-dimensional generalization of the constant-coefficient linear stability analysis while accounting for pressure sensitivity of the material response. Fressengeas and Molinari (1987) presented a modified linear stability approach based on the *relative* perturbations (which refer to the absolute perturbations normalized by the respective homogeneous solution) and showed better agreement with some nonlinear results. Burns (1989) used the linear stability theory to examine the effects of two dimensionless coefficients on the onset of localization. These coefficients are interpreted as the ratio of the momentum flux to the plastic flow stress as well as a measure of viscous damping. Shawki and Clifton (1989) presented, among several other analyses, necessary and sufficient conditions for the onset of shear localization along with upper and lower bounds for the critical wavelength of initial perturbations. However, the former work did not account for the time variation of the homogeneous solution.

The foregoing efforts served to illustrate some fundamental features related to the initiation of shear localization in thermal viscoplastic materials; however, they suffered from a number of drawbacks:

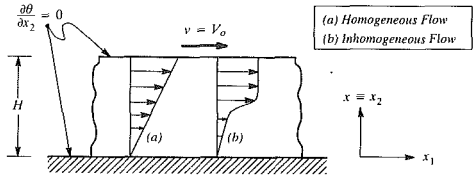


Fig. 1 The initial boundary value problem

(i) *Existence and uniqueness* properties of a homogeneous solution, for the considered initial boundary value problem, were not addressed.

(ii) Some of the works were concerned with *special constitutive models* which restrict the applicability of their results.

(iii) The *time dependence* of the homogeneous solution was almost always neglected.

(iv) The *notion of shear localization* was not consistent among various analyses.

These drawbacks resulted some confusion as regards the stability of plastic flow and the critical conditions for shear band formation. Hence, we present a linear stability theory that resolves the difficulties (i)–(iv) while allowing for a unified framework for the analysis of the pre-initiation regime of shear strain localization for the thermally sensitive, viscoplastic material response. A key feature of the present analysis is the introduction of a new mathematical description of flow *localization* which serves to identify the evolution of bounded, spatially inhomogeneous plastic flow while distinguishing it from the growth of spatially homogeneous flow. The foregoing description involves an appropriately selected energy norm in which the time dependence of the homogeneous solution *is retained*. This approach assumes a general description of material response and allows for the derivation of necessary and sufficient conditions for the onset of shear flow localization. It turns out that the onset of shear localization is associated with the increased importance of inertial effects. It should also be noted that this presentation applies strictly to the case of simple shear with velocity-controlled boundaries for which an exact, unique homogeneous solution exists. In Part II of this work, see Shawki (1994), a complete discussion regarding the effects of heat conduction, inertia, and time variation of the homogeneous solution is presented along with applications of the foregoing necessary and sufficient initiation conditions to a number of material constitutive descriptions.

2 Problem Formulation

Consider a simple shearing deformation of a plate with a finite thickness H in the x_2-direction whereas it is infinite in the other two rectangular cartesian directions (see Fig. 1). The lower edge of the plate is held fixed while a constant velocity V_o is applied at the upper edge. We assume that all physical quantities are uniform along the x_1 and x_3-directions so that the deformation depends only on the space coordinate x_2. A complete derivation of the governing system of equations is presented by Shawki and Clifton (1989). This system is given by

$$\rho \frac{\partial v}{\partial t} = \frac{\partial \sigma}{\partial x}, \tag{1}$$

$$\frac{\partial v}{\partial x} = \frac{1}{\mu}\frac{\partial \sigma}{\partial t} + \frac{\partial \gamma^p}{\partial t}, \tag{2}$$

$$\rho c \frac{\partial \theta}{\partial t} = \kappa \frac{\partial^2 \theta}{\partial x^2} + \beta\sigma \frac{\partial \gamma^p}{\partial t}, \tag{3}$$

$$\frac{\partial \gamma^p}{\partial t} = \phi(\sigma, \theta, \gamma^p). \tag{4}$$

Downloaded 03 May 2010 to 171.66.16.20. Redistribution subject to ASME license or copyright; see http://www.asme.org/terms/Terms_Use.cfm

Table 1 Deformation classifications

Static	Quasi-static	Dynamic	Adiabatic	Isothermal
$\rho \frac{\partial v}{\partial t} \doteq 0$	$0 < \rho \frac{\partial v}{\partial t} \ll 1$	$\rho \frac{\partial v}{\partial t} \gg 1$	$\kappa = 0$	$\theta(x, t) = \text{const.}$

In the above equations, (x, v, σ) are written for (x_2, v_1, σ_{12}), respectively. Further, v_1 is the particle velocity in the x_1-direction, σ_{12} is the shear stress, θ is the absolute temperature, and γ^p is the total accumulated plastic strain. Moreover, ρ is the mass density, μ is the elastic shear modulus, c is the specific heat, κ is the coefficient of thermal conduction and $\beta (0 < \beta \leq 1)$ represents the fraction of the power of dissipation that is converted to heat. Equations (1) and (3) represent the balance of linear momentum and energy, respectively. Equation (2) represents the additive decomposition of the total strain rate into an elastic strain rate plus a viscoplastic strain rate while Eq. (4) describes the considered class of material response in which the plastic strain rate depends on the total plastic strain, flow stress, and absolute temperature. The total plastic strain is given by

$$\gamma^p = \gamma_o^p + \int_0^t \phi dt. \tag{5}$$

It is often convenient to express the material behavior in the alternative form

$$\sigma = \psi(\phi, \theta, \gamma^p). \tag{6}$$

Further, we note that partial derivatives of the functions ϕ and ψ, with respect to their respective arguments, play an important role in the analysis of shear localization. These derivatives are denoted by

$$S_k \equiv \psi_{,k} \text{ and } F_k = \phi_{,k}, \ k = 1, 2, 3. \tag{7}$$

In Eq. (7), $\psi_{,k}$ denotes differentiation of the function ψ with respect to its kth argument. A material response is said to exhibit strain-rate hardening if $\{S_1 > 0, F_1 > 0\}$, thermal softening (hardening) if $\{S_2 < 0, F_2 > 0\}$ ($\{S_2 > 0, F_2 < 0\}$), strain hardening (softening) if $\{S_3 > 0, F_3 < 0\}(\{S_3 < 0, F_3 > 0\})$.

Table 1 illustrates the various deformation classifications used in our subsequent discussions. Furthermore, neglect of elastic effects can be mathematically achieved by letting $\mu \to \infty$ in Eq. (2). It is also convenient to rewrite the system of Eqs. (1)–(4) in a dimensionless form. The dimensionless quantities are chosen as follows:

$$\hat{t} = \frac{t}{t_o}, \ \hat{x} = \frac{x}{H}, \ \hat{\sigma} = \frac{\sigma}{\sigma_o}, \ \hat{v} = \frac{v t_o}{H}, \ \hat{\phi} = \phi t_o,$$

$$\hat{\theta} = \frac{\theta}{\theta_o}, \ \hat{\kappa} = \frac{\kappa \theta_o t_o}{\sigma_o H^2}, \ \hat{\rho} = \frac{\rho H^2}{\sigma_o t_o^2}, \ \hat{c} = \frac{c \theta_o t_o^2}{H^2},$$

$$\hat{\mu} = \frac{\mu}{\sigma_o}, \ \hat{F}_1 = F_1 \sigma_o t_o, \ \hat{F}_2 = F_2 \theta_o t_o, \ \hat{F}_3 = F_3 t_o,$$

$$\hat{S}_1 = \frac{S_1}{\sigma_o t_o}, \ \hat{S}_2 = \frac{S_2 \theta_o}{\sigma_o}, \ \hat{S}_3 = \frac{S_3}{\sigma_o}. \tag{8}$$

In Eqs. (8), the subscript "o" denotes constant reference values corresponding, for example, to the values these quantities have in a homogeneous solution at the time a perturbation is introduced. The characteristic time t_o is the time $t_o = 1/\phi_o = H/V_o$ required to obtain a unit shear strain at the strain rate ϕ_o. It is important to note that the three dimensionless groups

$$\hat{\rho} = \frac{\rho V_o^2}{\sigma_o}, \ \hat{r}_o = \frac{\kappa t_o}{\rho c H^2}, \ \hat{r}_1 = \frac{\beta \sigma_o}{\rho c \theta_o}, \tag{9}$$

represent, respectively, inertial effects, deformation adiabaticity, and heating due to plastic flow. Once the dimensionless groups, in Eq. (8), are introduced in the system of governing Eqs. (1)–(4), the resulting dimensionless equations retain the same form as their dimensional counterparts. For convenience of notations, we will drop the superposed "hat" from dimensionless quantities and use dimensionless quantities for the remainder of this work.

The *mechanical* boundary conditions are chosen as either the *velocity* boundary conditions

$$v(0, t) = 0 \text{ and } v(1, t) = 1, \tag{10}$$

or the *stress* boundary conditions

$$\sigma(0, t) = \sigma_b(t) \text{ and } \sigma(1, t) = \sigma_t(t), \tag{11}$$

where $\sigma_b(t)$ and $\sigma_t(t)$ are prescribed functions. Moreover, *thermal* boundary conditions correspond to thermally insulated boundaries; that is

$$\frac{\partial \theta(0, t)}{\partial x} = \frac{\partial \theta(1, t)}{\partial x} = 0. \tag{12}$$

3 Nonlinear Energy Estimates

Here, we examine the nature of energy balance in the boundary value problem described by the nonlinear system of governing Eqs. (1)–(4) together with the boundary conditions given by Eqs. (10) and (12). For this purpose, we put the system (1)–(4) in a vector form in terms of the solution vector $\mathbf{u} \equiv (v, \sigma, \theta, \gamma^p)^T$ where a superposed "T" denotes matrix transpose. The nonlinear system (1)–(4) reduces to

$$\mathbf{u}_{,t} = A_2 \mathbf{u}_{,xx} + A_1 \mathbf{u}_{,x} + \mathbf{h}(\mathbf{u}), \tag{13}$$

where the nonvanishing components of the above coefficient matrices are given by: $(A_2)_{33} = r_o$, $(A_1)_{12} = 1/\rho$, $(A_1)_{21} = \mu$, $h_2 = -\mu\phi$, $h_3 = r_1 \sigma \phi$ and $h_4 = \phi$. We note that the coefficient matrices A_2 and A_1 are constant matrices whereas the vector $\mathbf{h}$ reflects the nonlinearity of the considered system which is primarily due to the nonlinear material response, in Eq. (4), and the plastic power term in Eq. (3). We now introduce the change of variables $\mathbf{u} \equiv D\mathbf{z}$ where the nonvanishing elements of the transformation matrix D are provided by: $D_{11} = D_{12} = D_{33} = D_{44} = 1$, and $D_{22} = -D_{21} = \rho c_e$. Here, $c_e = \sqrt{\mu/\rho}$ is the elastic shear wave speed. Equation (13) is now reduced to the more convenient form

$$\mathbf{z}_{,t} = A_2 \mathbf{z}_{,xx} + S\mathbf{z}_{,x} + \mathbf{k}(\mathbf{z}), \tag{14}$$

where the nonvanishing elements of the above matrices are given by $S_{22} = -S_{11} = c_e$, $z_1 = [v - (\sigma/\rho c_e)]/2$, $z_2 = [v + (\sigma/\rho c_e)]/2$, $z_3 = \theta$, $z_4 = \gamma^p$, $k_1 = -k_2 = c_e \phi/2$, $k_3 = h_3$ and $k_4 = h_4$. We now define the $L2$-inner product of the two vector fields $\mathbf{a}(x, t)$ and $\mathbf{b}(x, t)$, denoted by $\langle \mathbf{a}, \mathbf{b} \rangle$, as well as the induced $L2$-*norm* by

$$\langle \mathbf{a}, \mathbf{b} \rangle \equiv \int_0^1 \{\mathbf{a}^*(\xi, t) \cdot \mathbf{b}(\xi, t)\} d\xi \text{ and } \|\mathbf{a}\|^2 = \langle \mathbf{a}, \mathbf{a} \rangle \tag{15}$$

where $\mathbf{a}^*$ denotes the complex conjugate of the vector field $\mathbf{a}$ while $\mathbf{a} \cdot \mathbf{b} = a_k b_k$ ($k = 1, 2, 3$) is the scalar (dot) product of the considered vectors. We now define

$$E(t) \equiv \langle \mathbf{z}, \mathbf{z} \rangle = \|\mathbf{z}(x, t)\|^2 \tag{16}$$

as the *energy norm* for our initial boundary value problem. Note that $E(t)$ is a scalar evolution measure of the solution behavior. The *rate of change* of the energy norm is given by

$$\dot{E}(t) = 2\langle \mathbf{z}, \mathbf{k}(\mathbf{z}) \rangle - 2\langle \mathbf{z}_{,x}, A_2^T \mathbf{z}_{,x} \rangle + [(\mathbf{z} \cdot S\mathbf{z}) + 2(\mathbf{z}_{,x} \cdot A_2^T \mathbf{z})]_0^1, \tag{17}$$

where the terms between square brackets depend, respectively, on the imposed mechanical and thermal boundary conditions. These boundary contributions are given by

$$(\mathbf{z} \cdot S\mathbf{z})|_0^1 = \frac{1}{\rho} \{v(1, t)\sigma(1, t) - v(0, t)\sigma(0, t)\},$$

$$(\mathbf{z}_{,x} \cdot A_2^T \mathbf{z})|_0^1 = r_o \{\theta(1, t)\theta_{,x}(1, t) - \theta(0, t)\theta_{,x}(0, t)\}. \tag{18}$$

Downloaded 03 May 2010 to 171.66.16.20. Redistribution subject to ASME license or copyright; see http://www.asme.org/terms/Terms_Use.cfm

The contribution given by the second of Eqs. (18) vanishes in the case of adiabatic boundary conditions or for adiabatic deformations while the contribution given by the first of Eqs. (18) reduces to $\sigma(1, t)/\rho$ for the case of prescribed velocities. Therefore, expression (17) reduces, in the case of insulated and velocity controlled boundaries, to the simpler form

$$\dot{E}(t) = 2\langle \mathbf{z}, \mathbf{k}(\mathbf{z})\rangle - 2\langle \mathbf{z}_{,x} A_2^T \mathbf{z}_{,x}\rangle + \frac{\sigma(1, t)}{\rho}. \tag{19}$$

The positive definiteness of the second inner product in (19) illustrates the stabilizing effect of heat conduction as regards the growth of the energy norm $E(t)$. Furthermore, we note that the elastic shear modulus μ does not appear explicitly in expression (19) which suggests that *elastic effects play no significant role towards the onset of shear strain localization* in the considered class of deformations. The former statement must be strictly tied to the onset of localization and not to the post-localization regime where elastic effects may play a more significant role. Since our current objectives are related to the initiation of shear localization; it seems reasonable to neglect elastic effects. Explicit evaluation of the various terms in Eq. (19) results in the familiar mechanical energy balance

$$\frac{d}{dt}\int_0^1 \frac{1}{2}\rho v^2(\xi, t)d\xi + \int_0^1 \sigma(\xi, t)\phi(\xi, t)d\xi = \sigma(1, t)v(1, t) = \sigma(1, t). \tag{20}$$

It is interesting to observe that for *quasi-static deformations*, the flow stress becomes almost independent of x; then the second integral in Eq. (20) reduces to the boundary stress $\sigma(1, t)$ for the case of prescribed boundary velocities and no elastic effects. This indicates that, for quasi-static deformations, the total kinetic energy remains almost unchanged. In this case, the input mechanical power is used primarily to increase the system's internal energy.

4 Existence and Uniqueness of a Homogeneous Solution

We seek a spatially homogeneous solution of the form

$$\sigma(x, t) = \bar{\sigma}(t),\ \gamma^p(x, t) = \bar{\gamma}^p(t),\ \theta(x, t) = \bar{\theta}(t). \tag{21}$$

Substitution of the above solution in Eq. (2) combined with spatial integration gives the consistent form of the "homogeneous" velocity profile

$$\bar{v}(x, t) = a(t)x + b(t). \tag{22}$$

Further substitution of Eq. (22) into Eq. (1) implies that the functions $a(t)$ and $b(t)$ must be independent of time. Hence, a homogeneous solution must satisfy

$$\frac{1}{\mu}\frac{d\bar{\sigma}}{dt} + \bar{\phi}(t) = a,\ \frac{d\bar{\theta}}{dt} = r_1\bar{\sigma}(t)\bar{\phi}(t),\ \bar{\gamma}^p(t) = \bar{\gamma}^p(0) + \int_0^1 \bar{\phi}(\eta)d\eta. \tag{23}$$

Consistent auxiliary conditions must satisfy that $\sigma_b(t) = \sigma_t(t) \equiv \sigma_B(t)$ and $\bar{\sigma}(0) = \sigma_B(0)$ in the case of *stress-controlled boundaries*. In this case, the second and third equations in (23) reduce to

$$\dot{\mathbf{w}} = \mathbf{f}_\sigma(\mathbf{w}, t);\ \mathbf{w} = (\bar{\theta}, \bar{\gamma}^p)^T,\ \mathbf{f}_\sigma = \{r_1\sigma_B(t)\bar{\phi}(t), \bar{\phi}(t)\}^T. \tag{24}$$

Assuming that a unique solution $\mathbf{w}(t)$ exists; the resulting homogeneous strain rate combined with the general loading $\sigma_B(t)$ will, in general, violate the first of Eqs. (23). Hence, we conclude that *there exists no homogeneous solution of the dynamic simple shear problem consistent with the case of stress-controlled boundaries*. In the case of a quasi-static deformation, the inertia term, based on the solution $\mathbf{w}(t)$ of Eq. (24), is given by

$$\rho\frac{\partial \bar{v}(x, t)}{\partial t} = \rho\dot{a}(t)x. \tag{25}$$

It is often argued that, for quasi-static deformations, the above inertia term is sufficiently small which suggests the acceptance of the solution $\mathbf{w}(t)$ as an *approximate* homogeneous solution. However, we discard this argument since, for linear stability studies of shear localization, the approximate homogeneous solution itself breaks down as soon as inertial effects become significant. This breakdown is often confused with shear band initiation which is incorrect.

On the other hand, for the case of *velocity-controlled boundaries*, Eqs. (10) and (22) indicate that $a = 1$ and $b = 0$; i.e., the "homogeneous" velocity profile is

$$\bar{v}(x, t) = x. \tag{26}$$

Thus, Eqs. (23) reduce to

$$\dot{\mathbf{s}}(t) = \mathbf{f}_v(\mathbf{s}) = \{\mu[1 - \bar{\phi}(t)], r_1\bar{\sigma}(t)\bar{\phi}(t), \bar{\phi}(t)\}^T,\quad \mathbf{s} = (\bar{\sigma}, \bar{\theta}, \bar{\gamma}^p)^T. \tag{27}$$

Sufficient conditions for the existence, uniqueness, and well-posedness of solutions for the system given by Eq. (27) are such that the function $\mathbf{f}_v(\mathbf{s})$ is continuous and satisfies a Lipschitz condition with respect to $\mathbf{s}$ in some domain $D(\mathbf{s}, t)$. Furthermore, it is evident that such solution is only consistent with adiabatic boundary conditions. For the remainder of this work, we will consider the case of insulated, velocity controlled boundaries combined with material models for which the foregoing sufficient conditions are met. It is also useful to note that the former homogeneous solution is the *unique static solution* to the dynamic simple shear Eqs. (1)–(4). In this case, the input power is used, in its entirety, to increase the system's internal energy.

5 Linear Energy Estimates

We impose a set of spatial perturbations of sufficiently small initial amplitude, consistent with insulated and velocity-controlled boundaries, on the homogeneous solution. Hence, we seek a solution to Eqs. (1)–(4) of the additive form

$$v(x, t) = x + \tilde{v}(x, t),\ \sigma(x, t) = \bar{\sigma}(t) + \tilde{\sigma}(x, t),\quad \phi(x, t) = \phi(t) + \tilde{\phi}(x, t),\quad \theta(x, t) = \bar{\theta}(t) + \tilde{\theta}(x, t),\ \gamma^p(x, t) = \bar{\gamma}(t) + \tilde{\gamma}^p(x, t) \tag{28}$$

where quantities with a superposed "tilde" represent the effect of the initial spatial perturbations. These contributions are assumed to be much smaller than their corresponding homogeneous counterparts; i.e.,

$$|\tilde{v}(x, t)| \ll 1,\ \left|\frac{\tilde{\sigma}(x, t)}{\bar{\sigma}(t)}\right| \ll 1,\ \left|\frac{\tilde{\theta}(x, t)}{\bar{\theta}(t)}\right| \ll 1,\ \left|\frac{\tilde{\phi}(x, t)}{\bar{\phi}(t)}\right| \ll 1,\ \left|\frac{\tilde{\gamma}^p(x, t)}{\gamma_o + t}\right| \ll 1,\ 0 \le x \le 1,\ 0 \le t \le T, \tag{29}$$

where T denotes the time at which a violation of any of the requirements (29) first takes place (i.e., the time at which nonlinear effects become significant). Here $t = 0$ is chosen, without loss of generality, as the time at which perturbations are introduced. The quotients enclosed by the absolute value signs in Eq. (29) are referred to as the *relative perturbations* and will be denoted by a subscript "r" in this discussion. Moreover, we note that admissible perturbations must satisfy the following boundary conditions:

$$\tilde{v}(0, t) = \tilde{v}(1, t) = 0 \text{ and } \tilde{\theta}_{,x}(0, t) = \tilde{\theta}_{,x}(1, t) = 0. \tag{30}$$

Substitution of the solution form (28), subject to the requirements (29), into the system (1)–(4) while retaining only first-order terms in the *absolute* perturbations gives the following system of *linear* partial differential equations:

Downloaded 03 May 2010 to 171.66.16.20. Redistribution subject to ASME license or copyright; see http://www.asme.org/terms/Terms_Use.cfm

$$\tilde{\mathbf{u}}_{,t} = A_2\tilde{\mathbf{u}}_{,xx} + A_1\tilde{\mathbf{u}}_{,x} + A_o(t)\tilde{\mathbf{u}}, \tag{31}$$

where

$$A_o(t) = \begin{pmatrix} 0 & 0 & 0 & 0 \\ 0 & -\mu\overline{F}_1(t) & -\mu\overline{F}_2(t) & -\mu\overline{F}_3(t) \\ 0 & r_1[\overline{\sigma}(t)\overline{F}_1(t) + \overline{\phi}(t)] & r_1\overline{\sigma}(t)\overline{F}_2(t) & r_1\overline{\sigma}(t)\overline{F}_3(t) \\ 0 & \overline{F}_1(t) & \overline{F}_2(t) & \overline{F}_3(t) \end{pmatrix},$$

$$\tilde{\mathbf{u}} = \begin{pmatrix} \tilde{v}(x, t) \\ \tilde{\sigma}(x, t) \\ \tilde{\theta}(x, t) \\ \tilde{\gamma}^p(x, t) \end{pmatrix}. \tag{32}$$

In Eq. (31), the coefficient matrices A_2 and A_1 are the same as those defined following Eq. (13) and all barred quantities refer to evaluations at the homogeneous, time-dependent solution. Now, we follow an identical procedure to that used in Section 3 and define

$$\tilde{\mathbf{z}} = D^{-1}\tilde{\mathbf{u}},\ \tilde{E}(t) = \langle \tilde{\mathbf{z}}, \tilde{\mathbf{z}} \rangle. \tag{33}$$

Hence, the rate of change of the energy norm associated with absolute perturbations is

$$\frac{d\tilde{E}}{dt} = -2\langle \tilde{\mathbf{z}}_{,x}, A_2\tilde{\mathbf{z}}_{,x} \rangle + 2\langle \tilde{\mathbf{z}}, B_o(t)\tilde{\mathbf{z}} \rangle;$$

$$B_o(t) = D^{-1}A_o(t)D. \tag{34}$$

The boundary conditions (30) have been used in deriving expression (34). Taking advantage of the positive definiteness of A_2, we can write

$$\frac{d\tilde{E}}{dt} \le 2\|B_o(t)\|\tilde{E}(t) \equiv 2R(t)\tilde{E}(t), \tag{35}$$

where $R(t)$ is the consistent $L2$ matrix norm corresponding to the spectral radius of the coefficient matrix $B_o(t)$ (i.e., the square root of the maximum eigenvalue of $B_o^tB_o$). The inequality (35) indicates that

$$\tilde{E}(t) \le \left\{ \exp\left[2\int_0^t R(\eta)d\eta \right] \right\} \tilde{E}(0),\ 0 \le t \le T. \tag{36}$$

The above estimate implies well-posedness of solutions to the linear system (31) as long as the spectral radius $R(t)$ is *integrable* for all times $0 \le t \le T$. The sufficient conditions, discussed in Section 4, for the existence, unique and well-posedness of the homogeneous solution guarantee the integrability of $R(t)$ for the considered initial boundary value problem. That is, the upper bound in (36) is finite. It is important to note that the exponent in (36) is an evolutionary term that reflects the time dependence of the homogeneous solution. However instructive, the estimate (36) is not directly useful as regards the necessary and sufficient conditions for shear localization. On the other hand, one can use the estimate (36) to derive a conservative expression for the time T at which the linear solution breaks down. This is achieved by assuming that the energy norm provides an appropriate measure of the "size" of the relevant solution vector. Hence, we consider the linear solution to be invalid as soon as

$$\tilde{E}(T) = \overline{E}(T), \tag{37}$$

which, through the use of the upper bound in (36), gives

$$\int_0^T R(\eta)d\eta = \ln\sqrt{\frac{\overline{E}(T)}{\tilde{E}(0)}}. \tag{38}$$

Expression (38) provides a nonlinear equation for a conservative estimate of the time T based on the criterion (37). A solution T exists if the rate of increase of the perturbation's energy norm is faster than that for the homogeneous solution energy norm. Following procedures identical to those used in Section 3, we arrive at the following mechanical energy balance law satisfied by the *absolute perturbations* (see Shawki (1988) for further details):

$$\frac{d}{dt}\int_0^1 \frac{1}{2}\rho\tilde{v}^2(\xi, t)d\xi + \int_0^1 \tilde{\sigma}(\xi, t)\tilde{\phi}(\xi, t)d\xi = 0. \tag{39}$$

That is, for the absolute perturbations, *a positive rate of change of the total kinetic energy is balanced by an equal decrease in the total dissipation power.*

6 Admissible Perturbations

Here we seek separable solutions of the form

$$\tilde{\mathbf{u}}(x, t) = \mathbf{s}(t)\sin\zeta x + \mathbf{n}(t)\cos\zeta x. \tag{40}$$

Consistency with the imposed boundary conditions corresponding to insulated and velocity-controlled boundaries reduces the general form (40) to the *admissible* form

$$\tilde{\mathbf{u}}(x, t) = \begin{pmatrix} V_n(t)\sin(n\pi x) \\ \Sigma_n(t)\cos(n\pi x) \\ \Theta_n(t)\cos(n\pi x) \\ \Gamma_n(t)\cos(n\pi x) \end{pmatrix},\ n = 1, 2, \ldots. \tag{41}$$

Substitution of the above admissible from into Eq. (31), while neglecting elastic effects, furnishes a system of linear, variable coefficient and first-order ordinary differential equations for the time-dependent functions in expression (41). This system is given by

$$\dot{\mathbf{d}}(t) = Z(t)\mathbf{d}(t), \tag{42}$$

where

$$Z(t) = \begin{pmatrix} -\zeta_n^2\overline{S}_1(t)/\rho & -\zeta_n\overline{S}_2(t)/\rho & -\zeta_n\overline{S}_3(t)/\rho \\ r_1\zeta_n[\overline{\sigma}(t) + \overline{S}_1(t)] & -r_o\zeta_n^2 + r_1\overline{S}_2(t) & r_1\overline{S}_3(t) \\ \zeta_n & 0 & 0 \end{pmatrix},$$

$$\mathbf{d}(t) \equiv \begin{pmatrix} V_n(t) \\ \Theta_n(t) \\ \Gamma_n(t) \end{pmatrix}, \tag{43}$$

and $\zeta_n = n\pi$ is the nth wave number. At this point, it is useful to derive the form of Eq. (42) corresponding to the quasi-static deformation limit which is obtained by considering sufficiently small values of inertia. The linearized version of the equation of motion (1) is given by

$$\rho\dot{V}_n(t) = -\zeta_n\Sigma_n(t) = -\zeta_n[\overline{S}_1(t)\dot{\Gamma}_n(t) + \overline{S}_2(t)\Theta_n(t) + \overline{S}_3(t)\Gamma_n(t)]. \tag{44}$$

In the absence of elastic effects, the linearized version of Eq. (2) is

$$\zeta_n V_n(t) = \dot{\Gamma}_n(t). \tag{45}$$

The *quasi-static approximation* is commonly obtained by assuming that the term $\rho\dot{V}_n(t)$ is much smaller than unity (in dimensionless form) which allows us, using Eqs. (44) and (45), to write

$$\Sigma_n(t) = \overline{S}_1(t)\dot{\Gamma}_n(t) + \overline{S}_2(t)\Theta_n(t) + \overline{S}_3(t)\Gamma_n(t) = \zeta_n\overline{S}_1(t)V_n(t) + \overline{S}_2(t)\Theta_n(t) + \overline{S}_3(t)\Gamma_n(t) = 0. \tag{46}$$

Elimination of $V(t)$ from the vector $\mathbf{d}(t)$, using Eq. (46), provides the relevant linear system of *time-dependent* ordinary differential equations for *quasi-static deformations*;

$$\dot{\mathbf{q}}(t) = Q(t)\mathbf{q}(t), \tag{47}$$

where

Downloaded 03 May 2010 to 171.66.16.20. Redistribution subject to ASME license or copyright; see http://www.asme.org/terms/Terms_Use.cfm

$$Q(t)=\begin{pmatrix} -\alpha_n + r_1\bar{\sigma}(t)\bar{F}_2(t) & r_1\bar{\sigma}(t)\bar{F}_3(t) \\ \bar{F}_2(t) & \bar{F}_3(t) \end{pmatrix},$$

$$\mathbf{q}(t)\equiv\begin{pmatrix}\Theta_n(t)\\ \Gamma_n(t)\end{pmatrix},\ \alpha_n\equiv r_o\zeta_n^2. \tag{48}$$

Note that the solution of the above system may be viewed as the zeroth-order contribution of a regular perturbation, for small values of the dimensionless ρ, of the solution of the system (42) in which inertial effects are present. Moreover, we note that the limit of an *adiabatic deformation* is obtained by setting $\alpha_n=0$. The term α_n, defined in Eq. (48), is called the *local adiabaticity parameter* which, in terms of *dimensional* quantities, takes the following form:

$$\alpha_n=\frac{\kappa t_o}{\rho c l_n^2};\ l_n=\frac{1}{\zeta_n} \tag{49}$$

It is evident that the dimensionless group α_n is the same as the dimensionless group r_o, see Eq. (9), except that it is normalized by the wavelength of the perturbation instead of being normalized by the specimen height H. This normalization explains the designation of α_n by the name "local" in contrast to the *global adiabaticity parameter* r_o.

Now, we turn our attention to the derivation of the relationships between the various energy norms. For this purpose, we observe that the approximate solution vector $\mathbf{a}(t)$—because of linearization—can be written as follows:

$$\mathbf{a}(x,\ t)=\bar{\mathbf{a}}(x,\ t)+\tilde{\mathbf{a}}(x,\ t), \tag{50}$$

where $\mathbf{a}\equiv(v(x,\ t),\ \theta(x,\ t),\ \gamma^p(x,\ t))^T$ and the homogeneous solution vector $\bar{\mathbf{a}}$ depends on x through the homogeneous particle velocity. Taking the *L2-norm* of both sides of (50) gives

$$\Delta E(t)\equiv E(t)-\bar{E}(t)=\tilde{E}(t)+2\langle\bar{\mathbf{a}},\ \tilde{\mathbf{a}}\rangle\simeq 2\langle\bar{\mathbf{a}},\ \tilde{\mathbf{a}}\rangle, \tag{51}$$

where $\Delta E(t)$ denotes the difference between the energies associated with the linear solution and the homogeneous reference solution. Hence, it is evident that this difference is directly related to the imposed perturbations. The energy $\tilde{E}(t)=\langle\tilde{\mathbf{a}},\ \tilde{\mathbf{a}}\rangle$, associated with the absolute perturbations, is neglected in view of the fact that it is much smaller than the other terms in Eq. (51) as long as $t\ll T$. Taking advantage of the admissible form of the perturbations, given by Eq. (41), together with the definition (15) of the *L2-inner* product yields

$$\Delta E(t)=(-1)^{n+1}\frac{2V_n(t)}{\zeta_n}. \tag{52}$$

It is interesting to observe that the *energy difference* $\Delta E(t)$ *depends only on the time-dependent amplitude* $V_n(t)$ *of the velocity perturbation.*

It is also useful to write the expression for the total kinetic energy as follows:

$$K(t)=\frac{\rho}{2}\int_0^1 v^2(\zeta,\ t)d\zeta=\frac{\rho}{2}\int_0^1(\bar{v}(\zeta)+\tilde{v}(\zeta,\ t))^2d\zeta,$$

$$=\frac{\rho}{2}\int_0^1\bar{v}^2(\zeta)d\zeta+\frac{\rho}{2}\int_0^1\tilde{v}^2(\zeta,\ t)d\zeta+\rho\int_0^1\bar{v}(\zeta)\tilde{v}(\zeta,\ t)d\zeta$$

$$=\bar{K}+\tilde{K}(t)+\frac{\rho}{2}\Delta E(t), \tag{53}$$

where we have used Eqs. (26), (28), (41), and (50). The time rate of change of the total kinetic energy $K(t)$ is given by

$$\frac{d}{dt}[K(t)-\tilde{K}(t)]=\frac{\rho}{2}\frac{d[\Delta E(t)]}{dt}. \tag{54}$$

In the case of a homogeneous solution (i.e., without perturbations), expression (54) implies that the total kinetic energy is time independent, which means that *the homogeneous solution is inertialess.* Furthermore, for sufficiently small-amplitude perturbations, expression (54) reduces to

$$\frac{dK(t)}{dt}\cong\frac{\rho}{2}\frac{d[\Delta E(t)]}{dt}. \tag{55}$$

That is, the rate of change of the energy difference is proportional to the rate of change of the total kinetic energy associated with the linear solution.

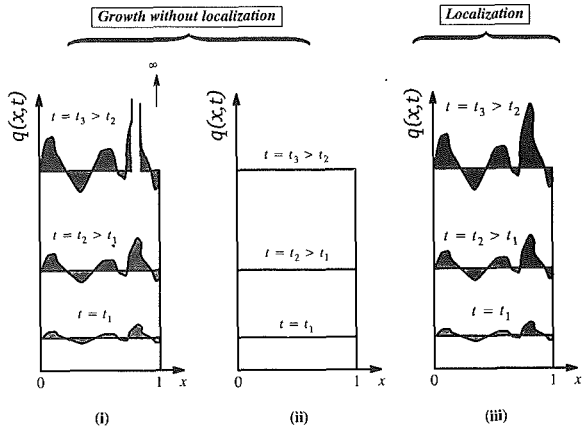


Fig. 2 The notion of strain localization

7 An Energy Criterion for the Onset of Shear Localization

We seek an appropriate mathematical characterization of shear flow localization that is capable of capturing the evolution of inhomogeneous plastic flow. Hence, we distinguish the following evolution types: (i) solution becomes unbounded at a finite time, (ii) monotonic temporal growth of a spatially homogeneous solution, and (iii) monotonic temporal growth of a bounded and spatially inhomogeneous solution. Figure 2 illustrates, schematically, the former three evolution cases where a typical field variable $q(x,\ t)$ is plotted versus the spatial dimension x at various time levels.

An inhomogeneous solution is represented as the superposition of a homogeneous part (the straight horizontal lines) and an inhomogeneous part (the superposed curve) while the inhomogeneous part is *not* necessarily restricted to be much smaller than the underlying homogeneous part. Evolution type (i) is characterized by the unboundness of the homogeneous *and* the inhomogeneous parts of q at a finite (albeit different) times. Evolution type (ii) is one in which a homogeneous solution remains bounded while it grows monotonically in time. Evolution type (iii) describes the behavior of an inhomogeneous solution which *remains bounded* for all times $t>t_l$ while the inhomogeneous part of the solution *grows at a faster rate* than the underlying homogeneous part. This type may also include the situation where the local rates of growth of the inhomogeneous part are different such that the solution exhibits a monotonic intensification of its spatial inhomogeneity as time proceeds. In this work, we select evolution type (iii) as the most appropriate for modeling observations of shear strain localization in dynamic deformations of viscoplastic solids. In fact, we discard evolution type (i) because the solution unboundness can be easily traced to the failure of the underlying mathematical model and, therefore; the model ceases to provide satisfactory description of the physical behavior considered. Next, we seek an appropriate mathematical description of evolution type (iii). Since our current analysis is based on the linear stability theory, we seek the derivation of appropriate mathematical criteria by which absolute perturbations behave according to evolution type (iii). In fact, the sufficient con-

Downloaded 03 May 2010 to 171.66.16.20. Redistribution subject to ASME license or copyright; see http://www.asme.org/terms/Terms_Use.cfm

ditions for existence, uniqueness and well-posedness of solutions to the system (27) guarantee the boundness of the homogeneous solution. Furthermore, the estimate (36) implies the boundness of the absolute perturbations. Hence, subject to the conditions cited in this work, the behavior of the linear solution will belong to either the evolution type (iii) or to its inverse in which the inhomogeneity of the linear solution decreases as time proceeds. It is important to note that the perturbations may grow monotonically while the overall inhomogeneity is reduced by means of a faster growth of the underlying homogeneous solution. The foregoing observation explains the effect of the time variation of the homogeneous solution on conclusions regarding shear localization. This time dependence of the homogeneous shear flow has often (if not always) been ignored in studies implementing the linear stability theory. Furthermore, Fressengeas and Molinari (1987) have examined the *asymptotic* stability of a homogeneous solution for late times. However, it should be noted that the validity of conclusions based on late times is related to whether or not the linear solution remains an accurate description of the deformation throughout the considered deformation history.

In this work, we select the *energy norm* as a suitable scalar measure for the solution vector of the system of governing equations. Hence, we examine the *relative* behavior of the energy norm associated with the linear solution with respect to the behavior of the energy norm associated with the *time-dependent*, homogeneous solution. In view of the foregoing discussion, we state our *mathematical characterization of deformation localization* as follows:

$$\frac{d}{dt}\,|\Delta E(t)|>0, \tag{56}$$

which, upon using Eq. (52), becomes

$$V_n(t)\,\dot{V}_n(t)>0. \tag{57}$$

That is, *localization of the deformation into a shear band mode is associated with the positive rate of change of the total kinetic energy of the absolute perturbations. Otherwise, there is no tendency for localization.*

8 Discussion

The criterion (56), or (57), provides a *necessary* and *sufficient* condition for shear localization in the sense of the continual departure of the system's total energy, including the effects of spatial perturbations, from the total energy associated with the underlying homogeneous solution. On the other hand, violation of the inequality (56) for $0\le t\le T$ provides a necessary and sufficient condition for deformation nonlocalization. A detailed description of further issues related to the application of criterion (56) towards the understanding of the onset of shear localization will be addressed in Part II of this work by Shawki (1994). Here, we note that the condition (56) for localization will also lead to the deterioration of the linear solution, at a critical time T, if it is met for all times $t\ge t_l$ where t_l denotes the instant at which condition (56) is first satisfied. Therefore; conclusions based on the criterion (56) should be viewed as being meaningful in the time interval $t_l\le t\le T$. Moreover, the satisfaction of condition (56) will also lead to the increase in the rate of change of the total kinetic energy of the system. In view of our earlier observation regarding the time independence of the kinetic energy associated with the homogeneous solution; it follows immediately that the *onset of localization can be directly tied to the increased importance of inertial effects.*

An alternative interpretation of the localization criterion (56) is possible by noting that

$$\frac{d\tilde{K}(t)}{dt}=\frac{\rho}{2}\,V_n(t)\,\dot{V}_n(t), \tag{58}$$

which, upon combining expression (39) and (56), reduces to

$$\int_0^1 \tilde{\sigma}(\zeta,\,t)\,\dot{\tilde{\phi}}(\zeta,\,t)\,d\zeta=\frac{1}{2}\,\Sigma_n(t)\,\dot{\Gamma}_n(t)<0. \tag{59}$$

The left side of the above inequality may be interpreted as the stress power or the power of dissipation associated with the absolute perturbations. Hence, we arrive at the following alternative interpretation of our energy-based localization criterion: *localization of the deformation into a shear band mode is associated with strictly negative values for the global power of dissipation associated with the absolute perturbations.*

In summary, we observe that the equivalent characterizations (56), (57), and (59) for the onset of the shear localization during dynamic deformations of thermal viscoplastic solids: (i) take full account for the time dependence of the homogeneous solution, (ii) are applied during the early time interval where the linear solution is meaningful, (iii) take full account of the imposed boundary conditions, (iv) apply to the initial boundary value problem in which a well-posed, unique homogeneous solution exists, and (v) they provide energy-based interpretations for the onset of shear flow localization in a general class of thermal viscoplastic material response.

Finally, we point out that the connection between the evolution of a spatially inhomogeneous deformation and a nonvanishing kinetic energy rate can be easily observed through the examination of the mechanical energy balance

$$\dot{K}(t)=\int_0^1 v(x,\,t)\,\frac{\partial\sigma(x,\,t)}{\partial x}\,dx$$

$$=[v(x,\,t)\sigma(x,\,t)]_0^1-\int_0^1 \sigma(x,\,t)\,\frac{\partial v(x,\,t)}{\partial x}\,dx. \tag{60}$$

Equation (60) holds for the *nonlinear* solution of Eqs. (1)–(4). In the case of *velocity boundary conditions* and rigid-viscoplastic material response, the above energy balance may be expressed in the instructive form

$$\dot{K}(t)=\int_0^1 [\sigma(1,\,t)-\sigma(x,\,t)]\dot{\phi}(x,\,t)dx. \tag{61}$$

It is evident that a spatially inhomogeneous stress field is necessary for the kinetic energy rate to be nonzero. Furthermore, for the case of *constant stress boundary conditions*, the energy balance takes the form

$$\dot{K}(t)=\Delta v(t)\dot{v}(t)-\int_0^1 \sigma(x,\,t)\,\frac{\partial\dot{v}(x,\,t)}{\partial x}\,dx,$$

$$\Delta v(t)\equiv v(1,\,t)-v(0,\,t). \tag{62}$$

Examination of the form (62) indicates that a constant stress solution (with the quasi-static assumption) leads to a vanishing kinetic energy rate. On the other hand, an inhomogeneous stress field satisfying the constant stress boundary conditions corresponds to a nonvanishing kinetic energy rate. The foregoing observations support the intimate connection between the evolutionary behavior of the total kinetic energy and the evolution of inhomogeneous deformation.

The second part of this work is concerned with the application of the equivalent criteria (56) and (57) to derive explicit localization conditions.

Acknowledgments

The support of the National Science Foundation through Grant #NSF MSM 87-09299 and the Presidential Young Investigator Award #NSF MSS 89-57180 PYI are gratefully acknowledged. Fruitful discussions with Dr. R. A. Sherif are appreciated.

Downloaded 03 May 2010 to 171.66.16.20. Redistribution subject to ASME license or copyright; see http://www.asme.org/terms/Terms_Use.cfm

References

Anand, L., Kim, K. H., and Shawki, T. G., 1987, "Onset of Shear Localization in Viscoplastic Solids," *J. Mech. Phys. Solids*, Vol. 35, p. 407.

Bai, Y. L., 1981, "A Criterion for Thermo-Plastic Shear Instability," *Shock Waves and High-Strain-Rate Phenomenon in Metals*, Proc. Int. Conf. on Metallurgical Effects of High-Strain-Rate Deformation and Fabrication, Albuquerque, NM, Plenum Press, p. 277.

Bai, Y. L., 1982, "Thermo-Plastic Instability in Simple Shear," *J. Mech. Phys. Solids*, Vol. 30, p. 195.

Burns, T. J., and Trucano, T. G., 1982, "Instability in Simple Shear Deformations of Strain-Softening Materials," *Mech. of Materials*, Vol. 1, p. 313.

Burns, T. J., 1985, "Approximate Linear Stability Analysis of a Model of Adiabatic Shear Band Formation," *Quart. Appl. Math.*, Vol. 43, p. 65.

Burns, T. J., 1989, "Similarity and Bifurcation in Unstable Viscoplastic Shear," *SIAM J. Appl. Math.*, Vol. 49, No. 1, p. 314.

Clifton, R. J., 1979, "Adiabatic Shear Banding," *Materials Response to Ultra-High Loading Rates*, NMAB-356, National Materials Advisory Board (NRC), Washington, D. C., Chapter 8.

Clifton, R. J., Duffy, J., Hartley, K. A., and Shawki, T. G., 1984, "On Critical Conditions for Shear Band Formation at High Strain Rates," *Scripta Metall.*, Vol. 18, p. 443.

Fressengeas, C., and Molinari, A., 1985, "Inertia and Thermal Effects on the Localization of Plastic Flow," *Acta. Metall.*, Vol. 33, p. 387.

Fressengeas, C., and Molinari, A., 1987, "Instability and Localization of Plastic Flow in Shear at High Strain Rates," *J. Mech. Phys. Solids*, Vol. 35, p. 185.

Johnson, J. W., 1987, "Henri Tresca as the Originator of Adiabatic Heat Lines," *Int. J. Mech. Sci*, Vol. 29, No. 5, p. 301.

Rogers, H. C., 1974, "Adiabatic Shearing—A Review," Drexel University Report.

Rogers, H. C., 1979, "Adiabatic Plastic Deformation," *Ann. Rev. Mater. Sci.*, Vol. 9, p. 283.

Rogers, H. C., 1983, "Adiabatic Shearing—General Nature and Material Aspects in Material Behavior under High Stress and Ultrahigh Loading Rates," *Segamore Army Materials Research Conference Proceedings*, Vol. 29, eds. J. Mescall and V. Weiss, eds., Plenum Press, p. 101.

Shawki, T. G., Clifton, R. J., and Majda, G., 1983, "Analysis of Shear Strain Localization in Thermal Viscoplastic Materials," Brown University Tech. Rep. #ARO DAAG29-81-K-0121/3, Division of Engineering, Brown University, Providence, RI.

Shawki, T. G., and Sherif, R. A., 1988, "A Model for Shear Band Thickness in Isothermal Simple Shearing Deformation of Thermal Viscoplastic Materials," Preprints of the 25th Ann. Tech. Mtg. of the Soc. Eng. Sci., No. ESP25.88041, University of California, Berkeley, CA.

Shawki, T. G., 1988, "Necessary and Sufficient Conditions for the Onset of Shear Strain Localization in Thermal Viscoplastic Materials," T.&A.M. Report No. 489, University of Illinois at Urbana-Champaign.

Shawki, T. G., and Clifton, R. J., 1989, "Shear Band Formation in Thermal Viscoplastic Materials," *Mech. of Materials*, Vol. 8, No. 1, pp. 13–43.

Shawki, T. G., 1994, "An Energy Criterion for the Onset of Shear Localization in Thermal Viscoplastic Materials: Part II—Applications and Implications," ASME JOURNAL OF APPLIED MECHANICS, Vol. 61, pp. 538–547.

Tresca, H., 1978, "On Further Applications of the Flow of Solids," *Proc. Inst. Mech. Engrs.*, Vol. 30, p. 301.

Zener, C., and Hollomon, J. H., 1944, "Effect of Strain Rate Upon Plastic Flow of Steel," ASME JOURNAL OF APPLIED MECHANICS, Vol. 15, p. 22.

Downloaded 03 May 2010 to 171.66.16.20. Redistribution subject to ASME license or copyright; see http://www.asme.org/terms/Terms_Use.cfm

An Energy Criterion for the Onset of Shear Localization in Thermal Viscoplastic Materials, Part II: Applications and Implications

T. G. Shawki
Department of Theoretical and Applied Mechanics,
University of Illinois at Urbana–Champaign,
Urbana, IL 61801

Necessary and/or sufficient conditions for the onset of shear flow localization in thermal viscoplastic materials were derived by Shawki (1994) through the analysis of a one-dimensional model of dynamic simple shear with velocity-controlled boundaries. In the former work, an energy-based viewpoint of localization allows for the association of the positive rate of change of the total kinetic energy of the absolute perturbations with the onset of shear strain localization. Here, we derive explicit conditions for the onset of shear localization without the need to obtain exact linear solutions. Explicit localization conditions are then applied to a number of empirical constitutive descriptions of material response. The effects of inertia, heat conduction, thermal softening, strain hardening, and strain rate sensitivity as regards the onset of shear localization are thoroughly discussed. Furthermore, the validity of conclusions based on a constant homogeneous solution is quantified together with the validity of conclusions based on a quasi-static approximation. Moreover, we examine the inadequacy of the notion of asymptotic stability for shear localization in the presence of heat conduction effects. A critical wavelength threshold is derived, for a general description of material response, below which perturbations will not grow. This threshold may also serve as a lower bound for shear band thickness.

1 Introduction

The initiation and subsequent propagation of regions of intense plastic deformation during dynamic deformations of thermal viscoplastic solids is an outstanding problem in mechanics. An extensive research activity has focused, during the past decade, on the derivation of critical conditions for the onset of shear localization (see Shawki and Clifton (1989) for a review of these efforts). The analysis of flow localization may be broadly classified into two major regimes: (1) analysis of the *pre-localization regime* and (2) analysis of the *post-localization regime*. Analysis of the pre-localization regime aims at deriving: (1a) an appropriate mathematical characterization of flow localization for the considered class of deformations, (1b) necessary and sufficient conditions for the initiation of localization, (1c) an estimate for the critical initiation strain, and (1d) an understanding of the interactive roles of strain hardening, strain-rate sensitivity, thermal softening, heat conduction, interia, boundary conditions, initial conditions, and loading rates on the evolution of the flow localization. On the other hand, analysis of the post-localization regime aims at the improved understanding of the following: (2a) elastic unloading and the band narrowing mechanism, (2b) characteristic shear band thickness and spacing, (2c) steady-state, late-time solutions, (2d) the connection between catastrophic material failure and shear localization, and (2e) the possible effects of phase transformations on the final stages of shear band formation.

This paper presents a mathematical framework for the analysis of the pre-localization regime through the implementation of the energy criterion for localization, introduced by Shawki (1988, 1994) within the context of a linear stability theory. The energy criterion associates the onset of flow localization with the positive rate of change of the total kinetic energy of absolute perturbations. Here, we formulate necessary and sufficient conditions for deformation homogeneity (and necessary conditions for localization) for large *classes* of thermal viscoplastic material response. Explicit localization conditions are derived for two classes of viscoplastic material response. These conditions are then applied to three widely used material description models. Validity of the quasi-static approximation is rigorously discussed together with the validity of conclusions

Contributed by the Applied Mechanics Division of THE AMERICAN SOCIETY OF MECHANICAL ENGINEERS for publication in the ASME JOURNAL OF APPLIED MECHANICS.

Discussion on this paper should be addressed to the Technical Editor, Professor Lewis T. Wheeler, Department of Mechanical Engineering, University of Houston, Houston, TX 77204-4792, and will be accepted until four months after final publication of the paper itself in the ASME JOURNAL OF APPLIED MECHANICS.

Manuscript received by the ASME Applied Mechanics Division, Apr. 5, 1991; final revision, July 29, 1993. Associate Technical Editor: C. F. Shih.

Copyright © 1994 by ASME
Downloaded 03 May 2010 to 171.66.16.20. Redistribution subject to ASME license or copyright; see http://www.asme.org/terms/Terms_Use.cfm

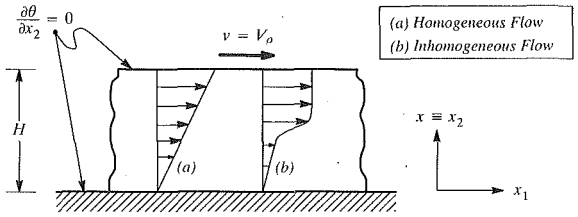


Fig. 1 The initial boundary value problem

based on linear stability analyses while the homogeneous solution is assumed to be stationary (i.e, the constant-coefficient approximation). Furthermore, the effects of heat conduction and perturbation wavelengths as regards the onset of localization are thoroughly addressed. A minimum wavelength threshold is established below which initial perturbations will not localize. This wavelength threshold illustrates the role of heat conduction as regards the introduction of a natural length scale to the problem besides providing a lower bound for the shear band thickness.

2 Problem Formulation

Consider a simple shearing motion of a plate with a finite thickness H in the x_2-direction whereas it is infinite in the other two rectangular cartesian directions (see Fig. 1). The lower edge of the plate is held fixed while a constant velocity V_o is applied at the upper edge. We assume that all physical quantities are uniform along the x_1 and x_3-directions so that the deformation depends only on the space coordinate x_2. A complete derivation of the governing system of equations is presented by Shawki and Clifton (1989). This system is given by

$$\rho \frac{\partial v}{\partial t} = \frac{\partial \sigma}{\partial x}, \tag{1}$$

$$\frac{\partial v}{\partial x} = \frac{1}{\mu}\frac{\partial \sigma}{\partial t} + \frac{\partial \gamma^p}{\partial t}, \tag{2}$$

$$\rho c \frac{\partial \theta}{\partial t} = \kappa \frac{\partial^2 \theta}{\partial x^2} + \beta \sigma \frac{\partial \gamma^p}{\partial t}, \tag{3}$$

$$\frac{\partial \gamma^p}{\partial t} = \phi(\sigma, \theta, \gamma^p). \tag{4}$$

In the foregoing equations, (x, v, σ) are written for (x_2, v_1, σ_{12}), respectively. Further, v_1 is the particle velocity in the x_1-direction, σ_{12} is the shear stress, θ is the absolute temperature, and γ^p is the total accumulated plastic strain. Moreover, ρ is the mass density, μ is the elastic shear modulus, c is the specific heat, κ is the coefficient of thermal conduction, and β $(0 < \beta \leq 1)$ represents the fraction of the power of dissipation that is converted to heat. Equations (1) and (3) represent the balance of linear momentum and energy, respectively. Equation (2) represents the additive decomposition of the total strain rate into an elastic strain rate plus a viscoplastic strain rate while Eq. (4) describes the considered class of material response in which the plastic strain rate depends on the total plastic strain, flow stress, and absolute temperature. The total plastic strain is given by

$$\gamma^p = \gamma_o^p + \int_0^t \phi \, dt. \tag{5}$$

It is often convenient to express the material behavior in the alternative form

$$\sigma = \psi(\phi, \theta, \gamma^p). \tag{6}$$

Further, we note that the partial derivatives of the functions ϕ and ψ, with respect to their respective arguments, play an important role in the analysis of shear localization. These derivatives are denoted by

$$S_k \equiv \psi_{,k} \quad \text{and} \quad F_k = \phi_{,k}, \quad k = 1, 2, 3 \tag{7}$$

where the above derivatives are further related by

$$F_1 = \frac{1}{S_1}, \quad F_2 = -\frac{S_2}{S_1}, \quad F_3 = -\frac{S_3}{S_1}. \tag{8}$$

It is also convenient to rewrite the system of Eqs. (1)-(4) in a dimensionless form. The dimensionless quantities are chosen as follows:

$$\hat{t} = \frac{t}{t_o}, \quad \hat{x} = \frac{x}{H}, \quad \hat{\sigma} = \frac{\sigma}{\sigma_o}, \quad \hat{v} = \frac{v t_o}{H}, \quad \hat{\phi} = \phi t_o,$$

$$\hat{\theta} = \frac{\theta}{\theta_o}, \quad \hat{\kappa} = \frac{\kappa \theta_o t_o}{\sigma_o H^2}, \quad \hat{\rho} = \frac{\rho H^2}{\sigma_o t_o^2}, \quad \hat{c} = \frac{c \theta_o t_o^2}{H^2},$$

$$\hat{\mu} = \frac{\mu}{\sigma_o}, \quad \hat{F}_1 = F_1 \sigma_o t_o, \quad \hat{F}_2 = F_2 \theta_o t_o, \quad \hat{F}_3 = F_3 t_o,$$

$$\hat{S}_1 = \frac{S_1}{\sigma_o t_o}, \quad \hat{S}_2 = \frac{S_2 \theta_o}{\sigma_o}, \quad \hat{S}_3 = \frac{S_3}{\sigma_o}. \tag{9}$$

In Eq. (9), the subscript "o" denotes constant reference values corresponding, for example, to the values these quantities have in a homogeneous solution at the time a perturbation is introduced. The characteristic time t_o is the time $t_o = 1/\phi_o = H/V_o$ required to obtain a unit shear strain at the strain rate ϕ_o. It is important to note that the three dimensionless groups

$$\hat{\rho} = \frac{\rho V_o^2}{\sigma_o}, \quad \hat{r}_o = \frac{\kappa t_o}{\rho c H^2}, \quad \hat{r}_1 = \frac{\beta \sigma_o}{\rho c \theta_o}, \tag{10}$$

represent, respectively, inertial effects, deformation adiabaticity, and heating due to plastic flow. Once the dimensionless groups, in Eq. (9), are introduced in the system of governing Eqs. (1)-(4), the resulting dimensionless equations retain the same form as their dimensional counterparts. For convenience of notations, we will drop the superposed "hat" from dimensionless quantities and use dimensionless quantities for the remainder of this work.

We consider the case of thermally insulated and velocity-controlled boundaries; that is,

$$v(0, t) = 0, \quad v(1, t) = 1, \quad \frac{\partial \theta(0, t)}{\partial x} = \frac{\partial \theta(1, t)}{\partial x} = 0. \tag{11}$$

This choice guarantees the existence of a unique and well-posed spatially homogeneous solution to Eqs. (1)-(4) as shown by Shawki (1994).

3 The Energy Criterion for Localization of Plastic Flow

In this section, we present a brief review of the energy criterion for the onset of shear strain localization which is derived by Shawki (1994). For this purpose, we seek a solution to Eqs. (1)-(4) of the additive form

$$v(x, t) + x + \tilde{v}(x, t), \quad \sigma(x, t) = \bar{\sigma}(t) + \tilde{\sigma}(x, t),$$
$$\phi(x, t) = 1 + \tilde{\phi}(x, t), \quad \theta(x, t) = \bar{\theta}(t) + \tilde{\theta}(x, t),$$
$$\gamma^p(x, t) = (\gamma_o + t) + \tilde{\gamma}^p(x, t). \tag{12}$$

where quantities with a superposed "tilde" represent the effect of the initial spatial perturbations while the "barred" quantities refer to the underlying homogeneous simple shear solution. The perturbations are assumed to be much smaller than their corresponding homogeneous counterparts. Moreover, we note that admissible perturbations must satisfy the following boundary conditions:

$$\tilde{v}(0, t) = \tilde{v}(1, t) = 0 \quad \text{and} \quad \tilde{\theta}_{,x}(0, t) = \tilde{\theta}_{,x}(1, t) = 0. \tag{13}$$

In the above discussion, the term "homogeneous solution"

Downloaded 03 May 2010 to 171.66.16.20. Redistribution subject to ASME license or copyright; see http://www.asme.org/terms/Terms_Use.cfm

refers to a spatially homogeneous solution to the system (1)–(4). We further follow the analysis of Shawki (1994) and neglect elastic effects while assuming the following separable form for the perturbations:

$$\tilde{\mathbf{u}}(x, t) = \begin{pmatrix} V_n(t) \sin(n\pi x) \\ \Sigma_n(t) \cos(n\pi x) \\ \Theta_n(t) \cos(n\pi x) \\ \Gamma_n(t) \cos(n\pi x) \end{pmatrix}, \quad n = 1, 2, \ldots . \tag{14}$$

Substitution of the solution form (14) into the system (1)–(4) while retaining only first-order terms in the *absolute* perturbations gives the following system of *linear* equations with variable coefficients:

$$\dot{\mathbf{d}}(t) = Z(t)\,\mathbf{d}(t), \tag{15}$$

where

$$Z(t) = \begin{pmatrix} -\zeta_n^2 \bar{S}_1(t)/\rho & -\zeta_n \bar{S}_2(t)/\rho & -\zeta_n \bar{S}_3(t)/\rho \\ r_1 \zeta_n [\bar{\sigma}(t) + \bar{S}_1(t)] & -r_o \zeta_n^2 + r_1 \bar{S}_2(t) & r_1 \bar{S}_3(t) \\ \zeta_n & 0 & 0 \end{pmatrix},$$

$$\mathbf{d}(t) \equiv \begin{pmatrix} V_n(t) \\ \Theta_n(t) \\ \Gamma_n(t) \end{pmatrix}, \tag{16}$$

and $\zeta_n = n\pi$ is the nth wave number (inverse of the wavelength l_n). The relevant linear system of time-dependent ordinary differential equations for *quasi-static deformations* is given by (see Shawki, 1994)

$$\dot{\mathbf{q}}(t) = Q(t)\,\mathbf{q}(t), \tag{17}$$

where

$$Q(t) = \begin{pmatrix} -\alpha_n + r_1 \bar{\sigma}(t) \bar{F}_2(t) & r_1 \bar{\sigma}(t) \bar{F}_3(t) \\ \bar{F}_2(t) & \bar{F}_3(t) \end{pmatrix},$$

$$\mathbf{q}(t) \equiv \begin{pmatrix} \Theta_n(t) \\ \Gamma_n(t) \end{pmatrix}, \quad \alpha_n \equiv r_o \zeta_n^2. \tag{18}$$

Shawki (1994) defines the energy $E(t)$ associated with a solution vector $\mathbf{a}(x, t)$ through the $L2$-norm

$$E(t) \equiv \langle \mathbf{a}, \mathbf{a} \rangle \equiv \int_0^1 \{\mathbf{a}^*(\xi, t) \cdot \mathbf{a}(\xi, t)\}\, d\xi. \tag{19}$$

Hence, the energy difference

$$\Delta E(t) \equiv E(t) - \bar{E}(t) = \tilde{E}(t) + 2\langle \bar{\mathbf{a}}, \tilde{\mathbf{a}} \rangle \simeq 2\langle \bar{\mathbf{a}}, \tilde{\mathbf{a}} \rangle, \tag{20}$$

describes the behavior of the perturbations with respect to the underlying *time-dependent* homogeneous solution. The energy criterion for the onset of shear flow localization (Shawki, 1994) is given by

$$\frac{d\tilde{K}(t)}{dt} = \frac{\rho}{2} V_n(t) \dot{V}_n(t) > 0, \quad \text{where} \quad \tilde{K}(t) \equiv \frac{\rho}{2} \int_0^1 \tilde{v}^2(\xi, t)\, d\xi. \tag{21}$$

The above criterion is obtained by requiring the absolute value of the energy difference, given by Eq. (20), to exhibit a positive rate of growth. Furthermore, the criterion (21) associates the onset of flow localization with the positive rate of growth of the total kinetic energy of absolute perturbations. This criterion takes full account of: (i) the time variation of the homogeneous solution and (ii) the imposed boundary conditions while being applicable at early times where the linear solution provides a satisfactory representation of the solution.

4 On the Quasi-Static Approximation

Here, we examine the validity of conclusions based on the quasi-static approximation as regards the *onset* of shear flow localization during *dynamic* deformations of thermal viscoplastic solids. For this purpose, it is useful to note that the rate of change of the total kinetic energy associated with the full linear solution is given by

$$\frac{dK(t)}{dt} = \int_0^1 \frac{1}{2} \rho v^2(\xi, t)\, d\xi = \frac{d\bar{K}(t)}{dt} + \frac{\rho}{2} \frac{d\Delta E(t)}{dt}$$

$$= \frac{\rho}{2} [V_n(t) \dot{V}_n(t) + (-1)^{n+1} l_n \dot{V}_n(t)]. \tag{22}$$

In the absence of perturbations, the right side of expression (22) vanishes, which implies that the kinetic energy associated with the homogeneous solution is time independent. In fact, the homogeneous solution for the considered problem is *static* (see Appendix B). Moreover, Shawki (1988) showed that the former homogeneous solution is the unique static solution to the nonlinear system of Eqs. (1)–(4), with no elastic and heat conduction effects, consistent with insulated and velocity-controlled boundaries. Now, we may rewrite Eq. (22), using the linearized version of Eqs. (1) and (2), as follows:

$$\frac{dK(t)}{dt} = \frac{\Sigma_n(t)}{2} [(-1)^n - \dot{\Gamma}_n(t)]. \tag{23}$$

Similarly, one may write

$$\frac{d\tilde{K}(t)}{dt} = -\frac{1}{2} \Sigma_n(t) \dot{\Gamma}_n(t). \tag{24}$$

During the time interval $t \in [0, T]$, where the perturbations remain much smaller than their homogeneous counterparts, one may establish the following bounds:

$$\left| \frac{dK(t)}{dt} \right| = \left| \frac{\Sigma_n(t)}{2} [(-1)^n - \dot{\Gamma}_n(t)] \right| \le \epsilon \bar{\sigma}(t) \le \epsilon \bar{\sigma}_m, \tag{25}$$

$$\left| \frac{d\tilde{K}(t)}{dt} \right| = \frac{1}{2} |\Sigma_n(t) \dot{\Gamma}_n(t)| \le \epsilon^2 \bar{\sigma}_m, \tag{26}$$

where $0 < \epsilon \ll 1$ is a typical acceptable size of the relative perturbations[1] while $\bar{\sigma}_m > 0$ is the maximum level of the homogeneous flow stress. In fact, it is reasonable, for studies of shear localization, to consider the class of material response in which such a maximum stress value exists. Inequality (25) implies that the rate of change of the kinetic energy associated with the full linear solution is at most of the order of relative perturbations. On the other hand, inequality (26) implies that the rate of change of the kinetic energy associated with the *absolute* perturbations is at most of order ϵ^2. Hence, it is evident that, for $t \in [0, T]$, the linear solution is indeed *quasi-static* in the sense illustrated above. Moreover, the energy criterion (21) for the onset of shear localization may also be viewed as a necessary condition for the deterioration of the quasi-static approximation. Therefore, we conclude that *it is mathematically consistent to ignore inertial effects when using the linear stability approach towards finding the critical conditions for the initiation of shear flow localization*. Hence, we will consider the system (17) corresponding to quasi-static deformation conditions in our subsequent discussions.

5 Explicit Localization Conditions

We are now concerned with the derivation of useful local-

[1] The linearized version of Eq. (2), in the absence of elastic effects, provides us with

$$|\zeta_n V_n(t)| = |\dot{\Gamma}_n(t)| \ll \frac{d\bar{\gamma}(t)}{dt} = 1,$$

Evaluation at the initial time gives

$$\zeta_n \epsilon \ll 1 \quad \text{or} \quad \epsilon \ll l_n.$$

The above inequality sets a bound for the admissible size of initial perturbations in terms of the considered wavelength.

Downloaded 03 May 2010 to 171.66.16.20. Redistribution subject to ASME license or copyright; see http://www.asme.org/terms/Terms_Use.cfm

ization conditions, based on the criterion (21), *without the need to obtain an exact solution of the linear system (17)*. Since the solution vector $\mathbf{q}$ does not include the velocity amplitude $V_n(t)$, we rewrite the energy criterion (21), using the linearized version of Eq. (2), as follows[2]:

$$\dot{\Gamma}_n(t)\ddot{\Gamma}_n(t) > 0. \tag{27}$$

Examination of the system (17) allows us to write[3]

$$\dot{\Gamma}_n(t) = \mathbf{w}_1(t)\cdot\mathbf{q}(t) \quad \text{and} \quad \ddot{\Gamma}_n(t) \equiv \mathbf{w}_2(t)\cdot\mathbf{q}(t), \tag{28}$$

where

$$\mathbf{w}_1(t) \equiv \begin{pmatrix} \overline{F}_2(t) \\ \overline{F}_3(t) \end{pmatrix},$$

$$\mathbf{w}_2(t) \equiv \begin{pmatrix} \dot{\overline{F}}_2(t) + r_1\overline{\sigma}(t)\overline{F}_2(t)^2 + \overline{F}_2(t)\overline{F}_3(t) - \alpha_n\overline{F}_2(t) \\ \dot{\overline{F}}_3(t) + r_1\overline{\sigma}(t)\overline{F}_2(t)\overline{F}_3(t) + \overline{F}_3(t)^2 \end{pmatrix}. \tag{29}$$

With the aid of the representations given by Eqs. (28) and (29), the localization criterion (27) may be expressed in the alternative form

$$\mathbf{q}(t)\cdot U(t)\mathbf{q}(t) > 0; \quad U(t) \equiv \mathbf{w}_1(t) \otimes \mathbf{w}_2(t). \tag{30}$$

In Eq. (30), the symbol $\otimes$ denotes the familiar dyadic (tensor) product of two vectors. Furthermore, the form (30) of our original localization criterion (21) implies that *conservative* localization conditions are associated with the *positive-definiteness* of the time-dependent tensor $U(t)$. It is interesting to observe that the tensor $U(t)$ depends entirely on the homogeneous solution as well as the wavelength of perturbations. Appendix A addresses the positive-definiteness problem for a tensor formed by the tensor product of two arbitrary vectors. This discussion implies that definiteness of the tensor $U(t)$ may only be rigorously established for the two classes of material response given by: (1) the material class exhibiting no strain sensitivity; i.e., $\dot{\gamma}^p = \phi(\sigma, \theta)$, $S_3 = F_3 = 0$, and (2) the material class exhibiting no thermal sensitivity; i.e., $\dot{\gamma}^p = \phi(\sigma, \gamma^p)$, thus $S_2 = F_2 = r_1 = r_o = 0$. The symmetric part of the tensor $U(t)$ is given by

$$U_s(t) = \frac{1}{2}\begin{pmatrix} 2\overline{F}_2^2(t)\hat{\Lambda}_2(t) & \overline{F}_2(t)\overline{F}_3(t)[\hat{\Lambda}_2(t) + \Lambda_3(t)] \\ \overline{F}_2(t)\overline{F}_3(t)[\hat{\Lambda}_2(t) + \Lambda_3(t)] & 2\overline{F}_3^2(t)\Lambda_3(t) \end{pmatrix}, \tag{31}$$

where

$$\Lambda_j(t) \equiv \frac{\dot{\overline{F}}_j(t)}{\overline{F}_j(t)} - \frac{\dot{\overline{C}}_p(t)}{\overline{S}_1(t)}, \quad \hat{\Lambda}_j = \Lambda_j - \alpha_n, \quad j = 2, 3 \tag{32}$$

and

$$C_p \equiv S_3 + r_1\sigma S_2 = -\frac{F_3 + r_1\sigma F_2}{F_1}. \tag{33}$$

In (33), the quantity C_p stands for the *slope of the adiabatic stress-strain curve at a constant strain rate.* Examination of the eigenvalues of the above tensor for the aforementioned material descriptions provide the following initiation conditions for shear localization:

Case 1: Materials With No Strain Sensitivity. Here, the positive semi-definiteness of the tensor $U(t)$ is related to the sign of its nonvanishing eigenvalue. Hence, the condition for the onset of shear localization (21) becomes

$$\hat{\Lambda}_2(t) = \frac{\dot{\overline{F}}_2(t)}{\overline{F}_2(t)} + r_1\overline{\sigma}(t)\overline{F}_2(t) - \alpha_n > 0. \tag{34}$$

Examination of the above inequality indicates that, for a heat-conducting material, a necessary condition for localization is that $\hat{\Lambda}_2(t) > 0$. Furthermore, the requirement (34) establishes *a critical value of the local adiabaticity parameter above which initial perturbations do not localize*. This critical value is given by

$$\alpha_{cr} = \frac{r_o}{l_{cr}^2} = \Lambda_2(0) \tag{35}$$

where l_{cr} is the associated *critical wavelength, below which* initial perturbations do not localize. Therefore, localization of a heat conducting material requires that the local adiabaticity parameter falls in the range

$$0 < \frac{\alpha_n}{\alpha_{cr}} < 1. \tag{36}$$

For cases where initial localization takes place, subsequent suppression of localization is possible at the critical time t^* which is the smallest, positive and real root (if any) of the equation

$$\Lambda_2(t^*) - \alpha_n = 0. \tag{37}$$

The former observations illustrate the role of heat conduction as a stabilizing mechanism towards shear strain localizations as well as its role towards the introduction of a natural *length scale* to the considered problem. In fact, the critical wavelength $l_{cr} = \sqrt{r_o/\Lambda_2(0)}$ may be viewed as a lower bound for *shear band thickness* for the considered class of materials. Moreover, the situation in which $l_{cr} \geq 1$ indicates no tendency for localization which may be viewed as a sufficient condition for no-localization. These ideas will be implemented in Section 6 for special forms of material description.

Case (2): Materials With No Thermal Sensitivity. Again, we use the tensor in (31) to express the condition for the onset of shear localization (21) as follows:

$$\Lambda_3(t) = \frac{\dot{\overline{F}}_3(t)}{\overline{F}_3(t)} + \overline{F}_3(t) > 0. \tag{38}$$

It is important to note that the violation of the onset criterion (21), or any of its equivalent forms, is viewed as a *necessary and sufficient* condition for *no localization*. On the other hand, the satisfaction of the criterion (21) is only viewed as a *necessary* condition for the *onset of localization*. The insufficiency of (21) is attributed to the fact that inertial and nonlinear effects may have a subsequent stabilizing effect that can not be accounted for through the present analysis. It is also useful to note that the explicit conditions (34) and (38) depend entirely on the homogeneous, time-dependent solution (often known in exact form) as well as the wavelength of initial perturbations (for heat-conducting materials).

6 Applications

In this section, we apply the onset criteria (34) and (38) to a number of widely used descriptions of viscoplastic response. Specifically, we consider the following material models:

Power-Law Model:

$$\sigma = \theta^v\left(\frac{\gamma^p}{\gamma_o}\right)^n (\dot{\gamma}^p)^m. \tag{39}$$

[2] Another alternative but equivalent form of (27) is obtained through using the linearized version of Eqs. (1), (2) to obtain

$$\Sigma_n(t)\dot{\Gamma}_n(t) < 0.$$

[3] It is useful to note that the vectors defined by Eq. (28) are the second rows of the matrices:

$$Q(t) \quad \text{and} \quad \dot{Q}(t) + Q(t)^2,$$

respectively.

Downloaded 03 May 2010 to 171.66.16.20. Redistribution subject to ASME license or copyright; see http://www.asme.org/terms/Terms_Use.cfm

Arrhenius-Law Model:

$$\sigma = \sigma_B(\gamma^p) - \left(\frac{K_b\theta}{V^*}\right)\ln\left(\frac{\omega}{\dot{\gamma}^p}\right). \tag{40}$$

Litonski Model:

$$\sigma = (1-a\theta)(\gamma_o+\gamma^p)^n(1+b\dot{\gamma}^p)^m. \tag{41}$$

Primary objectives of the current comparison include verification of the proposed energy criterion for localization against other proposed criteria as well as the analysis of the effect of constitutive description on predictions of shear flow localization. Here, we emphasize that the models (39) to (41) are all written in *dimensionless form*. In (40), σ_B is the amplitude of the stress barrier to dislocation motion (which depends generally on the plastic strain), ω is the frequency by which dislocations attempt to overcome obstacles, K_b is Boltzman's constant (1.38×10^{-23} JK^{-1}) and V^* is the activation volume. The associated dimensionless groups used in writing the Arrhenius law (40) are

$$\omega = \hat{\omega}\hat{t}_o, \quad \sigma_B = \frac{\hat{\sigma}_B}{\hat{\sigma}_o}, \quad \frac{K_b}{V^*} = \frac{\hat{K}_b\hat{\theta}_o}{\hat{\sigma}_o\hat{V}^*}, \tag{42}$$

where a superposed "hat" designates a dimensional quantity. Homogeneous solutions corresponding to the three material models described by Eqs. (39) to (41) are compiled in Appendix B.

6.1 The Power-Law Material Model. Here, we consider the subclass of power-law materials for which $n>-1$ and $v<1$ so that the associated homogeneous solutions remain finite for all times (see Appendix B). The necessary condition for the onset of localization (34) reduces to

$$r_1(1-p)+\alpha_n[1+r_1(1-v)t]<0; \quad p\equiv -\frac{v}{m}. \tag{43}$$

The above inequality applies to a non-Newtonian fluid with temperature-dependent viscosity (since $n=0$). Furthermore, a necessary condition for (43) to be *initially* met is $p>1+\alpha_n/r_1$. In the case of an adiabatic deformation (i.e., $r_0=0$) of a strain-rate-hardening material (i.e., $m>0$); the above inequality reduces to

$$p>1 \quad \text{or} \quad v+m<0. \tag{44}$$

However, for a heat-conducting material (i.e., nonadiabatic deformation) which also satisfies the inequality (44), the localization condition (43) establishes a *wavelength threshold l_{cr} below which initial perturbations will not localize*. This wavelength threshold is given by

$$l_{cr} = \sqrt{\frac{r_o}{r_1(p-1)}}. \tag{45}$$

The effect of heat conduction regarding the introduction of a thermal length scale to this problem is quite evident. Using expression (9) together with (45) allows us to write the *dimensional* form

$$\frac{l_{cr}}{H} = \sqrt{\frac{1}{p-1}\left(\frac{\kappa\theta_o/H^2}{\beta\sigma_o\phi_o}\right)}. \tag{46}$$

The sufficient condition for no-localization (discussed following expression (37)) is now given by

$$\frac{\kappa\theta_o/H^2}{\beta\sigma_o\phi_o} \geq p-1, \tag{47}$$

where the above quotient represents the ratio of the average, reference heat diffusion to the average reference power dissipation. In other words, a sufficient condition for deformation homogeneity is that the relative strength of heat diffusion to plastic power dissipation exceeds the critical, *material-dependent*, value $(p-1)$. Moreover, for materials satisfying the requirement (44) and for perturbations with a wavelength larger than the threshold value (given by (45)), the initial tendency for localization will eventually be suppressed by the diffusion effect of heat conduction at the critical time

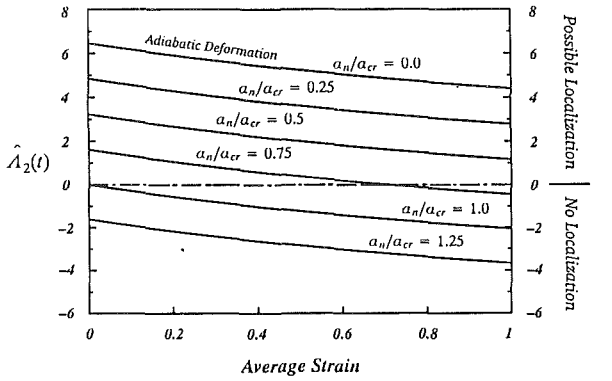


Fig. 2 Stabilizing effect of heat conduction on the onset of shear localization

$$t^* = \frac{p-1}{r_o(1-v)}(l_n^2 - l_{cr}^2). \tag{48}$$

The above expression is meaningful as long as $t^* \in [0, T]$. It is important to note that the condition (44) is necessary for the onset of localization of *all* wavelength disturbances in an adiabatic deformation whereas it is necessary for early-time localization of *some* wavelength disturbances in a nonadiabatic deformation. Moreover, the *range of nonlocalizing wavelengths* grows with continuing deformation according to

$$\frac{l_n(t)}{l_{cr}} > \sqrt{1+r_1(1-v)t}, \tag{49}$$

provided that $p>1$. This observation is consistent with the numerical results obtained by Shawki and Clifton (1989). Figure 2 illustrates the evolution of the eigenvalue $\hat{\Lambda}_2(t)$, defined by (32), for the case corresponding to a typical structural steel for which $r_1=0.34$, $v=-0.38$, $m=0.019$, and $\alpha_{cr}=r_o/l_{cr}^2=6.46$. It is important to note that the eigenvalue corresponding to adiabatic deformations ($\alpha_n=0$) remains positive for all times $t\geq 0$ while eigenvalues corresponding to values of the local adiabaticity parameter $0<\alpha_n/\alpha_{cr}<1$ show an initial tendency for localization that is suppressed at a later time due to the increasing significance of heat conduction (see, for example, the curve associated with $\alpha_n/\alpha_{cr}=0.75$ on Fig. 2). Whether or not shear localization will persist, for such wavelengths, depends on the post-initiation interactive roles of heat conduction, inertia, and nonlinear effects. Such roles are not expected to be revealed through the linear stability analysis.

The necessary condition (38) for the onset of localization reduces to

$$q>1 \quad \text{or} \quad n+m<0; \quad q\equiv -\frac{n}{m} \tag{50}$$

which strictly applies to the class of thermally insensitive viscoplastic solids described by the power-law model (39) with $v=0$. Figure 3 illustrates the evolution of the eigenvalue $\hat{\Lambda}_3(t)$ for a material characterized by the same overall properties as that used in Fig. 2 except that $v=0$ and thermal effects are assumed negligible. It is interesting to observe that materials for which $0<q<1$ show no tendency for localization, according to the current analysis, *while they exhibit strain softening* response. The necessary localization condition (50) implies that the "strength" of strain softening must overwhelm that of strain-rate hardening for possible localization.

Downloaded 03 May 2010 to 171.66.16.20. Redistribution subject to ASME license or copyright; see http://www.asme.org/terms/Terms_Use.cfm

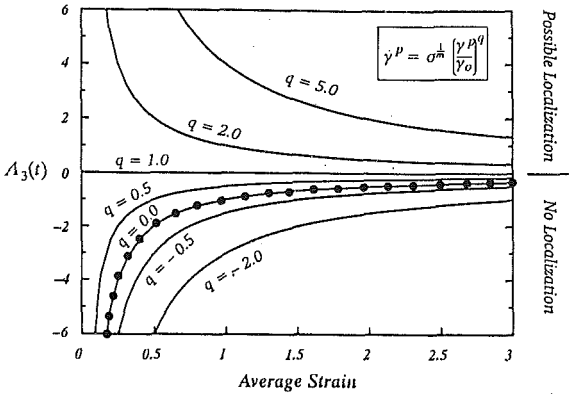


Fig. 3 Onset of shear localization for thermally insensitive materials

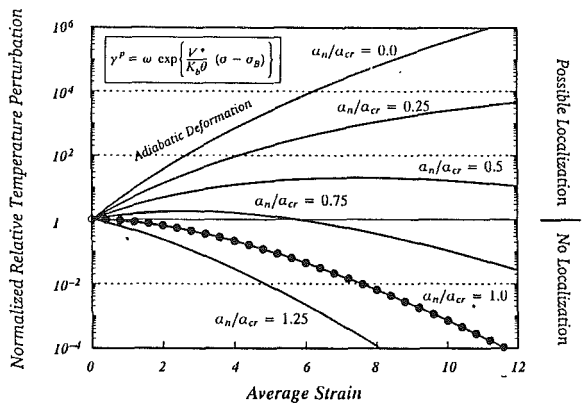


Fig. 4 Evolution of the normalized, relative temperature perturbation for the Arrhenius-law model

6.2 The Arrhenius-Law Material Model. Our current discussion will be limited to the case where the stress barrier amplitude σ_B in Eq. (40) is taken to be a constant. Appendix B gives the associated exact homogeneous solution for this class of materials. The necessary localization condition (34) reduces to

$$r_1\bar{\sigma}(t)(1-\ln\omega)+\alpha_n\bar{\theta}(t)<0. \tag{51}$$

Examination of the homogeneous solution (Appendix B) together with the above inequality indicates that a necessary condition for (51) to be met is

$$\ln\omega>1 \quad \text{or} \quad \omega>e. \tag{52}$$

A microscopic interpretation of shear strain localization emerges from the above requirement which states that the frequency by which dislocations attempt to overcome obstacles must exceed a critical threshold before macroscopic localization becomes possible. In the absence of heat conduction, the requirement (52) becomes a necessary condition for the onset of localization for *all* perturbation wavelengths. However, for a heat-conducting material, we obtain a wavelength threshold given by

$$l_{cr}=\sqrt{\frac{r_o}{r_1\sigma_B\ln(\omega/e)[1-(1/\bar{\theta}_\infty)]}} \tag{53}$$

below which initial perturbations will not localize. The qualitative behavior of the eigenvalue $\hat{\Lambda}_2(t)$ for the considered Arrhenius-law model is identical to that presented in Fig. 2 for the power-law model. In fact, the *exact* linear solution for quasi-static deformations of Arrhenius-law materials is given by

$$\frac{\Theta_n(t)}{\Theta_n(0)}=e^{-\alpha_n t}[\bar{\theta}(t)]^{\ln\omega}. \tag{54}$$

Hence, the exact, normalized and relative temperature perturbation is provided by

$$\Theta_r(t)\equiv\frac{\Theta_n(t)/\bar{\theta}(t)}{\Theta_n(0)}=e^{-\alpha_n t}[\bar{\theta}(t)]^{(\ln\omega)-1}. \tag{55}$$

Figure 4 illustrates the evolution of the above solution for different values of the local adiabaticity parameter. Note that the condition (52) is also a necessary condition for the relative temperature perturbation to grow. The qualitative features of the evolution in Fig. 4 are identical to those observed for the power-law model in Fig. 2. Values of the parameters used in Fig. 4 correspond to an aluminum alloy: $\sigma_o=\sigma_B=100$ MPa, $\theta_o=300°$C, $\kappa=249$ W/m°C, $\rho=2704$ kg/m^3, $c=903$ J/kg°C together with the values $\phi_o=10^3$ sec^{-1}, $H=2.5$ mm, $V^*=0.5\times10^{-26}$ m^3, $\omega=10^{12}$ sec^{-1}. Examination of Fig. 4 indicates that, for fixed values of the *global* adiabaticity parameter r_o, perturbations with longer wavelengths show higher tendency for shear localization as compared to perturbations with shorter wavelengths.

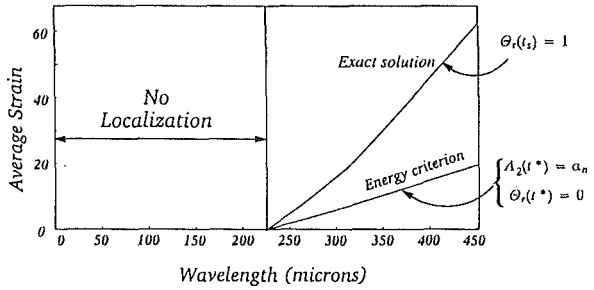


Fig. 5 Stabilization effect of heat conduction (Arrhenius law)

The above observation is qualified in view of the additional time available for the destabilizing effect of thermal softening to operate before the stabilizing effect of heat conduction becomes important. Suppression of localization by heat conduction is evident; however, one must note that the linear, quasi-static solution may break down before this can take place. Figure 5 illustrates the dependence of two critical times on the wavelength of perturbations. The critical time t^* is defined by Eq. (37). It is also interesting to note that t^* corresponds to the *maximum* of the relative, normalized temperature perturbation $\Theta_r(t)$. Furthermore, the critical time t_s is associated with the recovery of the relative perturbation to its initial value. Figure 5 shows that, for the model aluminum alloy, a lower bound for shear band thickness is about 226 μm. Moreover, it appears that localization of longer wavelength perturbations requires longer times before it can be suppressed. Hence, it seems that longer wavelengths are more likely to localize since inertial and nonlinear effects are likely to become significant before heat conduction effects become effective.

6.3 The Litonski Material Model. This model is described by Eq. (41) for which the necessary localization condition (34), corresponding to the case $n=0$ in Eq. (41), reduces to

$$ar_1(1+b)^m\left[1+\frac{1+b}{mb}\right]-\alpha_n>0. \tag{56}$$

It is important to note that the above condition is independent of *time* in contrast to the similar conditions (43) and (51) for the power law and Arrhenius law, respectively. For strain-rate-hardening materials belonging to the class (41), adiabatic deformations localize subject to the simple requirement that $a>0$. For nonadiabatic deformations, the requirement (56) establishes the wavelength threshold

Downloaded 03 May 2010 to 171.66.16.20. Redistribution subject to ASME license or copyright; see http://www.asme.org/terms/Terms_Use.cfm

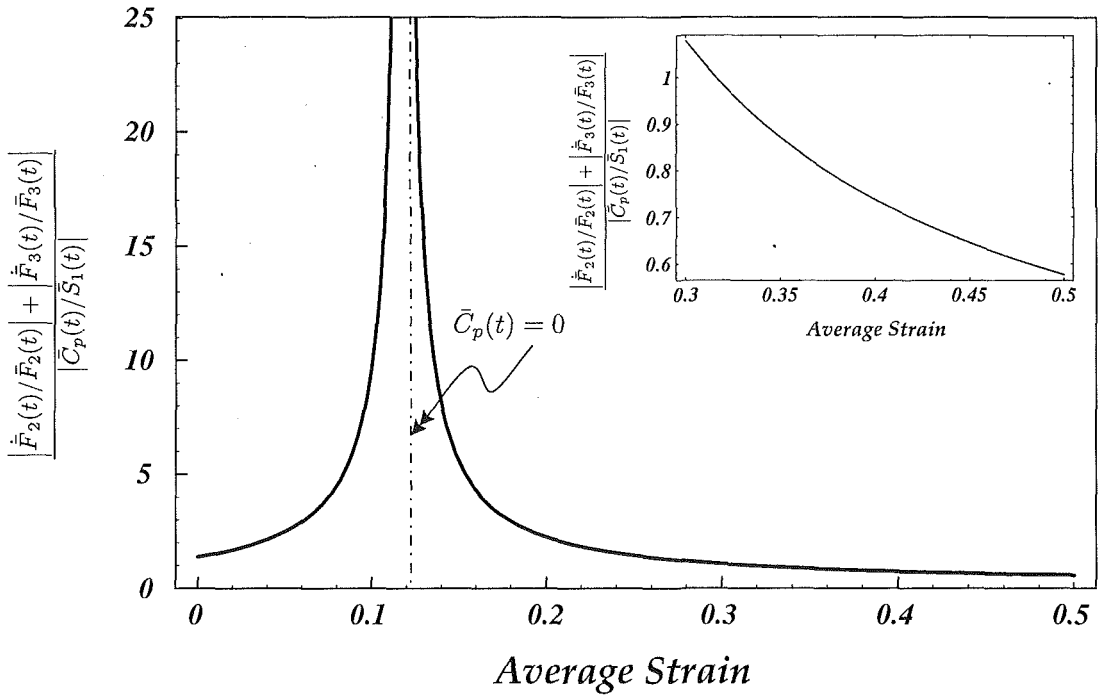


Fig. 6 Validity of the constant-coefficient approximation

$$l_{cr} = \sqrt{\frac{mr_o}{r_1[ab^m(1+m)]}}, \tag{57}$$

below which initial perturbations do not localize. The time independence of expression (56) indicates that the range of nonlocalizing wavelengths remains unchanged as deformation evolves for materials described by Litonski model (41). Furthermore, this feature implies that once localization initiates, heat conduction effects will *not* counterbalance the effects of thermal softening. The above feature is very special to the Litonski model that describes its strong localization tendencies which may not be observed for materials modeled by other constitutive descriptions. Examination of the necessary condition (38) in conjunction with the Litonski model gives rise to a condition identical to condition (50) which is derived for the power-law model.

7 Validity of the Constant-Coefficient Approximation

Difficulties associated with the attainment of an exact solution to the time-dependent system of Eqs. (15) or (17) have led to the widely used procedure in which the time dependence of the coefficient matrix $Z(t)$ (or $Q(t)$) is ignored. Results based on the constant-coefficient approximation are usually qualified in view of the assumption that the time scale of the evolution of perturbations is small relative to the time scale for the variation of the homogeneous solution. In view of our current results in which we take full account of the time variation of the homogeneous solution, we examine the validity of conclusions based on the constant-coefficient approximation. It is interesting to note that temporal rates of the homogeneous solution enter the symmetric matrix $U_s(t)$ only through the terms $\hat{\Lambda}_j(t)$, defined by Eq. (32).

Hence, the constant-coefficient approximation can be obtained by evaluating the matrix $U_s(t)$ at a fixed time, say t_o, while taking $\Lambda_j = -\bar{C}_p(t_o)/\bar{S}_1(t_o)$ for $j = 2, 3$. Therefore, it is now evident that *conclusions based on such approximation will provide useful information regarding the onset of shear localization as long as*

$$|\dot{\bar{F}}_2(t)/\bar{F}_2(t)| + |\dot{\bar{F}}_3(t)/\bar{F}_3(t)| \ll |\bar{C}_p(t)/\bar{S}_1(t)|, \quad t \in [0, T]. \tag{58}$$

Figure 6 examines the above requirement for the case of a power-law material with values for the parameters corresponding to a cold-rolled steel designated CRS-1018. This material has been examined thoroughly in the work by Shawki and Clifton (1989). It is evident that the criterion (58) is violated for all times considered in Fig. 6. It is also important to note that the worst performance of the constant-coefficient approximation takes place in the vicinity of the critical strain at which the slope of the adiabatic, homogeneous stress-strain curve vanishes. This behavior is expected for all materials in view of the requirement (58). The insert in Fig. 6 shows that the two sides of the inequality (58) are of the same order of magnitude even for average strains that are substantially larger than the critical (stress peak) strain. Further examination of our necessary conditions for localizations (23) and (27) indicates that localization, in the context of a constant-coefficient approximation, takes place as soon as the slope of the adiabatic, homogeneous stress-strain curve vanishes. The results illustrated in Fig. 6 as well as our earlier discussions in Section 6 point out that the constant-coefficient approximation is a poor choice as far as predictions of shear localization are concerned.

8 Discussion

This paper together with Part I by Shawki (1994) present a theoretical framework for the analysis of the *onset* of flow localization in thermal viscoplastic materials. This framework is based on a rigorous implementation of the classical linear stability theory. The five major difficulties usually associated with this implementation of linear stability are resolved. Namely, the five difficulties are: (i) the lack of a proper mathematical characterization of localization for the considered class of deformations, (ii) the existence, uniqueness and well-posedness of a homogeneous solution, (iii) effect of domain boundness (i.e., boundary conditions), (iv) the constant-coef-

Downloaded 03 May 2010 to 171.66.16.20. Redistribution subject to ASME license or copyright; see http://www.asme.org/terms/Terms_Use.cfm

Table 1 Comparison of several localization criteria

Study	Methodology & Results: *Other Criteria*	*Energy Criterion*
Tzavaras (1986a)	A priori estimates, nonlinear result for no localization	Linear stability, no localization requirements
$\sigma = \theta^{\nu} \dot{\gamma}^{m}$ *(Adiabatic case)*	$-m < \nu < 0$ as $t \to \infty$	$-m < \nu < 0$ for $t \in [0, T]$
Molinari & Clifton (1988)	L_∞ localization, nonlinear result for asymptotic localization	Linear stability, localization necessary condition
$\sigma = \theta^{\nu} \dot{\gamma}^{m}$ *(Adiabatic case)*	$-\nu > m > 0$ as $t \to \infty$	$-\nu > m > 0$ for $t \in [0, T]$
Tzavaras (1986b)	A priori estimates, nonlinear result for no localization	Linear stability, no localization requirements
$\sigma = \gamma^{n} \dot{\gamma}$	$-1 < n < \infty$ as $t \to \infty$	$n + 1 > 0$ for $t \in [0, T]$
Molinari & Clifton (1988)	L_∞ localization, nonlinear result for asymptotic localization	Linear stability, localization necessary condition
$\sigma = \gamma^{n} \dot{\gamma}^{m}$	$n < -m < 0$ as $t \to \infty$	$n < -m < 0$ for $t \in [0, T]$
Fressengeas & Molinari (1987)	Linear stability, relative perturbations, asymptotic localization.	Linear stability, localization necessary condition
$\sigma = \theta^{\nu} \dot{\gamma}^{m}$ *(Non-adiabatic case)*	No localization as $t \to \infty$ for all $\alpha_n > 0$	$-\nu > m > 0$ for $t \le t^* \in [0, T]$ $0 < (\alpha_n/\alpha_{cr}) < 1$

ficient approximation, and (v) the quasi-static approximation. The first three difficulties were thoroughly addressed in Part I of this paper where an $L2$-norm of the solution vector is selected as a scalar, time-dependent representative of the solution behavior while being identified as an energy measure. Furthermore, the existence, uniqueness, and well-posedness properties of a homogeneous solution to the posed *initial boundary value problem* are examined. The boundness of the considered domain along with the considered velocity boundary conditions dictate a class of *admissible* perturbations, given here by Eq. (14). Part I of this paper identifies the evolution of flow localization by a bounded and monotonic evolution of spatial inhomogeneity. Systematic mathematical development associates localization of the deformation with the positive rate of change of the total kinetic energy of the absolute perturbations. This characterization of localization is a direct consequence of our aforementioned view of localization as well as taking account of formal energy balance and the admissible classes of perturbations.

This paper addresses the two difficulties (iv) and (v) while providing a methodology by which the proposed energy criterion can be utilized to obtain the necessary conditions for the onset of localization. Here, we will present a comparison of our results based on the energy criterion to a number of earlier analytic efforts by Tzavaras (1986a,b), Molinari and Clifton (1988), Fressengeas and Molinari (1987), and Shawki and Clifton (1989). Those comparisons are restricted to the power-law description of material response which stands as a common factor between the selected works.

Table 1 illustrates this comparison with the first four articles where it is evident that predictions based on our proposed energy criterion agree with all other results (except Fressengeas and Molinari's work for a heat-conducting material) while the *notion of localization* varies widely in these works! It is also important to note that while predictions of Tzavaras' works and those based on the L_∞-localization hold for sufficiently large times (i.e., asymptotic results), conclusions based on our energy criterion hold for early times in which the linear, quasi-static solution remains valid. The interesting work by Fressengeas and Molinari (1987) introduces the implementation of relative perturbations which provides a better agreement with a number of related nonlinear results. On the other hand, Fressengeas and Molinari (1987) consider the late-time (asymptotic) response of the linear system which leads, in the case of a heat-conducting material, to a prediction of "no localization" in the presence of any nonvanishing heat conduction effect. This result does *not* agree with our current results (see condition (34) and the related analysis). This disagreement is directly related to the fundamental difference in localization characterization. Extensive numerical studies by Shawki and Clifton (1989) illustrate that plastic flow localization takes place, in a typical heat-conducting steel or aluminum, at strains less than 50 percent.

Finally, we point out that our proposed energy criterion and the associated conditions governing the onset of flow localization apply to a large *class* of thermal viscoplastic response rather than being only applicable to a special form of material description. Further, we emphasize that the energy criterion examines the question of *initiation* of flow localization while it does not provide an estimate for the critical initiation strain. Such an estimate as well as a detailed analysis of evolution rates of perturbations are the subject of a future article.

Acknowledgments

The support of the National Science Foundation through Grant # NSF MSM 87-09299 and the Presidential Young Investigator Award # NSF MSS 89-57180 PYI are gratefully acknowledged.

References

Fressengeas, C., and Molinari, A., 1987, "Instability and Localization of Plastic Flow in Shear at High Strain Rates," *J. Mech. Phys. Solids*, Vol. 35, p. 185.

Molinari, A., and Clifton, R. J., 1988, "Analytical Characterization of Shear Localization in Thermoviscoplastic Solids," ASME JOURNAL OF APPLIED MECHANICS, Vol. 54, p. 806.

Downloaded 03 May 2010 to 171.66.16.20. Redistribution subject to ASME license or copyright; see http://www.asme.org/terms/Terms_Use.cfm

Table A1 Homogeneous solutions for a number of constitutive descriptions

	Power Law	Arrhenius Law	Litonski Law
	$\sigma = \theta^{\nu}\left(\frac{\gamma^p}{\dot{\gamma}_o}\right)^n (\dot{\gamma}^p)^m$	$\sigma = \sigma_B - \left(\frac{K_b\theta}{V^*}\right)\ln\left(\frac{\omega}{\dot{\gamma}^p}\right)$	$\sigma = (1 - a\theta)(\gamma_o + \gamma^p)^n(1 + b\dot{\gamma}^p)^m$
Velocity & PlasticStrain Rate	$\bar{v}(x,t) = x\,, \quad \bar{\phi}(t) = 1$		
Plastic Strain	$\bar{\gamma}^p(t) = \gamma_o + t$	$\bar{\gamma}^p(t) = \gamma_o + t$	$\bar{\gamma}^p(t) = t$
Temperature	$\bar{\theta}(t) = g(t;\nu,n)^{\frac{1}{1-\nu}}$,	$\bar{\theta}(t) = \bar{\theta}_\infty - e^{Dt}(\bar{\theta}_\infty - 1)$,	$\bar{\theta}(t) = \frac{1 - (1-a)W(T)}{a}$,
	$g(t;\nu,n) = 1 + \frac{r_1\gamma_o(1-\nu)}{(1+n)}[T^{1+n} - 1]$, $T \equiv \frac{\gamma_o + t}{\gamma_o}$, $\bar{\gamma}_r(t) = \frac{\bar{\gamma}(t)}{\gamma_o}$	$\bar{\theta}_\infty = \lim_{t\to\infty}\bar{\theta}(t) = \frac{\sigma_B}{A\ln\omega}$, $A = \frac{K_b}{V^*}$, $D = -r_1 A\ln\omega$.	$W(T) = \exp[\delta\,[(1+T)^{1+n} - 1]]$, $T = \frac{t}{\gamma_o}$, $\delta = -\frac{r_1 a(1+b)^m\gamma_o^{1+n}}{1+n}$.
$\bar{S}_1(t)$	$m\,g(t;\nu,n)^{\frac{\nu}{1-\nu}}\,\bar{\gamma}_r(t)^n$	$A\bar{\theta}(t)$	$\frac{mb\bar{\sigma}(t)}{1+b}$
$\bar{S}_2(t)$	$\frac{\nu}{g(t;\nu,n)}\,\bar{\gamma}_r(t)^n$	$-A\ln\omega$	$-a(1+b)^m(\gamma_o + t)^n$
$\bar{S}_3(t)$	$\frac{n}{\gamma_o}\,g(t;\nu,n)^{\frac{\nu}{1-\nu}}\,\bar{\gamma}_r(t)^{n-1}$	0	$\frac{n\bar{\sigma}(t)}{\gamma_o + t}$
$\Lambda_2(t)$	$\frac{-r_1}{g(t;\nu,0)}\,(1-p)$	$-\left[1 + \frac{D}{A}\frac{\bar{\sigma}(t)}{\bar{\theta}(t)}\right]$	$\frac{ar_1\,[1 + (1+m)b]\,(1+b)^m}{mb}$
$\Lambda_3(t)$	$\frac{-(1-q)}{\bar{\gamma}^p(t)}$	$-\frac{D}{A}\frac{\bar{\sigma}(t)}{\bar{\theta}(t)}$	$\frac{[q - b(1-q)]}{b(\gamma_o + t)}$

Shawki, T. G., 1988, "Necessary and Sufficient Conditions for the Onset of Shear Strain Localization in Thermal Viscoplastic Materials," T.&A.M. Report No. 489, University of Illinois at Urbana-Champaign, Urbana, IL.

Shawki, T. G., and Clifton, R. J., 1989, "Shear Band Formation in Thermal Viscoplastic Materials," *Mech. of Materials*, Vol. 8, No. 1, pp. 13-43.

Shawki, T. G., 1994, "An Energy Criterion for the Onset of Localization in Thermal Viscoplastic Materials, Part I: Necessary and Sufficient Initiation Conditions," ASME JOURNAL OF APPLIED MECHANICS, Vol. 61, pp. 530-537.

Tzavaras, A. E., 1986a, "Shearing of Materials Exhibiting Thermal Softening or Temperature Dependent Viscosity," *Q. Appl. Math.*, Vol. 44, p. 1.

Tzavaras, A. E., 1986b, "Plastic Shearing of Materials Exhibiting Strain Hardening or Strain Softening," *Arch. Rat. Mech. Anal.*, Vol. 99, p. 39.

APPENDIX A

Positive-Definitness of a Dyadic Product of Two Arbitrary Vectors

Consider the tensor $\mathbf{A} = \mathbf{u}\otimes\mathbf{v}$ where $\mathbf{u}$ and $\mathbf{v}$ are two arbitrary vectors in a three-dimensional Euclidean space E while "$\otimes$" denotes the dyadic (tensor) product of the two vectors. The principal invariants of tensor $\mathbf{A}$ are given by

$$I_A = \mathbf{u}\cdot\mathbf{v}, \quad II_A = III_A = 0. \tag{A1}$$

Furthermore, the symmetric part of $\mathbf{A}$, denoted by $\mathbf{A}_s$, is given by $\mathbf{A}_s = [\mathbf{u}\otimes\mathbf{v} + \mathbf{v}\otimes\mathbf{u}]/2$, whose principal invariants are given by

$$I_{A_s} = I_A = \mathbf{u}\cdot\mathbf{v},$$

$$II_{A_s} = -\frac{1}{4}[(v_1u_2 - v_2u_1)^2 + (v_1u_3 - u_1v_3)^2 + (v_2u_3 - u_2v_3)^2],$$

$$III_{A_s} = III_A = 0. \tag{A2}$$

The characteristic equations for the above tensors are, therefore, provided by

$\mathbf{A} = \mathbf{u}\otimes\mathbf{v}$	$\mathbf{A}_s = \frac{1}{2}[\mathbf{u}\otimes\mathbf{v} + \mathbf{v}\otimes\mathbf{u}]$
$\eta^2(\eta - I_A) = 0$	$\lambda(\lambda^2 - I_{A_s}\lambda + II_{A_s}) = 0$
$\eta_1 = \eta_2 = 0, \quad \eta_3 = I_A$	$\lambda_1 = 0, \quad 2\lambda_{2,3} = I_{A_s} \pm \sqrt{(I_{A_s})^2 - 4(II_{A_s})}$.

It is simple to verify that

$$Q \equiv \mathbf{a}\cdot\mathbf{A}\mathbf{a} = \mathbf{a}\cdot\mathbf{A}_s\mathbf{a} = \mathbf{a}\cdot\sum_{k=1}^{k=3}\lambda_k(\mathbf{p}_k\otimes\mathbf{p}_k)\mathbf{a} = \sum_{k=1}^{k=3}\lambda_k(\mathbf{a}\cdot\mathbf{p}_k)^2, \tag{A3}$$

where the vectors $\mathbf{p}_k$ are three linearly independent eigenvectors of the symmetric part of $\mathbf{A}$. It follows immediately that strict definiteness of the tensor $\mathbf{A}$ require that the eigenvalues λ_k of $\mathbf{A}_s$ maintain the same sign. Examination of the characteristic equation for the symmetric tensor $\mathbf{A}_s$ indicate that the two nonvanishing eigenvalues have opposite signs as long as II_{A_s} is nonzero. Hence, the only situation in which the above procedure becomes conclusive is that in which

$$II_{A_s} = 0 \Rightarrow \lambda_{1,2} = 0, \quad \lambda_3 \equiv \lambda = I_{A_s} = \mathbf{u}\cdot\mathbf{v}.$$

Equation (A3) gives

$$Q = (\mathbf{u}\cdot\mathbf{v})(\mathbf{a}\cdot\mathbf{p}_3)^2. \tag{A4}$$

In this case, definiteness of the tensor $\mathbf{A}$ is tied to the angle formed between the two vectors $\mathbf{u}$ and $\mathbf{v}$.

Downloaded 03 May 2010 to 171.66.16.20. Redistribution subject to ASME license or copyright; see http://www.asme.org/terms/Terms_Use.cfm

Table A2 Limiting behaviors of selected constitutive models of material response

	Power Law	*Arrhenius Law*	*Litonski Law*
As:	$t \to \infty$	$t \to \infty$	$t \to t_L < \infty$
Then	$\bar{\theta}(t) \sim t^{\frac{1+n}{1-v}}$	$\bar{\theta}(t) \to \bar{\theta}_\infty = \frac{\sigma_B}{A \ln \omega}$	$\bar{\theta}(t_L) \to \frac{1}{a}$
	$\bar{\sigma}(t) \sim t^{\frac{v+n}{1-v}}$	$\bar{\sigma}(t) \to 0$	$\bar{\sigma}(t) \to 0$

APPENDIX B

Exact Homogeneous Solutions

Table A1 summarizes a number of homogeneous solutions for selected constitutive descriptions of material response. The former results assume a rigid, thermal-viscoplastic material response along with the following set of homogeneous, dimensionless initial conditions:

$$v(x, 0)=x, \quad \dot{\gamma}^p(x, 0)=1, \quad \gamma^p(x, 0)=\gamma_0,$$
$$\theta(x, 0)=1, \quad \sigma(x, 0)=\psi(1, 1, \gamma_o). \tag{B1}$$

For the Litonski model, the initial plastic strain is taken to be zero. Further, we note that

$$\Lambda_i \equiv \frac{d}{dt}(\ln[\bar{F}_i(t)]) - \frac{\bar{C}_p(t)}{\bar{S}_1(t)} \equiv \Lambda_i(\bar{S}_1, \bar{S}_2, \bar{S}_3, \bar{\sigma}). \tag{B2}$$

However, the values listed in the last two rows of Table A1 are those corresponding to

$$\Lambda_2(\bar{S}_1, \bar{S}_2, 0, \bar{\sigma}) \quad \text{and} \quad \Lambda_3(\bar{S}_1, 0, \bar{S}_3, \bar{\sigma}),$$

respectively. We also note that solutions for the Arrhenius-law model are obtained for the case of a constant stress barrier (i.e., no strain hardening).

Table A2 illustrates the asymptotic behaviors for the foregoing constitutive models of material description.

In Table A2, we considered the class of power-law materials for which $v<1$ and $n>-1$. Moreover, the critical time for the Litonski's model is provided by

$$\frac{t_L}{\gamma_o} = \left\{1 - \frac{1}{\delta}\ln(1-a)\right\}^{1/1+n} - 1.$$

Downloaded 03 May 2010 to 171.66.16.20. Redistribution subject to ASME license or copyright; see http://www.asme.org/terms/Terms_Use.cfm

Interactions Between Dislocations and Anisotropic Elastic Elliptical Inclusions

Wen J. Yen
Ph.D. Student.

Chyanbin Hwu[1]
Professor.

Institute of Aeronautics
and Astronautics,
National Cheng Kung University,
Tainan, Taiwan 70101,
Republic of China

A general field solution for the stresses and displacements of the interactions between dislocations and inclusions has been derived in this paper by applying the Stroh's formalism and the Muskhelishvili's method of analytical continuation. The solutions are valid for general elastic anisotropic media under two-dimensional deformation. The interaction energy between dislocations and elastic inclusions is obtained explicitly. The solutions in general are expressed in series form for elastic inclusions. However, for the special cases when the elastic inclusions are replaced by a hole or rigid inclusion, simple closed-form solutions are derived. The general solutions are verified by considering the isotropic media since it is the only solution available in the literature. For the general anisotropic media, a series of contour diagrams for the glide component of the force on a dislocation are provided in this paper to study the effects of inclusion hardness, shape, and matrix anisotropy.

1 Introduction

Interactions between dislocations and inclusions have been a topic of considerable research. Greater understanding of material defects can be gained through the solution of suitable elasticity problems. The solutions of dislocations are frequently used as a kernel function of an integral equation to consider the interactions between inclusions and cracks (Erdogan et al., 1974; Pattan and Santare, 1990). The problem of a circular elastic inclusion near an edge dislocation was solved in terms of Airy's stress potentials by Dundurs and Mura (1964). Later, Dundurs and Sedeckyj (1965) solved the related problem where the dislocation is within the circular inclusion. Recently, the analytic solutions of isotropic elliptic inhomogeneity were obtained by Stagni and Lizzio (1983) for a dislocation located outside an elliptic inhomogeneity and by Warren (1983) for a dislocation inside an elastic elliptic inhomogeneity. A closed-form solution is obtained by Santare and Keer (1986) for a dislocation near a rigid elliptical inclusion, in which particular attention is paid to the rigid-body rotation of the inclusion relative to the dislocation.

While these solutions are generally in isotropic materials, the concept of an elastically isotropic crystal is an idealization. All real crystals should be considered to be anisotropic. Isotropic theory may lead to useful results, but for some cases it is an inadequate approximation. Moreover, there are increasing numbers of observations of sufficient accuracy to warrant comparison with more precise anisotropic calculations. Also, some effects, such as the instability of some straight dislocations with respect to break up into zigzag shape, require anisotropic theory even for their qualitative explanation (Hirth and Lothe, 1982). Hence, it is necessary to analyze such interaction problems by using anisotropic theory. In this study, the Stroh's formalism (Stroh, 1958) for anisotropic elasticity combined with the method of analytical continuations (Muskhelishvili, 1954) is utilized to solve the general analytical solution for the interactions between dislocations and anisotropic elastic elliptical inclusions.

2 Anisotropic Elasticity

The stress-strain relation obeying Hooke's law for the generally anisotropic material is usually expressed as

$$\sigma_{ij} = C_{ijks}\epsilon_{ks}, \tag{1}$$

where σ_{ij} and ϵ_{ij} denote, respectively, the stresses and strains. C_{ijks} are the elastic constants which are assumed to be fully symmetric and positive definite. For a two-dimensional problem, it has been shown (Eshelby et al., 1953; Stroh, 1958; Lekhnitskii, 1963; Ting, 1986) that the elastic field can be represented in terms of three complex functions $f_1(z_1), f_2(z_2), f_3(z_3)$, each of which is holomorphic in its argument $z_\alpha (= x_1 + p_\alpha x_2)$. Here p_α, $\alpha = 1, 2, 3$, are the material eigenvalues which are complex numbers with positive imaginary part and can be solved as roots of a sixth-order polynomial (Eshelby et al., 1953). With these holomorphic functions, the displacements u_i, stress functions ϕ_i and stresses σ_{ij} can be represented as

[1] To whom all correspondence should be addressed.

Contributed by the Applied Mechanics Division of THE AMERICAN SOCIETY OF MECHANICAL ENGINEERS for publication in the ASME JOURNAL OF APPLIED MECHANICS.

Discussion on this paper should be addressed to the Technical Editor, Professor Lewis T. Wheeler, Department of Mechanical Engineering, University of Houston, Houston, TX 77204-4792, and will be accepted until four months after final publication of the paper itself in the ASME JOURNAL OF APPLIED MECHANICS.

Manuscript received by the ASME Applied Mechanics Division, Apr. 21, 1992; final revision, June 15, 1993. Associate Technical Editor: R. M. McMeeking.

Copyright © 1994 by ASME
Downloaded 03 May 2010 to 171.66.16.20. Redistribution subject to ASME license or copyright; see http://www.asme.org/terms/Terms_Use.cfm

$$\mathbf{u}=2\mathrm{Re}\left\{\sum_{\alpha=1}^{3}\mathbf{a}_\alpha f_\alpha(z_\alpha)\right\},\quad \boldsymbol{\phi}=2\mathrm{Re}\left\{\sum_{\alpha=1}^{3}\mathbf{b}_\alpha f_\alpha(z_\alpha)\right\},$$

$$\sigma_{i1}=-\phi_{i,2},\quad \sigma_{i2}=\phi_{i,1},\quad i=1,\ 2,\ 3, \tag{2}$$

where $\mathbf{u}$ and $\boldsymbol{\phi}$ are 3×1 column vectors whose components are u_i and ϕ_i, respectively. Re denotes the real part of a complex number and a comma in the subscript stands for differentiation. $(\mathbf{a}_\alpha,\ \mathbf{b}_\alpha)$ are the material eigenvectors associated with the eigenvalues p_α, and are related to the elastic constants (Eshelby et al., 1953; Hwu and Ting, 1989).

A well-known method treated extensively in isotropic elasticity is the Muskhelishvili's method of analytical continuation, which is powerful in dealing with the boundary value problem by complex variable formulation. To combine the above solution form Eq. (2) with the method of analytical continuation, another form is suggested by Suo (1990) and Hwu and Yen (1993) as

$$\mathbf{u}=\mathbf{A}\mathbf{f}(z)+\overline{\mathbf{A}}\,\overline{\mathbf{f}(z)},$$
$$\boldsymbol{\phi}=\mathbf{B}\mathbf{f}(z)+\overline{\mathbf{B}}\,\overline{\mathbf{f}(z)}, \tag{3a}$$

where

$$\mathbf{A}=[\mathbf{a}_1\ \mathbf{a}_2\ \mathbf{a}_3],\quad \mathbf{B}=[\mathbf{b}_1\ \mathbf{b}_2\ \mathbf{b}_3],\quad \mathbf{f}(z)=[f_1(z)\ f_2(z)\ f_3(z)]^T. \tag{3b}$$

The overbar denotes the complex conjugate and the superscript T stands for the transpose of a matrix. Note that the argument of each component function of $\mathbf{f}(z)$ is written as $z=x_1+px_2$ without referring to the associated eigenvalues p_α. Once the solution of $\mathbf{f}(z)$ is obtained for a given boundary value problem, a replacement of z_1, z_2, or z_3 should be made for each component function to calculate field quantities. Without the statement about the manipulation of $\mathbf{f}(z)$ before and after the solution procedure, Eq. (3*a*) is not a correct solution form since the subscript of z in the column vector $\mathbf{f}(z)$ is missing, which violates the requirement stated in Eq. (2) that $f_\alpha(z_\alpha)$ is a holomorphic function with argument z_α. It is also because of this slightly change for $\mathbf{f}(z)$ that the method of analytical continuation can be employed smoothly.

3 Dislocation in a Homogeneous Medium

Consider an isolated singularity in an infinite homogeneous anisotropic medium. If the singularity is a dislocation line in the direction perpendicular to the x_1x_2 plane with Burgers vector $\hat{\mathbf{b}}$ located at the point $(\hat{x}_1,\ \hat{x}_2)$, the complex function vector $\mathbf{f}_o$ associated with this problem may be written as

$$\mathbf{f}_o(z)=\langle\langle\log(z_\alpha-\hat{z}_\alpha)\rangle\rangle\mathbf{q}, \tag{4}$$

where $\mathbf{q}$ is to be determined in terms of $\hat{\mathbf{b}}$. The angular bracket stands for the diagonal matrix, i.e., $\langle\langle f_\alpha\rangle\rangle=\mathrm{diag}\{f_1\ f_2\ f_3\}$, which will be used throughout this paper. Using the condition that around any circle enclosing the point $(\hat{x}_1,\ \hat{x}_2)$, the total displacements and forces resulting from $\mathbf{f}_o(z)$ are $\hat{\mathbf{b}}$ and $\mathbf{0}$, we obtain

$$2\mathrm{Re}\{i\mathbf{B}\mathbf{q}\}=\mathbf{0},$$
$$2\mathrm{Re}\{i\mathbf{A}\mathbf{q}\}=\hat{\mathbf{b}}/2\pi. \tag{5}$$

To find $\mathbf{q}$ from (5), we recall the orthogonality relations among the eigenvectors (Stroh, 1958; Ting, 1988),

$$\begin{bmatrix}\mathbf{A}^T & \mathbf{B}^T\\ \overline{\mathbf{A}}^T & \overline{\mathbf{B}}^T\end{bmatrix}\begin{bmatrix}\mathbf{B} & \overline{\mathbf{B}}\\ \mathbf{A} & \overline{\mathbf{A}}\end{bmatrix}=\mathbf{I}$$

and obtain

$$\mathbf{q}=\mathbf{B}^T\hat{\mathbf{b}}/2\pi i. \tag{6}$$

4 Dislocation in an Anisotropic Matrix With an Inclusion

Consider an anisotropic elastic elliptical inclusion imbedded in an infinite matrix and the dislocation with Burgers vector $\hat{\mathbf{b}}$ located at the point $(\hat{x}_1,\ \hat{x}_2)$. The contour of the interface between the matrix and inclusion is represented by

$$x_1=a\cos\psi,\quad x_2=b\sin\psi,$$

where $2a$, $2b$ are the major and minor axes of the ellipse and ψ is a real parameter. If the inclusion and the matrix are assumed to be perfectly bonded along the interface, the displacements and surface tractions across the interface should be continuous. That is,

$$\left.\begin{aligned}\mathbf{u}_1&=\mathbf{u}_2\\ \boldsymbol{\phi}_1&=\boldsymbol{\phi}_2\end{aligned}\right\},\quad \text{along the interface} \tag{7}$$

where the second equation of (7) comes from the relation $\mathbf{t}=\partial\boldsymbol{\phi}/\partial s$ in which $\mathbf{t}$ is the surface traction and s is the arc length measured along the curved boundary. The subscripts 1 and 2 denote, respectively, the matrix and inclusion.

We are now trying to find an elasticity solution which satisfies the dislocation singularity (4) and the interface continuity condition (7). By a way similar to that used in (Hwu and Yen, 1993) for the problems of elastic inclusions subjected to arbitrary loadings, the general solution for the matrix and inclusion may be expressed as

$$\left.\begin{aligned}\mathbf{u}_1&=\mathbf{A}_1[\mathbf{f}_o(\zeta)+\mathbf{f}_1(\zeta)]+\overline{\mathbf{A}}_1[\overline{\mathbf{f}_o(\zeta)}+\overline{\mathbf{f}_1(\zeta)}]\\ \boldsymbol{\phi}_1&=\mathbf{B}_1[\mathbf{f}_o(\zeta)+\mathbf{f}_1(\zeta)]+\overline{\mathbf{B}}_1[\overline{\mathbf{f}_o(\zeta)}+\overline{\mathbf{f}_1(\zeta)}]\end{aligned}\right\},\quad \zeta\in S_1 \tag{8a}$$

$$\left.\begin{aligned}\mathbf{u}_2&=\mathbf{A}_1\mathbf{f}_2(\zeta^*)+\overline{\mathbf{A}}_2\overline{\mathbf{f}_2(\zeta^*)}\\ \boldsymbol{\phi}_2&=\mathbf{B}_1\mathbf{f}_2(\zeta^*)+\overline{\mathbf{B}}_2\overline{\mathbf{f}_2(\zeta^*)}\end{aligned}\right\},\quad \zeta^*\in S_2 \tag{8b}$$

where $\mathbf{f}_o$ can be chosen to represent exactly the solutions of homogeneous media, i.e., the equations shown in (4) and (6). However, it is inconvenient to use Eqs. (4) and (6) in calculation since our general solutions shown in Eqs. (8*a*, *b*) are expressed in terms of the variable ζ_α not z_α. An alternative choice for $\mathbf{f}_o$ is

$$\mathbf{f}_o(\zeta)=\frac{1}{2\pi i}\langle\langle\log(\zeta_\alpha-\hat{\zeta}_\alpha)\rangle\rangle\mathbf{B}_1^T\hat{\mathbf{b}}. \tag{8c}$$

This expression is more convenient than the one given in (4). Moreover, it also reflects the singularity characteristics of the dislocation considered in our problems. $\mathbf{f}_1$ (or $\mathbf{f}_2$) is the unknown complex function vector corresponding to the perturbed elastic field of matrix (or inclusion), which is holomorphic in region S_1 (or S_2). S_1 and S_2 denote, respectively, the regions occupied by the matrix and inclusion. ζ_α and ζ_α^* are related to the complex arguments z_α and $z_\alpha^*(=x_1+p_\alpha^*x_2)$ through the following transformation functions,

$$\zeta_\alpha=\frac{z_\alpha+\sqrt{z_\alpha^2-a^2-p_\alpha^2b^2}}{a-ip_\alpha b},$$
$$\zeta_\alpha^*=\frac{z_\alpha^*+\sqrt{z_\alpha^{*2}-a^2-p_\alpha^*b^2}}{a-ip_\alpha^*b}, \tag{9}$$

which map the region outside the elliptic inclusion onto the exterior of a unit circle. For the region inside the elliptic inclusion, certain restrictions should be satisfied to ensure that the transformation is single valued (Hwu and Yen, 1993). The inclusion in the z-plane is then mapped onto an annular ring in the ζ-plane. If $\mathbf{f}_2$ is holomorphic inside the elliptic inclusion and is represented by the Laurent's expansion, it has been shown that (Hwu and Yen, 1993) $\mathbf{f}_2$ has the following series form:

$$\mathbf{f}_2(\zeta^*)=\sum_{k=-\infty}^{\infty}\mathbf{c}_k\zeta^{*k}, \tag{10a}$$

Downloaded 03 May 2010 to 171.66.16.20. Redistribution subject to ASME license or copyright; see http://www.asme.org/terms/Terms_Use.cfm

where

$$\mathbf{c}_{-k}=\mathbf{\Gamma}_k^*\mathbf{c}_k,\quad \mathbf{\Gamma}_k^*=\left\langle\left\langle\left(\frac{a+ibp_\alpha^*}{a-ibp_\alpha^*}\right)^k\right\rangle\right\rangle. \tag{10b}$$

To determine $\mathbf{f}_1$ and $\mathbf{f}_2$ through the continuity conditions, we now apply the Muskhelishvili's method of analytical continuation. Using the continuity condition and the property that if $\mathbf{f}(\zeta)$ is holomorphic in S^+ then $\overline{\mathbf{f}(1/\bar{\zeta})}$ is holomorphic in S^-, one may introduce a function which is holomorphic in the entire domain including the interface. Applying the Liouville's theorem that if $\theta(\zeta)$ is holomorphic and single valued in the whole plane including the point at infinity then $\theta(\zeta)\equiv$ constant, one may derive two equations corresponding to the displacement and traction continuity conditions. From these two equations, the complex functions $\mathbf{f}_1$ and $\mathbf{f}_2$ are determined as follows (see Appendix):

$$\mathbf{f}_1(\zeta)=\mathbf{B}_1^{-1}\left\{\sum_{k=1}^{\infty}(\bar{\mathbf{B}}_2\bar{\mathbf{c}}_k+\mathbf{B}_2\mathbf{\Gamma}_k^*\mathbf{c}_k)\zeta^{-k}-\bar{\mathbf{B}}_1\bar{\mathbf{f}}_o(1/\zeta)\right\},$$

$$\mathbf{f}_2(\zeta^*)=\sum_{k=1}^{\infty}\{\mathbf{c}_k\zeta^{*k}+\mathbf{\Gamma}_k^*\mathbf{c}_k\zeta^{*-k}\}, \tag{11a}$$

where

$$\mathbf{c}_k=\{\mathbf{G}_o-\bar{\mathbf{G}}_k\bar{\mathbf{G}}_o^{-1}\mathbf{G}_k\}^{-1}\{\mathbf{t}_k-\bar{\mathbf{G}}_k\bar{\mathbf{G}}_o^{-1}\bar{\mathbf{t}}_k\},\quad k=1,\,2,\,\cdots\infty \tag{11b}$$

and

$$\begin{aligned}\mathbf{G}_o&=(\bar{\mathbf{M}}_1+\mathbf{M}_2)\mathbf{A}_2,\\ \mathbf{G}_k&=(\mathbf{M}_1-\mathbf{M}_2)\mathbf{A}_2\mathbf{\Gamma}_k^*,\\ \mathbf{t}_k&=\frac{-1}{2\pi}\mathbf{A}_1^{-T}\left\langle\left\langle-\frac{1}{k}\hat{\zeta}_\alpha^{-k}\right\rangle\right\rangle\mathbf{B}_1^T\hat{\mathbf{b}}.\end{aligned} \tag{11c}$$

$\mathbf{M}_k$ is the impedance matrix (Ingebrigtsen and Tonning, 1969) defined as

$$\mathbf{M}_k=-i\mathbf{B}_k\mathbf{A}_k^{-1}=\mathbf{H}_k^{-1}(\mathbf{I}+i\mathbf{S}_k), \tag{12a}$$

where

$$\begin{aligned}\mathbf{S}_k&=i(2\mathbf{A}_k\mathbf{B}_k^T-\mathbf{I}),\quad \mathbf{H}_k=2i\mathbf{A}_k\mathbf{A},\\ \mathbf{L}_k&=-2i\mathbf{B}_k\mathbf{B}_k^T,\quad k=1,\,2.\end{aligned} \tag{12b}$$

The second equality of (12a) has been given by Ting (1988) and $\mathbf{S}_k$, $\mathbf{H}_k$, $\mathbf{L}_k$ are real matrices composed of the elasticity constants. Moreover, $\mathbf{H}_k$ and $\mathbf{L}_k$ are positive definite if the strain energy is positive (Chadwick and Smith, 1977). Hence, the inverses of $\mathbf{H}_k$ and $\mathbf{L}_k$ exist. Note that the solutions associated with $\mathbf{c}_o$ are ignored because the constant stress function does not produce stress, which represents the rigid-body motion.

When the elastic inclusion is replaced by a traction-free hole, the boundary condition can be expressed as $\boldsymbol{\phi}=\mathbf{0}$. By a way similar to that described for the elastic inclusion, the solution can be found to be

$$\mathbf{f}(\zeta)=\sum_{k=1}^{3}\langle\langle\log(\zeta_\alpha^{-1}-\bar{\hat{\zeta}}_k)\rangle\rangle\mathbf{B}^{-1}\bar{\mathbf{B}}\mathbf{I}_k\bar{\mathbf{B}}^T\hat{\mathbf{b}}/2\pi i \tag{13a}$$

where

$$\mathbf{I}_1=\begin{bmatrix}1&0&0\\0&0&0\\0&0&0\end{bmatrix},\quad \mathbf{I}_2=\begin{bmatrix}0&0&0\\0&1&0\\0&0&0\end{bmatrix},\quad \mathbf{I}_3=\begin{bmatrix}0&0&0\\0&0&0\\0&0&1\end{bmatrix}. \tag{13b}$$

Here the subscripts denoting the matrix and inclusion are omitted since only the matrix is concerned. The solution of $\mathbf{f}_o(\zeta)$ related to the homogeneous media is the same as (8c).

Similarly, for a rigid inclusion interacted with the dislocation, the solution is found to be

$$\mathbf{f}(\zeta)=\sum_{k=1}^{3}\langle\langle\log(\zeta_\alpha^{-1}-\bar{\hat{\zeta}}_k)\rangle\rangle\mathbf{A}^{-1}\bar{\mathbf{A}}\mathbf{I}_k\bar{\mathbf{B}}^T\hat{\mathbf{b}}/2\pi i+\frac{\omega}{2}\langle\langle\zeta_\alpha^{-1}\rangle\rangle\mathbf{A}^{-1}\bar{\mathbf{k}} \tag{14a}$$

where

$$\mathbf{k}=\begin{Bmatrix}ib\\a\\0\end{Bmatrix}. \tag{14b}$$

ω denotes the rigid-body rotation relative to the matrix, which can be obtained by the condition that the total moment about the origin due to the traction along the surface of rigid inclusion vanishes. The result is

$$\omega=\frac{\mathrm{Re}\{\bar{\mathbf{k}}^T\mathbf{A}^{-T}\langle\langle\hat{\zeta}_\alpha^{-1}\rangle\rangle\mathbf{B}^T\}\hat{\mathbf{b}}}{\pi\mathrm{Im}\{\mathbf{k}^T\mathbf{B}\mathbf{A}^{-1}\bar{\mathbf{k}}\}}. \tag{14c}$$

5 Interaction Energy

In the absence of applied tractions, the interaction energy between the dislocation and the inclusion is equal to the elastic potential energy. Furthermore, all terms that are independent of the position of the dislocation, such as the divergent integrals corresponding to the energy of dislocation in the homogeneous materials, can be discarded in the computation of the interaction energy. Thus, the elastic potential energy for the dislocation with Burgers vector $\hat{\mathbf{b}}$ located on $\hat{\mathbf{x}}$, set up as the work required to introduce the dislocation in the material, is (Eshelby, 1956; Dundurs and Gangadharan, 1969)

$$E^i=\frac{1}{2}\int_{\hat{x}_1}^{\infty}(\hat{b}_1\sigma_{21}^i+\hat{b}_2\sigma_{22}^i+\hat{b}_3\sigma_{23}^i)dx_1 \tag{15a}$$

where $\sigma_{ij}^i=\sigma_{ij}-\sigma_{ij}^d$ and σ_{ij} is the stress field when the dislocation is located in an anisotropic matrix with an inclusion, which can be found by the results of Section 4. σ_{ij}^d is the self-stress of dislocation in an infinite homogeneous medium, which can be found by the results of Section 3. Since $\partial\boldsymbol{\phi}^i/\partial x_1=\{\sigma_{21}^i,\,\sigma_{22}^i,\,\sigma_{23}^i\}^T$, it follows that

$$E^i=-\frac{1}{2}\hat{b}^T\boldsymbol{\phi}^i(\hat{x}_1,\,\hat{x}_2), \tag{15b}$$

where $\boldsymbol{\phi}^i(\infty)$ is assumed to be zero. If the dislocation moves along the s direction, the generalized force F^i in the s direction on the dislocation is defined as the negative gradient of the interaction energy, i.e.,

$$F^i=-\frac{\partial E^i}{\partial s}. \tag{16}$$

The total stress function $\boldsymbol{\phi}$ ($=\boldsymbol{\phi}^i+\boldsymbol{\phi}^d$) for the dislocation in a general position with respect to the inclusion has been provided in the last section. To evaluate $\boldsymbol{\phi}^i$, a substraction of the self-stress function $\boldsymbol{\phi}^d$ from the total stress function should be made. Note that $\boldsymbol{\phi}^d$ is equal to

$$\boldsymbol{\phi}^d=2\mathrm{Re}\{\mathbf{B}\langle\langle\log(z_\alpha-\hat{z}_\alpha)\rangle\rangle\mathbf{B}^T\hat{\mathbf{b}}/2\pi i\}, \tag{17}$$

which is different from that obtained by $\mathbf{f}_o$ given in (8c). The total stress function of elastic inclusion with a dislocation is obtained from (8), in which (11) and (12) are used. Using the total stress function and Eqs. (15) and (17), we can obtain the interaction energy in an explicit form as

$$E^i=-\frac{1}{2}\hat{\mathbf{b}}^T\hat{\mathbf{\Phi}}\hat{\mathbf{b}}\,|_{\zeta_\alpha=\hat{\zeta}_\alpha}, \tag{18a}$$

where

$$\hat{\mathbf{\Phi}}=\frac{-1}{\pi}\mathrm{Im}\left\{\mathbf{B}_1\left\langle\left\langle\log\left(1-\frac{\zeta_\alpha^{o2}}{\zeta_\alpha\hat{\zeta}_\alpha}\right)\right\rangle\right\rangle\mathbf{B}_1^T\right\}+\frac{1}{\pi}\mathrm{Im}\left\{\mathbf{B}_1\sum_{k=1}^{\infty}\langle\langle\zeta_\alpha^{-k}\rangle\rangle\mathbf{B}_1^{-1}\hat{\mathbf{D}}_k\right\}$$

Downloaded 03 May 2010 to 171.66.16.20. Redistribution subject to ASME license or copyright; see http://www.asme.org/terms/Terms_Use.cfm

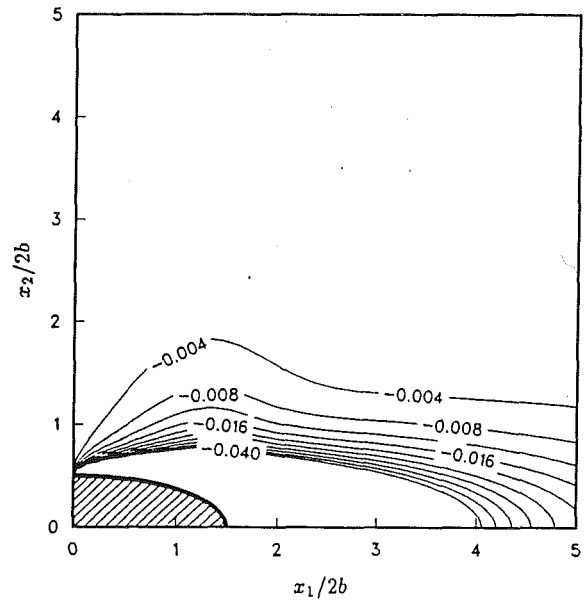


Fig. 1 Contour plots of the dimensionless glide force for anisotropic media with $k = 1/2$, $\hat{\mathbf{b}} = (\hat{b}_1, 0, 0)$, $a/b = 3$

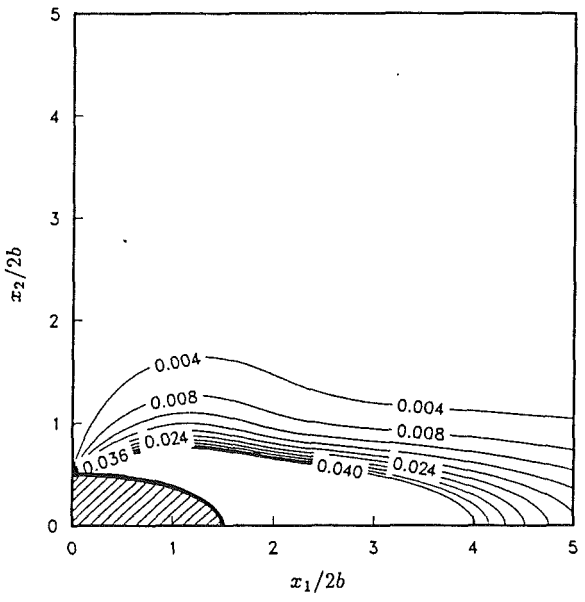


Fig. 2 Contour plots of the dimensionless glide force for anisotropic media with $k = 2$, $\hat{\mathbf{b}} = (\hat{b}_1, 0, 0)$, $a/b = 3$

$$+\frac{1}{\pi}\mathrm{Im}\left\{\mathbf{B}_1\sum_{k=1}^{3}\langle\langle\log(\zeta_\alpha^{-1}-\bar{\zeta}_k)\rangle\rangle\mathbf{B}_1^{-1}\bar{\mathbf{B}}_1\mathbf{I}_k\bar{\mathbf{B}}_1^T\right\}, \quad (18b)$$

$$\hat{\mathbf{D}}_k=\frac{i}{k}(\bar{\mathbf{B}}_2\bar{\mathbf{D}}_k-\mathbf{B}_2\boldsymbol{\Gamma}_k^*\mathbf{D}_k\mathbf{E}_k)\bar{\mathbf{A}}_1^{-T}\langle\langle\bar{\zeta}_\alpha^k\rangle\rangle\bar{\mathbf{B}}_1^T$$

$$+\frac{i}{k}(\mathbf{B}_2\boldsymbol{\Gamma}_k^*\mathbf{D}_k-\bar{\mathbf{B}}_2\bar{\mathbf{D}}_k\bar{\mathbf{E}}_k)\mathbf{A}_1^{-T}\langle\langle\hat{\zeta}_\alpha^{-k}\rangle\rangle\mathbf{B}_1^T, \quad (18c)$$

$$\mathbf{D}_k=\{\mathbf{G}_o-\bar{\mathbf{G}}_k\bar{\mathbf{G}}_o^{-1}\mathbf{G}_k\}^{-1},$$
$$\mathbf{E}_k=\bar{\mathbf{G}}_k\bar{\mathbf{G}}_o^{-1}. \quad (18d)$$

ζ_α^o is the critical point of the mapping function $(9)_1$, which is,

$$\zeta_\alpha^o=\pm\sqrt{\frac{a+ibp_\alpha}{a-ibp_\alpha}}. \quad (18e)$$

During the derivation of Eq. (18), the following relation has been employed:

$$\log(\zeta_\alpha-\hat{\zeta}_\alpha)=\log(z_\alpha-\hat{z}_\alpha)-\log\left(1-\frac{\zeta_\alpha^{o2}}{\zeta_\alpha\hat{\zeta}_\alpha}\right).$$

By a similar approach, the interaction energy between dislocations and holes can also be obtained in an explicit form as

$$2E^i=\hat{\mathbf{b}}^T\frac{1}{\pi}\mathrm{Im}\left\{\mathbf{B}\left\langle\left\langle\log\left(1-\frac{\zeta_\alpha^{o2}}{\hat{\zeta}_\alpha\hat{\zeta}_\alpha}\right)\right\rangle\right\rangle\mathbf{B}^T\right\}\hat{\mathbf{b}}$$

$$-\hat{\mathbf{b}}^T\frac{1}{\pi}\mathrm{Im}\left\{\mathbf{B}\sum_{k=1}^{3}\langle\langle\log(\hat{\zeta}_\alpha^{-1}-\bar{\zeta}_k)\rangle\rangle\mathbf{B}^{-1}\bar{\mathbf{B}}\mathbf{I}_k\bar{\mathbf{B}}^T\right\}\hat{\mathbf{b}}. \quad (19)$$

For rigid inclusions, we have

$$2E^i=\hat{\mathbf{b}}^T\frac{1}{\pi}\mathrm{Im}\left\{\mathbf{B}\left\langle\left\langle\log\left(1-\frac{\zeta_\alpha^{o2}}{\hat{\zeta}_\alpha\hat{\zeta}_\alpha}\right)\right\rangle\right\rangle\mathbf{B}^T\right\}\hat{\mathbf{b}}$$

$$-\hat{\mathbf{b}}^T\frac{1}{\pi}\mathrm{Im}\left\{\mathbf{B}\sum_{k=1}^{3}\langle\langle\log(\hat{\zeta}_\alpha^{-1}-\bar{\zeta}_k)\rangle\rangle\mathbf{A}^{-1}\bar{\mathbf{A}}\mathbf{I}_k\bar{\mathbf{B}}^T\right\}\hat{\mathbf{b}}$$

$$-\omega\hat{\mathbf{b}}^T\mathrm{Re}\left\{\mathbf{B}\left\langle\left\langle\frac{1}{\hat{\zeta}_\alpha}\right\rangle\right\rangle\mathbf{A}^{-1}\bar{\mathbf{k}}\right\}. \quad (20)$$

6 Results and Discussions

In the following, we consider an edge dislocation with Burgers vector $\hat{\mathbf{b}} = (\hat{b}_1, 0, 0)$ directed along the x_1-axis so that the slip plane is parallel to the plane $x_2 = 0$. The glide component of the force per unit length tending to move the dislocation towards or away from the x_2-axis may be found from (15) and (16), which is

$$F_1 = \sigma_{12}^i\hat{b}_1.$$

The interactions between dislocations and inclusions are then shown by the contour of the glide component of the force per unit length (F_1). The force is nondimensionalized by dividing $L_{11}\hat{b}_1/4\pi$ where L_{11} is the {11} component of the fundamental matrix $\mathbf{L}$ of the matrix and is proportional to the Young's modulus E_1 for orthotropic materials (Hwu, 1993). Moreover, $L_{11} = \mu/(\kappa+1)$ for isotropic materials where μ is the shear modulus of the matrix, $\kappa = 3-4\nu$ for the plane-strain problem, $\kappa = (3-\nu)/(1+\nu)$ for plane stress, where ν is the Poisson's ratio of the matrix. Note that when reduction to the case of isotropic materials, the nondimensionalized factor used in this paper is the same as that used by Santare and Keer (1986). Figures 1 and 2 show the contour diagrams of elastic inclusions interacted with dislocations, in which the material properties of the matrix are

$$E_1 = 144.8 \text{ Gpa}, \quad E_2 = E_3 = 10.7 \text{ Gpa}$$
$$\nu_{12} = \nu_{13} = \nu_{23} = 0.31$$
$$G_{12} = G_{13} = G_{23} = 4.5 \text{ Gpa} \quad (21)$$

while the properties of the inclusions are assumed to be proportional to the matrix as

$$k = \frac{(E_i)_2}{(E_i)_1} = \frac{(G_{ij})_2}{(G_{ij})_1}, \quad i, j = 1, 2, 3,$$

where k is the index of hardness (or softness). The Poisson's ratios ν_{ij} of the inclusions are assumed to be identical to those of the matrix. When $k<1$ the inclusion is softer than the matrix, while $k>1$ means hard. A hole or a rigid inclusion can therefore be approximated by letting $k\to 0$ or $k\to\infty$. The contour diagrams for the holes or rigid inclusions interacted with dislocations are then shown in Figs. 3 and 4. In regions where the glide components of the force are negative, the dislocation is attracted to the x_2-axis. A positive value indicates

Downloaded 03 May 2010 to 171.66.16.20. Redistribution subject to ASME license or copyright; see http://www.asme.org/terms/Terms_Use.cfm

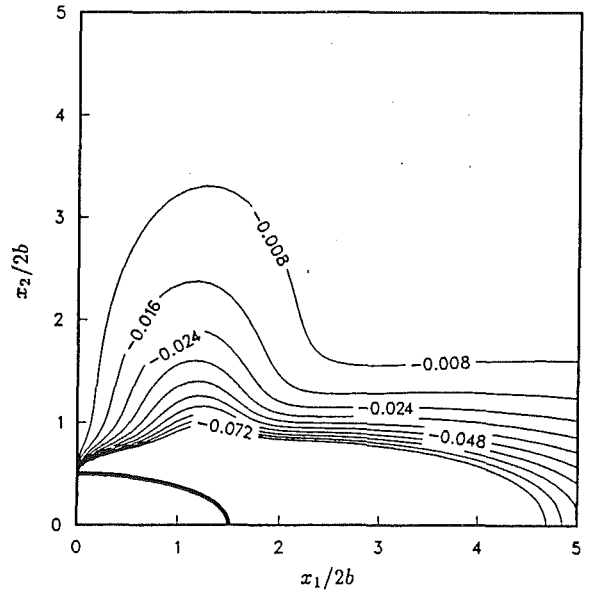


Fig. 3 Contour plots of the dimensionless glide force for anisotropic media containing a hole with $\hat{b} = (\hat{b}_1, 0, 0)$, $a/b = 3$

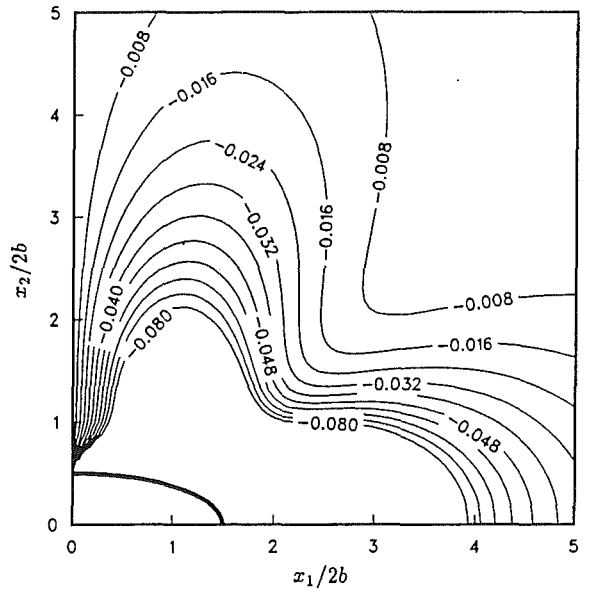


Fig. 5 Contour plots of the dimensionless glide force for isotropic media containing a hole with $\hat{b} = (\hat{b}_1, 0, 0)$, $a/b = 3$

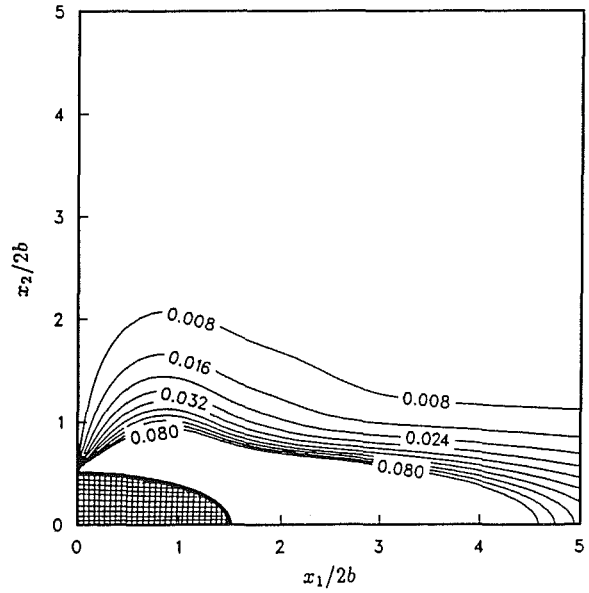


Fig. 4 Contour plots of the dimensionless glide force for anisotropic media containing a rigid inclusion with $\hat{b} = (\hat{b}_1, 0, 0)$, $a/b = 3$

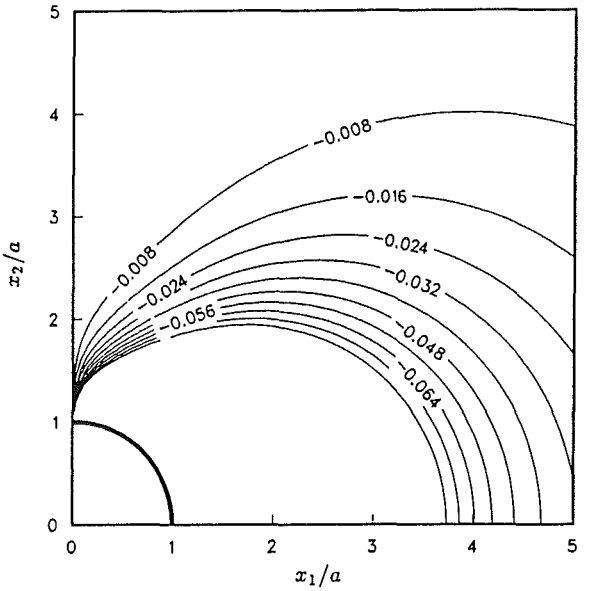


Fig. 6 Contour plots of the dimensionless glide force for isotropic media containing a hole with $\hat{b} = (\hat{b}_1, 0, 0)$, $a/b = 1$

that the dislocation is repelled from the x_2-axis. Therefore, when the glide force is zero, the position can be thought of as an equilibrium position for the dislocation. In all the plots, the x_2-axis is a line of zero glide force. The stability of the equilibrium can be judged from the attraction or repulsion condition around the equilibrium position. For example, the x_2-axis in Fig. 1 is a stable equilibrium position since the dislocations on both sides of the x_2-axis are attracted to the x_2-axis. Oppositely, the x_2-axis in Fig. 2 is an unstable equilibrium position. From the results of Figs. 1–4, we observe that the glide component of the force is positive for hard inclusions and is negative for soft inclusions. Moreover, the absolute values of the forces for the hard ($k = 2$) and soft ($k = 1/2$) inclusions are almost the same. If the holes and rigid inclusions are treated as the limiting cases of the soft and hard inclusions, it can be seen that the absolute value of the glide component of the force increases when the hard inclusions become harder or the soft inclusions become softer.

For the purpose of comparison, we now consider the matrix to be isotropic materials with $\nu = 0.1$ and the elastic inclusions is replaced by holes. Figures 5–7 show that they are really the same as those given by Stagni and Lizzo (1983). Moreover, from these figures, one may see the shape effects in the interactions between edge dislocations and holes, which have been discussed by Stagni and Lizzo (1983) and will not be repeated here. Note that in numerical calculation, a small perturbation of the material constants for isotropic materials has been used to avoid the problem of repeated eigenvalues p_α (Ting and Hwu, 1988).

The effects of matrix anisotropy may then be studied by observing the difference between Figs. 3 and 5 for the hole interaction problems, and Figs. 4 and 8 for the rigid inclusion interaction problems. These figures show that the outlooks of the force contour for the isotropic and anisotropic matrix are similar except that the latter looks like to be squeezed in the x_2-direction, which is due to the fact that the anisotropic matrix

Downloaded 03 May 2010 to 171.66.16.20. Redistribution subject to ASME license or copyright; see http://www.asme.org/terms/Terms_Use.cfm

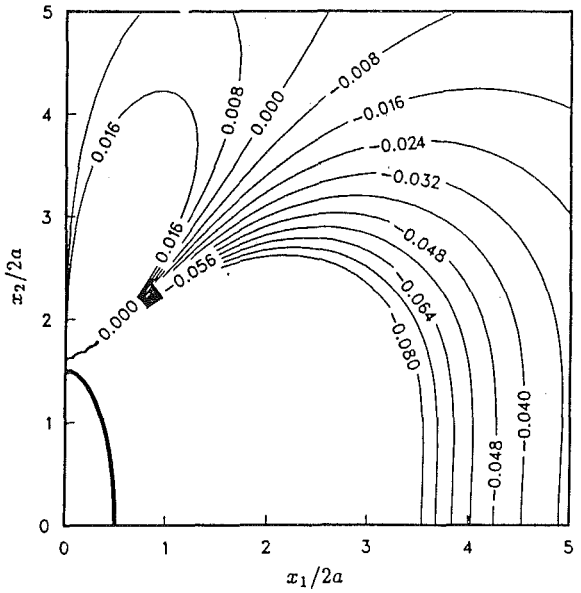


Fig. 7 Contour lots of the dimensionless glide force for isotropic media containing a hole with $\hat{\mathbf{b}} = (\hat{b}_1, 0, 0)$, $a/b = 1/3$

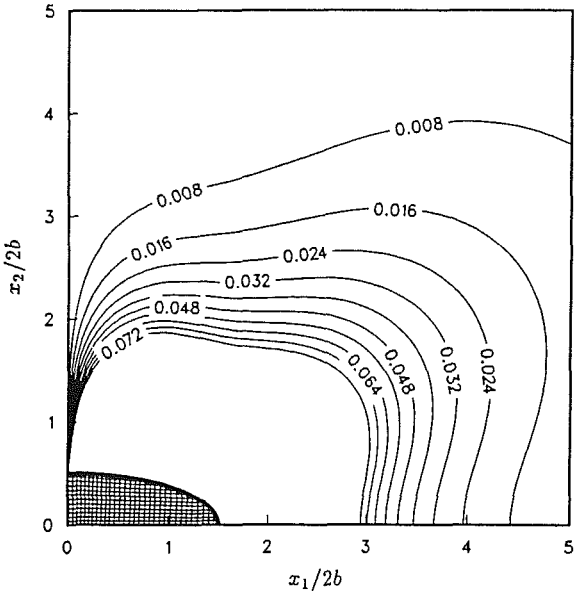


Fig. 8 Contour plots of the dimensionless glide force for isotropic media containing a rigid inclusion with $\hat{\mathbf{b}} = (\hat{b}_1, 0, 0)$, $a/b = 3$

considered has stronger stiffness in the x_1-direction than in the x_2-direction, i.e., $E_1 > E_2$.

7 Conclusions

An elasticity solution for the interactions between dislocations and inclusions has been provided in this paper. The inclusion and the matrix considered could be the general elastic anisotropic materials. Comparison with the existing solutions for the isotropic materials shows that the present results are exact and general. The effects of inclusion hardness, shape, and matrix anisotropy on the glide component of the force have also been discussed in this paper.

Acknowledgments

The authors would like to thank the support by National Science Council, Republic of China, through Grant No. NSC 81-0401-E006-12.

References

Dundurs, J., and Mura, T., 1964, "Interaction Between an Edge Dislocation and a Circular Inclusion," *J. Mech. Phys. Sol.*, Vol. 12, pp. 177–189.

Dundurs, J., and Sendeckyj, G. P., 1965, "Edge Dislocation Inside a Circular Inclusion," *J. Mech. Phys. Sol.*, Vol. 13, pp. 141–147.

Dundurs, J., and Gangadharan, A. C., 1969, "Edge Dislocation Near an Inclusion with a Slipping Interface," *J. Mech. Phys. Sol.*, Vol. 17, pp. 459–471.

Erdogan, F., Gupta, G. D., and Ratwani, M., 1974, "Interaction Between a Circular Inclusion and an Arbitrary Oriented Crack," ASME JOURNAL OF APPLIED MECHANICS, Vol. 41, pp. 382–385.

Eshelby, J. D., 1956, "The Continuum Theory of Lattice Defects," *Solid State Physics*, Vol. 3, pp. 79–144.

Eshelby, J. D., Read, W. T., and Shockley, W., 1953, "Anisotropic Elasticity with Applications to Dislocation Theory," *Act. Met.*, Vol. 1, pp. 251–259.

Hirth, J. P., and Lothe, J., 1982, *Theory of Dislocations*, McGraw-Hill, N.Y.

Hwu, C., 1993, "Fracture Parameters for Orthotropic Bimaterial Interface Cracks," *Engn. Frat. Mech.*, Vol. 45, pp. 89–97.

Hwu, C., and Ting, T. C. T., 1989, "Two-Dimensional Problems of an Anisotropic Elastic Solid with an Elliptic Inclusion," *Q. J. Mech. Appl. Math.*, Vol. 42, pp. 553–572.

Hwu, C., and Yen, W. J., 1993, "On Anisotropic Elastic Inclusions in Plane Elastostatics," ASME JOURNAL OF APPLIED MECHANICS, Vol. 60, pp. 626–632.

Lekhnitskii, S. G., 1963, *Theory of Elasticity of an Anisotropic Body*, Holden-Day, San Francisco, CA.

Muskhelishvili, N. I., 1954, *Some Basic Problem of the Mathematical Theory of Elasticity*, Noordhoff Pub., Groningen, The Netherlands.

Patton, E. M., and Santare, M. H., 1990, "The Effect of a Rigid Elliptical Inclusion on a Straight Crack," *Int. J. Fracture*, Vol. 46, pp. 71–79.

Santare, M. H., and Keer, L. M., 1986, "Interaction Between an Edge Dislocation and a Rigid Elliptical Inclusion," ASME JOURNAL OF APPLIED MECHANICS, Vol. 53, pp. 382–385.

Stagni, L., and Lizzio, R., 1983, "Shape Effects in the Interaction Between an Edge Dislocation and an Elliptic Inhomogeneity," *Appl. Phys. A*, Vol. 30, pp. 217–221.

Stroh, A. N., 1958, "Dislocations and Cracks in Anisotropic Elasticity," *Phil. Mag.*, Vol. 7, pp. 625–646.

Suo, Z., 1990, "Singularities, Interfaces and Cracks in Dissimilar Anisotropic Media," *Proc. R. Soc. Lond.*, Vol. A427, pp. 331–358.

Ting, T. C. T., 1988, "Some Identities and the Structure of N_i in the Stroh Formalism of Anisotropic Elasticity," *Q. Appl. Math.*, Vol. 46, pp. 109–120.

Ting, T. C. T., and Hwu, C., 1988, "Sextic Formalism in Anisotropic Elasticity for Almost Non-semisimple Matrix N," *Int. J. Solids Structures*, Vol. 24, pp. 65–76.

Warren, W. E., 1983, "The Edge Dislocation Inside an Elliptical Inclusion," *Mech. Materials*, Vol. 2, pp. 319–330.

APPENDIX

By using the general solution given in (8) and the expression for $\mathbf{f}_2(\zeta)$ given in (10), the traction continuity condition of (7) leads to

$$\mathbf{B}_1\mathbf{f}_1(\sigma) + \overline{\mathbf{B}}_1\overline{\mathbf{f}_o(\sigma)} - \sum_{k=1}^{\infty}\{\overline{\mathbf{B}}_2\bar{\mathbf{c}}_k + \mathbf{B}_1\boldsymbol{\Gamma}_k^*\mathbf{c}_k\}\sigma^{-k} = -\overline{\mathbf{B}\mathbf{f}_1(\sigma)} - \mathbf{B}_1\mathbf{f}_o(\sigma) + \sum_{k=1}^{\infty}\{\mathbf{B}_2\mathbf{c}_k + \overline{\mathbf{B}}_2\overline{\boldsymbol{\Gamma}}_k^*\bar{\mathbf{c}}_k\}\sigma^k, \quad \text{(A1)}$$

where $\sigma = e^{i\psi}$ is a point on the unit circle $|\zeta| = 1$. Base upon Eq. (A1) and the property of holomorphic function, we may now introduce a function which is holomorphic in the entire domain including the interface boundary, i.e.,

$$\theta(\zeta) = \begin{cases} \mathbf{B}_1\mathbf{f}_1(\zeta) + \overline{\mathbf{B}}_1\overline{\mathbf{f}_o(1/\bar{\zeta})} \\ \quad - \sum_{k=1}^{\infty}\{\overline{\mathbf{B}}_2\bar{\mathbf{c}}_k + \mathbf{B}_2\boldsymbol{\Gamma}_k^*\mathbf{c}_k\}\zeta^{-k}, & \zeta \in S_1 \\ -\overline{\mathbf{B}}_1\overline{\mathbf{f}_1(1/\bar{\zeta})} - \mathbf{B}_1\mathbf{f}_o(\zeta) \\ \quad + \sum_{k=1}^{\infty}\{\mathbf{B}_2\mathbf{c}_k + \overline{\mathbf{B}}_2\overline{\boldsymbol{\Gamma}}_k^*\bar{\mathbf{c}}_k\}\zeta^k, & \zeta \in S_2 + S_o \end{cases} \quad \text{(A2)}$$

where S_o denotes the region inside a circle of radius $\sqrt{m_\alpha}$ and $\sqrt{m_\alpha}$ is the modulus of the critical point ζ_α^o (Hwu and Yen, 1993). Since $\theta(\zeta)$ is now holomorphic and single valued in the whole plane including the point at infinity, by Liouville's theo-

Downloaded 03 May 2010 to 171.66.16.20. Redistribution subject to ASME license or copyright; see http://www.asme.org/terms/Terms_Use.cfm

rem we have $\theta(\zeta) = \text{constant}$. However, constant function $\mathbf{f}$ corresponds to rigid-body motion which may be neglected. Therefore, $\theta(\zeta) \equiv \mathbf{0}$. With this result, Eq. (A2) leads to

$$\sum_{k=1}^{\infty} \{\overline{\mathbf{B}}_2 \bar{\mathbf{c}}_k + \mathbf{B}_2 \boldsymbol{\Gamma}_k^* \mathbf{c}_k\} \zeta^{-k} = \mathbf{B}_1 \mathbf{f}_1(\zeta) + \overline{\mathbf{B}}_1 \bar{\mathbf{f}}_o(1/\zeta), \quad \zeta \in S_1,$$

$$\sum_{k=1}^{\infty} \{\mathbf{B}_2 \mathbf{c}_k + \overline{\mathbf{B}}_2 \overline{\boldsymbol{\Gamma}}_k^* \bar{\mathbf{c}}_k\} \zeta^{k} = \overline{\mathbf{B}}_1 \bar{\mathbf{f}}_1(1/\zeta) + \mathbf{B}_1 \mathbf{f}_o(\zeta), \quad \zeta \in S_2 + S_o. \tag{A3}$$

Similarly, the displacement continuity condition $\mathbf{u}_1 = \mathbf{u}_2$ provides

$$\sum_{k=1}^{\infty} \{\overline{\mathbf{A}}_2 \bar{\mathbf{c}}_k + \mathbf{A}_2 \boldsymbol{\Gamma}_k^* \mathbf{c}_k\} \zeta^{-k} = \mathbf{A}_1 \mathbf{f}_1(\zeta) + \overline{\mathbf{A}}_1 \mathbf{f}_o(1/\zeta), \quad \zeta \in S_1,$$

$$\sum_{k=1}^{\infty} \{\mathbf{A}_2 \mathbf{c}_k + \overline{\mathbf{A}}_2 \overline{\boldsymbol{\Gamma}}_k^* \bar{\mathbf{c}}_k\} \zeta^{k} = \overline{\mathbf{A}}_1 \bar{\mathbf{f}}_1(1/\zeta) + \mathbf{A}_1 \mathbf{f}_o(\zeta), \quad \zeta \in S_1 + S_o. \tag{A4}$$

Cancellation of $\mathbf{f}_1(\zeta)$ between (A3) and (A4) leads to

$$\mathbf{f}_o(\zeta) = \frac{1}{2} \sum_{k=1}^{\infty} \mathbf{A}_1^{-1} \mathbf{H}_1 \{(\overline{\mathbf{M}}_1 + \mathbf{M}_2) \mathbf{A}_2 \mathbf{c}_k + (\overline{\mathbf{M}}_1 - \overline{\mathbf{M}}_2) \overline{\mathbf{A}}_2 \overline{\boldsymbol{\Gamma}}_k^* \bar{\mathbf{c}}_k\} \zeta^k. \tag{A5}$$

Expressing $\mathbf{f}_o(\zeta)$ shown in Eq. (8*c*) by Taylor's series expansion and comparing the coefficients of corresponding terms in Eq. (A5), the unknown constants $\mathbf{c}_k$ may then be determined as those shown in Eqs. (11*b*,*c*). Having the solution of $\mathbf{c}_k$, function $\mathbf{f}_1(\zeta)$ can now be obtained from $(A3)_1$ or $(A4)_1$ with the understanding that the subscript of ζ in (A3) or (A4) are dropped. Once the solution of $\mathbf{f}_1(\zeta)$ is obtained from $(A3)_1$ or $(A4)_1$, a replacement of ζ_1, ζ_2, or ζ_3 should be made for each component function. The results of $\mathbf{f}_1(\zeta)$ and $\mathbf{f}_2(\zeta)$ are shown in Eq. (11*a*).

Downloaded 03 May 2010 to 171.66.16.20. Redistribution subject to ASME license or copyright; see http://www.asme.org/terms/Terms_Use.cfm

Norio Hasebe

Takuji Nakamura

Department of Civil Engineering,
Nagoya Institute of Technology,
Gokiso-cho, Showa-ku,
Nagoya 466, Japan

Yoshihiro Ito

Nagoya City Government,
Sannomaru 1,
Naka-ku, Nagoya 460, Japan

Analysis of the Second Mixed Boundary Value Problem for a Thin Plate

The second mixed boundary value problem is solved by the classical theory of thin plate bending. The mixed boundary consists of a boundary (M) *on which one respective component of external force and deflective angle are given, and on the remaining boundary the external forces are given. The boundary* (M) *is straight and the remaining boundary is arbitrary configuration. A closed solution is obtained. Complex stress functions and a rational mapping function are used. A half-plane with a crack is analyzed under a concentrated torsional moment. Stress distributions before and after the crack initiation, and stress intensity factors are obtained for from short to long cracks and for some Poisson's ratio.*

Introduction

Many analyses have been carried out for the bending problem of a thin plate by using the classical theory. It neglects transverse shear deformation. Many of them have been solved as an external force boundary value problem. Comparing this problem, analytical solutions of the mixed boundary value problem seem to be few. The problem is solved under the following boundary conditions: two components of the external force are given on a part of the boundary and two components of the displacement are given on the remaining boundary (Hasebe, 1984; Hasebe, et al., 1990).

In the present paper, a problem is analyzed under the following boundary conditions: one respective component of the external force and displacement are given on a part of the boundary (called boundary M) and two components of the external force are given on the remaining part (called boundary L).

However, a general solution of the problem seems not to have been obtained for arbitrary shapes, except for the solution of trigonometric series for rectangular plates with simply supported edges (Timoshenko and Woinowsky-Krieger, 1959). A problem of this type could be called the second mixed boundary value problem. Although the analysis of this problem is mathematically difficult, the analytical solution can be obtained in a closed form if M forms a straight boundary.

The first purpose presented in this paper is to obtain a general solution for the second mixed boundary value problem. A rational mapping function and complex stress functions are used for the analysis. The mapping function is used to obtain a solution for relatively general shapes and has the form of a sum of fractional expressions. The solution can also be used for the analysis of the symmetric shape by cutting on the symmetric axis which is regarded to be boundary M.

The second purpose is to analyze a problem of a half-plane with a simple support of the straight boundary and with a crack at an end of the simple support. The loading is a concentrated torsional moment at infinity. Stress distributions and stress intensity factors are obtained. This is a model of the shape shown in Fig. 2(*b*). This is also a model of two half-planes bonded in the finite length and with cracks at one end of the interface. Referring to the crack problem, this kind of analysis seems not to have been carried out (Murakami et al., 1987; Tada, 1973; Sih, 1973).

Mapping Function

As shown in Fig. 1, a mapping function that maps a half-plane with a vertical edge crack into a unit circle is obtained by the Schwarz-Christoffel's transformation.

$$z = -ib\sqrt{2}\,\frac{\sqrt{1+\zeta^2}}{1-\zeta}+\frac{a}{2} \tag{1}$$

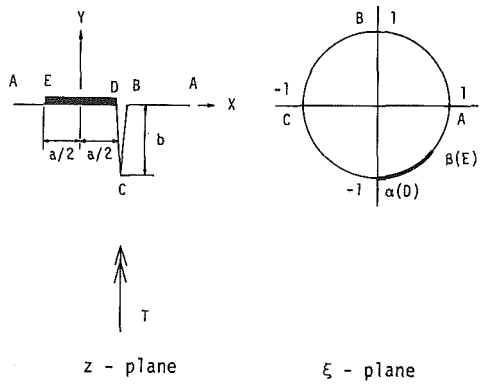


Fig. 1 Half-plane with an edge crack and the unit circle

Contributed by the Applied Mechanics Division of THE AMERICAN SOCIETY OF MECHANICAL ENGINEERS for publication in the ASME JOURNAL OF APPLIED MECHANICS.

Discussion on this paper should be addressed to the Technical Editor, Professor Lewis T. Wheeler, Department of Mechanical Engineering, University of Houston, Houston, TX 77204-4792, and will be accepted until four months after final publication of the paper itself in the ASME JOURNAL OF APPLIED MECHANICS.

Manuscript received by the ASME Applied Mechanics Division, June 11, 1991; final revision, Aug. 20, 1993. Associate Technical Editor: X. Markenscoff.

Copyright © 1994 by ASME

Downloaded 03 May 2010 to 171.66.16.20. Redistribution subject to ASME license or copyright; see http://www.asme.org/terms/Terms_Use.cfm

Table 1 Values of α_j and A_j in (2)

α_j	A_j	α_j	A_j
0.999 937 616 8	0.000 000 326 7	0.999 711 942 8	0.000 001 904 2
0.999 060 031 4	0.000 010 533 7	0.997 246 896 4	0.000 047 030 3
0.992 095 261 8	0.000 243 055 8	0.977 955 360 9	0.001 056 391 8
0.940 245 041 9	0.005 075 702 3	0.849 933 775 8	0.019 684 593 6
0.184 862 659 8	0.812 698 456 4	0.022 209 618 8	8.365 866 989 8
0.682 810 847 8	0.066 864 442 0	0.438 995 711 7	0.217 466 863 5

where a is the length of M and b is the crack length. Points α and β on the unit circle correspond to points D and E on the half-plane, respectively (see Fig. 1). Ratios a/b and b/a can be varied with a value of β.

Equation (1) is expressed as the following rational function in the form of a sum of fractional expressions (Hasebe, 1984):

$$z=\omega(\zeta)=\frac{-ib\sqrt{2}}{1-\zeta}\left[1+\sum_{j=1}^{12}\left(\frac{-A_j}{1+\alpha_j\zeta^2}+A_j\right)\right]+\frac{a}{2}$$

$$=\frac{E_0}{1-\zeta}+\sum_{k=1}^{n}\frac{E_k}{\zeta_k-\zeta}+E_c \tag{2}$$

where $n = 24$ is used in the present paper. If the half-plane occupies $y < 0$, then E_0 is a pure imaginary number. The method of obtaining A_j and α_j was described by Hasebe and Inohara (1980) and their values are contained in Table 1. The tip of the crack and points B and D have roundness, because (2) is a rational function. The radius of curvature ρ at the crack tip is small enough as $\rho/b = 0.7806 \times 10^{-13}$. The roundness at points B and D is $\rho/b = 0.00625$, and thus the value is also very small and can be considered as sharp corners.

Complex Stress Functions

Complex stress functions $\phi(\zeta)$ and $\psi(\zeta)$ for the thin plate are considered and they are regular inside of the unit circle. Using these functions, bending moments M_x and M_y, torsional moment M_{xy}, and shearing forces Q_x and Q_y are given as follows (Savin, 1961):

$$M_x+M_y=-4D(1+\nu)\mathrm{Re}\left[\frac{\phi'(\zeta)}{\omega'(\zeta)}\right] \tag{3a}$$

$$M_y-M_x+2iM_{xy}=2D(1-\nu)\frac{1}{\omega'(\zeta)}\left[\overline{\omega(\zeta)}\left\{\frac{\phi'(\zeta)}{\omega'(\zeta)}\right\}'+\psi'(\zeta)\right] \tag{3b}$$

$$Q_x-iQ_y=-4D\left[\frac{\phi'(\zeta)}{\omega'(\zeta)}\right]'\Big/\omega'(\zeta) \tag{3c}$$

where Re[•] is the real part of [•], and flexural rigidity D is $D = Eh^3/[12(1 - \nu^2)]$ in which E is Young's modulus, ν is Poisson's ratio, and h is the thickness of the plate.

Components of stress in (3) are rewritten with curvilinear coordinates, which are represented by the mapping function.

$$M_r+M_\theta=M_x+M_y \tag{4a}$$

$$M_\theta-M_r+2iM_{r\theta}=e^{2i\gamma}(M_y-M_x+2iM_{xy}) \tag{4b}$$

$$Q_r-iQ_\theta=e^{i\gamma}(Q_x-iQ_y) \tag{4c}$$

where $e^{i\gamma} = \zeta\omega'(\zeta)/|\zeta\omega'(\zeta)|$.

The external forces for the bending moment and the equivalent shearing force on the boundary are expressed as follows:

$$-\kappa\phi(\sigma)+\frac{\omega(\sigma)}{\overline{\omega'(\sigma)}}\overline{\phi'(\sigma)}+\overline{\psi(\sigma)}=\frac{1}{D(1-\nu)}\int[m(z)+i\int p(s)ds]dz \tag{5}$$

where $\kappa = (3 + \nu)/(1 - \nu)$, $\sigma = \zeta$ on the unit circle and $m(z)$ and $p(s)$ are the bending moment and the equivalent shearing force, respectively, per unit length along the boundary s.

The first derivatives of the deflection, i.e., the deflective angles are expressed as follows:

$$\phi(\sigma)+\frac{\omega(\sigma)}{\overline{\omega'(\sigma)}}\overline{\phi'(\sigma)}+\overline{\psi(\sigma)}=\frac{\partial w}{\partial x}+i\frac{\partial w}{\partial y} \tag{6}$$

where w is the deflection.

The stress function $\psi(\zeta)$ is given by analytic continuation for a traction-free boundary (Muskhelishvili, 1963),

$$\psi(\zeta)=\kappa\overline{\phi(1/\bar{\zeta})}-\frac{\overline{\omega(1/\bar{\zeta})}}{\omega'(\zeta)}\phi'(\zeta). \tag{7}$$

When ζ approaches σ on the unit circle, (7) becomes

$$\psi(\sigma)=\kappa\overline{\phi^-(\sigma)}-\frac{\overline{\omega(\sigma)}}{\omega'(\sigma)}\phi'^+(\sigma) \tag{8}$$

where $\phi^-(\sigma)$ denotes the value on the boundary approached from the outside region S^- and $\phi^+(\sigma)$ denotes the value from the inside region S^+ (see Fig. 1). On the unit circle, $\sigma = 1/\bar{\sigma}$. As the boundary condition, $m(s)$ and $\partial w/\partial x$ are given on M (DE), and $m(s)$ and $p(s)$ are given on L ($EABCD$). The external force boundary condition on L is obtained by substituting (8) in (5),

$$\phi^+(\sigma)-\phi^-(\sigma)=-\frac{1}{\kappa(1-\nu)D}\int_L[m(z)+i\int p(s)ds]dz.$$

$$\equiv f_L(\sigma) \tag{9}$$

Next, the external force boundary condition on M is obtained:

$$\phi^+(\sigma)-\phi^-(\sigma)=-\frac{1}{\kappa(1-\nu)D}\int_M[m(x)+i\int p(s)ds]dx \tag{10}$$

in which $dz = dx$, because M coincides with the x-axis. If (10) and its conjugate expression are added and the unknown $p(s)$ is eliminated from (10), the following equation is obtained:

$$[\phi^+(\sigma)-\phi^-(\sigma)]+[\overline{\phi^+(\sigma)}-\overline{\phi^-(\sigma)}]=-\frac{2}{\kappa(1-\nu)D}\int_M m(x)dx$$

$$\equiv N(\sigma). \tag{11}$$

Further, the displacement boundary condition is obtained by substituting (8) in (6) and then eliminating $\partial w/\partial y$ as follows:

$$[\phi^+(\sigma)+\kappa\phi^-(\sigma)]+[\overline{\phi^+(\sigma)}+\kappa\overline{\phi^-(\sigma)}]=2\frac{\partial w}{\partial x}$$

$$\equiv L(\sigma). \tag{12}$$

Equation (11) is expressed as follows:

$$\theta^+(\sigma)-\theta^-(\sigma)=N(\sigma) \tag{13}$$

where

$$\theta(\zeta)=\phi(\zeta)-\overline{\phi(1/\bar{\zeta})}. \tag{14}$$

The general solution of (13) is given by the following expression (Muskhelishvili, 1963):

$$\theta(\zeta)=\frac{1}{2\pi i}\int_M\frac{N(\sigma)}{\sigma-\zeta}d\sigma+R(\zeta)$$

$$\equiv M(\zeta)+R(\zeta) \tag{15}$$

Downloaded 03 May 2010 to 171.66.16.20. Redistribution subject to ASME license or copyright; see http://www.asme.org/terms/Terms_Use.cfm

where $R(\zeta)$ is an arbitrary rational function. Using (14) and (15),

$$\overline{\phi^-(\sigma)} = \phi^+(\sigma) - M^+(\sigma) - R(\sigma) \tag{16a}$$

$$\overline{\phi^+(\sigma)} = \phi^-(\sigma) - M^-(\sigma) - R(\sigma). \tag{16b}$$

Substituting (16) in (12), the following boundary condition on M is obtained:

$$\phi^+(\sigma) + \phi^-(\sigma) = \frac{1}{\kappa+1}[L(\sigma) + \kappa M^+(\sigma) + M^-(\sigma)] + R(\sigma)$$

$$\equiv f_M(\sigma) + R(\sigma). \tag{17}$$

Therefore, the problem has been reduced to a Riemann-Hilbert problem to find $\phi(\zeta)$, where $\phi(\zeta)$ has to satisfy (9) on L and (17) on M, respectively. The solution is obtained as follows (Muskhelishvili, 1963):

$$\phi(\zeta) = H(\zeta) + \frac{\chi(\zeta)}{2\pi i}\int_M \frac{R(\sigma)}{\chi(\sigma)(\sigma-\zeta)}\,d\sigma + Q(\zeta)\chi(\zeta) \tag{18}$$

where

$$H(\zeta) = \frac{\chi(\zeta)}{2\pi i}\int_L \frac{f_L(\sigma)}{\chi(\sigma)(\sigma-\zeta)}\,d\sigma + \frac{\chi(\zeta)}{2\pi i}\int_M \frac{f_M(\sigma)}{\chi(\sigma)(\sigma-\zeta)}\,d\sigma \tag{19}$$

and $Q(\zeta)$ is an arbitrary rational function which is regular in S^+ and $\chi(\zeta)$ is a Plemelj function; $\chi(\zeta) = (\zeta-\alpha)^{0.5}(\zeta-\beta)^{0.5}$. The index of $\chi(\zeta)$ is selected according to the condition at D and E, that is, the continuity of displacements and the discontinuity of stresses. Since $\chi(\zeta)$ is a multivalued function, the branch $\chi(\zeta)/\zeta \to 1$ is chosen for $\zeta \to \infty$.

The function $R(\zeta)$ is determined from now and is assumed as a sum of two kinds of regular terms in S^+ and S^-, respectively,

$$R(\zeta) = \sum_k \frac{C_{1k}}{\zeta_{1k}-\zeta} + \sum_k \frac{C_{2k}}{\zeta_{2k}-\zeta} \tag{20}$$

where $|\zeta_{1k}| > 1$, $|\zeta_{2k}| < 1$, C_{1k} and C_{2k} are undetermined complex coefficients.

Since poles with higher orders than the first finally become zero, (20) does not contain higher order terms (see (25)). Using (20), the integration in (18) is carried out as follows (Muskhelishvili, 1963):

$$\frac{\chi(\zeta)}{2\pi i}\int_M \frac{R(\sigma)}{\chi(\sigma)(\sigma-\zeta)}\,d\sigma = \frac{1}{2}\sum_k \frac{C_{1k}}{\zeta_{1k}-\zeta}\left[1-\frac{\chi(\zeta)}{\chi(\zeta_{1k})}\right] + \frac{1}{2}\sum_k \frac{C_{2k}}{\zeta_{2k}-\zeta}\left[1-\frac{\chi(\zeta)}{\chi(\zeta_{2k})}\right]. \tag{21}$$

The last term in (21) has no pole at points ζ_{2k} in S^+, since it has the limiting value: $[C_{2k}\chi'(\zeta_{2k})]/[2\chi(\zeta_{2k})]$ at $\zeta = \zeta_{2k}$. Similarly, the first term also has no pole at ζ_{1k} in S^-.

The function $Q(\zeta)$ in (18) is determined so that $\psi(\zeta)$ of (7) is regular in S^+. The last term in (7) is expanded in a Laurent series around $\zeta = 1/\bar{\zeta}_k \equiv \zeta_k'$

$$-\frac{\overline{\omega(1/\bar{\zeta})}}{\omega'(\zeta)}\phi'(\zeta) = \sum_{k=1}^n \frac{A_k\bar{B}_k\zeta_k'^2}{\zeta_k'-\zeta} + \text{regular part in } S^+ \tag{22}$$

where $B_k \equiv E_k/\overline{\omega'(\zeta_k')}$ are known and $A_k \equiv \phi'(\zeta_k')$ are undetermined coefficients.

Substituting (21) in (18), and using (7) and (22), $\psi(\zeta)$ is expressed as follows:

$$\psi(\zeta) = \kappa\overline{\chi(1/\bar{\zeta})Q(1/\bar{\zeta})} + \sum_{k=1}^n \frac{A_k\bar{B}_k\zeta_k'^2}{\zeta_k'-\zeta} + \text{regular part in } S^+ \tag{23}$$

In order for $\psi(\zeta)$ to be regular in S^+, the first and the second terms in (23) must cancel each other. Therefore, $Q(\zeta)$ is obtained as follows:

$$Q(\zeta) = \frac{1}{\kappa}\sum_{k=1}^n \frac{\bar{A}_kB_k}{\chi(\zeta_k)(\zeta_k-\zeta)}. \tag{24}$$

Substituting (21) and (24) in (18), and using (14), $\theta(\zeta)$ is expressed as follows:

$$\theta(\zeta) = M(\zeta) + R(\zeta) = H(\zeta) - \overline{H(1/\bar{\zeta})} + \frac{1}{2}\sum_k \frac{C_{1k}}{\zeta_{1k}-\zeta}\left[1-\frac{\chi(\zeta)}{\chi(\zeta_{1k})}\right] + \frac{1}{2}\sum_k \frac{\overline{C_{1k}}\zeta_{1k}'^2}{\zeta_{1k}'-\zeta}\left[1-\frac{\chi(\zeta)}{\chi(\zeta_{1k}')}\right] + \frac{1}{2}\sum_k \frac{C_{2k}}{\zeta_{2k}-\zeta}\left[1-\frac{\chi(\zeta)}{\chi(\zeta_{2k})}\right] + \frac{1}{2}\sum_k \frac{\overline{C_{2k}}\zeta_{2k}'^2}{\zeta_{2k}'-\zeta}\left[1-\frac{\chi(\zeta)}{\chi(\zeta_{2k}')}\right] + \frac{1}{\kappa}\sum_{k=1}^n \frac{\chi(\zeta)\bar{A}_kB_k}{\chi(\zeta_k)(\zeta_k-\zeta)} + \frac{1}{\kappa}\sum_{k=1}^n \frac{\chi(\zeta)A_k\bar{B}_k\zeta_k'^2}{\chi(\zeta_k')(\zeta_k'-\zeta)} + \text{const.} \tag{25}$$

where $\zeta_{1k}' \equiv 1/\overline{\zeta_{1k}}$ and $\zeta_{2k}' \equiv 1/\overline{\zeta_{2k}}$. Unknown coefficients in $R(\zeta)$ are determined to satisfy (25) identically. After the boundary condition is given, $H(\zeta)$ and $M(\zeta)$ are obtained. For the boundary condition in the present paper, $H(\zeta) - \overline{H(1/\bar{\zeta})} =$ constant (see (31) expressed later) and $M(\zeta) = 0$ because $m(s)$ is zero on M (see (11)). Then comparing coefficients and poles to satisfy (25) identically, C_{1k}, C_{2k}, ζ_{1k} and ζ_{2k} are determined and $R(\zeta)$ is obtained as follows:

$$R(\zeta) = \frac{1}{\kappa}\sum_{k=1}^n \left[\frac{\bar{A}_kB_k}{\zeta_k-\zeta} + \frac{A_k\bar{B}_k\zeta_k'^2}{\zeta_k'-\zeta}\right] \tag{26}$$

Finally $\phi(\zeta)$ is obtained as follows:

$$\phi(\zeta) = H(\zeta) + \frac{1}{2\kappa}\sum_{k=1}^n \left\{\frac{\bar{A}_kB_k}{\zeta_k-\zeta}\left[1+\frac{\chi(\zeta)}{\chi(\zeta_k)}\right] + \frac{A_k\bar{B}_k\zeta_k'^2}{\zeta_k'-\zeta}\left[1-\frac{\chi(\zeta)}{\chi(\zeta_k')}\right]\right\}. \tag{27}$$

Boundary Conditions

In the present paper, the following boundary conditions are considered: the external force does not apply on L; the concentrated torsional moment T applies at infinity and boundary M is rotated through an angle $\partial w/\partial x = \epsilon$.

Then, the boundary condition on L is

$$m(s) = 0 \qquad \text{on } L \tag{28a}$$

$$\int i\int p(s)\,ds\,dz = T \qquad \text{on } \widehat{ABCD} \text{ of } L \tag{28b}$$

$$= 0 \qquad \text{on } \widehat{EA} \text{ of } L \tag{28c}$$

and the boundary condition on M is

$$m(z) = 0 \tag{29a}$$

$$\frac{\partial w}{\partial x} = \epsilon. \tag{29b}$$

The concentrated torsional moment that applies at point A (at infinity) is in balance to the resultant torsional moment T on M. This moment corresponds to the reaction. The rotation ϵ on M is the same as the rigid rotation of the half-plane. Then, the rotation is independent of the stress that remains the same as that for $\epsilon = 0$. The boundary condition in (29) corresponds to that of the simple support. Thus, the boundary M is called a simple support for the boundary condition (29) hereafter.

Equations (9) and (17) are given for (28) and (29) as follows:

$$f_L(\sigma) = -\frac{iT}{\kappa(1-\nu)D} \text{ on } \widehat{ABCD} \text{ of } L \tag{30a}$$

$$= 0 \qquad \text{on } \widehat{EA} \text{ of } L \tag{30b}$$

$$f_M(\sigma) = 0 \qquad \text{on } M. \tag{30c}$$

Downloaded 03 May 2010 to 171.66.16.20. Redistribution subject to ASME license or copyright; see http://www.asme.org/terms/Terms_Use.cfm

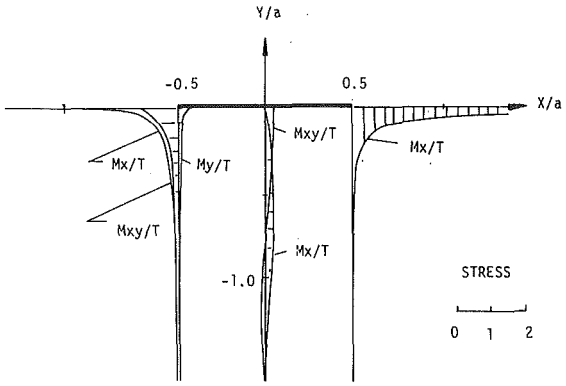


Fig. 2(*a*) Before the crack initiation ($\nu = 0.25$)

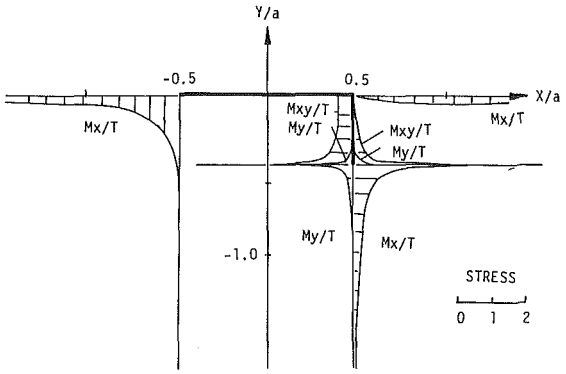


Fig. 2(*b*) After the crack initiation ($b/a = 0.4$, $\nu = 0.25$)

Fig. 2 Stress distributions

Substituting (30) in (19),

$$H(\zeta)=\frac{T}{\kappa(1-\nu)D}\frac{1}{2\pi}\log\frac{2\alpha\beta-\alpha-\beta+(2-\alpha-\beta)\zeta-2\chi(\zeta)\chi(1)}{1-\zeta} \tag{31}$$

and the first derivative $H'(\zeta)$ is given by the following simple expression:

$$H'(\zeta)=\frac{T}{2\pi\kappa(1-\nu)D}\frac{\chi(1)}{(1-\zeta)\chi(\zeta)}. \tag{32}$$

Stress Distributions

Figure 2(*a*) shows the stress distribution before the crack initiation ($b = 0$). In this case, the mapping function is used for $E_k = 0$ in (2). Thus, the stress function is $\phi(\zeta) = H(\zeta)$, because $B_k = 0$ in (27). Both ends of boundary M on the unit circle are $\alpha = -i$ and $\beta = \exp(-i\pi/4)$. In Fig. 2(*a*), the bending moments M_x and M_y, and the torsional moment M_{xy} are shown for $x/a = -0.5$, $x/a = 0$, and $x/a \geq 0.5$. The stress concentration occurs at both ends of the simple support, $x/a = \pm 0.5$. Thus, the crack initiation is anticipated at the ends of support. In Fig. 2(*b*), the stress distribution after the crack initiation is shown for the crack length $b/a = 0.4$. The stress has a square root singularity at points D and E before crack initiation. This singularity rises from the first derivative of Plemelj function included in the stress function $\phi(\zeta)$. The boundary condition satisfies Kirchhoff's assumption and thus the component of M_{xy} appears on the boundary. On the left surface of the crack, M_{xy}/T has the finite value at the end of the simple support and becomes negative infinite at the crack tip. On the right surface of the crack, M_{xy}/T has smaller value than that of left surface and becomes positive infinite at the crack tip. Thus the sign of M_{xy} changes at the crack tip. This fact is confirmed from the sign of torsional moment m_{xy} (see (34) expressed later) on the crack surfaces $\theta = \pi$ and $-\pi$ at the crack tip. We notice the difference of the stress distribution between the pre- and post-crack initiation. After the crack initiation, the stress components at point D have finite values. The first derivatives of $\phi(\zeta)$ has a square root singularity at point D ($\zeta = \alpha = -i$, see Fig. 1) because of Plemelj function. However, the mapping function (see (1)) has zero of square root at $\zeta = -i$ and thus $\omega'(\zeta)$ has a square root singularity. Therefore, we notice from (3*a*, *b*) and (8) that the stress components have finite values as a limit at $\zeta = -i$.

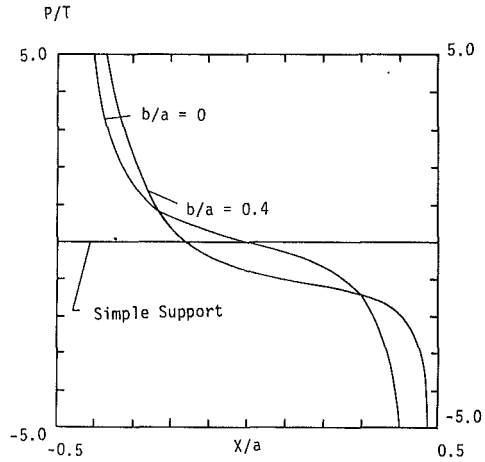


Fig. 3 Stress distributions of an equivalent shear force on the simple support ($b/a = 0$ and 0.4)

Figure 3 shows the distributions of equivalent shearing force p on the simple support before and after the crack initiation. Before the crack initiation, p/T is symmetric with respect to the origin. p/T increases as x/a approaches nearer to the end of support and becomes infinite. p has the same singularity as shearing force Q_x and Q_y. Therefore, p becomes infinite at points D and E with a singularity of $r^{-3/2}$ where r is the length from the singular point. This singularity arises due to the classical plate theory, in which the integration of the equivalent shearing force p (see (5)) has the singularity of the square root. However, after the crack initiation, the singularity at point D becomes a square root singularity due to the mapping function (see (3*c*)). After the crack initiation, p/T is unsymmetric and the point of $p = 0$ moves to the negative direction from the origin.

Stress Intensity Factors

In the vicinity of the crack tip, bending moments m_x and m_y, and torsional moment m_{xy} are expressed as follows (Sih et al., 1962; Isida, 1977; Hasebe and Inohara, 1980):

$$m_x+m_y=\frac{2}{\sqrt{2r}}\left(k_B\cos\frac{\theta}{2}-k_S\sin\frac{\theta}{2}\right) \tag{34a}$$

$$m_y-m_x+2im_{xy}=\frac{1}{2(1+\nu)\sqrt{2r}}\{[(7+\nu)k_B+i(5+3\nu)k_S]e^{-i\theta/2}+(1-\nu)(k_B-ik_S)e^{-5i\theta/2}\} \tag{34b}$$

where r and θ are polar coordinates with the origin at the crack tip; k_B and k_S are the stress intensity factors for the bending and torsional moments, respectively. The stress intensity factors k_B and k_S are calculated by the stress function $\phi(\zeta)$ and the mapping function $\omega(\zeta)$ as follows:

$$k_B-ik_S=-2D(1+\nu)e^{-i\delta/2}\frac{\phi'(\zeta_0)}{\sqrt{\omega''(\zeta_0)}} \tag{35}$$

where δ is an angle between a crack and x-axis, and ζ_0 is the coordinate on the unit circle corresponding to the crack tip. In the present paper, $\delta = -\pi/2$ and $\zeta_0 = -1$. As mentioned

Downloaded 03 May 2010 to 171.66.16.20. Redistribution subject to ASME license or copyright; see http://www.asme.org/terms/Terms_Use.cfm

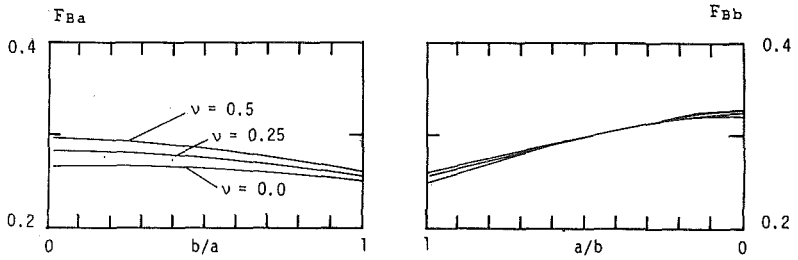


Fig. 4(*a*) Bending mode

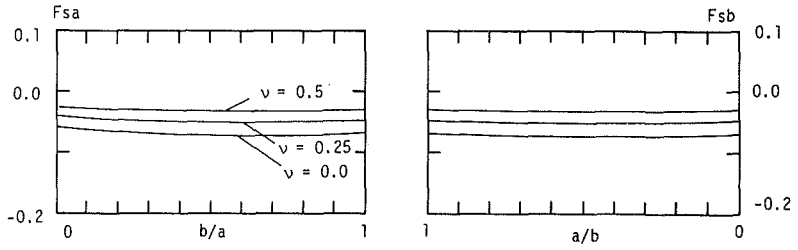


Fig. 4(*b*) Shearing mode

Fig. 4 Nondimensional stress intensity factors

Table 2 Nondimensional Stress Intensity Factors for Bending Mode and Shearing Mode

	Bending Mode			Shearing Mode		
	ν = 0.0	0.25	0.5	ν = 0.0	0.25	0.5
b/a = 0.0001	0.2655	0.2818	0.2957	−0.0525	−0.0356	−0.0217
0.001	0.2655	0.2818	0.2957	−0.0525	−0.0357	−0.0217
0.010	0.2656	0.2819	0.2957	−0.0530	−0.0360	−0.0219
0.100	0.2660	0.2818	0.2953	−0.0575	−0.0392	−0.0239
0.200	0.2662	0.2810	0.2939	−0.0617	−0.0421	−0.0258
0.300	0.2658	0.2796	0.2915	−0.0649	−0.0445	−0.0273
0.400	0.2648	0.2774	0.2883	−0.0672	−0.0461	−0.0283
0.500	0.2633	0.2745	0.2843	−0.0685	−0.0471	−0.0290
0.600	0.2612	0.2711	0.2797	−0.0690	−0.0474	−0.0292
0.700	0.2586	0.2672	0.2748	−0.0689	−0.0473	−0.0292
0.800	0.2555	0.2629	0.2695	−0.0682	−0.0469	−0.0289
0.900	0.2520	0.2583	0.2641	−0.0671	−0.0461	−0.0284
1.000	0.2483	0.2537	0.2586	−0.0658	−0.0452	−0.0279
a/b = 0.900	0.2571	0.2618	0.2662	−0.0677	−0.0465	−0.0287
0.800	0.2663	0.2703	0.2740	−0.0694	−0.0476	−0.0294
0.700	0.2760	0.2789	0.2820	−0.0708	−0.0486	−0.0299
0.600	0.2858	0.2877	0.2899	−0.0719	−0.0493	−0.0304
0.500	0.2954	0.2962	0.2975	−0.0725	−0.0497	−0.0306
0.400	0.3046	0.3042	0.3045	−0.0725	−0.0497	−0.0306
0.300	0.3127	0.3112	0.3106	−0.0720	−0.0493	−0.0303
0.200	0.3193	0.3167	0.3154	−0.0710	−0.0486	−0.0299
0.100	0.3238	0.3204	0.3185	−0.0699	−0.0478	−0.0294
0.050	0.3251	0.3214	0.3193	−0.0694	−0.0475	−0.0292
0.000	0.3257	0.3218	0.3196	−0.0691	−0.0473	−0.0291

in the section of mapping function, the crack tip has roundness, but it is very small. Therefore, there is no problem to calculate the stress intensity factors for accuracy.

The following nondimensional stress intensity factors are used:

$$F_{Ba}+iF_{Sa}=\frac{3+\nu}{1+\nu}\frac{(k_B+ik_S)\sqrt{a}}{T};\quad 0\le\frac{b}{a}\le 1 \tag{36}$$

$$F_{Bb}+iF_{Sb}=\frac{3+\nu}{1+\nu}\frac{(k_B+ik_S)\sqrt{b}}{T};\quad 0\le\frac{a}{b}\le 1. \tag{37}$$

Figures 4 and 5 and Table 2 contain these values versus b/a and a/b for three values of Poisson's ratio; ν = 0, 0.25, and 0.5. The values F_{Sa} and F_{Sb} are smaller than F_{Ba} and F_{Bb}. The value of F_{Ba} becomes large as ν becomes large, and decreases as b/a increases. The limit values of F_{Ba} and F_{Sa} exist for $b/a \to 0$.

Conclusions

The second mixed boundary value problem was solved for the thin plate bending. A closed solution was obtained. The geometry of the plate is arbitrary, except that the boundary M is straight. The boundary M expressed by a rational function is not completely straight and thus the boundary condition on M is approximately satisfied. However, there is no problem to obtain stress components because of the good accuracy of the rational function (2). The half-plane with an edge crack was analyzed for the simply supported boundary M [$m(z) = \partial w/\partial x = 0$], and a concentrated torsional moment T was applied on the half-plane. The mapping function for relatively general shapes can be made in the form of (2). For example, an oblique edge crack problem can be analyzed by using the mapping function of Hasebe and Inohara (1980). Since the limit value of stress intensity factor exists for the situation $b/a \to 0$, the crack propagation can be arrested by taking the fracture toughness value of a thin plate larger than the limit value.

References

Hasebe, N., and Inohara, S., 1980, "Stress Analysis of a Semiinfinite Plate with an Oblique Edge Crack," *Ingenieur Archiv.*, Springer-Verlag, Berlin, Vol. 49, pp. 51–62.

Hasebe, N., 1984, "Mixed Boundary Value Problem of Plate with Crack," *J. Eng. Mech.*, ASCE, Vol. 110, No. 1, pp. 37–48.

Hasebe, N., Miwa, M., and Nakamura, T., 1990, "A Mixed Boundary Value Problem of a Strip with a Crack Under Concentrated Bending and Torsional Moments," *Proc. of Japan Soc. of Civil Engineers*, No. 416, pp. 395–405 (in Japanese).

Isida, M., 1977, *Plate and Shells With Cracks*, by G. C. Sih, ed., Noordhoff, Leyden, Netherlands, Chapter 1.

Murakami, Y., et al., 1987, *Stress Intensity Factors Handbook*, Pergamon Press, Oxford, U.K.

Muskhelishvili, N. I., 1963, *Some Basic Problems of Mathematical Theory of Elasticity*, 2nd ed., Noordhoff, Leyden, Netherlands.

Savin, G. N., 1961, *Stress Concentration Around Holes*, 1st ed., Pergamon Press, Oxford, U.K.

Sih, G. C., Paris, P. C., and Erdogan, F., 1962, "Crack-Tip Stress Intensity Factors for Plane Extension and Plate Bending Problem," ASME JOURNAL OF APPLIED MECHANICS, Vol. 29, pp. 306–312.

Sih, G. C., 1973, *Handbook of Stress Intensity Factors*, Lehigh University, Pennsylvania.

Timoshenko, S., and Woinowsky-Krieger, S., 1959, *Theory of Plates and Shells*, 2nd ed., McGraw-Hill, New York.

Tada, H., 1973, *The Stress Analysis of Cracks Handbook*, Del Research Corporation, Pennsylvania.

Downloaded 03 May 2010 to 171.66.16.20. Redistribution subject to ASME license or copyright; see http://www.asme.org/terms/Terms_Use.cfm

Crack Propagation at and Near Bimaterial Interfaces: Linear Analysis[1]

P. H. Geubelle
Graduate Student.

W. G. Knauss
Professor of Aeronautics and Applied Mechanics.

California Institute of Technology, Pasadena, CA 91125

The problem of the growth of a crack located at the interface between two linearly elastic solids is considered when conditions promoting propagation along and/or away from the interface prevail. Both a stress and a maximum energy release rate criterion are examined. It is found that in contrast to the corresponding problem for crack growth in homogeneous solids, no unique propagation direction results when continuum considerations prevail alone. Uniqueness is established only upon invoking a presumably material dictated minimum crack extension size. The result for this linearized analysis are compared with experimental observations on kink fracture involving two elastomers of small strain capabilities.

1 Introduction

Although long-standing problems of adhesion mechanics have required consideration of failure and fracture at and near interfaces, it was only the advent of composite materials and the improved understanding of fracture in nonmonolithic solids which motivated a widespread interest in interfacial fracture studies. In addition, the need to better understand the failure characteristics of layered systems such as epitaxial layers of semiconductors in the electronics industry and electronic packaging in general require the same technology base for failure prediction and prevention. The early, geology-prompted discovery by Williams (1959) of the general differences between the stress field at the tip of a crack in a homogeneous, linearly elastic solid and that at an interface between two elastic solids established the odd oscillatory character of the stress field. Although this local crack-tip stress field has been confirmed repeatedly in the sequel (Rice and Sih, 1965, England, 1965, Erdogan, 1965), the physical reason for this behavior or its nonphysical aspects of material interpenetration along the crack plane have not been explained satisfactorily to this day. Various ways have been proposed to resolve this problem: some have eliminated the oscillatory term by postulating a frictionless contact zone (Comninou, 1977a, 1977b; Gautesen and Dundurs, 1987, 1988), by relinquishing the hypotheses of infinitesimal deformations (Knowles and Sternberg, 1983, Ravichandran and Knauss, 1989, Hermann, 1989) or by introducing a transition layer (Yang and Shih, 1990). Others (Shih and Asaro, 1988, 1989; Shih, 1991) have used a numerical plasticity model to compute the detailed stress and deformation fields at the crack-tip: the mere addition of nonlinear material response apparently did not eliminate the inconsistency although the region in which the oscillations occurred was now reduce still more below physically acceptable (atomic) dimensions. But the more widely used approach to deal with this problem for some engineering applications is the concept of small-scale contact (Rice, 1988) which essentially ignores its presence on the basis of its usually very small size.

The linearly elastic bimaterial asymptotic solution has other features which distinguish it from its homogeneous counterpart, most of which have been underlined by Rice (1988). Among these is the lack of self-similarity of the singular crack-tip expansion field. As illustrated by Symington (1987), the bimaterial situation leads to "rotational stress and deformation fields," at the crack-tip, which not only result in the stress and displacement oscillations extremely close to the crack-tip, but also extend to a region far outside of the contact zone.

In the past, we have favored the viewpoint that the small zone of mechanical inconsistency may be simply ignored on the basis of the small physical extent and that the major role of the special stress field for interfacial cracks is characterized by the general mixity of stress intensity. We feel now that such is not strictly admissible as an approximation unless one provides also a suitable reasoning to do so, especially when such an "approximation" leads to inconsistency in terms of what is accepted as normal in the fracture of homogeneous bodies. The implication of this statement will become clear.

It is the purpose of this paper to outline the effect of the stress field rotation at the crack-tip on criteria to determine the orientation of crack propagation when the latter moves along or kinks away from the interface, thus amplifying on the results of He and Hutchinson (1989). We show below that, in contrast to the case of fracture in a homogeneous body, the determination of kink direction from an interface cannot be

[1]This is the written version of an identically titled presentation given in March of 1991 at a symposium at the California Institute of Technology in honor of J. K. Knowles's 60th birthday.

Contributed by the Applied Mechanics Division of THE AMERICAN SOCIETY OF MECHANICAL ENGINEERS for publication in the ASME JOURNAL OF APPLIED MECHANICS.

Discussion on this paper should be addressed to the Technical Editor, Professor Lewis T. Wheeler, Department of Mechanical Engineering, University of Houston, Houston, TX 77204-4792, and will be accepted until four months after final publication of the paper itself in the ASME JOURNAL OF APPLIED MECHANICS.

Manuscript received by the ASME Applied Mechanics Division, Mar. 23, 1992; final revision, Nov. 12, 1992. Associate Technical Editor: M. E. Fourney.

Copyright © 1994 by ASME
Downloaded 03 May 2010 to 171.66.16.20. Redistribution subject to ASME license or copyright; see http://www.asme.org/terms/Terms_Use.cfm

accomplished uniquely without also specifying a fixed crack extension length, in agreement with the results of Mukai et al. (1990) who studied the effect of the kink length in the centered interfacial crack case. In the absence of such a length specification—as is the case in homogeneous fracture—the criteria of maximum circumferential stress (Erdogan and Sih, 1963) or the maximum energy release rate criterion (Palaniswamy and Knauss, 1978, Wu, 1978) cannot yield unique values for the kink angle.

The work is carried out numerically when closed-form analytical methods are too difficult. We make maximum use of the available analytical results to certify the requisite numerical precision. In the next section, we pass to the brief consideration of the Erdogan-Sih criterion and then deal in Section 3 with the energy release rate for the interface crack, followed in Section 4 by a condensed comparison of the results with some experimental data for this problem.

But before proceeding to further developments we summarize first the concepts and major notational conventions for later use. Following established notation, we use Dundur's mismatch parameters (Dundurs, 1969) defined as

$$\alpha=\frac{\mu_1(\kappa_2+1)-\mu_2(\kappa_1+1)}{\mu_1(\kappa_2+1)+\mu_2(\kappa_1+1)}=\frac{E_1'-E_2'}{E_1'+E_2'},$$
$$\beta=\frac{\mu_1(\kappa_2-1)-\mu_2(\kappa_1-1)}{\mu_1(\kappa_2+1)+\mu_2(\kappa_1+1)}, \tag{1}$$

where subscripts 1 and 2 refer to the materials above and below the interface, respectively; E_ρ^2, ν_ρ, and μ_ρ are Young's modulus, Poisson's ratio, and shear modulus of material ρ, respectively; $E'=E$ in plane stress and $E/(1-\nu^2)$ in plane strain, $\kappa=(3-\nu)/(1+\nu)$ in plane stress and $3-4\nu$ in plane strain.

The full-field expansion of the stresses at the tip of the interface crack as in Sun and Jih (1987) yields ahead of the crack-tip (along the interface)

$$\sigma_{22}+i\sigma_{12}|_{\theta=0}=\frac{K_1+iK_2}{\sqrt{2\pi r}}(r/l)^{i\epsilon}, \tag{2}$$

where K_α are the stress intensity factors, l is a characteristic length of the problem (e.g., the crack length) and $\epsilon=1/2\pi \ln[(1-\beta)/(1+\beta)]$ may be referred to as the oscillation parameter.

2 Maximum Opening Stress Criterion

The problem of crack-path prediction in a homogeneous linearly elastic solid has been extensively studied and its results are nowadays widely accepted. Several criteria have been introduced to relate the local loading conditions (characterized by the homogeneous stress intensity factors K_I and K_{II}) to the value of the crack kink angle; the primary criteria among these are most readily understood in terms of physical phenomenology, namely the maximum opening stress criterion (Erdogan and Sih, 1963) and the maximum energy release rate criterion (Palaniswamy and Knauss, 1978, Wu, 1978). Since these criteria provide fairly similar results in the homogeneous case, experimental work has not allowed to clearly distinguish between them, although the energy criteria is physically somewhat more appealing. This similarity in results for the two criteria does not hold for bimaterial interfaces between linearly elastic solids. Furthermore, as will be shown here later, the two approaches must be used with much caution—if they can be used at all—in most nonhomogeneous cases.

In this section, we examine first the case of the maximum opening stress criterion. The basic postulate behind this criterion is that the crack will propagate in the radial direction

[2]Greek indices take the values 1 and 2. Summation on repeated indices is implied.

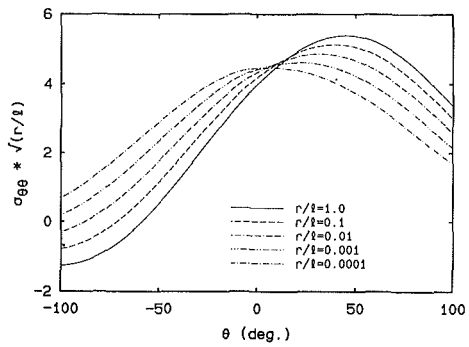


Fig. 1 Angular variation of the circumferential stress at various radii about the crack-tip ($\epsilon=-0.05$ $K_1=10$ $K_2=-5$)

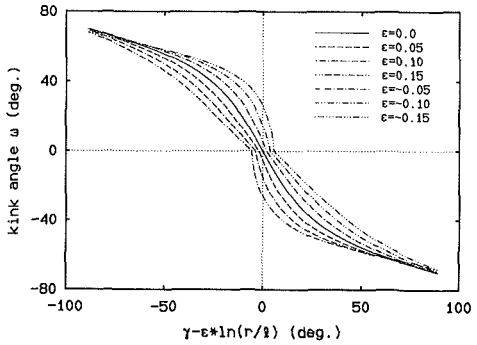


Fig. 2 Kink angle as predicted by the maximum circumferential stress criterion ($\gamma=\tan^{-1}(K_2/K_1)$)

along which the opening (or circumferential) stress $\sigma_{\theta\theta}$ is maximized. It can thus be simply expressed as

$$\lim_{r\to 0}\frac{\partial\sigma_{\theta\theta}}{\partial\theta}\bigg|_{\theta=\omega}=0 \text{ and } \lim_{r\to 0}\frac{\partial^2\sigma_{\theta\theta}}{\partial\theta^2}\bigg|_{\theta=\omega}<0,\ (-\pi<\omega<\pi). \tag{3}$$

As mentioned in the Introduction, the linearly elastic asymptotic stress field has a rotating character in those bimaterial case where $\epsilon\neq 0$; for the circumferential stress $\sigma_{\theta\theta}$, this character is illustrated in Fig. 1. Recall that for the homogeneous problem the value of $\sigma_{\theta\theta}\sqrt{r/l}$ (for $r/l\to 0$) is independent of the radius (i.e., all the curves in Fig. 1 are superposed). It is clear then that, in the present case, the value of the potential kink angle as determined by the stress criterion depends on the radius of the circle along which the "opening stress" is computed. This relationship between the local loading conditions (characterized by $\gamma=\tan-1\ (K_2/K_1)$) and the corresponding kink angle ω is given by the following implicit relation, which is illustrated in Fig. 2:

$$\tan\left(\gamma-\epsilon\ln\frac{r}{l}\right)=\frac{A(\omega;\epsilon)}{B(\omega;\epsilon)}, \tag{4}$$

where

$$A(\omega;\epsilon)=\epsilon\cosh(\pi-\omega)\cos\frac{3\omega}{2}+\frac{3}{2}\sinh\epsilon(\pi-\omega)\sin\frac{3\omega}{2}$$
$$+e^{\epsilon(\omega-\pi)}\sin\frac{\omega}{2}\cos\frac{\omega}{2}\left(\frac{3}{2}\cos\frac{\omega}{2}-2\epsilon\sin\frac{\omega}{2}+2\epsilon^2\cos\frac{\omega}{2}\right),$$
$$B(\omega;\epsilon)=\epsilon\sinh(\pi-\omega)\sin\frac{3\omega}{2}-\frac{3}{2}\cosh\epsilon(\pi-\omega)\cos\frac{3\omega}{2}$$
$$-e^{\epsilon(\omega-\pi)}\sin\frac{\omega}{2}\cos\frac{\omega}{2}\left(\frac{3}{2}\sin\frac{\omega}{2}+2\epsilon\cos\frac{\omega}{2}+2\epsilon^2\sin\frac{\omega}{2}\right). \tag{5}$$

This solution is valid for $0<\omega<\pi$; π has to be replaced by $-\pi$ for $-\pi<\omega<0$.

We note first that the curve for $\epsilon=0$ corresponds to that

Downloaded 03 May 2010 to 171.66.16.20. Redistribution subject to ASME license or copyright; see http://www.asme.org/terms/Terms_Use.cfm

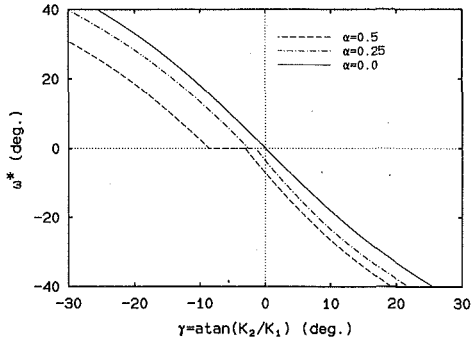


Fig. 3 Kink angle ω^* local loading parameter γ for various values of α (from He and Hutchinson (1989), $\beta = 0$)

obtained for the corresponding homogeneous fracture problem. The radial dependence of the kink angle ω appears then through a shift $\epsilon \ln(r/l)$ of the corresponding "master curve" described in Fig. 2. It would therefore appear that, in contrast to fracture in homogeneous solids, the maximum opening stress criterion does not produce a unique kink angle in the bimaterial case, unless an additional characteristic length is introduced; this length scale might be considered as a material parameter and would correspond to the value of the shift to be applied. We emphasize, however, that such a length scale is not an integral part of the fracture or kinking model, but constitutes a kind of "retrofit" to the linearized theory.

3 The Maximum Energy Release Criterion

The application of the maximum energy release rate criterion to the bimaterial case will be discussed in terms of analytical and numerical methods. We start with a brief review of the analytical results available to date.

3.1 Analytical Results. The maximum energy release rate criterion is based on the postulate that the crack will propagate along the path which maximizes the release of energy. If $G(\omega)$ is the energy release rate defined as the variation of potential energy Π corresponding to a virtual crack advance Δl in the direction ω, i.e.,

$$G = -\lim_{\Delta l \to 0} \frac{\Delta \Pi}{\Delta l}, \tag{6}$$

then this value is maximized for a kink angle ω^* satisfying the relations

$$\left.\frac{\partial G}{\partial w}\right|_{\omega=\omega^*} = 0 \text{ and } \left.\frac{\partial^2 G}{\partial \omega^2}\right|_{\omega=\omega^*} < 0, \ (-\pi < \omega^* < \pi). \tag{7}$$

The application of this criterion to the interfacial problem has been first documented by He and Hutchinson (1989) who used a method based on the superposition of dislocations which has been proven successful in the homogeneous case (Hayashi and Nemat-Nasser, 1981). Through an integral representation of the crack extension and a dimensional analysis, they were able to relate the local loading conditions at the tip of the extended crack to the stress intensity factors describing the asymptotic field at the tip of the semi-infinite interfacial crack prior to the extension. From this numerically obtained complex relationship, they compared the energy release rate of the kinked crack $G(\omega)$ to the variation of energy G_0 corresponding to an extension along the interface, the analytic expression of which has been derived by Malyshev and Salganik (1965) as

$$G_0 = \frac{(c_1 + c_2)(K_1^2 + K_2^2)}{16 \cosh^2 \pi\epsilon} \tag{8}$$

where the material constants $c_\rho = (\kappa_\rho + 1)/\mu_\rho$ (ρ not summed) and κ_ρ have been defined in Section 1.

He and Hutchinson (1989) first considered the case $\beta = \epsilon = 0$, then studied the effect of a nonzero β. The implicit assumption behind their investigation is that the energy release rate of the kinked crack is independent of the crack extension length Δl, except in a region very close to the crack-tip where the strong oscillations and the crack face interpenetration mentioned in the introduction take place. They invoked a weak influence of the second mismatch parameter β which ostensibly only affects in a mild manner the relationship between the energetically most favorable kink angle ω^* and the local loading parameter $\gamma(=\tan^{-1}(K_2/K_1))$. Some typical curves they obtained are shown in Fig. 3.

One notes that, in contrast to the maximum opening stress criterion, the maximum energy release rate criterion predicts that the relation between the kink angle ω^* and the local loading angle γ is not one-to-one: for a certain range of loading conditions, the crack will propagate along the interface, which seems to be more in accord with experimental observations (see Section 4). This result could be exploited to experimentally determine the interfacial fracture toughness. If the latter is of the same order as the fracture energies of the two materials, a curve similar to that shown in Fig. 3 is expected. If the interface is much weaker than either material, the crack will tend to propagate along the interface for a much wider range of load mixity conditions.

In the next section, we use the finite element technique to study the effect of β on the kinking behavior of the interface crack in more detail, using He and Hutchinson's special results to verify the numerical analysis.

3.2 Numerical Analysis. The finite element technique has been extensively used in the field of linearly elastic interfacial fracture mechanics, especially in order to relate the local loading parameters (i.e., the interface stress intensity factors K_1 and K_2) to the remote loading conditions, the geometry, and the material properties. In this analysis, the semi-energetic numerical scheme proposed by Matos et al. (1989) is used, which combines the values of the nodal crack opening displacements with the values of the J-integral (obtained through the domain-integration technique) to extract the two stress intensity factors. This method, which is relatively easy to implement, was shown in Matos et al. (1989) to provide an accuracy comparable to the more complex and fully energy-based methods.

The determination of the angular and radial variation of the energy release rate was carefully investigated in order to analyze the effect on the computed value of $G(\omega; \alpha, \beta, \Delta l)$ of the mesh refinement and distribution, which has been shown by Maiti (1990) to be of prime importance in the homogeneous case, especially when the kink angle is large. Since it was not possible, due to the presence of the interface, to adopt the doubly focussed mesh as suggested by Maiti, we chose the simpler mesh illustrated in Fig. 4.

The mesh is composed of approximately 2500 four-node bilinear elements concentrically focussed at the tip of the crack, the initial length of which was taken to be unity. The global geometry that was adopted is close to that of the bimaterial specimen used in the experiments (see Fig. 7). The problem was also solved by using a "boundary layer" approach in which a circular mesh is constructed around the crack tip and boundary conditions corresponding to a bimaterial K-field are applied along the outer circle. The second approach, which is applicable as long as the crack extension remains a small portion of the outer radius, allows to avoid the numerical error associated with the determination of the stress intensity factors (through the method described above) and to improve the mesh refinement around the crack-tip without increasing the number of elements. Both approaches yielded identical results. The number of nodes and their distribution was slightly varied depending on the length of the extension Δl. The number of

Downloaded 03 May 2010 to 171.66.16.20. Redistribution subject to ASME license or copyright; see http://www.asme.org/terms/Terms_Use.cfm

Table 1 Details on the precision of the computed values of the energy release rate as a function of Δl

$\frac{\Delta l}{l}$	G_0/J	error
10^{-2}	1.011	1.1%
10^{-3}	1.021	2.1%
10^{-4}	1.042	4.2%

released nodes was determined by a preliminary analysis of the homogeneous situation to allow comparison with analytic results. It was ascertained that a minimum number of five released nodes is need to guarantee an acceptable accuracy of the finite element scheme. We therefore selected six release nodes, equally spaced along the crack extension. The smallest element size was of the order of a tenth of the crack extension length. The question arises as to whether this type of meshing which suppresses the detail of the oscillation zone has serious consequences on the numerical results. This possible influence of the oscillation zone on the computed value of the energy release rate is examined separately and analytically by Geubelle and Knauss (1993) for the special case of interfacial separation. Using the relation developed there, it is possible to show that the maximum contribution of the contact zone (which is of the order of $5\ 10^{-8} l$) to the total energy release rate G is of the order of two percent in the present analysis summarized in Fig. 6(*b*).

Two independent methods were used to compute the energy release rate: the first corresponds to the "potential energy" definition of G described by Eq. (6) and the second is related to the crack closure work

$$G = \lim_{\Delta l \to 0} \frac{l}{2\Delta l} \int_0^{\Delta l} T_\alpha^{(1)} \Delta u_\alpha^{(2)}\, ds, \tag{9}$$

where $T_\alpha^{(1)}$ are the tractions existing along the crack extension prior to its opening and $\Delta u_\alpha^{(2)}$ are the opening displacements across the unloaded extension. Both methods gave almost identical values (within 0.01 percent) for the energy release rate G.

An idea of the accuracy of the computed value of G may be obtained by comparing the value of $G(\omega = 0) = G_0$ (extension along the interface) with the value of J-integral. The effect of the crack extension length on the obtained precision is summarized in Table 1. As expected, the error on the absolute value of G_0 increases with decreasing crack extension length due to the imprecision associated with higher crack-tip gradients. This problem can be solved by further refining the mesh but such studies showed that an increase in the number of elements can affect the absolute value of G, but does not change the ratio $G(\omega)/G_0$ nor the value of the kink angle corresponding to the maximum energy release rate.

3.3 Results and Discussion. A comparison between numerical and analytical results is presented in Fig. 5 for the case $\alpha = 0.5$ $\beta = 0$ and for three different crack extension lengths. The agreement with He and Hutchinson's analytical results is very satisfactory, except in the region near $\omega = 0$, where both analyses show some imprecision due to the flatness of the (G, ω) curve which makes the computation of the maximum relatively difficult. The independence of the energy release rate G, and therefore of the energetically most favorable kink angle ω^*, on the crack extension length Δl is obvious for the special case $\beta = 0$.

The more general case of $\beta \neq 0$ is illustrated in Figs. 6(*a*) and 6(*b*). In Fig. 6(*a*), the angular variation of the energy release

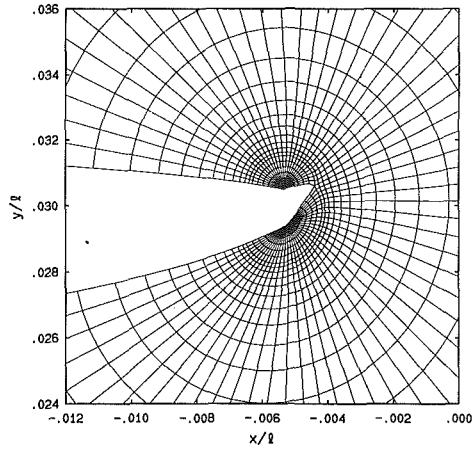


Fig. 4 Details of the deformed finite element mesh after crack extension

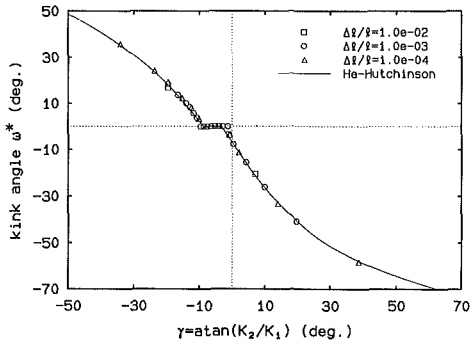


Fig. 5 Kink angle ω^* versus loading angle γ for $\alpha = 0.5$ $\beta = \epsilon = 0.0$

rate normalized by the value of the applied J-integral is presented for the loading conditions $\gamma = -45.0$ deg and for the three values of Δl. Except in the self-similar case of an extension along the interface ($\omega = 0$)[3], the energy release rate shows a definite dependence on the crack extension length Δl.

The complete relationship between the energetically most favorable kink angle ω^* and the local loading parameter γ is given in Fig. 6(*b*). If the individual curves are shifted by $\epsilon \ln(\Delta l/l)$, one obtains a unique "master" curve, also shown in Fig. 6(*b*), which is compared with He and Hutchinson's analytic solution obtained for the same value of α and β[4]. The difference that is apparent in Fig. 6(*b*) could not be explained by the coarseness of the finite element mesh since a much refined mesh (with close to 4000 elements and up to 15 released nodes) yields identical results[5] to that obtained with the coarser mesh. Thus, as was the case for the stress criterion and unlike for the homogeneous situation, the maximum energy release rate criterion does not provide a unique value of the kink angle in bimaterial cases when $\beta \neq 0$, but again, an additional length scale is necessary to make this criterion unique. This characteristic length Δl^*, which would most likely be considered as a property of the bimaterial combination, would be determined experimentally by computing the horizontal shift of the master curve necessary to fit the experimental (ω^*, γ) curve. Thus, as in Section 2, this length parameter is not part of the fracture model, but a retrofit parameter used "to make the linearized analysis work." The physical significance of the characteristic length Δl^* is still unknown at this point: it could, for example,

[3]The slight dependence of G_0 on the length of the extension is associated with the numerical imprecision described in Table 1.

[4]The error bars are associated with the imprecision of the determination of the maxima in Fig. 8 of He and Hutchinson (1989).

[5]Marked by asterisks in Fig. 6(*b*).

Downloaded 03 May 2010 to 171.66.16.20. Redistribution subject to ASME license or copyright; see http://www.asme.org/terms/Terms_Use.cfm

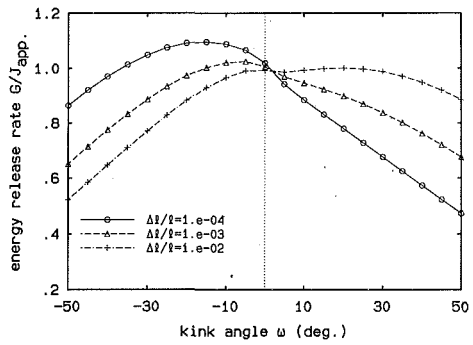


Fig. 6(*a*) Angular variation of the energy release rate for three different crack extension lengths Δl ($\alpha = 0.5$ $\beta = 0.25$ $\epsilon = -0.08$)

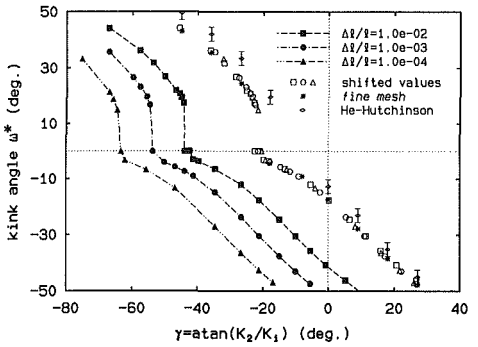


Fig. 6(*b*) Kink angle ω^* versus loading angle γ for $\alpha = 0.5$ $\beta = 0.25$: comparison of the numerical analysis with He and Hutchinson's (1989) results

correspond to a flaw size or an indicator of flaw distribution. It is also undetermined whether there is a unique characteristic length for each bimaterial combination or whether each component of the bimaterial combination has its own Δl^*— though that latter case could lead to nonunique values of the kink angle ω^* for every loading condition γ.

We note that the dependence of the energy release rate G on the crack extension length Δl has been suggested by Mukai et al. (1990) who studied the kinking behavior of a bimaterial crack of finite length; they concluded that a crack extension of a length which is at least equal to the (initial) length l of the crack was necessary to make ω^* appear to converge to a unique value. In the present context of small crack extension during the kink process, that configurational change is, however, inappropriate. The effect of Δl on the energy release rate has been acknowledged by Hutchinson in a private communication and in a recent publication by him and Suo (1991).

4 Information From Experiments

The issue of interfacial crack propagation has also been studied experimentally in our laboratories. Here, some of the experimental results are extracted from comparison with the results of the linear analysis described above. A more complete description of the experimental procedure is given by Bowen and Knauss (1993).

The fracture specimen, the geometry of which is given in Fig. 7, is composed of two co-cured sheets of Solithane 113, a polyurethane of small strain capabilities which has also been used previously to study the problem of crack propagation and kinking for the homogeneous case (Palaniswamy and Knauss, 1978). By adjusting the relative proportions of the base polymer and its crosslinking agent, the mechanical properties of the polyurethane are modified: the Young's modulus and Poisson's ratio of the two components used in the experiment, together with the corresponding plane stress[6] values of the mismatch parameters α, β and ϵ, are listed in Table 2. Excellent bond strength was achieved between the two sheets of Solithane by curing the two compositions almost simultaneously; as shown by Bowen and Knauss (1992), the interface toughness was comparable to at least the toughness of the weaker of the two components.

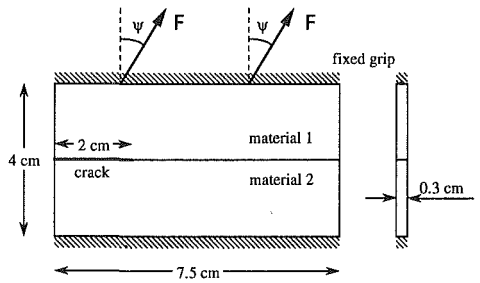


Fig. 7 Dimensions of the interfacial fracture specimen

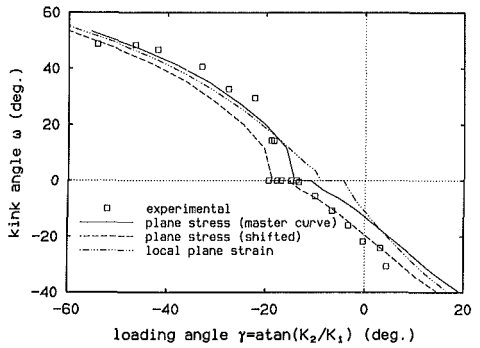


Fig. 8 Comparison of experimental and analytical results

Table 2 Material properties of the components used in the experiment and corresponding mismatch parameters. The composition is given in terms of the weight ratio "resin/crosslinking agent."

	material 1	material 2
composition	Solithane 55/45	Solithane 45/55
$E\,(N/cm^2)$	319	123
ν	0.499	0.499
$\alpha = 0.44$ $\beta = 0.11$ $\varepsilon = -0.036$		

The effect of the far-field loading conditions on the propagation behavior of the interfacial crack has been examined by rotating the bimaterial fracture specimen with respect to the loading axis. The relation between the far-field loading angle ψ(see Fig. 7) and the crack-tip local loading angle $\gamma(=\tan^{-1}(K_2/K_1))$ has been obtained numerically using the displacement-based semi-energetic method described in Section 3.2 assuming plane stress conditions. It has to be noted that the reference length l used in the definition of K_1, K_2 (and therefore γ) in (2) has been chosen as $l = 1$ cm, which is approximately half of the initial crack length.

The comparison between the experimental and analytical results is presented in Fig. 8 which shows the variation of the kink angle ω with respect to the local mixity parameter γ. The solid curve corresponds to the numerical solution (correspond-

[6]Due to the near incompressibility of the polymer, the plane-strain values of the mismatch parameters are $\alpha = 0.44 \beta \approx \epsilon \approx 0$.

Downloaded 03 May 2010 to 171.66.16.20. Redistribution subject to ASME license or copyright; see http://www.asme.org/terms/Terms_Use.cfm

ing to $\Delta l/l = 1$) and the dashed curve is the shifted analytical curve "fitted to the experimental points."

The shift was chosen to match the range of loading conditions for which the crack propagates along the interface ($\omega = 0$). The comparison with the experimental results shows good agreement also for negative values of the kink angle (i.e., when the crack propagates into the soft (lower modulus) material) but the agreement is less satisfactory when the crack propagates into the hard (higher modulus) material. The characteristic length Δl^*, determined from the value of the shift ($= \epsilon \ln(\Delta l^*/l)$) is approximately 1.1 mm. As mentioned earlier, the physical significance of this value is not clear at this time. It is, however, worth pointing out that there are at least two size scales that could be considered relative to this value: one is the plate thickness while the other is a measure of the zone in which deformations are nonlinear. Based on a finite strain analysis which matches Generalized Neo-Hookean material behavior to the mechanical response of the two components (Geubelle and Knauss, 1992), one finds that, in the experiments, the size of the nonlinear zone should be of the order of 0.5 mm in the softer material and less than 0.1 mm in the harder one. By comparison, the plate thickness was about 3 mm. The examination of the effects of large deformations on the propagation behavior of an interface crack is still ongoing and represents a problem that is too large to warrant inclusion in this presentation.

It might be appropriate at this point to discuss which of the plane-stress or plane-strain assumptions are more adequate to study the problem of crack propagation in the present experimental conditions. We understand that, although the specimen geometry suggests the use of the plane stress assumption, the stress and strain fields at the tip of the interface crack are three-dimensional, with conditions more akin to plane strain prevailing in the immediate vicinity of the crack-tip. A three-dimensional numerical investigation by Nakamura (1991) has analysed the respective extent of the plane stress, plane strain, and three-dimensional regions. It was shown there that, while the thickness-averaged value of the energy release rate is very close to the plane stress solution, a plane strain K-field exists within a radius of approximately 0.5 percent of the plate thickness near the midplane, for plates having a thickness to crack length ratio smaller than one. Let K^{σ}_{α} and $K^{\epsilon}_{\alpha}(\alpha = 1, 2)$ represent the components of the plane stress and plane strain stress intensity factors, respectively. The relationship between the plane stress phase angle $\gamma^{\sigma}(= \tan^{-1}(K^{\sigma}_2/K^{\sigma}_1))$ and the plane strain phase angle $\gamma^{\epsilon}(= \tan^{-1}(K^{\epsilon}_2/K^{\epsilon}_1))$ has been recently investigated numerically by Lee and Rosakis (1993). By assuming, as we will do here, the existence of a plane stress asymptotic field throughout the plate at a certain distance from the crack-tip they obtained

$$\gamma^{\sigma} + \epsilon^{\sigma} \ln h/l \approx \gamma^{\epsilon} + \epsilon^{\epsilon} \ln h/l, \tag{10}$$

where h is the plate thickness, l is the characteristic length used to define the two phase angles (1.2), and ϵ^{σ} and ϵ^{ϵ} are the plane-stress and plane-strain values of the oscillation index. This relation suggests that the "master" (ω^*, γ) curve corresponding to the plane-strain values of the mismatch parameters ($\alpha_{\epsilon} = 0.44$ $\epsilon_{\epsilon} \approx 0$) has to be shifted by $(\epsilon^{\epsilon} - \epsilon^{\sigma}) \ln(h/l)$ (≈ 2.4) to allow comparison with experimental results. The shifted "local plane strain" curve is also presented in Fig. 8. Note also that, if fully plane-strain conditions are assumed, no adjustment of the analytical results are possible through shifting ($= \epsilon^{\epsilon} \ln \Delta l/l$) at all since the oscillation index is then almost zero due to the high incompressibility of the two components. Although it seems likely that the phenomena dictating the propagation behavior of the interfacial crack involve distances that are much smaller than the thickness of the specimen, the agreement between the experimental results and the analytical curve obtained by assuming local plane-strain conditions is less satisfactory than for the fully plane-stress situation.

5 Conclusion

The propagation of a crack along and away from a bimaterial interface has been investigated analytically, using the linear theory of elasticity. Some major differences with the homogeneous situation have been noted: first, the maximum opening stress criterion and the maximum energy release rate criterion provide very different results in the bimaterial case, the energy criterion being more in accord with experimental observations; secondly, unlike in the homogeneous situation, the linear analysis of the kinking behavior of an interfacial crack necessitates an additional length parameter corresponding to the initial crack extension to bring the analysis into closer accord with measurements. This parameter, which constitutes a "retrofit to the theory," is not part of the fracture model but should probably be considered to be a property byproduct of the bimaterial combination. However, the experimentally obtained value of the additional length scale for the bimaterial specimen investigated in the present work is found to be orders of magnitude larger than any physically dictated characteristic length.

6 Acknowledgments

The authors are indebted to Dr. C. T. Liu, technical monitor on contract F04611-88-K-0024; additional support came from ONR Grant N00014-91-J-1427 under the direction of Dr. P. Schmidt. The computing facilities of the San Diego Supercomputing Center assisted materially in this work. We also wish to acknowledge repeated discussions with Prof. J. W. Hutchinson of Harvard University and with Dr. Noel O'Dowd, research fellow at Caltech.

References

Bowen, J. M., and Knauss, W. G., 1993, "An Experimental Study of Interfacial Crack Kinking," Galcit SM Report 91-15, Caltech, Paradena, CA.

Bowen, J. M., and Knauss, W. G., 1992, "The Characterization of the Energy of Fracture at and Near Interfaces Between Viscoelastic Solids," Galcit SM Report 91-14, Caltech, submitted to the *Journal of Adhesion*, submitted for publication.

Comninou, M., 1977a, "The Interface Crack," ASME JOURNAL OF APPLIED MECHANICS, Vol. 44, pp. 631–636.

Comninou, M., 1977b, "Interface Crack with Friction in the Contact Zone," ASME JOURNAL OF APPLIED MECHANICS, Vol. 44, pp. 780–781.

Dundurs, J., 1969, "Edge-Bonded Dissimilar Orthogonal Elastic Wedges Under Normal and Shear Loading," ASME JOURNAL OF APPLIED MECHANICS, Vol. 36, pp. 650–652.

England, A. H., 1965, "A Crack Between Dissimilar Media," ASME JOURNAL OF APPLIED MECHANICS, Vol. 32, pp. 400–402.

Erdogan, F., and Sih, G. E., 1963, "On the Crack Extension in Plates Under Plate Loading and Transverse Shear," *Journal of Basic Engineering*, Vol. 85, pp. 519–527.

Erdogan, F., 1965, "Stress Distribution in Bonded Dissimilar Materials with Cracks," ASME JOURNAL OF APPLIED MECHANICS, Vol. 32, pp. 403–410.

Gautesen, A. K., and Dundurs, J., 1987, "The Interface Crack in a Tension Field," ASME JOURNAL OF APPLIED MECHANICS, Vol. 54, pp. 93–98.

Gautesen, A. K., and Dundurs, J., 1988, "The Interface Crack Under Combined Loading," ASME JOURNAL OF APPLIED MECHANICS, Vol. 55, pp. 580–586.

Geubelle, P. H., and Knauss, W. G., 1993, "A Note Related to Energy Release Rate Computations for Kinking Interface Cracks," Galcit SM Report 91-17, Caltech, ASME JOURNAL OF APPLIED MECHANICS, submitted for publication.

Geubelle, P. H., and Knauss, W. G., 1992, "A Note on a Finite Deformation Analysis of the Nonlinear Zone Size in the Bimaterial Fracture Experiment," Galcit SM Report 92-34, Caltech, Pasadena, CA.

Hayashi, K., and Nemat-Nasser, S., 1981, "Energy Release Rate and Crack Kinking Under Combined loading," ASME JOURNAL OF APPLIED MECHANICS, Vol. 48, pp. 520–524.

Hutchinson, J. W., and Suo, Z., 1991, "Mixed Mode Cracking in Layered Materials," *Advances in Applied Mechanics*, Vol. 28, J. W. Hutchinson and T. Y. Wu, eds., Academic Press, New York.

He, M.-Y., and Hutchinson, J. W., 1989, "Kinking of a Crack out of an Interface," ASME JOURNAL OF APPLIED MECHANICS, Vol. 57, pp. 270–278.

Herrmann, J. M., 1989, "An Asymptotic Analysis of Finite Deformations Near the Tip of an Interface Crack," *Journal of Elasticity*, Vol. 21, pp. 227–269.

Knowles, J. K., and Sternberg, E., 1983, "Large Deformations Near a Tip of an Interface-Crack Between Two Neo-Hookean Sheets," *Journal of Elasticity*, Vol. 13, pp. 257–293.

Lee, Y.-J., and Rosakis, A. J., 1993, "Interfacial Cracks in Plates: Part I.

Downloaded 03 May 2010 to 171.66.16.20. Redistribution subject to ASME license or copyright; see http://www.asme.org/terms/Terms_Use.cfm

A Three-Dimensional Numerical Investigation," *International Journal of Solids and Structures*, Vol. 30, No. 22, pp. 3139–3158.

Maiti, S. K., 1990, "Finite Element Computation of the Strain Energy Release Rate for Kinking of a Crack," *International Journal of Fracture*, Vol. 43, pp. 161–170.

Malyshev, B. M., and Salganik, R. L., 1965, "The Strength of Adhesive Joints Using the Theory of Crack," *International Journal of Fracture Mechanics*, Vol. 1, pp. 114–128.

Matos, P. P. L., McMeeking, R. M., Charalambides, P. G., and Droy, M. D., 1989, "A Method for Calculating Stress Intensities in Bimaterial Fracture," *International Journal of Fracture*, Vol. 40, pp. 235–254.

Mukai, D. J., Ballarini, R., and Miller, G. R., 1990, "Analysis of Branched Interface Cracks," ASME JOURNAL OF APPLIED MECHANICS, Vol. 57, pp. 887–893.

Nakamura, T., 1991, "Three-Dimensional Stress Field of Elastic Interface Cracks," presented at the 1991 Annual Winter ASME Meeting in Atlanta, to appear in ASME JOURNAL OF APPLIED MECHANICS.

Palaniswamy, K., and Knauss, W. G., 1978, "On the Problem of Crack Extension in Brittle Solids Under General Loading," *Mechanics Today*, Vol. 4, S. Nemat-Nasser, ed., Pergamon Press, pp. 87–148.

Ravichandran, G., and Knauss, W. G., 1989, "A Finite Elastostatic Analysis of Bimaterial Interface Cracks," *International Journal of Fracture*, Vol. 39, pp. 235–253.

Rice, J. R., and Sih, G. C., 1965, "Plane Problems of Cracks in Dissimilar Media," ASME JOURNAL OF APPLIED MECHANICS, Vol. 32, pp. 418–423.

Rice, J. R., 1988, "Elastic Fracture Mechanics Concepts for Interfacial Cracks," ASME JOURNAL OF APPLIED MECHANICS, Vol. 55, pp. 98–103.

Shih, C. F., and Asaro, R. J., 1988, "Elastic-Plastic Analysis of Cracks on Bimaterial Interfaces: Part I—Small-Scale Yielding," ASME JOURNAL OF APPLIED MECHANICS, Vol. 55, pp. 299–316.

Shih, C. F., and Asaro, R. J., 1989, "Elastic-Plastic Analysis of Cracks on Bimaterial Interfaces: Part II—Structures on Small-Scale Yielding Fields," ASME JOURNAL OF APPLIED MECHANICS, Vol. 56, pp. 763–779.

Shih, C. F., 1991, "Cracks on Bimaterial Interfaces: Elasticity and Plasticity Aspects," *Materials Science and Engineering*, Vol. A143, pp. 77–90.

Sun, C. T., and Jih, C. J., 1987, "On Strain Energy Release Rates for Interfacial Cracks in Bi-Material Media," *Engineering Fracture Mechanics*, Vol. 28, No. 1, pp. 13–20.

Symington, M. F., 1987, "A Review of Some Aspects of the Linear Elastic Analysis of Bimaterial Cracks," Master Thesis, Division of Engineering, Brown University, Providence, R.I.

Williams, M. L., 1959, "The Stress Around a Fault or Crack in Dissimilar Media," *Bulletin of the Seismological Society of America*, Vol. 49, pp. 199–204.

Wu, C. H., 1978, "Maximum Energy Release Rate Criterion Applied to a Tension-Compression Specimen with Crack," *Journal of Elasticity*, Vol. 8, pp. 235–257.

Yang, Y., and Shin, C. F., 1990, "Fracture Along an Interlayer," Technical Report, Division of Engineering, Brown University, Providence, R.I.

Downloaded 03 May 2010 to 171.66.16.20. Redistribution subject to ASME license or copyright; see http://www.asme.org/terms/Terms_Use.cfm

Load Diffusion and Absorption Problems From a Finite Fiber to Elastic Infinite Matrix

Ven-Gen Lee
Assoc. Mem. ASME.

Toshio Mura
Fellow ASME.

Theoretical and Applied Mechanics,
Northwestern University,
Evanston, IL 60208

The load transfer behavior of a finite fiber perfectly bonded to an infinite matrix of distinct elastic moduli is investigated in this paper. The fiber is subjected to the uniformly distributed loading applied at infinity or on one cross-section of the fiber. The stress disturbance due to the existing fiber is simulated by the equivalent inclusion method, which formulates the inhomogeneity problem to a system of integral equations. By dividing the fiber into finite numbers of ring elements with uniform distributed eigenstrains, the integral equations can be further reduced to a system of algebraic equations with coefficients expressed in terms of the integrals of Lipschitz-Hankel type. Numerical results are presented for resultant axial force for various fiber length and material properties. The limiting cases of the infinite and semi-infinite fibers are also compared with the exact and approximate solutions.

1 Introduction

With the potential high strength and toughness, the fiber-reinforced composite materials have been widely used in engineering applications. Many research efforts have been directed towards studying the cracking process between the fiber and matrix. One of practical interest is to investigate the mechanical behavior of the transfer of force with the presence of fiber under applied loading.

Cohen and Romualdi (1967) proposed a numerical scheme to study the interaction forces at the fiber-matrix interface and the elastic fields of multifiber problem subjected to a remote tensile stress. By using the Fourier transform, Muki and Sternberg (1969) presented an exact analysis to the load transfer problem of an infinite cylindrical elastic bar in an infinite elastic medium of distinct elastic moduli. In the same paper, Muki and Sternberg also modeled the above problem by replacing the original bar with a one-dimension elastic bar, which has the Young's modules as the difference of the bar and matrix, in an isotropic infinite domain. Later, Muki and Sternberg (1970) used the same approximate scheme to study the load-absorption problem by a semi-infinite fiber in an infinite elastic body with remotely uniform applied stress. Recently, Slaughter and Lyell Sanders (1991) provided another approximate method for a load-diffusion problem of an axially loaded infinite fiber by assuming the rod with uniform axial stresses and ignoring shear strains. However, their model doesn't give correct stress fields near the loaded region in comparison with exact solution.

The idea of the equivalent inclusion method was first presented by Eshelby (1957) to solve an inhomogeneity problem. It has already been successfully applied to the isotropic matrix having ellipsoidal subdomain by the use of Eshelby's tensor, provided that the prescribed eigenstrain is uniform. But few applications for the other shape of the inhomogeneity can be found. In this paper, a theoretical study of the three-dimensional problem of a finite cylindrical fiber embedded in an infinite matrix with distinct elastic moduli is presented. In Section 2, the sound theory of the equivalent inclusion method is introduced. The equivalency of inclusion and inhomogeneity problems induces to a set of integral equations and the kernels in the integral equations are the function of the equivalent eigenstrain distribution and their derivative. In Section 3, an analysis method is proposed. By decomposing the fiber into finite sections of a uniformly distributed eigenstrain, the set of integral equations can be reduced to a system of algebraic equations, which is solved numerically. Finally, three cases are examined by the equivalent inclusion method. First, a finite fiber is considered and the matrix is subjected to uniform tensile stress at infinity. The limiting case of taking the length of fiber as infinite is compared with Eshelby's solutions. In Case 2, the length of fiber is taken as semi-infinite. In Case 3 we study the confined load applied on the central cross-section of a finite fiber. The resultant axial forces are displayed and compared with exact solutions and other approximate results.

2 Mathematical Formulation

Let D be the entire three-dimensional elastic space. Consider a finite cylindrical fiber Ω of length b and radius c perfectly bonded to an infinite matrix of different elastic moduli. The fiber is subjected to the uniform distributed stress applied at infinity or on the central cross-section of the fiber. Both the fiber and matrix are isotropic with elastic moduli C_{ijkl} for the

Contributed by the Applied Mechanics Division of THE AMERICAN SOCIETY OF MECHANICAL ENGINEERS for publication in the ASME JOURNAL OF APPLIED MECHANICS.

Discussion on this paper should be addressed to the Technical Editor, Professor Lewis T. Wheeler, Department of Mechanical Engineering, University of Houston, Houston, TX 77204-4792, and will be accepted until four months after final publication of the paper itself in the ASME JOURNAL OF APPLIED MECHANICS.

Manuscript received by the ASME Applied Mechanics Division, June 5, 1992; final revision, June 17, 1993. Associate Technical Editor: R. M. McMeeking.

Copyright © 1994 by ASME
Downloaded 03 May 2010 to 171.66.16.20. Redistribution subject to ASME license or copyright; see http://www.asme.org/terms/Terms_Use.cfm

matrix $D - \Omega$ and C^*_{ijkl} for the fiber Ω. A cylindrical coordinate $(r, \theta, z) = (x_1, x_2, x_3)$ is chosen such that the z-axis is coincident with the centroidal axis of the fiber. With the external applied stress σ^0_{ij}, the stress-strain relation for the inhomogeneous medium can be expressed as (see Mura, 1987)

$$\sigma_{ij} + \sigma^0_{ij} = C_{ijkl}(\epsilon_{kl} + \epsilon^0_{kl}) \quad \text{in } D - \Omega \tag{1}$$

$$\sigma_{ij} + \sigma^0_{ij} = C^*_{ijkl}(\epsilon_{kl} + \epsilon^0_{kl}) \quad \text{in } \Omega \tag{2}$$

where σ_{ij} and ϵ_{kl} represent the stress disturbance and related strain due to the existing inhomogeneity and $\sigma^0_{ij} = C_{ijkl}\epsilon^0_{kl}$ in D. The stress disturbance can also be simulated as the eigenstress resulting from the inclusion with equivalent eigenstrains. Consider an infinitely extended homogeneous solid D with elastic constants C_{ijkl}, which contains the subdomain Ω with the equivalent eigenstrain ϵ^*_{ij}. The eigenstrain ϵ^*_{ij} has been introduced here arbitrarily in order to simulate the inhomogeneity problem by use of the inclusion method. For the equivalent inclusion problem, the stress-strain relation is written as

$$\sigma_{ij} + \sigma^0_{ij} = C_{ijkl}(\epsilon_{kl} + \epsilon^0_{kl} - \epsilon^*_{kl}) \quad \text{in } \Omega. \tag{3}$$

From Eqs. (2) and (3), the necessary and sufficient condition for the equivalency of the stresses and strains in the inhomogeneity and inclusion problems is

$$C^*_{ijkl}(\epsilon_{kl} + \epsilon^0_{kl}) = C_{ijkl}(\epsilon_{kl} + \epsilon^0_{kl} - \epsilon^*_{kl}) \quad \text{in } \Omega \tag{4}$$

where ϵ_{kl} can be obtained as a function of ϵ^*_{kl} from the inclusion problem and is addressed below.

When an elastic solid is subjected to the distributed eigenstrain ϵ^*_{ij}, the total strain ϵ^T_{ij} is regarded as the sum of elastic strain e_{ij} and eigenstrain ϵ^*_{ij}, i.e.,

$$\epsilon^T_{ij} = \epsilon^*_{ij} + e_{ij} \tag{5}$$

and the corresponding stress is

$$\sigma_{ij} = C_{ijkl}e_{kl} = C_{ijkl}(\epsilon^T_{ij} - \epsilon^*_{ij}). \tag{6}$$

In general, the equilibrium equation for the homogeneous body without eigenstrain can be written as

$$C_{ijkl}e_{kl,j} = -X_i \tag{7}$$

where X_i is the body force. For the inclusion problem in the absence of body force, the equation of equilibrium can be written as

$$C_{ijkl}\epsilon_{kl,j} = C_{ijkl}\epsilon^*_{kl,j}. \tag{8}$$

Comparing Eqs. (7) and (8), the strain disturbance ϵ_{kl} caused by the eigenstrain ϵ^*_{kl} can be considered as the elastic strain due to the equivalent body force $-C_{ijkl}\epsilon^*_{kl,j}$. Therefore, the displacement can be considered as the displacement caused by the body force $-C_{jlmn}\epsilon^*_{mn,l}$ (in Cartesian coordinate)

$$u_i(\mathbf{x}) = -\int_\Omega \tilde{G}_{ij}(\mathbf{x}, \mathbf{x}')C_{jlmn}\epsilon^*_{mn,l}(\mathbf{x}')d\mathbf{x}' \tag{9}$$

where $\tilde{G}_{ij}(\mathbf{x}, \mathbf{x}')$ represents the displacement at point x in the x_i direction due to a unit body force applied at point $\mathbf{x}'$ in the x_j direction and the strain can be obtained from the strain-displacement relation. Particular emphasis has been placed on the case of ellipsoidal subdomain. It is noted that, for an ellipsoidal inclusion with uniform eigenstrain in an infinite body, the strain and stress inside the inclusion are also uniform. The resulting strain can be obtained by

$$\epsilon_{kl} = S_{klmn}\epsilon^*_{mn} \tag{10}$$

where S_{klmn} is known as the Eshelby's tensor for isotropic material. However, Chiu (1977) demonstrated the deviation of the stress distribution inside the cuboidal inclusion from that of the ellipsoidal inclusion. The application of the equivalent inclusion method shows much difficulty for other shape inhomogeneity. Since the cylindrical fiber is subjected to axially symmetric loading, the problem can be considered as an axially symmetric case. In order to obtain the strain caused by the eigenstrain prescribed in the cylindrical inclusion, Eq. (9) can be revised as the displacement caused by the ring body force F_j (equivalent body force)

$$u_i(\mathbf{x}) = \int_\Omega G_{ij}(\mathbf{x}, \mathbf{x}')F_j(\mathbf{x}')d\mathbf{x}' \tag{11}$$

where F_j is the function of eigenstrain and can be expressed as

$$F_1(\mathbf{x}') = (\lambda + 2\mu)\frac{\partial \epsilon^*_{rr}}{\partial \rho} + \lambda\frac{\partial \epsilon^*_{\theta\theta}}{\partial \rho} + \lambda\frac{\partial \epsilon^*_{zz}}{\partial \rho} + 2\mu\frac{\partial \epsilon^*_{rz}}{\partial z'} + \frac{2\mu}{\rho}(\epsilon^*_{rr} - \epsilon^*_{\theta\theta}) \tag{12}$$

$$F_2(\mathbf{x}') = 2\mu\frac{\partial \epsilon^*_{r\theta}}{\partial \rho} + 2\mu\frac{\partial \epsilon^*_{\theta z}}{\partial z'} + \frac{4\mu}{\rho}\epsilon^*_{r\theta} \tag{13}$$

$$F_3(\mathbf{x}') = \lambda\frac{\partial \epsilon^*_{rr}}{\partial z'} + \lambda\frac{\partial \epsilon^*_{\theta\theta}}{\partial z'} + (\lambda + 2\mu)\frac{\partial \epsilon^*_{zz}}{\partial z'} + 2\mu\frac{\partial \epsilon^*_{rz}}{\partial \rho} + \frac{2\mu}{\rho}\epsilon^*_{rz}. \tag{14}$$

The $G_{ij}(\mathbf{x}, \mathbf{x}')$ is the displacement in the x_i-direction at point $\mathbf{x} = (r, z)$ due to a distributed ring force acted along a circle $\mathbf{x}' = (\rho, z')$ in the x_j-direction in the infinitely extended medium. Due to the axisymmetric loading and geometry, the prescribed eigenstrain ϵ^*_{ij} is a function of r and z only. The solutions of displacement $G_{ij}(\mathbf{x}, \mathbf{x}')$ are shown in Appendix A.

In fact, Eq. (4) must hold for any shape of inclusion and applied load. As an axisymmetric case, Eq. (4) can be further expanded as

$$(\Gamma - 1)\{\epsilon_{\theta\theta} - \epsilon_{rr}\} - \epsilon^*_{rr} + \epsilon^*_{\theta\theta} = (\Gamma - 1)f_1 \tag{15}$$

$$(\Gamma - 1)\{\epsilon_{\theta\theta} - \epsilon_{zz}\} - \epsilon^*_{zz} + \epsilon^*_{\theta\theta} = (\Gamma - 1)f_2 \tag{16}$$

$$(\lambda^* - \lambda)\epsilon_{rr} + (\lambda^* + 2\mu^* - \lambda - 2\mu)\epsilon_{\theta\theta} - (\lambda - \lambda^*)\epsilon_{zz} + \lambda\epsilon^*_{rr} + (\lambda + 2\mu)\epsilon^*_{\theta\theta} + \lambda\epsilon^*_{zz} = -(\lambda^* - \lambda)f_3 \tag{17}$$

$$2(\Gamma - 1)\epsilon_{rz} + 2\epsilon^*_{rz} = -(\Gamma - 1)f_4 \tag{18}$$

where $\Gamma = \mu^*/\mu$, and

$$f_1 = \epsilon^0_{rr} - \epsilon^0_{\theta\theta}, \quad f_2 = \epsilon^0_{zz} - \epsilon^0_{\theta\theta},$$

$$f_3 = +\epsilon^0_{rr} + \{1 + (2\mu^* - 2\mu)/(\lambda^* - \lambda)\}\epsilon^0_{\theta\theta} + \epsilon^0_{zz}, \quad f_4 = +2\epsilon^0_{rz}. \tag{19}$$

The compatibility conditions in terms of a cylindrical system are

$$\epsilon_r(r, z) = \frac{\partial u_r}{\partial r} \tag{20}$$

$$\epsilon_\theta(r, z) = \frac{u_r}{r} \tag{21}$$

$$\epsilon_z(r, z) = \frac{\partial u_z}{\partial z} \tag{22}$$

$$\epsilon_{rz}(r, z) = \frac{1}{2}\left(\frac{\partial u_z}{\partial r} + \frac{\partial u_r}{\partial z}\right). \tag{23}$$

Hence, the strain components can be derived by taking the derivative of Eq. (11).

By substituting the corresponding strain into Eqs. (15)–(18), it yields

$$\int_\Omega [R_{11}(\mathbf{x}, \mathbf{x}')\epsilon^*_{rr}(\mathbf{x}') + R_{12}(\mathbf{x}, \mathbf{x}')\epsilon^*_{\theta\theta}(\mathbf{x}') + R_{13}(\mathbf{x}, \mathbf{x}')\epsilon^*_{zz}(\mathbf{x}') + R_{14}(\mathbf{x}, \mathbf{x}')\epsilon^*_{rz}(\mathbf{x}')]d\mathbf{x}' - \alpha(\epsilon^*_{rr}(\mathbf{x}) - \epsilon^*_{\theta\theta}(\mathbf{x})) = f_1(\mathbf{x}) \tag{24}$$

$$\int_\Omega [R_{21}(\mathbf{x}, \mathbf{x}')\epsilon^*_{rr}(\mathbf{x}') + R_{22}(\mathbf{x}, \mathbf{x}')\epsilon^*_{\theta\theta}(\mathbf{x}') + R_{23}(\mathbf{x}, \mathbf{x}')\epsilon^*_{zz}(\mathbf{x}') + R_{24}(\mathbf{x}, \mathbf{x}')\epsilon^*_{rz}(\mathbf{x}')]d\mathbf{x}' - \alpha(\epsilon^*_{zz}(\mathbf{x}) - \epsilon^*_{\theta\theta}(\mathbf{x})) = f_2(\mathbf{x}) \tag{25}$$

Downloaded 03 May 2010 to 171.66.16.20. Redistribution subject to ASME license or copyright; see http://www.asme.org/terms/Terms_Use.cfm

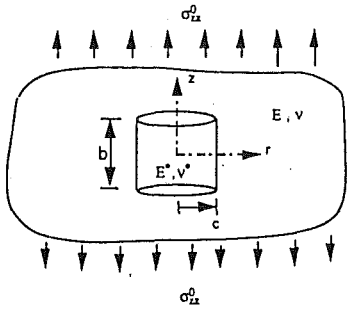


Fig. 1(*a*) Case 1: Load absorption by a finite fiber

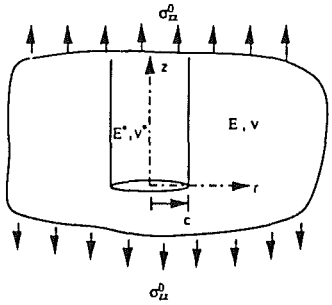


Fig. 1(*b*) Case 2: Load absorption by a semi-infinite fiber

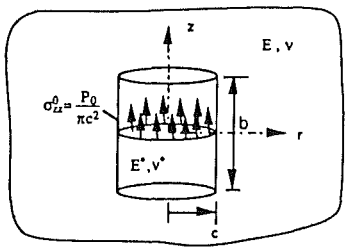


Fig. 1(*c*) Case 3: Load diffusion from a finite fiber

Fig. 1 Problem configuration

$$\int_\Omega [R_{31}(\mathbf{x}, \mathbf{x}')\epsilon^*_{rr}(\mathbf{x}') + R_{32}(\mathbf{x}, \mathbf{x}')\epsilon^*_{\theta\theta}(\mathbf{x}') + R_{33}(\mathbf{x}, \mathbf{x}')\epsilon^*_{zz}(\mathbf{x}') + R_{34}(\mathbf{x}, \mathbf{x}')\epsilon^*_{rz}(\mathbf{x}')]d\mathbf{x}' - \alpha_1(\epsilon^*_{rr}(\mathbf{x}) + \epsilon^*_{zz}(\mathbf{x})) - \alpha_2\epsilon^*_{\theta\theta}(\mathbf{x}) = f_3(\mathbf{x}) \tag{26}$$

$$\int_\Omega [R_{41}(\mathbf{x}, \mathbf{x}')\epsilon^*_{rr}(\mathbf{x}') + R_{42}(\mathbf{x}, \mathbf{x}')\epsilon^*_{\theta\theta}(\mathbf{x}') + R_{43}(\mathbf{x}, \mathbf{x}')\epsilon^*_{zz}(\mathbf{x}') + R_{44}(\mathbf{x}, \mathbf{x}')\epsilon^*_{rz}(\mathbf{x}')]d\mathbf{x}' - 2\alpha\epsilon^*_{rz}(\mathbf{x}) = f_4(\mathbf{x}) \tag{27}$$

where $R_{ij}(\mathbf{x}, \mathbf{x}')$ is given in Appendix B.

The α, α_1, and α_2 have the definition as

$$\alpha = 1/\{\mu^*/\mu - 1\}, \quad \alpha_1 = \lambda/\{\lambda^* - \lambda\},$$

$$\alpha_2 = \{\lambda + 2\mu\}/\{\lambda^* - \lambda\}. \tag{28}$$

Equations (24)–(27) are a set of coupled integral equations with unknown strength of the eigenstrain $\epsilon^*_{ij}(\mathbf{x})$.

With the solved eigenstrain, the stress fields can be obtained from

$$\sigma^{(in)}_{ij} = C_{ijkl}(\epsilon_{kl} + \epsilon^0_{kl} - \epsilon^*_{kl}) \quad \text{in } \Omega \tag{29}$$

$$\epsilon^{(ex)}_{ij} = C_{ijkl}(\epsilon_{kl} + \epsilon^0_{kl}) \quad \text{in } D - \Omega. \tag{30}$$

3 Numerical Analysis

First, in order to solve Eqs. (24)–(27) numerically, the fiber is divided into $M \times N$ ring elements, which include M sections in the radial direction and N sections in the vertical direction. For instance, the element (m, n) is defined as $c_m \le r \le c_{m+1}$, $b_n \le z \le b_{n+1}$ where $c_m = c(m-1)/M$ and $b_n = b(n-1)/N$. The collocation point in the element is located at the center of the element, i.e., $(r^m, z^n) = ((c_m + c_{m+1})/2, (b_n + b_{n+1})/2)$. For convenience, the eigenstrain ϵ^*_1, ϵ^*_2, ϵ^*_3, and ϵ^*_4 are used in the following to refer to ϵ^*_{rr}, $\epsilon^*_{\theta\theta}$, ϵ^*_{zz}, and ϵ^*_{rz} respectively. Each ring element is prescribed by the uniform eigenstrains. Thus, the eigenstrain in each element can be expressed as

$$\epsilon^*_k(m, n) = \overline{\epsilon^*_k}(m, n)\{H(r - c_m) - H(r - c_{m+1})\} \times \{H(z - b_n) - H(z - b_{n+1})\} \quad (m = 1, 2, \ldots, M \text{ and } n = 1, 2, \ldots, N) \tag{31}$$

where $\overline{\epsilon^*_k}$ represents the magnitude of the eigenstrain in each element. $H(\ )$ is the Heaviside function. From Eq. (31), the integrations in Eqs. (24)–(27) are split into

$$\int_\Omega \{\ \}d\mathbf{x}' = \sum_{m=1}^{M}\sum_{n=1}^{N}\left\{\overline{\epsilon^*}(m, n)\int_{c_m}^{c_{m+1}} d\rho \int_{b_n}^{b_{n+1}} \{\ \}dz'\right\}. \tag{32}$$

Therefore, Eqs. (24)–(27) can be reduced to a system of algebraic equations which are

$$\sum_{s=1}^{M}\sum_{t=1}^{N}\{[k^{st}_{ij}(r^m, z^n) + \delta_{sm}\delta_{tn}\alpha_{ij}]\epsilon^*_j(s, t)\} = f_i(r^m, z^n) \quad (i, j = 1, 2, 3, 4;\ m = 1, 2, \ldots, M;\ n = 1, 2, \ldots, N) \tag{33}$$

with

$$\alpha_{ij} = \begin{bmatrix} -\alpha & \alpha & 0 & 0 \\ 0 & \alpha & -\alpha & 0 \\ \alpha_1 & \alpha_2 & \alpha_1 & 0 \\ 0 & 0 & 0 & 2\alpha \end{bmatrix} \tag{34}$$

where δ_{sm} or δ_{tn} is the Kronecker delta.

Equations (33) are $4 \times M \times N$ algebraic equations with four unknown eigenstrain ϵ^*_k, $k = 1 - 4$ in each of $M \times N$ elements. The corresponding components $k^{st}_{ij}(r^m, z^n)$ and f_i are given in Appendix C.

4 Numerical Results and Discussion

The quantity of critical interest in the load transfer and the absorption problems is the resultant axial force in the fiber, which is defined by

$$p(z) = 2\pi \int_0^c \sigma^{(in)}_{zz}(r, z)rdr. \tag{35}$$

Three examples will be considered in this section, which include the load absorption problems of a finite and a semi-infinite fibers which are subjected to the applied stress at infinity and the load diffusion of a finite fiber which is loaded at the certain cross-section. The parameter $\beta = E^*/E$ is used to represent the ratio of the elastic modulus of the fiber to the matrix.

At first, consider a finite fiber is embedded in an elastic matrix with different elastic moduli as shown in Fig. 1(*a*). The uniform stress σ^0_{zz} is applied along the centroidal axis of fiber at infinity. Figure 2 represents the resultant axial force as a function of the location of the cross section along the z-axis for different fiber lengths. The material parameter is $\beta = 2$ and the Poisson's ratio $\nu = \nu^* = 0.25$. It is noted that the distribution of the resultant force is almost uniform as the length of fiber becomes very large. It is known that the strain and stress fields inside the ellipsoidal inclusion are uniform as the inclusion is subjected to the uniform applied stress σ^0_{ij}. The eigenstrain can be expressed explicitly in terms of applied stress through the use of Eshelby's tensor. As the length of fiber approaches infinity, $b/c \to \infty$, the expressions for the eigenstrain given in Mura (1987) can also be rederived from Eqs. (15)–(18), which are

Downloaded 03 May 2010 to 171.66.16.20. Redistribution subject to ASME license or copyright; see http://www.asme.org/terms/Terms_Use.cfm

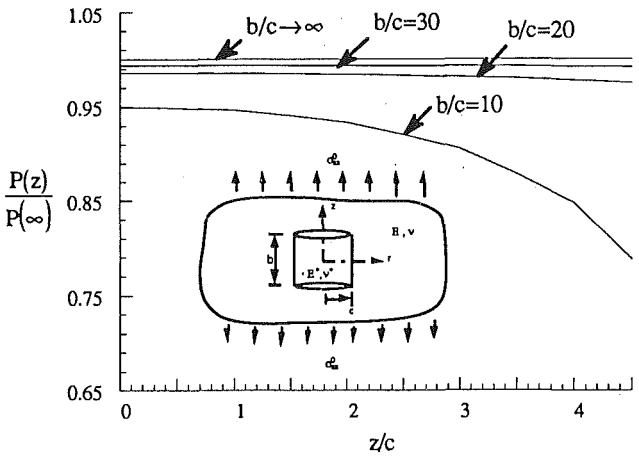


Fig. 2 Comparison of load absorption for varied normalized fiber length b/c with $\beta = 2$ and $\nu = \nu^* = 0.25$ (Case 1)

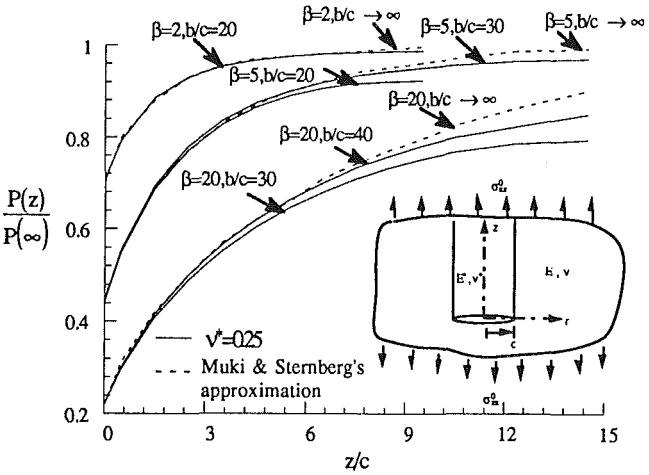


Fig. 3 Comparison of load absorption for varied normalized fiber length b/c and β with $\nu = 0.25$ (Case 2)

$$\epsilon^*_{rr} = \frac{\sigma^0_{zz}}{\mu} \times \frac{\dfrac{3\nu}{5(1-\nu)} + \dfrac{\alpha_1}{2} - \dfrac{\alpha}{5} + \dfrac{\nu\alpha_3}{(1+\nu)}\left(\alpha + \dfrac{1}{2(1-\nu)}\right)}{\det} \tag{36}$$

$$\epsilon^*_{\theta\theta} = \epsilon^*_{rr} \tag{37}$$

$$\epsilon^*_{zz} = \frac{\sigma^0_{zz}}{\mu} \times \frac{-\dfrac{3}{5(1-\nu)} - \dfrac{(\alpha_1+\alpha_2)}{2} - \dfrac{\alpha}{5} + \dfrac{\nu\alpha_3\alpha}{(1+\nu)} - \dfrac{\alpha_3}{2(1-\nu^2)}}{\det} \tag{38}$$

$$\epsilon^*_{rz} = 0 \tag{39}$$

with

$$\det = \left(\frac{1+\nu}{1-\nu} + 2\alpha_1 + \alpha_2 + \frac{1+\nu}{1-\nu}\alpha_3\right)\alpha + \frac{1}{2}\alpha_1 - \frac{\nu}{2(1-\nu)}\alpha_2 \tag{40}$$

where $\alpha_3 = \{\mu^* - \mu\}/\{\lambda^* - \lambda\}$.

As shown in Fig. 1(b), a semi-infinite fiber loaded by a remote applied stress is considered next. Figure 3 shows the resultant axial force as a function of the location of the cross-section along the z-axis for various combination of material parameter and fiber length. The Poisson's ratio is $\nu = \nu^* = 0.25$. The resultant axial force is normalized by the applied force $P(\infty)$, which is defined $P(\infty) = \pi c^2 \sigma_0 \beta$. The results are compared with those presented by Muki and Sternberg's approximation (1970). In the Muki and Sternberg's solution, the semi-infinite fiber is approximated as a one-dimensional filament by neglecting the Poisson's effect of the fiber. Thus,

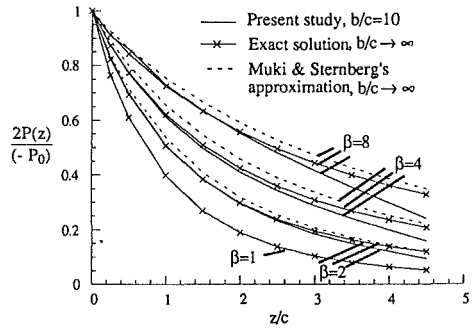


Fig. 4(a) Normalized fiber length b/c = 10

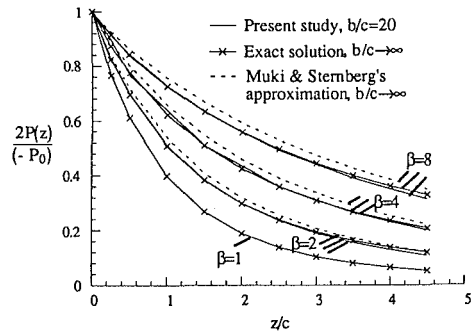


Fig. 4(b) Normalized fiber length b/c = 20

Fig. 4 Comparison of the axial fiber force for varied β with $\nu = \nu^* = 0.25$ (Case 3)

the discrepancy between the approximate solution and the presented results increase as the material parameter β becomes very large. It is noted that the axial force also changes rapidly near the end of the fiber, $z = 0$.

In the third example, the load diffusion problem of a finite fiber, which is loaded by uniformly applied stress at the cross-section of the fiber, $z = 0$, is shown in Fig. 1(c). The resultant forces along the axis of the fiber for various combinations of β and b/c are shown in Figs. 4(a)-(b) for $\nu = \nu^* = 0.25$ and Figs. 5(a)-(b) for $\nu = 0$ and $\nu^* = 0.25$. The axial force is normalized by the resultant force $P_0 = \pi c^2 \sigma_0$. As $b/c \to \infty$, the results are compared with the approximate solutions presented by Muki and Sternberg (1969), where the Poisson's ratio of fiber is neglected. It is noted that the stress component σ_{zz} at the loaded cross-section of the fiber $z = 0^+$ can be obtained from Eq. (29), which is

$$\sigma^{(in)}_{zz} \approx -\frac{c}{2}\int_0^\infty J_1(\eta c) J_0(\eta r) e^{-\eta|z|}\,\mathrm{sgn}(z)\,d\eta = -\frac{1}{2} \quad (r<c). \tag{41}$$

Therefore,

$$p(0^+) = 2\pi \int_0^c \sigma^{(in)}_{zz}(r, z) r dr = -\frac{\pi}{2} c^2. \tag{42}$$

It is observed that as $b/c > 20$, the presented results approaches the exact solutions derived by Muki and Sternberg (1969) for an infinite fiber. Figures 6(a)-(d) show the variation of the equivalent eigenstrains on some specific z plane as a function of r/c. The length of the fiber is assumed by $b/c = 20$ and material properties $\beta = 2$, $\nu = \nu^* = 0.25$. The eigenstrain has its maximum on the central part of the fiber and near the section of applied loading. Moreover, the distributions of eigenstrains become uniform as the cross-section moves away from the applied loading.

In conclusion, the equivalent inclusion method has been successfully applied to the cylindrical inhomogeneity problem. This method overcomes the restriction of fiber having larger

Downloaded 03 May 2010 to 171.66.16.20. Redistribution subject to ASME license or copyright; see http://www.asme.org/terms/Terms_Use.cfm

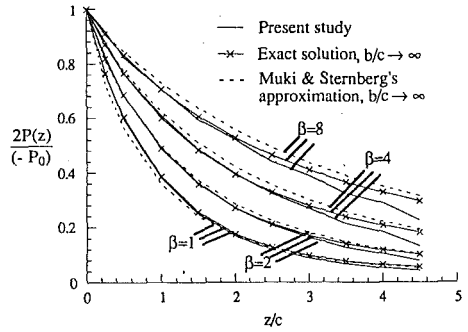


Fig. 5(*a*) Normalized fiber length *b/c* = 10

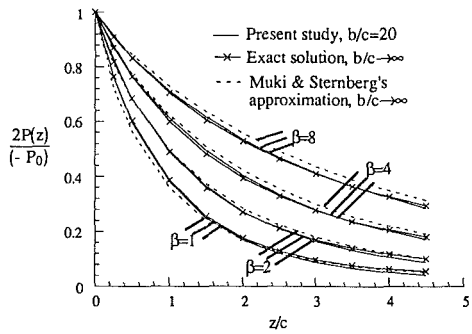


Fig. 5(*b*) Normalized fiber length *b/c* = 20

Fig. 5 Comparison of the axial fiber force for varied β with $\nu = 0$ and $\nu^* = 0.25$ (Case 3)

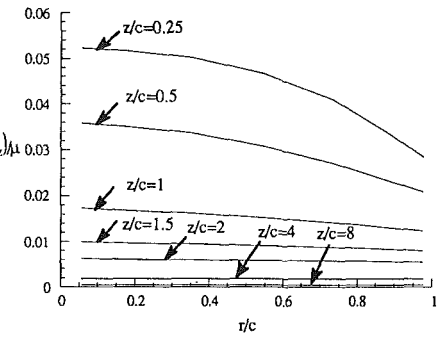


Fig. 6(*a*) The variation of ϵ^*_{rr}

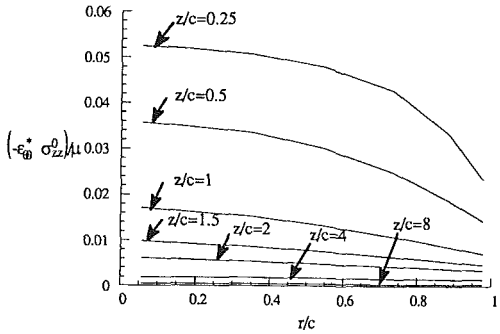


Fig. 6(*b*) The variation of $\epsilon^*_{\theta\theta}$

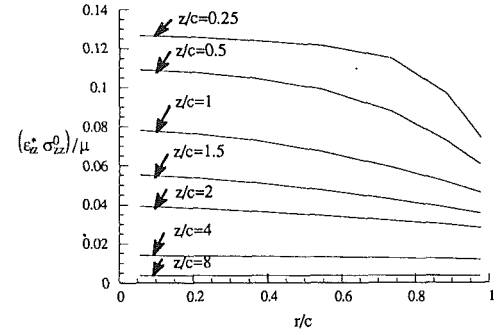


Fig. 6(*c*) The variation of ϵ^*_{zz}

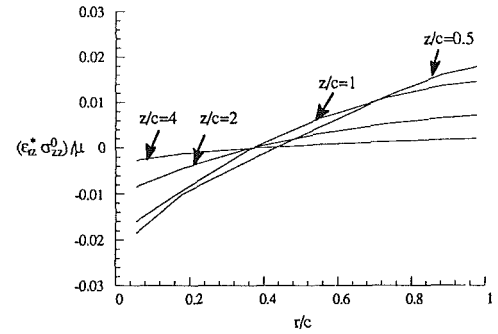


Fig. 6(*d*) The variation of ϵ^*_{rz}

Fig. 6 The eigenstrain distributions along the *r*-direction for various *z/c* (Case 3) with $\nu = \nu^* = 0.25$, $\beta = 2$, and *b/c* = 20

elastic modulus than matrix in Muki and Sternberg's approximation. The Poisson's ratio of the fiber can also be taken into consideration. The most important is that the results show favorable agreement with exact solutions.

Acknowledgment

This research is supported in part by the Air Force Office of Scientific Research under Grant No. AFOSR-F49620-92-J-0319 and in part by the Office of Naval Research under Grant No. N00014-91-J-4031/P3.

References

Abramowitz, M., and Stegun, I. A., 1972, *Handbook of Mathematical Functions*, 9th printing, Dover.

Byrd, P. F., and Friedman, M. D., 1971, *Handbook of Elliptic Integrals for Engineers and Scientists*, 2nd ed., Springer-Verlag, New York.

Chiu, Y. P., 1977, "On the Stress Field due to Initial Strains in Cuboid Surrounded by an Infinite Elastic Space," ASME Journal of Applied Mechanics, Vol. 44, pp. 587–590.

Cohen, L. J., and Romualdi, J. P., 1967, "Stress, Strain and Displacement Fields in a Composite Material Reinforced with Discontinuous Fibers," *Journal of the Franklin Institute*, Vol. 284, pp. 388–406.

Eason, G., Noble, B., and Sneddon, I. N., 1955, "On Certain Integrals of Lipschitz-Hankel Type Involving Products of Bessel Functions," *Philosophical Transaction of Royal Society, London*, Vol. A247, pp. 529–551.

Eshelby, J. D., 1957, "The Determination of the Elastic Field of an Ellipsoidal Inclusion and Related Problems," *Proceeding of the Royal Society, London*, Vol. A241, pp. 376–396.

Muki, R., and Sternberg, E., 1969, "On the Diffusion of an Axial Load from an Infinite Cylindrical Bar Embedded in an Elastic Medium," *International Journal of Solids and Structures*, Vol. 5, pp. 587–605.

Mura, T., 1987, *Micromechanics of Defects in Solids*, 2nd rev. ed., Martinus Nijhoff.

Slaughter, W. S., and Lyell Sanders, J., 1991, "A Model for Load-Transfer from an Embedded Fiber to an Elastic Matrix," *International Journal of Solids and Structures*, Vol. 28, pp. 1041–1052.

Sternberg, E., and Muki, R., 1970, "Load-Absorption by a Filament in a Fiber-Reinforced Material," *Zeitschrift Fur Angewandte Mathematik und Physik*, Vol. 21, pp. 552–569.

APPENDIX A

The fundamental solution $G_{ij}(\mathbf{x}, \mathbf{x}')$ is

(a) due to radial ring force

Downloaded 03 May 2010 to 171.66.16.20. Redistribution subject to ASME license or copyright; see http://www.asme.org/terms/Terms_Use.cfm

$$G_{rr}(\mathbf{x}, \mathbf{x}') = \frac{\rho}{8\mu(1-\nu)} \times \int_0^\infty \{\kappa - |z-z'|\eta\} J_1(\eta\rho) J_1(\eta r) e^{-\eta|z-z'|} d\eta \quad \text{(A1)}$$

$$G_{zr}(\mathbf{x}, \mathbf{x}') = \frac{\rho(z'-z)}{8\mu(1-\nu)} \int_0^\infty \eta J_1(\eta\rho) J_0(\eta r) e^{-\eta|z-z'|} d\eta, \quad \text{(A2)}$$

(b) due to hoop ring force

$$G_{\theta\theta}(\mathbf{x}, \mathbf{x}') = \frac{\rho}{2\mu} \int_0^\infty J_1'(\eta\rho) J_1(\eta r) e^{-\eta|z-z'|} d\eta, \quad \text{(A3)}$$

(c) due to vertical ring force

$$G_{rz}(\mathbf{x}, \mathbf{x}') = \frac{\rho(z-z')}{8\mu(1-\nu)} \int_0^\infty \eta J_0(\eta\rho) J_1(\eta r) e^{-\eta|z-z'|} d\eta \quad \text{(A4)}$$

$$G_{zz}(\mathbf{x}, \mathbf{x}') = \frac{\rho}{8\mu(1-\nu)} \times \int_0^\infty \{\kappa + |z-z'|\eta\} J_0(\eta\rho) J_0(\eta r) e^{-\eta|z-z'|} d\eta, \quad \text{(A5)}$$

where $J_n(\ )$ is a Bessel function of the first kind.

APPENDIX B

The operator $R_{ij}(\mathbf{x}, \mathbf{x}')$ is denoted as

$$R_{i1}(\mathbf{x}, \mathbf{x}') = (\lambda + 2\mu) A_i \frac{\partial}{\partial\rho} + A_i \frac{2\mu}{\rho} + \lambda B_i \frac{\partial}{\partial z'} \quad \text{(B1)}$$

$$R_{i2}(\mathbf{x}, \mathbf{x}') = \lambda A_i \frac{\partial}{\partial\rho} - A_i \frac{2\mu}{\rho} + \lambda B_i \frac{\partial}{\partial z'} \quad \text{(B2)}$$

$$R_{i3}(\mathbf{x}, \mathbf{x}') = \lambda A_i \frac{\partial}{\partial\rho} + (\lambda + 2\mu) B_i \frac{\partial}{\partial z'} \quad \text{(B3)}$$

$$R_{i4}(\mathbf{x}, \mathbf{x}') = 2\mu A_i \frac{\partial}{\partial z'} + 2\mu B_i \left(\frac{\partial}{\partial\rho} + \frac{1}{\rho}\right) \quad (i = 1, 2, 3, 4) \quad \text{(B4)}$$

where

$$A_1(\mathbf{x}, \mathbf{x}') = -\frac{G_{rr}(\mathbf{x}, \mathbf{x}')}{r} + \frac{\partial G_{rr}(\mathbf{x}, \mathbf{x}')}{\partial r} \quad \text{(B5)}$$

$$A_2(\mathbf{x}, \mathbf{x}') = -\frac{G_{rr}(\mathbf{x}, \mathbf{x}')}{r} + \frac{\partial G_{zr}(\mathbf{x}, \mathbf{x}')}{\partial z} \quad \text{(B6)}$$

$$A_3(\mathbf{x}, \mathbf{x}') = \frac{\{1 + 2(\mu^* - \mu)/(\lambda^* - \lambda)\}}{r} G_{rr}(\mathbf{x}, \mathbf{x}') + \frac{\partial G_{rr}(\mathbf{x}, \mathbf{x}')}{\partial r} + \frac{\partial G_{zr}(\mathbf{x}, \mathbf{x}')}{\partial z} \quad \text{(B7)}$$

$$A_4(\mathbf{x}, \mathbf{x}') = \frac{\partial G_{rr}(\mathbf{x}, \mathbf{x}')}{\partial z} + \frac{\partial G_{zr}(\mathbf{x}, \mathbf{x}')}{\partial r} \quad \text{(B8)}$$

$$B_1(\mathbf{x}, \mathbf{x}') = -\frac{G_{rz}(\mathbf{x}, \mathbf{x}')}{r} + \frac{\partial G_{rz}(\mathbf{x}, \mathbf{x}')}{\partial r} \quad \text{(B9)}$$

$$B_2(\mathbf{x}, \mathbf{x}') = -\frac{G_{rz}(\mathbf{x}, \mathbf{x}')}{r} + \frac{\partial G_{zz}(\mathbf{x}, \mathbf{x}')}{\partial z} \quad \text{(B10)}$$

$$B_3(\mathbf{x}, \mathbf{x}') = \frac{\{1 + 2(\mu^* - \mu)/(\lambda^* - \lambda)\}}{r} G_{rz}(\mathbf{x}, \mathbf{x}') + \frac{\partial G_{rz}(\mathbf{x}, \mathbf{x}')}{\partial r} + \frac{\partial G_{zz}(\mathbf{x}, \mathbf{x}')}{\partial z} \quad \text{(B11)}$$

$$B_4(\mathbf{x}, \mathbf{x}') = \frac{\partial G_{rz}(\mathbf{x}, \mathbf{x}')}{\partial z} + \frac{\partial G_{zz}(\mathbf{x}, \mathbf{x}')}{\partial r}. \quad \text{(B12)}$$

APPENDIX C

The component $k_{st}^{ij}(r^m, z^n)$ and f_i is expressed by using the following equations:

The integral of Lipschitz-Hankel type is of the form

$$I(\alpha, \beta, \nu; \zeta) = \int_0^\infty J_\alpha(\eta a) J_\beta(\eta b) e^{-\eta\zeta} \eta^\nu d\eta \quad \text{(C1)}$$

With different arguments, the following symbol is defined as

$$K(c^*, b^*) = \int_0^\infty J_\alpha(\eta c^*) J_\beta(\eta r) e^{-\eta\zeta} \eta^\nu d\eta \quad \text{(C2)}$$

$$L(b^*) = \int_0^\infty J_\alpha(\eta\rho) J_\beta(\eta r) e^{-\eta\xi} \eta^\nu d\eta \quad \text{(C3)}$$

where $\zeta = \zeta(z, b^*)$ is the function z and b^*.

Using the above definition, the different combinations of Lipschitz-Hankel integrations are shown as

$$I_1(\alpha, \beta, \nu; p) = c_i K(c_i, b_{j+1}) + c_{i+1} K(c_{i+1}, b_j) - c_i K(c_i, b_j) - c_{i+1} K(c_{i+1}, b_{j+1}) \quad \text{(C4)}$$

$$I_2(\alpha, \beta, \nu; p) = K(c_i, b_{j+1}) + K(c_{i+1}, b_j) - K(c_i, b_j) - K(c_{i+1}, b_{j+1}) \quad \text{(C5)}$$

$$I_3(\alpha, \beta, \nu; p) = c_i(z - b_{j+1}) K(c_i, b_{j+1}) + c_{i+1}(z - b_j) K(c_{i+1}, b_j) - c_i(z - b_j) K(c_i, b_j) - c_{i+1}(z - b_{j+1}) K(c_{i+1}, b_{j+1}) \quad \text{(C6)}$$

$$I_4(\alpha, \beta, \nu; p) = c_i|z - b_{j+1}| K(c_i, b_{j+1}) + c_{i+1}|z - b_j| K(c_{i+1}, b_j) - c_i|z - b_j| K(c_i, b_j) - c_{i+1}|z - b_{j+1}| K(c_{i+1}, b_{j+1}) \quad \text{(C7)}$$

$$I_5(\alpha, \beta, \nu; p) = |z - b_{j+1}| K(c_i, b_{j+1}) + |z - b_j| K(c_{i+1}, b_j) - |z - b_j| K(c_i, b_j) - |z - b_{j+1}| K(c_{i+1}, b_{j+1}) \quad \text{(C8)}$$

$$I_6(\alpha, \beta, \nu; p) = (z - b_{j+1}) K(c_i, b_{j+1}) + (z - b_j) K(c_{i+1}, b_j) - (z - b_j) K(c_i, b_j) - (z - b_{j+1}) K(c_{i+1}, b_{j+1}) \quad \text{(C9)}$$

$$I_7(\alpha, \beta, \nu; p) = c_i\, \mathrm{sgn}(z - b_{j+1}) K(c_i, b_{j+1}) + c_{i+1} \mathrm{sgn}(z - b_j) K(c_{i+1}, b_j) - c_i \mathrm{sgn}(z - b_j) K(c_i, b_j) - c_{i+1} \mathrm{sgn}(z - b_{j+1}) K(c_{i+1}, b_{j+1}) \quad \text{(C10)}$$

$$J_1(\alpha, \beta, \nu; \zeta) = \int_{c_i}^{c_{i+1}} L(b_j) d\rho - \int_{c_i}^{c_{i+1}} L(b_{j+1}) d\rho \quad \text{(C11)}$$

$$J_2(\alpha, \beta, \nu; \zeta) = (z - b_j) \int_{c_i}^{c_{i+1}} L(b_j) d\rho - (z - b_{j+1}) \int_{c_i}^{c_{i+1}} L(b_{j+1}) d\rho \quad \text{(C12)}$$

$$J_3(\alpha, \beta, \nu; \zeta) = |z - b_j| \int_{c_i}^{c_{i+1}} L(b_j) d\rho - |z - b_{j+1}| \int_{c_i}^{c_{i+1}} L(b_{j+1}) d\rho \quad \text{(C13)}$$

$$J_4(\alpha, \beta, \nu; \zeta) = \mathrm{sgn}(z - b_j) \int_{c_i}^{c_{i+1}} L(b_j) d\rho - \mathrm{sgn}(z - b_{j+1}) \int_{c_i}^{c_{i+1}} L(b_{j+1}) d\rho \quad \text{(C14)}$$

where

$$\mathrm{sgn}(z - b) = \begin{Bmatrix} 1 & z > b \\ -1 & z < b \\ 0 & z = b \end{Bmatrix}. \quad \text{(C15)}$$

Furthermore, the following integrations are defined as

$$D_1 = \int_0^\infty \frac{1}{\eta^2} J_1(\eta r) [J_0(\eta c_i) - J_0(\eta c_{i+1})] g_1 d\eta,$$

Downloaded 03 May 2010 to 171.66.16.20. Redistribution subject to ASME license or copyright; see http://www.asme.org/terms/Terms_Use.cfm

$$D_2=\int_0^\infty \frac{1}{\eta} J_0(\eta r)[J_0(\eta c_i)-J_0(\eta c_{i+1})]g_1 d\eta,$$

$$D_3=\int_0^\infty J_1(\eta r)[c_i J_0(\eta c_i)-c_{i+1}J_0(\eta c_{i+1})]g_1 d\eta,$$

$$D_4=\int_{c_i}^{c_{i+1}} d\rho \int_0^\infty J_0(\eta\rho)J_1(\eta r)g_1 d\eta \tag{C16}$$

with

$$g_1=\begin{cases} e^{-\eta(z-b_{j+1})}-e^{-\eta(z-b_j)} & z>b_{j+1} \\ 2-e^{-\eta(z-b_j)}-e^{\eta(z-b_{j+1})} & b_j<z<b_{j+1} \\ -e^{\eta(z-b_{j+1})}+e^{\eta(z-b_j)} & z<b_j \end{cases}. \tag{C17}$$

The components $k_{st}^{ij}(r^m, z^n)$ and f_i are shown as follows:

$$k_{11}^{ij}(r,z)=\frac{1}{\nu_1}\left\{-\frac{\nu_2}{r}D_1+\frac{\nu_2}{2}D_2+\frac{\nu_1}{2}I_1(1,0,0;p)\right.$$
$$-\frac{\nu_1}{r}I_1(1,1,-1;p)-\frac{1}{4}I_3(1,0,1;p)+\frac{1}{2r}I_3(1,1,0;p)$$
$$\left.-\frac{1}{4}I_6(0,0,0;m)+\frac{1}{2r}I_6(0,1,-1;m)\right\} \tag{C18}$$

$$k_{12}^{ij}(r,z)=\frac{1}{\nu_1}\left\{\frac{\nu_2}{r}D_1-\frac{\nu_2}{2}D_2+\frac{\nu}{2}I_1(1,0,0;p)\right.$$
$$-\frac{\nu}{r}I_1(1,1,-1;p)$$
$$\left.+\frac{1}{4}I_6(0,0,0;m)-\frac{1}{2r}I_6(0,1,-1;m)\right\} \tag{C19}$$

$$k_{13}^{ij}(r,z)=\frac{1}{\nu_1}\left\{\frac{\nu}{2}I_1(1,0,0;p)-\frac{\nu}{r}I_1(1,1,-1;p)\right.$$
$$\left.+\frac{1}{4}I_3(1,0,1;p)-\frac{1}{2r}I_3(1,1,0;p)\right\} \tag{C20}$$

$$k_{14}^{ij}(r,z)=\frac{1}{\nu_1}\left\{\frac{\nu_2}{2}J_1(0,0,0;p)-\frac{\nu_2}{r}J_1(1,0,-1;m)\right.$$
$$-\frac{1}{2}J_3(0,0,1;m)+\frac{1}{r}J_3(1,0,0;m)$$
$$-\frac{\nu_2}{2}I_1(0,0,0;p)+\frac{\kappa}{2r}I_1(0,1,-1;m)$$
$$-\frac{1}{2r}I_1(0,1,-1;p)+\frac{1}{4}I_3(0,0,1;p)-\frac{1}{2r}I_3(0,1,0;p)$$
$$\left.+\frac{1}{4}I_4(0,0,1;m)-\frac{1}{2r}I_4(0,1,0;m)\right\} \tag{C21}$$

$$k_{21}^{ij}(r,z)=\frac{1}{\nu_1}\left\{-\frac{\nu_2}{2r}D_1-\frac{\nu_1}{2r}I_1(1,1,-1;p)+\frac{1}{4}I_3(1,0,1;p)\right.$$
$$+\frac{1}{4r}I_3(1,1,0;p)+\frac{1}{4}I_6(0,0,0;m)$$
$$\left.+\frac{1}{4r}I_6(0,1,-1;m)-\frac{\nu}{2}I_7(1,0,0;m)\right\} \tag{C22}$$

$$k_{22}^{ij}(r,z)=\frac{1}{\nu_1}\left\{\frac{\nu_2}{2r}D_1-\frac{\nu}{2r}I_1(1,1,-1;p)-\frac{1}{4}I_6(0,0,0;m)\right.$$
$$\left.-\frac{1}{4r}I_6(0,1,-1;m)-\frac{\nu}{2}I_7(1,0,0;m)\right\} \tag{C23}$$

$$k_{23}^{ij}(r,z)=\frac{1}{\nu_1}\left\{-\frac{\nu}{2r}I_1(1,1,-1;p)-\frac{1}{4}I_3(1,0,1;p)\right.$$
$$\left.-\frac{1}{4r}I_3(1,1,0;p)-\frac{\nu_1}{2}I_7(1,0,0;m)\right\} \tag{C24}$$

$$k_{24}^{ij}(r,z)=\frac{1}{\nu_1}\left\{\frac{\nu_2}{2}J_1(0,0,0;p)-\frac{\nu_2}{2r}J_1(1,0,-1;m)\right.$$
$$+\frac{1}{2}J_3(0,0,1;m)+\frac{1}{2r}J_3(1,0,0;m)$$
$$-\frac{\nu_2}{2}I_1(0,0,0;p)+\frac{\kappa}{4r}I_1(0,1,-1;m)$$
$$-\frac{1}{4r}I_1(0,1,-1;p)-\frac{1}{4r}I_3(0,1,0;p)-\frac{1}{4}I_3(0,0,1;p)$$
$$\left.-\frac{1}{4}I_4(0,0,1;m)-\frac{1}{4r}I_4(0,1,0;m)\right\} \tag{C25}$$

$$k_{31}^{ij}(r,z)=\frac{1}{\nu_1}\left\{\frac{\nu_2\alpha_3}{r}D_1+\frac{\nu_2}{2}D_2+\frac{\nu_1\alpha_3}{r}I_1(1,1,-1;p)\right.$$
$$+\frac{\nu_1}{2}I_1(1,0,0;p)-\frac{\alpha_3}{2r}I_3(1,1,0;p)-\frac{\alpha_3}{2r}I_6(0,1,-1;m)$$
$$\left.-\frac{\nu}{2}I_7(1,0,0;m)\right\} \tag{C26}$$

$$k_{32}^{ij}(r,z)=\frac{1}{\nu_1}\left\{-\frac{\nu_2\alpha_3}{r}D_1-\frac{\nu_2}{2}D_2+\frac{\nu}{2}I_1(1,0,0;p)\right.$$
$$+\frac{\nu\alpha_3}{r}I_1(1,1,-1;p)+\frac{\alpha_3}{2r}I_6(0,1,-1;m)$$
$$\left.-\frac{\nu}{2}I_7(1,0,0;m)\right\} \tag{C27}$$

$$k_{33}^{ij}(r,z)=\frac{1}{\nu_1}\left\{\frac{\nu}{2}I_1(1,0,0;p)+\frac{\nu\alpha_3}{r}I_1(1,1,-1;p)\right.$$
$$\left.+\frac{\alpha_3}{2r}I_3(1,1,0;p)-\frac{\nu_1}{2}I_7(1,0,0;m)\right\} \tag{C28}$$

$$k_{34}^{ij}(r,z)=\frac{1}{\nu_1}\left\{\nu_2 J_1(0,0,0;p)+\frac{\nu_2\alpha_3}{r}J_1(1,0,-1;m)\right.$$
$$-\frac{\alpha_3}{r}J_3(1,0,0;m)-\nu_2 I_1(0,0,0;p)-\frac{\kappa\alpha_3}{2r}I_1(0,1,-1;m)$$
$$+\frac{\alpha_3}{2r}I_1(0,1,-1;p)+\frac{\alpha_3}{2r}I_3(0,1,0;p)$$
$$\left.+\frac{\alpha_3}{2r}I_4(0,1,0;m)\right\} \tag{C29}$$

$$k_{41}^{ij}(r,z)=\frac{1}{\nu_1}\left\{-\frac{1}{2}I_1(1,1,0;p)-\frac{\nu_2}{2}I_2(0,1,-1;m)\right.$$
$$\left.+\frac{1}{2}I_3(1,1,1;p)+\frac{1}{2}I_5(0,1,0;m)\right\} \tag{C30}$$

$$k_{42}^{ij}(r,z)=\frac{1}{\nu_1}\left\{-\nu I_1(1,1,0;p)+\frac{\nu_2}{2}I_2(0,1,-1;m)\right.$$
$$\left.-\frac{1}{2}I_5(0,1,0;m)\right\} \tag{C31}$$

$$k_{43}^{ij}(r,z)=\frac{1}{\nu_1}\left\{-\frac{1}{2}I_1(1,1,0;p)-\frac{1}{2}I_3(1,1,1;p)\right\} \tag{C32}$$

Downloaded 03 May 2010 to 171.66.16.20. Redistribution subject to ASME license or copyright; see http://www.asme.org/terms/Terms_Use.cfm

$$k_{44}^{ij}(r, z)=\frac{1}{\nu_1}\left\{-\nu_1 D_4+J_2(1, 0, 1; p)-\nu_1 J_4(1, 0, 0; m)\right.$$

$$\left.-\nu_1 I_1(0, 1, 0; p)-I_3(0, 1, 1; p)+\nu_1 I_7(0, 1, 0; m)\right\} \quad \text{(C33)}$$

where

$$\nu_1=1-\nu,\ \nu_2=1-2\nu \text{ and } \kappa=3-4\nu. \quad \text{(C34)}$$

The sub index m means $\zeta = |z - b|$, n means $\zeta = (z + b)$ and p means $\zeta = (z - b)$.

For Case 1 and Case 2:

$$f_1(r, z)=0 \qquad f_2(r, z)=\frac{1}{2\mu}$$

$$f_3(r, z)=+\frac{(1-2\nu-2\nu\Gamma_3)}{2\mu(1+\nu)} \qquad f_4(r, z)=0 \quad \text{(C35)}$$

For Case 3:

$$f_1(r, z)=\frac{z}{8\mu(1-\nu)} I_f(1, 0; 1)-\frac{z}{4\mu(1-\nu)r} I_f(1, 1; 0)$$

$$f_2(r, z)=-\frac{z}{8\mu(1-\nu)} I_f(1, 0; 1)-\frac{z}{8\mu(1-\nu)r} I_f(1, 1; 0)$$

$$-\frac{(1-2\nu)}{4\mu(1-\nu)} \operatorname{sgn}(z) I_f(1, 0; 0)$$

$$f_3(r, z)=+\frac{z\Gamma_3}{4\mu r(1-\nu)} I_f(1, 1; 0)-\frac{(1-2\nu)}{4\mu(1-\nu)} \operatorname{sgn}(z) I_f(1, 0; 0)$$

$$f_4(r, z)=-\frac{|z|}{4\mu(1-\nu)} I_f(1, 1; 1)-\frac{(1-2\nu)}{4\mu(1-\nu)} I_f(1, 1; 0) \quad \text{(C36)}$$

with

$$I_f(\alpha, \beta; \gamma)=\int_0^\infty J_\alpha(\eta c) J_\beta(\eta r) e^{-\eta|z|} \eta^\gamma d\eta. \quad \text{(C37)}$$

Downloaded 03 May 2010 to 171.66.16.20. Redistribution subject to ASME license or copyright; see http://www.asme.org/terms/Terms_Use.cfm

Hilbert Transform Generalization of a Classical Random Vibration Integral

P. D. Spanos
L. B. Ryon Chair in Engineering,
Fellow ASME.

S. M. Miller
Research Assistant.

Department of Mechanical Engineering,
and Materials Science,
Rice University,
P.O. Box 1892,
Houston, TX 77251

Integrals which represent the spectral moments of the stationary response of a linear and time-invariant system under random excitation are considered. It is shown that these integrals can be determined through the solution of linear algebraic equations. These equations are derived by considering differential equations for both the autocorrelation function of the system response and its Hilbert transform. The method can be applied to determine both even-order and odd-order spectral moments. Furthermore, it provides a potent generalization of a classical formula used in control engineering and applied mathematics. The applicability of the derived formula is demonstrated by considering random excitations with, among others, the white noise, "Gaussian," and Kanai-Tajimi seismic spectra. The results for the classical problem of a randomly excited single-degree-of-freedom oscillator are given in a concise and readily applicable format.

Introduction

A class of integrals often encountered in random vibrations and many other scientific fields is considered. Within the field of random vibrations, these integrals may represent the spectral moments of the response of a linear and time-invariant system to a stationary random excitation. Using the properties of correlation functions and the Hilbert transform (Papoulis, 1984), linear algebraic equations involving the response spectral moments are derived. The present approach is a generalization of that presented by Spanos (1983, 1987) and includes the classical James et al. (1965) integral of control engineering as a special case; it deals with the determination of odd-order spectral moments which cannot be determined by the formulae given in these references. The approach is particularly useful when the excitation spectrum has a rational polynomial form. It can, however, be applied when the excitation spectrum has any Fourier transformable form.

General formulae for use in calculating the response spectral moments when the excitation has a white noise, band-limited white noise, or "Gaussian" shaped spectrum are derived. Moreover, explicit expressions for the response spectral moments of a standard linear oscillator are derived for a variety of useful excitation spectra. These results could be supplemented by the work of Yang and Iwan (1972) on randomly excited linear multi-degree-of-freedom systems, of Shinozuka et al. (1986) on a class of random vibration integrals, and of Di Paola and Petrucci (1990) on spectral moments of nonstationary processes.

Contributed by the Applied Mechanics Division of THE AMERICAN SOCIETY OF MECHANICAL ENGINEERS for publication in the ASME JOURNAL OF APPLIED MECHANICS.

Discussion on this paper should be addressed to the Technical Editor, Professor Lewis T. Wheeler, Department of Mechanical Engineering, University of Houston, Houston, TX 77204-4792, and will be accepted until four months after final publication of the paper itself in the ASME JOURNAL OF APPLIED MECHANICS.

Manuscript received by the ASME Applied Mechanics Division, Feb. 17, 1993; final revision, May 18, 1993. Associate Technical Editor: L. T. Wheeler.

Differential Equations for Correlation Functions

Consider the response of an mth-order linear system under a stationary random excitation $f(t)$. The system response is governed by the differential equation

$$\lambda_m x^{(m)}(t) + \lambda_{m-1} x^{(m-1)}(t) + \ldots + \lambda_0 x(t) = f(t), \quad (1)$$

where $x^{(k)}(t) = d^k/dt^k\, x(t)$ and λ_k ($k = 0, 1, 2, \ldots, m$) are time-invariant constants. The autocorrelation function of the excitation, $R_{ff}(\tau)$, and the double-sided power spectral density function, $S_{ff}(\omega)$, are related by the Fourier transform pair

$$S(\omega) = \frac{1}{2\pi}\int_{-\infty}^{\infty} R(\tau) e^{-i\omega\tau} d\tau, \quad R(\tau) = \int_{-\infty}^{\infty} S(\omega) e^{i\omega\tau} d\omega, \quad (2)$$

where $i = \sqrt{-1}$. The one-sided power spectral density function, $G_{ff}(\omega)$, is related to its double-sided counterpart by the equation

$$G(\omega) = 2U(\omega)S(\omega) = S(\omega) + S(\omega)\mathrm{sgn}(\omega), \quad (3)$$

where $U(\omega)$ is the unit-step function and $\mathrm{sgn}(\omega)$ is the signum function. Furthermore, the excitation and the response spectral density functions are related by the equation

$$S_{xx}(\omega) = \frac{S_{ff}(\omega)}{|\Lambda(i\omega)|^2}, \quad (4)$$

where $\Lambda(s) = \lambda_m s^m + \lambda_{m-1} s^{m-1} + \ldots + \lambda_0$ is the characteristic polynomial of the linear system.

By noting the relations

$$E[x(t)x^{(k)}(t-\tau)] = (-1)^k R_{xx}^{(k)}(\tau), \quad (5)$$

and

$$E[x^{(k)}(t+\tau)f(t)] = R_{xf}^{(k)}(\tau), \quad (6)$$

Copyright © 1994 by ASME
Downloaded 03 May 2010 to 171.66.16.20. Redistribution subject to ASME license or copyright; see http://www.asme.org/terms/Terms_Use.cfm

where $(\cdot)^{(k)} = \partial^k/\partial\tau^k\,(\cdot)$ and $E[\cdot]$ denotes the mathematical expectation operator, it is possible to derive differential equations which govern $R_{xx}(\tau)$ and $R_{xf}(\tau)$. Specifically, one finds

$$\tilde{\lambda}_m R_{xx}^{(j+m)}(\tau) + \tilde{\lambda}_{m-1} R_{xx}^{(j+m-1)}(\tau) + \ldots + \tilde{\lambda}_0 R_{xx}^{(j)}(\tau) = R_{xf}^{(j)}(\tau) \quad (7)$$

and

$$\lambda_m R_{xf}^{(n+m)}(\tau) + \lambda_{m-1} R_{xf}^{(n+m-1)}(\tau) + \ldots + \lambda_0 R_{xf}^{(n)}(\tau) = R_{ff}^{(n)}(\tau), \quad (8)$$

where $\tilde{\lambda}_k = (-1)^k \lambda_k$ $(k = 0, 1, 2, \ldots, m)$. Clearly, these equations are valid only if the required differentiation is meaningful.

By setting n equal to zero in Eq. (8), it becomes the governing differential equation for a linear and time-invariant system with excitation expressed by $R_{ff}(\tau)$ and response given by $R_{xf}(\tau)$. Thus, one may write

$$R_{xf}(\tau) = \int_{-\infty}^{\infty} h(\tau - u) R_{ff}(u)\, du, \quad (9)$$

where $h(t)$ is the impulse response function of the linear system. Using Leibniz's rule to differentiate this expression with respect to τ gives

$$R_{xf}^{(k)}(\tau) = \int_{-\infty}^{\infty} h^{(k)}(\tau - u) R_{ff}(u)\, du. \quad (10)$$

Next, consider the Hilbert transform $\hat{x}(t)$ of $x(t)$ defined as (Papoulis, 1984)

$$\hat{x}(t) = \frac{1}{\pi} \int_{-\infty}^{\infty} \frac{x(\tau)}{t - \tau}\, d\tau = x(t) * \frac{1}{\pi t}, \quad (11)$$

where the asterisk denotes convolution. Note that the Hilbert transform operation commutes with the differentiation and the convolution operations. Thus, taking the Hilbert transform of Eqs. (7), (8), and (10) yields

$$\tilde{\lambda}_m \hat{R}_{xx}^{(j+m)}(\tau) + \tilde{\lambda}_{m-1} \hat{R}_{xx}^{(j+m-1)}(\tau) + \ldots + \tilde{\lambda}_0 \hat{R}_{xx}^{(j)}(\tau) = \hat{R}_{xf}^{(j)}(\tau), \quad (12)$$

$$\lambda_m \hat{R}_{xf}^{(n+m)}(\tau) + \lambda_{m-1} \hat{R}_{xf}^{(n+m-1)}(\tau) + \ldots + \lambda_0 \hat{R}_{xf}^{(n)}(\tau) = \hat{R}_{ff}^{(n)}(\tau), \quad (13)$$

and

$$\hat{R}_{xf}^{(k)}(\tau) = \int_{-\infty}^{\infty} h^{(k)}(\tau - u) \hat{R}_{ff}(u)\, du, \quad (14)$$

respectively, for $k = 0, 1, 2, \ldots, m-1$. Again, these equations are only valid if the differentiation is meaningful.

Equations for the Spectral Moments

Consider the kth spectral moment of the system response. In general, this is defined by the integral

$$M_k = \int_0^{\infty} \omega^k G_{xx}(\omega)\, d\omega = \int_0^{\infty} \frac{\omega^k G_{ff}(\omega)}{|\Lambda(i\omega)|^2}\, d\omega, \quad (15)$$

where $G_{xx}(\omega)$ is the one-sided spectral density of the response process, $G_{ff}(\omega)$ is the one-sided power spectral density of the excitation process; and $\Lambda(i\omega)$ is the characteristic polynomial of the linear system evaluated at $s = i\omega$.

Reserving the notation $S(\omega)$ to denote double-sided spectral density functions, an equivalent double-sided spectral density $S_{zz}(\omega)$ is introduced such that

$$S_{zz}(\omega) = G_{xx}(\omega) = S_{xx}(\omega) + S_{xx}(\omega)\,\mathrm{sgn}(\omega). \quad (16)$$

Taking the inverse Fourier transform of Eq. (16) yields

$$R_{zz}(\tau) = R_{xx}(\tau) + iR_{xx}(\tau) * \left(\frac{1}{\pi\tau}\right) = R_{xx}(\tau) + i\hat{R}_{xx}(\tau), \quad (17)$$

where $\hat{R}_{xx}(\tau)$ denotes the Hilbert transform of $R_{xx}(\tau)$.

With this new definition, the kth response spectral moment is given by the equation

$$M_k = \int_{-\infty}^{\infty} \omega^k S_{zz}(\omega)\, d\omega = (-i)^k R_{zz}^{(k)}(0), \quad (18)$$

where the inverse Fourier transform of $S_{xx}(\omega)$ has been differentiated and evaluated at $\tau = 0$. Recall that the autocorrelation function is an even function of τ for real-valued random processes. Furthermore, it can be shown that the Hilbert transform of an even function is an odd function. Hence, the odd-order derivatives of $R_{xx}(\tau)$ and the even-order derivatives of $\hat{R}_{xx}(\tau)$ must be zero when evaluated at $\tau = 0$. Thus, by substituting Eq. (17) into Eq. (18), the expressions for the even and the odd spectral moments become uncoupled. Specifically, one finds the equations

$$M_{2k} = (-1)^k R_{xx}^{(2k)}(0), \quad R_{xx}^{(2k+1)}(0) = 0, \quad (19)$$

and

$$M_{2k+1} = (-1)^k \hat{R}_{xx}^{(2k+1)}(0), \quad \hat{R}_{xx}^{(2k)}(0) = 0. \quad (20)$$

Now consider Eq. (7) for $\tau = 0$. This is simply a linear algebraic equation involving the even-order response spectral moments. Thus, it is possible to obtain m linear algebraic equations by setting j equal to $m-1$, $m-2$, $m-3$, ..., 0 in sequence. A similar procedure may be applied to Eq. (12) to obtain a set of linear algebraic equations involving the response spectral moments of odd order. These procedures yield

$$\begin{bmatrix} \lambda_{m-1} & -\lambda_{m-3} & \lambda_{m-5} & \cdot & \cdot & 0 & 0 & M_{2m-2} \\ -\lambda_m & \lambda_{m-2} & -\lambda_{m-4} & \cdot & \cdot & 0 & 0 & M_{2m-4} \\ 0 & -\lambda_{m-1} & \lambda_{m-3} & \cdot & \cdot & 0 & 0 & M_{2m-6} \\ \cdot & \cdot & \cdot & \cdot & \cdot & \cdot & \cdot & \cdot \\ 0 & \cdot & \cdot & \cdot & \lambda_2 & -\lambda_0 & 0 & M_4 \\ 0 & \cdot & \cdot & \cdot & -\lambda_3 & \lambda_1 & 0 & M_2 \\ 0 & \cdot & \cdot & \cdot & \lambda_4 & -\lambda_2 & \lambda_0 & M_0 \end{bmatrix} = \begin{Bmatrix} r_{m-1} \\ r_{m-2} \\ r_{m-3} \\ \cdot \\ r_2 \\ r_1 \\ r_0 \end{Bmatrix} \quad (21)$$

and

$$\begin{bmatrix} \lambda_m & -\lambda_{m-2} & \lambda_{m-4} & \cdot & \cdot & \cdot & 0 & M_{2m-1} \\ 0 & \lambda_{m-1} & -\lambda_{m-3} & \cdot & \cdot & \cdot & 0 & M_{2m-3} \\ 0 & -\lambda_m & \lambda_{m-2} & \cdot & \cdot & \cdot & 0 & M_{2m-5} \\ \cdot & \cdot & \cdot & \cdot & \cdot & \cdot & \cdot & \cdot \\ 0 & 0 & \cdot & \cdot & \lambda_3 & -\lambda_1 & 0 & M_5 \\ 0 & 0 & \cdot & \cdot & -\lambda_4 & \lambda_2 & -\lambda_0 & M_3 \\ 0 & 0 & \cdot & \cdot & \lambda_5 & -\lambda_3 & \lambda_1 & M_1 \end{bmatrix} = \begin{Bmatrix} \hat{r}_{m-1} \\ \hat{r}_{m-2} \\ \hat{r}_{m-3} \\ \cdot \\ \hat{r}_2 \\ \hat{r}_1 \\ \hat{r}_0 \end{Bmatrix}, \quad (22)$$

Downloaded 03 May 2010 to 171.66.16.20. Redistribution subject to ASME license or copyright; see http://www.asme.org/terms/Terms_Use.cfm

where Eqs. (10) and (14) evaluated at $\tau = 0$ give

$$r_k = R_{xf}^{(k)}(0) = \int_0^\infty h^{(k)}(u) R_{ff}(u)\, du, \tag{23}$$

and

$$\hat{r}_k = -\hat{R}_{xf}^{(k)}(0) = \int_0^\infty h^{(k)}(u) \hat{R}_{ff}(u)\, du. \tag{24}$$

Clearly, given the quantities $r_0, r_1, r_2, \ldots, r_{m-1}$, the value of any even-order spectral moment can be determined by solving the system of linear Eqs. (21). Similarly, given the quantities $\hat{r}_0, \hat{r}_1, \hat{r}_2, \ldots, \hat{r}_{m-1}$, the value of any odd-order spectral moment can be calculated by solving the system of linear Eqs. (22). Note that using Eqs. (7), (12), (19), and (20), recurrence relations for the determination of spectral moments of order higher than $2m - 1$ can be derived. Specifically,

$$\tilde{\lambda}_m R_{xx}^{(j+m)}(0) + \tilde{\lambda}_{m-1} R_{xx}^{(j+m-1)}(0) = r_j - \sum_{k=0}^{m-2} \tilde{\lambda}_k R_{xx}^{(j+k)}(0), \tag{25}$$

and

$$\tilde{\lambda}_m \hat{R}_{xx}^{(j+m)}(0) + \tilde{\lambda}_{m-1} \hat{R}_{xx}^{(j+m-1)}(0) = -\hat{r}_j - \sum_{k=0}^{m-2} \tilde{\lambda}_k \hat{R}_{xx}^{(j+k)}(0). \tag{26}$$

Clearly, in dealing with Eqs. (25) and (26), Eqs. (19) and (20) are used to relate the correlation functions with the response spectral moments. Furthermore, the values of r_j and $\hat{r}_j$ for $j \geq m$ can be calculated recursively from the equations

$$r_{n+m} = \left[R_{ff}^{(n)}(0) - \sum_{k=0}^{m-1} \lambda_k r_{n+k} \right] \Big/ \lambda_m, \tag{27}$$

and

$$\hat{r}_{n+m} = \left[-\hat{R}_{ff}^{(n)}(0) - \sum_{k=0}^{m-1} \lambda_k \hat{r}_{n+k} \right] \Big/ \lambda_m. \tag{28}$$

These have been derived from Eqs. (8) and (13).

Upon solving Eqs. (21) and (22), any linear combination of M_k, $k = 0, 1, 2, \ldots, 2m - 2$, can be determined. This allows one to consider integrals of the form

$$I_m = \int_0^\infty \frac{\Xi_m(\omega) G_{ff}(\omega)}{|\Lambda(i\omega)|^2}\, d\omega, \tag{29}$$

where $\Xi_m(\omega)$ is a polynomial in ω of order $2m - 1$. That is,

$$\Xi_m(\omega) = \xi_{m-1}\omega^{2m-1} + \xi_{m-1}\omega^{2m-2} + \xi_{m-2}\omega^{2m-3} + \xi_{m-2}\omega^{2m-4} + \ldots + \xi_0\omega + \xi_0, \tag{30}$$

where $\xi_0, \xi_1, \xi_2, \ldots, \xi_{m-1}$ are arbitrary constant coefficients for the even powers of ω, and $\hat{\xi}_0, \hat{\xi}_1, \hat{\xi}_2, \ldots, \hat{\xi}_{m-1}$ are arbitrary constant coefficients for the odd powers of ω. Note that integrals of this form appear, for example, when considering an excitation spectrum described by a rational polynomial, as well as when calculating the modal response spectral moments for multi-degree-of-freedom linear systems (Der Kiureghian, 1980). For the latter case it is necessary to determine integrals of the form

$$C_{n,jk} = \int_0^\infty \frac{\omega^n \Lambda_j^*(i\omega) \Lambda_k(i\omega) G_{ff}(\omega)}{|\Lambda(i\omega)|^2}\, d\omega, \tag{31}$$

where $\Lambda_p(s)$ denotes the characteristic equation for the pth modal differential equation and $\Lambda(s)$ is given by the equation

$$\Lambda(s) = \Lambda_j(s)\Lambda_k(s). \tag{32}$$

Thus, the required integrals can readily be put into the form of Eq. (29). Consequently, attention is focused on integrals of the form shown in Eq. (29).

Clearly, the integral I_m is a linear combination of integrals in the form of Eq. (15). That is

$$I_m = \hat{\xi}_{m-1} M_{2m-1} + \xi_{m-1} M_{2m-2} + \ldots + \hat{\xi}_0 M_1 + \xi_0 M_0. \tag{33}$$

Combining Eqs. (21) and (22) and taking into consideration the nullity of a determinant with two identical columns gives

$$I_m = \frac{\det \tilde{\Gamma}}{\det \Gamma} - 1, \tag{34}$$

where

$$\Gamma = \begin{bmatrix} \lambda_m & 0 & -\lambda_{m-2} & 0 & \cdot & \cdot & \cdot & 0 & 0 \\ 0 & \lambda_{m-1} & 0 & -\lambda_{m-3} & \cdot & \cdot & \cdot & 0 & 0 \\ 0 & 0 & \lambda_{m-1} & 0 & \cdot & \cdot & \cdot & 0 & 0 \\ 0 & -\lambda_m & 0 & \lambda_{m-2} & \cdot & \cdot & \cdot & 0 & 0 \\ \cdot & \cdot & \cdot & \cdot & \cdot & \cdot & \cdot & \cdot & \cdot \\ 0 & 0 & \cdot & \cdot & \cdot & \lambda_2 & 0 & -\lambda_0 & 0 \\ 0 & 0 & \cdot & \cdot & \cdot & 0 & \lambda_1 & 0 & 0 \\ 0 & 0 & \cdot & \cdot & \cdot & -\lambda_3 & 0 & \lambda_1 & 0 \\ 0 & 0 & \cdot & \cdot & \cdot & 0 & -\lambda_2 & 0 & \lambda_0 \end{bmatrix}, \tag{35}$$

and

$$\tilde{\Gamma} = \Gamma + \begin{Bmatrix} \hat{r}_{m-1} \\ r_{m-1} \\ \hat{r}_{m-2} \\ \vdots \\ r_1 \\ \hat{r}_0 \\ r_0 \end{Bmatrix} [\hat{\xi}_{m-1}, \xi_{m-1}, \hat{\xi}_{m-2}, \ldots, \xi_1, \hat{\xi}_0, \xi_0]. \tag{36}$$

Both Γ and $\tilde{\Gamma}$ are square matrices of order $(2m)$. Observe that Eq. (34) is simplified by noting that $\det\Gamma = \lambda_0 \lambda_m (\det\Gamma')^2$, where Γ' is the square matrix of order $(m - 1)$ given by the equation

$$\Gamma' = \begin{bmatrix} \lambda_{m-1} & -\lambda_{m-3} & \lambda_{m-5} & \cdot & \cdot & \cdot & 0 \\ -\lambda_m & \lambda_{m-2} & -\lambda_{m-4} & \cdot & \cdot & \cdot & 0 \\ 0 & -\lambda_{m-1} & \lambda_{m-3} & \cdot & \cdot & \cdot & 0 \\ \cdot & \cdot & \cdot & \cdot & \cdot & \cdot & \cdot \\ 0 & \cdot & \cdot & \cdot & \lambda_3 & -\lambda_1 & 0 \\ 0 & \cdot & \cdot & \cdot & -\lambda_4 & \lambda_2 & -\lambda_0 \\ 0 & \cdot & \cdot & \cdot & \lambda_5 & -\lambda_3 & \lambda_1 \end{bmatrix}. \tag{37}$$

Note that Γ' is found either by disregarding the last row and last column of Eq. (21) or by disregarding the first row and first column of Eq. (22).

Clearly, Eqs. (29) and (34) constitute a potent generalization

Downloaded 03 May 2010 to 171.66.16.20. Redistribution subject to ASME license or copyright; see http://www.asme.org/terms/Terms_Use.cfm

of the classical James et al. formula (1965), also given in the standard reference by Gradshteyn and Ryzhik (1980); they include not only even powers of ω as in these references, but odd powers of ω as well. Furthermore, $G_{ff}(\omega)$ can be arbitrary and not necessarily equal to unity for all ω as in these references.

Impulse Response Determination

Note that the characteristic polynomial of a linear, time-invariant system may be written in the form

$$\Lambda(s) = \lambda_m \sum_{j=1}^{n} (s+s_j)^{m_j}, \tag{38}$$

where $-s_j$ is the jth distinct root of the characteristic equation and has multiplicity m_j. The individual multiplicities must sum to the order of the system; that is, $\Sigma_{j=1}^{n} m_j = m$. Using this representation, it can be shown that the impulse response function can be expressed in the form (Korn and Korn, 1969)

$$h(t) = \sum_{j=1}^{n} \sum_{k=1}^{m_j} H_{jk} t^{m_j-k} e^{-s_j t}, \tag{39}$$

where H_{jk} is given by the equation

$$H_{jk} = \frac{1}{(k-1)!(m_j-k)!} \frac{d^{k-1}}{ds^{k-1}} \left[\frac{(s+s_j)_{m_j}}{\Lambda(s)} \right]_{s=-s_j}. \tag{40}$$

If all roots of the characteristic equation are simple, that is, if $m_j = 1$ for all $j = 1, 2, 3, \ldots, m$, then these expressions can be simplified as

$$h(t) = \sum_{j=1}^{m} h_j e^{-s_j t}, \quad h_j = \left[\frac{s+s_j}{\Lambda(s)} \right]_{s=-s_j}. \tag{41}$$

Differentiating Eq. (39) p times with respect to t yields

$$h^{(p)}(t) = \sum_{i=1}^{p} \sum_{j=1}^{n} \sum_{k=0}^{m_j-i} A_{ijk}^{(p-i)} t^{m_j-i-k} e^{-s_j t}, \tag{42}$$

where

$$A_{ijk}^{(p-i)} = i! \binom{p}{i} \binom{m_j-k}{i} (-s_j)^{p-i} H_{jk}. \tag{43}$$

for $p = 0, 1, 2, \ldots, m-1$, and the combinatorial notation

$$\binom{p}{i} = \frac{p!}{i!(p-i)!} \tag{44}$$

is used for brevity. Again, if the characteristic equation contains only simple roots, the expression reduces to the simpler form

$$h^{(p)}(t) = \sum_{j=1}^{m} h_j (-s_j)^p e^{-s_j t}. \tag{45}$$

Thus, it is feasible to derive general formulae for r_p and $\hat{r}_p$ using the expressions for $h^{(p)}(t)$. Note that the determination of $\hat{r}_p$ requires the Hilbert transform of $R_{ff}(\tau)$. This can be found either by calculating the Hilbert transform according to Eq. (11) or by performing the inverse Fourier transform of $-iS_{ff}(\omega)\text{sgn}(\omega)$.

Applications

White Noise Spectrum. Consider the excitation $f(t)$ to be a white noise process characterized by the double-sided power spectral density function

$$S_{ff}(\omega) = 1, \quad \text{for } -\infty < \omega < \infty. \tag{46}$$

Correspondingly, the autocorrelation function is given by $R_{ff}(\tau) = 2\pi\delta(\tau)$, where $\delta(\tau)$ denotes the Dirac delta function. Substituting into Eq. (11) gives

$$\hat{R}_{ff}(\tau) = 2/\tau. \tag{47}$$

Examining the definition of r_p and using the properties of the delta function, it becomes clear that r_p is simply a multiple of the pth derivative of the system impulse response function evaluated at $t = 0$. Thus,

$$r_p = \begin{cases} 0 & , 0 \le p < m-1 \\ \pi/\lambda_m & , p = m-1 \end{cases}. \tag{48}$$

Furthermore, it can be shown for the general case that $\hat{r}_p$ is given by the equation

$$\hat{r}_p = \begin{cases} 2\Sigma_{i=0}^{p} \Sigma_{j=1}^{n} \Sigma_{k=1}^{m_j-i-1} A_{ijk}^{(p-i)} F_k(s_j) & , 0 \le p < m-1 \\ \text{not finite} & , p = m-1 \end{cases}, \tag{49}$$

where $F_k(s_j)$ is defined as

$$F_k(s_j) = \begin{cases} (m_j-i-k-1)! s_j^{-m_j+i+k} & , 1 \le k < m_j - i \\ -\ln s_j & , k = m_j - i \end{cases}. \tag{50}$$

For the case of only simple roots of the characteristic equation, Eq. (49) reduces to

$$\hat{r}_p = \begin{cases} -2\Sigma_{j=1}^{m} h_j (-s_j)^p \ln s_j & , 0 \le p < m-1 \\ \text{not finite} & , p = m-1 \end{cases}. \tag{51}$$

Observe that Eq. (18) does not require the determination of the roots of the characteristic equation. Hence, this equation can be used regardless of the multiplicity of the roots to determine the even-order spectral moments; this is in essence the classical result given in James et al. (1965) and in the standard reference Gradshteyn and Ryzhik (1980). Regarding $\hat{r}_p$, $p = 0, 1, 2, \ldots, m-1$, which are required to determine the odd-order spectral moments, observe that $\hat{r}_{m-1}$ is not finite. Due to the mathematical peculiarity of the white noise, this result is expected. In fact, it is known that the response spectral moments of order higher than $2m-2$ for a linear system under white noise excitation do not exist. Since M_{2m-1} is known to be infinite, one may simply disregard the top row and first column of Eq. (22) and solve for the lower order response spectral moments.

Band-Limited White Noise Spectrum. Consider next an excitation $f(t)$ with a band-limited white noise spectrum. Recall that the double-sided spectral density is given by the equation

$$S_{ff}(\omega) = \begin{cases} 1 & , 0 \le \omega_a \le |\omega| \le \omega_b \\ 0 & , \text{elsewhere} \end{cases}. \tag{52}$$

Moreover, recall that its autocorrelation function is

$$R_{ff}(\tau) = \frac{2}{\tau} (\sin\omega_b\tau - \sin\omega_a\tau). \tag{53}$$

Here, ω_b and ω_a are the upper and lower cut-off frequencies of the spectral density, respectively. Furthermore, $\hat{R}_{ff}(\tau)$ can be expressed in the form

$$\hat{R}_{ff}(\tau) = \frac{2}{\tau} [\cos(\omega_a\tau) - \cos(\omega_b\tau)]. \tag{54}$$

Substituting these equations into the formulae for r_p, one finds

$$r_p = 2 \sum_{i=0}^{p} \sum_{j=1}^{n} \sum_{k=0}^{m_j-i} (-1)^{m_j-i-k} A_{ijk}^{(p-i)} G_k(s_j), \tag{55}$$

where $G_k(s_j)$ has been introduced for brevity. This function is defined as

$$G_k(s_j) = \begin{cases} -\dfrac{\partial^{m_j-i-k-1}}{\partial s_j^{m_j-i-k-1}} [N_k(s_j)], & , 0 \le k < m_j - i \\ \tan^{-1}\left(\dfrac{(\omega_b-\omega_a)s_j}{s_j^2 + \omega_a\omega_b} \right) & , k = m_j - i \end{cases} \tag{56}$$

where

Downloaded 03 May 2010 to 171.66.16.20. Redistribution subject to ASME license or copyright; see http://www.asme.org/terms/Terms_Use.cfm

$$N_k(s_j) = \left(\frac{(\omega_b - \omega_a)s_j^2 - \omega_a\omega_b(\omega_b - \omega_a)}{(s_j^2 + \omega_a^2)(s_j^2 + \omega_b^2)} \right). \quad (57)$$

Similarly, $\hat{r}_p$ is given by the equation

$$\hat{r}_p = -2 \sum_{i=0}^{p} \sum_{j=1}^{n} \sum_{k=0}^{m_j - 1} (-1)^{m_j - i - k} A_{ijk}^{(p-i)} \tilde{G}_k(s_j), \quad (58)$$

where $\tilde{G}_k(s_j)$ is expressed as

$$\tilde{G}_k(s_j) = \begin{cases} \dfrac{\partial^{m_j - i - k - 1}}{\partial s_j^{m_j - i - k - 1}} [\tilde{N}_k(s_j)] & , 0 \le k < m_j - i \\ \dfrac{1}{2} \ln \left(\dfrac{s_j^2 + \omega_a^2}{s_j^2 + \omega_b^2} \right) & , k = m_j - i \end{cases}, \quad (59)$$

and

$$\tilde{N}_k(s_j) = \left(\frac{(\omega_b^2 - \omega_a^2)s_j}{(s_j^2 + \omega_a^2)(s_j^2 + \omega_b^2)} \right). \quad (60)$$

Observe that these results simplify if the characteristic equation has only simple roots. Specifically,

$$r_p = 2 \sum_{j=1}^{m} h_j(-s_j)^p \tan^{-1} \left(\frac{(\omega_b - \omega_a)s_j}{s_j^2 + \omega_a\omega_b} \right), \quad (61)$$

and

$$\hat{r}_p = \sum_{j=1}^{m} h_j(-s_j)^p \ln \left(\frac{s_j^2 + \omega_b^2}{s_j^2 + \omega_a^2} \right). \quad (62)$$

"Gaussian" Spectrum. Consider next a random excitation with double-sided spectral density and autocorrelation function in the forms

$$S_{ff}(\omega) = e^{-\omega^2}, \quad R_{ff}(\tau) = \sqrt{\pi} e^{-\frac{\tau^2}{4}}. \quad (63)$$

Taking the inverse Fourier transform of $-i\text{sgn}(\omega)e^{-\omega^2}$ gives

$$\hat{R}_{ff}(\tau) = -i\sqrt{\pi} e^{-\frac{\tau^2}{4}} \Phi \left(\frac{i\tau}{2} \right), \quad (64)$$

where $\Phi(x)$ is the error function defined by the integral (Gradshteyn and Ryzhik, 1980)

$$\Phi(x) = \frac{2}{\sqrt{\pi}} \int_0^x e^{-t^2} dt. \quad (65)$$

Although Eq. (64) suggests that $\hat{R}_{ff}(\tau)$ is a complex-valued function, it can be shown that $\hat{R}_{ff}(\tau)$ is indeed purely real-valued.

Substituting these expressions into the equations for r_p and $\hat{r}_p$ and relying on Gradshteyn and Ryzhik (1980), one finds

$$r_p = \sqrt{\pi} \sum_{i=0}^{p} \sum_{j=1}^{n} \sum_{k=0}^{m_j - i} A_{ijk}^{(p-i)} I_{m_j - i - k}(s_j), \quad (66)$$

and

$$\hat{r}_p = -i\sqrt{\pi} \sum_{i=0}^{p} \sum_{j=1}^{n} \sum_{k=0}^{m_j - i} A_{ijk}^{(p-i)} \hat{I}_{m_j - i - k}(s_j), \quad (67)$$

Here, $I_k(s_j)$ and $\hat{I}_k(s_j)$ are defined by the equations

$$I_k(s_j) = \int_0^\infty t^k e^{-(t^2/4) - s_j t} dt \quad (68)$$

and

$$\hat{I}_k(s_j) = \int_0^\infty t^k e^{-(t^2/4) - s_j t} \Phi \left(\frac{it}{2} \right) dt, \quad (69)$$

and satisfy the recurrence relations

$$I_{k+2}(s_j) = 2s_j I_{k+1}(s_j) + 2(k+1) I_k(s_j) \quad (70)$$

and

$$\hat{I}_{k+2}(s_j) = -2s_j \hat{I}_{k+1}(s_j) + 2(k+1)\hat{I}_k(s_j) + \frac{2i}{\sqrt{\pi}} (k+1)! s_j^{-k-2}, \quad (71)$$

for $k = 0, 1, 2, \ldots$. The first two terms required to initiate the recursions are tabulated in Gradshteyn and Ryzhik (1980). These integrals are given by the equations

$$I_0(s_j) = \sqrt{\pi} e^{s_j^2} [1 - \Phi(s_j)], \quad (72)$$

$$I_1(s_j) = 2[1 - s_j I_0(s_j)], \quad (73)$$

$$\hat{I}_0(s_j) = \frac{-i}{\sqrt{\pi}} e^{s_j^2} \text{Ei}(-s_j^2), \quad (74)$$

$$\hat{I}_1(s_j) = \frac{2i}{s_j\sqrt{\pi}} [1 + i\sqrt{\pi} s_j^2 e^{-s_j^2} \hat{I}_0(s_j)], \quad (75)$$

where $\text{Ei}(x)$ refers to the exponential integral function (Gradshteyn and Ryzhik, 1980). Again, the formulae simplify if the characteristic equation has only simple roots. For this case one finds

$$r_p = \pi \sum_{j=1}^{m} h_j(-s_j)^p e^{s_j^2} [1 - \Phi(s_j)], \quad (76)$$

and

$$\hat{r}_p = -\sum_{j=1}^{m} h_j(-s_j)^p e^{s_j^2} \text{Ei}(-s_j^2). \quad (77)$$

Example: Standard Linear Oscillator

Consider the classical randomly excited second-order linear oscillator governed by the differential equation

$$\ddot{x}(t) + 2\zeta_0\omega_0\dot{x}(t) + \omega_0^2 x(t) = f(t). \quad (78)$$

Clearly, the characteristic polynomial is given by the equation

$$\Lambda(s) = s^2 + 2\zeta_0\omega_0 s + \omega_0^2. \quad (79)$$

The roots of the characteristic equation are then $s_1 = \zeta_0\omega_0 + i\omega_d$ and $s_2 = \zeta_0\omega_0 - i\omega_d$, where $\omega_d = \omega_0\sqrt{1 - \zeta_0^2}$. Furthermore, the impulse response function coefficients in Eq. (41) are $h_1 = -1/2i\omega_d$ and $h_2 = 1/2i\omega_d$. Solving Eqs. (21) and (22) gives

$$\begin{Bmatrix} M_2 \\ M_0 \end{Bmatrix} = \frac{1}{2\zeta_0\omega_0^3} \begin{bmatrix} \omega_0^2 & 0 \\ 1 & 2\zeta_0\omega_0 \end{bmatrix} \begin{Bmatrix} r_1 \\ r_0 \end{Bmatrix}, \quad (80)$$

and

$$\begin{Bmatrix} M_3 \\ M_1 \end{Bmatrix} = \frac{1}{2\zeta_0\omega_0} \begin{bmatrix} 2\zeta_0\omega_0 & \omega_0^2 \\ 0 & 1 \end{bmatrix} \begin{Bmatrix} \hat{r}_1 \\ \hat{r}_0 \end{Bmatrix}, \quad (81)$$

respectively. Note that these equations can be used for any random excitation process. In fact, by simply substituting the derived expressions for r_0, r_1, $\hat{r}_0$, and $\hat{r}_1$, the response spectral moments can be calculated in a closed form.

Excitation With White Noise Spectrum. If the random excitation is a white noise, then Eqs. (48) and (51) can be used to determine r_0, r_1, $\hat{r}_0$, and $\hat{r}_1$. Assuming that $0 < \zeta_0 < 1$, one finds

$$r_0 = 0, \quad r_1 = \pi, \quad (82)$$

and

$$\hat{r}_0 = \frac{2}{\omega_d} \tan^{-1} \left(\frac{\sqrt{1 - \zeta_0^2}}{\zeta_0} \right), \quad \hat{r}_1 = \text{not finite}. \quad (83)$$

Thus, the response spectral moments are given by the equations

Downloaded 03 May 2010 to 171.66.16.20. Redistribution subject to ASME license or copyright; see http://www.asme.org/terms/Terms_Use.cfm

$$M_0=\int_0^\infty \frac{2d\omega}{(\omega_0^2-\omega^2)^2+4\zeta_0^2\omega_0^2\omega^2}=\frac{\pi}{2\zeta_0\omega_0^3}, \tag{84}$$

$$M_1=\int_0^\infty \frac{2\omega d\omega}{(\omega_0^2-\omega^2)^2+4\zeta_0^2\omega_0^2\omega^2}=\frac{1}{\zeta_0\omega_0\omega_d}\tan^{-1}\left(\frac{\sqrt{1-\zeta_0^2}}{\zeta_0}\right), \tag{85}$$

$$M_2=\int_0^\infty \frac{2\omega^2 d\omega}{(\omega_0^2-\omega^2)^2+4\zeta_0^2\omega_0^2\omega^2}=\frac{\pi}{2\zeta_0\omega_0}, \tag{86}$$

$$M_3=\int_0^\infty \frac{2\omega^3 d\omega}{(\omega_0^2-\omega^2)^2+4\zeta_0^2\omega_0^2\omega^2}=\text{not finite}. \tag{87}$$

Note that some of these results can be verified by applying the theory of complex residua to evaluate the integrals (Lin, 1976). Furthermore, the response spectral moments of order greater than two will not be finite, as indicated by M_3 and as expected by the form of the integral.

Excitation With Band-Limited White Noise Spectrum. Next assume that the excitation spectrum is described by Eq. (52). Furthermore, assuming that $0 < \zeta_0 < 1$, Eqs. (61) and (62) yield

$$r_0=\frac{-1}{\omega_d}\tanh^{-1}\left(\frac{2\text{Im}\{z\}}{1+|z|^2}\right), \tag{88}$$

$$r_1=\tan^{-1}\left(\frac{2\text{Re}\{z\}}{1-|z|^2}\right)-\zeta_0\omega_0 r_0, \tag{89}$$

$$\hat{r}_0=\frac{1}{\omega_d}\tan^{-1}\left(\frac{\text{Im}\{\tilde{z}\}}{\text{Re}\{\tilde{z}\}}\right), \tag{90}$$

$$\hat{r}_1=-\ln(|\tilde{z}|^2)-\zeta_0\omega_0\hat{r}_0, \tag{91}$$

where $\text{Re}\{\cdot\}$ denotes the real part, $\text{Im}\{\cdot\}$ denotes the imaginary part,

$$z=\frac{(\omega_b-\omega_a)s_1}{s_1^2+\omega_a\omega_b}, \quad \tilde{z}=\frac{s_1^2+\omega_a^2}{s_1^2+\omega_b^2} \tag{92}$$

$$|z|^2=\frac{(\omega_b-\omega_a)^2\omega_0^2}{(\omega_a\omega_b-\omega_0^2)^2+4\zeta_0^2\omega_0^2\omega_a\omega_b}, \tag{93}$$

and

$$|\tilde{z}|^2=\frac{(\omega_a^2-\omega_0^2)^2+4\zeta_0^2\omega_0^2\omega_a^2}{(\omega_b^2-\omega_0^2)^2+4\zeta_0^2\omega_0^2\omega_b^2}. \tag{94}$$

The response spectral moments are then given by the equations

$$M_0=\frac{1}{2\zeta_0\omega_0^3}\left[\tan^{-1}\left(\frac{2\text{Re}\{z\}}{1-|z|^2}\right)-\frac{\zeta_0\omega_0}{\omega_d}\tanh^{-1}\left(\frac{2\text{Im}\{z\}}{1+|z|^2}\right)\right], \tag{95}$$

$$M_1=\frac{1}{2\zeta_0\omega_0\omega_d}\tan^{-1}\left(\frac{\text{Im}\{\tilde{z}\}}{\text{Re}\{\tilde{z}\}}\right), \tag{96}$$

$$M_2=\frac{1}{2\zeta_0\omega_0}\left[\tan^{-1}\left(\frac{2\text{Re}\{z\}}{1-|z|^2}\right)+\frac{\zeta_0\omega_0}{\omega_d}\tanh^{-2}\left(\frac{2\text{Im}\{z\}}{1+|z|^2}\right)\right], \tag{97}$$

$$M_3=-\ln(|\tilde{z}|^2)+\frac{\omega_0(1-2\zeta_0^2)}{2\zeta_0\omega_d}\tan^{-1}\left(\frac{\text{Im}\{\hat{z}\}}{\text{Re}\{\tilde{z}\}}\right). \tag{98}$$

If the excitation has a clipped white noise spectrum commonly encountered in engineering applications, then the expressions for r_0, r_1, $\hat{r}_0$, and $\hat{r}_1$ can be derived from the above equations by substituting $\omega_a = 0$. Note that upon determining M_0, M_1, M_2, and M_3, higher order spectral moments can be determined by relying on the recursive Eqs. (25) and (26).

Excitation With "Gaussian" Spectrum. Consider next a random excitation which has a spectrum described by Eq. (63). For this excitation, Eqs. (76) and (77) can be used to determine expressions for r_0, r_1, $\hat{r}_0$, and $\hat{r}_1$. Specifically, one finds

$$r_0=\frac{-\pi}{\omega_d}\text{Im}\{e^{s_1^2}[1-\Phi(s_1)]\}, \tag{99}$$

$$r_1=\pi\text{Re}\{e^{s_1^2}[1-\Phi(s_1)]\}-\zeta_0\omega_0 r_0, \tag{100}$$

$$\hat{r}_0=\frac{1}{\omega_d}\text{Im}\{e^{s_1^2}\text{Ei}(-s_1^2)\}, \tag{101}$$

$$\hat{r}_1=-\text{Re}\{e^{s_1^2}\text{Ei}(-s_1^2)\}-\zeta_0\omega_0\hat{r}_0. \tag{102}$$

Using these expressions, the response spectral moments are found to be

$$M_0=\frac{\pi}{2\zeta_0\omega_0^3}\text{Re}\left\{\left(1+\frac{i\zeta_0\omega_0}{\omega_d}\right)e^{s_1^2}[1-\Phi(s_1)]\right\}, \tag{103}$$

$$M_1=\frac{1}{2\zeta_0\omega_0\omega_d}\text{Im}\{e^{s_1^2}\text{Ei}(-s_1^2)\}, \tag{104}$$

$$M_2=\frac{\pi}{2\zeta_0\omega_0}Re\left\{\left(1-\frac{i\zeta_0\omega_0}{\omega_d}\right)e^{s_1^2}[1-\Phi(s_1)]\right\}, \tag{105}$$

and

$$M_3=-\text{Re}\left\{\left(1-\frac{i\omega_0(1-2\zeta_0^2)}{2\zeta_0\omega_d}\right)e^{s_1^2}\text{Ei}(-s_1^2)\right\}. \tag{106}$$

Upon determining M_0, M_1, M_2, and M_3, higher order spectral moments can be calculated by relying again on Eqs. (25) and (26), as in the case of band-limited white noise.

Alternatively, by writing the response spectral moments in integral form, one finds

$$M_k=\int_0^\infty \frac{2\omega^k e^{-\omega^2}d\omega}{(\omega_0^2-\omega^2)^2+4\zeta_0^2\omega_0^2\omega^2}. \tag{107}$$

Note that the authors have not been able to locate tabulated values of these integrals; this fact may attest to the pure mathematical merit of Eq. (34).

Excitation With Kanai-Tajimi Seismic Spectrum. Finally, assume that the excitation possesses the widely used Kanai-Tajimi seismic spectrum (Shinozuka and Deodatis, 1988; Roberts and Spanos, 1990). That is, its spectrum has the form

$$S_{ff}(\omega)=\frac{G_0[1+4\zeta_g^2(\omega/\omega_g)^2]}{\{[1-(\omega/\omega_g)^2]^2+4\zeta_g^2(\omega/\omega_g)^2\}}, \tag{108}$$

where G_0 is a scaling parameter, ζ_g is the ground critical damping factor, and ω_g is the predominant ground frequency. Clearly, the system response spectral moments are given by the equation

$$M_k=\int_0^\infty \frac{2G_0[\omega^k+4(\zeta_g/\omega_g)^2\omega^{k+2}]}{|\Lambda(i\omega)|^2}d\omega, \tag{109}$$

where $\Lambda(s) = \lambda_4 s^4 + \lambda_3 s^3 + \lambda_2 s^2 + \lambda_1 s + \lambda_0$ with

$$\lambda_4=\frac{1}{\omega_g^2}, \quad \lambda_3=\frac{2}{\omega_g^2}(\zeta_0\omega_0+\zeta_g\omega_g), \tag{110}$$

$$\lambda_2=1+4\zeta_0\zeta_g\left(\frac{\omega_0}{\omega_g}\right)+\left(\frac{\omega_0}{\omega_g}\right)^2, \tag{111}$$

$$\lambda_1=2\omega_0\left[\zeta_0+\zeta_g\left(\frac{\omega_0}{\omega_g}\right)\right], \quad \lambda_0=\omega_0^2. \tag{112}$$

That is, the response spectral moments are simply a linear combination of integrals of the form shown in Eq. (15); the excitation is a white noise process. Thus, combining Eqs. (34) through (37) with Eq. (109) gives

Downloaded 03 May 2010 to 171.66.16.20. Redistribution subject to ASME license or copyright; see http://www.asme.org/terms/Terms_Use.cfm

$$M_0 = \frac{\pi G_0}{\lambda_0 \det\Gamma'} [(\lambda_2\lambda_3 - \lambda_1\lambda_4) + 4(\zeta_g/\omega_g)^2\lambda_0\lambda_3], \quad (113)$$

$$M_1 = \frac{1}{\pi} [\lambda_0 \hat{f}_0 M_0 + (\lambda_3 \hat{f}_1 + \lambda_4 \hat{f}_2) M_2], \quad (114)$$

$$M_2 = \frac{\pi G_0}{\det\Gamma'} [\lambda_3 + 4(\zeta_g/\omega_g)^2\lambda_1], \quad (115)$$

$$M_3 = \frac{G_0}{\deg\Gamma'} [\lambda_4 + 4(\zeta_g/\omega_g)^2(\lambda_1\lambda_2 - \lambda_0\lambda_3)]\hat{f}_2 + \frac{1}{\pi}(\lambda_0\hat{f}_0 + \lambda_1\hat{f}_1)M_2, \quad (116)$$

where $\det\Gamma'$ is given by the equation

$$\det\Gamma' = \lambda_1(\lambda_2\lambda_3 - \lambda_1\lambda_4) - \lambda_0\lambda_3^2. \quad (117)$$

Note that Eq. (51) can be used to determine $\hat{f}_k$ which appear in Eqs. (114) and (116). The resulting formula can be written in the form

$$\hat{f}_k = -4 \sum_{n=1}^{2} \left[\ln(\omega_n) - \tan^{-1}\left(\frac{\sqrt{1-\zeta_n^2}}{\zeta_n}\right) \right] \times \begin{bmatrix} -\zeta_n\omega_n & \omega_n\sqrt{1-\zeta_n^2} \\ -\omega_n\sqrt{1-\zeta_n^2} & -\zeta_n\omega_n \end{bmatrix}^k \begin{Bmatrix} \mathrm{Re}\{h_n\} \\ \mathrm{Im}\{h_n\} \end{Bmatrix}, \quad (118)$$

where $\omega_1 = \omega_g$, $\zeta_1 = \zeta_g$, $\omega_2 = \omega_0$, and $\zeta_2 = \zeta_0$, and the impulse response coefficients are

$$h_1 = \frac{-(\zeta_0\omega_0 - \zeta_g\omega_g)}{\lambda_4 \det\Gamma'} + i\frac{[(\omega_0^2 - \omega_g^2) - 2\zeta_g\omega_g(\zeta_0\omega_0 - \zeta_g\omega_g)]}{2\lambda_4\omega_g\sqrt{1-\zeta_g^2}\det\Gamma'}, \quad (119)$$

$$h_2 = \frac{(\zeta_0\omega_0 - \zeta_g\omega_g)}{\lambda_4 \det\Gamma'} - i\frac{[(\omega_0^2 - \omega_g^2) - 2\zeta_0\omega_0(\zeta_0\omega_0 - \zeta_g\omega_g)]}{2\lambda_4\omega_0\sqrt{1-\zeta_0^2}\det\Gamma'}, \quad (120)$$

for $s_1 = \zeta_g\omega_g + i\omega_g\sqrt{1-\zeta_g^2}$, $s_2 = \zeta_0\omega_0 + i\omega_0\sqrt{1-\zeta_0^2}$, $s_3 = s_1^*$, and $s_4 = s_2^*$.

Concluding Remarks

Two sets of linear equations involving the response spectral moments of a linear system have been derived. Equation (21) can be solved to determine any even-order response spectral moment, while Eq. (22) can be similarly used to determine any odd-order response spectral moment. Both sets of linear equations are quite versatile. In fact, they have been combined to derive Eq. (34), which yields, as a special case, the classical James et al. (1965) integral used extensively in random vibration and control engineering. Furthermore, as demonstrated by the "Gaussian" spectrum, this equation has its own pure mathematical merit. In this respect, it can be useful in several technical fields, irrespective of the presence of a random vibration context.

It should also be noted that the derived formulae can be easily incorporated into problems where the excitation spectra are modeled as the response of linear filters to white noise excitation. Due to the linearity of the systems, $\Lambda(s)$ is simply the product of the characteristic polynomials of each system. Then, the integrals which represent the response spectral moments take the form of Eq. (15) or Eq. (29) and can be solved accordingly. Indeed, this approach was used to determine the response spectral moments of the standard linear oscillator under an excitation possessing the Kanai-Tajimi seismic spectrum.

It is noted that the application of Eq. (34) for the standard randomly excited linear oscillator has yielded results which are readily applicable for a variety of practical applications.

Acknowledgments

Some of the concepts of this work were conceived while the first author was visiting the University of Palermo, Italy. The stimulating discussions with Profs. M. Di Paola and G. Muscolino are acknowledged with pleasure.

The support of this research from the grant DE-FG05-91ER14215 from the Department of Energy is gratefully acknowledged.

References

Der Kiureghian, A., 1980, "Structural Response to Stationary Excitation," *ASCE Journal of the Engineering Mechanics Division*, Vol. 106, pp. 1195–1213.

Di Paola, M., and Petrucci, G., 1990, "Spectral Moments and Pre-Envelope Covariances of Nonseparable Processes," ASME JOURNAL OF APPLIED MECHANICS, Vol. 112, pp. 218–224.

Gradshteyn, I. S., and Ryzhik, I. M., 1980, *Tables of Integrals, Series and Products*, Academic Press, New York.

James, H. M., Nichols, N. B., and Philips, R. S., eds., 1965, *Theory of Servomechanisms*, Dover, New York.

Korn, A. G., and Korn, T. M., 1969, *Mathematical Handbook for Scientists and Engineers*, McGraw-Hill, New York.

Lin, Y. K., 1976, *Probabilistic Theory of Structural Dynamics*, R. E. Krieger, New York.

Papoulis, A., 1984, *Probability, Random Variables, and Stochastic Processes*, McGraw-Hill, New York.

Roberts, J. B., and Spanos, P. D., 1990, *Random Vibration and Statistical Linearization*, John Wiley and Sons, New York.

Shinozuka, M., and Deodatis, G., 1988, "Stochastic Process Models for Earthquake Ground Motion," *Probabilistic Engineering Mechanics*, Vol. 3, No. 3, pp. 114–123.

Shinozuka, M., Kako, T., and Tsurui, A., 1986, "Random Vibration Analysis in Finite Element Formulation," *Random Vibration-Status and Recent Developments*, I. Elishakoff and R. H. Lyon, eds., Elsevier, New York.

Spanos, P-T. D., 1983, "Spectral Moments Calculation of Linear System Output," ASME JOURNAL OF APPLIED MECHANICS, Vol. 50, pp. 901–903.

Spanos, P-T. D., 1987, "An Approach to Calculating Random Vibration Integrals," ASME JOURNAL OF APPLIED MECHANICS, Vol. 54, pp. 409–413.

Spanos, P. D., and Miller, S. M., 1992, "Linear System Spectral Moments Determination," *Probabilistic Mechanics, and Structural and Geotechnical Reliability*, Proceedings of the Sixth Specialty Conference, Denver, CO, Y. K. Lin, ed., ASCE, New York, pp. 192–195.

Yang, I. M., and Iwan, W. D., 1972, "Calculation of Correlation Matrices for Linear Systems Subjected to Nonwhite Excitation," ASME JOURNAL OF APPLIED MECHANICS, Vol. 39, pp. 559–562.

Downloaded 03 May 2010 to 171.66.16.20. Redistribution subject to ASME license or copyright; see http://www.asme.org/terms/Terms_Use.cfm

A Circular Crack System in an Infinite Elastic Medium Under Arbitrary Normal Loads

Zhou Yong

M. T. Hanson

Department of Engineering Mechanics,
University of Kentucky,
Lexington, KY 40506-0046

This analysis considers a circular crack system containing a penny-shaped crack and a concentric, coplanar external circular crack under arbitrary normal loading in a transversely isotropic body. The solution is obtained by transforming the governing two-dimensional integral equation to a set of algebraic equations which are easily solved numerically due to the special coefficient matrix. The normal stress component coplanar with the crack system is determined in power series form. The equations are solved and solutions for the stress intensity factors around the crack fronts are given for several different loading conditions. Including the rigid-body displacements at infinity allows the contact problem of an annular flat punch on an elastic half-space to be solved simultaneously.

1 Introduction

Crack problems under geometrically axisymmetric conditions with two coplanar crack contours have been examined by many researchers using various mathematical techniques for isotropic bodies. These problems can be divided into two categories; the problem of an annular crack, and the complementary problem of a penny-shaped crack coplanar and concentric with a circular external crack. The annular crack has been widely considered (Smetanin, 1968; Moss and Kobayashi, 1971; Erdol and Erdogan, 1978; Mastrojannis and Kermanidis, 1981; Choi and Shield, 1982; Neid and Erdogan, 1983; Mastrojannis, 1983; Selvadurai and Singh, 1985; Clements and Ang, 1988; Fabrikant, 1991a). In particular, axisymmetric loadings were examined by Smetanin (1968), Moss and Kobayashi (1971), Erdol and Erdogan (1978), Mastrojannis and Kermanidis (1981), Choi and Shield (1982), Selvadurai and Singh (1985), and Clements and Ang (1988), but only Neid and Erdogan (1983), Mastrojannis (1983), and Fabrikant (1991a) treat general nonaxisymmetric loading.

On the other hand, a detailed investigation of the complementary problem has not been undertaken in all generality, although several special cases have been examined. A special case which has been of great interest is the indentation of a half-space by a flat annular indenter. A review of this literature is given by Gladwell (1980). It is interesting to note that although the interior and exterior contact problems for a circular region have been given in closed form, a closed-form solution for the annular contact problem has not yet been found. The extension of the annular contact problem to include uniform normal pressure applied over the interior region has been made by Selvaduri and Singh (1987) and Shield and Bogy (1989). A recent paper by Fabrikant (1991b) has also analyzed the annular indenter problem loaded by a force or couple.

The combined penny-shaped external crack problem has an additional complication over the annular crack which is due specifically to the external crack: As pointed out by Stallybrass (1981a, 1981b), appropriate boundary conditions on the displacements at infinite distances from the bond region must be considered since two different situations may occur. If the infinite body is free of constraints at infinity, rigid-body displacements and rotations may occur there resulting from the unbalanced forces and moments on the plane of the external crack. The rigid-body terms are determined by adding appropriate homogeneous solutions which balance the applied forces and moments on this plane. Alternatively, if infinite distances are constrained from motion, the rigid displacements at infinity are zero and there is a resultant force and moment there balancing the resultants on the plane of the external crack. Comninou and Barber (1982) have noted that care must be taken when considering rigid-body rotations at infinity since interpenetration of the external crack faces will occur if the body is truly infinite. These aspects of external crack problems have been further discussed by Fabrikant et al. (1986) and Gao and Rice (1987).

The purpose of this paper is to develop a general formulation for analyzing the problem of a penny-shaped crack concentric and coplanar with a circular external crack in a transversely isotropic medium. In this analysis the crack plane is taken parallel to the planes of material isotropy which results in a solution which is identical to the isotropic case apart from a material constant. The crack faces are subjected to general nonaxisymmetric pressures and the appropriate boundary con-

Contributed by the Applied Mechanics Division of THE AMERICAN SOCIETY OF MECHANICAL ENGINEERS for publication in the ASME JOURNAL OF APPLIED MECHANICS.

Discussion on this paper should be addressed to the Technical Editor, Professor Lewis T. Wheeler, Department of Mechanical Engineering, University of Houston, Houston, TX 77204-4792, and will be accepted until four months after final publication of the paper itself in the ASME JOURNAL OF APPLIED MECHANICS.

Manuscript received by the ASME Applied Mechanics Division, Oct. 29, 1991; final revision, June 17, 1993. Associate Technical Editor: X. Markenscoff.

Copyright © 1994 by ASME
Downloaded 03 May 2010 to 171.66.16.20. Redistribution subject to ASME license or copyright; see http://www.asme.org/terms/Terms_Use.cfm

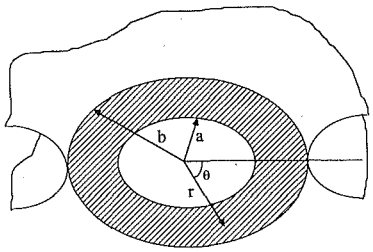


Fig. 1 A penny-shaped crack concentrically located in the bond ligament of a circular external crack

ditions at infinity are included. The only restriction is that the applied loadings are symmetrically applied to both crack faces (i.e., the problem is symmetric about the cracked plane). This is essentially equivalent to including arbitrarily distributed known normal tractions outside the contact region in the annular contact problem.

Although the method of Nied and Erdogan (1983) could be adopted to solve this problem, the method used by Yong (1989) is employed which alleviates the need for a numerical solution of singular integral equations. This method is similar in nature to the one applied by Mastrojannis (1983) to analyze the annular crack. The problem is formulated in terms of a two-dimensional integral equation governing the normal stress component in the annular bond region coplanar with the crack system. By adopting a series expansion formulation, the governing integral equation is transformed to a set of algebraic equations determining the coefficients of the expansions. These algebraic equations are easily solved due to the special coefficient matrix. The present solution involves only power series expansions and thus is an elementary solution procedure available to anyone with a basic knowledge in mathematics. No special quadrature or other numerical techniques, needed for solving singular integral equations, are required presently. This method is thus open to anyone within the engineering field to use in solving similar problems. The present solution procedure is first compared to the results of Selvadurai and Singh (1987) and then new numerical results are given for several different loading situations.

2 Formulation

The crack system under consideration is shown in Fig. 1. A penny-shaped crack of radius a is concentrically located in the bond region of a circular external crack of radius b $(a<b)$. The internal and external crack surfaces are subjected to arbitrary normal loading, symmetrically distributed on the upper and lower crack faces. From the symmetry of the geometry and loading, the problem is equivalent to a mixed boundary value problem for an elastic half-space $(z>0)$. Taking a cylindrical coordinate system (r, θ, z), the elastic half-space surface has the mixed boundary conditions

$$\tau_{zr}(r, \theta, 0)=\tau_{z\theta}(r, \theta, 0)=0, \quad 0\le\theta\le 2\pi, \ 0<r<\infty, \tag{1}$$

$$\sigma_{zz}(r, \theta, 0)=\begin{cases}-\sigma_A(r, \theta), & 0\le\theta\le 2\pi, \quad 0<r<a,\\ -\sigma_B(r, \theta), & 0\le\theta\le 2\pi, \quad b<r<\infty,\end{cases} \tag{2}$$

$$u_z(r, \theta, 0)=-w-\gamma r\cos(\theta)-\beta r\sin(\theta), \quad 0\le\theta\le 2\pi, \ a<r<b. \tag{3}$$

Equation (1) stems from the symmetry conditions while in Eq. (2), $\sigma_A(r, \theta)$ and $\sigma_B(r, \theta)$ are the known applied pressures on the faces of the internal and external crack, respectively.

The constants w, γ, and β represent the rigid-body displacement and rotations at $z=\infty$ which arise from the presence of the external crack. Typically for an external crack problem, Eq. (3) would be homogeneous since the crack plane $z=0$ is a reference and the rigid-body terms would occur at $z=\infty$ if no constraints were provided. However, since rigid-body displacements can be added in linear elasticity, Eq. (3) implies that all displacements vanish at $z=\infty$. The case $w=\gamma=\beta=0$ gives the result when a constraint is provided at infinity so that rigid displacements will vanish there. Obviously the boundary conditions in Eqs. (1)–(3) are equivalent to a flat, rigid, frictionless, annular indenter on a half-space with arbitrary normal loading applied inside and outside the contact region. The rigid-body displacements are related to the net force P_z and moments M_x and M_y of the normal stress on the plane $z=0$. These can be given as

$$P_z=-\int_0^{2\pi}\int_a^b \sigma_{zz}(\rho, \phi, 0)\rho d\rho d\phi+\int_0^{2\pi}\int_0^a \sigma_A(\rho, \phi)\rho d\rho d\phi+\int_0^{2\pi}\int_b^\infty \sigma_B(\rho, \phi)\rho d\rho d\phi, \tag{4}$$

$$M_y=-\int_0^{2\pi}\int_a^b \sigma_{zz}(\rho, \phi, 0)\rho\cos(\phi)\rho d\rho d\phi+\int_0^{2\pi}\int_0^a \sigma_A(\rho, \phi)\rho\cos(\phi)\rho d\rho d\phi+\int_0^{2\pi}\int_b^\infty \sigma_B(\rho, \phi)\rho\cos(\phi)\rho d\rho d\phi, \tag{5}$$

$$M_x=-\int_0^{2\pi}\int_a^b \sigma_{zz}(\rho, \phi, 0)\rho\sin(\phi)\rho d\rho d\phi+\int_0^{2\pi}\int_0^a \sigma_A(\rho, \phi)\rho\sin(\phi)\rho d\rho d\phi+\int_0^{2\pi}\int_b^\infty \sigma_B(\rho, \phi)\rho\sin(\phi)\rho d\rho d\phi. \tag{6}$$

Here x is the line $\theta=0$ while y corresponds to $\theta=\pi/2$ and $\sigma_{zz}(r, \theta, 0)$ is the unknown stress in the bond region between the two cracks.

It was pointed out by Comninou and Barber (1982), Fabrikant et al. (1986), and Gao and Rice (1987) that rigid-body rotations at infinity for an external crack problem will most likely result in overlapping of the external crack faces if the body is large as compared to the size of the bond ligament. Frictionless contact of the external crack faces is beyond the scope of the present investigation; however, the results obtained here are still valid and useful since they can also be applied to the annular contact problem.

3 Method of Solution

By using the Boussinesq solution for point normal loading of an elastic half-space (Fabrikant, 1989), a two-dimensional integral equation for the unknown normal stress $\sigma_{zz}(r, \theta, 0)$ $(0\le\theta\le 2\pi, a<r<b)$ in the bond ligament can be written down directly. The integral equation is given as

$$\int_0^{2\pi}\int_a^b K(r, \theta, \rho, \phi)\sigma_{zz}(\rho, \phi, 0)\rho d\rho d\phi=w_0+\gamma_0 r\cos\theta+\beta_0 r\sin(\theta)+\int_0^{2\pi}\int_0^a K(r, \theta, \rho, \phi)\sigma_A(\rho, \phi)\rho d\rho d\phi+\int_0^{2\pi}\int_b^\infty K(r, \theta, \rho, \phi)\sigma_B(\rho, \phi)\rho d\rho d\phi, \quad 0\le\theta\le 2\pi, \ a<r<b. \tag{7}$$

The function K is the normal surface displacement (apart from a constant multiplier) at the point (r, θ) resulting from a point normal load at (ρ, ϕ) and it is given as

Downloaded 03 May 2010 to 171.66.16.20. Redistribution subject to ASME license or copyright; see http://www.asme.org/terms/Terms_Use.cfm

$$K(r, \theta, \rho, \phi) = [r^2 + \rho^2 - 2r\rho\cos(\theta - \phi)]^{-1/2}, \quad (8)$$

and the rigid displacement terms are

$$w_0 = w/H, \quad \gamma_0 = \gamma/H, \quad \beta_0 = \beta/H. \quad (9)$$

Here H is a transversely isotropic elastic parameter defined by Fabrikant (1989). For isotropy, $H = (1-\nu^2)/(\pi E)$ where E is the elastic modulus and ν is Poisson's ratio. In subsequent calculations a solution even in θ is considered and β is taken as zero.

The solution procedure consists of using a Fourier expansion in the θ direction coupled with a power series expansion in the radial coordinate. The applied loadings $\sigma_A(r, \theta)$ and $\sigma_B(r, \theta)$ are taken in harmonic form as

$$\sigma_A(r, \theta) = \sigma_a Q_A(r/a)\cos(m\theta), \quad (10)$$

$$\sigma_B(r, \theta) = \sigma_b Q_B(b/r)\cos(m\theta), \quad (11)$$

where m is a positive integer or zero, σ_a and σ_b express uniform pressure and $Q_A(r/a)$, $Q_B(b/r)$ represent the axisymmetric parts of load. The unknown stress component $\sigma_{zz}(r, \theta, 0)$ is taken in the following series form:

$$\sigma_{zz}(r, \theta, 0) = \frac{a\cos(m\theta)}{\sqrt{r^2 - a^2}}\left(\frac{a}{r}\right)^m \sum_{\lambda=0}^{\infty} A_\lambda \left(\frac{a}{r}\right)^{2\lambda+2} + \frac{b\cos(m\theta)}{\sqrt{b^2 - r^2}}\left(\frac{r}{b}\right)^m \sum_{\lambda=0}^{\infty} B_\lambda \left(\frac{r}{b}\right)^{2\lambda}, \quad (12)$$

where the A_λ's and B_λ's are unknown constants.

After substitution of (10)–(12) into (7) and using the series expansion

$$[1 + y^2 - 2y\cos(\psi)]^{-1/2} = \sum_{n=0}^{\infty} P_n(\cos(\psi))y^n, \quad |y| < 1, \quad (13)$$

where $P_n(\cos(\psi))$ is the Legendre polynomial, the integral equation can be transformed to

$$\sum_{n=0}^{\infty} \Theta_n(\theta)\left[\left(\frac{a}{r}\right)^{n+1} X_n + \left(\frac{r}{b}\right)^n Y_n\right] + R_A + R_B - w_0 - \gamma_0 r\cos\theta = \sum_{n=0}^{\infty} \Theta_n(\theta)\left[\left(\frac{a}{r}\right)^{n+1} Q_A^n + \left(\frac{r}{b}\right)^n Q_B^n\right]. \quad (14)$$

Here the terms are given as

$$\Theta_n(\theta) = \int_0^{2\pi} P_n(\cos(\theta - \phi))\cos(m\phi)\, d\phi, \quad (15)$$

$$X_n = a\sum_{\lambda=0}^{\infty} [D_{\lambda,n} A_\lambda - \overline{D}_{\lambda,n} B_\lambda], \quad (16)$$

$$Y_n = b\sum_{\lambda=0}^{\infty} [-\alpha^3 \overline{D}_{\lambda,n} A_\lambda + D_{\lambda,n} B_\lambda], \quad \alpha = a/b, \quad (17)$$

$$D_{\lambda,n} = \sum_{k=0}^{\infty} \frac{d_k}{2k + 2\lambda + m - n + 1}, \quad d_k = \frac{\Gamma(k + 1/2)}{\sqrt{\pi} k!}, \quad (18)$$

$$\overline{D}_{\lambda,n} = \alpha^{2\lambda+m} \sum_{k=0}^{\infty} \frac{d_k \alpha^{2k}}{2k + 2\lambda + m + n + 2}, \quad (19)$$

$$Q_A^n = a\sigma_a \int_0^1 Q_A(x) x^{n+1} dx, \quad (20)$$

$$Q_B^n = b\sigma_b \int_0^1 Q_B(x) x^{n-2} dx, \quad (21)$$

$$R_A = a\sum_{n=0}^{\infty} \Theta_n(\theta) \sum_{\lambda=0}^{\infty} A_\lambda \sum_{k=0}^{\infty} d_k I_{k,\lambda,n} \left(\frac{a}{r}\right)^{2\lambda+2k+m+2}, \quad (22)$$

$$R_B = b\sum_{n=0}^{\infty} \Theta_n(\theta) \sum_{\lambda=0}^{\infty} B_\lambda \sum_{k=0}^{\infty} d_k I_{k,\lambda,n} \left(\frac{r}{b}\right)^{2\lambda+2k+m+1}, \quad (23)$$

$$I_{k,\lambda,n} = \frac{1}{2k + 2\lambda + n + m + 2} - \frac{1}{2k + 2\lambda + m - n + 1}. \quad (24)$$

The function $\Theta_n(\theta)$ has the following property:

$$\Theta_n(\theta) \doteq 0 \begin{cases} m > n \\ m < n \quad \text{and } n - m \text{ odd.} \end{cases} \quad (25)$$

Considering the nonzero terms ($n \geq m$, $n - m$ even) and defining a new integer $j = 1/2(n - m)$, $j = 0, 1, 2, \ldots$, the series in Eq. (18) can be summed as

$$D_{\lambda,n} = E_\lambda^j = \begin{cases} 0 & \lambda < j \\ \dfrac{\sqrt{\pi}}{2} \dfrac{\Gamma(\lambda - j + 1/2)}{\Gamma(\lambda - j + 1)} & \lambda \geq j, \end{cases} \quad (26)$$

and E_λ^j is introduced to show the dependence on the integer j. The coefficient $\overline{D}_{\lambda,n}$ can be written in the following integral form:

$$\overline{D}_{\lambda,n} = \overline{E}_\lambda^j = \alpha^{2\lambda+2m} \int_0^1 \frac{x^{2(\lambda+m+j)+1}}{\sqrt{1 - (\alpha x)^2}} dx, \quad (27)$$

where $\overline{E}_\lambda^j$ is analogously introduced. The integration can be performed analytically with the trigonometric substitution $\alpha x = \sin(t)$. Defining a new integer L as $L = \lambda + m + j$ ($L = 0, 1, 2, \ldots$), the result can be written as

$$\overline{E}_\lambda^j = \alpha^{-2L-2} \frac{4^L (L!)^2}{(2L+1)!} \left\{1 - \sqrt{1 - \alpha^2} \sum_{r=0}^{L} \frac{(2r)!}{4^r (r!)^2} \alpha^{2r}\right\}. \quad (28)$$

Finally, it can also be shown that R_A and R_B in Eqs. (14), (22), (23) are zero (the details of this are not included here for brevity since this point is discussed by Yong (1989)).

The unknown constants A_λ and B_λ in the power series expansions of Eq. (12) are found by equating coefficients of $\Theta_n(\theta)$ and powers of a/r and r/b in Eq. (14). The following algebraic equations are obtained:

$$\sum_{\lambda=0}^{\infty} [E_\lambda^j A_\lambda - \overline{E}_\lambda^j B_\lambda] = \sigma_a \int_0^1 Q_A(x) x^{2j+m+1} dx, \quad (j = 0, 1, \ldots, \infty), \quad (29)$$

$$\sum_{\lambda=0}^{\infty} [-\alpha^3 \overline{E}_\lambda^j A_\lambda + E_\lambda^j B_\lambda] = \sigma_b \int_0^1 Q_B(x) x^{2j+m-2} dx + \frac{1}{2\pi b} w_0 F(m, j) + \frac{1}{\pi} \gamma_0 F(m-1, j), \quad (j = 0, 1, \ldots, \infty), \quad (30)$$

where the rigid-body displacements are included by introducing the function $F(m, j)$ as

$$F(m, j) = \begin{cases} 1 & m = 0, j = 0 \\ 0 & \text{otherwise.} \end{cases} \quad (31)$$

For the purpose of a numerical solution the infinite system is truncated to one of finite dimension Λ and the equations are expressible in the following matrix form:

$$\left[\begin{array}{c|c} \mathbf{E} & -\overline{\mathbf{E}} \\ \hline -\alpha^3 \overline{\mathbf{E}} & \mathbf{E} \end{array}\right] \left[\begin{array}{c} \mathbf{A} \\ \hline \mathbf{B} \end{array}\right] = \left[\begin{array}{c} \mathbf{Q_A} \\ \hline \mathbf{Q_B} \end{array}\right], \quad (32)$$

where the submatrix $\mathbf{E}$ is an upper triangular matrix

Downloaded 03 May 2010 to 171.66.16.20. Redistribution subject to ASME license or copyright; see http://www.asme.org/terms/Terms_Use.cfm

$$\mathbf{E}=\begin{bmatrix} e_0\ e_1\ \cdots\cdots\ e_\Lambda \\ e_0\ e_1\cdots\cdots\ e_{\Lambda-1} \\ \cdots\cdots\cdots \\ 0\ \cdots\cdots\ e_0 \end{bmatrix},$$

$$e_i=\frac{\sqrt{\pi}}{2}\frac{\Gamma(i+1/2)}{\Gamma(i+1)},\quad i=0,\ 1,\ \ldots\Lambda, \tag{33}$$

$$\mathbf{A}=[A_0,\ A_1,\ \ldots,\ A_\Lambda]^T, \tag{34}$$

$$\mathbf{B}=[B_0,\ B_1,\ \ldots,\ B_\Lambda]^T, \tag{35}$$

$$\mathbf{Q}_A=[q_{A_0},\ q_{A_1},\ \ldots,\ q_{A_\Lambda}]^T, \tag{36}$$

$$q_{A_j}=\sigma_a\int_0^1 Q_A(x)x^{2j+m+1}dx, \tag{37}$$

$$\mathbf{Q}_B=[q_{B_0},\ q_{B_1},\ \ldots,\ q_{B_\Lambda}]^T, \tag{38}$$

$$q_{B_j}=\sigma_b\int_0^1 Q_B(x)x^{2j+m-2}dx+\frac{1}{2\pi b}w_0F(m,j)+\frac{1}{\pi}\gamma_0F(m-1,j). \tag{39}$$

The integral in the submatrix $\overline{\mathbf{E}}$ is symmetric by Eq. (27) since it only depends on the sum $\lambda+j$. For convenience in the solving process, Eq. (32) is rearranged in the form

$$[\mathbf{E}][\mathbf{A}]=[\mathbf{Q}_\mathbf{A}]+[\overline{\mathbf{E}}][\mathbf{B}] \tag{40}$$

$$[\mathbf{E}][\mathbf{B}]=[\mathbf{Q}_\mathbf{B}]+\alpha^3[\overline{\mathbf{E}}][\mathbf{A}]. \tag{41}$$

Because $\mathbf{E}$ and $\overline{\mathbf{E}}$ have the properties illustrated above, all of the elements in each of these matrices may be stored in one-dimensional arrays. The Eqs. (40), (41) are easily solved by means of an iteration method.

It is also necessary to determine expressions for the net force and moment on the crack plane. These are given in Eqs. (4), (5) where M_x in Eq. (6) is zero because solutions even in θ are considered. By substituting Eqs. (10), (11), (12) into Eq. (4), it is easy to see that $P_z=0$ for all m except $m=0$. Considering the axisymmetric case, the net force can be expressed as

$$\frac{P_z}{2\pi b^2}=-\sum_{\lambda=0}^{\Lambda}[-\overline{C}_\lambda A_\lambda+C_\lambda B_\lambda]+\sigma_b\int_0^1 Q_B(x)x^{-3}dx, \tag{42}$$

where the infinite sum has been truncated to Λ and

$$C_\lambda=\frac{\sqrt{\pi}\Gamma(\lambda+1)}{2\Gamma(\lambda+3/2)},\quad \overline{C}_\lambda=\alpha^{2\lambda+3}\int_0^1\frac{x^{2\lambda}}{\sqrt{1-(\alpha x)^2}}dx. \tag{43}$$

The integral can be evaluated as

$$\overline{C}_\lambda=\frac{\alpha^2(2\lambda)!}{4^\lambda(\lambda!)^2}\left\{\sin^{-1}(\alpha)-\sqrt{1-\alpha^2}\sum_{r=0}^{\lambda-1}\frac{4^r(r!)^2}{(2r+1)!}\alpha^{2r+1}\right\}. \tag{44}$$

The term containing $\sigma_A(\rho,\ \phi)$ in Eq. (42) has been eliminated by using Eq. (29) with $m=j=0$. It is also apparent that the net moment M_y vanishes for all m except $m=1$, in which case it may be expressed in truncated series as

$$\frac{M_y}{\pi b^3}=\sigma_b\int_0^1 Q_B(x)x^{-4}dx-\sum_{\lambda=0}^{\Lambda}[-\bar{f}_\lambda A_\lambda+f_\lambda B_\lambda], \tag{45}$$

where the coefficients are

$$f_\lambda=\frac{\sqrt{\pi}\Gamma(\lambda+2)}{2\Gamma(\lambda+5/2)},\quad \bar{f}_\lambda=\alpha^{2\lambda+4}\int_0^1\frac{x^{2\lambda}}{\sqrt{1-(\alpha x)^2}}dx, \tag{46}$$

and since $\bar{f}_\lambda=\alpha\overline{C}_\lambda$ the previous integral evaluation may be used here also. Equation (29) with $m=1$ and $j=0$ has been used to eliminate the term corresponding to $\sigma_A(\rho,\ \phi)$ in Eq. (45).

For the higher order harmonics ($m>1$), the rigid-body displacements do not enter into the analysis and Eqs. (29), (30) completely determine the A_λ's and B_λ's. The same is true for $m=0$, 1 if the rigid-body displacements are specified. In this case, the net force or moment may be found from Eqs. (42) or (45), respectively. The force or moment applied directly to the annular region (force or moment on the annular indenter for a contact problem) can be obtained by subtracting the contribution of the applied loadings from the total given in these equations. If the net force or moment is specified, the rigid-body displacements are unknown. In this case the appropriate Eq. (42) or (45) can be used in place of the one containing the unknown term. After determining the A_λ's and B_λ's, this extra equation may be used to evaluate either w_0 or γ_0 as follows:

$$\frac{w_0}{2\pi b}=-\sigma_b\int_0^1 Q_B(x)x^{-2}dx+\sum_{\lambda=0}^{\Lambda}[-\alpha^3\overline{E}^0_\lambda A_\lambda+E^0_\lambda B_\lambda],\quad (m=0), \tag{47}$$

$$\frac{\gamma_0}{\pi}=-\sigma_b\int_0^1 Q_B(x)x^{-1}dx+\sum_{\lambda=0}^{\Lambda}[-\alpha^3\overline{E}^0_\lambda A_\lambda+\overline{E}^0_\lambda B_\lambda],\quad (m=1). \tag{48}$$

4 Numerical Results

The quantity of interest is the normal stress in the annular region in the crack plane. This stress has square root singularities at $r=a$, b as illustrated in Eq. (12). The quantities to be considered in the present numerical results are the coefficients of these singularities (stress intensity factors) and are defined as

$$K_I^a=\lim_{r\to a}\sqrt{2(r-a)}\,\sigma_{zz}(r,\ \theta,\ 0), \tag{49}$$

$$K_I^b=\lim_{r\to b}\sqrt{2(b-r)}\,\sigma_{zz}(r,\ \theta,\ 0). \tag{50}$$

Substituting Eq. (12) into Eqs. (49), (50) leads to

$$K_I^a=\sqrt{a}\cos(m\theta)\sum_{\lambda=0}^{\Lambda}A_\lambda, \tag{51}$$

$$K_I^b=\sqrt{b}\cos(m\theta)\sum_{\lambda=0}^{\Lambda}B_\lambda, \tag{52}$$

where the values of the A_λ's and B_λ's are obtained as outlined above. It is noteworthy that when $\Lambda\to\infty$, theoretically speaking, the A_λ's and B_λ's will approach the exact solution. For the present numerical results a large enough Λ is used to reduce the error to approximately one percent. Numerical results will now be given for several different loading situations.

(i) Uniform Internal Pressure. The first loading to be analyzed consists of uniform pressure on the region $r<a$ while $r>b$ is traction-free. For this case $m=0$ and $Q_A(r/a)=1$ while $Q_B(b/r)=0$ in Eqs. (10), (11). The value of the internal pressure is σ_a. The rigid-body rotation γ is zero and the remaining condition must specify either the rigid displacement w or the total force P_z.

This loading has been considered previously (Selvadurai and Singh, 1987) where the condition $w=0$ was imposed. (This was not stated but it is implicit in their formulation of the problem.) Table 1(a) compares the present numerical results with the asymptotic series developed by them for various ratios of a/b. The nondimensionalized stress intensity factors are given as

$$\overline{K}_I^a=\frac{\xi}{\sqrt{a}}K_I^a,\quad \overline{K}_I^b=\frac{\xi}{\sqrt{b}}K_I^b, \tag{53}$$

where $\xi=\pi/(2\sigma_a)$ for this loading case. From the table it is evident that the present results agree very closely to the results of Salvadurai and Singh (1987) except for large a/b values.

Downloaded 03 May 2010 to 171.66.16.20. Redistribution subject to ASME license or copyright; see http://www.asme.org/terms/Terms_Use.cfm

Their results should be lower than the present solution for $a/b \to 1$ since their series expansion which was used to calculate the results in this table was only given to $O(c^9)$ where $c = a/b$. The results for $\bar{K}_I^b$ are in extremely good agreement while present calculations for $\bar{K}_I^a$ are about .007 below that predicted by the series solution. (The ratio $a/b = 0$ corresponds to the pressurized penny-shaped crack with a theoretical value of 1.0.) This error results from the truncation of the series in the present analysis to finite dimensions. However, the error here is only 0.7 percent from the more accurate series in Selvadurai and Singh (1987). The last column gives the resultant force on the crack plane nondimensionalized as

$$\bar{P}_z = \eta P_z, \tag{54}$$

where $\eta = 1/(\pi^2 \sigma_a b^2)$. Table 1($b$) gives the results for the case when the net force is taken as zero. Again the limiting value for $\bar{K}_I^a$ at $a/b = 0$ should be 1.00. The nondimensionalized rigid displacement is also given as

$$\bar{w}_0 = \chi w_0, \tag{55}$$

with $\chi = 1/(\pi^2 b \sigma_a)$.

(ii) Point Loading at the Origin. The equations above are not directly applicable to this loading but a slight alteration allows this problem to be solved. In Eqs. (2), (7) the applied loadings are taken in the form $\sigma_A(r, \theta) = 1/2\pi r\, P_0 \delta(r)$, $\sigma_B(r, \theta) = 0$ where P_0 is the magnitude of the point load. The resulting algebraic Eqs. (29), (30) can be used with $Q_A(x) = Q_B(x) = 0$, $m = 0$ and the additional term $1/2\pi a^2\, P_0 F(m, j)$ is added to the right-hand side of Eq. (29).

The numerical results are given in Table 2 with zero net force ($P_z = 0$) and $\xi = \pi^2 a^2/P_0$. For $b \to \infty$ the exact solution for the normal stress outside of a penny-shaped crack under point loading at its center is given as

$$\sigma_{zz}(r, \theta, 0) = \frac{P_0 \left(\frac{a}{r}\right)^2}{\pi^2 a \sqrt{r^2 - a^2}}, \tag{56}$$

which gives the limiting value of 1.0 for $\bar{K}_I^a$ and 0.0 for $\bar{K}_I^b$. The rigid-body displacement is also given with $\chi = a^2/(bP_0)$.

(iii) Uniform Displacement of the Annular Region. This case corresponds to the contact problem of a flat annular indenter attached to an elastic half-space. The exterior loadings $\sigma_A(r, \theta)$, $\sigma_B(r, \theta)$ and the parameter m are taken as zero and the net force P_z is that applied to the indenter. Table 3 gives the stress intensity factors with $\xi = 2\pi b^2/P_z$. The displacement of the indenter is also given with $\chi = 2b/(\pi P_z)$. The limit for $a/b \to 0$ corresponds to a circular rigid punch of radius b which gives a closed-form contact stress of

$$\sigma_{zz}(r, \theta, 0) = \frac{P_z}{2\pi b \sqrt{b^2 - r^2}}, \tag{57}$$

and limiting values of $\bar{K}_I^b = 1.0$ and $\bar{w}_o = 1.0$.

The limit of $\bar{K}_I^a = 0.634$ can be obtained by considering this problem as a superposition of two separate problems. The first problem corresponds to a rigid flat indenter of radius b in contact with a half-space and zero normal traction outside the contact region. The second solution removes the contact stress inside the circle $r < a$ while leaving the other boundary conditions homogeneous. This second solution corresponds to pressure over the region $r < a$, zero normal displacement in the annular region $a < r < b$, and zero normal tractions for $r > b$. As $a/b \to 0$ the second problem approaches a penny-shaped crack under uniform internal pressure of magnitude equal to

Table 1(a) Stress intensity factors for uniform internal pressure loading with zero displacement of the annular region

$\frac{a}{b}$	$\bar{K}_I^{a*}$	$\bar{K}_I^{b*}$	$\bar{P}_z^*$	$\bar{K}_I^a$	$\bar{K}_I^b$	$\bar{P}_z$
0	1	0	—	0.993	0	0
0.1	1.000	0.000	—	0.993	0.000	0.000
0.2	1.000	0.002	—	0.993	0.002	0.001
0.3	1.001	0.006	—	0.994	0.006	0.004
0.4	1.003	0.015	—	0.996	0.015	0.009
0.5	1.007	0.032	—	1.000	0.031	0.018
0.6	1.014	0.060	—	1.008	0.060	0.032
0.7	1.026	0.106	—	1.022	0.108	0.054
0.8	1.047	0.183	—	1.052	0.197	0.086
0.9	1.080	0.311	—	1.137	0.397	0.138
0.99	—	—	—	1.907	1.515	0.250

* Results from [11] (a factor of $2/\pi$ is missing from their results).

Table 1(b) Stress intensity factors for uniform internal pressure loading with zero net force

$\frac{a}{b}$	0	0.1	0.2	0.3	0.4	0.5	0.6	0.7	0.8	0.9	0.99
$\bar{K}_I^a$	0.993	0.993	0.994	0.999	1.006	1.020	1.046	1.094	1.189	1.440	3.662
$\bar{K}_I^b$	0	0.001	0.003	0.012	0.029	0.061	0.114	0.204	0.370	0.750	3.284
$\bar{w}_0$	0	0.000	0.002	0.006	0.014	0.029	0.052	0.090	0.150	0.263	0.644

Table 2 Stress intensity factors for point loading at the origin with zero net force

$\frac{a}{b}$	0	0.1	0.2	0.3	0.4	0.5	0.6	0.7	0.8	0.9	0.99
$\bar{K}_I^a$	1	1.001	1.004	1.015	1.038	1.080	1.154	1.282	1.530	2.144	6.822
$\bar{K}_I^b$	0	0.001	0.010	0.035	0.085	0.173	0.317	0.549	0.944	1.775	6.790
$\bar{w}_0$	0	0.001	0.005	0.017	0.042	0.084	0.151	0.254	0.415	0.669	1.544

Table 3 Stress intensity factors for uniform vertical displacement of the annular region

$\frac{a}{b}$	0	0.1	0.2	0.3	0.4	0.5	0.6	0.7	0.8	0.9	0.99
$\bar{K}_I^a$	0.634	0.634	0.642	0.655	0.678	0.713	0.767	0.855	1.016	1.403	4.373
$\bar{K}_I^b$	1	1.000	1.002	1.008	1.019	1.041	1.079	1.148	1.284	1.633	4.509
$\bar{w}_0$	1	1.000	1.001	1.004	1.009	1.019	1.036	1.064	1.114	1.217	1.643

Downloaded 03 May 2010 to 171.66.16.20. Redistribution subject to ASME license or copyright; see http://www.asme.org/terms/Terms_Use.cfm

Table 4 Stress intensity factors for uniform loading over an annular region of the external crack with zero net force

$\frac{a}{b}$	0	0.1	0.2	0.3	0.4	0.5	0.6	0.7	0.8	0.9	0.99
$\overline{K}_I^a$	0.149	0.149	0.152	0.157	0.165	0.179	0.199	0.234	0.300	0.467	1.803
$\overline{K}_I^b$	0.871	0.871	0.871	0.873	0.875	0.880	0.890	0.909	0.947	1.058	2.170
$\overline{w}_0$	0.219	0.219	0.219	0.220	0.221	0.223	0.228	0.235	0.249	0.284	0.447

Table 5 Stress intensity factors for a linearly varying internal pressure with zero net moment

$\frac{a}{b}$	0	0.1	0.2	0.3	0.4	0.5	0.6	0.7	0.8	0.9	0.99
$\overline{K}_I^a$	0.659	0.659	0.659	0.660	0.660	0.662	0.668	0.681	0.713	0.816	1.856
$\overline{K}_I^b$	0	0.000	0.001	0.002	0.006	0.016	0.036	0.074	0.150	0.125	0.335
$\overline{\gamma}_0$	0	0.000	0.000	0.001	0.002	0.005	0.010	0.020	0.039	0.077	0.221

Table 6 Stress intensity factors for uniform rotation of the annular region

$\frac{a}{b}$	0	0.1	0.2	0.3	0.4	0.5	0.6	0.7	0.8	0.9	0.99
$\overline{K}_I^a$	0	0.042	0.085	0.131	0.180	0.236	0.303	0.391	0.527	0.816	2.846
$\overline{K}_I^b$	1	1.000	1.000	1.000	1.002	1.005	1.015	1.039	1.099	1.286	3.104
$\overline{\gamma}_0$	1	1.000	1.000	1.000	1.001	1.004	1.011	1.027	1.063	1.159	1.664

the contact stress at the origin of the first problem given as $P_z/(2\pi b^2)$ from Eq. (57) with $r=0$. This limiting case gives a stress intensity factor of $\overline{K}_I^a = 2/\pi = 0.6366$ which is in excellent agreement with the present numerical result.

As a final point the results from Fabrikant (1991b) can be used to compare with present calculations. Fabrikant gives the nondimensional force P^* as 0.9989, 0.9907, 0.9651, 0.8976, 0.8210 for $a/b = 0.2$, 0.4, 0.6, 0.8 and 0.9, respectively. It can be shown that $P^* = 1/\overline{w}_o$. From Table 3 the values of $1/\overline{w}_o$ can be found for these a/b values as 0.9990, 0.9911, 0.9653, 0.8977, and 0.8217 and thus present results are in excellent agreement with Fabrikant's analysis.

(iv) Uniform Loading on the External Crack. The last axisymmetric ($m = 0$) loading considered here is uniform pressure over an annular region $b<r<b_1$. For a numerical solution the value of b_1 was taken as $b_1 = 1.25b$. The applied loadings are given as $Q_A(r/a) = 0$ while $Q_B(b/r) = H(b/r - 0.8)$ where $H(x)$ is the Heaviside function, and the uniform pressure has a magnitude of σ_b. Table 4 gives the numerical results with $\xi = \pi/(2\sigma_b)$, $\chi = 1/(\pi^2 b\sigma_b)$ and the net force is taken as zero. For $a/b \to 0$, the solution at $r = b$ approaches the external crack with an annular uniform loading. The limiting value in Table 4 of $\overline{K}_I^b = 0.871$ agrees well with the theoretical value of 0.8777 which can be obtained from the closed-form expression given by Tada et al. (1973). The limiting value of $\overline{K}_I^a$ can be evaluated in a manner analogous to the previous loading case. The Green's function for normal stress in the bond ligament of an external circular crack subjected to point normal loading and zero net force is given in Stallybrass (1981). Integrating this solution over the annular region $b<r<b_1$ and evaluating the stress at the origin gives the result

$$\lim_{r\to 0} \sigma_{zz}(r, \theta, 0) = \sigma_b \frac{1}{\pi}\left(\frac{b_1}{b}\right)^2 \left(\left(1 - 2\frac{b^2}{b_1^2}\right)\cos^{-1}\left(\frac{b}{b_1}\right) + \frac{b}{b_1}\left[1 - \left(\frac{b}{b_1}\right)\right]^{1/2}\right). \quad (58)$$

For the present ratio of $b_1 = 1.25b$, use of the above equation gives a value of $0.1491\sigma_b$ for the stress at the origin. Considering a penny-shaped crack of radius $r = a$ uniformly pressurized with this magnitude gives the theoretical limit appropriate for $\overline{K}_I^a$.

(v) Linear Variation of Internal Pressure. This case consists of internal pressure in the region $r<a$ which varies linearly in the $\theta = 0$ direction and vanishes at the center. This applied loading is mathematically expressed as $\sigma_A(r, \theta) = \sigma_a(r/a)\cos(\theta)$ and $\sigma_B(r, \theta) = 0$. For this loading $m = 1$ and Table 5 displays the numerical results for the condition of zero net moment ($M_y = 0$). The value of ξ in Eq. (53) is $\xi = \pi/(2\sigma_a \cos(\theta))$ and the nondimensionalized rotation $\overline{\gamma}_0$ is given as $\overline{\gamma}_0 = \zeta\gamma_0$ with $\zeta = 1/(\pi^2\sigma_a)$. For the limiting case $a/b \to 0$, $\overline{K}_I^b$ and $\overline{\gamma}_0$ vanish while $\overline{K}_I^a$ approaches the value for a penny-shaped crack. Integrating the point force solution in Tada et al. (1973) yields the theoretical limit of $\overline{K}_I^a = 2/3$ and the numerical error is just over one percent.

(vi) Uniform Rotation of the Annular Region. The last case corresponds to the contact problem of a tilted annular indenter attached to an elastic half-space. The external loadings $\sigma_A(r, \theta)$ an $\sigma_B(r, \theta)$ are taken as zero and the net moment M_y is the moment applied to the indenter. Again $m = 1$, and Table 6 gives the stress intensity factors and rotation with $\xi = 2\pi b^3/(3M_y \cos(\theta))$ and $\zeta = 4b^3/(3\pi M_y)$. The stress field for the limiting case $a/b \to 0$ is given as

$$\sigma_{zz}(r, \theta, 0) = \frac{3M_y}{2\pi b^3}\frac{r\cos(\theta)}{\sqrt{b^2 - r^2}}, \quad (59)$$

which corresponds to a tilted circular punch on an elastic half-space. From the above equation the limit of $\overline{K}_I^b$ can be easily obtained while at the origin the contact stress approaches $3M_y r\cos(\theta)/(2\pi b^4)$. The limiting case for $\overline{K}_I^a$ can be obtained by applying this stress to a penny-shaped crack in an infinite solid. Using the results from the previous section it is easy to verify that $\overline{K}_I^a$ behaves like $4a/(3\pi b)$ for $a/b \to 0$. The numerical results for $\overline{K}_I^a$ are very close to this leading term for a/b out to 0.3.

The present results for this case can also be compared to those in Fabrikant (1991b) who tabulated the nondimensionalized moment M^* as $M^* = 0.99996$, 0.99878, 0.98930, 0.94084, 0.86243, for $a/b = 0.2$, 0.4, 0.6, 0.8, 0.9, respectively.

Downloaded 03 May 2010 to 171.66.16.20. Redistribution subject to ASME license or copyright; see http://www.asme.org/terms/Terms_Use.cfm

It is easy to show that $M^* = 1/\bar{\gamma}_0$ and from Table 6 $1/\bar{\gamma}_0 = 1.000$, 0.9990, 0.9891, 0.9407, 0.8628 for these a/b values, showing excellent agreement.

5 Further Discussion

In the previous analysis a solution for radially arbitrary loading in cosine harmonic form was derived. For completely arbitrary loading conditions $\sigma_{zz}(r, \theta, 0)$ in Eq. (12) has the form

$$\sigma_{zz}(r, \theta, 0) = \frac{a}{\sqrt{r^2 - a^2}} \sum_{\lambda=0}^{\infty} A_\lambda(\theta) \left(\frac{a}{r}\right)^{\lambda+2} + \frac{b}{\sqrt{b^2 - r^2}} \sum_{\lambda=0}^{\infty} B_\lambda(\theta) \left(\frac{r}{b}\right)^{\lambda}, \quad \text{where} \tag{60}$$

$$A_\lambda(\theta) = \sum_{m=0}^{M} c_m^\lambda \cos(\lambda - 2m)\theta, \quad \lambda - 2M \geq 0, \tag{61}$$

$$B_\lambda(\theta) = \sum_{m=0}^{M} e_m^\lambda \cos(\lambda - 2m)\theta, \quad \lambda - 2M \geq 0, \tag{62}$$

are the polynomials of $\cos(m\theta)$ which are structurally correspondent with the Legendre polynomials and the c_m^λ's and e_m^λ's are unknown constants. Equation (60) still ensures that the nature of this solution is the same as that in Section 3. One obvious advantage of Eq. (60) is that the loading functions $\sigma_A(r, \theta)$ and $\sigma_B(r, \theta)$ can be taken as arbitrary mathematical forms instead of the special forms in Eqs. (10), (11). One of the differences caused by Eq. (60) is that $\Theta_n(\theta)$ on opposite sides of Eq. (14) has different expressions. This will increase the amount of calculations over that presently needed in Eqs. (29), (30).

References

Choi, I., and Shield, R. T., 1982, "A Note on a Flat Toroidal Crack in an Elastic Isotropic Body," *International Journal of Solids and Structures*, Vol. 18, pp. 479–486.

Clements, D. L., and Ang, W. T., 1988, "Stress Intensity Factors for the Circular Annulus Crack," *International Journal of Engineering Science*, Vol. 26, pp. 325–329.

Comninou, M., and Barber, J. R., 1982, "Letter to the Editor on the Plane External Crack," *Letters in Applied Engineering Sciences*, Vol. 20, pp. 695–696.

Erdol, R., and Erdogan, F., 1978, "A Thick-Walled Cylinder with an Axisymmetric Internal or Edge Crack," ASME JOURNAL OF APPLIED MECHANICS, Vol. 45, pp. 281–286.

Fabrikant, V. I., 1991a, "Non-Axisymmetric Normal Load on an Annular Crack," *Theoretical and Applied Fracture Mechanics*, Vol. 15, pp. 229–236.

Fabrikant, V. I., 1991b, "Nonaxisymmetric Annular Punch Problem," ASME JOURNAL OF APPLIED MECHANICS, Vol. 58, pp. 947–953.

Fabrikant, V. I., 1989, *Applications of Potential Theory in Mechanics: A Selection of New Results*, Kluwer Academic Publishers, The Netherlands, pp. 75–79.

Fabrikant, V. I., Sankar, T. S., and Xistris, G. D., 1986, "On the Conditions at Infinity in External Crack Problems," *Engineering Fracture Mechanics*, Vol. 23, pp. 921–924.

Gao, H., and Rice, J. R., 1987, "Nearly Circular Connections of Elastic Half Spaces," ASME JOURNAL OF APPLIED MECHANICS, Vol. 54, pp. 627–634.

Gladwell, G. M. L., 1980, *Contact Problems in the Classical Theory of Elasticity*, Sijthoff & Noordhoff, pp. 518–527.

Mastrojannis, E. N., 1983, "A Note on the Problem of an Annular Crack Subjected to an Arbitrary Normal Pressure," *Letters in Applied Engineering Sciences*, Vol. 21, pp. 1129–1136.

Mastrojannis, E. N., and Kermanidis, T. B., 1981, "An Approximate Solution of the Annular Crack Problem," *International Journal for Numerical Methods in Engineering*, Vol. 17, pp. 1605–1611.

Moss, L. W., and Kobayashi, A. S., 1971, "Approximate Analysis of Axisymmetric Problems in Fracture Mechanics with Application to a Flat Toroidal Crack," *International Journal of Fracture Mechanics*, Vol. 7, pp. 88–99.

Nied, H. F., and Erdogan, F., 1983, "The Elasticity Problem for a Thick-Walled Cylinder Containing a Circumferential Crack," *International Journal of Fracture*, Vol. 22, pp. 277–301.

Selvadurai, A. P. S., and Singh, B. M., 1985, "The Annular Crack Problem for an Isotropic Elastic Solid," *Quarterly Journal of Mechanics and Applied Mathematics*, Vol. 38, pp. 233–243.

Selvadurai, A. P. S., and Singh, B. M., 1987, "Axisymmetric Problems for an Externally Cracked Elastic Solid. I. Effect of a Penny-Shaped Crack," *International Journal of Engineering Science*, Vol. 25, pp. 1049–1057.

Shield, T. W., and Bogy, D. B., 1989, "Some Axisymmetric Problems for Layered Elastic Media: Part II—Solutions for Annular Indenters and Cracks," ASME JOURNAL OF APPLIED MECHANICS, Vol. 56, pp. 807–813.

Smetanin, B. T., 1968, "Problem of Extension of an Elastic Space Containing a Plane Annular Slit," *Journal of Applied Mathematics and Mechanics*, Vol. 32, pp. 461–466.

Stallybrass, M. P., 1981a, "Some Comments on External Crack Problems in 2-Dimensional Elastostatics," *International Journal of Engineering Science*, Vol. 19, pp. 57–61.

Stallybrass, M. P., 1981b, "On the Concentrated Loading of Certain Elastic Half-Space Problems and Related External Crack Problems. A New Approach," *International Journal of Engineering Science*, Vol. 19, pp. 1123–1144.

Tada, H., Paris, P. C., and Irwin, G. R., 1973, *The Stress Analysis of Cracks Handbook*, Del Research Corporation, Hellertown, PA.

Yong, Z., 1989, "A New Method for Solving the Circular Crack Problems Under Arbitrary Normal Loading," *Engineering Fracture Mechanics*, Vol. 34, pp. 201–207.

Downloaded 03 May 2010 to 171.66.16.20. Redistribution subject to ASME license or copyright; see http://www.asme.org/terms/Terms_Use.cfm

Simulation of Cone Bore Growth in Bearings With a Three-Ring Model

R. W. Neu[1]
Assoc. Mem. ASME.

Huseyin Sehitoglu
Mem. ASME.

Department of Mechanical and Industrial Engineering,
University of Illinois,
1206 W. Green Street,
Urbana, IL 61801

Cone bore growth in case-carburized bearings was modeled by incorporating the mechanisms of thermal-induced phase transformation and low temperature creep in an approximate model of the cone. The inner case, core, and outer case regions of the bearing cone are modeled by three concentric rings. Using a mechanics of materials approach with the aid of some simplifying assumptions (i.e., radial stresses remain zero throughout the ring thickness and net circumferential strain is the same for all three rings), the influence of temperature, interference fit stresses, initial case carburizing stresses, and stress relaxation on the change in bore diameter and circumferential stress during service could be determined. The model indicated that both thermal-induced transformation and low temperature creep may play a role in bore growth during service. As temperature was increased from 70°C to 200°C, the susceptibility to bore growth became greater. Also, an increase in the interference fit increased the initial cone bore growth rate. In addition, the effect of the recondition treatment on the bore diameter and residual stresses was studied. The bore diameter generally decreased during the recondition treatment, and this was attributed to the relaxation of residual stresses by low temperature creep.

Background

Understanding cone bore growth has become increasingly important in recent years, because of the desire to increase railcar loads. There is a strong requirement for higher reliability of bearings over a longer period of time. Currently, bearings are removed from service after a number of miles for inspection and reconditioning. The majority of bearings are reconditioned and put back in service. The bore diameter of the cones is measured, and if growth has occurred, the cone is reheated to a temperature around the tempering (177°C) and held there are two to four hours. After this recondition treatment, the bore diameter will usually be smaller. Reducing the interval when bearings need to be reconditioned, while keeping the same confidence in the bearings, will reduce cost and therefore benefit the railroad's competitiveness in the coming years.

In recent reviews of railroad bearing failure research (Moyar et al., 1988; Fec and Moyar, 1988), the concern of cone bore growth has increased since the mid-1970s, since it is not well understood. A schematic of the bearing is shown in Fig. 1. The load-carrying components in the bearing consist of the cup (also called the outer ring), rollers, and cone (inner ring). The cone bore diameter is also shown in Fig. 1. The entire bearing assembly, consisting of a pair of cones and rollers, is pressed fit onto the axle journal. The size of the axle journal must be 0.038 to 0.114 mm (0.0015 to 0.0045 in.) larger than the bore diameter to create an interference fit between the cone and journal. The cone is forged from 4320 steel, carburized, and then quenched and tempered. As a result, a case with carbon content near 1.0 percent and depth of about 2.0 mm (0.080 in.) exists around the cone. Because of the high carbon content, from 10 percent to 35 percent austenite is retained in the case.

It has been repeatedly found that the cone bore diameter becomes larger in service (Moyar et al., 1988; Fec and Moyar, 1988). A typical increase in bore diameter is 0.013 mm (0.0005 in.) (Gleeson, 1989). This is undesirable for a number of rea-

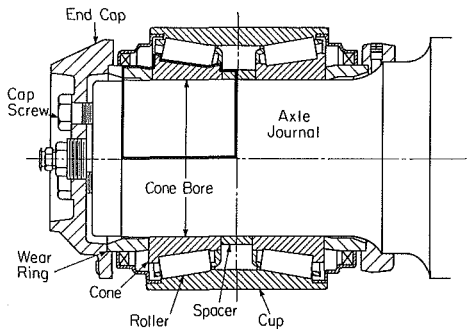


Fig. 1 Railroad roller bearing assembly

[1]Currently, Visiting Scientist, Wright Laboratory Materials Directorate, WL/MLLN, Wright-Patterson AFB, OH 45433.

Contributed by the Applied Mechanics Division of THE AMERICAN SOCIETY OF MECHANICAL ENGINEERS for publication in the ASME JOURNAL OF APPLIED MECHANICS.

Discussion on this paper should be addressed to the Technical Editor, Professor Lewis T. Wheeler, Department of Mechanical Engineering, University of Houston, Houston, TX 77204-4792, and will be accepted until four months after final publication of the paper itself in the ASME JOURNAL OF APPLIED MECHANICS.

Manuscript received by the ASME Applied Mechanics Division, Oct. 8, 1991; final revision, June 15, 1993. Associate Technical Editor: R. M. McMeeking.

Copyright © 1994 by ASME
Downloaded 03 May 2010 to 171.66.16.20. Redistribution subject to ASME license or copyright; see http://www.asme.org/terms/Terms_Use.cfm

sons. If the interference fit decreases due to cone bore growth, the turning of the cone relative to the journal can occur. This action tends to wear grooves in the journal (Orringer, 1988), which further reduces the interference fit. Heat can be generated from the severe sliding of the cone on the journal. The temperature gradients within the bearing change the dimensions of the close-tolerance components. This can lead to an increase in friction between roller and cone, generating additional heat. This heat generation can lead ultimately to journal burnoff, where the journal becomes so weak from the high temperatures that it no longer supports the load.

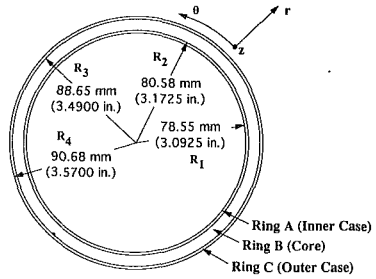
In 1982, Voskamp and Schalk (1982) presented results of roller bearing tests conducted on a test rig to study the cone bore growth phenomena. Three different mechanisms of cone bore growth were examined: (1) phase transformation of austenite, (2) cyclic plastic deformation, and (3) stress relaxation or creep. The study showed that the growth rate was directly related to the amount of initial retained austenite. Furthermore, Voskamp found that the growth increased with a larger case depth and with a higher operating temperature. Using X-ray diffraction techniques, retained austenite and residual stresses in the cone were found unchanged during the tests. Based on these observations and noting that growth increased with a higher operating temperature, Voskamp concluded that the creep phenomenon appeared to be the mechanism causing cone bore growth. The results of increasing growth rate with increasing retained austenite content were explained by the lower creep resistance of the steel with higher austenite amounts.

Even though Voskamp's results indicate otherwise, others (Fec and Moyar, 1988) tend to believe that cone bore growth is related to the transformation of retained austenite and the residual stresses that develop in the cone from the plastic deformation. One argument which supports the residual stress hypothesis is the fact that the cone bore diameter can be reduced with a reconditioning heat treatment of the bearing. The treatment (typically, 177°C for two to four hours) is sufficient to relieve some of the residual stresses.

Three-Ring Model

The effects of thermal-induced transformation of retained austenite, low temperature creep, and thermal expansion on the dimensions of a bearing cone were examined with the three-ring model, using a combined elasticity and mechanics of materials approach. The kinetics of both transformation and low temperature creep were independently determined from the transformation and creep experiments conducted on carburized 4320 steel (case material) and quenched and tempered 4320 steel (core material). The details of the experiments and expressions that describe thermal-induced transformation and low temperature creep are given in Neu and Sehitoglu (1993) and Neu and Sehitoglu (1992), respectively. Since no Hertzian stress is applied during the measurement of the cone bore, the Hertzian stress itself does not influence the bore diameter; however, any permanent change to the microstructure from cyclic plastic deformation resulting from the moving Hertzian contact may change the residual stress state and thus affect cone bore growth. Without resort to a plasticity analysis or complicated multiaxial plasticity experiments to simulate Hertzian contact, the influence of microstructural changes from cyclic plastic deformation on cone bore growth were undetermined and were omitted from the present analysis.

The axial center of the cone was modeled with three concentric rings (Fig. 2) representing the inner case (ring A), core (ring B), and the outer case (ring C). The elastic strains and stresses were computed using the theory of elasticity by satisfying compatibility and equilibrium at the interfaces between the rings and at the boundaries. The interference fit was imposed by displacing the inner radius of ring A. After the displacement was applied, the largest stress in the rings was a tensile circumferential stress.



6 1/2 × 12 (Class F)

Fig. 2 Geometry of the three-ring model

The axial stress was tensile when the interference fit was applied. If an axial compressive cap screw force was incorporated, the axial force would become compressive. However, the magnitude of the axial stress was still much smaller than the circumferential stress (Neu and Sehitoglu, 1990). The prediction of cone bore growth from the model was not very sensitive to axial stress as long as the axial stress was much smaller than the circumferential stress, so a zero resultant axial force was assumed. Even through the resultant axial force was zero, the individual axial ring forces were not zero when the rings had different material properties.

A thin-walled solution was used to simplify equations and computations. Consequently, the radial stress, σ_r, remained zero throughout the thickness and $\epsilon_\theta^{\text{net}}$ was the same for all three rings. Even though this wall thickness is not so small (radial thickness was about 14 percent of the average radius), the circumferential stress given by the three-ring model was within five percent of the average circumferential stress given by an axisymmetric finite element model that more closely approximated the geometry of the cone (Neu and Sehitoglu, 1990). The finite element model also confirmed that σ_r remained small relative to σ_θ.

For a given interference fit, temperature, geometry, and material, the radial displacements and circumferential and axial stresses were determined. The model predicted the change in bore diameter along with the mechanism causing this change. It also predicted whether the stress-relieving recondition treatment would sufficiently reduce the bore diameter. Residual stresses from the processing of case-carburized components could also be incorporated by imposing an initial strain in the case. The effects of stress-induced transformation strains and residual plastic strains could also be incorporated in the same way.

Methodology

During the first iteration, the net strains and elastic strain are computed based on the initial conditions of each ring and the radial displacement of the bore. The net strain (ϵ^{net}) is the sum of the elastic (ϵ^e), thermal (ϵ^{th}), thermal-induced transformation (ϵ^{tf}), and creep (ϵ^{cr}) strains, and in the uniaxial case is given as

$$\epsilon^{\text{net}} = \epsilon^e + \epsilon^* \tag{1}$$

where

$$\epsilon^* = \epsilon^{th} + \epsilon^{tf} + \epsilon^{cr}. \tag{2}$$

Once the strains are known, the radial displacement (bore growth or shrinkage) and stresses can be computed. The ring becomes loose when the resultant circumferential force becomes less than zero. When the ring is loose or the cone is not on the journal, the radial displacement is unknown, but the

Downloaded 03 May 2010 to 171.66.16.20. Redistribution subject to ASME license or copyright; see http://www.asme.org/terms/Terms_Use.cfm

resultant circumferential force is zero. Even when the cone is not loose, the radial displacement, which is bore growth divided by two, is determined by setting the resultant circumferential force to zero and computing the resulting change in the bore diameter.

For subsequent time steps, the time and temperature-dependent strains (ϵ^{th}, ϵ^{tl}, ϵ^{cr}) are computed before the elastic strain and stresses are computed. Since different boundary conditions exist when the cone is tight on the axle journal and when it is loose, each solution is discussed separately. When the cone is tight, the radial displacement at R_1 (u_1) is known, but the resultant circumferential stress, σ_θ^o, is unknown; when the cone is loose, σ_θ^o is zero, but u_1 is not known.

Tight Cone Solution. When the cone is tight on the axle journal, u_1 is known. Therefore, the net circumferential strain, $\epsilon_\theta^{\text{net}}$ can be computed,

$$\epsilon_\theta^{\text{net}} = \frac{u_1}{R_1}. \tag{3}$$

The diametral interference fit is defined as $2 \cdot u_1$ and typically ranges from 0.038 to 0.114 mm (0.0015 to 0.0045 in.). $\epsilon_\theta^{\text{net}}$ is the same for all three rings, or else radial planes will not remain plane.

The stresses and strains are determined at the outer and inner radii of each ring. First, the equations for determining the stresses and strains at one of the radii when the cone is tight will be derived. The net strains are given by

$$\epsilon_\theta^{\text{net}} = \frac{1}{E}\left[\sigma_\theta - \nu\sigma_z\right] + \epsilon_\theta^* \tag{4}$$

$$\epsilon_z^{\text{net}} = \frac{1}{E}\left[\sigma_z - \nu\sigma_\theta\right] + \epsilon_z^* \tag{5}$$

where $E = 200{,}000$ MPa and $\nu = 0.3$. In these equations, $\epsilon_\theta^{\text{net}}$ is known (from Eq. (3)); ϵ_z^{net} is unknown, but it must be constant for all three rings. The time and temperature-dependent strains (ϵ^*) are computed before each time increment. The stresses, σ_θ and σ_z, in each ring are unknown. Solving for σ_z in Eqs. (4) and (5),

$$\sigma_z = \frac{E\nu}{1-\nu^2}\left[\epsilon_\theta^{\text{net}} - \epsilon_\theta^* - \frac{1}{\nu}\left(\epsilon_z^* - \epsilon_z^{\text{net}}\right)\right]. \tag{6}$$

For three concentric rings, there are six equations:

$$\begin{aligned}
\sigma_{z1}^a &= \frac{E^a\nu^a}{1-\nu^{a2}}\left[\epsilon_\theta^{\text{net}} - \epsilon_{\theta1}^{*a} - \frac{1}{\nu^a}\left(\epsilon_{z1}^{*a} - \epsilon_z^{\text{net}}\right)\right] \\
\sigma_{z2}^a &= \frac{E^a\nu^a}{1-\nu^{a2}}\left[\epsilon_\theta^{\text{net}} - \epsilon_{\theta2}^{*a} - \frac{1}{\nu^a}\left(\epsilon_{z2}^{*a} - \epsilon_z^{\text{net}}\right)\right] \\
\sigma_{z2}^b &= \frac{E^b\nu^b}{1-\nu^{b2}}\left[\epsilon_\theta^{\text{net}} - \epsilon_{\theta2}^{*b} - \frac{1}{\nu^b}\left(\epsilon_{z2}^{*b} - \epsilon_z^{\text{net}}\right)\right] \\
\sigma_{z3}^b &= \frac{E^b\nu^b}{1-\nu^{b2}}\left[\epsilon_\theta^{\text{net}} - \epsilon_{\theta3}^{*b} - \frac{1}{\nu^b}\left(\epsilon_{z3}^{*b} - \epsilon_z^{\text{net}}\right)\right] \\
\sigma_{z3}^c &= \frac{E^c\nu^c}{1-\nu^{c2}}\left[\epsilon_\theta^{\text{net}} - \epsilon_{\theta3}^{*c} - \frac{1}{\nu^c}\left(\epsilon_{z3}^{*c} - \epsilon_z^{\text{net}}\right)\right] \\
\sigma_{z4}^c &= \frac{E^c\nu^c}{1-\nu^{c2}}\left[\epsilon_\theta^{\text{net}} - \epsilon_{\theta4}^{*c} - \frac{1}{\nu^c}\left(\epsilon_{z4}^{*c} - \epsilon_z^{\text{net}}\right)\right]
\end{aligned} \tag{7}$$

where the numerical subscripts represent the radius and the superscripts indicate the ring. The axial forces in the rings are given by the average axial stress in the ring multiplied by the cross-sectional area of the ring,

$$N_z^a = \frac{1}{2}\left(\sigma_{z1}^a + \sigma_{z2}^a\right)A_z^a$$

$$N_z^b = \frac{1}{2}\left(\sigma_{z2}^b + \sigma_{z3}^b\right)A_z^b$$

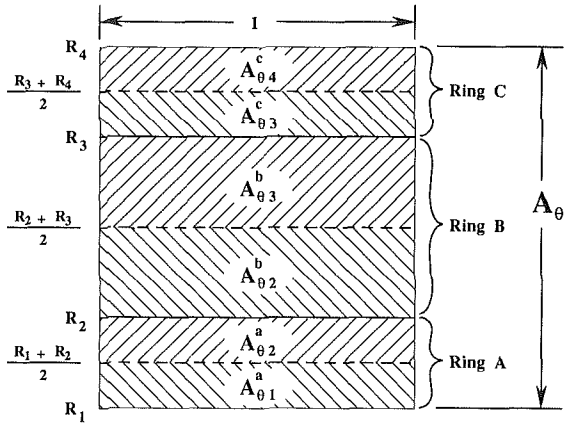


Fig. 3 Circumferential cross-section of three ring model

$$N_z^c = \frac{1}{2}\left(\sigma_{z3}^c + \sigma_{z4}^c\right)A_z^c. \tag{8}$$

For a short cylinder the resultant of the axial forces is zero,

$$N_z^a + N_z^b + N_z^c = 0. \tag{9}$$

The effect of an axial stress from the cap screw load can be applied by replacing the right-hand side of Eq. (9) with the desired axial stress. With Eqs. (3), (7), (8), and (9), ϵ_z^{net} can be determined. Once ϵ_z^{net} is known, the forces and stresses can be computed.

Before incrementing time at the end of the computations for each time increment, the cone is checked for detachment from journal. This is accomplished by computing the resultant circumferential stress, σ_θ^o. If $\sigma_\theta^o <= 0$, then the ring is loose. Since σ_θ^o can vary with r, this stress is computed by summing the circumferential forces,

$$\sigma_\theta^o = \frac{\Sigma N_\theta}{A_\theta} \tag{10}$$

where A_θ is the total area as shown in Fig. 3 and ΣN_θ is given by

$$\Sigma N_\theta = \sigma_{\theta1}^a A_{\theta1}^a + \sigma_{\theta2}^a A_{\theta2}^a + \sigma_{\theta2}^b A_{\theta2}^b + \sigma_{\theta3}^b A_{\theta3}^b + \sigma_{\theta3}^c A_{\theta3}^c + \sigma_{\theta4}^c A_{\theta4}^c \tag{11}$$

where the individual areas are also shown in Fig. 3. When the cone is loose, u_1 is no longer known, so a different methodology is required.

Loose Cone Solution. When the cone becomes loose or when it is removed from the journal, the pressure acting on the bore goes to zero; therefore, σ_θ^o (defined by Eq. (10)) must also become zero. However, neither $\epsilon_\theta^{\text{net}}$ or ϵ_z^{net} are known. A bit more algebra is required to solve for these strains. Two equations with $\epsilon_\theta^{\text{net}}$ and ϵ_z^{net} as the only unknowns are obtained, allowing these strains to be determined. The first of these equations is determined from Eqs. (7), (8), and (9):

$$A_1\epsilon_\theta^{\text{net}} + B_1\epsilon_z^{\text{net}} = C_1 \tag{12}$$

where

$$A_1 = A_z^a\frac{2E^a\nu^a}{1-\nu^{a2}} + A_z^b\frac{2E^b\nu^b}{1-\nu^{b2}} + A_z^c\frac{2E^c\nu^c}{1-\nu^{c2}}$$

$$B_1 = A_z^a\frac{2E^a}{1-\nu^{a2}} + A_z^b\frac{2E^b}{1-\nu^{b2}} + A_z^c\frac{2E^c}{1-\nu^{c2}}$$

$$\begin{aligned}
C_1 = {} & A_z^a\frac{E^a\nu^a}{1-\nu^{a2}}\left[\epsilon_{\theta1}^{*a} + \frac{1}{\nu^a}\left(\epsilon_{z1}^{*a}\right) + \epsilon_{\theta2}^{*a} + \frac{1}{\nu^a}\left(\epsilon_{z2}^{*a}\right)\right] \\
& + A_z^b\frac{E^b\nu^b}{1-\nu^{b2}}\left[\epsilon_{\theta2}^{*b} + \frac{1}{\nu^b}\left(\epsilon_{z2}^{*b}\right) + \epsilon_{\theta3}^{*b} + \frac{1}{\nu^b}\left(\epsilon_{z3}^{*b}\right)\right] \\
& + A_z^c\frac{E^c\nu^c}{1-\nu^{c2}}\left[\epsilon_{\theta3}^{*c} + \frac{1}{\nu^c}\left(\epsilon_{z3}^{*c}\right) + \epsilon_{\theta4}^{*c} + \frac{1}{\nu^c}\left(\epsilon_{z4}^{*c}\right)\right].
\end{aligned}$$

Downloaded 03 May 2010 to 171.66.16.20. Redistribution subject to ASME license or copyright; see http://www.asme.org/terms/Terms_Use.cfm

The second equation is derived from Eqs. (4), (5), (7), and (11):

$$A_2\epsilon_\theta^{\text{net}} + B_2\epsilon_z^{\text{net}} = C_2 \tag{13}$$

where

$$A_2 = (A_{\theta 1}^a + A_{\theta 2}^a)\frac{E^a}{1-\nu^{a2}} + (A_{\theta 2}^b + A_{\theta 3}^b)\frac{E^b}{1-\nu^{b2}} + (A_{\theta 3}^c + A_{\theta 4}^c)\frac{E^c}{1-\nu^{c2}}$$

$$B_2 = (A_{\theta 1}^a + A_{\theta 2}^a)\frac{\nu^a E^a}{1-\nu^{a2}} + (A_{\theta 2}^b + A_{\theta 3}^b)\frac{\nu^b E^b}{1-\nu^{b2}} + (A_{\theta 3}^c + A_{\theta 4}^c)\frac{\nu^c E^c}{1-\nu^{c2}}$$

$$C_2 = A_{\theta 1}^a \frac{E^a}{1-\nu^{a2}}[\epsilon_{\theta 1}^{*a} + \nu^a(\epsilon_{z1}^{*a})] + A_{\theta 2}^a \frac{E^a}{1-\nu^{a2}}[\epsilon_{\theta 2}^{*a} + \nu^a(\epsilon_{z2}^{*a})] + A_{\theta 2}^b \frac{E^b}{1-\nu^{b2}}[\epsilon_{\theta 2}^{*b} + \nu^b(\epsilon_{z2}^{*b})] + A_{\theta 3}^b \frac{E^b}{1-\nu^{b2}}[\epsilon_{\theta 3}^{*b} + \nu^b(\epsilon_{z3}^{*b})] + A_{\theta 3}^c \frac{E^c}{1-\nu^{c2}}[\epsilon_{\theta 3}^{*c} + \nu^c(\epsilon_{z3}^{*c})] + A_{\theta 4}^c \frac{E^c}{1-\nu^{c2}}[\epsilon_{\theta 4}^{*c} + \nu^c(\epsilon_{z4}^{*c})].$$

The net strains are determined using Cramer's rule

$$\epsilon_\theta^{\text{net}} = \frac{C_1B_2 - C_2B_1}{A_1B_2 - A_2B_1} \tag{14}$$

$$\epsilon_z^{\text{net}} = \frac{A_1C_2 - A_2C_1}{A_1B_2 - A_2B_1}. \tag{15}$$

The axial and circumferential stresses are computed using Eqs. (4) and (5). The elastic strain is computed by subtracting the thermal, creep, and transformation strains from the net strain. The radial displacement is computed from the net circumferential strain,

$$u_1 = \epsilon_\theta^{\text{net}} R_1. \tag{16}$$

After time is incremented, the new values for temperature and displacement are determined from the temperature-displacement history. Then, the thermal, transformation, and creep strains occurring during the time increment, Δt, are computed. The thermal strain increment, $\Delta\epsilon_i^{th}$, is computed at the radial interface of each ring,

$$\Delta\epsilon_i^{th} = \alpha_i(\Delta T) \tag{17}$$

where α_i is the coefficient of thermal expansion ($\alpha_\theta = \alpha_r = \alpha_z = 1.6\times10^{-5}$ 1/°C).

The transformation strain increment is determined from the kinetic model of thermal-induced transformation described in Neu and Sehitoglu (1993),

$$\Delta\epsilon_i^{tt} = \eta_i C \exp\left(-\frac{Q_o - \beta\sigma_H}{RT}\right)\left\{1 - \exp\left[\tau\left(\frac{\Delta V^{tt}}{V} - \frac{\Delta V^{tt}}{V_{\max}}\right)\right]\right\}\Delta t \tag{18}$$

where

- η_i is the anisotropy factor.
- $C\exp\left(-\frac{Q_o - \beta\sigma_H}{RT}\right)$ is the transformation rate, which is dependent on the temperature, T, activation energy for thermal-induced transformation, Q_o, and hydrostatic stress, σ_H. R is the gas constant and C, β are material constants.
- $\left\{1 - \exp\left[\tau\left(\frac{\Delta V^{tt}}{V} - \frac{\Delta V^{tt}}{V_{\max}}\right)\right]\right\}$ describes the decreasing amount of available retained austenite as transformation occurs. $\Delta V^{tt}/V$ is the current volumetric transformation strain, $\Delta V^{tt}/V_{\max}$ is the maximum possible transformation strain, and τ is a material constant representing the decrease in transformation rate as retained austenite diminishes. When $\Delta V^{tt}/V_{\max}$ is reached, no further thermal-induced transformation occurs.

The full description of the kinetic model for low-temperature creep is described in Neu and Sehitoglu (1992). Briefly, the creep strain increments are computed from the differential equation describing logarithmic creep (Schoeck, 1961),

$$\Delta\epsilon_i^{cr} = \alpha_i'\gamma\exp\left(\frac{-(\epsilon_i^{cr} - \epsilon_{oi}^{cr})}{\alpha_i'}\right)\Delta t \tag{19}$$

where the creep coefficient, α_i', is dependent on temperature, T, and deviatoric stress, S_i, which is normalized by the equivalent stress, σ_e,

$$\alpha_i' = \alpha_o RT\frac{S_i}{\sigma_e} \tag{20}$$

and the creep time factor, γ, is dependent on temperature, activation energy for creep, Q_c, and equivalent stress

$$\gamma = \gamma_o\exp\left(\frac{-(Q_c - h\sigma_e)}{RT}\right). \tag{21}$$

α_o, γ_o, and h are material constants.

Results

Effect of Temperature on Cone Bore Growth. To illustrate the capabilities of the model, a number of simulations were run. The first series of simulations examined the effect of the material, temperature, and interference fit on the bore growth. In these simulations, the cone was attached to the axle journal with a specified interference fit. The cone was then held at a constant temperature for a long period of time (up to a period greater than ten years).

The dimensions of the bearing cone used in the present analysis came from a 6 1/2×12″ (Class F) railroad bearing. The case thickness was 2.03 mm (0.080 in.). The dimensions of the rings are given in Fig. 2. First, a cone with a case containing 35 percent retained austenite (A_{ret}) was considered. The smallest allowable interference fit, 0.051 mm (0.002 in.), was imposed. The results of this simulation are shown in Fig. 4. Both the bore growth and circumferential stress are shown for various temperatures. At 140°C the cone became loose after 140 hours. When the cone became loose, the circumferential stress became zero and the bore growth reached the value of the initial interference fit. At 120°C the cone came loose after 1000 hours. At lower temperatures the cone did not become loose within the 1000 hours of the simulation, but there was some bore growth at both 100°C and 80°C. Since experiments indicated that both thermal-induced transformation of retained austenite to bainite and creep mechanisms operated at these temperatures in the $A_{\text{ret}} = 35$ percent steel, both these mechanisms contributed to the bore growth (Neu, 1991).

To examine the effect of typical operating temperatures (40°–100°C) of bearings, a longer time span was considered. The results of these simulations are shown in Fig. 5. Again, an initial interference fit of 0.051 mm (0.002 in.) was used. The model indicated that a cone held at 100°C will come loose after one year and at 80°C will come loose after six years. Even at 60°C some bore growth occurred during the ten-year period. Simulations with just creep strains and transformation strains indicated that most of the bore growth at these lower temperatures was due primarily to thermal-induced transformation of retained austenite (Neu, 1991). Since the model did not take into account the diminishing amount of retained austenite in the case of the cone with distance from the surface, it probably overpredicted the influence of transformation at these temperatures. A smaller case thickness could be used to take this into account.

Downloaded 03 May 2010 to 171.66.16.20. Redistribution subject to ASME license or copyright; see http://www.asme.org/terms/Terms_Use.cfm

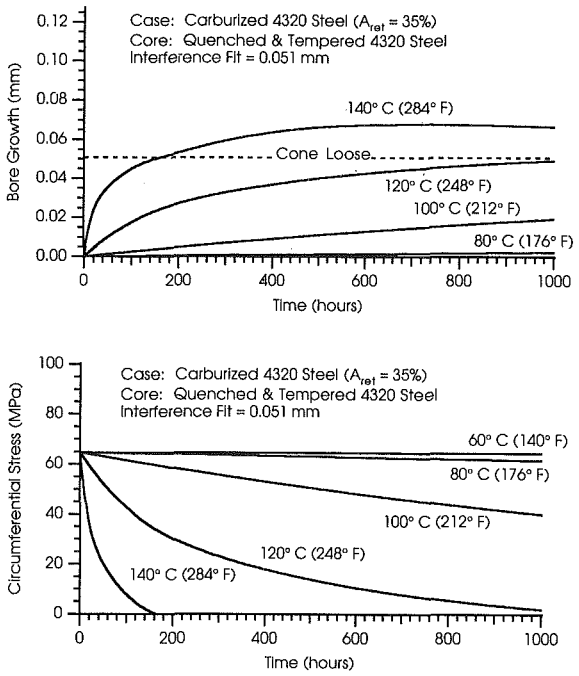


Fig. 4 Bore growth and circumferential stress when case contains 35 percent retained austenite, interference fit is 0.051 mm (0.002 in.), and temperature ranges from 80°C to 140°C

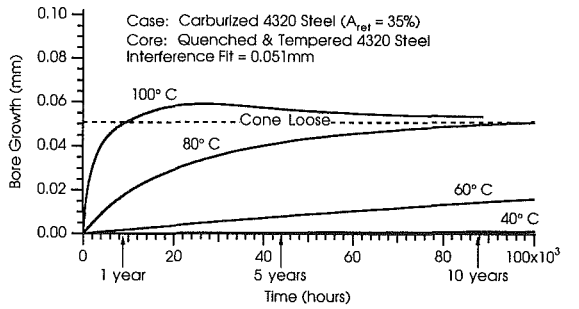


Fig. 5 Bore growth when case contains 35 percent retained austenite, interference fit is 0.051 mm (0.002 in.), and temperature ranges from 40°C to 100°C

Effect of Interference Fit on Cone Bore Growth. Using the material properties of the $A_{ret} = 35$ percent steel to represent the case material, a simulation with the larger interference fit of 0.102 mm (0.004 in.) is shown in Fig. 6, which can be compared to the 0.051 mm (0.002 in.) fit simulation in Fig. 5. Increasing the interference fit increased both the circumferential stress in the cone and the friction at the interface (Neu, 1991), reducing the likelihood that the cone would slip with respect to the axle journal. However, increasing the interference fit also increased the amount of bore growth. This was primarily attributed to the greater stress relaxation rate of the higher circumferential stress. Although the bore growth was greater, the cone did not come loose during the ten-year period of the simulation at the higher interference fit. Increasing the interference fit further continued to show these trends (Neu, 1991).

Effect of Service and Recondition Treatment on Cone Bore Growth. Another series of simulations examined both the effect of service temperatures over a one-month (720-hour) period and then a stress-relieving recondition treatment at 177°C for four hours with the cone off the axle journal. An actual bearing is at service temperature only a portion of the time, so a one-month period in the model represented a longer

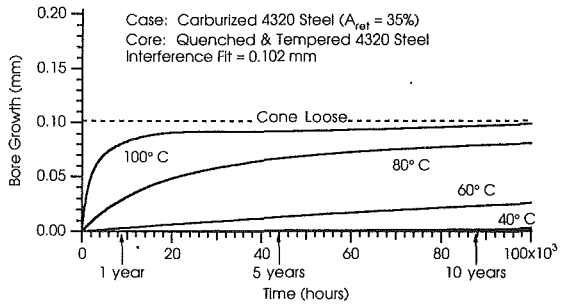


Fig. 6 Bore growth when case contains 35 percent retained austenite, interference fit is 0.102 mm (0.004 in.), and temperature ranges from 40°C to 100°C

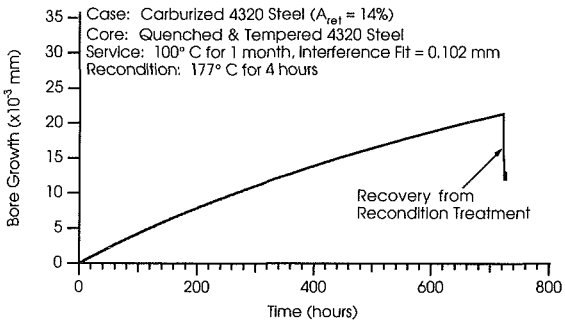


Fig. 7 Bore growth during simulated service (100°C for one-month, interference fit = 0.102 mm (0.004 in.)) and recondition treatment (177°C for four hours) when case contains 14 percent retained austenite

actual period of service. One of these simulations with the $A_{ret} = 14$ percent steel properties representing the case material is shown in Fig. 7. The service temperature was 100°C and the interference fit was 0.102 mm (0.004 in.). The bore growth after one month was over 0.020 mm (0.0008 in.). After the service period, the cone was removed (circumferential stress set to zero), and the recondition treatment was applied. During the recondition treatment, nearly half of this bore growth was recovered. Recovery was attributed to the relaxation of the residual stresses that developed during service. When the bore size no longer changed during the stress-relieving recondition treatment, the residual stresses have been completely relaxed. Most of the recovery occurred in the first 15 minutes of the recondition treatment. However, the model did not take into account the time it would take the cone to reach the reconditioning temperature.

The one-month simulation was also conducted with the $A_{ret} = 35$ percent steel properties representing the case material (Fig. 8). The amount of bore growth during service was about the same whether the $A_{ret} = 14$ percent or 35 percent steel properties represented the case. However, the model indicated that the recondition treatment would cause the bore diameter to increase, which contradicted what occurs when actual cones are reconditioned. The bore growth predicted by the model during the recondition treatment was attributed to the volume increase associated with thermal-induced transformation of retained austenite. If the transformation mechanism was suppressed in the $A_{ret} = 35$ percent steel, a reduction of the cone bore diameter was predicted during the recondition treatment (Neu, 1991). However, this recovery was less than that found when the $A_{ret} = 14$ percent steel represented the case.

At temperatures just above the recondition temperature (about 200°C), growth of the carbides would occur, resulting in a small volume decrease (Neu, 1991). The present model did not account for carbide growth. In addition, the stress-induced transformation of retained austenite to martensite was

Downloaded 03 May 2010 to 171.66.16.20. Redistribution subject to ASME license or copyright; see http://www.asme.org/terms/Terms_Use.cfm

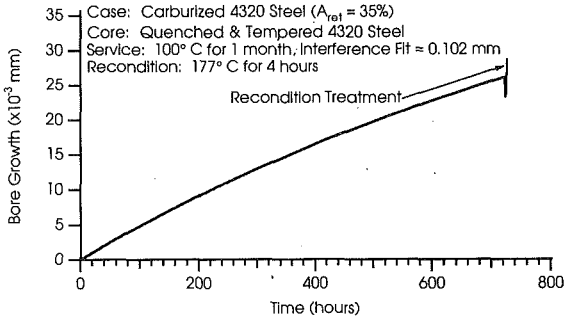


Fig. 8 Bore growth during simulated service (100°C for one-month, interference fit = 0.102 mm (0.004 in.)) and recondition treatment (177°C for four hours) when case contains 35 percent retained austenite

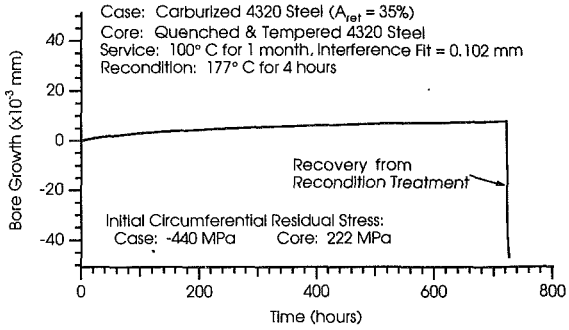


Fig. 9 Bore growth during simulated service (100°C for one-month, interference fit = 0.102 mm (0.004 in.)) and recondition treatment (177°C for four hours) when case contains 35 percent retained austenite and the initial residual stress in the case is −440 MPa

not modeled with a kinetic equation, although the stress-induced transformation strains could be incorporated if these are known a priori. Stress-induced transformation could occur due to the high contact stresses in the case material at the roller/cone contact. However, experiments did not show any clear evidence of time-dependent stress or strain-induced transformation. If stress-induced transformation occurred during service, the residual stresses would increase under the raceway. Consequently, there is a potential for a greater decrease in bore diameter during the stress-relieving recondition treatment from the relaxation of these residual stresses by low-temperature creep.

Effect of Residual Stresses From Case Carburizing. Up to this point, a new cone was assumed to be free from any initial residual stress. However, residual stresses are intentionally manufactured into the cone by the case-carburizing and subsequent hardening treatment to improve wear and fatigue resistance. Besides increasing the hardness of the surface, case carburizing also generates a compressive stress at the surface balanced by tensile stress in the core. An initial circumferential residual stress may be incorporated in the model. To demonstrate this effect on cone bore growth and reconditioning, the initial residual stress in the case was assumed to be −440 MPa, and to maintain equilibrium, the residual stress in the core was 222 MPa. The result of a simulated one-month service at 100°C with interference fit of 0.102 mm (0.004 in.) using the $A_{ret} = 35$ percent steel properties for the case is given in Fig. 9. The bore growth during service was less than that found in the simulation when no initial stresses were imposed (Fig. 8). Moreover, the reduction in bore diameter during the recondition treatment was 0.025 mm (0.001 in.) greater than the initial bore diameter before service. Recall that an increase in bore diameter was predicted when no initial stresses were imposed (Fig. 8). These trends were also predicted when either the $A_{ret} = 14$ percent steel properties represented the case or the service temperature was lower (80°C).

The circumferential stresses in a radial traverse of the cone at five significant events during service (100°C for one month with interference fit of 0.102 mm (0.004 in.)) and the recondition treatment (177°C for four hours) are shown in Fig. 10. These were the same conditions as in Fig. 9. At event A, the initial stress in the case was −440 MPa and in the core was 222 MPa. The tensile circumferential stress from the interference fit was superimposed with the initial residual stresses, resulting with the circumferential stress state shown at event B. After service, these stresses had relaxed to about 70 percent of their initial level (event C). Then the cone was removed from the journal (event D). After the recondition treatment (event E), the remaining stresses had further relaxed to about 25 percent of their initial level. Since there was a larger stress differential at event D when there were initial case-carburizing residual stresses compared to when the cone is initially stress-free, a greater amount of stress relaxation was possible resulting in a greater reduction in bore diameter (Neu, 1991).

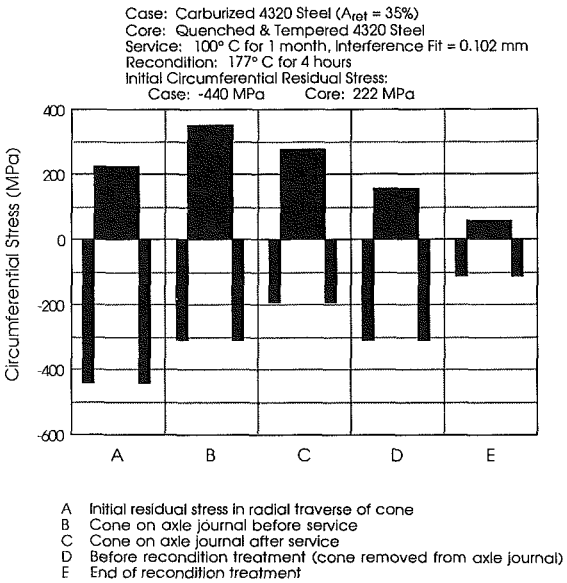


Fig. 10 Circumferential stress along a radial traverse in the cone at various events during service and reconditioning

Since initial residual stresses in the cone tended to relax during service and to a greater extent during the recondition treatment, reconditioned cones have lost some of the desired compressive residual stress in the case. Consequently, the fatigue life of a reconditioned cone may be lower than that of a new cone.

Conclusions

Both low-temperature creep and thermal-induced transformation of retained austenite to bainite with the accompanying volume expansion could contribute to bore growth as shown by the model. The creep mechanism manifested itself by the reduction of the tensile circumferential interference fit stress. The creep mechanism operated in both the case and core materials. However, since retained austenite existed only in the case, thermal-induced transformation was limited to the case. Nevertheless, the anisotropic volume expansion associated with the transformation was shown to contribute to bore growth. Important conclusions from the simulations to the three-ring model include the following:

1 Bore growth increased with temperature, since both creep and transformation kinetics increased with temperature.

2 Increasing the initial interference fit tended to increase

Downloaded 03 May 2010 to 171.66.16.20. Redistribution subject to ASME license or copyright; see http://www.asme.org/terms/Terms_Use.cfm

the amount of cone bore growth. The stress relaxation rate was greater due to the larger initial circumferential stress.

3 The model indicated that relaxation of residual stresses during the recondition treatment by a low-temperature creep mechanism was a probable explanation for the reduction of the cone bore.

4 Initial residual stresses from case carburizing were found to play an important role in both bore growth and recovery. These stresses tended to relax during service and even more during the recondition treatment. As a result, even though the bore diameter has been reduced, reconditioned cones have lost some of the desired compressive residual stress near the raceway surface, and fatigue life of the cone may suffer.

Acknowledgments

This work was supported by Brenco, Inc., Petersburg, VA, and the Association of American Railroads (AAR), Technical Center, Chicago, IL. The cooperation of Mr. Robert Lawrence and Mr. Arun Dhir of Brenco, Inc., and Dr. Dan Stone, Dr. Keith Hawthorne, and Mr. Michael Fec of AAR is appreciated. The heat treating of the specimens performed by Brenco personnel is greatly appreciated. Discussions with Dr. Gerald Moyar were insightful and highly valuable. Also, the assistance of Mr. Sean Murphy is acknowledged.

References

Fec, M. C., and Moyar, G. J., 1988, "Railroad Journal Roller Bearing Failure and Detection Past, Present and Future," *Railroad Journal Roller Bearing Failure and Detection*, RTD-Vol. 1, G. J. Moyar and S. K. Punwani, eds., ASME, New York, pp. 3–17.

Gleeson, J., 1989, "Freight Bearing Cone Bore Profile Measurement and Cap Screw Tension Measurement Surveys," Final Report to Dept. of Transportation, Trans. Syst. Center Contract No. DTRS-57-83-C-00090, Battelle, Columbus Div.

Moyar, G. J., Fec, M. C., and Lawrence, R. V., 1988, "A Review of Bearing Failure Research," *9th International Wheelset Congress*, pp. 1–10.

Neu, R. W., and Sehitoglu, H., 1990, "Determination of Cone Bore Growth Due to Microstructural Changes," ASME *Journal of Tribology*, Vol. 112, pp. 433–441.

Neu, R. W., 1991, "An Investigation into the Mechanisms of Cone Bore Growth in Railroad Bearings," Ph.D. Thesis, University of Illinois, Urbana, IL.

Neu, R. W., and Sehitoglu, H., 1992, "Low-Temperature Creep of a Carburized Steel," *Metallurgical Transactions A*, Vol. 23A, pp. 2619–2624.

Neu, R. W., and Sehitoglu, H., 1993, "Thermal-induced Transformation of Retained Austenite in the Simulated Case of a Carburized Steel," ASME *Journal of Engineering Materials and Technology*, Vol. 115, pp. 83–88.

Orringer, O., 1988, "Grooving Failure in Railroad Axle and Bearing Systems," 9th International Wheelset Congress, Montreal, Canada, pp. 4-4-1–4-4-11.

Schoeck, G., 1961, "Theories of Creep," *Mechanical Behavior of Materials at Elevated Temperatures*, John E. Dorn, ed., McGraw-Hill, New York, pp. 79–107.

Voskamp, A. P., and Schalk, B., 1982, "Ring Growth in Case Hardened Railway Journal Roller Bearings," *Proceedings 2nd International Heavy Haul Railway Conf.*, pp. 1–8.

Downloaded 03 May 2010 to 171.66.16.20. Redistribution subject to ASME license or copyright; see http://www.asme.org/terms/Terms_Use.cfm

Propagation of Surface Waves Across an Anisotropic Layer

E. N. Its

J. S. Lee
Mem. ASME.

Department of Civil and Environmental Engineering, Clarkson University, Potsdam, NY 13699-5710

Propagation of elastic surface waves across a thin anisotropic interface layer between two vertically inhomogeneous isotropic quarter-spaces is considered. The relationship between the surface wave fields at the opposite sides of the layer is obtained in the form of matrix differential operators. Based on the Green's function technique, an analytical method is developed to calculate reflection and transmission coefficients of Rayleigh waves at the layer. The reflection and transmission coefficients of Rayleigh waves at the interface layer are calculated as a function of the angle of incidence for various models of layers with hexagonal symmetry and results are discussed in some detail. Several isotropic layers of low or high velocity materials are also considered to examine the trade-off between anisotropy and inhomogeneity of the interface layer.

1 Introduction

With the increasing use of composite materials in many engineering applications and development of associated nondestructive evaluation techniques (Mase and Johnson, 1987; Bouden and Datta, 1990; Rose et al., 1990; Rokhlin and Wang, 1992; Lee and Its, 1992) and the increasing evidence of seismic anisotropy of geologic materials due to stress-induced cracks, or preferentially oriented pores and impurities (Anderson et al., 1974; Garbin and Knopoff, 1975; Hudson, 1982; Crampin, 1981, 1984; Fraser, 1990), propagation of elastic waves in inhomogeneous and/or anisotropic media has received considerable attention in the last two decades. In particular, problems of wave propagation in strongly inhomogeneous or discontinuous anisotropic media have been the topic of intensive research in recent years for possible application in seismology and nondestructive characterization of composite materials. The reflection and transmission of body waves at interfaces of similar or dissimilar anisotropic media have been studied by many investigators (e.g., Keith and Crampin, 1977; Banic, 1987; Roklin et al., 1986). Similar problems for surface waves were recently investigated by Its and Lee (1993b).

In the study of the reflection and transmission of elastic waves across a material discontinuity, the interface or interphase condition is of interest. An infinitely thin material interface is often used to describe a narrow fault zone, junction zone, or transition zone between dissimilar blocks when the elastic property of the zone is close to the property of the adjoining blocks or the bulk material. However, cracking and fracturing of materials, or the existence of various intrusions in the zone, may lead to a significant change of its elastic property, thereby rendering the infinitely thin interface not an adequate model of the zone. In this case, a thin layer with finite thickness whose elastic property is significantly different from that of the bulk material may be a more realistic model of the zone. The thin layer interface model can also be used to describe imperfect interfaces such as cracked welding, poorly bonded layers, or material interphases.

The problem involving a thin interfacial layer has received a considerable attention in recent years. Datta et al. (1988) studied the scattering by spherical inclusions surrounded by thin elastic layers. The tractions were assumed to be continuous across the layer, whereas displacements satisfy jump conditions that are linear in the thickness of the layer. Effects of thin interface layers on scattering of elastic waves by other shapes of inclusions were studied by Paskaramoorthy et al. (1988) by using a combination of the finite element method for the finite zone (including the scatterer) and the analytical approach for the exterior region, and later by Olsson et al. (1990) using the similar hybrid approach. Datta et al. (1990) studied the effect of interface layers on the scattering of waves by inclusions by including the inertial and curvature effects. They showed that these two effects have a strong influence on the scattering behavior. In these studies, the thin interface layers were described by equivalent boundary conditions which are approximate to the order of h, the thickness of the layer. Another important work relevant to the present method is the one by Rohklin and Huang (1992) where they introduced a set of boundary conditions to model a thin anisotropic layer between two generally anisotropic solids. As a generalization of previous works (Rokhlin et al., 1986; Rohklin and Wang, 1992) the boundary conditions are represented by a transfer matrix, which relates the stresses and displacements on each side of the interface layer. The transfer matrix, also approximate to the first order in h, was obtained as an asymptotic representation of the three-dimensional solution for a thin orthotropic

Contributed by the Applied Mechanics Division of The American Society of Mechanical Engineers for publication in the ASME Journal of Applied Mechanics.

Discussion on this paper should be addressed to the Technical Editor, Professor Lewis T. Wheeler, Department of Mechanical Engineering, University of Houston, Houston, TX 77204-4792, and will be accepted until four months after final publication of the paper itself in the ASME Journal of Applied Mechanics.

Manuscript received by the ASME Applied Mechanics Division, Aug. 24, 1992; final revision, June 23, 1993. Associate Technical Editor: S. K. Datta.

Copyright © 1994 by ASME
Downloaded 03 May 2010 to 171.66.16.20. Redistribution subject to ASME license or copyright; see http://www.asme.org/terms/Terms_Use.cfm

layer of arbitrary orientation between two solids. A review of recent advances on the subject was given by Rokhlin (1992). It should be noted, however, all of the aforementioned studies are limited to either isotropic materials or bulk waves.

Propagation of surface waves across lateral inhomogeneities, such as thin vertical layers in vertically homogeneous or inhomogeneous media, has received relatively little attention compared to its bulk wave counterpart. Propagation of Rayleigh waves across a vertical interface, normal to a free surface between two identical or different homogeneous quarter-planes, was studied by Li and Achenbach (1991a). The interface was represented by a layer of extensional and shear springs, and the boundary element method was used to solve the resulting system of singular integral equations. Later, they used the same approach to solve a similar problem involving a material interface which contains a discrete array of disbond (Li and Achenbach, 1991b). In studying the propagation of surface waves across a thin vertical layer between vertically heterogeneous isotropic quarter-spaces, Its (1991) introduces boundary conditions using the matrix-operator approach (both first and second-order approximation with respect to h) and developed a method based on the Green's function technique to calculate the reflection and transmission coefficients of surface waves at the interfacial layer. Accuracy of the matrix-operator approach was verified by ultrasonic experiments as well as by finite element modelings. Screening of Rayleigh waves by vertically layered thin wave barriers has been investigated by Its and Lee (1992, 1993a), where the nonwelded contact conditions were also introduced to describe the multilayered composite wave barriers. It should be noted, however, that all aforementioned studies of surface waves are limited to isotropic materials.

The primary objective of this work is to study the propagation of surface wave propagation in anisotropic media with strong lateral inhomogeneity by adopting the Green's function method reported in Its (1991). The validity of the method for predicting reliable reflection and transmission coefficients of surface waves at strong lateral inhomogeneities, such as material interfaces or thin isotropic layers between isotropic media, has been established by comparing results with those from the ultrasonic experiments, numerical (finite element) simulations, and other analytical techniques (Its and Yanovskaya, 1985; Its et al., 1989; Levshin et al., 1989; Biagi et al., 1990; Its, 1991). Therefore, in this work, principles of the method for isotropic media are adopted and further generalized to study the propagation of Rayleigh and Love waves in laterally inhomogeneous anisotropic media. The problem which we consider in this paper is a thin vertical interfacial layer of an anisotropic material between two vertically heterogeneous isotropic quarter-spaces. Based on the Green's function technique, an analytical approach for the estimation of the reflection and transmission coefficients of surface waves at the layer is presented. Matrix conditions involving differential operators are constructed to relate the surface wave fields at each side of the layer. A system of equations is then derived to determine the reflection and transmission coefficients of the surface waves at the interface layer. The reflection and transmission coefficients of Rayleigh waves at a transversely isotropic layer with the axis of symmetry parallel to the x-axis are presented as a function of the angle of incidence, and results are compared to those of isotropic layers. The trade-off between anisotropy and inhomogeneity of the interface is discussed in some detail.

2 The Method

Let the γth normal mode of a stationary Rayleigh or Love wave of frequency ω be incident with angle ϕ_γ to a vertical layer inserted between two quarter-spaces denoted by indices 1 and 2 (Fig. 1). All normal modes (corresponding to ω) of

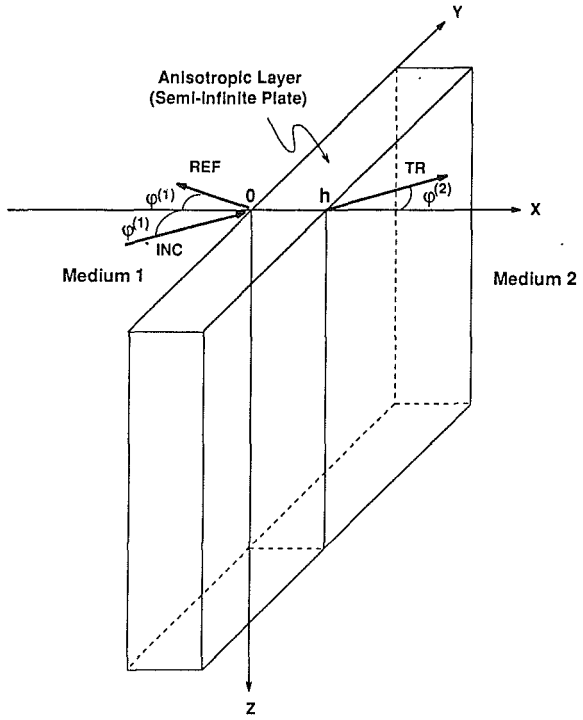


Fig. 1 Thin layer between two quarter-spaces

reflected and transmitted Rayleigh and Love waves, as well as body waves, arise due to the lateral inhomogeneity. Elastic parameters of the two quarter-spaces and the layer are denoted by $v_s^{(1)}(z)$, $v_p^{(1)}(z)$, $\rho^{(1)}(z)$, $v_s^{(2)}(z)$, $v_p^{(2)}(z)$, $\rho^{(2)}(z)$, and $C_{ij}(z)$, $\rho(z)$, respectively. For the most general case of anisotropy of the layer the elastic tensor, C_{ij} $(i, j = 1, 6)$ is determined by 21 independent elastic constants. The displacement and stress vectors of the ith medium, $\mathbf{U}^{(i)}$ and $\mathbf{T}_x^{(i)}$, can be written as follows:

$$\mathbf{U}^{(1)}(x, y, z) = \mathbf{V}_\gamma^{(1)}(z) \exp[i(\omega t - s_\gamma^{(1)} x \cos\phi_\gamma^{(1)} - s_\gamma^{(1)} y \sin\phi_\gamma^{(1)})] + \sum_{\alpha=1}^{A} a_\alpha \tilde{\mathbf{V}}_\alpha^{(1)}(z) \exp[i(\omega t + s_\alpha^{(1)} x \cos\phi_\alpha^{(1)} - s_\alpha^{(1)} y \sin\phi_\alpha^{(1)})] + \mathbf{U}_b^{(1)}$$

$$\mathbf{U}^{(2)}(x, y, z) = \sum_{\beta=1}^{B} b_\beta \mathbf{V}_\beta^{(2)}(z) \exp[i(\omega t - s_\beta^{(2)} x \cos\phi_\beta^{(2)} - s_\beta^{(2)} y \sin\phi_\beta^{(2)})] + \mathbf{U}_b^{(2)}$$

$$\mathbf{T}_x^{(1)}(x, y, z) = \mathbf{P}_\gamma^{(1)}(z) \exp[i(\omega t - s_\gamma^{(1)} x \cos\phi_\gamma^{(1)} - s_\gamma^{(1)} y \sin\phi_\gamma^{(1)})] + \sum_{\alpha=1}^{A} a_\alpha \tilde{\mathbf{P}}_\alpha^{(1)}(z) \exp[i(\omega t + s_\alpha^{(1)} x \cos\phi_\alpha^{(1)} - s_\alpha^{(1)} y \sin\phi_\alpha^{(1)})] + \mathbf{T}_b^{(1)}$$

$$\mathbf{T}_x^{(2)}(x, y, z) = \sum_{\beta=1}^{B} b_\beta \mathbf{P}^{(2)}\beta(z) \exp[i(\omega t + s_\beta^{(2)} x \cos\phi_\beta^{(2)} - s_\beta^{(2)} y \sin\phi_\beta^{(2)})] \mathbf{T}_b^{(2)}, \quad (1)$$

where a_α and b_β are the unknown reflection and transmission coefficients of surface waves; $\mathbf{U}_b$ and $\mathbf{T}_b$ are displacement and stress vectors of the body waves arising in the vicinity of layer boundaries; $s_\alpha^{(i)}$ and $\mathbf{V}_\alpha^{(i)}$ are the αth eigenvalue and eigenfunction, respectively, for the ith medium. The vector $\mathbf{V}^{(i)}$ has the following form:

$$V_x^{(i)} = \mp i W_r^{(i)} \cos\phi^{(i)}, \quad V_y^{(i)} = -i W_r^{(i)} \sin\phi^{(i)}, \quad V_z^{(i)} = W_z^{(i)}$$

for Rayleigh waves and

$$V_x^{(i)} = -i W_\theta^{(i)} \sin\phi^{(i)}, \quad V_y^{(i)} = \mp i W_\theta^{(i)} \cos\phi^{(i)}, \quad V_z^{(i)} = 0$$

for Love waves, where W_r, W_θ, and W_z are the radial, circumferential, and axial components of the eigenvector for the

Downloaded 03 May 2010 to 171.66.16.20. Redistribution subject to ASME license or copyright; see http://www.asme.org/terms/Terms_Use.cfm

homogeneous boundary value problem formed by the equations of motion and the traction-free surface condition in a half-space with elastic parameters of the ith medium (Levshin et al., 1989). In the above equations, the upper sign corresponds to the incident and transmitted waves ($i=1, 2$) and the lower one to the reflected waves. $\mathbf{P}_\alpha^{(i)}$ is the stress vector corresponding to $\mathbf{V}_\alpha^{(i)}$. $\tilde{\mathbf{V}}_\alpha$ and $\tilde{\mathbf{P}}_\alpha$ denote the similarly defined quantities for the reflected waves. A and B are the number of normal modes (Rayleigh and Love) corresponding to the given ω. The eigenfunctions are assumed to be normalized according to

$$\int_0^\infty (\mathbf{P}_\beta^{(i)*}\mathbf{V}_\alpha^{(i)} - \mathbf{P}_\alpha^{(i)}\mathbf{V}_\beta^{(i)*})dz = \begin{cases} 0 & \text{if } \alpha=\beta \\ \pm 2i\cos\phi_\alpha^{(i)} & \text{if } \alpha=\beta. \end{cases} \quad (2)$$

The layer is assumed to be in rigid contact with the host media. Therefore, the displacements and stresses are continuous at vertical layer boundaries

$$\begin{aligned} \mathbf{U}^{(1)}(0, y, z) &= \mathbf{U}(0, y, z) \\ \mathbf{T}_x^{(1)}(0, y, z) &= \mathbf{T}_x(0, y, z) \\ \mathbf{U}^{(2)}(h, y, z) &= \mathbf{U}(h, y, z) \\ \mathbf{T}_x^{(2)}(h, y, z) &= \mathbf{T}_x(h, y, z) \end{aligned} \quad (3)$$

where $\mathbf{U}$ and $\mathbf{T}_x$ are the displacement and stress vectors within the layer.

If the thickness of the layer is large compared to the wavelength, the propagation through the layer may be approximately considered as the propagation of the surface wave through the two layer boundaries separately, and the far-field solutions for vertical interfaces between two laterally homogeneous quarter-spaces may be used to construct the solution. In the case of isotropic media the relevant analytical method was discussed by Alsop et al. (1974) and Its and Yanovskaya (1979, 1985). The latter approach was used, for example, to study the surface wave transmission through a transition zone between lithospheric blocks in the South Kamchatka region by modeling the transition zone with a set of thick vertical layers with elastic parameters lying between the parameters of the lithospheric blocks (Levshin et al., 1989). In the case of anisotropic media, the analytical approach recently proposed by Its and Lee (1993b) for a vertical interface between two anisotropic quarter-spaces may be utilized.

If the thickness of the layer is small compared to the wavelength, however, the aforementioned approaches are no longer valid and other approaches must be found. Several approaches have been reported where the layer is replaced by equivalent boundary conditions (Li and Achenbach, 1991a; Its, 1991; Rokhlin, 1992). In the present paper we adopt the matrix operator approach of Its (1991) and generalize it to the case of anisotropic layer. To construct the equivalent boundary conditions, the displacement and stress fields within the layer $\mathbf{U}(x, y, z)$ and $\mathbf{T}_x(x, y, z)$ are expanded in the Taylor series with respect to x across the layer. Taking into account the equations of motion, Hooke's law, and boundary conditions of the layer, the displacement and stress fields at boundaries $x=0$ and $x=h$ (Fig. 1) can be related by the following matrix condition:

$$\begin{aligned} \mathbf{U}^{(2)}(h, y, z) &= \mathbf{Q}^{(U)}\mathbf{R}^{(1)}(0, y, z) \\ \mathbf{T}_x^{(2)}(h, y, z) &= \mathbf{Q}^{(T)}\mathbf{R}^{(1)}(0, y, z) \\ \mathbf{U}^{(1)}(0, y, z) &= \overline{\mathbf{Q}}^{(U)}\mathbf{R}^{(2)}(h, y, z) \\ \mathbf{T}_x^{(1)}(0, y, z) &= \overline{\mathbf{Q}}^{(T)}\mathbf{R}^{(2)}(h, y, z) \end{aligned} \quad (4)$$

where vectors $\mathbf{R}^{(1)}$ and $\mathbf{R}^{(2)}$ are defined by

$$\mathbf{R}^{(1)} = \begin{Bmatrix} \mathbf{U}^{(1)} \\ \mathbf{T}_x^{(1)} \end{Bmatrix} \quad \mathbf{R}^{(2)} = \begin{Bmatrix} \mathbf{U}^{(2)} \\ \mathbf{T}_x^{(2)} \end{Bmatrix}. \quad (5)$$

The matrix operators $\mathbf{Q}^{(U)}$, $\mathbf{Q}^{(T)}$, $\overline{\mathbf{Q}}^{(U)}$, and $\overline{\mathbf{Q}}^{(T)}$, which depend on the elastic parameters and the width of the layer as well as on the order of the Taylor series approximation, will be derived in the following section.

Once the expression for the fields of the reflected and transmitted surface waves at the interfaces $x=0$ and $x=h$ are determined from (4), the lth component of the displacement ($l=x, y, z$) at any point in medium 1 and 2 can be determined from the field at the interfaces according to the representation theorem:

$$\begin{aligned} U_l^{\text{ref}}(x_1, y_1, z_1) = \int_0^\infty \int_{-\infty}^\infty [\mathbf{G}_l^{(1)}(x_1, y_1, z_1, 0, y, z)\mathbf{T}_x^{ref} \\ - \mathbf{P}(\mathbf{G}_l^{(1)})\mathbf{U}^{\text{ref}}(0, y, z)]dydz \\ U_l^{tr}(x_2, y_2, z_2) = \int_0^\infty \int_{-\infty}^\infty [\mathbf{G}_l^{(1)}(x_2, y_2, z_2, h, y, z)\mathbf{T}_x^{tr} \\ - \mathbf{P}(\mathbf{G}_l^{(2)})\mathbf{U}^{tr}(h, y, z)]dydz \end{aligned} \quad (6)$$

where $\mathbf{G}_l^{(i)}$ and $\mathbf{P}(\mathbf{G}_l^{(i)})$ are the Green's function and the corresponding stress field for a half-space of the ith medium (Aki and Richards, 1980). Equations (1), (4), and (6) constitute the complete system for the determination of reflection and transmission coefficients of the surface waves.

3 Matrix Interlayer Conditions

We consider here a layer with hexagonal symmetry (transverse isotropy) with the axis of symmetry directed along the x-axis. The elasticity tensor $C_{ij}(z)$ in this case can be expressed as

$$C_{ij} = \begin{pmatrix} \lambda+2\mu-p & \lambda-l & \lambda-l & 0 & 0 & 0 \\ \lambda-l & \lambda+2\mu & \lambda & 0 & 0 & 0 \\ \lambda-l & \lambda & \lambda+2\mu & 0 & 0 & 0 \\ 0 & 0 & 0 & \mu & 0 & 0 \\ 0 & 0 & 0 & 0 & \mu-m & 0 \\ 0 & 0 & 0 & 0 & 0 & \mu-m \end{pmatrix} \quad (7)$$

where $\lambda(z), \mu(z), l(z), m(z), p(z)$ are the Lame's parameters and parameters of anisotropy. To obtain the matrix conditions (6), we use the Taylor series decomposition of $\mathbf{U}(x, y, z)$ and $\mathbf{T}(x, y, z)$ with respect to x. For a thin ($h/L \ll 1$ where L is the wavelength) layer, the displacement component U_x can be expanded in Taylor series as the following:

$$U_x(h, y, z) = U_x(0, y, z) + hU_{x,x}(0, y, z) + \frac{h^2}{2}U_{x,xx}(0, y, z) \quad (8)$$

where the quadratic term is also retained. Advantages of the second order approximation compared to the linear one were discussed in Its (1991). Using the Hooke's law for the T_{xx} component, the first derivative in (8) can be expressed as

$$U_{x,x} = \frac{T_{xx}}{\lambda+2\mu-p} - \frac{\lambda-l}{\lambda+2\mu-p}(U_{y,y} + U_{z,z}). \quad (9)$$

By using the equation of motion for the x component and Hooke's law, and taking into account that elastic parameters are laterally homogeneous throughout the layer, we can express the second derivative in (8) as the following:

$$\begin{aligned} U_{x,xx} = \frac{1}{\lambda+2\mu-p}\Bigg[-\rho\omega^2 U_x - \frac{\lambda-l}{\mu-m}\frac{\partial}{\partial y}[T_{xy} - (\mu-m)U_{x,y}] \\ - (\lambda-l)\frac{\partial}{\partial z}\left(\frac{T_{xz}}{\mu-m} - U_{x,z}\right) - T_{xy,y} - T_{xz,z}\Bigg]. \end{aligned} \quad (10)$$

Finally, combining (9) and (10) and using the boundary conditions (3), (8) can be written as

Downloaded 03 May 2010 to 171.66.16.20. Redistribution subject to ASME license or copyright; see http://www.asme.org/terms/Terms_Use.cfm

$$U_x^{(2)}(h, y, z) = U_x^{(1)}(0, y, z) + \frac{h}{\lambda+2\mu-p}[T_{xx}^{(1)} - (\lambda-l)(U_{y,y}^{(1)} + U_z^{(1)})] + \frac{h^2}{2(\lambda+2\mu-p)}\Big[-\rho\omega^2 U_x^{(1)} - T_{xy,y}^{(1)} - T_{xz,z} - \frac{\lambda+l}{\mu-m}\frac{\partial}{\partial y}(T_{xy}^{(1)} - (\mu-m)U_{x,y}^{(1)}) - (\lambda-l)\frac{\partial}{\partial z}\frac{1}{\mu-m}(T_{xz}^{(1)} - (\mu-m)U_{x,z}^{(1)})\Big] \quad (11)$$

Note that (11) in its form is valid for all points of the boundary except the line (0, y, 0). We adopt the assumption about the natural boundary conditions along the line of singularities (0, y, 0) and (h, y, 0) as discussed in Its (1991). Similar relationships can be obtained for other components of the displacement field and the stress field, and can be recast in the form of (4). Complete expressions for the matrix operators $\mathbf{Q}^{(U)}$ and $\mathbf{Q}^{(T)}$ are given in the Appendix. Operators $\overline{\mathbf{Q}}^{(U)}$ and $\overline{\mathbf{Q}}^{(T)}$ connecting the fields in the medium 1 and 2 can be obtained from $\mathbf{Q}^{(U)}$ and $\mathbf{Q}^{(T)}$ by replacing h with $-h$. The relationships (4) are to be used for the determination of the reflected and transmitted wave fields at the boundaries of the layer.

4 Reflection and Transmission Coefficients

Since the representation theorem (6) can be used for any single mode, we rewrite it for the αth mode of the reflected wave and the βth mode of the transmitted wave as

$$U_{\alpha l}^{\mathrm{ref}}(x_1, y_1, z_1) = \int_0^\infty\int_{-\infty}^\infty [\mathbf{T}(\mathbf{G}_{\alpha l}^{(1)})\mathbf{U}_\alpha^{\mathrm{ref}}(0, y, z) - \mathbf{T}_\alpha^{\mathrm{ref}}(0, y, z)\mathbf{G}_{\alpha l}^{(1)})(0, y, z; x_1, y_1, z_1)]dydz$$

$$U_{\beta l}^{tr}(x_2, y_2, z_2) = \int_0^\infty\int_{-\infty}^\infty [\mathbf{T}(\mathbf{G}_{\beta l}^{(2)})\mathbf{U}_\beta^{tr}(h, y, z) - \mathbf{T}_\beta^{tr}(h, y, z)\mathbf{G}_{\beta l}^{(2)}(h, y, z; x_2, y_2, z_2)]dydz \quad (12)$$

where $\mathbf{G}_{\alpha l}^{(1)}$ is the αth mode of the Green's function $\mathbf{G}_l^{(1)}$ in medium 1, and $\mathbf{G}_{\beta l}^{(2)}$ is the βth mode of the Green's function $\mathbf{G}_l^{(2)}$ in medium 2 (Aki and Richards, 1980).

Introducing vectors $\mathbf{r}_\gamma^{(1)}$, $\tilde{\mathbf{r}}_\alpha^{(1)}$, $\mathbf{r}_\beta^{(2)}$ as

$$\mathbf{r}_\gamma^{(1)} = \begin{pmatrix}\mathbf{V}_\gamma^{(1)}\\ \mathbf{P}_\gamma^{(1)}\end{pmatrix}, \quad \tilde{\mathbf{r}}_\alpha^{(1)} = \begin{pmatrix}\tilde{\mathbf{V}}_\alpha^{(1)}\\ \tilde{\mathbf{P}}_\alpha^{(1)}\end{pmatrix}, \quad \mathbf{r}_\beta^{(2)} = \begin{pmatrix}\tilde{\mathbf{V}}_\beta^{(2)}\\ \tilde{\mathbf{P}}_\beta^{(2)}\end{pmatrix}, \quad (13)$$

$\mathbf{R}^{(1)}$ and $\mathbf{R}^{(2)}$ may be rewritten as follows:

$$\mathbf{R}^{(1)}(x, y, z) = \mathbf{r}_\gamma^{(1)}(z)\exp[i(\omega t - s_\gamma^{(1)}x\cos\phi_\gamma^{(1)} - s_\gamma^{(1)}y\sin\phi_\gamma^{(1)})] + \sum_{\alpha=1}^{A} a_\alpha\tilde{\mathbf{r}}_\alpha^{(1)}(z)\exp[i(\omega t - s_\alpha^{(1)}x\cos\phi_\alpha^{(1)} - s_\alpha^{(1)}y\sin\phi_\alpha^{(1)})] + \mathbf{R}_b^{(1)}$$

$$\mathbf{R}^{(2)}(x, y, z) = \sum_{\beta=1}^{B} b_\beta\mathbf{r}_\beta^{(2)}(z)\exp[i(\omega t - s_\beta^{(2)}x\cos\phi_\beta^{(2)} - s_\beta^{(2)}y\sin\phi_\beta^{(2)})] + \mathbf{R}_b^{(2)}. \quad (14)$$

The relations (4) are used to define the stress and displacement fields at the boundaries:

$$\mathbf{U}_\alpha^{\mathrm{ref}}(0, y, z) = \sum_{\beta=1}^{B} b_\beta\overline{\mathbf{Q}}^{(U)}\mathbf{r}_\beta^{(2)}\exp[-is_\beta^{(2)}h\cos\phi_\beta^{(2)} - is_\beta^{(2)}y\sin\phi_\beta^{(2)}] + \overline{\mathbf{Q}}^{(U)}\mathbf{R}_b^{(2)} - \mathbf{V}_\gamma^{(1)}\exp[-is_\gamma^{(1)}y\sin\phi_\gamma^{(1)}[-\mathbf{U}_b^{(1)} - \sum_{\xi\neq\alpha} a_\xi\tilde{\mathbf{V}}_\xi^{(1)}\exp[-is_\xi^{(1)}y\sin\phi_\xi^{(1)}]$$

$$\mathbf{U}_\beta^{tr}(h, y, z) = \mathbf{Q}^{(U)}\mathbf{r}_\gamma^{(1)}\exp[-is_\gamma^{(1)}y\sin\phi_\gamma^{(1)}] + \sum_{\alpha=1}^{A} a_\alpha\mathbf{Q}^{(U)}\tilde{\mathbf{r}}_\alpha^{(1)}\exp[-is_\alpha^{(1)}y\sin\phi_\alpha^{(1)}] + \mathbf{Q}^{(U)}\mathbf{R}_b^{(1)} - \mathbf{U}_b^{(2)} - \sum_{\eta\neq\beta} b_\eta\mathbf{V}_\eta^{(2)}\exp[-is_\eta^{(2)}h\cos\phi_\eta^{(2)} - is_\eta^{(2)}y\sin\phi_\eta^{(2)}]. \quad (15)$$

The expression for stresses $\mathbf{T}_\alpha^{\mathrm{ref}}$ and $\mathbf{T}_\beta^{tr}$ can be similarly obtained by replacing the matrix operators $\mathbf{Q}^{(U)}$ and $\overline{\mathbf{Q}}^{(U)}$ by $\mathbf{Q}^{(T)}$ and $\overline{\mathbf{Q}}^{(T)}$. We now substitute (1) and (15) together with the far-field Green's function into (12) and integrate the resulting equations over y using the stationary phase method. Finally, assuming that the interaction between the surface and body waves is negligible (Levshin et al., 1989), the system of equations for the reflection and transmission coefficients can be obtained as the following:

$$a_\alpha\cos\phi_\alpha^{(1)} = -Z_{\alpha\gamma}^1 + \sum_{\beta=1}^{B} b_\beta\exp[-is_\beta^{(2)}h\cos\phi_\beta^{(2)}]Z_{\alpha\beta}^2 - \sum_{\xi\neq\alpha} a_\xi Z_{\alpha\xi}^3$$

$$b_\beta\cos\phi_\beta^{(2)} = \exp[-is_\beta^{(2)}h\cos\phi_\beta^{(2)}]Z_{\gamma\beta}^4 + \sum_{\alpha=1}^{A} a_\alpha Z_{\alpha\beta}^5 - \sum_{\eta\neq\beta} b_\eta Z_{\eta\beta}^6, \quad (16)$$

where the coupling coefficients Z^k ($k=1$ to 6) have the following form:

$$Z_{\alpha\gamma}^1 = \frac{1}{2i}\int_0^\infty (\mathbf{P}_\gamma^{(1)}\tilde{\mathbf{V}}_\alpha^{(1)} - \mathbf{V}_\gamma^{(1)}\tilde{\mathbf{P}}_\alpha^{(1)})dz$$

$$Z_{\alpha\beta}^2 = \frac{1}{2i}\int_0^\infty (\overline{\mathbf{K}}_{2\beta}^{(T)}\mathbf{r}_\beta^{(2)}\tilde{\mathbf{V}}_\alpha^{(1)} - (\overline{\mathbf{K}}_{2\beta}^{(U)}\mathbf{r}_\beta^{(2)}\tilde{\mathbf{P}}_\alpha^{(1)})dz$$

$$Z_{\alpha\xi}^3 = \frac{1}{2i}\int_0^\infty (\tilde{\mathbf{P}}_\xi^{(1)}\tilde{\mathbf{V}}_\alpha^{(1)} - \tilde{\mathbf{V}}_\xi^{(1)}\tilde{\mathbf{P}}_\alpha^{(1)})dz$$

$$Z_{\gamma\beta}^4 = \frac{1}{2i}\int_0^\infty (\mathbf{K}_{1\gamma}^{(T)}\mathbf{r}_\gamma^{(1)}\mathbf{V}_\beta^{(2)*} - \mathbf{K}_{1\gamma}^{(U)}\mathbf{r}_\gamma^{(1)}\mathbf{P}_\beta^{(2)*})dz$$

$$Z_{\alpha\beta}^5 = \frac{1}{2i}\int_0^\infty (\mathbf{K}_{1\alpha}^{(T)}\tilde{\mathbf{r}}_\alpha^{(1)}\mathbf{V}_\beta^{(2)*} - \mathbf{K}_{1\alpha}^{(U)}\tilde{\mathbf{r}}_\alpha^{(1)}\mathbf{P}_\beta^{(2)*})dz$$

$$Z_{\eta\beta}^6 = \frac{1}{2i}\int_0^\infty (\mathbf{P}_\eta^{(2)}\mathbf{V}_\beta^{(2)*} - \mathbf{V}_\eta^{(2)}\mathbf{P}_\beta^{(2)*})dz, \quad (17)$$

where the matrices $\mathbf{K}^{(T)}$, $K^{(U)}$, $\overline{\mathbf{K}}^{(T)}$, and $\overline{\mathbf{K}}^{(U)}$ may be obtained from the matrices $\mathbf{Q}^{(T)}$, $\mathbf{Q}^{(U)}$, $\overline{\mathbf{Q}}^{(U)}$, and $\overline{\mathbf{Q}}^{(T)}$, respectively, by replacing $\partial/\partial y$ with $-s_\alpha^{(i)}\sin\phi_\alpha^{(i)}$. The system of Eqs. (16) can be used to determine the reflection and transmission coefficients of surface waves at the thin anisotropic layer.

The method presented herein is a "far-field" method, as the far-field surface wave part (normal mode approximation) of the Green's function is used in the representation theorem (1). Therefore, the coefficients which can be obtained from (5) define the reflection and transmission of surface waves which are registered at a distance from the layer where the secondary waves can be considered as normal modes. Since the exact solution for the surface wave propagation across a vertical interface does not exist, the question whether the minimum distance from the layer for which the reflected and transmitted waves can be described by (5) may only be answered by physical ultrasonic experiments or numerical calculation. Previous experimental and numerical studies conducted for isotropic layers (Its et al., 1989) demonstrated that the distance must not be less than a wavelength. We postulate that the process of surface wave stabilization after an anisotropic disturbance has a similar physical character as the isotropic one. Therefore, the minimum distance at which the coefficients may be described by (5) has to be larger than the secondary wavelength.

Downloaded 03 May 2010 to 171.66.16.20. Redistribution subject to ASME license or copyright; see http://www.asme.org/terms/Terms_Use.cfm

Table 1 Elastic parameters for very thin layers (Example I)

Medium	$\rho(g/cm^3)$	$v_{sx}(km/sec)$	$v_{sy}(km/sec)$	$v_{px}(km/sec)$	$v_{py}(km/sec)$
Host medium	2.6	3.2	3.2	5.7	5.7
LI low velocity isotropic	1.8	2.0	2.0	3.6	3.6
LA1 low velocity weakly anisotropic	2.0	2.0	2.6	3.6	4.7
LA2 low velocity strongly anisotropic	2.2	2.0	3.2	3.6	5.7
HI high velocity isotropic	3.2	4.5	4.5	8.1	8.1
HA1 high velocity weakly anisotropic	2.8	3.9	3.2	7.0	5.7
HA2 high velocity strongly anisotropic	3.0	4.5	3.2	8.1	5.7

5 Results and Discussions

The technique developed in the previous sections has been used to study the reflection and transmission of Rayleigh waves at a thin anisotropic layer inserted between two isotropic quarter-spaces (or blocks). The primary goal of our present study was to examine the effects of anisotropy and inhomogeneity on the surface wave propagation. Trade-off between lateral inhomogeneity and azimuthal anisotropy, however, cannot be studied by a two-dimensional problem (normal incidence of Rayleigh or Love wave) which allows one to conduct one-wave experiments (i.e., no conversion of Rayleigh waves into Love waves at the inhomogeneity or vice versa) to study important characteristics of the wave motion. The only way to stay within the framework of a one-wave propagation problem and to avoid complications associated with the conversion of Rayleigh waves into Love waves in a three-dimensional model with azimuthal anisotropy is to consider homogeneous host media where only Rayleigh waves exist. Therefore, only homogeneous host materials have been considered in the present study. In this case, the eigenfunctions W_r and W_z have the following simple exponential form:

$$W_r = C\sqrt{\beta}\,(se^{-\alpha z} - \sqrt{\alpha\beta}e^{-\beta z})$$

$$W_z = C\sqrt{\alpha}\,(-\sqrt{\alpha\beta}e^{-\alpha z} + se^{-\beta z})$$

where s is the eigenvalue for Rayleigh wave, C is the normalization coefficient, and the exponents α and β are given by

$$\alpha = \sqrt{s^2 - \omega^2/v_p}, \quad \beta = \sqrt{s^2 - \omega^2/v_s}.$$

We considered transversely isotropic layer with the axis of symmetry parallel to the x-axis. This layer can be considered as a model of transition zones with ellipsoidal cracks or inclusions oriented along the interfaces (Anderson et al., 1974). In order to concentrate on the effect of anisotropy of the layer, the two quarter-spaces are assumed to be of the same material.

Example I: In this numerical example we considered very thin layers with $h/L_R = 0.05$ where L_R is the wavelength of the Rayleigh wave. In order to study the effect of anisotropy of the layer on the propagation of Rayleigh waves, we varied the ratios v_{sx}/v_{sy} and v_{px}/v_{py} of the layer to simulate the variation of the effective density and of the orientation of cracks (or inclusions). Three low-velocity layers were considered first: (1) LI: isotropic layer with $v_x/v_y = 1$; (2) LA1: anisotropic layer with $v_{sx}/v_{sy} = v_{px}/v_{py} = 0.77$ (referred as weakly anisotropic); and (3) LA2: anisotropic layer with $v_{sx}/v_{sy} = v_{px}/v_{py} = 0.62$ (referred as strongly anisotropic). Elastic parameters of the host medium and layers are given in Table 1. Figures 2(*a*) and 2(*b*) show the reflection and transmission coefficients of Rayleigh waves, respectively, as a function of the angle of incidence. In calculating the reflection and transmission coefficients we restricted the interval of the incident angle to the range between 0 and 70 deg, since the accuracy of the Green's function technique for this interval has been confirmed by ultrasonic experiments (Levshin et al., 1989; Biagi et al., 1990). As shown in Fig. 2(*a*), performances of the three layers are quite different. The reflection coefficient of the strongly anisotropic layer (LA2) demonstrates a weaker dependency on the angle of incidence compared to the other two cases (LI and LA1). The transmission coefficients of the three layers exhibit some different characteristic dependencies on the incident angle as shown in Fig. 2(*b*). According to the normalization condition (2), the square of the reflection and transmission coefficient is proportional to the energy of the reflected and transmitted Rayleigh wave, respectively. In the case of a vertical interface (infinitely thin layer), it was shown analytically that the reflection and transmission coefficients at a vertical interface calculated by the Green's function technique satisfy the energy conservation law and that the deficit of the energy of reflected and transmitted surface waves correspond to the energy of all other waves which may arise in the vicinity of the interface (Its and Yanovskaya, 1985). This statement cannot be proved analytically in the case of layers of finite width. However, in view of the fact that the second-order approximation of the layer provides a better agreement with the energy conservation law than the first-order approximation (Its, 1991), we assume that the energy leak at the layer may describe the energy of converted body and bodylike waves. Thus, it may be reasonable to assume that at least some part of the incident surface wave energy is converted into the energy of guided waves propa-

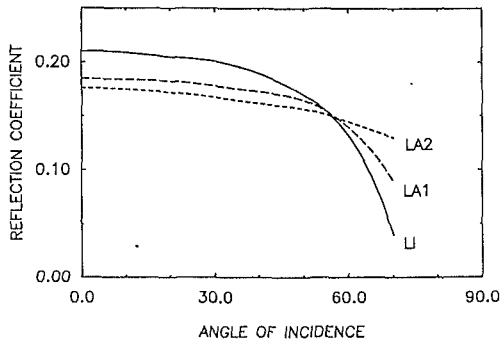


Fig. 2(*a*)

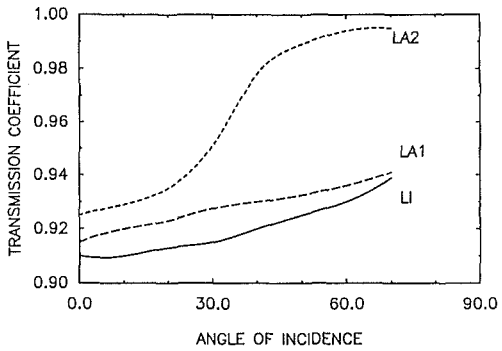


Fig. 2(*b*)

Fig. 2 Reflection and transmission coefficients at low-velocity layers with $h/L_R = 0.05$

Downloaded 03 May 2010 to 171.66.16.20. Redistribution subject to ASME license or copyright; see http://www.asme.org/terms/Terms_Use.cfm

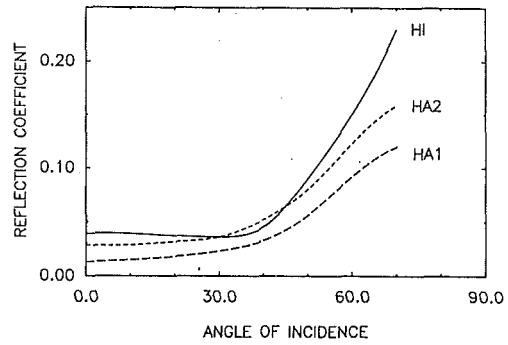


Fig. 3(*a*)

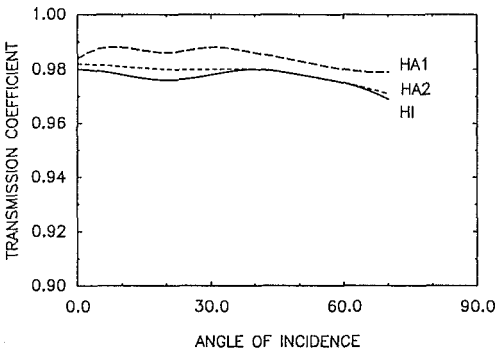


Fig. 3(*b*)

Fig. 3 Reflection and transmission coefficients at high-velocity layers with $h/L_R = 0.05$

gating inside the thin low-velocity layer considered in this example. This assumption can help to explain the difference between the transmission coefficients of the layers LI and LA1 and that of the layer LA2. Strictly speaking, the strongly anisotropic layer (LA2) is not a low-velocity layer with respect to v_y, so the characteristics and intensity of the guided wave in layer LA2 may differ significantly from those in the low velocity layers LI and LA1. Moreover, this suggests that the guided wave cease to exist if the velocity v_y increases further. We note that there is little lack of surface wave energy in the case of layer LA2 whose transmission coefficient approaches unity as the incident angle is increased.

Three high-velocity layers with the same width were considered next for comparison: (1) HI: isotropic layer with $v_x/v_y = 1$; (2) HA1: anisotropic layer with $v_{sx}/v_{sy} = v_{px}/v_{py} = 1.22$ (referred to as weakly anisotropic); and (3) HA2: anisotropic layer with $v_{sx}/v_{sy} = v_{px}/v_{py} = 1.41$ (referred as strongly anisotropic). The elastic parameters of these layers are also given in Table 1. The reflection and transmission coefficients as a function of the angle of incidence are shown in Figs. 3(*a*) and 3(*b*), respectively. As shown in the figures, the effect of anisotropy on the reflection and transmission is not significant compared to the effect of inhomogeneity in the case of high velocity layers.

Example II: In this example, we considered moderately thin layers with $h/L_R = 0.15$. Three layers of high velocity layers were considered first: An anisotropic layer (HA) and two isotropic layers (HI1 and HI2) with the same velocity as the velocity in the y and x direction of the anisotropic layer, respectively. Parameters of the host medium and the layers are given in Table 2. Figures 4(*a*) and 4(*b*) show the reflection and transmission coefficients of Rayleigh waves, respectively, as a function of the angle of incidence. It is noted in Fig. 4(*a*) that the reflection coefficient of the anisotropic layer (HA) is rather close to that of layer HI2 at the near normal incidence, but it tends to that of layer HI1 for large incident angles. For

Table 2 Elastic parameters of moderately thin layers (Example II)

Medium	$\rho(g/cm^3)$	v_{sx} (km/sec)	v_{sy} (km/sec)	v_{px} (km/sec)	v_{py} (km/sec)
Host medium	2.6	3.2	3.2	5.7	5.7
HI1 high velocity isotropic	2.8	3.5	3.5	6.3	6.3
HA high velocity anisotropic	3.0	4.5	3.5	8.1	6.3
HI2 high velocity isotropic	3.2	4.5	4.5	8.1	8.1
LI1 low velocity isotropic	1.8	2.0	2.0	3.6	3.6
LA low velocity anisotropic	2.0	2.0	3.0	3.6	5.4
LI2 low velocity isotropic	2.2	3.0	3.0	5.4	5.4

intermediate angles, however, the reflection coefficient of the anisotropic layer is quite different from that of the isotropic layers. One of the important characteristics of wave propagation from a low to a high-velocity medium is the existence of a critical angle which can be characterized by a sharp increase of the reflected wave. The propagation of surface waves across a thin isotropic high velocity layer is also characterized by a quasi-critical reflection with a sharp increase of the reflection coefficient after reaching a minimum (Its and Lee, 1992). In contrast to that of isotropic layers (HI1 and HI2), the reflection coefficient of the anisotropic layer (HA) exhibits a slow monotonic increase as the incident angle is increased. The "smearing" of the reflection at an interface between an anisotropic and an isotropic quarter-space (compared to the interface between two isotropic quarter-spaces) has been reported recently by Its and Lee (1993b). The same results were obtained in the case of a thin high-velocity anisotropic layer (HA). However, any conclusions on the significant "smearing" of the reflection coefficients by anisotropic properties of the layer should only be confirmed by physical ultrasonic experiments. The transmission coefficients are close to unity in all three cases as shown in Fig. 4(*b*). This implies that there exists very little leak of surface wave energy which may be interpreted as the absence of body and bodylike waves.

Next, we considered low-velocity layers ($h/L_R = 0.15$) whose elastic parameters are given in Table 2: an anisotropic layer (LA) and two corresponding isotropic layers (LI1 and LI2). Figures 5(*a*) and 5(*b*) show the reflection and transmission coefficients, respectively, as a function of the angle of incidence for the three models. The reflection at these low-velocity layers is still stronger than that at the high-velocity layers, given comparable material contrasts with respect to the host medium. As shown in Fig. 5(*a*), the anisotropic layer does not exhibit any distinctive behavior compared to the isotropic layers, and all three models exhibit very similar dependency on the incident angle. A possible explanation of this is that, since the low-velocity layer is a strong reflector for Rayleigh waves, the effect of anisotropy of the layer is overshadowed by the effect of low-velocity screening. Although the transmission coefficients shown in Fig. 5(*b*) suggest some leak of energy of the surface waves, no discriminating features are noted between the performances of the isotropic and anisotropic layers. It should

Downloaded 03 May 2010 to 171.66.16.20. Redistribution subject to ASME license or copyright; see http://www.asme.org/terms/Terms_Use.cfm

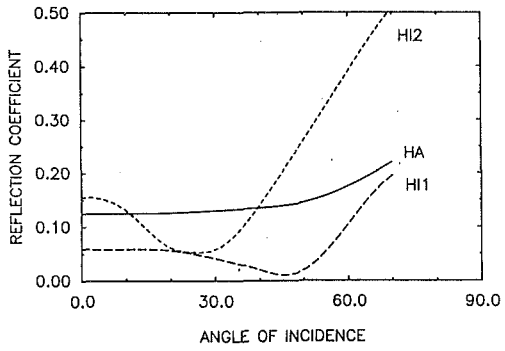


Fig. 4(*a*)

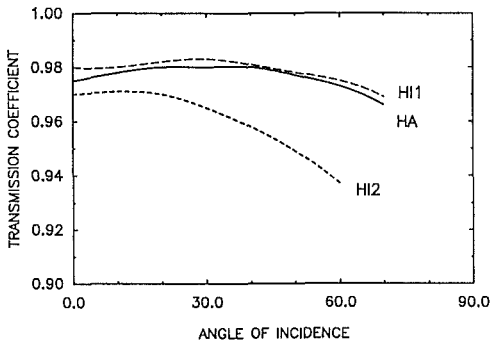


Fig. 4(*b*)

Fig. 4 Reflection and transmission coefficients at high-velocity layers with $h/L_R = 0.15$

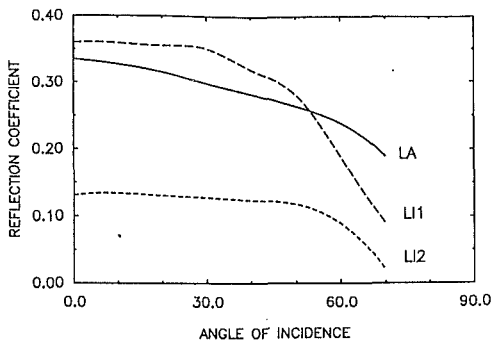


Fig. 5(*a*)

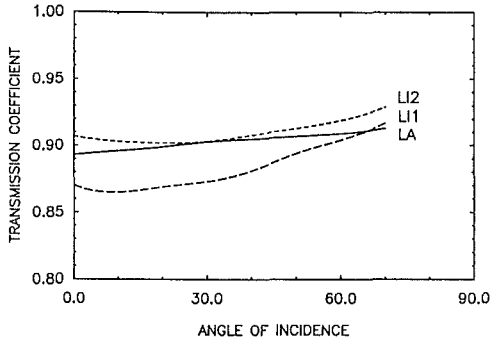


Fig. 5(*b*)

Fig. 5 Reflection and transmission coefficients at low-velocity layers with $h/L_R = 0.15$

be noted, however, that these observations are made from the consideration of layers with only the simplest form of anisotropy. Further investigations with more general anisotropic materials may provide more conclusive evidence on the trade-off between anisotropy and inhomogeneity of the interfacial layer.

6 Conclusions

An analytical approach based on the Green's function technique was developed to study the propagation of surface waves across a thin anisotropic layer inserted between two vertically inhomogeneous isotropic quarter-spaces. Using the proposed approach, reflection and transmission coefficients were calculated for several layer models of materials of hexagonal symmetry with the axis of symmetry oriented along the x-axis, and the trade-off between anisotropy and inhomogeneity of the interface layer was examined. The results demonstrated that, in the case of a very thin anisotropic layer with $h/L_R = 0.05$, the low-velocity layers generate larger reflection coefficients than the high-velocity layers, and the effect of anisotropy can not be distinguished from the effect of inhomogeneity for high-velocity layers. In the case of low-velocity layers, the reflection coefficient for the strongly anisotropic layer was shown to exhibit much weaker dependency on the angle of incidence than that of the isotropic or weakly anisotropic layers. Consideration of reflection and transmission coefficients and associated energy in the case of low-velocity layers suggests that there exists an energy leak which may be interpreted as the existence of a guided wave in the layer. It was also shown that the energy leak decreases for the case of strongly anisotropic low-velocity layer (LA2). For the high-velocity layers with $h/L_R = 0.15$, the dependency of reflection coefficients of the anisotropic layer on the angle of incidence is quite different from that of isotropic layers, and the anisotropy essentially "smears" the effect of the critical reflection which takes place at the high-velocity isotropic layers. For the low-velocity layers with $h/L = 0.15$, the effect of anisotropy is overshadowed by the effect of strong low-velocity reflection as in the case of very thin layers. The analytical approach presented here is equally valid for general anisotropic layer. Further investigations with general material anisotropy will shed more lights on this important issue of the trade-off between anisotropy and inhomogeneity of the interfacial layer.

Acknowledgments

The material presented herein is based upon work supported in part by the National Science Foundation under grants MSS-9009490 and MSS-9021973. These supports are gratefully acknowledged.

References

Aki, K., and Richards, P. G., 1980, *Quantitative Seismology*, Vol. 1, Freeman, San Francisco, CA.

Alsop, L. E., Goodman, A. S., and Gregerson, S., 1974, "Reflection and Transmission of Inhomogeneous Waves with Particular Application to Rayleigh Waves," *Bulletin of the Seismological Society of America*, Vol. 64, pp. 535–546.

Anderson, D. L., Minster, B., and Cole, D., 1974, "The Effect of Oriented Cracks on Seismic Velocities," *Journal of Geophysical Research*, Vol. 79, pp. 4011–4015.

Banik, N. C., 1987, "An Effective Anisotropy Parameter in Transversely Isotropic Media," *Geophysics*, Vol. 52, pp. 1654–1664.

Biagi, P. F., Gegechkory, T. S., Its, E. N., Manjgaladze, P., Scrigna, V., and Zilpimiani, D., 1990, "Transmission and Reflection of Rayleigh Waves at a Thin Low Velocity Layer: A Laboratory and Theoretical Study," *Pure and Applied Geophysics*, Vol. 133, pp. 317–327.

Bouden, M., and Datta, S. K., 1990, "Rayleigh and Love Waves in Cladded Anisotropic Medium," ASME JOURNAL OF APPLIED MECHANICS, Vol. 57, pp. 398–403.

Crampin, S., 1981, "A Review of Wave Motion in the Anisotropic and Cracked Elastic Media," *Wave Motion*, Vol. 3, pp. 343–391.

Crampin, S., 1984, "Effective Anisotropic Elastic Constants for Wave Propagating Through Cracked Solids," *Geophysical Journal of the Royal Astronomical Society*, Vol. 76, pp. 135–145.

Datta, S. K., Ledbetter, H. M., Shindo, Y., and Shah, A. H., 1988, "Phase Velocity and Attenuation of Plane Elastic Waves in a Particle-Reinforced Composite Medium," *Wave Motion*, Vol. 10, pp. 171–182.

Downloaded 03 May 2010 to 171.66.16.20. Redistribution subject to ASME license or copyright; see http://www.asme.org/terms/Terms_Use.cfm

Datta, S. K., Shah, A. H., Karusena, W., Olsson, P., and Bostrom, A., 1990, "Wave Propagation in the Presence of Interface Layers in Composites," *Materials Science and Engineering*, Vol. A126, pp.141–147.

Frazer, L. N., 1990, "Dynamic Elasticity of Microbedded and Fractured Rocks," *Journal of Geophysical Research*, Vol. 95, pp. 4821–4831.

Garbin, H. D., and Knopoff, L., 1975, "Elastic Moduli of a Medium with Liquid-Filled Cracks," *Quarterly of Applied Mathematics*, Vol. 33, pp. 301–303.

Hudson, J. A., 1982, "Overall Properties of a Cracked Solid," *Proceedings of the Cambridge Philosophical Society*, Vol. 88, pp. 371–384.

Its, E. N., and Yanovskaya, T. B., 1985, "Propagation of Surface Waves in Half-Space with Vertical, Inclined or Curved Interfaces," *Wave Motion*, Vol. 7, pp. 79–94.

Its, E. N., and Frolova, E. N., 1989, "Model Study of Rayleigh Wave Propagation Across Low Velocity Deep Faults," *Izvestiay Akademii Nauk SSSR, Fizika Zemli*, No. 9, pp. 16–25 (Physics of the Solid Earth, 1990).

Its, E. N., Frolova, E. N., and Vasiljeva, A. G., 1989, "Surface Wave Propagation Across the Deep Fault Zone," *Gerland Beitr Geophysik*, Vol. 98, pp. 346–352.

Its, E. N., 1991, "The Propagation of Surface Waves Across Vertical Thin Layer Between Horizontally Homogeneous Quarter Spaces," *Wave Motion*, Vol. 14, pp. 11–23.

Its, E. N., and Lee, J. S., 1992, "Screening of Surface Waves by Composite Wave Barriers," *Proceedings of the 10th World Conference on Earthquake Engineering*, pp. 1987–1992, Balkema, Rotterdam.

Its, E. N., and Lee, J. S., 1993a, "Propagation of Surface Waves Across a Vertical Layer with Non-Rigid Contacts," *International Journal of Engineering Science*, Vol. 31, No. 8, pp. 1151–1163.

Its, E. N., and Lee, J. S., 1993b, "Reflection and Transmission of Surface Waves at a Vertical Interface in Anisotropic Media," *Bulletin of the Seismological Society of America*, Vol. 83, No. 5, pp. 1355–1372.

Keith, C. M., and Crampin, S., 1977, "Seismic Body Waves in Anisotropic Media: Reflection and Refraction at a Plane Interface," *Geophysical Journal of the Royal Astronomical Society*, Vol. 49, pp. 181–208.

Lee, J. S., and Its, E. N., 1992, 'Propagation of Rayleigh Waves in Magneto-Elastic Media," ASME JOURNAL OF APPLIED MECHANICS, Vol. 59, No. 4, pp. 812–818.

Levshin, A. L., et al., 1989, *Seismic Surface Waves in Horizontally Inhomogeneous Earth*, Elsevier, Netherlands.

Li, Z. L., and Achenbach, J. D., 1991a, "Reflection and Transmission of Rayleigh Surface Waves by a Material Interphase," ASME JOURNAL OF APPLIED MECHANICS, Vol. 58, pp. 688–694.

Li, Z. L., and Achenbach, J. D., 1991b, "Interaction of Rayleigh Wave with a Disbond in a Material Interphase Normal to a Free Surface," *Ultrasonics*, Vol. 29, pp. 45–52.

Mase, T. G., and Johnson, D. C., 1987, "An Acoustoelastic Theory for Surface Waves in Anisotroic Media," ASME JOURNAL OF APPLIED MECHANICS, Vol. 54, pp. 127–135.

Olsson, P., Datta, S. K., and Bostrom, A., 1990, "Elastodynamic Scattering from Inclusions Surrounded by Thin Interface Layers," ASME JOURNAL OF APPLIED MECHANICS, Vol. 57, pp. 672–676.

Paskaramoorthy, R., Datta, S. K., and Shah, A. H, 1988, "Effect of Interface Layers on Scattering of Elastic Waves," ASME JOURNAL OF APPLIED MECHANICS, Vol. 55, pp. 871–878.

Rokhlin, S. I., Bolland, T. K., and Adler, L., 1986, "Reflection and Refraction of Elastic Waves on a Plane Interface Between Two Generally Anisotropic Media," *Journal of the Acoustical Society of America*, Vol. 79, pp. 906–918.

Rokhlin, S. I., and Wang, W., 1992, "Double Through-Transmission Bulk Wave Method for Ultrasonic Phase Velocity Measurement and Determination of Elastic Constants of Composite Materials," *Journal of the Acoustical Society of America*, Vol. 91, pp. 3303–3312.

Rokhlin, S. I., and Huang, W., 1992, "Ultrasonic Wave Interaction with a Thin Anisotropic Layer Between Two Anisotropic Solids: Exact and Asymptotic Boundary Condition Methods," *Journal of the Acoustical Society of America*, Vol. 92, pp. 1729–1742.

Rokhlin, S. I., 1992, "Recent Advances in Waves in Layered Media," *Journal de Physique IV*, Vol. 2, pp. 819–826.

Rose, J. L., Nayfeh, A., and Pilarski, A., 1990, "Surface Waves for Material Characterization," ASME JOURNAL OF APPLIED MECHANICS, Vol. 57, pp. 7–11.

Vasiljeva, A. G., and Its, E. N., 1988, "Mathematical Modeling of Love Wave Propagation in Medium Containing Low Velocity Zone," *Izvestiya Akademii Nauk SSSR, Fizika Zemli*, No. 1, pp. 16–25 (Physics of the Solid Earth, 1989).

APPENDIX

$$Q_{11}^{(U)} + 1 + \frac{h^2}{2} k_5 (-k_7 + k_3 \partial_{yy} + k_3 \partial_{zz})$$

$$Q_{12}^{(U)} = -h\partial_y$$

$$Q_{13}^{(U)} = -h\partial_z$$

$$Q_{21}^{(U)} = -hk_3 k_5 \partial_y$$

$$Q_{22}^{(U)} = 1 + \frac{h^2}{2} [k_0 \partial_{yy} + k_9 (-k_7 + k_{10}\partial_{yy} - k_6 \partial_{yy} - k_2 \partial_{zz})]$$

$$Q_{23}^{(U)} = \frac{h^2}{23} [\partial_z k_0 \partial_y + k_9 \partial_z (k_{10}\partial_y - k_1 \partial_y - k_1 \partial_y)]$$

$$Q_{31}^{(U)} = -hk_3 k_5 \partial_z$$

$$Q_{32}^{(U)} = \frac{h^2}{2} [k_0 \partial_{zz} + k_9 (k_{10}\partial_y \partial_z - k_1 \partial_y \partial_z - \partial_z k_2 \partial_y)]$$

$$Q_{33}^{(U)} = 1 + \frac{h^2}{2} [k_0 \partial_{zz} + k_9 (-k_7 + k_{10}\partial_{zz} - k_6 \partial_{zz} - k_2 \partial_{yy})]$$

$$Q_{41}^{(U)} = hk_5$$

$$Q_{42}^{(U)} = -\frac{h^2}{2} (k_9 k_{10} + k_5) \partial_y$$

$$Q_{43}^{(U)} = -\frac{h^2}{2} [k_9 \partial_z (k_0 + k_5)]$$

$$Q_{51}^{(U)} = \frac{h^2}{2} k_5 (\partial_z + k_8 \partial_y)$$

$$Q_{52}^{(U)} = hk_9$$

$$Q_{53}^{(U)} = 0$$

$$Q_{61}^{(U)} = \frac{h^2}{2} k_5 (\partial_z + k_8 \partial_y)$$

$$Q_{62}^{(U)} = 0$$

$$Q_{63}^{(U)} = hk_9$$

$$Q_{11}^{(T)} = -kh_7$$

$$Q_{12}^{(T)} = \frac{h^2}{2} [(k_7 k_{10} + k_7)\partial_y + (k_6 - k_{10}) \frac{\partial^3}{\partial^3 y} + 2k_2 \frac{\partial^3}{\partial^3 y} + (k_3 - k_{10}) \partial_{zz} \partial_y]$$

$$Q_{13}^{(T)} = \frac{h^2}{2} [(k_7 k_{10} + k_7)\partial_z + \partial_z (k_6 - k_{10}) \partial_{zz} + 2\partial_z k_2 \partial_y + (k_3 - k_{10}) \partial_{zz} \partial_y]$$

$$Q_{21}^{(T)} = \frac{h^2}{2} [(k_7 k_{10} + k_7)\partial_y + (k_6 - k_{10}) \frac{\partial^3}{\partial^3 y} + 2k_2 \partial_{zz} \partial_y + \partial_{zz} (k_3 - k_{10}) \partial_y]$$

$$Q_{22}^{(T)} = h[-k_7 - \partial_z k_2 \partial_z - (k_6 - k_{10}) \partial_{yy}]$$

$$Q_{23}^{(T)} = h(-k_2 \partial_y \partial_z - \partial_z k_1 \partial_y + k_{10} \partial_y \partial_z)$$

$$Q_{31}^{(T)} = \frac{h^2}{2} [(k_7 k_{10} \partial_z + \partial_z k_7) + \partial_z (k_6 - k_{10}) \partial_{zz} + 2\partial_z k_2 \partial_{yy} + (k_3 - k_{10}) \partial_{yy} \partial_z]$$

$$Q_{32}^{(T)} = h[\partial_z k_2 \partial_y - k_1 \partial_y \partial_z + k_{10} \partial_y \partial_z]$$

$$Q_{33}^{(T)} = h[-k_7 - k_2 \partial_{yy} - (k_6 - k_{10}) \partial_{zz}]$$

$$Q_{41}^{(T)} = 1 + \frac{h^2}{2} (-k_7 k_5 + k_0 \partial_{yy} + \partial_{zz} k_0)$$

$$Q_{42}^{(T)} = -kh_0 \partial_y$$

$$Q_{43}^{(T)} = -h\partial_z k_0$$

$$Q_{51}^{(T)} = -h\partial_y$$

$$Q_{52}^{(T)} = 1 + \frac{h^2}{2} [-k_7 k_9 - \partial_{zz} k_2 k_9 + (k_0 + k_{10} k_9) \partial_{yy} - k_6 k_9 \partial_{yy}]$$

$$Q_{53}^{(T)} = \frac{h^2}{2} [-k_2 \partial_z k_9 \partial_y + \partial_z (k_0 + k_{10} k_9) \partial_y - \partial_z k_{10} k_9 \partial_y]$$

Downloaded 03 May 2010 to 171.66.16.20. Redistribution subject to ASME license or copyright; see http://www.asme.org/terms/Terms_Use.cfm

$$Q_{61}^{(T)} = -h\partial_z$$

$$Q_{62}^{(T)} = \frac{h^2}{2}[-\partial_z k_2 k_9 \partial_y + (k_0 + k_{10}k_9)\partial_y\partial_z - k_1\partial_z k_9\partial_y]$$

$$Q_{63}^{(T)} = 1 + \frac{h^2}{2}[-k_7 k_9 - k_2 k_9 \partial_{yy} + \partial_y\partial_z(k_0 + k_{10}k_0) - \partial_z k_6 \partial_z k_9]$$

where

$$k_1 = \lambda,\quad k_2 = \mu,\quad k_3 = \lambda - l,\quad k_4 = \mu - m,$$

$$k_5 = \frac{1}{\lambda + 2\mu - p},\quad k_6 = \lambda + 2\mu,$$

$$k_7 = \rho\omega^2,\quad k_8 = \frac{\lambda - l}{\mu - m},\quad k_9 = \frac{1}{\mu - m},$$

$$k_{10} = \frac{\lambda - l}{\lambda + 2\mu - p},\quad k_0 = \frac{(\lambda - l)^2}{\lambda + 2\mu - p}.$$

Note that components of the matrices $\mathbf{Q}^{(T)}$ and $\mathbf{Q}^{(U)}$ are given for a vertically inhomogeneous layer.

Downloaded 03 May 2010 to 171.66.16.20. Redistribution subject to ASME license or copyright; see http://www.asme.org/terms/Terms_Use.cfm

Swerve During Three-Dimensional Impact of Rough Rigid Bodies

W. J. Stronge
Department of Engineering,
University of Cambridge,
Trumpington Street,
Cambridge, BC2 1PZ, U.K.

For collisions between rough bodies, dry friction can be represented by Coulomb's law; this relates the normal and tangential components of contact force by a coefficient of limiting friction if the contact is sliding. The friction force acts in a direction opposed to sliding. For a collision with planar changes in velocity, sliding is in either one direction or the other; the direction can reverse before separation only if the impact configuration is eccentric or noncollinear and the initial velocity of sliding is small. In general, however, friction results in nonplanar changes in velocity; for free bodies the velocity changes are three-dimensional or nonplanar unless the initial sliding velocity lies in the same plane as two principal axes of inertia for each body. Nonplanar velocity changes give a direction of sliding that continually changes or swerves during an initial phase of contact in an eccentric impact configuration. The present paper obtains changes in relative velocity during "rigid" body collisions as a function of impulse $\mathrm{P_n}$ *of the normal component of reaction force. The method of resolving changes in relative velocity as a function of impulse is demonstrated by obtaining the solution for a spherical pendulum colliding with a rough half-space. The solution depends on two independent material parameters—the coefficient of friction and an energetic coefficient of restitution.*

Introduction

Collisions between hard and compact bodies at moderate impact speeds result in changes in momentum and some loss of kinetic energy during a brief contact period. If the bodies are hard, a very large reaction force develops during contact but nevertheless there are only small displacements and these are confined to a small region around the contact patch. Consequently the contact area remains small. A very large reaction force acting in a small contact area implies that (a) the colliding bodies suffer large stresses and strains only very near the contact area, (b) the distribution of reaction force in the contact area is not significant, and (c) the contact period is so brief that any changes in orientation of the bodies during contact are negligible. These conditions form the basis of rigid-body impact theory. The conditions (small contact area combined with a very brief collision period) typically occur in high-speed assembly operations, impact printing processes and games such as baseball, billiards, or golf.

During moderate speed collisions between hard bodies there are continuous changes in relative velocity which can be calculated if we recognize that the bodies are not entirely rigid—there is a small region of deformation that surrounds the initial contact point. By considering an infinitesimally small deformable region between the contact points on two colliding rigid bodies, changes in relative velocity v_i between these points can be expressed as a function of impulse of the reaction force. The reaction impulse P_i that develops during a collision depends on the initial relative velocity $v_i(0)$ and both material and inertia properties for each body at the impact point. The relative velocity between the colliding bodies and the reaction impulse can be resolved into components normal and tangential to the common tangent plane for the contact surfaces at the point of contact. Let unit vector n be oriented normal to the tangent plane. The normal component of the impulse $P_n = P_i \cdot nn$ monotonically increases in magnitude during contact because the normal force F_n is compressive; thus, changes in relative velocity are obtained as a function of the scalar independent variable $P \equiv n \cdot P_n$.

The normal component of contact force $F_n = dP_n/dt$ does work on the bodies during an initial period of contact before the impulse at maximum compression P^c; this work compresses the bodies in a small region around the contact point while decreasing the sum of their kinetic energies. For subsequent impulse $P > P^c$, the normal component of contact force drives the bodies apart as the compressed region undergoes a release of elastic strain energy. Work done by F_n during the restitution period $P > P^c$ restores that part of the initial kinetic energy which was transformed into elastic strain energy during compression.

In addition to the normal component of relative velocity at the contact point there is also a tangential component of relative velocity called slip. If the bodies are rough a tangential contact force, termed friction, opposes any slip. The friction force complicates the analysis of impact problems, especially

Contributed by the Applied Mechanics Division of THE AMERICAN SOCIETY OF MECHANICAL ENGINEERS for publication in the ASME JOURNAL OF APPLIED MECHANICS.

Discussion on this paper should be addressed to the Technical Editor, Professor Lewis T. Wheeler, Department of Mechanical Engineering, University of Houston, Houston, TX 77204-4792, and will be accepted until four months after final publication of the paper itself in the ASME JOURNAL OF APPLIED MECHANICS.

Manuscript received by the ASME Applied Mechanics Division, Nov. 10, 1992; final revision, Apr. 26, 1993. Associate Technical Editor: R. L. Huston.

Copyright © 1994 by ASME
Downloaded 03 May 2010 to 171.66.16.20. Redistribution subject to ASME license or copyright; see http://www.asme.org/terms/Terms_Use.cfm

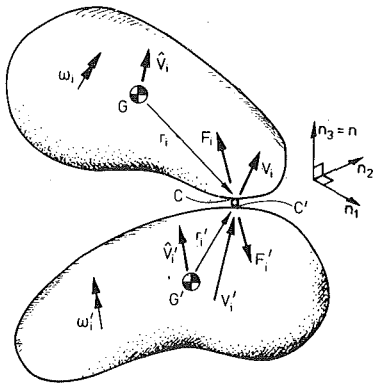


Fig. 1 Collision between two rough bodies. The rigid bodies have contact points C and C' that are separated by a deformable particle.

if friction and normal force components are coupled by the equations of motion. This coupling occurs if the impact configuration is eccentric or noncollinear; i.e., if the center of mass for each body is not on the common normal line through the contact point. The complications develop if the direction of slip varies during the contact period.

For eccentric collisions with changes in relative velocity that are planar, these complications due to friction have been overcome by dividing the total impulse into parts associated with successive phases of unidirectional slip (Bouligand, 1959; Stronge, 1991, 1992; Brach, 1993). In general, however, collisions between rough bodies result in changes in relative velocity at the contact point $v_i(P) - v_i(0)$ that are nonplanar unless the initial relative velocity $v_i(0)$ lies in the same plane as two principal axes of inertia for each body. We will show that in most cases the direction of slip changes continuously during contact if the collision configuration is eccentric. A general formulation for impact of two unconstrained rough rigid bodies will be developed. Then the effects of friction in three-dimensional or nonplanar collisions will be illustrated by two examples: the oblique impact of a sphere that has a component of initial rotation about the direction of initial translation and a collision of a spherical pendulum on a half-space. These examples represent collinear and eccentric impact configurations, respectively.

Collision of Two Free Bodies

Consider two bodies that collide at contact point C; the bodies have no displacement constraints except that they are mutually impenetrable at C. If the surface of at least one of the bodies has continous curvature at C, there is a common tangent plane that passes through C and perpendicular to this plane, a common normal direction n. Let n_i, $i=1, 2, 3$ be a set of mutually perpendicular unit vectors with n_1 and n_2 in the tangent plane while $n_3 = n$ is normal to this plane as shown in Fig. 1. The bodies have centers of mass located at G and G', respectively. There is a position vector r_i from G to the contact point C while r_i' locates C' from G'. The bodies have masses M and M' and each body has an inertia tensor I_{ij} or I_{ij}' for second moment of its mass at G or G', respectively. Let $\hat{V}_i$ and $\hat{V}_i'$ be the velocity at each respective center of mass while ω_i and ω_i' are corresponding angular velocities for the bodies in reference frame n_i. At the contact points C and C' the bodies are subjected to contact forces F_i and F_i'; these reactions apply an impulse on each body that is denoted by $P_i(t)$ and $P_i'(t)$ where

$$dP_i = F_i dt \quad \text{and} \quad dP_i' = F_i' dt. \tag{1}$$

The equations of motion for each body can be expressed as

$$M d\hat{V}_i = dP_i \tag{2a}$$

$$I_{ij} d\omega_j = \epsilon_{ijk} r_j dP_k \tag{3a}$$

and

$$M' d\hat{V}_i' = dP_i' \tag{2b}$$

$$I_{ij}' d\omega_j' = \epsilon_{ijk} r_j' dP_k' \tag{3b}$$

where a repeated index (e.g., j) indicates summation and the permutation tensor $\epsilon_{ijk} = +1$ if the indices are in cyclic order, $\epsilon_{ijk} = -1$ if the indices are in anticyclic order and $\epsilon_{ijk} = 0$ for repeated indices. Thus in index notation the vector product $\mathbf{r} \times d\mathbf{P} = \epsilon_{ijk} r_j dP_k$.

The reaction forces that act at the contact point during collision are large if the bodies are hard; in particular, these forces are very large in comparison with any body force. Consequently we assume that the only forces acting during a collision are the reactions at C and C'; the impulse of these reactions depends on changes in relative velocity across a small deforming region at C. The effect of a small deforming region can be represented by assuming that during a collision the contact points C and C' on the colliding bodies are separated by a negligibly small deformable element.[1] The components of velocity for each contact point V_i and V_i' can be obtained from the velocity relative to the respective center of mass

$$V_i = \hat{V}_i + \epsilon_{ijk} \omega_j r_k \quad \text{and} \quad V_i' = \hat{V}_i' + \epsilon_{ijk} \omega_j' r_k'. \tag{4}$$

Let components of *relative velocity* v_i between the contact points C and C' be defined as

$$v_i = V_i - V_i'. \tag{5}$$

Any incremental changes in reaction impulse acting on the rigid bodies are equal in magnitude but opposite in direction if the infinitesimally small deforming element has negligible mass; i.e.,

$$dp_i \equiv dP_i = -dP_i'. \tag{6}$$

Changes in relative velocity at C can be related to changes in impulse of the reaction by substituting Eqs. (2) and (3) into (4) and thence (5). This gives an equation of motion for changes in relative velocity v_i,

$$dv_i = m_{ij}^{-1} dp_j, \tag{7}$$

where the elements of the inverse inertia matrix for C are given by

$$m_{ij}^{-1} = \left(\frac{1}{M} + \frac{1}{M'}\right)\delta_{ij} + \epsilon_{ikm}\epsilon_{jln}(I_{kl}^{-1} r_m r_n + I_{kl}'^{-1} r_m' r_n'). \tag{8}$$

This matrix is symmetric, $m_{ij}^{-1} = m_{ji}^{-1}$. The following are representative elements:

$$\begin{aligned} m_{11}^{-1} &= (M^{-1} + r_2^2 I_{33}^{-1} - 2r_2 r_3 I_{23}^{-1} + r_3^2 I_{22}^{-1}) \\ &\quad + (M'^{-1} + r_2'^2 I_{33}'^{-1} - 2r_2' r_3' I_{23}'^{-1} + r_3'^2 I_{22}'^{-1}) \\ m_{12}^{-1} &= (r_1 r_3 I_{23}^{-1} - r_3^2 I_{21}^{-1} - r_1 r_2 I_{33}^{-1} + r_2 r_3 I_{31}^{-1}) \\ &\quad + (r_1' r_3' I_{23}'^{-1} - r_3'^2 I_{21}'^{-1} - r_1' r_2' I_{33}'^{-1} + r_2' r_3' I_{31}'^{-1}) \\ m_{13}^{-1} &= (r_1 r_2 I_{32}^{-1} - r_2^2 I_{31}^{-1} - r_1 r_3 I_{22}^{-1} + r_2 r_3 I_{21}^{-1}) \\ &\quad + (r_1' r_2' I_{32}'^{-1} - r_2'^2 I_{31}'^{-1} - r_1' r_3' I_{22}'^{-1} + r_2' r_3' I_{21}'^{-1}). \end{aligned} \tag{9}$$

Law of Friction for Rough Bodies. Dry friction between colliding bodies can be represented by the Amontons-Coulomb law of sliding friction (Johnson, 1985). This law relates the tangential component to the normal component of reaction force at the contact point by introducing a coefficient of limiting friction μ which acts if there is sliding, i.e., $v_1^2 + v_2^2 > 0$. Denoting the magnitude of the normal component of a differential increment of impulse by $dp \equiv dP \equiv n \cdot dp_3$, this law takes the form

[1] The physical construct of a deformable particle separating contact points on colliding rigid bodies is mathematically equivalent to Keller's (1986) asymptotic method of integrating with respect to time the equations for relative acceleration of deformable bodies and then taking the limit as the compliance (or contact period) becomes vanishingly small.

Downloaded 03 May 2010 to 171.66.16.20. Redistribution subject to ASME license or copyright; see http://www.asme.org/terms/Terms_Use.cfm

$$\sqrt{(dp_1)^2+(dp_2)^2}<\mu dp \quad \text{if} \quad v_1^2+v_2^2=0 \tag{10}$$

$$dp_1=-\frac{\mu v_1}{\sqrt{v_1^2+v_2^2}}dp,$$

$$dp_2=-\frac{\mu v_2}{\sqrt{v_1^2+v_2^2}}dp \quad \text{if} \quad v_1^2+v_2^2>0. \tag{11}$$

Equation (10) expresses an upper bound on the ratio of tangential to normal force for rolling contact; for force ratios less than μ the sliding speed $s\equiv\sqrt{v_1^2+v_2^2}$ vanishes. If sliding is present, $s>0$, the tangential increment of impulse or friction force at any impulse acts in a direction directly opposed to sliding. The sliding direction can be defined by angle ϕ measured in the tangent plane from n_1; thus $\phi\equiv\tan^{-1}(v_2/v_1)$ and

$$v_1=s\cos\phi \qquad v_2=s\sin\phi.$$

Since the normal contact force must be compressive, the impulse of the normal component of reaction is a monotonously increasing scalar function during the collision period. Hence rates of change for relative velocity at C can be expressed as a function of the rate of change of impulse for the normal component of reaction; i.e., the collision process can be resolved as a function of the independent variable p.

For sliding in direction $\phi(p)$ we obtain the equations of motion as a function of the impulse of the normal component of reaction,

$$dv_1/dp=-\mu m_{11}^{-1}\cos\phi-\mu m_{12}^{-1}\sin\phi+m_{13}^{-1} \tag{12}$$

$$dv_2/dp=-\mu m_{21}^{-1}\cos\phi-\mu m_{22}^{-1}\sin\phi+m_{23}^{-1} \tag{13}$$

$$dv_3/dp=-\mu m_{31}^{-1}\cos\phi-\mu m_{32}^{-1}\sin\phi+m_{33}^{-1}. \tag{14}$$

These equations of motion are not separable into independent expressions for each component of velocity unless $\mu=0$ or $m_{ij}^{-1}=0$ for $i\neq j$; i.e., either the contact surfaces are perfectly smooth or the impact configuration is collinear and the sliding velocity is in-plane with two principal axes of inertia for the center of mass of each body. Since the inertia terms in (12) and (13) are not proportional, the rates of change are generally different for each tangential component of slip; thus for nonplanar changes in relative velocity, the direction of slip $\phi(p)$ continually varies while $s>0$.

Sliding That Halts During Collision. If the collision is eccentric and the initial speed of sliding is small enough so that slip halts before separation, then after slip halts the contact patch subsequently either sticks or resumes sliding in a new direction. For a sufficiently large coefficient of friction, the contact patch sticks; i.e., after slip halts, $dv_1/dp=dv_2/dp=0$. This velocity constraint is imposed by a tangential force which corresponds to a differential impulse $(dp_1^2+dp_2^2)^{1/2}=f\,dp$ where $f<\mu$. The constraint force has a direction $\bar{\phi}-\pi$ and relative magnitude f that can be obtained by equating (12) and (13) to zero.

$$\bar{\phi}=\tan^{-1}\left[\frac{m_{11}^{-1}m_{23}^{-1}-m_{12}^{-1}m_{13}^{-1}}{m_{22}^{-1}m_{13}^{-1}-m_{23}^{-1}m_{12}^{-1}}\right]$$

$$f=\frac{[(m_{11}^{-1}m_{23}^{-1}-m_{12}^{-1}m_{13}^{-1})^2+(m_{22}^{-1}m_{13}^{-1}-m_{12}^{-1}m_{23}^{-1})^2]^{1/2}}{m_{11}^{-1}m_{22}^{-1}-m_{12}^{-1}m_{12}^{-1}}$$

Alternatively, if slip resumes after halting, it does so in direction $\bar{\phi}$ opposite to the constraint force for stick. Equations (12) and (13) indicate also that $\bar{\phi}=\tan^{-1}(dv_2/dv_1)$; thus the direction of slip is constant in any second phase of slip.

Energetic Definition of Coefficient of Restitution. A coefficient of restitution relates the normal impulse applied during the restitution phase to that during the compression phase; the sum of these impulses gives the terminal normal impulse p^f when the contact points finally separate. For situations where the direction of slip varies during collision, the only energetically consistent definition of this coefficient is the so-called *energetic coefficient of restitution* (Stronge, 1990, 1993)[2]. This directly relates the coefficient of restitution to irreversible deformation in the contact region and thus explicitly separates the dissipation due to hysteresis of contact forces from that due to friction between the colliding bodies.

The work W_3 done on the bodies by the normal component of reaction impulse is given by

$$W_3=\int_0^t F_3\cdot v_i\,dt=\int_0^p v_i\cdot dp. \tag{15}$$

During the compression phase of collision, the work done by the normal component of reaction impulse decreases the sum of the kinetic energies of the colliding bodies and brings the normal component of relative velocity to rest; this work equals the internal energy gained by the bodies during this period. The part of this internal energy known as elastic strain energy then drives the contact points apart during the subsequent restitution phase of collision. This restores some of the kinetic energy absorbed during compression. The difference between the work done to compress the bodies and the work done by the release of strain energy during restitution is the collision energy loss due to internal irreversible deformation. This work can be used to define an energetic coefficient of restitution that is independent of friction and the process of slip.

The square of the coefficient of restitution e_*^2 is the ratio of the elastic strain energy released during restitution to the internal energy of deformation absorbed during compression,

$$e_*^2=\frac{-\int_{p^c}^{p^f}v_3(p)\,dp}{\int_0^{p^c}v_3(p)\,dp} \tag{16}$$

where a characteristic normal impulse for the compression phase p^c is defined as the impulse that brings the normal component of relative velocity to rest; i.e., $v_3(p^c)=0$. This characteristic impulse for the compression phase can be calculated from the laws of motion. If the normal component of relative velocity is plotted as a function of impulse as shown in Fig. 2, the energetic coefficient of restitution is just the square root of the ratio of areas under the curve before and after p^c. Consequently, if the internal energy loss parameter e_* is known, the terminal impulse at separation p^f can be calculated and this provides the limit of integration to obtain the components of separation velocity $v_i(p^f)$ from Eqs. (12)–(14).

Further understanding of the process of slip during collision can be obtained from the following two examples. The first is a central or collinear collision of a rotating sphere on a rigid half-space; because of the initial rotation, the tangential component of translational relative velocity for the mass center is not parallel to the initial direction of slip. The second example is a noncollinear collision where the resultant of forces acting during contact is not in the plane of two principal axes of inertia for C so the changes in velocity are nonplanar.

Oblique Collision of Rotating Sphere on a Rough Half-Space

Consider a rigid sphere of radius R and mass M which has a center of mass G moving with translational velocity $\hat{v}_i(0)$ when it collides with a rough rigid half-space at a contact point C. Before the collision the sphere is rotating with angular velocity $\omega_i(0)$. Let the center of mass G have components of

[2] A similar definition was proposed by Boulanger (1939) for a time-dependent analysis. Although his statement overlooks the effect of friction during compression, his calculation of e_* is effectively the same as the energetic coefficient of restitution if tangential compliance is negligible.

Downloaded 03 May 2010 to 171.66.16.20. Redistribution subject to ASME license or copyright; see http://www.asme.org/terms/Terms_Use.cfm

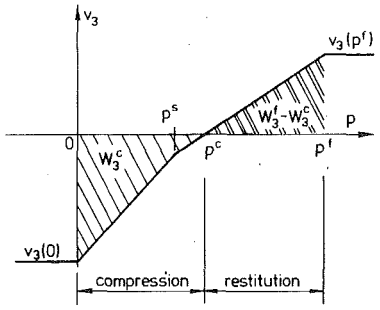


Fig. 2 Changes in the normal component of relative velocity during collision. The curve has slope that changes when the direction of slip changes. The cross-hatched areas under the curve are equal to the work done by the normal component of force during compression and restitution, respectively.

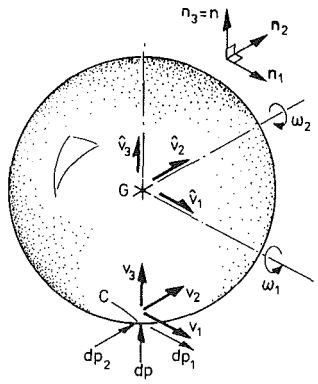


Fig. 3 Rotating sphere colliding with rough half-space at oblique angle of incidence

velocity $\hat{v}_1$ and $\hat{v}_2$ in the tangent plane and $\hat{v}_3$ in the normal direction n as shown in Fig. 3. At the contact point the reaction force gives a normal component of impulse $p_3 \equiv p$ and tangential components p_1 and p_2. Equations of motion for this sphere can be written as

$$d\hat{v}_1 = M^{-1}dp_1, \quad d\hat{v}_2 = M^{-1}dp_2, \quad d\hat{v}_3 = M^{-1}dp \tag{17}$$

$$d\omega_1 = \frac{R}{I_{11}}dp_2, \quad d\omega_2 = -\frac{R}{I_{22}}dp_1, \quad d\omega_3 = 0 \tag{18}$$

where the reaction is assumed to give no couple. While some experiments on spinning spheres by Horak (1948) have measured a mean reaction couple during collision, this couple is a consequence of development of a finite radius for the contact patch. A time-dependent analysis somewhat like the simulation of Brach (1993) is required to obtain the frictional reaction couple as a function of deformation of the colliding bodies. Hence these experimental results are outside the realm of rigid-body impact theory and not considered here.

At the contact point C the relative velocity v_i between the sphere and the surface of the half-space has a normal component $v_3 = \hat{v}_3$ and components of slip

$$v_1 = \hat{v}_1 - R\omega_2, \quad v_2 = \hat{v}_2 + R\omega_1. \tag{19}$$

The differential equations for change in relative velocity at the contact point are

$$\begin{Bmatrix} dv_1 \\ dv_2 \\ dv_3 \end{Bmatrix} = \frac{1}{M}\begin{bmatrix} 1+MR^2/I_{22} & 0 & 0 \\ 0 & 1+MR^2/I_{11} & 0 \\ 0 & 0 & 1 \end{bmatrix}\begin{Bmatrix} dp_1 \\ dp_2 \\ dp \end{Bmatrix}. \tag{20}$$

The slip speed $s(p)$ and the angle of slip $\phi(p)$ are defined as follows:

$$s^2 \equiv v_1^2 + v_2^2, \quad \phi \equiv \tan^{-1}(v_2/v_1) \tag{21}$$

so that

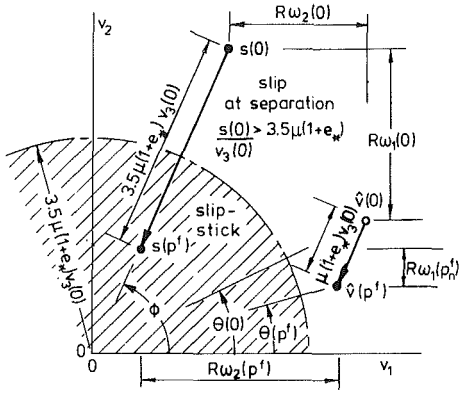


Fig. 4 Slip trajectory $s_i(p)$ and tangential velocity $\hat{v}_i(p) - \hat{v}_i(p) \cdot nn$ of center of mass during impact of solid sphere on rough half-space. Dashed curve denotes the largest initial speed $s(0)$ where slip is halted by friction before separation.

$$v_1 = s\cos\phi, \qquad v_2 = s\sin\phi. \tag{22}$$

If tangential components are related to the normal component of impulse by the Amontons-Coulomb law, then while the contact point is slipping,

$$dp_1 = -\mu\cos\phi\, dp, \qquad dp_2 = -\mu\sin\phi\, dp. \tag{23}$$

Instead of expressing slip in terms of velocity components v_1 and v_2 in the tangent plane, the equations of motion for a sphere can be written directly in terms of the slip speed s and angle of slip ϕ. Note that for a sphere the moment of inertia about a diametral axis is $I_{11} = I_{22} \equiv I$. Then from Eqs. (20)–(23) we obtain differential equations for slip of a sphere,

$$\frac{ds}{dp} = -\frac{\mu}{M}\left(1+\frac{MR^2}{I}\right), \quad \frac{d\phi}{dp} = 0. \tag{24}$$

Thus, for collinear or central collision of bodies that are axisymmetric about the common normal direction, the direction of slip does not vary.

From (24) the slip speed can be obtained as a function of impulse.

$$s(p) = s(0) - \frac{\mu}{M}\left(1+\frac{MR^2}{I}\right)p \tag{25}$$

The transition impulse p^c when compression terminates and separation begins is given by $p^c = -Mv_3(0)$ while in a collinear collision, the final impulse at separation is given by $p^f = (1+e_*)p^c$. This terminal impulse provides an upper limit on the change in slip velocity. If slip continues throughout the contact period, a solid sphere with $MR^2/I = 5/2$ has a final speed of slip

$$s(p^f) = s(0) + 3.5\mu(1+e_*)v_3(0) \tag{26}$$

where the coordinate system in Fig. 3 gives a normal component of relative velocity at incidence $v_3(0) < 0$.

Changes in tangential relative velocity of the contact point C and the center of mass G that develop during collision are illustrated in Fig. 4. The slip velocity is directed towards the origin. Slip continues throughout the collision if $s(0)/v_3(0) \geq 3.5\mu(1+e_*)$ while slip halts during collision and subsequently sticks if the initial slip speed is smaller than this limiting value. If the collision configuration is collinear, there is no tangential force after impulse p^s when slip halts, so there are no further changes in tangential relative velocity. At the center of mass G, the change in tangential velocity is parallel to that for the contact point C but the change in speed is only 2/7 as large. After slip halts, the sphere rolls in the direction of the tangential component of velocity for the center of mass G; the terminal velocity of the center of mass has a tangential component $\hat{v}_1(p^s)n_1 + \hat{v}_2(p^s)n_2$. The direction of slip is constant during the instant of collision and all changes in velocity

Downloaded 03 May 2010 to 171.66.16.20. Redistribution subject to ASME license or copyright; see http://www.asme.org/terms/Terms_Use.cfm

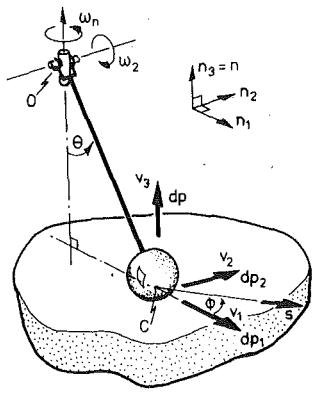


Fig. 5 Spherical simple pendulum colliding with rough half-space. Initially the pendulum is rotating about both n_2 and n_3.

are in this same direction (i.e., planar). Nevertheless most points in a rotating sphere do not have an initial velocity in the plane of the normal and the initial direction of slip; for points where the initial velocity is out of this plane, the velocity continuously changes in direction while the slip speed is changing. The direction of the tangential component of the translational velocity for G changes smoothly between the initial direction $\theta(0)$ and terminal direction $\theta(p^f)$ as shown in Fig. 4.

The center of mass has components of final velocity at separation $\hat{v}_i^f \equiv \hat{v}_i(p^f)$ that are given by

$$\frac{\hat{v}_i(p^f)}{\hat{v}_3(0)} = \begin{cases} \dfrac{\hat{v}_i(0)}{\hat{v}_3(0)} - \dfrac{2}{7}\dfrac{v_i(0)}{\hat{v}_3(0)} & \text{if } \left|\dfrac{s(0)}{\hat{v}_3(0)}\right| < 3.5\mu(1+e_*) \\ \dfrac{\hat{v}_i(0)}{\hat{v}_3(0)} + \mu(1+e_*)\cos\phi(0) & \text{if } \left|\dfrac{s(0)}{\hat{v}_3(0)}\right| > 3.5\mu(1+e_*) \end{cases} \quad (i=1,\ 2)$$

$$\frac{\hat{v}_3(p^f)}{\hat{v}_3(0)} = -e_*. \tag{27}$$

Spherical Pendulum Colliding on a Rough Half-Space

As an example of an eccentric impact configuration, consider a spherical simple pendulum that collides on a rough half-space. The pendulum is a rigid body of length L with one end pivoted at a stationary point O. At the instant of impact the pendulum is inclined at an angle θ from the normal to a massive half-space so the support is located a perpendicular distance $L\cos\theta$ from the plane surface of the half-space as illustrated in Fig. 5.

During collision the pendulum is subjected to reactions at both the contact point C and the fixed support O so the free-body impact Eqs. (7)–(9) are not directly applicable. The impulse of the reaction at O can be eliminated from consideration, however, by obtaining equations of motion in terms of moments about this fixed point. Since the motion of the pendulum is a pure rotation about O, it is convenient to use a cylindrical coordinate system with axis n directed normal to the surface of the half-space and a radial unit vector n_1 directed from the projection of O on the surface towards the contact point C. The differential equations for rotations about these unit vectors can be obtained as follows:

$$\hat{I}_{ij}\,d\omega_j = \epsilon_{ijk} r_j\, dp_k \tag{28}$$

where dp_i is the differential of impulse at C, r_i is the position vector of C from the fixed point O, and $\hat{I}_{ij}$ is the second moment of mass for point O in reference frame n_i. Therefore the relative velocity v_i at the contact point can be calculated from

$$v_i = \epsilon_{ijk}\omega_j r_k \tag{29}$$

so that differential equations for changes in relative velocity can be expressed in terms of the differential impulse of the reaction at C,

$$dv_i = \epsilon_{ikm}\epsilon_{jln}\hat{I}_{kl}^{-1} r_m r_n\, dp_j. \tag{30}$$

In this simple pendulum, however, the bob is assumed to be a particle of mass M at the contact point C. This idealization has a moment of inertia that vanishes for line OC, so an additional constraint is required to obtain a unique solution (this constrains rotations about OC). For this purpose let $\omega_1 = 0$.

This additional constraint reduces the number of equations of motion to the same as the number of degrees-of-freedom, namely two. Nevertheless, separate equations for the rates of change of components of relative velocity at the contact point can be obtained as a function of the reaction impulse.

$$\begin{aligned} M dv_1 &= \cos^2\theta\, dp_1 + \sin\theta\cos\theta\, dp \\ M dv_2 &= dp_2 \\ M dv_3 &= \sin\theta\cos\theta\, dp_1 + \sin^2\theta\, dp \end{aligned} \tag{31}$$

where a spherical simple pendulum has moments of inertia for O about n_i, $\hat{I}_{11} = ML^2\cos^2\theta$, $\hat{I}_{22} = ML^2$ and $\hat{I}_{33} = ML^2\sin^2\theta$.

If there is slip at the contact point, $v_1^2 + v_2^2 > 0$; in this case the Amontons-Coulomb law of friction gives

$$\begin{aligned} M dv_1/dp &= \sin\theta\cos\theta - \mu\cos^2\theta\cos\phi \\ M dv_2/dp &= -\mu\sin\phi \\ M dv_3/dp &= \sin^2\theta - \mu\sin\theta\cos\theta\cos\phi \end{aligned} \tag{32}$$

where $\phi(p) \equiv \tan^{-1}(v_2/v_1)$ is the angle of slip. These equations can be integrated to give

$$\begin{aligned} v_1(p) &= v_1(0) + \frac{p}{M}\sin\theta\cos\theta - \frac{\mu\cos^2\theta}{M}\int_0^p \cos\phi(p)\,dp \\ v_2(p) &= v_2(0) - \frac{\mu}{M}\int_0^p \sin\phi(p)\,dp \\ v_3(p) &= v_3(0) + \frac{p}{M}\sin^2\theta - \frac{\mu}{M}\sin\theta\cos\theta\int_0^p \cos\phi(p)\,dp \end{aligned} \tag{33}$$

where initial conditions for a spherical pendulum (0, $\omega_2(0)$, $\omega_3(0)$) give normal and tangential components of initial relative velocity at C,

$$v_1(0) = -L\omega_2(0)\cos\theta$$

$$v_2(0) = L\omega_3(0)\sin\theta \quad v_3(0) = -L\omega_2(0)\sin\theta.$$

Additional information about behavior during impact can be gained by considering the slip trajectory dv_2/dv_1 at any impulse p,

$$\frac{dv_2}{dv_1} = \frac{-\mu\sec^2\theta\sin\phi}{\tan\theta - \mu\cos\phi}.$$

Suppose the angle of slip $\phi(p)$ is a constant throughout the compression phase of collision and that slip vanishes simultaneously with the normal component of relative velocity at impulse p^c. For $0 < \phi < \pi$ this condition can be expressed as

$$\tan\phi(p) = \frac{dv_2(p)/dp}{dv_1(p)/dp} = \tan\phi(0), \quad 0 \le p < p^c.$$

After substitution from (33) this constant direction of slip results from a critical value μ_c for the coefficient of friction,

$$\mu_c = -\cot\theta/\cos\phi(0). \tag{34}$$

Downloaded 03 May 2010 to 171.66.16.20. Redistribution subject to ASME license or copyright; see http://www.asme.org/terms/Terms_Use.cfm

Note that the spherical pendulum has initial conditions $v_1(0)<0$ and $v_2(0)>0$ which gives $-1<\cos\phi(0)<0$ and consequently a critical value $\mu_c>0$.

At this point we can anticipate a few results. If $\mu>\mu_c$, the circumferential component of slip vanishes at impulse p^c where compression terminates, while if $\mu<\mu_c$ and $\mu<\tan\theta$, the circumferential component of slip asymptotically approaches zero but never completely vanishes during the collision. In either case the direction of slip is continuously changing unless $\mu=\mu_c$.

For the spherical pendulum the kinematic constraints give

$$v_3(0)/v_1(0)=\tan\theta \qquad v_3(0)/v_2(0)=\tan\theta\cot\phi(0).$$

Together with these relations, the velocities (33) can be expressed as a function of the normal component of reaction impulse p.

$$\frac{v_1(p)}{v_3(0)}=\left\{1+\frac{p\sin^2\theta}{Mv_3(0)}+\frac{\mu}{\mu_c}\frac{\cos^2\theta}{Mv_3(0)}\int_0^p\frac{\cos\phi(p)}{\cos\phi(0)}dp\right\}\cot\theta$$

$$\frac{v_2(p)}{v_3(0)}=\left\{1+\frac{\mu}{\mu_c Mv_3(0)}\int_0^p\frac{\sin\phi(p)}{\sin\phi(0)}dp\right\}\cot\theta\tan\phi(0)$$

$$\frac{v_3(p)}{v_3(0)}=\left\{1+\frac{p\sin^2\theta}{Mv_3(0)}+\frac{\mu}{\mu_c}\frac{\cos^2\theta}{Mv_3(0)}\int_0^p\frac{\cos\phi(p)}{\cos\phi(0)}dp\right\} \tag{35}$$

Here it is worth noting that an alternative derivation of the equations of motion can be expressed directly in terms of angular speeds rather than the normal and slip velocity components at the contact point. For the spherical simple pendulum this gives

$$\hat{I}_{22}\begin{bmatrix}1 & 0\\ 0 & \sin^2\theta\end{bmatrix}\begin{Bmatrix}d\omega_2\\ d\omega_3\end{Bmatrix}=\begin{bmatrix}-L\cos\theta & 0 & -L\sin\theta\\ 0 & L\sin\theta & 0\end{bmatrix}\begin{Bmatrix}dp_1\\ dp_2\\ dp\end{Bmatrix}.$$

These equations relating changes in generalized momentum and impulse, can also be obtained from Smith's (1991) general formulation of equations of impulsive motion for colliding bodies with velocity constraints. If rates of change of tangential components of impulse are related to the normal component by the Amontons-Coulomb law, $dp_1=-\mu\cos\phi\,dp$ and $dp_2=-\mu\sin\phi\,dp$. Hence,

$$\frac{d\omega_2}{\omega_2(0)}=-\left[1+\frac{\mu}{\mu_c}\frac{\cos\phi(p)}{\cos\phi(0)}\cot^2\theta\right]\frac{dp}{p^c}$$

$$\frac{d\omega_3}{\omega_3(0)}=-\frac{\mu}{\mu_c}\frac{\sin\phi(p)}{\sin\phi(0)}\csc^2\theta\frac{dp}{p^c} \tag{36}$$

where a characteristic impulse p^c that brings the normal component of relative velocity to a halt in the absence of friction is obtained as

$$p^c=\frac{Mk_2^2\omega_2(0)}{L\sin\theta}=-\frac{Mv_3(0)}{\sin^2\theta} \tag{37}$$

To integrate these differential equations, the angle of slip $\phi(p)$ must be expressed in terms of the rotation rates

$$\sin\phi=\frac{\omega_3\sin\theta}{\sqrt{\omega_2^2\cos^2\theta+\omega_3^2\sin^2\theta}} \qquad \cos\phi=\frac{-\omega_2\cos\theta}{\sqrt{\omega_2^2\cos^2\theta+\omega_3^2\sin^2\theta}}.$$

The components of slip are directly related to the angular velocities so a comparison of (36) with the combination of (32), (34), and (37) gives

$$\frac{dv_3}{v_3(0)}=\frac{d\omega_2}{\omega_2(0)} \qquad \frac{dv_2}{v_3(0)}=\frac{-d\omega_3}{\omega_2(0)}.$$

The terminal impulse p^f that corresponds to any specific value of the energetic coefficient of restitution e_* can be calculated by either integrating the last equation in (35) or by double integration of the first equation in (36). This terminal impulse is the upper limit of integration for each component of relative velocity; it depends on any variation in the angle of slip.

Numerical Results for $\theta=\pi/3$ and $\pi/4$ Rad. The critical friction coefficient μ_c that gives a steady direction of slip during compression is listed in Table 1 for a variety of initial conditions and impact configurations. For most of these conditions the critical value is rather large in comparison with typical friction measurements.

During collision the normal and tangential components of velocity are continuously changing as a function of impulse. The changes in components of slip are shown in Fig. 6; this illustrates that unless $\mu/\mu_c=1.0$ the direction of slip is continuously varying. In this figure, the radial component of slip v_1 is negative during compression and positive during the restitution phase of collision. The curvature of the slip trajectories indicates that the pendulum bob in this system has a radial acceleration that is larger than the circumferential acceleration during the compression phase while the circumferential acceleration is the largest component during the restitution phase. If $\mu<\mu_c$ and $\mu<\tan\theta$ the circumferential component of velocity monotonically decreases throughout the collision whereas if $\tan\theta<\mu<\mu_c$ circumferential slip vanishes during restitution. After circumferential slip vanishes the slip velocity is radial and decreasing. Furthermore, if $\mu\geq\mu_c$, the circumferential and radial components of slip vanish simultaneously at the end of the compressive phase of collision. In the latter case, Eqs. (32a) and (34) show that friction is sufficient to prevent the radial component of slip from reversing. Consequently, if $\mu\geq\mu_c$, there is no final separation as the pendulum is stuck in the compressed state.

A previous attempt at solving this problem by Brach (1991) assumed that the radial component of slip was necessarily zero; this implied that the direction of slip was solely circumferential. If changes in relative velocity across contact points are obtained as a function of impulse, however, this constraint is a mistake that leads to erroneous results (Stronge, 1991). The reaction impulses acting at contact point C and support O of a spherical pendulum result in nonplanar forces acting on a noncollinear

Table 1 Critical friction coefficient μ_c for spherical pendulum

Inclination at Impact θ (deg)	Initial Direction of Slip $\phi(0)$ (deg)	Ratio of Initial Comp. of Slip $v_2(0)/v_1(0)$	Ratio of Initial Angular Speeds $\omega_3(0)/\omega_2(0)$	Critical Coefficient of Friction μ_c
45	165	−0.27	0.27	1.03
45	154	−0.50	0.50	1.12
45	150	−0.58	0.58	1.16
45	135	−1.00	1.00	1.42
45	120	−1.75	1.75	2.01
45	117	−2.00	2.00	2.24
60	165	−0.28	0.16	0.59
60	150	−0.59	0.34	0.67
60	139	−0.86	0.50	0.76
60	135	−1.00	0.58	0.82
60	120	−1.74	1.01	1.16
60	106	−3.47	2.00	2.10

Downloaded 03 May 2010 to 171.66.16.20. Redistribution subject to ASME license or copyright; see http://www.asme.org/terms/Terms_Use.cfm

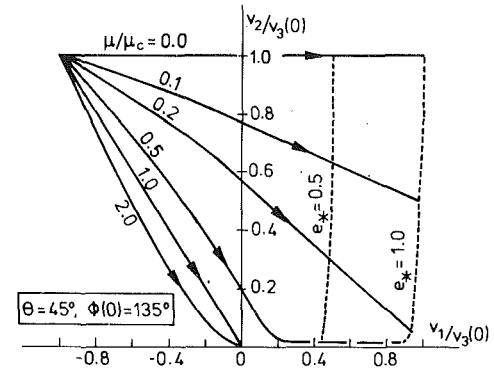


Fig. 6(*a*)

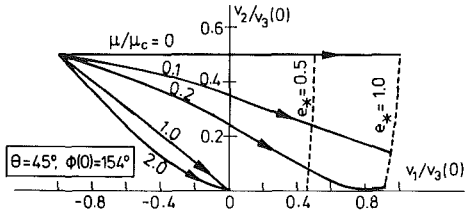


Fig. 6(*b*)

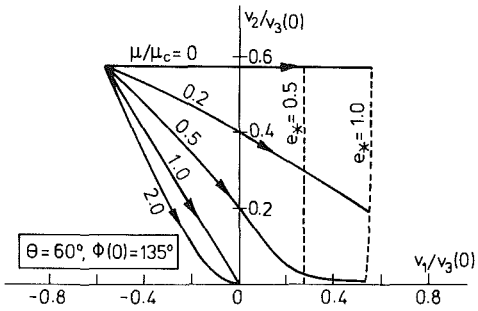


Fig. 6(*c*)

Fig. 6 Slip trajectories for spherical pendulum (*a*) $\theta = 45$ deg, $\phi(0) = 135$ deg; (*b*) $\theta = 45$ deg, $\phi(0) = 154$ deg; (*c*) $\theta = 60$ deg, $\phi(0) = 135$ deg.

collision configuration so the direction of slip is continually changing.

The present analysis gives ratios of angular speeds at separation to those at incidence (final/initial angular speed) that can be obtained from Fig. 6 for several initial conditions. The separation velocity is diminished if either the coefficient of friction increases or the coefficient of restitution decreases. If some energy is dissipated by friction, both the radial and the circumferential slip speeds at separation are smaller than the initial values even if the coefficient of restitution $e_* = 1$.

Conclusion

Some of the results obtained in this paper are not original. It was Coriolis in his *Jeu de Billiard* (1835) who first proved that the contact points on two rough spheres have the same direction of slip throughout any collision. Later, Ed Phillips generalized this result in *Liouville's Journal*, Vol. 14 (1849). He showed that in a collinear collision between two rough bodies, the direction of slip is constant if each body has a principal axis of inertia in the direction of initial slip. If each body does not have a principal axis of inertia parallel to the direction of initial slip, however, the contact points have a rate of change of relative tangential velocity with impulse $d(v_i - v_i \cdot nn)/dp$ that is not parallel to the direction of slip so the direction of slip changes continuously. While the direction of slip swerves only if the impact configuration is eccentric, the tangential velocity of the center of mass swerves whenever there is friction and the body has a component of initial angular velocity parallel to the initial tangential velocity of the center of mass. These changes in direction occur smoothly as a function of impulse. Slip can halt before separation only if the coefficient of friction is larger than a characteristic value. Slip that halts can immediately resume in a different direction only if the impact configuration is eccentric.

Here, changes in relative velocity that occur during an instant of impact have been obtained from ordinary differential equations of motion using the normal impulse of the reaction at the contact point as an independent variable. These equations represent collisions between hard bodies where deformation is limited to an infinitesimally small region around the contact point. By considering that contact points on two colliding bodies are separated by a deformable particle, we are able to follow the process of slip. This gives a method of dividing the energy loss into separate parts due to friction and irreversible deformations; e.g., by calculating separately the work done by normal and tangential components of the reaction impulse. In fact, the advance of the present analytical method compared with a semigraphical method presented by Routh (1877) and an analytical method given by Keller (1986) is the use of an *energetic coefficient of restitution* to calculate the terminal impulse at final separation. This coefficient of restitution represents hysteresis of contact force due to internal irreversible deformation. It is calculable from the kinetic equations for rigid-body motions. This method of obtaining changes in velocity as a function of impulse represents collisions between slightly deformable solids where the contact patch remains small.

Acknowledgment

I thank a reviewer who brought the French literature on energetic coefficient of restitution to my attention and gratefully acknowledge communication with V. Bhatt and J. Koechling. In the example of a spherical pendulum they drew attention to the region $\tan\theta < \mu < \mu_c$ where circumferential slip halts during restitution.

References

Boulanger, G., 1939, "Sur le choc avec frottement des corps non parfaitement élastiques," *Revue Scientifique*, Vol. 77, pp. 325–327.

Bouligand, G., 1959, *Mécanique Rationnelle*, Vuibert, Paris, pp. 477–483.

Brach, R. M., 1991, *Mechanical Impact Dynamics*, John Wiley and Sons, New York, pp. 155–157.

Brach, R. M., 1993, "Classical Planar Impact Theory and the Tip Impact of a Slender Rod," *International Journal of Impact Engineering*, Vol. 13, pp. 21–33.

Horak, Z., 1948, "Impact of a Rough Ball Spinning Round Its Vertical Axis onto a Horizontal Plane," Trans. Dept. Tech. Phys., Tech. Univ. Prague.

Johnson, K. L., 1985, *Contact Mechanics*, Cambridge University Press, Cambridge, U.K.

Keller, J. B., 1986, "Impact With Friction," ASME JOURNAL OF APPLIED MECHANICS, Vol. 53, pp. 1–4.

Routh, E. J., 1877, *Dynamics of a System with Rigid Bodies*, Part I, Macmillan, London, pp. 247–254.

Smith, C. E., 1991, "Predicting Rebounds using Rigid-Body Dynamics," ASME JOURNAL OF APPLIED MECHANICS, Vol. 58, pp. 754–758.

Stronge, W. J., 1990, "Rigid Body Collisions with Friction," *Proceedings of the Royal Society, London*, Vol. A431, pp. 169–181.

Stronge, W. J., 1991, "Friction in Collisions: Resolution of a Paradox," *Journal of Applied Physics*, Vol. 69, No. 2, pp. 610–612.

Stronge, W. J., 1992, "Energy Dissipated in Planar Collision," ASME JOURNAL OF APPLIED MECHANICS, Vol. 59, pp. 681–682.

Stronge, W. J., 1993, "Two-Dimensional Rigid-Body Collisions with Friction," (discussion) ASME JOURNAL OF APPLIED MECHANICS, Vol. 60, pp. 564–566.

Downloaded 03 May 2010 to 171.66.16.20. Redistribution subject to ASME license or copyright; see http://www.asme.org/terms/Terms_Use.cfm

Bending of a Layered Isotropic Plate With Periodic Debondings

E. Danicki
Polish Academy of Sciences, IFTR,
21 Swietokrzyska St.,
00-049 Warsaw, Poland

A layered, isotropic, and infinite elastic plate which has periodic cracks (debondings) between the layers is considered. The plate is subjected to a surface traction. The traction is spatially sinusoidal but is oriented arbitrarily. A solution for the particle displacement is obtained in form of a Fourier series expansion which accounts for the field singularities at the edges of the cracks. An average elastic property (homogenization) of the sample plate is discussed.

Formulation of the Boundary Problem

In this paper we deal with an isotropic, homogeneous, and infinite elastic layer of thickness $2h$ which contains infinitely long periodic cuts in its midplane.

Let us consider an elastic body subjected to a stress T. The linear equation for the balance of force is

$$\frac{\partial}{\partial x_j} T_{ij} = 0 \tag{1}$$

where T_{ij} is the stress tensor, and $i = 1, 2, 3$ represent, respectively, x, y, and z. T_{ij} is related to the particle displacement u_j by

$$T_{ij} = c^s_{ijkl} \frac{\partial}{\partial x_k} u_l \tag{2}$$

where, for the isotropic body considered in this paper, the stiffness tensor, c^s_{ijkl} can be expressed by two Lamé elastic constants, μ and λ (see Thurston, 1964).

In this paper, we consider two plates of thickness h bonded to each other at $y = 0$. The bonding is perfect in some periodic regions with period Λ along the x-axis and there are stress-free cracks (perfect debondings) between them (Fig. 1). The regions of perfect bondings are $2w$ wide and infinitely long along the z-axis. The stress can have a nonzero value in these regions at $y = 0$, while in the regions of cracks, on both sides of the plane $y = 0$, say at $y = +0$ and $y = -0$, the corresponding stress components must vanish. The resulting boundary conditions are

$$\begin{aligned} &T_{yi}(x, y = +0, z) = T_{yi}(x, y = -0, z) = T_{yi}(x, z) \\ &T_{yi}(x, z) = 0, \text{ on cracks, } (l-1)\Lambda + w < x < l\Lambda - w \\ &2\Delta u_i(x, z) = u_i(x, y = +0, z) - u_i(x, y = -0, z) \\ &\Delta u_i = 0, \text{ between cracks, } l\Lambda - w < x < l\Lambda + w \end{aligned} \tag{3}$$

where z is arbitrary and l is the integer number.

It is necessary to assume, additionally, that $\Delta u_y \geq 0$ in the area of cracks. In this paper we avoid this condition on the basis of the following consideration. In accordance with the theory of linear elasticity, the stress and strain are infinitesimally small and thus the superposition rule can be applied. Let us then apply an additional small and uniform tensile stress to both sides of the layered plate that is large enough to keep cracks open. This additional stress, however, does not contribute to the plate bending, thus we will not include it explicitly in the considerations that follow. Similarly, to keep cracks closed, we can applied the opposite uniform stress to both sides of the plate which will result in $\Delta u_y = 0$ at $y = 0$ and $-\infty < x < \infty$.

In the simple case considered in this paper we assume a sinusoidal traction applied to the upper side of the layered plate, while its bottom side is traction-free. One can consider the sinusoidal traction as a Fourier component of some more complicated function.

$$\begin{aligned} &T_{yi}(x, y = h, z) = t^o_i \exp(-jp_x x - jp_z z) \\ &T_{yi}(x, y = -h, z) = 0, \quad i = x, y, z \end{aligned} \tag{4}$$

We seek the particle displacement vector, $u_i(x, y, z)$, which is the solution of the boundary problem (1)–(4). The solution for vectors $\Delta\mathbf{u} = (\Delta u_x, \Delta u_y, \Delta u_z)$ and $\mathbf{T} = (T_{yx}, T_{yy}, T_{yz})$ at the plane of cracks $y = 0$, as well as an average sinusoidal particle displacement $\bar{\mathbf{u}}$ in this plane, dependent on the applied traction $\mathbf{t}^o = (t^o_x, t^o_y, t^o_z)$, will be presented in the paper.

Green's Function for an Elastic Slab

Let us consider a homogeneous elastic slab $-h < y < 0$, with its upper surface at $y = 0$ subjected to a traction $T_{yi}(x, y = 0, z) = T_{yi} \exp(-jp_x x - jp_z z)$, $i = 1, 2, 3$, and its bottom side ($y = -h$) stress-free. We need the solution for the particle dis-

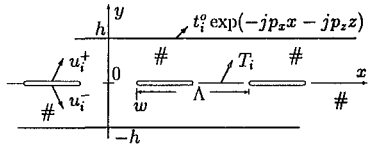


Fig. 1 Elastic plate with periodic cracks

Contributed by the Applied Mechanics Division of JOURNAL OF APPLIED MECHANICS for publication in the ASME THE AMERICAN SOCIETY OF MECHANICAL ENGINEERS.

Discussion on this paper should be addressed to the Technical Editor, Professor Lewis T. Wheeler, Department of Mechanical Engineering, University of Houston, Houston, TX 77204-4792, and will be accepted until four months after final publication of the paper itself in the ASME JOURNAL OF APPLIED MECHANICS.

Manuscript received by the ASME Applied Mechanics Division, Feb. 6, 1992; final revision, May 10, 1993. Associate Technical Editor: X. Markenscoff.

Copyright © 1994 by ASME
Downloaded 03 May 2010 to 171.66.16.20. Redistribution subject to ASME license or copyright; see http://www.asme.org/terms/Terms_Use.cfm

displacement vector components which must have the form $u_i \exp(-jp_x x - jp_z z)$, where $u_i = u_i(y)$.

The problem can be considerably simplified, if we rotate the system of coordinates around the y-axis so that the new x'-axis coincides with the vector $(p_x, 0, p_z)$. The transformation of the coordinates is governed by $(p = (p_x^2 + p_z^2)^{1/2})$

$$\mathbf{x}' = \mathbf{cx}, \quad \mathbf{c} = \begin{bmatrix} p_x/p & 0 & p_z/p \\ 0 & 1 & 0 \\ -p_z/p & 0 & p_x/p \end{bmatrix} \tag{5}$$

In the new "primed" system of coordinates $(x', y' = y, z')$ we have transformed tensors $\mathbf{T}'$, $\mathbf{u}'$ representing stress and particle displacements instead of $\mathbf{T}$, $\mathbf{u}$ in the old system. It is essential that the vector product $\mathbf{px}$ becomes px' so that the applied surface traction is a one-dimensional harmonic function $T'_{yi} \exp(-jpx')$. Hence, the solution will be independent of z'.

Assuming a particle displacement of the form $u_i'(y)\exp(-jpx')$, Eqs. (1), (2) yield the following relations for u_z':

$$T'_{yz} = \mu \frac{d}{dy} u_z'$$

$$\mu \frac{d^2}{dy^2} u_z' - \mu u_z' = 0. \tag{6}$$

The resulting boundary problem ($T'_{yz} = T'_{yz} \exp(-jpx')$ on the upper side of the slab, and 0 at its lower side) can be easily solved.

Analogously, the remaining components of stress tensor and displacement vector are governed by the equations

$$T'_{yx} = \mu \frac{d}{dy} u_x' - jp\mu u_y'$$

$$T'_{yy} = -jp\lambda u_x' + (\lambda + 2\mu) \frac{d}{dy} u_y' \tag{7}$$

and

$$\mu \frac{d^2}{dy^2} u_x' - p^2(\lambda + 2\mu) u_x' - jp(\lambda + \mu) \frac{d}{dy} u_y' = 0$$

$$(\lambda + 2\mu) \frac{d^2}{dy^2} u_y' - p^2 \mu u_y' - jp(\lambda + \mu) \frac{d}{dy} u_x' = 0 \tag{8}$$

for which the solution should be assumed in form of $\exp(\pm qy)$ and $y \exp(\pm qy)$, where $q = |p|$ for p real, otherwise $q = \sqrt{p^2}$, $\mathrm{Im}\{q\} < 0$ uniquely determines q as dependent on p (see Danicki, 1991).

Some simple but cumbersome mathematics yields (the second equation will be explained later)

$$\mathbf{u}^{-\prime} = \mathbf{G}'\mathbf{T}'$$

$$\mathbf{u}^{+\prime} = \overline{\mathbf{G}}'\mathbf{T}' + \mathbf{F}'\mathbf{t}^{o\prime} \tag{9}$$

where $\mathbf{u}^{-\prime} = [u_1', u_2', u_3']^T$ is particle displacement vector at $y = -0$ ("$-$" marks the displacement of the plate stretching for $y < 0$), $\mathbf{T}' = [T_1', T_2', T_3']^T$. Corresponding matrices $\mathbf{G}'$, $\overline{\mathbf{G}}'$, and $\mathbf{F}'$ will be presented later below.

The second relation Eqs. (9) has been derived for $\mathbf{u}^{+\prime}$, the particle displacement on the bottom side of a plate stretching for $0 < y < h$ that results from traction $\mathbf{T} \exp(-j\mathbf{px})$ applied to the bottom side of the plate $y = 0$ (Fig. 1), while its upper side is subjected to a traction $\mathbf{t}^o \exp(-j\mathbf{px})$ (denotation analogous to $\mathbf{T}$). After the transformation to the new coordinate system, these tractions become $\mathbf{T}' \exp(-jpx')$ and $\mathbf{t}^{o\prime} \exp(-jpx')$. To obtain $\overline{\mathbf{G}}'$ one should apply simultaneous substitutions $q \to -q$ and $h \to -h$ in equation for $\mathbf{G}'$.

In the next sections we use the quantities $\Delta\mathbf{u} = (\mathbf{u}^+ - \mathbf{u}^-)/2$ and $\overline{\mathbf{u}} = (\mathbf{u}^+ + \mathbf{u}^-)/2$. Our final explicit relations are (formally, $-\infty < p < \infty$ is allowed as follows)

$$\Delta\mathbf{u}' = -\frac{1}{\mu q} \mathbf{g}'(p)\mathbf{T}' + \frac{1}{\mu q} \mathbf{f}'(p)\mathbf{t}^{o\prime}$$

$$\overline{\mathbf{u}}' = \mathbf{G}'(p)\mathbf{T}' + \Delta\mathbf{u}' \tag{10}$$

where

$$\mathbf{g}'(p) = \frac{\mu q}{2}(\overline{\mathbf{G}}' - \mathbf{G}')$$

$$= \begin{bmatrix} A\dfrac{1 - H^4 - 4qhH^2}{2W} & 0 & 0 \\ 0 & A\dfrac{1 - H^4 + 4qhH^2}{2W} & 0 \\ 0 & 0 & \dfrac{1 + H^2}{1 - H^2} \end{bmatrix} \tag{11}$$

$$\mathbf{G}' = \frac{1}{\mu q} \begin{bmatrix} A\dfrac{1 - H^4 - 4qhH^2}{2W} & j\dfrac{p}{q}\dfrac{\frac{\mu}{\lambda + \mu}(1 - H^2)^2 + 4q^2h^2H^2}{2W} & 0 \\ -j\dfrac{p}{q}\dfrac{\frac{\mu}{\lambda + \mu}(1 - H^2)^2 + 4q^2h^2H^2}{2W} & A\dfrac{1 - H^4 + 4qhH^2}{2W} & 0 \\ 0 & 0 & \dfrac{1 + H^2}{1 - H^2} \end{bmatrix} \tag{12}$$

$$\mathbf{f}'(p) = \frac{\mu q}{2} \mathbf{F}' = H \times \begin{bmatrix} A\dfrac{1 - H^2 - qh(1 + H^2)}{2W} & -jphA\dfrac{1 - H^2}{2W} & 0 \\ -jphA\dfrac{1 - H^2}{2W} & A\dfrac{1 - H^2 + qh(1 + H^2)}{2W} & 0 \\ 0 & 0 & \dfrac{1}{1 - H^2} \end{bmatrix} \tag{13}$$

and

$$A = \frac{\lambda + 2\mu}{\lambda + \mu}, \quad H = e^{-qh}, \; q = |p|$$

$$W = (1 - H^2)^2 - 4q^2h^2H^2.$$

We will also need the above relations for certain values of the wave number p, namely for $p \to \infty$ and for $p \to 0$. In the later case we introduce parameter $e = (qh)^{-1}$. We obtain

$$\mathbf{g}'(\infty) = \begin{bmatrix} A/2 & 0 & 0 \\ 0 & A/2 & 0 \\ 0 & 0 & 1 \end{bmatrix}, \quad \mathbf{g}'(0) = \begin{bmatrix} Ae & 0 & 0 \\ 0 & 3Ae^3 & 0 \\ 0 & 0 & e \end{bmatrix}$$

Downloaded 03 May 2010 to 171.66.16.20. Redistribution subject to ASME license or copyright; see http://www.asme.org/terms/Terms_Use.cfm

$$\mathbf{G}'(0)=\frac{1}{\mu q}\begin{bmatrix} Ae & j\frac{3}{2}e^2A\frac{p}{q} & 0 \\ -j\frac{3}{2}e^2A\frac{p}{q} & 3Ae^3 & 0 \\ 0 & 0 & e \end{bmatrix},$$

$$\mathbf{f}'(0)=\frac{1}{2}\begin{bmatrix} -\frac{1}{2}Ae & -j\frac{3}{2}e^2A\frac{p}{q} & 0 \\ -j\frac{3}{2}e^2A\frac{p}{q} & 3Ae^3 & 0 \\ 0 & 0 & e \end{bmatrix}. \quad (14)$$

In order to obtain the corresponding quantities in the original system of coordinates one must apply

$$\mathbf{u}'=\mathbf{cu},\ \mathbf{T}'=\mathbf{cT},\ \mathbf{c}^{-1}=\mathbf{c}^T.$$

Ultimately we obtain the solution of the boundary problem formulated at the beginning of this section. Below, it is presented after introducing yet another function $j(\partial/\partial x)\Delta\mathbf{u}(x,z)=\mathbf{v}\exp(-j\mathbf{px})$

$$\mathbf{v}=p_x\Delta\mathbf{u}=-\frac{1}{\mu}C_p\mathbf{g}(\mathbf{p})\mathbf{T}+\frac{1}{\mu}C_p\mathbf{f}(\mathbf{p})\mathbf{t}^o$$
$$\bar{\mathbf{u}}=\mathbf{G}(\mathbf{p})\mathbf{T}+\mathbf{v}/p_x \quad (15)$$

where

$$\mathbf{g}=\mathbf{c}^T\mathbf{g}'\mathbf{c},\ \mathbf{G}=\mathbf{c}^T\mathbf{G}'\mathbf{c},\ \mathbf{f}=\mathbf{c}^T\mathbf{f}'\mathbf{c},$$
$$p=q=\sqrt{p_x^2+p_z^2},\ C_p=p_x/q. \quad (16)$$

Note that, due to the dependence of $\mathbf{c}$ on both p_x and p_z, shown explicitly in Eq. (5), all the foregoing functions also depend on $\mathbf{p}=(p_x, 0, p_z)$.

It results from Eqs. (14), (16) taken for $p_x\to\pm\infty$ that

$$\mathbf{g}(p_x\pm\to\infty, p_z)=\mathbf{g}_\infty=\mathbf{c}^T\mathbf{g}'(\infty)\mathbf{c}$$
$$\bar{\mathbf{g}}=\mathbf{g}(\mathbf{p})\mathbf{g}_\infty^{-}=\mathbf{c}^T\mathbf{g}'(p)\mathbf{g}_\infty'^{-1}\mathbf{c}=\mathbf{c}^t\bar{\mathbf{g}}'(p)\mathbf{c} \quad (17)$$

where

$$\bar{\mathbf{g}}'(p)=\begin{bmatrix} \frac{1-H^4-4qhH^2}{W} & 0 & 0 \\ 0 & \frac{1-H^4+4qhH^2}{W} & 0 \\ 0 & 0 & \frac{1+H^2}{1-H^2} \end{bmatrix}. \quad (18)$$

It is worth noting that

$$\bar{\mathbf{g}}(p_x\to\pm\infty, p_z)=\bar{\mathbf{g}}'(\infty)=\mathbf{I},\ \bar{\mathbf{g}}'(0)=\begin{bmatrix} 2e & 0 & 0 \\ 0 & 6e^3 & 0 \\ 0 & 0 & e \end{bmatrix} \quad (19)$$

where $\mathbf{I}$ is identity matrix. In what follows we will assume that $\bar{\mathbf{g}}(\mathbf{p})=\bar{\mathbf{g}}(\infty)$ if $\|\mathbf{p}\|>p_\infty$, where p_∞ is chosen sufficiently large.

A Method of Solution

Equations (19) allows the considered boundary problem to be formulated at the $y=0$ plane only

$$\mathbf{T}(x,z)=\begin{cases}=0, \text{ on cracks,} & (l-1)\Lambda+w<x<l\Lambda-w \\ \neq 0, \text{ between cracks,} & l\Lambda-w<x<l\Lambda+w\end{cases} \quad (20)$$

correspondingly to the first condition in Eqs. (3), and

$$\frac{\partial}{\partial x}\Delta\mathbf{u}(x,z)=j\mathbf{v}(x,z)$$
$$=\begin{cases}\neq 0, \text{ on cracks,} & (l-1)\Lambda+w<x<l\Lambda-w \\ =0, \text{ between cracks,} & l\Lambda-w<x<l\Lambda+w\end{cases} \quad (21)$$

together with

$$\Delta\mathbf{u}(l\Lambda,z)=-j\int\mathbf{v}(x,z)dx=0,\ l=0,\pm1,\ldots \quad (22)$$

gives a sufficient condition for perfect contact between two plates in the area between cracks at $y=0$.

In Eqs. (4), the applied traction $\mathbf{t}^o$ on the surface $y=h$ is harmonic function with wave numbers p_x and p_z in the x and z directions correspondingly. It will be convenient to represent p_x as $p_x=r+JK$, where $0<r<K$ and $K=2\pi/\Lambda$ is the wave number of periodic system of cracks considered. For convenience, we introduce notation $p_z=s$ which is considered constant in this paper. Thus the applied traction is

$$\mathbf{t}^o e^{-j(r+JK)x-jsz}. \quad (23)$$

The dependence of the mechanical fields, stress, and particle displacement on z is the same as of the applied traction, that is $\exp(-jsz)$. There is periodic system of cracks thus, on the strength of Floquet theorem, we apply the following Fourier expansion for $\mathbf{v}(x, z)$ and $\mathbf{T}(x, z)$:

$$\mathbf{v}(x,z)=\sum_{k=-\infty}^{\infty}\mathbf{v}_k e^{-j(r+kK)x}e^{-jsz}$$
$$\mathbf{T}(x,z)=\sum_{k=-\infty}^{\infty}\mathbf{t}_k e^{-j(r+kK)x}e^{-jsz} \quad (24)$$

where the spatial harmonics $\mathbf{v}_k$ and $\mathbf{t}_k$ depend on one another as described by Eqs. (15) evaluated for $\mathbf{p}=(r+kK, 0, s)$. We have

$$\mathbf{v}_k=\frac{1}{\mu}C_k[-\mathbf{g}(r+kK, s)\mathbf{t}_k+\mathbf{f}(r+kK, s)\mathbf{t}^o\delta_{kJ}],$$
$$C_k=\frac{r+kK}{\sqrt{(r+kK)^2+s^2}} \quad (25)$$

where δ_{kJ} is Kroenecker delta.

Note, that approximately $\mathbf{g}(\mathbf{p})=\mathbf{g}(\infty)$ if $|p_x|>p_\infty$. Thus, for any k satisfying the inequalities $r+kK<-p_\infty$ and $r+kK>p_\infty$, Eqs. (25) yield

$$\mathbf{v}_k=-\frac{1}{\mu}S_k\mathbf{g}_\infty\mathbf{t}_k,\ S_k=k/|k|=\pm1, \quad (26)$$

provided that $k\neq J$. There are an infinite number of equations.

It is a consequence of the applied solution (24) that, if the boundary conditions are fulfilled in one period of x, they will be fulfilled for any $x\in(-\infty, \infty)$ so that we can consider $-\Lambda/2<x<\Lambda/2$ only. As required by the boundary conditions (20), (21), the functions $\mathbf{T}(x, z)$ and $\mathbf{v}(x, z)$ must vanish of the adjoining areas in the domain $-\Lambda/2<x<\Lambda/2$, they are also expected to have square-root singularities at the crack edges. In the Appendix, a complementary pair of functions is presented which has such properties, thus applying the expansion ($S_\nu=1$ for $\nu\geq0$ and -1 otherwise)

$$\mathbf{t}_k=\mu\sum_m\mathbf{a}^{(m)}P_{k-m}(\cos\Delta)$$
$$\mathbf{v}_k=\sum_m S_{k-m}\mathbf{b}^{(m)}P_{k-m}(\cos\Delta) \quad (27)$$

where $\Delta=Kw$, we not only satisfy Eqs. (20), (21), but also include the required square-root singularities to the solution for mechanical fields. In the above expansion we assume m to take values in some large, but finite limits, $N\leq m\leq M+1$, $N\leq0$, $M\geq0$. We also assume that $J\in[N, M]$ (see Eq. (23)), and $r+(N-1)K<-p_\infty$ and $r+(M+1)K>p_\infty$.

Let us apply Eqs. (26) to the above expansion for $\mathbf{t}_k$ and $\mathbf{v}_k$. We obtain, that for $0<r<K$ as assumed before, and for any k in infinite regions $-\infty<k<N$ and $M<k<\infty$, the following relation takes place independently on m in the above-mentioned limits

Downloaded 03 May 2010 to 171.66.16.20. Redistribution subject to ASME license or copyright; see http://www.asme.org/terms/Terms_Use.cfm

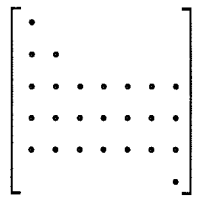
$$\mathbf{b}^{(m)} = -\mathbf{g}_\infty \mathbf{a}^{(m)}. \tag{28}$$

In the remaining domain of k, that is for $N \le k \le M$, $C_k \mathbf{g}(r+kK, s) \neq S_k \mathbf{g}_\infty$ and Eqs. (25) yield

$$\sum_{m=N}^{M+1} [S_{k-m}\mathbf{I} - C_k \bar{\mathbf{g}}(r+kK, s)]\mathbf{b}^{(m)} P_{k-m}(\Delta) = \frac{1}{\mu} C_k \mathbf{f}(r+kK, s)\mathbf{t}^o \delta_{kJ} \tag{29}$$

which is a set of $M-N+1$ equations for $M-N+2$ unknowns $\mathbf{b}^{(m)}$ (C_k is defined in Eqs. (25)).

It is easy to note ($\bar{\mathbf{g}}(r+kK, s) \to \mathbf{I}$ and $C_k \to S_k = S_{k-m}$ for large $|k|$, $k<N$ or $k>M$ and $N \le m \le M+1$) that the matrix of Eqs. (29) has the form



In the above example we can choose $N+2$ and $M-1$ instead of N and M, if only J still remains in the new limits. The advantage of the applied method which was first presented by Blotekjaer et al. (1973) in analysis of certain electrostatic problem is that the limits for m and k are usually narrow, so there is not a very large system of Eqs. (29) to handle. This is a result of the chosen expansion (27) that properly models the mechanical field at the plane of cracks, accounting for its square-root singularities.

The additional condition for particle displacements Eqs. (22) will be satisfied if we apply

$$\Delta \mathbf{u}(0, z) = \sum_{k=-\infty}^{\infty} \frac{1}{r+kK} \mathbf{v}_k = 0$$

that yields (Appendix)

$$\sum_{m=N}^{M+1} (-1)^m \mathbf{b}^{(m)} P_{-\nu-m}(-\cos\Delta) = 0 \tag{30}$$

where $\nu = r/K$. Equations (29) and (30) are set of linear inhomogeneous equations sufficient for evaluation of all unknowns $\mathbf{a}^{(m)} = -\mathbf{g}_\infty^{-1}\mathbf{b}^{(m)}$ and $\mathbf{b}^{(m)}$ as dependent on $\mathbf{t}^o$. In conclusion of this section, let us note that Eq. (19), which is asymptotic property of the Green's function of a plate, is essential for the method of solution we have presented.

The mechanical field, for example the particle displacement at the $y=0$ plane, can be evaluated from the foregoing relations. The average sinusoidal displacement, having the same wave vector $\mathbf{p} = (r+JK, 0, s)$ as the applied traction $\mathbf{t}^o$, can be determined with the help of Eqs. (15), explicitly

$$\bar{\mathbf{u}}(x, z) = [\mathbf{G}(\mathbf{p})\mathbf{t}_J + \mathbf{v}_J/p_x]\exp(-j\mathbf{p}\mathbf{x}). \tag{31}$$

Examples, Thin Plate With Dense Slots

In the sample calculations that will be presented as follows, we will consider a plate, thin in comparison to a wavelength of the applied traction ($qh \ll$ will be assumed). Another simplifying assumption is that the period of cracks is considerably smaller than the plate thickness (this is the assumption of dense cracks, $Kh \gg 1$). These two assumptions allow us to obtain closed solutions with relative ease.

Two cases will be considered. In the first one the harmonic "wave" of applied traction has wave vector $\mathbf{p} = (r, 0, 0)$ that is perpendicular to cracks. This is a two-dimensional case, fully independent of the z-axis. Closed cracks will also be discussed. In the second case, the traction wave the vector is $\mathbf{p} = (0, 0, s)$, that is along the cracks. The applied traction has only one component t_y^o which is nonzero. The solution for $\bar{u}_y$ will be presented. In these examples, we use $\lambda = 0$, $E = 2\mu$, $A = 2$, $\bar{\mathbf{g}} = \mathbf{I}$ and as a result $\mathbf{b}^{(m)} = -\mathbf{a}^{(m)}$.

Before considering the layered plate with cracks, let us apply Eqs. (9) to evaluate the displacement $u_y = u_y^-$ of a thin uniform plate subjected to a surface traction T_{yy}. Applying $\mathbf{p} = (p, 0, 0)$, $p \to 0$, we obtain $G_{22} = G'_{22}$, and thus based on Eqs. (14) we obtain

$$u_y(x) = \frac{6}{\mu q}\left(\frac{1}{qh}\right)^3 T_{yy} e^{-jpx}, \quad q = |p|.$$

This can be rewritten as

$$EI \frac{d^4}{dx^4} u_y(x) = T_{yy}(x) \tag{32}$$

where $I = h^3/12$, and we exploited the formal relation $d/dx = -jp$. The above equation is the known equation for an elastic beam (plate). In summary for p small or for h small as compared to $2\pi/p$, which is the period of the applied sinusoidal traction, $\exp(-qh) \to 1$, and Eqs. (9) gives the known equation for a thin elastic plate.

- Case $\mathbf{p} = (r, 0, 0)$.

In this case $C_p = S_p = p_x/q = (r+kK)/|r+kK| = S_k = \pm 1$, for $0 < r < K$. Moreover, $\bar{\mathbf{g}} = \mathbf{g}'$ and $J = 0$. Following the assumptions of a thin plate $rh \ll 1$ and dense cracks $Kh \gg 1$, we can choose $N = M = 0$ in Eqs. (29), which thus become

$$(\mathbf{I} - \mathbf{g}'(0))\mathbf{b}^{(0)} P_0(\cos\Delta) + (-\mathbf{I} - \mathbf{g}'(0))\mathbf{b}^{(1)} P_{-1}(\cos\Delta) = \frac{1}{\mu}\mathbf{f}'(0)[0, t_y^o, 0]^T.$$

Taking into account that with these approximations $\mathbf{v}_0 = \mathbf{b}^{(0)} - \mathbf{b}^{(1)}$, $\mathbf{t}_0 = -\mu(\mathbf{b}^{(0)} + \mathbf{b}^{(1)})$, and $P_\nu(-\cos\Delta) = 1 + B\nu$, $\nu = r/K$ (see Appendix), we can rewrite the previous equation and Eqs. (30) in the following form:

$$\mathbf{v}_0 + \frac{1}{\mu}\begin{bmatrix} 2e & 0 & 0 \\ 0 & 6e^3 & 0 \\ 0 & 0 & e \end{bmatrix}\mathbf{t}_0 = \frac{1}{E}\begin{bmatrix} -j3e^2 \\ 6e^3 \\ 0 \end{bmatrix} t_y^o$$

$$\mathbf{v}_0 + B\frac{\nu}{\mu}\mathbf{t}_0 = 0.$$

The solution is ($\mathbf{t}_0 = (t_x, t_y, t_z)$, similarly $\mathbf{v}_0$)

$$t_x = -j\frac{3}{4} e \frac{t_y^o}{1 - B\nu/(2e)}, \quad t_y = \frac{1}{2}\frac{t_y^o}{1 - B\nu/(6e^3)}, \quad t_z = 0$$

$$v_x = j\frac{3}{2} e \frac{B\nu t_y^o/E}{1 - B\nu/(2e)}, \quad v_y = -\frac{B\nu t_y^o/E}{1 - B\nu/(6e^3)}, \quad v_z = 0$$

which substituted into Eq. (31) finally gives

$$\bar{u}_y = \frac{1}{rE}\left(-\frac{9e^3/2}{1 - B\nu/(2e)} + \frac{6e^2}{1 - B\nu/(6e^3)}\right) t_y^o - \frac{1}{rE}\frac{B\nu}{1 - B\nu/(6e^3)} t_y^o. \tag{33}$$

Let us consider two particular cases.

For $B\nu \approx 0$, that is for $\cos\Delta \approx -1$ (narrow cracks, $w/\Lambda \approx 1$), $r/K \approx 0$, or for $rh \approx 0$, we obtain

$$\bar{u}_y \approx \frac{3}{2}\frac{e^3}{E} t_y^o$$

that can be rewritten in equation for "thin" plate which is $2h$ thick ($I = (2h)^3/12 = 2/3\ h^3$)

$$EI \frac{d^4}{dx^4}\bar{u}(x) = t_y^o e^{-jrx}.$$

This is the "homogenized" equation for a plate in this case.

For $B \to -\infty$, what happens if $\cos\Delta \to 1$ (wide cracks), we obtain $t_x \approx t_y \approx 0$, and

$$\bar{u}_y = (u_y^+ + u_y^-)/2 \approx \frac{v_y}{r} = (u_y^+ - u_y^-)/2 = 3e^3 \frac{t_y^o}{\mu r}.$$

Downloaded 03 May 2010 to 171.66.16.20. Redistribution subject to ASME license or copyright; see http://www.asme.org/terms/Terms_Use.cfm

In this case we obtain Eq. (32), which is exactly the equation for the h-thick plate. That is because the lower plate does not work in this case as $\mathbf{t}_0 \to 0$ and $\bar{u_y} = 0$.

Let us now consider briefly the case of closed cracks, $\Delta u_y = 0$. Equations (15) yield

$$\Delta u_y \sim -6e^3 T_{yy} + 6e^3 t_y^o = 0.$$

That is $T_{yy} = t_y^o/2$, thus $t_y = t_y^o/2$. From Eqs. (29) and (30), applied to the x-components of the corresponding vectors, we get

$$v_x + 2e\frac{1}{\mu} t_x = -j3e_2 t_y^o/E, \quad v_x + B\nu t_x/\mu = 0.$$

Finally, we obtain ($\bar{u}_y = G_{21} t_x + G_{22} t_y$)

$$\bar{u}_y = \frac{1}{r}\left(-\frac{9e^3/2}{1 - B\nu/(2e)} + 6e^3\right) t_y^o/E. \tag{34}$$

This yields

$$\bar{u}_y = \frac{3}{2r} e^3 t_y^o/E, \text{ for } B \to 0$$

and

$$\bar{u}_y = \frac{1}{r} 6e^3 t_y^o/E, \text{ for } B \to -\infty, \text{ or } rh \to 0$$

which are identical results to those presented above for open cracks.

- Case $r \to 0$, $s \approx 0$, $e = (sh)^{-1}$

There is ($p = \sqrt{r^2 + s^2} \to s > 0$)

$$\mathbf{c} = \begin{bmatrix} r/p & 0 & s/p \\ 0 & 1 & 0 \\ -s/p & 0 & r/p \end{bmatrix} \to \begin{bmatrix} 0 & 0 & 1 \\ 0 & 1 & 0 \\ -1 & 0 & 0 \end{bmatrix}$$

$$\mathbf{g} = \mathbf{c}^T \mathbf{g}' \mathbf{c}, \; \bar{\mathbf{g}}(0) = \begin{bmatrix} e & 0 & 0 \\ 0 & 6e^3 & 0 \\ 0 & 0 & 2e \end{bmatrix},$$

and

$$\mathbf{G}(0) = \frac{1}{\mu q}\begin{bmatrix} e & 0 & 0 \\ 0 & 6e^3 & -j3e^2 \\ 0 & j3e^2 & 2e \end{bmatrix}, \quad \mathbf{f}(0) = \frac{1}{2}\begin{bmatrix} e & 0 & 0 \\ 0 & 6e^3 & -j3e^2 \\ 0 & -j3e^2 & -e \end{bmatrix}.$$

Equation (30) yields

$$\mathbf{v}_0 = -B\nu \mathbf{t}_0/\mu$$

when substituted into Eqs. (29) gives

$$\begin{bmatrix} \frac{r}{p} e - B\nu & 0 & 0 \\ 0 & \frac{r}{p} 6e^3 - B\nu & 0 \\ 0 & 0 & \frac{r}{p} 2e - B\nu \end{bmatrix} \mathbf{t}_0 = \frac{1}{2}\frac{r}{p}\begin{bmatrix} 0 \\ 6e^3 \\ -j3e^2 \end{bmatrix} t_y^o,$$

the solution for which is straightforward. In the foregoing relations $\nu = r/K \to 0$, but $B\nu p/r = Bs/K = B\nu' = \text{const} \neq 0$ in the considered case. We thus obtain ($\nu' = s/K$)

$$\bar{u}_y = \frac{1}{sE}\left(\frac{6e^3}{1 - B\nu'/(6e^3)} - \frac{9e^3/2}{1 - B\nu'/(2e)} - \frac{B\nu'}{1 - B\nu'/(6e^3)}\right) t_y^o \tag{35}$$

where is the same relation as obtained previously for case $s = 0$, if only we substitute ν' for ν.

Conclusion

Equations (33)–(35) can be transformed into differential equations for $\bar{u}_y(x)$ in a similar way to that applied to obtain Eq. (32). These will be the homogenized equations for plates with periodic debondings. We see that higher derivatives (up to the tenth order in the case of Eqs. (33) and (35), or up to sixth order in the case of Eq. (34)) of $\bar{u}_y$ will be involved in these equations. This is not an unexpected result as we consider two plates with some elastic constraints between them.

The method presented in this paper for analyzing an elastic body with in-plane periodic cracks can be applied also in the case of an anisotropic body. Corresponding equations may not be, however, as simple as Eqs. (6)–(13). Another possible application of the method concerns a multilayered body, with cracks between the layers having different periods and orientations. A generalization of the method to dynamical cases is presented by Danicki (1992).

Acknowledgment

The author wishes to express his deep gratitude to Prof. William D. Hunt of Georgia Institute of Technology for his editorial comments with regard to the paper style and grammar. The author is also indebted to an anonymous reviewer for valuable comments and correction of typographical errors in the manuscript.

This work was supported by the Polish National Scientific Committee, Grant 3 1212 9101.

References

Bløtekjaer, K., Ingebrigtsen, K. A., and Skeie, H., 1973, "A Method for Analyzing Waves in Structures Consisting of Metal Strips on Dispersive Media," *IEEE Transactions*, Vol. ED-20, pp. 1133–1138.

Danicki, E., 1991, "Analysis of Surface Acoustic Wave in a Layered Structure with Periodic Delamination," *Physical Acoustics, Fundamentals and Applications*, O. Leroy and M. A. Breazeale, eds., Plenum Press, New York, pp. 281–285.

Danicki, E., 1992, "A Method for Analysis EM-wave Scattering by Periodic Strips," *Journal of Technical Physics*, Vol. 33, pp. 375–399.

Erdélyi, A., Magnus, W., Oberhettinger, F., and Tricomi, F. G., 1953, *Higher Transcendental Functions*, Vol. 1, McGraw-Hill, New York, Chapter 3, pp. 146–149.

Thurston, R., 1964, "Wave Propagation in Liquids and Solids," *Physical Acoustics*, Vol. 1A, W. P. Mason, ed., Academic Press, New York, Chapter 1.

APPENDIX

In this paper we exploit the following identity for a certain square-root singular and periodic function with period 2π given by Erdélyi et al. (1953) (it is assumed that $0 < \theta < \pi$ and $\text{Re}\{\mu\} < 1/2$):

$$\Gamma\left(\frac{1}{2} - \mu\right) \sum_{n=0}^{\infty} P_n^{\mu}(\cos\theta) \cos\left(n + \frac{1}{2}\right) v = \begin{cases} \dfrac{(\pi/2)^{1/2} \sin^{\mu}\theta}{(\cos v - \cos\theta)^{\mu + 1/2}}; & 0 \leq v < \theta \\ 0; & \theta < v < \pi \end{cases} \tag{36}$$

where P is the Legendre function, $P_{\nu} = P_{\nu}^0$,

$$P_{-\nu-1}^{\mu} = P_{\nu}^{\mu}; \text{ and } P_n(-x) = (-1)^n P_n(x), \text{ for } n \geq 0. \tag{37}$$

Equations (25) can be rewritten as follows for $-\pi < \theta < \pi$, $0 < \Delta < \pi$ (see Blotekjaer, 1973, for details):

$$\sum_{n=-\infty}^{\infty} \alpha_m P_{n-m}(\cos\Delta) e^{-jn\theta} = \begin{cases} \sqrt{2}\, \dfrac{\alpha_m \exp(-jm\theta)}{\sqrt{\cos\theta - \cos\Delta}} e^{j\theta/2}; & |\theta| < \Delta \\ 0; & \Delta < |\theta| < \pi \end{cases} \tag{38}$$

and (apply $\Delta \to \pi - \Delta$ and $\theta \to \pi - \theta$)

Downloaded 03 May 2010 to 171.66.16.20. Redistribution subject to ASME license or copyright; see http://www.asme.org/terms/Terms_Use.cfm

$$\sum_{n=-\infty}^{\infty} \beta_m S_{n-m} P_{n-m}(\cos\Delta) e^{-jn\theta} = \begin{cases} 0; & |\theta| < \Delta \\ -jS_\theta \sqrt{2}\, \dfrac{\beta_m \exp(-jm\theta)}{\sqrt{\cos\Delta - \cos\theta}}\, e^{j\theta/2}; & \Delta < |\theta| < \pi \end{cases} \tag{39}$$

where $S_\nu = 1$ for $\nu \geq 0$, and -1 otherwise, α_m and β_m are arbitrary constants.

As it can be easily noticed, the foregoing pair of functions allows us to model any periodic function, vanishing in one domain of the period, and having square-root singularities at the edges of the other domain, provided that the function is smooth enough to be represented by a finite Fourier series $\exp(-jm\theta)$ (see numerators above).

Useful identities resulting from Dougall's expansion (see Erdélyi et al., 1953) are

$$P_{-\nu}(-\cos\Delta) = \frac{\sin\pi\nu}{\pi} \sum_{n=-\infty}^{\infty} \frac{S_n P_n(\cos\Delta)}{\nu + n}$$

$$P_{-\nu}(\cos\Delta) = \frac{\sin\pi\nu}{\pi} \sum_{n=-\infty}^{\infty} \frac{(-1)^n P_n(\cos\Delta)}{\nu + n}, \tag{40}$$

the first of which was applied in evaluation of the series leading to Eqs. (30). There are also the following approximations valid for $0 < \nu \ll 1$ and $\cos\Delta \approx 1$:

$$P_\nu(0) = \frac{1}{\pi} \frac{\Gamma\left(\frac{1}{2} + \frac{\nu}{2}\right)}{\Gamma\left(1 + \frac{\nu}{2}\right)} \cos\left(\frac{\pi}{2}\nu\right) \approx 1 - \frac{\nu}{2}\ln 2$$

$$P_\nu(-\cos\Delta) \approx 1 + \nu \ln\frac{1-\cos\Delta}{2}. \tag{41}$$

Downloaded 03 May 2010 to 171.66.16.20. Redistribution subject to ASME license or copyright; see http://www.asme.org/terms/Terms_Use.cfm

W. Q. Zhu[1]

T. T. Soong

Department of Civil Engineering,
State University of New York,
Buffalo, NY 14260

Y. Lei

Department of Architectural Engineering,
Shantou University,
Shantou, Guangdong, China

Equivalent Nonlinear System Method for Stochastically Excited Hamiltonian Systems

An equivalent nonlinear system method is presented to obtain the approximate probability density for the stationary response of multi-degree-of-freedom nonlinear Hamiltonian systems to Gaussian white noise parametric and/or external excitations. The equivalent nonlinear systems are obtained on the basis of one of the following three criteria: least mean-squared deficiency of damping forces, dissipation energy balancing, and least mean-squared deficiency of dissipation energies. An example is given to illustrate the application and validity of the method and the differences in the three equivalence criteria.

1 Introduction

A relatively newly developed approximate approach to predicting stochastic response of nonlinear systems is the so-called equivalent nonlinear system method (Soong and Grigoriu, 1992; Zhu, 1992). The basic idea of the method is to replace a given nonlinear stochastic system with another nonlinear stochastic system whose behavior is close to the original one in some statistical sense and whose exact stationary solution is obtainable. The idea was originally suggested by Caughey about two decades ago and applied to particular problems by Lutes (1970) and Kirk (1974). In 1986, Caughey (1986) published his method of equivalent nonlinear equation for a class of oscillators with linear stiffness and nonlinear damping subject to Gaussian white noise external excitation. Later, Caughey's technique was verified by Lin (1988) using digital simulation and generalized to include systems with both nonlinear damping and nonlinear stiffness. Recently, it was further generalized by To and Li (1991) to include the case of stochastically parametric excitation.

At the same time, an equivalent nonlinear system method for stochastically parametrically and (or) externally excited nonlinear conservative systems was proposed by Zhu and Yu (1989) based on the equivalence of averaged total energies of the original and equivalent systems. An approximate technique to obtain the probability density for the stationary response of a nonlinear oscillator under Gaussian white noise parametric and (or) external excitations was presented by Cai and Lin (1988b) on the basis of the equivalence of averaged energy dissipations of the original and substitutive systems.

Recently, an equivalent statistical quadratization method was developed by Donley and Spanos (1990) and Spanos and Donley (1991, 1992). It is another version of the equivalent nonlinear system method which is different from the above mentioned versions in that the exact stationary solution for the equivalent quadratic system is usually not obtainable.

It is interesting to note that, for a given nonlinear stochastic system, different equivalence criteria may lead to the same result. It has been shown (Hennig and Roberts, 1986) that, in the case of Gaussian white noise external excitation, Caughey's technique, the dissipation energy balancing technique, and the stochastic averaging method (Roberts and Spanos, 1986; Zhu, 1988) lead to the same result. It has also been shown (Zhu and Yu, 1989; Zhu and Lin, 1991) that the equivalent nonlinear system method (Zhu and Yu, 1989) and the dissipation energy balancing technique (Cai and Lin, 1988b) yield the same stationary joint probability density for the displacement and velocity as that obtained from the stochastic averaging of energy envelope (Zhu and Lin, 1991) for stochastically parametrically and (or) externally excited nonlinear systems.

The equivalent nonlinear system method can be considered as a generalization of equivalent linearization (Spanos, 1981; Roberts and Spanos, 1990; Socha and Soong, 1992). Compared with equivalent linearization, the equivalent nonlinear system method has a remarkable advantage. That is, it may be applicable to systems which are strongly nonlinear and whose responses are essentially non-Gaussian. The method is specially useful for systems which may exhibit essential nonlinear phenomena such as limit cycle and parametric excitation (Cai and Lin, 1988b; Zhu and Yu, 1989), etc.

A prerequisite for developing an equivalent nonlinear system technique is the availability of the exact stationary solutions for some classes of nonlinear stochastic systems. The various versions (Caughey, 1986; Cai and Lin, 1988b; Zhu and Yu, 1989) of the equivalent nonlinear system method developed so far are for one-degree-of-freedom nonlinear stochastic systems. Recently, the exact stationary solutions have been obtained for a class of stochastically excited multiple-degree-of-

[1]Present address: Department of Mechanics, Zhejiang University, Hangzhou 310027, China.

Contributed by the Applied Mechanics Division of THE AMERICAN SOCIETY OF MECHANICAL ENGINEERS for publication in the ASME JOURNAL OF APPLIED MECHANICS.

Discussion on this paper should be addressed to the Technical Editor, Professor Lewis T. Wheeler, Department of Mechanical Engineering, University of Houston, Houston, TX 77204-4792, and will be accepted until four months after final publication of the paper itself in the ASME JOURNAL OF APPLIED MECHANICS.

Manuscript received by the ASME Applied Mechanics Division, Sept. 4, 1992; final revision, May 12, 1993. Associate Technical Editor: P. D. Spanos.

Copyright © 1994 by ASME

Downloaded 03 May 2010 to 171.66.16.20. Redistribution subject to ASME license or copyright; see http://www.asme.org/terms/Terms_Use.cfm

freedom dissipative Hamiltonian systems (Zhu, Cai and Lin, 1990, 1992; Soize, 1991). Thus, it is possible to develop an equivalent nonlinear system technique for a class of similar nonlinear stochastic systems whose exact stationary solutions are not obtainable.

In the present paper, the equivalent nonlinear system method for stochastically excited Hamiltonian systems is formulated on the basis of three different equivalence criteria. The validity of the method and the differences in the three equivalence criteria are examined via an example.

2 Exact Stationary Solutions

Consider an n-degree-of-freedom stochastically excited Hamiltonian system governed by the following equations of motion:

$$\dot{Q} = \nabla_P H$$

$$\dot{P} = -\nabla_Q H - f(H) M \nabla_P H + g(H)\sigma W(t) \tag{1}$$

where $Q = [Q_1 Q_2 \dots Q_n]^T$ and $P = [P_1 P_2 \dots P_n]^T$ are generalized displacement vector and generalized momentum vector, respectively;

$$\nabla_Q = \left[\frac{\partial}{\partial Q_1}\frac{\partial}{\partial Q_2}\cdots\frac{\partial}{\partial Q_N}\right]^T \text{ and } \nabla_P = \left[\frac{\partial}{\partial P_1}\frac{\partial}{\partial P_2}\cdots\frac{\partial}{\partial P_n}\right]^T$$

are vectors of gradient operators; $H = H(Q, P)$ is a Hamiltonian with continuous second-order derivatives; $f(H)$ and $g(H)$ are once and twice differentiable functions, respectively; M is an $n \times n$ matrix with elements $m_{ij} = m_{ij}(Q, P)$ which are differentiable functions; σ is an $n \times m$ matrix with elements $\sigma_{ik} = \sigma_{ik}(Q, P)$ which are twice differentiable functions; $W(t)$ is an m-dimensional vector of Gaussian white noises in the sense of Stratonovich with correlation matrix

$$E[W(t)W^T(t+\tau)] = 2D\delta(\tau) = 2\pi S\delta(\tau) \tag{2}$$

in which $2D$ and S are $m \times m$ constant intensity matrix and spectral density matrix of $W(t)$, respectively.

The system governed by Eq. (1) is generally nonlinear. The first term on the right-hand side of the second equation represents a set of linear and/or nonlinear damping mechanisms while the second term may include both external (additive) and parametric (multiplicative) stochastic excitations. This system is called a stochastically excited Hamiltonian system.

The diffusion matrix of the Fokker-Planck equation associated with Eq. (1) is g^2B with $B = 2\sigma D\sigma^T$. To provide for additional flexibility in obtaining an exact stationary solution to the reduced Fokker-Planck equation, matrix B with elements b_{ij} is split (Cai and Lin, 1988a) into two parts $B^{(1)}$ and $B^{(2)}$ with elements $b_{ij}^{(i)}$ and $b_{ji}^{(j)}$, respectively, i.e., $B = B^{(1)} + B^{(2)}$ or $b_{ij} = b_{ij}^{(i)} + b_{ji}^{(j)}$. Note that this split retains the symmetry condition for the diffusion matrix g^2B.

It has been shown by solving the reduced Fokker-Planck equation for Eq. (1) (Zhu, Cai, and Lin, 1990, 1992) that the exact stationary solution for Eq. (1) can be obtained under the following conditions:

1 If g is a constant, m_{ij} and σ_{ik} are functions of Q only, and

$$M = \eta B^{(1)} \tag{3}$$

or

$$M + M^T = \eta B \tag{4}$$

then the exact stationary probability density of the response of the system is

$$p_s(q, p) = C \exp\left[-\frac{\eta}{g^2}\int_0^H f(u)du\right]\Bigg|_{H=H(q,p)} \tag{5}$$

where C is a normalizing constant.

2 If g is a function of H, m_{ij}, and σ_{ik} are functions of Q only, and

$$M = M^T = (\eta/2)B \tag{6}$$

then the exact stationary probability density of the response of the system is

$$p_s(q, p) = Cg^{-1}(H) \exp\left[-\eta\int_0^H \frac{f(u)}{g^2(u)}du\right]\Bigg|_{H=H(q,p)}. \tag{7}$$

Exact stationary solutions have also been obtained for a more general class of systems, which include Eq. (1) as a special case (Zhu, Cai and Lin, 1990, 1992). Several examples were also given in (Zhu, Cai and Lin, 1990, 1992) to illustrate the aforementioned exact stationary solutions.

3 Equivalent Nonlinear System Method

Equations (3), (4), and (6) are usually severe restrictive and hardly satisfied by most engineering systems. For a given system of the form similar to Eq. (1), however, it may be possible to find an equivalent nonlinear system which has an exact stationary solution and whose behavior is close to the original one in some statistical sense.

Suppose we are given an n-degree-of-freedom stochastically excited Hamiltonian system whose equations of motion are of the form

$$\dot{Q} = \nabla_P H$$

$$\dot{P} = -\nabla_Q H - C\nabla_P + g(H)\sigma W(t) \tag{8}$$

where Q, P, H, $g(H)$, σ, and $W(t)$ are the same as those in Eq. (1); C is a matrix with elements $c_{ij} = c_{ij}(Q, P)$ which are differentiable functions. Assume that none of conditions (3), (4), and (6) is satisfied by Eq. (8). Our purpose is to find an equivalent nonlinear system for Eq. (8).

First consider the case where matrix C is not symmetrical and g is a constant. Let $g = 1$. Obviously, if there exists an $\lambda(H)$ such that

$$C = \lambda(H)B^{(1)} \tag{9}$$

then the system, Eq. (8), possesses the exact stationary probability density

$$p_s(q, p) = C \exp\left[-\int_0^H \lambda(u)du\right]\Bigg|_{H=H(q,p)}. \tag{10}$$

However, the condition, Eq. (9), is actually not satisfied. The difference between Eq. (8) and the one having exact stationary solution is in the damping forces and can be expressed as a vector

$$\epsilon = (C - \lambda(H)B^{(1)})\nabla_P H. \tag{11}$$

Once $\lambda(H)$ is found based on some criterion, an equivalent nonlinear system is found and Eq. (10) can be regarded as the approximate stationary probability density for the given system, Eq. (8).

There are several possible criteria based on which $\lambda(H)$ is determined. Three of them are presented in the following. The first criterion to find $\lambda(H)$ is to minimize the mean-squared ϵ with respect to $\lambda(H)$, i.e., $E[\epsilon^T\epsilon] = \min$. It means that if $\lambda(H)$ in Eq. (11) is replaced by $\lambda(H) + \mu\eta(H)$, where μ is a constant and $\eta(H)$ is a function of H similar to $\lambda(H)$, then $E[\epsilon^T\epsilon]$, as a function of μ, is minimized by letting $\mu = 0$, i.e.,

$$\frac{\partial}{\partial\mu}E[\epsilon^T\epsilon]\,|_{\mu=0} = 0. \tag{12}$$

Equation (12) is equivalent to $\partial/\partial\lambda\ E[\epsilon^T\epsilon] = 0$, i.e.,

$$\int \nabla_p^T H[C - \lambda(H)B^{(1)}]^T[-B^{(1)}]\nabla_p H p_s(q, p)dqdp = 0 \tag{13}$$

where $p_s(q, p)$ is determined by $\lambda(H)$ according to Eq. (10).

Downloaded 03 May 2010 to 171.66.16.20. Redistribution subject to ASME license or copyright; see http://www.asme.org/terms/Terms_Use.cfm

The multifold integral in Eq. (13) may be simplified by a transformation from $q_1, \ldots, q_n, p_1, \ldots, p_n$ to $q_1, \ldots, q_n, H, p_2, \ldots, p_n$. After the transformation, Eq. (13) is converted to

$$\int_0^\infty p_s(H)dH \int_\Omega (\nabla_p^T H[C-\lambda(H)B^{(1)}]^T[-B^{(1)}] \times \nabla_p H/(\partial H/\partial p_1))dq_1 \ldots dq_n\, dp_2 \ldots dp_n = 0. \quad (14)$$

In Eq. (14), p_1 is replaced by $q_1, \ldots, q_n, p_2 \ldots, p_n, H$ and is the solution of $H = H(q_1 \ldots, q_n, p_1 \ldots p_n)$, and the integration domain Ω is determined by inequality $H(q_1, \ldots, q_n, 0, p_2, \ldots, p_n) \leq H$. Note that q_1 generally has at least two values. Correspondingly, Ω can be divided into at least two domains.

Since $p_s(H)$ is unknown, to proceed further Eq. (14) is replaced by a more restrictive sufficient condition requiring that the integration on $q_1, \ldots, q_n, p_2, \ldots, p_n$ vanishes for every H. This condition leads to an expression for $\lambda(H)$, i.e.,

$$\lambda(H) = \frac{\int_\Omega (\nabla_p^T HC^T B^{(1)} \nabla_p H/(\partial H/\partial p_1))dq_1 \ldots dq_n\, dp_2 \ldots dp_n}{\int_\Omega (\nabla_p^T HB^{(1)T} B^{(1)} \nabla_p H/(\partial h/\partial p_1))dq_1 \ldots dq_n\, dp_2 \ldots dp_n} \quad (15)$$

where $p_1 = p_1(q_1, \ldots, q_n, p_2, \ldots, p_n, H)$.

The second criterion to find $\lambda(H)$ is to make the deficiency of dissipation energies vanish in the original system and equivalent system, i.e.,

$$E[\nabla_p^T H\epsilon] = 0. \quad (16)$$

Then similar derivation as that used in going from Eq. (12) to Eq. (15) leads to

$$\lambda(H) = \frac{\int_\Omega (\nabla_p^T HC \nabla_p H/(\partial H/\partial p_1))dq_1 \ldots dq_n\, dp_2 \ldots dp_n}{\int_\Omega (\nabla_p^T HB^{(1)} \nabla_p H/(\partial H/\partial p_1))dq_1 \ldots dq_n\, dp_2 \ldots dp_n}. \quad (17)$$

The third criterion to find $\lambda(H)$ is to minimize the mean-squared deficiency of the dissipation energies in the original and equivalent systems, i.e.,

$$E[(\nabla_p^T H\epsilon)^2] = \min. \quad (18)$$

Similar derivation loads to

$$\lambda(H) = \frac{\int_\Omega (\nabla_p^T HC \nabla_p H \nabla_p^T HB^{(1)} \nabla_p H/(\partial H/\partial p_1))dq_1 \ldots dq_n\, dp_2 \ldots dp_n}{\int_\Omega (\nabla_p^T HB^{(1)} \nabla_p^T HB^{(1)} \nabla_p H/(\partial H/\partial p_1))dq_1 \ldots dq_n\, dp_2 \ldots dp_n}. \quad (19)$$

Now consider the case where C is symmetrical and g is a function of H. Obviously, if there is an $\lambda(H)$ such that

$$C = C^T = \frac{1}{2}\lambda(H)B \quad (20)$$

then the system, Eq. (8), possesses the exact stationary probability density

$$p_s(q, p) = Cg^{-1}(H) \exp\left[-\int_0^H \frac{\lambda(u)}{g^2(u)}\,du\right]\Bigg|_{H=H(q,p)}. \quad (21)$$

On the other hand, if we find an $\lambda(H)$ according to Eqs. (15), (17), or (19) with $B^{(1)}$ replaced by $B/2$, then Eq. (21) can be regarded as the approximate stationary probability density for the given system, Eq. (8).

The above procedure can be further extended to a more general class of systems, which includes Eq. (8) as a special case. The equivalent systems for this class of systems may be chosen from the class of systems given by Zhu, Cai, and Lin (1990, 1992).

4 Example of Application

As an example of the application of the equivalent nonlinear system method developed in the last section, consider two linearly and nonlinearly coupled van der Pol oscillators subject to Gaussian white noise parametric excitations. The equation of motion of the system is of the form

$$\ddot{X} - \lambda_1\dot{X} + \alpha_1 X^2\dot{X} + \omega_1^2 X + aY + b(X-Y)^3 = c_1 XW_1(t)$$
$$\ddot{Y} - (\lambda_1 - \lambda_2)\dot{Y} + \alpha_2 Y^2\dot{Y} + \omega_2^2 Y + aX + b(Y-X)^3 = c_2 YW_2(t) \quad (22)$$

where λ_1, λ_2, α_1, α_2, ω_1, ω_2, a, b, c_1 and c_2 are constants; $W_1(t)$ and $W_2(t)$ are uncorrelated Gaussian white noises with spectral densities S_1 and S_2, respectively. This system has been studied by To and Lin (1989) using the stochastic averaging method for the case of light damping, weak coupling and excitation. The results obtained by them are for the two uncoupled van der Pol oscillators subject to uncorrelated Gaussian white noise parametric excitations. In fact, the same results can be obtained by using the stochastic averaging of energy envelope (Zhu and Lin, 1991) or the dissipation energy balancing technique (Cai and Lin, 1988b) for one-degree-of-freedom nonlinear stochastic systems.

The Hamiltonian of system (22) is the total energy

$$H = \frac{1}{2}\dot{X}^2 + \frac{1}{2}\dot{Y}^2 + U(X, Y) \quad (23)$$

where

$$U(X, Y) = \frac{1}{2}\omega_1^2 X^2 + \frac{1}{2}\omega_2^2 Y^2 + aXY + \frac{1}{4}b(X-Y)^4 \quad (24)$$

is the potential energy of the two coupled oscillators. The equivalent nonlinear system for system (22) is of the form

$$\ddot{X} + \lambda(H)b_{11}\dot{X} + \frac{\partial U}{\partial X} = C_1 XW_1(t)$$
$$\ddot{Y} + \lambda(H)b_{22}\dot{Y} + \frac{\partial U}{\partial Y} = C_2 YW_2(t) \quad (25)$$

where

$$b_{11} = 2c_1^2 X^2 \pi S_1, \quad b_{22} = 2c_2^2 Y^2 \pi S_2. \quad (26)$$

It is easy to rewrite Eqs. (22) and (25) in the forms of Eqs. (1) and (8), respectively. System (25) possesses the exact stationary joint probability density of the displacements and velocities

$$p_s(x, y, \dot{x}, \dot{y}) = c \exp\left[-\int_0^H \lambda(u)du\right]\Bigg|_{H=H(x,y,\dot{x},\dot{y})} \quad (27)$$

where c is a normalizing constant, H is defined by Eq. (23) and $\lambda(H)$ is to be determined.

Based on the criterion of least mean-squared deficiency of damping forces, according to Eq. (15),

$$\lambda(H) = \frac{\int_\Omega \{(-\lambda_1 + \alpha_1 x^2)b_{11}\dot{x} + [-(\lambda_1 - \lambda_2) + \alpha_2 y^2]b_{22}\dot{y}^2/\dot{x}\}\,|_{\dot{x}=\pm\sqrt{2H-2U(x,y)-\dot{y}^2}}\,dxdyd\dot{y}}{\int_\Omega (b_{11}\dot{x} + b_{22}\dot{y})(b_{11} + b_{22}\dot{y}/\dot{x})\,|_{\dot{x}=\pm\sqrt{2H-2U(x,y)-\dot{y}^2}}\,dxdyd\dot{y}} \quad (28)$$

and Ω is a three-dimensional domain which satisfies the following inequality:

$$\dot{y}^2/2 + U(x, y) \leq H. \quad (29)$$

Downloaded 03 May 2010 to 171.66.16.20. Redistribution subject to ASME license or copyright; see http://www.asme.org/terms/Terms_Use.cfm

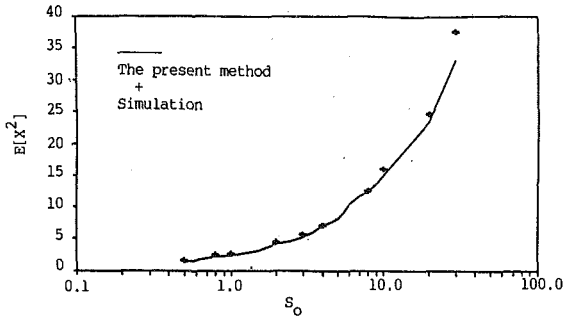


Fig. 1 Variance $E[X^2]$ of stationary response of system (22) based on criterion of least mean-squared deficiency of damping forces. $\lambda_1 = \lambda_2 = 0.01$, $\alpha_1 = 0.01$, $\alpha_2 = 0.02$, $\omega_2 = 1.0$, $\omega_2 = 2.0$, $a = 0.01$, $b = 1.0$, $c_1 = c_2 = 0.2$, $S_1 = S_2 = S_0$.

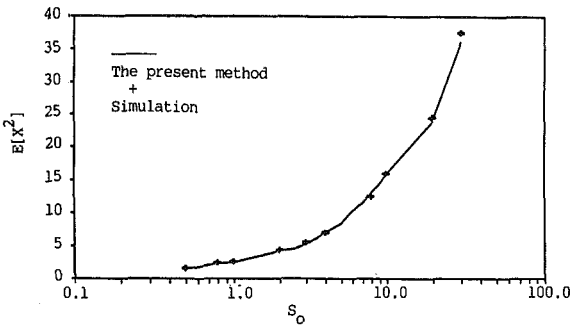


Fig. 2 Variance $E[X^2]$ of stationary response of system (22) based on dissipation energy balancing criterion. The parameters are the same as in Fig. 1.

The function $\lambda(H)$ can also be obtained based on the dissipation energy balancing criterion. Instead of Eq. (28), $\lambda(H)$ in this case is

$$\lambda(H)=\frac{2\int_\Omega (e_1/\dot{x})\,|_{\dot{x}=\pm\sqrt{2H-2U(x,y)-\dot{y}^2}}dxdyd\dot{y}}{\int_\Omega (b_{11}\dot{x}+b_{22}\dot{y}^2/\dot{x})\,|_{\dot{x}=\pm\sqrt{2H-2U(x,y)-\dot{y}^2}}dxdyd\dot{y}} \tag{30}$$

where

$$e_1=-\lambda_1\dot{x}^2+\alpha_1 x^2\dot{x}^2-(\lambda_1-\lambda_2)\dot{y}^2+\alpha_2 y^2\dot{y}^2. \tag{31}$$

On the basis of least mean-squared deficiency of dissipation energies, instead of Eq. (28), $\lambda(H)$ is

$$\lambda(H)=\frac{2\int_\Omega e_1(b_{11}\dot{x}+b_{22}\dot{y}^2/\dot{x})\,|_{\dot{x}=\pm\sqrt{2H-2U(x,y)-\dot{y}^2}}dxdyd\dot{y}}{\int_\Omega (b_{11}\dot{x}^2+b_{22}\dot{y}^2)(b_{11}\dot{x}+b_{22}\dot{y}^2/\dot{x})\,|_{\dot{x}=\pm\sqrt{2H-2U(x,y)-\dot{y}^2}}dxdyd\dot{y}}. \tag{32}$$

Completing the integration in Eq. (28), (30), or (32) (see Appendix A) and substituting the resultant $\lambda(H)$ into Eq. (27), one obtains the approximate stationary probability density $p_s(x, y, \dot{x}, \dot{y})$ for the original system (22), from which all the approximate statistical information with regard to the stationary response of system (22) can be obtained.

For example, the mean-squared displacement of X may be computed from

$$E[X^2]=c\int x^2 p_s(x, y, \dot{x}, \dot{y})dxdyd\dot{x}d\dot{y} \tag{33}$$

which can be transformed into

$$E[X^2]=c\int_0^\infty \rho(h)dh\int_\Omega \frac{x^2}{\pm\sqrt{2h-2U(x, y)-\dot{y}^2}}dxdyd\dot{y} \tag{34}$$

where

$$\rho(h)=\exp\left(-\int_0^h \lambda(u)du\right). \tag{35}$$

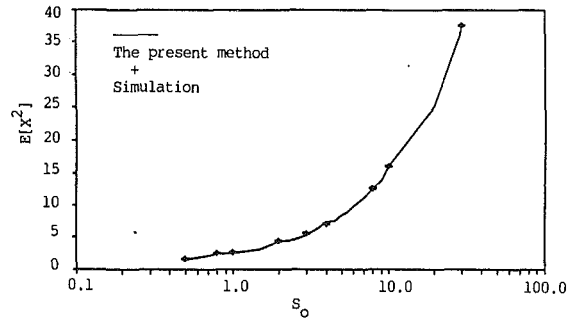


Fig. 3 Variance $E[X^2]$ of stationary response of system (22) based on criterion of least mean-squared deficiency of dissipation energies. The parameters are the same as in Fig. 1.

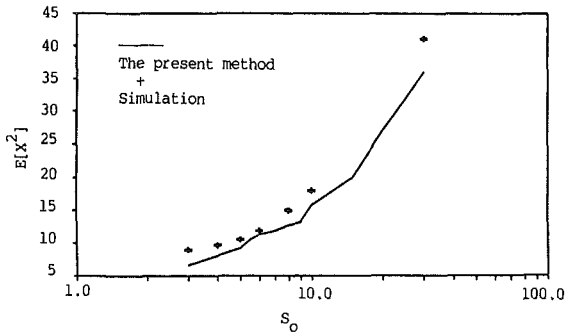


Fig. 4 Variance $E[X^2]$ of stationary response of system (22) based on criterion of least mean-squared deficiency of damping forces. $\lambda_1 = \lambda_2 = 0.05$; the other parameters are the same as in Fig. 1.

Completing the integration in Eq. (34) with respect to $\dot{y}$, Eq. (34) is reduced to

$$E[X^2]=2\pi c\int_0^\infty \rho(h)dh\int_{\Omega_1} x^2dxdy \tag{36}$$

where the integration domain Ω_1 is determined by the inequality

$$U(x, y)\le h. \tag{37}$$

Some numerical results for the stationary variance $E[X^2]$ of system (22) obtained by using the present method based on the three different criteria, i.e., least mean-squared deficiency of damping forces, dissipation energy balancing, and least mean-squared deficiency of dissipation energy, are shown in Figs. 1-7. Results from digital simulation are also shown in these figures for comparison. Similar results for $E[\dot{X}^2]$, $E[Y^2]$, $E[\dot{Y}^2]$, and $E[XY]$ have also been obtained. It is seen from Figs. 1-3 that, for small values of λ_1 and λ_2, the present method yields excellent results for $S_1 = S_2 = S_0 \ge 0.5$ and no great differences exist among the results based on three different criteria. For larger values of λ_1 and λ_2, it is seen from Figs. 4-6 that the present method still yields quite good results for stronger excitations, i.e., $S_1 = S_2 = S_0 \ge 5.0$. In this case, the results from the criteria based on dissipation energy consideration are better than those from the criterion based on least mean-squared deficiency of damping forces, especially for $E[\dot{X}^2]$ and $E[\dot{Y}^2]$. The results shown in Fig. 7 indicate that the present method yields better results for stronger nonlinear coupling between the two van der Pol oscillators.

5 Concluding Remarks

In the present paper, an equivalent nonlinear system method

Downloaded 03 May 2010 to 171.66.16.20. Redistribution subject to ASME license or copyright; see http://www.asme.org/terms/Terms_Use.cfm

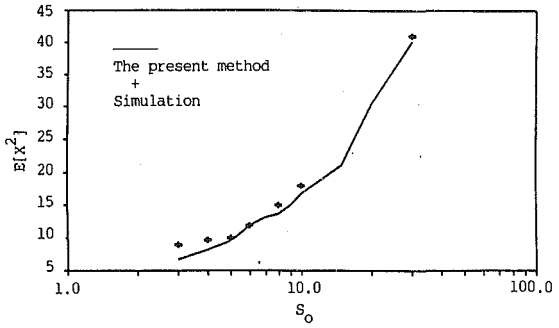


Fig. 5 Variance $E[X^2]$ of stationary response of system (22) based on dissipation energy balance criterion. The parameters are the same as in Fig. 4.

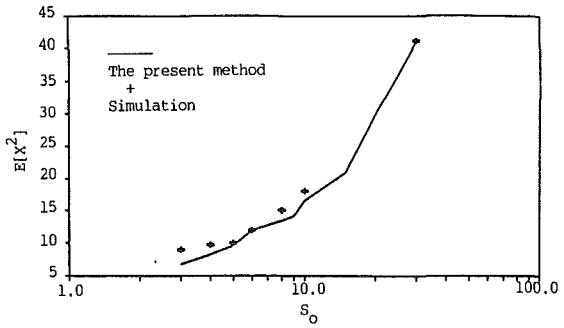


Fig. 6 Variance $E[X^2]$ of stationary response of system (22) based on criterion of least mean-squared deficiency of dissipation energies. The parameters are the same as in Fig. 4.

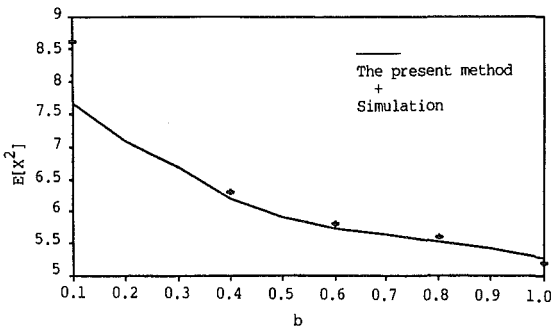


Fig. 7 Variance $E[X^2]$ of stationary response of system (22) based on criterion of least mean-squared deficiency of damping forces. $S_0 = 3.0$; the other parameters are the same as in Fig. 1.

is proposed to obtain the approximate probability density for the stationary response of multi-degree-of-freedom nonlinear Hamiltonian systems under Gaussian white noise parametric and/or external excitations. In this method the original nonlinear system is replaced by an equivalent nonlinear system whose behavior is close to the original one in some statistical sense and for which the exact stationary solution is obtainable. The equivalent nonlinear system is obtained on the basis of one of three criteria: least mean-squared deficiency of damping forces, dissipation energy balancing, and least mean-squared deficiency of dissipation energies. Numerical integration is usually required but the computation is simple and straightforward. The comparisons of the results given by the present method with those from digital simulation for two linearly and nonlinearly coupled van der Pol oscillators subject to uncorrelated Gaussian white noise parametric excitations indicate that the proposed method provides a feasible procedure for solving random vibration problems involving strongly coupled multi-degree-of-freedom nonlinear systems under Gaussian white noise parameter and (or) external excitations.

Acknowledgment

The authors thank Mr. C. D. Huang for reprinting the figures in the present paper.

References

Cai, G. Q., and Lin, Y. K., 1988a, "On Exact Stationary Solutions of Equivalent Non-Linear Stochastic Systems," *International Journal of Non-Linear Mechanics*, Vol. 23, pp. 315–325.

Cai, G. Q., and Lin, Y. K., 1988b, "A New Approximate Solution Technique for Randomly Excited Nonlinear Oscillators," *International Journal of Non-Linear Mechanics*, Vol. 23, pp. 409–420.

Caughey, T. K., 1986, "On Response of Nonlinear Oscillators to Stochastic Excitation," *Probabilistic Engineering Mechanics*, Vol. 1, pp. 2–4.

Donley, M. G., and Spanos, P. D., 1990, *Dynamic Analysis of Non-Linear Structures by the Method of Statistical Quadratization* (Lecture Notes in Engineering), Springer-Verlag, Berlin.

Hennig, K., and Roberts, J. B., 1986, "Averaging Method for Randomly Excited Non-Linear Oscillators," *Random Vibration: Status and Recent Developments*, I. Elishakoff and R. H. Lyon, eds., Elsevier, Amsterdam.

Kirk, C. L., 1974, "Application of the Fokker-Planck Equation to Random Vibration of Non-Linear Systems," *Cranfield Report Aero*, No. 20, Cranfield Institute of Technology, United Kingdom.

Lin, A., 1988, "A Numerical Evaluation of the Method of Equivalent Nonlinearization," Ph.D. Thesis, California Institute of Technology, Pasadena, CA.

Lutes, L. D., 1970, "Approximate Technique for Treating Random Vibration of Hysteretic Systems," *Journal of Acoustical Society of America*, Vol. 48, pp. 299–306.

Roberts, J. B., and Spanos, P. D., 1986, "Stochastic Averaging: An Approximate Method of Solving Random Vibration Problems," *International Journal of Non-Linear Mechanics*, Vol. 21, pp. 111–134.

Roberts, J. B., and Spanos, P. D., 1990, *Random Vibration and Statistical Linearization*, John Wiley and Sons, New York.

Socha, L., and Soong, T. T., 1991, "Linearization in Analysis of Nonlinear Stochastic Systems," ASME *Applied Mechanics Review*, Vol. 44, pp. 399–422.

Soize, C., 1991, "Exact Stationary Response of Multi-Dimensional Non-Linear Hamiltonian Dynamical Systems under Parametric and External Stochastic Excitations," *Journal of Sound and Vibration*, Vol. 149, pp. 1–24.

Soong, T. T., and Grigoriu, M., 1992, *Random Vibration in Mechanical and Structurarl Systems*, Prentice-Hall, Englewood Cliffs, NJ.

Spanos, P. D., 1981, "Stochastic Linearization in Structural Dynamics," ASME *Applied Mechanics Review*, Vol. 34, pp. 1–8.

Spanos, P. D., and Donley, M. G., 1991, "Equivalent Statistical Quadratization for Nonlinear Systems," *ASCE Journal of Engineering Mechanics*, Vol. 117, pp. 1289–1310.

Spanos, P. D., and Donley, M. G., 1992, "Non-Linear Multi-Degree-of-Freedom System Random Vibration by Equivalent Statistical Quadratization," *International Journal of Non-Linear Mechanics*, Vol. 27, pp. 735–748.

To, C. W. S., and Li, D. M., 1991, "Equivalent Nonlinearization of Nonlinear Systems to Random Excitations," *Probabilistic Engineering Mechanics*, Vol. 6, pp. 184–192.

To, C. W. S., and Lin, R., 1989, "Bifurcation in a Stochastically Disturbed Nonlinear Two-Degree-of-Freedom System," *Structural Safety*, Vol. 6, pp. 223–231.

Zhu, W. Q., 1988, "Stochastic Averaging Methods in Random Vibration," ASME *Applied Mechanics Review*, Vol. 41, pp. 189–199.

Zhu, W. Q., 1992, *Random Vibration*, Science Press, Beijing, China (in Chinese).

Zhu, W. Q., Cai, G. Q., and Lin, Y. K., 1990, "On Exact Stationary Solutions of Stochastically Perturbed Hamiltonian Systems," *Probabilistic Engineering Mechanics*, Vol. 5, pp. 84–87.

Zhu, W. Q., Cai, G. Q., and Lin, Y. K., 1992, "Stochastically Excited Hamiltonian Systems," *Nonlinear Stochastic Mechanics*, N. Bellomo, and F. Casciati, eds., Springer-Verlag, Berlin.

Zhu, W. Q., and Lin, Y. K., 1991, "Stochastic Averaging of Energy Envelope," *ASCE Journal of Engineering Mechanics*, Vol. 117, pp. 1890–1905.

Zhu, W. Q., and Yu, J. S., 1989, "The Equivalent Non-Linear System Method," *Journal of Sound and Vibration*, Vol. 129, pp. 385–395.

APPENDIX

Threefold integrals in Eqs. (28), (30), (32), and (36) can be reduced to three singlefold integrals by introducing polar coordinates

$$x = r\cos\theta$$

$$y = r\sin\theta. \tag{A1}$$

For example, Eq. (28) can be rewritten as

Downloaded 03 May 2010 to 171.66.16.20. Redistribution subject to ASME license or copyright; see http://www.asme.org/terms/Terms_Use.cfm

$$\lambda(H)=\frac{2\int_0^{2\pi}d\theta\int_0^{r(\theta)}rdr\int_{-\sqrt{2H-2U(r,\theta)}}^{\sqrt{2H-2U(r,\theta)}}\{(-\lambda_1+\alpha_1x^2)b_{11}\dot{x}+[-(\lambda_1-\lambda_2)+d_2y^2]b_{22}\dot{y}^2/\dot{x}\}|_{\dot{x}=\pm\sqrt{2H-2U(r,\theta)-\dot{y}^2}}d\dot{y}}{\int_0^{2\pi}d\theta\int_0^{r(\theta)}rdr\int_{-\sqrt{2H-2U(r,\theta)}}^{\sqrt{2H-2U(r,\theta)}}(b_{11}\dot{x}+b_{22}\dot{y})(b_{11}+b_{22}\dot{y}/\dot{x})|_{\dot{x}=\pm\sqrt{2H-2U(r,\theta)-\dot{y}^2}}d\dot{y}} \tag{A2}$$

where $r(\theta)$ is the root of equation

$$U(r,\theta)=H \tag{A3}$$

i.e.,

$$\frac{1}{2}\omega_1^2r^2\cos^2\theta+\frac{1}{2}\omega_2^2r^2\sin^2\theta+ar^2\sin\theta\cos\theta+\frac{br^4}{4}(\cos\theta-\sin\theta)^4=H. \tag{A4}$$

Using the transformation (A1), Eq. (36) can be further rewritten as

$$E[X^2]=2\pi c\int_0^{\infty}\rho(h)dh\int_0^{\pi}d\theta\int_{r_1}^{r_2}r^3\cos^2\theta dr \tag{A5}$$

where r_1 and r_2 are the two roots of equation

$$U(r,\theta)=h. \tag{A6}$$

Similarly, the normalizing constant c may be determined from

$$1=2\pi c\int_0^{\infty}\rho(h)dh\int_0^{\pi}d\theta\int_{r_1}^{r_2}rdr. \tag{A7}$$

Downloaded 03 May 2010 to 171.66.16.20. Redistribution subject to ASME license or copyright; see http://www.asme.org/terms/Terms_Use.cfm

An Inverse Mode Problem for the Continuous Model of an Axially Vibrating Rod

Y. M. Ram
Department of Mechanical Engineering,
University of Adelaide,
GPO Box 498,
Adelaide 5001, Australia

An inverse mode problem for the continuous model of an axially vibrating rod is formulated and solved. It is shown that the density and axial rigidity functions are determined by two eigenvalues, their corresponding eigenfunctions, and the total mass of the rod. The necessary and sufficient conditions for the construction of a physically realizable rod with positive parameters are given. It is shown that when these conditions are satisfied, the solution is unique. Since the data required for the construction may be available from measurements, the presented approach is well-suited for modal analysis applications.

1 Introduction

The problem of reconstructing the continuous variations in axial rigidity $r(x)$ and density $\rho(x)$ of a longitudinally vibrating rod is considered. The reconstruction is based on the knowledge of only two eigenvalues, together with their corresponding eigenfunctions and the total mass of the rod. The necessary and sufficient conditions required for the construction of a physically realizable rod, with positive rigidity and density functions, are derived. It is further shown that if these conditions are satisfied the resulting realizable solution is unique. These results are presented in Section 2.

An inverse mode problem for the discrete finite difference model of a vibrating rod has been studied by Gladwell (1986b). In a recent paper, Ram and Gladwell (1993) have investigated the associated problem of reconstructing the *discrete* finite element model of an axial vibrating rod, fixed at one end and free at the other. They have shown that the mass and stiffness matrices, which are both tridiagonal, may be reconstructed from one eigenvalue, two eigenvectors and the total mass of the rod. In Section 3 we show that when the rod is subject to fixed-free boundary conditions, the *continuous* model is similarly determined by a single eigenvalue, two eigenfunctions, and the total mass of the rod.

The subject of inverse problems for vibrating systems is covered in the book by Gladwell (1986a) *Inverse Problems in Vibration*. Gladwell and Gbadeyan (1985) have shown that a simply connected mass-spring system, fixed at one end and free at the other end, may be reconstructed uniquely from two spectral sequences and the total mass of the system. These results are also applicable to the construction of a discrete finite difference model of the nonuniform axially vibrating rod, where two sets of spectral data, corresponding to the fixed-fixed and fixed-free boundary conditions, determine the model uniquely. Ram and Caldwell (1992) have shown that the physical parameters of a free multiconnected mass-spring system may be determined from certain spectral data as well. The problem of constructing the physical parameters of a multi-dimensional mass-spring lattice from eigenvalue data has been recently posed and solved by Gladwell and Zhu (1992). Barcilon (1976, 1972, 1982) has shown that the discrete mass-spring-rod model associated with the transversely vibrating beam can be reconstructed from three spectral sequences associated with three different boundary conditions. The necessary and sufficient conditions applicable to the spectral data to permit the construction of a realizable beam have been derived by Gladwell (1984). The classical inverse problem of the continuous model of the axial vibrating rod is associated with the inverse Sturm-Liouville problem. The inverse Sturm-Liouville problem has been studied by Levinson (1949), Hald (1978), Levitan (1968), and Hochstadet (1973, 1975). Their main results, associated with the vibrating rod, are expounded by Gladwell (1986a).

It should be noted that the novel inverse mode problem studied here differs from the classical inverse problem of the continuous rod in two main aspects:

(a) The construction here is mainly based on eigenfunctions, whereas the classical approach constructs the parameters of the rod from eigenvalues, and

(b) in the classical inverse problem it is assumed that the cross-sectional area of the rod is variable, while the Young's modulus of elasticity and the rod density are constants. In the present analysis we allow the cross-sectional area, the Young's modulus of elasticity, and the density of the rod to be variable functions of the axial position x.

The low-frequency eigenvalues and their corresponding mode shapes for a vibrating structure may be measured by using model analysis techniques. Thus the data required for the construction of the physical properties are readily available from measurements. On the contrary, the classical approach constructs the model from a large number of natural frequencies. Since the high-frequency eigenvalues cannot be determined

Contributed by the Applied Mechanics Division of THE AMERICAN SOCIETY OF MECHANICAL ENGINEERS for publication in the ASME JOURNAL OF APPLIED MECHANICS.

Discussion on this paper should be addressed to the Technical Editor, Professor Lewis T. Wheeler, Department of Mechanical Engineering, University of Houston, Houston, TX 77204-4792, and will be accepted until four months after final publication of the paper itself in the ASME JOURNAL OF APPLIED MECHANICS.

Manuscript received by the ASME Applied Mechanics Division, Sept. 21, 1992; final revision, Apr. 5, 1993. Associate Technical Editor: D. J. Inman.

Copyright © 1994 by ASME
Downloaded 03 May 2010 to 171.66.16.20. Redistribution subject to ASME license or copyright; see http://www.asme.org/terms/Terms_Use.cfm

accurately by available measurement techniques, the data required by the classical approach is difficult to obtain. As a result, the present method lends itself naturally to the use of modal analysis data. The actual application is demonstrated in Section 4.

2 Main Results

The equation of motion governing the infinitesimal longitudinal oscillations $u(x, t)$ of a rod is

$$\frac{\partial}{\partial x}\left(r\frac{\partial u}{\partial x}\right)=\rho\frac{\partial^2 u}{\partial t^2},\quad 0<x<L,\ t>0 \tag{1a}$$

where $r(x)>0$ and $\rho(x)>0$ are the axial rigidity and the rod mass per unit length, respectively. For the purpose of the analysis we assume that r and ρ are continuous differentiable functions in the closed interval $0\le x\le L$, and that r and its derivatives of all order are bounded there. If the rod is supported by two springs of constants k_0 and k_L at its ends $x=0$ and $x=L$, respectively, then the boundary conditions have the form

$$\alpha_0 u(0, t)-\beta_0\frac{\partial u(0, t)}{\partial x}=0$$

and

$$\alpha_L u(L, t)+\beta_L\frac{\partial u(L, t)}{\partial x}=0. \tag{1b}$$

When the rod is not fixed at its ends; i.e., $\beta_0\neq 0$ and $\beta_L\neq 0$, then $k_0=\alpha_0 r(0)/\beta_0$ and $k_L=\alpha_L r(L)/\beta_L$.

For harmonic motion with frequency ω expressed by

$$u(x, t)=v(x)\sin(\omega t-\phi), \tag{2}$$

the following eigenvalue system is obtained:

$$\begin{cases}\dfrac{d}{dx}\left(r\dfrac{dv}{dx}\right)+\lambda\rho v=0,\quad \lambda\equiv\omega^2,\quad 0<x<L;\\[2ex] \alpha_0 v(0)-\beta_0\dfrac{\partial v(0)}{\partial x}=0\\[2ex] \alpha_L v(L)+\beta_L\dfrac{\partial v(L)}{\partial x}=0.\end{cases} \tag{3}$$

Let λ_1 and λ_2 be two eigenvalues of Eq. (3) with corresponding eigenfunctions $v_1(x)$ and $v_2(x)$, respectively. Then for λ_1 and v_1 Eq. (3) yields

$$r'v_1'+rv_1''+\lambda_1\rho v_1=0,\quad 0<x<L \tag{4a}$$

and, similarly, for λ_2 and v_2 we have

$$r'v_2'+rv_2''+\lambda_2\rho v_2=0,\quad 0<x<L \tag{4b}$$

where primes denote derivatives with respect to x. Multiplying Eqs. (4a) and (4b) by $\lambda_2 v_2$ and $\lambda_1 v_1$, respectively, the following equations are determined:

$$\lambda_2 v_2(r'v_1'+rv_1'')+\lambda_1\lambda_2\rho v_1 v_2=0,\quad 0<x<L \tag{5a}$$

and

$$\lambda_2 v_1(r'v_2'+rv_2'')+\lambda_1\lambda_2\rho v_1 v_2=0,\quad 0<x<L. \tag{5b}$$

Subtracting Eq. (5b) from (5a) results in

$$r'+\psi(x)r=0 \tag{6}$$

where

$$\psi(x)=\frac{\lambda_2 v_1''-\lambda_1 v_1 v_2''}{\lambda_2 v_1 v_1'-\lambda_1 v_1 v_2'},\quad 0<x<L; \tag{7}$$

provided that $\lambda_2 v_1 v_1'-\lambda_1 v_1 v_2'\neq 0$ for $0<x<L$. With the assumption that r and its derivatives are bounded in $[0, L]$, it is found (Appendix) that if ψ is unbounded at a particular value $\xi\in(0, L)$ then $r(\xi)=0$. It follows therefore that $\psi(x)$ must be finite for all arguments $x\in(0, L)$.

The first-order linear differential Eq. (6) has the solution

$$r(x)=Ce^{-\int^x\psi(\xi)d\xi} \tag{8}$$

where C is a constant of integration. Equation (4a) implies that for points x where $v_1(x)\neq 0$, the density function ρ can be found from

$$\rho=-\frac{r'v_1'+rv_1''}{\lambda_1 v_1}, \tag{9}$$

where limiting values may be obtained for points where $v_1(x)=0$. Hence, by using Eqs. (6) and (8) the density $\rho(x)$ may be written in the form

$$\rho(x)=\frac{C}{\lambda_1 v_1}(\psi v_1'-v_1'')e^{-\int^x\psi(\xi)d\xi}. \tag{10}$$

The axial rigidity $r(x)$ and the mass density $\rho(x)$ may be thus reconstructed, subject to a normalization constant C, from two eigenvalues λ_1, λ_2 and their corresponding eigenfunctions $v_1(x)$, $v_2(x)$, by using Eqs. (7), (8), and (10). If the total mass of the rod $w>0$ is also known, then the positive constant C is determined uniquely from

$$\int_0^L\rho(x)dx=w. \tag{11}$$

The conditions which we have imposed on $r(x)$ and $\rho(x)>0$ imply that the data λ_1, v_1, λ_2, and v_2 are interrelated. Since the natural exponential function is always positive, and $\psi(x)$ is required to be finite at $x\in(0, L)$, the rigidity function obtained from Eqs. (8) and (11) necessarily satisfies $r(x)>0$ for $0>x>L$. Also, since $\rho(x)>0$ for $0\ge x\ge L$ it may be deduced from Eq. (10) that

$$\frac{\psi v_1'-v_1''}{\lambda_1 v_1}>0,\quad 0>x>L \tag{12}$$

is another condition that must be satisfied.

The boundary conditions in Eq. (3) imply the additional constraints $v_1'(0)v_2(0)-v_1(0)v_2'(0)=0$, $v_1'(0)v_1(0)\ge 0$, $v_2'(0)v_2(0)\ge 0$ at one end, and $v_1'(L)v_2(L)-v_1(L)v_2'(L)=0$, $v_1'(L)v_1(L)\le 0$, $v_2'(L)v_2(L)\le 0$ at the other end of the rod. The constants of the supporting springs are thus $k_0=r(0)v_1'(0)/v_1(0)$ and $k_L=-r(L)v_1'(L)/v_1(L)$. Further investigation shows that there are no additional constraints on the construction. We, therefore, conclude that the *necessary and sufficient* conditions to ensure the construction of the rod parameters are

(a) $\psi(x)$ must be finite for all $0<x<L$,
(b) $(\psi v_1'-v_1'')/\lambda_1 v_1>0$ for all arguments $0<x<L$, and
(c) $v_1'(0)v_2(0)-v_1(0)v_2'(0)=0$, $v_1'(0)v_1(0)\ge 0$, $v_2'(0)v_2(0)\ge 0$ and $v_1'(L)v_2(L)-v_1(L)v_2'(L)=0$, $v_1'(L)v_1(L)\le 0$, $v_2'(L)v_2(L)\le 0$.

Moreover, the procedure of construction indicates that if these conditions are satisfied, the resulting solution is unique.

Example 1. Consider the following eigenvalue problem

$$\begin{cases}(e^x v')'+\lambda e^x v=0,\quad 0<x<1,\ t>0\\ v(0)=0\\ v'(1)=0\end{cases}$$

associated with the axial motion of a nonuniform rod, fixed at $x=0$ and free at $x=1$. The natural frequencies of this system are the roots of

$$2\sqrt{\omega_i^2-1/4}=\tan\sqrt{\omega_i^2-1/4}$$

and their corresponding eigenfunctions are given by

$$v_i=e^{-x/2}\sin\sqrt{\omega_i^2-1/4}\,x$$

for $i=1, 2, \ldots$.

Suppose that $\lambda_1=\omega_1^2$, v_1, $\lambda_2=\omega_2^2$, and v_2 are given. Then differentiating v_j w.r.t. x gives

Downloaded 03 May 2010 to 171.66.16.20. Redistribution subject to ASME license or copyright; see http://www.asme.org/terms/Terms_Use.cfm

$$v_j' = -1/2e^{-x/2}\sin\sqrt{\omega_j^2-1/4}\,x + e^{-x/2}\sqrt{\omega_j^2-1/4} \times \cos\sqrt{\omega_j^2-1/4}\,x$$

and

$$v_j'' = 1/2e^{-x/2}\sin\sqrt{\omega_j^2-1/4}\,x - e^{-x/2}\sqrt{\omega_j^2-1/4} \times \cos\sqrt{\omega_j^2-1/4}\,x - e^{-x/2}\omega_j^2\sin\sqrt{\omega_j^2-1/4}\,x$$

for $j=1, 2$.

We recognize that here

$$v_j'' = -(v_j' + \omega_j^2 v_j)$$

which implies

$$\lambda_2 v_2 v_1'' - \lambda_1 v_1 v_2'' = -\omega_2^2 v_2(v_1' + \omega_1^2 v_1) + \omega_1^2 v_1(v_2' + \omega_2^2 v_2) = -\lambda_2 v_2 v_1' + \lambda_1 v_1 v_2'.$$

Equations (7), (8), and (9) therefore yield

$$\psi(x) = -1, \quad 0<x<1,$$
$$r(x) = Ce^x \text{ and}$$
$$\rho(x) = \frac{-Ce^x v_1' + Ce^x(v_1' + \lambda_1 v_1)}{\lambda_1 v_1} = Ce^x,$$

respectively.

At $x=0$ the conditions $v_1'(0)v_2(0) - v_1(0)v_2'(0) = 0$, $v_1'(0)v_1(0) = 0$ and $v_2'(0)v_2(0) = 0$ are obviously satisfied since $v_1(0) = 0 = v_2(0)$. Since the eigenvalues $\lambda_1 = \omega_1^2$ and $\lambda_2 = \omega_2^2$ satisfy

$$2\sqrt{\omega_1^2-1/4} = \tan\sqrt{\omega_1^2-1/4} \text{ and } 2\sqrt{\omega_2^2-1/4} = \tan\sqrt{\omega_2^2-1/4},$$

it follows that

$$\begin{aligned} &v_1'(1)v_2(1) - v_1(1)v_2'(1) \\ &= \sqrt{\omega_1^2-1/4}\cos\sqrt{\omega_1^2-1/4}\sin\sqrt{\omega_2^2-1/4} \\ &\quad - \sin\sqrt{\omega_1^2-1/4}\sqrt{\omega_2^2-1/4}\cos\sqrt{\omega_2^2-1/4} \\ &= 1/2\sin\sqrt{\omega_1^2-1/4}\sin\sqrt{\omega_2^2-1/4} \\ &\quad - 1/2\sin\sqrt{\omega_1^2-1/4}\sin\sqrt{\omega_2^2-1/4} \\ &= 0. \end{aligned}$$

We also have $v_1'(1)v_1(1) = 0 = v_2'(1)v_2(1)$. Hence, the conditions for the construction are fully satisfied.

Example 2. (The hanging cable).

The differential equation with the conditions

$$\begin{cases} \dfrac{\partial}{\partial x}\left(x\dfrac{\partial u}{\partial x}\right) = \dfrac{\partial^2 u}{\partial t^2}, & 0<x<1, \quad t>0 \\ u(1) = 0, \\ u \text{ is bounded in } x \in [0, 1], \end{cases}$$

govern the lateral motion of a flexible cable supported at the upper end and free to oscillate under the influence of a unit gravity field. The natural frequencies ω_i, $i=1, 2, 3, \ldots$, of this system are the roots of the zeroth-order Bessel function $J_0(2\omega_i) = 0$ and their corresponding eigenfunctions are $J_0(2\omega_i\sqrt{x})$.

We note that since the rigidity function approaches zero at the free end, our requirement regarding the positivity of r is not satisfied. Also, the formulation of this problem is different from the problem under consideration, which is defined by Eq. (3). Nevertheless the above results may, with some slight changes, still be employed as the following analysis shows.

Suppose $\lambda_1 = \omega_1^2 = 1.4457965$, $v_1 = J_0(2\omega_1\sqrt{x})$, $\lambda_2 = \omega_2^2 = 7.6178155$, $v_2 = J_0(2\omega_2\sqrt{x})$ and $w=1$ are given. Then differentiation yields

$$v_j' = -\frac{\omega_j}{\sqrt{x}}J_1(2\omega_j\sqrt{x})$$

and

$$v_j'' = \frac{\omega_j}{x\sqrt{x}}J_1(2\omega_j\sqrt{x}) - \frac{\omega_j^2}{z}J_0(2\omega_j\sqrt{x})$$

for $j=1, 2$.

It follows, therefore, that

$$\lambda_2 v_2 v_1'' - \lambda_1 v_1 v_2'' = \frac{\omega_1\omega_2}{x\sqrt{x}}(\omega_2 J_0(2\omega_2\sqrt{x})J_1(2\omega_1\sqrt{x}) - \omega_1 J_0(2\omega_1\sqrt{x})J_1(2\omega_2\sqrt{x}))$$

and

$$\lambda_2 v_2 v_1' - \lambda_1 v_1 v_2' = \frac{\omega_1\omega_2}{\sqrt{x}}(-\omega_2 J_0(2\omega_2\sqrt{x})J_1(2\omega_1\sqrt{x}) + \omega_1 J_0(2\omega_1\sqrt{x})J_1(2\omega_2\sqrt{x})),$$

which imply through Eq. (7) $\psi = -x^{-1}$. The rigidity function may be evaluated from Eq. (8)

$$r(x) = Ce^{-\int x - \xi^{-1}d\xi} = Ce^{\ln(x)} = Cx$$

and by Eq. (9) we have

$$\rho = -\frac{r'v_1' + rv_1''}{\lambda_1 v_1} = -C\frac{-\frac{\omega_1}{\sqrt{x}}J_1(2\omega_1\sqrt{x}) + \frac{\omega_1}{\sqrt{x}}J_1(2\omega_1\sqrt{x}) - \omega_1^2 J_0(2\omega_1\sqrt{x})}{\omega_1^2 J_0(2\omega_1\sqrt{x})} = C.$$

Finally, the assumption that the total mass $w=1$ yields $C=1$. The rigidity and density functions, $r(x) = x$ and $\rho(x) = 1$, have thus been reconstructed.

Since $J_0(2\omega_1) = 0 = J_0(2\omega_2)$, the conditions for the construction at $x=1$ are satisfied. However, at $x=0$, the only condition to be satisfied is that the eigenfunctions and their derivatives are bounded.

The function $\psi(x)$ plays a major role in the present analysis. However, when the rod is either fixed, or free, at one of its boundaries the denominator in Eq. (7) vanishes locally, and consequently ψ is indeterminate when $x \to 0$ or $x \to L$. Attention will be focused in the next section on the rod with fixed-free boundary conditions. A similar analysis may then be applied to other configurations involving either fixed or free-end conditions.

3 The Fixed-Free Configuration

Suppose that the rod is fixed at $x=0$ and free at $x=L$. Then $\beta_0 = 0 = \alpha_L$, $\alpha_0 \neq 0$ and $\beta_L \neq 0$ in this case. The differential equation and boundary conditions are

$$\begin{cases} \dfrac{d}{dx}\left(r\dfrac{dv}{dx}\right) + \lambda\rho v = 0, & 0<x<L \\ v(0) = 0 \\ v'(L) = 0. \end{cases} \tag{13}$$

If $v_1(x)$, $v_2(x)$ and their first two derivatives are continuous bounded functions in $x \in [0, L]$ then it follows from their continuity and the requirements which we have imposed on r and ρ, that Eqs. (4a) and (4b) hold also at the end points $x=0$ and $x=L$. For $x=L$ these equations together with $v_1'(L) = 0 = v_2'(L)$ give

$$\begin{aligned} r(L)v_1''(L) + \lambda_1\rho(L)v_1(L) &= 0 \\ r(L)v_2''(L) + \lambda_2\rho(L)v_2(L) &= 0, \end{aligned} \tag{14}$$

Downloaded 03 May 2010 to 171.66.16.20. Redistribution subject to ASME license or copyright; see http://www.asme.org/terms/Terms_Use.cfm

and, equivalently, we obtain

$$\begin{bmatrix} v_1''(L) & \lambda_1 v_1(L) \\ v_2''(L) & \lambda_2 v_2(L) \end{bmatrix} \begin{pmatrix} r(L) \\ \rho(L) \end{pmatrix} = \begin{pmatrix} 0 \\ 0 \end{pmatrix}. \tag{15}$$

The trivial solution $r(L)=0=\rho(L)$ is not valid. Hence the left-hand side matrix of Eq. (15) must be singular, i.e.,

$$\begin{vmatrix} v_1''(L) & \lambda_1 v_1(L) \\ v_2''(L) & \lambda_2 v_2(L) \end{vmatrix} = 0 \tag{16}$$

which yields

$$\lambda_2 = \lambda_1 \frac{v_1(L) v_2''(L)}{v_1''(L) v_2(L)}. \tag{17}$$

Therefore, as the discrete model analogy indicates in Ram and Gladwell (1993), the functions $r(x)$ and $\rho(x)$ may be reconstructed from two eigenfunctions $v_1(x)$, $v_2(x)$ and a single eigenvalue λ_1.

It has been observed that at the free end the denominator in (7) vanishes. We note that in satisfying Eq. (17) the numerator in Eq. (7) vanishes as well. As a result $\psi(L)$ is not necessarily unbounded at $x=L$.

Consider now the boundary condition at $x=0$. With the previous continuity assumptions we may substitute $v_1(0)=0=v_2(0)$ in Eqs. (4*a*) and (4*b*) and obtain

$$\begin{aligned} r'(0)v_1'(0) + r(0)v_1''(0) &= 0, \\ r'(0)v_2'(0) + r(0)v_2''(0) &= 0. \end{aligned} \tag{18}$$

To avoid the unrealizable trivial solution $r(0)=0=r'(0)$ it is required that

$$\begin{vmatrix} v_1'(0) & v_1''(0) \\ v_2'(0) & v_2''(0) \end{vmatrix} = 0. \tag{19}$$

It follows, therefore, that

$$v_1'(0)v_2''(0) - v_1''(0)v_2''(0) = 0 \tag{20}$$

necessarily holds in this case. The limit of ψ at $x \to 0$ may be determined by L'Hospital's rule. It is noted that if (20) is satisfied then $\psi(0)$ is finite, and vice versa.

For demonstration purposes the following example is presented:

Example 3. Consider the fixed-free uniform rod of length $L=1$, axial rigidity $r(x)=1$, and density $\rho(x)=1$. The natural frequencies of the rod are $\omega_k=(k-1/2)\pi$, and their corresponding eigenfunctions are $\sin(\omega_k x)$; $(k=1, 2, \ldots)$. Suppose that $\lambda_1=((i-1/2)\pi)^2$, $v_1(x)=\sin((i-1/2)\pi x)$, $v_2(x)=\sin((j-1/2)\pi x)$ for $i \neq j$, and the total mass $w=1$ are given. Then we may reconstruct the rod parameters from the given data as follows. From Eq. (17) we have

$$\begin{aligned} \lambda_2 &= ((i-1/2)\pi)^2 \\ &\quad \times \frac{\sin((i-1/2)\pi)(-1)((j-1/2)\pi)^2 \sin((j-1/2)\pi)}{(-1)((i-1/2)\pi)^2 \sin((i-1/2)\pi)\sin((j-1/2)\pi)} \\ &= ((j-1/2)\pi)^2. \end{aligned}$$

Since

$$\begin{aligned} &\lambda_2 v_2 v_1'' - \lambda_1 v_1 v_2'' \\ &= ((j-1/2)\pi)^2 \sin((j-1/2)\pi x)(-1) \\ &\qquad \times ((i-1/2)\pi)^2 \sin((i-1/2)\pi x) \\ &\quad - ((i-1/2)\pi)^2 \sin((i-1/2)\pi x)(-1) \\ &\qquad \times ((j-1/2)\pi)^2 \sin((j-1/2)\pi x) \\ &\equiv 0 \end{aligned}$$

whereas the denominator of Eq. (7) $\lambda_2 v_2 v_1' - \lambda_1 v_1 v_2'$ vanishes only at finite points it follows from L'Hospital's rule that $\psi(x)=0$ for all $0 \le x \le L$. Hence, Eq. (8) gives

$$r(x) = C$$

where C is a constant of integration. Equation (10) reduces in this case to

$$\rho(x) = -\frac{C v_1''}{\lambda_1 v_1} = -\frac{C(-1)((i-1/2)\pi)^2 \sin((i-1/2)\pi x)}{((i-1/2)\pi)^2 \sin((i-1/2)\pi x)} = C.$$

By using Eq. (11) we have

$$w = 1 = \int_0^1 \rho(x)dx = \int_0^1 C dx = C.$$

Hence, as expected, the uniform rigidity and density functions, $r(x)=1=\rho(x)$, have been reconstructed from the given data.

Example 4. Consider again the fixed-free rod of Example 1, but suppose now that only $\lambda_1=1.60853$, $v_1=e^{-x/2}\sin(1.1655612x)$ and $v_2=e^{-x/2}\sin(4.6042168x)$ are given. Then the following numerical data can be found:

$$\begin{aligned} &v_1(1)=0.5574076, \quad v_1'(1)=0, \quad v_1''(1)=-0.896608, \\ &v_2(1)=-0.6029855, \quad v_2'(1)=0, \quad v_2''(1)=12.933324. \end{aligned}$$

Using Eq. (17) we obtain $\lambda_2=21.4488$.

For this value we have $2\sqrt{\lambda_2 - 1/4} = 9.208 = \tan\sqrt{\lambda_2 - 1/4}$ which confirms the result.

We note, however, that the counterpart of Eq. (17), employed in Example 4,

$$\lambda_2 = \lambda_1 \frac{v_1(0) v_2''(0)}{v_1''(0) v_2(0)},$$

does not hold at the free end $x=0$ of the hanging cable problem, defined in Example 2. Due to the irregularity of r at $x=0$, *the slope of the hanging cable eigenfunctions are not equal to zero at the free end.* Consequently Eqs. (4) do not imply (14), and therefore Eq. (17) cannot be used in this case.

4 Applications

The low-frequency eigenvalues and the corresponding mode shapes of the axially vibrating rod may be determined experimentally by means of modal analysis methods. The measured eigendata correspond to the continuous model of the rod. Hence, we may apply the results of Sections 2 and 3 to reconstruct the rigidity and density functions of the rod. Since the measured mode shapes consist of the finite sampled data obtained from the continuous eigenfunctions, we may evaluate $r(x)$ and $\rho(x)$ *numerically*, as demonstrated by the following example:

Example 5. Consider the fixed-fixed uniform rod, of length $L=1$, with rigidity and density functions $\rho(x)=1=r(x)$. Suppose that the following data are given:

$$\begin{aligned} &\lambda_1=\pi^2, \quad \lambda_2=4\pi^2, \\ &v_1(ih)=\sin(ih\pi), \quad v_2(ih)=\sin(2ih\pi) \\ &\text{for } i=0, 1, \ldots, 10, \quad h=0.1, \text{ and } w=1. \end{aligned}$$

For convenience we denote $v(i) \equiv v(ih)$, and use similar notation for v' and v''. Then, the derivatives of $v_1(x)$ and $v_2(x)$ may be approximated by the discrete functions $\tilde{v}_j'(i)$ and $\tilde{v}_j''(i)$, for $j=1, 2$, using the following finite difference schemes:

$$\tilde{v}_j'(i) = \begin{cases} (v_j(1) - v_j(0))/h; & i=0 \\ (v_j(i+1) - v_j(i-1))/2h; & i=1, 2, \ldots, 9 \\ (v_j(10) - v_j(9))/h; & i=10 \end{cases}$$

$$\tilde{v}_j''(i) = \begin{cases} (\tilde{v}_j'(1) - \tilde{v}_j'(0))/h; & i=0 \\ (v_j(i-1) - 2v_j(i) + v_j(i+1))/h^2; & i=1, 2, \ldots, 9 \\ (\tilde{v}_j'(10) - \tilde{v}_j'(9))/h; & i=10. \end{cases}$$

Downloaded 03 May 2010 to 171.66.16.20. Redistribution subject to ASME license or copyright; see http://www.asme.org/terms/Terms_Use.cfm

Table 1 Eigenfunctions and their numerical derivatives

i	$v_1(i)$	$\tilde{v}_1'(i)$	$\tilde{v}_1''(i)$	$v_2(i)$	$\tilde{v}_2'(i)$	$\tilde{v}_2''(i)$
0	0.0	3.0902	−1.5130	0.0	5.8779	−11.2260
1	0.3090	2.9389	−3.0249	0.5878	4.7553	−22.4514
2	0.5878	2.5	−5.7537	0.9511	1.8164	−36.3271
3	0.8090	1.8164	−7.9192	0.9511	−1.8164	−36.3271
4	0.9511	0.9549	−9.3096	0.5878	−4.7553	−22.4514
5	1.0	0.0	−9.7887	0.0	−5.8779	0.0
6	0.9511	−0.9549	−9.3096	−0.5878	−4.7553	22.4514
7	0.8090	−1.8164	−7.9192	−0.9511	−1.8164	36.3271
8	0.5878	−2.5	−5.7537	−0.9511	1.8164	36.3271
9	0.3090	−2.9389	−3.0249	−0.5878	4.7553	22.4514
10	0.0	−3.0902	1.5130	0.0	5.8779	11.2260

Table 2 Approximated parameters for the rod

i	$\tilde{\psi}_i$	$\int^{ih}\tilde{\psi}dx$	$\tilde{r}_i$	$\tilde{\rho}_i$
0	0.0	0.0	1.0135	1.0135
1	−0.0320	−0.0016	1.0151	0.9755
2	−0.0634	−0.0064	1.0199	0.9837
3	−0.0880	−0.0139	1.0277	0.9987
4	−0.0791	−0.0223	1.0363	1.0195
5	0.0	−0.0263	1.0396	1.0319
6	0.0791	−0.0223	1.0363	1.0195
7	0.0880	−0.0139	1.0277	0.9987
8	0.0634	−0.0064	1.0199	0.9838
9	0.0320	−0.0016	1.0151	0.9755
10	0.0	0.0	1.0135	1.0135

These functions are listed in Table 1.

Then $\psi(x)$ may be approximated by the discrete function $\tilde{\psi}_i$ where

$$\tilde{\psi}_2=\frac{\lambda_2 v_2(i)\tilde{v}_1''(i)-\lambda_1 v_1(i)\tilde{v}_2''(i)}{\lambda_2 v_2(i)\tilde{v}_1'(i)-\lambda_1 v_1(i)\tilde{v}_2'(i)},\quad i=1, 2, \ldots, 10;$$

and the integral of $\tilde{\psi}$ may be evaluated numerically by the trapezoid rule

$$\int^{ih}\tilde{\psi}dx=\frac{1}{2}h(\tilde{\psi}_{i-1}+\tilde{\psi}_i)+\int^{(i-1)h}\tilde{\psi}dx;\quad i=1, 2, \ldots, 10.$$

Finally, the approximated rigidity and density functions are found from

$$\tilde{r}_i=\tilde{C}e^{-\int^{ih}\tilde{\psi}_i dx},\quad \tilde{\rho}_i=\frac{\tilde{r}_i}{\lambda_1 v_1}(\tilde{\psi}_i\tilde{v}_1'(i)-\tilde{v}_1''(i))$$

where using the trapezoidal formula again

$$\tilde{C}=\frac{w}{\frac{h}{2}\left(-(\tilde{\rho}_0+\tilde{\rho}_{10})+2\sum_{i=0}^{10}\tilde{\rho}_i\right)}=0.99997.$$

The numerical data which have been obtained by these equations are shown in Table 2. Despite the simplicity of the numerical schemes, a good approximation of the uniform rod parameters has been achieved.

5 Conclusions

The problem of reconstructing the rigidity and density functions of the longitudinally vibrating continuous rod from eigendata has been studied. Unlike the traditional approach which constructs the finite difference model of the rod from a large number of natural frequencies, subject to different end conditions, the method here constructs the rod from only two eigenvalues, their corresponding eigenfunctions, and the total mass of the rod. This novel procedure overcomes the following main disadvantages associated with the traditional method:

(a) The inherent inconsistency in the high-frequency eigenvalues of the discrete model, with respect to the rod which is a continuous system, plays no role at all.

(b) The large number of natural frequencies required by the traditional approach cannot usually be obtained from measurements.

(c) The need to impose additional (unnatural) boundary conditions limits the applicability of the traditional method.

The necessary and sufficient conditions for the construction of a physically realizable rod have been established. It has been shown that if the rod is subject to fixed-free boundary conditions then one eigenvalue, two eigenfunctions, and the total mass are all that is needed to reconstruct the rod. Numerical example demonstrating the method have been presented.

References

Barcilon, V., 1976, "Inverse Problem for a Vibrating Beam," *Journal of Applied Mathematics and Physics*, Vol. 24, pp. 346-358.

Barcilon, V., 1979, "On the Multiplicity of Solutions of the Inverse Problem for a Vibrating Beam," *SIAM Journal on Applied Mathematics*, Vol. 37, pp. 605-613.

Barcilon, V., 1982, "Inverse Problems for the Vibrating Beam in the Free-Clamped Configuration," *Philosophical Transactions of the Royal Society of London*, Vol. A304, pp. 211-252.

Hald, O. H., 1978, "The Inverse Sturm-Liouville Problem and the Rayleigh-Ritz Method," *Mathematics of Computation*, Vol. 32, pp. 687-705.

Hochstadet, H., 1973, "The Inverse Sturm-Liouville Problem," *Communications on Pure and Applied Mathematics*, Vol. 26, pp. 715-729.

Hochstadet, H., 1975, "Well-Posed Inverse Spectral Problem," *Proceedings of the National Academy of Sciences of the U.S.A.*, Vol. 72, pp. 2496-2497.

Gladwell, G. M. L., 1984, "The Inverse Problem for the Vibrating Beam," *Proceedings of the Royal Society of London: Series A—Mathematical and Physical Sciences*, Vol. 393, pp. 277-295.

Gladwell, G. M. L., and Gbadeyan, J. A., 1985, "On the Inverse Problem of the Vibrating String and Rod," *Quarterly Journal of Mechanics and Applied Mathematics*, Vol. 38, pp. 169-174.

Gladwell, G. M. L., 1986a, *Inverse Problems in Vibration*, Martinus Nijhoff Publishers, Dordrecht, The Netherlands.

Gladwell, G. M. L., 1986b, "The Inverse Mode Problem for Lumped-Mass Systems," *Quarterly Journal of Mechanics and Applied Mathematics*, Vol. 39, pp. 297-307.

Gladwell, G. M. L., and Zhu, B. R., 1992, "Inverse Problems for Multidimensional Vibrating Systems," *Proceedings of the Royal Society of London: Series A—Mathematical and Physical Sciences*, Vol. 439, pp. 511-530.

Levinson, N., 1945, "The Inverse Sturm-Liouville Problem," *Matematicheskii Tidsskrift B*, pp. 25-30.

Levitan, B. M., 1968, "On the Determination of a Sturm-Liouville Equation by Two Spectra," *American Mathematical Society—Translations*, Vol. 68, No. 2, pp. 1-20.

Ram, Y. M., and Caldwell, J., 1992, "Physical Parameters Reconstruction of a Free-Free Mass-Spring System From its Spectra," *SIAM Journal on Applied Mathematics*, Vol. 52, pp. 140-152.

Ram, Y. M., and Gladwell, G. M. L., 1994, "Constructing a Finite-Element Model of a Vibratory Rod From Eigendata," *Journal of Sound and Vibration*, Vol. 169, pp. 229-237.

APPENDIX A

Subtracting Eq. (5*b*) from (5*a*) yields

$$Pr'+Qr=0,\quad 0<x<L \tag{A1}$$

where $P=\lambda_2 v_2 v_1'-\lambda_1 v_1 v_2'$ and $Q=\lambda_2 v_2 v_1''-\lambda_1 v_1 v_2''$. If $P(\xi)=0$ and $Q(\xi)\neq 0$ at $\xi\in(0, L)$ then with the assumption that r' is bounded in $[0, L]$ it follows from (A1) that $r(\xi)=0$. If $P(\xi)=0=Q(\xi)$ then we may examine the derivative of (A1)

$$P'r'+Pr''+Q'r+Qr'=0,\quad 0<x<L. \tag{A2}$$

Since $P(\xi)=0=Q(\xi)$ and $r'(\xi)$ and $r''(\xi)$ are bounded we have

$$P'(\xi)r'(\xi)+Q'(\xi)r(\xi)=0 \tag{A3}$$

which implies again at $r(\xi)=0$ when $P'(\xi)=0$ and $Q'(\xi)\neq 0$. If $P'(\xi)=0=Q'(\xi)$, then differentiating (A2) and substituting $P(\xi)=P'(\xi)=Q(\xi)=Q'(\xi)=0$ we obtain

$$P''(\xi)r'(\xi)+Q''(\xi)r(\xi)=0. \tag{A4}$$

Equation (A4) may lead to a similar conclusion regarding $r(\xi)$ when $P''(\xi)=0$ and $Q''(\xi)\neq 0$. If $P''(\xi)=0=Q''(\xi)$ then we may continue in this manner until $P^{(k)}(\xi)$ and $Q^{(k)}(\xi)$ do not vanish simultaneously and conclude that $r(\xi)=0$ if $P^{(k)}(\xi)=0$ and $Q^{(k)}(\xi)\neq 0$.

Noting that this process is equivalent to the method of testing the limit of the indeterminate $\psi\equiv P/Q$ at $x=\xi$, we deduce that when $\psi(\xi)$ is unbounded then $r(\xi)=0$.

Downloaded 03 May 2010 to 171.66.16.20. Redistribution subject to ASME license or copyright; see http://www.asme.org/terms/Terms_Use.cfm

An Exact Solution of the Unsteady Navier-Stokes Equations Resulting From a Stretching Surface

S. H. Smith
Department of Mathematics,
University of Toronto,
Toronto, ON M5S 1A1,
Canada

When a stretching surface is moved quickly, for a short period of time, a pulse is transmitted to the surrounding fluid. Here we describe an exact solution in terms of a similarity variable for the Navier-Stokes equations which represents the effect of this pulse for two-dimensional flow. The unusual feature is that this solution is only valid for a limited range of the Reynolds number; outside this domain unbounded velocities result.

1 Introduction

In the extrusion process for the drawing of plastic films, a sheet issues from a slit with a velocity, which is proportional to the distance from the slit. The fluid above the sheet is otherwise at rest, and the pressure away from the boundary layer, which forms on the sheet, is constant. This situation was first considered by Crane (1970), who presented a very simple exact solution to the Navier-Stokes equations for the steady flow in terms of exponential functions. Since then there have been a number of extensions for steady behaviors in both two and three-dimensional situations as well as for time-dependent situations (for example, Wang (1984), Brady and Acrivos (1981), Wang (1991a), Devi et al. (1986)); many of these studies concentrated on thermodynamic consequences of the behavior. Interest in these results has been, on the one hand, because of practical engineering questions involved in the manufacturing process, and on the other, because of the fact that new similarity solutions to the complete Navier-Stokes equations are obtained.

Although exact solutions represent highly specialized situations, they do give clues concerning the nature of more realistic behavior. The major review was given in the encyclopaedic article by Berker (1963) many years ago, but recently there have been two valuable updates of steady flows by Wang (1991b) and unsteady flows also by Wang (1989).

Here we present a new exact solution of the unsteady Navier-Stokes equations for the stretching surface, which displays a number of novel features. It corresponds to the flow created by a pulse-like motion of the surface, where we use the term "pulse" to represent rapid motion for a short time. More precisely, when a body is given the velocity V for a time T, then we are interested in the limiting situation with V large and T small, such that the product VT has finite magnitude; this product is a measure of the distance traveled by the body. When the viscosity of the fluid is ν, then we can define the Reynolds number for such a motion as $V(T/\nu)^{1/2}$.

We first formulate the problem generally, and then proceed to investigate the motion for very small Reynolds numbers to help give an intuitive understanding of the role of the pulse before eventually considering the finite Reynolds number behavior. In all our discussions we restrict ourselves to just the fluid mechanical properties.

2 Two-Dimensional Stretching Surface

For the general formulation we introduce the cartesian coordinate system (x, y), where fluid occupies the region above the infinite plane $y = 0$. The velocities parallel and perpendicular to the plane are u, v, respectively, where all the variables have been made nondimensional with respect to a time scale T, a length scale $(\nu T)^{1/2}$, and a velocity scale $(\nu/T)^{1/2}$; this scaling ensures that the Reynolds number is absorbed into the basic equation. We then proceed to consider the motion which develops in the fluid when the surface $y = 0$ is at rest at $t < 0$, given the velocity Ux for $0 \le t < \tau$, and then held at rest again for all subsequent time $t \ge \tau$; U and τ are given (nondimensional) constants.

With the simple geometry of this model we can remove the variable x through defining the stream function

$$\psi = xf(y, t) \text{ for } y,\ t \ge 0, \tag{1}$$

where $u = xf_y$ and $v = -f$; the Navier-Stokes equations are then completely satisfied if

$$f_{yt} + f_y^2 - ff_{yy} = f_{yyy}. \tag{2}$$

The boundary conditions are

$$f = 0,\quad f_y = U\{H(t) - H(t-\tau)\} \text{ on } y = 0, \tag{3a}$$

$$f_y \to 0 \text{ as } y \to \infty, \tag{3b}$$

where $H(t)$ is the Heaviside step function.

2.1 Linear Approximation. Now if the velocities produced by this stretching action are very small, we can write f

Contributed by the Applied Mechanics Division of THE AMERICAN SOCIETY OF MECHANICAL ENGINEERS for publication in the ASME JOURNAL OF APPLIED MECHANICS.

Discussion on this paper should be addressed to the Technical Editor, Professor Lewis T. Wheeler, Department of Mechanical Engineering, University of Houston, Houston, TX 77204-4792, and will be accepted until four months after final publication of the paper itself in the ASME JOURNAL OF APPLIED MECHANICS.

Manuscript received by the ASME Applied Mechanics Division, Apr. 9, 1992; final revision, Mar. 23, 1993. Associate Technical Editor: T. R. Akylas.

Copyright © 1994 by ASME
Downloaded 03 May 2010 to 171.66.16.20. Redistribution subject to ASME license or copyright; see http://www.asme.org/terms/Terms_Use.cfm

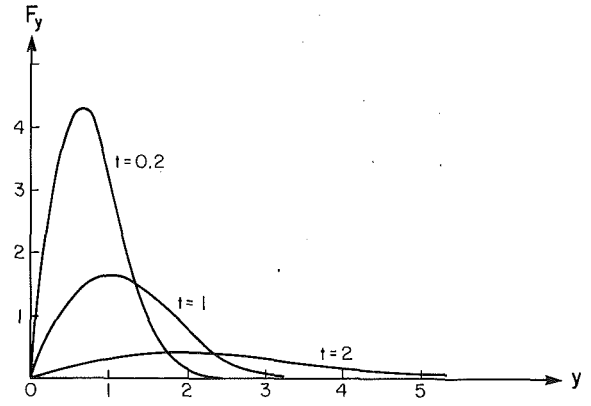


Fig. 1 Graph of the velocity for the weak pulse as given by (8)

$\cong \mathcal{F}(y, t)$, and proceed to neglect all the quadratic terms in $\mathcal{F}$ to provide the linear differential equation

$$\mathcal{F}_{yt} = \mathcal{F}_{yyy} \tag{4}$$

as the approximation to Eq. (2); this step is justified a posteriori. The boundary conditions for (4) are still given by (3). To solve for $\mathcal{F}$ we define the Laplace transform $\overline{\mathcal{F}}(y, s) = \int_0^\infty e^{-st}\mathcal{F}(y, t)dt$, from which it follows that

$$\overline{\mathcal{F}}_y = Us^{-1}(1-e^{-s\tau})e^{-s^{1/2}y}. \tag{5}$$

When the inverse transform of (5) is taken, it is then seen, in particular, that

$$\mathcal{F}_y = U\left\{erfc\left(\frac{y}{2t^{1/2}}\right) - erfc\left(\frac{y}{2(t-\tau)^{1/2}}\right)\right\} \text{ for } t>\tau. \tag{6}$$

The first term represents the basic Rayleigh flow for the diffusion of vorticity from the surface $y = 0$ which begins to move at $t = 0$, while the second term represents the equivalent Rayleigh flow for the stopping of the surface at $t = \tau$, thereby ensuring that there is no slip on $y = 0$ for $t > \tau$.

The limit as $\tau \to 0$ and $U \to \infty$ such that $U\tau \to \lambda$ is now taken, and when we write $\mathcal{F}_p$ as the corresponding limit for $\mathcal{F}$ as given in (6), we see that

$$\mathcal{F}_{py} = \frac{\lambda y}{2\pi^{1/2}t^{3/2}}\, e^{-(y^2/4t)} \text{ for } t>0, \tag{7}$$

and therefore

$$\mathcal{F}_p = \frac{\lambda}{(\pi t)^{1/2}}\{1-e^{-(y^2/4t)}\} \text{ for } t>0, \tag{8}$$

which represents the basic solution for the weak pulse—see Fig. 1. The basic linearization which led to (4) is now seen to be legitimate when λ is sufficiently small; that is, when the strength of the pulse is sufficiently small.

Some comments are appropriate at this point before proceeding. First, the expression (8) could have been gained directly by setting the condition $(\mathcal{F}_y)_{y=0} = \lambda\delta(t)$ in place of (3*a*), or, equivalently, by differentiating with respect to t the solution which follows when $(\mathcal{F}_y)_{y=0} = \lambda H(t)$. The basic effect of the pulse is to create an intense shear layer along the plate for $t = 0+$, which then diffuses away into the fluid, and the result (8) describes that diffusive process. The function $\mathcal{F}_p$, as given in (8) satisfies the boundary value problem defined by the differential Eq. (4) plus the boundary conditions $\mathcal{F} = \mathcal{F}_y = 0$ on $y = 0$ and $\mathcal{F}_y \to 0$ as $y \to \infty$ for all $t > 0$. This boundary value problem is homogeneous for $t > 0$ because the nonhomogeneous condition (3*a*) collapses into just $(\mathcal{F}_y)_{y=0} = \lambda\delta(t)$ when the limit as $\tau \to 0$ is taken to obtain (7).

An alternate understanding is to see the basic effect of the pulse as creating an intense shear layer on the plate for $t = 0+$, which then diffuses away into the fluid, and it is the role of (8) to describe this diffusive process. That is, we could solve the initial value problem with (4) plus the conditions $\mathcal{F} = \mathcal{F}_y = 0$, $\mathcal{F}_{yy} = 1/2\,\lambda\pi^{-1/2}t^{-3/2}$ on $y = 0$ for $t > 0$ to obtain (8).

In a similar vein we observe that the function $\mathcal{F}_p(y, t)$, given in (8), is unbounded as $t \to 0$; this behavior should be understood in the sense of singular perturbations. When the limit as $\tau \to 0$ was found, t was taken to be finite so that (8) essentially represents the flow when $t/\tau \gg 1$; the flow for $t/\tau = O(1)$ still requires the more complete description given by (6). Mathematically, the nature of this singularity is most clearly seen from the expression

$$\mathcal{F}(\infty, t) = 2U\pi^{-1/2}\{t^{1/2} - (t-\tau)^{1/2}\} \text{ for } t>\tau,$$

gained from (6) after intregration, which leads to the limiting form $\lambda(\pi t)^{-1/2}$ as $U\tau \to \lambda$ (c.f. Eq. (8)).

2.2 Nonlinear Solution. We now turn to the nonlinear flow, and continue the description for larger pulse strengths by substituting the series

$$f = \sum_{n=1}^{\infty} \lambda^n f_n(y, t) \text{ for } y,\ t \geq 0 \tag{9}$$

into (2); the first term is given, from (8), by

$$f_1 = (\pi t)^{-1/2}(1-e^{-\zeta^2}), \text{ where } \zeta = \frac{1}{2}yt^{-1/2}.$$

So far the nonlinear convection terms of (2) have been ignored through retaining only the linear terms of the diffusion equation; when we proceed to the second order, it is found that we can write $f_2 = t^{-1/2}F_2(\zeta)$ where

$$F_2''' + 2\zeta F_2'' + 4F_2' = 4\pi^{-1}\{e^{-2\zeta^2} + (2\zeta^2-1)e^{-\zeta^2}\}, \tag{10}$$

subject to $F_2(0) = F_2'(0) = F_2'(\infty) = 0$. The solution of (10) is straightforward but lengthy and we do not present it here. However, when this process is continued further, it is seen that all the terms f_n can be written as $t^{-1/2}$ multiplying a function of ζ. Consequently, if such a series expansion (9) is in fact convergent, a point which is by no means yet certain, it follows that a similarity variable solution for the problem in the form

$$f(y, t) = t^{-1/2}F(\zeta) \tag{11}$$

would then exist to Eq. (2); the resulting equation shows

$$F''' + 2\zeta F'' + 4F' = 2(F'^2 - FF'') \tag{12}$$

exactly. The boundary conditions we would then need to impose for this equation are

$$F(0) = F'(0) = F'(\infty) = 0; \tag{13}$$

the first two require that the velocity is zero on the plane $y = 0$ for $t > 0$ (that is, after the pulse is complete), while the third indicates that the finite pulse cannot give rise to a translational velocity at infinity. This similarity variable expression (11) was one of the examples presented by Birkhoff (1960) and, after a simple translation for t, was considered by Yang (1958) for a particular forced stagnation point flow, which required $F'(\infty)$ to be nonzero, and by Devi et al. (1986) for the corresponding flow due to a stretching surface. Essentially, the present discussion is giving a physical context to this mathematical solution of Birkhoff. The stress on the wall is measured by $x(f_{yy})_{y=0}$, and just after the pulse has acted this is proportional to $xt^{-3/2}$; the resulting motion therefore describes how the intense shear layer thus created along the wall dissipates with no external forces acting. A consequence of the simple solution (11) is that the stress is proportional to $xt^{-3/2}$ for all time. Viscous and inertial terms in the Navier-Stokes equations balance throughout this process when $\lambda = O(1)$.

It is most convenient when numerical solutions are considered for the boundary value problem (12), (13), that the conditions (13) are replaced with the initial conditions

$$F(0) = F'(0) = 0, \quad F''(0) = \alpha \tag{14}$$

Downloaded 03 May 2010 to 171.66.16.20. Redistribution subject to ASME license or copyright; see http://www.asme.org/terms/Terms_Use.cfm

for different values of α. It is known that there is a unique solution to this initial value problem when α is given (c.f., Coddington and Levinson, 1955), and the computations are straightforward, though clearly the only solutions which are valid for the physical problem posed must require $F'(\zeta)$ to tend to zero as ζ tends to infinity. Further, changing the value of α is equivalent to changing the strength of the pulse. This approach also recalls the comment made earlier that the effect of the pulse is to create an intense shear layer which diffuses away into the fluid, and so increasing the value of α increases the strength of the initial stress on the surface. When $\alpha > 0$, the pulse motion of the stretching surface is outwards, but we can also include the situation when $\alpha < 0$, when the surface moves inward. In the numerical solutions satisfactory results were obtained using a fourth-order Runge-Kutta method; in particular cases (for larger α) these were checked by applying predictor-corrector methods associated with Adams-Moulton and Adams-Bashforth which have a built-in check for possible divergence of the solution (c.f. Shampine and Gordon, 1975). A set of graphs for $F(\zeta)$ and $F'(\zeta)$ are shown in Fig. 2.

The first conclusion to observe is that a bounded solution for $F(\zeta)$ exists only when $\alpha_1 < \alpha < \alpha_2$, where $\alpha_1 \simeq -3.940$ and $\alpha_2 \simeq 3.692$; outside this domain the velocity becomes unbounded a large distance from the plate, which is physically unacceptable. An increase in $|\alpha|$ measures an increase in the strength of the pulse, and so there is a clear limit to its magnitude for this approach through the similarity solution (11) to be valid. The fact that the exact solution is present for only a finite range of the Reynolds number is distinctive. It is reasonable to conjecture that the greater strengths give rise to instantaneous explosive separation from the plane, which is beyond the capability of (11), (12) to describe.

For $\alpha_3 < \alpha < 0$, where $\alpha_3 \simeq -1.802$, $F(\zeta)$ is negative for all ζ with a minimum before F tends to some (negative) constant value c, depending on α. When we write $F(\zeta) = \Sigma_{n=1}^{\infty} \lambda^n F_n(\zeta)$ corresponding to (9), it is seen that the decay to the constant is exponential in the linear solution represented by F_1; but that $F_2' = O(\zeta^{-2})$ as $\zeta \to \infty$, and this pattern continues for F_3, F_4, ... When $\alpha = \alpha_3$, $F(\zeta)$ tends to zero as $\zeta \to \infty$.

Next, when $\alpha_1 < \alpha < \alpha_3$, the one difference from the previous situation is that now $F(\zeta)$ changes sign and tends to a positive constant value c as $\zeta \to \infty$. Consequently, there is a flow reversal with a free streamline parallel to the surface marking the separated flow; this streamline is designated by a constant value of ζ, and so moves away from the surface as t increases with a velocity proportional to $t^{-1/2}$. Some comparison can be made with the separation described by Proudman and Johnson (1962) for the impulsive flow past a rear stagnation point, though they found the separated region grow exponentially in time.

For $0 < \alpha < \alpha_2$ which represents the extrusion process, $F(\zeta)$ is a monotonic increasing function with $F(\zeta)$ tending to a positive constant as $\zeta \to \infty$, with the same algebraic decay; there is an inward flow from infinity to compensate for the pulse motion of the surface, and there is really only a quantitative difference from the representation given by the linear solution. In Fig. 3 we represent graphically the relation between the values of $F''(0)$ and $F(\infty)$. Because the value of $F(\infty)$ is already very large for α some distance from the boundary quantities α_1, and α_2, it can be expected physically that instabilities will develop before α takes on these limiting values.

When $\alpha = \alpha_1$ and $\alpha = \alpha_2$, the numerical solutions show that $F'(\zeta) \to 2$ as $\zeta \to \infty$, corresponding to the solution of Yang (1958); whereas for $\alpha < \alpha_1$ and $\alpha > \alpha_2$, the solution for $F(\zeta)$ grows exponentially in ζ. In the particular case $\alpha = -5$, this behavior is represented by $F \simeq 3.81 \exp(1/2\zeta)$ as $\zeta \to \infty$.

3 Discussion

It is not difficult to see that a similar approach is also successful for the axisymmetric flow due to the pulse. We introduce the model of a stretching surface which is drawn out of a small hole with a large velocity (which is proportional to the distance from the hole) for a short time, and then take the limiting case where the distance moved is finite. The geometry is the same as that considered for the steady-state situation by Wang (1984); the surface is represented by $z = 0$, and in a polar coordinate system (r, θ, z) based on the axis of symmetry the radial and axial velocities $\mathfrak{U}$ and $\mathfrak{W}$ can be written as

$$\mathfrak{U} = rh(z, t), \quad \mathfrak{W} = -2h(z, t). \tag{15}$$

The Navier-Stokes equations are satisfied exactly when

$$h_{zt} + h_z^2 - 2hh_{zz} = h_{zzz}, \quad t > 0, \tag{16}$$

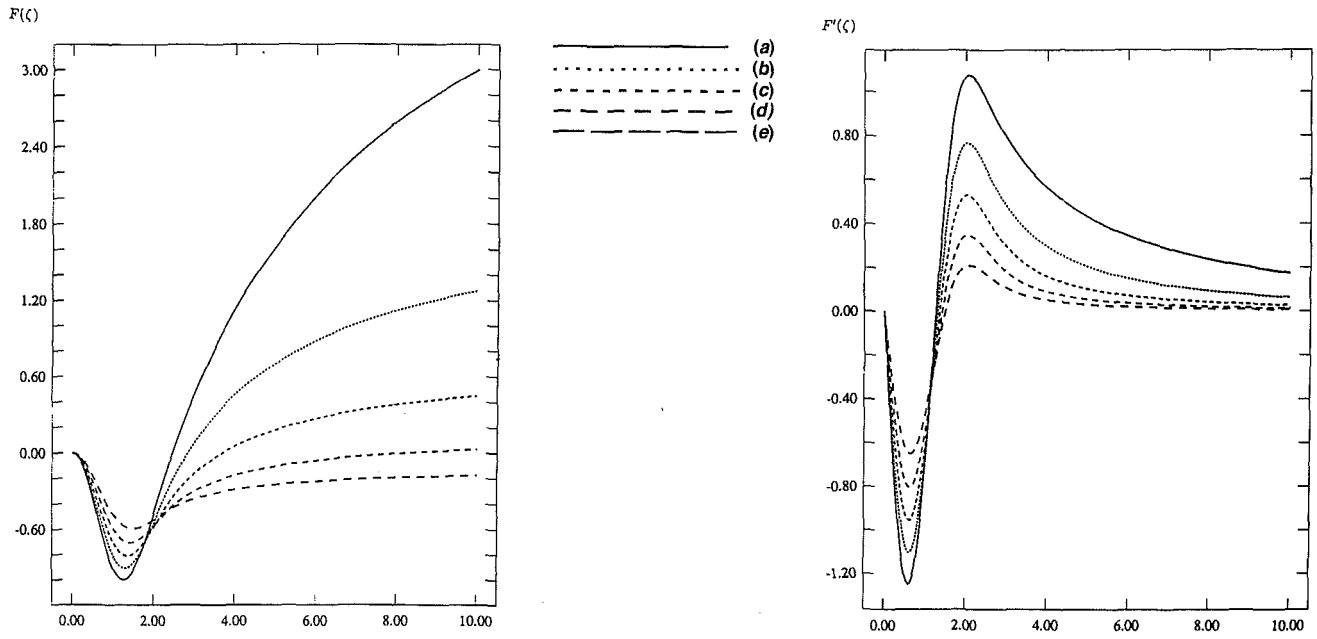


Fig. 2, Pt. 1

Downloaded 03 May 2010 to 171.66.16.20. Redistribution subject to ASME license or copyright; see http://www.asme.org/terms/Terms_Use.cfm

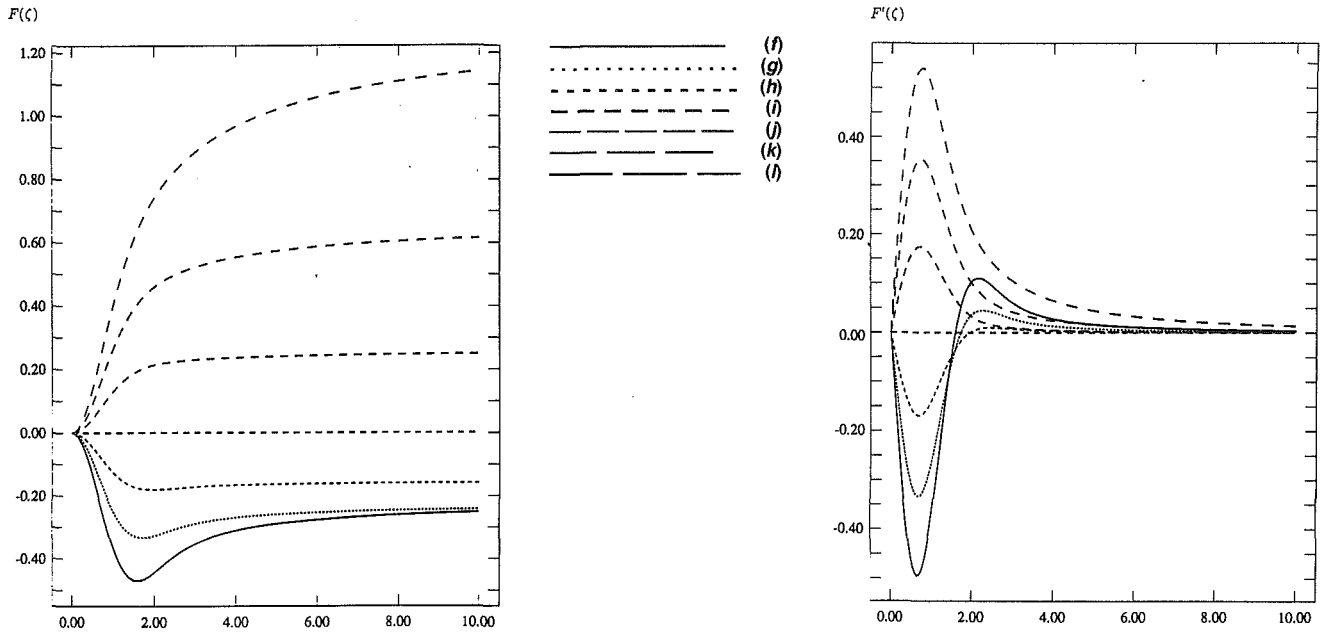


Fig. 2, Pt. 2

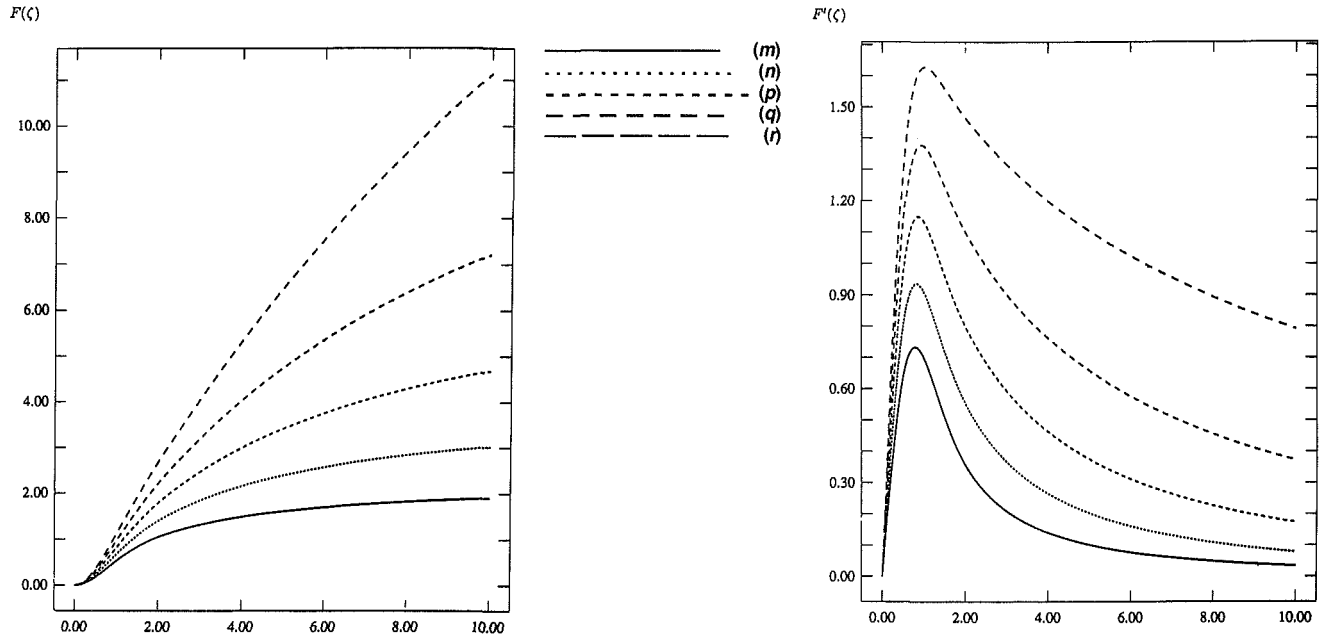


Fig. 2, Pt. 3

Fig. 2 Numerical solutions for $F(\zeta)$ and $F'(\zeta)$ from (12) and (14) for the indicated values of α; (*a*) $\alpha = -3.2$, (*b*) $\alpha = -2.8$, (*c*) $\alpha = -2.4$, (*d*) $\alpha = -2.0$, (*e*) $\alpha = -1.6$, (*f*) $\alpha = -1.2$, (*g*) $\alpha = -0.8$, (*h*) $\alpha = -0.4$, (*i*) $\alpha = 0.0$, (*j*) $\alpha = 0.4$, (*k*) $\alpha = 0.8$, (*l*) $\alpha = 1.2$, (*m*) $\alpha = 1.6$, (*n*) $\alpha = 2.0$, (*p*) $\alpha = 2.4$, (*q*) $\alpha = 2.8$, (*r*) $\alpha = 3.2$

where all the variables have been made nondimensional and the Reynolds number has been absorbed into the definition of h. The similarity solution equivalent to (11) can be justified through corresponding arguments, so that we can write

$$h(z, t) = t^{-1/2} H(\xi) \text{ where } \xi = \frac{1}{2} z t^{-1/2},$$

for the ordinary differential equation

$$H''' + 2\xi H'' + 4H' = 2(H'^2 - 2HH''), \tag{17}$$

plus

$$H(0) = H'(0) = H'(\infty) = 0. \tag{18}$$

As before, we solve an initial value problem with the conditions $H(0) = H'(0) = 0$, $H''(0) = \beta$, for different values of β, and look for solutions where $H'(\xi) \to 0$ as $\xi \to \infty$.

The general features of the solution are virtually identical with those already described in Section 2, with the graphs of $H(\xi)$ being topologically the same as those for $F(\zeta)$. Solutions with bounded values for $H(\xi)$ exist for $\beta_1 < \beta < \beta_2$ where $\beta_1 \cong -2.476$ and $\beta_2 \cong 4.140$; the graph connecting $H''(0)$ with

Downloaded 03 May 2010 to 171.66.16.20. Redistribution subject to ASME license or copyright; see http://www.asme.org/terms/Terms_Use.cfm

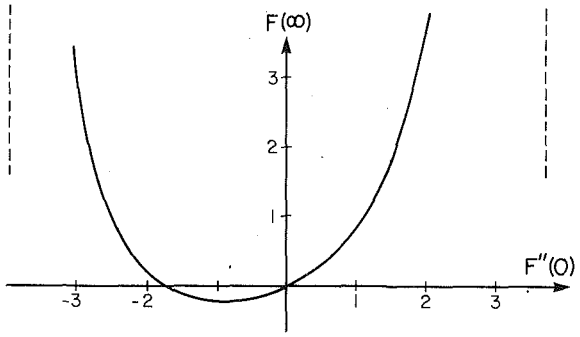


Fig. 3 The relation between the values of $F''(0)$ and $F(\infty)$ from the solution of (12) and (13); the asymptotes are also given

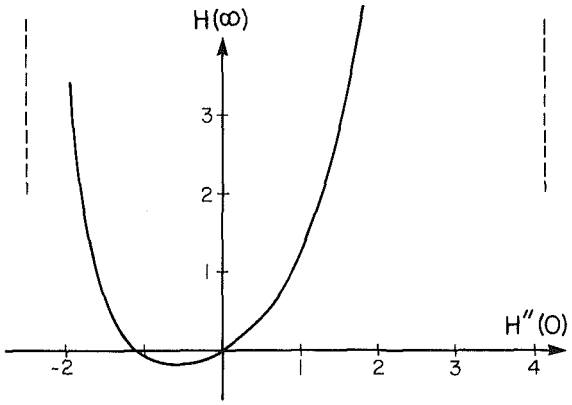


Fig. 4 The relation between the values of $H''(0)$ and $H(\infty)$ from the solution of (17) and (18); the asymptotes are also given

$H(\infty)$ is given in Fig. 4. The only basic difference to note is that the asymptotic solution for large ξ is parabolic in the domains $\beta < \beta_1$ and $\beta > \beta_2$ with $H(\xi) \cong A\xi^2 + 3\xi\ln\xi + B\xi + O\{(\ln\xi)^2\}$ as $\xi \to \infty$; in the particular case $\beta = -4$ it is found that $A \cong 3.14$ and $B \cong -7.21$.

The author wishes to thank Dr. David Pravica for his assistance in completing all the numerical computations. A grant in aid of research from the Navier Sciences and Engineering Research Council of Canada is gratefully acknowledged.

References

Berker, R., 1963, "Intégration des Équations du Mouvement d'un Fluide Visqueux Incompressible," *Handbuch der Physik*, Vol. VIII/2, Springer, Berlin, pp. 1–384.

Birkhoff, G., 1960, *Hydrodynamics, a Study in Logic, Fact and Similitude*, Princeton Univ. Press, Princeton, NJ.

Brady, J. F., and Acrivos, A., 1981, "Steady Flow in a Channel or Tube with an Accelerating Surface: An Exact Solution to the Navier-Stokes Equations with Reverse Flow," *Journal of Fluid Mechanics*, Vol. 112, pp. 127–150.

Coddington, E. A., and Levinson, N., 1955, *Theory of Ordinary Differential Equations*, McGraw-Hill, New York.

Crane, L. J., 1970, "Flow Past a Stretching Plate," *Zeitschrift für Angewandte Mathematik und Physik*, Vol. 21, pp. 645–647.

Devi, C. D. S., Takhar, H. S., and Nath, G., 1986, "Unsteady, Three-dimensional Boundary Layer Flow due to a Stretching Surface," *International Journal of Heat and Mass Transfer*, Vol. 29, pp. 1996–1999.

Proudman, I., and Johnson, K., 1962, "Boundary-layer Growth Near a Rear Stagnation Point," *Journal of Fluid Mechanics*, Vol. 12, pp. 161–168.

Shampine, L. F., and Gordon, M. K., 1975, *Computer Solutions of Ordinary Differential Equations*, W. H. Freeman, San Francisco, CA.

Wang, C. Y., 1984, "The Three Dimensional Flow due to a Stretching Surface," *Physics of Fluids*, Vol. 27, pp. 1915–1917.

Wang, C. Y., 1989, "Exact Solutions of the Unsteady Navier-Stokes Equations," ASME *Applied Mechanics Reviews*, Vol. 42, pp. 269–282.

Wang, C. Y., 1991a, "Flow Across a Stretching Surface," ASME JOURNAL OF APPLIED MECHANICS, Vol. 58, pp. 579–580.

Wang, C. Y., 1991b, "Exact Solutions of the Steady-State Navier-Stokes Equations," *Annual Review of Fluid Mechanics*, Vol. 23, pp. 159–178.

Yang, K. T., 1958, "Unsteady Laminar Boundary Layers in an Incompressible Stagnation Flow," ASME JOURNAL OF APPLIED MECHANICS, Vol. 25, pp. 421–427.

Downloaded 03 May 2010 to 171.66.16.20. Redistribution subject to ASME license or copyright; see http://www.asme.org/terms/Terms_Use.cfm

A Theory of Hydrodynamic Lubrication Involving the Mixture of Two Fluids

F. Dai[1]
Assoc. Mem. ASME.

M. M. Khonsari[2]
William Kepler Whiteford Faculty Fellow, Mem. ASME.

Department of Mechanical Engineering, University of Pittsburgh, Pittsburgh, PA 15261

Based on the principles of continuum mechanics, we drive the governing equations for the hydrodynamic lubrication involving the mixture of two incompressible fluids. The governing equations are general in the sense that they can be applied to the mixture of any simple non-Newtonian fluid with a Newtonian fluid. A mixture thus formed is considered to be nonhomogeneous and non-Newtonian. In the theoretical development, the interaction between the constituents is taken into consideration. It is shown that a number of currently available models are special cases of the theory presented in this paper. As an example, results are presented for journal bearing performance lubricated with a mixture of a power-law fluid mixed with Newtonian oil.

1 Introduction

There are many applications where one is interested in examining the behavior of a mixture of two fluids. A familiar example is an emulsion which is the dispersion of one liquid within another liquid. Typical emulsions are oil dispersed within water (O/W) or water within oil (W/O). Some emulsions are regarded as contamination and some are made by design. For instance, the lubricant used in steam turbines is often contaminated with water, making an W/O emulsion. On the other hand, in metal-working application, W/O emulsions are commonly used as they are known to be fire-resistant. This type of emulsion is of practical interest because noncombustible synthetic fluids tend to be more toxic than mineral oils and are more expensive (Hamaguchi et al., 1977).

Discussed in the foregoing paragraph is the emulsion problem that involves the mixture of two liquids; each of which may be considered as a Newtonian fluid. The behavior of the droplets of one fluid within another and, in general, the rheology of emulsions within the context of lubrication is of significant interest. To this end, various experimental and theoretical research efforts have been directed toward the understanding of the lubrication characteristic of W/O emulsions (cf. Nakahara et al., 1988; Dow, 1977; Lunberg et al., 1988). Another application where the mixture of fluids plays an important role is in multigrade oils. To enhance the lubrication properties of mineral oils, such as the viscosity index, polymeric-type fluids are added to the base oil. Additives, in general, can have a pronounced influence on the performance of lubricants particularly in hydrodynamic bearings. Unlike the emulsion problems discussed previously, however, the mixture of the polymer in oil normally results in a fluid that cannot be regarded as linearly viscous or Newtonian. A mixture thus formed is, in general, nonhomogeneous and non-Newtonian.

There are numerous models available in the literature that describe the behavior of non-Newtonian fluids. Nevertheless, a common feature in many of the existing non-Newtonian fluid models is the assumption of the homogeneity of the mixture; that is when two liquids are mixed, the resulting fluid is homogeneous and if one is non-Newtonian, the resulting mixture is regarded as non-Newtonian. While this assumption may be reasonable for certain applications, it is clearly deficient for emulsion problems.

In this paper we develop general governing equations for hydrodynamic lubrication of two incompressible fluids. The base fluid is assumed to Newtonian and the other fluid is classified as a simple non-Newtonian fluid. The resulting mixture is nonhomogeneous. The governing equations are general and well-suited for application to a variety of hydrodynamic lubrication problems. It is shown that these equations can be reduced to the generalized Reynolds equations for non-Newtonian fluids developed by Paranjpe (1992). The equations developed in this paper may be useful for the modeling of emulsion problems. As an example for the application of the theory, we present numerical solutions for the performance parameters of a journal bearing lubricated with a mixture of power-law fluid and Newtonian fluid.

In Section 2, the governing equations for the mixture of two non-Newtonian fluids are developed using the mixture theory. A subclass of the problem involving the mixture of a simple non-Newtonian fluid and a linearly viscous (Newtonian) fluid is studied. A number of limiting cases are discussed. In Section 3, the special case of the homogeneous mixture is investigated. Numerical results are presented for the mixture composed of

[1]Current address: Department of Mechanical Engineering, University of California, Berkeley, CA 94720.

[2]To whom all correspondence should be addressed.

Contributed by the Applied Mechanics Division of THE AMERICAN SOCIETY OF MECHANICAL ENGINEERS for publication in the ASME JOURNAL OF APPLIED MECHANICS.

Discussion on this paper should be addressed to the Technical Editor, Professor Lewis T. Wheeler, Department of Mechanical Engineering, University of Houston, Houston, TX 77204-4792, and will be accepted until four months after final publication of the paper itself in the ASME JOURNAL OF APPLIED MECHANICS.

Manuscript received by the ASME Applied Mechanics Division, Feb. 10, 1992; final revision, Apr. 19, 1993. Associate Technical Editor: S. A. Berger.

Copyright © 1994 by ASME
Downloaded 03 May 2010 to 171.66.16.20. Redistribution subject to ASME license or copyright; see http://www.asme.org/terms/Terms_Use.cfm

a power-law fluid and a Newtonian fluid in Section 4. The last section is devoted to concluding remarks.

2 Theory

Preliminaries and Notation. Consider a mixture containing two fluids, S_1 and S_2. According to the theory of interacting continua, a point in the mixture can be considered to be simultaneously occupied by two particles belonging to each constituent S_1 and S_2 and that the motion of each constituent is described independently by continuous functions of position. In the development that follows we shall adopt the notation listed below as follows:

	fluid 1	fluid 2
constituent	S_1	S_2
kinematics	u_1, v_1, w_1	u_2, v_2, w_2
pressure	p_1	p_2
density	ρ_1	ρ_2
viscosity coefficient	μ_{s_1}	μ_{s_2}
volume fraction	ν_1	ν_2
second invariant of strain rate tensor	I_1	I_2

Interacting Body Force. For the mixture of two incompressible fluids we have $\nu_1 + \nu_2 = 1$. For convenience, let $\nu_1 = \nu$. Therefore, it follows that $\nu_2 = 1 - \nu$. We shall assume that the constituents involved are chemically inert, that is no chemical reaction is allowed to take place between them. However, the constituents can interact mechanically. A general form for interacting body forces that includes effects due to drag force, density gradient, and virtual mass is given by Homsy et al. (1980). We assume that the virtual mass and density gradient effects are negligibly small when compared to that of the drag term $\alpha(\mathbf{u}_1 - \mathbf{u}_2)$, where α is the interaction coefficient which is a function of the volume fraction, $\alpha = \alpha(\nu)$. In the theory of interacting continua, namely the theory of mixture, the interaction term appears in the conservation laws written for each of the constituents. The interested reader may refer to recent articles by the authors (Dai and Khonsari, 1991, 1993) where we treated the problem involving the mixture of granular material inserted into Newtonian fluid. There, a similar approach was adopted in characterizing the interaction of particulate solids inserted into a lubricating oil.

Mixture of Two Non-Newtonian Fluids. Restricting our analysis now to hydrodynamic lubrication problems involving relatively narrow film gaps with non-Newtonian fluids, we assume that the flow is laminar and that the inertia effects are absent. Under the premise of these assumptions, Tanner (1963) shows that for simple non-Newtonian fluids the cross-film velocity gradients are responsible for all deformation. We shall begin by extending his approach to the mixture of two simple non-Newtonian fluids. A simple order-of-magnitude analysis shows that *momentum equations* for the mixture can be written as given as follows:

Fluid 1.

$$\frac{\partial}{\partial z}\left[\mu_{s_1}(I_1, \nu)\frac{\partial u_1}{\partial z}\right] = \frac{\partial p_1}{\partial x} + \alpha(\nu)(u_1 - u_2), \tag{1}$$

$$\frac{\partial}{\partial z}\left[\mu_{s_1}(I_1, \nu)\frac{\partial v_1}{\partial z}\right] = \frac{\partial p_1}{\partial y} + \alpha(\nu)(v_1 - v_2), \tag{2}$$

$$\frac{\partial p_1}{\partial z} = 0, \tag{3}$$

Fluid 2.

$$\frac{\partial}{\partial z}\left[\mu_{s_2}(I_2, \nu)\frac{\partial u_2}{\partial z}\right] = \frac{\partial p_2}{\partial x} - \alpha(\nu)(u_1 - u_2), \tag{4}$$

$$\frac{\partial}{\partial z}\left[\mu_{s_2}(I_2, \nu)\frac{\partial v_2}{\partial z}\right] = \frac{\partial p_2}{\partial y} - \alpha(\nu)(v_1 - v_2), \tag{5}$$

$$\frac{\partial p_2}{\partial z} = 0, \tag{6}$$

where the viscosity coefficients, μ_{s_i} $(i = 1, 2)$, are dependent upon the second invariant of the strain rate tensor and the volume fractions. The second invariant of the rate of deformation tensor for each fluid takes on the following form:

$$I_1 = \left(\frac{\partial u_1}{\partial z}\right)^2 + \left(\frac{\partial v_1}{\partial z}\right)^2, \quad I_2 = \left(\frac{\partial u_2}{\partial z}\right)^2 + \left(\frac{\partial v_2}{\partial z}\right)^2.$$

According to the theory of mixtures, the *continuity equations* for the constituents, S_1 and S_2, are given, respectively, by

$$\frac{\partial}{\partial x}(\nu u_1) + \frac{\partial}{\partial y}(\nu v_1) + \frac{\partial}{\partial z}(\nu w_1) = 0, \tag{7}$$

and

$$\frac{\partial}{\partial x}[(1-\nu)u_2] + \frac{\partial}{\partial y}[(1-\nu)v_2] + \frac{\partial}{\partial z}[(1-\nu)w_2] = 0. \tag{8}$$

In the above system, there are eight Eqs. (1)–(8), for nine unknown variables: ν, p_i, u_i, v_i and w_i, $(i = 1, 2)$. The final equation may be obtained by assuming that the pressure, p, in the mixture flow is shared by both of constituents according to their volume fractions, that is

$$p_1 = \nu p, \quad p_2 = (1-\nu)p.$$

Furthermore, we shall assume that the viscosity coefficients, μ_{s_1} and μ_{s_2}, depend linearly on the volume fraction, ν. Since the momentum Eq. (1)–(6) for the mixture flow should reduce to those for a simple fluid, the following expressions for the constitutive relations for μ_{s_1} and μ_{s_2} are introduced:

$$\mu_{s_1} = \nu\mu_1(I_1), \quad \mu_{s_2} = (1-\nu)\mu_2(I_2),$$

where μ_1 and μ_2 are functions of the second invariants only.

The equations governing the *conservation of momentum* now reduce to those listed as follows:

Fluid 1:

$$\frac{\partial}{\partial z}\left[\nu\mu_1(I_1)\frac{\partial u_1}{\partial z}\right] = \frac{\partial(\nu p)}{\partial x} + \alpha(\nu)(u_1 - u_2), \tag{9}$$

$$\frac{\partial}{\partial z}\left[\nu\mu_1(I_1)\frac{\partial v_1}{\partial z}\right] = \frac{\partial(\nu p)}{\partial y} + \alpha(\nu)(v_1 - v_2), \tag{10}$$

$$\frac{\partial(\nu p)}{\partial z} = 0. \tag{11}$$

Fluid 2:

$$\frac{\partial}{\partial z}\left[(1-\nu)\mu_2(I_2)\frac{\partial u_2}{\partial z}\right] = \frac{\partial[(1-\nu)p]}{\partial x} - \alpha(\nu)(u_1 - u_2), \tag{12}$$

$$\frac{\partial}{\partial z}\left[(1-\nu)\mu_2(I_2)\frac{\partial v_2}{\partial z}\right] = \frac{\partial[(1-\nu)p]}{\partial y} - \alpha(\nu)(v_1 - v_2), \tag{13}$$

$$\frac{\partial[(1-\mu)p]}{\partial z} = 0. \tag{14}$$

The foregoing system of equations are general in the sense that once the functional forms of α, μ_1 and μ_2 are known, they can be solved by numerical schemes to determine the velocity fields and pressure distribution in the mixture of the two simple non-Newtonian fluids within the context of hydrodynamic lubrication theory and subject to the assumptions discussed heretofore.

Before proceeding to more specific derivation for the gov-

Downloaded 03 May 2010 to 171.66.16.20. Redistribution subject to ASME license or copyright; see http://www.asme.org/terms/Terms_Use.cfm

erning equations, we point out the interaction coefficient α must be evaluated by considering the drag forces on a fluid drop while it moves in another fluid. Evaluation of such a coefficient is indeed a difficult task. In the absence of available data in the open literature, one simple approach for estimating the value of α is to make use of the Hadamard-Rebczynski solution as a *first approximation* (cf. Hetsroni, 1982). They showed that the drag coefficient exerted on a spherical liquid particle of diameter a as it moves in another liquid in an infinite domain is

$$6a\pi\mu_1 \frac{2\mu_1+3\mu_2}{3(\mu_1+\mu_2)},$$

where μ_1 is the viscosity of the carrying liquid and μ_2 is that of the liquid droplet. Since the number of fluid particles in a unite volume of the mixture is $3\nu/4\pi a^3$, the interaction coefficient becomes

$$\alpha = k\frac{3\nu}{2a^2h}\int_0^h \frac{\mu_1(2\mu_1+3\mu_2)}{\mu_1+\mu_2}\,dz,$$

where an average value of the drag forces across the film thickness h has been taken and a correction factor k is introduced to account for the retardation effects due to the bounding surface. For the mixture of two Newtonian fluids with viscosities μ_{N_1} and μ_{N_2}, the above interaction coefficient reduces to

$$\alpha = k\frac{3\mu_{N_1}\nu(2\mu_{N_1}+3\mu_{N_2})}{2a^2(\mu_{N_1}+\mu_{N_2})}.$$

Mixture of a Simple Non-Newtonian Fluid and a Newtonian Fluid. We now turn our attention to a specific subclass of lubrication problems that involves the mixture of linearly viscous (Newtonian) fluid to which a simple non-Newtonian fluid is added. An example of such a mixture is a conventional lubricant (Newtonian) with additives that are intentionally included therein to improve the characteristics of the lubricant, such as the Viscosity Index (V.I.). These lubricants are often classified as multigrade oils. We proceed by first deriving a generalized Reynolds equation for such a class of mixture. In the absence of thermal effects, we assume that the viscosity of the Newtonian fluid, μ_1, remains constant and that the volume fraction remains uniform across the film, z, but it is allowed to vary in x and y directions: $\nu = \nu(x, y)$.

Equations (9)–(11) now become

$$\nu\mu\frac{\partial^2 u_1}{\partial z^2} = \frac{\partial(\nu p)}{\partial x} + \alpha(\nu)(u_1-u_2), \tag{15}$$

$$\nu\mu\frac{\partial^2 v_1}{\partial z^2} = \frac{\partial(\nu p)}{\partial y} + \alpha(\nu)(v_1-v_2), \tag{16}$$

$$\frac{\partial p}{\partial z} = 0, \tag{17}$$

where μ is the viscosity of the Newtonian fluid which is a constant.

The boundary conditions are

$$u_1|_{z=0} = u_2|_{z=0} = U_1,\ u_1|_{z=h} = u_2|_{z=h} = U_2,$$
$$v_1|_{z=0} = v_2|_{z=0} = v_1|_{z=h} = v_2|_{z=h} = 0, \tag{18}$$

$$w_1|_{z=0} = w_2|_{z=0} = 0,\ w_1|_{z=h} = w_2|_{z=h} = \frac{\partial h}{\partial t}. \tag{19}$$

The components of velocity u_i and v_i, (i = 1, 2), can now be determined by integrating Eqs. (12), (13), (15), and (16), subject to the boundary conditions (18) and (19). The results are given as follows:

$$u_1 = U_1 + (U_2-U_1)\frac{z}{h} - \frac{z(h-z)}{2\mu}\frac{\partial(\nu p)}{\partial x} + \frac{\alpha(\nu)}{\mu}\left[z\int_0^z (u_1-u_2)dz - \int_0^z z(u_1-u_2)dz - z\int_0^h \left(1-\frac{z}{h}\right)(u_1-u_2)dz\right], \tag{20}$$

$$v_1 = -\frac{z(h-z)}{2\mu}\frac{\partial(\nu p)}{\partial y} + \frac{\alpha(\nu)}{\mu}\left[z\int_0^z (u_1-u_2)dz - \int_0^z z(u_1-u_2)dz - z\int_0^h \left(1-\frac{z}{h}\right)(u_1-u_2)dz\right], \tag{21}$$

$$u_2 = U_1 + \frac{\int_0^z \frac{1}{\mu_2}dz}{\int_0^h \frac{1}{\mu_2}dz}\left[(U_2-U_1) + \int_0^h \left(\frac{\mu}{\mu_2}\frac{\partial u_1}{\partial z} - \frac{z}{\mu_2}\frac{\partial p}{\partial x}\right)dz\right] - \int_0^z \left(\frac{\mu}{\mu_2}\frac{\partial u_1}{\partial z} - \frac{z}{\mu_2}\frac{\partial p}{\partial x}\right)dz, \tag{22}$$

$$v_2 = \frac{\int_0^z \frac{1}{\mu_2}dz}{\int_0^h \frac{1}{\mu_2}dz}\int_0^h \left(\frac{\mu}{\mu_2}\frac{\partial u_1}{\partial z} - \frac{z}{\mu_2}\frac{\partial p}{\partial y}\right)dz - \int_0^z \left(\frac{\mu}{\mu_2}\frac{\partial u_1}{\partial z} - \frac{z}{\mu_2}\frac{\partial p}{\partial y}\right)dz, \tag{23}$$

where $\mu_2 = \mu_2(I_2)$. The preceding velocity profiles are composed of three distinct portions caused by the sliding movement of boundary surfaces, pressure gradient, and the interaction between the two fluids.

Substitution of Eqs. (20)–(23) into the continuity Eqs. (7) and (8) yields the following two partial differential equations for each fluid phase in the mixture flow:

$$\frac{\partial}{\partial x}\left[\frac{\nu h^3}{12\mu}\frac{\partial(\nu p)}{\partial x} + \alpha(\nu)\nu F_1\right] + \frac{\partial}{\partial y}\left[\frac{\nu h^3}{12\mu}\frac{\partial(\nu p)}{\partial y} + \alpha(\nu)\nu F_1\right] = \frac{\partial}{\partial x}\left[U_1\nu h + (U_2-U_1)\frac{\nu h}{2}\right] + \nu\frac{\partial h}{\partial t}, \tag{24}$$

and

$$\frac{\partial}{\partial x}\left[(1-\nu)\left(F_5 - \frac{F_3^2}{F_2}\right)\frac{\partial[(1-\nu)p]}{\partial x} - \alpha(\nu)(1-\nu)F_4\right] + \frac{\partial}{\partial y}\left[(1-\nu)\left(F_5 - \frac{F_3^2}{F_2}\right)\frac{\partial[(1-\nu)p]}{\partial y} - \alpha(\nu)(1-\nu)F_4\right] = U_1\frac{\partial}{\partial x}\left[(1-\nu)\frac{F_3}{F_2}\right] + U_2\frac{\partial}{\partial x}\left[(1-\nu)\left(h - \frac{F_3}{F_2}\right)\right] + (1-\nu)\frac{\partial h}{\partial t}, \tag{25}$$

where

$$F_1 = \frac{1}{2\mu}\int_0^h z(h-z)(u_1-u_2)dz,\quad F_2 = \int_0^h \frac{1}{\mu_2}dz,\ F_3 = \int_0^h \frac{z}{\mu_2}dz,$$
$$F_4 = \int_0^h \left[\frac{1}{\mu_2}\left(z - \frac{F_3}{F_2}\right)\int_0^z (u_1-u_2)dz\right]dz,\ F_5 = \int_0^h \frac{z^2}{\mu_2}dz.$$

Downloaded 03 May 2010 to 171.66.16.20. Redistribution subject to ASME license or copyright; see http://www.asme.org/terms/Terms_Use.cfm

The left-hand members of Eqs. (24) and (25) essentially represent the volumetric flow rates in the circumferential and transverse directions induced by pressure gradients and the interaction between the fluids. The pressure across the film is uniform as dictated by Eqs. (11) and (14). The right-hand members of terms in Eqs. (24) and (25) represent the physical wedge, $\partial/\partial x$, and squeeze motion, $\partial h/\partial t$. When the film thickness profile, h, is specified and the operating conditions are known, that is, when the bearing type and the speeds, U_1, U_2, and $\partial h/\partial t$ are given, these two coupled equations must be solved simultaneously for the volume fraction and pressure distribution in the mixture flow. The problem can be treated by an iterative numerical scheme.

Once possible approach is to assume trial velocity distributions for u_1, u_2, v_1, and v_2 so that function F_i, (i = 1, 2, ..., 5), can be evaluated. Then, Eqs. (24) and (25) can be solved simultaneously for the volume fraction ν and the pressure distribution, respectively. In the absence of the squeeze action, i.e., when $\partial h/\partial t = 0$, Eqs. (24) and (25) are both elliptic partial differential equations and can be solved numerically (see Section 4 for solutions of a special case). Once converged solutions for pressure and volume fraction have been determined, one may use Eqs. (20)–(23) to update the velocity distributions, u_i and v_i, (i = 1, 2). Again the functions F_i, (i = 1, 2, ..., 5), will have to be evaluated and the iteration cycle repeated until the system converges, that is the errors for ν and p between two successive iterations fall below a tolerance value(s). This numerical procedure requires extensive computational time.

Limiting Cases. Equations (24) and (25) result in two limiting cases: $\nu = 1$, the Reynolds equation for a Newtonian fluid:

$$\frac{\partial}{\partial x}\left(\frac{h^3}{12\mu}\frac{\partial p}{\partial x}\right)+\frac{\partial}{\partial y}\left(\frac{h^3}{12\mu}\frac{\partial p}{\partial y}\right)=U_1\frac{\partial h}{\partial x}+\frac{\partial h}{\partial t}, \tag{26}$$

and $\nu = 0$, the Reynolds equation for a simple non-Newtonian fluid:

$$\frac{\partial}{\partial x}\left[\left(F_5-\frac{F_3^2}{F_2}\right)\frac{\partial p}{\partial x}\right]+\frac{\partial}{\partial y}\left[\left(F_5-\frac{F_3^2}{F_2}\right)\frac{\partial p}{\partial y}\right]$$
$$=U_1\frac{\partial}{\partial x}\left(\frac{F_3}{F_2}\right)+U_2\frac{\partial}{\partial x}\left(h-\frac{F_3}{F_2}\right)+\frac{\partial h}{\partial t}, \tag{27}$$

while Eq. (26) is the classical form of the Reynolds equation, the limiting case of $\nu = 0$ corresponds exactly to Reynolds equation for a simple non-Newtonian fluid recently presented by Paranjpe (1992). Equation (27) is considerably easier to solve than the coupled equations given in (24) and (25), since the terms F_1 and F_4 do not appear in the formulation. These terms contain the velocity distributions u_1 and u_2 that are a priori unknown. The terms emerge in present formulations since we deal with the nonhomogeneous mixture of two fluids, whereas Eq. (27) is restricted to simple, homogeneous non-Newtonian fluids.

In the following sections we shall examine a somewhat restrictive mixture problem and present results for a number of pertinent bearing parameters.

3 The Special Case of the Homogeneous Mixture

Let us now turn our attention to a restricted form of the problem where the droplets of one fluid completely dissolve in the other in such a manner that the resulting mixture is homogeneous. Again, we will assume that no chemical reaction takes place and the fluids both retain their original mechanical properties after they are mixed. For such a mixture, depending on the application, it may be reasonable to assume that the diameter of the particles belonging to the fluidic additive—which uniformly disperses in the base fluid—diminishes; that is in the limiting case $a \to 0$. Consequently, the coefficient of interaction characterized by the drag force between the two constituents $\alpha \to \infty$. Therefore, with reference to the momentum Eqs. (9) and (10), or (15) and (16), one can see that the fluid particles belonging to each constituent must possess the same velocity at each point in the mixed region, that is $u_1 = u_2$ and $v_1 = v_2$. As shown below, these considerations result in a significant simplification of the governing equations. From Eqs. (9)–(14), we have

$$\frac{\partial}{\partial z}\left[\mu_h(I,\nu)\frac{\partial u}{\partial z}\right]=\frac{\partial p}{\partial x}, \tag{28}$$

$$\frac{\partial}{\partial z}\left[\mu_h(I,\nu)\frac{\partial v}{\partial z}\right]=\frac{\partial p}{\partial y}, \tag{29}$$

$$\frac{\partial p}{\partial z}=0, \tag{30}$$

where $u = u_1 = u_2$, $v = v_1 = v_2$, $I = I_1 = I_2$, and

$$\mu_h=\nu\mu_1+(1-\nu)\mu_2. \tag{31}$$

Here ν is essentially constant, and the drag force between the two constituents vanishes.

3.1 Couette-Dominated Non-Newtonian Mixture. Let us now further examine the behavior of such a mixture. Clearly, in the case of the Newtonian fluid, the velocities and their derivatives vary linearly with the pressure gradient. For simple non-Newtonian fluids, one may refer to the work of Dien and Elrod (1983) whose analysis is also based on the assumption asserting that for hydrodynamic lubrication problems, the strain rates in the flow are principally generated by the relative surface velocities. As pointed out by the authors, such an assumption restricts the analysis to either the simple non-Newtonian fluids that are Couette-dominated, or to Newtonian fluids with arbitrary Couette-Poiseuille components. Following the procedure of Dien and Elrod (1983), using the usual perturbation method, the following results for Couette-dominated mixture composed of two fluid constituents can be obtained:

$$u=U\frac{z}{h}-\frac{z(h-z)}{2}$$
$$\times\left[\frac{1}{\mu_h^0}\frac{\partial p}{\partial x}-\frac{U}{h}\left(\frac{U}{h}\frac{\partial p}{\partial x}+\frac{V}{h}\frac{\partial p}{\partial y}\right)\frac{2\left.\frac{\partial\mu_h}{\partial I}\right|_{I=I_0}}{(\mu_h^0)^2\left(1+\left.\frac{\partial ln\mu_h}{\partial ln\sqrt{I}}\right|_{I=I_0}\right)}\right], \tag{32}$$

$$v=V\frac{z}{h}-\frac{z(h-z)}{2}$$
$$\times\left[\frac{1}{\mu_h^0}\frac{\partial p}{\partial y}-\frac{V}{h}\left(\frac{U}{h}\frac{\partial p}{\partial x}+\frac{V}{h}\frac{\partial p}{\partial y}\right)\frac{2\left.\frac{\partial\mu_h}{\partial I}\right|_{I=I_0}}{(\mu_h^0)^2\left(1+\left.\frac{\partial ln\mu_h}{\partial ln\sqrt{I}}\right|_{I=I_0}\right)}\right], \tag{33}$$

$$\dot{\mathbf{m}}=\frac{\rho h\mathbf{S}}{2}-\frac{\rho h^3}{12\mu_h^0}\left[\nabla p-\frac{\mathbf{s}(\mathbf{s}\cdot\nabla p)}{1+\left.\frac{\partial ln\sqrt{I}}{\partial ln\mu_h}\right|_{I=I_0}}\right], \tag{34}$$

where

Downloaded 03 May 2010 to 171.66.16.20. Redistribution subject to ASME license or copyright; see http://www.asme.org/terms/Terms_Use.cfm

$$I_0=\left(\frac{U}{h}\right)^2+\left(\frac{V}{h}\right)^2,\ \mu_h^0=\mu_h(I_0),\quad \mathbf{S}=U\mathbf{i}+V\mathbf{j},\ \mathbf{s}=\frac{\mathbf{S}}{\sqrt{U^2+V^2}}.$$

In Eqs. (32) and (33), U and V represent the surface velocities in the x and y directions at $z = h$, respectively. The system of Eqs. (32)–(34) are identical, in form, to those Dien and Elrod (1983) obtained for non-Newtonian fluids. Except, here, for this class of mixture the definition of the viscosity, μ_h is given by Eq. (31).

3.2 Application. Consider a mixture of a Newtonian fluid and a power-law fluid. The total shear stress is shared by the two fluid constituents, that is

$$\tau_{zx}^M=\tau_{zx}^N+\tau_{zx}^P=\mu_N\nu_N\frac{\partial u}{\partial z}+\mu_P\nu_P\left(\frac{\partial u}{\partial z}\right)^n=\mu_h\frac{\partial u}{\partial z},\tag{35}$$

where

$$\mu_h=\mu_N\nu_N+\mu_P\nu_P\left[\left(\frac{\partial u}{\partial z}\right)^2\right]^{(n-1)/2}=\mu(1-\nu_P)+\mu_P\nu_P I^{(n-1)/2},\tag{36}$$

and μ and $\nu_N\ (=1-\nu_P)$ are the viscosity and volume fraction of Newtonian fluid, respectively; μ_P and ν_P are the viscosity and volume fraction of the power-law fluid, respectively.

From Eq. (36) we have

$$1+\frac{\partial ln\sqrt{I}}{\partial ln\mu_h}=\frac{\mu(1-\nu_P)+n\mu_P\nu_P I^{(n-1)/2}}{\mu_P\nu_P(n-1)I^{(n-1)/2}},\tag{37}$$

and

$$1+\frac{\partial ln\mu_h}{\partial ln\sqrt{I}}=\frac{\mu(1-\nu_P)+n\mu_P\nu_P I^{(n-1)/2}}{\mu(1-\nu_P)+\mu_P\nu_P I^{(n-1)/2}}.\tag{38}$$

Substitution of Eqs. (37) and (38) into (32) and (33) yields the velocity distributions

$$u=U\frac{z}{h}-\frac{z(z-h)}{2\left[\mu(1-\nu_P)+n\mu_P\nu_P\left(\frac{U}{h}\right)^{n-1}\right]}\frac{\partial p}{\partial x},\tag{39}$$

$$v=-\frac{z(z-h)}{2\left[\mu(1-\nu_P)+n\mu_P\nu_P\left(\frac{U}{h}\right)^{n-1}\right]}\frac{\partial p}{\partial y}.\tag{40}$$

Similarly, substituting Eq. (37) into (34) and taking the divergent of the result, we obtain a form of the Reynolds equation valid for the mixture of power-law fluid inserted into a Newtonian fluid:

$$\frac{\partial}{\partial x}\left[\frac{h^3}{\mu(1-\nu_P)+n\mu_P\nu_P\left(\frac{U}{h}\right)^{n-1}}\frac{\partial p}{\partial x}\right]+\frac{\partial}{\partial y}\left[\frac{h^3}{\mu(1-\nu_P)+\mu_P\nu_P\left(\frac{U}{h}\right)^{n-1}}\frac{\partial p}{\partial y}\right]=6U\frac{\partial h}{\partial x},\tag{41}$$

where we have assumed that squeeze term $\partial h/\partial t$ is absent. The shear stress of this mixture, τ_{zx}^M, is obtained from Eqs. (35), (36), and (39):

$$\tau_{zx}^M=\left[\mu(1-\nu_P)+\mu_P\nu_P\left(\frac{U}{h}\right)^{n-1}\right]\frac{U}{h}-\frac{h-2z}{2}\frac{\partial p}{\partial x}.\tag{42}$$

3.3 Journal Bearings. Equations (41) and (42) can be applied to study the performance of a hydrodynamic bearing of an arbitrary shape lubricated with the mixture described in Section 3.2. In this section we present solutions for a journal bearing. The geometric function of the film thickness in a journal bearing is given by

$$h(x)=c+e\cos\theta,$$

where c is the bearing clearance, e denotes the eccentricity of the center of the rotating journal from that of the stationary bushing, $\theta = x/R$, and R is the radius of the journal.

The following dimensionless parameters are introduced:

$$\bar{x}=\theta=\frac{x}{R},\ \bar{y}=\frac{y}{L},\ \bar{h}=\frac{h}{c},\ \bar{u}=\frac{u}{U},\ \bar{v}=\frac{v}{U},$$

$$\bar{p}=\left(\frac{R}{c}\right)^2\frac{R}{\mu U}p,\ \bar{\tau}_{zx}^M=\frac{c}{\mu U}\tau_{zx}^M,\ \bar{\mu}_P=\frac{U^{n-1}}{\mu c^{n-1}}\mu_P,$$

where L is the length of the bearing in the axial direction. The dimensionless forms of Eqs. (39)–(42) are

$$\bar{u}=\frac{\bar{z}}{\bar{h}}-\frac{\bar{z}(\bar{z}-\bar{h})}{2\left(1-\nu_P+\frac{n\bar{\mu}_P\nu_P}{\bar{h}^{n-1}}\right)}\frac{\partial\bar{p}}{\partial\theta},$$

$$\bar{v}=-\frac{\bar{z}(\bar{z}-\bar{h})}{2\left(1-\nu_P+\frac{n\bar{\mu}_P\nu_P}{\bar{h}^{n-1}}\right)}\frac{\partial\bar{p}}{\partial\bar{y}},$$

$$\frac{\partial}{\partial\theta}\left(\frac{\bar{h}^3}{1-\nu_P+\frac{n\bar{\mu}_P\nu_P}{\bar{h}^{n-1}}}\frac{\partial\bar{p}}{\partial\theta}\right)+\left(\frac{R}{L}\right)^2\frac{\partial}{\partial\bar{y}}\left(\frac{\bar{h}^3}{1-\nu_P+\frac{\bar{\mu}_P\nu_P}{\bar{h}^{n-1}}}\frac{\partial\bar{p}}{\partial\bar{y}}\right)=6\frac{\partial\bar{h}}{\partial\theta},\tag{43}$$

$$\bar{\tau}_{zx}^M=\left(1-\nu_P+\frac{\bar{\mu}_P\nu_P}{\bar{h}^{n-1}}\right)\frac{1}{\bar{h}}-\frac{\bar{h}-2\bar{z}}{2}\frac{\partial\bar{p}}{\partial\theta}.$$

The boundary conditions for Eq. (43) are

$$\bar{p}\,|_{\theta=0}=0,\ \left.\frac{\partial\bar{p}}{\partial\theta}\right|_{\theta=\theta_{cav}}=0,$$

where θ_{cav} is the position at which fluid-film cavitates. This condition is known as the Swift-Stieber boundary condition.

Once the pressure distribution has been determined, other bearing performance parameters such as the load-carrying capacity, friction force, and the friction coefficient are determined from the following equations written in dimensionless form:

$$\bar{W}=\int_0^{\theta_{cav}}\bar{p}d\bar{x},\ \bar{F}=\int_0^{\theta_{cav}}\bar{\tau}_{zx}^M d\theta,\ f=\frac{\bar{F}}{\bar{W}}\left(\frac{c}{R}\right).\tag{44}$$

4 Results and Discussion

In this section we will present some numerical results for the Couette-dominated flow of a homogeneous mixture composed of a power-law fluid and a Newtonian fluid. Assuming that a journal bearing is lubricated with such a mixture, we will show that the volume fraction of the non-Newtonian constituent, i.e., the power-law fluid, plays an important role on the performance of the bearing even under the restricted case of the homogeneous mixture.

Equation (43) is an elliptic partial differential equation and was solved numerically using the finite difference method with a successive-over-relaxation procedure. All results presented in this section pertain to a journal bearing with $L/R = 1$. For the purpose of simulations, unless stated otherwise, the following parameters are assumed:

$$n=0.6,\ \nu_P=0.5,\ \bar{\mu}_P=0.6,\ \epsilon=0.8,$$

where $\epsilon = e/c$ is the dimensionless eccentricity ratio.

For the purpose of comparison, we begin by presenting the pressure distributions in the mixture flow for three cases: "pure" Newtonian fluid ($\nu_P = 0$), the mixture of Newtonian

Downloaded 03 May 2010 to 171.66.16.20. Redistribution subject to ASME license or copyright; see http://www.asme.org/terms/Terms_Use.cfm

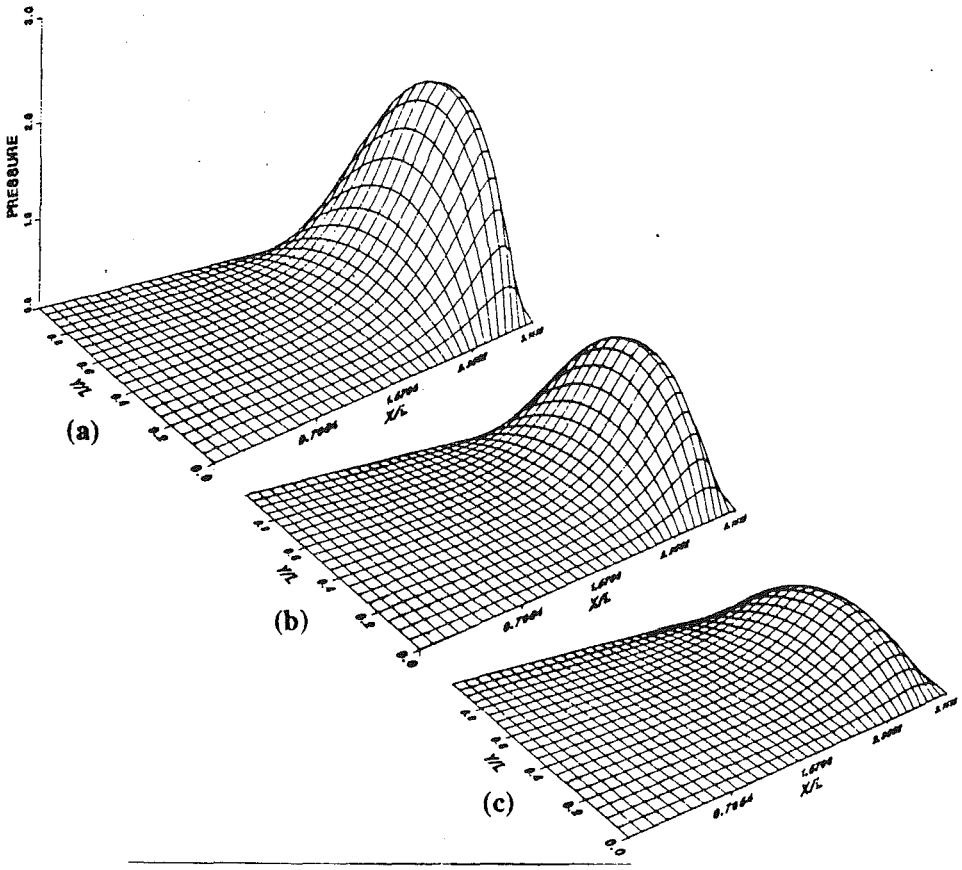


Fig. 1 Pressure distributions; (*a*) Newtonian fluid, (*b*) mixture of power-law fluid (ν_P = 0.5), (*c*) power-law fluid

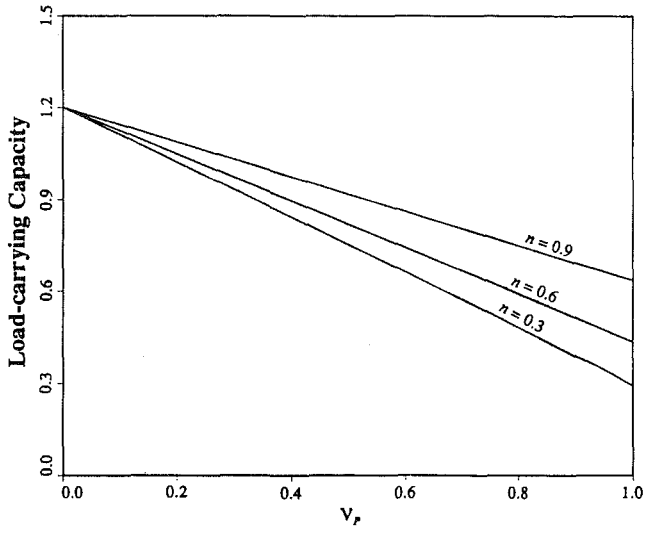


Fig. 2 Variation of load-carrying capacity with the viscosity of power-law fluid

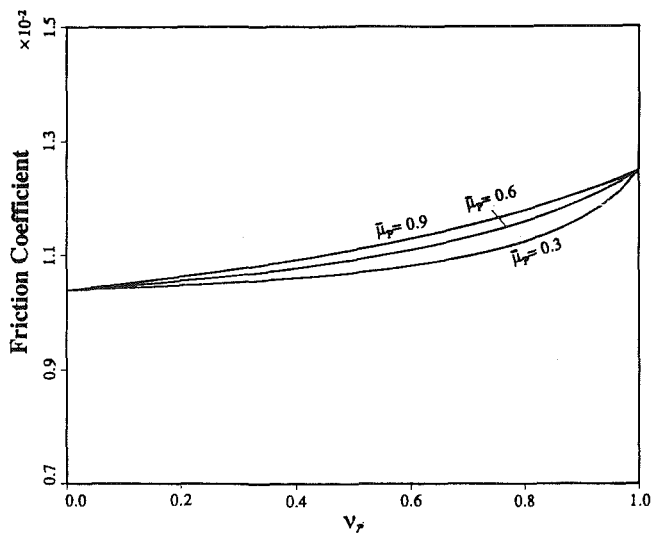


Fig. 3 Variation of friction coefficient with the viscosity of power-law fluid

fluid and power-law fluid with volume fraction of 0.5 (i.e., ν_P = 0.5), and a "pure" power-law fluid (ν_P = 1). These are shown in Fig. 1. It can be seen that for the given parameters the pure Newtonian fluid case results in the largest magnitude of pressure distribution and the pressure is reduced as the volume fraction of the given power-law fluid increases.

Figure 2 shows the variation of load-carrying capacity with the volume fraction and the viscosity of the power-law fluid. The limiting cases corresponding to ν_P = 0 (pure Newtonian fluid) and ν_P = 1 (pure power-law fluid) are also shown for comparison. Clearly, the load-carrying capacity is affected by the volume fraction of the power-law fluid. It drops roughly linearly with the increase in the volume fraction of the power-law fluid. Also shown in the figure is the parametric study of the power-law viscosity coefficient $\bar{\mu}_P$. The higher the value of $\bar{\mu}_P$, the better the load-carrying capacity. Nevertheless, the highest load-carrying capacity is when the fluid is purely Newtonian. Another parameter of interest is the friction coefficient. The variation of friction coefficient with the volume fraction and the viscosity of the power-law fluid is given in Fig. 3. One

Downloaded 03 May 2010 to 171.66.16.20. Redistribution subject to ASME license or copyright; see http://www.asme.org/terms/Terms_Use.cfm

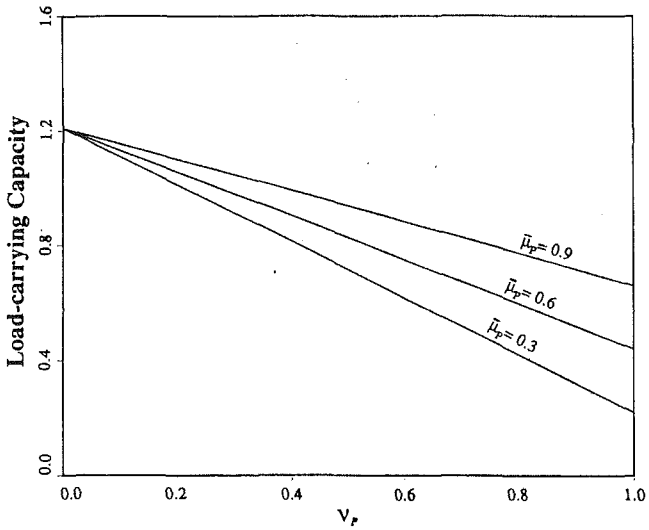


Fig. 4 Variation of load-carrying capacity with the index of power-law fluid

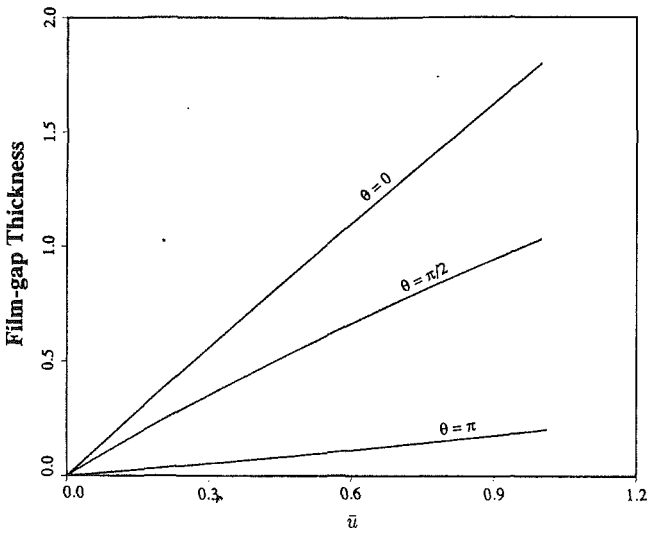


Fig. 6 Velocity distribution $\bar{u}$

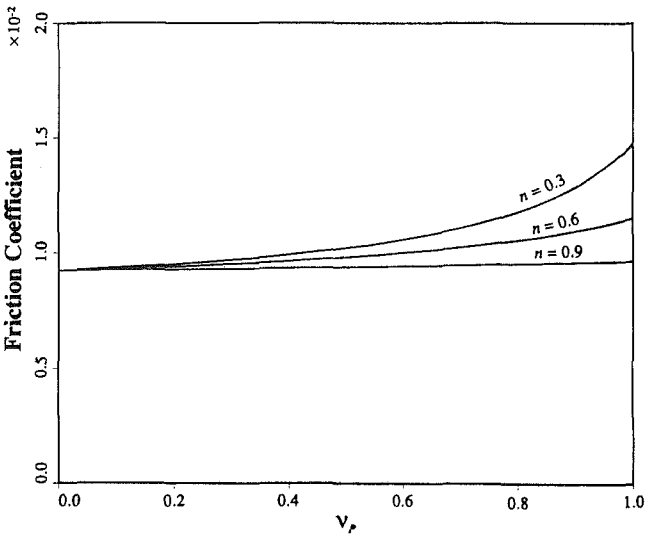


Fig. 5 Variation of friction coefficient with the index of power-law fluid

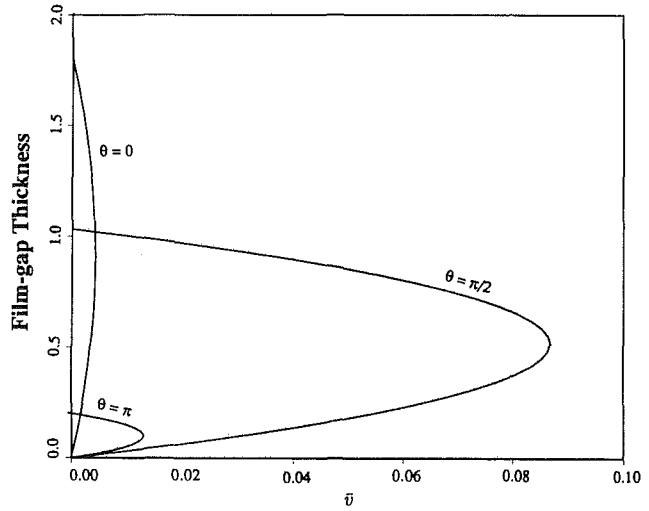


Fig. 7 Velocity distribution $\bar{v}$

can see that the friction coefficient increases with the volume fraction as well as the viscosity of the power-law fluid.

The variation of load-carrying capacity and the friction coefficient with the index of power-law fluid are shown in Figs. 4 and 5, respectively. Three different values of the index are given: $n = 0.3$, $n = 0.6$, and $n = 0.9$. Power-law fluids with $n < 1$ are sometimes referred to as shear-thinning (pseudoplastic) fluids. When $n = 1$, we recover the Newtonian case. It is seen that the load-carrying capacity increases as the index is increased and that the friction coefficient increases with the increasing the value of the index.

For emulsion-type problems where the mixture is nonhomogeneous, particles of each constituent would move independently at velocities u_1, u_2 in the circumferential direction and v_1, v_2 in the axial direction. As was discussed before, for the restricted class presented in this section, the mixture is homogeneous and at a given point in the mixture the particles belonging to both constituents have the same velocity. Shown in Fig. 6 are three velocity profiles in the sliding direction at the bearing midplane for a mixture of power-law fluid and Newtonian fluid with volume fraction of 0.5. The position where the velocities are plotted are: inlet, middle, and outlet ($\theta = 0$, $\theta = \pi/2$ and $\theta = \pi$). The distributions of velocity in the axial direction, $\bar{v}$, for the points on the boundary at inlet, middle, and outlet are plotted in Fig. 7.

5 Concluding Remarks

The general governing equations for the hydrodynamic lubrication involving the mixture of two incompressible fluids are derived. The theory is different from many existing non-Newtonian fluid models in that it considers the mixture as nonhomogeneous. A subclass of the problem, the mixture of a non-Newtonian fluid and a Newtonian fluid is considered as a special case. The classical Reynolds equation for a Newtonian fluid and the generalized Reynolds equation for a simple non-Newtonian fluid (cf., Paranjpe, 1992) are essentially two limiting cases of the equations presented in this paper. Furthermore, it is shown that the formulation of Dien and Elrod (1983) for Couette-dominated flows of non-Newtonian fluids can be derived from the general equations presented. Finally, as an application study, numerical results are presented for the performance parameters of a steadily loaded finite journal bearing lubricated with a mixture of a power-law fluid and a Newtonian fluid.

Downloaded 03 May 2010 to 171.66.16.20. Redistribution subject to ASME license or copyright; see http://www.asme.org/terms/Terms_Use.cfm

Acknowledgments

The authors wish to acknowledge the National Science Foundation and the Pittsburgh Supercomputing Center for the support of this research.

References

Dai, F., and Khonsari, M. M., 1991, "On the Solution of a Lubrication Problem with Particulate Solids," *Int. J. Engng. Sci.*, Vol. 29, p. 1019.

Dai, F., and Khonsari, M. M., 1993, "A Continuum Theory of a Lubrication Problem with Solid Particles," ASME JOURNAL OF APPLIED MECHANICS, Vol. 60, p. 48.

Dien, I. K., and Elrod, H. G., 1983, "A Generalized Steady-State Reynolds Equation for non-Newtonian Fluids, with Application to Journal Bearings," *J. Lubrication Technology*, Vol. 105, p. 385.

Dow, T., 1977, "A Rheology Model for Oil-in-Water," CASA Technical Paper #Ms77-339.

Hamaguchi, H., Spikes, H., and Cameron, A., 1977, "Elastohydrodynamic Properties of Water in Oil Emulsions," *Wear*, Vol. 43, p. 17.

Hetsroni, G., ed., 1982, *Handbook of Multiphase System*, McGraw-Hill, New York.

Homsy, G., El-Kaissy, M., and Didwania, A., 1980, "Instability Waves and the Origin of Bubbles in Fluidized Beds II," *Int. J. Multi-Phase Flow*, Vol. 6, p. 305.

Lunberg, J., 1988, "Rheological Model of a Dilute Emulsion," *STLE Tribology Transactions*, Vol. 31, p. 83.

Nakahara, T., Màkino, T., and Kyogoku, K., 1988, "Observation of Liquid Droplet Behavior and Oil Film Formation in O/W Type Emulsion Lubrication," ASME *Journal of Tribology*, Vol. 110, p. 348.

Paranjpe, R. S., 1992, "Analysis of Non-Newtonian Effects in Dynamically Loaded Finite Journal Bearings Including Mass Conserving Cavitation," ASME *Journal of Tribology*, Vol. 114, p. 736.

Tanner, R. I., 1963, "Non-Newtonian Theory and its Application to the Short Journal Bearing," *Aust. J. Appl. Sci.*, Vol. 14, p. 129.

Downloaded 03 May 2010 to 171.66.16.20. Redistribution subject to ASME license or copyright; see http://www.asme.org/terms/Terms_Use.cfm

Finite Element Analysis of Quasi-static Contact Problems Using Minimum Dissipation of the Energy Principle

N. N. Kishore
Professor.

A. Ghosh
Professor.

S. K. Rathore
Graduate Student.

P. V. Kishore
Graduate Student.

Department of Mechanical Engineering,
Indian Institute of Technology,
Kanpur 208016, India

There are many practical situations where two bodies are directly in contact and are subjected to dynamic or varying loads. The contact area and the contact conditions are functions of load and load history and are not known a priori at any load thus making the problems nonlinear. The conditions of contact are determined by the kinematic constraints and the Coulomb's law of friction. Direct solutions do not give unique results if the load steps are large and the finite element mesh is coarse. In the present work a method using the principle of minimum dissipation of energy is proposed and is applied to finite element analysis of a two-dimensional elastic contact problem under quasi-static loading. A combined incremental and iterative procedure is adopted to solve this problem. The results obtained are in good agreement with physical reasoning. The proposed method obtains new results apart from greatly reducing computational time and efforts.

1 Introduction

There are many instances of engineering structures, such as shrunk-fit shaft and rotor, gear teeth in mesh, flanged connections of pressure vessels, dovetails of turbine blades, rolling wheel, etc., wherein the components are in mechanical contact and transfer of external forces takes place through the contact surfaces. Accurate stress and deformation analysis of such systems requires careful understanding of the frictional contact conditions.

Simplest contact problems occur when two smooth bodies with no friction come in contact with each other along a plane surface under static conditions. This is a linear problem as the contact area remains unchanged during loading and is reversible as the system is conservative. When two curved bodies with smooth surfaces come in contact, the area of contact is a function of load applied. The change in contact area with loads renders the problem nonlinear. However, it is still of reversible nature due to absence of nonconservative forces. When the contact area varies with load and when friction is present, the system becomes irreversible and nonlinear. This, in fact, is the most general case of a contact problem.

Since Hertz (1882) gave his well-known classical solution of a frictionless contact problem further developments have taken place. The need for these in-depth studies has come from practical considerations, particularly with respect to the influence of interfacial friction. The earliest solutions using integral equation methods have been contributed by Muskhelishvili (1963) and Gladwell (1973), etc. In later development, contact problems were considered as special cases of constrained optimization of either total potential or complementary potential energy.

The flexibility method was developed by Francavilla and Zienkiewicz (1975) for frictionless elastic contact problems and then extended to frictional contact by Sachdeva and Ramakrishnan (1981). Jing and Liao (1990) introduced the concept of relative displacements and contact double forces. Total loading and compatibility of displacements were used to determine the contact forces. Wilson and Parsons (1970) used differential displacements and a load incremental process to treat the frictionless contact problems. Chan and Tuba (1971) and Ohte (1973) studied the frictional contact problems for plane and axisymmetric elastic problems. Fredricksson (1976) proposed a constitutive model to account for friction at contact surface. Gaertner (1977) used an experimetnal friction law and a modified element to treat the connecting rod and Hertz problem. Okamoto and Nakajawa (1979) gave a finite element solution using incremental load theory. Torstenfelt (1983) and Rahman, Cook, and Rowlands (1984) used iterative procedure for analysis of elastostatic contact problem with friction. A variational approach, where the equilibrium and the boundary conditions were put into variational form, was adopted by Oden and Pires (1983). They used a nonclassical, nonlocal friction law and variational principle under which these laws hold.

While determining locked displacements in the contact region during the unloading process by minimization of the error approach it was observed by Kishore (1979) that the evaluation

Contributed by the Applied Mechanics Division of THE AMERICAN SOCIETY OF MECHANICAL ENGINEERS for publication in the ASME JOURNAL OF APPLIED MECHANICS.

Discussion on this paper should be addressed to the Technical Editor, Professor Lewis T. Wheeler, Department of Mechanical Engineering, University of Houston, Houston, TX 77204-4792, and will be accepted until four months after final publication of the paper itself in the ASME JOURNAL OF APPLIED MECHANICS.

Manuscript received by the ASME Applied Mechanics Division, May 18, 1992; final revision, Nov. 5, 1993. Associate Technical Editor: A. K. Noor.

Copyright © 1994 by ASME
Downloaded 03 May 2010 to 171.66.16.20. Redistribution subject to ASME license or copyright; see http://www.asme.org/terms/Terms_Use.cfm

evaluation of the displacements was ambiguous and leads to multiple solutions if the load step was finite. It was felt that the unambiguous determination would require an additional principle.

The present work on the dynamic contact is an attempt to solve the problem by the finite element method without assuming any distribution of tractions on the contact patch and without regularizing the friction conditions. The law of Coulomb's friction is assumed. Use is made of the principle of least dissipation of energy of Onsager (1931) to propose an efficient algorithm which does not require any assumption.

2 Theory of Contact Problems and Minimum Dissipation of Energy Approach

2.1 Theory of Contact Problem. Consider two generic bodies which are arbitrarily denoted as contactor and target (Fig. 1(*a*)). The bodies are brought in contact by prescribed tractions and displacements applied on the surface S_t and S_u, respectively. The target body can be either rigid or deformable. On coming in contact, the contact forces develop in the region of contact (Fig. 1(*c*)), where neither the contact pressure nor the area of contact S_c is known a priori.

(i) The stick or no-slip conditions are as follows:

$$u_n^A = u_n^B$$
$$u_t^A = u_t^B$$
$$F_n^A = -F_n^B$$
$$F_t^A = -F_t^B \tag{1}$$

where

u_n^A, u_n^B = normal displacements of adjacent points of body A and B, which are in contact;
u_t^A, u_t^B = tangential displacements of adjacent points of body A and B, which are in contact.
F_n, F_t = corresponding normal and tangential contact forces.

(ii) The slip conditions are as follows:

$$u_n^A = u_n^B$$
$$u_t^A \neq u_t^B$$
$$F_n^A = -F_n^B$$
$$F_t^A = -F_n^B$$
$$F_t = \pm \mu |F_n| \tag{2}$$

where μ is the coefficient of friction and the directions of F_t and the tangential displacement are opposite.

The same conditions of contact and friction apply to both quasi = static and rolling contact problems. When a roller moves on a rigid plane surface without sliding, the contact develops between the roller and the ground. In free rolling, i.e., rolling under the action of a purely normal load, the extent of slip is small whereas when the contact surfaces transmit an externally applied tangential force or twisting couple, an appreciable amount of slip occurs. Uniform rolling motion is a steady process in which the loads and the fields of stress, strain, and deformation do not change with time with respect to an observer translating with the speed of the roller.

2.2 Minimum Dissipation of Energy. The elastic contact problem with finite friction is an irreversible problem, the solution to which depends upon the loading history. The loading or unloading are done gradually, and the process is assumed to be quasi-static. The principle of least dissipation of energy was originally formulated by Onsager (1931) for a particular case of heat conduction and later extended by Onsager and Machlup (1953) to the case of adiabatically isolated noncontinuous systems. In the following procedure the problem is solved in an incremental and iterative manner in which the normal contact pressures are found and the minimum dissipation of energy principle is applied alternately, thus making the problem an associated one.

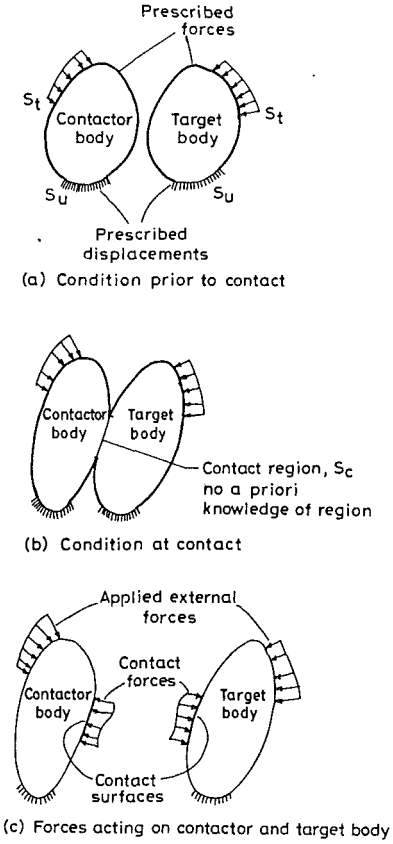


Fig. 1 Schematic representation of contact problem

The approach adopted in the present work is that after establishing the total contact area, the principle of minimum dissipation of energy is employed to determine the extent of tangential displacement in the slip region. The procedure of minimization of the energy dissipation and the search for the feasible state is formulated as a constrained minimization problem, with the dissipated energy expression, ϕ_d, as the objective function together with a penalty, e, due to constraints at the contact. The expression for ϕ_d is given as

$$\phi_d = \sum_{k=1}^{m} |(\alpha_k^i - \alpha_k^{i-1})(F_{t_k}^{i-1} + F_{t_k}^i)/2| \tag{3}$$

where the summation is over all m-contact nodes, α_k^i denote the tangential displacement of the node k on the contact surface at ith load step and $F_{t_k}^i$ represents the tangential nodal force at ith load step.

The penalty term e takes into account the friction conditions and is given by

$$e = \sum_{k=1}^{m} \left\{ \frac{(|F_{t_k}^i| - \mu |F_{n_k}^i|)^2}{\sqrt{\lambda}} + C|(\alpha_k^i - \alpha_k^{i-1})(|F_{t_k}^i| - \mu |F_{n_k}^i|)| \right\} \tag{4}$$

where $F_{n_k}^i$ represents the normal nodal force at ith load step.

The first term in the foregoing expression is considered only for those nodes where $|F_t| \geq \mu |F_n|$. λ and C are the penalty parameter and weighting factors, respectively.

Downloaded 03 May 2010 to 171.66.16.20. Redistribution subject to ASME license or copyright; see http://www.asme.org/terms/Terms_Use.cfm

Thus, the objective function to be minimized is

$$\psi = \phi_d + e. \tag{5}$$

When ψ is minimized, e usually becomes zero showing that all the nodes satisfy contact conditions and ϕ_d also assumes a minimum value of such possible states, and that state is characterized as a feasible state.

With the above notation, the sticking status of any node is represented as follows:

$$\text{When } \alpha_k^i = \alpha_k^{i-1}$$
$$e = 0 \text{ and } \phi_d = 0. \tag{6}$$

When e is not equal to zero, then the set of unknowns α_k^i are found by minimizing ψ. Thus, the extent of slip is determined.

3 Finite Element Method and Solution Algorithm

The solution of the contact problem is determined in two stages. The first part is to determine the area of contact and the second part is to find the feasible state by using principle of minimum dissipation of energy. The second part is computer time intensive and substructuring methods are used to simplify the repeated calculations.

To obtain a finite element solution, the assumptions made are as follows: the materials are linear elastic, the deformations are small, plane-strain conditions prevail, and the body forces are negligible. In the present investigation, for simplicity, it is assumed that one of the two contacting bodies is rigid whereas the other one is deformable and needs to be discretized. The domain is discretized into a standard triangular element mesh.

Symmetry has been made use of wherever present. At the contact surface, a local coordinate system in the tangential and normal directions is used to facilitate the application of contact conditions. For solving the above equations the contact conditions are enforced as follows:

Phase I: Determination of Contact Area. Initially, a set of possible nodes is considered in contact and the response is obtained at a given load level. If at a node, the normal contact force turns out to be tensile, then that node is set free. Whereas, if the displacement of any free node in a normal direction of contact surface appears to penetrate geometrically or touches the rigid surface, it is included in the contact region.

Thus, the following conditions are imposed when the nodes change their state:

(*i*) *Change From Contact to Separation.* In the separated condition, the node is treated as a free node and their nodal force components are equated to zero. Thus,

$$F_n = 0$$
$$F_t = 0 \tag{7}$$

where F_n, F_t are the normal and tangential contact forces, respectively.

(*ii*) *Change From Separation to Contact.* The displacement conditions in normal and tangential directions are modified so that the given node becomes a contact node as

$$u_n = \delta$$
$$u_t = 0 \tag{8}$$

where u_n is a normal nodal displacement, δ is a clearance between the rigid surface and the corresponding node in a normal direction before application of the given load, and u_t is the tangential nodal displacement.

Using the above conditions at the contact nodes, the reaction forces at the contact zone and the displacements of the free nodes are obtained. Again, the conditions of contact are checked and the above procedure is repeated, until the changes are below a certain value in successive iterations at the given load.

Phase II: Determination of Slip and No-Slip Zones in the Contact Region. Having determined the contact area at a load level, the next phase is to check the friction condition to establish the regions of slip and no-slip as given below:

(i) When $|F_t| \leq \mu |F_n|$, there is no relative tangential displacement between the node and the rigid surface.

For this case, the following conditions are imposed:

$$u_n = \delta$$
$$u_t = 0 \tag{9}$$

(ii) When $|F_t| > \mu |F_n|$, the nodes are allowed to slip and the following conditions are imposed:

$$u_n = \delta. \tag{10}$$

The slip allowed until $|F_t| = \mu |F_n|$. The direction of F_t is chosen such that it opposes the tangential movement of the node with respect to the rigid surface.

In these problems, the contact conditions such as a node coming into contact or a node separating or change in friction status of slipping or sticking will modify the stiffness matrix. These modifications change in every iteration, and a multilevel substructuring scheme is made use of so that smaller matrices are handled in the iterative procedure. The substructuring scheme is necessary not only to save computational time but also to minimize memory storage requirement as the contact relations, when imposed as such otherwise, render the stiffness matrix unsymmetrical, requiring full storage of the matrices.

4 Results

As an example a plate with a hole with an oversized rigid inclusion is studied. The plate is subjected to far-field uniform loading. The loading and unloading processes are gradual and after each load increment the solution is updated. The load increments are chosen in such a manner that at a time either one node comes into contact or just one node separates, and the changed contact conditions are assumed to become operative for subsequent load increments. The expressions for interpolating the incremental load is discussed as follows:

First, solve for a nodal displacement increment $\{\Delta U_n\}$ and a contact force increment vector $\{\Delta F_n\}$ using the contact conditions of previous step and a test load $\{\Delta P\}$. $\{U_n\}$ and $\{F_n\}$ is the solution at load P_n.

The new load P_{n+1} is found as

$$\{P_{n+1}\} = \{P_n\} + \alpha_n \{\Delta P\} \tag{11}$$

where α_n is a load incremental ratio. The value of α_n is the smallest of α_n^* (load incremental ratio at different nodes) for the nodes violating their existing contact conditions. The objective function ψ, which includes the penalty e and the dissipation of energy, ϕ_d, is minimized by a suitable unconstrained minimization technique. Hookes and Jeeves pattern search method (Rao S. S., 1990; Kuesterl-Mize, 1973), which is a unimodal, sequential-search type, is adopted in determining the tangential displacements, represented as the geometric variables α_k, such that the dissipation is minimum and all other constraints are satisfied. A finite plate with $a/r = 6$ is taken to model a large plate (Fig. 2(*a*)). Because of symmetry it is enough to analyze one quarter of the plate and the geometry is shown in Fig. 2(*b*) along with finite element mesh. As shown in the figure, there is a fine mesh near the hole boundary and coarser mesh away with a total 360 elements and 207 nodes.

In what follows the amount of shrinkage is expressed in terms of an equivalent initial precompression stress, T_{pre}, as

Downloaded 03 May 2010 to 171.66.16.20. Redistribution subject to ASME license or copyright; see http://www.asme.org/terms/Terms_Use.cfm

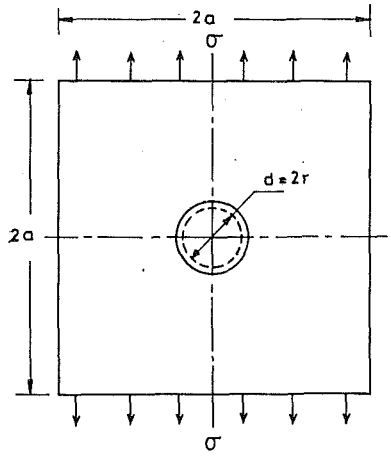


Fig. 2(*a*) A plate with a oversized rigid inclusion

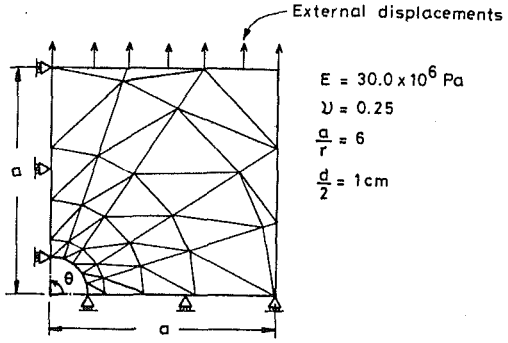


Fig. 2(*b*) Representative mesh and prescribed boundary conditions

$$T_{\text{pre}} = -\frac{\delta}{r}\frac{E}{(1+\nu)} \tag{12}$$

where δ is the amount of shrinkage, r is the radius of the hole, E is the modulus of elasticity, and ν is the Poisson's ratio.

The material properties and the geometry of the plate are taken as follows: $E = 30.0 \times 10^6$ Pa; $\nu = 0.25$; $a = 6$ cm; $r = 1$ cm; $\delta = 1.5 \times 10^{-4}$ cm, $\mu = 0.4$.

It is assumed that there are no locked displacements initially and the tensile load is applied gradually. Studies have been conducted on the sensitiveness of the solution with the load increment and it is found that with the new method the solutions were quite stable with a moderate step size of T (in comparison to T_{pre}).

4.1 Comparison of the Solution Methods.

Method I: Objective function, ψ, consists of the term due to constraints, e only. (This method is referred to as "without dissipation of energy").

Method II: The objective function consists of the terms due to constraints, e, and the energy dissipated, ϕ_d. (This method is referred to as "with dissipation of energy.")

Figure 3 presents the contact zones as functions of load T while the loading is done in tension for a coefficient of friction, μ, of 0.4 by Method I and Fig. 4 presents the results of the same problem by Method II. From the figures it can be observed that with the increase in load, the slip zone appears first and expands. Later separation occurs near 90 degrees and spreads inward. It can be observed that there is no difference in the results by the two methods, though the first method requires interpolation of load for any node going from the no-slip to slip state. Because of the coarseness of the mesh the

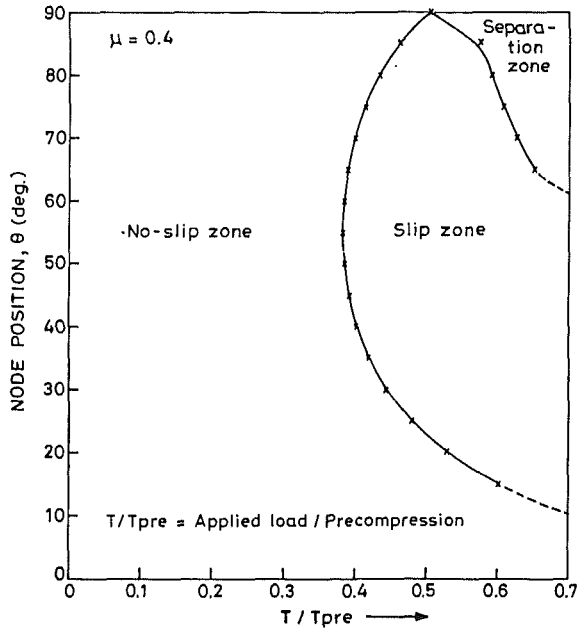


Fig. 3 Interface zones while loading in tension from undeformed state (without dissipation) $\mu = .4$

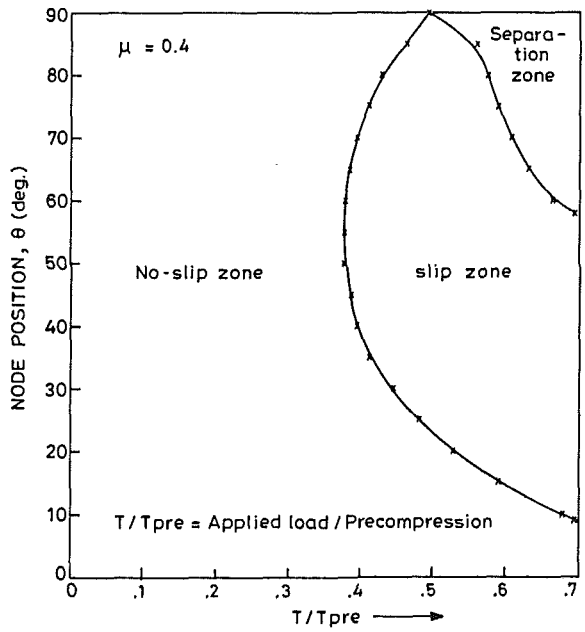


Fig. 4 Interface zones while loading in tension from undeformed state (with dissipation) $\mu = .4$

data are not available very near to 0 deg and 90 deg, and curves are extrapolated (shown by broken line) for the sake of completeness and understanding.

Figures 5 and 6 present the variation of contact zones with load when the load is decreased from the maximum tensile load. During this unloading process the nodes tend to slip in the direction opposite to that while loading and for a small load step the slip zone completely becomes no-slip. Later the nodes in the no-slip zone begin to slip gradually and the size of the separation zone decreases. It can be seen that the behaviors obtained by the methods are different. In the case of Method I (Fig. 5) when any node enters the contact zone from separation, it slips and later the nodes near 90 deg go to no-slip zone. On the other hand, Method II (Fig. 6) shows that the nodes near 90 deg directly go to no-slip zone. After in-

Downloaded 03 May 2010 to 171.66.16.20. Redistribution subject to ASME license or copyright; see http://www.asme.org/terms/Terms_Use.cfm

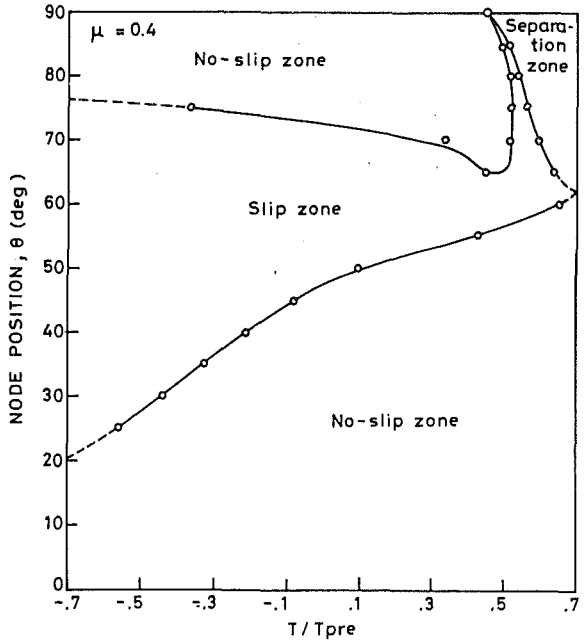


Fig. 5 Interface zones while unloading tension and loading in compression (without dissipation) $\mu = .4$

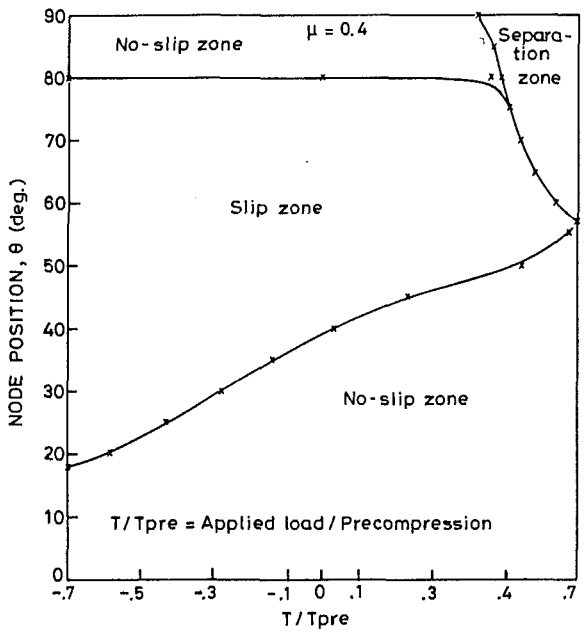


Fig. 6 Interface zones while unloading tension and loading in compression (with dissipation) $\mu = .4$

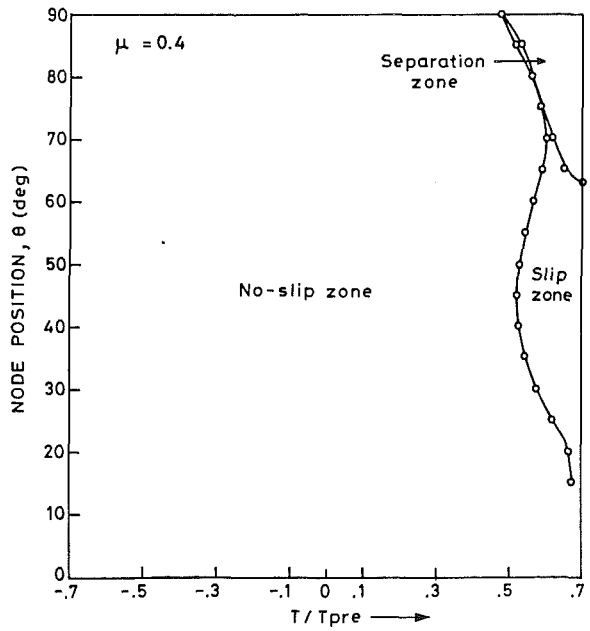


Fig. 7 Interface zones while unloading compression and loading in tension (without dissipation) $\mu = .4$

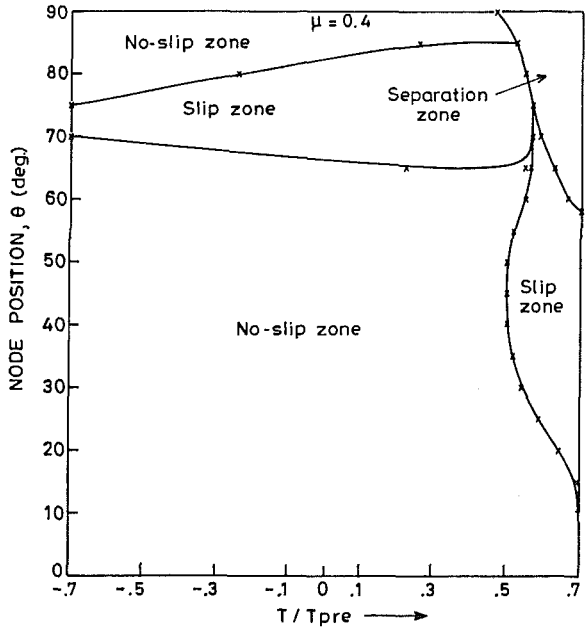


Fig. 8 Interface zones while unloading compression and loading in tension (with dissipation) $\mu = .4$

vestigating the two methods, it was found that in the case of Method I, during iterations the nodes near 90 deg oscillate between slip and no-slip conditions. It requires a finer mesh to obtain the correct solution with Method I, whereas Method II can solve such problems effectively with any mesh, even if it is coarse.

After complete unloading, it is loaded in compression to the same maximum value as that in tension. Figures 5 and 6 also show the behavior during that process and the results are comparable to both methods.

During unloading from maximum compression, in the case of Method I, Fig. 7 shows that there is complete no-slip zone at the interface initially and slip zone appears as unloading continues whereas, by the Method II (Fig. 8), some of the nodes continue to slip in the same direction as that while loading. As the unloading proceeds some of those nodes stick for some time and then start slipping in the reverse direction. This complex behavior is not obtained by the Method I procedure. The distributions of normal and tangential stresses at the interface are presented in Figs. 9 to 12. There is slight deviation near the plane of symmetry which may be due to angular contact area (Gaertner, 1977) and use of lower order element in the region of high stress gradient. There exists a separation zone also at this load, shown as zero contact stresses.

5 Conclusions

(1) Using the minimum dissipation of energy approach there is no requirement to keep track of the direction of frictional resistance during the various stages of loading. The procedure itself takes care of all such situations.

Downloaded 03 May 2010 to 171.66.16.20. Redistribution subject to ASME license or copyright; see http://www.asme.org/terms/Terms_Use.cfm

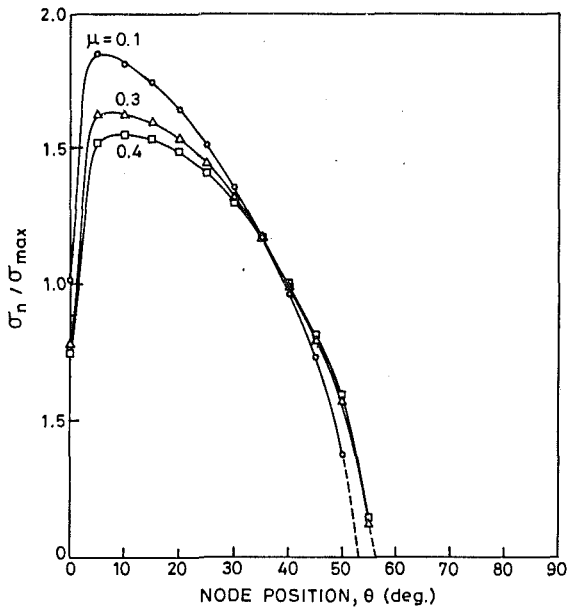


Fig. 9 Variation of normal stress over contact length, for different μ (at maximum tensile load, $T/T_{pre} = 0.7$)

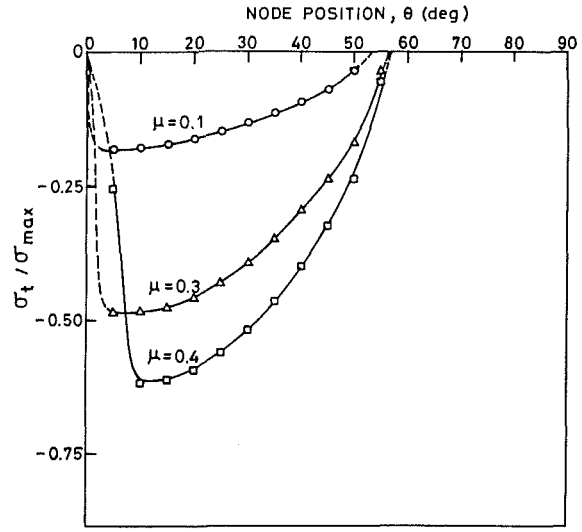


Fig. 10 Variation of tangential stress over contact length, for different μ (at maximum tensile load, $T/T_{pre} = 0.7$)

(2) In complex contact conditions the present method leads, with ease, to more accurate results. To achieve the same accuracy by the method without dissipation energy will require very fine mesh and very small load steps.

6 References

Chan, S. K., and Tuba, I. S., 1971, "A Finite Element Method for Contact Problems of Solid Bodies—Part I: Theory and Validation," *Int. J. of Mech. Sci.*, Vol. 13, pp. 615–625.

Francavilla, A., and Zienkiewicz, O. C., 1975, "A Note on Numerical Computation of Elastic Contact Problems," *International Journal for Numerical Methods in Engineering*, Vol. 9, pp. 913–924.

Fredriksson, B., 1976, "Finite Element Solution of Surface Non-Linearities in Structural Mechanics with Special Emphasis to Contact and Fracture Mechanics Problems," *Computers & Structures*, Vol. 6, pp. 281–290.

Gaertner, R., 1977, "Investigation of Plane Elastic Contact Allowing for Friction," *Computers & Structures*, Vol. 7, pp. 59–63.

Gladwell, G. M. L., 1973, *Contact Problems in Classical Theory of Elasticity*, Sijthoff and Nordhoff, The Netherlands.

Hertz, H. J., 1882, Miscellaneous papers (in German) Vol.92, 156–171); (in English) Macmillan, London, 1896.

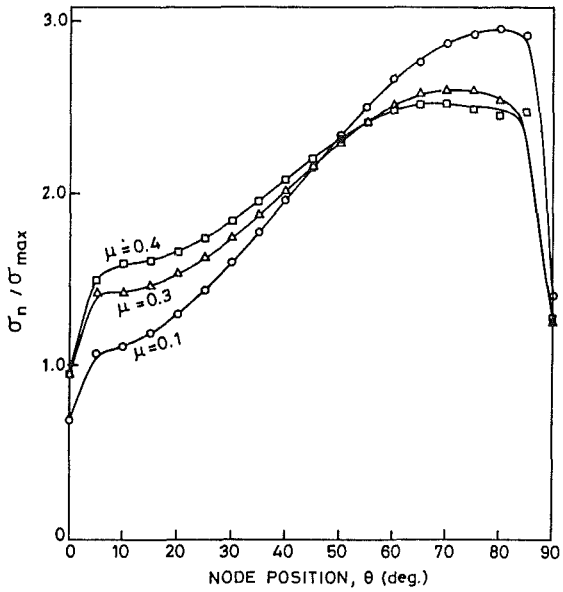


Fig. 11 Variation of normal stress over contact length, for different μ (at maximum compressive load, $T/T_{pre} = -0.7$)

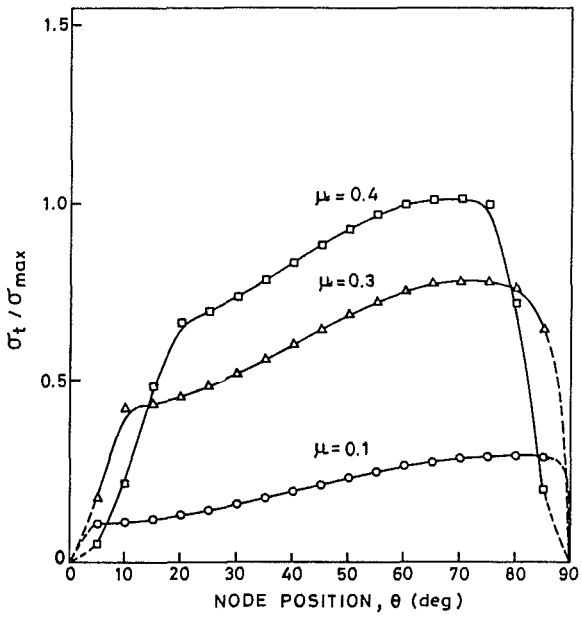


Fig. 12 Variation of tangential stress over contact length, for different μ (at maximum compressive load, $T/T_{pre} = -0.7$)

Jing, H.-S., and Liao, M. L., 1990, "An Improved Finite Element Scheme for Elastic Contact Problems with Friction," *Computers & Structures*, Vol. 35, pp. 571–578.

Johnson, K. L., 1958, "Effect of Tangential Contact Force upon the Rolling Motion of an Elastic Sphere on a Plane," ASME Journal of Applied Mechanics, Vol. 25.

Kishore, N. N., 1979, 'Development and Analysis of High Damping Composites through Imperfect Bonding," Ph.D. Thesis, I. I. T. Kanpur.

Kuester, J. L., and Mize, J. H., 1973, *Optimization Techniques with Fortaran*, McGraw-Hill, New York.

Muskhelishville, N. I., 1963, "Some Basic Problems of the Mathematical Theory of Elasticity," Sijthoff and Nordhoff, The Netherlands.

Oden and Pires, 1983, "Non-Local and Non-Linear Friction Laws and Variational Princples for Contact Problems in Elasticity," ASME Journal of Applied Mechanics, Vol. 50, pp. 67–76.

Okamoto, N., and Nakazawa, M., 1979, "Finite Element Incremental Contact Analysis with Various Frictional Conditions," *International Journal for Numerical Methods in Engineering*, Vol. 14, pp. 337–357.

Ohte, S., 1973, "Finite Element Analysis of Elastic Contact Problems," *Bulletin of JSME*, Vol. 16, pp. 797–804.

Downloaded 03 May 2010 to 171.66.16.20. Redistribution subject to ASME license or copyright; see http://www.asme.org/terms/Terms_Use.cfm

Onsager, L., 1931, *Phy. Rev.*, Vol. 37, p. 405; Vol. 38, p. 2265.

Onsager, L., and Machlup, S., 1953, *Phy. Rev.*, Vol. 91, pp. 1505–1512.

Rahman, M. U., Rowlands, R. E., and Cook, R. D., 1984, "An Iterative Procedure for Finite Element Stress Analysis of Frictional Contact Problems," *Comptuers & Structures*, Vol. 18, pp. 947–954.

Rao, S. S., 1990, *Optimization Theory and Application*, 2nd ed., Wiley Eastern Ltd.

Sachdeva, T. D., and Ramakrishnan, C. V., 1981, "A Finite Element Solution for the Two-Dimensional Elastic Contact Problems with Friction," *International Journal for Numerical Methods in Engineering*, Vol. 17, pp. 1257–1271.

Torstenfelt, Bo, 1983, "Contact Problems with Friction in General Purpose Finite Element Computer Program," *Computers & Structures*, Vol. 16, pp. 487–493.

Wilson and Parsons, 1970, "Finite Element Analysis of Contact Problems Using Differential Displacements," *Computers & Structures*, Vol. 2, pp. 387–395.

Downloaded 03 May 2010 to 171.66.16.20. Redistribution subject to ASME license or copyright; see http://www.asme.org/terms/Terms_Use.cfm

Exact Transient Full-Field Analysis of an Antiplane Subsurface Crack Subjected to Dynamic Impact Loading

Chien-Ching Ma
Professor.

Szu-Kuzi Chen
Graduate Student.

Department of Mechanical Engineering,
National Taiwan University,
Taipei, Taiwan 10764, R.O.C.

The transient problem of a half-space containing a subsurface inclined semi-infinite crack subjected to dynamic antiplane loading on the boundary of the half-space has been investigated to gain insight into the phenomenon of the interaction of stress waves with material defects. The solutions are determined by superposition of the fundamental solution in the Laplace transform domain. The fundamental solution is the exponentially distributed traction on crack faces. The exact close-form transient solutions of stresses and displacement are obtained in this study. These solutions are valid for an infinitely long time and have accounted for the contributions of incident, reflected, and diffracted waves. Numerical results of the transient stresses are obtained and compared with the corresponding static values. The transient solution has been shown to approach the static value after the first few diffracted waves generated from the crack tip have passed the observation point.

1 Introduction

The difficulty in determining the transient stress field in a cracked-elastic body subjected to dynamic loading is a well-known problem. A considerable amount of research has been directed towards the solution of problems involving the interaction of stress waves with the crack and boundary to improve understanding of the behavior of material failure under dynamic loading. The investigation of an idealized semi-infinite crack can provide some information for a realistic elastodynamic fracture problem. It is noted that while the analysis has been carried out assuming a semi-infinite crack, the results remain valid for a finite crack up until the time at which waves diffracted from the far tip reach the tip near the boundary.

In conventional studies of a semi-infinite crack in an unbounded medium subjected to dynamic loading, the complete solution is obtained by integral transform methods together with direct application of the Wiener-Hopf technique (Noble, 1958) and the Cagniard-de Hoop method (de Hoop, 1958) of Laplace inversion. If the loading is replaced by a nonuniform distribution having a characteristic length, then the same procedure using integral transformation methods does not apply. The problem of an elastic solid containing a half-plane crack subjected to concentrated impact loading on the faces of the crack has been previously studied by Freund (1974). He proposed a fundamental solution arising from an edge dislocation climbing along the line ahead of the crack tip with a constant speed to overcome these difficulties of the case with a characteristic length. The solution can be constructed by taking an integration over a climbing dislocation of different moving velocity. Basing his procedure on this method, Brock (1982, 1984, 1985) and Ma and Hou (1990, 1991) have recently analyzed a series problems of a semi-infinite crack subjected to impact loading. Lee and Freund (1990) analyzed fracture initiation of an edge cracked plate subjected to an asymmetric impact.

Whenever dynamic loading is applied to a body with an internal crack, the resulting stress waves may initiate crack growth. Few solutions for a cracked elastic solid subjected to dynamic loading are available. Exact transient close-form solutions for a stationary semi-infinite crack subjected to a suddenly applied dynamic body force in an unbounded medium have been obtained by Tsai and Ma (1992) for the in-plane case and by Ma and Chen (1993) and Brock (1986) for the antiplane case. The problem to be considered in this study is the antiplane response of an elastic half-plane, with an inclined crack extending from infinity to a location near the half-plane surface, which is subjected to dynamic antiplane loading on the half-plane surface as shown in Fig. 1. The propagation of stress waves through an unbounded medium, which are due to applying dynamic loading on the boundary, is not a difficult subject. A pre-existing fault inside the medium would disturb the propagation waves and make the theoretical analysis much more difficult than in an homogeneous medium. In this study, a free boundary and crack are incorporated into the analysis

Contributed by the Applied Mechanics Division of THE AMERICAN SOCIETY OF MECHANICAL ENGINEERS for publication in the ASME JOURNAL OF APPLIED MECHANICS.

Discussion on this paper should be addressed to the Technical Editor, Professor Lewis T. Wheeler, Department of Mechanical Engineering, University of Houston, Houston, TX 77204-4792, and will be accepted until four months after final publication of the paper itself in the ASME JOURNAL OF APPLIED MECHANICS.

Manuscript received by the ASME Applied Mechanics Division, Sept. 30, 1992; final revision, June 12, 1993. Associate Technical Editor: S. K. Datta.

Copyright © 1994 by ASME
Downloaded 03 May 2010 to 171.66.16.20. Redistribution subject to ASME license or copyright; see http://www.asme.org/terms/Terms_Use.cfm

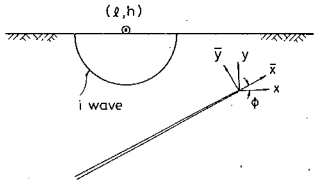


Fig. 1 Configuration, coordinate systems of a subsurface inclined crack subjected to impact loading on the half-space

which made the analysis extremely difficult. In analyzing this problem, the reflections and diffractions of stress waves by the boundary and by the crack which will generate infinite waves, must be taken into account. This problem involves a characteristic length which makes a direct solution by standard techniques difficult. Since none of the methods proposed by Freund (1974) and Brock et al. (1985) have worked for this problem, some other approach must be followed. A new fundamental solution is used for overcoming these difficulties. This alternative fundamental solution is successfully applied towards solving the problem and is to be demonstrated as an efficient methodology. The final formulations are expressed explicitly and the dynamic effect of each wave is presented in a closed form. The results are valid for the infinitely many waves that are scattered from the crack tip and reflected by the free boundary. In some classes of dynamic problems, the ability to find a static field may hinge on waiting for the wave fronts to pass and the transient effect to die away. The characteristic time after which the transient effect can be neglected is also investigated in this study.

2 Required Fundamental Solutions

As usual in problems of the type considered here, superposition of solutions plays a significant role. The solutions to the problem considered in this study can be determined by superposition of the following problems. Problem A treats the dynamic concentrated force acting on a half-plane medium without a crack, which induces a traction on the planes that will eventually define the initial crack faces. In problem B, an infinite body containing a semi-infinite crack is considered in which the faces are subjected to tractions which are equal and opposite to those on the corresponding planes in problem A. Problem C considers a half-plane free surface subjected the incident waves which are generated by the crack in problem B. The reflected waves coming from the free boundary can be constructed by employing the method of images.

Problem B in the above-mentioned three fundamental problems is the only one which needs careful analysis. Reflected and diffracted waves are generated from physical considerations, thus eliminating the stress induced by incident waves on the traction-free boundaries of crack faces. For most of the dynamic problems, the incident waves can be represented in an exponential functional form in the Laplace transform domain of time. The reflected and diffracted waves generated by the crack can thus be constructed by the superposition method; that is, if the responses toward an applied exponentially distributed traction on the crack face in the Laplace transform domain can be obtained preliminarily. The superposition scheme proposed in this study, unlike usual superposition methods which are performed in the time domain, is performed in the Laplace transform domain.

This solution for an exponentially distributed loading applied to the crack faces in the Laplace transform domain will be referred to as the fundamental solution. The problem can be viewed as a half-plane problem with the material occupying the region $y \geq 0$, subject to the following boundary conditions:

$$\bar{\tau}_{yz}(x, 0, p) = e^{p\eta x} \quad -\infty < x < 0, \tag{1}$$

$$\bar{w}(x, 0, p) = 0 \quad 0 < x < \infty, \tag{2}$$

where p is the Laplace transform parameter and η is a constant. The overbar symbol is used for denoting the transform on time t. The governing equation can be represented by the two-dimensional wave equation

$$\frac{\partial^2 w}{\partial x^2} + \frac{\partial^2 w}{\partial y^2} = b^2 \frac{\partial^2 w}{\partial t^2}, \tag{3}$$

where b is the slowness of the transverse wave given by

$$b = 1/v = \sqrt{\rho/\mu},$$

in which $w(x, y, t)$ is the displacement normal to the xy-plane, v is the shear wave speed, and μ and ρ are the respective shear modulus and the mass density of the material. The nonvanishing shear stresses are

$$\tau_{yz} = \mu \frac{\partial w}{\partial y}, \quad \tau_{xz} = \mu \frac{\partial w}{\partial x}. \tag{4}$$

This problem can be solved by the application of integral transforms. Applying the one-sided Laplace transform over time, the two-sided Laplace transform over x under the restriction of $\mathrm{Re}(\eta) > \mathrm{Re}(\lambda)$, finally the Wiener-Hopf technique is implemented. The solutions of stresses and displacement for the boundary conditions (1) and (2) in the transform domain are

$$\bar{\tau}_{yz}(x, y, p) = \frac{1}{2\pi i} \int_{\Gamma_\lambda} \frac{(b+\lambda)^{1/2} e^{-p(\alpha y - \lambda x)}}{(b+\eta)^{1/2}(\eta - \lambda)} d\lambda, \tag{5}$$

$$\bar{\tau}_{xz}(x, y, p) = -\frac{1}{2\pi i} \int_{\Gamma_\lambda} \frac{\lambda e^{-p(\alpha y - \lambda x)}}{(b+\eta)^{1/2}(\eta - \lambda)(b-\lambda)^{1/2}} d\lambda, \tag{6}$$

$$\bar{w}(x, y, p) = -\frac{1}{2\pi i} \int_{\Gamma_\lambda} \frac{e^{-p(\alpha y - \lambda x)}}{\mu p (b+\eta)^{1/2}(\eta - \lambda)(b-\lambda)^{1/2}} d\lambda, \tag{7}$$

where

$$\alpha = (b^2 - \lambda^2)^{1/2}.$$

3 Transient Full-Field Analysis

The investigation of a subsurface crack subjected to dynamic loading is an important topic in material failure analysis. The problem considered here is an inclined semi-infinite crack located under the surface of a half-plane. Having two coordinate systems in the following analysis is convenient, since the surface of the half-plane is not parallel to the crack faces. The origins of the two coordinate systems $(\bar{x}, \bar{y})$ and (x, y) are both located at the crack tip as shown in Fig. 1. The planar crack lies in the plane $\bar{y} = 0$, $\bar{x} < 0$ and the inclined angle of the crack is ϕ. The coordinate transforms and stress relations between these two systems are

$$\bar{x} = x \cos\phi + y \sin\phi, \tag{8}$$

$$\bar{y} = -x \sin\phi + y \cos\phi, \tag{9}$$

$$\tau_{xz} = \tau_{\bar{x}\bar{z}} \cos\phi - \tau_{\bar{y}\bar{z}} \sin\phi, \tag{10}$$

$$\tau_{yz} = \tau_{\bar{x}\bar{z}} \sin\phi + \tau_{\bar{y}\bar{z}} \cos\phi. \tag{11}$$

This problem has a characteristic length. A direct attempt towards solving this problem by transform and Wiener-Hopf techniques is not applicable. The transient elastodynamic problem is solved by superposition of the fundamental solutions obtained in the previous section in the Laplace transform domain. The transient solutions are composed of an incident field, reflected field, and diffracted field, which are denoted by superscripts of i, r, and d, respectively. The incident wave is the response to loading applied to a semi-infinite unbounded medium. The reflected and diffracted waves are generated through application of an opposite traction at the crack surface thus eliminating the stress induced by incident wave.

Downloaded 03 May 2010 to 171.66.16.20. Redistribution subject to ASME license or copyright; see http://www.asme.org/terms/Terms_Use.cfm

Consider a half-plane body which is stress-free and at rest. At time $t = 0$, an anti-plane concentrated dynamic force is applied at the free surface of a half-plane at position (l, h). The time dependence of the loading is represented by the Heaviside step function $H(t)$. The incident fields in the Laplace transform domain can be obtained as follows:

$$\bar{w}^i(x, y, p) = \frac{1}{2\pi i} \int_{\Gamma_\lambda} \frac{1}{\mu p \alpha} e^{p[\alpha(y-h)+\lambda(x-l)]} d\lambda, \quad (12)$$

$$\bar{\tau}^i_{yz}(x, y, p) = \frac{1}{2\pi i} \int_{\Gamma_\lambda} e^{p[\alpha(y-h)+\lambda(x-l)]} d\lambda, \quad (13)$$

$$\bar{\tau}^i_{xz}(x, y, p) = \frac{1}{2\pi i} \int_{\Gamma_\lambda} \frac{\lambda}{\alpha} e^{p[\alpha(y-h)+\lambda(x-l)]} d\lambda. \quad (14)$$

The incident stress field $\bar{\tau}^i_{\bar{y}\bar{z}}(\bar{x}, 0, p)$ induced in the crack face at $\bar{y} = 0$ expressed in the $\bar{x} - \bar{y}$ coordinate system is

$$\bar{\tau}^i_{\bar{y}\bar{z}}(\bar{x}, 0, p) = \frac{1}{2\pi i} \int_{\Gamma_\lambda} e^{-p\alpha h_0 + p\lambda(\bar{x}-l_0)} d\lambda, \quad (15)$$

where

$$l_0 = l \cos\phi + h \sin\phi, \quad h_0 = -l \sin\phi + h \cos\phi.$$

The applied traction on the crack face, in order to eliminate the incident wave as indicated in (15) has the functional form $e^{p\lambda\bar{x}}$. Since the solutions of applying traction $e^{p\eta\bar{x}}$ on crack faces have been solved in Section 2, the reflected and diffracted fields generated from the inclined crack can be constructed by superimposing the incident wave traction that is equal and opposite to (15). When we combine Eqs. (5) and (15), the solution of reflected and diffracted waves for $\bar{\tau}_{\bar{y}\bar{z}}$ and $\bar{\tau}_{\bar{x}\bar{z}}$ in the Laplace transform domain can be expressed as follows:

$$\bar{\tau}^{d+r}_{\bar{y}\bar{z}}(\bar{x}, \bar{y}, p) = \frac{1}{4\pi^2} \int_{\Gamma_{\eta_1}} \int_{\Gamma_{\eta_2}} G(\eta_1, \eta_2) e^{-p(\alpha_1 h_0 + \eta_1 l_0)} \times e^{-p(\alpha_2 \bar{y} - \eta_2 \bar{x})} d\eta_2 d\eta_1, \quad (16)$$

$$\bar{\tau}^{d+r}_{\bar{x}\bar{z}}(\bar{x}, \bar{y}, p) = -\frac{1}{4\pi^2} \int_{\Gamma_{\eta_1}} \int_{\Gamma_{\eta_2}} \frac{\eta_2}{\alpha_2} G(\eta_1, \eta_2) e^{-p(\alpha_1 h_0 + \eta_1 l_0)} \times e^{-p(\alpha_2 \bar{y} - \eta_2 \bar{x})} d\eta_2 d\eta_1,$$

where

$$G(\eta_1, \eta_2) = \frac{(b+\eta_2)^{1/2}}{(b+\eta_1)^{1/2}(\eta_1 - \eta_2)},$$

$$\alpha_1 = (b^2 - \eta_1^2)^{1/2}, \quad \alpha_2 = (b^2 - \eta_2^2)^{1/2}.$$

The above solutions for stresses are expressed in the $\bar{x} - \bar{y}$ coordinate system. If the solutions are expressed in the $x - y$ coordinate system, then a small modification should be made to account the effect of coordinate transformation, and the result for $\bar{\tau}_{yz}$ is

$$\bar{\tau}^{d+r}_{yz}(x, y, p) = \frac{1}{4\pi} \int_{\Gamma_{\eta_1}} \int_{\Gamma_{\eta_2}} K_1(\eta_2) G(\eta_1, \eta_2) e^{-p(\alpha_1 h_0 + \eta_1 l_0)} \times e^{-p(\alpha_2 \bar{y} - \eta_2 \bar{x})} d\eta_2 d\eta_1,$$

where

$$K_1(\eta_2) = \cos\phi - \frac{\eta_2}{\alpha_2} \sin\phi.$$

Equation (16) constitutes a double inversion integral where the path Γ_{η_1} and Γ_{η_2} refer to Laplace inversion contours in the η_1-plane and the η_2-plane, respectively. The inverse transformation is carried out here through use of the Cagniard-de Hoop technique. Cagniard contours are introduced here in both η_1- and η_2-plane by setting

$$\alpha_1 h_0 + \eta_1 l_0 = t_1, \quad (17)$$

$$\alpha_2 \bar{y} - \eta_2 \bar{x} = t_2. \quad (18)$$

Equations (17) and (18) can be solved for η_1 and η_2 to yield

$$\eta_1^{\pm} = \frac{t_1 \cos\Theta_0}{R_0} \pm i \frac{\sin\Theta_0}{R_0} (t_1^2 - b^2 R_0^2)^{1/2}, \quad (19)$$

$$\eta_2^{\pm} = \frac{t_2 \cos\psi}{d} \pm i \frac{\sin\psi}{d} (t_2^2 - b^2 d^2)^{1/2}, \quad (20)$$

where (R_0, Θ_0) and (d, ψ) are the respective polar coordinates of the source point and field point, and

$$R_0 = (l_0^2 + h_0^2)^{1/2}, \quad \Theta_0 = \cos^{-1}(l_0/R_0),$$

$$d = (\bar{x}^2 + \bar{y}^2)^{1/2}, \quad \psi = \cos^{-1}(\bar{x}/d).$$

In the η_1-plane (or η_2-plane), (19) (or (20)) describes a hyperbola which is denoted as the Cagniard contour. The η_1- and η_2-integrations are then shifted onto Cagniard contours along which t_1 and t_2 are both real and positive. The two Cagniard contours must be superimposed in this technique for different locations of source and field points. Continuing from this, the reflected and diffracted waves can be automatically constructed. Because $G(\eta_1, \eta_2)$ possesses a pole at $\eta_1 = \eta_2$, the contribution of the pole has to be taken into account in the change of integral paths from η_1 to t_1 and η_2 to t_2. Recall from (16) that a pole term arises, representing the reflected waves. The contribution of this pole represents the reflected r wave generated from the crack surface. The reflected r waves can be concluded to pass the region for $\psi > \pi - \Theta_0$. By using the Cagniard-de Hoop method of Laplace inversion, reflected field in the time domain is obtained in a simple closed form

$$\tau^r_{yz}(x, y, t) = -\frac{t \sin\theta_1 H(t - br_1)}{\pi r_1 (t^2 - b^2 r_1^2)^{1/2}}, \quad (21)$$

where

$$r_1 = [(x-l_1)^2 + (y+h_1)^2]^{1/2}, \quad \theta_1 = \cos^{-1}\left(\frac{x-l_1}{r_1}\right),$$

$$l_1 = l \cos(2\phi) + h \sin(2\phi), \quad h_1 = l \sin(2\phi) - h \cos(2\phi).$$

The diffracted wave generated from the crack tip is considered next. Recalling that p is real and positive, the η_1- and η_2-integrations are shifted here onto Cagniard contours. The stress τ^d_{yz} induced by the diffracted wave from the crack tip is found to be

$$\tau^d_{yz}(x, y, t) = \frac{1}{2\pi^2} \int_{bR_0}^{t-bd} \mathrm{Re}\left[K_1(\eta_2^+) \left(G(\eta_1^+, \eta_2^+) \frac{\partial \eta_1^+}{\partial t_1} \frac{\partial \eta_2^+}{\partial t_2} - G(\eta_1^-, \eta_2^+) \frac{\partial \eta_1^-}{\partial t_1} \frac{\partial \eta_2^+}{\partial t_2} \right) \right] dt_1, \quad (22)$$

where

$$t_2 = t - t_1.$$

The incident shear wave (i wave) will generate a reflected wave (r wave) and a diffracted wave (d wave) from the subsurface crack. After some later time, these two waves are to reflect from the free half-surface which is to be indicated as the rr wave and dr wave. The solutions for rr and dr waves can be constructed by employing the method of images, which are easily obtained from the solutions of r and d waves, hence the results are omitted here. The reflected rr and dr waves will arrive at the crack tip at later time. The reflected waves (rrr and drr waves) and diffracted waves (rrd and drd waves) generated from the crack can be constructed following the previously indicated similar analysis.

The complete full-field solutions that account for the contributions of all the reflected and diffracted waves are finally

Downloaded 03 May 2010 to 171.66.16.20. Redistribution subject to ASME license or copyright; see http://www.asme.org/terms/Terms_Use.cfm

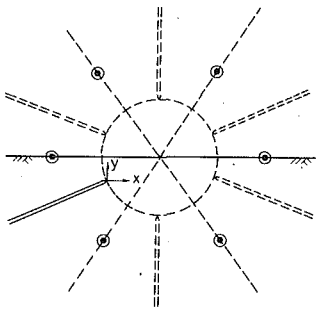


Fig. 2 Image method used to construct the transient full-field solutions

obtained explicitly. The image method shown in Fig. 2 is used for constructing the solution. The complete solutions for stresses and displacement can be simplified into a very compact form as follows:

$$\tau_{yz}=\sum_{i=0}^{s}\tau_{yz}^{i}+\sum_{k=0}^{n}\sum_{l=0}^{\infty}\sum_{j=0}^{m}\tau_{yz}^{j,k,l}, \tag{23a}$$

$$\tau_{xz}=\sum_{i=0}^{s}\tau_{xz}^{i}+\sum_{k=0}^{n}\sum_{l=0}^{\infty}\sum_{j=0}^{m}\tau_{xz}^{j,k,l}, \tag{23b}$$

$$w=\sum_{i=0}^{s}w^{i}+\sum_{k=0}^{n}\sum_{l=0}^{\infty}\sum_{j=0}^{m}w^{j,k,l}. \tag{23c}$$

The complete solutions consist of two terms as shown in (23). The first term with one summation is the contributions of incident wave and reflected waves which are only generated by reflected waves, i.e., $i = 0$ for incident wave, $i = 1$ for r wave, $i = 2$ for rr wave, $i = 3$ for rrr wave. The explicit forms are expressed as follows:

$$\tau_{yz}^{i}=(-1)^{i}\frac{t\sin\theta_i H(t-br_i)}{\pi r_i(t^2-b^2r_i^2)^{1/2}}, \tag{24a}$$

$$\tau_{xz}^{i}=-\frac{t\cos\theta_i H(t-br_i)}{\pi r_i(t^2-b^2r_i^2)^{1/2}}, \tag{24b}$$

$$w^{i}=\frac{1}{\pi\mu}\ln\left[\frac{t}{br_i}+\sqrt{\left(\frac{t}{br_i}\right)^2-1}\right]H(t-br_i), \tag{24c}$$

where

$$r_i=((x-l_i)^2+(y-h_i)^2)^{1/2},\quad \theta_i=\cos^{-1}\left(\frac{x-l_i}{r_i}\right),$$

$$l_0=l,\quad h_0=h,$$

$$l_1=l\cos(2\phi)+h\sin(2\phi),\quad h_1=l\sin(2\phi)-h\cos(2\phi),$$

$$l_i=l\cos((i+1)\phi)+h\sin((i+1)\phi)+\sum_{m=1}^{(i-1)/2}2h\sin(2m\phi),\quad i=3,5,7,\ldots$$

$$h_i=l\sin((i+1)\phi)-h\cos((i+1)\phi)-\sum_{m=1}^{(i-1)/2}2h\cos(2m\phi),\quad i=3,5,7,\ldots.$$

The second term in (23) with three summations comes from the contributions for diffracted waves and reflected waves which are generated by diffracted waves, i.e., $k = 0$, $l = 0$, $j = 0$ for d wave, $j = 1$ for dr wave, $j = 2$ for drr wave; $k = 0$, $l = 1$, $j = 0$ for drd wave, $j = 1$ for $drdr$ wave, $j = 2$ for $drdrr$ wave; $k = 0$, $l = 2$, $j = 0$ for $drdrd$ wave, $j = 1$ for $drdrdr$ wave; $k = 1$, $l = 0$, $j = 0$ for rrd wave, $j = 1$ for $rrdr$ wave; and $k = 1$, $l = 1$, $j = 0$ for $rrdrd$ wave, $j = 1$ for $rrdrdr$ wave. $k = 0$ can be seen here to consist of the diffracted d wave which is diffracted by the incident wave and the sequence of diffracted waves and reflected waves which are generated by the d wave. $k = 1$ consists of the diffracted rrd wave which is diffracted from the rr wave by the crack tip and the sequence of diffracted and reflected waves which are generated by the rrd wave. The index notation $j = 0$ will stand for the diffracted waves and $j \neq 0$ stands for the reflected waves. The results are expressed as follows:

$$\tau_{yz}^{j,k,l}=\frac{i^q}{2\pi^2(2\pi i)^l}\int_{bR_{0,2k}}^{a_1}\int_{2hb}^{a_2}\cdots\int_{2hb}^{a_{l+1}}\times FUN1_{j,k,l}\,dt_{k+l+1}dt_{k+l}\cdots dt_{k+1}, \tag{25a}$$

$$\tau_{xz}^{j,k,l}=\frac{-1}{2\pi^2(2\pi)^l}\int_{bR_{0,2k}}^{a_1}\int_{2hb}^{a_2}\cdots\int_{2hb}^{a_{l+1}}\times FUN2_{j,k,l}\,dt_{k+l+1}dt_{k+l}\cdots dt_{k+1}, \tag{25b}$$

$$w^{j,k,l}=\frac{-1}{2\pi^2(2\pi)^l\mu}\int_{bk}^{t}\int_{bR_{0,2k}}^{a_1'}\int_{2hb}^{a_2'}\cdots\int_{2hb}^{a_{l+1}'}\times FUN3_{j,k,l}\,dt_{k+l+1}dt_{k+l}\cdots dt_{k+1}, \tag{25c}$$

where

$$bk=b(R_{0,2k}+d_j+2lh),$$

$$a_1=t-bd_j-2lhb,\quad a_1'=\tau-bd_j-2lhb,$$

$$a_{v+1}=t-bd_j-t_1-t_2-\cdots-t_v-2(l-v)hb,\quad v=1,2,3.\ldots,l$$

$$a_{v+1}'=\tau-bd_j-t_1-t_2-\cdots-t_v-2(l-v)hb,\quad v=1,2,3.\ldots,l$$

$$FUN1_{j,k,l}=\mathrm{Op}\,(G(S_{2,k+1}^{\pm},\eta_{k+2}^{\pm})G(S_{2,k+2}^{\pm},\eta_{k+3}^{\pm})\cdots\times G(S_{2,k+2}^{\pm},\eta_{k+3}^{\pm})\cdots$$

$$\times\left(\pm\frac{\partial S_{2,k+1}^{\pm}}{\partial t_{k+1}}\right)\left(\pm\frac{\partial S_{2,k+2}^{\pm}}{\partial t_{k+2}}\right)\cdots\left(\pm\frac{\partial S_{2,k+l+1}^{\pm}}{\partial t_{k+l+1}}\right)\left(\frac{\partial S_{1,k+l+p+2}^{+}}{\partial t_{k+l+p+2}}\right)\Bigg),$$

$$l_i=l\cos(i\phi)+h\sin(i\phi)+\sum_{m=0}^{i/2-1}2h\sin(2m\phi),\quad i=2,4,6,\ldots$$

$$h_i=-l\sin(i\phi)+h\cos(i\phi)+\sum_{m=0}^{i/2-1}2h\cos(2m\phi),\quad i=2,4,6,\ldots$$

$$FUN2_{j,k,l}=\mathrm{Op}\left(\left(\frac{S_{1,l+k+p+2}^{+}}{(b^2-S_{1,l+k+p+2}^{+2})^{1/2}}\right)G(S_{2,k+1}^{\pm},\eta_{k+2}^{\pm})\times G(S_{2,k+2}^{\pm},\eta_{k+3}^{\pm})\cdots\times G(S_{2,k+l+1}^{\pm},\eta_{k+l+2}^{+})\left(\pm\frac{\partial S_{2,k+1}^{\pm}}{\partial t_{k+1}}\right)\right)$$

Downloaded 03 May 2010 to 171.66.16.20. Redistribution subject to ASME license or copyright; see http://www.asme.org/terms/Terms_Use.cfm

$$\times\left(\pm\frac{\partial S^{\pm}_{2,k+2}}{\partial t_{k+2}}\right).\ .\ .\ .\ .\left(\pm\frac{\partial S^{\pm}_{2,k+l+1}}{\partial t_{k+l+1}}\right)\left(\frac{\partial S^{+}_{1,k+l+p+2}}{\partial t_{k+l+p+2}}\right)\Bigg),$$

$$FUN3_{j,k,l}=\mathrm{Op}\left(\left(\frac{1}{(b^2-S^{+2}_{1,l+k+p+2})^{1/2}}\right)G(S^{\pm}_{2,k+1},\ \eta^{\pm}_{k+2})\right.$$

$$\times G(S^{\pm}_{2,k+2},\ \eta^{\pm}_{k+3}).\ .\ .\ .$$

$$\times G(S^{\pm}_{2,k+l+1},\ \eta^{+}_{k+l+2})\left(\pm\frac{\partial S^{\pm}_{2,k+1}}{\partial t_{k+1}}\right)\left(\pm\frac{\partial S^{\pm}_{2,k+2}}{\partial t_{k+2}}\right).\ .\ .\ .\ .$$

$$\left.\times\left(\pm\frac{\partial S^{\pm}_{2,k+l+1}}{\partial t_{k+l+1}}\right)\left(\frac{\partial \eta^{+}_{k+l+p+2}}{\partial t_{k+l+p+2}}\right)\right),$$

in which the operator "Op" is "Re" or "Im" depending on whether l is even or odd and

$$S^{+}_{1,k+l+p+2}=-\frac{t_{k+l+p+2}\cos\psi'_j}{s_j}+i\frac{\sin\psi'_j}{s_j}(t^2_{k+l+p+2}-b^2d^2_j)^{1/2},$$

$$S^{\pm}_{2,k+1}=\frac{t_{k+1}\cos\Theta_{0,2k}}{R_{0,2k}}\pm i\frac{\sin\Theta_{0,2k}}{R_{0,2k}}(t^2_{k+1}-b^2R^2_{0,2k})^{1/2},$$

$$S^{\pm}_{2,k+v+1}=\frac{t_{k+v+1}\sin\phi}{2h}\pm i\frac{\cos\phi}{2h}(t^2_{k+v+1}-4b^2h^2)^{1/2},$$

$$v=1,2,3,\ .\ .\ .\ ,l$$

$$\eta^{+}_{k+l+2}=-\frac{t_{k+l+2}\cos\psi_j}{d_j}+i\frac{\sin\psi_j}{d_j}(t^2_{k+l+2}-b^2d^2_j)^{1/2},$$

$$\eta^{\pm}_{k+v+1}=-\frac{t_{k+v+1}\sin\phi}{2h}\pm i\frac{\cos\phi}{2h}(t^2_{k+v+1}-4b^2h^2)^{1/2},$$

$$v=1,2,3,\ .\ .\ .\ ,$$

$S_{2,1}=\eta_1$, $t_{k+l+p+2}=t-t_{k+1}-t_{k+2}-.\ .\ .\ .\ .-t_{k+l+1}$,

$q=0$, when $l=0,2,4,6,\ .\ .\ .\ .\ .$; $q=1$,

when $l=1,3,5,7,\ .\ .\ .\ .\ .$

$p=j/2$, when $j=0,2,4,6,\ .\ .\ .\ .\ .$; $p=(j-1)/2$,

when $j=1,3,5,7,\ .\ .\ .\ .\ .$

$$R_{0,2k}=(l^2_{0,2k}+h^2_{0,2k})^{1/2};\ d_j=(x^2_j+y^2_j)^{1/2},$$

$$s_j=((x-l_j)^2+(y-h_j)^2)^{1/2};\ \cos\psi'_j=\frac{x-l_j}{s_j},$$

$$\cos\psi_j=\frac{x_j}{d_j};\ \cos\Theta_{0,2k}=\frac{l_{0,2k}}{R_{0,2k}},$$

$$l_{0,2k}=l\cos(2k+1)\phi+h\sin(2k+1)\phi+\sum_{m=0}^{k-1}2h\sin(2m+1)\phi,$$

$$h_{0,2k}=-l\sin(2k+1)\phi+h\cos(2k+1)\phi$$

$$+\sum_{m=0}^{k-1}2h\cos(2m+1)\phi,$$

$$x_j=(x-l_j)\cos(j+1)\phi+(y-h_j)\sin(j+1)\phi,$$

$$j=0,2,4,6,\ .\ .\ .\ .\ .$$

$$y_j=-(x-l_j)\sin(j+1)\phi+(y-h_j)\cos(j+1)\phi,$$

$$j=0,2,4,6,\ .\ .\ .\ .\ .$$

$$x_j=(x-l_j)\cos(j\phi)+(y-h_j)\sin(j\phi),\ j=1,3,5,7,\ .\ .\ .\ .\ .$$

$$y_j=-(x-l_j)\sin(j\phi)+(y-h_j)\cos(j\phi),$$

$$j=1,3,5,7,\ .\ .\ .\ .\ .$$

$l_0=0$; $h_0=0$,

$$l_j=\sum_{m=1}^{j/2}2h\sin(2m\phi),\ j=2,4,6,\ .\ .\ .\ .\ .$$

$$h_j=-\sum_{m=1}^{j/2}2h\cos(2m\phi),\ j=2,4,6,\ .\ .\ .\ .\ .$$

$$l_j=\sum_{m=0}^{(j-1)/2}2h\sin(2m\phi),\ j=1,3,5,7,\ .\ .\ .\ .\ .$$

$$h_j=\sum_{m=0}^{(j-1)/2}2h\cos(2m\phi),\ j=1,3,5,7,\ .\ .\ .\ .\ .$$

The number of reflected waves (i.e., n, s, and m) is dependent on the location and the inclined angle ϕ of the crack, and the position where the dynamic point loading is applied. The results are expressed as follows:

If $\phi_{2j+1}<\pi/2<\phi_{2j-1}$, then $n=j$.

If $(2v-1)\phi<\phi_{2n+1}<2v\phi$, then $s=2(n+v)+1$.

If $2v\phi<\phi_{2n+1}<(2v+1)\phi$, then $s=2(n+v)+2$.

If $(2v-1)\phi<\pi/2<2v\phi$, then $m=2v$.

If $2v\phi<\pi/2<(2v+1)\phi$, then $m=2v+1$

where

$$\phi_{2j+1}=\cos^{-1}\left(\frac{l_{2j+1}}{R_{2j+1}}\right),$$

$$R_{2j+1}=(l^2_{2j+1}+h^2_{2j+1})^{1/2},$$

$$l_{2j+1}=l\cos2(j+1)\phi+h\sin2(j+1)\phi+\sum_{p=1}^{j}2h\sin(2p\phi),$$

$$h_{2j+1}=l\sin2(j+1)\phi-h\cos2(j+1)\phi-\sum_{p=1}^{j}2h\cos(2p\phi).$$

4 Numerical Results of Transient Solutions

The geometric configuration considered in this study is an inclined semi-infinite crack located under the surface of a half-plane. The incident wave generated by the dynamic antiplane loading will be diffracted from the crack tip and reflected from the crack surface as d and r waves, which will be reflected from the half-plane and interact with the inclined crack again at later time. The complete structure of the wave fronts for the incident, reflected, and diffracted waves over a short time period are expressed in Fig. 3.

The exact full-field solutions have been determined in the previous section. The transient response for a point dynamic

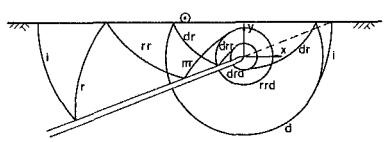


Fig. 3 Wave fronts of the incident, reflected, and diffracted waves for a short time period after the impact loading is applied on the half-space

Downloaded 03 May 2010 to 171.66.16.20. Redistribution subject to ASME license or copyright; see http://www.asme.org/terms/Terms_Use.cfm

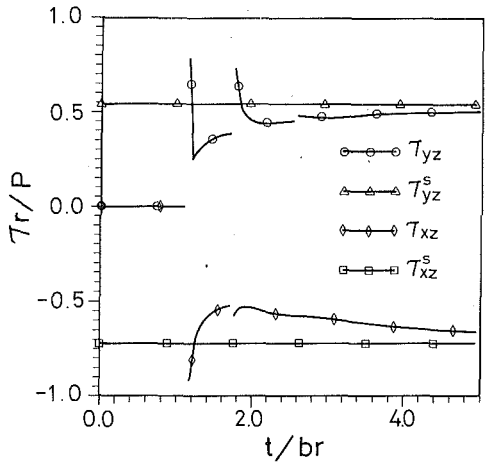


Fig. 4 Transient shear stresses for the field point located at $r = 5$, $\theta = 30$ deg due to impact loading applied at (−25, 10)

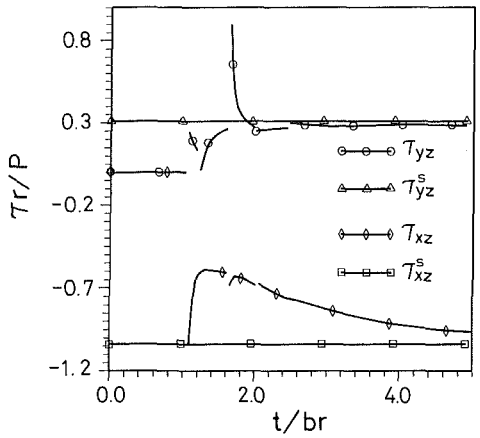


Fig. 5 Transient shear stresses for the field point located at $r = 5$, $\theta = 60$ deg due to impact loading applied at (−25, 10)

loading is next investigated here with a Heaviside function $H(t)$ time dependence and with a magnitude P applied at (−25, 10) which is at the left-hand side of the crack tip. The inclined angle ϕ of the crack is chosen to be 30 deg and the shear wave speed is assumed to be 3200 m/sec. It is worthy to note that only the incident wave and the second reflected *rr* wave will pass through the crack tip and generate a sequence of diffracted waves; the other pure reflected waves (i.e., *rrr*, *rrrr*, etc.) will only reflect back and forth between the crack face and the half-plane surface. Hence, in this particular case, k is equal to 0 and 1 and the associated wave fronts are shown in Fig. 3. The field points located at $r = 5$, $\theta = 30$ deg, 60 deg, and 120 deg are selected for analyzing the transient response. The transient shear stresses of these points are expressed in Figs. 4–6. The time has been normalized by dividing *br*. The corresponding static solutions are also indicated in these figures. The incident and purely reflected waves are singular at their wave fronts while the diffracted waves have finite jumps at their wave fronts. In these figures the transient stresses tend toward the corresponding static value after the third diffracted wave has passed the field points. Next, we consider the point loading being applied directly above the crack tip, so that $l = 0$ and $h = 10$. The field points to be investigated are at $r = 5$, $\theta = 0$ deg and 120 deg. In this case, only the incident wave will generate a sequence of diffracted waves, hence $k = 0$. The transient shear stresses are plotted in Figs. 7–8. It is indicated in these figures that after the second diffracted wave has passed, the transient stresses will approach the static value.

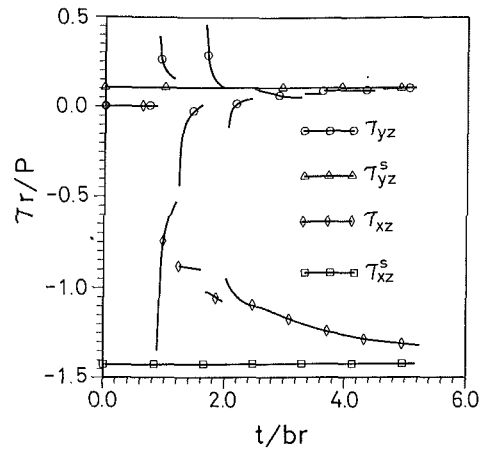


Fig. 6 Transient shear stresses for the field point located at $r = 5$, $\theta = 120$ deg due to impact loading applied at (−25, 10)

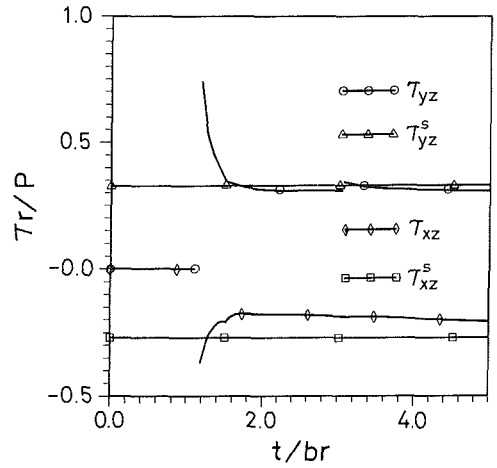


Fig. 7 Transient shear stresses for the field point located at $r = 5$, $\theta = 0$ deg due to impact loading applied at (0, 10)

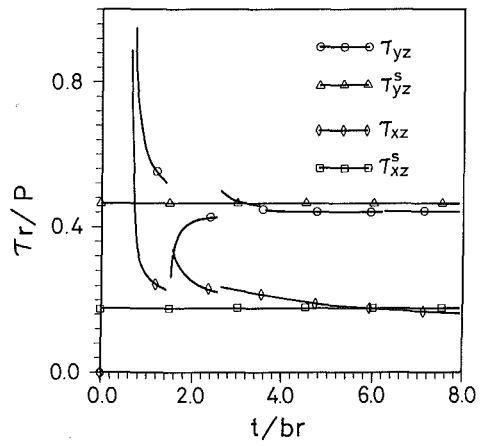


Fig. 8 Transient shear stresses for the field point located at $r = 5$, $\theta = 120$ deg due to impact loading applied at (0, 10)

5 Conclusions

Most of the problems which have been studied in the development of fracture mechanics are quasi-static. Because of

Downloaded 03 May 2010 to 171.66.16.20. Redistribution subject to ASME license or copyright; see http://www.asme.org/terms/Terms_Use.cfm

loading conditions and material properties, numerous problems have existed for which the assumption of quasi-static deformation is invalid, and the inertia of the material must be taken into account. It would be difficult to state precise conditions under which inertia effects might be neglected. The propagation of stress waves through an unbounded medium has not been a difficult subject. However, if boundaries are introduced, reflected and diffracted waves will be generated from boundaries, making the problem much more complicated.

The transient response of a half-space containing a subsurface inclined crack has been considered here to gain understanding of the interaction of stress waves with material defects. This problem contains a characteristic length and is solved by superposition of the fundamental solutions in the Laplace transform domain. The exact transient full-field solutions for stresses and displacement over a long period of time are obtained in this study. The complicated close-form transient solutions are expressed in a very simple formulation which account for all contributions coming from incident, reflected, and diffracted waves. The transient stresses near the crack tip can be used for analyzing the condition for unstable crack propagation. The transient displacement responses at the half-plane surface could possibly be used to detect the location of the subsurface crack and its orientation.

One of the main objectives in this study is to investigate the characteristic time in which the transient solution would approach the correspondent static value in dynamic fracture problems. With the exact analytic solutions at hand, numerical calculations for the transient stresses have been presented and compared to corresponding static values. It is found in this study that the transient effect in this problem can be neglected after the first few diffracted waves being generated from the crack tip have passed the field points.

Acknowledgments

The research support of the National Science Council, Republic of China, through Grant NSC 81-0401-E002-18 at National Taiwan University is gratefully acknowledged.

References

Brock, L. M., 1982, "Shear and Normal Impact Loadings on One Face of a Narrow Slit," *International Journal of Solids and Structures*, Vol. 18, pp. 467–477.

Brock, L. M., 1984, "Stresses in a Surface Obstacle Undercut Due to Rapid Indentation," *Journal of Elasticity*, Vol. 14, pp. 415–424.

Brock, L. M., Jolles, M., and Schroedl, M., 1985, "Dynamic Impact Over a Subsurface Crack: Applications to the Dynamic Tear Test," ASME JOURNAL OF APPLIED MECHANICS, Vol. 52, pp. 287–290.

Brock, L. M., 1986, "Transient Dynamic Green's Functions for a Cracked Plane," *Quarterly of Applied Mathematics*, Vol. 44, pp. 265–275.

de Hoop, A. T., 1958, "Representation Theorems for the Displacement in an Elastic Solid and Their Application to Elastodynamic Diffraction Theory," Doctoral Dissertation, Technische Hoegschool, Delft, The Netherlands.

Freund, L. B., 1974, "The Stress Intensity Factor Due to Normal Impact Loading of the Faces of a Crack," *International Journal of Engineering Science*, Vol. 12, pp. 179–189.

Lee, Y. J., and Freund, L.B., 1990, "Fracture Initiation Due to Asymmetric Impact Loading of an Edge Cracked Plate," ASME JOURNAL OF APPLIED MECHANICS, Vol. 57, pp. 104–111.

Ma, C. C., and Chen, S. K., 1993, "Exact Transient Analysis of an Antiplane Semiinfinite Crack Subjected to Dynamic Body Forces," *Wave Motion*, Vol. 17, pp. 161–171.

Ma, C. C., and Hou, Y. C., 1990, "Theoretical Analysis of the Transient Response for a Stationary Inplane Crack Subjected to Dynamic Impact Loading," *International Journal of Engineering Science*, Vol. 28, pp. 1321–1329.

Ma, C. C., and Hou, Y. C., 1991, "Transient Analysis for Antiplane Crack Subjected to Dynamic Loadings," ASME JOURNAL OF APPLIED MECHANICS, Vol. 58, pp. 703–709.

Noble, B., 1958, *The Wiener-Hopf Technique*, Pergamon Press, New York.

Tsai, C. H., and Ma, C. C., 1992, "Transient Analysis of a Semi-infinite Crack Subjected to Dynamic Concentrated Forces," ASME JOURNAL OF APPLIED MECHANICS, Vol. 59, pp. 804–811.

Downloaded 03 May 2010 to 171.66.16.20. Redistribution subject to ASME license or copyright; see http://www.asme.org/terms/Terms_Use.cfm

Transient Response of Multiple Rigid Foundations on an Elastic, Homogeneous Half-Space

F. Guan

M. Novak

Department of Civil Engineering,
University of Western Ontario,
London, ON N6A 5B9, Canada

Three-dimensional transient response of both massless and massive multiple, rigid foundations, bonded to an elastic, homogeneous half-space, is investigated to study the effect of dynamic interaction through-soil. The numerical procedure is formulated in terms of the boundary element approach by means of the transient fundamental solutions developed by the authors (1994). This procedure works efficiently for the problem addressed here since the separated foundations are analyzed without discretizing the surface of the half-space outside the contact areas between the half-space and the foundations. It also provides the possibility to study nonlinear problems involved with semi-infinite soils.

1 Introduction

It is well known that soil-structure interaction is important for the response of structures and also that the dynamic through-the-soil coupling of closely spaced structures may have a significant effect on the responses. An analysis was made by Warburton et al. (1971) to investigate the effect of the interaction between two rigid circular foundations. The corresponding experimental study was carried out by MaCalden et al. (1972). Richardson obtained the solution of two rigid cylinders resting on a half-space when one of them was excited by external harmonic loading (1969). Roesset and Gonzalez (1977) analyzed the interaction through underlying soil between two rigid masses idealized as a one-degree-of-freedom system. An antiplane through-soil coupling problem for two structures resting on semi-cylindrical foundations was implemented for the case of two structures by Luco and Contesse (1977) and by Murakami and Luco (1977) for a periodic array of structures. An approach based on integral technique to calculate dynamic response of rigid surface foundations bonded to a layered viscoelastic half-space subjected to external forces and seismic motions was presented by Wong and Luco (1986). Kawakami and Tasaki (1988) developed a numerical procedure for the study of the seismic response of a group of rigid structures with arbitrarily shaped bases attached to the surface of an elastic half-space. A comprehensive parametric study of responses for surface or embedded three-dimensional adjacent foundations was made by Lin et al. (1987). More recently, the dynamic response of a system of flexible strip foundation resting in smooth contact on a homogeneous isotropic viscoelastic half-space was studied by Wang et al. (1991). Finally, harmonic response of a number of rectangular or circular rigid foundations was studied by Triantafyllidis and Prange (1987, 1989).

The aforementioned studies were all carried out in the frequency domain, and were limited to linear problems. Herein, a numerical procedure is developed in the sense of boundary element method to investigate the three-dimensional transient responses of multiple foundations taking advantage of the Green's function developed by the authors (1994). The multiple foundations are assumed bonded to an elastic, homogeneous half-space. The advantages of the proposed procedure, compared with most of the other time domain boundary element methods, are that the multiple foundations can be analyzed without discretizing the regions outside the contact areas between the half-space and foundations and that no additional computational effort arises as the distances between the foundations increase. The transient response of a single surface foundation was studied by Karabalis and Beskos (1984) approximately using the Stokes solution as Green's function for the half-space. Since this problem has many parameters, only some of the more important aspects are examined in this paper.

2 Formulations

The multiple, rigid foundations, as shown in Fig. 1, are assumed to rest on an elastic, homogeneous half-space described by shear modulus μ, mass density, ρ, and Poisson's ratio σ. The P, SV, and Rayleigh wave velocities are denoted by α, β, and C_R, respectively.

The problem addressed here is formulated in the boundary element sense using constant elements (subregions) in both space and time. The multiple foundations are discretized into n rectangular subregions and the incremental stresses under each subregion are assumed uniformly distributed over its area and constant within every time interval $(m\Delta t, (m + 1)\Delta t)$, where Δt is the incremental time step. There are two sets of

Contributed by the Applied Mechanics Division of THE AMERICAN SOCIETY OF MECHANICAL ENGINEERS for publication in the ASME JOURNAL OF APPLIED MECHANICS.

Discussion on this paper should be addressed to the Technical Editor, Professor Lewis T. Wheeler, Department of Mechanical Engineering, University of Houston, Houston, TX 77204-4792, and will be accepted until four months after final publication of the paper itself in the ASME JOURNAL OF APPLIED MECHANICS.

Manuscript received by the ASME Applied Mechanics Division, Dec. 11, 1992; final revision, June 17, 1993. Associate Technical Editor: S. K. Datta.

Copyright © 1994 by ASME
Downloaded 03 May 2010 to 171.66.16.20. Redistribution subject to ASME license or copyright; see http://www.asme.org/terms/Terms_Use.cfm

unknowns, i.e., the displacements and resultant forces over the subregions of the half-space. The displacement-force relationship can be found using the Green functions developed by the authors.

2.1 Impedance of the Half-Space. The Green's function due to a suddenly applied load, uniformly distributed over a rectangular area $2a \times 2b$ is (Guan and Novak, 1993)

$$\Delta_{jk}(x, y, t) = \int_0^{2\pi} \Delta_{jk}^{(1)} \chi_{jk}(x, y, \theta, C_R, t)\, d\theta + \int_0^{2\pi} \int_\beta^\alpha \Delta_{jk}^{(2)} \chi_{jk}(x, y, \theta, \eta, t)\, d\eta d\theta + \int_0^{2\pi} \int_\alpha^\infty \Delta_{jk}^{(3)} \chi_{jk}(x, y, \theta, \eta, t)\, d\eta d\theta \quad (1)$$

where

$$\chi_{lj}(x, y, \theta, c, t) = \chi_{jl}(x, y, \theta, c, t)$$

$$\chi_{jl}(x, y, \theta, c, t) = \frac{1}{4ab \sin\theta \cos\theta} \times \sum_{m,n}^{2} (-1)^{m+n+1} \begin{cases} f_{mn}(x, y, \theta, c, t) & j=3,\ l\neq 3 \\ g_{mn}(x, y, \theta, c, t) & \text{otherwise} \end{cases} \quad (2)$$

in which

$$f_{mn}(x, y, \theta, c, t) = \frac{c_{mn}}{2} \ln\left|\frac{c_{mn}^2 - c^2t^2}{c_{mn}^2}\right| + \frac{ct}{2} \ln\left|\frac{c_{mn}+ct}{c_{mn}-ct}\right| \quad (3a)$$

$$g_{mn}(x, y, \theta, c, t) = \begin{cases} \frac{\pi}{2}(ct - |c_{mn}|) & |c_{mn}| \le ct \\ 0 & |c_{mn}| \ge ct \end{cases} \quad (3b)$$

$$c_{mn} = (x + (-1)^m a)\cos\theta + (y + (-1)^n b)\sin\theta. \quad (3c)$$

The expressions for $\Delta_{jk}^{(i)}(\theta, \eta)$ can be found in the Appendix.

The response of an elastic and homogeneous half-space can be determined by successive applications of the incremental tractions in the time intervals using the solutions above. Therefore, at the mth time step, the response of the subregions can be expressed as by means of the Green functions given above.

$$\begin{Bmatrix} \mathbf{U}_1 \\ \mathbf{U}_2 \\ \vdots \\ \mathbf{U}_n \end{Bmatrix}_{(m+1)} = \sum_{j=0}^{m} \begin{bmatrix} F_{11} & F_{12} & \dots & F_{1n} \\ F_{21} & F_{22} & \dots & F_{2n} \\ \dots & \dots & \dots & \dots \\ F_{n1} & F_{n2} & \dots & F_{nn} \end{bmatrix}_j \begin{Bmatrix} \Delta\mathbf{T}_1^{m-j} \\ \Delta\mathbf{T}_2^{m-j} \\ \vdots \\ \Delta\mathbf{T}_n^{m-j} \end{Bmatrix}$$

$$= \sum_{j=0}^{m} \begin{bmatrix} F_{11} & F_{12} & \dots & F_{1n} \\ F_{21} & F_{22} & \dots & F_{2n} \\ \dots & \dots & \dots & \dots \\ F_{n1} & F_{n2} & \dots & F_{nn} \end{bmatrix}_j \begin{Bmatrix} \mathbf{T}_1^{m-j} - \mathbf{T}_1^{m-j-1} \\ \mathbf{T}_2^{m-j} - \mathbf{T}_2^{m-j-1} \\ \vdots \\ \mathbf{T}_n^{m-j} - \mathbf{T}_n^{m-j-1} \end{Bmatrix}$$

$$= \sum_{j=0}^{m} \begin{bmatrix} \Delta F_{11} & \Delta F_{12} & \dots & \Delta F_{1n} \\ \Delta F_{21} & \Delta F_{22} & \dots & \Delta F_{2n} \\ \dots & \dots & \dots & \dots \\ \Delta F_{n1} & \Delta F_{n2} & \dots & \Delta F_{nn} \end{bmatrix}_j \begin{Bmatrix} \mathbf{T}_1^{m-j} \\ \mathbf{T}_2^{m-j} \\ \vdots \\ \mathbf{T}_n^{m-j} \end{Bmatrix} \quad (4)$$

where

$$[\Delta F]_j = [F]_j - [F]_{j-1}. \quad (5)$$

The matrix $[F]_j$ and vector $\{T^{m-j}\}$ denote the influence matrix in the time interval $[j\Delta t, (j+1)\Delta t]$ and the interaction forces on the half-space between the times $[(m-j)\Delta t, (m-j+1)\Delta t]$. The matrix $[F]_j$ is symmetric if the foundations are meshed by subelements with same size. If the system is also subjected to seismic motion, (4) can be expressed as

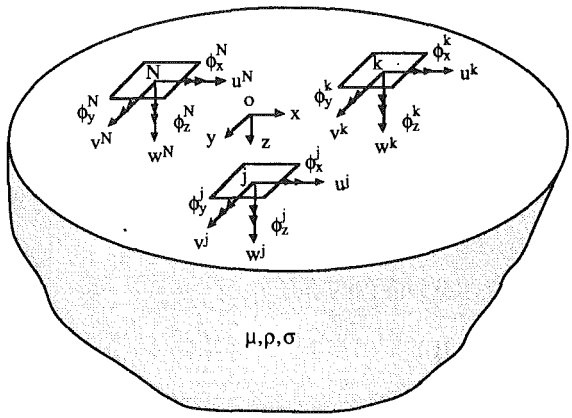


Fig. 1 Multiple, rigid foundations resting on a half-space

$$\{U\}_{(m+1)} - \{U\}_{(m+1)}^{f} = \sum_{j=0}^{m} \Delta F_j \{T\}^{m-j}) \quad (6)$$

in which the superscript f represents the free-field seismic motion. Therefore, the displacement-force relationship for the half-space can be established

$$\{T\}^m = F_0^{-1}(\{U\}_{(m+1)} - \{U\}_{(m+1)}^{f} - \sum_{j=1}^{m} \Delta F_j \{T\}^{m-j}). \quad (7)$$

2.2 Geometry Conditions. For rigid-body motions, the displacements of each foundation can be condensed to six degrees-of-freedom: two horizontal displacements $u(t)$, $v(t)$ and one vertical displacement $w(t)$ at the foundation centroid and rotation angles $\phi_1(t)$, $\phi_2(t)$, and $\phi_3(t)$ around the axes. For convenience, the subscripts indicating the foundation number are deleted. The displacements of any foundation can be expressed as

$$u_1(x_1, x_2, t) = u(t) + \phi_3 x_2 \quad (8a)$$

$$u_2(x_1, x_2, t) = v(t) - \phi_3 x_1 \quad (8b)$$

$$u_3(x_1, x_2, t) = w(t) - \phi_1 x_2 + \phi_2 x_1 \quad (8c)$$

where (x_1, x_2) is the local coordinate system with the origin at the centroid of the foundation.

Assembling the equations for all foundations leads to

$$\{u\} = D\{\Delta\} \quad (9)$$

where D and $\{\Delta\}$ are the transformation matrix and displacement vector, respectively. The submatrices of them are defined as

$$\begin{bmatrix} 1 & 0 & 0 & 0 & 0 & -x_2 \\ 0 & 1 & 0 & 0 & 0 & x_1 \\ 0 & 0 & 1 & x_2 & -x_1 & 0 \end{bmatrix} \quad (10)$$

and

$$\{u\ v\ w\ \phi_1\ \phi_2\ \phi_3\}^T. \quad (11)$$

2.3 Equilibrium Conditions. The equilibrium conditions can be stated as

$$P_1(t) - M\ddot{u}(t) = -\sum t_1(t) \quad (12a)$$

$$P_2(t) - M\ddot{v}(t) = -\sum t_2(t) \quad (12b)$$

$$P_3(t) - M\ddot{w}(t) = -\sum t_3(t) \quad (12c)$$

for translational motions and

$$P_1^M(t) - I_1\ddot{\phi}_1 = -\sum t_3(t)x_2 \quad (13a)$$

$$P_2^M(t) - I_2\ddot{\phi}_2 = \sum t_3(t)x_1 \quad (13b)$$

Downloaded 03 May 2010 to 171.66.16.20. Redistribution subject to ASME license or copyright; see http://www.asme.org/terms/Terms_Use.cfm

$$P_3^M(t) - I_3\ddot{\phi}_3 = \sum (t_1(t)x_2 - t_2(t)x_1) \tag{13c}$$

for rotational motions, where M and I_j ($j = 1, 3$) are, respectively, the mass and mass moments of inertia with respect to the axes passing through the foundation centroid, and t_i are the interaction forces over the subregions of foundations. With the force equilibrium conditions at the interfaces between the foundations and half-space, (12) and (13) can be written in a compact form

$$\{P(m\Delta t)\} - [M]\{\ddot{\Delta}\} = [D]^T\{T^m\}. \tag{14}$$

Substituting (14) into (7) yields

$$[M]\{\ddot{\Delta}^m\} + [K]\{\Delta^m\} = \{P^m\} + D^T F_0^{-1}\left(\{u^f\} + \sum_{j=1}^{m} \Delta F_j T^{m-j}\right) \tag{15}$$

where

$$[K] = DF_0^{-1}D^T. \tag{16}$$

The solution of (15) can be obtained by the numerical integration scheme. Here the Newmark numerical integration algorithm is employed.

The numerical procedure is carried out in such a way that the displacement in (15) is solved first using the interaction forces determined in the previous steps; then the interaction force at the current time step follows from (7).

If the foundations are appropriately discretized in both space and time, this procedure will be an effective tool to solve the transient interaction between the foundations. The numerical procedure is found to be conditionally convergent. For a given time step Δt, it is required that $\Delta b < 2.5\beta\Delta t$, where Δb is the maximum size of the mesh. Therefore, the efficiency of the procedure is also dependent on the type of the applied loading. For a loading with high-frequency components, a finer time step is needed.

3 Numerical Results

To check the accuracy of the procedure, the harmonic response of a massless, rigid, square footing $2b \times 2b$ was evaluated first, assuming either 16 or 25 equal subregions or using discretization into 25 refined subregions with finer meshes at edges and corners to account for the stress concentrations in these areas. The nondimensional frequency is defined as $a_0 = \Omega b/\beta$, where Ω is circular frequency. The Poisson's ratio for the underlying soil is assumed to be 1/3. The numerical results are plotted in Fig. 2, where they are compared with the results by Wong and Luco (1976), who discretized the foundation by 8×8 equal subregions under the assumption of relaxed boundary conditions between the foundation and the half-space.

Figure 2 shows that if the square foundation is discretized equally by no less than 4×4 subregions, the solution of the translational motion is accurate enough. However, more subelements are needed for the rotational motion to obtain a sufficiently accurate solution. The accuracy of the rotational motion solution can also be improved by using finer mesh size near the edges and corners without increasing the total number of subelements. Such a nonuniform mesh was used for the cases indicated as "refined" in the Fig. 2.

In the rest of the paper, dynamic through-soil interaction between the foundations subjected to impulsive loading is investigated. The foundations are assumed to be massive or massless, equal and square, and each of them is discretized by 25 equal elements. Poisson's ratio for the half-space is 1/3. The time is nondimensionalized by $\tau = \beta t/2b$. The time-step is selected as $\Delta t = 0.2b/\beta$.

For a twin foundation system with different spacing ratios $L/2b$, the horizontal responses of the loaded foundation to horizontal impulsive loading are given in Fig. 3(*a*). It is observed that the contributions by the feedback waves from the adjacent foundation to the horizontal response are negligible. The rocking motions resulting from the horizontally applied loading due to coupling are illustrated for various nondimensional distances in Fig. 3(*b*). The rotations (rocking) are denoted by Φ_{ij}, with the first subscript indicating the axis of the rotation and the second subscript identifying the direction of the applied load. The responses differ due to the feedback waves coming from the contiguous foundation. When the responses coincide, the feedback waves have not arrived at the loaded foundation (cases 2, 3 and 4 for $\tau < 0.9$). However, when the feedback waves arrive, the responses for 2, 3, and 4 diverge.

The responses of a loaded foundation due to vertical loading are illustrated in Figs. 3(*c*)-(*d*). The contributions by the feedback waves to the responses in the vertical direction are very slight. It is interesting to note that rocking motions are induced at the loaded foundation by the feedback waves solely, though the peak response is only about 20 percent of the ones induced by the horizontal loading for case 1. It can be seen that the rocking motions of the loaded foundation decay quite fast as the distance between the foundations increases. Note also that the rocking motions are vibratory.

In Fig. 4, the responses of the adjacent foundations are plotted. It is observed that the rocking motion due to horizontal loading (Fig. 4(*b*)) is significant. In general, the response of the passive foundation decreases with the increase of the nondimensional distance between the foundations; however, the rocking response for case 2 ($L/2b = 0.5$) is greater than in the other cases. It is known that for surface response, the Rayleigh wave is very important. At a certain distance, the Rayleigh wave may be well developed and can contribute greatly to the rocking observed. The maximum horizontal displacement induced is about 20 percent that of the loaded foundation.

The vertical response of the passive, contiguous foundation due to vertical loading of the loaded foundation (Fig. 4(*c*)) is very slight. But again, marked rocking responses are excited. Unlike the rocking motions induced by the horizontal loading, the peak responses decrease with the increasing distance between the foundations. It is found that the rocking motions of the adjacent foundation are greater than those of the foundation loaded vertically since the wave inducing the rocking motion in the loaded foundation travels twice as far as that causing the rocking motions in the adjacent foundation.

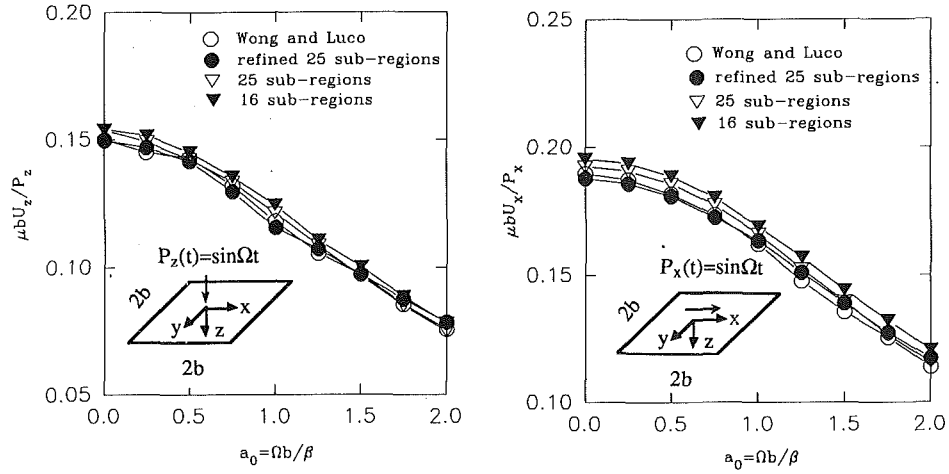
The responses of massive foundations are presented for various mass ratios. The mass ratio is defined as

$$\gamma = \frac{M_i}{\rho b^3}. \tag{17}$$

The responses of the loaded foundation are depicted in Fig. 5. It is observed that the displacements in the direction of the applied impulse loading decrease with the increase of the mass ratios. However, for the rocking motions due to vertical loading, the mass inertia may increase the peak response as shown in Fig. 5(*b*). Marked differences can be found between the responses of massless and mass foundations. The responses of massive foundation decay slowly and exhibit characteristic frequencies. For the massless foundation, the responses attain peak values when the loading is removed, then decrease with time monotonically. However, the nondimensional times of the peak responses in the massive foundation are delayed. It is noted that the rocking motion for $\gamma = 1, 2$ is greater than the responses for other mass ratios.

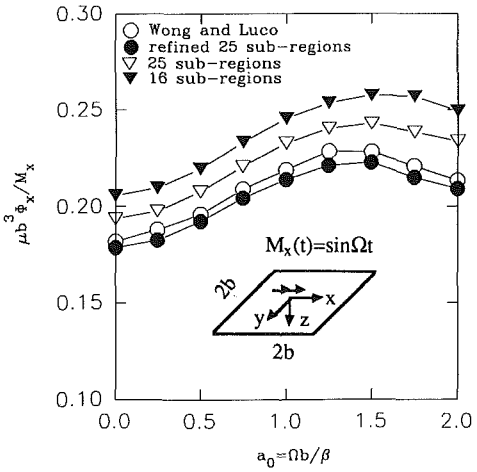
Pronounced responses are induced in the contiguous, massive foundation shown in Fig. 6. For the massless foundation system, most of the wave energy radiates to infinity while for the massive foundation system, some of the energy builds up in the masses to be released later. This explains, to some degree,

Downloaded 03 May 2010 to 171.66.16.20. Redistribution subject to ASME license or copyright; see http://www.asme.org/terms/Terms_Use.cfm



(a) vertical compliance

(b) horizontal compliance



(c) rocking compliance

Fig. 2 Compliance of a 2*b* × 2*b* square foundation for different numbers of the foundation subregions versus nondimensional frequency a_0

why the through-soil interaction effect for the massive foundation system is so different.

The comparisons between the responses of the massless triple and twin foundation systems are illustrated in Fig. 7. It has been found that, though the results are not presented here, for the responses of the middle foundation, slight differences are observed between the triple foundation system and the twin foundation system (without the presence of the right foundation). This indicates that the contribution to the response by the feedback waves from the right foundation is very small.

However, the effect of the middle foundation on the response of the right foundation is considerable. It is noted that the peak responses in the direction of the applied loadings increase slightly. On the other hand, for the rocking motion, the peak responses decrease somewhat. The time histories of the response are quite different for the triple and twin foundation systems since the middle foundation greatly affects the wave propagation. It reduces the time needed for the wave generated at the loaded foundation to arrive at the right foundation. Therefore, an advance in the time of the peak responses for the triple foundation system occurs as can be seen in Fig. 7(*b*).

The mass inertia effect of the middle foundation on the response of the right foundation is presented in Fig. 8, where $\gamma_M = 0$ represents the case without the middle foundation. The mass ratios of the left and right foundations equal two. For the case studied here, the presence of the massive middle foundation increases the response of the right foundation for all the mass ratios. Greater responses are obtained in the right foundation when the mass ratio of the middle one is the same as that of the others. It appears that the inertia of the middle foundation hardly affects the characteristic frequency of the response of the right one. Again, it can be concluded that the middle foundation affects the wave propagation between the left and right foundations. It makes the energy of the wave propagate easily and less energy is dissipated through the travelled distance. The characteristics of the response to the horizontal loading were found to be similar to those shown in Figs. 5 to 8.

4 Conclusions

A numerical procedure for the analysis of transient dynamic responses of three-dimensional multiple foundations on an elastic, homogeneous half-space under external excitation is developed. Adequate agreement with the known numerical results is obtained for harmonic excitation. Based on the studies, the following conclusions emerge:

Downloaded 03 May 2010 to 171.66.16.20. Redistribution subject to ASME license or copyright; see http://www.asme.org/terms/Terms_Use.cfm

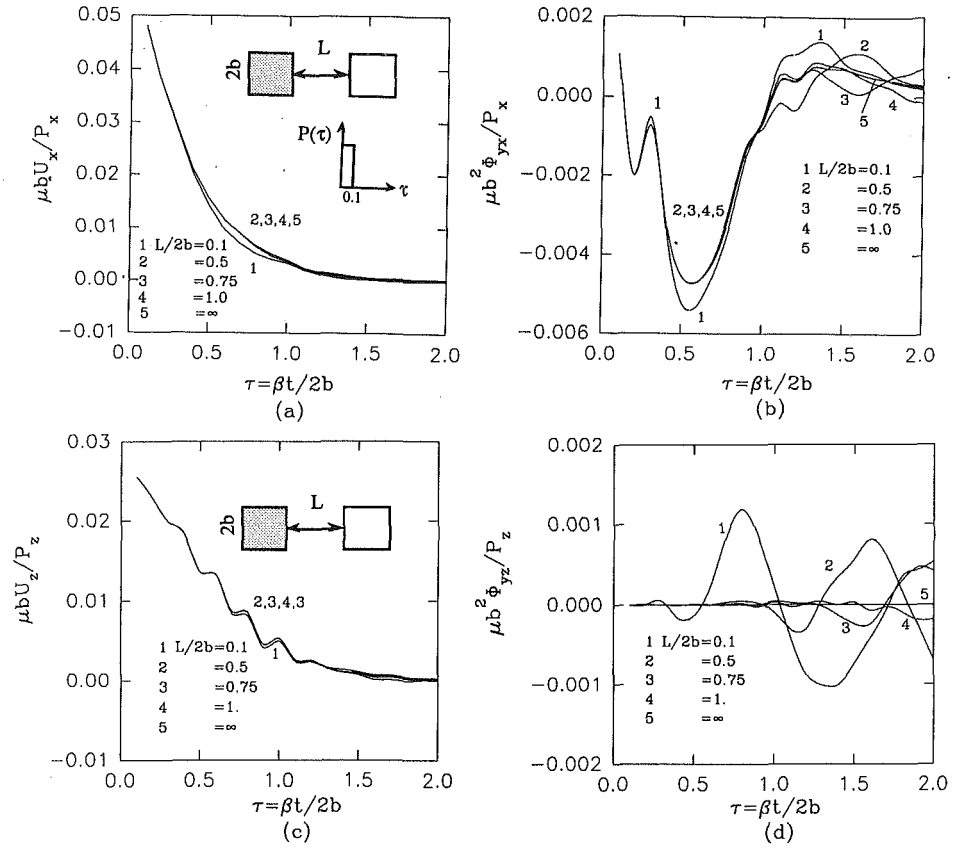


Fig. 3 Effect of the contiguous, passive foundation on the response of the loaded massless foundation versus nondimensional time τ for various distances

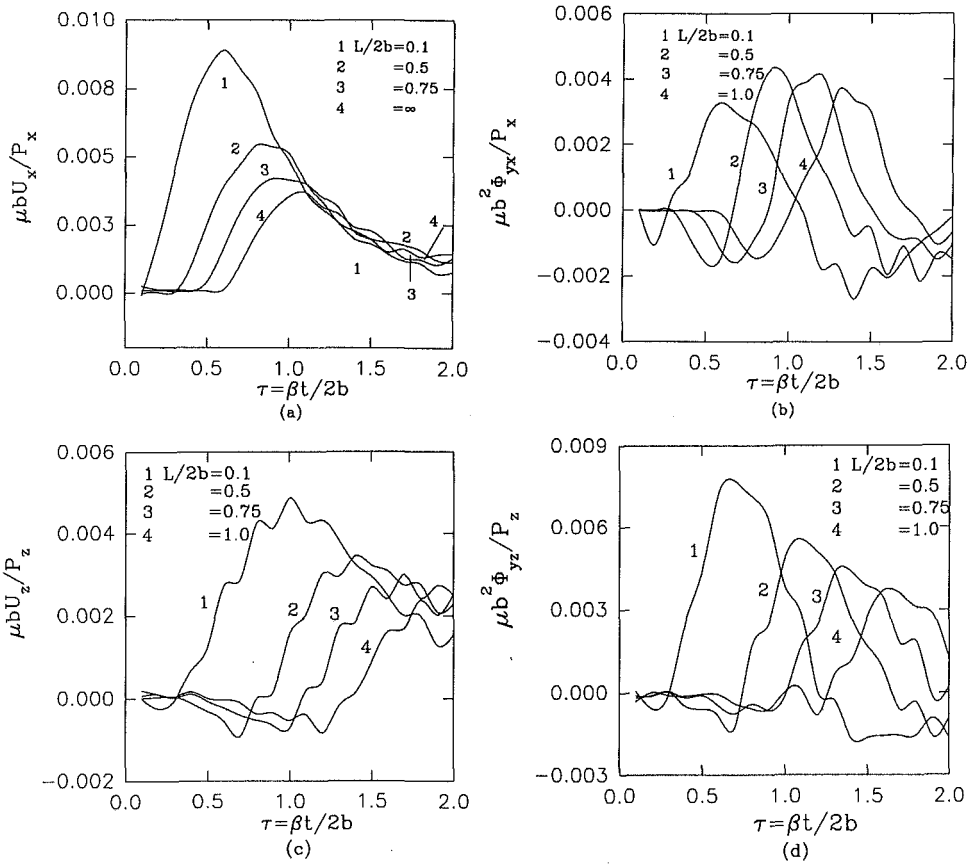


Fig. 4 Responses of the contiguous, passive massless foundation versus nondimensional time τ for various distances

Downloaded 03 May 2010 to 171.66.16.20. Redistribution subject to ASME license or copyright; see http://www.asme.org/terms/Terms_Use.cfm

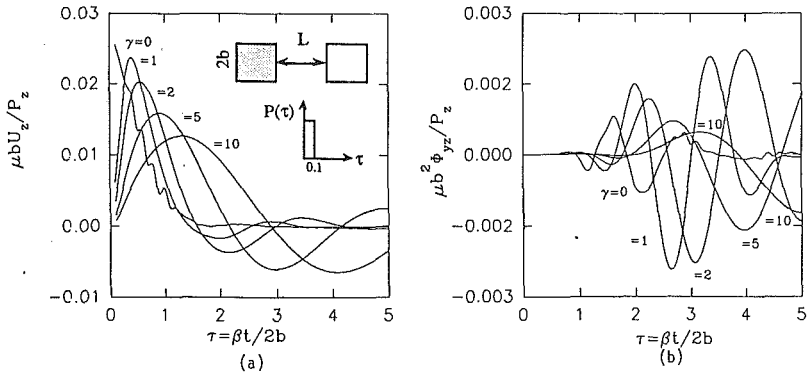


Fig. 5 Responses of the loaded, massive foundation versus nondimensional time τ for different mass ratios

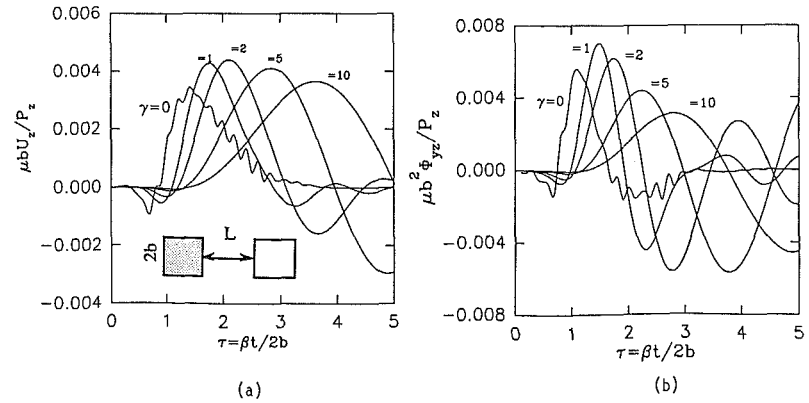


Fig. 6 Responses of the contiguous, unloaded massive foundation versus nondimensional time τ for different mass ratios

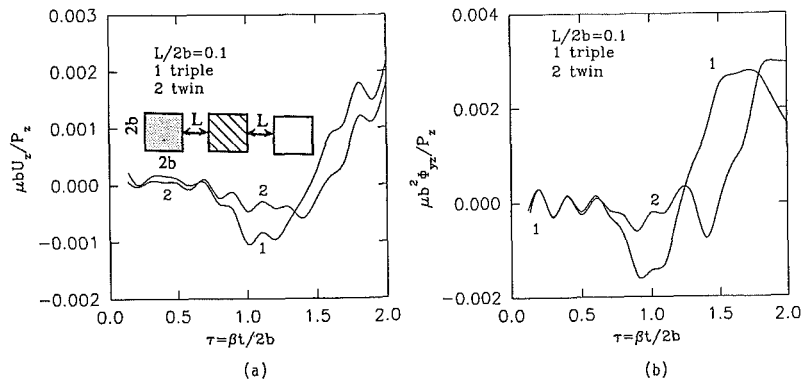


Fig. 7 Responses of the right, passive foundation versus nondimensional time τ with or without the presence of the middle foundation (massless foundations, left one loaded)

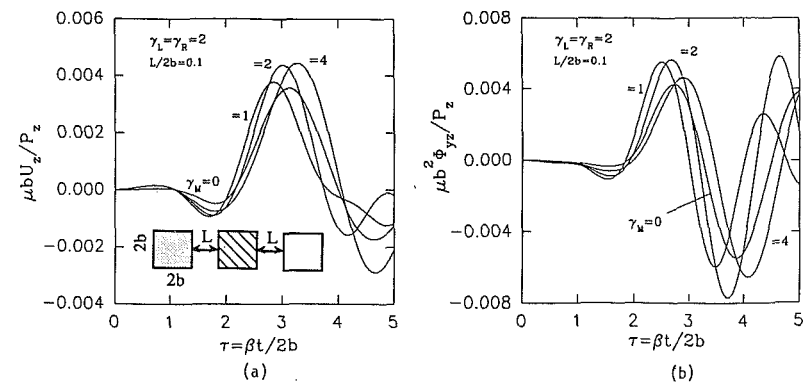


Fig. 8 The inertia effect of the middle foundation on the responses of the unloaded right foundation (left one loaded)

Downloaded 03 May 2010 to 171.66.16.20. Redistribution subject to ASME license or copyright; see http://www.asme.org/terms/Terms_Use.cfm

1 The advantage of the procedure proposed is that only the contact area between the soil and foundation has to be discretized. For the other numerical analyses available, the region in the vicinity of the multiple foundation system has to be discretized also.

2 The stability and accuracy of the solution is guaranteed for any incremental time step if appropriate discretization of the foundations is made.

3 The response of the contiguous, passive foundation is greatly affected by the loaded foundation. Significant rocking motions are induced in the adjacent foundation.

4 In contrast to the passive foundation, the through-soil interaction effect on the loaded foundation is negligible. The feedback wave generated by the contiguous foundation and transmitted to the loaded foundation decays greatly as it arrives and has little effect.

5 The inertia of the foundation greatly affects the response. It reduces the response of the loaded foundation and either increases or decreases the response of the adjacent foundation, depending on its mass ratio. It also makes the response decay very slowly with the increase of γ.

6 The effect of the middle foundation in the triple, massless foundation systems is not very pronounced for the peak responses. Nevertheless, the middle foundation does affect the wave propagation between the foundations. For the closely spaced masses, the presence of the middle foundation may amplify the response of the right one.

Acknowledgments

The support by the National Sciences and Engineering Research Council of Canada is appreciated.

References

Guan, F., and Novak, M., 1994, "Transient Response of an Elastic Homogeneous Half-Space to Suddenly Applied Rectangular Loading," ASME JOURNAL OF APPLIED MECHANICS, Vol. 61, pp. 256–263.

Karabalis, D. L., and Beskos, D. E., 1984, "Dynamic Response of 3-D Rigid Surface Foundations by Time Domain Boundary Element Method," *Earthq. Engr. & Struc. Dyn.*, Vol. 12, pp. 73–93.

Kawakami, H., and Tasaki, S., 1988, "Soil-Structure Interaction of Rigid Structures Considering Through-Soil Coupling Between Adjacent Structures," *Proc. 9th World Conf. Earthq. Engr.*, Tokyo-Kyoto, Japan, Vol. III, pp. 385–390.

Lin, H.-T., Roesset, J. M., and Tassoulas, J. L., 1987, "Dynamic Interaction Between Adjacent Foundations," *Earthq. Engr. Struct. Dyn.*, Vol. 5, pp. 323–343.

Luco, J. E., and Contesse, L., 1973, "Dynamic Structure-Soil-Structure Interaction," *Bull. Seism. Soc. Am.*, Vol. 63, No. 4, pp. 1289–1303.

MaCalden, P. B., and Mathiesen, R. B., 1973, "Coupled Response of Two Foundations," *Proc. 5th World Conf. Earthq. Engr.*, Rome, Italy, Paper No. 238.

Richardson, J. D., 1969, "Forced Vibration of Rigid Bodies on a Semi-Infinite Medium," Ph.D. Thesis, University of Nottingham, U.K.

Roesset, J. M., and Gonzalez, J. J., 1977, "Dynamic Interaction Between Adjacent Structures," *Proc. of DMSR 77*, Karlsruhe, Germany, 5–16, Vol. 1, pp. 127–166.

Murakami, H., and Luco, J. E., 1977, "Seismic Response of a Periodic Array of Structures," *J. of the Eng. Mech. Div., ASCE*, Vol. 103, No. EM5, pp. 965–977.

Triantafyllidis, Th., and Prange, B., 1987, "Dynamic Subsoil Coupling Between Rigid, Rectangular Foundations," *Soil. Dyn. Earthq. Eng.*, Vol. 6, pp. 164–179.

Triantafyllidis, Th., and Prange, B., 1989, "Dynamic Subsoil-Coupling Between Rigid, Circular Foundations on the Half-Space," *Soil. Dyn. Earthq. Eng.*, Vol. 8, pp. 9–21.

Wang, Y., Rajapakse, R. K. N. D., and Shah, A. H., 1991, "Dynamic Interaction Between Flexible Strip Foundations," *Earthq. Eng. Struct. Dyn.*, Vol. 5, pp. 441–454.

Warburton, G. B., Richardson, J. D., and Webster, J. J., 1971, "Forced Vibrations of Two Masses on an Elastic Half Space," ASME JOURNAL OF APPLIED MECHANICS, Vol. 38, pp. 148–156.

Wong, H. L., and Luco, J. E., 1986, "Dynamic Interaction Between Rigid Foundations in a Layered Half-Space," *Soil. Dyn. Earthq. Eng.*, Vol. 3, pp. 149–158.

Wong, H. L., and Luco, J. E., 1976, "Dynamic Response of Rigid Foundation of Arbitrary Shape," *Earthq. Engng. Struct. Dyn.*, Vol. 4, pp. 579–587.

APPENDIX

The Green's function can be written as (see Guan and Novak, 1993)

$$\Delta_{jk}(x, y, t) = \int_0^{2\pi} \Delta_{jk}^{(1)} \chi_{jk}(x, y, \theta, C_R, t)\, d\theta + \int_0^{2\pi} \int_\beta^\alpha \Delta_{jk}^{(2)} \chi_{jk}(x, y, \theta, \eta, t)\, d\eta d\theta + \int_0^{2\pi} \int_\alpha^\infty \Delta_{jk}^{(3)} \chi_{jk}(x, y, \theta, \eta, t)\, d\eta d\theta \quad \text{(A1)}$$

in which $\Delta_{jk}^{(i)}$ can be expressed as

$$\Delta_{jk}^{(i)} = \begin{cases} G^{(i)}(\delta_{jk} - \delta_j\delta_k) - G_{jk}^{(i)}\delta_j\delta_k & j \le 2 \text{ and } k \le 2 \\ -G_{jk}^{(i)}\delta_j\delta_k & \text{otherwise} \end{cases} \quad \text{(A2)}$$

where

$$G_{11}^{(i)} = G_{22}^{(i)} = G_{12}^{(i)} = G_{21}^{(i)}$$

$$G_{31}^{(i)} = -G_{13}^{(i)}, \quad G_{32}^{(i)} = -G_{23}^{(i)}$$

$$G_{13}^{(i)} = G_{23}^{(i)}$$

$$\delta_1 = \cos\theta, \quad \delta_2 = \sin\theta, \quad \delta_3 = 1 \quad \text{(A3)}$$

and

$$\delta_{jk} = \begin{cases} 1 & j = k \\ 0 & j \ne k \end{cases} \quad \text{(A4)}$$

$$G_{11}^{(1)} = \frac{C_R^2/\beta^2\sqrt{1 - C_R^2/\beta^2}}{2\mu K(C_R)}$$

$$G_{11}^{(2)} = -\frac{2}{\pi\mu} \frac{\eta^2/\beta^2(2 - \eta^2/\beta^2)^2\sqrt{\eta^2/\beta^2 - 1}}{(2 - \eta^2/\beta^2)^4 + 16(1 - \eta^2/\alpha^2)(\eta^2/\beta^2 - 1)}$$

$$G_{11}^{(3)} = -\frac{2}{\pi\mu} \frac{\eta^2/\beta^2\sqrt{\eta^2/\beta^2 - 1}}{(2 - \eta^2/\beta^2)^2 + 4\sqrt{\eta^2/\beta^2 - 1}\sqrt{\eta^2/\alpha^2 - 1}} \quad \text{(A5)}$$

$$G_{13}^{(1)} = \frac{C_R^2/\beta^2(2 - C_R^2/\beta^2)}{4\mu K(C_R)}$$

$$G_{13}^{(2)} = -\frac{4}{\pi\mu} \frac{\eta^2/\beta^2(2 - \eta^2/\beta^2)\sqrt{1 - \eta^2/\alpha^2}\sqrt{\eta^2/\beta^2 - 1}}{(2 - \eta^2/\beta^2)^4 + 16(1 - \eta^2/\alpha^2)(\eta^2/\beta^2 - 1)}$$

$$G_{13}^{(3)} = 0 \quad \text{(A6)}$$

$$G_{33}^{(1)} = \frac{C_R^2/\beta^2\sqrt{1 - C_R^2/\alpha^2}}{2\mu K(C_R)}$$

$$G_{33}^{(2)} = -\frac{8}{\pi\mu} \frac{\eta^2/\beta^2(1 - \eta^2/\alpha^2)\sqrt{\eta^2/\beta^2 - 1}}{(2 - \eta^2/\beta^2)^4 + 16(1 - \eta^2/\alpha^2)(\eta^2/\beta^2 - 1)}$$

$$G_{33}^{(3)} = -\frac{2}{\pi\mu} \frac{\eta^2/\beta^2\sqrt{\eta^2/\alpha^2 - 1}}{(2 - \eta^2/\beta^2)^2 + 4\sqrt{\eta^2/\beta^2 - 1}\sqrt{\eta^2/\alpha^2 - 1}} \quad \text{(A7)}$$

$$G^{(1)} = 0$$

Downloaded 03 May 2010 to 171.66.16.20. Redistribution subject to ASME license or copyright; see http://www.asme.org/terms/Terms_Use.cfm

$$G^{(2)} = -\frac{2}{\pi\mu}\frac{1}{\sqrt{\eta^2/\beta^2 - 1}}$$

$$G^{(3)} = G^{(2)} \tag{A8}$$

where $K(C_R)$ denotes

$$K(C_R) = C_R\left\{\frac{1}{\beta^2}\left(2 - \frac{C_R^2}{\beta^2}\right) - \frac{1}{\alpha^2}\frac{\sqrt{1 - C_R^2/\beta^2}}{\sqrt{1 - C_R^2/\alpha^2}} - \frac{1}{\beta^2}\frac{\sqrt{1 - C_R^2/\alpha^2}}{\sqrt{1 - C_R^2/\beta^2}}\right\}. \tag{A9}$$

Downloaded 03 May 2010 to 171.66.16.20. Redistribution subject to ASME license or copyright; see http://www.asme.org/terms/Terms_Use.cfm

Nondimensional Parameters and Equations for Buckling of Anisotropic Shallow Shells

M. P. Nemeth
Senior Research Engineer,
Structural Mechanics Division,
NASA Langley Research Center,
Hampton, VA 23681-0001

A procedure for deriving nondimensional parameters and equations for bifurcation buckling of anisotropic shallow shells subjected to combined loads is presented. First, the Donnell-Mushtari-Vlasov equations governing buckling of symmetrically laminated doubly curved thin elastic shallow shells are presented. Then, the rationale used to perform the nondimensionalization of the buckling equations is presented, and fundamental parameters are identified that represent measures of the shell orthotropy and anisotropy. In addition, nondimensional curvature parameters are identified that are analogues of the well-known Batdorf Z parameter for isotropic shells, and analogues of Dunnell's and Batdorf's shell buckling equations are presented. Selected results are presented for shear buckling of balanced symmetric laminated shells that illustrate the usefulness of the nondimensional parameters.

Introduction

Understanding the buckling behavior of anisotropic shallow shells made of laminated composite materials is important for the structural design of future high performance aircraft. Identifying fundamental parameters that characterize buckling behavior of shells for a wide range of laminate configurations and materials will greatly aid the preliminary design of aircraft components such as the fuselage and empennage. More specifically, nondimensional parameters permit results to be presented as a series of curves, on one or more plots, that span a wide range of shell dimensions, loading combinations, boundary conditions, and material properties. Design charts of this general nature allow for quick evaluation of several design alternatives and furnish the designer with insight into the sensitivity of a particular design to changes in geometry, loading conditions, boundary conditions, or material properties. Of equal importance is the potential for nondimensional parameters to provide insight into the development of scaling laws for composite shells that will be valuable for relating subscale tests to full-scale tests during the certificiation phase of aircraft design. Potentially, well-defined scaling laws would minimize the amount of full-scale structural testing by using a series of less expensive subscale tests to complement the full-scale tests.

Characterizing the buckling behavior of anisotropic shells is not a trivial task due to the complex deformational coupling they exhibit. However, there are classes of practical laminated composite shells that do not exhibit total deformational coupling. The present study focuses on one such class of shells commonly known as symmetrically laminated shells. These shells exhibit anisotropy in the form of material-induced coupling between pure bending and twisting deformations and coupling between pure biaxial stretching and membrane shearing.

The objectives of the present paper are to present a method of deriving nondimensional equations for doubly curved anisotropic shallow shells subjected to combined loads, and to identify the fundamental parameters associated with bifurcation buckling of these shells. Shells with a high degree of curvature are known to be sensitive to small imperfections in their geometry under certain loading conditions, and this imperfection sensitivity leads to collapse loads often substantially lower than a predicted bifurcation buckling load (Almroth and Brogan, 1972). However, a class of shallow shells exists for which imperfection sensitivity is minimal under certain loading conditions (Stein and McElman, 1965). In this case, results obtained from a bifurcation buckling analysis can be used to obtain credible estimates of the collapse load. Moreover, in studying the general collapse behavior of shells, the researcher is often interested in knowing the bifurcation-type response for the sake of comparison. Furthermore, the parameters identified in a simpler bifurcation shell buckling analysis may be adequate for use in characterizing the actual nonlinear collapse behavior. A significant example of this approach is the well-known nondimensional Batdorf Z parameter that has seen wide use in buckling analyses of isotropic cylindrical shells (Gerard, 1962).

The present paper begins with a presentation of the Donnell-Mushtari-Vlasov equations governing bifurcation buckling of shallow shells that are thin, symmetrically laminated, and elastic. The equations are put into a form suitable for nondimensionalization, and the rationale used to perform the nondimensionalization of the buckling equations is presented.

Contributed by the Applied Mechanics Division of THE AMERICAN SOCIETY OF MECHANICAL ENGINEERS for publication in the ASME JOURNAL OF APPLIED MECHANICS.

Discussion on this paper should be addressed to the Technical Editor, Professor Lewis T. Wheeler, Department of Mechanical Engineering, University of Houston, Houston, TX 77204-4792, and will be accepted until four months after final publication of the paper itself in the ASME JOURNAL OF APPLIED MECHANICS.

Manuscript received by the ASME Applied Mechanics Division, Dec. 12, 1992; final revision, Apr. 12, 1993. Associate Technical Editor: X. Markenscoff.

Copyright © 1994 by ASME
Downloaded 03 May 2010 to 171.66.16.20. Redistribution subject to ASME license or copyright; see http://www.asme.org/terms/Terms_Use.cfm

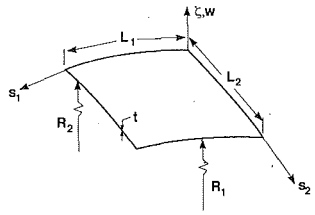


Fig. 1 Geometry of a shallow shell

Fundamental parameters are then identified that represent measures of the membrane and bending orthotropy and anisotropy. Curvature parameters for symmetrically laminated shells are then presented that are analogues of the Batdorf Z parameter. Next, analogues to Donnell's and Batdorf's shell buckling equations are presented. Last, selected results are presented for shear buckling of balanced symmetrically laminated shells to illustrate the usefulness of the nondimensional parameters.

The analysis presented in the present paper was inspired by the work presented by Stein (1982). For this reason, and for many useful discussions on this subject, the author would like to dedicate this paper to the late Dr. Manuel Stein of NASA Langley Research Center who spent nearly 50 years studying the buckling behavior of plates and shells.

Equations Governing Buckling

Equations governing buckling of thin elastic doubly curved shallow shells have been derived by Nemeth (1991) from the Donnell-Mushtari-Vlasov nonlinear equations in terms of lines-of-curvature coordinates using the method of adjacent equilibrium states. In the derivation, prebuckling displacements normal to the surface are neglected and the lines-of-curvature coordinates s_1 and s_2 with units of length are used to simplify the form of the equations (see Fig. 1). The use of two arc-length coordinates to parametrize the shell reference surface, which is not developable in general, is consistent with the assumptions of shallow shell theory that the surface metric tensor equals the Kronecker delta function and that the surface compatibility equation of Gauss is approximately satisfied. The linearized equilibrium equations are given by

$$\frac{\partial N_1}{\partial s_1}+\frac{\partial N_{12}}{\partial s_2}=0 \tag{1a}$$

$$\frac{\partial N_{12}}{\partial s_1}+\frac{\partial N_2}{\partial s_2}=0 \tag{1b}$$

$$\frac{\partial^2 M_1}{\partial s_1^2}+2\frac{\partial^2 M_{12}}{\partial s_1 \partial s_2}+\frac{\partial^2 M_2}{\partial s_2^2}-\frac{N_1}{R_1}-\frac{N_2}{R_2}+N_1^0\frac{\partial^2 w}{\partial s_1^2}+N_2^0\frac{\partial^2 w}{\partial s_2^2}+2N_{12}^0\frac{\partial^2 w}{\partial s_1 \partial s_2}=0 \tag{1c}$$

where N_1, N_2, and N_{12} are the membrane stress resultants and M_1, M_2, and M_{12} are the bending stress resultants of the adjacent equilibrium state. The quantities N_1^0, N_2^0, and N_{12}^0 are the membrane stress resultants of the primary equilibrium state and are referred to herein as the prebuckling stress resultants. The quantity w is the normal deflection of the shell at the onset of buckling and is referred to herein as the buckling displacement. The symbols R_1 and R_2 denote the principal radii of curvature of the shell middle surface along the s_1 and s_2 coordinate directions, respectively. Similarly, the linearized buckling compatibility equation is given by

$$\frac{\partial^2 \epsilon_1}{\partial s_2^2}+\frac{\partial^2 \epsilon_2}{\partial s_1^2}-\frac{\partial^2 \gamma_{12}}{\partial s_1 \partial s_2}=\frac{1}{R_2}\frac{\partial^2 w}{\partial s_1^2}+\frac{1}{R_1}\frac{\partial^2 w}{\partial s_2^2} \tag{2}$$

where ϵ_1, ϵ_2, and γ_{12} are the membrane strains of the adjacent equilibrium state. The constitutive equations for a symmetrically laminated anisotropic shell are given by

$$N_1=A_{11}\epsilon_1+A_{12}\epsilon_2+A_{16}\gamma_{12} \tag{3a}$$

$$N_2=A_{12}\epsilon_1+A_{22}\epsilon_2+A_{26}\gamma_{12} \tag{3b}$$

$$N_{12}=A_{16}\epsilon_1+A_{26}\epsilon_2+A_{66}\gamma_{12} \tag{3c}$$

$$M_1=-D_{11}\frac{\partial^2 w}{\partial s_1^2}-D_{12}\frac{\partial^2 w}{\partial s_2^2}-2D_{16}\frac{\partial^2 w}{\partial s_1 \partial s_2} \tag{4a}$$

$$M_2=-D_{12}\frac{\partial^2 w}{\partial s_1^2}-D_{22}\frac{\partial^2 w}{\partial s_2^2}-2D_{26}\frac{\partial^2 w}{\partial s_1 \partial s_2} \tag{4b}$$

$$M_{12}=-D_{16}\frac{\partial^2 w}{\partial s_1^2}-D_{26}\frac{\partial^2 w}{\partial s_2^2}-2D_{66}\frac{\partial^2 w}{\partial s_1 \partial s_2} \tag{4c}$$

where A_{11}, A_{12}, A_{22}, and A_{66} are the orthotropic membrane stiffnesses; A_{16} and A_{26} are the anisotropic membrane stiffnesses; D_{11}, D_{12}, D_{22}, and D_{66} are the orthotropic bending stiffnesses; and D_{16} and D_{26} are the anisotropic bending stiffnesses of classical laminated thin-shell theory (Dong, Pister, and Taylor, 1962). The corresponding boundary conditions of the boundary value problem are homogeneous and are not listed herein for brevity.

Nondimensionalization Procedure and Parameters

Nondimensional parameters for the buckling of shallow shells are obtained by building upon the procedure presented by Batdorf (1947*a–c*) for isotropic curved plates, by Stein (1982) for flat specially orthotropic laminated plates, and by Nemeth (1986) for flat symmetrically laminated plates. The basic premise of the procedure is to make the field variables and their derivatives of order one, to minimize the number of independent parameters required to characterize the behavior, and to avoid introducing a preferential direction into the nondimensional equations.

The first step in the nondimensionalization procedure is to formulate the boundary valve problem in terms of a single equilibrium equation and a compatibility equation. This step yields two coupled homogeneous linear partial differential equations. To obtain these equations, the membrane stress resultants of the adjacent equilibrium state are expressed in terms of a stress function Φ by

$$N_1=\frac{\partial^2 \Phi}{\partial s_2^2} \tag{5a}$$

$$N_2=\frac{\partial^2 \Phi}{\partial s_1^2} \tag{5b}$$

$$N_{12}=-\frac{\partial^2 \Phi}{\partial s_1 \partial s_2} \tag{5c}$$

This stress function satisfies Eqs. (1*a*) and (1*b*) identically. Eliminating these two equations from the boundary value problem by introducing a stress function requires that the buckling compatibility equation given by Eq. (2) be satisfied. To put the buckling compatibility equation into a convenient form, the inverted form of constitutive Eqs. (3*a*) through (3*c*) is used to express the buckling strains in terms of the stress function; i.e.,

$$\epsilon_1=a_{11}\frac{\partial^2 \Phi}{\partial s_2^2}+a_{12}\frac{\partial^2 \Phi}{\partial s_1^2}-a_{16}\frac{\partial^2 \Phi}{\partial s_1 \partial s_2} \tag{6a}$$

$$\epsilon_2=a_{12}\frac{\partial^2 \Phi}{\partial s_2^2}+a_{22}\frac{\partial^2 \Phi}{\partial s_1^2}-a_{26}\frac{\partial^2 \Phi}{\partial s_1 \partial s_2} \tag{6b}$$

$$\gamma_{12}=a_{16}\frac{\partial^2 \Phi}{\partial s_2^2}+a_{26}\frac{\partial^2 \Phi}{\partial s_1^2}-a_{66}\frac{\partial^2 \Phi}{\partial s_1 \partial s_2} \tag{6c}$$

where a_{11}, a_{12}, a_{22}, a_{16}, a_{26}, and a_{66} are the membrane flexibility coefficients of the shell and are functions of the membrane

Downloaded 03 May 2010 to 171.66.16.20. Redistribution subject to ASME license or copyright; see http://www.asme.org/terms/Terms_Use.cfm

stiffnesses only. Substituting Eqs. (6) into Eq. (2) converts the buckling compatibility equation into an equation in terms of the stress function and buckling displacement. Following Stein (1982), the following nondimensional coordinates are used:

$$S_1 = s_1/L_1 \text{ and } S_2 = s_2/L_2 \tag{7}$$

where L_1 and L_2 are characteristic dimensions of the shell shown in Fig. 1. Substituting these nondimensional coordinates into the buckling compatibility equation and normalizing by a weighted geometric mean flexibility; i.e., multiplying through by $L_1^2 L_2^2/\sqrt{a_{11}a_{22}}$, yields

$$\alpha_m^2 \frac{\partial^4 \Phi}{\partial S_1^4} + 2\alpha_m\gamma_m \frac{\partial^4 \Phi}{\partial S_1^3 \partial S_2} + 2\mu \frac{\partial^4 \Phi}{\partial S_1^2 \partial S_2^2} + 2\frac{\delta_m}{\alpha_m}\frac{\partial^4 \Phi}{\partial S_1 \partial S_2^3} + \frac{1}{\alpha_m^2}\frac{\partial^4 \Phi}{\partial S_2^4} = \frac{1}{\sqrt{a_{11}a_{22}}}\left[\frac{L_2^2}{R_2}\frac{\partial^2 w}{\partial S_1^2} + \frac{L_1^2}{R_1}\frac{\partial^2 w}{\partial S_2^2}\right] \tag{8}$$

where the nondimensional parameters appearing in the equation are given by

$$\alpha_m = \frac{L_2}{L_1}(a_{22}/a_{11})^{1/4} \tag{9a}$$

$$\mu = \frac{2a_{12} + a_{66}}{2\sqrt{a_{11}a_{22}}} \tag{9b}$$

$$\gamma_m = -\frac{a_{26}}{(a_{11}a_{22}^3)^{1/4}} \tag{9c}$$

and

$$\delta_m = -\frac{a_{16}}{(a_{11}^3 a_{22})^{1/4}}. \tag{9d}$$

Expressions for these parameters written in terms of shell membrane stiffness coefficients are presented in the Appendix.

The next step in the nondimensionalization procedure is to express the normal-direction equilibrium equation in terms of the buckling displacement w and stress function Φ by substituting Eqs. (4) and (5) into Eq. (1c). Performing this step, introducing the nondimensional coordinates, and normalizing by a weighted geometric mean stiffness; i.e., multiplying through by $L_1^2 L_2^2/\sqrt{D_{11}D_{22}}$, yields

$$\alpha_b^2 \frac{\partial^4 w}{\partial S_1^4} + 4\alpha_b\gamma_b \frac{\partial^4 w}{\partial S_1^3 \partial S_2} + 2\beta \frac{\partial^4 w}{\partial S_1^2 \partial S_2^2} + 4\frac{\delta_b}{\alpha_b}\frac{\partial^4 w}{\partial S_1 \partial S_2^3} + \frac{1}{\alpha_b^2}\frac{\partial^2 w}{\partial S_2^4} + \frac{L_1^2}{R_1\sqrt{D_{11}D_{22}}}\frac{\partial^2 \Phi}{\partial S_2^2} + \frac{L_2^2}{R_2\sqrt{D_{11}D_{22}}}\frac{\partial^2 \Phi}{\partial S_1^2} - K_1\pi^2 \frac{\partial^2 w}{\partial S_1^2} - K_2\pi^2 \frac{\partial^2 w}{\partial S_2^2} - 2\frac{K_{12}\pi^2}{\alpha_b}\frac{\partial^2 w}{\partial S_1 \partial S_2} = 0 \tag{10}$$

where the nondimensional parameters appearing in the equation are given by

$$\alpha_b = \frac{L_2}{L_1}(D_{11}/D_{22})^{1/4} \tag{11a}$$

$$\beta = \frac{D_{12} + 2D_{66}}{\sqrt{D_{11}D_{22}}} \tag{11b}$$

$$\gamma_b = \frac{D_{16}}{(D_{11}^3 D_{22})^{1/4}} \tag{11c}$$

$$\delta_b = \frac{D_{26}}{(D_{11}D_{22}^3)^{1/4}} \tag{11d}$$

$$K_1 = \frac{N_1^0 L_2^2}{\pi^2\sqrt{D_{11}D_{22}}} \tag{11e}$$

$$K_2 = \frac{N_2^0 L_1^2}{\pi^2\sqrt{D_{11}D_{22}}} \tag{11f}$$

$$K_{12} = \frac{N_{12}^0 L_2^2}{\pi^2 (D_{11}D_{22}^3)^{1/4}}. \tag{11g}$$

The parameters α_b, β, γ_b, and δ_b are parameters used to characterize plate buckling (see Stein, 1982; Nemeth, 1986). Similarly, the nondimensional functions K_1, K_2, and K_{12} give rise to the usual definitions of buckling coefficients.

To obtain nondimensional equilibrium and compatibility equations of order one, a new stress resultant function defined by

$$F = \Phi/\sqrt{D_{11}D_{22}} \tag{12}$$

is introduced into Eqs. (8) and (10). Equilibrium Eq. (10) becomes

$$\alpha_b^2 \frac{\partial^4 w}{\partial S_1^4} + 4\alpha_b\gamma_b \frac{\partial^4 w}{\partial S_1^3 \partial S_2} + 2\beta \frac{\partial^4 w}{\partial S_1^2 \partial S_2^2} + 4\frac{\delta_b}{\alpha_b}\frac{\partial^4 w}{\partial S_1 \partial S_2^3} + \frac{1}{\alpha_b^2}\frac{\partial^4 w}{\partial S_2^4} + \frac{L_1^2}{R_1}\frac{\partial^2 F}{\partial S_2^2} + \frac{L_2^2}{R_2}\frac{\partial^2 F}{\partial S_1^2} - K_1\pi^2 \frac{\partial^2 w}{\partial S_1^2} - K_2\pi^2 \frac{\partial^2 w}{\partial S_2^2} - 2\frac{K_{12}\pi^2}{\alpha_b}\frac{\partial^2 w}{\partial S_1 \partial S_2} = 0. \tag{13}$$

Similarly, substituting Eq. (12) into compatibility Eq. (8) and simplifying gives

$$\alpha_m^2 \frac{\partial^4 F}{\partial S_1^4} + 2\alpha_m\gamma_m \frac{\partial^4 F}{\partial S_1^3 \partial S_2} + 2\mu \frac{\partial^4 F}{\partial S_1^2 \partial S_2^2} + 2\frac{\delta_m}{\alpha_m}\frac{\partial^4 F}{\partial S_1 \partial S_2^3} + \frac{1}{\alpha_m^2}\frac{\partial^4 F}{\partial S_2^4} = \frac{1}{\sqrt{a_{11}a_{22}D_{11}D_{22}}}\left[\frac{L_2^2}{R_2}\frac{\partial^2 w}{\partial S_1^2} + \frac{L_1^2}{R_1}\frac{\partial^2 w}{\partial S_2^2}\right]. \tag{14}$$

A factor of the right-hand-side of Eq. (14) is given by

$$\frac{1}{(a_{11}a_{22}D_{11}D_{22})^{1/4}}$$

and has dimension $1/t$, where t is the shell wall thickness. To put Eq. (14) into a form of order one, a nondimensional buckling displacement W is introduced; i.e.,

$$W = \frac{w}{(a_{11}a_{22}D_{11}D_{22})^{1/4}}. \tag{15}$$

The nondimensional displacement W defined in Eq. (15) has a character that is similar to w/t. Using Eq. (15), Eq. (14) simplifies to

$$\alpha_m^2 \frac{\partial^4 F}{\partial S_1^4} + 2\alpha_m\gamma_m \frac{\partial^4 F}{\partial S_1^3 \partial S_2} + 2\mu \frac{\partial^4 F}{\partial S_1^2 \partial S_2^2} + 2\frac{\delta_m}{\alpha_m}\frac{\partial^4 F}{\partial S_1 \partial S_2^3} + \frac{1}{\alpha_m^2}\frac{\partial^4 F}{\partial S_2^4} = \sqrt{12}\left\{Z_2 \frac{\partial^2 W}{\partial S_1^2} + Z_1 \frac{\partial^2 W}{\partial S_2^2}\right\} \tag{16}$$

where

$$Z_1 = \frac{L_1^2}{R_1\sqrt{12}(a_{11}a_{22}D_{11}D_{22})^{1/4}} \tag{17a}$$

$$Z_2 = \frac{L_2^2}{R_2\sqrt{12}(a_{11}a_{22}D_{11}D_{22})^{1/4}}. \tag{17b}$$

The term $\sqrt{12}$ is factored out of the right-hand side of Eq. (16) to cancel out a $1/\sqrt{12}$ term that arises when Eqs. (17) are specialized to isotropic shells. Expressions for Z_1 and Z_2 written in terms of shell membrane and bending stiffness coefficients are presented in the Appendix. Equilibrium Eq. (13) also simplifies to

$$\alpha_b^2 \frac{\partial^4 W}{\partial S_1^4} + 4\alpha_b\gamma_b \frac{\partial^4 W}{\partial S_1^3 \partial S_2} + 2\beta \frac{\partial^4 W}{\partial S_1^2 \partial S_2^2} + 4\frac{\delta_b}{\alpha_b}\frac{\partial^4 W}{\partial S_1 \partial S_2^3} + \frac{1}{\alpha_b^2}\frac{\partial^4 W}{\partial S_2^4} + \sqrt{12}\left[Z_1 \frac{\partial^2 F}{\partial S_2^2} + Z_2 \frac{\partial^2 F}{\partial S_1^2}\right] - K_1\pi^2 \frac{\partial^2 W}{\partial S_1^2} - K_2\pi^2 \frac{\partial^2 W}{\partial S_2^2} - 2\frac{K_{12}\pi^2}{\alpha_b}\frac{\partial^2 W}{\partial S_1 \partial S_2} = 0. \tag{18}$$

Compatibility Eq. (16) can be expressed in operator form as

$$D_m(F) - \sqrt{12}D_c(W) = 0 \tag{19}$$

Downloaded 03 May 2010 to 171.66.16.20. Redistribution subject to ASME license or copyright; see http://www.asme.org/terms/Terms_Use.cfm

where $D_m(\ )$ and $D_c(\ )$ are membrane and shell curvature operators, respectively, given by

$$D_m(F) \equiv \alpha_m^2 \frac{\partial^4 F}{\partial S_1^4} + 2\alpha_m\gamma_m \frac{\partial^4 F}{\partial S_1^3 \partial S_2} + 2\mu \frac{\partial^4 F}{\partial S_1^2 \partial S_2^2} + 2\frac{\delta_m}{\alpha_m} \frac{\partial^4 F}{\partial S_1 \partial S_2^3} + \frac{1}{\alpha_m^2} \frac{\partial^4 F}{\partial S_2^4} \quad (20)$$

and

$$D_c(W) \equiv Z_2 \frac{\partial^2 W}{\partial S_1^2} + Z_1 \frac{\partial^2 W}{\partial S_2^2}. \quad (21)$$

The membrane operator given above simplifies to a nondimensional form of the biharmonic operator for isotropic shells.

To put equilibrium Eq. (18) into a useful form, the nondimensional functions K_1, K_2, and K_{12} are expressed in terms of a loading parameter $\tilde{p}$. These relationships are given by

$$K_1 = -P_1 g_1(S_1, S_2)\tilde{p} \quad (22a)$$

$$K_2 = -P_2 g_2(S_1, S_2)\tilde{p} \quad (22b)$$

$$K_{12} = P_3 g_3(S_1, S_2)\tilde{p} \quad (22c)$$

where the minus signs are introduced to make compression loads correspond to positive eigenvalues. The parameters P_1, P_2, and P_3 are load factors that indicate the relative magnitudes of the nondimensional membrane stress resultants prior to buckling, and the functions $g_1(S_1, S_2)$ through $g_3(S_1, S_2)$ indicate the corresponding spatial variations. Using these relations, Eq. (18) is expressed in operator form as

$$D_b(W) + \sqrt{12} D_c(F) = \tilde{p} K_g(W) \quad (23)$$

where $D_b(\ )$ is a bending operator and $K_g(\ )$ is a geometric stiffness operator defined by

$$D_b(W) \equiv \alpha_b^2 \frac{\partial^4 W}{\partial S_1^4} + 4\alpha_b\gamma_b \frac{\partial^4 W}{\partial S_1^3 \partial S_2} + 2\beta \frac{\partial^4 W}{\partial S_1^2 \partial S_2^2} + 4\frac{\delta_b}{\alpha_b} \frac{\partial^4 W}{\partial S_1 \partial S_2^3} + \frac{1}{\alpha_b^2} \frac{\partial^4 W}{\partial S_2^4} \quad (24)$$

$$K_g(W) \equiv -P_1 g_1(S_1, S_2)\pi^2 \frac{\partial^2 W}{\partial S_1^2} - P_2 g_2(S_1, S_2)\pi^2 \frac{\partial^2 W}{\partial S_2^2} + 2P_3 g_3(S_1, S_2) \frac{\pi^2}{\alpha_b} \frac{\partial^2 W}{\partial S_1 \partial S_2}. \quad (25)$$

The bending operator given above also simplifies to a nondimensional form of the biharmonic operator for isotropic shells.

Equations (19) and (23) and the corresponding homogeneous boundary conditions constitute an eigenvalue problem. The smallest value of the loading parameter $\tilde{p}$ for which the equations are satisfied constitutes buckling of the shell. The equations are nondimensional and each derivative is typically of order one for buckle patterns that do not exhibit severe gradients. Thus, the magnitude of the parameters multiplying each derivative term is often a direct indication of the importance of that term to the shell response. Moreover, the parameters defined by Eqs. (11*a*) and (11*b*) and those defined by Eqs. (11*c*) and (11*d*) characterize shell bending orthotropy and bending anisotropy, respectively. Likewise, the parameters defined by Eqs. (9) characterize shell membrane orthotropy and anisotropy. The parameters Z_1 and Z_2 are analogues of the Batdorf Z parameter (Batdorf, 1947a-c) that has long been used to characterize the effects of shell curvature on buckling of isotropic cylindrical shells. The identification of these generalized shell curvature parameters in the present paper was influenced to a great extent by Stein's work (1982), and thus are referred to herein as the Batdorf-Stein Z parameters.

Analogues of Donnell's and Batdorf's Equations

Donnell showed that a single eighth-order differential equation could be obtained for isotropic cylindrical shells by eliminating the stress function appearing in the buckling equations (see Batdorf, 1947a). Applying Donnell's approach to the equations derived herein, Eq. (19) is operated on by the curvature operator $D_c(\ )$ to give

$$D_m(D_c(F)) = \sqrt{12} D_c^2(W) \quad (26)$$

where the order of the operators has been exchanged, in accordance with the commutative property of linear operators with constant coefficients. Next, operating on Eq. (23) with the membrane stiffness operator yields

$$D_m(D_b(W)) + \sqrt{12} D_m(D_c(F)) = \tilde{p} D_m K_g(W). \quad (27)$$

Substituting the right-hand side of Eq. (26) into Eq. (27) yields an eighth-order partial differential equation referred to herein as the Donnell-Stein equation; i.e.,

$$D_m(D_b(W)) + 12 D_c^2(W) = \tilde{p} D_m K_g(W). \quad (28)$$

This equation simplifies to a nondimensional equivalent of Donnell's equation for isotropic shells.

Batdorf (1947b,c, 1969) presented an alternative to Donnell's equation that made use of inverse differential operators. The equivalent of Batdorf's equation is obtained by expressing Eq. (19) as

$$F = \sqrt{12} D_m^{-1}(D_c(W)) \quad (29)$$

where $D_m^{-1}(\ )$ denotes the inverse differential operator. Commuting the order of the linear constant coefficient operators in Eq. (29) and substituting the resulting equation into Eq. (23) yields the desired equation; i.e.,

$$D_b(W) + 12 D_c^2[D_m^{-1}(W)] - \tilde{p} K_g(W) = 0. \quad (30)$$

This equation is an analogue of Batdorf's modified equilibrium equation (Batdorf, 1947b) and is referred to herein as the modified Batdorf-Stein equation. Equation (30) also simplifies to a nondimensional equivalent of Batdorf's modified equation for isotropic shells.

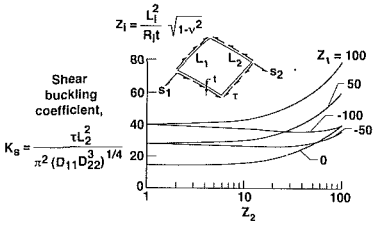


Fig. 2 Effect of shell curvature on shear buckling resistance of isotropic shallow shells ($L_1/L_2 = 1$)

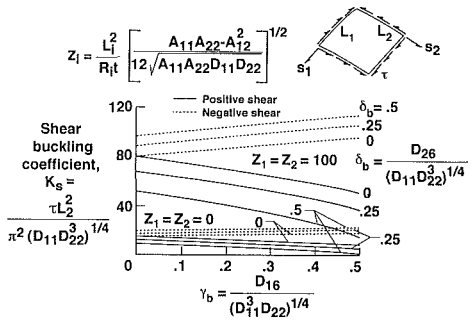


Fig. 3 Effects of bending anisotropy and shell curvature on shear buckling resistance ($L_1/L_2 = 1$)

Selected Results and Discussion

Some selected results are presented in Figs. 2 and 3 for shear buckling of balanced symmetrically laminated shallow shells to demonstrate the usefulness of the nondimensional param-

Downloaded 03 May 2010 to 171.66.16.20. Redistribution subject to ASME license or copyright; see http://www.asme.org/terms/Terms_Use.cfm

eters identified herein. The results were obtained from a Bubnov-Galerkin approximate solution to the modified Batdorf-Stein equation given by Eq. (30). Details of the analytical solution have been presented by Nemeth (1991). A typical shell is loaded on its edges by a uniform tangential shearing traction τ as shown in Fig. 2. For this loading, $N^0_{12}(s_1, s_2) = \tau$ is the only nonzero prebuckling stress resultant. The shell is supported such that the buckling displacement w and the rotations $\partial w/\partial s_1$ and $\partial w/\partial s_2$ vanish along all the edges of the shell. In addition, the membrane displacements normal to each edge of the shell are restrained and no additional tangential shearing tractions occur due to buckling. The buckling resistance of a shell is indicated in the figures by the nondimensional shear buckling coefficient K_s defined by

$$K_s = \frac{\tau L_2^2}{\pi^2 (D_{11} D_{22}^3)^{1/4}} \tag{31}$$

where τ is the applied uniform shearing traction. For the results presented in the figures, the orthotropic parameters (α_b, β, α_m, and μ) and the anisotropic parameters (γ_b, δ_b, γ_m, and δ_m) that are not varied are set equal to one and zero, respectively. This baseline set of values corresponds to an isotropic shell with sides of equal length ($L_1 = L_2$).

Results showing shear buckling coefficient as a function of the Batdorf-Stein shell curvature parameters, Z_1 and Z_2, are presented in Fig. 2. The abscissa of the plot shown in Fig. 2 is measured by a logarithmic scale. Results are shown in this figure for $Z_1 = 0$ and $Z_2 = 1$, which correspond essentially to flat plates, and for shells with zero ($Z_1 Z_2 = 0$), negative ($Z_1 Z_2 < 0$), and positive ($Z_1 Z_2 > 0$) Gaussian curvature with magnitudes of Z_1 and Z_2 ranging from 0 to 100. The analytical results presented in Fig. 2 predict that the shear buckling resistance of a shell is significantly influenced by shell curvature, especially for the larger values of Z_1 and Z_2 shown in the figure. The results also indicate that the shells with positive Gaussian curvature are more buckling resistant than those with negative Gaussian curvature, which, in turn, are typically more buckling resistant than those with zero Gaussian curvature. Flat plates exhibit the lowest buckling resistance.

Results showing shear buckling coefficient as a function of the curvature parameters, Z_1 and Z_2, and the bending anisotropy parameters γ_b and δ_b are presented in Fig. 3. Results are shown in this figure for flat plates ($Z_1 = Z_2 = 0$) and for shells with positive Gaussian curvature corresponding to $Z_1 = Z_2 = 100$. Values of the anisotropic parameters range from 0 to 0.5. This range of values is considered to be representative of a large class of laminated plates (Nemeth, 1986). Results are presented in Fig. 3 corresponding to both positive (as shown in the figure) and negative directions of the applied shearing traction, in accordance with the presence of bending anisotropy.

The results presented in Fig. 3 predict that the shear buckling resistance of a shell with positive Gaussian curvature is more sensitive to variations in the anisotropic (bending) parameters than a corresponding flat plate. The results show substantial reductions in buckling resistance with increasing values of the anisotropic parameters for shells loaded in positive shear, and similar increases in buckling resistance for shells loaded in negative shear. Similar results were obtained for a corresponding shell with negative Gaussian curvature that indicate the same trend, but not to as large as extent as exhibited by the shell with positive Gaussian curvature.

The generic results presented in Figs. 2 and 3 apply to many laminate constructions, and show that varying parameters independently can give insight into the factors strongly affecting the structural response. For example, by independently varying the parameters associated with shell curvature, positive values of Gaussian curvature are found to improve substantially the shear buckling resistance of a shell. In addition, shell curvature was determined to affect significantly the importance of the bending anisotropy on the shear buckling resistance. Both of these observations clearly indicate the benefits of using nondimensional parameters to formulate the analysis and to perform parametric studies.

Concluding Remarks

A method of deriving nondimensional equations and identifying the fundamental parameters associated with bifurcation buckling of shallow, anisotropic shells subjected to combined loads has been presented. Specifically, analysis has been presented for symmetrically laminated doubly curved shells that exhibit both membrane and bending anisotropy, and the procedure and rationale required to obtain useful nondimensional forms of the transverse equilibrium and compatibility equations for buckling have been discussed. The analysis presented herein yields fundamental parameters that explicitly and compactly indicate the effects of both membrane and bending orthotropy and anisotropy, and the effects of curvature on shallow shell buckling behavior. An important contribution of this work is the development of anisotropic analogues of the well-known Batdorf Z shell curvature parameter for symmetrically laminated anisotropic shells with compound curvature, and corresponding analogues of Donnell's and Batdorf's shell buckling equations.

Results obtained from a Bubnov-Galerkin solution to a representative example problem have also been presented. The results indicate the utility of recasting the shell buckling equations in terms of nondimensional parameters to conduct parametric studies that are generic and well suited to the preliminary design of laminated composite shells. Moreover, the analytical results predict that shells with positive Gaussian curvature are much more resistant to shear buckling than corresponding flat plates or shells with negative and zero Gaussian curvature. In addition, the results predict that the importance of bending anisotropy on shear buckling resistance is significantly affected by shell curvature.

References

Almroth, B. O., and Brogan, F. A., 1972, "Bifurcation Buckling as an Approximation of the Collapse Load for General Shells," *AIAA Journal*, Vol. 10, No. 4, pp. 463–467.

Batdorf, S. B., 1947a, "A Simplified Method of Elastic-Stability Analysis for Thin Cylindrical Shells, I—Donnell's Equation," NACA Technical Note No. 1341.

Batdorf, S. B., 1947b, "A Simplified Method of Elastic-Stability Analysis for Thin Cylindrical Shells, II—Modified Equilibrium Equation," NACA Technical Note No. 1342.

Batdorf, S. B., 1947c, "A Simplified Method of Elastic-Stability Analysis for Thin Cylindrical Shells," NACA Technical Report No. 874.

Batdorf, S. B., 1969, "On the Application of Inverse Differential Operators to the Solution of Cylinder Buckling and Other Problems," *Proceedings of the AIAA/ASME 10th Structures, Structural Dynamics, and Materials Conference.*

Dong, S. B., Pister, K. S., and Taylor, R. L., 1962, "On the Theory of Laminated Anisotropic Shells and Plates," *Journal of the Aerospace Sciences*, Vol. 29, pp. 969–975.

Gerard, G., 1962, *Introduction to Structural Stability Theory*, McGraw-Hill, New York, pp. 129–155.

Nemeth, M. P., 1986, "Importance of Anisotropy on Buckling of Compression-Loaded Symmetric Composite Plates," *AIAA Journal*, Vol. 24, No. 11, pp. 1831–1835.

Nemeth, M. P., 1991, "Nondimensional Parameters and Equations for Buckling of Symmetrically Laminated Thin Elastic Shallow Shells," NASA Technical Memorandum 104060.

Stein, M., and McElman, J. A., 1965, "Buckling of Segments of Toroidal Shells," *AIAA Journal*, Vol. 3, No. 9, pp. 1704–1709.

Stein, M., 1982, "Postbuckling of Orthotropic Composite Plates Loaded in Compression," Presented at the AIAA/ASME/ASCE/AHS 23rd Structures, Structural Dynamics, and Materials Conference, AIAA Paper No. 82-0778, New Orleans, LA.

APPENDIX

Parameters in Terms of Membrane Stiffnesses

The parameters α_m, μ, γ_m, δ_m, Z_1, and Z_2 have been given

Downloaded 03 May 2010 to 171.66.16.20. Redistribution subject to ASME license or copyright; see http://www.asme.org/terms/Terms_Use.cfm

in the present paper in terms of membrane flexibility coefficients. More convenient forms of these parameters are obtained by expressing them in terms of the membrane stiffness coefficients. Inverting the membrane stiffness matrix $[A]$ associated with Eqs. (6) and substituting the resulting expressions into the expressions for the nondimensional parameters gives

$$\alpha_m = \frac{L_2}{L_1}\left(\frac{A_{11}A_{66}-A_{16}^2}{A_{22}A_{66}-A_{26}^2}\right)^{1/4} \tag{A1}$$

$$\mu = \frac{A_{11}A_{22}-A_{12}^2-2A_{12}A_{66}+2A_{16}A_{26}}{2[(A_{11}A_{66}-A_{16}^2)(A_{22}A_{66}-A_{26}^2)]^{1/2}} \tag{A2}$$

$$\gamma_m = \frac{A_{11}A_{26}-A_{12}A_{16}}{[(A_{11}A_{66}-A_{16}^2)^3(A_{22}A_{66}-A_{26}^2)]^{1/4}} \tag{A3}$$

$$\delta_m = \frac{A_{22}A_{16}-A_{12}A_{26}}{[(A_{11}A_{66}-A_{16}^2)(A_{22}A_{66}-A_{26}^2)^3]^{1/4}} \tag{A4}$$

$$Z_i = \frac{L_i^2}{R_i}\left[\frac{(A_{11}A_{22}-A_{12}^2)A_{66}-A_{11}A_{26}^2-A_{22}A_{16}^2+2A_{12}A_{16}A_{26}}{12[(A_{11}A_{66}-A_{16}^2)(A_{22}A_{66}-A_{26}^2)D_{11}D_{22}]^{1/2}}\right]^{1/2} \tag{A5}$$

where i appearing in Eq. (A5) is a free index that takes on the values of 1 and 2. For balanced symmetric laminates with A_{16} and A_{26} that are zero valued, $\gamma_m = 0$ and $\delta_m = 0$. The remaining nonzero parameters simplify to

$$\alpha_m = \frac{L_2}{L_1}(A_{11}/A_{22})^{1/4} \tag{A6}$$

$$\mu = \frac{A_{11}A_{22}-A_{12}^2-2A_{12}A_{66}}{2A_{66}\sqrt{A_{11}A_{22}}} \tag{A7}$$

$$Z_i = \frac{L_i^2}{R_i}\left[\frac{A_{11}A_{22}-A_{12}^2}{12\sqrt{A_{11}A_{22}D_{11}D_{22}}}\right]^{1/2}. \tag{A8}$$

In addition, when the bending stiffnesses D_{16} and D_{26} are zero valued, $\gamma_b = \delta_b = 0$. Similarly, for isotropic shells, the nonzero parameters are given by

$$\alpha_m = \alpha_b = \frac{L_2}{L_1} \tag{A9}$$

$$\mu = \beta = 1 \tag{A10}$$

$$Z_i = \frac{L_i^2}{R_i t}(1-\nu^2)^{1/2} \tag{A11}$$

where t is the total shell thickness and ν is Poisson's ratio.

Downloaded 03 May 2010 to 171.66.16.20. Redistribution subject to ASME license or copyright; see http://www.asme.org/terms/Terms_Use.cfm

V. Berdichevsky

O. Özbek

W. W. Kim

Georgia Institute of Technology,
Atlanta, GA 30332-0150

Thermodynamics of Duffing's Oscillator

We study the averaged characteristics of the response of Duffing's oscillator to harmonic excitation. We show that, as in classical thermodynamics, response characteristics are potential functions of excitation characteristics.

Introduction

Classical equilibrium thermodynamics studies the response of mechanical and physical systems to slow changes of control parameters. Usually it is implied that the systems which obey the thermodynamical laws have very large numbers of degrees-of-freedom. Discovery of the surprising complexity of the behavior of simple low-dimensional mechanical systems raises the question on the possibility of formulating thermodynamical laws for such systems. Since thermodynamics has proven to be the necessary tool in the study of complex systems, the achievement of this goal seems very important. It was shown (Berdichevsky 1988) that thermodynamical laws stay unchanged for all finite-dimensional ergodic Hamiltonian systems. Thermodynamical laws are valid approximately if the Hamiltonian system is approximately ergodic (Berdichevsky et al., 1991).

Most engineering equations, however, are not Hamiltonian: they differ from the Hamiltonian equations by dissipative terms. For such systems thermodynamical laws should be modified (Berdichevsky, 1993). The most essential change relates to entropy: entropy drops out of the thermodynamical relations due to the fact that initial data is forgotten in dissipative systems. In general, thermodynamical laws for systems with small dissipation are reduced to the potentiality of the constitutive relations. Herein, we study this property for one of the most important nonlinear systems-Duffing's oscillator.

Vibrations of Duffing's oscillator are governed by the equation

$$m\ddot{x}+k\dot{x}+Ex+Gx^3=A+B\sin\omega t. \tag{1}$$

This equation was first formulated by Duffing (1918). It has received a lot of attention in the last few decades as it presents one of the simplest nonlinear systems that demonstrates extremely complex behavior. (Ueda, 1980, 1985; Moon, 1979; Holmes, 1983; Dowell et al., 1986; Fang, et al. 1987.)

The main statement of "thermodynamics of Duffing's oscillator" is as follows. The extreme complexity of the solutions suggests the description of the response of Duffing's oscillator in terms of some average characteristics. By averaging, we mean time averaging along a trajectory: for any function $\varphi(\dot{x},x,t)$,

$$\langle\varphi\rangle=\lim_{\Theta\to\infty}\frac{1}{\Theta}\int_0^{\Theta}\varphi(\dot{x}(t),\,x(t),\,t)dt. \tag{2}$$

Since each trajectory approaches to some attractor (damping k is assumed to be positive), the average value $\langle\varphi\rangle$ is unique for each attractor. For each attractor $\langle\varphi\rangle$ is some function of the force parameters A, B, and ω and of the oscillator characteristics m, k, E, and G. Typically, attractors of Duffing's oscillator with periodic excitation are limit cycles with periods $2\pi n/\omega$, where n is an integer, or strange attractors.

For limit cycles with the minimal period $2\pi/\omega$ the most important characteristics of the response are the amplitudes of the first two Fourier modes:

$$\bar{x}=\langle x(t)\rangle \quad \hat{x}=\langle x\sin\omega t\rangle. \tag{3}$$

These modes play a distinctive role because the averaged potential of the external force $F=A+B\sin\omega t$ can be expressed in terms of $\bar{x}$ and $\hat{x}$

$$\langle F(t)x(t)\rangle=A\bar{x}+B\hat{x}.$$

For each limit cycle the quantities $\bar{x}$ and $\hat{x}$ are functions of the oscillator characteristics and the applied force parameter:

$$\bar{x}=\bar{x}(A,B,\omega,m,k,E,G)$$

$$\hat{x}=\hat{x}(A,B,\omega,m,k,E,G). \tag{4}$$

Equations (4) describe averaged dynamics of the oscillator, its "macroscopic behavior." They are analogous to constitutive equations of classical thermodynamics, and their study is the subject of "thermodynamics of Duffing's oscillator." Note that damping coefficient k is small but nonzero: for zero damping the right-hand side of (4) does not have sense since it depends also on initial data.

Thermodynamics of Duffing's oscillator states (Berdichevsky, 1993), that for $k\to 0$ functions (4) can be derived from a dynamical potential function P, such that

$$\bar{x}=\frac{\partial P}{\partial A},\quad \hat{x}=\frac{\partial P}{\partial B}. \tag{5}$$

The function P contains all of the information on the "macrobehavior" of Duffing's oscillator and is analogous

Contributed by the Applied Mechanics Division of THE AMERICAN SOCIETY OF MECHANICAL ENGINEERS for publication in the ASME JOURNAL OF APPLIED MECHANICS.

Discussion on this paper should be addressed to the Technical Editor, Professor Lewis T. Wheeler, Department of Mechanical Engineering, University of Houston, Houston, TX 77204-4792, and will be accepted until four months after final publication of the paper itself in the ASME JOURNAL OF APPLIED MECHANICS.

Manuscript received by the ASME Applied Mechanics Division, Jan. 15, 1993; final revision, Apr. 26, 1993. Associate Technical Editor: R. L. Huston.

Copyright © 1994 by ASME

Downloaded 03 May 2010 to 171.66.16.20. Redistribution subject to ASME license or copyright; see http://www.asme.org/terms/Terms_Use.cfm

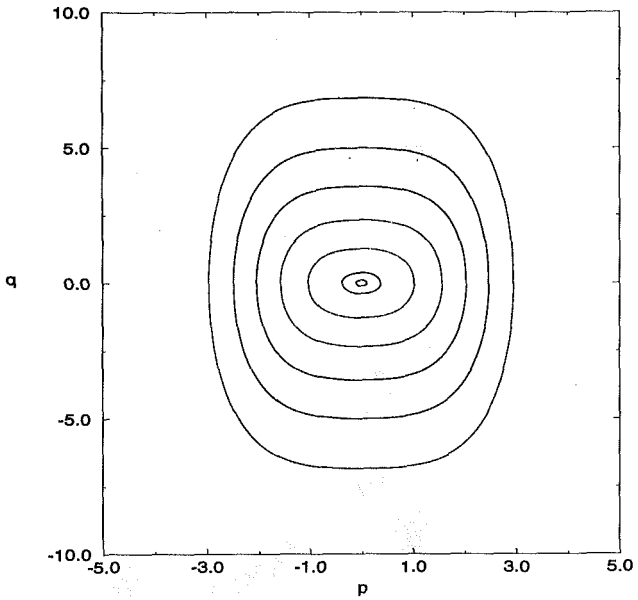


Fig. 1 Poincare map for $\alpha = 1$, $a = b = \mu = 0$

to the internal energy in classical thermodynamics. To know the macrodynamics of Duffing's oscillator means to know the function P.

The potentiality simplifies the description of macrobehavior: one needs to know only one function P instead of two functions (4). The potentiality reflected in Eq. (5) means that the following reciprocal relation is valid:

$$\frac{\partial \bar{x}}{\partial B} = \frac{\partial \hat{x}}{\partial A}. \tag{6}$$

Our aim is to check the error of Eq. (5) by numerical simulations and *find the dynamical potential* numerically. We show that this error is very small for small damping: it does not exceed 0.01 percent if dimensionless friction $\mu = 2\pi k/m\omega$ is less than 0.5. The error grows with μ and reaches about 10 percent for $\mu = 8$.

Concluding this Introduction it is worthy to note that Eq. (1) can be considered as Hamiltonian with Lagrange's function of the form

$$L = \left(\frac{1}{2} m\dot{x}^2 - \frac{1}{2} Ex^2 - \frac{1}{4} Gx^4 + Ax + Bx \sin \omega t\right) \exp\left(\frac{kt}{m}\right). \tag{7}$$

Other forms of similar type are also possible (see, for example, Berdichevsky, 1983). Unfortunately, they have some peculiarities which inhibit the direct use of approaches developed in statistical mechanics. For example, Lagrange's function written above degenerates when $t \to \infty$. On the other hand, this example shows that there exists time-dependent Hamiltonian systems which possess attractors.

Geometry of Trajectories of Duffing's Oscillator

To get a better understanding of the behavior of Duffing's oscillator for small dissipation, it is very useful to study the geometry of the trajectories for zero dissipation first. This will be investigated in this section.

First, let us transform Duffing's equation to nondimensional form

$$\frac{d^2q}{d\theta^2} + \mu \frac{dq}{d\theta} + \alpha q + \beta q^3 = a + b \sin 2\pi\theta \tag{8}$$

where

$$\alpha = \frac{E\left(\frac{2\pi}{\omega}\right)^2}{m}, \quad \beta = \frac{\lambda^2 G\left(\frac{2\pi}{\omega}\right)^2}{m\lambda}, \quad a = \frac{A\left(\frac{2\pi}{\omega}\right)^2}{m\lambda}, \quad b = \frac{B\left(\frac{2\pi}{\omega}\right)^2}{m\lambda}$$

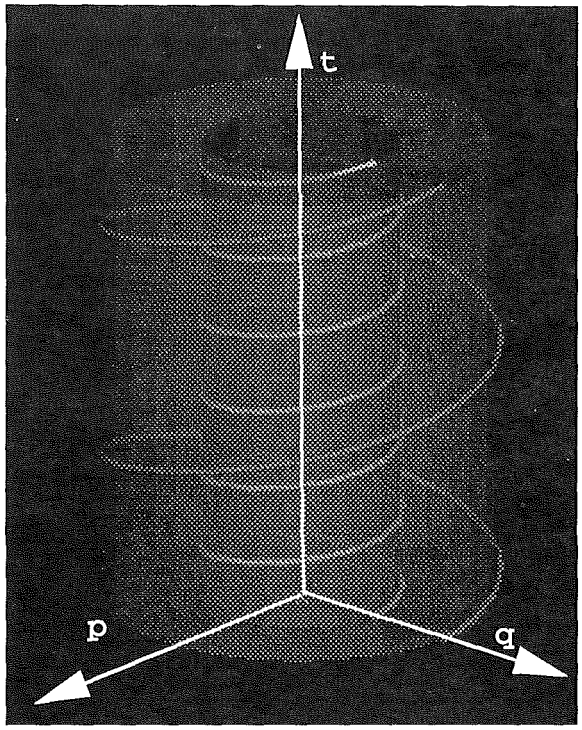


Fig. 2 Phase picture of two trajectories for $\alpha = 1$, $a = b = \mu = 0$

and

$$\lambda = \sqrt{\frac{G}{m}} \frac{2\pi}{\omega}, \quad \theta = \frac{\omega}{2\pi} t, \quad \mu = \frac{2\pi k}{m\omega}.$$

Let us start from the case of zero external force. We then have an autonomous nonharmonic oscillator with the Hamiltonian

$$H = \frac{p^2}{2} + \alpha \frac{q^2}{2} + \beta \frac{q^4}{4}, \quad p = \frac{dg}{d\theta}. \tag{9}$$

Trajectories of this oscillator are closed curves $H(p,q) = E = \text{const}$. They are shown in Fig. 1 for the $\alpha = \beta = 1$.

Since we are going to investigate the nonautonomous case, it is convenient to view the trajectories in three-dimensional phase space $\{p, q, t\}$.

All trajectories lie on cylinders (Fig. 2) the bases of which are the closed curves of Fig. 1. Figure 2 shows the trajectories starting from various initial points.

Now let us add a periodical force. The oscillator is still Hamiltonian with Hamilton function of the form

$$H = \frac{p^2}{2} + \alpha \frac{q^2}{2} + \beta \frac{q^4}{4} - aq - bq \sin 2\pi\theta. \tag{10}$$

If amplitudes a and b are small then most of the cyclinders are simply disturbed periodically, while others are destroyed and replaced by chaotic trajectories (Arnold, 1986, 1989).

A good method of visualizing the trajectories is to utilize Poincare maps, which show successive positions of points for time $t = 0, \tau, 2\tau, \ldots$, where $\tau = 2\pi/\omega$ is the period of the exciting force. A typical Poincare map for small excitation ($a = 0$, $b = 1$) is shown in Fig. 3. It can be seen that most of the trajectories are on invariant tori. General theory predicts the existence of destroyed tori for arbitrary small values of b, but for b which are very small it is not easy to find destroyed tori by computer simulations: they occupy a small part of the phase space and, in addition, can be hidden by computational errors.

If b is large enough, chaotic sea emerging from the destroyed

Downloaded 03 May 2010 to 171.66.16.20. Redistribution subject to ASME license or copyright; see http://www.asme.org/terms/Terms_Use.cfm

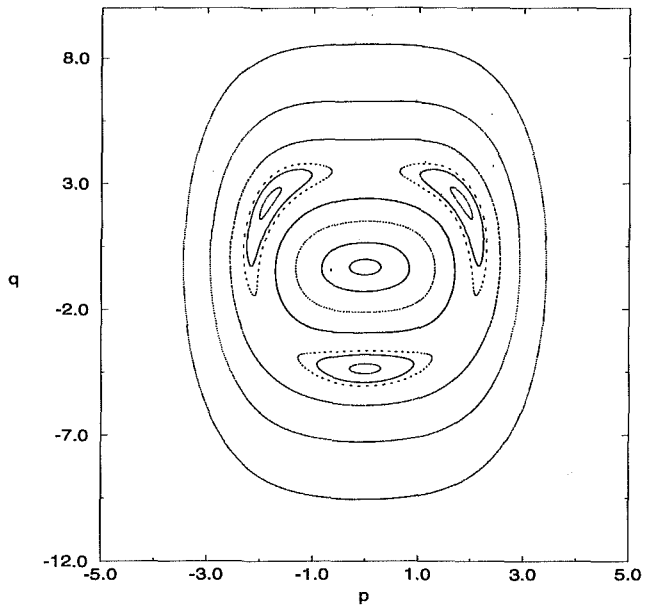


Fig. 3 Poincare map for $\alpha = 1$, $a = 0$, $b = 2$, and $\mu = 0$

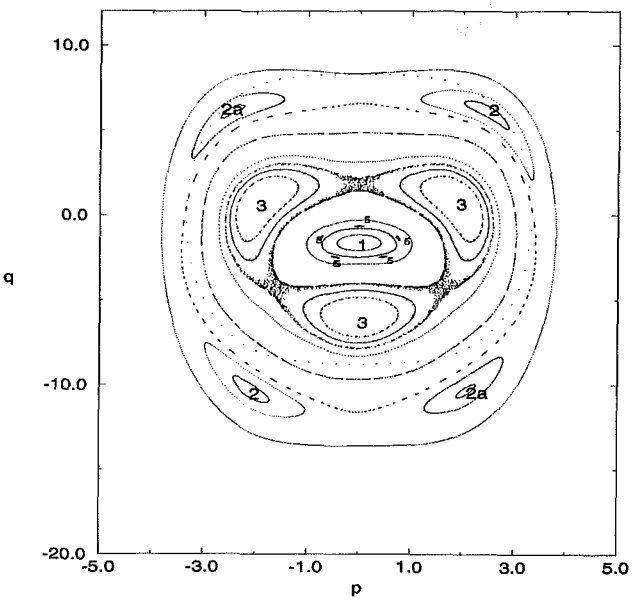


Fig. 4 Poincare map for $\alpha = 1$, $a = \mu = 0$, and $b = 10$

tori, can easily be seen (Fig. 4). An interesting peculiarity of this picture is the appearance of subharmonic resonances: periodic tubes in three-dimensional phase space with periods 2τ, 3τ, 5τ. Closed curves in Figs. 3 and 4 are cross-sections of these tubes. The central line of each family of tubes is the periodic trajectory. The families of tubes are numbered in Fig. 4 by their periods. A family of tubes with period 1 can be observed. These tubes are embedded with other tubes of period 5. The period-1 family is surrounded by the family with period 3. On the periphery of this figure we see two families of period 2. The (p, q, t) phase space picture of two tubes from the families with periods 1 and 3 is shown in Fig. 5. The darker tube corresponds to vibrations with the period 1 while the lighter tube represents the vibrations with period 3.

Increasing the amplitude of the excitation leads to more and more complex pictures of motion. Poincare maps are shown in Figs. 6–8 for $a = 0$, $b = 12$, 16, 20. For example, in Fig. 8, periodic tubes with various periods are marked by their periods

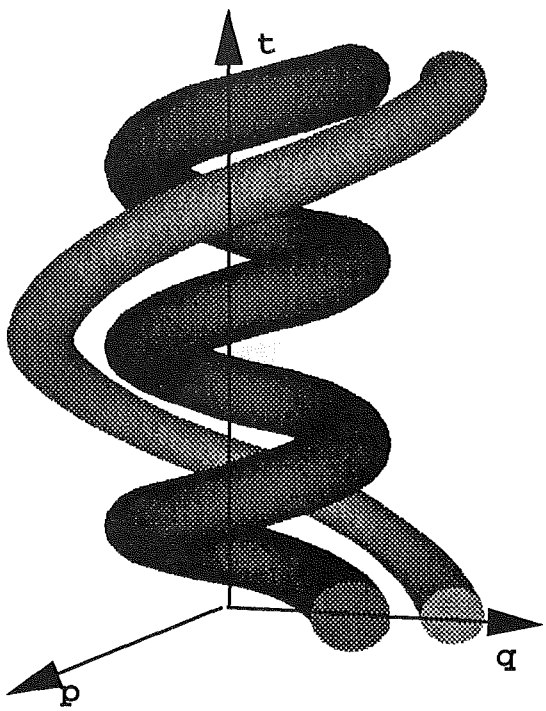


Fig. 5 Three-dimensional picture for two tubes with periods 1 and 3

varying from 1 to 35, and tubes of the same period that are close are marked by letters.

Influence of Dissipation

At first glance the vibrations of Duffing's oscillator look so complicated that no simple characteristic relations can be suggested. The only tool seems to be direct numerical simulation of the equation. It turns out, however, that dissipation significantly simplifies the complex pictures we have considered in the previous section.

Dissipation causes all the complex "microstructure" of the phase space to disappear, and all trajectories fall on a number of attractors. For very small a and b, dissipation causes all trajectories to leave the tubes and approach the central trajectory, which becomes a limit cycle. This limit cycle corresponds to linear vibrations.

If one adds small dissipation to Duffing's equation for the case shown in Fig. 5, then each tube collapses to the corresponding central trajectory, and one gets a number of limit cycles. This number, N, depends on the value of the dissipation, μ, and the parameters a, b, α, and β. If dissipation μ is small enough, limit cycles survive. For a sufficiently large value of μ there is only one limit cycle. In general, tubes with smaller periods do survive for larger values of dissipation, and the ones with large periods disappear with even small dissipation. The number, N of limit cycles which exist for given values of the parameters μ, a, b, α, and β, is an important characteristic of the oscillator. It has not been studied in a systematic way yet.

For large amplitudes a, b, a strange attractor might appear. It is natural to assume that a strange attractor emerges at the place occupied previously by a chaotic sea of Hamiltonian system. This assumption is supported by the Poincare maps in Figs. 9 and 10. Figure 9 shows the Poincare map of the Hamiltonian system for $a = 0$, $b = 2975$, $(\mu = 0)$, Figs. 10, 11 and 12 are the Poincare maps for $\mu = .01$, $\mu = .05$ and $\mu = 1.0$, respectively.

We are going to consider the thermodynamical relations for the central attractor of Fig. 4. The situation for the strange attractor will be discussed in the following section.

Downloaded 03 May 2010 to 171.66.16.20. Redistribution subject to ASME license or copyright; see http://www.asme.org/terms/Terms_Use.cfm

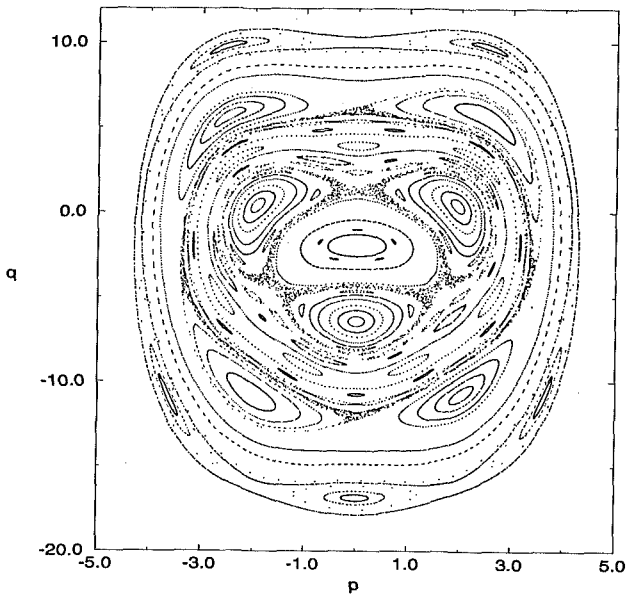


Fig. 6 Poincare map for $\alpha = 1$, $a = \mu = 0$, and $b = 12$

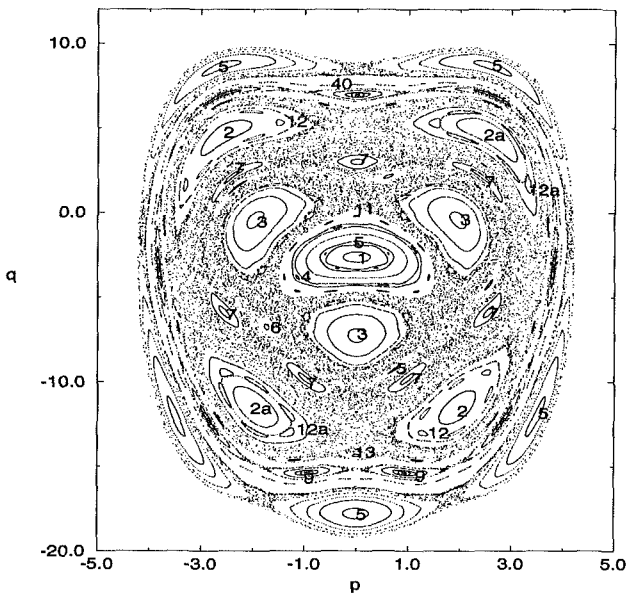


Fig. 8 Poincare map for $\alpha = 1$, $a = \mu = 0$, and $b = 16$

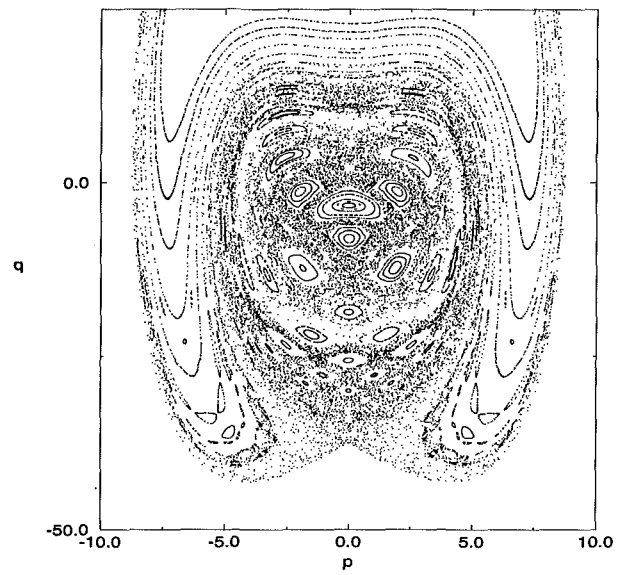


Fig. 7 Poincare map for $\alpha = 1$, $a = \mu = 0$, and $b = 20$

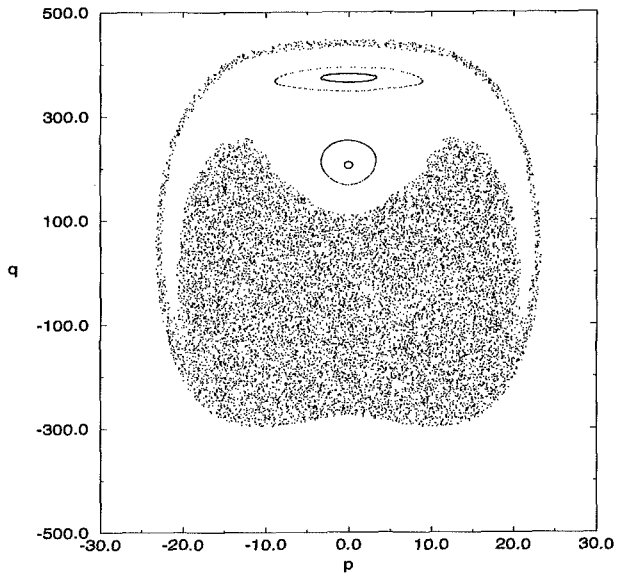


Fig. 9 Poincare map for $\alpha = 1$, $a = \mu = 0$, and $b = 2975$

Numerical Simulations

The central attractor of Fig. 4 is a limit cycle with period 1. For this limit cycle the averaged characteristics of the response $\bar{q}$ and $\hat{q}$ are

$$\bar{q} = \int_0^1 q(t)dt \quad \hat{q} = \int_0^1 q(t)\sin 2\pi t dt. \tag{11}$$

These quantities are functions of a and b, and we will try to determine if they possess the dynamical potential

$$\bar{q} = \frac{\partial P}{\partial a}, \quad \hat{q} = \frac{\partial P}{\partial b}. \tag{12}$$

We verify this by numerically integrating Eq. (8). As it should be, errors grow with increasing friction coefficient. For small dissipation ($\mu \leq 0.1$) the reciprocal relations are practically exact, with errors in the 10^{-6} range. The error grows and reaches about eight percent when $\mu = 5$.

Dynamical potential is obtained by fitting a surface to the numerically generated function $L(a,b)$. The resulting expression is

$$\bar{L}(a,b) = \alpha_0 + \alpha_1 a + \alpha_2 a^2 + \alpha_3 b^2 + \alpha_4 a^2 b \tag{13}$$

where

$$\alpha_0 = -0.1584, \quad \alpha_1 = 0.3835, \quad \alpha_2 = 0.1787,$$
$$\alpha_3 = -0.0065, \quad \alpha_4 = -0.0003.$$

Constitutive equations take the form

$$\bar{q} = \frac{\partial \bar{L}}{\partial a} = \alpha_1 + 2\alpha_2 a + 2\alpha_4 ab$$

$$\hat{q} = \frac{\partial \bar{L}}{\partial b} = \alpha_3 + \alpha_4 a^2. \tag{14}$$

The accuracy of the constitutive relations shows the same trend as the reciprocal relations. For $\mu < 0.1$, the error is less than 0.1 percent. For $\mu = 10$, error reaches eight percent.

Downloaded 03 May 2010 to 171.66.16.20. Redistribution subject to ASME license or copyright; see http://www.asme.org/terms/Terms_Use.cfm

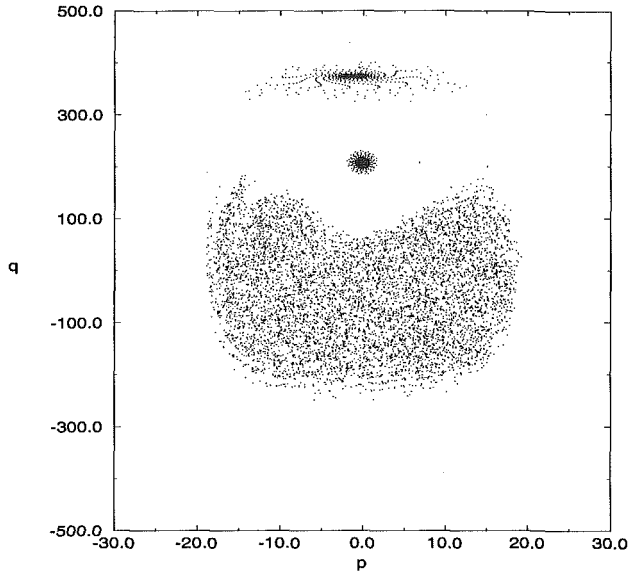


Fig. 10 Poincare map for $\alpha = 1$, $a = 0$, $\mu = 0.01$, and $b = 2975$

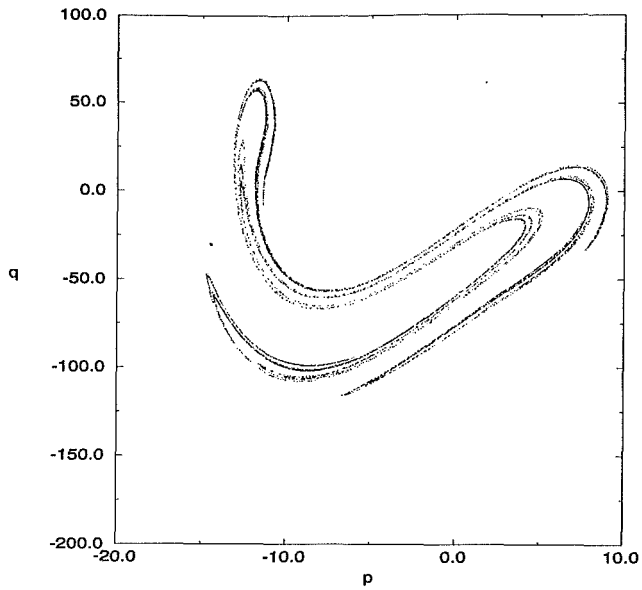


Fig. 12 Poincare map for $\alpha = 1$, $a = 0$, $\mu = 1.0$, and $b = 2975$

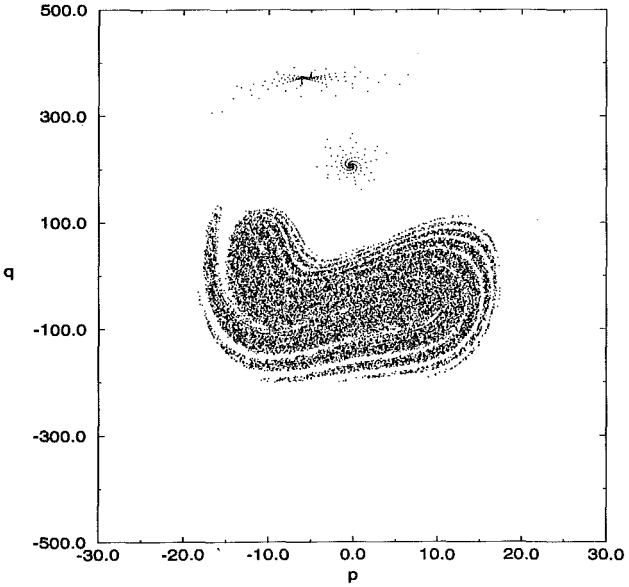


Fig. 11 Poincare map for $\alpha = 1$, $a = 0$, $\mu = 0.05$, and $b = 2975$

Transitional Chaos

We tried to validate the reciprocal relations for a strange attractor. However, we encountered some difficulties. The first one is that we were not able to find strange attractors with very small dissipation. In numerical simulations, we set $\alpha = \beta = 1$ and vary a from 1 to 10 and b around 3000. In this case, if one puts dissipation equal to zero, one gets two central trajectories with period 1 and a chaotic sea, as shown in Fig. 9. It seemed that the addition of small dissipation ($\mu = 0.01$) would transform the chaotic sea into a strange attractor. Figure 10 shows the Poincare map made of $0 \le t \le 100000$. It looks like a strange attractor. However, when we took longer periods of time ($t > 100000$), we observed that trajectories leave this "attractor" and fall onto one of the two limit cycles. It stays unclear whether this is a result of numerical errors, and the closeness of the basins of the limit cycle and the "attractor." However, this behavior persists under different time steps and integration orders, as well as various initial conditions.

It is also conceivable that the chaotic region in Fig. 10 is not an attractor. The phenomenon of "transitional chaos" is observed for other systems (Lichtenberg et al., 1983, E. H. Dowell, 1988); however, there is no clear evidence that this is really transitional chaos and not just a result of intertangled basins and numerical errors.

When the dissipation is increased to $\mu = 0.1$ we do get a stable strange attractor. Increasing damping coefficient we arrive at the usually observed worm-like form of the attractor. This is shown in Fig. 12 for $\mu = 1$. For these large values of friction the attractors differ significantly from underlying Hamiltonian chaotic sea, pure potentiality does not take place, as we checked, and the constitutive relations should be complicated by additional terms related to dissipation.

For small damping we have also encountered another problem related to the calculation of $\bar{q}$, and $\hat{q}$. It turns out that the quantity

$$\frac{1}{T}\int_0^T q(t)dt$$

does not converge when T grows, and continued vibrating even for very large T ($T > 1000000$) consequently preventing the accurate calculation of derivatives. A possible explanation is that the strange attractor is not metrically transitive and consists of a number of components. The solution to this problem is also far from clear.

Conclusions

We have discussed the geometry of the phase space of Duffing's oscillator and showed that the reciprocal relations are valid for a limit cycle of Duffing's oscillator. We have also found its dynamical potential.

Acknowledgments

The authors thank V. Afraimovich and L. Bunimovich for useful discussions, and D. Hodges for many helpful suggestions. The authors would like to acknowledge the use of Dynamics program (Yorke, 1991).

This research was partially supported by Air Force Office of Scientific Research under contract F49620-91-C-0074. Akif Özbek was supported by the National Science Foundation under grant MSS-8822003.

Downloaded 03 May 2010 to 171.66.16.20. Redistribution subject to ASME license or copyright; see http://www.asme.org/terms/Terms_Use.cfm

References

Afraimovich, V., Rabinovich, M., and Ugodchikov, A., 1984, "Appearance of a Strange Attractor in the Systems Close to Hamiltonian Ones," *Radiophysics*, Vol. 27, pp. 1346–1349.

Arnol'd, V. I., 1986, *Dynamical Systems*, Vol. 3, Springer-Verlag, New York.

Arnol'd, V. I., 1989, *Mathematical Methods of Classical Mechanics*, (Translation of *Mathematicheskie Metody Klassicheskoi Mekhaniki*), Springer-Verlag, New York.

Berdichevsky, V., 1983, *Variational Principles of Continuum Mechanics*, Nauka, Moscow.

Berdichevsky, V., 1988, "A Connection Between Thermodynamical Entropy and Probability," *Journal of Applied Mathematics and Mechanics (PMM)*, Vol. 52, No. 36, pp. 738–746.

Berdichevsky, V., 1993, "Reciprocal Relations in Nonlinear Vibrations," *International Journal of Engineering Science*, Vol. 31, No. 8, pp. 1215–1218.

Berdichevsky, V., and von Alberti, M., 1991, "Statistical Mechanics of Henon-Heiles Oscillators," *Physical Review A*, Vol. 44, No. 2, pp. 858–865.

Dowell, E. H., 1988, "Chaotic Oscillations in Mechanical Systems," *Computational Mechanics*, Vol. 3, pp. 199–218.

Dowell, E. H., and Pezeshki, C., 1986 "On the Understanding of Chaos in the Duffing's Equation Including a Comparison With Experiment," ASME JOURNAL OF APPLIED MECHANICS, Vol. 52, pp. 949–957.

Duffing, G., 1918, *Erzwungene Schwingungen bei Veranderlicher Eigenfrequenz*, Braunschweig: F. Vieweg u. Shon.

Fang, T., and Dowell, E. H., 1987 "Numerical Simulations of Jump Phenomena in Stable Duffing Systems," *International Journal of Non-Linear Mechanics*, Vol. 22, No. 3, pp. 267–274.

Holmes, P. J., and Moon, F. C., 1983, "Strange attractors and Chaos in Non-Linear Mechanics," ASME JOURNAL OF APPLIED MECHANICS, Vol. 50, pp. 1021–1032.

Lichtenberg, A. J., and Lieberman, M. A., 1983, *Regular and Stochastic Motion*, Springer-Verlag, New York.

Moon, F. C., 1979, "Experiments on Chaotic Motions of a Forced Nonlinear Oscillator: Strange Attractor," Theoretical and Applied Mechanics Preprint, Cornell University, Ithaca, New York.

Ueda, Y., 1980, "Steady Motions Exhibited by Duffing's Equation: A Picture-book of Regular and Chaotic Motions," *New Approaches to Nonlinear Problems in Dynamics*, P. J. Holmes, ed., pp. 311–322.

Ueda, Y., 1985, "Random Phenomena Resulting From Nonlinearity in the System Described by Duffing's Equation," *International Journal of Non-Linear Mechanics*, Vol. 20, No. 5–6, pp. 481–491.

Yorke, J. A., "Dynamics," a Software Package for Nonlinear Dynamics.

Downloaded 03 May 2010 to 171.66.16.20. Redistribution subject to ASME license or copyright; see http://www.asme.org/terms/Terms_Use.cfm

Reconsideration of the Stress-Focusing Effect in a Uniformly Heated Solid Cylinder

T. Hata

Department of Technology,
Faculty of Education,
Shizuoka University,
Shizuoka City 422, Japan

The stress-focusing effect is the phenomenon that, under an instantaneous heating, stress waves reflected from the free surface of the cylinder result in very high stresses at the center. Ho solved the problem by using Laplace transform on time and presented the solution as infinite series summations, which converge very slowly for certain combinations of time and the radius of a cylinder. However, adopting a concept of the ray theory, the solution of stress waves in the cylinder is sorted out into rays according to the ray path of multiply reflected waves. The results expressed in an infinite series reveal that stresses peak out periodically at a constant period and the order of singularity of the stresses in a cylinder is $O(\rho^{-2})$.

Introduction

The analysis of a long cylindrical rod subjected to a sudden rise in temperature uniformly over its cross-section has been studied by Ho (1976). This type of temperature distribution may be caused by the absorption of electromagnetic radiant energy or gammy ray of nuclear energy. One important conclusion by Ho (1976) is that, due to the instantaneous heating, stress waves reflected from the cylindrical surface of the rod may accumulate at the center and give rise to very high stresses, even though the initial thermal stress is relatively small.

In the analysis, the results are obtained by use of the Laplace transform on time. The solutions in the transformed plane are given by using the modified Bessel functions. The inversion of the transformed solutions is obtained by use of the Bromwich contour integration. But, in the numerical computations, the final series converge so slowly that a Kummer transformation must be used to obtain reasonable accuracy. Ho made some numerical errors in his figures. In Fig. 2 in his paper the radial stress exhibits singular behavior at the wave front. But we can prove that the radial stress has no singularities at the wave front except at the center. He merely showed the effect numerically in figures. The problem of the analysis by Ho is the omission of mathematical proof of the stress-focusing effect.

However, recently Hata (1991) solved precisely the problem of stress-focusing effects in a uniformly heated solid sphere. In the analysis, by using the ray theory, the Laplace transformed solution of stress waves in the sphere is sorted out into rays according to the ray path of multiply reflected waves. Therefore, Hata shows that the ray theory is the most appropriate method to solve the stress-focusing effect in a solid.

In this paper, we reconsider Ho's solution in the problem of stress-focusing effect in a cylinder and clarify the physical meaning of the stress-focusing effect in a cylinder. In the analysis, beginning with Ho's solution and adopting a concept of the ray theory for the solution, the series of Bessel functions in the solution decompose to the ray series of Hankel functions. Each term of the ray series expresses the wave propagation between the surface and the center of a cylinder. Therefore, the convergence of the ray series is so fast that we can get the reasonable solution without using a Kummer transformation.

As for the singularities at the center of the cylinder, Ho only showed that there are some infinite peak stresses indicated in figures, but Mann-Nachbar and Nachbar (1970) pointed out that the peak tensile stress at the center becomes infinite for a cylinder in the limit as heating time goes to zero at the arrival time of the first ray. The result of Mann-Nachbar and Nachbar is shown only for the first ray arrival to the center.

Here, adopting a concept of the ray theory to the problem of stress-focusing effect in a uniformly heated solid cylinder, each path of stress waves can be represented in terms of ray series. Using these formulas, we can show mathematically the behavior of stresses at the center of the cylinder, discuss precisely the nature of the singularity at the center, and obtain the order of the singularity of the stresses in a cylinder.

Formulation of Problem

An isotropic, homogeneous, elastic solid cylinder of radius b has uniform temperature $T = 0$, prior to time $t = 0$. The temperature is assumed to be brought to a sudden uniform temperature T_0 rise over its cross-section at $t = 0$, because the singularities exist only for the instantaneous heating case as mentioned by Ho. The temperature distribution is given by the following form with the Heaviside step-function:

Contributed by the Applied Mechanics Division of THE AMERICAN SOCIETY OF MECHANICAL ENGINEERS for publication in the ASME JOURNAL OF APPLIED MECHANICS.

Discussion on this paper should be addressed to the Technical Editor, Professor Lewis T. Wheeler, Department of Mechanical Engineering, University of Houston, Houston, TX 77204-4792, and will be accepted until four months after final publication of the paper itself in the ASME JOURNAL OF APPLIED MECHANICS.

Manuscript received by the ASME Applied Mechanics Division, Oct. 30, 1992; final revision, June 22, 1993. Associate Technical Editor: S. K. Datta.

Copyright © 1994 by ASME
Downloaded 03 May 2010 to 171.66.16.20. Redistribution subject to ASME license or copyright; see http://www.asme.org/terms/Terms_Use.cfm

$$T = T_0 H(t) \tag{1}$$

where $H(t)$ is the Heaviside step function. The cylinder is at rest prior to time $t = 0$ and the initial conditions are

$$u(r, t) = \partial u(r, t)/\partial t = 0 \quad \text{at } t = 0. \tag{2}$$

The radial displacement u is then the only nonzero displacement in the cylindrical coordinates (r, θ, z). The equation of motion for thermoelasticity is

$$\frac{\partial^2 u}{\partial r^2} + \frac{1}{r}\frac{\partial u}{\partial r} - \frac{u}{r^2} = \frac{1}{C_L^2}\frac{\partial^2 u}{\partial t^2} + \alpha\frac{(1+\nu)}{(1-\nu)}\frac{\partial T}{\partial r} \tag{3}$$

where α is the coefficient of thermal expansion and ν is Poisson's ratio and C_L is the dilatational wave speed, which is denoted as follows:

$$C_L = \sqrt{\frac{(\lambda + 2\mu)}{\rho_0}} \tag{4}$$

where λ and μ are Lame's constants and ρ_0 is the mass density of the material. In cylindrical coordinates (r, ϑ, z), the stress-strain relations in plane strain are expressed as

$$\left.\begin{aligned} \sigma_r &= 2\mu\frac{\partial u}{\partial r} + \lambda\left(\frac{\partial u}{\partial r} + \frac{u}{r}\right) - (3\lambda + 2\mu)\alpha T \\ \sigma_\vartheta &= 2\mu\frac{u}{r} + \lambda\left(\frac{\partial u}{\partial r} + \frac{u}{r}\right) - (3\lambda + 2\mu)\alpha T \\ \sigma_z &= \lambda\left(\frac{\partial u}{\partial r} + \frac{u}{r}\right) - (3\lambda + 2\mu)\alpha T \end{aligned}\right\}. \tag{5}$$

The boundary condition is that the radial displacement at $r = 0$ vanishes and the radial stress σ_r satisfies the condition

$$\sigma_r(r, t) = 0 \quad \text{at } r = b. \tag{6}$$

As the temperature distribution of Eq. (1) is independent of r, the thermal stresses are given by Eq. (5) as follows:

$$\left.\begin{aligned} \sigma_r^T &= -T_0\alpha\rho_0 C_L^2\{(1+\nu)/(1-\nu)\}H(t) \\ \sigma_\vartheta^T &= -T_0\alpha\rho_0 C_L^2\{(1+\nu)/(1-\nu)\}H(t) \end{aligned}\right\}. \tag{7}$$

These stresses give nonzero boundary tractions on the surface of the cylinder. The effects of removing these stresses are found by solving an ordinary dynamic stress problem.

Therefore, the total stresses σ_r and σ_ϑ consist of a sum of two components as

$$\sigma_j = \sigma_j^T + \sigma_j^S \quad (j = r, \vartheta). \tag{8}$$

Upon introduction of the following dimensionless variables

$$\left.\begin{aligned} &\zeta^l = u^l/\{\alpha T_0 b(1+\nu)/(1-2\nu)\}, \\ &\tau = tC_L/b, \quad \rho = r/b, \quad \sigma_\rho^l = \sigma_r^l/(3K\alpha T_0) \\ &\sigma_\theta^l = \sigma_\vartheta^l/(3K\alpha T_0), \quad K = E/3(1-2\nu) \quad (l = T, S) \end{aligned}\right\} \tag{9}$$

and a displacement potential $\psi(r, t)$ which satisfies the relation

$$\zeta^S = \partial\psi/\partial\rho, \tag{10}$$

the equation of motion may be expressed as (Achenbach, 1973)

$$\frac{\partial^2\psi}{\partial\rho^2} + \frac{1}{\rho}\frac{\partial\psi}{\partial\rho} = \frac{\partial^2\psi}{\partial\tau^2}. \tag{11}$$

The stress components are related to a displacement potential by

$$\left.\begin{aligned} \sigma_\rho^S &= \frac{(1-\nu)}{(1-2\nu)}\frac{\partial\zeta^S}{\partial\rho} + \frac{\nu}{(1-2\nu)}\frac{\zeta^S}{\rho} \\ \sigma_\theta^S &= \frac{\nu}{(1-2\nu)}\frac{\partial\zeta^S}{\partial\rho} + \frac{(1-\nu)}{(1-2\nu)}\frac{\zeta^S}{\rho} \end{aligned}\right\} \tag{12}$$

The boundary condition of Eq. (6) is

$$\sigma_\rho^S(\rho, \tau) = -\sigma_\rho^T \quad \text{at } \rho = 1. \tag{13}$$

We shall make use of the Laplace transform on τ, defined as

$$\left.\begin{aligned} \bar{\zeta}(\rho, p) &= \int_0^\infty \zeta(\rho, \tau)e^{-p\tau}d\tau \\ \zeta(\rho, \tau) &= \frac{1}{2\pi i}\int_{\epsilon - i\infty}^{\epsilon + i\infty} \bar{\zeta}(\rho, p)e^{p\tau}dp \end{aligned}\right\}. \tag{14}$$

Ho's Solution

Applying the Laplace transform to Eqs. (10) to (12), and invoking the relation that the temperature distribution is independent of ρ, the general solution of the transformed radial displacement is expressed in terms of modified Bessel functions I_1 and K_1. The constant can be determined by the requirement of bounded displacement at $\rho = 0$ and zero radial stress at the surface of a cylinder. Finally, Ho (1976) obtained the displacement in the transformed plane as follows:

$$\bar{\zeta}^S(\rho, p) = -\bar{\sigma}_\rho^T\frac{(1-2\nu)I_1(p\rho)}{pI_2(p)/(1+\kappa_0) + I_1(p)} \tag{15}$$

where $I_2(p)$ is the modified Bessel function of order two and

$$\kappa_0 = \nu/(1-\nu). \tag{16}$$

The corresponding transformed stresses are given from Eq. (12) by

$$\bar{\sigma}_\rho^S(\rho, p) = -\bar{\sigma}_\rho^T\frac{pI_2(p\rho)/(1+\kappa_0) + I_1(p\rho)/\rho}{pI_2(p)/(1+\kappa_0) + I_1(p)}. \tag{17}$$

The complete inversion of Eq. (15) is given by

$$\begin{aligned} \zeta^S = &-(1-2\nu)\sigma_\rho^T\rho H[\tau - 1 + \rho] \\ &+ 2\sigma_\rho^T\sum_{n=1}^{\infty}\frac{J_1(\beta_n\rho)e^{-i\beta_n\tau}}{\beta_n(1-2\kappa+\kappa^2\beta_n^2)J_0(\beta_n)}H[\tau - 1 + \rho] \end{aligned} \tag{18}$$

where β_n is a nontrivial root of equation

$$\kappa\beta_n J_0(\beta_n) - J_1(\beta_n) = 0 \tag{19}$$

and

$$\kappa = (1-\nu)/(1-2\nu). \tag{20}$$

The roots of Eq. (19) are given in Nelson (1968). The corresponding stresses are

$$\begin{aligned} \sigma_\rho^S(\rho, \tau) = &-\sigma_\rho^T H[\tau - 1 + \rho] \\ &+ 2\sigma_\rho^T\sum_{n=1}^{\infty}\frac{\{\kappa\beta_n J_0(\beta_n\rho) - J_1(\beta_n\rho)/\rho\}e^{-i\beta_n\tau}}{\beta_n(1-2\kappa+\kappa^2\beta_n^2)J_0(\beta_n)}H[\tau - 1 + \rho]. \end{aligned} \tag{21}$$

The infinite series in Eq. (18) converge very slowly for certain combinations of τ and ρ. Nelson (1968, 1969) used the Kummer transformation technique for summation of each of these series. Ho also used the same method for the instantaneous heating case. However, it is very difficult to discuss the stress-focussing effect by using the numerical method.

Author's Method

Beginning with Ho's solution and adopting a concept of ray theory, we obtain the ray series of Hankel functions. Since each term of the ray series corresponds well with the wave propagation, numerical results express clearly the stress-focusing effect in a cylinder, where it appears that some further insight is needed.

The Bessel function $J_n(z)$ can be expressed in terms of Hankel functions of the first and second kinds as

$$J_n(z) = \{H_n^{(1)}(z) + H_n^{(2)}(z)\}/2 \tag{22}$$

where $J_n(z)$ is the Bessel function of the first kind of order n and $H_n^{(1)}(z)$ and $H_n^{(2)}(z)$ are the Hankel functions of the first

Downloaded 03 May 2010 to 171.66.16.20. Redistribution subject to ASME license or copyright; see http://www.asme.org/terms/Terms_Use.cfm

and second kind of order n, respectively. Substitution of Eq. (22) into Ho's solution of Eq. (18) yields

$$\zeta^S = -(1-2\nu)\sigma_\rho^T \rho H[\tau-1+\rho] + 2\sigma_\rho^T \sum_{n=1}^{\infty} \frac{[H_1^{(1)}(\beta_n\rho)+H_1^{(2)}(\beta_n\rho)]e^{-i\beta_n\tau}H[\tau-1+\rho]}{\beta_n(1-2\kappa+\kappa^2\beta_n^2)[H_0^{(1)}(\beta_n)+H_0^{(2)}(\beta_n)]}. \quad (23)$$

Here, we introduce the reflection coefficient $R(\beta_n)$, which is defined as

$$R(\beta_n) = -\frac{H_0^{(1)}(\beta_n)}{H_0^{(2)}(\beta_n)}. \quad (24)$$

It should be noted that, since β_n given by Eq. (19) are real, the absolute value of Eq. (24) is

$$|R(\beta_n)| = \left|\frac{J_0(\beta_n+iY_0(\beta_n)}{J_0(\beta_n)-iY_0(\beta_n)}\right| = 1 \quad (25)$$

where $Y_0(\beta_n)$ is the Bessel function of the second kind of order zero.

The physical meaning of Eq. (25) is that the system of elastic motion in the paper is nondispersive.

Substituting the coefficient R into Eq. (23), we have

$$\zeta^S = -(1-2\nu)\sigma_\rho^T \rho H[\tau-1+\rho] + 2\sigma_\rho^T \sum_{n=1}^{\infty} \frac{[H_1^{(1)}(\beta_n\rho)+H_1^{(2)}(\beta_n\rho)]e^{-i\beta_n\tau}}{\beta_n(1-2\kappa+\kappa^2\beta_n^2)H_0^{(2)}(\beta_n)} \times (1+R+R^2+R^3+\ldots)H[\tau-1+\rho]. \quad (26)$$

Therefore, the displacement ζ^S may be given by

$$\zeta^S = -(1-2\nu)\sigma_\rho^T \rho H[\tau-1+\rho] + 2\sigma_\rho^T \sum_{j=0}^{\infty}\sum_{n=1}^{\infty} \{\psi_n^{(2j)}(\rho,\tau)+\psi_n^{(2j+1)}(\rho,\tau)\}H[\tau-1+\rho] \quad (27)$$

where

$$\left.\begin{aligned}
\varphi_{\rho n}^{(0)}(\rho,\tau) &= \frac{\{\kappa\beta_n H_0^{(2)}(\beta_n\rho) - H_1^{(2)}(\beta_n\rho)/\rho\}e^{-i\beta_n\tau}}{\beta_n(1-2\kappa+\kappa^2\beta_n^2)H_0^{(2)}(\beta_n)} \\
\varphi_{\rho n}^{(1)}(\rho,\tau) &= \frac{\{\kappa\beta_n H_0^{(1)}(\beta_n\rho) - H_1^{(1)}(\beta_n\rho)/\rho\}e^{-i\beta_n\tau}}{\beta_n(1-2\kappa+\kappa^2\beta_n^2)H_0^{(2)}(\beta_n)} \\
\varphi_{\rho n}^{(2j)}(\rho,\tau) &= R\varphi_{\rho n}^{(2j-2)}(\rho,\tau) \\
\varphi_{\rho n}^{(2j+1)}(\rho,\tau) &= R\varphi_{\rho n}^{(2j-1)}(\rho,\tau) \qquad (j=1,2,3,\ldots)
\end{aligned}\right\} \quad (30)$$

$$\left.\begin{aligned}
\varphi_{\theta n}^{(0)}(\rho,\tau) &= \frac{\left\{\left(\frac{\nu}{1-2\nu}\right)\beta_n H_0^{(2)}(\beta_n\rho) + H_1^{(2)}(\beta_n\rho)/\rho\right\}e^{-i\beta_n\tau}}{\beta_n(1-2\kappa+\kappa^2\beta_n^2)H_0^{(2)}(\beta_n)} \\
\varphi_{\theta n}^{(1)}(\rho,\tau) &= \frac{\left\{\left(\frac{\nu}{1-2\nu}\right)\beta_n H_0^{(1)}(\beta_n\rho) + H_1^{(1)}(\beta_n\rho)/\rho\right\}e^{-i\beta_n\tau}}{\beta_n(1-2\kappa+\kappa^2\beta_n^2)H_0^{(2)}(\beta_n)} \\
\varphi_{\theta n}^{(2j)}(\rho,\tau) &= R\varphi_{\theta n}^{(2j-2)}(\rho,\tau) \\
\varphi_{\theta n}^{(2j+1)}(\rho,\tau) &= R\varphi_{\theta n}^{(2j-1)}(\rho,\tau) \qquad (j=1,2,3,\ldots).
\end{aligned}\right\} \quad (31)$$

Comparing Eq. (27) with Ho's solution of Eq. (18), it is found that Eq. (27) is useful to express the wave propagation exactly. The nature of the wave motions represented by Eq. (27) becomes evident by introducing the asymmetric representations of the Hankel functions for large values of z. In a handbook of mathematical functions (Abramowitz and Stegun, 1965) the following asymptotic representations of Hankel functions can be found:

$$\left.\begin{aligned}
H_\nu^{(1)}(z) &= \sqrt{2/(\pi z)}\{P(\nu,z)+iQ(\nu,z)\}e^{i\chi} \qquad (-\pi<\arg z<2\pi) \\
H_\nu^{(2)}(z) &= \sqrt{2/(\pi z)}\{P(\nu,z)-iQ(\nu,z)\}e^{-i\chi} \qquad (-2\pi<\arg z<\pi)
\end{aligned}\right\} \quad (32)$$

where $\chi = z - (1/2\nu + 1/4)\pi$ and, with $4\nu^2$ denoted by μ,

$$\left.\begin{aligned}
P(\nu,z) &\sim 1 - \frac{(\mu-1)(\mu-9)}{2!(8z)^2} + \frac{(\mu-1)(\mu-9)(\mu-25)(\mu-49)}{4!(8z)^4} - \ldots \\
Q(\nu,z) &\sim \frac{(\mu-1)}{8z} - \frac{(\mu-1)(\mu-9)(\mu-25)}{3!(8z)^3} + \ldots
\end{aligned}\right\}. \quad (33)$$

where

$$\left.\begin{aligned}
\psi_n^{(0)}(\rho,\tau) &= \frac{H_1^{(2)}(\beta_n\rho)e^{-i\beta_n\tau}}{\beta_n(1-2\kappa+\kappa^2\beta_n^2)H_0^{(2)}(\beta_n)} \\
\psi_n^{(1)}(\rho,\tau) &= \frac{H_1^{(1)}(\beta_n\rho)e^{-i\beta_n\tau}}{\beta_n(1-2\kappa+\kappa^2\beta_n^2)H_0^{(2)}(\beta_n)} \\
\psi_n^{(2j)}(\rho,\tau) &= R\psi_n^{(2j-2)}(\rho,\tau) \\
\psi_n^{(2j+1)}(\rho,\tau) &= R\psi_n^{(2j-1)}(\rho,\tau) \\
&\qquad (j=1,2,3,\ldots)
\end{aligned}\right\}. \quad (28)$$

It is now apparent that the function $\psi_n^{(0)}(\rho,\tau)$ in Eq. (28) represents a wave converging toward $\rho = 0$, while the function $\psi_n^{(1)}(\rho,\tau)$ in Eq. (28) represents a wave diverging from $\rho = 0$. Similarly, the function $\psi_n^{(2j)}(\rho,\tau)$ in Eq. (28) represents a wave converging toward $\rho = 0$, while the function $\psi_n^{(2j+1)}(\rho,\tau)$ in Eq. (28) represents a wave diverging from $\rho = 0$. Hence, substituting (32) into (28), we find

$$\left.\begin{aligned}
\psi_n^{(0)}(\rho,\tau) &= \frac{ie^{-i\beta_n(\tau+\rho-1)}}{\beta_n(1-2\kappa+\kappa^2\beta_n^2)\sqrt{\rho}} \frac{[P(1,\beta_n\rho)-iQ(1,\beta_n\rho)]}{[P(0,\beta_n)-iQ(0,\beta_n)]} \\
\psi_n^{(1)}(\rho,\tau) &= \frac{-e^{-i\beta_n(\tau-\rho-1)}}{\beta_n(1-2\kappa+\kappa^2\beta_n^2)\sqrt{\rho}} \frac{[P(1,\beta_n\rho)+iQ(1,\beta_n\rho)]}{[P(0,\beta_n)-iQ(0,\beta_n)]}
\end{aligned}\right\}. \quad (34)$$

The corresponding stresses may be given by

$$\left.\begin{aligned}
\sigma_\rho^S &= -\sigma_\rho^T H[\tau-1+\rho] + 2\sigma_\rho^T \sum_{j=0}^{\infty}\sum_{n=1}^{\infty} \{\varphi_{\rho n}^{(2j)}(\rho,\tau)+\varphi_{\rho n}^{(2j+1)}(\rho,\tau)\}H[\tau-1+\rho] \\
\sigma_\theta^S &= -\sigma_\rho^T H[\tau-1+\rho] + 2\sigma_\rho^T \sum_{j=0}^{\infty}\sum_{n=1}^{\infty} \{\varphi_{\theta n}^{(2j)}(\rho,\tau)+\varphi_{\theta n}^{(2j+1)}(\rho,\tau)\}H[\tau-1+\rho]
\end{aligned}\right\} \quad (29)$$

Downloaded 03 May 2010 to 171.66.16.20. Redistribution subject to ASME license or copyright; see http://www.asme.org/terms/Terms_Use.cfm

An inspection of Eq. (34) suggests that the function $\psi_n^{(0)}$ denotes the first incoming wave with the phase of $\beta_n(\tau + \rho - 1)$, while the function $\psi_n^{(1)}$ denotes the first outgoing wave with the phase of $\beta_n(\tau - \rho - 1)$. Hence, these two waves interfere with each other in the neighborhood of $\rho = 0$ at time $\tau = 1$.

Next, substituting Eqs. (32) into (24), we have

$$R(\beta_n) = i\,\frac{[P(0,\beta_n)+iQ(0,\beta_n)]}{[P(0,\beta_n)-iQ(0,\beta_n)]}\,e^{2i\beta_n}. \tag{35}$$

The functions $\psi_n^{(2j)}$ and $\psi_n^{(2j+1)}$ in Eq. (28) are expressed by using Eq. (35) as follows:

$$\left.\begin{aligned}
\psi_n^{(2j)}(\rho,\tau) &= \{R(\beta_n)\}^j\psi_n^{(0)}(\rho,\tau)\\
&= \left\{ i\,\frac{[P(0,\beta_n)+iQ(0,\beta_n)]}{[P(0,\beta_n)-iQ(0,\beta_n)]}\right\}^j \frac{ie^{-i\beta_n(\tau+\rho-1-2j)}}{\beta_n(1-2\kappa+\kappa^2\beta_n^2)\sqrt{\rho}}\\
&\quad\times\frac{[P(1,\beta_n\rho)-iQ(1,\beta_n\rho)]}{[P(0,\beta_n)-iQ(0,\beta_n)]}\\
\psi_n^{(2j+1)}(\rho,\tau) &= \{R(\beta_n)\}^j\psi_n^{(1)}(\rho,\tau)\\
&= \left\{ i\,\frac{[P(0,\beta_n)+iQ(0,\beta_n)]}{[P(0,\beta_n)-iQ(0,\beta_n)]}\right\}^j \frac{-e^{-i\beta_n(\tau-\rho-1-2j)}}{\beta_n(1-2\kappa+\kappa^2\beta_n^2)\sqrt{\rho}}\\
&\quad\times\frac{[P(1,\beta_n\rho)+iQ(1,\beta_n\rho)]}{[P(0,\beta_n)-iQ(0,\beta_n)]}
\end{aligned}\right\}. \tag{36}$$

An inspection of Eq. (36) suggests that the phase of the jth incoming wave denoted by $\psi_n^{(2j)}$ is $\beta_n(\tau + \rho - 1 - 2j)$, while the phase of the jth outgoing wave denoted by $\psi_n^{(2j+1)}$ is $\beta_n(\tau - \rho - 1 - 2j)$. Therefore, these waves also interfere with each other in the neighborhood of $\rho = 0$ at time $\tau = 1 + 2j$. It should be noted the displacement at $\rho = 0$ can not be obtained from Eq. (36), because the asymptotic functions of Eq. (32) are not true for $\rho = 0$.

Singularity of Stresses

Further investigation of singular behavior of both displacement and stresses in the neighborhood of the center of a cylinder for time $\tau = 1 + 2j$ is carried out in this section. In a handbook of mathematical functions (Abramowitz and Stegun, 1965) the Hankel functions near $z = 0$ can be found:

$$\left.\begin{aligned}
&H_0^{(2)}(z) \approx -i\left(\frac{2}{\pi}\right)\log(z) \quad H_\nu^{(2)}(z) \approx i\left(\frac{1}{\pi}\right)\Gamma(\nu)\left(\frac{2}{z}\right)^\nu\\
&H_\nu^{(2)}(z) \approx -H_\nu^{(1)}(z) \quad (\text{Real } \nu > 0)
\end{aligned}\right\}. \tag{37}$$

To determine the displacement at the center for time $\tau = 1$, we consider the displacement at a neighboring point $\rho = \epsilon$ in the time interval $1 - \epsilon \le \tau < 1 + \epsilon$, where ϵ is a quantity approaching zero. When we analyze the functions $\psi_n^{(0)}$ and $\psi_n^{(1)}$ in the neighborhood of the center of the cylinder, the Hankel function $H_0^{(2)}(\beta_n)$ is evaluated from Eq. (32), but the Hankel functions $H_1^{(1)}(\beta_n\rho)$ and $H_1^{(2)}(\beta_n\rho)$ must be evaluated from Eq. (37). Then the functions $\psi_n^{(0)}$ and $\psi_n^{(1)}$ near $\rho = \epsilon$ may be given by

$$\left.\begin{aligned}
\psi_n^{(0)}(\epsilon,\tau) &= \frac{(i+1)e^{-i\beta_n(\tau-1)}}{\sqrt{\pi\beta_n}\beta_n(1-2\kappa+\kappa^2\beta_n^2)[P(0,\beta_n)-iQ(0,\beta_n)]}\,\frac{1}{\epsilon}\\
\psi_n^{(1)}(\epsilon,\tau) &= \frac{-(1+i)e^{-i\beta_n(\tau-1)}}{\sqrt{\pi\beta_n}\beta_n(1-2\kappa+\kappa^2\beta_n^2)[P(0,\beta_n)-iQ(0,\beta_n)]}\,\frac{1}{\epsilon}
\end{aligned}\right\} \tag{38}$$

In Eq. (38) we find that the function $\psi_n^{(0)}(\rho,\tau)$ increases in the order of ϵ^{-1} as ϵ approaches zero, while the function $\psi_n^{(1)}(\rho,\tau)$ falls with the same order of opposite sign. In the limit, as $\epsilon \to 0$, the sum of these two functions behaves as a Dirac delta function. Similarly other couple of waves behaves as a Dirac delta function near the center at time $\tau = 1 + 2j$.

Next, we discuss the behavior of stresses at the center of the cylinder. The stress wave motion generated in an initially undisturbed cylinder by the application of a uniform temperature may be analyzed from Eqs. (29) to (31). Substituting Eqs. (32) into (30) and (31), we find that the phase of the jth incoming stress waves denoted by the functions $\varphi_{\rho n}^{(2j)}$ and $\varphi_{\theta n}^{(2j)}$ is $\beta_n(\tau + \rho - 1 - 2j)$, while the phase of the jth outgoing stress waves denoted by the functions $\varphi_{\rho n}^{(2j+1)}$ and $\varphi_{\theta n}^{(2j+1)}$ is $\beta_n(\tau - \rho - 1 - 2j)$. These stress waves also interfere with each other in the neighborhood of $\rho = 0$ at time $\tau = 1 + 2j$ as the functions of Eq. (36) in the displacement do.

To determine the radial stress at the center for time $\tau = 1 + 2j$, we consider the radial stress at a neighboring point $\rho = \epsilon$ in the time interval $1 + 2j - \epsilon \le \tau < 1 + 2j + \epsilon$, ($j = 0, 1, 2, 3, \ldots$). The function $\varphi_{\rho n}^{(j)}$ near $\rho = \epsilon$ may be given by

$$\left.\begin{aligned}
\varphi_{\rho n}^{(0)}(\epsilon,\tau) &= -\frac{(i+1)e^{-i\beta_n(\tau-1)}}{\sqrt{\pi\beta_n}\beta_n(1-2\kappa+\kappa^2\beta_n^2)[P(0,\beta_n)-iQ(0,\beta_n)]}\,\frac{1}{\epsilon^2}\\
\varphi_{\rho n}^{(1)}(\epsilon,\tau) &= \frac{(1+i)e^{-i\beta_n(\tau-1)}}{\sqrt{\pi\beta_n}\beta_n(1-2\kappa+\kappa^2\beta_n^2)[P(0,\beta_n)-iQ(0,\beta_n)]}\,\frac{1}{\epsilon^2}\\
\varphi_{\rho n}^{(2j)}(\epsilon,\tau) &= -\frac{(i+1)e^{-i\beta_n(\tau-1-2j)}}{\sqrt{\pi\beta_n}\beta_n(1-2\kappa+\kappa^2\beta_n^2)[P(0,\beta_n)-iQ(0,\beta_n)]}\left\{ i\,\frac{[P(0,\beta_n)+iQ(0,\beta_n)]}{[P(0,\beta_n)-iQ(0,\beta_n)]}\right\}^j\frac{1}{\epsilon^2}\\
\varphi_{\rho n}^{(2j+1)}(\epsilon,\tau) &= \frac{(1+i)e^{-i\beta_n(\tau-1-2j)}}{\sqrt{\pi\beta_n}\beta_n(1-2\kappa+\kappa^2\beta_n^2)[P(0,\beta_n)-iQ(0,\beta_n)]}\left\{ i\,\frac{[P(0,\beta_n)+iQ(0,\beta_n)]}{P(0,\beta_n)-iQ(0,\beta_n)]}\right\}^j\frac{1}{\epsilon^2}
\end{aligned}\right\}. \tag{39}$$

An inspection of Eq. (39) suggests that the jth incoming waves denoted by $\varphi_{\rho n}^{(2j)}$ rises sharply in the order of ϵ^{-2}, while the jth outgoing stress waves denoted by $\varphi_{\rho n}^{(2j+1)}$ falls sharply in the order of ϵ^{-2}. Therefore, the radial stress in the neighborhood of $\epsilon = 0$ at time $\tau = 1 + 2j$ behaves as a Dirac delta function. The singularity of the radial stress in a uniformly heated solid cylinder may be $O(\rho^{-2})$. The same discussion is true for the case of tangential stress focusing.

Numerical Results and Discussion

To show the stress-focusing effect in a uniformly heated solid cylinder, we performed numerical calculations for a cylinder with Poisson's ratio $\nu = 0.3$. The numerical integrations were carried out using Simpson's formula. The numerical results are shown in Figs. 1 to 4. These figures have been computed by taking $n = 1$ to 20 and $j = 0$ to 6.

In Fig. 1 the stress σ_ρ is initially compressive because of instantaneous heating. After this period, the wave reflects from the surface and accumulates to the center. As the waves approach to the center, the maximum values of σ_ρ increase higher as shown in Fig. 1. The peaks of stress σ_ρ near $\rho = 0$ indicated by arrows in Fig. 1, which are calculated from Eq. (39), peaks

Downloaded 03 May 2010 to 171.66.16.20. Redistribution subject to ASME license or copyright; see http://www.asme.org/terms/Terms_Use.cfm

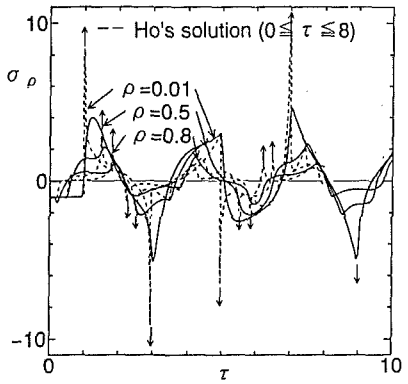


Fig. 1

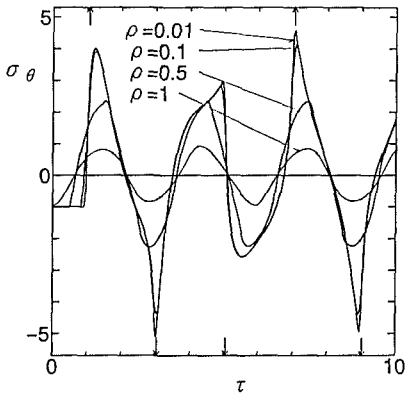


Fig. 2

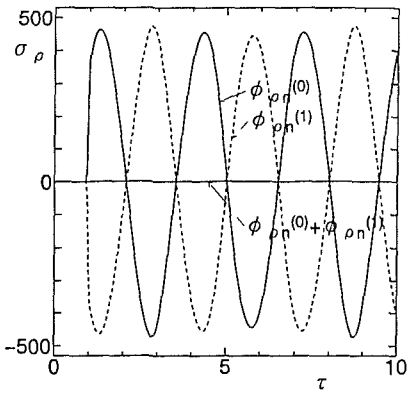


Fig. 3

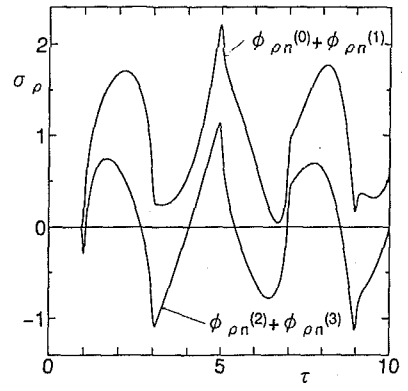


Fig. 4

out periodically. The shape of stress variation from $\tau = 0$ to 5 is almost the same as the shape of stress variation from $\tau =$ 5 to 10. In the figure, the dotted curves represent the radial stress variation given by Ho. The arrows in the figure designate the infinity. It is noticed that the solid curves have no peaks except in the neighborhood of the center, while the dotted curves have many peaks at the wave front. That is different from the results of Ho. The numerical errors at the wave front in his work may come out from a Kummer transformation.

Figure 2 shows the variation of tangential stress σ_θ at different ρ values as a function of time. The behavior of tangential stress σ_θ is similar to that of the radial stress. In the figure we also observe that the shape of stress variation of σ_θ in the time interval from $\tau = 0$ to 5 is almost the same as that in the time interval from $\tau = 5$ to 10.

Here, in order to explain the relation between the stress functions $\varphi_{\rho n}^{(j)}$, we show the variations of $\varphi_{\rho n}^{(0)}$ and $\varphi_{\rho n}^{(1)}$ and the sum of these two functions as a function of time at $\rho = 0.01$ in Fig. 3. In Fig. 3 the function $\varphi_{\rho n}^{(0)}$ varies periodically as a sine function, while the function $\varphi_{\rho n}^{(1)}$ varies similar to the function $\varphi_{\rho n}^{(0)}$ with opposite sign. Therefore the sum of two functions $\varphi_{\rho n}^{(0)} + \varphi_{\rho n}^{(1)}$ are 100 times smaller than the function $\varphi_{\rho n}^{(1)}$.

Figure 4 shows the variations of the sum of two functions $\varphi_{\rho n}^{(2j)} + \varphi_{\rho n}^{(2j+1)}$ $(j = 0, 1)$ at $\rho = 0.01$ as a function of time. The graph of $\varphi_{\rho n}^{(0)} + \varphi_{\rho n}^{(1)}$ in Fig. 4 is the enlargement of that in Fig. 3. Since the waves arrive at $\rho = 0.01$ periodically, the graphs have discontinuities at $\tau = 1, 3, 5, 7, 9$.

Conclusion

The major accomplishment of this study has been in gaining a better understanding of the stress-focusing effect in a uniformly heated solid cylinder. The stress-focusing effects occur when stress waves reflect from the surface of the cylinder and accumulate radially inward to the center.

The solution are carried out by using Laplace transform on time and presented as the infinite series summations by Ho. Since these infinite series, which are expressed in terms of modified Bessel functions, converge very slowly, Nelson and Ho used the Kummer transformation technique for summation of each of these series. However, adopting a concept of the ray theory, we found the method of ray series, which is significantly easier for evaluation of the series of Bessel functions. Following the method, we could obtain mathematically the order of singularity of the stresses in a cylinder subjected to the instantaneous heating, which is $O(\rho^{-2})$. Numerical results also shows the stress-focusing effects explicitly.

Acknowledgments

The author is especially grateful to Emeritus Professor A. Atsumi of Tohoku University for his invaluable suggestions. This work was partly supported by Grant-in-Aid of the Tokai Foundation for Technology, Japan.

References

Abramowitz, M., and Stegun, I. A., 1965, *Handbook of Mathematical Functions*, Dover Publications, New York.

Achenbach, J. D., 1973, *Wave Propagation in Elastic Solids*, North-Holland, Amsterdam, The Netherlands.

Hata, T., 1991, "Stress-Focusing Effect in a Uniformly Heated Solid Sphere," ASME Journal of Applied Mechanics, Vol. 58, pp. 58–63.

Ho, C. H., 1976, "Stress-Focusing Effect in a Uniformly Heated Cylindrical Rod," ASME Journal of Applied Mechanics, Vol. 43, pp. 404–468.

Mann-Nachbar, P., and Nachbar, W., 1970, "Thermal Shock Following Rapid Uniform Heating of Spheres and Long Cylindrical Rods," *Aerospace Corp. Report*, TR-0066 (S5816-71)-1.

Nelson, C. W., 1968, "Transient Axially Symmetric Excitation of a Circular Elastic Rod in Plane Strain," ASME Journal of Applied Mechanics, Vol. 35, pp. 306–312.

Nelson, C. W., 1969, "The Ramp Unloading Case of Transient Axially Symmetric Excitation of a Circular Elastic Rod in Plane Strain," *Journal of Franklin Institute*, Vol. 287, pp. 125–142.

Downloaded 03 May 2010 to 171.66.16.20. Redistribution subject to ASME license or copyright; see http://www.asme.org/terms/Terms_Use.cfm

F. McCaughan
Professor,
Assoc. Mem. ASME.

H. Bedir
Graduate Student.

Department of Mechanical and Aerospace Engineering,
Case Western Reserve University,
Cleveland, OH 44106

Marangoni Convection With a Deformable Surface

Double diffusive convection is considered in a semi-infinite domain, bounded below by a solid surface and above by a gas interface. Temperature and concentration gradients are imposed normal to the free surface and the linear stability of the fluid is examined. Traditional analyses are extended to include the effects of a deformable free surface. The governing equations are nondimensionalized and the parameter groupings are identified. We particularly focus on the effects of the capillary number, the Nusselt number and the Marangoni temperature and concentration numbers.

1 Introduction

Thermal-solutal convection problems are characterized by a layer of fluid with both temperature and concentration gradients imposed. Linear instability occurs when a small perturbation of a specified base flow grows with time. The temperature and concentration gradients may be stabilizing or destabilizing. Our attention is limited to flows driven by surface tension (Marangoni effect) and buoyancy effects are neglected.

The motivation for the study of this class of problems is the desire to understand the behavior of the fluids in space. One of the primary goals of the space station program is the possibility of improved material processing (e.g., crystal growth, manufacturing of alloys, fabrication of drugs, condensing of melts) in a low-gravity environment. Other applications of Marangoni convection can be found in oil extraction from porous media, energy storage in molten salts, chemical engineering of paints, colloids and detergents, and also in thin film processes in chemical microelectronic industries.

Surface tension driven convection was first discussed by Pearson (1958) with reference to drying paint films. In that study the gas-liquid interface is assumed to be flat. Scriven and Sternling (1964) extended Pearson's analysis by accounting for the possibility of shape deformations of the free surface. McTaggert (1983) examined the stability of a single layer with a planar-free surface, with double diffusion (heat and mass), and Ho and Chang (1988) extended this work by considering oscillatory solutions. Benguria and Depassier (1987, 1989) have investigated the effects of surface deformation on buoyancy driven flows, showing the presence of a bifurcation to an oscillatory solution, which is not possible when the surface is planar. Herein, we build on these problems, examining the significant effects of surface deformation on the linear stability of surface tension-driven double-diffusive convection.

Contributed by the Applied Mechanics Division of THE AMERICAN SOCIETY OF MECHANICAL ENGINEERS for publication in the ASME JOURNAL OF APPLIED MECHANICS.

Discussion on this paper should be addressed to the Technical Editor, Professor Lewis T. Wheeler, Department of Mechanical Engineering, University of Houston, Houston, TX 77204-4792, and will be accepted until four months after final publication of the paper itself in the ASME JOURNAL OF APPLIED MECHANICS.

Manuscript received by the ASME Applied Mechanics Division, July 13, 1992; final revision, Apr. 14, 1993. Associate Technical Editor: R. M. Bowen.

2 Physical Problem

A semi-infinite single layer of fluid, bounded below by a rigid boundary and above by a free surface, has temperature and concentration gradients imposed normal to the free surface (Fig. 1). Following the earlier work (Ho and Chang, 1988) we will rstrict our analysis to two-dimensional flow. The fluid is Newtonian with constant properties, except surface tension, which is assumed to be a linear function of both temperature and solutal concentration at the free surface. Assuming that the Bond number (ratio of gravitational force to surface tension force) is very small, we can neglect the body force term. The fluid evolves according to the Navier-Stokes equation, the continuity equation for incompressible flow, and the heat and mass transfer equations.

The base conduction solution is easily found to be

$$\tilde{\psi}_b = 0 \tag{1}$$

$$\tilde{T}_b(y) = (\tilde{T}_\infty - \tilde{T}_0)\frac{\mathrm{Nu}}{1+\mathrm{Nu}}\frac{\tilde{y}}{L} + \tilde{T}_0 \tag{2}$$

$$\tilde{C}_b(y) = (\tilde{C}_\infty - \tilde{C}_0)\frac{\mathrm{Sh}}{1+\mathrm{Sh}}\frac{\tilde{y}}{L} + \tilde{C}_0 \tag{3}$$

where Nusselt number Nu, and Sherwood number Sh are defined as

$$\mathrm{Nu} = \frac{h_T L}{\rho C_p \kappa} \quad \mathrm{Sh} = \frac{h_C L}{\rho D}$$

and $\tilde{\psi}$, $\tilde{T}$, $\tilde{C}$, h_T, h_C, ρ, κ, D, C_p, are, respectively, stream function, temperature, solutal concentration, heat and mass transfer coefficients, density, thermal diffusivity, mass diffusivity, and specific heat. The characteristic temperature difference, $\Delta\tilde{T}_0$, and the characteristic solutal concentration difference, $\Delta\tilde{C}_0$, are defined as

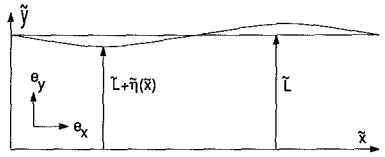


Fig. 1 Schematic of the fluid domain

Copyright © 1994 by ASME
Downloaded 03 May 2010 to 171.66.16.20. Redistribution subject to ASME license or copyright; see http://www.asme.org/terms/Terms_Use.cfm

$$\Delta\tilde{T}_0 \equiv \tilde{T}(\tilde{y}=L) - \tilde{T}(\tilde{y}=0) = \frac{\mathrm{Nu}}{1+\mathrm{Nu}}\frac{\tilde{y}}{L}(\tilde{T}_\infty - \tilde{T}_0)$$

$$\Delta\tilde{C}_0 \equiv \tilde{C}(\tilde{y}=L) - \tilde{C}(\tilde{y}=0) = \frac{\mathrm{Sh}}{1+\mathrm{Sh}}\frac{\tilde{y}}{L}(\tilde{C}_\infty - \tilde{C}_0).$$

The variables are nondimensionalized as follows:

$$\psi = \frac{\tilde{\psi}}{UL} \quad T = \frac{\tilde{T}-\tilde{T}_0}{\Delta\tilde{T}_0} \quad C = \frac{\tilde{C}-\tilde{C}_0}{\Delta\tilde{C}_0}$$

where L and U are characteristic length and velocity. Thus, the base conduction solution becomes

$$\psi_b = 0 \quad T_b(y) = y \quad C_b(y) = y.$$

Linearizing the governing equations about this solution gives

$$\frac{\partial}{\partial t}(\nabla^2\psi) = \frac{\nu}{UL}(\nabla^4\psi) \tag{4}$$

$$\frac{\partial T}{\partial t} + \frac{\partial\psi}{\partial x} = \frac{\kappa}{UL}(\nabla^2 T) \tag{5}$$

$$\frac{\partial C}{\partial t} + \frac{\partial\psi}{\partial x} = \frac{D}{UL}(\nabla^2 C) \tag{6}$$

where ν, ψ, T, C, denote kinematic viscosity, perturbed stream function, perturbed temperature, and perturbed solutal concentration, respectively. Assuming a viscous velocity scale, $U=\nu/L$ the coefficients on the right-hand sides of Eqs. (4)–(6) become: 1, $1/\mathrm{Pr}=\kappa/\nu$, $1/\mathrm{Sc}=D/\nu$, respectively. The velocity scale is chosen to maintain the symmetry of the heat and mass diffusion terms. Taking no-slip conditions, and, constant temperature and solutal concentration at the bottom boundary, the boundary conditions at the right bottom surface $y=0$ are

$$\psi = \psi_{,y} = T = C = 0. \tag{7}$$

The unit normal vector, $\mathbf{n}$, and the unit tangent vector, $\mathbf{t}$, to the surface are defined by

$$\mathbf{n} = \frac{-\eta_{,x}\mathbf{e_x} + \mathbf{e_y}}{\sqrt{1+\eta_{,x}^2}} \quad \mathbf{t} = \frac{\mathbf{e_x} + \eta_{,x}\mathbf{e_y}}{\sqrt{1+\eta_{,x}^2}}.$$

At the free surface $y=1+\eta(x,\ t)$ the conditions are (Davis, 1987)

$$-(\mathbf{n}.\nabla)(T+T_b) = \mathrm{Nu}(T+T_b-T_\infty) \tag{8}$$

$$-(\mathbf{n}.\nabla)(C+C_b) = \mathrm{Sh}(C+C_b-C_\infty) \tag{9}$$

$$(\mathbf{t}.\nabla)\sigma = \tau_{nt} \tag{10}$$

$$(p-p_{\mathrm{atm}}) - \tau_{nn} = \frac{\sigma}{R} \tag{11}$$

$$\frac{D\eta}{Dt} = \psi_{,x} \tag{12}$$

where D/Dt, τ_{nt}, τ_{nn}, σ, p, p_{atm} are material derivative, tangential and normal stresses, surface tension, pressure in the layer, and atmospheric pressure, respectively. R is the radius of curvature defined by

$$R \equiv \frac{-\eta_{,xx}}{L\sqrt[3]{1+\eta_{,x}^2}}$$

Equations (8)–(12) represent energy balance, mass diffusion balance, tangential force and normal force balances and the kinematic condition at the free surface. The analysis of Scriven and Sternling (1964) included the viscous resistance force to the dilatation of the surface in the tangential force balance equation. Since we have assumed two-dimensional flow, the surface continuity equation (Aris, 1962) gives zero surface dilatation, and so the surface viscosity term drops from the tangential force balance equation.

Assuming the surface tension is a linear function of both the temperature and solutal concentration of the free surface, we have the following equation:

$$\sigma = \sigma_0 + \sigma_T\Delta\tilde{T}_0(T+T_b) + \sigma_C\Delta\tilde{C}_0(C+C_b) \tag{13}$$

After linearization the boundary conditions become

$y=0$:

$$\psi = \psi_{,y} = T = C = 0 \tag{14}$$

$y=1+\eta(x,\ t)$:

$$T_{,y} + \mathrm{Nu}(T+\eta) = 0 \tag{15}$$

$$C_{,y} + \mathrm{Sh}(C+\eta) = 0 \tag{16}$$

$$\frac{\mathrm{Ma}_T}{\mathrm{Pr}}(T_{,x}+\eta_{,x}) + \frac{\mathrm{Ma}_C}{\mathrm{Sc}}(C_{,x}+\eta_{,x}) + \psi_{,xx} + \psi_{,yy} = 0 \tag{17}$$

$$\psi_{,xxxx} + K(\psi_{,ytt} - \psi_{,yyyt} - 3\psi_{,xxyt}) = 0 \tag{18}$$

$$K = \frac{\mu\nu}{\sigma L} \quad \mathrm{Ma}_T = \frac{\sigma_T\Delta\tilde{T}_0 L}{\kappa\mu} \quad \mathrm{Ma}_C = \frac{\sigma_C\Delta\tilde{C}_0 L}{D\mu}$$

where μ is viscosity. K is the capillary number and in the limit as $K\to 0$ the free surface becomes planar. Scriven and Sternling (1964) use crispation number to measure surface deflection. Note that we used kinematic viscosity in the definition of K, rather than thermal diffusivity, therefore crispation number corresponds to our capillary number times Prandtl number. The boundary conditions at the free surface apply at $y=1+\eta(x,\ t)$, but a Taylor series expansion shows that in the linear analysis, they are actually applied at $y=1$.

This work focuses primarily on the qualitative difference between previously known results with $K=0$ and the new results for a range of values of K.

3 Linear Stability

We wish to examine the stability of a zero base flow, to small perturbations. Implementing the normal mode approach, viz.,

$$\psi(x,\ y,\ t) = f(y)e^{\omega t + i\alpha x} \tag{19}$$

$$T(x,\ y,\ t) = g(y)e^{\omega t + i\alpha x} \tag{20}$$

$$C(x,\ y,\ t) = h(y)e^{\omega t + i\alpha x} \tag{21}$$

the problem reduces to the following system of ordinary differential equations:

$$(D^2-\alpha^2)(D^2-\alpha^2\beta^2)f(y) = 0 \tag{22}$$

$$(D^2-\alpha^2\gamma^2)g(y) = i\alpha\mathrm{Pr}f(y) \tag{23}$$

$$(D^2-\alpha^2\epsilon^2)h(y) = i\alpha\mathrm{Sc}f(y) \tag{24}$$

where

$$D^2 = \frac{d^2}{dy^2} \quad \beta^2 = 1+\omega/\alpha^2$$

$$\gamma^2 = 1+\mathrm{Pr}\omega/\alpha^2 \quad \epsilon^2 = 1+\mathrm{Sc}\omega/\alpha^2.$$

The boundary conditions become

$y=0$

$$f = f' = g = h = 0 \tag{25}$$

$y=1$

$$\omega g' + \mathrm{Nu}(\omega g + i\alpha f) = 0 \tag{26}$$

$$\omega h' + \mathrm{Sh}(\omega h + i\alpha f) = 0 \tag{27}$$

$$\frac{\mathrm{Ma}_T}{\mathrm{Pr}}(\omega i\alpha g - \alpha^2 f) + \frac{\mathrm{Ma}_C}{\mathrm{Sc}}(\omega i\alpha h - \alpha^2 f) + \omega f'' + \omega\alpha^2 f = 0 \tag{28}$$

$$\alpha^4 f + K(-\omega f'''' + f'(\omega^2 + 3\alpha^2\omega)) = 0. \tag{29}$$

Downloaded 03 May 2010 to 171.66.16.20. Redistribution subject to ASME license or copyright; see http://www.asme.org/terms/Terms_Use.cfm

Variables in the reduced set of equations have solutions in terms of hyperbolic sines and cosines:

$$f(y) = a_1 \sinh(\alpha y) + a_2 \cosh(\alpha y) + a_3 \sinh(\alpha\beta y) + a_4 \cosh(\alpha\beta y) \quad (30)$$

$$g(y) = b_1 \sinh(\alpha y) + b_2 \cosh(\alpha y) + b_3 \sinh(\alpha\beta y) + b_4 \cosh(\alpha\beta y) + a_5 \sinh(\alpha\gamma y) + a_6 \cosh(\alpha\gamma y) \quad (31)$$

$$h(y) = c_1 \sin(\alpha y) + c_2 \cosh(\alpha y) + c_3 \sinh(\alpha\beta y) + c_4 \cosh(\alpha\beta y) + a_7 \sinh(\alpha\epsilon y) + a_8 \cosh(\alpha\epsilon y). \quad (32)$$

Terms preceded by b_1 through b_4 and c_1 through c_4 are the particular solutions associated with the nonhomogeneous terms in the governing Eqs. (22)–(24). Hence these coefficients can be found by direct substitution. The remaining coefficients are required to satisfy the boundary conditions (25)–(29). After obtaining the particular solutions (using *Mathematica*) and applying the boundary conditions, the problem reduces to

$$[A]\begin{bmatrix} a_1 \\ \vdots \\ a_8 \end{bmatrix} = 0. \quad (33)$$

A nontrivial solution of Eq. (33) exists only when the determinant of the matrix A is zero. The resulting expression relates the parameters Pr, Sc, Ma_T, Ma_C, K, Sh, Nu to the wave number α and the associated eigenvalue ω.

4 Exchange of Stability

An exchange of stability occurs when the eigenvalue ω is zero. This problem needs to be treated as a special case of the previous analysis since the particular solution of the Eqs. (30)–(32) now take the form

$$f(y) = a_1 \sinh(\alpha y) + a_2 \cosh(\alpha y) + a_3 y \sinh(\alpha y) + a_4 y \cosh(\alpha y). \quad (34)$$

The following boundary conditions need to be treated with care in the limits as $\omega \to 0$:

$y = 1$

$$g' + \mathrm{Nu}\left(g + \frac{i\alpha f}{\omega}\right) = 0 \quad (35)$$

$$h' + \mathrm{Sh}\left(h + \frac{i\alpha f}{\omega}\right) = 0 \quad (36)$$

$$\frac{\mathrm{Ma}_T}{\mathrm{Pr}}\left(i\alpha g - \frac{\alpha^2 f}{\omega}\right) + \frac{\mathrm{Ma}_C}{\mathrm{Sc}}\left(i\alpha h - \frac{\alpha^2 f}{\omega}\right) + f'' + \alpha^2 f = 0 \quad (37)$$

$$\alpha^4 f + K(-\omega f'''' + f'(\omega^2 + 3\alpha^2\omega)) = 0 \quad (38)$$

The term $i\alpha f/\omega$ in Eqs. (35), (36), and the term $\alpha^2 f/\omega$ in Eq. (37) need to be replaced by the appropriate expression involving K from Eq. (38), so that the boundary conditions become

$y = 1$

$$g' + \mathrm{Nu}\left(g - \frac{iK}{\alpha^3}(-f''' + 3\alpha^2 f')\right) = 0 \quad (39)$$

$$h' + \mathrm{Sh}\left(h - \frac{iK}{\alpha^3}(-f''' + 4\alpha^2 f')\right) = 0 \quad (40)$$

$$i\alpha\left(\frac{\mathrm{Ma}_T}{\mathrm{Pr}} g + \frac{\mathrm{Ma}_C}{\mathrm{Sc}} h\right) + \frac{K}{\alpha^2}(-f''' + 3\alpha^2 f) \times \left(\frac{\mathrm{Ma}_T}{\mathrm{Pr}} + \frac{\mathrm{Ma}_C}{\mathrm{Sc}}\right) + f'' + \alpha^2 f = 0 \quad (41)$$

$$f = 0. \quad (42)$$

Following the procedure described in the previous section, we determine the expression relating the parameter values when $\omega = 0$, and the result is given in the following expression.

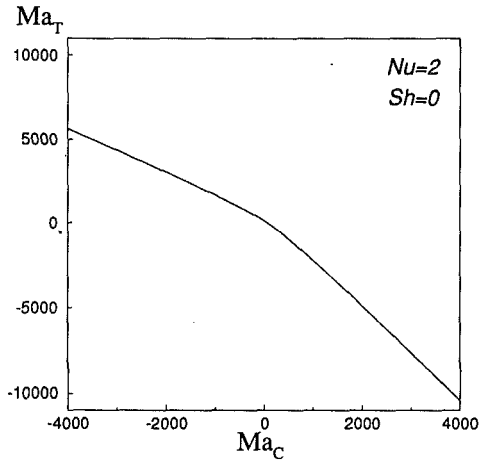


Fig. 2 Envelope of exchange of stability bifurcations for various wave numbers, Sh = 0, Nu = 2

$$\frac{\mathrm{Ma}_T}{E_1 E_3} + \frac{\mathrm{Ma}_C}{E_2 E_4} - \frac{4\alpha(\sin 2\alpha - 2\alpha)}{E_1 E_2} = 0 \quad (43)$$

where

$$E_1 = \sinh^3\alpha - \alpha^3 \cosh\alpha + \frac{8K\alpha^3}{\mathrm{Sc}} \cosh\alpha$$

$$E_2 = \sinh^3\alpha - \alpha^3 \cosh\alpha + \frac{8K\alpha^3}{\mathrm{Pr}} \cosh\alpha$$

$$E_3 = \mathrm{Nu} \sinh\alpha + \alpha \cosh\alpha$$

$$E_4 = \mathrm{Sh} \sinh\alpha + \alpha \cosh\alpha.$$

Scriven and Sternling (1964) give an equivalent expression for the case of single diffusion (heat), and in that equation they have a term with surface viscosity, but as explained before, in our two-dimensional flow analysis surface viscosity does not play any role. Equation (43) reduces to the equivalent expression for the $K = 0$ case which was given by McTaggert (1983). While the case with $K = 0$ is independent of Prandtl and Schmidt numbers, both of these parameters are present in the general case. This result differs from the conclusions of Benguira and Depassier (1987), for the buoyancy-driven problem. In that problem they showed that the presence of the deformable free surface has no impact on the exchange of stability.

4.1 Nu = 0, K = 0 Case. Throughout we assume no mass transfer at the free surface, Sh = 0. If we also assume the surface is insulated, Nu = 0, and that the effect of deformability vanishes, i.e., $K = 0$, Eq. (43) reduces to

$$\mathrm{Ma}_T = -\mathrm{Ma}_C + \frac{8\alpha^2 \cos\alpha(\sinh\alpha\cosh\alpha - \alpha)}{\sinh^3\alpha - \alpha^3\cosh\alpha}. \quad (44)$$

With *Mathematica*, we determine the minimum wave number to be 1.9929. In that case

$$\mathrm{Ma}_T = -\mathrm{Ma}_C + 79.6067.$$

Base states with parameter values which fall below this line in the (Ma_T, Ma_C) space, (such as $\mathrm{Ma}_T = \mathrm{Ma}_C = 0$) are stable. This is consistent with Pearson (1958), where the critical value of Ma_T was found to be 80. That analysis was for the single diffusion case, so that Ma_C would be zero.

4.2 K = 0 Results. When Nu is not equal to Sh, there is no longer a single critical wave number. Instead, an envelope of critical wave numbers is formed in the Marangoni temperature and concentration space. Positive and negative Marangoni numbers correspond respectively to destabilizing and stabilizing situations. In the lower left region of Fig. 2, the

Downloaded 03 May 2010 to 171.66.16.20. Redistribution subject to ASME license or copyright; see http://www.asme.org/terms/Terms_Use.cfm

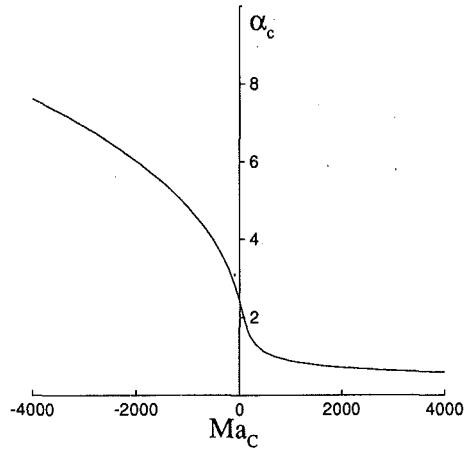


Fig. 3 Minimum wave numbers along the envelope of bifurcations in Fig. 2

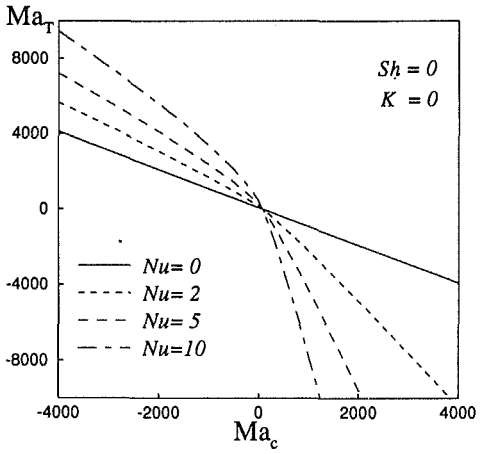


Fig. 5 Envelopes of simple bifurcations for various Nu, with $K=0$

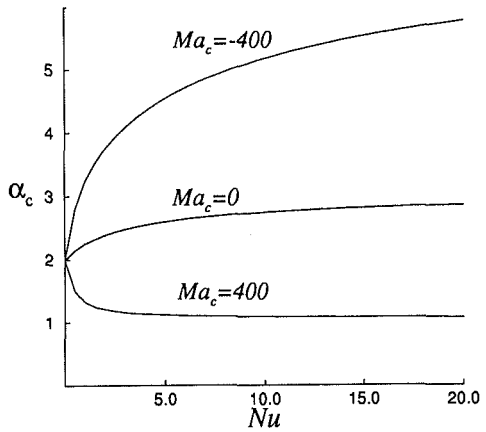


Fig. 4 Minimum wave number as function of Nusselt number for various Ma_C, with $K=0$

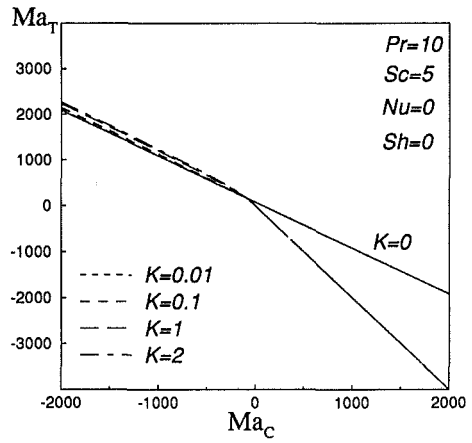


Fig. 6 Envelopes of simple bifurcations for a range of values of capillary number

base flow is linearly stable and when the envelope of bifurcation lines is crossed, the conduction solution loses stability and a new steady flow develops. The wave number where instability first occurs is called the critical wave number. Using *Mathematica* we can determine a functional relationship for the dependence of minimum Marangoni number on the critical wave number as we move along the envelope in Fig. 2, where Nu = 2. This result, shown in Fig. 3, indicates that when the temperature gradients drives the instability, and the concentration Marangoni number is negative, then the flow first loses stability to large wave numbers. On the other hand when the concentration Marangoni number is positive so that the concentration gradient is the driving force for the instability, the flow first loses stability to small wave numbers, that is to long wave perturbations.

In Fig. 4, we see how the minimum wave number varies with Nu number for three different values of Ma_C. As mentioned in Section 4.1, the critical wave number for the Nu = 0 case is 1.9929, independent of Ma_C. As Nu is increased from zero this is no longer the case. When $Ma_C = 400$, the wave number decreases to a minimum value. Once the Nusselt number is increased beyond 2 or 3, is ceases to have any significant influence on the critical wave number. In the limiting case as $Nu \to \infty$, the temperature at the free surface is the same as the environmental temperature, T_∞. However, as Ma_C decreases, the behavior qualitatively changes. For the other two cases shown $Ma_C = 0$, and $Ma_C = -400$, the critical wave number increases with Nusselt number. In the second case, the critical wave number increases from 2 to 5 and will continue to increase further until it eventually asymptotes to a value of ~20. Although the tables which McTaggert (1983) gives are consistent with our results, she mistakenly states that as L (equivalent to Nu) increases, the corresponding wave number increases for all Ma_C.

As the Nusselt number is varied for a particular value of Ma_C the temperature Marangoni number is also affected, so that the location of the bifurcation envelope shifts in the Marangoni space. Various envelopes of simple bifurcations for different values of Nu are shown in Fig. 5. If we choose a specific negative value of Ma_C, and increase Nu, instability is delayed until larger temperature Marangoni numbers are achieved. Hence fluids which allow greater heat transfer at the free surface, that is exhibit larger Nu, will remain linearly stable for larger values of temperature difference across the layer.

4.3 Deformable Free Surface, $K=0$. We now proceed to examine the effects of a deformable surface on these results. In Fig. 6 the envelope of simple bifurcation is shown for various values of K. First we note the difference between the rigid surface $K=0$ and the deformable surface, $K \neq 0$. Instead of the smooth curves shown in Fig. 5, the critical Marangoni numbers now lie on a piecewise continuous function. At some point along the envelope, the critical wave number discretely changes from a value close to 2 down to 0, see Fig. 7. In the lower right of Fig. 6, as the parametes are varied to cross the envelope of simple bifurcations, the conduction solution loses stability first to infinitely long-wave perturbations. We also note that the bifurcation envelope now passes through the origin so there is no range of positive temperature Marangoni numbers where the base solution is stable if the concentration

Downloaded 03 May 2010 to 171.66.16.20. Redistribution subject to ASME license or copyright; see http://www.asme.org/terms/Terms_Use.cfm

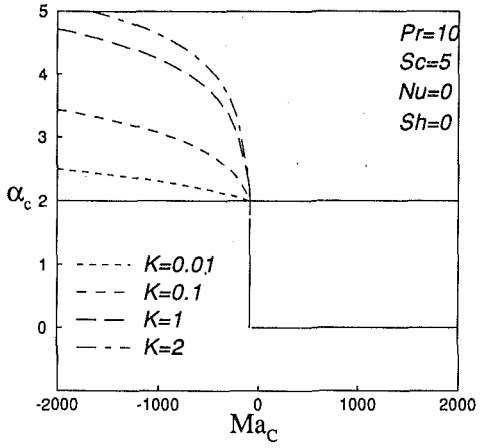


Fig. 7 Variation of the critical number along the envelopes shown in Fig. 6

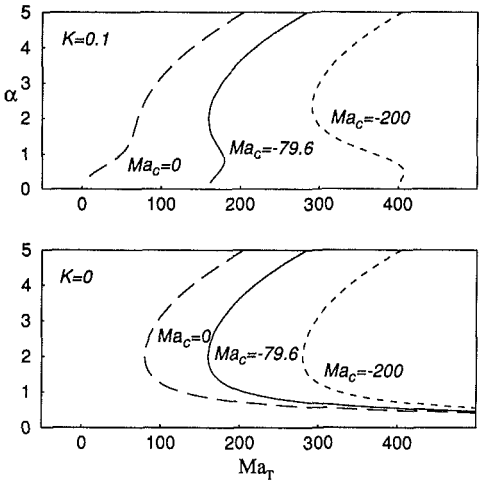


Fig. 8 Wave number versus Ma_T for various values of Ma_C. The critical wave number occurs when Ma_T is a minimum.

Marangoni number is zero, i.e., single diffusion case. This is consistent with Scriven and Sternling (1964).

The jump in the critical wave number is readily explained when we examine the graph of wave number versus temperature Marangoni number for a fixed value of concentration Marangoni number, Fig. 8. We include for reference the original results of Pearson for the $K=0$, $Ma_C=0$ case. When $K=0$, the critical wave number is only weakly dependent on the concentration Marangoni number. When $K=0.1$ and $Ma_C=-200$, the critical wave number remains close to this value. However, as Ma_C increases, the function changes shape until it reaches a point, $Ma_C=-79.6$ where the critical wave number drops to zero. Thereafter the critical wave number is unchanged, indicating that the base flow loses stability first to perturbations of infinitely long-wave length.

It is clear from Fig. 6 that as long as the capillary number is not equal to zero, its actual magnitude has little effect on the critial values of Marangoni number. The bifurcations on the left-hand side of Fig. 6 lie very close to the $K=0$ envelope and the bifurcations on the right-hand side lie on the $\alpha=0$ line which is independent of K, and can be found asymptotically using *Mathematica* to be

$$Ma_T + Ma_C \frac{(1+Nu)}{(1+Sh)} \frac{Pr}{Sc} = 0. \tag{45}$$

On the other hand, the critical wave numbers change significantly with K, Fig. 7. As K is increased the critical wave number

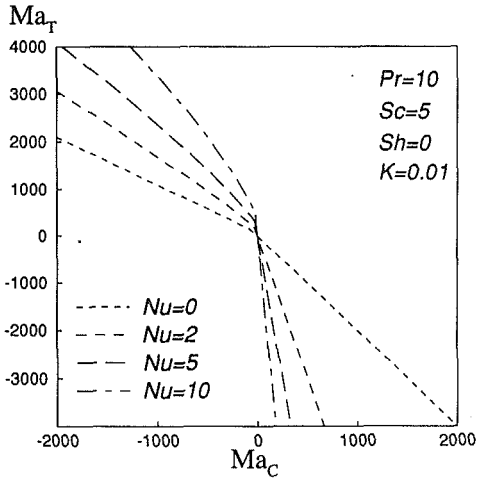


Fig. 9 Effect of Nusselt number on the bifurcation envelopes

Table 1 Nusselt number and Ma_C and Ma_T values at the point of jump

Nu	Ma_C	Ma_T
0	−79.61	159.22
2	−35.74	214.44
5	−34.81	348.10
10	−23.54	517.88

increases, so that the base solution will be unstable first to shorter wave disturbances.

The effect of Nusselt number (Fig. 9) is qualitatively the same as that observed in the $K=0$ case, shown in Fig. 5. The major quantitative change is that the unstable region increases in size, since the bifurcation envelope is lower than before. Table 1 shows how the values of Ma_C and Ma_T at the point where the jump occurs depend on Nusselt number. As Nusselt number increases, the jump occurs at large Ma_C.

The exchange of stability loci shown in this section indicate the loss of stability of the base flow to steady convective cellular flow. This information may have no physical relevance if the flow has already lost stability through a Hopf bifurcation resulting in a new oscillatory solution. In the next section we explore the parameter space looking for that behavior.

5 Hopf Bifurcations

An equilibrium solution may also lose stability when a complex pair of eigenvalues assumes positive real part. The new solution which then develops will be periodic. From the linear analysis we cannot deduce whether the ensuing oscillatory solution will be stable or unstale. This information can only be determined from a weakly nonlinear analysis. If the Hopf bifurcation is supercritical, a small stable periodic solution appears at the bifurcation point and as the parameters are varied away from this point, the orbit grows. If the Hopf bifurcation is subcritical, the periodic which develops is unstable. However, it often acquire stability near the Hopf bifurcation point and when the steady solution loses stability, a transient occurs resulting in an oscillation of finite amplitude. In order to determine the location of the Hopf bifurcation points in the Marangoni parameters space, we set $\omega = i\lambda$ in

$$|A| = 0. \tag{46}$$

As before, this results in an expression relating the parameters: Nu, Sh, Pr, Sc, K, the two Marangoni numbers, and the wave number. In fact the expression is now complex and includes the additional unknown λ. It would be desirable to take the real and imaginary parts of the equation and use these to eliminate λ. Unfortunately, this is impossible since λ appears

Downloaded 03 May 2010 to 171.66.16.20. Redistribution subject to ASME license or copyright; see http://www.asme.org/terms/Terms_Use.cfm

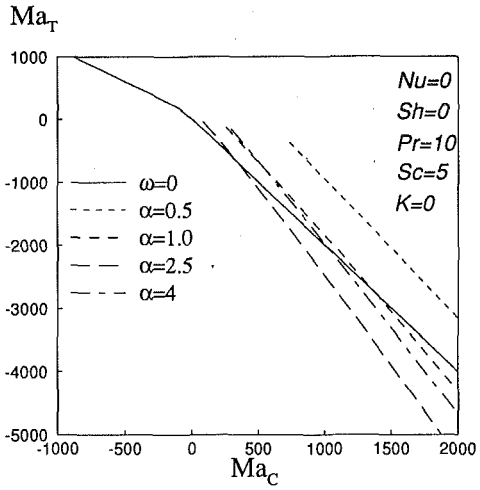


Fig. 10 Effect of wave number on the Hopf bifurcation curves when capillary number is zero

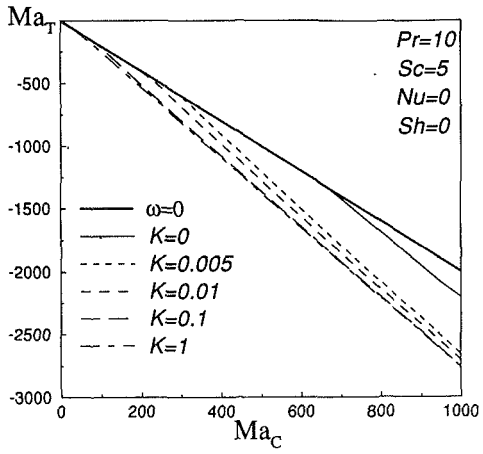


Fig. 11 Envelopes of Hopf bifurcation points for different capillary numbers Pr > Sc

Table 2 As we move along the Hopf bifurcations, the critical wave number increases slightly (Pr = 10, Sc = 5, Nu = 2, Sh = 10, K = 0)

α_c	Ma_T	Ma_C
2.91	−150	716.744
2.80	−500	979.505
2.91	−1000	1305.714
2.96	−3000	2351.942

in the hyperbolic functions and so we are unable to produce a single expression of the same form as Eq. (43). However, we continue to use *Mathematica* to reduce the system and produce the data for the Hopf bifurcation diagrams shown in the next sections.

5.1 Nondeformable Case: $K = 0$. We first consider the classic case where the upper boundary is planar. The assumption of no mass transfer at the free surface, Sh = 0, is maintained and we first consider the case of Nu = 0. As shown by Ho and Chang (1988) the Hopf bifurcation envelope can lie either in upper left or lower right quadrant in the Marangoni space depending upon the values of Pr, Sc, Nu, and Sh. For Nu = Sh the loci lie in the upper left quadrant if Sc > Pr and in the lower right quadrant if Pr > Sc.

In Fig. 10, the bifurcation loci are presented for a range of wave numbers. The dashed lines denote $\omega = i\lambda$, and the unbroken line is the minimum curve for the simple bifurcation case $\omega = 0$ discussed in Section 4. A Hopf bifurcation point is calculated by choosing a value of λ and then solving the complex expression (46) for Ma_T and Ma_C with all other parameters given. As λ is varied, the locus of Hopf bifurcation points is traced out. The loci are always traced from the origin outwards as λ is increased.

In the lower left quadrant the conduction solution is stable. If the temperature Marangoni number is increased to positive values, then the conduction solution will bifurcate to a new steady flow. However, if the concentration Marangoni number is increased, the conduction solution loses stability in a Hopf bifurcation suggesting that the new flow will be oscillatory. There is only a slight change in the critical wave number along the Hopf bifurcation envelope, ($\alpha_c \approx 2.4$). Ho and Chang (1988) focused on the case where the parameter values were Pr = 10, Sc = 5, Nu = 2, Sh = 10, $K = 0$, and found the critical wave number to be $\alpha_c = 2.69$ with $Ma_T = -150$, $Ma_C = 716.6$. Using our procedure we found $\alpha_c = 2.71$ with $Ma_T = -150.00$, $Ma_C = 716.744$. In addition we found a weak dependence of critical wave number on the minimum value of Ma_C, Table 2, while Ho and Chang (1988) found that $\alpha_c = 2.69$ for the Hopf bifurcations.

Note that these results are consistent with the work of (Vidal and Acrivos, 1966), where it was observed that for the single diffusion case ($Ma_C = 0$) no bifurcation to an oscillatory solution is possible.

5.2 Deformable Case $K \neq 0$. We now choose a small value of K, and determine the critical values of the wave number where the flow will first go unstable via a Hopf bifurcation. We used *Mathematica* to determine the critical parameter values where the Hopf bifurcations occur and to extract the correspondng wave numbers for a range of values of capillary number.

In Fig. 11, the case Pr > Sc is presented for a range of K values. The nonzero K results fall on the left of the results for the planar free surface. Even for very small values of K, (0.005) the jump of minimum Marangoni numbers is significant. The Hopf bifurcations also lie much closer to the origin. As K increases, the Hopf bifurcation envelopes asymptote to a single line, and for $K > 0.1$ there is no longer any discernible change in behavior. The Hopf bifurcation curves for Pr > Sc lie only in the lower right quadrant and never intersect the Ma_T axis. Therefore, with the parameter values chosen, a bifurcation to an oscillatory solution is not possible for the single diffusion case with a deformable surface. As K increases, the intersection point of the Hopf and the simple bifurcation curves move towards the origin. For capillary values of 0.005, 0.01, 0.1, 1, the values of Ma_C at double zero eigenvalue points are respectively, 278.26, 194.96, 63.57, and 31.66. The corresponding critical wave numbers are shown in Fig. 12. When $K = 0$ the critical wave numbers lie in the range from 2.3 to 2.5. For any value of capillary number greater than zero, a local minimum occurs close to these values, but the absolute minimum is much smaller, so that Hopf bifurcations will occur first for disturbances with wave number less than 1. As K increases the critical wave number also increases slightly. However, as Ma_C increases the curves asymptote to critical wave number 0.22.

The case of Sc > Pr is shown in Fig. 13. An examination of Eqs. (22)–(29) will show that there is a symmetry between Pr and Sc when Nu = Sh. As a result of this symmetry the effect of Pr on Ma_T is similar to the effect of Sc on Ma_C. Therefore, the Hopf bifurcation lines for the case shown in Fig. 13 (which has the switched values of Pr and Sc of the previous case) are like mirror images of the Hopf bifurcation lines for Pr > Sc. The Hopf bifurcation lines lie in the upper left quadrant instead of lower right quadrant. The effect of capillary number on this case is similar to that just discussed. As capillary number

Downloaded 03 May 2010 to 171.66.16.20. Redistribution subject to ASME license or copyright; see http://www.asme.org/terms/Terms_Use.cfm

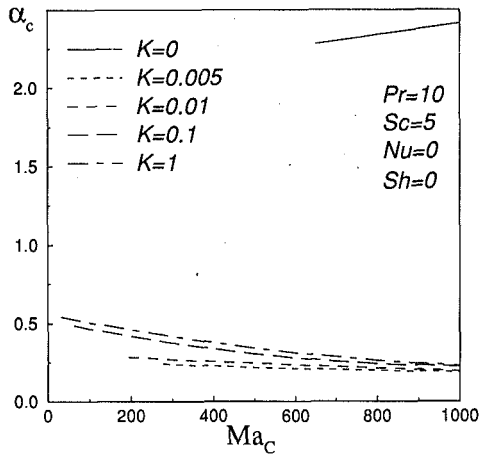


Fig. 12 Critical wave numbers corresponding to the Hopf bifurcation envelopes in Fig. 11

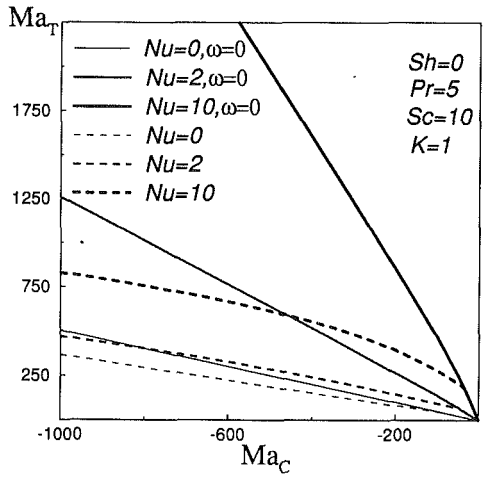


Fig. 14 Envelopes of Hopf bifurcation for different values of Nusselt number

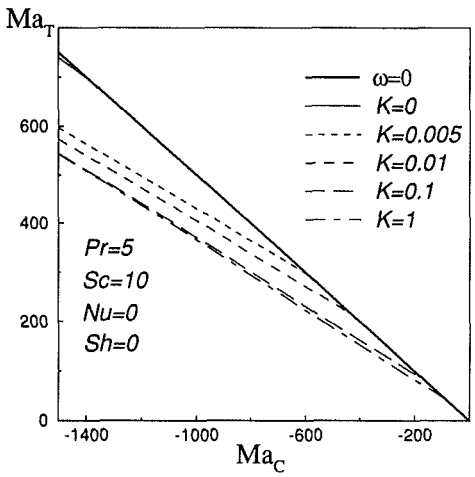


Fig. 13 Envelopes of Hopf bifurcation points for different capillary numbers Sc > Pr

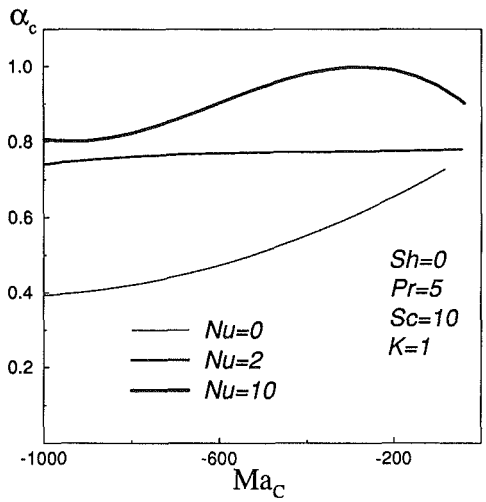


Fig. 15 Critical wave numbers corresponding to the Hopf bifurcation envelopes in Fig. 14

increases, the Hopf bifurcation loci drop. For capillary values of 0.005, 0.01, 0.1, 1, the values of Ma_C at double zero eigenvalue points are, respectively, -591.52, -426.80, -158.29, and -81.67. For nonzero K values the critical wave number is less than 1. Like the previously described case, increasing capillary number increases the critical wave number.

5.3 Nonzero Nusselt Number. In the discussion of the Hopf bifurcation loci in the last sections we have assumed that the Nusselt number and the Sherwood number were both zero. We now examine the case where the free surface is no longer assumed to be insulated. Figure 14 shows how bifurcation envelopes change as Nu is increased. The unbroken lines are the simple bifurcation lines and the dashed lines are the Hopf bifurcation lines. For any given Nusselt number, the stable region is bounded by the lower of the corresponding Hopf or simple bifurcation lines. For Ma_C values close to zero, the flow loses stability through a simple bifurcation; however, for larger negative values of Ma_C the flow loses stability through a Hopf bifurcation, suggesting that the new flow will be oscillatory. As Nusselt number is increased, the size of the stable region is increased. This result is expected, because transferring heat to the environment decreases the gradient of temperature along the surface which is the driving force for instability in the upper left quadrant. Critical wave numbers are increased as one increases Nusselt number (see Figure 15). Therefore with a conducting surface the flow loses stability to shorter wave perturbations.

5.4 Conclusions. The influence of a deformable free surface, reflected by the parameter K, on the linear stability of a single layer of fluid with double diffusion is considerable. When viewed in the space of the Marangoni numbers, the base conduction solution is stable when both these numbers are negative. The upper right quadrant is completely unstable. In the upper left and lower right quadrant, there is a balance between the stabilizing effect of one of the quantities and the destabilizing effect of the other. In these two quadrants the region of stability is significantly reduced when we permit the surface to deform by taking nonzero values of capillary number. Increasing capillary number decreases the size of the stable region. Nonzero capillary number also has a strong effect on the values of the critical wave number, which in turn influences the nature of the new flow that will develop when the base conduction solution loses stability.

Larger Nusselt number reflects increased heat transfer from the surface to the gas phase, and decreased temperature gradient on the surface. Therefore when the temperature gradient is the driving force for instability ($Ma_T > 0$), increasing the Nusselt number decreases the destabilizing force and increases the size of the stable region. On the other hand, when the temperature gradient is the stabilizing force ($Ma_T < 0$), increasing the Nusselt number decreases the size of the stable region by decreasing the stabilizing force.

The result that there is no longer any region where the flow

Downloaded 03 May 2010 to 171.66.16.20. Redistribution subject to ASME license or copyright; see http://www.asme.org/terms/Terms_Use.cfm

is linearly stable in the upper right quadrant is not guaranteed since in our analysis we neglect gravity waves. In fact, for the single diffusion case, Smith (1966) shows that the gravity waves generated stabilize the long-wave perturbations.

References

Aris, R., 1962, *Vectors, Tensors, and the Basic Equations of Fluid Mechanics*, Dover Publications, New York, pp. 226–244.

Benguria, R., and Depassier, M., 1987, "Oscillatory Instabilities in the Rayleigh-Benard Problem with a Free Surface," *Physics of Fluids*, Vol. 30, pp. 1678–1682.

Benguria, R., and Depassier, M., 1989, "On the Linear Stability Theory of Benard-Marangoni Convection," *Physics of Fluids A*, Vol. 1, pp. 1123–1127.

Davis, S. H., 1987, "Thermocapillary Instabilities," *Annual Review of Fluid Mechanics*, Vol. 19, pp. 403–435.

Ho, K., and Chang, H., 1988, "On Nonlinear Double Diffusive Marangoni Instability," *AIChE Journal*, Vol. 34, pp. 705–722.

McTaggert, C., 1983, "Convection Driven by Concentration and Temperature Dependent Surface Tension," *Journal of Fluid Mechanics*, Vol. 134, pp. 301–310.

Pearson, J. R. A., 1958, "On Convection Cells Induced by Surface Tension," *Journal of Fluid Mechanics*, Vol. 4, pp. 489–500.

Scriven, L. E., and Sternling, C. V., 1964, "On Cellular Convection Driven by Surface Tension Gradients: Effect of Mean Surface Tension and Viscosity," *Journal of Fluid Mechanics*, Vol. 19, pp. 321–340.

Smith, K. A., 1966, "On Convective Instability Induced by Surface Tension Gradients," *Journal of Fluid Mechanics*, Vol. 24, pp. 401–414.

Vidal, A., and Acrivos, A., 1966, "Nature of the Neutral State in Surface Tension Driven Convection," *Physics of Fluids*, Vol. 9, p. 615.

Downloaded 03 May 2010 to 171.66.16.20. Redistribution subject to ASME license or copyright; see http://www.asme.org/terms/Terms_Use.cfm

On the Geometry of Nonholonomic Dynamics

H. Essén
Department of Mechanics,
Royal Institute of Technology,
S-100 44 Stockholm, Sweden

The formulation and derivation of equations of motion for finite degree-of-freedom nonholonomic systems, is discussed. The starting point is Newton's equation of motion in the 3K-dimensional unconstrained configuration space of K particles. Constraints represent knowledge that motion is only possible along some directions in the local tangent spaces. Only projections of the 3K-dimensional vector equation onto these allowed directions are of interest. The formalism is essentially that of Kane-Appell cast into an abstract form. It is shown to give the same equations as Hamel's generalization of Lagrange's method. The algorithmic advantage of the Kane-Appell projection approach is stressed.

1 Introduction

Even modern textbooks and monographs normally present Lagrange's method in a way that is strongly influenced by various historical approaches such as the "principle of virtual work" and "d'Alembert's principle." It is the opinion of this author that this practice is pointless, sometimes even misleading. Except for certain advanced variational principles, there are no deeper principles in mechanics than those given by Newton's laws. Lagrange's equations are therefore best seen as mathematical consequences of these laws. Some textbooks emphasize that Lagrange's equations arise when Newton's laws are transformed to arbitrary curvilinear coordinates and this is at least part of the the truth.

The intellectually most economic point of view is that Lagrange's equations arise by projection of Newton's equations ($\dot{\mathbf{p}}_k = \mathbf{F}_k$) from some original unconstrained configuration space ($3K$-dimensional for K particles) to a lower dimensional configuration space consistent with the (holonomic) constraints. This space can be seen as a surface embedded in the original space. Lesser (1992) developed this projection idea in connection with Kane's (1961, 1985) method, but it applies equally to the Lagrange formalism. The number of projected equations is equal to the number of dimensions, n of the holonomically constrained configuration space. The number n is also the number of degrees-of-freedom unless there are nonholonomic constraints.

One of the drawbacks of the Lagrange method is that it does not produce Euler's dynamic equations for the rigid body as a special case. The reason is that these are expressed in terms of angular velocities which are not time derivatives of any generalized coordinates. Another drawback is that it does not naturally handle nonholonomic constraints. These two shortcomings of the Lagrange method disappear when it is generalized to "quasi-coordinates." Quasi-coordinates, or more properly, noncoordinate (or anholonomic) velocity component, were developed in the early twentieth century by Hamel (1904). Hamel, however, was preceded by Poincaré (1901) and the idea appears already in work by men like Lagrange, Kirchoff, Gibbs, and Volterra. The traditional quasi-coordinate approach is mentioned in Pars (1965), discussed in Whittaker (1927), and treated fully in Neĭmark and Fufaev (1972). The main purpose of the present work is to present these ideas in the light of more modern different geometric ideas and to consider their connection with Kane's method.

The quasi-velocities introduced via the quasi-coordinates turn to to be equivalent to the so-called "generalized speeds" introduced in the much used Kane's method (Kane and Levinson 1985). This method may be regarded as a modern elaboration of methods that originated with Gibbs and Appell. The present work thus throws some light on the relationship between Kane's equations and older methods in analytical mechanics. In particular it seems that there is a close mathematical correspondence between Kane's equations of motion and Lagrange's equation in terms of quasi-coordinates. One must note, however, that Kane's method entails an entire methodology for setting up the equations of motion in a practical way that surpasses many of his predecessors.

2 Notation and Background

We shall assume that the mechanical system of interest can be obtained by adding constraints to an underlying unconstrained K-particle system. Let the masses of these particles be m_k, their position vectors in some coordinate system $\mathbf{r}_k$, and the (total) forces on them $\mathbf{F}_k$, where $k = 1, \ldots, K$. To simplify the expressions in the rest of this article we introduce the following notation:

$$R \equiv (\mathbf{r}_1, \mathbf{r}_2, \ldots, \mathbf{r}_K) \tag{1}$$

Contributed by the Applied Mechanics Division of THE AMERICAN SOCIETY OF MECHANICAL ENGINEERS for publication in the JOURNAL OF APPLIED MECHANICS.

Discussion on this paper should be addressed to the Technical Editor, Professor Lewis T. Wheeler, Department of Mechanical Engineering, University of Houston, Houston, TX 77204-4792, and will be accepted until four months after final publication of the paper itself in the JOURNAL OF APPLIED MECHANICS.

Manuscript received by the ASME Applied Mechanics Division, Mar. 5, 1993; final revision, May 26 1993.

Associate Technical Editor: R. L. Huston.

Copyright © 1994 by ASME
Downloaded 03 May 2010 to 171.66.16.20. Redistribution subject to ASME license or copyright; see http://www.asme.org/terms/Terms_Use.cfm

$$V \equiv (\mathbf{v}_1, \mathbf{v}_2, \ldots, \mathbf{v}_K) = \dot{R} \tag{2}$$

$$P \equiv (\mathbf{p}_1, \mathbf{p}_2, \ldots, \mathbf{p}_K) = \hat{\mathbf{M}} V \tag{3}$$

$$F \equiv (\mathbf{F}_1, \mathbf{F}_2, \ldots, \mathbf{F}_K). \tag{4}$$

Here $\hat{\mathbf{M}}$ is a linear operator on the space (with the masses as diagonal elements) which turns the velocity vector into the momentum vector. Using this notation Newton's equations of motion for the system can be written

$$\dot{P} = F. \tag{5}$$

Following Lesser (1992) we introduce a scalar product on the $3K$-dimensional unconstrained configuration space as the sum of the K ordinary scalar products. We shall denote this scalar product by $\bullet$ so that

$$A \bullet B \equiv \sum_{k=1}^{K} \mathbf{a}_k \bullet \mathbf{b}_k. \tag{6}$$

The kinetic energy can, for example, be written in the compact form

$$T = \frac{1}{2} P \bullet V \tag{7}$$

when this scalar product is used.

We now assume that the holonomic constraints of the system are taken into account by giving a parametrization $q = q^1, \ldots, q^n$ of an n-dimensional surface embedded in the unconstrained configuration space

$$R = R(q, t) \equiv (\mathbf{r}_1(q, t), \ldots, \mathbf{r}_K(q, t)). \tag{8}$$

For time-dependent constraints one gets one such surface for each value of the time t. If the constraints are time-independent (scleronomic system) the time t will not appear in the parameterization. This surface is the (instantaneous) configuration space of the system. Since a single parametrization cannot, in general, cover the entire configuration space, the theory given here is local.

3 Projection Onto Coordinate Tangent Vectors

A constraint represents knowledge about the motion of the system that one has prior to solving the equations of motion. Since one already knows that the motion will take place on the embedded surface (8) implied by the holonomic constraints, there is no need to solve all $3K$ equations of motion (5). It is enough to solve the equations that are the components of the vector Eq. (5) along the tangent vectors of the surface (8).

One obtains n linearly independent tangent vectors of the (instantaneous) configuration space (surface) by taking the partial derivatives of the position vector (8) with respect to the generalized coordinates

$$\tau_a(q, t) \equiv \frac{\partial R}{\partial q^a}, \quad a = 1, \ldots, n. \tag{9}$$

The projected equations of motion that will be of interest are thus

$$\dot{P}(\dot{q}, q, t) \bullet \tau_a(q, t) = F(\dot{q}, q, t) \bullet \tau_a(q, t) \quad a = 1, \ldots, n \tag{10}$$

since these describe the motion along directions allowed by the constraints. The ideas involved here are not really more advanced than those used when Newton's equations are projected onto so called moving basis vectors associated with polar coordinates. Yet these equations are, in fact, the (Euler-) Lagrange equations as we will show in the next section. One notes that, even if there are no constraints, the procedure is useful just for changing coordinates.

4 Lagrange's Equations

We denote the partial time derivative of the position vector by

$$\tau_t(q, t) \equiv \frac{\partial R}{\partial t}. \tag{11}$$

The total time derivative d/dt, sometimes denoted simply by an overdot, should be thought of as the operator

$$\frac{d}{dt} \equiv \ddot{q}^a \frac{\partial}{\partial \dot{q}^a} + \dot{q}^a \frac{\partial}{\partial q^a} + \frac{\partial}{\partial t}, \tag{12}$$

when it acts on a function of the independent variables $\dot{q}$, q, and t. Here $\dot{q}^a \equiv dq^a/dt$ are the so called "generalized velocities," or more properly, the (holonomic) contravariant components of the system velocity vector. In this formula summation is implied over repeated upper lower indices. We will use this summation convention below. The $3K$-dimensional velocity vector, $V = dR/dt$, is now given by

$$V(q, \dot{q}, t) = \dot{q}^a \tau_a(q, t) + \tau_t(q, t). \tag{13}$$

The generalized velocities, which are regarded as independent variables in the Lagrange formalism, can thus be seen as coordinates in velocity space; when they vary the vector V sweeps over an n-dimensional hyperplane. For the case of the scleronomic system the vector τ_t is a null vector ($\tau_t = \mathbf{0}$) and this hyperplane can be identified with the tangent plane of the configuration surface (8).

In terms of the independent variables q, $\dot{q}$, and t we can now write the kinetic energy, $T = \hat{\mathbf{M}} V \bullet V/2$, as follows:

$$T(q, \dot{q}, t) = \frac{1}{2} g_{ab}(q, t) \dot{q}^a \dot{q}^b + a_a(q, t) \dot{q}^a + b(q, t) \tag{14}$$

where we have introduced

$$g_{ab}(q, t) \equiv \hat{\mathbf{M}} \tau_a \bullet \tau_b, \tag{15}$$

$$a_a(q, t) \equiv \hat{\mathbf{M}} \tau_a \bullet \tau_t, \tag{16}$$

$$b(q, t) \equiv \frac{1}{2} \hat{\mathbf{M}} \tau_t \bullet \tau_t. \tag{17}$$

In the scleronomic case only the first term appears and the kinetic energy is purely quadratic in the generalized velocities.

We now proceed to differentiate the kinetic energy to find Lagrange's equations. We first note that

$$\frac{\partial V}{\partial \dot{q}^a} = \tau_a = \frac{\partial R}{\partial q^a} \tag{18}$$

according to (13) and (9). This is sometimes referred to as the "cancellation of the dots." Using this one finds that

$$\frac{\partial T}{\partial \dot{q}^a} = \frac{\partial}{\partial \dot{q}^a} \frac{1}{2} \mathbf{M} V \bullet V = P \bullet \frac{\partial V}{\partial \dot{q}^a} = P \bullet \frac{\partial R}{\partial q^a} = P \bullet \tau_a \equiv p_a. \tag{19}$$

The quantities p_a are the generalized momenta and the above equation shows that these are projections of the $3K$-dimensional momentum vector P onto the tangent vector τ_a. If we now take the total time derivative of this we get

$$\frac{d}{dt} \frac{\partial T}{\partial \dot{q}^a} = \frac{d}{dt} (P \bullet \tau_a) = \frac{dP}{dt} \bullet \tau_a + P \bullet \frac{d\tau_a}{dt}. \tag{20}$$

If we differentiate T with respect to q^a we find

$$\frac{\partial T}{\partial q^a} = \frac{\partial}{\partial q^a} \frac{1}{2} \hat{\mathbf{M}} V \bullet V = P \bullet \frac{\partial V}{\partial q^a}. \tag{21}$$

We now form the difference

$$\frac{d}{dt} \frac{\partial T}{\partial \dot{q}^a} - \frac{\partial T}{\partial q^a} = \frac{dP}{dt} \bullet \tau_a + P \bullet \left(\frac{d\tau_a}{dt} - \frac{\partial V}{\partial q^a} \right) \tag{22}$$

and note that the vector

$$\left(\frac{d\tau_a}{dt} - \frac{\partial V}{\partial q^a} \right) = \left(\frac{d}{dt} \frac{\partial}{\partial q^a} - \frac{\partial}{\partial q^a} \frac{d}{dt} \right) R = \mathbf{0} \tag{23}$$

is the null vector since the differential operators commute (see Eq. (12)). If one now makes the natural definition that the

Downloaded 03 May 2010 to 171.66.16.20. Redistribution subject to ASME license or copyright; see http://www.asme.org/terms/Terms_Use.cfm

projection of the $3K$-dimensional force vector $\boldsymbol{F}$ onto the tangent vector τ_a,

$$\frac{d\boldsymbol{P}}{dt} \bullet \tau_a = \boldsymbol{F} \bullet \tau_a \equiv Q_a, \tag{24}$$

is the generalized force Q_a one finally ends up with

$$\frac{d}{dt}\frac{\partial T}{\partial \dot{q}^a} - \frac{\partial T}{\partial q^a} = Q_a; \tag{25}$$

i.e., the (Euler-) Lagrange equations in one of their traditional forms. These are thus simply the projected Newton Eq. (10).

5 Generalization to a Noncoordinate Basis

We now generalize the above treatment and introduce anholonomic (contravariant) velocity components, $\dot{\pi}^\alpha$, as linear expression in terms of the generalized velocities (the holonomic components)

$$\dot{\pi}^\alpha \equiv A^\alpha_a(q, t)\dot{q}^a + B^\alpha(q, t), \ \alpha = 1, \ldots, n. \tag{26}$$

In Kane's approach these are called generalized speeds. The notation here follows Neĭmark and Fufaev (1972) and the original work by Hamel (1904) in denoting this quantity as if it was the derivative with respect to time of some quantity which in fact does not exist but which nevertheless is called a "quasi-coordinate" and is denoted by π^α. The present treatment is, however, somewhat more general than most earlier ones in allowing time-dependence in the transformation matrix $A^\alpha_a(q, t)$ and in allowing an in-homogeneous part $B^\alpha(q, t)$ in the transformation. One should note that the $\dot{\pi}^\alpha$ are to be regarded as independent variables, together with q and t, just as the $\dot{q}^a$ before. The dependence of the transformation on q and t only means that these are different independent variables at each point of configuration space and at each time when regarded as functions of the $\dot{q}^a$.

By solving the linear Eqs. (26) for the $\dot{q}^a$ one finds

$$\dot{q}^a = A^a_\alpha(q, t)\dot{\pi}^\alpha + B^a(q, t), \ a = 1, \ldots, n \tag{27}$$

where the same summation convention is used for the α-index as for the index a and where we have introduced the inverse of the transformation matrix so that

$$A^a_\alpha A^\alpha_b = \delta^a_b \text{ and } A^a_\beta A^\alpha_a = \delta^\alpha_\beta \tag{28}$$

are Kronecker deltas. It is thus necessary that this matrix is nonsingular. We have also introduced the quantities

$$B^a \equiv -A^a_\alpha B^\alpha. \tag{29}$$

We now introduce the generalized speeds $\dot{\pi}^\alpha$ into the expression for the velocity $\boldsymbol{V}$ by inserting the expressions (27) into Eq. (13). The result is

$$\boldsymbol{V}(q, \dot{\pi}, t) = \dot{\pi}^\alpha \tau_\alpha(q, t) + \tau^*_t(q, t), \tag{30}$$

where the vectors τ_α are new tangent vectors defined as the following linear combinations of the old

$$\tau_\alpha(q, t) \equiv A^a_\alpha(q, t)\tau_a(q, t) \tag{31}$$

and where finally

$$\tau^*_t(q, t) \equiv B^a(q, t)\tau_a(q, t) + \tau_t(q, t) \tag{32}$$

gives the last term in the expression for $\boldsymbol{V}$.

6 Nonholonomic Constraints

One advantage of introducing the quasi-velocities of Eq. (26) is that components of the angular velocity vector are such velocities and thus can be used as independent dynamical variables. Another advantage is that nonholonomic constraints often can naturally be expressed in terms of them. If there are $m(<n)$ nonholonomic constraints of the form

$$A^\alpha_a(q, t)q^a + B^\alpha(q, t) = 0 \quad \alpha = n_u + 1, \ldots, n \tag{33}$$

the number of independent coordinates in velocity space is $n_u = n - m$ and is thus less than n, the number of generalized coordinates of the configuration space. If we compare with Eq. (26) we see that the above nonholonomic constraints can be expressed simply as the vanishing of the last m generalized speeds:

$$\dot{\pi}^\alpha = 0 \quad \alpha = n_u + 1, \ldots, n. \tag{34}$$

Geometrically this means that we have some knowledge about the allowed behavior of the velocity vector (30) prior to solving the equations of motion. This knowledge is that the velocity will not have components along the directions of tangent space defined by the tangent vectors τ_a for $\alpha = n_u + 1, \ldots, n$; it can only vary along the first n_u directions. There is then no need to solve equations of motion projected onto the m the last noncoordinate tangent vectors. Instead of all the n Eq. (10) we need only

$$\boldsymbol{P}(\dot{\pi}_u, q, t) \bullet \tau_\lambda(q, t) = \boldsymbol{F}(\dot{\pi}_u, q, t) \bullet \tau_\lambda(q, t) \quad \lambda = 1, \ldots, n_u \tag{35}$$

where the symbol $\dot{\pi}_u$ stands for the first n_u unconstrained generalized speeds. We have also introduced the convention that a Greek index from the middle of the alphabet only runs over these unconstrained speeds $1, \ldots, n_u$.

Now that our independent variables are $\dot{\pi}$, q, and t the total time derivative operator, Eq. (12), is

$$\frac{d}{dt} \equiv \ddot{\pi}^\alpha \frac{\partial}{\partial \dot{\pi}^\alpha} + \dot{q}^a \frac{\partial}{\partial q^a} + \frac{\partial}{\partial t}. \tag{36}$$

Using

$$\boldsymbol{P} = \hat{\mathbf{M}}\boldsymbol{V} = \hat{\mathbf{M}}(\dot{\pi}^\mu \tau_\mu + \tau^*_t) \tag{37}$$

we find that

$$\dot{\boldsymbol{P}} \bullet \tau_\lambda = \hat{\mathbf{M}}\left(\ddot{\pi}^\mu \tau_\mu + \dot{\pi}^\mu \frac{d\tau_\mu}{dt} + \frac{d\tau^*_t}{dt}\right) \bullet \tau_\lambda. \tag{38}$$

The $\dot{q}$ arising because of the time derivatives must be replaced with $\dot{\pi}_u$ using equations (27). A more explicit expression for this quantity will be given below.

In the next section we will show that Lagrange's equations, when generalized to handle quasi-velocities and nonholonomic constraints are in fact these projected Newton's equations of motion (35). This generalization is usually attributed to Hamel (1904) in the mechanics literature. The author first thought that the somewhat more general treatment given below, that can handle inhomogeneous [$B^\alpha \neq 0$ in (26)] nonholonomic constraints, was new. Later, however, I discovered precisely these equations in a book by Chetaev (1989). Chetaev attributes the restricted form of the equations to Poincaré (1901) who thus published them before Hamel, but who did not apply them to any examples.

The amount of work done on the problem of making the Langrange method useful also for the case of nonholonomic constraints is large. Some of this work is reviewed by Passerello and Huston (1973) who also present a solution to the problem. Their solution corresponds to making the projection to the subspace of allowed directions in the tangent space on the Lagrange equations. It is, however, more algebraic in spirit than the present approach. These authors have also generalized their treatment to more general, nonlinear nonholonomic constraints (Huston and Passerello 1976).

7 The Lagrange-Hamel Equations

Equipped with the expression (30) we can now define the kinetic energy $T = \hat{M}\,\boldsymbol{V} \bullet \boldsymbol{V}/2$ as a function of q, $\dot{\pi}$, and t. (It should be noted that, even in the case of nonholonomic constraints, all n generalized speeds must be included in the derivations below.) We obtain expressions completely analogous to the expressions (14) and (15) to (17) above. These expressions are

Downloaded 03 May 2010 to 171.66.16.20. Redistribution subject to ASME license or copyright; see http://www.asme.org/terms/Terms_Use.cfm

$$T(q,\dot{\pi},t)=\frac{1}{2}\,g_{\alpha\beta}(q,t)\dot{\pi}^{\alpha}\pi^{\beta}+a_{\alpha}(q,t)\dot{\pi}^{\alpha}+b^{*}(q,t) \quad (39)$$

where we now have

$$g_{\alpha\beta}(q,t)\equiv\hat{\mathbf{M}}\tau_{\alpha}\bullet\tau_{\beta}=A^{a}_{\alpha}A^{b}_{\beta}\,g_{ab}, \quad (40)$$

$$a_{\alpha}(q,t)\equiv\hat{\mathbf{M}}\tau_{\alpha}\bullet\tau^{*}_{t}=A^{a}_{\alpha}(B^{b}g_{ab}+a_{a}), \quad (41)$$

$$b^{*}(q,t)\equiv\frac{1}{2}\,\hat{\mathbf{M}}\tau^{*}_{t}\bullet\tau^{*}_{t}=\frac{1}{2}\,B^{a}B^{b}g_{ab}+B^{a}a_{a}+b. \quad (42)$$

Even in the scleronomic case the second and third terms may appear if the B^{α} are nonzero.

We must now try to carry out the steps from Eq. (18) to the result, Eq. (25), to see what must be modified when we use noncoordinate velocities. We first of all find that Eq. (18) now gives

$$\frac{\partial V}{\partial\dot{\pi}^{\alpha}}=\tau_{\alpha}=A^{a}_{\alpha}\tau_{a}=A^{a}_{\alpha}\frac{\partial\boldsymbol{R}}{\partial\dot{q}^{a}}. \quad (43)$$

If we define the differential operator

$$\frac{\delta}{\partial\pi^{\alpha}}\equiv A^{a}_{\alpha}\frac{\partial}{\partial q^{a}}, \quad (44)$$

(the "partial derivative with respect to the quasi-coordinate π^{α}") we can rewrite this as

$$\frac{\partial V}{\partial\dot{\pi}^{\alpha}}=\tau_{\alpha}=\frac{\delta\boldsymbol{R}}{\partial\pi^{\alpha}}. \quad (45)$$

When this is used, Eq. (19) translates to

$$\frac{\partial T}{\partial\dot{\pi}^{\alpha}}=\boldsymbol{P}\bullet\frac{\delta\boldsymbol{R}}{\partial\pi^{\alpha}}=\boldsymbol{P}\bullet\tau_{\alpha}\equiv p_{\alpha}. \quad (46)$$

In Eq. (20) the only change needed is the replacement of qa with $\dot{\pi}^{\alpha}$ and the replacement of τ_{a} with τ_{α}. Eq. (21) now gets the form

$$\frac{\delta T}{\partial\pi^{\alpha}}=\boldsymbol{P}\bullet\frac{\delta V}{\partial\pi^{\alpha}} \quad (47)$$

so the difference Eq. (22) now becomes

$$\frac{d}{dt}\frac{\partial T}{\partial\dot{\pi}^{\alpha}}-\frac{\delta T}{\partial\pi^{\alpha}}=\frac{d\boldsymbol{P}}{dt}\bullet\tau_{\alpha}+\boldsymbol{P}\bullet\left(\frac{d\tau_{\alpha}}{dt}-\frac{\delta V}{\partial\pi^{\alpha}}\right). \quad (48)$$

The vector difference in the parenthesis, however, no longer cancels

$$\left(\frac{d\tau_{\alpha}}{dt}-\frac{\delta V}{\partial\pi^{\alpha}}\right)=\left(\frac{d}{dt}\frac{\delta}{\partial\pi^{\alpha}}-\frac{\delta}{\partial\pi^{\alpha}}\frac{d}{dt}\right)\boldsymbol{R}\equiv\left[\frac{d}{dt},\frac{\delta}{\partial\pi^{\alpha}}\right]\boldsymbol{R}\neq\boldsymbol{0} \quad (49)$$

since the differential operators no longer commute. The generalization of the Lagrange's Eq. (25) can now be written

$$\frac{d}{dt}\frac{\partial T}{\partial\dot{\pi}^{\alpha}}-\frac{\delta T}{\partial\pi^{\alpha}}+\boldsymbol{P}\bullet\left[\frac{\delta}{\partial\pi^{\alpha}},\frac{d}{dt}\right]\boldsymbol{R}=Q_{\alpha}. \quad (50)$$

To calculate the commutator it is convenient to first express the total time-derivative operator (36) in terms of $\dot{\pi}$ and $\delta/\partial\pi$ using Eqs. (27) and (44). Since it operates on functions of q and t only ($\boldsymbol{R}(q,t)$) we can skip the first term involving the $\dot{\pi}$ and use the expression

$$\frac{d}{dt}=(\dot{\pi}^{\alpha}-B^{\alpha})\frac{\delta}{\partial\pi^{\alpha}}+\frac{\partial}{\partial t}. \quad (51)$$

Use of this allows us to express the commutator term, Eq. (49), as follows:

$$\left[\frac{d}{dt},\frac{\delta}{\partial\pi^{\alpha}}\right]\boldsymbol{R}=\left((\dot{\pi}^{\beta}-B^{\beta})\left[\frac{\delta}{\partial\pi^{\beta}},\frac{\delta}{\partial\pi^{\alpha}}\right]+\frac{\delta B^{\beta}}{\partial\pi^{\alpha}}\frac{\delta}{\partial\pi^{\beta}}+\left[\frac{\partial}{\partial t},\frac{\delta}{\partial\pi^{\alpha}}\right]\right)\boldsymbol{R}. \quad (52)$$

If we now make the definitions

$$\gamma^{\gamma}_{\beta\alpha}(q,t)\equiv A^{a}_{\beta}\,A^{b}_{\alpha}\left(\frac{\partial A^{\gamma}_{b}}{\partial q^{a}}-\frac{\partial A^{\gamma}_{a}}{\partial q^{b}}\right) \quad (53)$$

$$f^{\gamma}_{\alpha}(q,t)\equiv-\frac{\delta B^{\gamma}}{\partial\pi^{\alpha}}-A^{\gamma}_{a}\frac{\partial A^{a}_{\alpha}}{\partial t}=-A^{a}_{\alpha}\left(\frac{\partial B^{\gamma}}{\partial q^{a}}-\frac{\partial A^{\gamma}_{a}}{\partial t}\right) \quad (54)$$

we can write this

$$\left[\frac{d}{dt},\frac{\delta}{\partial\pi^{\alpha}}\right]\boldsymbol{R}=\left(-\gamma^{\gamma}_{\beta\alpha}(\dot{\pi}^{\beta}-B^{\beta})\frac{\delta}{\partial\pi^{\gamma}}-f^{\gamma}_{\alpha}\frac{\delta}{\partial\pi^{\gamma}}\right)\boldsymbol{R}. \quad (55)$$

We now put

$$e^{\gamma}_{\alpha}(q,t)\equiv f^{\gamma}_{\alpha}(q,t)-\gamma^{\gamma}_{\beta\alpha}(q,t)\,B^{\beta}(q,t). \quad (56)$$

Using this, the results above and Eqs. (45) and (46) we now find that

$$\boldsymbol{P}\bullet\left[\frac{\delta}{\partial\pi^{\alpha}},\frac{d}{dt}\right]\boldsymbol{R}=\boldsymbol{P}\bullet(\gamma^{\gamma}_{\beta\alpha}\dot{\pi}^{\beta}+e^{\gamma}_{\alpha})\tau_{\gamma}=(\gamma^{\gamma}_{\beta\alpha}\dot{\pi}^{\beta}+e^{\gamma}_{\alpha})\frac{\partial T}{\partial\dot{\pi}^{\gamma}}. \quad (57)$$

Insertion of this into Eq. (50) now gives our final result for (Euler-) Lagrange's equations with noncoordinate velocities (generalized speeds), in the form

$$\frac{d}{dt}\frac{\partial T}{\partial\dot{\pi}^{\alpha}}+(\gamma^{\gamma}_{\beta\alpha}\dot{\pi}^{\beta}+e^{\gamma}_{\alpha})\frac{\partial T}{\partial\dot{\pi}^{\gamma}}-\frac{\delta T}{\partial\pi^{\alpha}}=Q_{\alpha}. \quad (58)$$

One notes that for the special case of a homogeneous ($B^{\alpha}=0$) time-independent ($A^{\alpha}_{a}=A^{\alpha}_{a}(q)$) transformation (26), which is the case treated by Poincaré (1901), Hamel (1904), and most previous literature with the exception of Chetaev (1989), the e^{γ}_{α} vanish. The quantities of Eq. (53), which can be considered as defined by the commutator

$$\left[\frac{\delta}{\partial\pi^{\beta}},\frac{\delta}{\partial\pi^{\alpha}}\right]=-\gamma^{\gamma}_{\beta\alpha}\frac{\delta}{\partial\pi^{\gamma}}, \quad (59)$$

are sometimes called the "object of anholonomicity" in the literature. One should note that Euler's dynamic equations for a rigid body with inertia tensor $\hat{\mathbf{J}}$, angular velocity vector $\boldsymbol{\omega}$, and moment of force $\mathbf{M}$, (in body-fixed axes)

$$\hat{\mathbf{J}}\dot{\boldsymbol{\omega}}+\boldsymbol{\omega}\times\hat{\mathbf{J}}\boldsymbol{\omega}=\mathbf{M}, \quad (60)$$

represent a special form of the Eqs. (58), but not of the conventional Lagrange Eqs. (25).

8 The Projected Equation of Motion

The amount of algebra involved in setting up the Eqs. (58) by differentiating the kinetic energy, as done above, is often considerable (see example below). The more direct approach based on directly projecting the equations of motion will usually be advantageous. Let us return to Eq. (38) for the projected momentum time derivative, ignoring nonholonomic constraints for the time being. By means of equation (51) it can be written in the form

$$\dot{\boldsymbol{P}}\bullet\tau_{\alpha}=\hat{\mathbf{M}}\left(\ddot{\pi}^{\beta}\tau_{\beta}+\dot{\pi}^{\beta}(\dot{\pi}^{\alpha}-B^{\alpha})\frac{\delta\tau_{\beta}}{\partial\pi^{\alpha}}+\dot{\pi}^{\beta}\frac{\partial\tau_{\beta}}{\partial t}+(\dot{\pi}^{\alpha}-B^{\alpha})\frac{\delta\tau^{*}_{t}}{\partial\pi^{\alpha}}+\frac{\partial\tau^{*}_{t}}{\partial t}\right)\bullet\tau_{\alpha}. \quad (61)$$

Some calculations show that this can be written

$$\boldsymbol{P}\bullet\tau_{\alpha}=g_{\alpha\beta}\ddot{\pi}^{\beta}+\Gamma_{\alpha,\beta\gamma}\dot{\pi}^{\beta}\dot{\pi}^{\gamma}+h_{\alpha\beta}\dot{\pi}^{\beta}+\phi_{\alpha}. \quad (62)$$

Here the quantities

$$\Gamma_{\alpha,\beta\gamma}\equiv\hat{\mathbf{M}}\tau_{\alpha}\bullet\frac{\delta\tau_{\beta}}{\partial\pi^{\gamma}}= \quad (63)$$

$$=\frac{1}{2}\left(\frac{\delta g_{\alpha\beta}}{\partial\pi^{\gamma}}+\frac{\delta g_{\alpha\gamma}}{\partial\pi^{\beta}}-\frac{\delta g_{\beta\gamma}}{\partial\pi^{\alpha}}\right)-\frac{1}{2}(\gamma_{\alpha\beta\gamma}+\gamma_{\alpha\gamma\beta}-\gamma_{\beta\gamma\alpha}), \quad (64)$$

Downloaded 03 May 2010 to 171.66.16.20. Redistribution subject to ASME license or copyright; see http://www.asme.org/terms/Terms_Use.cfm

(see Golab 1974, or Schouten 1954, for anholonomic tensor calculus) where

$$\gamma_{\alpha\beta\gamma} \equiv g_{\gamma\delta}\gamma^{\delta}_{\alpha\beta} \tag{65}$$

represent the connection on the manifold with metric $g_{\alpha\beta}$. We have also introduced

$$h_{\alpha\beta} \equiv -B^{\gamma}\Gamma_{\alpha,\,\beta\gamma} + \hat{\mathbf{M}}\tau_{\alpha} \bullet \left(\frac{\partial \tau_{\beta}}{\partial t} + \frac{\delta \tau_{t}^{*}}{\partial \pi^{\beta}}\right) \tag{66}$$

and

$$\phi_{\alpha} \equiv \hat{\mathbf{M}}\tau_{\alpha} \bullet \left(-B^{\beta}\frac{\delta \tau_{t}^{*}}{\partial \pi^{\beta}} + \frac{\partial \tau_{t}^{*}}{\partial t}\right). \tag{67}$$

If one now raises an index with the inverse metric tensor $g^{\alpha\beta}$ (i.e., $g^{\alpha\beta}g_{\beta\gamma} = \delta^{\alpha}_{\gamma}$) in the usual way, one gets the projected equations of motion in the form

$$\ddot{\pi}^{\alpha} + \Gamma^{\alpha}_{\beta\gamma}\dot{\pi}^{\beta}\dot{\pi}^{\gamma} + h^{\alpha}_{\beta}\dot{\pi}^{\beta} + \phi^{\alpha} = Q^{\alpha}. \tag{68}$$

Here Q^{α} are the components of the $3K$-dimensional force vector F that survive the projection; all constraint forces have disappeared. The last two terms on the left-hand side represent, if formally transferred to the right-hand side, inertial (or fictitious) forces that arise when the constraints are time dependent or when the nonholonomic constraints are inhomogeneous. If these two and Q^{α} are zero, the equation of motion (68) is the equation for a geodesic.

In case of nonholonomic constraints ($\dot{\pi}^{\alpha} = 0$, $\alpha = n_u + 1, \ldots, n$) one simply restricts the indices in Eqs. (68) to the allowed range $1, \ldots, n_u$. The motions will then take place on a lower dimensional point set (of dimension $n_u < n$).

One notes that the amount of algebraic computation required in finding Eq. (62), and thus the projected equations of motion, is much less than that needed to get the equations via the (Poincaré-) Hamel method (58). This is illustrated by an example in the next section. One should also mention that, the fact that the quantities in Eq. (63) are the nonholonomic Christoffel symbols (i.e., the connection) as given by the second line, formula (64), is computationally irrelevant. It is only by considering the formalism in the present, more abstract setting that the fact can be discovered.

9 Example: Ball Rolling on Turntable

Consider a ball of mass m, radius a, and radius of gyration k so that the moment of inertia for any axis through its center is $J = mk^2$. Let this ball roll on a horizontal table which rotates around a vertical axis with angular velocity Ω. Chose Cartesian coordinates with vertical z-axis, the plane of the table coinciding with the xy-plane, and the origin at the fixed point where the rotation axis goes through table. We then have $\boldsymbol{\Omega} = \Omega\mathbf{e}_z$ and the condition that the ball rolls without slipping can be written

$$\mathbf{v} + a\,\mathbf{e}_z \times \boldsymbol{\omega} = \boldsymbol{\Omega} \times \mathbf{r}. \tag{69}$$

Here

$$\mathbf{r} = x\mathbf{e}_x + y\mathbf{e}_y, \tag{70}$$

$$\mathbf{v} = \dot{x}\mathbf{e}_x + \dot{y}\mathbf{e}_y, \tag{71}$$

$$\boldsymbol{\omega} = \omega_x\mathbf{e}_x + \omega_y\mathbf{e}_y + \omega_z\mathbf{e}_z \tag{72}$$

represent the position vector of the contact point of the ball with the table, the velocity of the center of mass of the ball, and the angular velocity vector of the ball (in the space-fixed, inertial, system), respectively. The nonholonomic rolling constraints are now

$$\dot{x} - a\omega_y + \Omega_y = 0, \tag{73}$$

$$\dot{y} + a\omega_x - \Omega x = 0. \tag{74}$$

With standard Euler angles for the rotational degrees-of-freedom we have

$$\omega_x = \dot{\theta}\cos\psi + \dot{\varphi}\sin\theta\sin\psi, \tag{75}$$

$$\omega_y = \dot{\theta}\sin\psi - \dot{\varphi}\sin\theta\cos\psi, \tag{76}$$

$$\omega_z = \dot{\psi} + \dot{\varphi}\cos\theta. \tag{77}$$

We now introduce generalized coordinates as follows:

$$q^1 = \theta,\ q^2 = \varphi,\ q^3 = \psi,\ q^4 = x,\ q^5 = y. \tag{78}$$

Using these we introduce quasi-velocities according to formula (26) as follows:

$$\begin{aligned}
\dot{\pi}^1 &= \dot{q}^1\cos q^3 + \dot{q}^2\sin q^1\sin q^3 \\
\dot{\pi}^2 &= \dot{q}^1\sin q^3 - \dot{q}^2\sin q^1\cos q^3 \\
\dot{\pi}^3 &= \dot{q}^2\cos q^1 + \dot{q}^3 \\
\dot{\pi}^4 &= -\dot{q}^1 a\sin q^3 + \dot{q}^2 a\sin q^1\cos q^3 + \dot{q}^4 + \Omega q^5 \\
\dot{\pi}^5 &= \dot{q}^1 a\cos q^3 + \dot{q}^2 a\sin q^1\sin q^3 + \dot{q}^5 - \Omega q^4.
\end{aligned} \tag{79}$$

Our nonholonomic (rolling) constraints are now

$$\dot{\pi}^4 = 0,\ \dot{\pi}^5 = 0 \tag{80}$$

and the quantities represented by A^{α}_{a} and B^{α} can be summarized as follows:

A^{α}_{a}	$a=1$	$a=2$	$a=3$	$a=4$	$a=5$	B^{α}
$\alpha=1$	$\cos q^3$	$\sin q^1\sin q^3$	0	0	0	0
$\alpha=2$	$\sin q^3$	$-\sin q^1\cos q^3$	0	0	0	0
$\alpha=3$	0	$\cos q^1$	1	0	0	0
$\alpha=4$	$-a\sin q^3$	$a\sin q^1\cos q^3$	0	1	0	Ωq^5
$\alpha=5$	$a\cos q^3$	$a\sin q^1\sin q^3$	0	0	1	$-\Omega q^4$.

(81)

The corresponding inverse quantities appearing in $\dot{q}^a = A^{a}_{\alpha}\dot{\pi}^{\alpha} + B^{a}$ are then given by

A^{a}_{α}	$\alpha=1$	$\alpha=2$	$\alpha=3$	$\alpha=4$	$\alpha=5$	B^{a}
$a=1$	$\cos q^3$	$\sin q^3$	0	0	0	0
$a=2$	$\sin q^3/\sin q^1$	$-\cos q^3/\sin q^1$	0	0	0	0
$a=3$	$-\sin q^3\cot q^1$	$\cos q^3\cot q^1$	1	0	0	0
$a=4$	0	a	0	1	0	$-\Omega q^5$
$a=5$	$-a$	0	0	0	1	Ωq^4.

(82)

The kinetic energy in terms of the generalized velocities is

$$T(q,\dot{q}) = \frac{m}{2}\{k^2[(\dot{q}^1)^2 + (\dot{q}^2)^2 + (\dot{q}^3)^2 + 2\dot{q}^2\dot{q}^3\cos q^1] + [(\dot{q}^4)^2 + (\dot{q}^5)^2]\}. \tag{83}$$

When it is expressed in terms of the quasi-velocities it takes the form

$$T(q,\dot{\pi}) = \frac{m}{2}\{k^2[(\dot{\pi}^1)^2 + (\dot{\pi}^2)^2 + (\dot{\pi}^3)^2] + (a\dot{\pi}^2 + \dot{\pi}^4 - \Omega q^5)^2 + (-a\dot{\pi}^1 + \dot{\pi}^5 + \Omega q^4)^2\}. \tag{84}$$

(One may not take advantage of the nonholonomic constraints at this stage and put $\dot{\pi}^4 = \dot{\pi}^5 = 0$; this would not give the correct equations of motion.) We now wish to derive the Hamel Eqs. (58). We thus need the object of anholonomicity $\gamma^{\gamma}_{\beta\alpha}$, which may be calculated from formula (59). The result is that

$$\gamma^{1}_{23} = -\gamma^{1}_{32} = \gamma^{2}_{31} = -\gamma^{2}_{13} = \gamma^{3}_{12} = -\gamma^{3}_{21} = 1 \tag{85}$$

$$\gamma^{4}_{13} = -\gamma^{4}_{31} = \gamma^{5}_{23} = -\gamma^{5}_{32} = a \tag{86}$$

while all the rest are zero. The quantities e^{γ}_{α} must now be calculated from Eqs. (54) and and (56). The result of this is that

Downloaded 03 May 2010 to 171.66.16.20. Redistribution subject to ASME license or copyright; see http://www.asme.org/terms/Terms_Use.cfm

$$e_1^4 = e_2^5 = a\Omega,\ e_3^4 = -e_4^5 = -\Omega \tag{87}$$

while all the rest are zero. After much further differention and algebra, and use of the nonholonomic constraints once the differentiations have been done, one finds that the first three equations of motion are

$$(k^2 + a^2)\ddot{\pi}^1 - a\Omega(a\dot{\pi}^2 - \Omega q^5) - a\dot{\Omega}q^4 = 0, \tag{88}$$

$$(k^2 + a^2)\ddot{\pi}^2 + a\Omega(a\dot{\pi}^1 - \Omega q^4) - a\dot{\Omega}q^5 = 0, \tag{89}$$

$$k^2\ddot{\pi}^3 = 0. \tag{90}$$

One might note that the first two equations, after the initial algebra, consist of 13 terms each but nine of these add up to zero, so that the four terms given above remain. This is an indication that some unnecessary work may have been done.

If one assumes that the angular velocity $\dot{\Omega}$ of the turntable is constant, so that the terms containing $\dot{\Omega}$ in the equations of motion above vanish, one can solve the resulting equations in closed form (Neĭmark and Fufaev 1972). Use of the rolling constraints allows one to write them in a form that can be integrated once with respect to time. Elimination of the angular velocities, again using the rolling constraints, then gives

$$\dot{x} = -\Omega^* y + aC_2, \tag{91}$$

$$\dot{y} = +\Omega^* x - aC_1, \tag{92}$$

where

$$\Omega^* \equiv \frac{1}{1 + a^2/k^2}\,\Omega, \tag{93}$$

and where the integration constants are

$$C_1 = \omega_x(0) - a\Omega x(0)/(a^2 + k^2),\ C_2 = \omega_y(0) - a\Omega y(0)/(a^2 + k^2). \tag{94}$$

Formally these equations of motion are the same as for a particle in a constant magnetic field. The solutions are circles that are traversed with angular velocity Ω^* and which have centers and radii that depend on the initial conditions, but which are independent of the position on the turntable.

The above solution to this nontrivial and surprising problem may be contrasted with solutions based directly on Newton's equations for the center of mass motion and Euler's dynamic Eq. (60) for the rotational motion. Such solutions have been given in the literature several times. Two more recent ones are by Lévy-Leblond (1986) and by Gersten et al. (1991). The equations are

$$m\dot{\mathbf{v}} = \mathbf{F}, \tag{95}$$

$$J\dot{\boldsymbol{\omega}} = -a\mathbf{e}_z \times \mathbf{F}. \tag{96}$$

These together with the rolling constraint, Eq. (69), give the desired solution after some elementary manipulations that start with elimination of the friction force from the two equations above. One should note that this vectorial method is essentially the same as the projection method discussed above; Euler's dynamic equations arise in a first projection step that introduces the angular velocities, then the force is eliminated by a second projection.

It is often stated that the Lagrange and Kane methods eliminate "nonworking" constraint forces. In the present problem the (static) friction force does work (on the rotational degrees-of-freedom, due to the motion of the table surface) but it is nevertheless eliminated by the projection technique. Finally one should mention that the direct vectorial projection technique gives much shorter and simpler computations since one avoids the unnecessary detour of first calculating the scalar kinetic energy and then go back to higher dimensions again by differentiation. This fact has been stressed by Kane (1985).

Acknowledgments

I am grateful to Prof. Martin Lesser for inspiration, encouragement, and discussions. Thanks are also due to the Swedish Research Council for Engineering Sciences (TFR) and the Göran Gustafsson Foundation for financial support.

References

Chetaev, N., G., 1989, *Theoretical Mechanics*, Mir Publishers, Moscow and Springer-Verlag, Berlin (translated from the Russian 1987 edition).

Gersten, J., Soodak, H., and Tiersten, M. S., 1991, "Ball Moving on Stationary or Rotating Horizontal Surface," *American Journal of Physics*, Vol. 60, pp. 43-47.

Golab, S., 1974, *Tensor Calculus*, Elsevier, Amsterdam (translated form the 1970 Polish edition).

Hamel, G., 1904, "Die Lagrange-Eulersche Gleichungen der Mechanik," *Zeitschrift für Mathematik und Physik*, Vol. 50, pp. 1-57.

Huston, R. L., and Passerello, C. E., 1976, "Nonholonomic Systems with Nonlinear Constraint Equations," *International Journal of Non-Linear Mechanics*, Vol. 11, pp. 331-336.

Kane, T. R., 1961, "Dynamics of Nonholonomic Systems," ASME JOURNAL OF APPLIED MECHANICS, Vol. 28, pp. 574-578.

Kane, T. R., and Levinson, D. A., 1985, *Dynamics: Theory and Applications*, McGraw-Hill, New York.

Lesser, M., 1992, "A Geometrical Interpretation of Kane's Equations," *Proceedings of the Royal Society, London*, Vol. A436, pp. 69-87.

Lévy-Leblond, J. M., 1986, "Le Billard d'ANAIS," *European Journal of Physics*, Vol. 7, pp. 252-258.

Neĭmark, Ju. I., and Fufaev, N. A., 1972, *Dynamics of Nonholonomic Systems*, Volume Thirty-Three (Translations of Mathematical Monographs), American Mathematical Society, Providence, RI (translation of 1967 *Dinamika negolonomnysk sistem*, Moscow).

Pars, L. A., 1965, *A Treatise on Analytical Dynamics*, Heinemann, London.

Passerello, C. E., and Huston, R. L, 1973, "Another Look at Nonholonomic Systems," ASME JOURNAL OF APPLIED MECHANICS, Vol. 40, pp. 101-104.

Poincaré, H., 1901, "Sur une Forme Nouvelle des Équations de la Mécanique," *Comptes rendus de l'Acadèmie des Sciences*, Vol. 132, pp. 369-371.

Schouten, J.A., 1954, *Tensor Analysis for Physicists*, 2nd ed., Clarendon Press, Oxford, U.K.

Whittaker, E. T., 1927, *A Treatise on the Analytical Dynamics of Particles and Rigid Bodies*, Cambridge University Press, Cambridge, UK.

Downloaded 03 May 2010 to 171.66.16.20. Redistribution subject to ASME license or copyright; see http://www.asme.org/terms/Terms_Use.cfm

Plausibility of Structural Constitutive Equations for Isotropic Soft Tissues in Finite Static Deformations

Y. Lanir
Department of Biomedical Engineering,
Julius Silver Institute for Biomedical
Engineering Sciences
Technion—Israel Institute of Technology,
Haifa, 32000, Israel

Soft tissues are binary systems of fibers embedded in a fluid matrix. Their equilibrium response to external loading is the sum of the fibers' stress and the matrix osmotic pressure. The present study examines the conditions under which the elastic response of isotropic tissues, as modeled by structural constitutive equations, is physically plausible. The analysis shows that plausibility is ensured if the fibers' stretch force increases monotonically with the stretch and if the matrix osmotic pressure increases convexly with the concentration. Published data shows that both conditions prevail in soft tissues. It is thus concluded that structural modeling is compatible with physically plausible response.

1 Introduction

Constitutive equations must satisfy certain restrictions "such as to ensure physically reasonable behavior in any possible deformation" (Truesdell and Noll, 1965). Examples of simple restrictions are the following: Any material must not shear in an opposite direction to the shear stress, nor reduce its length when pulled.

A detailed discussion of the restrictions on the constitutive equations of elastic material is given by Truesdell and Noll (1965). One group of restrictions relates to plausibility in statics. The applications of these restrictions to soft biological tissues is the subject of the present study.

Soft tissues are in general nonlinear, anisotropic, and nonhomogeneous. Several classes of constitutive equations have been proposed for various tissues. One class is phenomenological models which attempt to reproduce measured responses by mathematical expressions. Most influential are the exponential models of Fung (e.g., Fung, 1972). A second class are constitutive equations derived from the tissue morphological structure. In this approach (e.g., Lanir, 1983), the strain energy function of an elastic tissue is considered as the sum of strain energies of its components (networks of fibers embedded in a fluid matrix). The bulk averaged stress is then derived from the total strain energy function following the formalism of hyperelasticity. A third class of constitutive models are "hybrid" ones which consider the tissues' local properties phenomenologically but relate to their nonhomogeneity in a structural manner following morphological observations (e.g., Humphrey and Yin, 1987; Hunter et al., 1988; Huyghe et al., 1991). Another class of models accounts for the binary nature of tissues, i.e., solid fibers embedded in a fluid-like matrix. The solid response is represented either by a phenomenological or by a structural constitutive equation.

No matter which constitutive law is used, the resulting response must be physically sound. Otherwise stress analysis based on inappropriate constitutive law may produce erroneous results. This problem may be especially acute in cases of nonhomogeneous multidimensional deformations where such errors are difficult to detect. In spite of the practical importance of this topic in stress analysis, it seems that hitherto no attention was paid to it.

The present study will focus on binary structural constitutive equations. They perform well descriptively (goodness of fit to data, e.g., Horowitz et al., 1988), as well as explanatorily (physical significance of the model parameters). The equilibrium response of a tissue to external loading is determined in this approach by three parameters: the structure of the tissue's fibrous network, the fibers' axial constitutive equations, and the matrix osmotic properties. The latter gives rise to swelling of soft tissues—under loading they swell or deswell until equilibrium with the loading is achieved (e.g., Maroudas and Urban, 1980). Consequently, soft tissues are inherently compressible. This assertion does not contradict the frequently used assumption of incompressibility under dynamic loadings, where the loading time constant is much shorter than the characteristic time constant of fluid filtration (which gives rise to volume changes).

In the present study, the plausibility of binary structural constitutive equations for isotropic tissues in static deformations will be examined. The study will focus on the conse-

Contributed by the Applied Mechanics Division of THE AMERICAN SOCIETY OF MECHANICAL ENGINEERS for publication in the ASME JOURNAL OF APPLIED MECHANICS.

Discussion on this paper should be addressed to the Technical Editor, Professor Lewis T. Wheeler, Department of Mechanical Engineering, University of Houston, Houston, TX 77204-4792, and will be accepted until four months after final publication of the paper itself in the ASME JOURNAL OF APPLIED MECHANICS.

Manuscript received by the ASME Applied Mechanics Division, June 19, 1992; final revision, Apr. 13, 1993. Associate Technical Editor: R. Abeyaratne.

Copyright © 1994 by ASME
Downloaded 03 May 2010 to 171.66.16.20. Redistribution subject to ASME license or copyright; see http://www.asme.org/terms/Terms_Use.cfm

quences of general restrictions on the uniaxial constitutive laws of tissue fibers and on the matrix swelling properties. The possible restrictions on the structure of the fibrous network in anisotropic tissues are a subject of a separate study.

2 Tissue as Binary Structures

The thermodynamics and mechanics of binary systems have been studied by several authors (e.g., Bowen, 1980; Silberberg, 1982). These studies form the basis for the present analysis.

From the mechanical point of view, soft tissues consist of networks of fibers (the solid) embedded in a fluid-like matrix (the ground substance). The fluid matrix contains large macromolecules of proteoglycans which contain negatively charged groups in their structure (Maroudas, 1990). This polyelectrolyte nature of the tissue space results in swelling potential represented by "osmotic pressure." The tissue will swell by increasing its water content. Swelling is accompanied by stretching of the tissue fibers and a concomitant increase of the fluid hydrostatic pressure required for mechanical balance. Equilibrium is reached when the fluid osmotic pressure (representing the concentration component of its chemical potential) is balanced by the fluid hydrostatic pressure, while the latter is balanced mechanically by the stress in the tissue fibers.

The mechanical interaction between two adjacent material points in binary systems under static equilibrium consists of the combined contributions of the fibers and that of the fluid pressure (Appendix A). Consequently, it is the total stress $\mathbf{t}$ which must be considered in examining the plausibility of elastic response. It is given by

$$\mathbf{t} = \mathbf{t}_f(\mathbf{E}) - P\mathbf{I} \tag{1}$$

where $\mathbf{t}_f(\mathbf{E})$ is the stress due to the bulk-averaged effect of the tension in the tissue fibers (the solid stress), $\mathbf{E}$ is the overall Green-Lagrange strain tensor, P is the pore fluid hydrostatic pressure, and $\mathbf{I}$ is the unit matrix. In view of Eq. (A9) the expression for the total stress at equilibrium can be written as

$$\mathbf{t}(\mathbf{E}, c) = \mathbf{t}_f(\mathbf{E}) - \Psi(c)\mathbf{I}. \tag{2}$$

The quantity on the R.H.S. of Eq. (2) with a negative sign was termed "swelling stress" (Lanir, 1987) since it expresses the net tissue swelling potential. Equation (2) indicates then that two distinct constitutive laws must be examined: the stress-strain relationship for the fibrous network $\mathbf{t}_f(\mathbf{E})$ and the osmotic pressure-concentration law $\Psi(c)$.

2.1 The Tissue Osmotic Pressure. A few factors contribute to the tissue osmotic pressure (Maroudas, 1990). The major contribution arises from the Donnan effect: The negatively charged groups of the proteoglycans are surrounded by positive cations which maintain electroneutrality. The elevated cationic concentration in the tissue space results in reduced chemical potential of the tissue water and a tendency to increase it by swelling.

The Donnan osmotic pressure is compounded by an entropic component (Maroudas, 1990) due to excluded volume: A volume occupied by a proteoglycan macromolecule is sterically excluded for all other molecules and for the solution itself. This results in increased osmotic pressure and swelling potential.

Another contribution to swelling of tissues may arise from the mutual expulsion of the proteoglycan negative groups (Lai et al., 1991).

Although there have been attempts to evaluate the osmotic pressure of tissues on the basis of theoretical considerations, complete formulation is not yet available for all components, and an experimental approach is required.

2.2 Structural Constitutive Equations. The structural approach towards constitutive formulation of tissues (Lanir, 1983) considers a representative elementary volume which is large enough to be statistically representative of its vicinity yet small enough compared to the whole tissue so that its stress and strain can be considered as homogeneous. The representative elementary volume contains a fixed mass of fibers and deforms with it. The volume of fluid in the representative elementary volume changes with the deformation.

The fibrous network of soft tissues consists of a large number of fibers oriented in different directions. Although some tissues have predominantly uniaxial (tendon—Viidik, 1972) or biaxial (mesentery—Chu et al., 1972) fibrous networks, they are in fact three-dimensional, a requisite for structural integrity. It is, nevertheless, convenient to carry out the formulation in two steps: consider first a uniaxial ensemble of fibers and then the three-dimensional fibers' network.

2.2.1 Uniaxial Fiber Ensemble: It consists of a large number of long thin fibers aligned parallel to each other. The fibers are, however, undulated (wavy) in a nonuniform manner. Their stiffness when wavy is negligibly small due to their thinness, (i.e., high ratio of length to diameter). For the same reason they have negligible compressive stiffness. As the whole ensemble is stretched, a gradually increasing number of wavy fibers become straight and load-bearing, thus increasing the ensemble stiffness (Viidik, 1972). Mechanically, this gradual recruitment results in increasing stiffness with strain. The process can be described as follows: The strain energy function of a single fiber when straight (w^*) is a function of its true strain e_t, or alternatively, a function of its true stretch λ_t where $e_t = (\lambda_t^2 - 1)/2$. Under contraction ($e_t \leq 0$), the fiber is undulated and transmits no load. A wavy fiber is characterized by the stretch λs (or strain $e_s\,[=(\lambda_s^2 - 1)/2]$) at which it becomes straight. Hence at an overall tissue stretch λ (or strain $e[=(\lambda^2 - 1)/2]$), the corresponding true values for the fiber are

$$\lambda_t = \lambda/\lambda_s; \quad e_t = (e - e_s)/(1 + 2e_s). \tag{3}$$

The waviness distribution of the entire ensemble of unidirectional fibers is represented by a density distribution $D(e_s)$ such that in the range of strain between e_s and $e_s + de_s$, the fraction of all fibers in the ensemble which become straight is $D(e_s)\cdot de_s$. The strain energy function of this subensemble is thus $D(e_s)w^*(e_t)\cdot de_s$. Hence the strain energy of the entire fiber ensemble $w(e)$ is given by the sum of strain energies of all fibers, i.e.,

$$w(e) = \int_0^e D(x)\cdot w^*(e_t)dx. \tag{4}$$

In elastic fibers the uniaxial second Piola-Kirchhoff stress of the ensemble is derived from $w(e)$ by (using Eq. (3))

$$s(e) = dw/de = \int_0^e D(x)\cdot dw^*/de_t\cdot \partial e_t/\partial e\cdot dx$$

$$= \int_0^e D(x)[1 + 2x]^{-1}s^*(e_t)dx \tag{5}$$

where $s^*(e_t) = dw^*/de_t$, and $s^*(o) = 0$.

Equation (4) describes the process of increasing recruitment of fibers with strain. This gives rise to the typical exponential type stress-strain law (Fung, 1972) as shown analytically by Lanir (1980), and experimentally by Viidik (1972).

2.2.2 Network of Tissues' Fibers: Tissues' fibers are arranged in various directions. Their orientation distribution determines the tissue anisotropy. Random orientation gives rise to isotropic response. The orientation distribution can be prescribed by a density distribution function $R(\phi, \theta)$ where the arguments are the two polar angles. Hence $R(\phi, \theta)\cdot d\phi\cdot d\theta$ is the fraction of fibers oriented between (ϕ, θ) and $(\phi + d\phi, \theta + d\theta)$. A unit vector in direction (ϕ, θ) is given by

$$\mathbf{N} = \sin\phi\cos\theta\cdot\mathbf{1}_1 + \sin\phi\sin\theta\cdot\mathbf{1}_2 + \cos\phi\cdot\mathbf{1}_3, \tag{6}$$

Downloaded 03 May 2010 to 171.66.16.20. Redistribution subject to ASME license or copyright; see http://www.asme.org/terms/Terms_Use.cfm

$\mathbf{1}_i$ being unit base vectors in a Cartesian coordinate system.

Since the subsequent development for isotropic and general anisotropic tissues is identical except for the specific form of $R(\phi, \theta)$, the analysis will consider the general anisotropic case and later use the isotropic constraint when required.

Due to the high degree of interconnectivity between fibers, it is reasonable to consider the deformation as affine, i.e., each element deforms as if it were a part of a continuum. Under this assumption the uniaxial strain along each direction $\mathbf{N}$ in the tissue space is given by

$$e = \mathbf{N}^T \mathbf{E} \mathbf{N} \quad (2\mathbf{E} = \mathbf{F}^T\mathbf{F} - \mathbf{I}) \tag{7}$$

where $\mathbf{E}$ is the Green-Lagrange strain tensor and $\mathbf{F}$ is the deformation gradient tensor. The strain energy function of the whole fibrous network is considered to be the sum of the strain energies of all uniaxial ensembles ($w(e)$ – Eq. (4)) so that

$$W_f(\mathbf{E}) = \phi_f^0 \int_\phi \int_\theta R(\phi, \theta) w(e) d\phi d\theta \tag{8}$$

where ϕ_f^0 is the volume fraction occupied by the fibers in the reference configuration. The second Piola-Kirchhoff fibers stress ($\mathbf{S}_f$) is related to $W_f(\mathbf{E})$ by $\mathbf{S}_f = \partial W_f / \partial \mathbf{E}$. By using Eqs. (5), (7), and (8) it follows that

$$\mathbf{S}_f(\mathbf{E}) = \phi_f^0 \int_\phi \int_\theta R(\phi, \theta) \cdot dw/de \cdot de/d\mathbf{E}\, d\phi d\theta$$

$$= \phi_f^0 \int_\phi \int_\theta R(\phi, \theta) s(e)\ [\mathbf{N} \otimes \mathbf{N}] d\phi d\theta \tag{9}$$

where $\otimes$ stands for external multiplication so that $[\mathbf{N} \otimes \mathbf{N}]_{ij} = N_i N_j$ where N_i are given by Eq. (6). From Eq. (7) and the constraint $s(o) = 0$ it follows that $\mathbf{S}_f(\mathbf{O}) = \mathbf{O}$.

In cases where there are more than one type of fibers (e.g., skin which has collagen and elastin), their contribution to the tissue SEF is added up, and the fibers' stress is thus given by:

$$\mathbf{S}_f(\mathbf{E}) = \sum_k \phi_{fk}^o \int_\phi \int_\theta R_k(\phi, \theta) s_k(e)\ [\mathbf{N} \otimes \mathbf{N}] d\phi d\theta \tag{10}$$

where the subscript k indicates a property of the type k fibers.

The Cauchy fiber-stress $\mathbf{t}_f$ of Eq. (1) is related to the second Piola-Kirchhoff stress $\mathbf{S}_f$ by

$$\mathbf{t}_f = J^{-1} \mathbf{F}\, \mathbf{S}_f \mathbf{F}^T \quad J = \det(\mathbf{F}) \tag{11}$$

where J is the deformed to reference volume ratio. Hence the total Cauchy stress $\mathbf{t}$ in Eq. (2) is given by

$$\mathbf{t}(\mathbf{E}, c) = J^{-1} \mathbf{F}\, \mathbf{S}_f(\mathbf{E}) \mathbf{F}^T - \Psi(c) \mathbf{I} \tag{12}$$

where $\mathbf{S}_f(\mathbf{E})$ is given by Eqs. (9) or (10) and $\Psi(c)$ is the concentration-dependent tissue osmotic pressure. The total second Piola-Kirchhoff stress $\mathbf{S}$ is given by

$$\mathbf{S}(\mathbf{E}, c) = \mathbf{S}_f(\mathbf{E}) - J\, \Psi(c) \mathbf{C}^{-1} \quad \mathbf{C} = \mathbf{F}^T\mathbf{F} = 2\mathbf{E} + \mathbf{I} \tag{13}$$

where $\mathbf{C}$ is the right Cauchy-Green deformation tensor. An overall expression for the stress-strain relation in swelling tissue can now be written by using Eqs. (6) and (13):

$$\mathbf{S}(\mathbf{E}, c) = \phi_f^o \int_\phi \int_\theta R(\phi, \theta) s(e) \begin{bmatrix} \sin^2\phi \cos^2\theta & \sin^2\phi \sin\theta \cos\theta & \sin\phi \cos\phi \cos\theta \\ & \sin^2\phi \sin^2\theta & \sin\phi \cos\phi \sin\theta \\ \text{SYM} & & \cos^2\phi \end{bmatrix} d\phi d\theta - J\Psi(c)\mathbf{C}^{-1}. \tag{14}$$

On the elastic constitutive equations which ensure physically reasonable response, can be related to the principal strains and principal stresses. Truesdell and Noll (1965) show that the use of principal forces, rather than principal stresses, lead to simpler and more plausible forms of the restrictions. A summarized list of the restrictions for isotropic compressible elastic materials as prescribed by Truesdell and Noll (1965) is given in the following:

(a) The P-C ("Pressure-Compression") inequality: This inequality requires that in mean, each principal force is tension or compression accordingly as the corresponding principal stretch is a contraction or elongation. Hence

$$\sum_i T_i(\lambda_i - 1) > 0 \quad i = 1, 2, 3, \tag{15}$$

if not all $\lambda_i = 1.0$. In Eq. (15) λ_i and T_i are the principal stretches and principal forces, respectively. Equation (15) is a generalization of the condition that the volume decreases under hydrostatic pressure and vice versa. The latter can be reduced from Eq. (15) by setting $\lambda_1 = \lambda_2 = \lambda_3 = \lambda$ and $T_1 = T_2 = T_3 = T$.

(b) The *T-E* ("Tension-Extension") inequalities require that tensile forces must increase when a cube is lengthened in one principal direction while other dimensions are constant, and vice versa. Hence

$$(T_i^* - T_i)(\lambda_i^* - \lambda_i) > 0, \tag{16}$$

provided $\lambda_j^* = \lambda_j$ if $i \neq j$, where λ and T are the stretch ratio and principal force in one configuration while λ^*, T^* are the corresponding terms of another configuration. Equation (16) imposes a restriction on the response function $T_i^* = T(\lambda_1^*, \lambda_2^*, \lambda_3^*)$.

(c) The IFS ("Invertibility of Force-Stretch") condition requires that the force-stretch relationship $T_i = T_i(\lambda_1, \lambda_2, \lambda_3)$ be uniquely invertible. This is fulfilled when

$$\det \|J_{ij}\| \neq 0, \quad J_{ij} \equiv \partial T_i / \partial \lambda_j. \tag{17}$$

(d) The E-T ("Extension-Tension") inequalities,

$$(T_i^* - T_i)(\lambda_i^* - \lambda_i) > 0, \tag{18}$$

if $T_j^* = T_j$ for $j \neq i$, i.e., a cube will lengthen in the direction of increased principal forces when other principal forces are constant, and vice versa. Equation (18) imposes a restriction on the response function $\lambda_i^* = \lambda(T_1^*, T_2^*, T_3^*)$. In general it is not implied by restriction (16) and vice versa.

(e) The O-F ("Ordered-Forces") inequalities

$$(T_i - T_j)(\lambda_i - \lambda_j) > 0 \tag{19}$$

if $\lambda_i \neq \lambda_j$. This restriction states that greater stretch must occur in the direction of greater force.

In Truesdall and Noll (1965) it is shown that restrictions *a* to *e* above are satisfied when $\|J_{ij}\|$ in Eq. (17) is non-negative, i.e.,

$$\sum_{ij} J_{ij} w_i w_j \geq 0 \quad i, j = 1, 2, 3 \tag{20}$$

3 Plausibility in Static Deformations

3.1 Criteria of Plausibility. Since in isotropic materials the principal axes of strain and stress coincide, the restrictions for arbitrary numbers w_k. Equation (20) is termed in Truesdall and Noll (1965) as the GCN_o condition.

The following further restrictions must be satisfied in addition to the GCN_o condition:

Downloaded 03 May 2010 to 171.66.16.20. Redistribution subject to ASME license or copyright; see http://www.asme.org/terms/Terms_Use.cfm

(f) The B-E ("Baker-Ericksen") inequalities require that greater principal Cauchy stress occurs in the direction of the greater principal stretch. Hence

$$(t_i - t_j)(\lambda_i - \lambda_j) > 0 \tag{21}$$

if $\lambda_i \neq \lambda_j$. In spite of its similar form to the O-F restriction (Eq. (20)), restriction O-F does not imply restriction B-E, and vice versa.

3.2 Principal Stresses and Forces. The criteria for plausibility are expressed in terms of principal forces or principal Cauchy stresses. The constitutive equation (Section 2) is expressed in terms of second Piola-Kirchhoff stress. Before commencing with examination of these criteria it is necessary to establish the relationship between these quantities for general deformations of isotropic materials.

By the polar decomposition theorem, the deformation gradient $\mathbf{F}$ can be decomposed into two alternate forms:

$$\mathbf{F} = \mathbf{RU} = \mathbf{VR} \tag{22}$$

where $\mathbf{R}$ is orthogonal matrix and $\mathbf{U}$ and $\mathbf{V}$ are symmetric and positive definite ones. The matrices $\mathbf{U}$ and $\mathbf{V}$ have the same principal values $\lambda_i (i = 1, 2, 3)$ which are the stretches.

The first Piola-Kirchhoff stress ($\mathbf{P}$) is related to Cauchy ($\mathbf{t}$) and to the second Piola-Kirchhoff stress ($\mathbf{S}$) by

$$\mathbf{P} = J\mathbf{t}(\mathbf{F}^{-1})^T = \mathbf{F}\,\mathbf{S} \tag{23}$$

which, by Eq. (22) using the equalities $(\mathbf{V}^{-1})^T = \mathbf{V}^{-1}$, $(\mathbf{R}^{-1})^T = \mathbf{R}$, can be written as

$$\mathbf{P} = (J\mathbf{t}\mathbf{V}^{-1})\mathbf{R} = \mathbf{R}(\mathbf{US}) \tag{24}$$

where $J = \det(\mathbf{F}) = \det(\mathbf{V}) = \det(\mathbf{U}) = \lambda_1 \lambda_2 \lambda_3$.

It was shown (Truesdell and Noll, 1965, Sect. 48) that in isotropic materials the principal values of $(J\mathbf{t}\mathbf{V}^{-1})$ in Eq. (24) are the principal forces $T_i (i = 1, 2, 3)$ given by

$$T_i = J\, t_i \lambda_i^{-1} \quad i = 1, 2, 3 \text{ (not summed)} \tag{25}$$

where t_i are the principal values to $\mathbf{t}$.

It can be shown (Appendix B) that in isotropic materials T_i are also the principal values of ($\mathbf{U}$ $\mathbf{S}$) and are thus given by

$$T_i = \lambda_i S_i \quad i = 1, 2, 3 \text{ (not summed)} \tag{26}$$

where S_i are the principal values of λ_i and $\mathbf{S}$.

4 Condition of Plausibility in Structural Models

The form taken by the general restrictions in the framework of the structural constitutive laws will be developed first for an ensemble of parallel fibers, and then for a three-dimensional fibers network of tissues. The study of parallel fiber ensemble relates directly to the fibers' axial properties. The three-dimensional analysis allows to consider restriction on the osmotic properties.

4.1 The GCN_o Restriction in a Unidirectional Fiber Ensemble. The discussion here will be restricted to isotropic fibers (where GCN_o applies) loaded solely in the fibers direction, say direction 1. Thus the only nonvanishing stress component is S_{11} which is also the principal stress S_1, and the only nonzero principal force (Eq. (26)) is T_1. Hence, the only nonvanishing components of J_{ij} in Eq. (17) is J_{11} and the GCN_o restriction (Eq. (20)) reduces to

$$J_{11} w_1^2 \geq 0 \quad J_{ij} = 0 \quad i \neq 1, j \neq 1. \tag{27}$$

The stress S_1 is given by $s(e)$ in Eq. (5). Now since $w_1^2 > 0$ when $w_1 \neq 0$, the GCN_o restriction reduces further to $J_{11} \geq 0$. From the definition of J_{ij} (Eq. (17)) and from Eq. (26) it follows that the GCN_o condition in this case reduces to

$$J_{11} = dT_1/d\lambda \geq 0, \tag{28}$$

which says that in a unidirectional ensemble, the stretching force T must be increasing with the stretch ratio λ. To check the consequences of this condition on the intrinsic properties of the fiber, it is convenient to express the ensemble uniaxial stress s in terms of the stretch ratio λ rather than of the strain e. Denoting this by $\hat{s}(\lambda)$, we have, from Eq. (5),

$$\hat{s}(\lambda) = \int_{1.0}^{\lambda} \frac{\hat{D}(y)}{y^2}\, \hat{s}^*(\lambda_t)\, dy; \quad \lambda_t = \lambda/\lambda_s, \tag{29}$$

where λ_s is the straightening stretch ratio ($\lambda_s^2 = 1 + 2e_s$), $\hat{D}(y)$ is the waviness distribution in terms of λ_s (or y in the integrand), and λ_t and $\hat{s}^*(\lambda_t)$ are the true stretch ratio (Eq. (3)) and the axial stress of a wavy fiber when stretched, respectively. From Eqs. (26) and (29) it follows that

$$T_1^f(\lambda) = \lambda \hat{s}(\lambda) = \int_{1.0}^{\lambda} \frac{\hat{D}(y)}{y}\, T^*(\lambda_t)\, dy \tag{30}$$

where T_1^f and T^* ($= \lambda_t \hat{s}^*$) are the principal forces of the ensemble and of a single stretched fiber, respectively, and $T^*(1) = T_1^f = 0$. By introducing Eq. (30) in Eq. (28) while using Eq. $(29)_2$ in the chain differentiation, it follows that the GCN_o restriction reduces to

$$J_{11} = dT_1^f/d\lambda = \int_{1.0}^{\lambda} \frac{\hat{D}(y)}{y^2}\, [dT^*(\lambda_t)/d\lambda_t]\, dy \geq 0. \tag{31}$$

Since $\hat{D}(y)$ and y^2 are always positive, it follows that if

$$dT^*(\lambda_t)/d\lambda_t \geq 0, \tag{32}$$

then the GCN_o condition is satisfied. Equation (32) says that the stretching force in a straight fiber must increase with the true fiber's stretch ratio.

4.2 The B-E Restriction in a Unidirectional Fiber Ensemble. The B-E restriction for isotropic elastic materials (Eq. (21)) relates to the Cauchy stresses and states that

$$(t_i - t_j)(\lambda_i - \lambda_j) > 0 \quad \lambda_i \neq \lambda_j. \tag{33}$$

In a uniaxial stretch of a fiber ensemble in direction 1, $\lambda_1 > 0$, $t_1 > 0$ while $t_2 = t_3 = 0$. Hence the B-E restriction reduces in this case to

$$\lambda_1 > \lambda_2, \lambda_3 \tag{34}$$

which says that when stretched, the fibers ensemble cannot expand transversely more than it elongates in the stretching direction.

4.3 The GCN_o Restriction in Tissues. The plausibility restrictions in tissues must consider the contributions of both their three-dimensional fibers network and of their matrix osmotic properties. The analysis starts with the stress due to the fibers. From Eq. (9) the principal value of the fiber stress $\mathbf{S}_f$ is given by

$$S_f^i = \phi_f^0 \int_{\phi} \int_{\theta} R(\phi, \theta) s(e) N_i^2 d\phi d\theta \quad i = 1, 2, 3 \tag{35}$$

where N_i are the components of $\mathbf{N}$ (Eq. (6)) in the principal coordinate system. By using Eq. (13) in Eq. (26) one gets for the principal forces

$$T_i = \phi_f^0 \lambda_i \int_{\phi} \int_{\theta} R(\phi, \theta) s(e) N_i^2 d\phi d\theta - J\Psi(c)/\lambda_i. \tag{36}$$

From here on, unless otherwise indicated, repeated indices are not summed. For the sake of consistency, the uniaxial stress-strain law $s(e)$ will be replaced by a corresponding stress-stretch $\hat{s}(\lambda)$ relationship (Eq. (29)) λ being the stretch along the fiber direction ($\mathbf{N}$) given by

Downloaded 03 May 2010 to 171.66.16.20. Redistribution subject to ASME license or copyright; see http://www.asme.org/terms/Terms_Use.cfm

$$\lambda^2 = \sum_{i=1}^{3} \lambda_i^2 N_i^2 = (1 + 2e). \tag{37}$$

In addition, the osmotic constitutive law $\Psi(c)$ will be replaced by a corresponding law $\hat{\Psi}(J)$ with the volume ratio J as the argument. This is permissible since the concentration of the fixed charges in the tissue changes due to swelling/deswelling, and is uniquely related to changes in the volume ratio J (Appendix C).

Following this, Eq. (36) can be written in an alternative form as

$$T_i = \phi_f^0 \cdot \int_\phi \int_\theta R(\phi, \theta) \cdot \hat{s}(\lambda) \lambda_i N_i^2 d\phi d\theta - J\hat{\Psi}(J)/\lambda_i. \tag{38}$$

In Appendix D it is shown that from Eq. (38) the GCN_o restriction (Eq. (20)) reduces in the case of isotropic tissues to

$$\hat{s}(\lambda) \geq 0, \quad d\hat{s}(\lambda)/d\lambda \geq 0 \tag{39}$$

for the fiber ensembles, while the condition for the osmotic pressure $\Psi(J)$ is

$$|\hat{\Psi}/J| < |d\hat{\Psi}(J)/dJ|. \tag{40}$$

Equation (39) can be further reduced to a form relating to the intrinsic properties of the fibers. This is carried out by using Eq. (29) and following a derivation similar to the one leading to Eq. (32). The resulting expressions in terms of single fiber properties are

$$\hat{s}^*(\lambda_t) \geq 0, \quad d\hat{s}^*(\lambda_t)/d\lambda_t \geq 0, \tag{41}$$

i.e., when the inequalities (Eq. (41)) hold, the GCN_o restriction for the fibers is satisfied.

4.4 The B-E Restriction in Tissues. The B-E inequalities (Eq. (21)) relate to principal Cauchy stresses (t_i) and principal stretches λ_i ($i = 1, 2, 3$). The expression for t_i in terms of the second Piola-Kirchhoff stress components (S_i) is derived from Eq. (12) resulting in

$$t_i = J^{-1}(S_f^i)\lambda_i - \Psi(c) \quad i = 1, 2, 3. \tag{42}$$

Here again, repeated indices are not summed. Since the material is isotropic, the specific choice of $i = 1$, $j = 2$ in Eq. (21) can be made without loss of generality. Consider the case of $\lambda_1 - \lambda_2 > 0$. The B-E inequalities (Eq. (21)) require that in this case $t_1 - t_2 > 0$. From Eqs. (2), (9), and (14), while replacing $s(e)$ by $\hat{s}(\lambda)$, it follows that

$$t_1 - t_2 = (\phi_f^o/J) \int_\phi \int_\theta \hat{s}(\lambda) R(\phi, \theta) [\lambda_1^2 N_1^2 - \lambda_2^2 N_2^2] d\phi d\theta > 0 \tag{43}$$

where $N_1 = \sin\theta \cos\theta$ and $N_2 = \sin\phi \sin\theta$. The osmotic term does not appear in Eq. (43); it dropped out in the subtraction of $t_1 - t_2$. This means that the osmotic properties in isotropic tissues are not restricted by the B-E condition.

5 Examination of Plausibility

Collagen and elastin fibers are the major fibrous constituents of soft tissue. In the following, their compatibility with the plausibility conditions will be examined.

Viidik (1972) has shown that in tendon of the rat tail there is a process of gradual straightening (reduction in undulation) and a subsequent recruitment with stretch of the parallel ensemble of collagen fibers. This process is accompanied by an increase in stiffness with stretch. The resulting behavior is of an exponential type. Beyond a certain stretch, all fibers are straight and the load-stretch curve becomes straight or slightly convex, indicating that stretched fibers have a nearly constant stiffness. These observations show that the GCN_o condition for a unidirectional fiber ensemble ($dT/d\lambda \geq 0$—Eq. (28)) is satisfied, and that the stronger restriction (Eq. (32)) for stretched fibers is satisfied as well, i.e., $dT^*/d\lambda_t \geq 0$.

Carton et al. (1962) showed that in elastin fibers the force-stretch relationship is exponentially convex. Hence these fibers satisfy the GCN_o restriction for a unidirectional ensemble in both its forms (Eqs. (28) and (32)).

The B-E restriction for a unidirectional ensemble requires (Eq. (34)) that when stretched it will not expand transversely more than it elongates in the stretching direction. In reality, biological fibers contract transversely when stretched (e.g., collagen fiber ensemble in rat tail tendon—Lanir et al., 1988), so that the B-E restriction is satisfied.

In tissues with three-dimensional fiber structure, the GCN_o restriction is reduced to condition (41) for the fibers and Eq. (40) for the osmotic pressure term. The first inequality in Eq. (41) holds since the long and thin fibers can resist only tensile forces. The second inequality (i.e., $d\hat{s}^*/d\lambda_t \geq 0$) seems to hold as well in light of experimental evidence from collagen and elastin fibers (e.g., Viidik, 1972; Carton et al., 1962) that the force-stretch curve is either convex or at least linear but not concave.

The reduced GCN_o condition for the osmotic pressure Eq. (40) can be written in a more convenient form. Since the osmotic pressure is always positive ($\hat{\Psi} > 0$) and decreases when the tissue swells (when J increases) due to decreased concentration of the negative groups (i.e., $d\hat{\Psi}/dJ < 0$), then it follows that $|\hat{\Psi}/J| = \hat{\Psi}/J$ and $|d\hat{\Psi}/dJ| = -d\hat{\Psi}/dJ$, so that Eq. (40) can be written as

$$\hat{\Psi}/J < -d\hat{\Psi}/dJ. \tag{44}$$

By transforming $\hat{\Psi}(J)$ back to concentration dependence $\Psi(c)$ (using Eq. (C5)) one obtains another form of Eq. (44), namely,

$$\Psi/(1 + c \cdot K_2/K_1) < c(d\Psi/dc). \tag{45}$$

Since $c \cdot K_2/K_1 \geq 0$ for any concentration c, then Eq. (45) holds if

$$\Psi/c < d\Psi/dc. \tag{46}$$

This is the final form of the GCN_o condition for the osmotic pressure.

Experimental results (e.g., Maroudas and Urban, 1980; Urban et al., 1979) show that the osmotic pressure is convexly related to the concentration of negative charged groups of the PG (the Fixed Charge Density—FCD). The FCD is proportional to the concentration c, hence the $\Psi(c)$ relationship is convex and the following relationship holds:

$$\Psi(o) = 0; \quad \Psi(c) > 0; \quad d\Psi/dc > 0; \quad d^2\Psi/dc^2 > 0. \tag{47}$$

The experimental observations expressed in Eq. (47) guarantee that inequality Eq. (46) holds. To prove this claim, recall the Mean Value Theorem. It states that if $f(x)$ is continuous in $[a, b]$ and differentiable in (a, b), then there exists a point ζ in (a, b) such that

$$[f(b) - f(a)]/(b - a) = f'(\zeta). \tag{48}$$

Now set $a = 0$, $b = c$ so that $\Psi(a) = 0$ $\Psi(b) = \Psi(c) = \Psi$. Hence by Eq. (48)

$$\Psi/c = d\Psi/dc|_\zeta. \tag{49}$$

Since $d^2\Psi/dc^2 > 0$ and $\zeta \leq c$, then it follows that

$$d\Psi/dc|_\zeta < d\Psi/dc|_c. \tag{50}$$

By introducing Eq. (50) into Eq. (49), the GCN_o restriction (Eq. (46)) is obtained.

To summarize: It has been shown that in Eq. (D4) $I_{(f)} \geq 0$ and $I_{(\Psi)} < 0$ except when $w_1 = w_2 = w_3 = 0$. Hence the total quadratic form in Eq. (D4) is positive definite, i.e.,

$$I = I_{(f)} - I_{(\Psi)} = \sum_{i,j} J_{ij} w_i w_j > 0 \tag{51}$$

Downloaded 03 May 2010 to 171.66.16.20. Redistribution subject to ASME license or copyright; see http://www.asme.org/terms/Terms_Use.cfm

except when $w_1 = w_2 = w_3 = 0$. This is more restrictive than the GCN_o condition and has been termed the GCN_o^+ in Truesdall and Noll (1965).

It can be readily shown that the GCN_o^+ condition is also satisfied when there exists more than one type of fibers. Equation (10) leads (by using Eqs. (26) and (17)) to

$$I_{(J)} = \sum_k I^k_{(J)} \tag{52}$$

where $I^k_{(J)}$ is $I_{(J)}$ for the type k fibers (Eqs. (D2)-(D4)). Since for each fiber k $\hat{s}_k(\lambda)$, $d\hat{s}_k/d\lambda \geq 0$, then it can be shown in a similar way that for each k, $I^k_{(J)} \geq 0$ so that, in Eq. (52), $I_{(J)} \geq 0$.

The B-E restriction in tissues is given by Eq. (43). It will be shown that it is satisfied by virtue of $\hat{s}(\lambda) \geq 0$ and $d\hat{s}/d\lambda \geq 0$ (the GCN_o restriction for tissues—Eq. (39)). The proof is as follows: Equation (43) can be written in an alternative form as

$$t_1 - t_2 = (\phi^o_f/J) \int_\phi \sin^2\phi \left\{ \int_\theta R(\phi, \theta)\hat{s}(\lambda)[\lambda_1^2 \cos^2\theta - \lambda_2^2 \sin^2\theta]d\theta \right\} d\phi > 0. \tag{53}$$

Since the case $\lambda_1 > \lambda_2$ is considered without loss of generality (Section 4.2), then it follows that

$$\lambda_1^2 \cos^2\theta - \lambda_2^2 \sin^2\theta > \lambda_2^2[\cos^2\theta - \sin^2\theta] \tag{54a}$$

$$\lambda = (\lambda_1^2 \sin^2\phi \cos^2\theta + \lambda_2^2 \sin^2\phi \sin^2\theta + \lambda_3^2 \cos^2\phi)^{1/2} > (\lambda_2^2 \sin^2\phi)^{1/2}. \tag{54b}$$

Since $\hat{s}(\lambda) \geq 0$, $d\hat{s}/d\lambda \geq 0$, then it follows from Eqs. (54) that for the internal integral in Eq. (53),

$$\int_\theta R(\phi, \theta)\hat{s}(\lambda)[\lambda_1^2 \cos^2\theta - \lambda_2^2 \sin^2\theta]d\theta > \lambda_2^2 \hat{s}(\lambda_2 \sin\phi) \int_\theta R(\phi, \theta)\,[\cos^2\theta - \sin^2\theta]d\theta. \tag{55}$$

In isotropic tissues, the integral on the R.H.S. of Eq. (55) vanishes (Appendix E). Since in the argument of the integral in Eq. (53) $\sin^2\phi > 0$, then it follows from Eq. (55) that in Eq. (53) $t_1 - t_2 > 0$, and the B-E condition is thus satisfied.

6 Discussion

Although the conditions listed in Section 3.1 are based on intuitive *ad hoc* reasoning for an isotropic material, they have been shown to result from two basic mechanical considerations (Truesdell and Noll, 1965, Section 83): If the GCN_o^+ condition is satisfied at any point in a certain region, then there is at most one solution to a given mixed boundary value problem that is different from the given deformation by infinitesimal pure stretch only. Hence satisfaction of GCN_o^+ is associated with uniqueness of solution.

The B-E condition is related to a basic principle as well. It is a consequence of another general restriction on elastic materials, the S-E condition (Truesdell and Noll, 1965, Section 52). In a hyperelastic material, satisfaction of the S-E condition ensures the uniqueness and stability for a boundary value problem of superimposed infinitesimal deformation (Truesdell and Noll, 1965, Section 68). It also ensures the existence of acoustical waves with real (rather than imaginary) velocities in every direction in the body (Truesdell and Noll, 1965, Section 71).

The constitutive model studied in the present work is a binary structural one. The basic assertion is that the morphological structure is a pivotal parameter in the tissue's overall response. Other determinants are: the binary nature of the tissues' space (solid fiber embedded in fluid-like matrix), the volume fraction occupied by the fibers at the reference state, the waviness distribution of the fibers, the stress-strain relationship for a stretched fiber, and the osmotic properties of the fluid matrix.

The present work concentrated on the properties of the fibers (their volume fraction, waviness and stress-strain response) and of the matrix osmotic pressure. The fibers orientation distribution in isotropic tissues is assumed to be known *a priori* (e.g., random distribution).

The structural model relies on two basic assumptions: First, the strain energy in the fibrous network is stored as extensional energy in the fibers. The second is the assumption of affine deformation—each fibrous element deforms with the global strain as if it were a part of a continuum.

The first assumption is reasonable for a wide range of biological interest. The assumption of affine deformation seems intuitively reasonable in fibrous tissues, due to the high degree of interconnectivity. The author is not aware of an experimental observation refuting this assumption in multicomponent fibrous tissues. Some doubt was raised regarding its applicability in the lung parenchyma where, unlike in more amorphous fibrous networks, the basic structural unit is a regular structured membranous alveolus with a typical size of hundreds of microns. Budiansky and Kimmel (1987) analyzed a representative alveolus idealized as a regular, pin-jointed, dodecahedral space truss loaded by the macroscopic stress. The stress-carrying elements are interconnected tension members which represent the lumped effects of the alveolar walls, the fibrous extensions of the pleural membranes, the reinforced alveolar opening and the small bronchioles, and blood vessels. From their analysis, they concluded that assuming affine deformation leads to unbounded stiffness in their model. It is doubtful whether this result can be taken as a sufficient argument against the assumption of affine deformation in view of the considerable simplification in their analysis.

7 Conclusions

(1) Constitutive laws for soft fibrous tissues have been derived on the basis of their structure, the fibers stress-strain law, and the fluid matrix osmotic properties.

(2) The resulting constitutive equations have been examined in the light of general restrictions which ensure physically reasonable response.

(3) By considering isotropic tissues, it has been shown that the observed convexities of both the fibers stress-strain law and of the matrix osmotic pressure-concentration law are essential features which guarantee that the tissue response will be physically acceptable.

References

Bowen, R. M., 1980, "Incompressible Porous Media Models by Use of the Theory of Mixtures," *International Journal of Engineering Sciences*, Vol. 18, pp. 1129–1148.

Carton, R. W., Dainauskas, J., and Clark, J. W., 1962, "Elastic Properties of Single Elastic Fibers," *Journal of Applied Physiology*, Vol. 17, pp. 547–551.

Chu, B. M., Frasher, W. G., and Wayland, H., 1972, "Hysteretic Behavior of Soft Living Animal Tissue," *Annals of Biomedical Engineering*, Vol. 1, pp. 182–203.

Fung, Y. C., 1972, "Stress-Strain-History Relations of Soft Tissues in Simple Elongation," *Biomechanics—Its Foundations and Objectives*, Y. C. Fung, N. Perrone, and M. Anliker, eds., Prentice-Hall, Englewood Cliffs, NJ, pp. 181–208.

Horowitz, A., Lanir, Y., Yin, F. C. P., Sheinman, I., Strumpf, R. P., Perl, M., and Sideman, S., 1988, "Structural Three-Dimensional Constitutive Law for the Passive Myocardium," ASME *Journal of Biomechanical Engineering*, Vol. 110, pp. 200–207.

Humphrey, J. D., and Yin, F. C. P., 1987, "A New Constitutive Formulation for Characterizing the Mechanical Behavior of Soft Tissues," *Biophysical Journal*, Vol. 52, pp. 563–570.

Hunter, P. J., McCulloch, A. D., Nielsen, P. M. F., and Smaill, B. H., 1988, "A Finite Element Model of Passive Ventricular Mechanics," *Computational Methods in Bioengineering*, R. Spilker and B. Simon, eds., ASME New York, pp. 387–397.

Huyghe, J. M., van Campen, D. H., Arts, T., and Heethaar, R. M., 1991,

Downloaded 03 May 2010 to 171.66.16.20. Redistribution subject to ASME license or copyright; see http://www.asme.org/terms/Terms_Use.cfm

"A Two-Phase Finite Element Model of the Diastolic Left Ventricle," *Journal of Biomechanics*, Vol. 24, pp. 527–538.

Lai, W. M., Hou, J. S., and Mow, V. C., 1991, "A Triphasic Theory for the Swelling and Deformation Behaviors of Articular Cartilage," ASME *Journal of Biomechanical Engineering*, Vol. 113, pp. 245–258.

Lanir, Y., 1980, "A Microstructure Model for the Rheology of Mammalian Tendon," ASME *Journal of Biomechanical Engineering*, Vol. 102, pp. 332–339.

Lanir, Y., 1983, "Constitutive Equations for Fibrous Connective Tissues," *Journal of Biomechanics*, Vol. 16, pp. 1–12.

Lanir, Y., 1987, "Biorheology and Fluid Flux in Swelling Tissues. I: Biocomponent Theory for Small Deformation, Including Concentration Effects," *Biorheology*, Vol. 24, pp. 173–187.

Lanir, Y., Salant, E. L., and Foux, A., 1988, "Physico-Chemical and Microstructural Changes in Collagen Fiber Bundles Following Stretch *In Vitro*," *Biorheology*, Vol. 25, pp. 591–603.

Maroudas, A., 1990, "Different Ways of Expressing Concentration of Cartilage Constituents With Special Reference to the Tissue's Organization and Functional Properties," *Methods in Cartilage Research*, Ch. 53, A. Maroudas and K. Kuettner, eds., Academic Press, London, pp. 221–219.

Maroudas, A., and Urban, J. P. G., 1980, "Swelling Pressures of Cartilaginous Tissues," *Studies in Joint Disease 1*, A. Maroudas and E. J. Holborow, eds., Pitman Medical, Kent, U.K., pp. 87–116.

Silberberg, A., 1982, "The Mechanics and Thermodynamics of Separation Flow Through Porous Molecularly Dispersed, Solid Media," *The Poiseulle Lecture, 1981, Biorheology*, Vol. 19, pp. 111–127.

Truesdell, C., and Noll, W., 1965, "The Nonlinear Field Theories of Mechanics," *Encyclopedia of Physics*, Vol. III/3, S. Flugge, ed., Springer-Verlag, Berlin, pp. 1–579.

Urban, J. P. G., Maroudas, A., Bayliss, M. T., and Dillon, J., 1979, "Swelling Pressures of Proteoglycans at the Concentrations Found in Cartilaginous Tissues," *Biorheology*, Vol. 16, pp. 447–464.

Viidik, A., 1972, "Simultaneous Mechanical and Light Microscopic Studies of Collagen Fibers," *Zeitschrift fuer Anatomie und entwicklungsgeschichte.*, Vol. 136, pp. 204–212.

APPENDIX A

Equations of Motion in Binary Swelling Tissues

The kinematics and dynamics of swelling tissues as binary solid-fluid systems has been worked out in Lanir (1987). The motions of both solid (fibers) and fluid is governed by force balance conditions expressed by

$$\text{div } \mathbf{t}_s + \phi_s\,(\psi_s + \text{grad } \Psi_s + \mathbf{b}_s) = \rho_s \mathbf{a}_s \tag{A1}$$

$$\text{div } \mathbf{t}_m + \phi_m\,(\psi_m + \text{grad } \Psi_m + \mathbf{b}_m) = \rho_m \mathbf{a}_s \tag{A2}$$

where $\mathbf{t}$'s are the Cauchy stresses, ϕ's are the volume fractions, ψ's are the viscous interaction forces, Ψ's are the concentration forces, $\mathbf{b}$'s the body forces, ρ's the bulk densities, and $\mathbf{a}$'s are the accelerations. The subscripts s and m denote the solid and fluid (matrix) components, respectively. The viscous interaction forces balance each other, so that

$$\phi_s \psi_s + \phi_m \psi_m = 0 \tag{A3}$$

The Gibbs-Duhem equation asserts that the concentration forces balance each other as well, so that

$$\phi_s \cdot \text{grad } \Psi_s + \phi_m \cdot \text{grad } \Psi_m = 0. \tag{A4}$$

In most cases related to tissues, the body forces vanish. Hence, $\mathbf{b}_s = \mathbf{b}_m = 0$.

Under equilibrium, $\psi_s = \psi_m = 0$ and $\mathbf{a}_s = \mathbf{a}_m = 0$. If both solid and fluid are incompressible (as in soft tissues), then the first terms in Eqs. (A1), (A2) are given by (Silberberg, 1982):

$$\text{div } \mathbf{t}_s = \text{div}(\mathbf{t}_f - \phi_s P\mathbf{I}); \quad \text{div } t_m = -\phi_m \text{ grad } P \tag{A5}$$

so that by summing Eqs. (A1) and (A2) one gets

$$\text{div}(\mathbf{t}_f - P\mathbf{I}) = 0 \tag{A6}$$

while Eq. (A2) yields for the fluid component

$$\text{grad}(P - \Psi_m) = 0. \tag{A7}$$

The bracketed term in Eq. (A6) is the total stress $\mathbf{t}$. Comparing Eq. (A6) with the equilibrium equation in classical solid mechanics (div $\mathbf{t}$ = 0) shows that the total stress in binary systems replaces the regular stress in uniphasic solid. Integration of (A7) yields

$$P - \Psi = P_{ex} - \Psi_{ex} \tag{8}$$

where $\Psi \equiv \Psi_m$. Since P_{ex} and Ψ_{ex} are deformation independent, the R.H.S. of Eq. (A8) can be neglected without loss of generality. Hence, under equilibrium we take

$$P = \Psi. \tag{A9}$$

APPENDIX B

Principal Values of the Matrices in Eq. (24)

For brevity denote $\mathbf{G} \equiv J\mathbf{t}\mathbf{V}^{-1}$, $\mathbf{M} = \mathbf{US}$. Then from Eq. (24) $\mathbf{GR} = \mathbf{RM}$. Hence $\mathbf{R}^T\mathbf{GR} = \mathbf{R}^T\mathbf{RM} = \mathbf{M}$, since $\mathbf{R}^T\mathbf{R} = \mathbf{I}$. Since T_i are the principal values of $\mathbf{G}$, it follows that

$$(\mathbf{G} - T_i\mathbf{I}) \cdot \mathbf{A}^{(i)} = 0 \tag{B1}$$

where $\mathbf{A}^{(i)}$ is a unit vector in the principal direction i.

Hence

$$\mathbf{R}^T(\mathbf{G} - T_i\mathbf{I})\mathbf{R}\mathbf{R}^T\mathbf{A}^{(i)} = 0 \tag{B2}$$

or

$$(\mathbf{R}^T\mathbf{G}\,\mathbf{R} - T_i\mathbf{R}^T\mathbf{I}\,\mathbf{R})\mathbf{R}^T\mathbf{A}^{(i)} = 0 \tag{B3}$$

which can be written as

$$(\mathbf{M} - T_i\mathbf{I})\mathbf{R}^T\mathbf{A}^{(i)} = 0. \tag{B4}$$

Equation (B4) shows that T_i are also the principal values of $\mathbf{M} \equiv \mathbf{US}$. Since in an isotropic material $\mathbf{U}$ and $\mathbf{S}$ have the same principal directions, Eq. (26) follows.

APPENDIX C

Relationship Between Concentration (c) and Volume Ratio (J)

In most tissues the negatively charged groups on the PG are effectively trapped in the fiber network. Their concentration in the fluid phase in the reference configuration is thus $c^o = KV_f^o/V_w^o$, K being proportional to the FCD, and V_f and V_w are the volumes of fibers and fluid in the representative elementary volume, respectively. The superscript o denotes the reference configuration (J = 1). We follow changes in concentration in a representative elementary volume containing a fixed ensemble of fibers. The fibers are taken to be incompressible. Hence $V_f = V_f^o$ and thus

$$c = KV_f^o/V_w = K(V_f^o/V_w^o)\,(V_w^o/V^o)\,(V^o/V)\,(V/V_w). \tag{C1}$$

By introducing the volume fractions $\phi_f = V_f/V$, $\phi_w = V_w/V$, Eq. (C1) can be written as

$$c = c^o\phi_w^o/J\phi_w, \quad J = V/V^o. \tag{C2}$$

But since $\phi_f + \phi_w = 1$, we have

$$\phi_w = V_w/V = 1 - V_f^o/V = 1 - (V_f^o/V^o)\,(V^o/V) = 1 - \phi_f^o/J \tag{C3}$$

so that from Eq. (C2), using $\phi_w^o = 1 - \phi_f^o$, one gets

$$c = c^o(1 - \phi_f^o)/(J - \phi_f^o) = K_1/(J - K_2) \tag{C4}$$

where $K_1 = c^o(1 - \phi_f^o)$, $K_2 = \phi_f^o$. Equation (C4) establishes the relationship between the concentration c and volume ratio J. It follows that

$$d/dJ = (d/dc)\,(dc/dJ) = [-K_1/(J - K_2)^2]\,(d/dc) = -[c^2/K_1]\,(d/dc) \tag{C5}$$

and thus

$$J(d/dJ) = -c(1 + c \cdot K_2/K_1)\,(d/dc) \tag{C6}$$

Equation (C5) indicates that the derivatives w.r.t. J and c are of mutually opposite signs.

Downloaded 03 May 2010 to 171.66.16.20. Redistribution subject to ASME license or copyright; see http://www.asme.org/terms/Terms_Use.cfm

APPENDIX D

The GCN_o Restriction—Eqs. (39)-(40)

The components J_{ij} in Eq. (17) can be divided into two parts as

$$J_{ij} = J_{ij}^{(f)} - J_{ij}^{(\Psi)} \tag{D1}$$

where superscripts f and Ψ relate to the fibers and osmotic terms, respectively. Thus from Eq. (36)

$$J_{ij}^{(f)} = \partial T_i^f / \partial \lambda_j; \quad J_{ij}^{(\Psi)} = \partial (J\hat{\Psi}/\lambda_i)/\partial \lambda_j \tag{D2}$$

where T_i^f is the first term on the R.H.S. of Eq. (38).

The quadratic forms of the GCN_o condition (Eq. (20)) can be likewise divided as

$$I = I_{(f)} - I_{(\Psi)} \tag{D3}$$

where

$$I = \sum_{i,j} J_{ij} w_i w_j; \quad I_{(f)} = \sum_{i,j} J_{ij}^{(f)}\, w_i w_j; \quad I_{(\Psi)} = \sum_{i,j} J_{ij}^{(\Psi)}\, w_i w_j. \tag{D4}$$

To examine whether the GCN_o condition is satisfied by the structural material laws, consider first $J_{ij}^{(f)}$. From Eqs. (37), (38), and (D2) one gets

$$J_{ij}^{(f)} = \phi_f^0 \int_\phi \int_\theta R(\phi, \theta) \lambda^{-1} [d\hat{s}/d\lambda] \lambda_i \lambda_j N_i^2 N_j^2 \, d\phi d\theta, \quad i \neq j \tag{D5a}$$

$$J_{ii}^{(f)} = \phi_f^0 \int_\phi \int_\theta R(\phi, \theta)\, [\hat{s}(\lambda) N_i^2 + \lambda^{-1} [d\hat{s}/d\lambda] \lambda_i^2 N_i^4] \, d\phi d\theta. \tag{D5b}$$

By summing Eq. (D5*a*) for all i, j with Eq. (D5*b*) it follows that the GCN_o condition requires that

$$I_{(f)} = \phi_f^0 \int_\phi \int_\theta R(\phi, \theta)\, [\hat{s}(\lambda) G + \lambda^{-1} \cdot (d\hat{s}/d\lambda) \cdot Q] d\phi d\theta \geq 0 \tag{D6}$$

where G and Q are given by

$$G = N_1^2 w_1^2 + N_2^2 w_2^2 + N_3^2 w_3^2;$$

$$Q = (w_1 \lambda_1 N_1^2 + w_2 \lambda_2 N_2^2 + w_3 \lambda_3 N_3^2)^2. \tag{D7}$$

Since $G, Q \geq 0$ for any deformation, it follows from Eq. (D7) that the GCN_o condition for $I_{(f)}$ will always be satisfied if $\hat{s}(\lambda) \geq 0$ and $d\hat{s}/d\lambda \geq 0$.

In the foregoing, although the specific form of the orientation distribution $R(\phi, \theta)$ for isotropic tissues was not used, isotropy was nevertheless assumed in stating (Eq. (25) and Appendix B) that the principal directions of stress and strain coincide.

Consider next $I_{(\Psi)}$ in Eq. (D4). From Eq. (D2) it follows that

$$J_{ij}^{(\Psi)} = \lambda_k [\hat{\Psi} + \lambda_j (\partial \hat{\Psi}/\partial \lambda_j)] = J\lambda_k [\hat{\Psi}/J + d\hat{\Psi}/dJ]; \quad i \neq j,\ i,j = 1, 2, 3 \tag{D8a}$$

$$J_{ii}^{(\Psi)} = \lambda_j \lambda_k (\partial \hat{\Psi}/\partial \lambda_i) = \lambda_j^2 \lambda_k^2 (d\hat{\Psi}/dJ) \tag{D8b}$$

where $i \neq j \neq k \neq i$. Hence, it follows (after some algebra), that the GCN_o condition for $I_{(\Psi)}$ in Eq. (D4) will be satisfied if

$$I_{(\Psi)} = (\hat{\Psi}/J + d\hat{\Psi}/dJ) B_1 + (d\hat{\Psi}/dJ) B_2 \leq 0 \tag{D9}$$

where

$$B_1 = 2\lambda_1^2 \lambda_2 \lambda_3 w_2 w_3 + 2\lambda_2^2 \lambda_1 \lambda_3 w_1 w_3 + 2\lambda_3^2 \lambda_1 \lambda_2 w_1 w_2$$

$$B_2 = w_1^2 \lambda_2^2 \lambda_3^2 + w_2^2 \lambda_1^2 \lambda_3^2 + w_3^2 \lambda_1^2 \lambda_2^2. \tag{D10}$$

From Eq. (D10) it is seen that

$$B_1 + B_2 = (w_1 \lambda_2 \lambda_3 + w_2 \lambda_1 \lambda_3 + w_3 \lambda_1 \lambda_2)^2. \tag{D11}$$

Hence $B_2 \geq 0$ and $B_1 + B_2 \geq 0$. It follows then that $B_2 \geq |B_1|$. Hence if $|\hat{\Psi}/J| < |d\hat{\Psi}/dJ|$, then regardless of the sign of B_1, $I_{(\Psi)}$ in Eq. (D9) will always be of the same sign as $d\hat{\Psi}/dJ$. Since the osmotic pressure always increases with decreasing volume (= reduced water content), then $d\hat{\Psi}/dJ < 0$ and it follows that $I_{(\Psi)} < 0$ as well if the following exist:

$$|\Psi/J| < |d\Psi/dJ|. \tag{D12}$$

Equation (D12) is the reduced GCN_o condition for the osmotic pressure portion of the total stress.

APPENDIX E

Proof of Statement Following Eq. (55)

When an isotropic material is stretched uniformly in the directions of the coordinates x_1, x_2, x_3, then the three corresponding stress components must be mutually equal. The global deformation in this case is given by $\mathbf{E} = e_o \mathbf{I}$ and the fiber's strain by $e = e_o$ (Eq. (7)). Hence from Eq. (14) it follows that

$$S_{11} - S_{22} = s(e_o) \int_\phi \sin^2\phi \left\{ \int_\theta R(\phi, \theta)\, [\cos^2\theta - \sin^2\theta] d\theta \right\} d\phi = 0. \tag{E1}$$

Since $s(e_o)$, $\sin^2\phi \geq 0$, then it follows that the internal integral in Eq. (E1) (and hence also the one on the R.H.S. of Eq. (55)) must vanish in isotropic materials.

Downloaded 03 May 2010 to 171.66.16.20. Redistribution subject to ASME license or copyright; see http://www.asme.org/terms/Terms_Use.cfm

J. K. Park
Ph.D. Student.

B. M. Kwak[1]
Professor,
Mem. ASME.

Department of Mechanical Engineering,
Korea Advanced Institute
of Science and Technology,
373-1, Kusong-dong, Yusung-gu,
Taejon 305-701, Korea

Three-Dimensional Frictional Contact Analysis Using the Homotopy Method

A three-dimensional contact problem with the orthotropic Coulomb friction is formulated in the form of a system of nonlinear equations. The nonlinear complementarity formulation derived naturally from the three-dimensional frictional contact phenomenon is used in the numerical analysis without such linearization as previously introduced. The probability-one homotopy method known as a globally convergent zero-finding algorithm is implemented as an exact method and applied to each incremental step. The method is illustrated by two three-dimensional problems and the results are compared with those of commercial package and other approximations.

1 Introduction

As seen from the literature, notwithstanding the importance and intensive study for several decades, the frictional contact problem has still remained as one of the most difficult problem. Especially three-dimensional frictional contact problems have rarely been treated. No attempt of exact approach seemed available until now. In general, numerical methods for the contact problem with friction can be divided into two categories, that is, iterative trial and error methods and mathematical formulations such as variational inequality and complementarity. In the former methods, the solution for the contact problem is sought iteratively by a trial and error scheme until it satisfies some contact and friction conditions in the discretized formulation (Okamato and Nakazawa, 1979; Rahman, Rowlands and Cook, 1984; Torstenfelt, 1984; Bathe and Chaudhary, 1985). Contact or interface elements are often used in this approach. In the latter category, the variational inequality is useful in obtaining mathematical properties of the solution such as existence and uniqueness (Duvaut and Lions, 1976; Panagiotopoulos, 1985). However, it has been limited to the case in which either normal pressure or contact area is known, or some mathematical assumptions on smoothness of friction law are used (Oden and Pires, 1983). Complementarity formulation where a subdifferential analysis is used under the restriction that contact area is constant has been derived by Klarbring (1986). Kwak et al. (Lee and Kwak, 1988; Kwak, 1990; Kwak, 1991) have derived a complementarity principle directly from the natural law for the frictional contact phenomenon, which leads to a linear complementarity problem (LCP) for a two-dimensional case and a nonlinear complementarity problem for general three-dimensional cases. In the latter case, by introducing a polyhedral law of friction, the problem has been transformed to a linear complementarity problem, but the nonlinear complementarity per se has not been treated yet.

The complementarity problem has relevant equivalences to a certain type of variational inequality, fixed point problem, system of nonlinear equations and so on (Cottle, Giannessi and Lions, 1980). In this line, a useful theorem regarding the equivalence between a complementarity problem and a system of nonlinear equations was developed by Mangasarian (1976). In his theorem, it was shown that the resulting nonlinear equations preserve the useful properties such as continuity and differentiability. Watson (1979) proposed a numerical scheme for a general nonlinear complementarity problem using this theorem and homotopy method.

The Newton-type methods and the continuation methods are two major branches of solution methods for the system of nonlinear equations. Both have some disadvantages. Due to the first proposition by Chow et al. (1978), the homotopy-based continuation method is gaining interest as a valuable tool for the numerical solution of tough nonlinear equations in several variables. Theoretically, this method has the probability-one convergence property under mild conditions. It has been successfully applied to several difficult problems (Watson and Wang, 1981).

In this paper the nonlinear complementarity formulation of three-dimensional frictional contact presented by Kwak (1991) is transformed to a system of nonlinear equations using Mangasarian's theorem and solved by the homotopy method with an ordinary differential equation based, zero-curve following method in HOMPACK (Watson, Billups and Morgan, 1987). Considering inherent nonlinearities of the contact problem, the updated Lagrangian formulation is adopted with the finite element discretization. The internal degrees-of-freedom can be statically condensed out. For the numerical examples, the three-

[1]To whom all correspondence should be addressed.

Contributed by the Applied Mechanics Division of THE AMERICAN SOCIETY OF MECHANICAL ENGINEERS for publication in the ASME JOURNAL OF APPLIED MECHANICS.

Discussion on this paper should be addressed to the Technical Editor, Professor Lewis T. Wheeler, Department of Mechanical Engineering, University of Houston, Houston, TX 77204-4792, and will be accepted until four months after final publication of the paper itself in the ASME JOURNAL OF APPLIED MECHANICS.

Manuscript received by the ASME Applied Mechanics Division, Nov. 16, 1992; final revision, June 17, 1993. Associate Technical Editor: J. N. Reddy.

Copyright © 1994 by ASME
Downloaded 03 May 2010 to 171.66.16.20. Redistribution subject to ASME license or copyright; see http://www.asme.org/terms/Terms_Use.cfm

dimensional contact of an elastic body on a rigid surface is considered and changes of pressure distribution and slips on the contact surface are observed and compared with ABAQUS. The problem of a flat-ended square rigid punch on the elastic half surface is also solved and the results are compared with others in the literature (Klarbring, 1986).

2 Formulation of Three-Dimensional Contact Problem With The Coulomb Friction

2.1 Finite Element Approximation and Condensation of the Internal DOF. Considering the loading-path dependent nature of friction phenomena and other nonlinearities, an incremental formulation is used. The description based on the updated Lagrangian incremental approach as in Kwak (1991) is adopted. The configuration and state up to loading step t are known and those at $t + \Delta t$ are sought. Employing a usual finite element discretization scheme to the linearized variational form of the equation of motion and imposing traction and displacement boundary conditions, the governing finite element matrix equation is obtained.

$$(\mathbf{K}_L + \mathbf{K}_{NL})\mathbf{u} = {}^{t+\Delta t}\mathbf{R} - {}^{t+\Delta t}\mathbf{F} \tag{1}$$

where

$\mathbf{u}$ = the nodal displacement increment vector
$\mathbf{K}_L$ = the linear incremental stiffness matrix
$\mathbf{K}_{NL}$ = the nonlinear incremental stiffness matrix
${}^{t+\Delta t}\mathbf{F}$ = the internal force vector

and ${}^{t+\Delta t}\mathbf{R}$ is the external force vector which involves the body force, the surface traction, and the unknown contact traction at the potential contact surface, which is selected sufficiently large to cover the real contact area.

Partitioning $\mathbf{u}$ into the nodal displacement increments $\mathbf{u}_c$ on the potential contact surface Γ_c and internal nodal displacement increments $\mathbf{u}_i$, the matrix equation is rewritten as

$$\begin{bmatrix} \mathbf{K}_{ii} & \mathbf{K}_{ic} \\ \mathbf{K}_{ci} & \mathbf{K}_{cc} \end{bmatrix} \begin{Bmatrix} \mathbf{u}_i \\ \mathbf{u}_c \end{Bmatrix} = \begin{Bmatrix} \mathbf{F}_i \\ \mathbf{S}_c \end{Bmatrix}. \tag{2}$$

The internal degrees of freedom $\mathbf{u}_i$ can be condensed out and then the matrix equation for $\mathbf{u}_c$ is obtained as follows:

$$\hat{\mathbf{K}}\mathbf{u}_c = \mathbf{S}_c - \mathbf{K}_f\mathbf{F}_i, \tag{3}$$

where $\hat{\mathbf{K}} = \mathbf{K}_{cc} - \mathbf{K}_{ci}\mathbf{K}_{ii}^{-1}\mathbf{K}_{ic}$ and $\mathbf{K}_f = \mathbf{K}_{ci}\mathbf{K}_{ii}^{-1}$.

So the relationship between the displacement increment and the force at the potential contact surface for the kth body is expressed as

$$\mathbf{u}_c^k = \mathbf{B}^k\mathbf{S}_c^k + \mathbf{T}^k\mathbf{F}_i^k, \tag{4}$$

where $\mathbf{B}^k = \hat{\mathbf{K}}^{-1}$ and $\mathbf{T}^k = -\hat{\mathbf{K}}^{-1}\mathbf{K}_f$.

The displacement increment $\mathbf{u}_c^k$ on the contact surface and the contact force $\mathbf{S}_c^k$ in Eq. (4) are unknown and these must satisfy the contact and friction conditions described in Kwak (1991). They are briefly summarized with the same notations as used there.

(1) Global Equilibrium. For configuration at $t + \Delta t$, the global equilibrium equation for body 1 where rigid-body motion is allowed is obtained as follows:

$$\int_{{}^{t+\Delta t}\Gamma_f^1} {}^{t+\Delta t}F_i H_{ij}\, {}^{t+\Delta t}d\Gamma + \int_{{}^{t+\Delta t}\Gamma_c^1} {}^{t+\Delta t}S_i A_{ij}\, {}^{t+\Delta t}d\Gamma = 0. \tag{5}$$

(2) Compatibility Condition. Since either contact gap $D_n(a_i^1)$ or contact normal force ${}^{t+\Delta t}P$ between the mating contact points a_i^1 and a_i^2 after load increment Δt must be equal to zero, the following condition is satisfied:

$${}^{t+\Delta t}P \cdot D_n(a_i^1) = 0 \quad \text{for all } a_i^1 \text{ on } \Gamma_c^1. \tag{6}$$

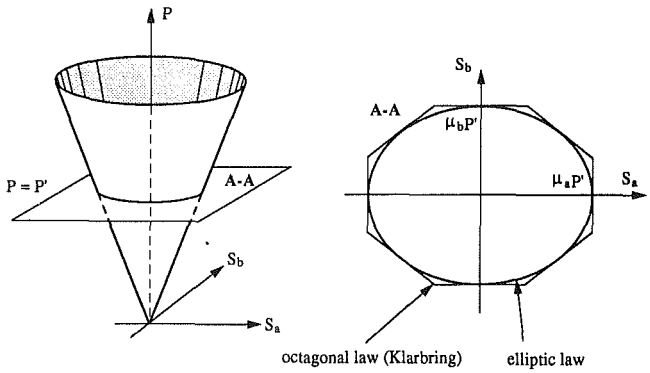


Fig. 1 Elliptic Coulomb friction law and octagonal approximation

(3) Coulomb friction condition. The form of the static friction law is described by the following inequality between the tangential traction component S_a and S_b, and the normal P and shown in Fig. 1:

$$C_E = \left\{ (S_a, S_b, P) \,\middle|\, \left[\left(\frac{{}^{t+\Delta t}S_a}{\mu_a} \right)^2 + \left(\frac{{}^{t+\Delta t}S_b}{\mu_b} \right)^2 \right]^{1/2} \le {}^{t+\Delta t}P \right\}. \tag{7}$$

If strict inequality holds, there is no slip. Otherwise, a relative motion is imminent.

In this latter case it is known (Panagiotopoulos, 1985) that there exists a non-negative λ such that

$$D_a = -\lambda \frac{{}^{t+\Delta t}S_a}{\mu_a^2} \text{ and } D_b = -\lambda \frac{{}^{t+\Delta t}S_b}{\mu_b^2} \tag{8}$$

where D_a and D_b are appropriately defined relative tangential displacements along the principal axes of the friction.

2.2 Nonlinear Complementarity Problem Formulation. The relative displacements and all tangential components are well defined in Fig. 3 and Eq. (22) in Kwak (1991). Here and in the following, the exact same definitions and notations are adopted to avoid unnecessary repeating.

The unknown displacement vector on the potential contact region Γ_c^k of body k was expressed as a function of the contact traction vector in (4). Symbolically it can be expressed as follows:

$$u_c^k = u_c^k\,({}^{t+\Delta t}S_c^k;\ {}^{t+\Delta t}F^k), \quad k = 1, 2 \tag{9}$$

where the subscript c refers to the potential contact region; and ${}^{t+\Delta t}S_c^k$ denotes a traction vector with both normal and tangential components and can be expressed by ${}^{t+\Delta t}S_a$, ${}^{t+\Delta t}S_b$, and ${}^{t+\Delta t}S_n$. If Eq. (9) is used, the gap function can be expressed in the following functional form

$$D_n({}^t a_i^1) = D_n({}^{t+\Delta t}S_c,\ q;\ {}^t a_i^2) \tag{10}$$

where ${}^t a_i^1$ and ${}^t a_i^2$ are mating contact points predetermined at configuration t, and q denotes the rigid-body displacement. Then the condition in Eq. (6) becomes

$${}^{t+\Delta t}P D_n = 0 \tag{11}$$

where ${}^{t+\Delta t}P \ge 0$ and $D_n \ge 0$

The Coulomb friction law, (7), can be directly transformed to a complementarity form. First, introduce a non-negative real number ${}^{t+\Delta t}P^*$ and ${}^{t+\Delta t}\theta_f$ such that

$$\frac{{}^{t+\Delta t}S_a}{\mu_a} = {}^{t+\Delta t}P^* \cos {}^{t+\Delta t}\theta_f, \text{ and}$$

$$\frac{{}^{t+\Delta t}S_b}{\mu_b} = {}^{t+\Delta t}P^* \sin {}^{t+\Delta t}\theta_f. \tag{12}$$

Also introduce D_t and θ_u such that

$$D_a = D_t \cos\theta_u \text{ and } D_b = D_t \sin\theta_u, \tag{13}$$

Downloaded 03 May 2010 to 171.66.16.20. Redistribution subject to ASME license or copyright; see http://www.asme.org/terms/Terms_Use.cfm

where D_t denotes the magnitude of slip or the relative displacement between a pair of contacting points and can be defined as

$$D_t = (D_a^2 + D_b^2)^{1/2}. \tag{14}$$

Since D_a, D_b, and D_t are functions of u_c^1 and u_u^2, they can also be expressed in terms of ${}^{t+\Delta t}S_a$, ${}^{t+\Delta t}S_b$, and ${}^{t+\Delta t}S_n$ using Eq. (4). Symbolically then

$$D_a = D_a({}^{t+\Delta t}S_a, {}^{t+\Delta t}S_b, {}^{t+\Delta t}S_n),$$

$$D_b = D_b({}^{t+\Delta t}S_a, {}^{t+\Delta t}S_b, {}^{t+\Delta t}S_n) \tag{15}$$

and $$D_t = D_t({}^{t+\Delta t}S_a, {}^{t+\Delta t}S_b, {}^{t+\Delta t}S_n).$$

Introducing a slack variable T, the friction condition (7) can be expressed as

$${}^{t+\Delta t}P^* + T = {}^{t+\Delta t}P \tag{16}$$

with the complementarity rule

$$TD_t = 0 \tag{17}$$

where $$T \geq 0 \text{ and } D_t \geq 0.$$

Another relation is derived from Eq. (8) using Eqs. (12) and (13) as follows:

$$\tan\theta_u = \frac{\mu_a}{\mu_b} \tan {}^{t+\Delta t}\theta_f. \tag{18}$$

This indicates that the direction of tangential contact force can be different from the direction of slip for the orthotropic law.

By similar fashion, the global equilibrium Eq. (5) can be expressed symbolically as follows:

$$E({}^{t+\Delta t}S_c; {}^{t+\Delta t}F) = 0. \tag{19}$$

From (12) and (16),

$${}^{t+\Delta t}S_a = \mu_a({}^{t+\Delta t}P - T)\cos {}^{t+\Delta t}\theta_f \text{ and}$$

$${}^{t+\Delta t}S_b = \mu_b({}^{t+\Delta t}P - T)\cos {}^{t+\Delta t}\theta_f. \tag{20}$$

By substituting (20) to (10), (15) and (19), we can express them only in terms of ${}^{t+\Delta t}P$, T, ${}^{t+\Delta t}\theta_f$ and q as follows:

$$D_n = D_n({}^{t+\Delta t}P, T, {}^{t+\Delta t}\theta_f, q) \tag{21}$$

$$D_a = D_a({}^{t+\Delta t}P, T, {}^{t+\Delta t}\theta_f, q) \tag{22}$$

$$D_b = D_b({}^{t+\Delta t}P, T, {}^{t+\Delta t}\theta_f, q) \tag{23}$$

and

$$E({}^{t+\Delta t}P, T, {}^{t+\Delta t}\theta_f, q) = 0. \tag{24}$$

Also from (13) and (18) the following relation is obtained:

$$\frac{D_b}{D_a} = \frac{\mu_a}{\mu_b} \tan {}^{t+\Delta t}\theta_f. \tag{25}$$

Now, the complete description of three-dimensional friction contact problems with the orthogonal Coulomb law is obtained by two complementarity conditions (11), (17) and the two equality conditions (24), (25). The unknowns are ${}^{t+\Delta t}P$, T, ${}^{t+\Delta t}\theta_f$, and q. But the two complementarity conditions are nonlinear because of (12). The only treatment in the literature is to approximate the elliptic or circular type friction law by polygons (Klarbring, 1986; Kwak, 1991) as shown in Fig. 1, resulting in a set of linear complementarity. But, in the next section a solution method to solve the nonlinear complementarity problem without such approximation is proposed. For this purpose, the nonlinear complementarity problem is transformed to a system of nonlinear equations suitable for the application of the homotopy method.

2.3 System of Nonlinear Equations Formulation. One such transformation of the complementarity problem to a system of nonlinear equations has been shown by Mangasarian (1976), and is given in the following theorem: Let F: $R^n \to R^n$, let $z \in R^n$ and let F_i and z_i, $i = 1, \ldots, n$, denote the components of F and z, respectively. The problem of finding a $z \in R^n$ such that

$$zF(z) = 0, \quad F(z) \geq 0, \quad z \geq 0 \tag{26}$$

is a so-called complementarity problem. Let θ be any strictly increasing function from R into R, that is $a > b \Leftrightarrow \theta(a) > \theta(b)$, and let $\theta(0) = 0$. Then z solves complementarity problem (26) if and only if

$$\theta(|F_i(z) - z_i|) - \theta(F_i(z)) - \theta(z_i) = 0, \quad i = 1, \ldots, n. \tag{27}$$

By taking $\theta(t) = t^3$, the nonlinear complementarity conditions can be converted to the system of nonlinear equations as follows:

$$|F_i(z) - z_i|^3 - F_i(z)^3 - z_i^3 = 0. \tag{28}$$

The choice $\theta(t) = t^3$ is taken because it is the simplest strictly increasing function satisfying C^2 continuity and $\theta(0) = 0$.

Using (28), we can transform the nonlinear complementarity conditions (11) and (17) to the system of equations

$$H1: \ -|D_{n_i} - {}^{t+\Delta t}P_i|^3 + D_{n_i}^3 + {}^{t+\Delta t}P_i^3 = 0 \quad i = 1, \ldots, n_c \tag{29}$$

and

$$H2: \ -|D_{t_i} - T_i|^3 + D_{t_i}^3 + T_i^3 = 0 \quad i = 1, \ldots, n_c, \tag{30}$$

where subscript i represents each contact point and n_c is the total number of contact points.

For numerical efficiency in treating the direction of friction force θ_f, we introduce two independent variable u and v such that

$$u \equiv \sin\theta_f \text{ and } v \equiv \cos\theta_f. \tag{31}$$

Substituting (31), global equilibrium Eq. (24) can be rewritten as

$$H3: \ E_i({}^{t+\Delta t}P, T, u, v, q) = 0 \quad i = 1, \ldots, n_r \tag{32}$$

where n_r is the number of independent rigid-body motions.

By the same fashion, (21), (22), and (23) are rewritten as follows:

$$D_n = D_n({}^{t+\Delta t}P, T, u, v, q) \tag{33}$$

$$D_a = D_n({}^{t+\Delta t}P, T, u, v, q) \tag{34}$$

$$D_b = D_n({}^{t+\Delta t}P, T, u, v, q). \tag{35}$$

Equations (13) and (18) can be rewritten and applied to each point on the potential contact surface. Then,

$$H4: \ [(\mu_a u_i)^2 + (\mu_b v_i)^2]^{1/2} D_{a_i} + \mu_b D_{t_i} v_i = 0 \quad i = 1, \ldots, n_c \tag{36}$$

$$H5: \ [(\mu_a u_i)^2 + (\mu_b v_i)^2]^{1/2} D_{b_i} + \mu_a D_{t_i} u_i = 0 \quad i = 1, \ldots, n_c \tag{37}$$

where n_c is the number of total potential contact points.

In the case of isotropic friction, (36) and (37) are reduced to simpler forms as follows:

$$D_{a_i} + D_{t_i} v_i = 0 \quad i = 1, \ldots, n_c \tag{38}$$

$$D_{b_i} + D_{t_i} u_i = 0 \quad i = 1, \ldots, n_c. \tag{39}$$

Obviously, (29), (30), (32), (36) (or (38)) and (37) (or (39)) represent the complete system of equations for the three-dimensional contact problem with the Coulomb friction and the total number of variables is $4n_c + n_r$.

3 Homotopy Method

Newton-type methods have been widely used to solve nonlinear equations in engineering and science for their fast convergence near the solution. But there are many difficult problems that cannot be solved by these methods. For an attempt to those difficult problems, the continuation methods have been used in various forms. Incremental loading, incremental displacement, and arc-length methods in nonlinear structural analysis are particular types of continuation. The homotopy method is a new class of continuation methods for

Downloaded 03 May 2010 to 171.66.16.20. Redistribution subject to ASME license or copyright; see http://www.asme.org/terms/Terms_Use.cfm

computing (Brouwer) fixed points and zeros of nonlinear systems. It is robust and converges from an arbitrary starting point almost surely under mild conditions, such as C^2 continuities and asymptotic similarity conditions (Watson, 1986). This method is globally convergent as opposed to local convergence of most iterative methods. Useful theorems with an abstract algorithm regarding homotopy method were first published by Chow, Paret, and Yorke (1978). From that time, many efforts to complete the background theory and to establish numerical algorithms had been performed by Watson et al. (Watson, 1986; Watson, 1979; Watson, Billups, and Morgan, 1987).

The general idea of probability-one homotopy methods is as follows: Suppose that a root of a system of nonlinear equations $F(x)$ is to be found where F: $R^n \rightarrow R^n$ is a C^2 map. Construct a homotopy map such that

$$\rho_a(\lambda, x) = \lambda F(x) + (1-\lambda)(x-a). \tag{40}$$

From this it can be easily shown that $\rho_a(0, x) = (x - a)$ and $\rho_a(1, x) = F(x)$. A zero curve of (40) is tracked by varying λ from 0 to 1. Starting from $(\lambda, x) = (0, a)$, where a is an arbitrarily chosen starting point, it reaches to a point $(\lambda, x) = (1, \bar{x})$, where $F(\bar{x}) = 0$. There are many algorithms that can be used for tracking the zero curve $\rho_a(\lambda, x)$ such as an ordinary differential equation based algorithm, Davidenko's normal flow algorithm and Rheinboldt's augmented Jacobian matrix algorithm (Rheinboldt and Burkardt, 1983).

In solving the previously formulated nonlinear system of equations for the three-dimensional frictional contact problem, it is very difficult to choose the starting points especially for the direction of slips which can change abruptly. Because of this, the probability-one homotopy method is adopted with the homotopy as follows:

$$\rho_a = \lambda F(z) + (1-\lambda)(z-a) \tag{41}$$

where

$$F(z) = \begin{pmatrix} -|D_n - P|^3 + D_n^3 + P^3 \\ -|D_t - T|^3 + D_t^3 + T^3 \\ [(\mu_a u)^2 + (\mu_b v)^2]^{1/2} D_a + \mu_b D_t v \\ [(\mu_a u)^2 + (\mu_b v)^2]^{1/2} D_b + \mu_a D_t u \\ E(P, T, u, v, q) \end{pmatrix} \in R^{4n_c + n_r},$$

$$z = (P, T, u, v, q) \in R^{4n_c+n_r},\ a \in R^{4n_c+n_r}.$$

The subscript i previously used to refer to the ith contact point is omitted to avoid notational complexity.

It is apparent that $F(z)$ is a C^2 map but difficult to check the asymptotic similarity condition necessary for the guarantee of global or probability-one convergency. No failure, however, has been experienced in solving several three-dimensional contact problems. For the tracking of zero curves, the ordinary differential equation based method in HOMPACK (Watson, Billups and Morgan, 1987) is used. Detailed theory and algorithm regarding this method can be found in Watson (1986). To increase the accuracy of solutions, the Newton iteration is adopted near $\lambda = 1$ of the zero curve of the homotopy map.

4 Numerical Examples

Due to scarcity of solved problems in the literature and therefore difficulty of comparisons, only constant contact area problems with the isotropic friction law are considered. The present formulation, however, does not differentiate between these problems and more general problems with variable contact area and orthotropic friction case.

Example 1. Elastic Body on a Flat Rigid Surface. To test the proposed method, three-dimensional frictional contact between a rectangular elastic body and a flat rigid surface is considered. The size of the elastic body is 20 × 20 × 25 (mm^3)

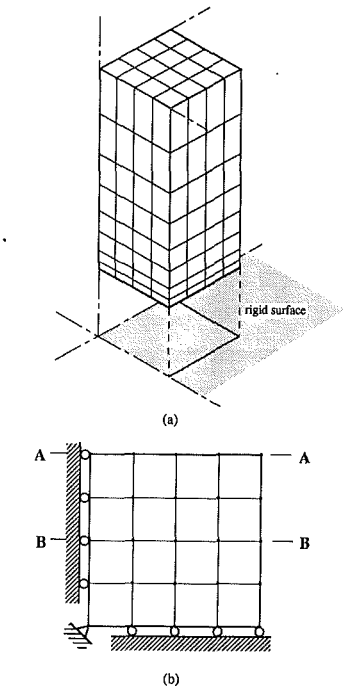


Fig. 2 Modeling of elastic body; (*a*) FEM model; (*b*) FEM mesh and contact points on the bottom surface

and only a one-quarter model is used because of symmetry as shown in Fig. 2. For the FEM model, 128 isoparametric eight-noded brick elements and 225 nodes are used. Twenty-five contact nodes are on the bottom surface as shown in Fig. 2. A constant pressure is applied on the top surface of the elastic body by two steps of 30 percent and 100 percent of the maximum load level and unloaded by four steps corresponding to 95 percent, 70 percent, 50 percent, and 30 percent of the maximum level. Poisson's ratio is taken to be 0.3 and Young's modulus 206 GPa. Directions of slips and pressure distributions on the contact surface at loading and unloading steps are shown in Fig. 3 and 4 when the friction coefficient is 0.1. The arrows represent the directions of slips not magnitudes and the pressure distributions are scaled by the maximum applied pressure. Rapid changes of pressure distributions and contact status such as the process of outward slip-adhesion-inward slip, mentioned and shown by other authors for two-dimensional and axisymmetric contact (Torstenfelt, 1984; Lee and Kwak, 1988) at unloading steps, are well observed in Fig. 3 and 4. Pressure distribution and slips at 100 percent loading are compared with the results of a commercial package, ABAQUS for 10^7 of "stiffness in stick" which is a penalty parameter used to impose zero relative slip when the friction force does not exceed the friction limit. Their agreement is good as shown in Figs. 5 and 6. Slight differences are observed in the pressure though probably due to the approximation nature specific to the method used in ABAQUS as compared to the present exact treatment. The results of ABAQUS converged to those of the proposed method as the value of "stiffness in stick" was increased and obviously, more computing time was needed. For the value larger than 10^7 ABAQUS failed to converge.

Example 2. Rigid Punch on the Elastic Half Surface. Indentation of an elastic half-space by a flat-ended square rigid punch as treated in Klarbring (1986) is solved by the proposed method. The material is isotropic and homogeneous and friction coefficient is 0.1848. Material properties are given in a consistent unit. Poisson's ratio and Young's modulus are taken to be 0.3 and 2000, respectively. Only one quarter of the half-space is modeled considering the symmetry of the problem.

Downloaded 03 May 2010 to 171.66.16.20. Redistribution subject to ASME license or copyright; see http://www.asme.org/terms/Terms_Use.cfm

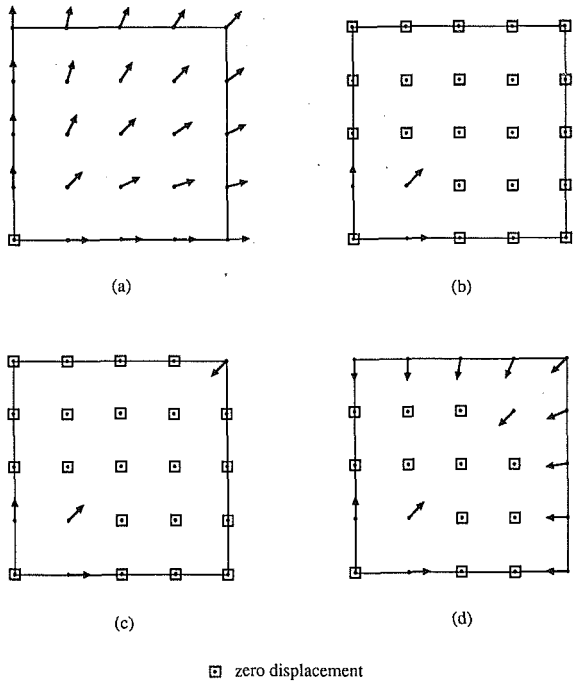


Fig. 3 Direction of slips during unloading ($\mu_a = 0.1$, $\mu_b = 0.1$); at loading level of (*a*) 100 percent; (*b*) 95 percent; (*c*) 70 percent; (*d*) 50 percent

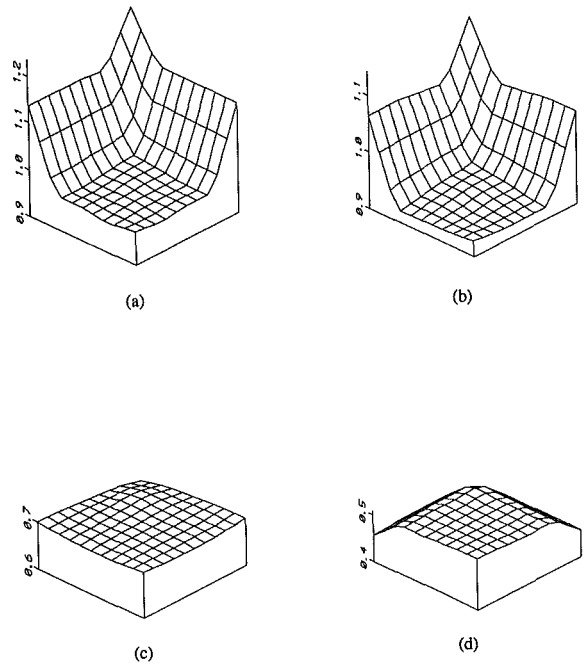


Fig. 4 Pressure distributions during unloading ($\mu_a = 0.1$, $\mu_b = 0.1$); at load level of (*a*) 100 percent; (*b*) 95 percent; (*c*) 70 percent; (*d*) 50 percent

The dimension of the quarter model is 10.0 × 10.0 × 10.0 and the area of contact surface is 1.0 × 1.0. For the FEM model, 1575 nodes, 1176 eight-noded brick elements, and 49 contact nodes are used as shown in Fig. 7, which is coarser than that of Klarbring (1986). The same loading cases as in Klarbring (1986) are used for comparison, that is monotonically increasing vertical displacement of the rigid punch and gradually removing it. In Fig. 8 tangential displacements and stick points are represented at various loading steps. At unloading steps, a new stick zone begins to develop at the edge of punch and gradually moves inwardly. Reverse slip occurs as mentioned by other authors (Torstenfelt, 1984; Klarbring,

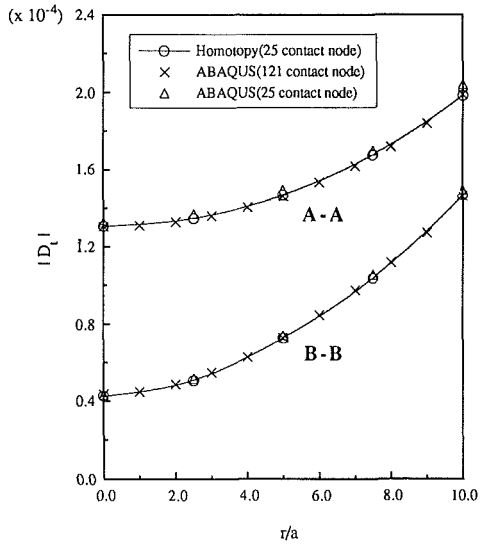


Fig. 5 Comparison of tangential displacement with ABAQUS

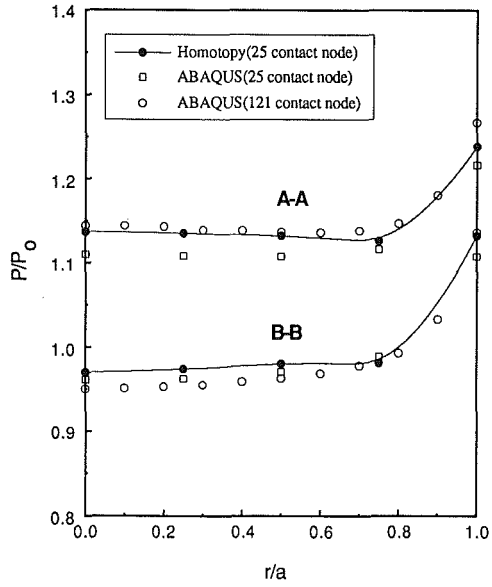


Fig. 6 Comparison of pressure with ABAQUS

1986). The general behavior of contact status is nearly similar to the result by linear complementarity formulation using octagonal friction law (Klarbring, 1986) but more reasonable smooth changes of slip angles are obtained in this work. Pressure distribution at 100 percent loading is compared with Klarbring (1986) in Fig. 9. The discrepancies observed are presumably due to the difference in the two discretizations and especially the linearization of the friction law in Klarbring (1986). Comparison of the magnitude of tangential displacements on the contact surface is shown in Fig. 10. Slips of the present work are relatively larger than those of Klarbring (1986) in the region from 0.6 to 0.95 of r/a. This region approximately corresponds to the situation where the octagonal approximation of the circular-type friction law causes relatively large error. An underestimate of the tangential displacements by Klarbring (1986) is plausible.

5 Conclusions

A new solution method for three-dimensional contact problems with the orthotropic Coulomb friction using a homotopy method has been presented. The nonlinear complementarity

Downloaded 03 May 2010 to 171.66.16.20. Redistribution subject to ASME license or copyright; see http://www.asme.org/terms/Terms_Use.cfm

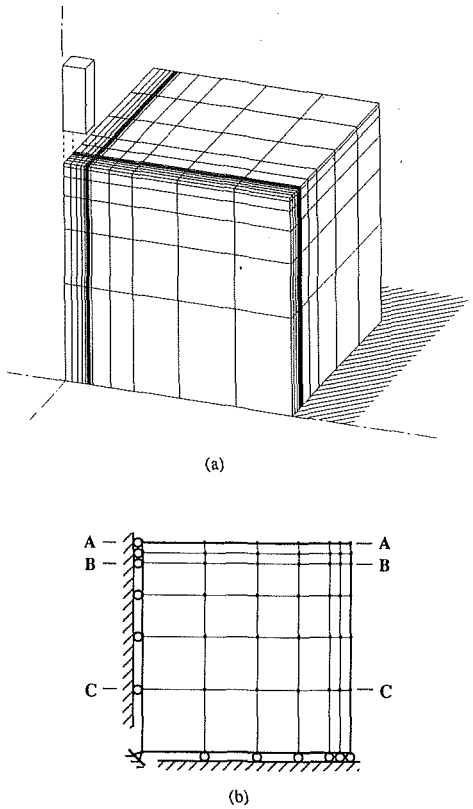


Fig. 7 Modeling of half-space; (*a*) FEM model; (*b*) FEM mesh and contact points on the contact surface

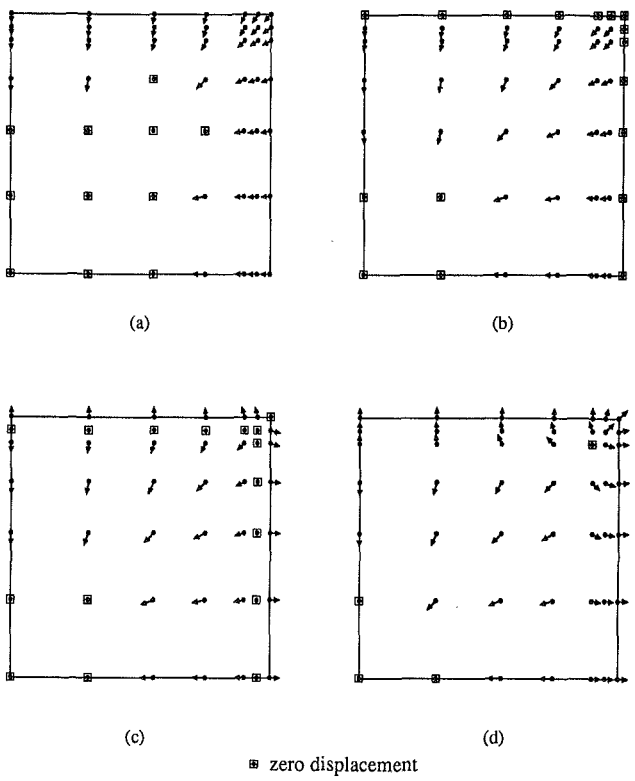


Fig. 8 Direction of tangential displacement; at load level of (*a*) 100 percent; (*b*) 39.8 percent; (*c*) 29.3 percent; (*d*) 17.9 percent

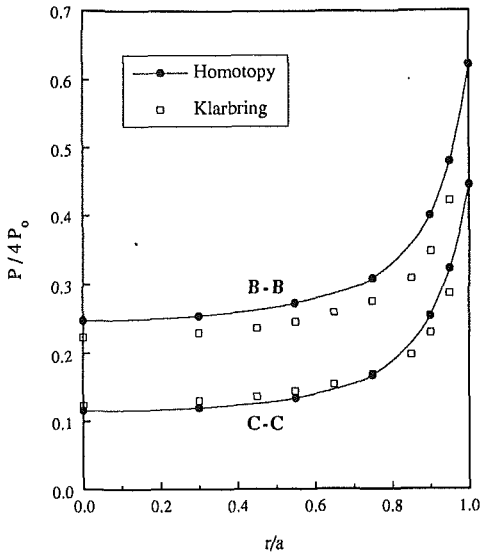


Fig. 9 Comparison of pressure on the contact surface with Klarbring (1986)

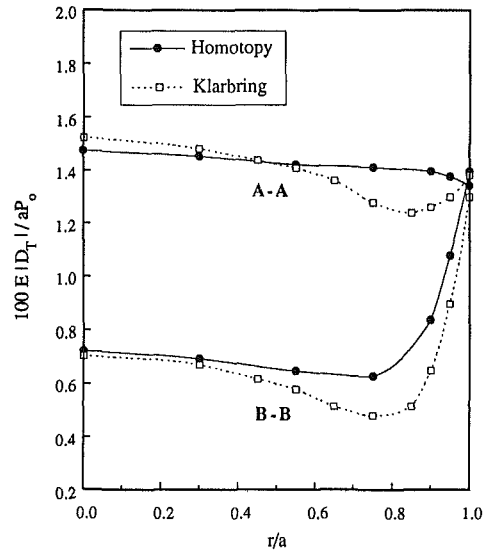


Fig. 10 Comparison of tangential displacement with Klarbring (1986)

problem exactly describing three-dimensional frictional contact phenomena has been transformed to a system of nonlinear equations and solved by the probability-one homotopy method. The formulation is very general without any specific restrictions as previously introduced on the normal contact force and on the contact area. Also, no linearization scheme of the orthotropic Coulomb friction law has been necessary. Moreover, the problem of large matrix size in solving LCP is alleviated in this solution method because the number of variables is only $4n_c + n_r$ after condensation, where n_c is the number of potential contact points and n_r is the number of rigid degrees-of-freedom. Although no comparisons under the exact same conditions are possible due to the difference in the nature of approximation and discretization, the results of two examples have been presented together with those from a commercial package and literature.

Acknowledgment

This work is partially supported by the Korea Science and Engineering Foundation.

Downloaded 03 May 2010 to 171.66.16.20. Redistribution subject to ASME license or copyright; see http://www.asme.org/terms/Terms_Use.cfm

References

Allgower, E., and Georg, K., 1980, "Simplicial and Continuation Methods for Approximating Fixed Points," *SIAM Review*, Vol. 22, pp. 28–85.

Bathe, K. J., and Chaudhary, A., 1985, "A Solution Method for Planar and Axisymmetric Contact Problems," *International Journal for Numerical Methods in Engineering*, Vol. 21, pp. 65–88.

Boehm, J., 1987, "A Comparison of Different Contact Algorithms with Applications," *Computers and Structures*, Vol. 26, pp. 207–221.

Chow, S. N., Mallet-Paret, J., and Yorke, J. A., 1978, "Finding Zeros of Maps: Homotopy Methods that are Constructive with Probability One," *Mathematics of Computation*, Vol. 32,.pp. 887–899.

Cottle, R. W., Giannessi, F., and Lions, J. L., 1980, *Variational Inequalities and Complementarity Problems*, John Wiley and Sons, New York.

Dennis, J. E., and Schnabel, R., 1983, *Numerical Methods for Unconstrained Optimization and Nonlinear Equations*, Prentice-Hall, Englewood Cliffs, N.J.

Duvaut, G., and Lions, J. L., 1976, *Inequalities in Mechanics and Physics*, Springer-Verlag, Berlin.

Hibbitt, Karlsson & Sorensen, Inc., 1988, *ABAQUS User's Manual*.

Joo, J. W., and Kwak, B. M., 1986, "Analysis and Application of Elastoplastic Contact Problems Considering Large Deformations," *Computers and Structures*, Vol. 24, pp. 958–961.

Klarbring, A., 1986, "A Mathematical Programming Approach to Three-Dimension Contact Problems with Friction," *Computer Methods in Applied Mechanics and Engineering*, Vol. 58, pp. 175–200.

Klarbring, A., and Bjorkman, G., 1988, "A Mathematical Programming Approach to Contact Problems with Friction and Varying Contact Surface," *Computers and Structures*, Vol. 30, pp. 1185–1198.

Kwak, B. M., 1990, "Numerical Implementation of Three-Dimensional Frictional Contact by a Linear Complementarity Problem," *KSME Journal*, Vol. 4, pp. 23–31.

Kwak, B. M., 1991, "Complementarity Problem Formulation of Three-Dimensional Frictional Contact," ASME JOURNAL OF APPLIED MECHANICS, Vol. 58, pp. 134–140.

Lee, S. S., and Kwak, B. M., 1988, "A Complementarity Problem Formulation for Two-Dimensional Frictional Contact Problem," *Computers and Structures*, Vol. 28, pp. 469–480.

Mangasarian, O. L., 1976, "Equivalence of the Complementarity Problem to a System of Nonlinear Equations," *SIAM Journal on Applied Mathematics*, Vol. 31, pp. 89–92.

Oden, J. T., and Pires, E. B., 1983, "Nonlocal and Nonlinear Friction Laws and Variational Principles for Contact Problems in Elasticity," ASME JOURNAL OF APPLIED MECHANICS, Vol. 50, pp. 67–76.

Okamato, N., and Nakazawa, M., 1979, "Finite Element Incremental Contact Analysis with Various Frictional Conditions," *International Journal for Numerical Methods in Engineering*, Vol. 14, pp. 337–357.

Panagiotopoulos, P. D., 1985, *Inequality Problems in Mechanics and Applications*, Birkhaeuser.

Rahman, M. U., Rowlands, R. E., and Cook, R. D., 1984, "An Iterative Procedure for Finite Element Stress Analysis of Frictional Contact Problems," *Computers and Structures*, Vol. 18, pp. 947–954.

Rheinboldt, W. C., 1986, *Numerical Analysis of Parameterized Nonlinear Equations*, John Wiley and Sons, New York.

Rheinboldt, W. C., and Burkardt, J. V., 1983, "Algorithm 596: A Program for a Locally Parameterized Continuation Process," *ACM Transactions on Mathematical Software*, Vol. 9, pp. 236–241.

Torstenfelt, B., 1984, "An Automatic Incrementation Technique for Contact Problems with Friction," *Computers and Structures*, Vol. 19, pp. 393–400.

Watson, L. T., 1986, "Numerical Linear Algebra Aspects of Globally Convergent Homotopy Methods," *SIAM Review*, Vol. 28, pp. 529–545.

Watson, L. T., 1979, "Solving the Nonlinear Complementarity Problem by a Homotopy Method," *SIAM Journal on Control and Optimization*, Vol. 17, pp. 36–46.

Watson, L. T., Billups, S. C., and Morgan, A. P., 1987, "Algorithm 652: HOMPACK: A Suite of Codes for Globally Convergent Homotopy Algorithms," *ACM Transactions on Mathematical Software*, Vol. 13, pp. 281–310.

Watson, L. T., and Wang, C. Y., 1981, "A Homotopy Method Applied to Elastica Problems," *International Journal of Solids and Structures*, Vol. 17, pp. 29–37.

Downloaded 03 May 2010 to 171.66.16.20. Redistribution subject to ASME license or copyright; see http://www.asme.org/terms/Terms_Use.cfm

Journal of Applied Mechanics

Brief Notes

A Brief Note is a short paper that presents a specific solution of technical interest in mechanics but which does not necessarily contain new general methods or results. A Brief Note should not exceed 1500 words *or equivalent* (a typical one-column figure or table is equivalent to 250 words; a one line equation to 30 words). Brief Notes will be subject to the usual review procedures prior to publication. After approval such Notes will be published as soon as possible. The Notes should be submitted to the Technical Editor of the JOURNAL OF APPLIED MECHANICS. Discussions on the Brief Notes should be addressed to the Editorial Department, ASME, United Engineering Center, 345 East 47th Street, New York, N. Y. 10017, or to the Technical Editor of the JOURNAL OF APPLIED MECHANICS. Discussions on Brief Notes appearing in this issue will be accepted until two months after publication. Readers who need more time to prepare a Discussion should request an extension of the deadline from the Editorial Department.

On the Modeling of Fracture of Brittle Solids

Y. V. Petrov[1] and N. F. Morozov[2]

1 Introduction

Dynamic fracture initiation in brittle solids is remarkable for some principal effects that have no interpretation within the framework of traditional models of brittle failure.

The traditional ways of modeling of the dynamic failure effects and testing of the dynamic strength properties of the material are usually reduced to the measuring of the fracture toughness and strength rate dependencies, proclaimed as material functions.

The approach suggested in the present paper associates the dynamic strength peculiarities of the brittle media with the existence of a special physical constant with dimension of time. In special cases, the introduced structure time may be interpreted as an incubation time in well-known minimum time criterion proposed and explored by Kalthoff and Shockey (1977), Homma et al. (1983), and Shockey et al. (1986). The brittle fracture criterion assumed in the present paper allows us to calculate the fracture toughness rate dependencies on the basis of a system of fixed material parameters and so to explain some of the principal effects of dynamic tests. The results of some of the well-known experiments (Ravi-Chandar and Knauss, 1984; Shockey et al., 1986) are discussed in terms of the suggested structure-time fracture criterion.

2 Brittle Fracture Criterion

Analysis of the experiments shows that the main contradictions of the traditional models reveal themselves when failure occurs during the short time intervals after the start of the loading process.

Morozov and Petrov (1990) proposed an approach to the analysis of brittle failure in dynamic based on the structure-time fracture criterion:

$$\frac{1}{\tau}\int_{t-\tau}^{t}\frac{1}{d}\int_{0}^{d}\sigma(r, t')drdt' \le \sigma_c. \tag{1}$$

Here d and τ are the structure size and structure time of failure, σ_c is static strength of the material, and $\sigma(r, t)$ is the maximum tension stress at the crack tip ($r = 0$). The structure size d is to be determined in accordance with the data of quasi-statical tests of crack-containing specimens, and in case of a plane deformation state it may be expressed by the simple formula (Morozov, 1984): $d = 2\,K_{Ic}^2/(\pi\sigma_c^2)$. The structure time τ is responsible for the dynamic peculiarities of the macrofracture process and for each material should be found from experiments. In accordance with this approach σ_c, K_{Ic}, and τ do make up the system of fixed material constants describing macro strength properties of the material. Petrov (1991) has shown that the criterion (1) reflects the discrete nature of dynamic fracture of brittle solids.

In the special case of slow deformation the quasi-statical criterion by Neuber-Novozilov (Neuber, 1937; Novozilov, 1969) from (1) comes out.

Criterion (1) may also be written in the form $J(t) \le J_c$, $J_c = \sigma_c\tau\, d$. This form has the physical meaning of critical structure momentum. Time at fracture t_* must be determined by equation $J(t_*) = J_c$. The threshold condition

$$J(t_*) = \max_t J(t) = J_c \tag{2}$$

may be considered as a condition of instability.

We shall demonstrate below that some of the effects of cracks instability and rate dependence of fracture toughness of brittle materials can be obtained and analyzed within the framework of linear elasticity and suggested criterion.

3 Instability of Cracks Under Short Pulse Loads and Loading Rate Effect

The semi-infinite straight crack ($x \le 0$, $y = 0$) is situated in the infinite plate and loaded on its faces by the rectangular stress pulse of amplitude P and duration T:

$$\sigma_y = P[H(t) - H(t-T)], \quad \sigma_{xy} = 0. \tag{3}$$

$H(t)$ is the Heaviside function. The appropriate expression for the maximal tearing stress on the prospective crack line is well known and given by

[1]IPTRAN, Academy of Sciences of Russia, 12 Linia, 13, St. Petersburg, 199178, Russia.

[2]Department of Elasticity, St. Petersburg State University, Petrodvorets, St. Petersburg, 198904, Russia.

Contributed by the Applied Mechanics Division of THE AMERICAN SOCIETY OF MECHANICAL ENGINEERS for publication in the ASME JOURNAL OF APPLIED MECHANICS. Manuscript received by the ASME Applied Mechanics Division, June 5, 1992; final revision, Apr. 12, 1993. Associate Technical Editor: X. Markenscoff.

Copyright © 1994 by ASME
Downloaded 03 May 2010 to 171.66.16.20. Redistribution subject to ASME license or copyright; see http://www.asme.org/terms/Terms_Use.cfm

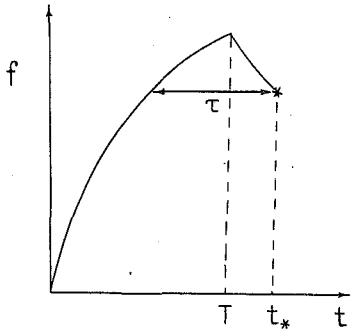


Fig. 1 The stress intensity function $f(t)$ in conditions of crack instability

$$\sigma_y = K_I(t)/\sqrt{2\pi x} + 0(1), \quad x \to 0;$$

$$K_I(t) = P\phi(c_1, c_2)f(t), \quad f(t) = \sqrt{t}\,H(t) - \sqrt{t-T}\,H(t-T),$$

$$\phi(c_1, c_2) = 4c_2\sqrt{c_1^2 - c_2^2}/(c_1\sqrt{\pi c_1}), \tag{4}$$

where c_1, c_2 are velocities of longitudinal and shear waves.

We are interested in critical pulse amplitude for crack instability. It may be determined from (2) and (4) and expressed by simple formula:

$$P_1 = \frac{\tau K_{Ic}}{\phi(c_1, c_2)\max\limits_t \int_{t-\tau}^{t} f(s)\,ds}. \tag{5}$$

On the other hand, from traditional criterion of maximum stress intensity, $\max\limits_t K_I(t) = K_{Ic}$ (Sih, 1968) becomes

$$P_2 = \frac{K_{Ic}}{\phi(c_1, c_2)\max\limits_t f(t)}. \tag{6}$$

In our case we find that

$$\max_t \frac{1}{\tau}\int_{t-\tau}^{t} f(s)\,ds < \max_t f(t), \tag{7}$$

and so it follows from (5), (6), and (7) that

$$P_1 > P_2. \tag{8}$$

This result conforms with the experiments on short pulse crack instability (Shockey et al., 1986), in which it was shown that for very short-duration pulses (so, that the stress intensity history were independent of crack length), the critical values of the stress amplitudes were greater than the same values calculated from maximum stress intensity criteria and could not be explained by classical fracture mechanics.

The dependence of stress intensity at the crack tip on time is schematically shown in Fig. 1. At the moment of fracture t_* inegral $\int_{t-\tau}^{t} f(s)ds$ reaches its maximum value, therefore $f(t_* - \tau) = f(t_*)$. Due to monotony properties of function $f(t)$ we can conclude that $K_I(t)$ exceeds the value $K_{Id} = K(t_*)$ for the period τ. Thus, theoretical analysis of the crack instability shows that structure parameter τ has the features of incubation time t_{inc}, introduced by Kalthoff and Shockey (1977), and so for the problems of crack growth initiation it may be taken

$$\tau = t_{\text{inc}}. \tag{9}$$

Taking, for example, the characteristics of 4340 steel $c_1 = 6$ mm/μsec, $\nu = 0.3$, $K_{Ic} = 47$ MPa, $\tau_{\text{inc}} = 7$ μsec and duration of pulse $T = 18$ μsec we receive from (5), (9) the value of critical stress amplitude $P_1 = 155$ MPa that well corroborates with the experiments by Homma et al. (1983).

It is noteworthy that dynamic fracture toughness may here be regarded as a calculated characteristic. The values of the dynamic fracture toughness become less than the appropriate quasi-statical value

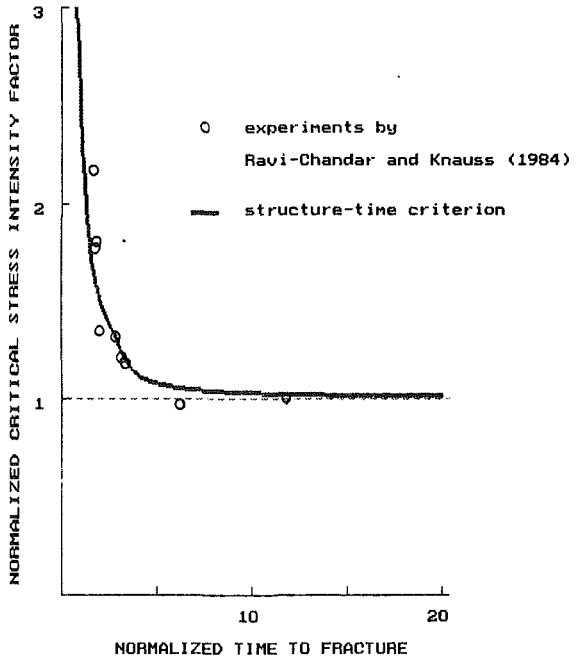


Fig. 2 The dependence of normalized critical stress intensity factor of crack growth initiation K_{Iq}/K_{Ic} on normalized time to fracture, t_*/τ calculated for $t_O = 25$ μsec, $K_{Ic} = 0.48$ MPa$\sqrt{m}$, $\tau = 9$ μsec

$$K_{Id} = P_1\phi(c_1, c_2)f(t_*) = \frac{\tau K_{Ic} f(t_*)}{\int_{t_*-\tau}^{t_*} f(s)\,ds} < K_{Ic}, \tag{10}$$

that was observed in the aforementioned crack instability experiments.

Let us now consider the semi-infinite straight crack loaded on its faces by the endless trapezoidal normal stress of amplitude P:

$$\sigma_y = P/t_O[tH(t) - (t-t_O)H(t-t_O)], \quad \sigma_{xy} = 0, \tag{11}$$

where t_O is the rise time of the pulse. The appropriate asymptotic for the maximal normal stress on the prospective crack line is given by the expression (4) where

$$f(t) = 2[t^{3/2}H(t) - (t-t_O)^{3/2}H(t-t_O)]/(3t_O). \tag{12}$$

Let t_* be time to fracture, and t_O is fixed. Using (1), (4), and (12) we can find the corresponding term to t_* fracture amplitude P_*. After the calculation of the critical stress intensity factor of initiation of crack growth $K_{Iq} = K_I(t_*) = P_*\phi(c_1, c_2)f(t_*)$ we receive

$$\frac{K_{Iq}}{K_{Ic}} = \frac{5}{2}\frac{\bar{t}_*^{3/2} - (\bar{t}_* - \bar{t}_O)^{3/2}}{\bar{t}^{5/2}{}_* - (\bar{t}_* - 1)^{5/2} - (\bar{t}_* - \bar{t}_O)^{5/2} + (\bar{t}_* - \bar{t}_O - 1)^{5/2}} \tag{13}$$

where $\bar{t}_* = t_*/\tau$, $\bar{t}_O = t_O/\tau$. Here the values of power functions for the negative values of their arguments are supposed equal to zero.

Ravi-Chandar and Knauss (1984) conducted dynamic tests under comparable conditions using specimens made of Homalite-100. We do not know the structure time for that material but can try to evaluate it assuming the coincidence between theoretical and experimental results. The calculated curve in Fig. 2 was obtained for $t_O = 25$ μsec, $K_{Ic} = 0.48$ MPa $\sqrt{m}$, and $\tau = 9$ μsec. The results are very similar with what in the experiments was observed. There is an obvious dependence of critical stress intensity factor of crack growth initiation on the loading history. Analytical formula (13) shows that it depends

Downloaded 03 May 2010 to 171.66.16.20. Redistribution subject to ASME license or copyright; see http://www.asme.org/terms/Terms_Use.cfm

on the rise time t_O. In the case of finite bodies this connection will depend on the geometrical parameters of the problem. For instance, if L is the size of the crack and $K_I(t) = PG(t, L)$, then from (1) becomes

$$\frac{K_{Iq}}{K_{Ic}} = \frac{\tau G(t_*, L)}{\int_{t_*-\tau}^{t_*} G(s, L)\, ds}. \tag{17}$$

Unlike the crack instability problem here, the load on the crack faces acts up to the moment of macrofracture. It provides the monotonic growth of the stress intensity factor during the whole time interval τ, so that the inequality $K_{Iq} > K_{Ic}$ comes out. The same relation in numerous experiments was observed (Ravi-Chandar and Knauss, 1984; Kalthoff, 1986; Dally and Barker, 1988).

4 Conclusions

In the present paper the structure-time model was considered that allowed us to obtain analytically some of the general effects of fast fracture observed in well-known experiments. According to the suggested approach the principal parameter that is responsible for dynamic reaction by brittle failure is the certain structure time τ, which supplements the quasi-statical fracture characteristics system σ_c and K_{Ic} (or d). Analysis of instability of cracks under short pulse loads has shown that introduced structure time might be interpreted as an incubation time in well-known minimum time criterion. Structure time τ should be found from the experiments on fast fracture of brittle solids. It may be considered as a parameter given for each material and an appropriate class of problem. Having σ_c, K_{Ic}, and τ, we can obtain the united description of the limiting loads both for slow and for high-rate deformation processes. The rate dependencies of dynamic fracture toughness (effects of rate of loading) for each material and the chosen way of loading by means of structure-time criterion can be theoretically constructed. Analysis shows that the critical stress intensity factor of a crack growth initiation may be either less or bigger than its corresponding value in static, depending on the mode and history of loading.

References

Dally, J. W., and Barker, D. B., 1988, "Dynamic Measurements of Initiation Toughness at High Loading Rates," *Experimental Mechanics*, Vol. 28, pp. 298–303.

Homma, H., Shockey, D. A., and Murayama, Y., 1983, "Response of Cracks in Structural Materials to Short Pulse Loads," *J. Mech. Phys. Solids*, Vol. 31, pp. 261–279.

Kalthoff, J. F., and Shockey, D. A., 1977, "Instability of Cracks Under Impulse Loads," *Journal of Applied Physics*, Vol. 48, pp. 986–993.

Kalthoff, J. F., 1986, "Fracture Behavior Under High Rates of Loading," *Engineering Fracture Mechanics*, Vol. 23, pp. 289–298.

Morozov, N. F., 1984, *Mathematical Questions of Crack Theory*, Nauka, Moscow (in Russian).

Morozov, N. F., and Petrov, Yu. V., 1990, "Dynamic Fracture Toughness in Crack Growth Initiation Problems," *Izv. AN SSSR. MTT* (Solid Mechanics), No. 6, pp. 108–111 (in Russian).

Neuber, H., 1937, *Kerbspannungslehre* (*Notch Stresses*), Verlag von Julius Springer, Berlin.

Novozilov, V. V., 1969, "Necessary and Sufficient Criterion of Brittle Strength," *Prikladnaja Matematika i Mechanika*, Vol. 33, pp. 212–222 (in Russian).

Petrov, Yu. V., 1991, "On 'Quantum' Nature of Dynamic Fracture of Brittle Media," *Dokl. AN SSSR*, Vol. 321, pp. 66–68 (in Russian).

Ravi-Chandar, K., and Knauss, W. G., 1984, "An Experimental Investigation into Dynamic Fracture: 1. Crack Initiation and Arrest," *International Journal of Fracture*, Vol. 25, pp. 247–262.

Shockey, D. A., Erlich, D. C., Kalthoff, J. F., and Homma, H., 1986, "Short-Pulse Fracture Mechanics," *Engineering Fracture Mechanics*, Vol. 23, pp. 311–319.

Sih, G. C., 1968, "Some Elastodynamic Problems of Cracks," *Int. J. Fract. Mech.*, Vol. 4, pp. 51–68.

A Note on Peel Stresses in Single-Lap Adhesive Joints

Ming-Yi Tsai[3] and J. Morton[3, 4]

Introduction

The single-lap joint is a bonding configuration widely used in the aerospace, automotive, and wood and plastic industries. Theoretical analyses for the lap joint have been developed over the last 50 years. Among these analyses, the most widely quoted is that due to Goland and Reissner (1944). The Goland and Reissner approach, especially the adhesive peel stress section, has been modified and *corrected* by many other researchers. These revisions have, however, resulted in confusion and inconsistencies in the literature. The purpose of this note is to illustrate these inconsistencies and to identify a consistent solution for the peel stresses in a single-lap adhesive joint.

A schematic representation of a single-lap joint is shown in Fig. 1 in which the geometrical and material parameters are defined in Fig. 1(*a*), and the joint edge moment M_0, edge shear V_0, and edge tensile force T per unit width are defined in the free-body diagram, Fig. 1(*b*). The Goland and Reissner adhesive peel stress (σ_0) and maximum stress solutions are

$$\frac{\sigma_o}{p} = \frac{t^2}{c^2}\frac{1}{\Delta}\left[\left(R_2\lambda^2\frac{k}{2} + \lambda k'\cosh\lambda\cos\lambda\right)\times\cosh\left(\lambda\frac{x}{c}\right)\cos\left(\lambda\frac{x}{c}\right) + \left(R_1\lambda^2\frac{k}{2} + \lambda k'\sinh\lambda\sin\lambda\right)\sinh\left(\lambda\frac{x}{c}\right)\sin\left(\lambda\frac{x}{c}\right)\right] \tag{1}$$

and

$$\frac{(\sigma_0)_{\max}}{p} = \frac{t^2}{c^2}\left(\lambda^2\frac{k}{2}\frac{\sinh 2\lambda - \sin 2\lambda}{\sinh 2\lambda + \sin 2\lambda} + \lambda k'\frac{\cosh 2\lambda + \cos 2\lambda}{\sinh 2\lambda + \sin 2\lambda}\right) \tag{2}$$

where

$$\gamma^4 = \frac{6E_c}{E}\frac{t}{\eta}$$

$$\lambda = \gamma\frac{c}{t}$$

$$R_1 = \cosh\lambda\sin\lambda + \sinh\lambda\cos\lambda$$

$$R_2 = \sinh\lambda\cos\lambda - \cosh\lambda\sin\lambda$$

$$\Delta = \frac{1}{2}(\sinh 2\lambda + \sin 2\lambda) \tag{3}$$

and

$$k = \frac{2M_o}{p\,t^2} \text{ and } k' = \frac{cV_o}{p\,t^2} \tag{4}$$

in which p is the applied average stress (T/t).

Sneddon (1961) produced revised versions of Eqs. (1), (2), and (3) as

[3]Department of Engineering Science and Mechanics, Virginia Polytechnic Institute and State University, Blacksburg, VA 24061-0219.

[4]Mem. ASME.

Contributed by the Applied Mechanics Division of THE AMERICAN SOCIETY OF MECHANICAL ENGINEERS for publication in the JOURNAL OF APPLIED MECHANICS. Manuscript received by the ASME Applied Mechanics Division, Sept. 29, 1992; final revision, May 21, 1993. Associate Technical Editor: J. N. Reddy.

Downloaded 03 May 2010 to 171.66.16.20. Redistribution subject to ASME license or copyright; see http://www.asme.org/terms/Terms_Use.cfm

on the rise time t_O. In the case of finite bodies this connection will depend on the geometrical parameters of the problem. For instance, if L is the size of the crack and $K_I(t) = PG(t, L)$, then from (1) becomes

$$\frac{K_{Iq}}{K_{Ic}} = \frac{\tau G(t_*, L)}{\int_{t_*-\tau}^{t_*} G(s, L)\, ds}. \tag{17}$$

Unlike the crack instability problem here, the load on the crack faces acts up to the moment of macrofracture. It provides the monotonic growth of the stress intensity factor during the whole time interval τ, so that the inequality $K_{Iq} > K_{Ic}$ comes out. The same relation in numerous experiments was observed (Ravi-Chandar and Knauss, 1984; Kalthoff, 1986; Dally and Barker, 1988).

4 Conclusions

In the present paper the structure-time model was considered that allowed us to obtain analytically some of the general effects of fast fracture observed in well-known experiments. According to the suggested approach the principal parameter that is responsible for dynamic reaction by brittle failure is the certain structure time τ, which supplements the quasi-statical fracture characteristics system σ_c and K_{Ic} (or d). Analysis of instability of cracks under short pulse loads has shown that introduced structure time might be interpreted as an incubation time in well-known minimum time criterion. Structure time τ should be found from the experiments on fast fracture of brittle solids. It may be considered as a parameter given for each material and an appropriate class of problem. Having σ_c, K_{Ic}, and τ, we can obtain the united description of the limiting loads both for slow and for high-rate deformation processes. The rate dependencies of dynamic fracture toughness (effects of rate of loading) for each material and the chosen way of loading by means of structure-time criterion can be theoretically constructed. Analysis shows that the critical stress intensity factor of a crack growth initiation may be either less or bigger than its corresponding value in static, depending on the mode and history of loading.

References

Dally, J. W., and Barker, D. B., 1988, "Dynamic Measurements of Initiation Toughness at High Loading Rates," *Experimental Mechanics*, Vol. 28, pp. 298–303.

Homma, H., Shockey, D. A., and Murayama, Y., 1983, "Response of Cracks in Structural Materials to Short Pulse Loads," *J. Mech. Phys. Solids*, Vol. 31, pp. 261–279.

Kalthoff, J. F., and Shockey, D. A., 1977, "Instability of Cracks Under Impulse Loads," *Journal of Applied Physics*, Vol. 48, pp. 986–993.

Kalthoff, J. F., 1986, "Fracture Behavior Under High Rates of Loading," *Engineering Fracture Mechanics*, Vol. 23, pp. 289–298.

Morozov, N. F., 1984, *Mathematical Questions of Crack Theory*, Nauka, Moscow (in Russian).

Morozov, N. F., and Petrov, Yu. V., 1990, "Dynamic Fracture Toughness in Crack Growth Initiation Problems," *Izv. AN SSSR. MTT* (Solid Mechanics), No. 6, pp. 108–111 (in Russian).

Neuber, H., 1937, *Kerbspannungslehre* (*Notch Stresses*), Verlag von Julius Springer, Berlin.

Novozilov, V. V., 1969, "Necessary and Sufficient Criterion of Brittle Strength," *Prikladnaja Matematika i Mechanika*, Vol. 33, pp. 212–222 (in Russian).

Petrov, Yu. V., 1991, "On 'Quantum' Nature of Dynamic Fracture of Brittle Media," *Dokl. AN SSSR*, Vol. 321, pp. 66–68 (in Russian).

Ravi-Chandar, K., and Knauss, W. G., 1984, "An Experimental Investigation into Dynamic Fracture: 1. Crack Initiation and Arrest," *International Journal of Fracture*, Vol. 25, pp. 247–262.

Shockey, D. A., Erlich, D. C., Kalthoff, J. F., and Homma, H., 1986, "Short-Pulse Fracture Mechanics," *Engineering Fracture Mechanics*, Vol. 23, pp. 311–319.

Sih, G. C., 1968, "Some Elastodynamic Problems of Cracks," *Int. J. Fract. Mech.*, Vol. 4, pp. 51–68.

A Note on Peel Stresses in Single-Lap Adhesive Joints

Ming-Yi Tsai[3] and J. Morton[3, 4]

Introduction

The single-lap joint is a bonding configuration widely used in the aerospace, automotive, and wood and plastic industries. Theoretical analyses for the lap joint have been developed over the last 50 years. Among these analyses, the most widely quoted is that due to Goland and Reissner (1944). The Goland and Reissner approach, especially the adhesive peel stress section, has been modified and *corrected* by many other researchers. These revisions have, however, resulted in confusion and inconsistencies in the literature. The purpose of this note is to illustrate these inconsistencies and to identify a consistent solution for the peel stresses in a single-lap adhesive joint.

A schematic representation of a single-lap joint is shown in Fig. 1 in which the geometrical and material parameters are defined in Fig. 1(*a*), and the joint edge moment M_0, edge shear V_0, and edge tensile force T per unit width are defined in the free-body diagram, Fig. 1(*b*). The Goland and Reissner adhesive peel stress (σ_0) and maximum stress solutions are

$$\frac{\sigma_o}{p} = \frac{t^2}{c^2}\frac{1}{\Delta}\left[\left(R_2\lambda^2\frac{k}{2} + \lambda k'\cosh\lambda\cos\lambda\right)\times\cosh\left(\lambda\frac{x}{c}\right)\cos\left(\lambda\frac{x}{c}\right) + \left(R_1\lambda^2\frac{k}{2} + \lambda k'\sinh\lambda\sin\lambda\right)\sinh\left(\lambda\frac{x}{c}\right)\sin\left(\lambda\frac{x}{c}\right)\right] \tag{1}$$

and

$$\frac{(\sigma_0)_{\max}}{p} = \frac{t^2}{c^2}\left(\lambda^2\frac{k}{2}\frac{\sinh 2\lambda - \sin 2\lambda}{\sinh 2\lambda + \sin 2\lambda} + \lambda k'\frac{\cosh 2\lambda + \cos 2\lambda}{\sinh 2\lambda + \sin 2\lambda}\right) \tag{2}$$

where

$$\gamma^4 = \frac{6E_c}{E}\frac{t}{\eta}$$

$$\lambda = \gamma\frac{c}{t}$$

$$R_1 = \cosh\lambda\sin\lambda + \sinh\lambda\cos\lambda$$

$$R_2 = \sinh\lambda\cos\lambda - \cosh\lambda\sin\lambda$$

$$\Delta = \frac{1}{2}(\sinh 2\lambda + \sin 2\lambda) \tag{3}$$

and

$$k = \frac{2M_o}{p\,t^2} \text{ and } k' = \frac{cV_o}{p\,t^2} \tag{4}$$

in which p is the applied average stress (T/t).

Sneddon (1961) produced revised versions of Eqs. (1), (2), and (3) as

[3]Department of Engineering Science and Mechanics, Virginia Polytechnic Institute and State University, Blacksburg, VA 24061-0219.

[4]Mem. ASME.

Contributed by the Applied Mechanics Division of THE AMERICAN SOCIETY OF MECHANICAL ENGINEERS for publication in the JOURNAL OF APPLIED MECHANICS. Manuscript received by the ASME Applied Mechanics Division, Sept. 29, 1992; final revision, May 21, 1993. Associate Technical Editor: J. N. Reddy.

Copyright © 1994 by ASME
Downloaded 03 May 2010 to 171.66.16.20. Redistribution subject to ASME license or copyright; see http://www.asme.org/terms/Terms_Use.cfm

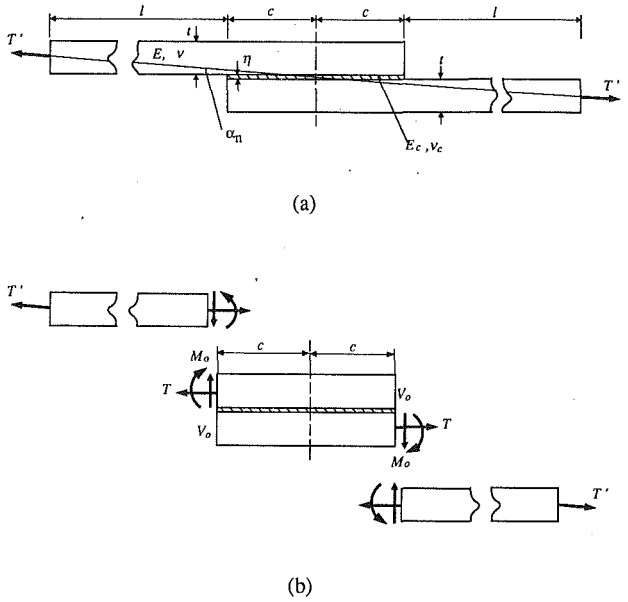


Fig. 1 Schematic configuration of a single-lap joint; (*a*) geometrical and material parameters; (*b*) force equilibrium free-body diagram

$$\frac{\sigma_o}{p}=\frac{t^2}{c^2}\frac{1}{\Delta}\left[\left(R_2\lambda^2\frac{k}{2}-\lambda k'\cosh\lambda\cos\lambda\right)\times\cosh\left(\lambda\frac{x}{c}\right)\cos\left(\lambda\frac{x}{c}\right)+\left(R_1\lambda^2\frac{k}{2}-\lambda k'\sinh\lambda\sin\lambda\right)\sinh\left(\lambda\frac{x}{c}\right)\sin\left(\lambda\frac{x}{c}\right)\right] \quad (5)$$

$$\frac{(\sigma_0)_{\max}}{p}=\frac{t^2}{c^2}\left(\lambda^2\frac{k}{2}\frac{\sinh 2\lambda-\sin 2\lambda}{\sinh 2\lambda+\sin 2\lambda}-\lambda k'\frac{\cosh 2\lambda+\cos 2\lambda}{\sinh 2\lambda+\sin 2\lambda}\right). \quad (6)$$

That is, the terms in k' are negative in Eqs. (5) and (6), as derived by Sneddon and positive in Eqs. (1) and (2) from Goland and Reissner. Sneddon also proposed that Eq. (3) be revised to

$$\gamma^4=\frac{6\,E_c\,(1-\nu^2)}{E}\frac{t}{\eta}, \quad (7)$$

since the Goland and Reissner solution was inconsistent in its incorporation of the Poisson effect.

In addition to these two sets of equations, there are, in effect, several other versions, which mix the Goland and Reissner, and Sneddon equations, or quote either one but with minor inconsistencies in the definition of the edge shear V_0. For example, Adams and Wake (1984) used Eqs. (3), (5), and (6), Anderson, Bennett, and DeVries (1977) employed the Goland and Reissner equations with a different sign of V_o. Chen and Cheng (1983) adopted Goland and Reissner's equations with V_o, obtained from the joint moment-equilibrium (shown in Fig. 1(*b*)) equation

$$V_o=\frac{1}{2c}\left[(t+\eta)T-2M_o\right] \quad (8)$$

rather than Goland and Reissner's original equation

$$V_o=kT\sqrt{3(1-\nu^2)\frac{p}{E}} \quad (9)$$

which is based on "small bending of thin, cylindrically bent plates" but including the effects of the transverse deflections of the joint. Equation (9) does not include the thickness of the adhesive layer. The result of these approaches has been sets of equations for the peel stress, which are neither identical nor consistent, leading to the problem of deciding which equations are correct?

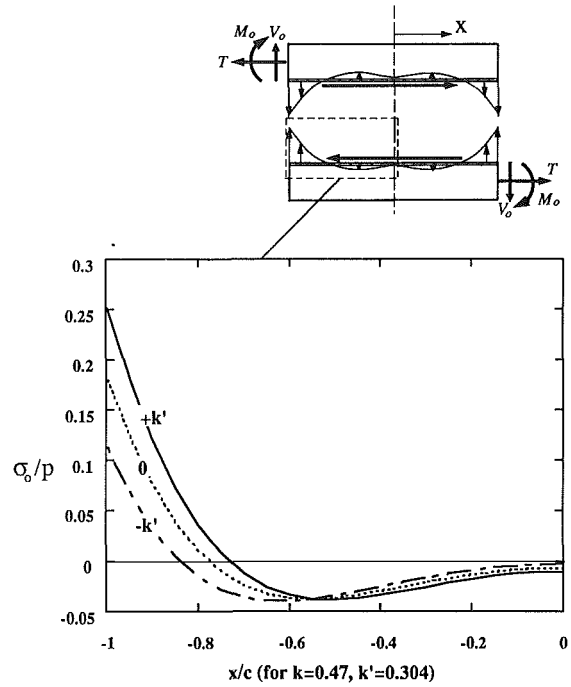


Fig. 2 Normalized adhesive peel stress distribution along a half length of the overlap for the joint with $l/c=10$, $c/t=4$, $\eta/t=0.078$, $E_c/E=0.008$, $k=0.47$ and $k'=0.304$, 0 and -0.304

The Sign of k'

Errors in Derivation. Goland and Reissner made an error in the sign of V_o in the boundary conditions of their derivation (see Eqs. (38) and (48) of the Goland and Reissner paper). The correct V_o in Eqs. (38) and (48) should be

$$V_l=-V_o \text{ at } x=c$$

$$V_u=-V_o \text{ at } x=-c \quad (10)$$

and

$$\frac{d^3\sigma_0}{dx^3}=-\frac{E_c}{\eta D}V_o \text{ at } x=c$$

$$\frac{d^3\sigma_0}{dx^3}=\frac{E_c}{\eta D}V_o \text{ at } x=-c. \quad (11)$$

Apparently, the effects of these errors on σ_0 were removed in the algebraic development of their analysis from Eqs. (48) to (53), so that Eq. (1) is still correct. Sneddon pointed out the error in Eq. (38) of Goland and Reissner's formulation of the boundary conditions and corrected it (but did not correct Eq. (48) of the Goland and Reissner paper). Sneddon then obtained an expression similar to Eq. (1) but with negative signs for the k' terms.

Mechanics Considerations. To support to the statement that Eq. (1) is correct, Eq. (1) is plotted in Fig. 2 for $+k'$, 0 and $-k'$, taking $k=0.47$ and $k'=0.304$. Note that the values of k and k' chosen for the data in Fig. 2 were selected from a parallel experimental and numerical study (Tsai and Morton (1993a)). The value for $k=0.47$ is close to the value of 0.45 provided in Table 1 of Goland and Reissner. However, the value of $k'=0.304$ is not close to the value of 0.094 presented

Downloaded 03 May 2010 to 171.66.16.20. Redistribution subject to ASME license or copyright; see http://www.asme.org/terms/Terms_Use.cfm

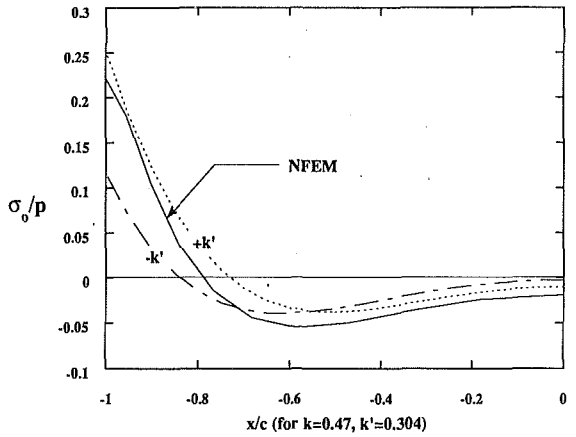


Fig. 3 A comparison of normalized adhesive peel stress distributions from nonlinear finite element method (NFEM) and theoretical solution, along a half length of the overlap for the joint with $l/c = 10$, $c/t = 4$, $\eta/t = 0.078$, $E_c/E = 0.008$, $k = 0.47$ and $k' = 0.304$

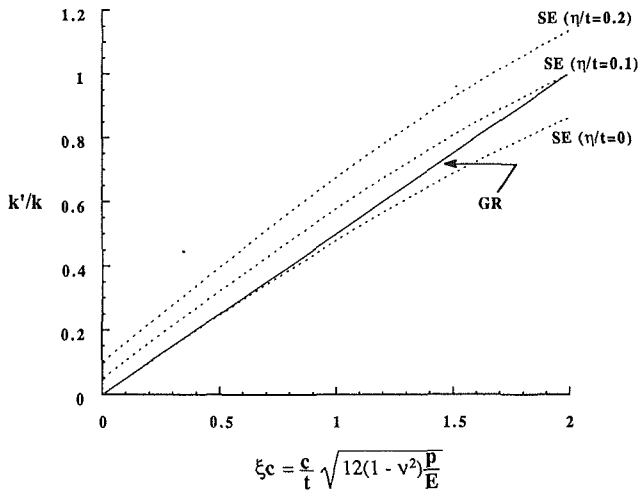


Fig. 4 k'/k versus ξc for Eq. (9), Goland and Reissner's equation (GR), and Eq. (8), self-equilibrium equation (SE), for various η/t.

in the table. An error in the tabulated values of k' has been noted by Sneddon (1961). Since T' is tensile, the generated V_o is positive (with reference to the free-body diagram in Fig. 1(*b*)). Based on force equilibrium in the transverse (y) direction, $\int_{-c}^{c} \sigma_0\, dx$ equals zero for $k' = 0$ (representing $V_o = 0$), or $\int_{-c}^{c} \sigma_0\, dx$ is positive (tensile) values for $+k'$ in order to balance the positive V_o. However, the $-k'$, resulting in a negative value of $\int_{-c}^{c} \sigma_o\, dx$, violates equilibrium for positive V_o. Further evidence is shown in Fig. 3 which provides a comparison of peel stress distributions determined from a two-dimensional nonlinear finite element analysis (NFEM, from Tsai and Morton (1993b)) and Eq. (1) and (5) (representing $+k'$ and $-k'$, respectively). It is clear that the result from Eq. (1) agrees more closely with the NFEM than that from Eq. (5). It should be noted that Carpenter (1989) has also concluded that Eq. (1) is correct and verified his conclusion with a special adhesive element finite element model.

Roles of V_o and ν

The joint edge shear V_o formulation, Eq. (9), developed by Goland and Reissner ignores the thickness of the adhesive layer, is based on small deflection cylindrical bending theory. Following Goland and Reissner's derivation, Eqs. (9) and (4) yield

$$k' = \frac{kc}{t}\sqrt{3(1-\nu^2)\,\frac{p}{E}} = \frac{k\xi c}{2} \tag{12}$$

where $\xi = \frac{1}{t}\sqrt{12(1-\nu^2)\,\frac{p}{E}}$. However, the free-body diagram in Fig. 1(*b*), Eqs. (8) and (4), k' can also be expressed as

$$k' = \frac{(1-k)}{2} + \frac{\eta}{2t} = k\left[\frac{1}{2}\left(\frac{1}{k} - 1\right) + \frac{\eta}{2t\,k}\right] \tag{13}$$

where $k = \left[1 + 2\sqrt{2}\,\tanh\left(\frac{\xi c}{2\sqrt{2}}\right)\right]^{-1}$.

It is interesting then to determine how the selection of Eq. (12) or (13) affects the maximum adhesive peel stress. Equations (12) and (13) can be plotted in Fig. 4 as k'/k versus ξc for various values of η/t. Figure 4 shows that the k'/k from Eq. (9), suggested by Goland and Reissner, is close to that from Eq. (8), the self-equilibrium (SE) equation, *only* for a short joint ($\xi c < 1$) *and* zero-thickness adhesive $\eta/t \cong 0$, whereas

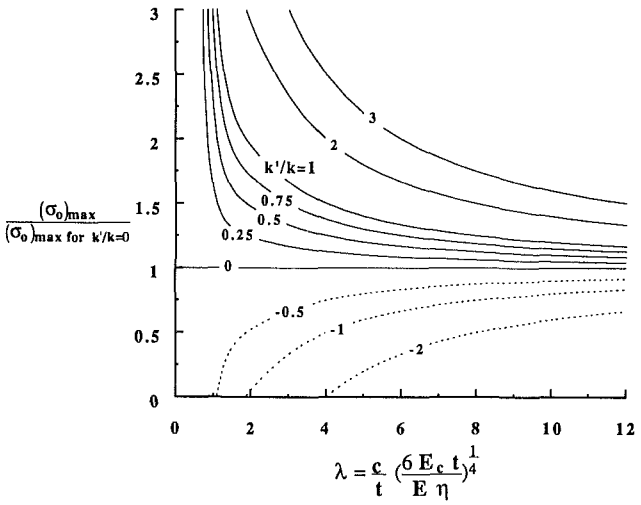


Fig. 5 The sensitivity of the maximum peel stress, normalized by $(\sigma_o)_{max}$ for $k'/k = 0$, to k'/k and λ

both diverge for $\xi c > 1$. Also, Eq. (9) underestimates k'/k for the short joint with a relatively large thickness of adhesive layer. Increasing η/t is associated with increasing k'/k, according to Eq. (8). In order to illustrate the sensitivity of k'/k to the peel stress σ_o, Eq. (2) normalized by $(\sigma_o)_{max}$ for $k'/k = 0$

$$\frac{(\sigma_o)_{max}}{(\sigma_o)_{max\ for\ k'/k=0}} = 1 + \frac{2}{\lambda}\,\frac{k'}{k}\left(\frac{\cosh 2\lambda + \cos 2\lambda}{\sinh 2\lambda - \sin 2\lambda}\right) \tag{14}$$

is plotted against λ for various values of k'/k in Fig. 5. The results indicate that for $\lambda > 5$ the variations in the values of $(\sigma_o)_{max}$, corresponding to a change of 0.1 in k'/k, are less than five percent $(\sigma_o)_{max\ for\ k'/k=0}$, and for $5 > \lambda > 2$ a 0.05 difference corresponds to less than five percent. Also, $(\sigma_o)_{max}$ increases in value as k'/k (or V_o) increases. It is also shown that the negative k' would yield a significant error. From Fig. 4 and 5, the differences due to V_o calculated from Eqs. (8) and (9) on $(\sigma_o)_{max}$ are negligible for short joints ($\xi c < 1$) with a very thin adhesive ($\eta/t < 0.05$), otherwise Eq. (8) is recommended. Both figures also indicate that, as applied load T (or stress p) is increased, the influence of V_o on $(\sigma_o)_{max}$ becomes more significant.

The Poisson's ratio ν effect on σ_o was omitted by Goland and Reissner in Eq. (3), but included by Sneddon in Eq. (7).

Downloaded 03 May 2010 to 171.66.16.20. Redistribution subject to ASME license or copyright; see http://www.asme.org/terms/Terms_Use.cfm

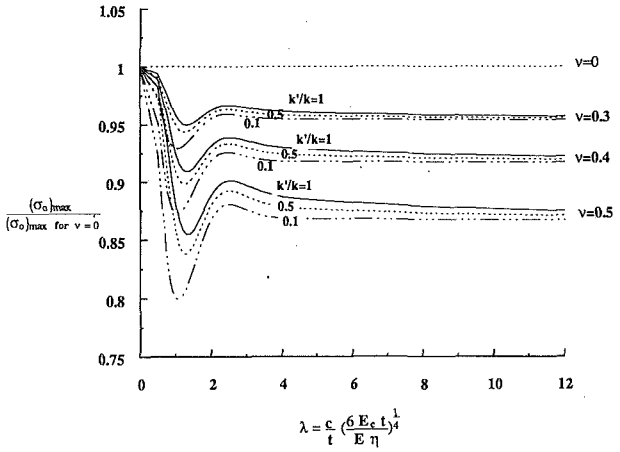


Fig. 6 The sensitivity of the maximum peel stress, normalized by $(\sigma_o)_{max}$ for $\nu = 0$, to ν, k'/k and λ

In order to understand the sensitivity of the solution to ν, $(\sigma_o)_{max}$ Eq. (2) is normalized by $(\sigma_o)_{max\ for\ \nu=0}$:

$$\frac{(\sigma_o)_{max}}{(\sigma_o)_{max\ for\ \nu=0}} = \frac{\lambda_o^2 \frac{1}{2}\frac{\sinh 2\lambda_o - \sinh 2\lambda_o}{\sinh 2\lambda_o + \sin 2\lambda_o} + \lambda_o \frac{k'}{k}\frac{\cosh 2\lambda_o + \cos 2\lambda_o}{\sinh 2\lambda_o + \sin 2\lambda_o}}{\lambda^2 \frac{1}{2}\frac{\sinh 2\lambda - \sin 2\lambda}{\sinh 2\lambda + \sin 2\lambda} + \lambda \frac{k'}{k}\frac{\cosh 2\lambda + \cos 2\lambda}{\sinh 2\lambda + \sin 2\lambda}} \quad (15)$$

where $\lambda_o = \lambda\,(1-\nu^2)^{1/4}$. Equation (15) is then plotted against λ in Fig. 6. It is shown that increasing ν leads to reduced $(\sigma_o)_{max}$. That is, for $\lambda > 3$ and $\nu = 0.3 \sim 0.4$, Eq. (3) without the Poisson effect ($\nu = 0$) gives five ~ seven percent more for $(\sigma_o)_{max}$ than Eq. (7).

Conclusions

It has been shown, through inspection of the original derivation, equilibrium considerations, and numerical analyses, that the original Goland and Reissner solutions for adhesive peel stress, which has been misused and misquoted by several researchers, is correct, even though there were some errors in the derivation. However, there are still some minor discrepancies in the peel stress equations, which are related to neglecting the Poisson effect, and accurately determining edge shear force, V_o. It has been demonstrated that Poisson effect should be included so that Eq. (3) should be replaced by Eq. (7). It is also suggested that the edge shear V_o expression in Eq. (8) be used in Eq. (4).

References

Adams, R. D., and Wake, W. C., 1984, *Structural Adhesive Joints in Engineering*, Elsevier, New York.

Anderson, G. P., Bennett, S. J., and DeVries, K. L., 1977, *Analysis and Testing of Adhesive Bonds*, Academic Press, New York.

Carpenter, W. C., 1989, "Goland and Reissner were Correct," *Journal of Strain Analysis*, Vol. 24, No. 3, pp. 185–187.

Chen, D., and Cheng, S., 1983, "An Analysis of Adhesive-Bonded Single-Lap Joints," ASME JOURNAL OF APPLIED MECHANICS, Vol. 50, pp. 109–115.

Goland, M., and Reissner, E., 1944, "The Stresses in Cemented Joints," ASME JOURNAL OF APPLIED MECHANICS, Vol. 11, p. A17–A27.

Sneddon, I., 1961, "The Distribution of Stress in Adhesive Joints," *Adhesion*, by D. D. Eley, ed., Oxford University Press, Cambridge, U. K., Chapter 9.

Tsai, M. Y., and Morton, J., 1993a, "An Experimental Investigation of Nonlinear Deformations in Single-Lap Joints," submitted to *Mechanics of Materials*.

Tsai, M. Y., and Morton, J., 1993b, "An Evaluation of Analysis and Numerical Solutions to the Single-Lap Joint," *International Journal of Solids and Structures* (in press).

A Sufficient Stability Condition for Linear Conservative Gyroscopic Systems

Jinn-Wen Wu[5] and Tsu-Chin Tsao[5,6]

A sufficient stability condition for linear conservative gyroscopic systems with negative definite stiffness matrices is given. The condition for the stability is stated in terms of the coefficients of system matrices without solving the spectrum of the entire system. An example is given for comparison with existing results.

1 Introduction

One interesting phenomenon for gyroscopic dynamic systems is that unstable conservative systems can be stabilized by increasing the gyroscopic forces. Criteria to determine reasonably small gyroscopic forces for stabilization are important for practical problems, for example, in the spacecraft attitude control problem, the artillery shell moving problem, and the flexible rotating shaft problem (Chetayev, 1961; Hughes, 1986). Recent results (Inman, 1988; Walker, 1991) have stimulated new interest in providing simple stability conditions for such systems without resorting to eigenvalue calculation.

Linear conservative gyroscopic systems can be described by a set of ordinary differential equations satisfying

$$\ddot{x}(t) + G\dot{x}(t) + Kx(t) = 0, \quad (1)$$

where $G^T = -G$, $K^T = K$. The special case of interest here is when K is negative definite and G is nonsingular. The stability used here is in the sense of Lyapunov (see, for instance, Bellman, 1953).

It is well known that the system described by Eq. (1) is stable if and only if the latent values associated with (1) are purely imaginary and nonzero (see, for instance, Huseyin, 1978) since if λ is a latent value so is $-\lambda$. It has also been known that dissipative damping can easily violate gyroscopic stabilization. Hence in a practical sense, since dissipative forces almost always exist, the gyroscopic stability is only temporary.

2 Previous Results

It has been known that when the determinant of G is sufficiently large, Eq. (1) is stable (Müller, 1985; Roseau, 1987). However, so far only a few criteria to determining the strength of the gyroscopic force for stabilizing the system are available. Summaries of results to date are given in Inman (1988) and Walker (1991).

For a two-degree-of-freedom system, Teschner (1977) showed that the stability for negative definite K results if $4K - G^2$ is positive definite. Inman and Saggio (1985) showed that the stability results if the trace of $4K - G^2$ and the determinant of K are both positive and applied the result to the design of a dynamically tuned gyroscope. In fact, for a two-

[5]Department of Mechanical and Industrial Engineering, University of Illinois at Urbana-Champaign, Urbana, IL 61801.

[6]Mem. ASME.

Contributed by the Applied Mechanics Division of THE AMERICAN SOCIETY OF MECHANICAL ENGINEERS for publication in the ASME JOURNAL OF APPLIED MECHANICS. Manuscript received by the ASME Applied Mechanics Division, Feb. 19, 1993; final revision, Apr. 30, 1993. Associate Technical Editor: P. D. Spanos.

Downloaded 03 May 2010 to 171.66.16.20. Redistribution subject to ASME license or copyright; see http://www.asme.org/terms/Terms_Use.cfm

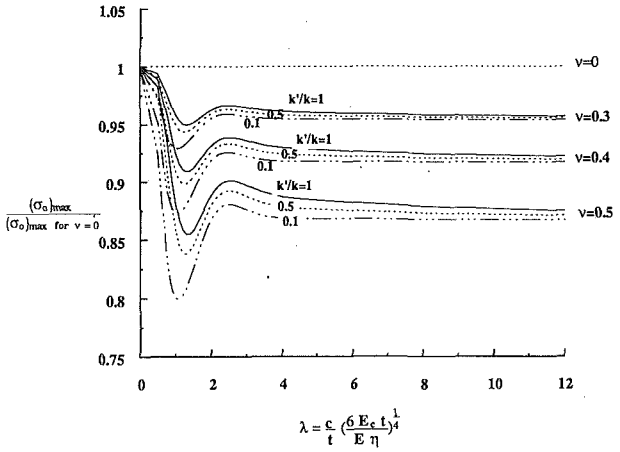


Fig. 6 The sensitivity of the maximum peel stress, normalized by $(\sigma_o)_{max}$ for $\nu = 0$, to ν, k'/k and λ

In order to understand the sensitivity of the solution to ν, $(\sigma_o)_{max}$ Eq. (2) is normalized by $(\sigma_o)_{max\ for\ \nu=0}$:

$$\frac{(\sigma_o)_{max}}{(\sigma_o)_{max\ for\ \nu=0}} = \frac{\lambda_o^2 \frac{1}{2}\frac{\sinh 2\lambda_o - \sinh 2\lambda_o}{\sinh 2\lambda_o + \sin 2\lambda_o} + \lambda_o \frac{k'}{k}\frac{\cosh 2\lambda_o + \cos 2\lambda_o}{\sinh 2\lambda_o + \sin 2\lambda_o}}{\lambda^2 \frac{1}{2}\frac{\sinh 2\lambda - \sin 2\lambda}{\sinh 2\lambda + \sin 2\lambda} + \lambda \frac{k'}{k}\frac{\cosh 2\lambda + \cos 2\lambda}{\sinh 2\lambda + \sin 2\lambda}} \quad (15)$$

where $\lambda_o = \lambda\,(1-\nu^2)^{1/4}$. Equation (15) is then plotted against λ in Fig. 6. It is shown that increasing ν leads to reduced $(\sigma_o)_{max}$. That is, for $\lambda > 3$ and $\nu = 0.3 \sim 0.4$, Eq. (3) without the Poisson effect ($\nu = 0$) gives five ~ seven percent more for $(\sigma_o)_{max}$ than Eq. (7).

Conclusions

It has been shown, through inspection of the original derivation, equilibrium considerations, and numerical analyses, that the original Goland and Reissner solutions for adhesive peel stress, which has been misused and misquoted by several researchers, is correct, even though there were some errors in the derivation. However, there are still some minor discrepancies in the peel stress equations, which are related to neglecting the Poisson effect, and accurately determining edge shear force, V_o. It has been demonstrated that Poisson effect should be included so that Eq. (3) should be replaced by Eq. (7). It is also suggested that the edge shear V_o expression in Eq. (8) be used in Eq. (4).

References

Adams, R. D., and Wake, W. C., 1984, *Structural Adhesive Joints in Engineering*, Elsevier, New York.

Anderson, G. P., Bennett, S. J., and DeVries, K. L., 1977, *Analysis and Testing of Adhesive Bonds*, Academic Press, New York.

Carpenter, W. C., 1989, "Goland and Reissner were Correct," *Journal of Strain Analysis*, Vol. 24, No. 3, pp. 185–187.

Chen, D., and Cheng, S., 1983, "An Analysis of Adhesive-Bonded Single-Lap Joints," ASME JOURNAL OF APPLIED MECHANICS, Vol. 50, pp. 109–115.

Goland, M., and Reissner, E., 1944, "The Stresses in Cemented Joints," ASME JOURNAL OF APPLIED MECHANICS, Vol. 11, p. A17–A27.

Sneddon, I., 1961, "The Distribution of Stress in Adhesive Joints," *Adhesion*, by D. D. Eley, ed., Oxford University Press, Cambridge, U. K., Chapter 9.

Tsai, M. Y., and Morton, J., 1993a, "An Experimental Investigation of Nonlinear Deformations in Single-Lap Joints," submitted to *Mechanics of Materials*.

Tsai, M. Y., and Morton, J., 1993b, "An Evaluation of Analysis and Numerical Solutions to the Single-Lap Joint," *International Journal of Solids and Structures* (in press).

A Sufficient Stability Condition for Linear Conservative Gyroscopic Systems

Jinn-Wen Wu[5] and Tsu-Chin Tsao[5,6]

A sufficient stability condition for linear conservative gyroscopic systems with negative definite stiffness matrices is given. The condition for the stability is stated in terms of the coefficients of system matrices without solving the spectrum of the entire system. An example is given for comparison with existing results.

1 Introduction

One interesting phenomenon for gyroscopic dynamic systems is that unstable conservative systems can be stabilized by increasing the gyroscopic forces. Criteria to determine reasonably small gyroscopic forces for stabilization are important for practical problems, for example, in the spacecraft attitude control problem, the artillery shell moving problem, and the flexible rotating shaft problem (Chetayev, 1961; Hughes, 1986). Recent results (Inman, 1988; Walker, 1991) have stimulated new interest in providing simple stability conditions for such systems without resorting to eigenvalue calculation.

Linear conservative gyroscopic systems can be described by a set of ordinary differential equations satisfying

$$\ddot{x}(t) + G\dot{x}(t) + Kx(t) = 0, \quad (1)$$

where $G^T = -G$, $K^T = K$. The special case of interest here is when K is negative definite and G is nonsingular. The stability used here is in the sense of Lyapunov (see, for instance, Bellman, 1953).

It is well known that the system described by Eq. (1) is stable if and only if the latent values associated with (1) are purely imaginary and nonzero (see, for instance, Huseyin, 1978) since if λ is a latent value so is $-\lambda$. It has also been known that dissipative damping can easily violate gyroscopic stabilization. Hence in a practical sense, since dissipative forces almost always exist, the gyroscopic stability is only temporary.

2 Previous Results

It has been known that when the determinant of G is sufficiently large, Eq. (1) is stable (Müller, 1985; Roseau, 1987). However, so far only a few criteria to determining the strength of the gyroscopic force for stabilizing the system are available. Summaries of results to date are given in Inman (1988) and Walker (1991).

For a two-degree-of-freedom system, Teschner (1977) showed that the stability for negative definite K results if $4K - G^2$ is positive definite. Inman and Saggio (1985) showed that the stability results if the trace of $4K - G^2$ and the determinant of K are both positive and applied the result to the design of a dynamically tuned gyroscope. In fact, for a two-

[5]Department of Mechanical and Industrial Engineering, University of Illinois at Urbana-Champaign, Urbana, IL 61801.

[6]Mem. ASME.

Contributed by the Applied Mechanics Division of THE AMERICAN SOCIETY OF MECHANICAL ENGINEERS for publication in the ASME JOURNAL OF APPLIED MECHANICS. Manuscript received by the ASME Applied Mechanics Division, Feb. 19, 1993; final revision, Apr. 30, 1993. Associate Technical Editor: P. D. Spanos.

Copyright © 1994 by ASME
Downloaded 03 May 2010 to 171.66.16.20. Redistribution subject to ASME license or copyright; see http://www.asme.org/terms/Terms_Use.cfm

degree-of-freedom system, eigenvalues can be evaluated directly. Thus the following necessary and sufficient condition not appeared in the literature previously can be derived:

$$[\det(G)]^2+\mathrm{tr}(K)>2\sqrt{\det(K)}>0. \tag{2}$$

Our main interest here is to provide simple stability criteria for n-degree-of-freedom systems. Huseyin (1983) obtained the following result: Suppose $GK = KG$. Then Eq. (1) is stable if and only if

$$4K-G^2>0. \tag{3}$$

When G and K does not commute, the construction of stability conditions becomes much more difficult. Inman (1988) proposed that the system described by Eq. (1) is stable if

$$4K-G^2-\epsilon I>0, \text{ where } 2\epsilon=\lambda_{\max}(-G^2). \tag{4}$$

However, a rigorous proof was not given as pointed out by Walker (1991). Based on the Lyapunov approach, Walker (1991) derived that the system described by Eq. (1) is stable if there exists a real number α such that

$$K(K-\alpha I)>0 \text{ and } K-\alpha I-\alpha G^T(K-\alpha I)^{-1}G>0. \tag{5}$$

The evaluation of this stability condition requires searches of the α values. Our main result of this paper is a simple sufficient stability condition with a rigorous proof.

3 Main Results

Lemma 1: (Huseyin, 1978): Consider the system described by Eq. (1). The system is stable if and only if for every latent vector q the following is true:

$$4\langle Kq, q\rangle-\langle Gq, q\rangle^2>0 \text{ and } \langle Kq, q\rangle\neq 0.$$

Proof: The solution of Eq. (1) is stable if and only if every latent value λ is purely imaginary. Let C^n be the n-dimensional complex Euclidean space and for all $z, w \in C^n$ define the inner product $\langle z, w\rangle = \Sigma_{i=1}^n z_i\overline{w_i}$ and norm $\|z\|^2 = \langle z, z\rangle$. It is not difficult to verify that $\forall\, x \in C^n$, $\langle Gx, x\rangle$ is pure imaginary and $\langle Kx, x\rangle$ is real. Suppose λ is a latent value of Eq. (1) and q is the corresponding latent vector, where $\lambda \in C$, $q \in C^n$. Then

$$x(t)=e^{\lambda t}q \tag{6}$$

is a fundamental solution of Eq. (1). Substitute Eq. (6) into Eq. (1). It follows that

$$\lambda^2 q+\lambda Gq+Kq=0. \tag{7}$$

Take the inner product to the both sides of Eq. (7) with q:

$$\lambda^2\langle q, q\rangle+\lambda\langle Gq, q\rangle+\langle Kq, q\rangle=0. \tag{8}$$

Assume that the latent vector q has unit length, i.e., $\|q\| = 1$. Then

$$\lambda^2+\lambda\langle Gq, q\rangle+\langle Kq, q\rangle=0. \tag{9}$$

Let $\lambda = i\omega$, $k = -\langle Kq, q\rangle$ and $\langle Gq, q\rangle = i\beta$. Then Eq. (9) becomes

$$\omega^2+\beta\omega+k=0. \tag{10}$$

To show that λ is purely imaginary and nonzero is equivalent to showing that ω is real and non-zero, which is true if and only if

$$\beta^2-4k=-\langle Gq, q\rangle^2+4\langle Kq, q\rangle>0 \text{ and } k\neq 0. \quad \text{QED.}$$

Although Lemma 1 gives the necessary and sufficient condition for stability, it requires the knowledge of a system latent vector and hence it is not useful for the stability investigation when the system dimension becomes large. A sufficient stability condition which does not require the calculation of system latent vectors or values is given next.

Theorem 1: The system described by Eq. (1), with $K < 0$ and $\det. G \neq 0$, is stable if

$$3K+\frac{1}{\delta}K^2-G^2>0. \tag{11}$$

where $\delta < 0$ is the maximum eigenvalue of K.

Proof: Suppose there exists a latent value $\lambda = i\omega$ and the corresponding latent vector q, satisfying $\beta^2 - 4k = -\langle Gq, q\rangle^2 + 4\langle Kq, q\rangle \leq 0$. Then the roots ω of Eq. (10) are complex conjugates and $|\omega|^2 = k > 0$. A contradiction is verified in the following.

By Eq. (9), $\langle Gq, q\rangle = -1/\lambda\,(\langle Kq, q\rangle + \lambda^2)$. Then

$$-\langle Gq, q\rangle^2=|\langle Gq, q\rangle|^2$$

$$=\left(\frac{|k-\lambda^2|}{|\lambda|}\right)^2=\frac{(k-\lambda^2)(k-\overline{\lambda^2})}{|\lambda|^2}$$

$$=\frac{k^2-2\mathrm{Re}(\lambda^2)k+|\lambda|^4}{|\lambda|^2}$$

$$=\frac{1}{|\omega|^2}\{k^2+2\mathrm{Re}(\omega^2)k+|\omega|^4\}. \tag{12}$$

By Eq. (7), it follows $Gq = -1/\lambda\,(Kq + \lambda^2 q)$. Then

$$\langle -G^2q, q\rangle=\langle Gq, Gq\rangle$$

$$=\left\langle\frac{1}{\lambda}(Kq+\lambda^2q), \frac{1}{\lambda}(Kq+\lambda^2q)\right\rangle$$

$$=\frac{1}{|\lambda|^2}\langle Kq+\lambda^2q, Kq+\lambda^2q\rangle$$

$$=\frac{1}{|\lambda|^2}\{\|Kq\|^2$$

$$+\overline{\lambda^2}\langle Kq, q\rangle+\lambda^2\langle Kq, q\rangle+\langle\lambda^2q, \lambda^2q\rangle\}$$

$$=\frac{1}{|\lambda|^2}\{\|Kq\|^2-2\mathrm{Re}(\lambda^2)k+|\lambda|^4\}$$

$$=\frac{1}{|\omega|^2}\{\|Kq\|^2+2\mathrm{Re}(\omega^2)k+|\omega|^4\}. \tag{13}$$

Since $3K + 1/\delta\, K^2 - G^2 > 0$,

$$\rightarrow 3\langle Kq, q\rangle+\frac{1}{\delta}\langle K^2q, q\rangle-\langle -G^2q, q\rangle>0$$

$$\rightarrow -3k|\omega|^2+\frac{|\omega|^2}{\delta}\|Kq\|^2+\|Kq\|^2+2\mathrm{Re}(\omega^2)k+|\omega|^4>0. \tag{14}$$

Noting that $\dfrac{|\omega|^2}{\delta}=\dfrac{k}{\delta}=\dfrac{-\langle Kq, q\rangle}{\max\limits_{x\in C^n}\langle Kx, x\rangle}\leq -1$,

$$\rightarrow -3k^2-\|Kq\|^2+\|Kq\|^2+2\mathrm{Re}(\omega^2)k+k^2>0.$$

$$\rightarrow \mathrm{Re}(\omega^2)k>k^2. \tag{15}$$

Then by Eqs. (12) and (15) we have

$$-\langle Gq, q\rangle^2+4\langle Kq, q\rangle$$

$$=\frac{2\mathrm{Re}(\omega^2)k-2k^2}{k}$$

$$>0.$$

Downloaded 03 May 2010 to 171.66.16.20. Redistribution subject to ASME license or copyright; see http://www.asme.org/terms/Terms_Use.cfm

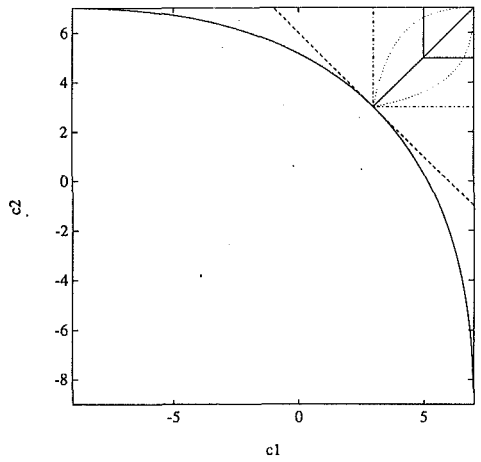


Fig. 1 Stability region predicted by various stability criteria

A contradiction is concluded. Therefore, every latent vector must satisfy $4\langle Kq, q\rangle - \langle Gq, q\rangle^2 > 0$ and the system is stable by The Lemma. QED.

Since for the case that $GK = KG$, the stability condition is $4K - G^2 > 0$, it is natural to ask whether the premises could be relaxed. The following stability criterion does not require K and G be commutative.

Theorem 2: Consider Eq. (1) in the following form:

$$G=\begin{bmatrix} 0 & B \\ -B^T & 0 \end{bmatrix},\ K=-\begin{bmatrix} k_1 I & 0 \\ 0 & k_2 I \end{bmatrix} \tag{16}$$

where B is an arbitrary nonsingular $n \times n$ matrix, k_1, k_2, are nonzero positive real numbers, and I is the $n \times n$ identity matrix. If $4K - G^2 > 0$, then the system is stable.

Proof: Let

$$\phi = \det(\lambda^2 I_{2n} + \lambda G + K). \tag{17}$$

It follows that

$$\phi = \det((\lambda^2 - k_1)I)\det((\lambda^2 - k_2)I + \lambda^2 B^T B(\lambda^2 - k_1)^{-1} I)$$

$$= \lambda^{2n}\det\left(\frac{(\lambda^2 - k_1)(\lambda^2 - k_2)}{\lambda^2} I + B^T B\right) \tag{18}$$

since

$$-G^2 + 4K > 0 \text{ implies } BB^T - 4k_1 I > 0 \text{ and } B^T B - 4k_2 I > 0 \text{ and} \tag{19}$$

since BB^T and $B^T B$ have the same eigenvalues,

$$\mu > \lambda_{\min}(B^T B) > \text{Max}\{4k_1, 4k_2\}, \tag{20}$$

where μ is any eigenvalue of $B^T B$. From Eq. (20), every root of $\phi(\lambda) = 0$ must satisfy

$$\frac{(\lambda^2 - k_1)(\lambda^2 - k_2)}{\lambda^2} + \mu = 0. \tag{21}$$

Let $\omega = \lambda^2$. Then Eq. (21) is equivalent to

$$\omega^2 + (\mu - (k_1 + k_2))\omega + k_1 k_2 = 0. \tag{22}$$

Then the roots of Eq. (22) can be expressed as

$$\omega_{\pm} = \frac{[(k_1 + k_2) - \mu] \pm \sqrt{(\mu - (k_1 + k_2))^2 - 4k_1 k_2}}{2}.$$

By (20), it follows that

$$k_1 + k_2 - \mu < 0, \text{ and } (\mu - (k_1 + k_2))^2 - 4k_1 k_2 > \mu^2$$
$$- 2\mu(k_1 + k_2) > \mu^2 - 4\mu(\text{Max}(k_1, k_2)) > 0. \tag{23}$$

Therefore $\omega_{\pm}$ are negative real. Therefore, all roots are purely imaginary and hence the system is stable. QED.

4 An Example

Consider a simplified model of a mass mounted on a noncircular weightless rotating shaft (Inman, 1991). The equation of motion in the rotating reference frame is (Huseyin, 1976)

$$\ddot{x} + 2\xi\begin{bmatrix} 0 & -1 \\ 1 & 0 \end{bmatrix}\dot{x} + \begin{bmatrix} c_1 - \xi^2 - \eta & 0 \\ 0 & c_2 - \xi^2 - \eta \end{bmatrix} x = 0, \tag{24}$$

where x represents the displacements of the mass in the rotating reference coordinate frame, ξ is the shaft angular velocity, η is the axial compression force, and $c_1 \geq c_2 \geq 0$ are elastic rigidities in the two principle directions. Using the same parameter values as those in Inman's example (1988), $\xi^2 = 4$, $\eta = 3$, Fig. 1 shows the stability regions for c_1 and c_2 obtained from various stability criteria. The wing shape enclosed by the solid curve and lines $c_1 = 7$ and $c_2 = 7$ is the stability region predicted by the necessary and sufficient condition for two-degree-of-freedom systems per Eq. (2). The triangular shape enclosed by the dashed line is the stability region predicted by Inman and Saggio's (1985) sufficient condition for two-degree-of-freedom systems. The square enclosed by the dash-dotted lines is the stability region predicted by Teschner's (1977) sufficient condition for two-degree-of-freedom systems and also by the sufficient condition for n-degree-of-freedom systems per Theorem 2. The football shaped dotted curves enclose the stability region predicted by the sufficient condition for n-degree-of-freedom systems per Theorem 1. The 45-deg straight solid line represents Huseyin's (1983) necessary and sufficient condition for the case $GK = KG$. The smaller square enclosed by the solid line is the stability region predicted by Inman's (1988) sufficient condition for n-degree-of-freedom systems per Eq. (4).

Since the simple stability conditions developed herein are meant for systems of large degree-of-freedom, where direct eigenvalue evaluation becomes cumbersome, this two-degree-of-freedom example is only for the purpose of graphical illustration of various stability conditions.

References

Bellman, R., 1953, *Stability Theory of Differential Equations*, McGraw-Hill, New York, Chapter 2.

Chetayev, N. G., 1961, *The Stability of Motion*, Pergamon Press, New York, pp. 101–105.

Hagedorn, P., 1975, "Über die Instabilität Konservativer Systeme mit Gyroskopischen Kräften," *Arch. Rat. Mech. Anal.*, Vol. 58, pp. 1–9.

Hughes, P., 1986, *Spacecraft Attitude Dynamics*, John Wiley and Sons, New York, pp. 515–521.

Huseyin, K., 1978, *Vibrations and Stability of Multiple Parameter Systems*, Noordholl International Publishing, pp. 115.

Huseyin, K., Hagedorn, P., and Teschner, W., 1983, "On the Stability of Linear Conservative Gyroscopic Systems," *Journal of Applied Mathematics and Physics*, Vol. 34, No. 6, pp. 807–815.

Inman, D. J., and Saggio, III, F., 1985, "Stability Analysis of Gyroscopic Systems by Matrix Methods," *J. Guidance*, Vol. 8, No. 1, pp. 150–152.

Inman, D. J., 1988, "A Sufficient Condition for the Stability of Conservative Gyroscopic Systems," ASME JOURNAL OF APPLIED MECHANICS, Vol. 55, pp. 895–898.

Lancaster, P., 1983, *Lambda Matrices and Vibrating Systems*, Pergamon Press, pp. 135–136.

Müller, P. C., and Schiehlen, W. O., 1985, Linear Vibrations, Martinus Nijhoff Publishers, Dordrecht, The Netherlands, p. 122.

Ortega, J. A., 1988, *Matrix Theory: A Second Course*, Plenum Press, New York, 1988.

Roseau, M., 1987, *Vibrations in Mechanical Systems*, Spring-Verlag, New York, pp. 78–81.

Walker, J. A., 1991, "Stability of Linear Conservative Gyroscopic Systems," ASME JOURNAL OF APPLIED MECHANICS, Vol. 58, pp. 229–232.

Downloaded 03 May 2010 to 171.66.16.20. Redistribution subject to ASME license or copyright; see http://www.asme.org/terms/Terms_Use.cfm

Buckling Load of Composite Conical Shells Under Axial Compression

Liyong Tong[7]

1 Introduction

Due to their extensive use, particularly in the aeronautical industry, the buckling of conical shells has been studied by many researchers. Much literature exists on the buckling of isotropic conical shells under compressive axial loads. A simple formula was developed for buckling load of isotropic conical shells under axial compression by Seide (1956) and later verified by Lackman and Renzien (1960). Seide's formula may be written as

$$p_{cl}=\frac{2\pi Eh^2\cos^2\alpha}{\sqrt{3(1-\mu^2)}} \tag{1}$$

where P_{cl} is the critical buckling load, E and μ denote the Young's modulus and the Poisson ratio, respectively, h represents the wall thickness, and α is the semivertex angle of the conical shell. It is evident that this formula is independent of boundary conditions and is best used for long shells. For orthotropic shells and composite laminated shells with bending-stretching coupling there have been fewer studies. In this technical Note, we suggest a simple formula for the critical buckling loads of laminated conical shells, with stretching-bending coupling, under axial compression. Using this suggested formula, numerical results are obtained and compared with these computed using series method (Tong and Wang, 1992).

2 Series Solution Method and Buckling Load

Consider a composite laminated circular conical shell subjected to an axially compressive load P. The geometry and notations of the conical shell are shown in Fig. 1, where R_1 and R_2 indicate the radii of the cone at its small and large ends, respectively, α denotes semivertex angle of the cone, and L is the cone length along its generator. The coordinate x is measured along the cone's generator starting at middle length and ϕ is the circumferential coordinate. The displacements of the shell's middle surface are denoted by U and V along the x and ϕ directions, respectively, and by W along the normal of the surface (inward positive). In terms of these variables the cone's radius at any point along its length may be expressed as

$$R(x)=R_o+x\sin\alpha \tag{2}$$

where R_o is the average radius.

The shell is laminated with layers and each layer is fabricated by plying the same amount of fiber in two opposite directions, namely, positive and negative ply angles. In this case, there exists only the bending-stretching coupling, and no twisting-stretching coupling. Similar to orthotropic material, only orthotropic coupling terms exist.

Using the classical Donnell-type shallow shell theory (Seide, 1957), we may derive the governing equations, in terms of the displacements U, V, and W, for linear buckling analysis of

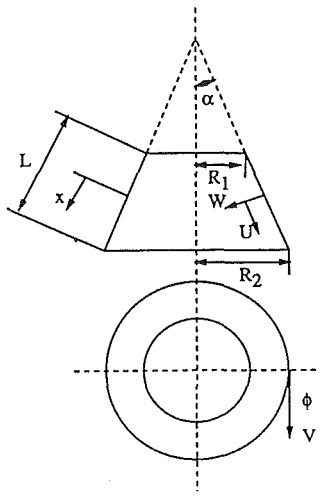


Fig. 1 Geometry and notation

composite laminated conical shell under axial compression. These equations may be solved by assuming solutions of the following form:

$$U=\sum_{m=0}^{\infty}a_m x^m\cos n\phi \quad V=\sum_{m=0}^{\infty}b_m x^m\sin n\phi$$

$$W=\sum_{m=0}^{\infty}c_m x^m\cos n\phi \tag{3}$$

where n is an integer representing the circumferential wave number of the buckled shell, a_m, b_m, and c_m are unknowns to be determined later. On substituting from Eqs. (3) into the governing equations and using Eq. (2) we develop three linear algebraic equations, by matching the terms of same order in x, and further we obtain the recurrence relations for a_m, b_m, and c_m. Convergence analysis shows that these series solutions are applicable to both truncated and complete conical shells. The solution procedure was given in detail by Tong and Wang (1992).

Using the above series solution method, we have computed the buckling loads and the associated wave number for a variety of composite conical shells with orthotropic conical shells under axial compression. Numerical results show that the Seide's formula may be extended as

$$P_{\text{conical}}=P_{\text{cylindrical}}\cos^2\alpha \tag{4}$$

where P_{conical} denotes the buckling load of the composite cones, $P_{\text{cylindrical}}$ indicates the buckling load of the equivalent composite cylindrical shells with radius being the average radius R_o of the cone, and α is the semivertex angle of the cone. As we know, there exists much literature on computation of the buckling load of cylindrical shells, with orthotropic coupling terms, under axial compression (Tennyson, 1975; Tong et al., 1988).

3 Numerical Results and Discussions

In this section the buckling loads are computed using the series method and Eq. (4) for a particular set of laminated cones, namely, regularly antisymmetric cross-plied cones. For this case, we have

$$A_{11}=A_{22}=\frac{1}{2}(Q_{11}+Q_{22})h \quad A_{12}=Q_{12}h \quad A_{66}=Q_{66}h$$

$$B_{11}=-B_{22}=\pm\frac{1}{4N}(Q_{11}-Q_{22})h^2 \quad A_{12}=A_{66}=0$$

$$D_{11}=D_{22}=\frac{1}{24}(Q_{11}+Q_{22})h^3 \quad D_{12}=\frac{1}{12}Q_{12}h^3 \quad D_{66}=\frac{1}{12}Q_{66}h^3$$

[7]Department of Mechanical Engineering, University of Victoria, Victoria, BC V8W 3P6. Canada. Assoc. Mem. ASME. Present address: Cooperative Research Center for Aerospace Structures, 361 Milperra Road, Bankstown, New South Wales 2200, Australia.

Contributed by the Applied Mechanics Division of The American Society of Mechanical Engineers for publication in the ASME Journal of Applied Mechanics. Manuscript received by the ASME Applied Mechanics Division, Dec. 30, 1991; final revision, June 21, 1993. Associate Technical Editor: G. J. Drovak.

Copyright © 1994 by ASME
Downloaded 03 May 2010 to 171.66.16.20. Redistribution subject to ASME license or copyright; see http://www.asme.org/terms/Terms_Use.cfm

Table 1 ρ_{cr} and n for SS_3 boundary condition

$\bar{N}$	0°	10°	30°	45°	60°
2	1.000(7)	1.033(9)	1.032(6)	0.997(6)	1.027(6)
4	1.000(6)	1.000(6)	1.011(6)	1.045(5)	1.108(5)
6	1.000(6)	1.000(6)	1.028(6)	1.052(5)	1.114(4)
∞	1.000(6)	1.001(6)	1.036(6)	1.054(5)	1.121(4)

Table 2 ρ_{cr} and n for CC_1 boundary condition

$\bar{N}$	0°	10°	30°	45°	60°
2	1.000(8)	1.006(8)	1.020(8)	0.986(6)	1.050(6)
4	1.000(7)	1.006(7)	1.022(6)	1.065(5)	1.093(4)
6	1.000(6)	1.002(6)	1.029(6)	1.066(5)	1.090(4)
∞	1.000(6)	1.003(6)	1.034(6)	1.067(5)	1.085(4)

where Q_{ij} $(i,j = 1, 2, 6)$ are material parameters (Jones, 1975), $\bar{N}$ is the total number of layers which must be even, and h denotes the total wall thickness. The elementary material parameters of each carbon/epoxy layer are given as

$$\frac{E_x}{E_\phi} = 40.0 \quad \mu_{x\phi} = 0.25 \quad \frac{G_{x\phi}}{E_\phi} = 0.5.$$

Before presenting the results, let us introduce the following notation:

$$\rho_{cr} = \frac{P_{\text{series}}}{P_{\text{conical}}} \tag{5}$$

where P_{series} is the critical buckling load obtained from the series method, and P_{conical} is the critical buckling load using Eq. (4).

Numerical results for ρ_{cr} are given for composite cones with $L/R_o = 1.0$, semivertex angles α and different boundary conditions, i.e., SS_3 in Table 1 and CC_1 in Table 2, where SS_3 and CC_1 are given by

$$SS_3: \quad N_x = V = W = M_x = 0$$

$$CC_1: \quad U = V = W = \frac{\partial W}{\partial x} = 0.$$

It can be seen that ρ_{cr} tends to be larger than unity as α increases. For α less than 45 deg, good agreement can be observed. In Tables 1 and 2, the numbers in round brackets denote the circumferential wave number computed using the series solution method. It is worth pointing out that the length-to-radius ratio L/R_o has a strong influence on the ratio ρ_{cr}, namely, short shells yield larger ρ_{cr} than long cones. This means that, similar to Seide's formula Eq. (1), Eq. (4) applies for moderately long or long conical shells.

4 Concluding Remarks

The salient points in this study include: (1) a simple formula for the critical buckling loads of the composite laminated conical shells, with orthotropic stretching-bending coupling, under axial compression is suggested; (2) the comparison to these calculated by using the series solution procedure shows that the suggested formula can yield simple and reasonable prediction for the buckling loads of moderately long and long conical shells.

References

Jones, R. M., 1975, *Mechanics of Composite Materials*, Script Book Co.

Lackman, L., and Renzien, J., 1960, "Buckling of Circular Cones Under Axial Compression," ASME JOURNAL OF APPLIED MECHANICS, Vol. 27, pp. 458-460.

Seide, P., 1956, "Axisymmetrical Buckling of Circular Cones Under Axial Compression," ASME JOURNAL OF APPLIED MECHANICS, Vol. 23, pp. 626-628.

Seide, P., 1957, "A Donnell-Type Theory for Asymmetrical Bending and Buckling of Thin Conical Shells," ASME JOURNAL OF APPLIED MECHANICS, Vol. 24, pp. 547-552.

Tennyson, R. C., 1975, "Buckling of Laminated Composite Cylinders: A Review," *Composites*, Vol. 6, pp. 17-24.

Tong, L., and Wang, T. K., 1988, "An Eight-order Equation of Fiber Reinforced Laminated Cylinders and Its Solutions," *Acta Aeronautica and Astronautica Sinica*, Vol. 19, pp. A388-392.

Tong, L., and Wang, T. K., 1992, "Simple Solutions for Buckling of Laminated Conical Shells," *International Journal of Mechanical Science*, Vol. 34, pp. 93-111.

Stress Intensity Factors for Plate Bending and Shearing Problems

A. T. Zehnder[8,10] and Chung-Yuen Hui[9,10]

Stress intensity factors for a finite crack in an infinite plate are calculated assuming Kirchhoff plate theory. Two problems are considered: a cracked plate subjected to uniform far-field shearing, and a cracked plate subjected to uniform far-field bending moment. In both cases the crack is oriented at an arbitrary angle to the axis of loading.

Introduction

The stress intensity factors for a cracked plate subjected to bending, twisting, and shearing were first calculated in the pioneering work of Sih et al. (1962) and have since been incorporated into handbooks of stress intensity factors such as Murakami (1987). Recently we tried to use these solutions to help verify the results of some finite element computations of stress intensity factors. After many interations and refinements to our finite element mesh we found that the computed stress intensity factors always differed from the published results by a consistent amount. In order to reconcile the differences we performed a careful study of the solutions of Sih et al. Upon reworking the problems, we found that some of the published solutions contained errors. After correcting those errors, our computational results agreed with the analytical results to within a few percent (Hui and Zehnder, 1993; Potyondy et al., 1993). Thus in this paper we present the corrected solutions and contrast them with the solutions of Sih et al.

The stresses near the tip of a crack in a plate were first calculated by Williams (1961) in the context of Kirchhoff plate theory. The singular crack-tip stresses are represented by a symmetric mode stress intensity factor, k_1, and an antisymmetric mode stress intensity factor, k_2. Using the definitions for k_1 and k_2 given by Sih et al. and in the (r, θ, z) coordinate system of Fig. 1, the stresses on a line ahead of the crack, $\theta = 0$, are

[8]Assistant Professor, Assoc. Mem. ASME.

[9]Associate Professor.

[10]Department of Theoretical and Applied Mechanics, Cornell University, Ithaca, NY 14853.

Contributed by the Applied Mechanics Division of THE AMERICAN SOCIETY OF MECHANICAL ENGINEERS for publication in the ASME JOURNAL OF APPLIED MECHANICS. Manuscript received by the ASME Applied Mechanics Division, Sept. 8, 1992; final revision, June 24, 1993. Associate Technical Editor: S. K. Datta.

Downloaded 03 May 2010 to 171.66.16.20. Redistribution subject to ASME license or copyright; see http://www.asme.org/terms/Terms_Use.cfm

Table 1 ρ_{cr} and n for SS_3 boundary condition

$\bar{N}$	0°	10°	30°	45°	60°
2	1.000(7)	1.033(9)	1.032(6)	0.997(6)	1.027(6)
4	1.000(6)	1.000(6)	1.011(6)	1.045(5)	1.108(5)
6	1.000(6)	1.000(6)	1.028(6)	1.052(5)	1.114(4)
∞	1.000(6)	1.001(6)	1.036(6)	1.054(5)	1.121(4)

Table 2 ρ_{cr} and n for CC_1 boundary condition

$\bar{N}$	0°	10°	30°	45°	60°
2	1.000(8)	1.006(8)	1.020(8)	0.986(6)	1.050(6)
4	1.000(7)	1.006(7)	1.022(6)	1.065(5)	1.093(4)
6	1.000(6)	1.002(6)	1.029(6)	1.066(5)	1.090(4)
∞	1.000(6)	1.003(6)	1.034(6)	1.067(5)	1.085(4)

where Q_{ij} $(i,j = 1, 2, 6)$ are material parameters (Jones, 1975), $\bar{N}$ is the total number of layers which must be even, and h denotes the total wall thickness. The elementary material parameters of each carbon/epoxy layer are given as

$$\frac{E_x}{E_\phi} = 40.0 \quad \mu_{x\phi} = 0.25 \quad \frac{G_{x\phi}}{E_\phi} = 0.5.$$

Before presenting the results, let us introduce the following notation:

$$\rho_{cr} = \frac{P_{\text{series}}}{P_{\text{conical}}} \tag{5}$$

where P_{series} is the critical buckling load obtained from the series method, and P_{conical} is the critical buckling load using Eq. (4).

Numerical results for ρ_{cr} are given for composite cones with $L/R_o = 1.0$, semivertex angles α and different boundary conditions, i.e., SS_3 in Table 1 and CC_1 in Table 2, where SS_3 and CC_1 are given by

$$SS_3: \quad N_x = V = W = M_x = 0$$

$$CC_1: \quad U = V = W = \frac{\partial W}{\partial x} = 0.$$

It can be seen that ρ_{cr} tends to be larger than unity as α increases. For α less than 45 deg, good agreement can be observed. In Tables 1 and 2, the numbers in round brackets denote the circumferential wave number computed using the series solution method. It is worth pointing out that the length-to-radius ratio L/R_o has a strong influence on the ratio ρ_{cr}, namely, short shells yield larger ρ_{cr} than long cones. This means that, similar to Seide's formula Eq. (1), Eq. (4) applies for moderately long or long conical shells.

4 Concluding Remarks

The salient points in this study include: (1) a simple formula for the critical buckling loads of the composite laminated conical shells, with orthotropic stretching-bending coupling, under axial compression is suggested; (2) the comparison to these calculated by using the series solution procedure shows that the suggested formula can yield simple and reasonable prediction for the buckling loads of moderately long and long conical shells.

References

Jones, R. M., 1975, *Mechanics of Composite Materials*, Script Book Co.

Lackman, L., and Renzien, J., 1960, "Buckling of Circular Cones Under Axial Compression," ASME JOURNAL OF APPLIED MECHANICS, Vol. 27, pp. 458-460.

Seide, P., 1956, "Axisymmetrical Buckling of Circular Cones Under Axial Compression," ASME JOURNAL OF APPLIED MECHANICS, Vol. 23, pp. 626-628.

Seide, P., 1957, "A Donnell-Type Theory for Asymmetrical Bending and Buckling of Thin Conical Shells," ASME JOURNAL OF APPLIED MECHANICS, Vol. 24, pp. 547-552.

Tennyson, R. C., 1975, "Buckling of Laminated Composite Cylinders: A Review," *Composites*, Vol. 6, pp. 17-24.

Tong, L., and Wang, T. K., 1988, "An Eight-order Equation of Fiber Reinforced Laminated Cylinders and Its Solutions," *Acta Aeronautica and Astronautica Sinica*, Vol. 19, pp. A388-392.

Tong, L., and Wang, T. K., 1992, "Simple Solutions for Buckling of Laminated Conical Shells," *International Journal of Mechanical Science*, Vol. 34, pp. 93-111.

Stress Intensity Factors for Plate Bending and Shearing Problems

A. T. Zehnder[8,10] and Chung-Yuen Hui[9,10]

Stress intensity factors for a finite crack in an infinite plate are calculated assuming Kirchhoff plate theory. Two problems are considered: a cracked plate subjected to uniform far-field shearing, and a cracked plate subjected to uniform far-field bending moment. In both cases the crack is oriented at an arbitrary angle to the axis of loading.

Introduction

The stress intensity factors for a cracked plate subjected to bending, twisting, and shearing were first calculated in the pioneering work of Sih et al. (1962) and have since been incorporated into handbooks of stress intensity factors such as Murakami (1987). Recently we tried to use these solutions to help verify the results of some finite element computations of stress intensity factors. After many interations and refinements to our finite element mesh we found that the computed stress intensity factors always differed from the published results by a consistent amount. In order to reconcile the differences we performed a careful study of the solutions of Sih et al. Upon reworking the problems, we found that some of the published solutions contained errors. After correcting those errors, our computational results agreed with the analytical results to within a few percent (Hui and Zehnder, 1993; Potyondy et al., 1993). Thus in this paper we present the corrected solutions and contrast them with the solutions of Sih et al.

The stresses near the tip of a crack in a plate were first calculated by Williams (1961) in the context of Kirchhoff plate theory. The singular crack-tip stresses are represented by a symmetric mode stress intensity factor, k_1, and an antisymmetric mode stress intensity factor, k_2. Using the definitions for k_1 and k_2 given by Sih et al. and in the (r, θ, z) coordinate system of Fig. 1, the stresses on a line ahead of the crack, $\theta = 0$, are

[8]Assistant Professor, Assoc. Mem. ASME.

[9]Associate Professor.

[10]Department of Theoretical and Applied Mechanics, Cornell University, Ithaca, NY 14853.

Contributed by the Applied Mechanics Division of THE AMERICAN SOCIETY OF MECHANICAL ENGINEERS for publication in the ASME JOURNAL OF APPLIED MECHANICS. Manuscript received by the ASME Applied Mechanics Division, Sept. 8, 1992; final revision, June 24, 1993. Associate Technical Editor: S. K. Datta.

Copyright © 1994 by ASME

Downloaded 03 May 2010 to 171.66.16.20. Redistribution subject to ASME license or copyright; see http://www.asme.org/terms/Terms_Use.cfm

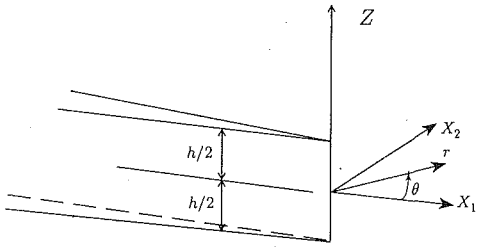


Fig. 1 Coordinate system for a crack in a plate

$$\sigma_{22}=\frac{k_1}{\sqrt{2r}}\frac{2z}{h},$$

$$\sigma_{21}=\frac{k_2}{\sqrt{2r}}\left(\frac{1+\nu}{3+\nu}\right)\frac{2z}{h},$$

$$\sigma_{2z}=\frac{-k_2}{(2r)^{3/2}}\frac{(h/2)}{3+\nu}\left[1-\left(\frac{2z}{h}\right)^2\right], \tag{1}$$

where h is the plate thickness, ν is the Poisson's ratio, and the two Kirchhoff theory stress intensity factors k_1 and k_2 have dimensions of force/length$^{3/2}$.

Problem Formulation and Solution

We will solve for the stress intensity factors at the tip of a finite crack of length $2a$ oriented at angle β to the axis of loading as shown in Fig. 2. The far-field loading is either uniform transverse shear, Fig. 2(a), or uniform bending, Fig. 2(b).

The deflection w of a cracked plate without pressure loading is governed by the biharmonic equation (Timoshenko and Woinowsky-Krieger, 1959)

$$\nabla^4 w=0. \tag{2}$$

In the (x, y) coordinate system of Fig. 2, the boundary conditions along the crack line, ($y = 0$, $-a \le x \le a$), are the free-edge conditions

$$M_y=0,$$

$$Q_y+\frac{\partial M_{yx}}{\partial x}=0. \tag{3}$$

The resultant moments and shears are related to w by

$$M_x=-D[w_{,xx}+\nu w_{,yy}],$$

$$M_y=-D[w_{,yy}+\nu w_{,xx}],$$

$$M_{xy}=M_{yx}=-D(1-\nu)w_{,yx},$$

$$Q_x=-D(\nabla^2 w)_{,x},$$

$$Q_y=-D(\nabla^2 w)_{,y}, \tag{4}$$

where $D = Eh^3/12(1 - \nu^2)$, E is the modulus of elasticity and ν is the Poisson's ratio.

Uniform Transverse Shear. The far-field conditions ($x^2 + y^2 \to \infty$) for the transverse shear problem of Fig. 2(a) are (Yu, 1954)

$$Q_x=Q_0\cos\beta,\quad Q_y=Q_0\sin\beta,$$

$$M_x=Q_0 x\cos\beta+\nu Q_0 y\sin\beta,$$

$$M_y=\nu Q_0 x\cos\beta+Q_0 y\sin\beta,\quad M_{yx}=0. \tag{5}$$

We solve this problem using conformal mapping and the solution given by Yu (1954) for a hole in a plate under shear.

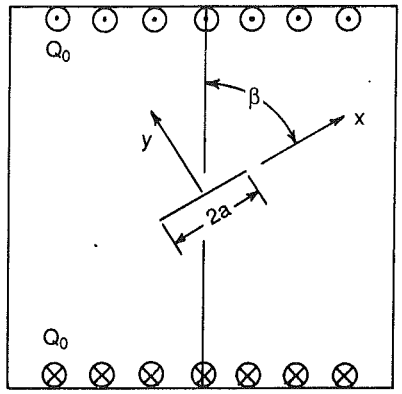


Fig. 2(a)

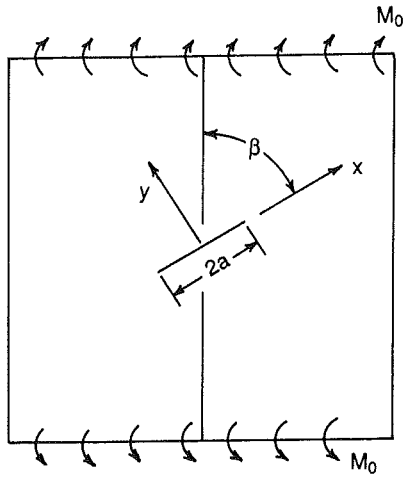


Fig. 2(b)

Fig. 2 Finite crack at an angle β to the loading in an infinite plate; (a) uniform far-field transverse shearing, (b) uniform far-field bending moment

As discussed by Yu the solution to Eq. (2) can be expressed in terms of analytic functions, φ and ψ of $z = x + iy$, as

$$w=\mathrm{Re}[z\varphi(z)+\chi(z)],\quad \chi=\int\psi(z)dz, \tag{6}$$

and

$$M_x+M_y=-4D(1+\nu)\mathrm{Re}[\varphi'(z)]. \tag{7}$$

Note that $\varphi = 2\varphi_1$, $\psi = 2\psi_1$, where φ_1 and ψ_1 are the symbols used by Yu.

Under the mapping $z = \Omega(\zeta) = a(\zeta + 1/\zeta)/2$, that transforms a straight crack of length $2a$ into a unit circle, Sih et al. (1962) show that the crack-tip stress intensity factor is related to φ by

$$k\equiv k_1+ik_2=\frac{-12D(3+\nu)}{h^2\sqrt{a}}\varphi_b'(\zeta)\,|_{\zeta=1}, \tag{8}$$

where $\varphi_b(\zeta) = \varphi(\Omega(\zeta))$ is the stress function for a plate containing a unit radius circular hole with the crack-tip boundary conditions, Eq. (3) mapped to the surface of the hole. For a hole oriented at angle β to the shear Q_0, Yu gives

$$\varphi_b(\zeta)=\frac{Q_0a^2}{32D}\left[\zeta^2e^{-i\beta}+\left(\frac{1-\nu}{3+\nu}\right)\frac{e^{-i\beta}+2e^{i\beta}}{\zeta^2}\right]. \tag{9}$$

Evaluating $\varphi_b'(\zeta)$ and using Eq. (8), the stress intensity factors for the uniform far-field shearing problem in Fig. 2(a) are

$$k_1=\frac{3Q_0a^{3/2}\nu\cos\beta}{h^2},$$

$$k_2=\frac{3Q_0a^{3/2}\sin\beta}{h^2}. \tag{10}$$

Downloaded 03 May 2010 to 171.66.16.20. Redistribution subject to ASME license or copyright; see http://www.asme.org/terms/Terms_Use.cfm

These stress intensity factors and the resulting near crack-tip displacement field, which is governed by k_1 and k_2, agree with results of our finite element computations (Hui and Zehnder, 1993, and Potyondy et al., 1993) to within a few percent. The agreement, while not proof that Eqs. (10) are correct, is at least evidence that the results are correct.

Uniform Bending. The far-field conditions for the bending problem of Fig. 2(*b*) are (Yu, 1954)

$$M_x = M_0 \cos^2 \beta, \quad M_y = M_0 \sin^2 \beta,$$

$$M_{yx} = M_0 \cos \beta \sin \beta, \quad Q_y = Q_x = 0. \tag{11}$$

Although the following result can be calculated using conformal mapping as indicated above, it is simpler to solve the problem using the following arguments.

Decompose the loading into the sum of three problems: (1) Pure bending parallel to the crack line, $M_x = M_0 \cos^2 \beta$, $M_y = M_{yx} = 0$, (2) pure bending perpendicular to the crack line, $M_x = M_{yx} = 0$, $M_y = M_0 \sin^2 \beta$, and (3) pure twisting, $M_x = M_y = 0$, $M_{yx} = M_{xy} = M_0 \sin \beta \cos \beta$.

Problem (1) results in no singularities since all of the stresses are parallel to the crack line. Problem (2) results in singular tensile and compressive stresses at the crack tip. The stress intensity factors for this case are (Sih et al., 1962) $k_1 = 6M_0/h^2 \sin^2 \beta \sqrt{a}$, $k_2 = 0$.

We now consider problem (3) pure twisting of the plate. The solution for an *uncracked* plate with uniform twisting moment $M_0 \cos \beta \sin \beta$ imposed on its boundaries is

$$w = \frac{-M_0 \cos \beta \sin \beta}{D(1-\nu)} xy. \tag{12}$$

To check this solution observe that $\nabla^4 w = 0$ since $\nabla^2 w = 0$. Furthermore, $M_x = M_y = Q_x = Q_y = 0$ everywhere since all second derivatives of w with respect to x or y vanish. One also can verify that $M_{yx} = -D(1-\nu)w_{,yx} = M_0 \cos \beta \sin \beta$ everywhere so that the boundary condition at infinity is satisfied.

Equation (12) is also the solution to the problem of a plate with *any number of cracks lying along the x-axis*. The first of the free-edge boundary conditions in Eq. (3) is satisfied since $M_y = 0$ everywhere. The second is also satisfied since $Q_y = 0$ and M_{yx} is a constant. Thus Eq. (12) is the exact solution of both the cracked and uncracked plate problems. None of the stresses in this problem are singular, thus $k_1 = 0$ and $k_2 = 0$.

In summary the stress intensity factors for the bending problem shown in Fig. 2(*b*) are

$$k_1 = \frac{6M_0 \sin^2 \beta \sqrt{a}}{h^2},$$

$$k_2 = 0. \tag{13}$$

The result that in pure twisting $k_2 = 0$ is supported by looking at the results for the equivalent problem using the Reissner plate theory, solving the same problem using conformal mapping and Yu's solutions, and by looking at the results of finite element computations.

Using the J-integral, Hui and Zehnder (1993) showed that for a "thin plate" ($h/a \to 0$) the Reissner theory stress intensity factors K_2 and K_3 are related to the Kirchhoff theory stress intensity factor k_2 by

$$k_2^2 \frac{1+\nu}{3+\nu} = K_2^2 + K_3^2 \frac{8(1+\nu)}{5}. \tag{14}$$

The Reissner theory solutions for K_2 and K_3 for a plate under pure twisting, calculated by Tamate (1975) and Wang (1970) as functions of the plate thickness, are $K_2 \propto M_0 \cos \beta \sin \beta F_2(h/a, \nu)\sqrt{a}$, $K_3 \propto M_0 \cos \beta \sin \beta F_3(h/a, \nu)\sqrt{a}$. The plots of the functions F_2 and F_3 in Tamate (1975) and Wang (1970) show that as $h/a \to 0$, $K_2 \to 0$ and $K_3 \to 0$. Thus Tamate and Wang's results and Eq. (14) imply that $k_2 = 0$.

One can also specialize Yu's results to the problems of pure bending (problem 2) and pure twisting (problem 3). Following the procedure outlined in the section on uniform transverse shear, we confirmed the k_1 result of Eq. (13). We also found that $\varphi_b(\zeta) = 0$ and hence $k_2 = 0$ for problem 3.

As we were at first still not convinced of the veracity of our results, we performed a simple finite element computation of a square, center cracked plate under pure twisting. The finite element model used just 32 four-noded elements, with five nodes along the crack. The ratio of crack length to plate width was 1:2. The computation showed that there is no relative displacement across the crack and that there are no stress concentrations. Using the same mesh, a stress concentration factor of ten was computed when the plate was loaded in tension perpendicular to the crack line, indicating that the mesh, while very coarse, was sufficient to indicate the presence of stress concentrations.

Comparison to Previous Results

For the shearing problem, Fig. 2(*a*), Sih et al. calculated $k_1 = 8Q_0 a^{3/2} \nu \cos \beta/h^2$, and $k_2 = 8Q_0 a^{3/2} \sin \beta/h^2$. Thus our new results differ from the old by a factor of 3/8. The reason for the difference in results can be traced to the $\varphi_b(\zeta)$ function given in Sih et al. They have a 12 in the place where we have a 32 in Eq. (9). We arrived at Eq. (9) by taking the general results of Yu and specializing them to the crack problem. It appears that Sih et al. arrived at their $\varphi_b(\zeta)$ in the same way, so the discrepancy must be due to calculation errors in that step. Yu's paper also contains a number of typographical errors and uses a notation where the φ_1 of Yu differs from the φ defined by Sih et al. by a factor of 2.

For the uniform bending problem of Fig. 2(*b*) Sih et al. give the correct symmetric mode solution, $k_1 = 6M_0 \sin^2 \beta \sqrt{a}/h^2$, but give a nonzero solution for the antisymmetric mode $k_2 = 6M_0 \cos \beta \sin \beta \sqrt{a}/h^2$. The $\varphi_b(\zeta)$ function used to obtain this result comes from Savin (1956), which is a Russian paper translated into German. It appears that that function is incorrect. Since it is a formidable task to delve into Savin's paper, and since we are sure that our results are correct based on simple, fundamental arguments, we have not attempted to track down the source of the problem in Savin. It does appear, however, that results from that paper should be checked very carefully before being applied.

Acknowledgments

Support for A. T. Zehnder from NASA Langley, contract NAG-1-1311, is gratefully acknowledged. C. Y. Hui is supported by the Materials Science Center at Cornell, NSF/MSC DMR-9121654.

References

Hui, C. Y., and Zehnder, A. T., 1993, "A Theory for the Fracture of Thin Plates Subjected to Bending and Twisting Moments," *International Journal of Fracture*, Vol. 61, pp. 211–229.

Murakami, Y., eds., 1987, *Stress Intensity Factor Handbook—Vol. 2*, Pergamon Press, Elmsford, New York.

Potyondy, D., Rankin, C., Riks, E., Viz, M., and Zehnder, A. T., 1993, "Computation of Membrane and Bending Stress Intensity Factors for Thin, Cracked Plates," ASME JOURNAL OF APPLIED MECHANICS, submitted for publication.

Savin, G. N., 1956, "Spannungoerhöhung am Rande von Löchern," *VEB Verlag Technik*, Berlin (in German).

Sih, G. C., Paris, P. C., and Erdogan, F., 1962, "Crack Tip Stress-Intensity Factors for Plane Extension and Plate Bending Problems," ASME JOURNAL OF APPLIED MECHANICS, Vol. 29, pp. 306–312.

Tamate, O., 1975, "A Theory of Dislocations in the Plate under Flexure with Applications to Crack Problems," *Technology Reports*, Tohoku University, Vol. 40, pp. 67–88.

Downloaded 03 May 2010 to 171.66.16.20. Redistribution subject to ASME license or copyright; see http://www.asme.org/terms/Terms_Use.cfm

Timoshenko, S., and Woinowsky-Krieger, S., 1959, *Theory of Plates and Shells*, McGraw-Hill, New York.

Wang, N. M., 1970, "Twisting of an Elastic Plate Containing a Crack," *International Journal of Fracture*, Vol. 6, pp. 367–378.

Williams, M. L., 1961, "The Bending Stress Distribution at the Base of a Stationary Crack," ASME JOURNAL OF APPLIED MECHANICS, Vol. 28, pp. 78–82.

Yu, Yi-Yuan, 1954, "The Influence of a Small Hole or Rigid Inclusion on the Transverse Flexure of Thin Plates," *Proceedings of the Second U.S. National Congress of Applied Mechanics*, pp. 381–387.

Response of a Disk Mass on a Half-Space to Dilatational Waves

Tierang Liu[11] and Xiangzhou Zhang[12]

Introduction

This investigation deals with the elastodynamics problem for a disk mass lying on an elastic half-space, impinged upon by dilatational waves, a problem of considerable technical interest in the design of transducers or seismological design of on-ground apparatuses and structures.

Counterpart problems, where the elastic half-space is disturbed by sinusoidal forces exerted on a circular or rectangular body resting on its surface, have been treated by Bycroft (1956), Robertson (1966), Karasudhi et al. (1968), Krenk and Schmidt (1981), and other authors. However, the more complicated problem of transient response to wave incidence is considered here. This involves reflection and scattering of transient waves by the disk and does not seem to have been discussed.

In the present Note, based on the theory of elastodynamics and Reissner's assumption, the equation of motion for the disk mass under the action of a uniformly incoming dilatational waves is first derived. The Laplace transformed solutions for the displacement of the disk mass is then obtained via solving for the transformed equation. By employing a number of analytic techniques, the explicit expression for the displacement is developed, with which other unknowns, for instance the contact stress between the disk mass and the half-space, can be determined directly. The numerical result depicted in diagrams shows that for a large disk mass, the displacement response vibrates rather slowly with large amplitudes, whereas that of a small disk mass oscillates with small amplitudes and high frequencies.

Problem and Transformed Solution

An elastic half-space of density ρ, Lame constants λ and μ, and dilatational wave speed c_d is depicted in Fig. 1, with a rigid circular disk of radius a and mass m resting on its surface. A uniform, one-dimensional displacement wave, in association with uniform dynamic stress $s(c_d z + t)$ and coming from the infinity, reaches the surface plane $z = 0$ at the instant $t = 0$. The elastodynamic process taking place in the disk mass and the half-space ensuing that instant is to be investigated.

Since it is difficult to treat exactly such a transient mixed boundaries value problem, Reissner's assumption will be used in the following. Reissner's assumption (Bycroft, 1956) includes (1) allowing no friction between the rigid circular disk and the half-space, and neglecting the gravitational force in the disk; (2) supposing a constant normal contact stress over the circle $0 \le r \le a$; and (3) taking the displacement at the center of the circle as the displacement of the rigid disk.

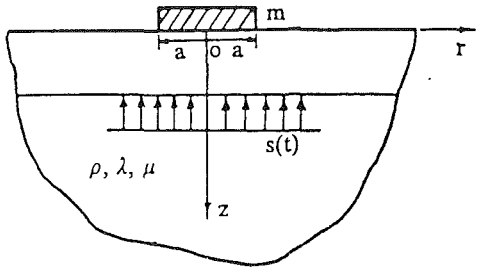


Fig. 1 The half-space and the disk mass

The displacements and stresses in the half-space are composed of those induced by the incoming, the reflecting, and the scattering waves. These waves are distinguished by subscripts 1, 2, and 3, respectively. The displacements and stresses corresponding to the first two waves can be determined directly. They are (Eringen and Suhubi, 1975)

$$w_1(r, z, t) = -\frac{1}{\rho c_d} H\left(t+\frac{z}{c_d}\right) \int_0^{t+\frac{z}{c_d}} s(\tau)d\tau,$$

$$u_{r1}(r, z, t) = 0 \qquad (1a,b)$$

$$\sigma_{z1}(r, z, t) = -H(t+z/c_d)s(t+z/c_d),$$

$$\sigma_{zr1}(r, z, t) = 0 \qquad (2a,b)$$

and

$$w_2(r, z, t) = -\frac{1}{\rho c_d} H\left(t-\frac{z}{c_d}\right) \int_0^{t-\frac{z}{c_d}} s(\tau)d\tau,$$

$$u_{r2}(r, z, t) = 0 \qquad (3a,b)$$

$$\sigma_{z2}(r, z, t) = H(t-z/c_d)s(t-z/c_d), \quad \sigma_{zr2}(r, z, t) = 0 \qquad (4a,b)$$

where $H(t)$ is the Heaviside unit function. The determination of the scattering field is rather complicated. However, once $\sigma(t)$, the normal contact stress between the disk mass and the half-space over the area $r \le a$, is known, the displacements and stresses in the half-space can be found, lengthily yet straightforwardly, through a procedure described in Eringen and Suhubi (1975) and Graff (1975). Neglecting the details of the derivation, the displacement at the origin in the z direction in Laplace transform domain, $\overline{w}_3(0, 0, p)$, is written as follows:

$$\overline{w}_3(0, 0, p) = \frac{a\overline{\sigma}(p)}{\mu} \int_0^\infty \eta_d k_s^2 \frac{J_1(\kappa a)}{R(\kappa, p)} d\kappa \qquad (5)$$

where

$$R(\kappa, p) = (k_s^2 + 2\kappa^2)^2 - 4\kappa^2\eta_d\eta_s \qquad (6)$$

$$\eta_d = \sqrt{k_d^2+\kappa^2}, \quad \eta_s = \sqrt{k_s^2+\kappa^2}$$

$$k_d = p/c_d, \quad k_s = p/c_s \qquad (7a,b,c,d)$$

$J_1(x)$ is the Bessel function of the first kind, c_s is the shear wave speed of the material, p is the Laplace transform parameter, and η_d and η_s stand for the branches that are real and positive for real p. $\overline{\sigma}(p)$ should be determined from the displacement continuity condition over the contact area $r \le a$.

Since the disk mass is rigid and the motion is axisymmetric, the displacement of the disk mass during the dynamic response can only be an upward (regarded as positive) or downward (negative) translation. Denoting this displacement with w_m, from the Reissner's assumption the displacement continuity

[11]Department of Aircraft Engineering, Nanjing University of Aeronautics and Astronautics, Nanjing 210016, People's Republic of China.

[12]Department of Aircraft Engineering, Northwestern Polytechnical University, Xian 710072, People's Republic of China.

Contributed by the Applied Mechanics Division of THE AMERICAN SOCIETY OF MECHANICAL ENGINEERS for publication in the ASME JOURNAL OF APPLIED MECHANICS. Manuscript received by the ASME Applied Mechanics Division, Nov. 12, 1992; final revision, Mar. 30, 1993. Associate Technical Editor: S. K. Datta.

Downloaded 03 May 2010 to 171.66.16.20. Redistribution subject to ASME license or copyright; see http://www.asme.org/terms/Terms_Use.cfm

Timoshenko, S., and Woinowsky-Krieger, S., 1959, *Theory of Plates and Shells*, McGraw-Hill, New York.

Wang, N. M., 1970, "Twisting of an Elastic Plate Containing a Crack," *International Journal of Fracture*, Vol. 6, pp. 367–378.

Williams, M. L., 1961, "The Bending Stress Distribution at the Base of a Stationary Crack," ASME JOURNAL OF APPLIED MECHANICS, Vol. 28, pp. 78–82.

Yu, Yi-Yuan, 1954, "The Influence of a Small Hole or Rigid Inclusion on the Transverse Flexure of Thin Plates," *Proceedings of the Second U.S. National Congress of Applied Mechanics*, pp. 381–387.

Response of a Disk Mass on a Half-Space to Dilatational Waves

Tierang Liu[11] and Xiangzhou Zhang[12]

Introduction

This investigation deals with the elastodynamics problem for a disk mass lying on an elastic half-space, impinged upon by dilatational waves, a problem of considerable technical interest in the design of transducers or seismological design of on-ground apparatuses and structures.

Counterpart problems, where the elastic half-space is disturbed by sinusoidal forces exerted on a circular or rectangular body resting on its surface, have been treated by Bycroft (1956), Robertson (1966), Karasudhi et al. (1968), Krenk and Schmidt (1981), and other authors. However, the more complicated problem of transient response to wave incidence is considered here. This involves reflection and scattering of transient waves by the disk and does not seem to have been discussed.

In the present Note, based on the theory of elastodynamics and Reissner's assumption, the equation of motion for the disk mass under the action of a uniformly incoming dilatational waves is first derived. The Laplace transformed solutions for the displacement of the disk mass is then obtained via solving for the transformed equation. By employing a number of analytic techniques, the explicit expression for the displacement is developed, with which other unknowns, for instance the contact stress between the disk mass and the half-space, can be determined directly. The numerical result depicted in diagrams shows that for a large disk mass, the displacement response vibrates rather slowly with large amplitudes, whereas that of a small disk mass oscillates with small amplitudes and high frequencies.

Problem and Transformed Solution

An elastic half-space of density ρ, Lame constants λ and μ, and dilatational wave speed c_d is depicted in Fig. 1, with a rigid circular disk of radius a and mass m resting on its surface. A uniform, one-dimensional displacement wave, in association with uniform dynamic stress $s(c_d z + t)$ and coming from the infinity, reaches the surface plane $z = 0$ at the instant $t = 0$. The elastodynamic process taking place in the disk mass and the half-space ensuing that instant is to be investigated.

Since it is difficult to treat exactly such a transient mixed boundaries value problem, Reissner's assumption will be used

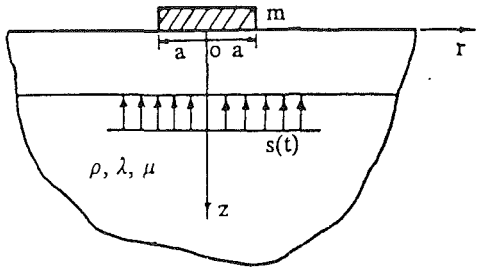


Fig. 1 The half-space and the disk mass

in the following. Reissner's assumption (Bycroft, 1956) includes (1) allowing no friction between the rigid circular disk and the half-space, and neglecting the gravitational force in the disk; (2) supposing a constant normal contact stress over the circle $0 \le r \le a$; and (3) taking the displacement at the center of the circle as the displacement of the rigid disk.

The displacements and stresses in the half-space are composed of those induced by the incoming, the reflecting, and the scattering waves. These waves are distinguished by subscripts 1, 2, and 3, respectively. The displacements and stresses corresponding to the first two waves can be determined directly. They are (Eringen and Suhubi, 1975)

$$w_1(r, z, t) = -\frac{1}{\rho c_d} H\left(t+\frac{z}{c_d}\right) \int_0^{t+\frac{z}{c_d}} s(\tau)d\tau,$$

$$u_{r1}(r, z, t) = 0 \qquad (1a,b)$$

$$\sigma_{z1}(r, z, t) = -H(t+z/c_d)s(t+z/c_d),$$

$$\sigma_{zr1}(r, z, t) = 0 \qquad (2a,b)$$

and

$$w_2(r, z, t) = -\frac{1}{\rho c_d} H\left(t-\frac{z}{c_d}\right) \int_0^{t-\frac{z}{c_d}} s(\tau)d\tau,$$

$$u_{r2}(r, z, t) = 0 \qquad (3a,b)$$

$$\sigma_{z2}(r, z, t) = H(t-z/c_d)s(t-z/c_d), \quad \sigma_{zr2}(r, z, t) = 0 \qquad (4a,b)$$

where $H(t)$ is the Heaviside unit function. The determination of the scattering field is rather complicated. However, once $\sigma(t)$, the normal contact stress between the disk mass and the half-space over the area $r \le a$, is known, the displacements and stresses in the half-space can be found, lengthily yet straightforwardly, through a procedure described in Eringen and Suhubi (1975) and Graff (1975). Neglecting the details of the derivation, the displacement at the origin in the z direction in Laplace transform domain, $\overline{w}_3(0, 0, p)$, is written as follows:

$$\overline{w}_3(0, 0, p) = \frac{a\overline{\sigma}(p)}{\mu} \int_0^\infty \eta_d k_s^2 \frac{J_1(\kappa a)}{R(\kappa, p)} d\kappa \qquad (5)$$

where

$$R(\kappa, p) = (k_s^2 + 2\kappa^2)^2 - 4\kappa^2\eta_d\eta_s \qquad (6)$$

$$\eta_d = \sqrt{k_d^2+\kappa^2}, \quad \eta_s = \sqrt{k_s^2+\kappa^2}$$

$$k_d = p/c_d, \quad k_s = p/c_s \qquad (7a,b,c,d)$$

$J_1(x)$ is the Bessel function of the first kind, c_s is the shear wave speed of the material, p is the Laplace transform parameter, and η_d and η_s stand for the branches that are real and positive for real p. $\overline{\sigma}(p)$ should be determined from the displacement continuity condition over the contact area $r \le a$.

Since the disk mass is rigid and the motion is axisymmetric, the displacement of the disk mass during the dynamic response can only be an upward (regarded as positive) or downward (negative) translation. Denoting this displacement with w_m, from the Reissner's assumption the displacement continuity

[11]Department of Aircraft Engineering, Nanjing University of Aeronautics and Astronautics, Nanjing 210016, People's Republic of China.

[12]Department of Aircraft Engineering, Northwestern Polytechnical University, Xian 710072, People's Republic of China.

Contributed by the Applied Mechanics Division of THE AMERICAN SOCIETY OF MECHANICAL ENGINEERS for publication in the ASME JOURNAL OF APPLIED MECHANICS. Manuscript received by the ASME Applied Mechanics Division, Nov. 12, 1992; final revision, Mar. 30, 1993. Associate Technical Editor: S. K. Datta.

Copyright © 1994 by ASME
Downloaded 03 May 2010 to 171.66.16.20. Redistribution subject to ASME license or copyright; see http://www.asme.org/terms/Terms_Use.cfm

condition between the disk mass and the half-space can then be expressed as

$$w_m(t) = -w_1(0, 0, t) - w_2(0, 0, t) - w_3(0, 0, t). \quad (8)$$

Now consider the motion of the disk mass. The equation of motion is simply

$$m\frac{d^2w_m(t)}{dt^2} = \sigma(t). \quad (9)$$

Substituting Eqs. (8), (1*a*), and (2*a*) into Eq. (9), operating Laplace transform on the resulted equation and noticing the initial conditions for the disk mass

$$w_m(0) = 0, \quad \left.\frac{dw_m(t)}{dt}\right|_{t=0} = 0 \quad (10a,b)$$

we obtain

$$\bar{w}_3(0, 0, p) = \frac{2}{\rho c_d}\frac{1}{p}\bar{s}(p) - \frac{1}{mp^2}\bar{\sigma}(p). \quad (11)$$

Simultaneously solving Eqs. (5) and (11) yields the following transformed solutions for $\bar{\sigma}(p)$ and $\bar{w}_m(p)$:

$$\bar{\sigma}(p) = \frac{2}{\rho c_d p}\frac{\bar{s}(p)}{\dfrac{1}{mp^2} + \dfrac{a}{\mu}\displaystyle\int_0^\infty \eta_d k_s^2 \frac{J_1(\kappa a)}{R(\kappa, p)}\,d\kappa} \quad (12)$$

$$\bar{w}_m(p) = \frac{2c_s^3}{\mu k p^3}\cdot\frac{\bar{s}(p)}{\dfrac{c_s^2}{p^2} + \dfrac{am}{\rho}\displaystyle\int_0^\infty \eta_d k_s^2 \frac{J_1(\kappa a)}{R(\kappa, p)}\,d\kappa} \quad (13)$$

where $k = c_d/c_s$.

The displacement $w_m(t)$ serves a basic unknown in the problem. Since once $w_m(t)$ is determined, $\sigma(t)$, and subsequently all displacements and stresses in the half-space, can directly be found.

Two special cases deserve attention. In the first case, when $m \to \infty$, from Eq. (13) we have

$$\bar{w}_m(p) = 0. \quad (14)$$

That is, this case is equivalent to that the area $r \le a$ is a fixed boundary. In the second case, when $m \to 0$, we have, from Eq. (12),

$$\bar{\sigma}(p) = 0. \quad (15)$$

Therefore, this case is equivalent to the situation where the area $r \le a$ is a free boundary.

Inversion

Inversion of Eq. (13) will be discussed particularly in this section. The analysis developed below applies essentially to incoming waves of any particular form; however, for definiteness we suppose in the following that the incoming wave is of a rectangular type such as

$$s(\theta) = H(\theta) - H(\theta - T) \quad (16)$$

where T is a time interval standing for the width of the rectangle.

Employing Eq. (16), Eq. (13) is first nondimensionalized by introducing a length parameter L,

$$\frac{\mu c_s}{L^2}\bar{w}_m(\tilde{p}) = \frac{2}{k}\frac{1 - e^{-\tilde{p}\tilde{T}}}{\tilde{p}^2(1 + c\tilde{p}^2 I)} \quad (17)$$

where

$$\tilde{p} = p/c_s, \quad \tilde{T} = c_s T/L, \quad c = am/(\rho L^2) \quad (18a,b,c)$$

and

$$I = \int_0^\infty \tilde{\eta}_d \tilde{p}^2 \frac{J_1(\kappa\tilde{a})}{\tilde{R}(\kappa, \tilde{p})}\,d\kappa \quad (19)$$

with

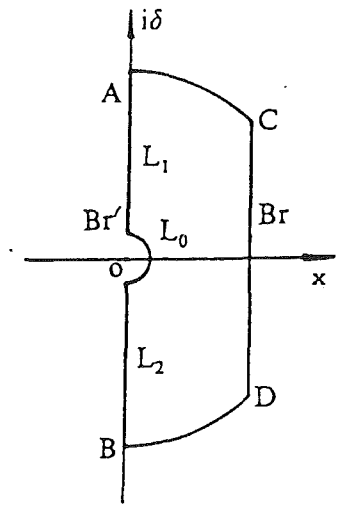


Fig. 2 Integration path in complex plane $\tilde{p} = x + i\delta$

$$\tilde{\eta}_d = \sqrt{\tilde{p}^2/k^2 + \kappa^2}, \quad \tilde{a} = a/L \quad (20a,b)$$

$$\tilde{R}(\kappa, \tilde{p}) = (\tilde{p}^2 + 2\kappa^2)^2 - 4\kappa^2(\tilde{p}^2/k^2 + \kappa^2)^{1/2}(\tilde{p}^2 + \kappa^2)^{1/2}. \quad (21)$$

Furthermore, using the complex inversion formula of the Laplace transform (Spiegel, 1965) the expression for w_m is obtained:

$$\frac{\mu}{L}w_m(\tau) = \frac{1}{2\pi i}\int_{Br}\frac{\mu c_s}{L^2}\bar{w}_m(\tilde{p})e^{\tilde{p}\tau}d\tilde{p} \quad (22)$$

where $\tau = c_s t/L$.

By analysis (Miklowitz, 1978) and numerical searching, it is found that the integrand in Eq. (22) has no singularities in the right half $\tilde{p} = x + i\delta$ complex plane except a pole of order 2 at $x + i\delta = 0$. In view of this, the integration path Br in Eq. (22) can be replaced by Br' as indicated in Fig. 2. We have

$$\frac{\mu}{L}w_m(\tau) = \frac{1}{2\pi i}\left(\int_{L_0} + \int_{L_1} + \int_{L_2}\right)\frac{\mu c_s}{L^2}\bar{w}_m(\tilde{p})e^{\tilde{p}\tau}d\tilde{p}. \quad (23)$$

Examining the first integral in Eq. (23) and noticing that the latter two integrals are mutually conjugate numbers, give rise to

$$\frac{\mu}{L}w_m(\tau) = \frac{\tilde{T}}{2} + 2\mathrm{Re}\int_{L_1}\frac{\mu c_s}{L^2}\bar{w}_m(\tilde{p})e^{\tilde{p}\tau}d\tilde{p}. \quad (24)$$

In order to treat further the integral in Eq. (24), the integral I contained therein (see Eq. (17)) must be evaluated. Through a lengthy procedure, the final result of the integral I is obtained as follows:

$$I = \frac{1}{k\tilde{p}\tilde{a}} + \frac{2}{\pi}\int_0^\infty \mathrm{Im}[n(iy)]K_1(\tilde{p}\tilde{a}y)dy \quad (25)$$

where

$$\mathrm{Im}[n(iy)] = 0, \quad 0 \le y < \frac{1}{k} \quad (26a)$$

$$\mathrm{Im}[n(iy)] = \frac{(y^2 - 1/k^2)^{1/2}(1 - 2y^2)^2}{1 - 8y^2 + 8(3 - 2/k^2)y^4 - 16(1 - 1/k^2)y^6}, \quad \frac{1}{k} \le y < 1 \quad (26b)$$

$$\mathrm{Im}[n(iy)] = \frac{(y^2 - 1/k^2)^{1/2}}{(1 - 2y^2)^2 - 4y^2(y^2 - 1/k^2)^{1/2}(y^2 - 1)^{1/2}}, \quad y \ge 1. \quad (26c)$$

Since on L_1, $\tilde{p} = i\delta$ besides (Abramowitz and Stegun, 1964),

$$K_1(ix) = \pi[-J_1(x) + iY_1(x)]/2 \quad (27)$$

where $Y_1(x)$ and $K_1(x)$ stand for the Bessel function of the

Downloaded 03 May 2010 to 171.66.16.20. Redistribution subject to ASME license or copyright; see http://www.asme.org/terms/Terms_Use.cfm

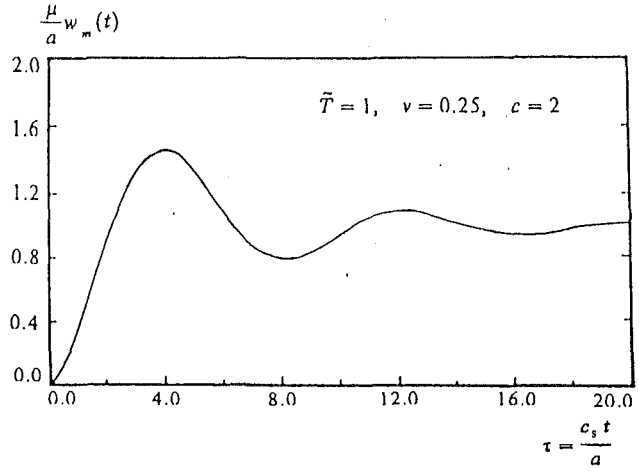


Fig. 3 Displacement response of the disk mass (*a*)

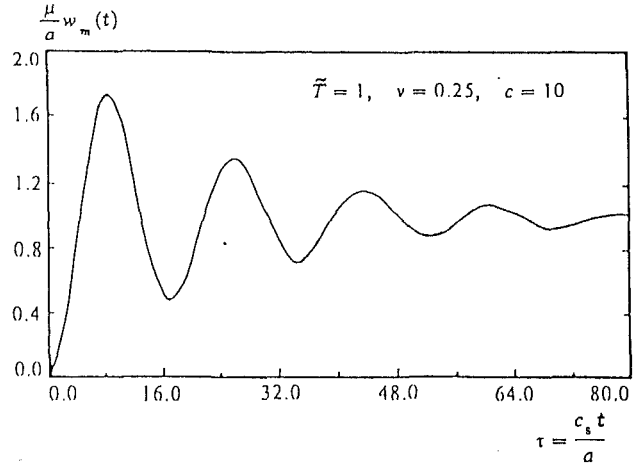


Fig. 4 Displacement response of the disk mass (*b*)

second kind and the modifying Bessel function of the first kind, respectively, therefore the integral I can be written in an alternate form as follows:

$$I = 1/(k\tilde{p}\tilde{a}) - P_1 + iP_2 \tag{28}$$

$$\begin{matrix} P_1 \\ P_2 \end{matrix} = \int_0^\infty \mathrm{Im}[n(iy)] \begin{matrix} J_1(\delta\tilde{a}y) \\ Y_1(\delta\tilde{a}y) \end{matrix} dy. \tag{29}$$

Substituting Eqs. (28), (17) into Eq. (24) and using the notations

$$E = 1 + c\delta^2 P_1, \quad F = c\delta[1/(k\tilde{a}) - \delta P_2] \tag{30a,b}$$

we finally obtain

$$\frac{\mu}{L} w_m(\tau) = \frac{\tilde{T}}{k} - \frac{2}{k\pi}\int_0^\infty \frac{E[(1-\cos\tilde{T}\delta)\cos\tau\delta - \sin\tilde{T}\delta\sin\tau\delta] + F[\sin\tilde{T}\delta\cos\tau\delta + (1-\cos\tilde{T}\delta)\sin\tau\delta]}{\delta^2(E^2+F^2)} d\delta. \tag{31}$$

This is the exact expression for the basic unknown $w_m(\tau)$.

Numerical Values and Discussion

Based on formulas presented in the preceding sections, numerical values of $w_m(\tau)$ are shown in Figs. 3-4 for two different values of c (see Eq. (18*c*)), with the Poission's ratio $\nu = 0.25$ and the nondimensionalized width of the rectangular pulse $\tilde{T} = 1.0$ (see Eqs. (16), (18*b*)).

It is seen that in all cases w_m approaches the stationary value, $\tilde{T}$, as t enlarges. This stationary value has numerically been computed to $(1 \pm 0.001)\tilde{T}$, a fact manifesting the validity of our analysis and computation.

For small values of c (which represents the ratio of the mass density of the disk mass to that of the half-space), w_m oscillates with small amplitudes and relatively high frequencies, whereas for large c, the disk mass vibrates rather slowly with large amplitudes. In the latter case, the energy in the incoming wave is largely absorbed by the disk mass during the initial stage of the dynamic response. From Eq. (12), the contact stress $\sigma(t)$ can be determined directly, once $w_m(t)$ has been determined. The displacement and stress responses in the half-space can then be found through a standard approach.

References

Abramowitz, M., and Stegun, A., 1964, *Handbook of Mathematical Functions*, U.S. Government Printing Office, Washington, D.C.

Bycrobt, G. N., 1956, "Forced Vibrations of a Rigid Circular Plate on a Semi-Infinite Elastic Space and on an Elastic Stratum," *Philosophical Transactions of Royal Society London*, Vol. A248, pp. 327-368.

Eringen, A. C., and Suhubi, E. S., 1975, *Elastodynamics*, Vol. 2, Academic Press, New York.

Graff, K. F., *Wave Motion in Elastic Solids*, Clarendon Press, Oxford, U.K.

Karasudhi, P., Keer, L. M., and Lee, S. L., 1968, "Vibratory Motion of a Body on an Elastic Half Plane," ASME JOURNAL OF APPLIED MECHANICS, Vol. 35, pp. 697-705.

Krenk, S., and Schmidt, H., 1981, "Vibration of an Elastic Circular Plate on an Elastic Half Space—A Direct Approach," ASME JOURNAL OF APPLIED MECHANICS, Vol. 48, pp. 161-168.

Miklowitz, J., 1978, *Elastic Waves and Waveguides*, North Holland, Amsterdam, the Netherland.

Robertson, I. A., 1966, "Forced Vertical Vibration of a Rigid Circular Disc on a Semi-Infinite Elastic Solid," *Proc. Camb. Phil. Soc.*, Vol. 62A, pp. 547-553.

Spiegel, M. R., 1965, *Laplace Transforms*, McGraw-Hill, New York.

Rayleigh Waves on a Rotating Surface

N. S. Clarke[13,15] and J. S. Burdess[14,15]

Introduction

In a recent paper (Clarke and Burdess, 1994) the authors discussed a possible device which could act as a rotation rate sensor. This was based upon previous work on a Rayleigh resonator (Clarke and Burdess, 1991), and extended to account for the effects of rotation upon Rayleigh waves on the surface of a linearly elastic half-space. For the purposes of that work only the first-order effects of the rotation (assumed small when compared to the wave frequency) were required. It is, however,

[13] Department of Engineering Mathematics.
[14] Department of Mechanical, Materials, and Manufacturing Engineering.
[15] University of Newcastle upon Tyne, NE1 7RU, England.

Contributed by the Applied Mechanics Division of THE AMERICAN SOCIETY OF MECHANICAL ENGINEERS for publication in the ASME JOURNAL OF APPLIED MECHANICS. Manuscript received by the ASME Applied Mechanics Division, Apr. 28, 1993; final revision, June 23, 1993. Associate Technical Editor: S. K. Datta.

Downloaded 03 May 2010 to 171.66.16.20. Redistribution subject to ASME license or copyright; see http://www.asme.org/terms/Terms_Use.cfm

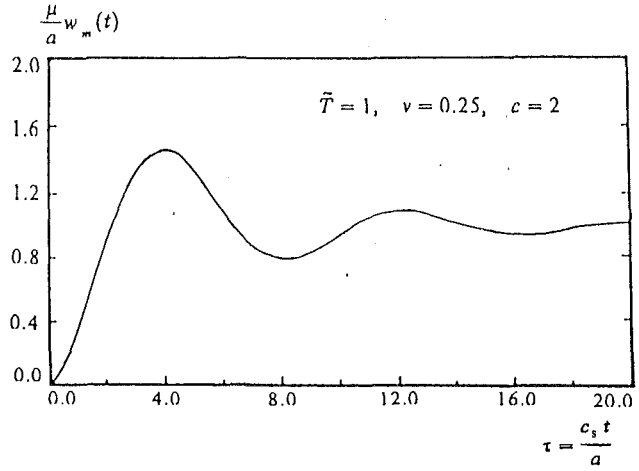


Fig. 3 Displacement response of the disk mass (*a*)

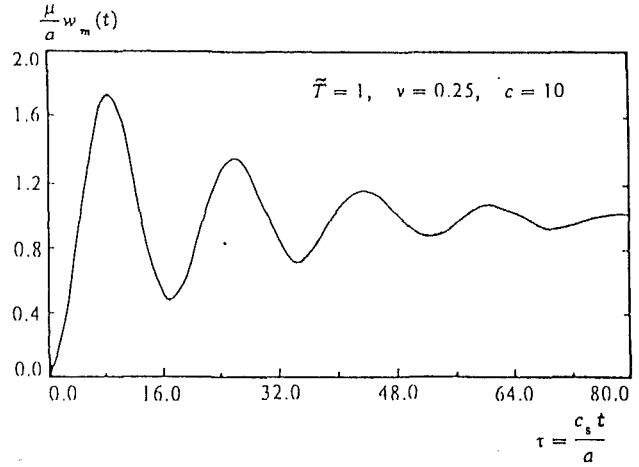


Fig. 4 Displacement response of the disk mass (*b*)

second kind and the modifying Bessel function of the first kind, respectively, therefore the integral I can be written in an alternate form as follows:

$$I = 1/(k\tilde{p}\tilde{a}) - P_1 + iP_2 \tag{28}$$

$$\begin{matrix} P_1 \\ P_2 \end{matrix} = \int_0^\infty \mathrm{Im}[n(iy)] \begin{matrix} J_1(\delta\tilde{a}y) \\ Y_1(\delta\tilde{a}y) \end{matrix} dy. \tag{29}$$

Substituting Eqs. (28), (17) into Eq. (24) and using the notations

$$E = 1 + c\delta^2 P_1, \quad F = c\delta[1/(k\tilde{a}) - \delta P_2] \tag{30a,b}$$

we finally obtain

$$\frac{\mu}{L} w_m(\tau) = \frac{\tilde{T}}{k} - \frac{2}{k\pi}\int_0^\infty \frac{E[(1-\cos\tilde{T}\delta)\cos\tau\delta - \sin\tilde{T}\delta\sin\tau\delta] + F[\sin\tilde{T}\delta\cos\tau\delta + (1-\cos\tilde{T}\delta)\sin\tau\delta]}{\delta^2(E^2+F^2)} d\delta. \tag{31}$$

This is the exact expression for the basic unknown $w_m(\tau)$.

Numerical Values and Discussion

Based on formulas presented in the preceding sections, numerical values of $w_m(\tau)$ are shown in Figs. 3-4 for two different values of c (see Eq. (18*c*)), with the Poission's ratio $\nu = 0.25$ and the nondimensionalized width of the rectangular pulse $\tilde{T} = 1.0$ (see Eqs. (16), (18*b*)).

It is seen that in all cases w_m approaches the stationary value, $\tilde{T}$, as t enlarges. This stationary value has numerically been computed to $(1 \pm 0.001)\tilde{T}$, a fact manifesting the validity of our analysis and computation.

For small values of c (which represents the ratio of the mass density of the disk mass to that of the half-space), w_m oscillates with small amplitudes and relatively high frequencies, whereas for large c, the disk mass vibrates rather slowly with large amplitudes. In the latter case, the energy in the incoming wave is largely absorbed by the disk mass during the initial stage of the dynamic response. From Eq. (12), the contact stress $\sigma(t)$ can be determined directly, once $w_m(t)$ has been determined. The displacement and stress responses in the half-space can then be found through a standard approach.

References

Abramowitz, M., and Stegun, A., 1964, *Handbook of Mathematical Functions*, U.S. Government Printing Office, Washington, D.C.

Bycrobt, G. N., 1956, "Forced Vibrations of a Rigid Circular Plate on a Semi-Infinite Elastic Space and on an Elastic Stratum," *Philosophical Transactions of Royal Society London*, Vol. A248, pp. 327-368.

Eringen, A. C., and Suhubi, E. S., 1975, *Elastodynamics*, Vol. 2, Academic Press, New York.

Graff, K. F., *Wave Motion in Elastic Solids*, Clarendon Press, Oxford, U.K.

Karasudhi, P., Keer, L. M., and Lee, S. L., 1968, "Vibratory Motion of a Body on an Elastic Half Plane," ASME JOURNAL OF APPLIED MECHANICS, Vol. 35, pp. 697-705.

Krenk, S., and Schmidt, H., 1981, "Vibration of an Elastic Circular Plate on an Elastic Half Space—A Direct Approach," ASME JOURNAL OF APPLIED MECHANICS, Vol. 48, pp. 161-168.

Miklowitz, J., 1978, *Elastic Waves and Waveguides*, North Holland, Amsterdam, the Netherland.

Robertson, I. A., 1966, "Forced Vertical Vibration of a Rigid Circular Disc on a Semi-Infinite Elastic Solid," *Proc. Camb. Phil. Soc.*, Vol. 62A, pp. 547-553.

Spiegel, M. R., 1965, *Laplace Transforms*, McGraw-Hill, New York.

Rayleigh Waves on a Rotating Surface

N. S. Clarke[13,15] and J. S. Burdess[14,15]

Introduction

In a recent paper (Clarke and Burdess, 1994) the authors discussed a possible device which could act as a rotation rate sensor. This was based upon previous work on a Rayleigh resonator (Clarke and Burdess, 1991), and extended to account for the effects of rotation upon Rayleigh waves on the surface of a linearly elastic half-space. For the purposes of that work only the first-order effects of the rotation (assumed small when compared to the wave frequency) were required. It is, however,

[13] Department of Engineering Mathematics.
[14] Department of Mechanical, Materials, and Manufacturing Engineering.
[15] University of Newcastle upon Tyne, NE1 7RU, England.

Contributed by the Applied Mechanics Division of THE AMERICAN SOCIETY OF MECHANICAL ENGINEERS for publication in the ASME JOURNAL OF APPLIED MECHANICS. Manuscript received by the ASME Applied Mechanics Division, Apr. 28, 1993; final revision, June 23, 1993. Associate Technical Editor: S. K. Datta.

Copyright © 1994 by ASME
Downloaded 03 May 2010 to 171.66.16.20. Redistribution subject to ASME license or copyright; see http://www.asme.org/terms/Terms_Use.cfm

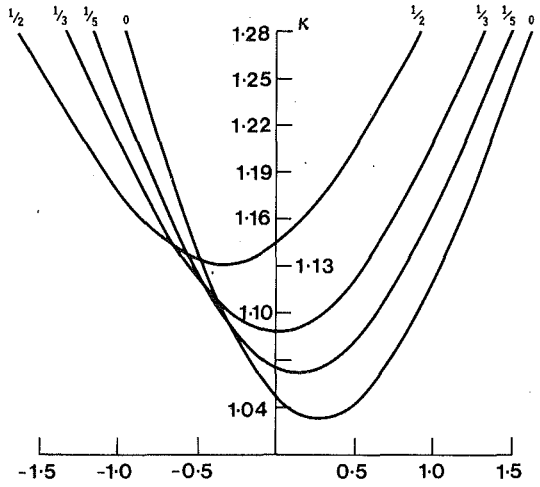


Fig. 1 κ versus δ for various α

quite conceivable that for other problems, no such approximation will be appropriate. In this Note it is shown how the wave number may be calculated for all rotation rates. The method taken to achieve this is simple and straightfoward, whereas previous attempts (Wren and Burdess, 1987) were somewhat more complicated and led only to the first-order effects.

Analysis

The plane Rayleigh wave travels "along" the surface $y=0$ of the linearly elastic material, occupying the half-space $y<0$, in the x-direction in such a way that it is independent of the z-coordinate. The whole space rotates about the z-axis with constant angular speed Ω.

Two dimensionless parameters appear in the problem. One is a material parameter

$$\alpha=(1-2\sigma)/(2-2\sigma), \tag{1}$$

$(0\le\alpha\le 1/2)$, where σ is Poisson's ratio, and the other is δ where

$$(1-\alpha)=2\Omega/\omega. \tag{2}$$

Here ω is the frequency of the Rayleigh wave and so δ measures the relative strength of the rotational effects.

When time and space variables are rendered dimensionless with respect to $1/\omega$ and $(\mu/\rho\omega^2)^{1/2}$, respectively (μ and ρ being a Lamé constant and density of the material), then the dimensionless form of the field equations for the displacements $(u_1, u_2, 0)$ are, in $y<0$,

$$\frac{\partial^2 u_1}{\partial x^2}+\alpha\frac{\partial^2 u_1}{\partial y^2}+(1-\alpha)\frac{\partial^2 u_2}{\partial x\partial y}=\alpha\frac{\partial^2 u_1}{\partial t^2}-\delta\alpha(1-\alpha)\frac{\partial u_2}{\partial t}-\frac{1}{4}\delta^2\alpha(1-\alpha)^2u_1,$$

$$(1-\alpha)\frac{\partial^2 u_1}{\partial x\partial y}+\alpha\frac{\partial^2 u_2}{\partial x^2}+\frac{\partial^2 u_2}{\partial y^2}=\alpha\frac{\partial^2 u_2}{\partial t^2}+\delta\alpha(1-\alpha)\frac{\partial u_1}{\partial t}-\frac{1}{4}\delta^2\alpha(1-\alpha)^2u_2. \tag{3}$$

The boundary conditions (stress-free) on $y=0$ are

$$\frac{\partial u_1}{\partial y}+\frac{\partial u_2}{\partial x}=0,$$

$$(1-2\alpha)\frac{\partial u_1}{\partial x}+\frac{\partial u_2}{\partial y}=0. \tag{4}$$

The solution which corresponds to a Rayleigh wave is of the form

$$u_j(x, y, t)=C_j\exp(i\kappa x+\nu y-it), \tag{5}$$

for $j=1, 2$ and with $\nu>0$. For a right-moving wave $\kappa>0$, and for a left moving wave $\kappa<0$. It is the wave number κ and its dependence upon δ and α which we seek.

When (5) is put into (3) the latter yields

$$(\alpha\nu^2-\kappa^2+\alpha\gamma)C_1+i(1-\alpha)(\kappa\nu-\delta\alpha)C_2=0,$$
$$i(1-\alpha)(\kappa\nu+\delta\alpha)C_1+(\nu^2-\alpha\kappa^2+\alpha\gamma)C_2=0, \tag{6}$$

where

$$\gamma=1+\delta^2(1-\alpha)^2/4. \tag{7}$$

For consistency it follows that ν satisfies a quartic equation whose positive roots are

$$\nu_1=(\kappa^2-\eta_1)^{1/2} \quad \text{and} \quad \nu_2=(\kappa^2-\eta_2)^{1/2}$$

where

$$\eta_1=\alpha\gamma-(1-\alpha)\psi, \quad \eta_2=\gamma+(1-\alpha)\psi, \tag{8}$$

and

$$\psi=[-\gamma+(\gamma^2+4\alpha\delta^2)^{1/2}]/2.$$

Equations (6) also give the relationship between the C_i for each ν_i so that the solutions are necessarily of the form

$$u_1=e^{i(\kappa x-t)}\{A(\kappa^2+\psi)e^{\nu_1 y}+iB(\kappa\nu_2-\alpha\delta)e^{\nu_2 y}\},$$
$$u_2=e^{i(\kappa x-t)}\{-iA(\kappa\nu_1+\alpha\delta)e^{\nu_1 y}+B(\kappa^2+\alpha\psi)e^{\nu_2 y}\}. \tag{9}$$

The boundary conditions (4) are now used by inserting into them the forms (9). A pair of homogeneous equations for A and B are derived, and for these to be consistent we have the following equation for κ to be satisfied:

$$(2\kappa^2+\psi)^2(\kappa^2-\eta_1)^{1/2}(\kappa^2-\eta_2)^{1/2}-\kappa^2(2\kappa^2-\gamma+\psi)\times\{2\kappa^2-\gamma-(1-2\alpha)\psi\}+\delta\kappa\{\alpha(4\kappa^2+2\psi-\gamma)(\kappa^2-\eta_2)^{1/2}-[4\alpha\kappa^2-\gamma-2(1-2\alpha)\psi](\kappa^2-\eta_1)^{1/2}\}+\delta^2\alpha\{(1-2\alpha)\kappa^2+(\kappa^2-\eta_1)^{1/2}(\kappa^2-\eta_2)^{1/2}\}=0. \tag{10}$$

This equation is exact and so is valid for all δ and α.

For $\delta=0$, (10) reduces to the static case $f(\kappa)=0$ where

$$f(\kappa)=4\kappa^2(\kappa^2-1)^{1/2}(\kappa^2-\alpha)^{1/2}-(2\kappa^2-1)^2. \tag{11}$$

The real positive root $\kappa=k_0(\alpha)$ is well known (see Achenbach, 1980). For small and large values of δ the limiting forms are readily obtained as

$$\kappa=k_0+\delta k_1+0(\delta^2) \quad \text{as} \quad \delta\to 0,$$

and

$$\kappa=|\delta|[(1-\alpha)k_0/2+2\delta^{-1}k_1/(1-\alpha)+0(\delta^{-2})] \quad \text{as} \quad \delta\to\infty, \tag{12}$$

where

$$k_1=\{\alpha k_0(k_0^2-1)^{-1/2}-(k_0^2-\alpha)^{1/2}/k_0\}/f'(k_0). \tag{13}$$

Curiously, for the material for which $\alpha=1/3$ (corresponding to Poisson's ratio 1/4), it is possible to find the wave number explicitly for all δ. It is given by

$$\kappa=\{3+\delta^2/3+(3+10\delta^2/3+\delta^4/27)^{1/2}\}^{1/2}/2, \tag{14}$$

and, it should be noted, is an even function of δ. This means that for this material the wave number is independent of the

Downloaded 03 May 2010 to 171.66.16.20. Redistribution subject to ASME license or copyright; see http://www.asme.org/terms/Terms_Use.cfm

sense of rotation. This is the only value of α for which this is so.

For other values of α, (10) has been solved numerically giving κ as a function of δ. Several cases are displayed graphically in the Fig. 1.

References

Achenbach, J. D.,.1980, *Wave Propagation in Elastic Solids*, North-Holland, Amsterdam, pp. 187–190.

Clarke, N. S., and Burdess, J. S., 1994, "A Rotation Rate Sensor Based upon a Rayleigh Resonator," ASME JOURNAL OF APPLIED MECHANICS, Vol. 61, pp. 139–143.

Clarke, N. S., and Burdess, J. S., 1991, "A Rayleigh Resonator," *Wave Motion*, Vol. 13, pp. 193–200.

Wren, T., and Burdess, J. S., 1987, "Surface Waves Perturbed by Rotation," ASME JOURNAL OF APPLIED MECHANICS, Vol. 54, pp. 464–466.

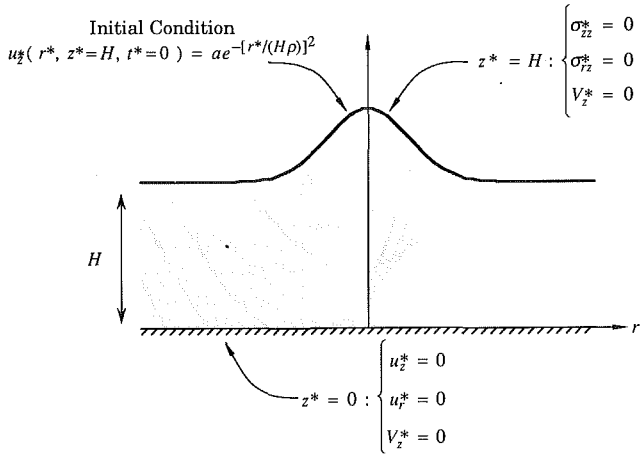


Fig. 1 The geometry and boundary conditions. An infinite axisymmetric layer of undeformed height H is shown here in cross-section. The bottom adheres to an impermeable base plate so that there is no motion of the solid matrix, and no vertical flux of fluid at $z = 0$. At the top, $z^* = H$, no fluid flux is allowed normal to the surface, and normal and shear forces on the surface are assumed to be insignificant. The no-normal-flow condition, $\mathbf{n} \cdot \mathbf{V}^* = 0$ at $z^* = H + u_z^*$, with $\mathbf{n}$ the unit surface normal, has been linearized. At $r = \infty$ all fields are zero.

Linear Flow and Deformation in a Poroelastic Disk With a Free Surface

J. R. Sachs[16], M. R. Glucksberg[17], O. E. Jensen[18], and J. B. Grotberg[17,19]

The equilibration of an axisymmetric, linearly poroelastic layer of finite thickness is determined given an immobile, impermeable base and an impermeable, stress-free top surface. Analytical and numerical studies show that there are eigenfunctions corresponding to sites of fluid injection and removal. Numerical studies also show that an increase in effective stiffness accelerates the equilibration of initial disturbances with longer wavelengths. A Gaussian initial displacement is shown to spread radially rather than simply decaying in amplitude.

Introduction

Poroelasticity has recently been used to model the deformation, flow, and pressure fields in many biological tissues[20]. We will determine the solid displacements and fluid velocities in the axially symmetric, poroelastic layer of Fig. (1) given an initial configuration corresponding to fluid injection-induced deformations. This boundary value problem is particularly applicable to understanding fluid flow in the interstitium (Ford et al., 1991), the equilibration of the area around a subcutaneous injection, and, because of the analogy described by Biot (1956a), a locally heated thermoelastic layer.

The poroelastic model equations used here are those of Biot (1941, 1956b) and Biot and Willis (1957). Several approaches have been used to derive varying forms of these equations and determine their range of validity (Craine, Green, and Naghdi, 1970; Green and Naghdi, 1970; Kenyon, 1976; Rice and Cleary, 1976; Bowen, 1980; Burridge and Keller, 1981; Bowen and Lockett, 1983), and various axisymmetric problems with free-surface boundary conditions have been studied (Paria, 1958; McNamee and Gibson, 1960; Gibson, Schiffman, and Pu, 1970; Sanyal, 1972; Chiarella and Booker, 1975; Szefer and Gaszyński, 1975; Mak, Lai, and Mow, 1987)[20]. Many of these studies use displacement or stress potential functions along with Laplace/Laplace-Hankel transforms to calculate the deformations produced by different loads, whereas we use transform methods to solve the equations directly (Sachs and Grodzinsky, 1989). The resulting analytical and asymptotic solutions describe the re-equilibration to the undeformed state without surface loading of a finite-depth, axisymmetric poroelastic layer with a free-surface boundary condition and an arbitrary initial configuration. We will predict the vertical displacement at the surface, $u_z^*(r^*, z^* = H, t^*)$ of the layer in Fig. 1, because this is a measurable quantity of interest.

The Model and Boundary Conditions

We use the simplest form of the Biot model consisting of conservation of mass and momentum:

$$\nabla \cdot (\mathbf{V}^* + \partial_{t^*}\mathbf{u}^*) = 0 \quad \nabla \cdot \boldsymbol{\sigma}^* = 0 \qquad (1, 2)$$

with the constitutive relation and Darcy's Law

$$\sigma_{ij}^* = 2Ge_{ij} + \delta_{ij}(\lambda e_{kk} - P^*) \quad \nabla P^* = -b\mathbf{V}^*. \qquad (3, 4)$$

Here $\mathbf{V}^*$ is the local area-averaged velocity of the fluid relative to the solid matrix, $\mathbf{u}^*$ is the displacement of the solid matrix, $\boldsymbol{\sigma}^*$ is the total (fluid plus solid) stress based on total area, G and λ are the Lamé coefficients of the solid matrix, P^* is the fluid pressure (per unit total area), b is the fluid resistivity, and e_{ij} is the small-strain tensor $\boldsymbol{e} = 1/2(\nabla\mathbf{u}^* + (\nabla\mathbf{u}^*)^T)$. Figure 1 depicts the geometry and boundary conditions. Displacements and velocities at $t = 0$ are assumed to be known and consistent with the model equations.

Solution

We solve (1)–(4) using separation of variables and Hankel transforms. Equations (1)–(4) show that the dilatation of the

[16]Author to whom all correspondence should be addressed. D. H. Wagner Associates, 894 Ross Drive, Suite 205, Sunnyvale, CA 94089-1443.

[17]Biomedical Engineering Department, McCormick School of Engineering and Applied Science, Northwestern University, Evanston, IL 60208.

[18]Department of Mathematics and Statistics, University of Newcastle upon Tyne, Newcastle upon Tyne, NE1 7RU, U.K.

[19]Department of Anesthesia, Northwestern University Medical School, 303 E. Chicago Avenue, Chicago, IL 60611. Assoc. Mem. ASME.

Contributed by the Applied Mechanics Division of THE AMERICAN SOCIETY OF MECHANICAL ENGINEERS for publication in the ASME JOURNAL OF APPLIED MECHANICS. Manuscript received by the ASME Applied Mechanics Division, Sept. 14, 1992; final revision, Jan. 4, 1993. Associate Technical Editor: R. M. Bowen.

[20]Due to length limitations, the reader is referred to the literature for further references and details.

Downloaded 03 May 2010 to 171.66.16.20. Redistribution subject to ASME license or copyright; see http://www.asme.org/terms/Terms_Use.cfm

sense of rotation. This is the only value of α for which this is so.

For other values of α, (10) has been solved numerically giving κ as a function of δ. Several cases are displayed graphically in the Fig. 1.

References

Achenbach, J. D.,.1980, *Wave Propagation in Elastic Solids*, North-Holland, Amsterdam, pp. 187–190.

Clarke, N. S., and Burdess, J. S., 1994, "A Rotation Rate Sensor Based upon a Rayleigh Resonator," ASME JOURNAL OF APPLIED MECHANICS, Vol. 61, pp. 139–143.

Clarke, N. S., and Burdess, J. S., 1991, "A Rayleigh Resonator," *Wave Motion*, Vol. 13, pp. 193–200.

Wren, T., and Burdess, J. S., 1987, "Surface Waves Perturbed by Rotation," ASME JOURNAL OF APPLIED MECHANICS, Vol. 54, pp. 464–466.

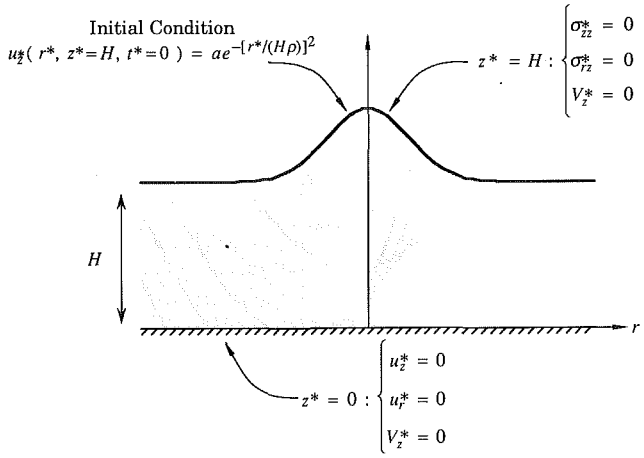


Fig. 1 The geometry and boundary conditions. An infinite axisymmetric layer of undeformed height H is shown here in cross-section. The bottom adheres to an impermeable base plate so that there is no motion of the solid matrix, and no vertical flux of fluid at $z = 0$. At the top, $z^* = H$, no fluid flux is allowed normal to the surface, and normal and shear forces on the surface are assumed to be insignificant. The no-normal-flow condition, $\mathbf{n} \cdot \mathbf{V}^* = 0$ at $z^* = H + u_z^*$, with $\mathbf{n}$ the unit surface normal, has been linearized. At $r = \infty$ all fields are zero.

Linear Flow and Deformation in a Poroelastic Disk With a Free Surface

J. R. Sachs[16], M. R. Glucksberg[17], O. E. Jensen[18], and J. B. Grotberg[17,19]

The equilibration of an axisymmetric, linearly poroelastic layer of finite thickness is determined given an immobile, impermeable base and an impermeable, stress-free top surface. Analytical and numerical studies show that there are eigenfunctions corresponding to sites of fluid injection and removal. Numerical studies also show that an increase in effective stiffness accelerates the equilibration of initial disturbances with longer wavelengths. A Gaussian initial displacement is shown to spread radially rather than simply decaying in amplitude.

Introduction

Poroelasticity has recently been used to model the deformation, flow, and pressure fields in many biological tissues[20]. We will determine the solid displacements and fluid velocities in the axially symmetric, poroelastic layer of Fig. (1) given an initial configuration corresponding to fluid injection-induced deformations. This boundary value problem is particularly applicable to understanding fluid flow in the interstitium (Ford et al., 1991), the equilibration of the area around a subcutaneous injection, and, because of the analogy described by Biot (1956a), a locally heated thermoelastic layer.

The poroelastic model equations used here are those of Biot (1941, 1956b) and Biot and Willis (1957). Several approaches have been used to derive varying forms of these equations and determine their range of validity (Craine, Green, and Naghdi, 1970; Green and Naghdi, 1970; Kenyon, 1976; Rice and Cleary, 1976; Bowen, 1980; Burridge and Keller, 1981; Bowen and Lockett, 1983), and various axisymmetric problems with free-surface boundary conditions have been studied (Paria, 1958; McNamee and Gibson, 1960; Gibson, Schiffman, and Pu, 1970; Sanyal, 1972; Chiarella and Booker, 1975; Szefer and Gaszyński, 1975; Mak, Lai, and Mow, 1987)[20]. Many of these studies use displacement or stress potential functions along with Laplace/Laplace-Hankel transforms to calculate the deformations produced by different loads, whereas we use transform methods to solve the equations directly (Sachs and Grodzinsky, 1989). The resulting analytical and asymptotic solutions describe the re-equilibration to the undeformed state without surface loading of a finite-depth, axisymmetric poroelastic layer with a free-surface boundary condition and an arbitrary initial configuration. We will predict the vertical displacement at the surface, $u_z^*(r^*, z^* = H, t^*)$ of the layer in Fig. 1, because this is a measurable quantity of interest.

The Model and Boundary Conditions

We use the simplest form of the Biot model consisting of conservation of mass and momentum:

$$\nabla \cdot (\mathbf{V}^* + \partial_{t^*}\mathbf{u}^*) = 0 \quad \nabla \cdot \boldsymbol{\sigma}^* = 0 \qquad (1, 2)$$

with the constitutive relation and Darcy's Law

$$\sigma_{ij}^* = 2Ge_{ij} + \delta_{ij}(\lambda e_{kk} - P^*) \quad \nabla P^* = -b\mathbf{V}^*. \qquad (3, 4)$$

Here $\mathbf{V}^*$ is the local area-averaged velocity of the fluid relative to the solid matrix, $\mathbf{u}^*$ is the displacement of the solid matrix, $\boldsymbol{\sigma}^*$ is the total (fluid plus solid) stress based on total area, G and λ are the Lamé coefficients of the solid matrix, P^* is the fluid pressure (per unit total area), b is the fluid resistivity, and e_{ij} is the small-strain tensor $\boldsymbol{e} = 1/2(\nabla\mathbf{u}^* + (\nabla\mathbf{u}^*)^T)$. Figure 1 depicts the geometry and boundary conditions. Displacements and velocities at $t = 0$ are assumed to be known and consistent with the model equations.

Solution

We solve (1)–(4) using separation of variables and Hankel transforms. Equations (1)–(4) show that the dilatation of the

[16]Author to whom all correspondence should be addressed. D. H. Wagner Associates, 894 Ross Drive, Suite 205, Sunnyvale, CA 94089-1443.

[17]Biomedical Engineering Department, McCormick School of Engineering and Applied Science, Northwestern University, Evanston, IL 60208.

[18]Department of Mathematics and Statistics, University of Newcastle upon Tyne, Newcastle upon Tyne, NE1 7RU, U.K.

[19]Department of Anesthesia, Northwestern University Medical School, 303 E. Chicago Avenue, Chicago, IL 60611. Assoc. Mem. ASME.

Contributed by the Applied Mechanics Division of THE AMERICAN SOCIETY OF MECHANICAL ENGINEERS for publication in the ASME JOURNAL OF APPLIED MECHANICS. Manuscript received by the ASME Applied Mechanics Division, Sept. 14, 1992; final revision, Jan. 4, 1993. Associate Technical Editor: R. M. Bowen.

[20]Due to length limitations, the reader is referred to the literature for further references and details.

Copyright © 1994 by ASME

Downloaded 03 May 2010 to 171.66.16.20. Redistribution subject to ASME license or copyright; see http://www.asme.org/terms/Terms_Use.cfm

solid matrix, $d^* = \nabla \cdot \mathbf{u}^*$, obeys the diffusion equation $\partial_t{}^* d^* = D\nabla^2 d^*$ with $D \equiv (2G + \lambda)/b$. If a is the height of the surface deformation we use the diffusion scaling $t^* = (H^2/D)t$, $\mathbf{x}^* = H\mathbf{x}$, $\mathbf{u}^* = a\mathbf{u}$, $\mathbf{V}^* = (aD/H^2)\mathbf{V}$, $P^* = a[(2G + \lambda)/H]P$, and $\sigma^* = a[(2G + \lambda)/H]\sigma$, where the unstarred variables are nondimensional. Linearity requires that $a \ll H$.

The transformed displacement, $\hat{u}_z$, is defined by

$$u_z(r, z, t) = \int_0^\infty \hat{u}_z(z; k, \gamma) e^{-k^2\gamma t} J_0(kr)\, k dk \tag{5}$$

and similarly for $\hat{V}_z$, $\hat{P}$, and $\hat{\sigma}_{zz}$. The transforms $\hat{u}_r$, $\hat{V}_r$, and $\hat{\sigma}_{rz}$ are defined similarly with J_1 replacing J_0. Here γ is a separation constant called the *decay rate*, and k is effectively a radial wave number. Transforming and nondimensionalizing Eqs. (1)–(4) yields the equations

$$(k\hat{V}_r + \hat{V}_z') - k^2\gamma(k\hat{u}_r + \hat{u}_z') = 0 \tag{6}$$

$$N\hat{u}_r'' - k\hat{u}_z' - (1+N)k^2\hat{u}_r + (1+N)\hat{V}_r = 0 \tag{7}$$

$$(1+N)\hat{u}_z'' + k\hat{u}_r' - k^2 N\hat{u}_z + (1+N)\hat{V}_z = 0 \tag{8}$$

$$\hat{V}_r' + k\hat{V}_z = 0 \tag{9}$$

where f' denotes df/dz, and $N \equiv 1 - 2\nu = G/(G + \lambda)$ (ν is the Poisson ratio). The six boundary conditions in Fig. 1 become

$$z = 0: \quad \hat{V}_z = 0; \quad \hat{u}_r = 0; \quad \hat{u}_z = 0$$

$$z = 1: \quad \hat{V}_z = 0; \quad \hat{\sigma}_{rz} = \frac{\beta}{2}(\hat{u}_r' - k\hat{u}_z) = 0;$$

$$\hat{\sigma}_{zz} = \frac{-1}{k}\left[\hat{V}_r - k\hat{u}_z' - k^2\frac{1-N}{1+N}\hat{u}_r\right] = 0 \tag{10}$$

where $\beta \equiv 2N/(1 + N)$. Equations (6)–(10) determine the field transforms $\hat{u}_r$, $\hat{u}_z$, $\hat{V}_r$, and $\hat{V}_z$ as functions of z with parametric dependence on k, γ, and N. ($\hat{P}$ is determined from $\hat{\mathbf{V}}$ via Eq. (4): $k\hat{P} - \hat{V}_r = 0$.) The only nondimensional material parameter in the Eqs. (6)–(10) is N, which is a measure of the relative compressibility of the material, with $N = 0$ for an incompressible matrix, and $0 \le N \le 1$ for materials of interest.

The general solution of the ordinary differential Eqs. (6)–(9) is

$$\hat{u}_r = \left(-1, 1, -\left(z + \frac{1}{k}\right), z - \frac{1}{k}, -1, 1\right) \cdot \mathbf{c}(z)$$

$$\hat{u}_z = (1, 1, z, z, \Lambda, \Lambda) \cdot \mathbf{c}(z)$$

$$\hat{V}_r = (0, 0, \beta k, \beta k, -k^2\gamma, k^2\gamma) \cdot \mathbf{c}(z)$$

$$\hat{V}_z = (0, 0, -\beta k, \beta k, \Lambda k^2\gamma, \Lambda k^2\gamma) \cdot \mathbf{c}(z)$$

$$\hat{P} = (0, 0, \beta, \beta, -k\gamma, k\gamma) \cdot \mathbf{c}(z)$$

$$\hat{\sigma}_{rz} = \left(-\beta k, -\beta k, -\beta k\left(z + \frac{1}{k}\right), \beta k\left(\frac{1}{k} - z\right), -\Lambda\beta k, -\Lambda\beta k\right) \cdot \mathbf{c}(z)$$

$$\hat{\sigma}_{zz} = (\beta k, -\beta k, \beta k z, -\beta k z, \beta k, -\beta k) \cdot \mathbf{c}(z) \tag{11}$$

where $\mathbf{c}(z) \equiv (c_1 e^{kz}, c_2 e^{-kz}, c_3 e^{kz}, c_4 e^{-kz}, c_5 e^{\Lambda kz}, c_6 e^{-\Lambda kz})^T$, $\Lambda = \sqrt{1 - \gamma}$, and $c_1, \ldots, c_6$ are constants (in r, z, and t).

The problem has now been reduced to using the six boundary conditions (10) to determine the c_i. An initial condition will be satisfied by superposing these solutions for different k. Substituting Eq. (11) into the boundary conditions (10) gives an equation of the form $M\mathbf{c}(0) = 0$. This has nonzero solutions only when $\Delta(\gamma, k; N) \equiv \det M = 0$. The value of N is fixed for a given material, so the dispersion equation $\Delta = 0$ determines γ as a function of k. The value $\gamma = 1$ corresponds to purely diffusive behavior.

For every value of k, numerical and asymptotic solutions show that there is one solution (eigenfunction) with $\gamma \equiv \gamma^{(0)}(k) < 1$, and one eigenfunction for each $\gamma \equiv \gamma^{(n)}(k)$, $1 < \gamma^{(1)} < \gamma^{(2)} < \ldots$. The fields are calculated using

$$u_z(r, z, t) = \int_0^\infty \sum_{n=0}^{\infty} a_n(k)\hat{u}_z^{(n)}(z; k) e^{-k^2\gamma^{(n)}t} J_0(kr)\, k dk \tag{12}$$

and similarly for the other fields as described for Eqs. (5). Here $\hat{u}_z^{(n)}(z; k)$ signifies the $\hat{u}_z$ field corresponding to the eigenvalue $\gamma^{(n)}(k)$. This solution method is roughly equivalent to a Laplace-Hankel transform, but avoids some technical difficulties. The coefficients $a_n(k)$ are determined by the initial conditions (see below).

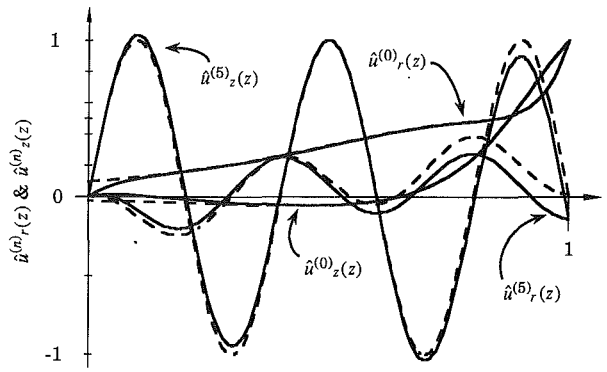


Fig. 2 Displacement eigenfunctions $\hat{u}_r^{(n)}(z; k, \gamma)$ and $\hat{u}_z^{(n)}(z; k, \gamma)$ versus z for $n = 0$, $k = 10$, $N = 1/5$, and $\gamma = \gamma^{(0)} \approx 0.930993$, and for $n = 5$, $k = 3$, $N = 1/5$, and $\gamma = \gamma^{(5)} \approx 28.4205$. c(0) is normalized so that $\hat{u}_z^{(0)}(z = 1) = 1$ ($n = 0$), and $\hat{u}_z^{(5)\prime}(1) = -5\pi$ ($n = 5$). The solid lines were determined numerically and the dashed lines are from shortwave approximations to the fields for $n = 0$, and from the large-n approximations for $n = 5$. (When $n \gg k/\pi$, $\hat{u}_r^{(n)} \sim k[\cos n\pi z - 1 + \alpha(n, k)z(1 - z/2)]/(n\pi)$ and $\hat{u}_z^{(n)} \sim \sin n\pi z$.) When only a single wave number, k, and nth decay rate, $\gamma^{(n)}(k)$, are present, Eq. (12) shows that the eigenfunctions have the form $[u_r, u_z](r, z, t) = [\hat{u}_r^{(n)}, \hat{u}_r^{(n)}](z; k, \gamma^{(n)}(k))J_l(kr)e^{-k^2\gamma^{(n)}t}$, with $l = 0$ for u_z and $l = 1$ for u_r. $N = 1/5$ was chosen because it is an accepted value for bovine femoropatellar articular cartilage (Sachs and Grodzinsky, 1989).

Results and Analysis

Figure 2 shows the numerically and asymptotically calculated displacement $\hat{\mathbf{u}}^{(n)}(z; k)$ for $n = 0$, $k = 10$ and $n = 5$, $k = 3$. For $n = 0$, the upward and (radially) outward displacements are accompanied by a predominantly horizontal flow of fluid. For $n \ge 1$, the $\gamma^{(n)}(k)$ solution has n local extrema, like the eigenfunctions for a Sturm-Liouville problem. Each maximum (minimum) in u_r effectively represents a site of local fluid injection (removal), where the matrix has been pushed radially outward (inward) and vertically away from the source.

The numerical results may be confirmed and better understood using asymptotics for the slowest decaying mode ($n = 0$) with $k \ll 1$ and $k \gg 1$, and for the other modes with $n \gg k/\pi$. In the long-wave (shallow layer) limit, $k \ll 1$, a regular perturbation expansion in k yields the following: $\gamma^{(0)} \sim 1 + O(k^2)$, $\hat{u}_r^{(0)} \sim kz(4 - z)/2$, $\hat{u}_z^{(0)} \sim z$, $\hat{V}_r^{(0)} \sim k$, and $\hat{V}_z^{(0)} \sim O(k^4)$. Asymptotic and numerically calculated fields are almost indistinguishable when $k = 0.1$ and $N = 1/5$. In this limit, finite slope effects produce significant V_z and concomitant changes in equilibration rates (Jensen et al., 1994).

For the short-wave (infinitely deep) limit $k \gg 1$, boundary layer theory gives $c_2 = c_4 = c_6 = 0$ in Eq. (11). The fields have a nested boundary layer structure with layers of thickness $1/k$ and $1/(k\Lambda)$ at $z = 1$ representing purely elastic and fluid-solid friction responses, respectively, visible in Fig. (2). The dispersion equation $\Delta(\gamma, k; N) = 0$ may be approximated $\gamma^{(0)} \sim (1 - 2\beta + \sqrt{1 + 4\beta})/2$. Thus, $\gamma^{(0)} = 1$ for $N = 0$ (representing incompressibility), with $\gamma^{(0)}$ decreasing to 0.62 as N increases to 1 (corresponding to Poisson ratio $\nu = 0$), so that

Downloaded 03 May 2010 to 171.66.16.20. Redistribution subject to ASME license or copyright; see http://www.asme.org/terms/Terms_Use.cfm

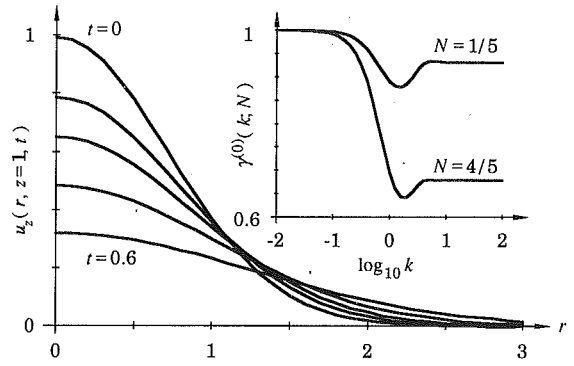


Fig. 3 The surface displacement, $u_z(r, z = 1, t)$, versus r for $t = 0, 0.075, 0.15, 0.3$, and 0.6 with $\rho = 1$ and $N = 1/5$. The force of the radial fluid motion on the top surface causes u_z to increase in t temporarily for $r > 1.2$ so that the bump spreads radially rather than just decreasing in amplitude. Note the roughly equal decrements of $u_z(r = 0, z = 1, t)$ for these t, so that the values of $0.21 - 0.22 \log t$ fit the numerically calculated values of $u_z(r = 0, z = 1, t)$ well for $0.075 \le t \le 1$. Inset: The decay rate, $\gamma^{(0)}(k; N)$, versus $\log_{10} k$ for $N = 1/5$ (upper curve) and $N = 4/5$ (lower curve). Both curves show that small k disturbances decay faster (relative to a diffusion time), and that there is a minimum in equilibration rate for wave number $k \sim 1.5$. The more compressible medium ($N = 4/5$) equilibrates more slowly.

the equilibration rate decreases dramatically as the dilatational restoring force is weakened (i.e., N is increased).

The dependence of $\gamma^{(0)}$ on N and k is depicted in the inset in Fig. 3. For fixed $0.2 < N \le 0.8$, $\gamma^{(0)}(k < 1) > \gamma^{(0)}(k > 2)$, with $\gamma^{(0)}(k)$ minimum near $k = 1.5$. Consider the equilibration of the layer to be characterized by an effective diffusivity, $D^e = M^e/b^e$, resulting from an effective stiffness M^e and resistivity b^e. b^e should increase for a thin layer ($k \ll 1$) due to the boundary conditions $V_z(z = 0) = 0$ and $V_z(z = 1) = 0$, thus decreasing D^e (and so causing slower equilibration) for small k. But the decrease in $\gamma^{(0)}$ with k in Fig. 3 indicates that D^e decreases as k increases, so that thin layers are stiffened (i.e., M^e increases) by the fixed boundary at $z = 0$, and equilibrate faster. This is also true for higher modes: $\gamma^{(n)} \sim n^2\pi^2/k^2 + 1$ for $n \gg k/\pi$, so that $\gamma^{(n)}$ decreases with k. Because the shorter wavelengths decay more rapidly than the longer ones for all n (as expected in a diffusive process), the long-time behavior of any initial condition is determined by the long-wave behavior.

An Example

An initial condition generated from a single (perhaps diffuse) source at $r = 0$ would contain upward and radially outward displacement, resulting in a bulge like that in Fig. 1. Since these characteristics may be described using only $n = 0$ eigenmodes, only the $n = 0$ term is retained in Eq. (12). We assume that the initial surface shape is Gaussian, $u_z^*(r^*, z^* = H, t^* = 0) = ae^{-[r^*/(H\rho)]^2}$, so that inverting the Hankel transform (Miles, 1971) gives $a_0(k) = (\rho^2/2)e^{-(k\rho)^2/4}$, which determines all of the fields via Eq. (12) and the following comments.

Figure 3 shows the evolution of the vertical surface displacement, u_z, for $\rho = 1$. Initially, the hump spreads radially, with motion downward near $r = 0$ and upward for $r > 1.2$. In the absence of interaction with the fluid ($b = 0$), the purely elastic forces predicted by the constitutive relation (3) would result in a simple decrease in hump amplitude. For a shallow layer, spreading of the hump would be expected from the conservation of mass, but it is seen even for deeper layers in which vertical mass transfer might reduce this effect. This suggests that the outward radial fluid velocity produces a significant radial drag force on the matrix.

Because the long-time behavior is governed by the longer wavelengths, and because the radial velocity is uniform (in z) in the long-wave limit regardless of N, the radial spread probably arises irresepctive of the value of N. The behavior of $\gamma^{(0)}(k)$ (Fig. 3) indicates that narrower bumps (relative to H) decay faster. Asymptotics show that, for $0.2 < N < 0.8$, bumps with $\rho < 1/2$ will behave as though γ is between its minimum and large k behavior (i.e., decay slower than expected based on diffusion scaling), whereas those with $\rho > 6$ act as though $\gamma = 1$, as expected from the diffusive nature of long wave asymptotics (Jensen et al., 1994). This difference results in $u_z(r/\rho, t/\rho^2)$ being several percent (depending on N) larger at a given r and $t > 0$ for $\rho < 1/2$ than for $\rho > 6$, even though it would be identical for a purely diffusive process.

Acknowledgments

This work was supported by NIH grants R01-HL41126 and K04-HL01818, NSF grant CTS-9013083, the Whitaker Foundation, and the American Lung Association. JRS performed this work largely at Northwestern University and at the Biotechnology Division of the National Institute of Standards and Technology.

References

Biot, M. A., 1941, "General Theory of Three-Dimensional Consolidation," *J. Appl. Phys.*, Vol. 12, pp. 155–164.

Biot, M. A., 1956a, "Thermoelasticity and Irreversible Thermodynamics," *J. Appl. Phys.*, Vol. 27, pp. 240–253.

Biot, M. A., 1956b, "General Solutions of the Equations of Elasticity and Consolidation for a Porous Material," ASME JOURNAL OF APPLIED MECHANICS, Vol. 78, pp. 91–96.

Biot, M. A., and Willis, D. G., 1957, "The Elastic Coefficients of the Theory of Consolidation," ASME JOURNAL OF APPLIED MECHANICS, Vol. 24, pp. 594–601.

Bowen, R. M., 1980, "Incompressible Porous Media Models by Use of the Theory of Mixtures," *Int. J. Engng. Sci.*, Vol. 18, pp. 1129–1148.

Bowen, R. M., and Lockett, R. R., 1983, "Inertial Effects in Poroelasticity," ASME JOURNAL OF APPLIED MECHANICS, Vol. 50, pp. 334–342.

Burridge, R., and Keller, J. B., 1981, "Poroelasticity Equations Derived from Microstructure," *J. Acoust. Soc. Am.*, Vol. 70, pp. 1140–1146.

Chiarella, C., Booker, J. R., 1975, "The Time-Settlement Behaviour of a Rigid Die Resting on a Deep Clay Layer," *Quart. J. Mech. and Applied Math.*, Vol. 28, pp. 317–328.

Craine, R. E., Green, A. E., and Naghdi, P. M., 1970, "A Mixture of Viscous Elastic Materials with Different Constituent Temperatures," *Quart. J. Applied Math.*, Vol. 23, pp. 171–184.

Ford, T. R., Sachs, J. R., Grotberg, J. B., and Glucksberg, M. R., 1991, "Perialveolar Interstitial Resistance and Compliance in the Isolated Rat Lung," *J. Appl. Physiol.*, Vol. 70, pp. 2750–2756.

Gibson, R. E., Schiffman, R. L., and Pu, S. L., 1970, "Plane Strain and Axially Symmetric Consolidation of a Clay Layer on a Smooth Impervious Base," *Quart. J. Mech. and Applied Math.*, Vol. 23, pp. 505–520.

Green, A. E., and Naghdi, P. M., 1970, "The Flow of Fluid through an Elastic Solid," *Acta Mechanica*, Vol. 9, pp. 329–340.

Jensen, O. E., Glucksberg, M. R., Sachs, J. R., and Grotberg, J. B., 1994, "Weakly Nonlinear Deformation of a Thin Poroelastic Layer with a Free Surface," ASME JOURNAL OF APPLIED MECHANICS, Vol. 61, pp. 729–731.

Kenyon, D. E., 1976, "The Theory of an Incompressible Solid-Fluid Mixture," *Arch. Ration. Mech. Anal.*, Vol. 62, pp. 131–147.

Mak, A. F., Lai, W. M., and Mow, V. C., 1987, "Biphasic Indentation of Articular Cartilage—I. Theoretical Analysis," *J. Biomechanics*, Vol. 20, pp. 703–714.

McNamee, J., and Gibson, R. E., 1960, "Plane Strain and Axially Symmetric Problems of the Consolidation of a Semi-infinite Clay Stratum," *Quart. J. Mech. & Applied Math.*, Vol. 13, pp. 210–227.

Miles, J. W., 1971, *Integral Transforms in Applied Mathematics*, Cambridge University Press, Cambridge, U.K.

Paria, G., 1958, "Axisymmetric Consolidation for a Porous Elastic Material Containing a Fluid," *Quart. J. Math. & Phys.*, Vol. 36, pp. 338–346.

Rice, J. R., and Cleary, M. P., 1976, "Some Basic Stress Diffusion Solutions for Fluid-Saturated Elastic Porous Media with Compressible Constituents," *Rev. Geophys. and Space Phys.*, Vol. 14, pp. 227–241.

Sachs, J. R., and Grodzinsky, A. J., 1989, "An Electromechanically Coupled Poroelastic Medium Driven by an Applied Electric Current: Surface Detection of Bulk Material Properties," *Physicochemical Hydrodynamics*, Vol. 11, pp. 585–614.

Sanyal, D. C., 1972, "On the Two-dimensional Deformation of a Semi-infinite Porous Elastic Medium," *Appl. Sci. Res.*, Vol. 26, pp. 227–245.

Szefer, G., and Gaszyński, J., 1975, "Axisymmetric Punch Problem under Condition of Consolidation," *Arch. of Mechanics*, Vol. 27, pp. 497–515.

Downloaded 03 May 2010 to 171.66.16.20. Redistribution subject to ASME license or copyright; see http://www.asme.org/terms/Terms_Use.cfm

Weakly Nonlinear Deformation of a Thin Poroelastic Layer With a Free Surface

O. E. Jensen,[21,24] M. R. Glucksberg,[21] J. R. Sachs[23,25] and J. B. Grotberg[21,22,26]

Using the biphasic theory of Biot (1941), we examine the evolution of deformations of a poroelastic layer, secured at its base to a rigid plane and having a stress-free, impermeable upper surface. By identifying a limit in which the layer is very thin but the wavelength of disturbances is very long, we show how nonlinear effects due to the finite slope of the free surface cause local elevations of the free surface to decay more slowly than depressions.

Introduction

A number of biological tissues, such as mesentery, pulmonary interstitium, or subcutaneous tissue, may be modeled as poroelastic materials. To describe some of the physical processes underlying fluid flow in the interstitium, for example, Sachs et al. (1994) (referred to herein as I; see this accompanying Note for further references) consider the behavior of a poroelastic layer, the lower surface of which is attached to a rigid plane while the impermeable, stress-free upper surface is free to move vertically. They consider small deformations of the free surface about an equilibrium configuration: the vertical strains induced by a localized deformation generate pressure gradients that drive flows, leading to the decay of the perturbations. They use the biphasic theory of Biot (1941), which couples linear elasticity to the Darcy equations for flow in a porous medium.

Although the calculation in I is valid for arbitrary aspect ratios, it is completely linear: vertical deflections of the layer are required to be much smaller than the layer depth in order to satisfy linear elasticity, and the boundary conditions at the upper surface are linearized about the unperturbed position. Larger deformations introduce nonlinearities to this problem partly because the assumptions of linear elasticity fail (e.g., see Holmes, Lai and Mow (1985) for a study of large stress and strain-rate nonlinearities, or the quasi-static, isothermal, Lagrangian approach of Biot (1972)), partly because of variation in material parameters such as porosity-dependent permeability (e.g., see Kwan, Lai and Mow (1990), Grimshaw et al. (1990), Parker, Mehta and Caro (1987)), and partly because of geometrically more complex boundary conditions at the free surface. Here we wish to investigate the effect of the last, but we do so while remaining within the framework of linear elasticity by identifying a limit in which the layer is very thin but the wavelength of disturbances is very long. We show that the slope of the free surface induces a vertical velocity that is absent in the corresponding linear problem. This flow is downward irrespective of the direction of the surface deflection, so that the rate at which disturbances decay is dependent on whether the film is compressed or dilated.

The Model

We consider a thin layer of poroelastic material attached to a rigid plane and having an impermeable free surface. For simplicity we consider a planar geometry; the free surface is at $z = h(x, t)$. Our notation follows that in I, except that subscripts x, z will be used to denote the components of the displacement and velocity fields $\mathbf{u}$ and $\mathbf{V}$, and also, following commas, derivatives. Thus $u_{x,x} \equiv \partial_x u_x$, etc. The dimensional governing equations of the model are given by equations (1)–(4) in I. The layer's elastic moduli G and λ and fluid resistance b are all assumed constant.

We choose scalings for these equations as follows. If H is the height of the undeformed film, we assume that H/ϵ is a typical horizontal lengthscale, where $\epsilon \ll 1$, and that δH is a typical vertical displacement of the film. The condition $\delta \ll 1$ will ensure that strains are small, so that linear elasticity may be employed. Variables are scaled as follows: x by H/ϵ; z and h by H; u_x by $\epsilon\delta H$; u_z by δH; V_x by $U = (2G + \lambda)\epsilon\delta/bH$; V_z by ϵU; t by $T = H^2 b/[\epsilon^2(2G + \lambda)]$ (the timescale for horizontal diffusion of a deformation); and p by $P = (2G + \lambda)\delta$. Hereafter all variables are written in nondimensional form.

In scaled variables, the mass conservation equation (Eq. (1) in I) becomes

$$V_{x,x} + V_{z,z} + u_{z,zt} = -\epsilon^2 u_{x,xt}. \tag{1}$$

Darcy's Law (Eq. (4) in I) becomes

$$p_{,x} + V_x = 0, \quad p_{,z} = -\epsilon^2 V_z. \tag{2}$$

Equations (2) and (3) of I give

$$\frac{(G+\lambda)u_{z,zx} + Gu_{x,zz}}{2G+\lambda} - p_{,x} = -\epsilon^2 u_{x,xx},$$

$$u_{z,zz} - p_{,z} = -\epsilon^2\left(\frac{(G+\lambda)u_{x,xz} + Gu_{z,xx}}{2G+\lambda}\right). \tag{3}$$

The boundary conditions are as follows. At the rigid plane, $z = 0$, there is zero displacement and zero normal velocity,

$$u_x = 0, \quad u_z = 0, \quad V_z = 0. \tag{4}$$

The free surface at $z = h(x, t)$ is covered by a membrane that is impermeable (so $\mathbf{V} \cdot \mathbf{n} = 0$) and stress-free (so $\mathbf{t} \cdot \boldsymbol{\sigma} \cdot \mathbf{n} = \mathbf{n} \cdot \boldsymbol{\sigma} \cdot \mathbf{n} = 0$, where $\mathbf{t}$ and $\mathbf{n}$ are the unit tangent and normal to this surface and $\boldsymbol{\sigma}$ is the stress tensor). In addition, there is a kinematic condition relating the displacement of the layer to the layer depth. These four boundary conditions may be written as follows:

$$\begin{aligned} V_z - h_{,x}V_x &= 0, \\ (1-\epsilon^2 h_{,x}^2)(u_{z,x} + u_{x,z}) + 2h_{,x}(u_{z,z} - \epsilon^2 u_{x,x}) &= 0, \\ u_{z,z}\left(1 + \frac{\lambda}{2G+\lambda}\epsilon^2 h_{,x}^2\right) + \epsilon^2 u_{x,x}\left(\frac{\lambda}{2G+\lambda} + \epsilon^2 h_{,x}^2\right) & \\ - \frac{2G}{2G+\lambda}\epsilon^2 h_{,x}(u_{z,x} + u_{x,z}) - p(1+\epsilon^2 h_{,x}^2) &= 0, \\ \delta u_z(z=h) &= h - 1. \end{aligned} \tag{5}$$

Asymptotic Analysis

We wish to describe the leading-order effects of the slope of the free surface. To do so we must relate δ, the size of the

[21]Department of Biomedical Engineering, Northwestern University, Evanston, IL 60208.
[22]Department of Anesthesia, Northwestern University Medical School, Chicago, IL 60611.
[23]Biotechnology Division, National Institute of Standards and Technology, Gaithersburg, MD 20899.
[24]Author to whom correspondence should be addressed. Present address: Department of Mathematics and Statistics, University of Newcastle upon Tyne, Newcastle upon Tyne NE1 7RU, U.K.
[25]Present address: Daniel H. Wagner Associates, 894 Ross Drive, Suite 205, Sunnyvale, CA 94089-1443.
[26]Assoc. Mem. ASME.

Contributed by the Applied Mechanics Division of THE AMERICAN SOCIETY OF MECHANICAL ENGINEERS for publication in the ASME JOURNAL OF APPLIED MECHANICS. Manuscript received by the ASME Applied Mechanics Division, Sept. 14, 1994; final revision, Jan. 4, 1993. Associate Technical Editor: R. M. Bowen.

Copyright © 1994 by ASME
Downloaded 03 May 2010 to 171.66.16.20. Redistribution subject to ASME license or copyright; see http://www.asme.org/terms/Terms_Use.cfm

vertical strain, to ϵ, the ratio of layer depth to disturbance wavelength. We will consider the regime in which $\epsilon^2 \ll \delta \ll 1$; the limit implicitly assumed in the long-wavelength analysis of I is $\delta \ll \epsilon^2 \ll 1$. We expand all variables in powers of δ as follows:

$$\frac{h-1}{\delta} = h^{(0)} + \delta h^{(1)} + O(\epsilon^2, \delta^2), \qquad p = p^{(0)} + \delta p^{(1)} + O(\epsilon^2, \delta^2),$$
$$V_j = V_j^{(0)} + \delta V_j^{(1)} + O(\epsilon^2, \delta^2), \quad u_j = u_j^{(0)} + \delta u_j^{(1)} + O(\epsilon^2, \delta^2), \tag{6}$$

(where $j = x$ or z). Inserting these expansions into the governing equations and boundary conditions (1)–(5), we obtain at leading order equations identical to Eqs. (1)–(4) with the right-hand sides set to zero and all variables having a superscript (0), together with boundary conditions at $z = 1$

$$V_z^{(0)} = 0, \quad u_{x,z}^{(0)} + u_{z,x}^{(0)} = 0, \quad u_{z,z}^{(0)} - p^{(0)} = 0, \quad u_z^{(0)} - h^{(0)} = 0. \tag{7}$$

It is straightforward to show that these equations have a simple solution corresponding to the long-wave limit in I, namely $u_z^{(0)} = h^{(0)}z$, $p^{(0)} = h^{(0)}(x, t)$, $V_x^{(0)} = -h_{,x}^{(0)}(x, t)$ and $V_z^{(0)} = 0$, where

$$h_{,t}^{(0)} = h_{,xx}^{(0)}. \tag{8}$$

Small disturbances to the film decay like solutions of the diffusion equation, with horizontal flows driven by horizontal pressure gradients; vertical flows do not arise at this order. Because the layer is very thin, diffusion of the deformation field across the layer is very rapid, so there is a uniform vertical strain throughout the layer, proportional to the local pressure. The horizontal deformation $u_x^{(0)} = p_{,x}^{(0)}(z^2/2 - 2z)$ does not have a leading-order influence on the evolution of the layer.

Proceeding to the next order in δ, Eqs. (1)–(4) again give equations identical to those obtained at leading order, except that the superscripts (0) are replaced by (1). Inhomogeneous contributions due to the finite slope of the impermeable membrane arise in three of the four boundary conditions at $z = 1$ (5),

$$V_z^{(1)} = h_{,x}^{(0)} V_x^{(0)} \qquad u_{x,z}^{(1)} + u_{z,x}^{(1)} = -2h_{,x}^{(0)} u_{z,z}^{(0)}$$
$$u_{z,z}^{(1)} - p^{(1)} = 0 \qquad u_z^{(1)} - h^{(1)} = -u_{z,z}^{(0)}. \tag{9}$$

Again, $p^{(1)}$, $u_{z,z}^{(1)}$, and $V_x^{(1)}$ are independent of z. Integrating, we find that $u_z^{(1)}(z = 1) = p^{(1)}z$ and that $h^{(1)} = h^{(0)} + p^{(1)}$. From the continuity equation we again see that $V_{z,z}^{(1)}$ is independent of z, but that now the kinematic boundary condition at $z = 1$ generates a downwards vertical velocity, $V_z^{(1)} = -(h_{,x}^{(0)})^2 z$, and the continuity condition then implies that

$$h_{,t}^{(1)} - h_{,xx}^{(1)} = (h_{,x}^{(0)})^2. \tag{10}$$

The corresponding horizontal displacement field is

$$u_x^{(1)} = -p_{,x}^{(1)}\left(2z - \frac{z^2}{2}\right) - (h^{(0)2})_{,x} z. \tag{11}$$

Notice the final term in (11) is a nonlinear contribution from the tangential stress condition (9*b*).

Results

We now consider the evolution of a typical disturbance to the poroelastic layer. Let us suppose that the film height is deformed such that $h(0, 0) = 1 \pm \delta$. We take advantage of a similarity solution of (8) consistent with this initial condition: $h(x, t) = 1 + \delta h^{(0)}$ where $h^{(0)} = \pm(t + 1)^{-1/2} \exp[-x^2/(4(t + 1))]$ (solid curves in Figs. 1 and 2). The appropriate higher-order contribution (a solution of (10) satisfying $h^{(1)}(0, 0) = 0$) is

$$h^{(1)} = \frac{1}{2}(\pm h^{(0)} - (h^{(0)})^2), \quad p^{(1)} = \frac{1}{2}((\pm 1 - 2)h^{(0)} - (h^{(0)})^2). \tag{12}$$

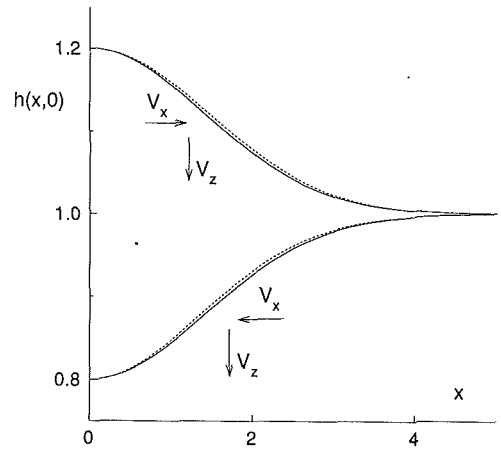


Fig. 1 Free surface profiles at $t = 1$. Solid curves show leading-order film displacements $h = 1 + \delta h^{(0)}$, dashed curves include nonlinear contribution $h = 1 + \delta h^{(0)} + \delta^2 h^{(1)}$, with $h^{(1)}$ given by (12) and $\delta = 0.2$. The solutions are symmetrical about $x = 0$. Upward ($h > 1$) and downward ($h < 1$) displacements both generate downward vertical velocities.

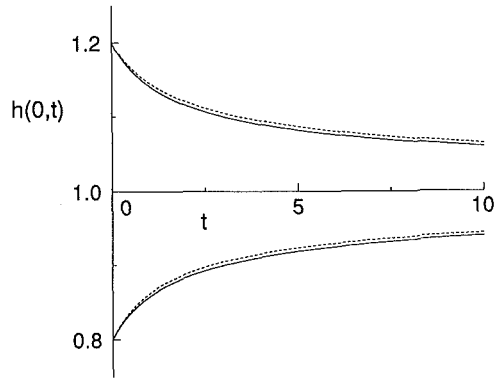


Fig. 2 Time evolution of extrema of the free surface. Solid curves show leading-order (linear) film displacements $h = 1 + \delta h^{(0)}$. Dashed curves include $0(\delta^2)$ contribution, showing how nonlinear effects increase the decay times of elevations of the layer but reduce decay times of depressions.

A localized elevation of the layer evolves as follows: the outward horizontal flow is deflected downward by the sloping free surface towards the impermeable lower plane, resulting in a slight upward displacement of the free surface ($h > 1$ in Fig. 1, dashed curve), a corresponding reduction in the horizontal velocity, and a downwards vertical velocity. The inward flow due to a localized depression is also deflected downwards, again resulting in an upward displacement of the free surface ($h < 1$ in Fig. 1, dashed curve), reduced horizontal velocities, and a downwards velocity. The rate of decay of a disturbance is therefore reduced if the film is displaced upwards, but increased if it is displaced downwards ($h(0, t) = 1 \pm \delta(1 + t)^{-1/2} + \delta^2((1 + t)^{-1/2} - (1 + t)^{-1})/2 + O(\delta^3)$), as shown in Fig. 2.

The finite-slope effect described here may arise for finite deformations of all wavelengths, although it was demonstrated here only in the long-wave limit. If deflections are sufficiently large, however, the effect will compete with other nonlinear elastic effects, so further studies are required to determine its significance.

Acknowledgments

This work was supported by NIH grants K04-HL01818, R01-HL41126, NSF grant CTS-9013083, the Whitaker Foundation and the American Lung Association.

Downloaded 03 May 2010 to 171.66.16.20. Redistribution subject to ASME license or copyright; see http://www.asme.org/terms/Terms_Use.cfm

References

Biot, M. A., 1941, "General Theory of Three-Dimensional Consolidation," *J. Appl. Phys.*, Vol. 12, pp. 155–164.

Biot, M. A., 1972, "Theory of Finite Deformations of Porous Solids," *Indiana Univ. Math J.*, Vol. 21, pp. 597–620.

Grimshaw, P. E., Nussbaum, J. H., Grodzinsky, A. J., and Yarmush, M. L., 1990, "Kinetics of Electrically and Chemically Induced Swelling in Polyelectrolyte Gels," *J. Chem. Phys.*, Vol. 93, pp. 4462–4472.

Holmes, M. H., Lai, W. M., and Mow, V. C., 1985, "Singular Perturbation Analysis for Stress Relaxation Test of Articular Cartilage," *J. Biomech Engng.*, Vol. 107, pp. 206–218.

Kwan, S. C., Lai, W. M., and Mow. V. C., 1990, "A Finite Deformation Theory for Cartilage and Other Soft Hydrated Connective Tissues—I. Equilibrium Results," *J. Biomech*, Vol. 23, pp. 145–155.

Parker, K. H., Mehta, R. V., and Caro, C. G.,. 1987, "Steady Flow in Porous, Elastically Deformable Materials," ASME JOURNAL OF APPLIED MECHANICS, Vol. 54, pp. 794–799.

Sachs, J. R., Glucksberg, M. R., Jensen, O. E., and Grotberg, J. B., 1994, "Linear Flow and Deformation in a Poroelastic Disk With a Free Surface," ASME JOURNAL OF APPLIED MECHANICS, Vol. 61, pp. 726–728.

Stress Intensity Factors of Two-Dimensional and Three-Dimensional Cracks Next to a Thermally Mismatched Inclusion

W. H. Müller,[27,28,29] D. O. Harris,[29,30] and D. D. Dedhia[28,29]

Stress intensity factors for two-dimensional matrix cracks next to cylindrical inclusions have been subject of various publications. The general case in which the matrix and the inclusion have different elastic and thermal constants can only be treated numerically, e.g., in two dimensions by using the method of integral equations (cf., Erdogan et al., 1974; Müller and Schmauder, 1993). However, if the elastic constants of both constituents are equal, and if the geometry is not too complex, it is possible to derive analytical solutions for the stress intensity factors, which can conveniently be used to assess the fracture-mechanical performance of composites subjected to severe thermal stress.

The purpose of this Brief Note is, first, to outline how these analytical formulae for two-dimensional cracks can be obtained from point-force solutions using the principle of linear superposition. Second, the same technique will be used to study the axisymmetric case of a penny-shaped crack centered above the pole of a spherical inclusion. Third, the root-mean-square-averaged stress intensity factors of an elliptical crack at the same position as in the previous case will be computed numerically using influence functions. The study concludes with the numerical computation of penny-shaped and elliptical cracks in front of a spherical inclusion. In order to show the accuracy of the numerical results they will be compared with an analytical formula which, however, is only valid for small elliptical cracks.

Consider the two-dimensional crack in front or above a thermally mismatched, cylindrical inclusion (Fig. 1). The stress intensity factors resulting from the thermomechanical stresses can be computed using the point force solutions 5.10 and 5.10a in Tada et al. (1985):

$$K_I(\pm l) = \int_{-l}^{+l} \frac{\sigma_{yy}(x)}{\sqrt{\pi l}} \frac{[l^2-x^2]^{1/2}}{l \mp x}\, dx,$$

$$K_{II}(\pm l) = \int_{-l}^{+l} \frac{\sigma_{xy}(x)}{\sqrt{\pi l}} \frac{[l^2-x^2]^{1/2}}{l \mp x}\, dx \tag{1}$$

where $\sigma_{yy}(x)$ and $\sigma_{xy}(x)$ denote the thermal stresses developing in the matrix without the crack of length l. For a crack in front of an inclusion these stresses read (Müller, 1990)

$$\sigma_{yy}(x) = \sigma + \frac{E'\Delta\alpha\Delta T}{2} \frac{R^2}{(x+b)^2}, \quad \sigma_{xy}(x) = 0, \tag{2}$$

and for a crack above an inclusion one may write

$$\sigma_{yy}(x) = \sigma + \frac{E'\Delta\alpha\Delta T}{2} \frac{R^2(x^2-d^2)}{(x^2+d^2)^2},$$

$$\sigma_{xy}(x) = -E'\Delta\alpha\Delta T \frac{dR^2 x}{(x^2+d^2)^2}. \tag{3}$$

In these expressions the following contractions were used:

	plane stress	plane strain
$\Delta\alpha\Delta T$	$(\alpha_2-\alpha_1)(T-T_R)$	$(1+\nu)(\alpha_2-\alpha_1)(T-T_R)$
E'	E	$E/(1-\nu^2)$

(4)

E being Young's modulus, and ν being Poisson's ratio. σ denotes a constant external load, T is the current temperature, T_R is any reference temperature, and α_1 and α_2 are the thermal expansion coefficients of the matrix and the inclusion, respectively.

Thus, by performing the necessary integrations (for details see Müller, 1990), one finally arrives at

$$K_I(\pm l) = \left(\sigma + \frac{E'\Delta\alpha\Delta T R^2}{2(b^2-l^2)^{1/2}(b \pm l)}\right)\sqrt{\pi l}, \quad K_{II}(\pm l) = 0 \tag{5}$$

for the crack in front of an inclusion, and at

$$K_I(\pm l) = \left(\sigma - \frac{E'\Delta\alpha\Delta T R^2 d}{2(d^2+l^2)^{3/2}}\right)\sqrt{\pi l},$$

$$K_{II}(\pm l) = \mp \frac{E'\Delta\alpha\Delta T R^2 l}{2(d^2+l^2)^{3/2}}\sqrt{\pi l} \tag{6}$$

for a crack above an inclusion.

Next, consider the penny-shaped crack above the pole of a thermally mismatched, spherical inclusion (Fig. 2). The stress intensity factors resulting from thermomechanical stresses can be computed using the point force solutions for a penny-shaped crack 24.5 and 24.24 in Tada et al. (1985):

$$K_I = \frac{2}{\sqrt{\pi l}} \int_0^l \frac{\sigma_{zz}\rho d\rho}{\sqrt{l^2-\rho^2}}, \quad K_{II} = \frac{2}{\sqrt{\pi l} l} \int_0^l \frac{\sigma_{\rho z}\rho^2 d\rho}{\sqrt{l^2-\rho^2}} \tag{7}$$

in which $\sigma_{\rho z}$ and σ_{zz} denote the thermal stresses developing in the matrix without the crack

$$\sigma_{\rho z} = E'\Delta\alpha\Delta T \frac{dR^3\rho}{(\rho^2+d^2)^{5/2}},$$

$$\sigma_{zz} = \sigma + \frac{E'\Delta\alpha\Delta T}{3} \frac{R^3(\rho^2-2d^2)}{(\rho^2+d^2)^{5/2}}, \quad d > R \tag{8}$$

in which $E' = E/(1-\nu)$. Performing the necessary integrations results in

[27]Currently address: the Hochschuldozent für Strukturmechanik at the Universität Paderborn, FB 10, Pohlweg 47-49, 33098 Paderborn, Germany.

[28]Failure Analysis Associates, Inc., 149 Commonwealth Drive, Menlo Park, CA 94025.

[29]Senior Engineer. Assoc. Mem. ASME.

[30]Managing Engineer. Mem. ASME.

Contributed by the Applied Mechanics Division of THE AMERICAN SOCIETY OF MECHANICAL ENGINEERS for publication in the ASME JOURNAL OF APPLIED MECHANICS. Manuscript received by the ASME Applied Mechanics Division, Sept. 28, 1992; final revision, Aug. 9, 1993.

Downloaded 03 May 2010 to 171.66.16.20. Redistribution subject to ASME license or copyright; see http://www.asme.org/terms/Terms_Use.cfm

References

Biot, M. A., 1941, "General Theory of Three-Dimensional Consolidation," *J. Appl. Phys.*, Vol. 12, pp. 155–164.

Biot, M. A., 1972, "Theory of Finite Deformations of Porous Solids," *Indiana Univ. Math J.*, Vol. 21, pp. 597–620.

Grimshaw, P. E., Nussbaum, J. H., Grodzinsky, A. J., and Yarmush, M. L., 1990, "Kinetics of Electrically and Chemically Induced Swelling in Polyelectrolyte Gels," *J. Chem. Phys.*, Vol. 93, pp. 4462–4472.

Holmes, M. H., Lai, W. M., and Mow, V. C., 1985, "Singular Perturbation Analysis for Stress Relaxation Test of Articular Cartilage," *J. Biomech Engng.*, Vol. 107, pp. 206–218.

Kwan, S. C., Lai, W. M., and Mow. V. C., 1990, "A Finite Deformation Theory for Cartilage and Other Soft Hydrated Connective Tissues—I. Equilibrium Results," *J. Biomech*, Vol. 23, pp. 145–155.

Parker, K. H., Mehta, R. V., and Caro, C. G.,. 1987, "Steady Flow in Porous, Elastically Deformable Materials," ASME JOURNAL OF APPLIED MECHANICS, Vol. 54, pp. 794–799.

Sachs, J. R., Glucksberg, M. R., Jensen, O. E., and Grotberg, J. B., 1994, "Linear Flow and Deformation in a Poroelastic Disk With a Free Surface," ASME JOURNAL OF APPLIED MECHANICS, Vol. 61, pp. 726–728.

Stress Intensity Factors of Two-Dimensional and Three-Dimensional Cracks Next to a Thermally Mismatched Inclusion

W. H. Müller,[27,28,29] D. O. Harris,[29,30] and D. D. Dedhia[28,29]

Stress intensity factors for two-dimensional matrix cracks next to cylindrical inclusions have been subject of various publications. The general case in which the matrix and the inclusion have different elastic and thermal constants can only be treated numerically, e.g., in two dimensions by using the method of integral equations (cf., Erdogan et al., 1974; Müller and Schmauder, 1993). However, if the elastic constants of both constituents are equal, and if the geometry is not too complex, it is possible to derive analytical solutions for the stress intensity factors, which can conveniently be used to assess the fracture-mechanical performance of composites subjected to severe thermal stress.

The purpose of this Brief Note is, first, to outline how these analytical formulae for two-dimensional cracks can be obtained from point-force solutions using the principle of linear superposition. Second, the same technique will be used to study the axisymmetric case of a penny-shaped crack centered above the pole of a spherical inclusion. Third, the root-mean-square-averaged stress intensity factors of an elliptical crack at the same position as in the previous case will be computed numerically using influence functions. The study concludes with the numerical computation of penny-shaped and elliptical cracks in front of a spherical inclusion. In order to show the accuracy of the numerical results they will be compared with an analytical formula which, however, is only valid for small elliptical cracks.

Consider the two-dimensional crack in front or above a thermally mismatched, cylindrical inclusion (Fig. 1). The stress intensity factors resulting from the thermomechanical stresses can be computed using the point force solutions 5.10 and 5.10a in Tada et al. (1985):

$$K_I(\pm l) = \int_{-l}^{+l} \frac{\sigma_{yy}(x)}{\sqrt{\pi l}} \frac{[l^2-x^2]^{1/2}}{l \mp x}\, dx,$$

$$K_{II}(\pm l) = \int_{-l}^{+l} \frac{\sigma_{xy}(x)}{\sqrt{\pi l}} \frac{[l^2-x^2]^{1/2}}{l \mp x}\, dx \tag{1}$$

where $\sigma_{yy}(x)$ and $\sigma_{xy}(x)$ denote the thermal stresses developing in the matrix without the crack of length l. For a crack in front of an inclusion these stresses read (Müller, 1990)

$$\sigma_{yy}(x) = \sigma + \frac{E'\Delta\alpha\Delta T}{2} \frac{R^2}{(x+b)^2}, \quad \sigma_{xy}(x) = 0, \tag{2}$$

and for a crack above an inclusion one may write

$$\sigma_{yy}(x) = \sigma + \frac{E'\Delta\alpha\Delta T}{2} \frac{R^2(x^2-d^2)}{(x^2+d^2)^2},$$

$$\sigma_{xy}(x) = -E'\Delta\alpha\Delta T \frac{dR^2 x}{(x^2+d^2)^2}. \tag{3}$$

In these expressions the following contractions were used:

	plane stress	plane strain
$\Delta\alpha\Delta T$	$(\alpha_2-\alpha_1)(T-T_R)$	$(1+\nu)(\alpha_2-\alpha_1)(T-T_R)$
E'	E	$E/(1-\nu^2)$

(4)

E being Young's modulus, and ν being Poisson's ratio. σ denotes a constant external load, T is the current temperature, T_R is any reference temperature, and α_1 and α_2 are the thermal expansion coefficients of the matrix and the inclusion, respectively.

Thus, by performing the necessary integrations (for details see Müller, 1990), one finally arrives at

$$K_I(\pm l) = \left(\sigma + \frac{E'\Delta\alpha\Delta T R^2}{2(b^2-l^2)^{1/2}(b \pm l)}\right)\sqrt{\pi l}, \quad K_{II}(\pm l) = 0 \tag{5}$$

for the crack in front of an inclusion, and at

$$K_I(\pm l) = \left(\sigma - \frac{E'\Delta\alpha\Delta T R^2 d}{2(d^2+l^2)^{3/2}}\right)\sqrt{\pi l},$$

$$K_{II}(\pm l) = \mp \frac{E'\Delta\alpha\Delta T R^2 l}{2(d^2+l^2)^{3/2}}\sqrt{\pi l} \tag{6}$$

for a crack above an inclusion.

Next, consider the penny-shaped crack above the pole of a thermally mismatched, spherical inclusion (Fig. 2). The stress intensity factors resulting from thermomechanical stresses can be computed using the point force solutions for a penny-shaped crack 24.5 and 24.24 in Tada et al. (1985):

$$K_I = \frac{2}{\sqrt{\pi l}} \int_0^l \frac{\sigma_{zz}\rho d\rho}{\sqrt{l^2-\rho^2}}, \quad K_{II} = \frac{2}{\sqrt{\pi l} l} \int_0^l \frac{\sigma_{\rho z}\rho^2 d\rho}{\sqrt{l^2-\rho^2}} \tag{7}$$

in which $\sigma_{\rho z}$ and σ_{zz} denote the thermal stresses developing in the matrix without the crack

$$\sigma_{\rho z} = E'\Delta\alpha\Delta T \frac{dR^3\rho}{(\rho^2+d^2)^{5/2}},$$

$$\sigma_{zz} = \sigma + \frac{E'\Delta\alpha\Delta T}{3} \frac{R^3(\rho^2-2d^2)}{(\rho^2+d^2)^{5/2}}, \quad d > R \tag{8}$$

in which $E' = E/(1-\nu)$. Performing the necessary integrations results in

[27]Currently address: the Hochschuldozent für Strukturmechanik at the Universität Paderborn, FB 10, Pohlweg 47-49, 33098 Paderborn, Germany.

[28]Failure Analysis Associates, Inc., 149 Commonwealth Drive, Menlo Park, CA 94025.

[29]Senior Engineer. Assoc. Mem. ASME.

[30]Managing Engineer. Mem. ASME.

Contributed by the Applied Mechanics Division of THE AMERICAN SOCIETY OF MECHANICAL ENGINEERS for publication in the ASME JOURNAL OF APPLIED MECHANICS. Manuscript received by the ASME Applied Mechanics Division, Sept. 28, 1992; final revision, Aug. 9, 1993.

Copyright © 1994 by ASME
Downloaded 03 May 2010 to 171.66.16.20. Redistribution subject to ASME license or copyright; see http://www.asme.org/terms/Terms_Use.cfm

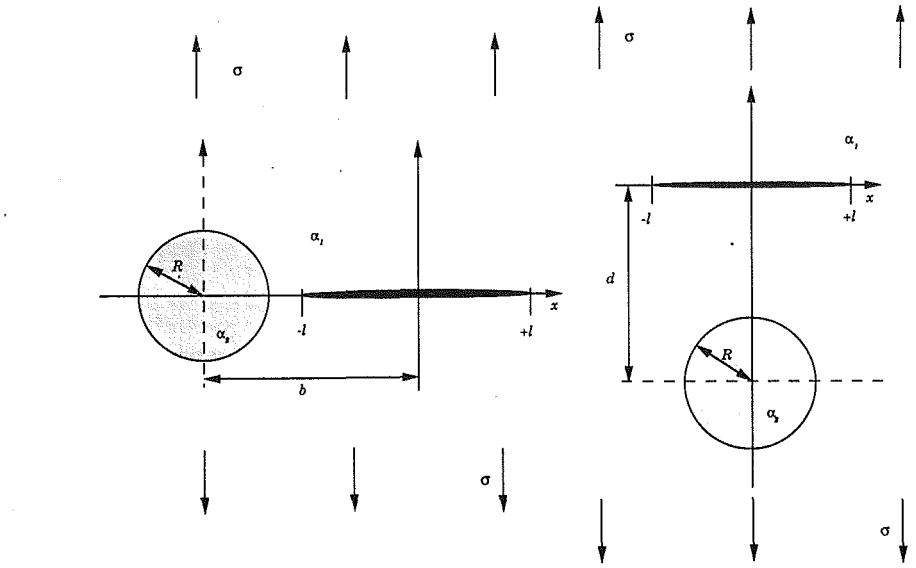


Fig. 1 Two-dimensional crack configurations

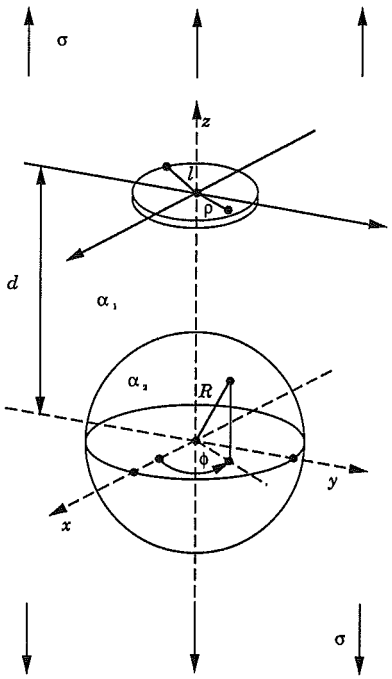


Fig. 2 Penny-shaped crack above spherical inclusion

$$K_I = \left(\sigma - \frac{2E'\Delta\alpha\Delta T R^3 d}{3(d^2+l^2)^2}\right) 2\sqrt{\frac{l}{\pi}},$$

$$K_{II} = \frac{4E'\Delta\alpha\Delta T R^3 l}{3(d^2+l^2)^2}\sqrt{\frac{l}{\pi}}. \tag{9}$$

Note that the formulae shown in Eq. (9) are very similar to their two-dimensional counterparts in Eq. (6). Figure 3 shows Mode I stress intensity factors based on the last equation, plotted as a function of crack size for various distances from the inclusion. Obviously, thermal mismatch is only important in the immediate neighborhood of the particle.

Next, consider the three-dimensional elliptical crack above a spherical inclusion shown in Fig. 4. For this crack geometry it is customary (cf., NASCRAC™-Theory Manual, 1990) to consider the so-called root-mean-square-averaged stress intensity factors which are defined as follows:[31]

$$\overline{K}_{Ii} = \sqrt{\frac{1}{\Delta A_i}\int_0^{\pi/2} K_I^2(\theta)\, d[\Delta A_i(\theta)]}, \quad i \in \{a, b\} \tag{10}$$

where $K_I(\theta)$ denotes the stress intensity factor at an angular position, θ, of the crack flank, and ΔA_a is the incremental area when the semi-minor axis, a, is increased by Δa while keeping the semi-major axis, b, constant.[32] Following the work of Besuner (1977), Eq. (10) can be integrated analytically for a crack subjected to a constant stress field σ normal to its surface ($b > a$):

$$\overline{K}_{Ia} = 2\sigma\sqrt{a}\left\{\frac{1}{3E(k)}\left(2 + \frac{a^2}{b^2-a^2}\left[1 - \frac{K(k)}{E(k)}\right]\right)\right\}^{1/2},$$

$$\overline{K}_{Ib} = 2\sigma\sqrt{a}\left\{\frac{1}{3E(k)}\left(1 - \frac{a^2}{b^2-a^2}\left[1 - \frac{K(k)}{E(k)}\right]\right)\right\}^{1/2}, \quad k^2 = 1 - \frac{a^2}{b^2} \tag{11}$$

where $E(k)$ and $K(k)$ are the complete elliptic integrals of the first and second kind, respectively. However, for a spatially varying stress field, such as in the case of the thermally mismatched inclusion, the corresponding integration can no longer be performed analytically and numerical integration schemes (based on influence functions) of the NASCRAC Computer Code were used with the stress σ_{zz} from Eq. (8) as input parameter.

Typical results for the root-mean-square stress intensity factors of both axis, $\overline{K}_{Ia}$ and $\overline{K}_{Ib}$, normalized by $-E'\Delta\alpha\Delta T2\sqrt{a/\pi}$, are shown in Fig. 5 for two elliptical cracks with aspect ratios $b/a = 2$ and 4, respectively. The SIF for the minor axis, $\overline{K}_{Ia}$, is clearly higher than the corresponding SIF for the major axis, $\overline{K}_{Ib}$, indicating that an elliptical crack tends to become a crack of circular shape. Note that in the limit $a/R \to 0$, $\overline{K}_{Ia,b}$ can be calculated analytically from Eq. (11) using the expres-

[31]Note that, depending upon the stress field, a maximum of four different SIFs can result, i.e., two for the minor and two for the major axes of the elliptical crack.

[32]Analogous definition holds for ΔA_b.

Downloaded 03 May 2010 to 171.66.16.20. Redistribution subject to ASME license or copyright; see http://www.asme.org/terms/Terms_Use.cfm

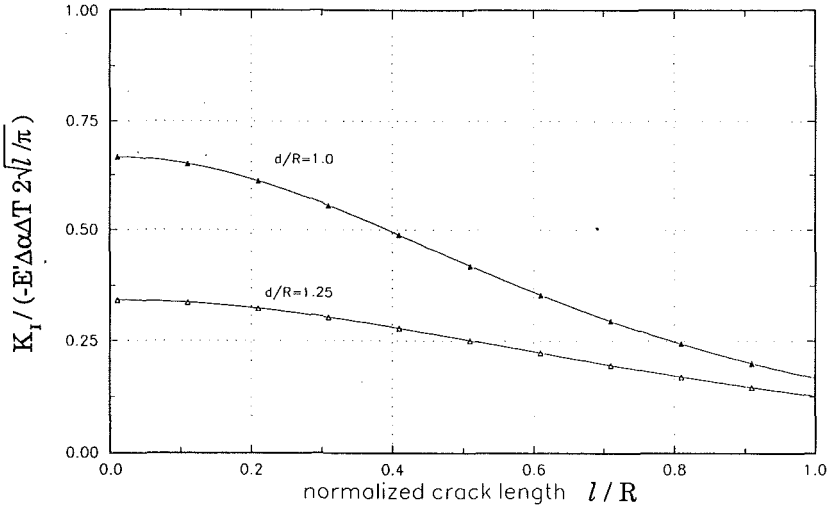


Fig. 3 Stress intensity factors of a penny-shaped crack above an inclusion

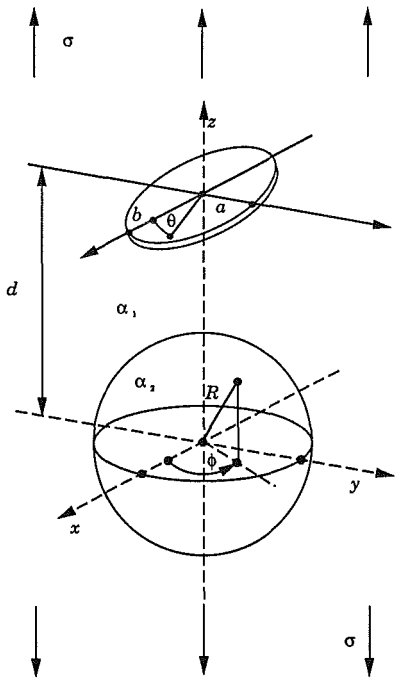


Fig. 4 Elliptical crack above spherical inclusion

sion for $\sigma_{zz}(\rho = 0)$ of Eq. (8). The numbers resulting for specific choices of b/a and d/R agree perfectly well with the corresponding data of Fig. 5, indicating high accuracy of the numerical procedures involved. Another check of the accuracy is obtained by looking at the case of a penny-shaped crack, i.e., an aspect ratio of 1. The triangles of Fig. 3 are the result of NASCRAC computations for this specific choice. They obviously agree with the corresponding data from the analytic formula (solid lines).

Finally, consider the elliptical crack in front of a spherical inclusion shown in Fig. 6. Analogously to the previous case, root-mean-square stress intensity factors were computed using influence function implemented in the NASCRAC Code, based on the following expression for the thermal stress:

$$\sigma_{zz} = \frac{E'\Delta\alpha\Delta T}{3}\frac{R^3}{[(d+x)^2+y^2]^{3/2}}, \quad d>R \tag{12}$$

d being the distance between the centers of the inclusion and the crack.

Typical results for positions 1, 2, and 3 on the crack flanks (cf., Fig. 6) are shown in Fig. 7 for ratios $b/a = 2$, 0.5, and 1 (i.e., a penny-shaped crack, $a = b = l$). The stress intensity factor for the axis closest to the inclusion (position 2) is always greater than the stress intensity factors at positions 1 and 3, and increases significantly for increasing crack length. The stress intensity factor at the far-away end of the crack from the inclusion (position 1), however, decreases with increasing crack length. Finally, increasing the distance d of the crack from the inclusion results in a general decrease of stress intensity factors. All these features are a consequence of the rapid decrease of the stress field around an inclusion (cp., Eq. (12)). As before, the stress intensity factors can be computed analytically from Eq. (11)[33] for small cracks, i.e., in the limit $a/R \rightarrow 0$, showing perfect agreement with the numerically obtained data.

References

Besuner, P., 1977, "The Influence Function Method for Fracture Mechanics and Residual Life Analysis of Cracked Components under Complex Stress Fields," *Nuclear Engineering and Design*, Vol. 43, No. 1, pp. 115-154.

Erdogan, F., Gupta, G. D., and Ratwani, M., 1974, "Interaction Between a Circular Inclusion and an Arbitrarily Oriented Crack," ASME JOURNAL OF APPLIED MECHANICS, Vol. 41, pp. 1007-1013.

NASCRAC, 1990, NASA CRack Analysis Code, Version 2.2, Theory Manual, Failure Analysis Associates, Menlo Park, CA.

Müller, W. H., 1990, "An Analytical Approach for the Calculation of Stress Intensity Factors in Transformation Toughened Ceramics," *Cont. Mech. Thermodyn.*, Vol. 2, pp. 279-299.

Müller, W. H., and Schmauder, S., 1993, "Stress-Intensity Factors of r-Cracks in Fiber-Reinforced Composites under Thermal and Mechanical Loading," *International Journal of Fracture*, Vol. 59, pp. 307-343.

Tada, H., Paris, P. C., and Irwin, G. R., 1985, "The Stress Analysis of Crack Handbook," St. Louis, MO.

[33]For penny-shaped cracks, i.e., $a = b = l$, Eq. (11) reduces to $K_I = \overline{K}_{Ia} = \overline{K}_{Ib} = 2\,\sigma\sqrt{\frac{l}{\pi}}$.

Downloaded 03 May 2010 to 171.66.16.20. Redistribution subject to ASME license or copyright; see http://www.asme.org/terms/Terms_Use.cfm

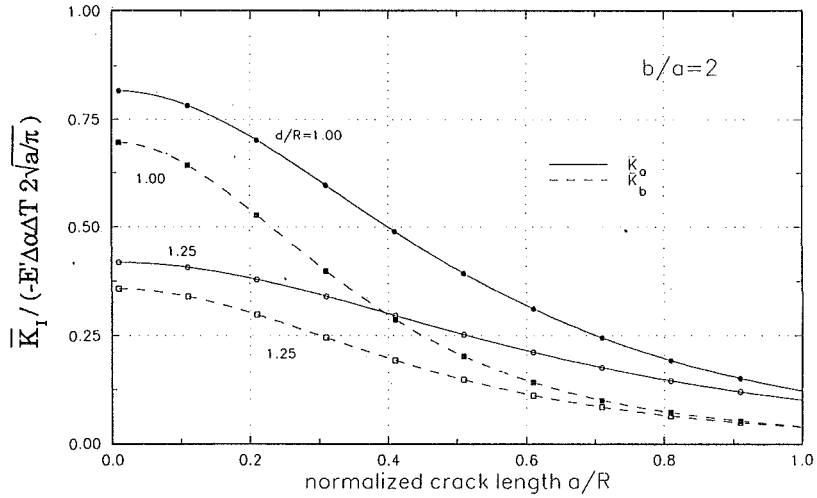


Fig. 5(*a*) Stress intensity factors of an elliptical crack above an inclusion (part 1)

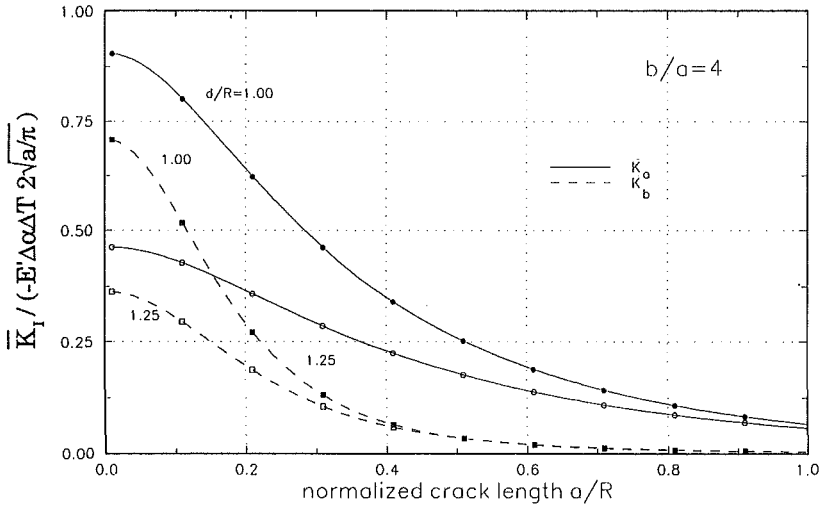


Fig. 5(*b*) Stress intensity factors of an elliptical crack above an inclusion (part 2)

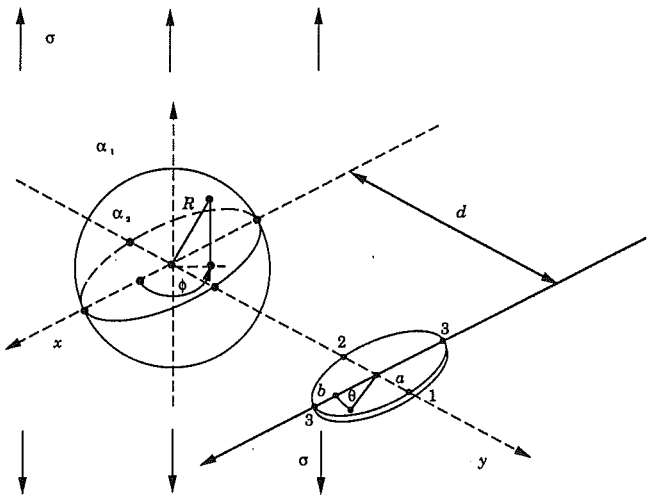


Fig. 6 Elliptical crack in front of a spherical inclusion

Downloaded 03 May 2010 to 171.66.16.20. Redistribution subject to ASME license or copyright; see http://www.asme.org/terms/Terms_Use.cfm

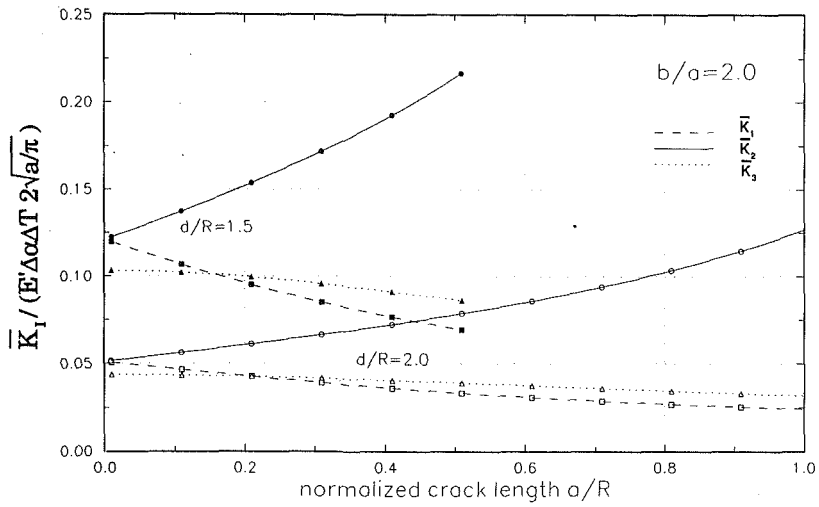


Fig. 7(*a*) Stress intensity factors of elliptical and penny-shaped cracks in front of an inclusion (part 1)

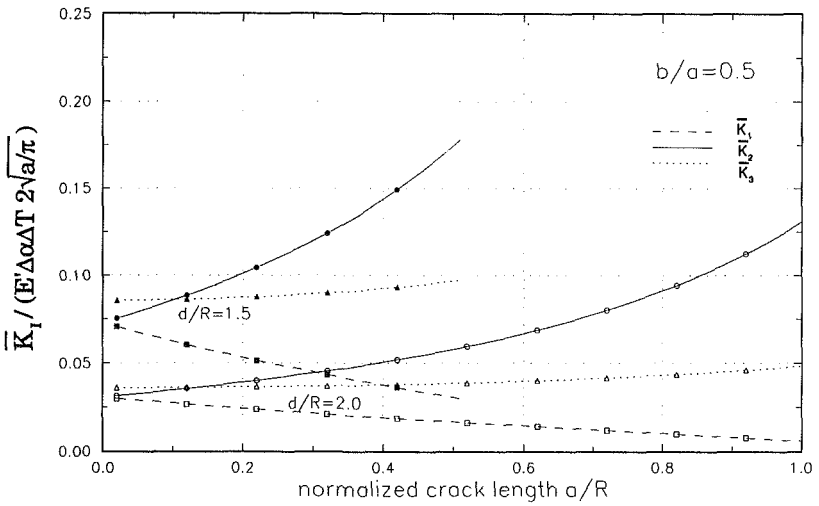


Fig. 7(*b*) Stress intensity factors of elliptical and penny-shaped cracks in front of an inclusion (part 2)

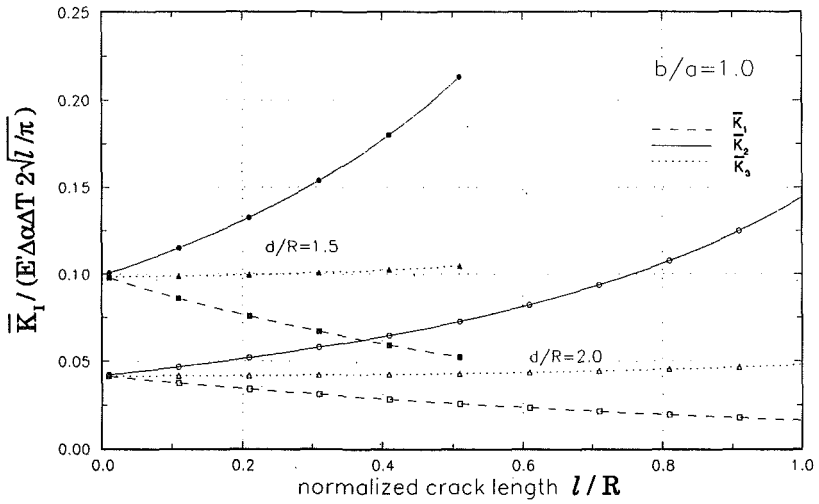


Fig. 7(*c*) Stress intensity factors of elliptical and penny-shaped cracks in front of an inclusion (part 3)

Downloaded 03 May 2010 to 171.66.16.20. Redistribution subject to ASME license or copyright; see http://www.asme.org/terms/Terms_Use.cfm

Coupled Transient Thermoelastic Contact Problem in an Edge-Cracked Plate

Cha'o-Kuang Chen[34,36] and Bor-Lih Kuo[35,36]

Introduction

For a cracked strip subjected to thermal loading, two possible conditions may occur: the crack either opens wider or progressively closes. When the surface of the strip is subjected to the sudden cooling, it could result in very high tensile thermal stresses near the surface which tend to open the crack wider. Several studies have solved the crack opening problems. Nied (1983) analyzed the problem of thermal shock fracture in an edge-cracked plate by the concept of superposition. Chen and Weng (1991) obtained coupled transient thermoelastic response in an edge-cracked plate by the finite element/Laplace transform method. When the surface of the strip is subjected to heating, the surface experiences compressive thermal stresses which cause the opposing faces of the crack to come into contact. Nied (1987) analyzed this kind of problem for an infinite edge-cracked strip by the method of superposition and a singular integral formulation. In the previous studies, both the effects of the inertia term and the thermoelastic coupling term are neglected. However, the effect due to these terms may be significant and shall be taken into consideration in some actual applications. Therefore, a general coupled thermoelastic theory is adopted in this paper to deal with this thermal crack contact problem. In the present study, the edge crack problem in an infinite plate is the same as described by Nied (1987). The elastic strip of thickness L, at an initial temperature T_0, is assumed to be insulated along the surface $y = 0$. The upper surface, $y = L$, contains an edge crack of length a, with the crack tip located at $y = b$. At time $t = 0$ the surface $y = L$ is suddenly subjected to Newtonian convective heating with the heat-transfer coefficient given by h and the ambient temperature maintained at T_a. It is assumed that the existence of the crack does not alter the temperature distribution, the problem can be separated into the following two parts and solved by the principle of superposition. First, the temperature and stress distributions in the imaginary body without a crack are calculated by the finite element/implicit time integration method. Secondly, the opposite sense of the stress distributions along the crack surface, which were obtained previously, are treated as the traction boundary conditions, and the contact length and stress intensity factor of the real cracked body are obtained by the modified elimination finite element scheme.

Formulation of the Problem

Part 1. The Thermal Stress Distribution in the Uncracked Strip. The basic equations of a classical coupled thermoelasticity theory are summarized herein.

Balance Equations.

(a) Mass conservation

$$\frac{\rho_0}{\rho} = 1 + u_{k,k}. \tag{1}$$

(b) Momentum

$$\sigma_{ij,j} + \rho b_i = \rho \ddot{u}_i \tag{2}$$

$$\sigma_{ij} = \sigma_{ji}.$$

(c) Energy (heat conduction)

$$\rho T \dot{\eta} = -q_{k,k} + Q \tag{3}$$

where ρ_0 is the mass density in reference configuration,
ρ is the mass density in current configuration,
u_i is the displacement vector,
σ_{ij} is the stress tensor,
b_i is the body force vector,
T is the absolute temperature,
η is the entropy density,
q_i is the heat flux vector, and
Q is the heat source.

A superposed dot ($\dot{}$) is used to denote material time differentiation and a comma ($,j$) to denote partial time differentiation with respect to coordinate x_j ($j = 1, 2, 3$).

Generalized Constitutive Equations.

$$\sigma_{ij} = C_{ijkl}\epsilon_{kl} - \beta_{ij} T_m \theta$$

$$q_i = -K_{ij} T_m \theta_{,j}$$

$$\eta = \eta_0 + C_e \theta + \frac{1}{\rho} \beta_{ij} \epsilon_{ij} \tag{4}$$

where C_{ijkl} is the tensor of elastic moduli,
β_{ij} is the tensor of thermal moduli,
ϵ_{ij} is the strain tensor,
K_{ij} is the thermal conductivity tensor,
C_e is the specific heat,
T_m is the maximum temperature difference between the applied temperature on the plate and T_0, and
θ is the dimensionless temperature, $\theta = (T - T_0)/T_m$.

Substituting Eq. (4) into Eq. (2) and Eq. (3), we have the resulting field equations in terms of displacements and temperature as follows:

$$\rho \ddot{u}_i + (\beta_{ij} T_m \theta - C_{ijkl} u_{k,l})_{,j} = \rho b_i \tag{5}$$

$$\rho C_e \dot{\theta} + \beta_{ij} T \dot{u}_{i,j}/T_m - (K_{ij}\theta_{,j})_{,i} = Q/T_m \tag{6}$$

where $\beta_{ij} T \dot{u}_{i,j}/T_m$ is called the thermoelastic coupling term. The nonlinear energy balance Eq. (6) can be linearized to the following form if the reference temperature T_0 is chosen such that $(T - T_0)/T_0 \ll 1$. So Eq. (6) becomes

$$\rho C_e \dot{\theta} + \beta_{ij} T_0 \dot{u}_{i,j}/T_m - (K_{ij}\theta_{,j})_{,i} = Q/T_m. \tag{7}$$

In the finite element method, the variation within any element is described in terms of the nodal values by means of two sets of shape functions of the displacement and temperature field. We solved this time-dependent problem by implicit one-step time integration method. And we also obtained the transient thermal stress distribution by the Gaussian integration method.

Part 2. The Contact Problem in an Isothermal Cracked Strip. When the surface of an elastic strip with an edge crack is subjected to heating, it may induce very high compressive thermal stress near the strip surface, which forces the crack surface together over a contact length, and a region of tensile stress near the tip of crack, which tends to open the crack as shown in Fig. 1(*a*). The contact forces and area are determined iteratively by eliminating the nodes having tensile normal contact forces and imposing the compatibility conditions along

[34]Professor.
[35]Graduate Student.
[36]Department of Mechanical Engineering, National Cheng Kung University, Tainan, Taiwan, Republic of China.

Contributed by the Applied Mechanics Division of THE AMERICAN SOCIETY OF MECHANICAL ENGINEERS for publication in the ASME JOURNAL OF APPLIED MECHANICS. Manuscript received by the ASME Applied Mechanics Division, Nov. 13, 1992; final revision, Aug. 2, 1993. Associate Technical Editor: S. K. Datta.

Copyright © 1994 by ASME
Downloaded 03 May 2010 to 171.66.16.20. Redistribution subject to ASME license or copyright; see http://www.asme.org/terms/Terms_Use.cfm

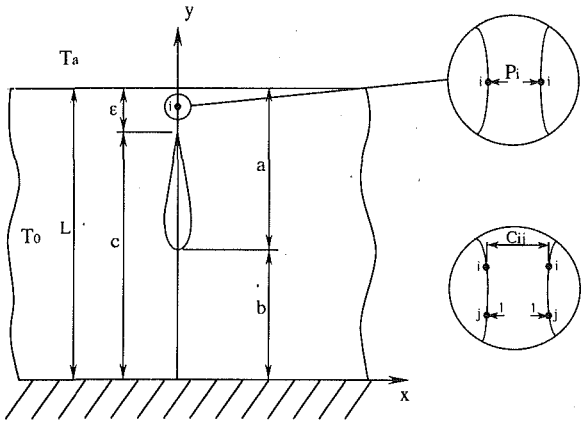


Fig. 1(*a*) Edge-cracked strip heated on surface $y = L$ with crack contact length ϵ; (*b*) the concept of contact double force; (*c*) determination of compliance coefficient C_{ij} for contact pairs

the contact surface. The concept of contact node pairs, relative displacements or penetration, contact double force, and compliance matrix are introduced in a modified elimination finite element scheme. The compliance matrix is defined as a relative displacement induced by two unit contact forces, i.e., unit double force. In Fig. 1(*b*), along the crack contact area, the forces and displacements at node pair i are denoted by p_i and δ_i. The compliance coefficient C_{ij} represents the relative displacement of node pair i produced by a unit contact double force acting at node pair j as shown in Fig. 1(*c*). The problem of an isothermal cracked elastic body may be conducted using the stresses obtained in Part 1. These stresses, with opposite sign, become the crack surface tractions in the boundary value problem and can be solved by the finite element method with a triangular quarter-point isoparametric singular element. The first mode of stress intensity factor can be expressed as follows:

$$K_I = \sqrt{\frac{2}{l_e}} \frac{G}{1+\kappa} [4(v_b - b_d) - (v_c - v_e)] \tag{8}$$

where $\kappa = 3 - 4\nu$ for a plane-strain problem; u_b, u_c, u_d, u_e and v_b, v_c, v_d, v_e are the nodal displacements in the tangential and normal direction with respect to the crack surface, respectively; G is the shear modulus, and l_e is the element length of the triangular element.

Results and Conclusions

In the present paper a powerful numerical analysis, which is called implicit finite element method, is employed to analyze the effect due to the thermoelastic coupling term in the transient response of a cracked strip subjected to heating. The calculated temperature and thermal stress distributions are in good agreement with the values predicted by the analytical method, and a simple numerical procedure is used to analyze the cracked surface contact problem by using the concepts of contact node pairs and contact double forces. The results of the contact length and normal pressure are very close to the analytical solutions, and this scheme needs very few iterations to reach convergence. The normalized stress intensity factors for the uncoupled case are in good agreement with the analytical solutions. Figure 2 compares the stress intensity factor for different values of coupling coefficient and is defined as $\delta = E\alpha_t^2(1+\nu)T_0/\rho C_e(1-\nu)(1-2\nu)$ and crack length ratio is a/L. Increasing the values of the crack length increases the magnitude of the stress intensity factors. Figure 3 shows the stress intensity factors for different values of the Biot number and various δ. Decreasing the values of the Biot number not only reduces the magnitude of the stress intensity factors but also slightly delays the time that the peak of the stress intensity

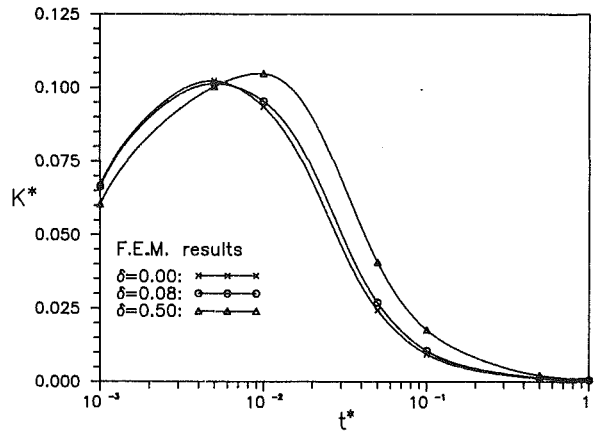


Fig. 2(*a*) Transient stress intensity factor at crack tip for various δ ($a = 0.3L$, $K^* = (1-\nu) \cdot K_I/E\alpha_t \cdot (T_a - T_0)$, $\beta = \infty$, $\delta = 0., 0.08, 0.5$)

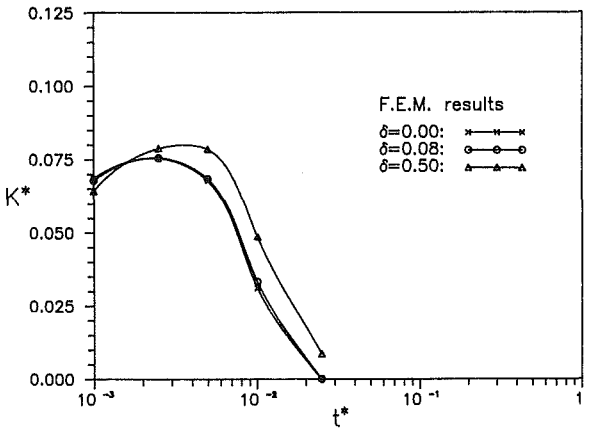


Fig. 2(*b*) Transient stress intensity factor at crack tip for various δ ($a = 0.2L$, $K^* = (1-\nu) \cdot K_I/E\alpha_t \cdot (T_a - T_0)$, $\beta = \infty$, $\delta = 0., 0.08, 0.5$)

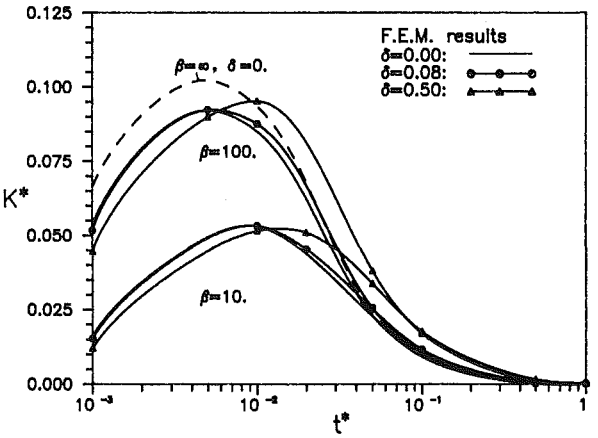


Fig. 3 Transient stress intensity factor at crack tip for $\beta = \infty$, 100, 10 ($a = 0.3L$, $K^* = (1-\nu) \cdot K_I/E\alpha_t \cdot (T_a - T_0)$, $\delta = 0., 0.08, 0.5$)

factor is reached. These results show that as the coupling coefficients are larger, the peaks of the stress intensity factor are higher, and the effect of the thermoelastic coupling term will also result in a small time lag in the stress intensity factor.

References

Nied, H. F., 1983, "Thermal Shock Fracture in an Edge-cracked Plate," *Journal of Thermal Stresses*, Vol. 6, pp. 217–229.

Chen, T. C., and Weng, C. I., 1991, "Coupled Transient Thermoelastic

Downloaded 03 May 2010 to 171.66.16.20. Redistribution subject to ASME license or copyright; see http://www.asme.org/terms/Terms_Use.cfm

Response in an Edge-cracked Plate," *Engineering Fracture Mechanics*, Vol. 39, pp. 915-925.

Nied, H. F., 1987, "Thermal Shock in an Edge-cracked Plate Subjected to Uni-form Surface Heating," *Engineering Fracture Mechanics*, Vol. 26, pp. 239-246.

Jing, H. S., and Liao, M. L., 1990, "An Improved Finite Element Scheme for Elastic Contact Problems with Friction," *Computers & Structures*, Vol. 35, pp. 571-578.

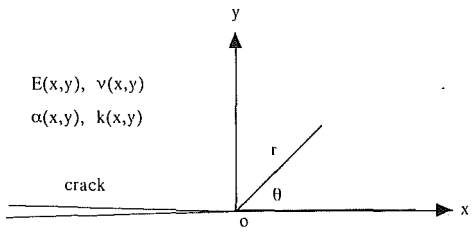


Fig. 1 A crack lying at the weak physics discontinuity line

Crack-Tip Singular Fields in Nonhomogeneous Materials

Zhi-He Jin[37,39] and Naotake Noda[38,39]

Introduction

In recent years, the concept of so-called functionally gradient materials (FGM) has been introduced and applied to the development of structural components. Usually, FGM are expected to be mixtures of metals and ceramics and thus have both thermal and mechanical nonhomogeneities. The advantages of FGM are that the materials can resist high temperature effectively due to the ceramics composition and, at the same time, the thermal stresses in the materials could be relaxed significantly by the appropriate continuous variation of material properties. The interest in FGM research is growing rapidly due to these advantages.

From the viewpoints of applied mechanics and heat conduction, FGM materials are nonhomogeneous solids. Thus the nonhomogeneous continuum theories can offer the basis for evaluating the mechanical and thermal properties of FGM. Erdogan (1985) and Delale and Erdogan (1988) solved some crack problems for nonhomogeneous materials with cracks subjected to mechanical loading. Jin and Noda (1993) and Noda and Jin (1993) studied the crack problems in nonhomogeneous solids under thermal loading. In all those studies, the material properties were specifically selected so that the crack-tip stresses have a square root singularity and the stress intensity factor concept can be well defined. Erdogan (1985) and Delale and Erdogan (1988) proposed that the square root singularity of stresses will not be affected by nonhomogeneities of materials if the material properties are continuous and piecewise differentiable. For the antiplane crack problem, Schovanec and Walton (1988) verified the above conjecture.

In this Note, singular stress and heat flux fields at the tip of the crack in a general nonhomogeneous material are studied, and the plastic stress singularity is also considered. It is found that the crack-tip field singularities and angular distributions are the same as those in the homogeneous material provided that the properties of the material are continuous and piecewise differentiable and some of them do not vanish at the crack tip. In this study, only two-dimensional isotropic problems are considered but the results can be extended to three-dimensional and anisotropic cases.

Temperature Distribution Near a Crack Tip

The heat conduction in nonhomogeneous materials is governed by the following equation:

$$T_{,ii}+\frac{1}{k}k_{,i}T_{,i}=\frac{1}{\kappa}T_{,t} \tag{1}$$

and the heat fluxes are given by

$$q_i=-kT_{,i} \tag{2}$$

where T is the temperature, q_i are the heat fluxes, t is the time, k is the heat conductivity, and κ is the thermal diffusivity. It is assumed that k and κ are continuous and piece-wise differentiable functions of space positions. The boundaries between the differentiable pieces are refereed as "weak physics discontinuity line."

It is first assumed that the crack is at a weak physics discontinuity line as shown in Fig. 1. The polar coordinates (r, θ) are centered at the crack tip. For the singular solutions near the crack tip $(r\to 0)$, the first term in the left-hand side of Eq. (1) dominates over the others if k and κ do not vanish at the tip, hence the equation governing the singular solution becomes

$$T_{,ii}=0. \tag{3}$$

Since k is piece-wise differentiable, the above equation holds both in the upper piece $(y>0)$ and the lower piece $(y<0)$.

The crack faces are supposed to be completely insulated, which corresponds to the following boundary conditions:

$$\frac{\partial T}{\partial \theta}=0 \quad \theta=\pm\pi. \tag{4}$$

Since k is continuous, the continuity conditions require that both the temperature T and its derivatives are continuous across the weak physics discontinuity line ahead of the crack tip. The above asymptotic boundary value problem with the requirement with heat which flows over any finite arc is finite has the following asymptotic solutions near the crack tip:

$$T(r,\theta,t)=R(t)\sqrt{2r}\sin\frac{\theta}{2} \tag{5}$$

and the heat fluxes are

$$q_r=-k^0\frac{\partial T}{\partial r}=-\frac{k^0R(t)}{\sqrt{2r}}\sin\frac{\theta}{2}$$

$$q_\theta=-k^0\frac{\partial T}{r\partial\theta}=-\frac{k^0R(t)}{\sqrt{2r}}\cos\frac{\theta}{2} \tag{6}$$

where k^0 is the value of k at the crack tip and $R(t)$ is a parameter which cannot be determined by the local analysis. The fields (5) and (6) are the same as that in the homogeneous material (Sih, 1965). Here the word "same" means that the singularity and the angular distribution of the fields for nonhomogeneous and homogeneous materials are identical. For a crack terminating at a weak physics discontinuity line as shown in Fig. 2, similar results can be obtained.

[37] Research Associate.

[38] Professor. Corresponding author.

[39] Department of Mechanical Engineering, Shizuoka University, 3-5-1 Johoku, Hamamatsu, Shizouka 432, Japan.

Contributed by the Applied Mechanics Division of THE AMERICAN SOCIETY OF MECHANICAL ENGINEERS for publication in the ASME JOURNAL OF APPLIED MECHANICS. Manuscript received by the ASME Applied Mechanics Division, Jan. 11, 1993; final revision, Aug. 23, 1993. Associate Technical Editor: X. Makenscoff.

Downloaded 03 May 2010 to 171.66.16.20. Redistribution subject to ASME license or copyright; see http://www.asme.org/terms/Terms_Use.cfm

Response in an Edge-cracked Plate," *Engineering Fracture Mechanics*, Vol. 39, pp. 915-925.

Nied, H. F., 1987, "Thermal Shock in an Edge-cracked Plate Subjected to Uni-form Surface Heating," *Engineering Fracture Mechanics*, Vol. 26, pp. 239-246.

Jing, H. S., and Liao, M. L., 1990, "An Improved Finite Element Scheme for Elastic Contact Problems with Friction," *Computers & Structures*, Vol. 35, pp. 571-578.

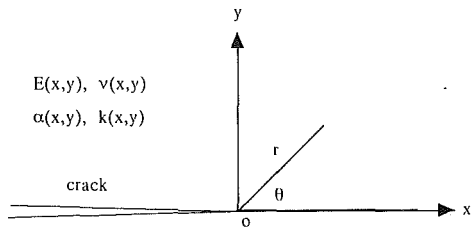


Fig. 1 A crack lying at the weak physics discontinuity line

Crack-Tip Singular Fields in Nonhomogeneous Materials

Zhi-He Jin[37,39] **and Naotake Noda**[38,39]

Introduction

In recent years, the concept of so-called functionally gradient materials (FGM) has been introduced and applied to the development of structural components. Usually, FGM are expected to be mixtures of metals and ceramics and thus have both thermal and mechanical nonhomogeneities. The advantages of FGM are that the materials can resist high temperature effectively due to the ceramics composition and, at the same time, the thermal stresses in the materials could be relaxed significantly by the appropriate continuous variation of material properties. The interest in FGM research is growing rapidly due to these advantages.

From the viewpoints of applied mechanics and heat conduction, FGM materials are nonhomogeneous solids. Thus the nonhomogeneous continuum theories can offer the basis for evaluating the mechanical and thermal properties of FGM. Erdogan (1985) and Delale and Erdogan (1988) solved some crack problems for nonhomogeneous materials with cracks subjected to mechanical loading. Jin and Noda (1993) and Noda and Jin (1993) studied the crack problems in nonhomogeneous solids under thermal loading. In all those studies, the material properties were specifically selected so that the crack-tip stresses have a square root singularity and the stress intensity factor concept can be well defined. Erdogan (1985) and Delale and Erdogan (1988) proposed that the square root singularity of stresses will not be affected by nonhomogeneities of materials if the material properties are continuous and piecewise differentiable. For the antiplane crack problem, Schovanec and Walton (1988) verified the above conjecture.

In this Note, singular stress and heat flux fields at the tip of the crack in a general nonhomogeneous material are studied, and the plastic stress singularity is also considered. It is found that the crack-tip field singularities and angular distributions are the same as those in the homogeneous material provided that the properties of the material are continuous and piecewise differentiable and some of them do not vanish at the crack tip. In this study, only two-dimensional isotropic problems are considered but the results can be extended to three-dimensional and anisotropic cases.

Temperature Distribution Near a Crack Tip

The heat conduction in nonhomogeneous materials is governed by the following equation:

$$T_{,ii}+\frac{1}{k}k_{,i}T_{,i}=\frac{1}{\kappa}T_{,t} \tag{1}$$

and the heat fluxes are given by

$$q_i=-kT_{,i} \tag{2}$$

where T is the temperature, q_i are the heat fluxes, t is the time, k is the heat conductivity, and κ is the thermal diffusivity. It is assumed that k and κ are continuous and piece-wise differentiable functions of space positions. The boundaries between the differentiable pieces are refereed as "weak physics discontinuity line."

It is first assumed that the crack is at a weak physics discontinuity line as shown in Fig. 1. The polar coordinates (r, θ) are centered at the crack tip. For the singular solutions near the crack tip $(r\to 0)$, the first term in the left-hand side of Eq. (1) dominates over the others if k and κ do not vanish at the tip, hence the equation governing the singular solution becomes

$$T_{,ii}=0. \tag{3}$$

Since k is piece-wise differentiable, the above equation holds both in the upper piece $(y>0)$ and the lower piece $(y<0)$.

The crack faces are supposed to be completely insulated, which corresponds to the following boundary conditions:

$$\frac{\partial T}{\partial \theta}=0 \quad \theta=\pm\pi. \tag{4}$$

Since k is continuous, the continuity conditions require that both the temperature T and its derivatives are continuous across the weak physics discontinuity line ahead of the crack tip. The above asymptotic boundary value problem with the requirement with heat which flows over any finite arc is finite has the following asymptotic solutions near the crack tip:

$$T(r,\theta,t)=R(t)\sqrt{2r}\sin\frac{\theta}{2} \tag{5}$$

and the heat fluxes are

$$q_r=-k^0\frac{\partial T}{\partial r}=-\frac{k^0R(t)}{\sqrt{2r}}\sin\frac{\theta}{2}$$

$$q_\theta=-k^0\frac{\partial T}{r\partial\theta}=-\frac{k^0R(t)}{\sqrt{2r}}\cos\frac{\theta}{2} \tag{6}$$

where k^0 is the value of k at the crack tip and $R(t)$ is a parameter which cannot be determined by the local analysis. The fields (5) and (6) are the same as that in the homogeneous material (Sih, 1965). Here the word "same" means that the singularity and the angular distribution of the fields for nonhomogeneous and homogeneous materials are identical. For a crack terminating at a weak physics discontinuity line as shown in Fig. 2, similar results can be obtained.

[37] Research Associate.

[38] Professor. Corresponding author.

[39] Department of Mechanical Engineering, Shizuoka University, 3-5-1 Johoku, Hamamatsu, Shizouka 432, Japan.

Contributed by the Applied Mechanics Division of THE AMERICAN SOCIETY OF MECHANICAL ENGINEERS for publication in the ASME JOURNAL OF APPLIED MECHANICS. Manuscript received by the ASME Applied Mechanics Division, Jan. 11, 1993; final revision, Aug. 23, 1993. Associate Technical Editor: X. Makenscoff.

Copyright © 1994 by ASME
Downloaded 03 May 2010 to 171.66.16.20. Redistribution subject to ASME license or copyright; see http://www.asme.org/terms/Terms_Use.cfm

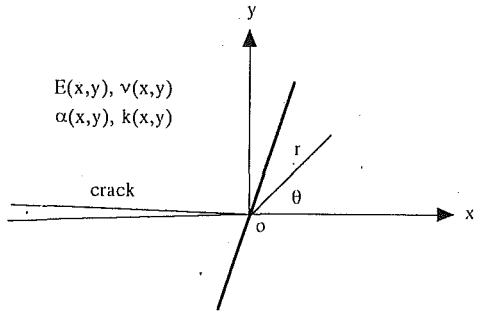


Fig. 2 A crack terminating at the weak physics discontinuity line

Elastic Crack-Tip Singular Fields

The thermoelastic constitutive equations for nonhomogeneous materials are

$$\epsilon_{ij}=\frac{1+\nu}{E}\sigma_{ij}-\frac{\nu}{E}\sigma_{kk}\delta_{ij}+\alpha T\delta_{ij} \tag{7}$$

where E and ν are the Young's modulus and the Poisson's ratio, respectively, and α is the coefficient of linear thermal expansion. It is assumed that E, ν, and α are continuous and piecewise differentiable functions of space positions. Under plane stress conditions, the equation satisfied by the Airy stress function F can be obtained as follows:

$$\nabla^2\left(\frac{1}{E}\nabla^2F\right)-\frac{\partial^2}{\partial y^2}\left(\frac{1+\nu}{E}\right)\frac{\partial^2F}{\partial x^2}-\frac{\partial^2}{\partial x^2}\left(\frac{1+\nu}{E}\right)\frac{\partial^2F}{\partial y^2}+2\frac{\partial^2}{\partial x\partial y}\left(\frac{1+\nu}{E}\right)\frac{\partial^2F}{\partial x\partial y}+\nabla^2(\alpha T)=0. \tag{8}$$

For plane strain, E, ν, and α are substituted by $E/(1-\nu^2)$, $\nu/(1-\nu)$ and $(1+\nu)\alpha$, respectively. In Eq. (8), ∇^2 is the Laplacian operator.

It is assumed that the crack is either located or terminated at a weak physics discontinuity line as shown in Figs. 1 and 2. Since E, ν, and α are piece-wise differentiable, when E does not vanish at the crack tip, the governing equation for the singular solution near the tip in each pieces becomes

$$\nabla^2\nabla^2F=0. \tag{9}$$

The singular solution to the homogeneous material satisfies the same equation. Therefore, it is also the solution to the nonhomogeneous material in every differentiable pieces. The continuities in displacements and traction across the weak physics discontinuity lines are maintained by this solution, so long as the material properties are continuous. Therefore, one can come to the conclusion that the singularity and the angular distribution of the crack-tip stress field for the nonhomogeneous material are identical to those in the homogeneous material.

For the elastic or elastic-plastic thermal crack problems, Aoki et al. (1981) introduced a path-independent integral $\hat{J}$ defined as follows:

$$\hat{J}=-\int_L\sigma_{ij}n_j\frac{\partial u_i}{\partial x}dl+\int\int_S\sigma_{ij}\frac{\partial\epsilon_{ij}}{\partial x}dS \tag{10}$$

where L denotes any curve surrounding the crack tip, S is the area enclosed by L, and n_i is the unit outward normal vector on L. Aoki et al. showed that the path independence of $\hat{J}$ even hold for fully nonhomogeneous materials and the following relation is valid for the materials with homogeneity in the x-direction

$$\hat{J}=\frac{1}{E'}(K_I^2+K_{II}^2) \tag{11}$$

in which E' is E^0 for plane stress and $E^0/[1-(\nu^0)^2]$ for the plane strain, respectively, where E^0 and ν^0 are the limiting values of E and ν at the crack tip, respectively (note that E and ν are continuous). It can be easily shown that even if for fully nonhomogeneous materials, Eq. (11) is still valid.

Plastic Crack-Tip Fields

In the plastic case, the total strains are expressed as

$$\epsilon_{ij}=\frac{1+\nu}{E}\sigma_{ij}-\frac{\nu}{E}\sigma_{kk}\delta_{ij}+\alpha T\delta_{ij}+\epsilon_{ij}^p. \tag{12}$$

For stationary cracks and without unloading, it is approximately justified that the deformation theory can be used to describe the plastic behavior near the crack tip (Rice and Rosengren, 1968; Hutchinson, 1968). In the present study, therefore, the deformation theory is used:

$$\epsilon_{ij}^p=\frac{3\epsilon_e^p}{2\sigma_e}s_{ij},\quad s_{ij}=\sigma_{ij}-\frac{1}{3}\sigma_{kk}\delta_{ij} \tag{13}$$

where ϵ_e^p and σ_e are the effective plastic strain and the effective stress, respectively, defined by

$$\epsilon_e^p=\sqrt{\frac{2}{3}\epsilon_{ij}^p\epsilon_{ij}^p},\quad \sigma_e=\sqrt{\frac{3}{2}s_{ij}s_{ij}}. \tag{14}$$

For the power-law material, we have

$$\epsilon_e^p=A(\sigma_e)^n \tag{15}$$

where the material properties A and n are continuous and piecewise differentiable.

In plane stress, the Airy stress function F satisfies the following compatibility equation:

$$\frac{\partial^2}{\partial y^2}\left\{\frac{1}{E}\left(\frac{\partial^2F}{\partial y^2}-\nu\frac{\partial^2F}{\partial x^2}\right)+A\sigma_e^{n-1}\left(\frac{\partial^2F}{\partial y^2}-\frac{1}{2}\frac{\partial^2F}{\partial x^2}\right)\right\}+\frac{\partial^2}{\partial x^2}\left\{\frac{1}{E}\left(\frac{\partial^2F}{\partial x^2}-\nu\frac{\partial^2F}{\partial y^2}\right)+A\sigma_e^{n-1}\left(\frac{\partial^2F}{\partial x^2}-\frac{1}{2}\frac{\partial^2F}{\partial y^2}\right)\right\}+\frac{\partial^2}{\partial x\partial y}\left\{\frac{1+\nu}{E}\frac{\partial^2F}{\partial x\partial y}+\frac{3}{2}A\sigma_e^{n-1}\frac{\partial^2F}{\partial x\partial y}\right\}+\nabla^2(\alpha T)=0 \tag{16}$$

As in the elastic case, when E and A do not vanish at the crack tip, the governing equation for the singular solution near the tip in each differential pieces becomes

$$\frac{\partial^2}{\partial y^2}\left\{\sigma_e^{n^0-1}\left(\frac{\partial^2F}{\partial y^2}-\frac{1}{2}\frac{\partial^2F}{\partial x^2}\right)\right\}+\frac{\partial^2}{\partial x^2}\left\{\sigma_e^{n^0-1}\left(\frac{\partial^2F}{\partial x^2}-\frac{1}{2}\frac{\partial^2F}{\partial y^2}\right)\right\}+3\frac{\partial^2}{\partial x\partial y}\left\{\sigma_e^{n^0-1}\left(\frac{\partial^2F}{\partial x\partial y}\right)\right\}=0 \tag{17}$$

where n^0 is the value of n calculated at the crack tip. The asymptotic Eq. (17) is the same as that in a homogeneous material with its index n being n^0 (Rice and Rosengren, 1968; Hutchinson, 1968). Therefore, the crack-tip field is the same as the well-known HRR singular field.

Acknowledgment

This work was supported by the Grant-Aid of the National Science Foundation from the Ministry of Education of Japan. The authors would like to thank the reviewers for their suggestions.

References

Aoki, S., Kishimoto, K., and Sakata, M., 1981, "Crack-Tip Stress and Strain Singularity in Thermally Loaded Elastic-Plastic Materials," ASME JOURNAL OF APPLIED MECHANICS, Vol. 48, pp. 428-429.

Delale, F., and Erdogan, F., 1988, "Interface Crack in a Nonhomogeneous Elastic Medium," *International Journal of Engineering Science*, Vol. 26, pp. 559-568.

Erdogan, F., 1985, "The Crack Problem for Bonded Nonhomogeneous Ma-

Downloaded 03 May 2010 to 171.66.16.20. Redistribution subject to ASME license or copyright; see http://www.asme.org/terms/Terms_Use.cfm

terials under Antiplane Shear Loading," ASME JOURNAL OF APPLIED MECHANICS, Vol. 52, pp. 823–828.

Hutchinson, J. W., 1968, "Singular Behavior at the End of a Tensile Crack in a Hardening Material," *Journal of the Mechanics and Physics of Solids*, Vol. 16, pp. 13–31.

Jin, Z.-H., and Noda, N., 1993, "Minimization of Thermal Stress Intensity Factors for a Crack in a Metal-Ceramic Mixture," *Ceramic Transactions, Vol. 34: Functionally Gradient Materials*, J. B. Holt et al., eds., The American Ceramic Society, Westerville, OH, pp. 47–54.

Noda, N., and Jin, Z.-H., 1993, "Thermal Stress Intensity Factors for a Crack in a Strip of a Functionally Gradient Material," *International Journal of Solids and Structures*, Vol. 30, pp. 1039–1056.

Rice, J. R., and Rosengren, G. F., 1968, "Plane Strain Deformation Near a Crack Tip in a Power-Law Hardening Material," *Journal of the Mechanics and Physics of Solids*, Vol. 16, pp. 1–12.

Schovanec, L., and Walton, J. R., 1988, "On the Order of Stress Singularity for an Antiplane Shear Crack at the Interface of Two Bonded Inhomogeneous Elastic Materials," ASME JOURNAL OF APPLIED MECHANICS, Vol. 55, pp. 234–236.

Sih, G. C., 1965, "Heat Conduction in the Infinite Medium with Lines of Discontinuities," ASME *Journal of Heat Transfer*, Vol. 87, pp. 293–298.

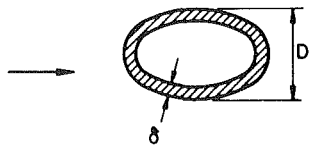


Fig. 1(*a*) Transport in a particle of a porous medium

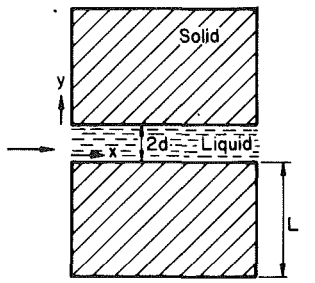


Fig. 1(*b*) Equivalent model in Cartesian coordinates

An Analytical Solution for Adsorption and Desorption Problems in Porous Media

K. Muralidhar[40] and J. Swarup[40]

Introduction

Heat and mass transfer problems in a fluid-saturated porous medium are encountered in the study of spreading of radioactive and chemical wastes by groundwater. At steady state it is commonly assumed that an equilibrium, in terms of the concentration of a chemical species and temperature, exists between the fluid phase and the solid matrix. A local volume-averaged concentration and temperature can then be defined for each point in the porous medium (Kladius and Prasad, 1990). In transient problems this equilibrium will not exist in general. Deviation from equilibrium will be significant when the porosity is low and when the conductivity ratio between the solid and the fluid is small. In such problems the transport processes in each of the phases along with an interface equation relating them must be separately considered. Equations governing these processes have been solved analytically in the present work.

Theoretical Model

Consider a water-saturated porous region that is suddenly exposed to water contaminated with a radioactive species at its in-flow plane. Since the porosity of commonly encountered formations under the earth is small ($\epsilon > 0.01$) the solid fraction is large and has a large surface area. Further the solid phase conductivity, with respect to the diffusing species, is usually much smaller than that for water. Under these conditions the diffusion process in the solid phase is close to one-dimensional in a direction normal to the surface of the solid particle. This is sketched in Fig. 1(*a*). Here δ is the depth of penetration of the solid particle of size D. The assumptions of small ϵ and conductivity guarantee that δ/D is also small, i.e., $\delta/D \ll 1$ and gradients normal to the particle surface predominate over those parallel to it. Further curvature effects can be neglected and the interface between the fluid and solid phases can be treated as planar. This is shown in Fig. 1(*b*). Hence species transport is reduced to a two-dimensional flow problem in the small parallel gap of opening $2d$ and one-dimensional diffusion in the y-direction in the solid phase of size L. The ratio d/L now represents ϵ, the porosity of the region.

Mathematical Formulation

Let C be the concentration of a species in the liquid phase and c^s be its concentration in the solid phase. The equations, initial and boundary conditions governing C and c^s, are as follows.

Liquid:

$$C_t + uC_x + vC_y = DC_{xx} + D_t C_{yy} - \lambda C$$

$$C(x, y, 0) = 0,\ C(0, y, t) = c_o e^{-\lambda t} \quad \text{and} \quad C(\infty, y, t) = 0. \tag{1}$$

Solid Phase:

$$c^s_t = D_s c^s_{yy} - \lambda c^s$$

$$c^s(x, y, 0) = c_s,\quad \frac{-\partial c^s}{\partial y}(x, 0, t) = k(c - c^s) \tag{2}$$

and

$$\frac{\partial c^s}{\partial y}(x, L, t) = 0.$$

In Eqs. (1) and (2), u and v are the x and y components of velocity, λ is the decay constant ($= 0.693/T_{1/2}$ where $T_{1/2}$ is the half-life), D and D_t are the longitudinal and transverse dispersivities of the species under study in water, D_s is the molecular diffusivity of the species in the solid phase, and k is an interface heat/mass transfer coefficient. Suffixes such y in c_y represent the partial derivatives $\partial c/\partial y$. Equation (2) is general enough to handle both adsorption and desorption since the sign of $\partial c^s/\partial y$ changes according to whether $c > c^s$ or $c < c^s$. Here c is an average value of C in the fluid gap. The boundary condition at $y = L$ reflects the fact that it is a symmetry plane. The limit of a heat transfer problem is reached when λ is set equal to zero. In a pure desorption problem, Eq. (1) is modified by the boundary condition $x = 0$, $C = 0$. In an initially clean solid, c_s in Eq. (2) is zero.

[40] Department of Mechanical Engineering, Indian Institute of Technology, Kanpur, P.O. IIT, Kanpur, 208 016, India.

Contributed by the Applied Mechanics Division of THE AMERICAN SOCIETY OF MECHANICAL ENGINEERS for publication in the ASME JOURNAL OF APPLIED MECHANICS. Manuscript received by the ASME Applied Mechanics Division, Jan. 11, 1993; final revision, July 12, 1993. Associate Technical Editor: R. M. Bowen.

Downloaded 03 May 2010 to 171.66.16.20. Redistribution subject to ASME license or copyright; see http://www.asme.org/terms/Terms_Use.cfm

terials under Antiplane Shear Loading," ASME JOURNAL OF APPLIED MECHANICS, Vol. 52, pp. 823–828.

Hutchinson, J. W., 1968, "Singular Behavior at the End of a Tensile Crack in a Hardening Material," *Journal of the Mechanics and Physics of Solids*, Vol. 16, pp. 13–31.

Jin, Z.-H., and Noda, N., 1993, "Minimization of Thermal Stress Intensity Factors for a Crack in a Metal-Ceramic Mixture," *Ceramic Transactions, Vol. 34: Functionally Gradient Materials*, J. B. Holt et al., eds., The American Ceramic Society, Westerville, OH, pp. 47–54.

Noda, N., and Jin, Z.-H., 1993, "Thermal Stress Intensity Factors for a Crack in a Strip of a Functionally Gradient Material," *International Journal of Solids and Structures*, Vol. 30, pp. 1039–1056.

Rice, J. R., and Rosengren, G. F., 1968, "Plane Strain Deformation Near a Crack Tip in a Power-Law Hardening Material," *Journal of the Mechanics and Physics of Solids*, Vol. 16, pp. 1–12.

Schovanec, L., and Walton, J. R., 1988, "On the Order of Stress Singularity for an Antiplane Shear Crack at the Interface of Two Bonded Inhomogeneous Elastic Materials," ASME JOURNAL OF APPLIED MECHANICS, Vol. 55, pp. 234–236.

Sih, G. C., 1965, "Heat Conduction in the Infinite Medium with Lines of Discontinuities," ASME *Journal of Heat Transfer*, Vol. 87, pp. 293–298.

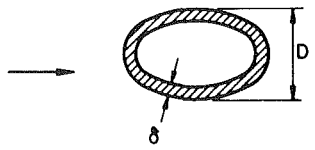


Fig. 1(*a*) Transport in a particle of a porous medium

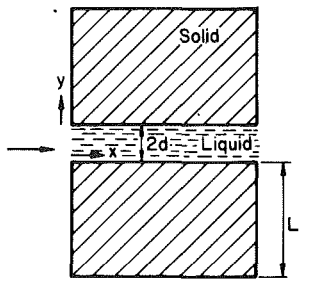


Fig. 1(*b*) Equivalent model in Cartesian coordinates

An Analytical Solution for Adsorption and Desorption Problems in Porous Media

K. Muralidhar[40] and J. Swarup[40]

Introduction

Heat and mass transfer problems in a fluid-saturated porous medium are encountered in the study of spreading of radioactive and chemical wastes by groundwater. At steady state it is commonly assumed that an equilibrium, in terms of the concentration of a chemical species and temperature, exists between the fluid phase and the solid matrix. A local volume-averaged concentration and temperature can then be defined for each point in the porous medium (Kladius and Prasad, 1990). In transient problems this equilibrium will not exist in general. Deviation from equilibrium will be significant when the porosity is low and when the conductivity ratio between the solid and the fluid is small. In such problems the transport processes in each of the phases along with an interface equation relating them must be separately considered. Equations governing these processes have been solved analytically in the present work.

Theoretical Model

Consider a water-saturated porous region that is suddenly exposed to water contaminated with a radioactive species at its in-flow plane. Since the porosity of commonly encountered formations under the earth is small ($\epsilon > 0.01$) the solid fraction is large and has a large surface area. Further the solid phase conductivity, with respect to the diffusing species, is usually much smaller than that for water. Under these conditions the diffusion process in the solid phase is close to one-dimensional in a direction normal to the surface of the solid particle. This is sketched in Fig. 1(*a*). Here δ is the depth of penetration of the solid particle of size D. The assumptions of small ϵ and conductivity guarantee that δ/D is also small, i.e., $\delta/D \ll 1$ and gradients normal to the particle surface predominate over those parallel to it. Further curvature effects can be neglected and the interface between the fluid and solid phases can be treated as planar. This is shown in Fig. 1(*b*). Hence species transport is reduced to a two-dimensional flow problem in the small parallel gap of opening $2d$ and one-dimensional diffusion in the y-direction in the solid phase of size L. The ratio d/L now represents ϵ, the porosity of the region.

Mathematical Formulation

Let C be the concentration of a species in the liquid phase and c^s be its concentration in the solid phase. The equations, initial and boundary conditions governing C and c^s, are as follows.

Liquid:

$$C_t + uC_x + vC_y = DC_{xx} + D_t C_{yy} - \lambda C$$

$$C(x, y, 0) = 0,\ C(0, y, t) = c_o e^{-\lambda t} \quad \text{and} \quad C(\infty, y, t) = 0. \tag{1}$$

Solid Phase:

$$c^s_t = D_s c^s_{yy} - \lambda c^s$$

$$c^s(x, y, 0) = c_s,\quad \frac{-\partial c^s}{\partial y}(x, 0, t) = k(c - c^s) \tag{2}$$

and

$$\frac{\partial c^s}{\partial y}(x, L, t) = 0.$$

In Eqs. (1) and (2), u and v are the x and y components of velocity, λ is the decay constant ($= 0.693/T_{1/2}$ where $T_{1/2}$ is the half-life), D and D_t are the longitudinal and transverse dispersivities of the species under study in water, D_s is the molecular diffusivity of the species in the solid phase, and k is an interface heat/mass transfer coefficient. Suffixes such y in c_y represent the partial derivatives $\partial c/\partial y$. Equation (2) is general enough to handle both adsorption and desorption since the sign of $\partial c^s/\partial y$ changes according to whether $c > c^s$ or $c < c^s$. Here c is an average value of C in the fluid gap. The boundary condition at $y = L$ reflects the fact that it is a symmetry plane. The limit of a heat transfer problem is reached when λ is set equal to zero. In a pure desorption problem, Eq. (1) is modified by the boundary condition $x = 0$, $C = 0$. In an initially clean solid, c_s in Eq. (2) is zero.

[40] Department of Mechanical Engineering, Indian Institute of Technology, Kanpur, P.O. IIT, Kanpur, 208 016, India.

Contributed by the Applied Mechanics Division of THE AMERICAN SOCIETY OF MECHANICAL ENGINEERS for publication in the ASME JOURNAL OF APPLIED MECHANICS. Manuscript received by the ASME Applied Mechanics Division, Jan. 11, 1993; final revision, July 12, 1993. Associate Technical Editor: R. M. Bowen.

Copyright © 1994 by ASME
Downloaded 03 May 2010 to 171.66.16.20. Redistribution subject to ASME license or copyright; see http://www.asme.org/terms/Terms_Use.cfm

Since d/L is assumed to be small in the present study, the liquid phase equations can be simplified by defining an average liquid concentration,

$$c(x, t) = \frac{1}{2dc_0}\int_{-2d}^{0} C(x, y, t)dy.$$

The process of depth-averaging generates a one-dimensional transient problem in the x-direction for flow and the y-direction for diffusion into the solid. The equation governing c is as follows:

$$c_t + uc_x = Dc_{xx} - \left(\lambda + \frac{D_s k}{d}\right)c + \frac{D_s k}{d}c^s|_{y=0} \qquad (3)$$

with $c(x, o) = 0$, $c(o, t) = e^{-\lambda t}$ and $c(\infty, t) = 0$.

In the present work λ, D, D_s, and d/L are treated as constants and u and k are prescribed parameters.

Analytical Solution

Equations (2) and (3) are coupled and the process of decoupling them produces an integral equation for $c(x, t)$. Let the length scales in the x and y directions and the time scale be $X = \sqrt{DT}$, $Y = \sqrt{D_s T}$ and $T = 1/[\lambda + (u^2/4D) + (D_s k/d)]$. In the expressions given as follows, x, y, t and λ are nondimensionalized using these scales. Let $U(x, t) = (V_1(x, t) + V_2(x, t))$ where V_1 and V_2 are intermediate functions given as

$$V_1(x, t) = \frac{1}{2}e^{(1-\lambda)t}\left[e^{(\sqrt{1-\lambda})x}\operatorname{erfc}\left(\frac{x+2\sqrt{1-\lambda}t}{2\sqrt{t}}\right) + e^{-(\sqrt{1-\lambda})x}\operatorname{erfc}\left(\frac{x-2\sqrt{1-\lambda}}{2\sqrt{t}}\right)\right]$$

and

$$V_2 = \frac{1}{2}wc_s\int_0^t d\tau\left[e^{w(\tau-t)}\left[\operatorname{erfc}\left(\frac{2b(t-\tau)-x}{2\sqrt{t-\tau}}\right) - e^{2bx}\operatorname{erfc}\left(\frac{2b(t-\tau)+x}{2\sqrt{t-\tau}}\right)\right]\right] * \sum_{m=1}^{\infty} c_m e^{-\beta_m^2\tau}.$$

Here $w = D_s kT/d$, $b = uX/2D$, $c_m = 2k/((k^2+\beta_m^2)L + k)$ and β_m are the roots of the equation $\beta_m \tan \beta_m L = k$. The solution for $c(x, t)$ is of the form $U(x, t)\exp(-\lambda t) + G(x, t)$ where G contains integrals in c.

To solve the integral equation for $c(x, t)$, we assume a solution in the form $c(x, t) = U(x, t).Z(x, t)e^{-\lambda t}$ where U is given above and

$$Z(x, t) = \sum_{i,j}\frac{a_{ij}t^i}{i!(1+x)^j}.$$

The a_{ij} are undetermined coefficients which depend on the parameters such as u, λ, and k. Substituting the assumed form of $c(x, t)$ in the integral equation produces the following equation for a_{ij}:

$$U(x, t) + \sum_{i,j} F_{ij}a_{ij} = 0$$

where

$$F_{ij} = -\frac{Ut^i}{i!(1+x)^j} + \frac{w}{i!\sqrt{\pi}}\int_0^t \frac{d\tau}{\sqrt{t-\tau}}\int_0^\infty \frac{\Psi dp}{(1+p)^j} \times \left[\mu U(p, \tau)\tau^i + \sum_m \beta_m^2 c_m \tau^{i+1}\int_0^1 \phi^i U(p, \phi\tau)e^{\beta_m^2(\phi-1)\tau}d\phi\right],$$

$$\mu = 1 - \sum_m c_m$$

and

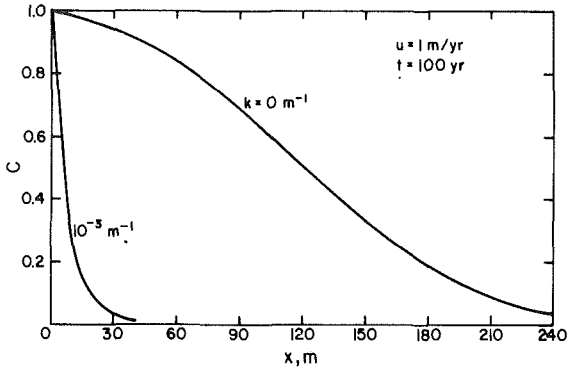


Fig. 2 Concentration distribution as a function of distance (stable species). $t = 100$ years.

$$\Psi = \left[\exp\left(-\frac{(x-p)^2}{4(t-\tau)}\right) - \exp\left(-\frac{(x+p)^2}{4(t-\tau)}\right)\right] \times \exp(b(x-p) - (1-\lambda).(t-\tau)).$$

For $i = 0, 1, \ldots M-1$ and $j = 0, 1, \ldots M-1$ one requires M^2 equations for a unique solution of a_{ij}. The M^2 equations are generated by requiring that the expansion for $Z(x, t)$ be linearly independent with respect to each polynomial in x and t of order less than M. Hence, with $l = 0, 1, \ldots M-1$ and $k = 0, 1, \ldots M-1$ we require

$$\int_{-1}^{1}\int_{-1}^{1}\left(U - \sum_{i,j}F_{ij}a_{ij}\right)\frac{T_l(x)T_k(t)dx\,dt}{\sqrt{1-x^2}\sqrt{1-t^2}} = 0 \quad \text{each } l, k \qquad (4)$$

where T_l and T_k are lth and kth order Chebyshev polynomials in x and t, respectively. The matrix equation arising from Eq. (4) is inverted using Gaussian elimination to determine a_{ij}.

Definite integrals appearing in Eq. (4) are evaluated using powerful quadratures (Krylov and Kruglikova, 1969). In the present work, infinite series are summed using 20 terms, quadratures employ a tenth-order polynomial, and the indices i and j in the expansion for $Z(x, t)$ vary from 0 to 5. The solution is seen to converge for larger values of these parameters. The results of the analytical solution derived here have been compared with the full numerical solution of Eqs. (2) and (3) and the comparison is seen to be good (Muralidhar, 1992).

Results

The following data has been used in the present study to generate results for the concentration distribution in the fluid phase as a function of x and t: $d = 0.005$ m, $L = 1$ m, $D_s = 2.52$ m^2/year, $D = 25.2$ m^2/year, $u = 1$m/year, $k = 0$ and 10^{-3}m^{-1} and half-life = 100 years and infinity. Figure 2 shows a plot of $c(x, t)$ as a function of x when $u = 1$m/year at $t = 100$ years. The half-life is taken as infinity and hence c may be interpreted as the temperature of the fluid. Two values of k, namely 0 and 0.001 m^{-1}, have been considered. For $k = 0$, the time scale $T = 60$ years and for $k = 0.001$ m^{-1}, $T = 2$ years. Hence, $k = 0.001$ m^{-1} represents a strong adsorption problem. A temperature front steady moves through fluid region for $k = 0$. However, when $k > 0$, the front becomes immobile for $t > 100$ years. Under these conditions an equilibrium exists in the porous medium with the concentration flux at $x = 0$ being completely passed into the solid medium.

Figure 3 shows the concentration profiles in the fluid phase in a desorption problem at two different instants ($t = 10$ and 100 years) and for two different velocities ($u = 1$ and 10 m/year). The species half-life is 100 years. It can be seen that c increases from zero at the in-flow boundary to attain a steady equilibrium value. Once $c(x, t)$ becomes equal to $c^s(x, 0, t)$,

Downloaded 03 May 2010 to 171.66.16.20. Redistribution subject to ASME license or copyright; see http://www.asme.org/terms/Terms_Use.cfm

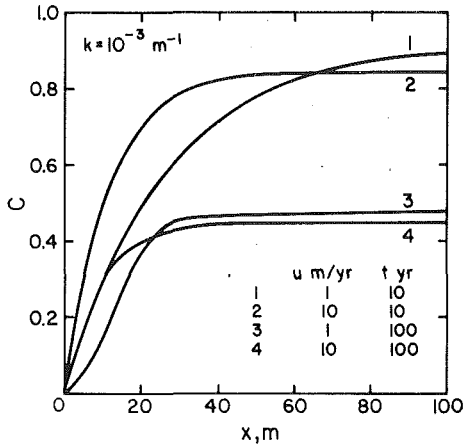


Fig. 3 Desorption problem: Concentration distribution as a function of distance

the concentration in the solid phase the net transport (advection + diffusion) is reduced to zero and $c(x, t)$ decays as $\exp(-\lambda t)$. The solid and fluid phases will then be in equilibrium with each other even during the transient period.

References

Kladius, N., and Prasad, V., 1990, "Flow Transition in Buoyancy-Induced Non-Darcy Convection in a Porous Medium Heated from Below," Trans. ASME *Journal of Heat Transfer*, Vol. 112, pp. 675–684.

Krylov, V. I., and Kruglikova, L. G., 1969, "Handbook of Numerical Harmonic Analysis," Israel Program for Scientific Translations.

Muralidhar, K., 1992, "Flow, Heat and Mass Transfer from Buried Nuclear Waste Canisters," Final Report, Project Number DAE/ME/1989, sponsored by Department of Atomic Energy, Government of India.

Half-Space Instabilities and Short Wavelength Bifurcations in Cylinders and Rectangular Blocks

K. T. Chau[41]

1 Introduction

The problem of surface instability of a half-space was first considered by Biot (1965) and was motivated by its possible application in geophysics, such as the formation of parallel mountain ranges. A similar problem was also studied by Nowinski (1969a,b) for an incompressible hyperelastic half-space under uniaxial and biaxial compressions. Motivated by its possible explanations for earthquake initiation and for prehistoric landmass formations, Brunelle (1973) reexamined the problem by using a linearized theory from the nonlinear theory of elasticity. The bifurcation analysis was extended to frictional materials by Horii and Nemat-Nasser (1982). Surface instability of a half-space was also used to explain the bursting phenomenon of rock (Vardoulakis, 1984; Vardoulakis and Muhlhaus, 1986) and borehole instability (Papanastasiou and Vardoulakis, 1989; Vardoulakis et al., 1988).

Besides geotechnical applications, the surface instability of a half-space is also related to the stability problems of rubber under compression (Guz, 1970; Usmani and Beatty, 1974; Meijers, 1987), under an indentation test (Beatty and Usmani, 1975), and under frictional sliding contact (Best et al., 1981). Hutchinson and Tvergaard (1980) attributed the surface roughness and surface wave pattern observed by Larsson et al. (1982) on pressurized ductile metal cylinders to the same phenomenon. More recent theoretical studies include the works by Wu and Cao (1983), Triantafyllidis (1984), Guz (1986), and Klyushnikov and Mustyatsa (1990). Numerical methods include the finite element analyses by Bardet (1990), Tvergaard (1982), and Triantafyllidis et al. (1982). In addition, surface instabilities are also often observed in metals (e.g., Onyewuenyi and Hirth, 1982; Rittel and Roman, 1989; Rittel, 1990; Rittel et al., 1991) and in soils (Alsiny et al., 1992).

The half-space bifurcation condition also emerges naturally as a special case of the stability problems of a spherical cavity in an infinite medium (Bassini et al., 1980), of pure bending of beam (Triantafyllidis, 1980), of rectangular blocks under plane deformation (Hill and Hutchinson, 1975; Young, 1976; Chau and Rudnicki, 1990), and of circular cylinders under axisymmetric loads (Chau, 1992, 1993a,b). However, the conclusion by Chau and Rudnicki (1990) and by Chau (1992, 1993a,b) is restricted to incompressible solids satisfying plastic normality.

In this Brief Note, we show analytically that the equivalence between the short wavelength limit of bifurcations in rectangular blocks and circular cylinders and the half-space instabilities actually applies to compressible pressure-sensitive materials and to all circumferential bifurcation mode types in circular cylinders.

2 Half-Space Instabilities

We consider here a bifurcation analysis for a half-space of compressible pressure-sensitive material and the result is compared to the short wavelength limit of the geometric diffuse mode bifurcations obtained by Chau and Rudnicki (1990) and by Chau (1922, 1993a). First, we consider a half-space occupying $x_3 \leq 0$ subjected to (i) zero surface traction rate on $x_3 = 0$; and (ii) a triaxial stress state (i.e., $\sigma_{33} = \sigma_{11} = \sigma_c$ and $\sigma_{22} = \sigma_a$). Note that this triaxial stress state is similar to those near the curved surface of a circular cylinder. The uniqueness of a homogeneous deforming state is questioned. Under plane deformation ($v_1 = 0$; v_2 and v_3 are independent of x_1), the subsequent deformation of the half-space is characterized by the following time and rate-independent incrementally linear model:

$$\overset{\nabla}{\boldsymbol{\sigma}}_{22} = a\mathbf{D}_{22} + b\mathbf{D}_{33}, \quad \overset{\nabla}{\boldsymbol{\sigma}}_{33} = c\mathbf{D}_{22} + d\mathbf{D}_{33}, \quad \overset{\nabla}{\boldsymbol{\sigma}}_{23} = 2e\mathbf{D}_{23}, \quad (1)$$

where $\boldsymbol{\sigma}$ is the Cauchy stress tensor, the superposed ∇ denotes the Jaumann rate, and $\mathbf{D}$ is the rate of deformation tensor. There are five incrementally linear material parameters, namely, a, b, c, d, and e. Note that we do not assume $b = c$, and this choice is motivated by the pressure-sensitive model of Rudnicki (1977). That is, the present analysis is applicable to geomaterials.

The continued equilibrium of the incremental solutions, $\dot{t}^*_{ij,i} = 0$ (where $\dot{\mathbf{t}}$ is material rate of the nominal stress), can be written as

$$v_{2,22}a + v_{2,33}e(1-s) + v_{3,32}[b + e(1+s)] = 0,$$

$$v_{3,33}d + v_{3,22}e(1+s) + v_{2,23}[c + e(1-s)] = 0, \quad (2)$$

where $s = (\sigma_a - \sigma_c)/2e$. The zero traction rate boundary conditions are

$$v_{3,3}d + v_{2,2}(c + \sigma_c) = 0,$$

$$v_{2,3}e(1-s) + v_{3,2}e(1-s-\sigma_c/e) = 0, \quad (3)$$

on $x_3 = 0$. We consider the following bifurcation modes

[41]Department of Civil and Structural Engineering, Hong Kong Polytechnic, Hung Hom, Hong Kong. Mem. ASME.

Contributed by the Applied Mechanics Division of THE AMERICAN SOCIETY OF MECHANICAL ENGINEERS for publication in the ASME JOURNAL OF APPLIED MECHANICS. Manuscript received by the ASME Applied Mechanics Division, Oct. 12, 1993; final revision, Sept. 8, 1993.

Downloaded 03 May 2010 to 171.66.16.20. Redistribution subject to ASME license or copyright; see http://www.asme.org/terms/Terms_Use.cfm

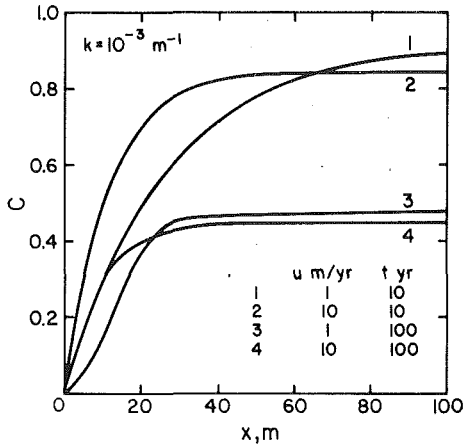


Fig. 3 Desorption problem: Concentration distribution as a function of distance

the concentration in the solid phase the net transport (advection + diffusion) is reduced to zero and $c(x, t)$ decays as $\exp(-\lambda t)$. The solid and fluid phases will then be in equilibrium with each other even during the transient period.

References

Kladius, N., and Prasad, V., 1990, "Flow Transition in Buoyancy-Induced Non-Darcy Convection in a Porous Medium Heated from Below," Trans. ASME *Journal of Heat Transfer*, Vol. 112, pp. 675–684.

Krylov, V. I., and Kruglikova, L. G., 1969, "Handbook of Numerical Harmonic Analysis," Israel Program for Scientific Translations.

Muralidhar, K., 1992, "Flow, Heat and Mass Transfer from Buried Nuclear Waste Canisters," Final Report, Project Number DAE/ME/1989, sponsored by Department of Atomic Energy, Government of India.

Half-Space Instabilities and Short Wavelength Bifurcations in Cylinders and Rectangular Blocks

K. T. Chau[41]

1 Introduction

The problem of surface instability of a half-space was first considered by Biot (1965) and was motivated by its possible application in geophysics, such as the formation of parallel mountain ranges. A similar problem was also studied by Nowinski (1969a,b) for an incompressible hyperelastic half-space under uniaxial and biaxial compressions. Motivated by its possible explanations for earthquake initiation and for prehistoric landmass formations, Brunelle (1973) reexamined the problem by using a linearized theory from the nonlinear theory of elasticity. The bifurcation analysis was extended to frictional materials by Horii and Nemat-Nasser (1982). Surface instability of a half-space was also used to explain the bursting phenomenon of rock (Vardoulakis, 1984; Vardoulakis and Muhlhaus, 1986) and borehole instability (Papanastasiou and Vardoulakis, 1989; Vardoulakis et al., 1988).

Besides geotechnical applications, the surface instability of a half-space is also related to the stability problems of rubber under compression (Guz, 1970; Usmani and Beatty, 1974; Meijers, 1987), under an indentation test (Beatty and Usmani, 1975), and under frictional sliding contact (Best et al., 1981). Hutchinson and Tvergaard (1980) attributed the surface roughness and surface wave pattern observed by Larsson et al. (1982) on pressurized ductile metal cylinders to the same phenomenon. More recent theoretical studies include the works by Wu and Cao (1983), Triantafyllidis (1984), Guz (1986), and Klyushnikov and Mustyatsa (1990). Numerical methods include the finite element analyses by Bardet (1990), Tvergaard (1982), and Triantafyllidis et al. (1982). In addition, surface instabilities are also often observed in metals (e.g., Onyewuenyi and Hirth, 1982; Rittel and Roman, 1989; Rittel, 1990; Rittel et al., 1991) and in soils (Alsiny et al., 1992).

The half-space bifurcation condition also emerges naturally as a special case of the stability problems of a spherical cavity in an infinite medium (Bassini et al., 1980), of pure bending of beam (Triantafyllidis, 1980), of rectangular blocks under plane deformation (Hill and Hutchinson, 1975; Young, 1976; Chau and Rudnicki, 1990), and of circular cylinders under axisymmetric loads (Chau, 1992, 1993a,b). However, the conclusion by Chau and Rudnicki (1990) and by Chau (1992, 1993a,b) is restricted to incompressible solids satisfying plastic normality.

In this Brief Note, we show analytically that the equivalence between the short wavelength limit of bifurcations in rectangular blocks and circular cylinders and the half-space instabilities actually applies to compressible pressure-sensitive materials and to all circumferential bifurcation mode types in circular cylinders.

2 Half-Space Instabilities

We consider here a bifurcation analysis for a half-space of compressible pressure-sensitive material and the result is compared to the short wavelength limit of the geometric diffuse mode bifurcations obtained by Chau and Rudnicki (1990) and by Chau (1922, 1993a). First, we consider a half-space occupying $x_3 \leq 0$ subjected to (i) zero surface traction rate on $x_3 = 0$; and (ii) a triaxial stress state (i.e., $\sigma_{33} = \sigma_{11} = \sigma_c$ and $\sigma_{22} = \sigma_a$). Note that this triaxial stress state is similar to those near the curved surface of a circular cylinder. The uniqueness of a homogeneous deforming state is questioned. Under plane deformation ($v_1 = 0$; v_2 and v_3 are independent of x_1), the subsequent deformation of the half-space is characterized by the following time and rate-independent incrementally linear model:

$$\overset{\nabla}{\boldsymbol{\sigma}}_{22} = a\mathbf{D}_{22} + b\mathbf{D}_{33}, \quad \overset{\nabla}{\boldsymbol{\sigma}}_{33} = c\mathbf{D}_{22} + d\mathbf{D}_{33}, \quad \overset{\nabla}{\boldsymbol{\sigma}}_{23} = 2e\mathbf{D}_{23}, \quad (1)$$

where $\boldsymbol{\sigma}$ is the Cauchy stress tensor, the superposed ∇ denotes the Jaumann rate, and $\mathbf{D}$ is the rate of deformation tensor. There are five incrementally linear material parameters, namely, a, b, c, d, and e. Note that we do not assume $b = c$, and this choice is motivated by the pressure-sensitive model of Rudnicki (1977). That is, the present analysis is applicable to geomaterials.

The continued equilibrium of the incremental solutions, $\dot{t}^*_{ij,i} = 0$ (where $\dot{\mathbf{t}}$ is material rate of the nominal stress), can be written as

$$v_{2,22}a + v_{2,33}e(1-s) + v_{3,32}[b + e(1+s)] = 0,$$

$$v_{3,33}d + v_{3,22}e(1+s) + v_{2,23}[c + e(1-s)] = 0, \quad (2)$$

where $s = (\sigma_a - \sigma_c)/2e$. The zero traction rate boundary conditions are

$$v_{3,3}d + v_{2,2}(c + \sigma_c) = 0,$$

$$v_{2,3}e(1-s) + v_{3,2}e(1-s-\sigma_c/e) = 0, \quad (3)$$

on $x_3 = 0$. We consider the following bifurcation modes

[41]Department of Civil and Structural Engineering, Hong Kong Polytechnic, Hung Hom, Hong Kong. Mem. ASME.

Contributed by the Applied Mechanics Division of THE AMERICAN SOCIETY OF MECHANICAL ENGINEERS for publication in the ASME JOURNAL OF APPLIED MECHANICS. Manuscript received by the ASME Applied Mechanics Division, Oct. 12, 1993; final revision, Sept. 8, 1993.

Copyright © 1994 by ASME
Downloaded 03 May 2010 to 171.66.16.20. Redistribution subject to ASME license or copyright; see http://www.asme.org/terms/Terms_Use.cfm

$$v_2 = A_2 \exp(\rho x_3)\sin(\rho_2 x_2), \quad v_3 = A_3 \exp(\rho x_3)\cos(\rho_2 x_2), \quad (4)$$

with $v_1 = 0$ and A_2 and A_3 are constants. Substitution of (4) into (2) gives two simultaneous equations for A_2 and A_3. For nontrivial solutions, we require

$$A(\rho/\rho_2)^4 - B(\rho/\rho_2)^2 + C = 0, \quad (5)$$

where A, B, and C are defined as

$$A = de(1-s), \quad B = ad - bc - e(b+c) + e(b-c)s,$$

$$C = ae(1+s). \quad (6)$$

For exponential decay in the x_3 direction, we require the real part of ρ greater than zero (i.e., $\mathrm{Re}(\rho) > 0$). Replacing ρ/ρ_2 by $\sqrt{(-1)g/g_z}$ in (5), we recover the characteristic equation for shear band (see Chau, 1992), if proper identification of the material parameters is used. In both the hyperbolic and parabolic regimes (Chau, 1992), because the combination of the material parameters gives a real root for g/g_z, we have $\mathrm{Re}(\rho/\rho_2) = 0$. That is, exponentially decaying solution is possible only in the elliptic regime, which can further be subdivided into the elliptic complex (EC) and elliptic imaginary (EI) subregimes (Hill and Hutchinson, 1975; Chau, 1992). By using the two simultaneous equations for A_2 and A_3, we obtain the following relation between A_2 and A_3:

$$A_2 = \frac{[b+e(1+s)]\eta}{e(1-s)\eta^2 - a} A_3 = F(\eta)A_3, \quad (7)$$

where $\eta = \rho/\rho_2$.

By using (7), the bifurcation field in the EC subregime becomes

$$v_2 = [F(\eta)A_0 \exp(\rho x_3) + \overline{F}(\eta)\overline{A}_0 \exp(\overline{\rho} x_3)]\sin(\rho_2 x_2), \quad (8)$$

$$v_3 = [A_0 \exp(\rho x_3) + \overline{A}_0 \exp(\overline{\rho} x_3)]\cos(\rho_2 x_2), \quad (9)$$

where $\overline{A}_0$ is the complex conjugate of A_0. And η and $\overline{\eta}$ are defined as

$$\eta^2 + \overline{\eta}^2 = B/A, \quad (\eta\overline{\eta})^2 = C/A, \quad (10)$$

where A, B, and C are defined in (6). For the elliptic imaginary subregime, the surface mode becomes

$$v_2 = [A_1 F(p/\rho_2)\exp(px_3) + A_2 F(q/\rho_2)\exp(qx_3)]\sin(\rho_2 x_2), \quad (11)$$

$$v_3 = [A_1 \exp(px_3) + A_2 \exp(qx_3)]\cos(\rho_2 x_2), \quad (12)$$

where p and q are given by

$$p^2 + q^2 = \rho_2^2 B/A, \quad p^2 - q^2 = \rho_2^2 (B^2 - 4AC)^{1/2}/A. \quad (13)$$

Note that (13) equals (6.15) of Chau (1993a) if $\rho_2 = 1$. The zero traction rate boundary conditions (3) yield the following eigenvalue equation:

$$(Z_2 Z_3 - Z_1 Z_4)(AC)^{1/2} - AZ_2 Z_4 - Z_1(CZ_3 + BZ_4) = 0, \quad (14)$$

for both the EC and EI subregimes and where

$$Z_1 = de(1-s), \quad Z_2 = [b+e(1+s)](c+\sigma_c) - da,$$

$$Z_3 = [b+e(1+s)](1-s) - e(1-s)(1-s-\sigma_c/e),$$

$$Z_4 = a(1-s-\sigma_c/e). \quad (15)$$

3 Comparison With the Short Wavelength Limit

To show that (14) equals the short wavelength limit (6.23) of Chau (1993a), we note the following identities:

$$(Z_2 Z_3 - Z_1 Z_4) = (1-s)[b+e(1+s)] \times [(b+2se+\sigma_c)(c+\sigma_c) - da], \quad (16)$$

$$AZ_2 Z_4 + Z_1(CZ_3 + BZ_4) = 2ade(1+s)\left[es(1-s) + \sigma_c(1-s) - \frac{\sigma_c^2}{2e}\right]. \quad (17)$$

Substitution of (16)-(17) into (14) gives

$$[cd(1-s)(1+s)]^{1/2}[(b+2se+\sigma_c)(c+\sigma_c) - da] - 2da\left[es(1-s) + \sigma_c(1-s) - \frac{\sigma_c^2}{2e}\right] = 0. \quad (18)$$

It is straightforward to show that (18) is identical to (6.23) of Chau (1993a) if we set $\sigma_a = \sigma_{zz}$ and $\sigma_c = \sigma_{rr}$ and use the following identifications:

$$a \leftarrow \left(\frac{E + 9Kr^*\nu}{2}\right), \quad b \leftarrow \frac{9Kr^*}{4}, \quad c \leftarrow \frac{9K\nu}{2},$$

$$d \leftarrow G_t + \frac{9K}{4}, \quad e \leftarrow G_1, \quad (19)$$

where K, r^*, G_1, G_t, ν, and E are the in-plane bulk modulus, the pressure-sensitivity parameter, the longitudinal shear modulus, the transverse shear modulus, the effective Poisson's ratio, and the instantaneous Young's modulus (see Rudnicki, 1977). Thus, we have shown that the eigenstress for the short wavelength limit of a circular cylinder equals the condition for half-space instabilities even though the material is compressible and pressure sensitive. Furthermore, Chau (1993b) showed that (6.23) of Chau (1993a) holds for all circumferential bifurcations modes. Therefore, the above proof is valid for all bifurcation modes provided that the circumferential mode number remains finite.

Furthermore, by comparing (1) and the Chau-Rudnicki (1990) model, we have

$$d \leftarrow \frac{G^*}{1-\alpha\delta}[\kappa(1+\delta) + (1+\alpha)],$$

$$c \leftarrow \frac{G^*}{1-\alpha\delta}[\kappa(1+\delta) - (1+\alpha)], \quad e \leftarrow G,$$

$$b \leftarrow \frac{G^*}{1-\alpha\delta}[\kappa(1-\delta) - (1-\alpha)], \quad a \leftarrow \frac{G^*}{1-\alpha\delta}[\kappa(1-\delta) + (1-\alpha)], \quad (20)$$

where α, δ, κ, G^*, and G are the factor of plastic dilatancy, pressure-sensitivity coefficient, in-plane bulk modulus, modulus governing shearing at 45 deg to coordinate axes, and modulus governing shearing relative to the coordinate axes. See Chau and Rudnicki (1990) for more detailed discussion of these parameters. Substitution of (20) into (14) and setting $\sigma_a = \sigma_{11}$ and $\sigma_c = \sigma_{22}$ gives

$$(1-s)(\sigma_{11}^{\max} - \sigma_{11})\{(1+\delta-(1+\alpha)/\kappa] + (1-\alpha\delta)\sigma_{22}/\kappa G^*\}/G + [1-\delta+(1-\alpha)/\kappa][1-s^2-(1-\sigma)^2] \times \left\{\frac{(1-s)[1+\delta+(1+\alpha)/\kappa]}{(1+s)[1-\delta+(1-\alpha)/\kappa]}\right\}^{1/2} = 0, \quad (21)$$

where $\sigma = (\sigma_{11} + \sigma_{22})/2G$, $s = (\sigma_{11} - \sigma_{22})/2G$ and $\sigma_{11}^{\max}$ is the stress at maximum load under plane-strain condition. This eigenvalue equation has been obtained previously by Chau and Rudnicki (1990) as the short wavelength limit for a rectangular specimen under plane-strain deformation. That is, the short wavelength bifurcation of a compressible pressure-sensitive rectangular block corresponds to the half-space rumpling mode bifurcation of the same material.

4 Conclusion

In summary, we have shown that both the short wavelength limit of geometric diffuse modes bifurcations for circular cylinders and rectangular blocks corresponds to half-space instabilities regardless of the details of the constitutive response of (1). Although we arrive at this conclusion by using the con-

Downloaded 03 May 2010 to 171.66.16.20. Redistribution subject to ASME license or copyright; see http://www.asme.org/terms/Terms_Use.cfm

stitutive models by Rudnicki (1977) and by Chau and Rudnicki (1990), the conclusion applies for all incrementally linear solids that can be characterized by (1).

Note also that there is no length scale in the stability problem of a half-space, and surface modes emerge simultaneously for all wavelength (e.g., see Wu and Cao, 1983). In real materials, the wavelength of surface modes cannot be arbitrary small. In particular, as remarked by Rittel (1990), the wavelength of surface modes is inevitably controlled by the microstructure of the material. The natural length scale governed by the size of microstructures, such as microcracks, should be incorporated in the analysis (e.g., see Papamichos and Vardoulakis, 1989; Rittel, 1990). However, such analysis is out of the scope of this Note.

Acknowledgment

The author is grateful to Prof. John W. Rudnicki of Northwestern University for suggesting this proof and providing some helpful comments. The suggestion by an anonymous reviewer is also appreciated.

References

Alsiny, A., Vardoulakis, I., and Drescher, A., 1992, "Deformation Localization in Cavity Inflation Experiments on Dry Sand," *Geotechnique*, Vol. 42, pp. 395–410.

Bardet, J., 1990, "Finite Element Analysis of Surface Instability in Hypoelastic Solids," *Computer Methods in Applied Mechanics and Engineering*, Vol. 78, pp. 273–296.

Bassini, J. L., Duran, D., and Hutchinson, J. W., 1980, "Bifurcations at a Spherical Hole in an Infinite Elastoplastic Medium," *Mathematical Proceedings of the Cambridge Philosophical Society*, Vol. 87, pp. 339–356.

Beatty, M. F., and Usmani, S. A., 1975, "On the Indentation of Highly Elastic Half-space," *Quarterly Journal of Mechanics and Applied Mathematics*, Vol. 28, pp. 47–62.

Best, B., Meijers, P., and Savkoor, A. R., 1981, "The Formation of Schallamach Waves," *Wear*, Vol. 65, pp. 385–396.

Biot, M. A., 1965, *Mechanics of Incremental Deformations*, John Wiley and Sons, New York.

Brunelle, E. J., 1973, "Surface Instability due to Initial Compressive Stress," *Bulletin of the Seismological Society of America*, Vol. 63, pp. 1885–1893.

Chau, K. T., 1992, "Non-normality and Bifurcation in a Compressible Pressure-sensitive Circular Cylinder under Tension and Compression," *International Journal of Solids and Structures*, Vol. 29, pp. 801–824.

Chau, K. T., 1993a, "Antisymmetric Bifurcations in a Compressible Pressure-Sensitive Circular Cylinder Under Axisymmetric Tension and Compression," ASME JOURNAL OF APPLIED MECHANICS, Vol. 60, pp. 282–289.

Chau, K. T., 1993b, "Buckling, Barrelling, and Surface Instabilities of a Finite, Transversely Isotropic Circular Cylinder," *Quarterly of Applied Mathematics*, in press.

Chau, K. T., and Rudnicki, J. W., 1990, "Bifurcation of Compressible Pressure-sensitive Materials in Plane Strain Tension and Compression," *Journal of the Mechanics and Physics of Solids*, Vol. 38, pp. 875–898.

Guz, A. N., 1970, "Surface Instability of Highly-elastic Materials," *Polymer Mechanics*, Vol. 6, No. 6, pp. 966–968.

Guz, A. N., 1986, "Three-dimensional Stability Theory of Deformable Bodies. Surface Instability," *Soviet Applied Mechanics*, Vol. 22, No. 1, pp. 24–35.

Hill, R., and Hutchinson, J. W., 1975, "Bifurcation Phenomena in Plane Tension Test," *Journal of the Mechanics and Physics of Solids*, Vol. 23, pp. 239–264.

Horii, H., and Nemat-Nasser, S., 1982, "Instability of a Half-space with Frictional Materials," *Journal of Applied Mathematics and Physics*, Vol. 33, pp. 1–16.

Hutchinson, J. W., and Tvergaard, V., 1980, "Surface Instabilities on Statically Strained Plastic Solids," *International Journal of Mechanical Science*, Vol. 22, pp. 339–354.

Klyushnikov, V. D., and Mustyatsa, S. V., 1990, "Some Features of the Solution of the Surface-Instability Problem," *Mechanics of Solids* (English Translation), Vol. 25, No. 4, pp. 41–43.

Larsson, M., Needleman, A., Tvergaard, V., and Storakers, B., 1982, "Instability and Failure of Internally Pressurized Ductile Metal Cylinders," *Journal of the Mechanics and Physics of Solids*, Vol. 30, pp. 121–154.

Meijers, P., 1987, "Stability of a Rubber Half-space," *Journal of Elasticity*, Vol. 17, pp. 143–158.

Nowinski, J. L., 1969a, "Surface Instability of a Half-space under Highly Two-dimensional Compression," *Journal of The Franklin Institute*, Vol. 228, pp. 367–376.

Nowinski, J. L., 1969b, "On the Surface Instability of an Isotropic Highly Elastic Half-space," *Indian Journal of Mechanics and Mathematics*, Anniversary Volume, pp 1–10.

Onyewuenyi, O. A., and Hirth, J. P., 1982, "Plastic Instability in U-notched Bend Specimens of Spheroidized AISI 1090 Steel," *Metallurgy Transaction A*, Vol. 13, pp. 2209–2218.

Papamichos, E., and Vardoulakis, I., 1989, "The Coupling Effect of Surface Instabilities and Surface Parallel Griffith Cracks," *Proceedings of the International Symposium of Rock Mechanics and Rock Physics at Great Depth*, Pau, France, Aug. 28–31, pp. 481–487.

Papanastasiou, P., and Vardoulakis, I., 1989, "Bifurcation Analysis of Deep Boreholes: II Scale Effect," *International Journal for Numerical and Analytical Methods in Geomechanics*, Vol. 13, pp. 183–198.

Rittel, D., 1990, "The Influence of Microstructures on the Macroscopic Patterns of Surface Instabilities in Metals," *Scripta Metallurgica et Materialia*, Vol. 24, pp. 1759–1764.

Rittel, D., Aharonov, R., Feigin, G., and Roman, I., 1991, "Experimental Investigation of Surface Instabilities in Cylindrical Tensile Metallic Specimens," *Acta Metallurgy and Materials*, Vol. 39, pp. 719–724.

Rittel, D., and Roman, I., 1989, "Tensile Deformation of Coarse-grained Cast Austenitic Manganese Steels," *Material Science and Engineering*, Vol. 110, pp. 77–87.

Rudnicki, J. W., 1977, "The Effect of Stress-Induced Anisotropy on a Model of Brittle Rock Failure as Localization of Deformation," *Energy Resources and Excavation Technology, Proceedings of the Eighteenth U.S. Symposium on Rock Mechanics*, Keystone, CO, June 22–24, pp. 3B4-1–3B4-8.

Triantafyllidis, N., 1980, "Bifurcation Phenomena in Pure Bending," *Journal of the Mechanics and Physics of Solids*, Vol. 28, pp. 221–245.

Triantafyllidis, N., 1984, "Surface Instabilities in Finitely Strained Solids under Static Loading," *International Journal of Engineering Science*, Vol. 22, pp. 1187–1192.

Triantafyllidis, N., and Needleman, A., and Tvergaard, V., 1982, "On the Development of Shear Bands in Pure Bending," *International Journal of Solids and Structures*, Vol. 18, pp. 121–138.

Tvergaard, V., 1982, "Influence of Void Nucleation on Ductile Shear Fracture at a Free Surface," *Journal of the Mechanics and Physics of Solids*, Vol. 30, pp. 399–425.

Usmani, S. A., and Beatty, M. F., 1974, "On the Surface Instability of a Highly Elastic Half-space," *Journal of Elasticity*, Vol. 4, pp. 249–263.

Vardoulakis, I., 1984, "Rock Bursting as a Surface Instability," *International Journal of Rock Mechanics and Mining Science & Geomechanics Abstract*, Vol. 21, pp. 137–144.

Vardoulakis, I., and Muhlhaus, H. B., 1986, "Local Rock Surface Instabilities," *International Journal of Rock Mechanics and Mining Science & Geomechanics Abstract*, Vol. 23, pp. 379–383.

Vardoulakis, I., Sulem, J., and Guenot, A., 1988, "A Borehole Instabilities as Bifurcation Phenomena," *International Journal of Rock Mechanics and Mining Science & Geomechanics Abstract*, Vol. 25, pp. 159–170.

Wu, C. H., and Cao, G., 1983, "Buckling of an Axially Compressed Incompressible Half Space," *Journal of Structural Mechanics*, Vol. 11, pp. 37–48.

Young, N. J. B., 1976, "Bifurcation Phenomena in the Plane Compression Test," *Journal of the Mechanics and Physics of Solids*, Vol. 24, pp. 77–91.

To the Construction of Uniformly Valid Forward-Area Asymptotics in Terms of the Ray Method in Dynamic Problems in Linear Viscoelasticity

Y. A. Rossikhin[42,44] and M. V. Shitikova[43,44]

Introduction

Once the ray method based on the combination of the ray theory with the theory of propagating surfaces of discontinuity due to Thomas (1961) has been proposed by Achenbach and Reddy (1967), the papers in which this method has been used for solving various boundary value problems have evolved. However, the authors know isolated papers (Sun, 1970; Rossikhin and Shitikova, 1991) wherein the question is posed con-

[42] Professor, Department of Theoretical Mechanics.

[43] Senior Research Scientist, Department of Structural Mechanics.

[44] Voronezh Civil Engineering Institute, Voronezh 394006, Russia.

Contributed by the Applied Mechanics Division of THE AMERICAN SOCIETY OF MECHANICAL ENGINEERS for publication in the ASME JOURNAL OF APPLIED MECHANICS. Manuscript received by the ASME Applied Mechanics Division, June 11, 1993; final revision, June 23, 1993. Associate Technical Editor: S. K. Datta.

Downloaded 03 May 2010 to 171.66.16.20. Redistribution subject to ASME license or copyright; see http://www.asme.org/terms/Terms_Use.cfm

stitutive models by Rudnicki (1977) and by Chau and Rudnicki (1990), the conclusion applies for all incrementally linear solids that can be characterized by (1).

Note also that there is no length scale in the stability problem of a half-space, and surface modes emerge simultaneously for all wavelength (e.g., see Wu and Cao, 1983). In real materials, the wavelength of surface modes cannot be arbitrary small. In particular, as remarked by Rittel (1990), the wavelength of surface modes is inevitably controlled by the microstructure of the material. The natural length scale governed by the size of microstructures, such as microcracks, should be incorporated in the analysis (e.g., see Papamichos and Vardoulakis, 1989; Rittel, 1990). However, such analysis is out of the scope of this Note.

Acknowledgment

The author is grateful to Prof. John W. Rudnicki of Northwestern University for suggesting this proof and providing some helpful comments. The suggestion by an anonymous reviewer is also appreciated.

References

Alsiny, A., Vardoulakis, I., and Drescher, A., 1992, "Deformation Localization in Cavity Inflation Experiments on Dry Sand," *Geotechnique*, Vol. 42, pp. 395–410.

Bardet, J., 1990, "Finite Element Analysis of Surface Instability in Hypoelastic Solids," *Computer Methods in Applied Mechanics and Engineering*, Vol. 78, pp. 273–296.

Bassini, J. L., Duran, D., and Hutchinson, J. W., 1980, "Bifurcations at a Spherical Hole in an Infinite Elastoplastic Medium," *Mathematical Proceedings of the Cambridge Philosophical Society*, Vol. 87, pp. 339–356.

Beatty, M. F., and Usmani, S. A., 1975, "On the Indentation of Highly Elastic Half-space," *Quarterly Journal of Mechanics and Applied Mathematics*, Vol. 28, pp. 47–62.

Best, B., Meijers, P., and Savkoor, A. R., 1981, "The Formation of Schallamach Waves," *Wear*, Vol. 65, pp. 385–396.

Biot, M. A., 1965, *Mechanics of Incremental Deformations*, John Wiley and Sons, New York.

Brunelle, E. J., 1973, "Surface Instability due to Initial Compressive Stress," *Bulletin of the Seismological Society of America*, Vol. 63, pp. 1885–1893.

Chau, K. T., 1992, "Non-normality and Bifurcation in a Compressible Pressure-sensitive Circular Cylinder under Tension and Compression," *International Journal of Solids and Structures*, Vol. 29, pp. 801–824.

Chau, K. T., 1993a, "Antisymmetric Bifurcations in a Compressible Pressure-Sensitive Circular Cylinder Under Axisymmetric Tension and Compression," ASME JOURNAL OF APPLIED MECHANICS, Vol. 60, pp. 282–289.

Chau, K. T., 1993b, "Buckling, Barrelling, and Surface Instabilities of a Finite, Transversely Isotropic Circular Cylinder," *Quarterly of Applied Mathematics*, in press.

Chau, K. T., and Rudnicki, J. W., 1990, "Bifurcation of Compressible Pressure-sensitive Materials in Plane Strain Tension and Compression," *Journal of the Mechanics and Physics of Solids*, Vol. 38, pp. 875–898.

Guz, A. N., 1970, "Surface Instability of Highly-elastic Materials," *Polymer Mechanics*, Vol. 6, No. 6, pp. 966–968.

Guz, A. N., 1986, "Three-dimensional Stability Theory of Deformable Bodies. Surface Instability," *Soviet Applied Mechanics*, Vol. 22, No. 1, pp. 24–35.

Hill, R., and Hutchinson, J. W., 1975, "Bifurcation Phenomena in Plane Tension Test," *Journal of the Mechanics and Physics of Solids*, Vol. 23, pp. 239–264.

Horii, H., and Nemat-Nasser, S., 1982, "Instability of a Half-space with Frictional Materials," *Journal of Applied Mathematics and Physics*, Vol. 33, pp. 1–16.

Hutchinson, J. W., and Tvergaard, V., 1980, "Surface Instabilities on Statically Strained Plastic Solids," *International Journal of Mechanical Science*, Vol. 22, pp. 339–354.

Klyushnikov, V. D., and Mustyatsa, S. V., 1990, "Some Features of the Solution of the Surface-Instability Problem," *Mechanics of Solids* (English Translation), Vol. 25, No. 4, pp. 41–43.

Larsson, M., Needleman, A., Tvergaard, V., and Storakers, B., 1982, "Instability and Failure of Internally Pressurized Ductile Metal Cylinders," *Journal of the Mechanics and Physics of Solids*, Vol. 30, pp. 121–154.

Meijers, P., 1987, "Stability of a Rubber Half-space," *Journal of Elasticity*, Vol. 17, pp. 143–158.

Nowinski, J. L., 1969a, "Surface Instability of a Half-space under Highly Two-dimensional Compression," *Journal of The Franklin Institute*, Vol. 228, pp. 367–376.

Nowinski, J. L., 1969b, "On the Surface Instability of an Isotropic Highly Elastic Half-space," *Indian Journal of Mechanics and Mathematics*, Anniversary Volume, pp 1–10.

Onyewuenyi, O. A., and Hirth, J. P., 1982, "Plastic Instability in U-notched Bend Specimens of Spheroidized AISI 1090 Steel," *Metallurgy Transaction A*, Vol. 13, pp. 2209–2218.

Papamichos, E., and Vardoulakis, I., 1989, "The Coupling Effect of Surface Instabilities and Surface Parallel Griffith Cracks," *Proceedings of the International Symposium of Rock Mechanics and Rock Physics at Great Depth*, Pau, France, Aug. 28–31, pp. 481–487.

Papanastasiou, P., and Vardoulakis, I., 1989, "Bifurcation Analysis of Deep Boreholes: II Scale Effect," *International Journal for Numerical and Analytical Methods in Geomechanics*, Vol. 13, pp. 183–198.

Rittel, D., 1990, "The Influence of Microstructures on the Macroscopic Patterns of Surface Instabilities in Metals," *Scripta Metallurgica et Materialia*, Vol. 24, pp. 1759–1764.

Rittel, D., Aharonov, R., Feigin, G., and Roman, I., 1991, "Experimental Investigation of Surface Instabilities in Cylindrical Tensile Metallic Specimens," *Acta Metallurgy and Materials*, Vol. 39, pp. 719–724.

Rittel, D., and Roman, I., 1989, "Tensile Deformation of Coarse-grained Cast Austenitic Manganese Steels," *Material Science and Engineering*, Vol. 110, pp. 77–87.

Rudnicki, J. W., 1977, "The Effect of Stress-Induced Anisotropy on a Model of Brittle Rock Failure as Localization of Deformation," *Energy Resources and Excavation Technology, Proceedings of the Eighteenth U.S. Symposium on Rock Mechanics*, Keystone, CO, June 22–24, pp. 3B4-1–3B4-8.

Triantafyllidis, N., 1980, "Bifurcation Phenomena in Pure Bending," *Journal of the Mechanics and Physics of Solids*, Vol. 28, pp. 221–245.

Triantafyllidis, N., 1984, "Surface Instabilities in Finitely Strained Solids under Static Loading," *International Journal of Engineering Science*, Vol. 22, pp. 1187–1192.

Triantafyllidis, N., and Needleman, A., and Tvergaard, V., 1982, "On the Development of Shear Bands in Pure Bending," *International Journal of Solids and Structures*, Vol. 18, pp. 121–138.

Tvergaard, V., 1982, "Influence of Void Nucleation on Ductile Shear Fracture at a Free Surface," *Journal of the Mechanics and Physics of Solids*, Vol. 30, pp. 399–425.

Usmani, S. A., and Beatty, M. F., 1974, "On the Surface Instability of a Highly Elastic Half-space," *Journal of Elasticity*, Vol. 4, pp. 249–263.

Vardoulakis, I., 1984, "Rock Bursting as a Surface Instability," *International Journal of Rock Mechanics and Mining Science & Geomechanics Abstract*, Vol. 21, pp. 137–144.

Vardoulakis, I., and Muhlhaus, H. B., 1986, "Local Rock Surface Instabilities," *International Journal of Rock Mechanics and Mining Science & Geomechanics Abstract*, Vol. 23, pp. 379–383.

Vardoulakis, I., Sulem, J., and Guenot, A., 1988, "A Borehole Instabilities as Bifurcation Phenomena," *International Journal of Rock Mechanics and Mining Science & Geomechanics Abstract*, Vol. 25, pp. 159–170.

Wu, C. H., and Cao, G., 1983, "Buckling of an Axially Compressed Incompressible Half Space," *Journal of Structural Mechanics*, Vol. 11, pp. 37–48.

Young, N. J. B., 1976, "Bifurcation Phenomena in the Plane Compression Test," *Journal of the Mechanics and Physics of Solids*, Vol. 24, pp. 77–91.

To the Construction of Uniformly Valid Forward-Area Asymptotics in Terms of the Ray Method in Dynamic Problems in Linear Viscoelasticity

Y. A. Rossikhin[42,44] and M. V. Shitikova[43,44]

Introduction

Once the ray method based on the combination of the ray theory with the theory of propagating surfaces of discontinuity due to Thomas (1961) has been proposed by Achenbach and Reddy (1967), the papers in which this method has been used for solving various boundary value problems have evolved. However, the authors know isolated papers (Sun, 1970; Rossikhin and Shitikova, 1991) wherein the question is posed con-

[42] Professor, Department of Theoretical Mechanics.

[43] Senior Research Scientist, Department of Structural Mechanics.

[44] Voronezh Civil Engineering Institute, Voronezh 394006, Russia.

Contributed by the Applied Mechanics Division of THE AMERICAN SOCIETY OF MECHANICAL ENGINEERS for publication in the ASME JOURNAL OF APPLIED MECHANICS. Manuscript received by the ASME Applied Mechanics Division, June 11, 1993; final revision, June 23, 1993. Associate Technical Editor: S. K. Datta.

Copyright © 1994 by ASME
Downloaded 03 May 2010 to 171.66.16.20. Redistribution subject to ASME license or copyright; see http://www.asme.org/terms/Terms_Use.cfm

cerning the improvement of the ray series convergence or the uniform validity of truncated ray series.

In this Note, an attempt is made to obtain the uniformly suitable forward-area asymptotics in terms of recurrent equations of the ray method for bodies of significant extent in space. As an illustration it is considered a thin semi-infinite linearly viscoelastic homogeneous rod which is assumed to be initially undisturbed but subjected to a constant velocity at one end or subjected to a constant stress impact at the initial instant of time.

Analysis

The given problem was considered by Achenbach and Reddy (1967) wherein the stress $\sigma(x, t)$ $(0 \le x < \infty)$ behind the front of the strong discontinuity surface was obtained using the ray series

$$\sigma(x, t) = \sum_{n=0}^{\infty} \frac{1}{n!}\left(t - \frac{x}{G}\right)^n \left[\frac{\partial^n \sigma}{\partial t^n}\right]_{t=x/G} \tag{1}$$

where $[\partial^n \sigma/\partial t^n]$ and $[\partial^n v/\partial t^n]$ are the discontinuities in the n-order time derivatives of the stress, t is the time, $G = (\rho J_o)^{-1/2}$ is the propagation velocity of the discontinuity surface, ρ is the mass density, and $J_0 = J(0)$, $J(t)$ is the uniaxial creep function.

The coefficients of the ray series (1) were determined from the recurrent equation

$$\frac{d}{dt}\left[\frac{\partial^n \sigma}{\partial t^n}\right] + \alpha_1 \left[\frac{\partial^n \sigma}{\partial t^n}\right] = F_{n-1}$$

$$F_{n-1}(t) = \frac{1}{2}\frac{d^2}{dt^2}\left[\frac{\partial^{n-1}\sigma}{\partial t^{n-1}}\right] - \sum_{i=1}^{n} \alpha_{i+1}\left[\frac{\partial^{n-i}\sigma}{\partial t^{n-i}}\right], \quad \alpha_i = \frac{J_0^{(i)}}{2J_0} \tag{2}$$

which was obtained from the equation of motion and the constitutive equation for linear viscoelastic material behavior by employing the geometric and kinematic condition of compatibility (Thomas, 1961). In Eq. (2), $J_0^{(i)} = J^{(i)}(0)$, and $J^{(i)}(t) = d^i J/dt^i$.

Sun (1970) applied Eqs. (1) and (2) to a viscoelastic rod of linear Maxwell material subjected to a particle velocity v_0 for $t > 0$ and a rod of a standard linear solid subjected to a constant stress σ_0 for $t > 0$. In both examples, the relations for the dimensionless stress Z can be obtained as

$$Z = \exp(-\alpha\xi) \sum_{k=0}^{5} z_k(\xi)(\tau - \xi)^k \tag{3}$$

where $Z = \sigma^* = -\sigma(\rho G v_0)^{-1}$ and $Z = \sigma_* = \sigma\sigma_0^{-1}$ for the first and second examples, respectively, $z_k(\xi)$ are the polynomials of degree k in the variable ξ which harbor k arbitrary constants to be determined from the initial conditions, $\xi = x(2G\tau_0)^{-1}$, τ_0 is the relaxation time, $\tau = t(2\tau_0)^{-1}$, and α is a certain constant.

Sun (1970) has compared the results due to the formulas (3) with the exact solutions obtained by Lee and Kanter (1953) and Morrison (1956) by employing the Laplace transform technique to the first and second problems, respectively. It has been shown that for short-time range elapsed after the moment of the load application it has been observed that there is good agreement between the approximate and exact solutions in the whole domain of the wave motion existence. But as time increases, the ray expansions show characteristics of forward-area asymptotics, i.e.,

$$Z = \exp(-\alpha\xi) \sum_{k=0}^{5} z_k(\xi)\epsilon^k \tag{4}$$

where ϵ is a small value.

However, for a rod of significant extent, the near front domains, wherein the exact solutions are closely approximated by the truncated ray series (4), are rapidly narrowed down

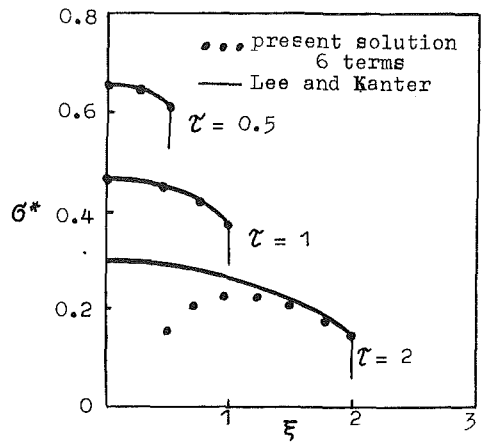


Fig. 1 Stress distribution for a rod of Maxwell material subjected to a velocity impact

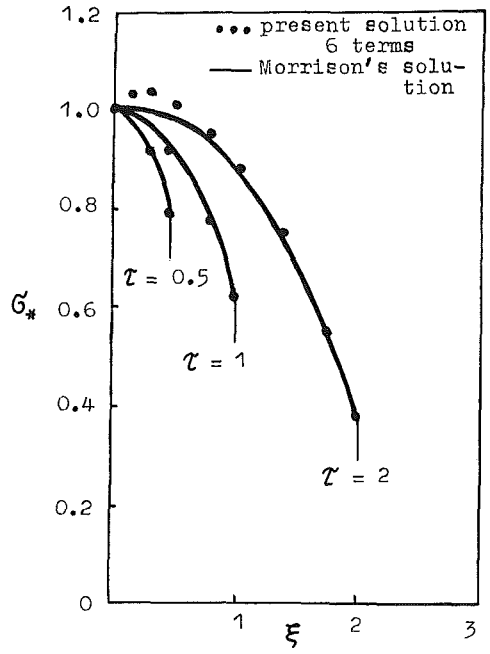


Fig. 2 Stress distribution for a rod of a standard linear solid subjected to a constant stress

contracting to the wavefront with increase in ξ. The reason is that though the ray series (1) is a convergent series, its convergence is slow, and one fails to represent the solution for all ξ by a finite number of terms of (4). Slow convergence is governed by the fact that for the expansion (4) the ratio of the following term to the preceding term increases without bound with $\xi \to \infty$, i.e., the condition for uniform validity (Nayfeh, 1973) is violated for this expansion, the further the wave surface gets from the boundary $\xi = 0$.

To adjust the ray expansions and thereby expand the region of their uniform fitness, we show that the expression (4) satisfies the equation

$$\frac{dZ}{dt} + \alpha_1 Z = \frac{1}{2}\epsilon\frac{d^2 Z}{dt^2} - \sum_{i=1}^{n} \alpha_{i+1}\epsilon^i Z. \tag{5}$$

To prove (5), we substitute (4) into Eq. (5) and equate coefficients of like powers of ϵ. As a result, we come to the recurrent Eq. (2). To solve Eq. (5), we use the method of multiple scales (Nayfeh, 1973). For this purpose we represent the value Z as

Downloaded 03 May 2010 to 171.66.16.20. Redistribution subject to ASME license or copyright; see http://www.asme.org/terms/Terms_Use.cfm

$$Z = Z_0(T_0, T_1, T_2, ..) + \epsilon Z_1(T_0, T_1, T_2, ..) + \epsilon^2 Z_2(T_0, T_1, T_2, ..) + .. \quad (6)$$

where $T_n = \epsilon^n t$ $(n = 0, 1, 2, \ldots)$ are new independent variables.

Substituting (6) into Eq. (5), equating the coefficients of like powers of ϵ, and eliminating secular terms, we obtain

$$Z = [a_0 + \epsilon a_1 + \ldots + \epsilon^n a_n]\exp[(b_0 + \epsilon b_0 + \ldots + \epsilon^n b_n)t] \quad (7)$$

where α_n are constants dependent on boundary conditions, $b_0 = -\alpha_1$,

$$b_n = \begin{cases} -\alpha_{n+1} + \frac{1}{2} b^2_{(n-1)/2} + \sum_{i=0}^{(n-3)/2} b_i b_{n-i-1} & \text{for an even } n \\ -\alpha_{n+1} + \sum_{i=0}^{(n-2)/2} b_i b_{n-i-1} & \text{for an uneven } n. \end{cases}$$

For the expansion (7) to be treated as a uniformly applicable forward-area asymptotic, it is necessary to replace τ with ξ and the value ϵ^n by $(\tau - \xi)^n/n!$, assuming that ξ varies from 0 to τ.

The method resulting in the expansions (7) will be named as the method of "forward-area regularization."

Figures 1 and 2 give the dimensionless stress distribution for a rod of a Maxwell material and for a rod of a standard linear solid due to (7), respectively, for several values of τ. It is seen that the expressions (7) give us forward-area asymptotics stable with reference to the wavefront movement.

Thus, a formal increase in the number of ray series terms may not give the wanted result in the improvement of the solution approximation if the wavefront is at a considerable distance from a boundary surface. To eliminate such a contradiction, it is coincidently necessary, with the increase in the number of terms of a ray series, to eliminate singular items entering into these terms due to the method of forward-area regularization.

References

Achenbach, J. D., and Reddy, D. P., 1967, "Note on Wave Propagation in Linearly Viscoelastic Media," *Zeitschrift fur angewandte Mathematik und Physik*, Vol. 18, pp. 141–144.

Lee, E. H., and Kanter, I., 1953, "Wave Propagation in Finite Rods of Viscoelastic Materials," *Journal of Applied Physics*, Vol. 24, pp. 1115–1122.

Morrison, J. A., 1956, "Wave Propagation in Rods of Voigt Materials and Viscoelastic Materials with Three-Parameter Models," *Quarterly of Applied Mathematics*, Vol. 14, pp. 153–169.

Nayfeh, A. H., 1973, *Perturbation Methods*, John Wiley and Sons, New York.

Rossikhin, Yu. A., and Shitikova, M. V., 1991, "Construction of Uniformly Fit Beam Decompositions for Solution of Dynamic Problems of Linear Viscoelasticity," *Prikladnaja Mekhanika*, Vol. 27, pp. 89–95 (in Russian).

Sun, C. T., 1970, "Transient Wave Propagation in Viscoelastic Rods," Transactions of the ASME JOURNAL OF APPLIED MECHANICS, Vol. 37, pp. 1141–1144.

Thomas, T. Y., 1961, *Plastic Flow and Fracture in Solids*, Academic Press, New York.

Downloaded 03 May 2010 to 171.66.16.20. Redistribution subject to ASME license or copyright; see http://www.asme.org/terms/Terms_Use.cfm

Journal of Applied Mechanics

Discussion

Characteristics of Modal Coupling in Nonclassically Damped Systems Under Harmonic Excitation[1]

S. M. Shahruz[2]. The authors study the nature of modal coupling in nonclassically damped systems under harmonic excitation. They consider the system

$$\ddot{q}(t) + D\dot{q}(t) + \Omega q(t) = [f_1\ f_2\ \cdots\ f_n]^T u(t), \qquad (3)$$

for all $t \geq 0$, where $q(t) \in \mathbf{R}^n$, $u(t)$ is a scalar-valued harmonic function of time of frequency ω_f and amplitude one, $D = D^T \in \mathbf{R}^{n\times n}$ is a positive definite matrix, and $\Omega = \text{diag}[\omega_1^2, \ldots, \omega_n^2]$.

For simplicity of the presentation, we let $n = 3$, and write (14) in Section 2 of the paper for $i = 1$:

$$Q_1(s) = \frac{1}{s^2 + d_{11}s + \omega_1^2} \times \left[f_1 - \frac{d_{12}f_2 s}{s^2 + (d_{22} + d_{21}Q_1(s)/Q_2(s) + d_{23}Q_3(s)/Q_2(s))s + \omega_2^2} - \frac{d_{13}f_3 s}{s^2 + (d_{33} + d_{31}Q_1(s)/Q_3(s) + d_{32}Q_2(s)/Q_3(s))s + \omega_3^2} \right] U(s), \qquad (D1)$$

where $Q_i(s)$ and $U(s)$ are, respectively, the Laplace transforms of $q_i(\cdot)$ for $i = 1, 2, 3$ and $u(\cdot)$. The authors interpret the coefficient of $U(s)$ in (D1) as the transfer function from the input $U(s)$ to the response $Q_1(s)$. We note that the coefficient of $U(s)$ cannot be the transfer function from $U(s)$ to $Q_1(s)$, because in this coefficient the response $Q_1(s)$ is present.

Referring to (D1), the authors define the coupling coefficients

$$\gamma_{12}(s) = -\frac{d_{12}f_2 s}{s^2 + (d_{22} + d_{21}Q_1(s)/Q_2(s) + d_{23}Q_3(s)/Q_2(s))s + \omega_2^2}, \qquad (D2)$$

and $\gamma_{13}(s)$, which is the third term in the square bracket in (D1). The authors state that the coupling coefficients $\gamma_{12}(s)$ and $\gamma_{13}(s)$ are, respectively, a measure of the effect of the coupling exerted by the second and third modes on the first mode $Q_1(s)$. This statement is incorrect, because $\gamma_{12}(s)$ and $\gamma_{13}(s)$ are not functions of $Q_2(s)$ and $Q_3(s)$ only; they do incorporate $Q_1(s)$. Therefore, $\gamma_{12}(s)$ and $\gamma_{13}(s)$ cannot determine the effect of $Q_2(s)$ and $Q_3(s)$ on $Q_1(s)$ explicitly. The authors' argument could have been correct if $Q_1(s)$ was not present in $\gamma_{12}(s)$ and $\gamma_{13}(s)$.

Next, the authors introduce the coupling index. The coupling index for the first mode is $\Gamma_1(s) = \gamma_{12}(s) + \gamma_{13}(s)$. According to the authors' statement, a large magnitude of $\Gamma_1(s)$ at $s = J\omega_f$, $J = \sqrt{-1}$, implies a significant effect of the modal coupling on $Q_1(s)$. This statement is incorrect, because $\Gamma_1(s)$ incorporates $Q_1(s)$, and hence its direct effect on $Q_1(s)$ is not clear. If the authors' statement was correct, then the computed value of $|\Gamma_i(J\omega_f)|$ for each i could help decide on the approximate decoupling of the system (3) by neglecting the off-diagonal elements of the matrix D. We, however, note that in order to compute $|\Gamma_i(J\omega_f)|$ for any i, we have to know the exact responses of the system, $Q_i(s)$, for all i. The question is: So what do we achieve by computing $|\Gamma_i(J\omega_f)|$ if we are supposed to solve the system for $Q_i(s)$ for all i? If we solve the system, then there is no need to know the extent of the modal coupling that would possibly help us decide on the approximate decoupling of the system.

In Section 4, the authors analyze the effect of the separation of the natural and excitation frequencies on the decoupling of the modes. They first define $\alpha_i = \text{Re}[\Delta_i(J\omega_f)]$ and $\beta_i = \text{Im}[\Delta_i(J\omega_f)]$. Next, they derive expressions (22) and (23) for $|Q_i(J\omega_f)|$ and $arg(Q_i(J\omega_f))$. We note that (22) and (23) express $|Q_i(J\omega_f)|$ and $arg(Q_i(J\omega_f))$ implicitly, because they incorporate α_i and β_i, which in turn are functions of $Q_i(J\omega_f)$. Using (22) and (23), the authors draw conclusions (*a*), (*b*), (*c*), and (*d*). The validity of these conclusions is questionable, because (22) and (23) are not explicit expressions for $|Q_i(J\omega_f)|$ and $arg(Q_i(J\omega_f))$; the response $Q_i(J\omega_f)$ is embedded in the right-hand sides of (22) and (23).

Authors' Closure[3]

The purpose of our paper is to demonstrate that, within the practical range of engineering applications, neither diagonal dominance of the modal damping matrix nor frequency separation of the natural modes would be sufficient for neglecting modal coupling. The discussion by Dr. S. M. Shahruz is much appreciated. However, the issues brought up in the discussion are rather minor and stylistic. These issues can be readily clarified in the following paragraphs.

It was stated in our paper that the coefficient of $U(s)$ in Eq. (14) could be thought of as a transfer function of the modal response. While it is useful to intuitively look at Eq. (14) that way, it is also clear that the coefficient of $U(s)$ cannot be a transfer function from a strict mathematical viewpoint. An obvious reason is that the Laplace transform of the input is not just $U(s)$, the elements f_i ($i = 1, 2, \ldots, n$) of the amplitude vector must also be included. The coefficient of $U(s)$ was never formally defined as a transfer function, nor was any property of a transfer function invoked on it. In our paper, it is suggested that the coupling term γ_{12}, for example,

[1] By I. W. Park, J. S. Kim, and F. Ma and published in the Mar. 1994 issue of ASME JOURNAL OF APPLIED MECHANICS, Vol. 61, pp. 77–83.

[2] Research Scientist, Berkeley Engineering Research Institute, P.O. Box 9984, Berkeley, CA 94709.

[3] I. W. Park, J. S. Kim, and F. Ma, Department of Mechanical Engineering, University of California, Berkeley, CA 94720.

Copyright © 1994 by ASME
Downloaded 03 May 2010 to 171.66.16.20. Redistribution subject to ASME license or copyright; see http://www.asme.org/terms/Terms_Use.cfm

Journal of Applied Mechanics

Book Reviews

Elasticity, by J. R. Barber. Kluwer. Dordrecht, 1992. 293 pages. Price: $119.00.

REVIEWED BY C. O. HORGAN[1]

This book is described on its back cover as

"a first year graduate textbook in Linear Elasticity, being based on a one semester course taught by the author at the University of Michigan. It is written with the practical engineering reader in mind, dependence on previous knowledge of Solid Mechanics, Continuum Mechanics or Mathematics being minimized. Most of the test should be readily intelligible to a reader with an undergraduate background of one or two courses in elementary Strength of Materials and a rudimentary knowledge of partial differentiation. Emphasis is placed on engineering applications of elasticity and examples are generally worked through to final expressions for the stress and displacement fields in order to explore the engineering consequences of the results. The topics covered were chosen with a view to modern research applications in Fracture Mechanics, Composite Materials, Tribology and Numerical Methods. Thus, significant attention is given to crack and contact problems, problems involving interfaces between dissimilar media, thermoelasticity, singular asymptotic stress fields and three-dimensional problems. Problems suitable for class use are included at the end of most of the chapters. These are expressed wherever possible in the form they would arise in Engineering—i.e. as a body of a given geometry subjected to prescribed loading—instead of inviting the student to "verify" that a given candidate stress function is appropriate to the problem. The text is therefore written in such a way as to enable the student to approach such problems deductively."

The book is in three parts: I General Considerations (2 chapters), II Two-Dimensional Problems (12 chapters), III Three-Dimensional Problems (11 chapters). Part I consists of 28 pages outlining notation and developing the equilibrium equations and compatibility conditions. Part II (156 pages) provides extensive treatment of the plane strain and plane stress problems of linear isotropic elastostatics. The extent of coverage can be gleaned from the chapter titles: 3 Plane strain and plane stress; 4 Stress function formulation; 5 Problems in rectangular coordinates; 6 End effects; 7 Body forces; 8 Problems in polar coordinates; 9 Calculation of displacements; 10 Curved beam problems; 11 Wedge problems; 12 Plane contact problems; 13 Forces, dislocations and cracks; 14 Thermoelasticity. Part III (102 pages) covers a number of topics in three-dimensional elasticity: 15 Displacement function solutions; 16 The Boussinesq potentials; 17 Thermoelastic displacement potentials; 18 Singular solutions; 19 Spherical harmonics; 20 Axisymmetric problems, 21 Frictionless contact; 22 The boundary value problem; 23 The Penny-shaped crack; 24 The interface crack; 25 The Reciprocal theorem.

From the foregoing, it can be seen that this book covers a variety of topics of contemporary interest in linear isotropic elastostatics. The emphasis throughout is on applications, rather than theory. The most important areas are covered, with the exclusion of complex variable methods which the author states "would need most of a book of this length to itself." The book is clearly written, the problems considered are well motivated and it is certainly suitable as a graduate textbook. It is a viable alternative to the book of Timoshenko and Goodier and may, indeed, be regarded as a modern version of this classic.

Plasticity and Creep, by J. J. Skrzypek (English ed. edited by R. B. Hetnarski). CRC Press, 1993. 542 pages.

REVIEWED BY Z. MRÓZ[2]

The present book provides a comprehensive introduction to plasticity and creep of materials and structures. It is addressed to students of applied mechanics and can be used within mechanical and civil engineering undergraduate or graduate programs. The present version originated from the Polish edition of 1986, which was based on courses taught by the author at the Cracow Technical University.

The book is divided into six parts: I Basic Definitions, pp. 1-36; II Foundations of Plasticity, pp. 37-235; III Solutions of Elastic-Plastic Problems, pp. 235-355; IV Foundations of Creep, pp. 355-425; V Solution of Creep Problems, pp. 425-465; VI Creep Rupture, pp. 465-511.

Part I is composed of two chapters: Stress and Strain State, and Finite Deformations. First, the stress and linear strain tensors are introduced and equilibrium and compatibility equations are derived. The principal stress and strain components are determined together with principal invariants. Next, the finite strain tensors of Green and Almansi are introduced in both rectangular and curvilinear coordinates. The Cauchy and Piola-Kirchhoff stress tensors are also briefly discussed with respective equilibrium and virtual work equations.

Part II consists of three chapters: Basic Equations of Perfect Plasticity, Basic Equations of Plastic Hardening, and Methods of the Theory of Plasticity. The fundamental assumptions of the perfectly plastic model are outlined with several yield conditions discussed in detail. The flow rule and the Hencky deformation theory are next introduced and their applicability is illustrated. For hardening description isotropic, kinematic, and combined hardening models are introduced. The concepts of cyclic plasticity and shake down are briefly

[1]Department of Applied Mathematics, University of Virginia, Charlottesville, VA 22901. Fellow ASME.

[2]Institute of Fundamental Technological Research, Warsaw, Poland. Mailing address: c/o R. B. Hetnarski, Department of Mechanical Engineering, P. O. Box 9887, Rochester Institute of Technology, Rochester, NY 14623.

Copyright © 1994 by ASME
Downloaded 03 May 2010 to 171.66.16.20. Redistribution subject to ASME license or copyright; see http://www.asme.org/terms/Terms_Use.cfm